# Electronic Warfare Receivers and Receiving Systems

Richard A. Poisel

# Table of Contents

# Preface

Receiver systems can be considered to be the core of electronic warfare (EW) intercept systems. Without them the fundamental purpose of such systems is null and void. In this work we consider the major elements that make up receiver systems and the receivers that go in them.

Receiver system architectures are introduced in Chapter 1. Basic nomenclature and system functioning are covered, including the key system performance parameters. Spread spectrum signaling is introduced as that, along with non-spread digital signaling, is the foundation of most communication systems in which we are interested. The chapter concludes with an overview of collection management on the battlefield. EW signal collection is but one of many ways information is collected, and it is useful to see where EW fits with some of the other disciplines.

Chapter 2 covers communication signals and the modulation systems they use. Mathematical representations of these signals are introduced. The principal focus is on digital techniques as digital signaling is the basis for modern spread spectrum communications. An introduction to random modulation is provided because most realistic communication signals are contaminated with at least thermal noise and that yields them at least partially stochastic in nature. We introduce the primary spectrum access methods to include the relatively new one, spatial division multiple access. The chapter concludes with a brief discussion of two of the most popular types of signal filtering methods.

Beginning in Chapter 3, we delve into the major elements comprising receivers. Chapter 3 specifically covers the RF stage at the target signal entry point. Major noise sources are considered with particular emphasis on low noise amplifiers. Thermal noise is a particular nemesis because target signals of interest are typically very weak for EW systems. Low noise amplifiers are required to minimize this source of noise. Although the coverage is far from exhaustive, we consider low noise amplifiers designed with both bipolar junction transistors and metal oxide semiconductor transistors. The effects of mismatches between the antenna and receiver input are covered. The chapter concludes by considering band select/preselector filters and why they are required.

The low noise amplifier (LNA) in the receiver RF stage must be as wideband as possible in EW receivers. These receivers typically have a very wide frequency

range and usually multiple LNAs. Of course, the more of these amplifiers, the more costly the receiver becomes, both in terms of price and the amount of space occupied by the receivers. In addition, the receiver requires more power, which is usually at a premium. The preselection filters also must be wideband, but usually not as wide as the LNA. Suboctave preselector filters are frequently employed. Relatively narrowband (i.e., 10% of tuned frequency) amplifiers are also used. Thus, in Chapter 4 we introduce some techniques for enhancing the bandwidth of amplifiers.

The next stage in the signals path through the receiver is usually the mixer, which we introduce in Chapter 5. The fundamental parameters are discussed and the limitations on the mixer are covered. Some simple mixers are introduced, concluding with a discussion on the Gilbert mixer, popular for system-on-a-chip receivers. Chapter 5 concludes with a presentation on oscillators. The local oscillator plays a large role in establishing the receiver performance.

The mixer stage usually drives the intermediate frequency (IF) chain, which we introduce in the next two chapters. In Chapter 6 the RF amplifiers used for the IF amplification function are considered. Chapter 7 examines analog filters and their characteristics. These filtering stages are normally narrowband, with the same frequency used irrespective of the RF frequency to which the receiver is tuned.

Analog narrowband receivers, which have formed the majority of EW receivers up until relatively recently, are discussed in Chapter 8. The superheterodyne receiver is introduced along with its popular cousin, the homodyne receiver (which is really a special type of superheterodyne receiver). Tuned radio frequency receivers are briefly mentioned, although they do not comprise a widely used architecture for EW receivers. In some applications they can be used because of their simplicity and therefore low cost.

We consider compressive receiver architectures in Chapter 9. They form a family of architectures that, while being wideband, can detect signals that are changing frequency rapidly, as one type of spread spectrum does, and, coupled with the necessary signal processing, allows for intercept of these signals. The modules that allow for this fast processing are introduced and key performance parameters examined.

Another popular family of wideband receivers useful for processing spread spectrum signals is digital, which we introduce in Chapter 10. This chapter forms an introduction to the following five chapters, which delve deeper into particular topics for digital receivers. Chapter 11 covers the important topic of sampling signals as well as how this is accomplished—with analog-to-digital converters. The principal architectures and performance parameters for analog-to-digital converters are covered. Chapter 12 provides an introduction to digital filters and their performance. Methods for digital demodulation of signals are covered in Chapter 13. Converting signals from the digital domain back into the analog domain is sometimes (although not always) required. These devices and their main

architectures are introduced in Chapter 14. Finally, in Chapter 15 we consider direct digital converters, a method of extracting narrowband signals from wideband ones that are comprised of several of the narrowband signals. This is a key requirement of modern wideband EW receiving systems.

The methods of spreading narrowband signals into wideband ones are reviewed in Chapter 16. Direct spread, frequency hopping, and time hopping methods are discussed and their characteristics are assessed.

The next three chapters cover some receiver architectures for these three types of spread spectrum signals. Chapter 17 provides two representative architectures for direct spread signals. The difficulty in intercepting this type of signal should become clear after reading this chapter. Chapter 18 examines some popular digital architectures for intercepting frequency hopping signals, as well as the use of compressive receivers for this purpose. These signals are considerably easier to process. Finally, Chapter 19 illustrates receiver architectures for time hopping signals. The method of accomplishing time hopping consists of using pulse position modulation and very wide bandwidths (several gigahertz). As such, they can easily interfere with many other types of communications if their power is not carefully controlled. Because of this, they are currently limited to very short range links (personal area networks). The receiver architecture that can address this signal type is the time-channelized radiometer, and we discuss that architecture.

We introduce receiver techniques for direction finding in the final chapter, Chapter 20. We examine the architectures for the most popular forms of signal processing and discuss most of the sources of error introduced both internally and externally in EW systems. We conclude the chapter with a brief discussion of using the compressive receiver for this purpose primarily for frequency hopping targets.

Some symbols are duplicated. In a book such as this that covers a wide variety of subjects, it is difficult to avoid reusing symbols and still adhering to common standards ($f$ for both frequency and noise factor, e.g.). While every effort has been made to minimize this, some duplication is unavoidable. In those cases, it is hoped that the meaning of the symbols is clear from the context.

Any errors of commission or omission are the responsibility of the author. As always, constructive feedback is welcomed.

# Chapter 1

## Receiving Systems and Receiving System Architectures

### 1.1 Introduction

In this chapter we present the fundamental electronic warfare (EW) receiving system architectures. Since this book is about EW receivers, a great deal more will be said about receivers in the later chapters. This chapter presents the big picture of receiver architectures.

The modern taxonomy of EW is illustrated in Figure 1.1. This functional area is usually split into three fundamental areas as shown: (1) *electronic support* (ES), *electronic attack* (EA), and *electronic protect* (EP) as shown:

- ES is comprised of all the processes necessary to intercept battlefield transmissions for the purpose of generating combat information. This includes determining targets for EA.
- EA is the actions taken to insert false signals into equipment meant to receive the transmissions. This includes jamming receivers.
- EP is the actions taken to protect friendly forces from being successfully attacked by opposing forces using ES and EA.

Here we are mainly concerned with the ES function, and, in particular, the receivers and receiver systems that are used to intercept adversarial communication systems. We explicitly preclude discussions on other types of transmission systems (e.g., radars) to keep the discussions limited in scope.

This chapter is oriented as follows. We begin with a summary of ES functionality and the command and control process. We then present the electromagnetic spectrum for future reference. The second part of the chapter is

```
                    ┌─────────────────────┐
                    │  Electronic Warfare │
                    └─────────────────────┘
        ┌───────────────────┼───────────────────┐
┌─────────────────┐ ┌─────────────────┐ ┌─────────────────┐
│Electronic Support│ │Electronic Attack │ │Electronic Protect│
└─────────────────┘ └─────────────────┘ └─────────────────┘
```
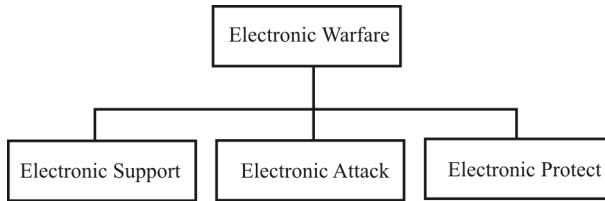
**Figure 1.1** Electronic warfare taxonomy.

devoted to a dialog on how EW receiving systems are configured to accomplish the functions identified in the first part. The chapter concludes with a brief discussion on collection management, which outlines the way targets are derived for ES (and other) systems.

## 1.2 Electronic Support Systems

In the context of this chapter and the remainder of this book, a receiving system is defined as those elements necessary for the noncooperative intercept of targeted communication systems.

### 1.2.1 Electronic Support

ES is action taken to search for, intercept, locate, and analyze radiated *electromagnetic* (EM) energy for the purpose of exploiting these in support of military operations. This information is sometimes referred to as *combat information*, and it is generally used for support of immediate activities. When further analyzed, it can also be used for intelligence generation.

One of the most important, but difficult, problems associated with electronic surveillance and countermeasures involves the recognition of signals in an extremely complex multisignal environment. In many RF environments of interest every, or almost every, channel is occupied. The signals acquisition receiver must search a wide frequency band, while providing an interception capability with extreme speed, large dynamic range, and high sensitivity. These characteristics are especially important when the threat signals are frequency agile. The use of frequency agile *electronic counter-countermeasures* (ECCM) techniques by the opposing side is a significant threat to the ability of denying effective use of the EM spectrum. Faced with a frequency agile threat, the countermeasures system must locate each dwell frequency rapidly enough so that jamming interference can be applied in a manner and for a time sufficient to cause loss of message intelligence.

The modern EW environment is characterized by communication systems emissions that are increasing in number and sophistication. As the demand for communications continues to expand, the electronic technologies will continue to

be driven by the need to gather and process ever-increasing amounts of information. This will place even greater demands on the digital technologies and on the application of more exotic frequency agile techniques.

It used to be true that the frequency bands of primary interest to tactical military EW systems started at about 2 MHz and reached about 500 MHz. With the advent of modern forms of communication, such as cellular phones and various networking capabilities, this frequency range has expanded up to 5 GHz and beyond in some cases. These signal transmissions utilize conventional forms of modulation, as well as *low probability of intercept* (LPI) formats.

ES has the important advantage as a detector of enemy systems in being completely passive. Active sensors such as radar and sonar can generally be detected at ranges much greater than the maximum range at which the active system can detect targets. ES systems, on the other hand, have no sensor signals that an adversary can detect. (There are C2 signals that emanate from ES systems in order to control the system. However, these signals are normally the same type as used by other forces in the area so they do not compromise the ES system as such.)

## 1.2.2 Command and Control

A concise definition of *command and control* (C2) was provided by MG John B. Marks (Ret.) as follows:

> **Definition 1.1:** *Command and Control*
> Command: All the means necessary to direct actions.
> Control: All the means necessary to ensure that directed actions
> are being carried out [1].

It has been true through the ages that to successfully engage in combat, a military leader must have effective C2 of his forces. This is true whether the forces consist of armies, groups of tanks, a naval flotilla, aircraft, or some combination of these. A commander needs to have communications links for transmitting directions to his forces. Superior C2 executed by a commander, and the communications to carry out these orders, can often offset the disadvantages of having forces that are smaller in number of those of an enemy force.

It is a generally held opinion that in modern warfare, victory goes to the side that can effectively control the spectrum.

Thus we see that communications places a large role in C2. In many tactical situations that communication is via RF transmissions. Commanders must communicate both with their subordinates and their superiors in order to effectively execute the C2 functions. It is precisely this feature that is exploited by ES systems, and the better the ES functions, the better exploitation ensues.
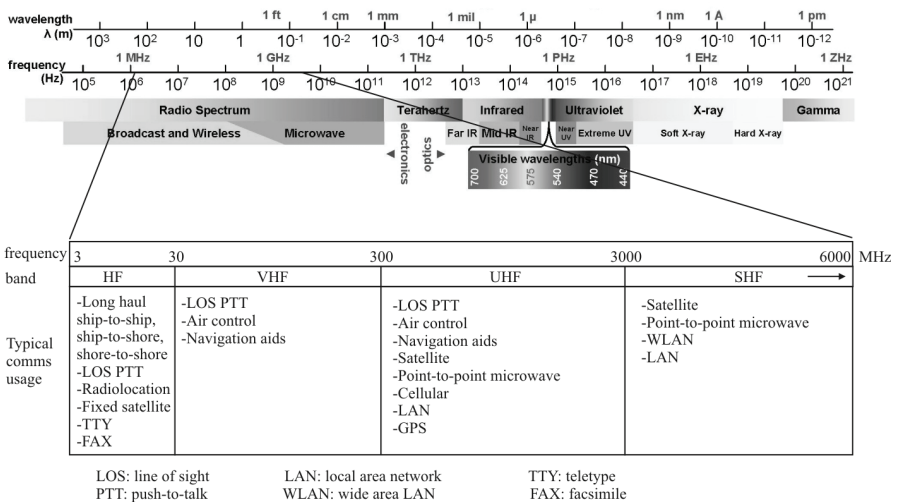
**Figure 1.2** The electromagnetic spectrum used for communication.

# 1.3 The Electromagnetic Spectrum

We show the *electromagnetic spectrum* (EMS) in Figure 1.2. The portion of the band that is normally used for communication purposes is shown at the bottom of the chart (this excludes some forms of communication by the Navy for communications with submarines). The band extends from the *high frequency* (HF) through the lower end of the *super high frequency* (SHF) spectrums. This is the band of concern to most modern ES systems. This is not to say that a single system needs to cover this entire region, but the entire region must be included when considering the requirements for ES systems.

The types of communication transmissions that transpire in these zones are also indicated in Figure 1.2, although this list should not be considered complete. Special communications systems and capabilities can be found in almost all regions of the frequency spectrum, for example. It is also important to note that while radars are not normally used for communications (although some can be), they can be found in all of the regions shown in Figure 1.2 as well. For communications ES, radars are a source of interference and noise.

# 1.4 Receiving System Architectures

In this section we present the basics of receiving system architectures to provide a baseline for detailed discussions of receiving systems in the subsequent chapters.
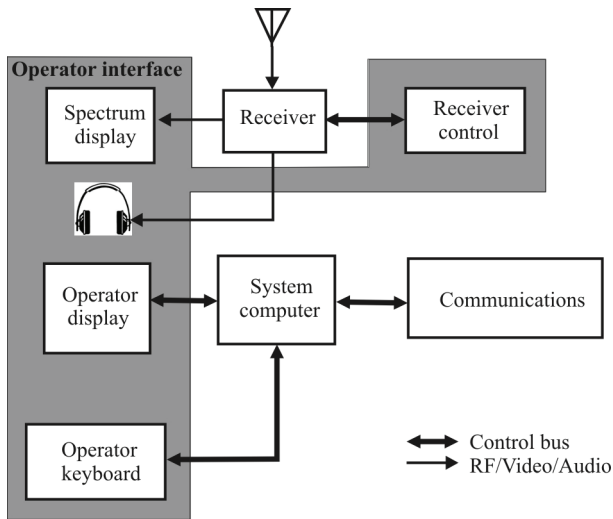
**Figure 1.3** A simple receiving system.

By far the most prolific receiver architecture in use for EW systems is the superheterodyne structure.

## 1.4.1 Fundamental Receiving System Model

A diagram of a simple (maybe the simplest) receiving system is shown in Figure 1.3. The receiving subsystem consists of an antenna, a *receiver* (Rx), a *spectral display unit* (SDU), and a *receiver control unit* (RCU). The operator subsystem consists of a system computer and the necessary equipment for an operator to interface with it. The ability to communicate with the outside world is also included. Signal paths [*radio frequency* (RF) and *intermediate frequency* (IF) in this case] are shown with light lines while dark lines indicate control lines.

The Rx may actually consist of several receivers, each of which covers a portion of the total frequency spectrum (receivers for the HF range are typically much different from those for the VHF range, e.g., and two receivers would be implemented in this case). The SDU displays the portion of the frequency spectrum of current interest to the operator. The signal sent from the receiver to the SDU is normally the IF signal in the receiver or some other video (pre-detected) signal useful for the purpose. Sometimes the SDU signal information is implemented on the operator's display. The presence of a signal at a frequency/channel is indicated by some mechanism on the screen of the SDU. The RCU performs the function of controlling the receiver and may, in reality, be the receiver front panel or a function implemented by the system computer, in which

case the operator's control of the receiver is via the keyboard and display. Control signals are sent from the RCU to the receiver to change the receiver settings, such as frequency. In return, status signals are sent from the receiver back to the RCU to indicate the health of the receiver.

The operator subsystem, while not literally part of the receiving subsystem, is shown for completeness to illustrate where the operator fits into the receiving process. The keyboard and display permit the operator to interface with the system computer to facilitate receiving tasking from the C2 source as well as to communicate the results of the receiving process to a destination.

The architecture, while simple in this case, is extensible and not much changes. A receiving system with many operators each with one or more receivers would look like Figure 1.3 replicated the necessary number of times. The system computer would likely be more powerful. The operator interfaces would likely be some sort of standard control bus such as MIL-STD-1555 or 10baseT or 100baseT Ethernet.

In the largest of such receiving system, the functions of searching the spectrum and subsequent copying of targets of interest would typically be separated and executed by operators specializing in one subset of the overall functions.

1.4.1.1 Signal Searching

The system shown in Figure 1.3 could be used to search the spectrum for signals of interest, or it could be used to tune to specific frequencies to see if there is current activity at a frequency. The former is referred to as *general search* and normally the search is executed from some start frequency to some stop frequency, typically linearly.

The latter search method is referred to as *directed search*, and specific frequencies are programmed into the RCU. This is the mode when the target frequencies of interest are a priori known.

The two search modes can be mixed. One implementation of an algorithm that combines the two is illustrated in Figure 1.4 [2]. In this architecture a revisit timer is used to cycle between the two search modes. It represents the amount of time the system spends in the general search mode before entering the directed search mode. Starting in the general search mode, the next scan frequency is selected to examine for energy presence. If there is energy present at that channel, the signal is copied, which may or may not be accompanied by recording of the signal. Other functions may also be executed at that time, such as obtaining a geoposition (fix) of the target, as illustrated in Figure 1.4. If the target is of interest, typically the channel is entered onto the directed search list. When copying is completed the scan process proceeds. If there is no energy detected at the tuned channel, the revisit timer is examined to see if it has expired. If not, the next channel is chosen. If it has expired, the directed search mode is entered. In this mode, each directed
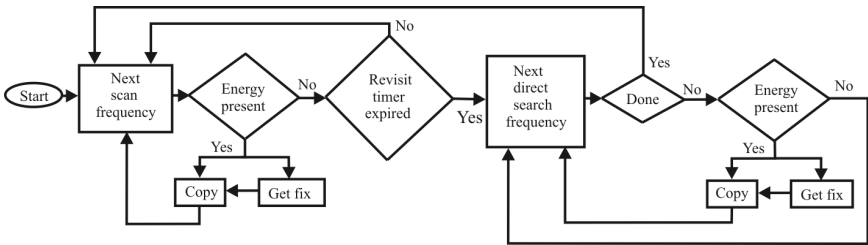
**Figure 1.4** An EW signal collection process. (Source: [2], ©Artech House, 2002. Reprinted with permission.)

search frequency is examined in sequence. If energy is detected at one of these frequencies, then, as in the general search mode, the target is copied, and possibly other functions are executed. Once all the directed frequencies are examined, the general search mode is started again.

A somewhat more extensive receiving system is illustrated in Figure 1.5. In this case the search receiver/receiving subsystem is separate from the receiver used for the copy function. The monitor receivers are typically queued from the search
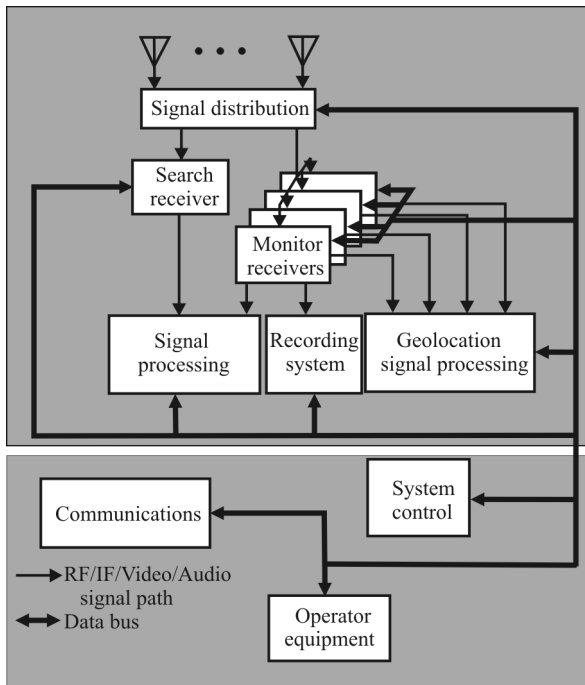


**Figure 1.5** Receiving system with a separate search function.
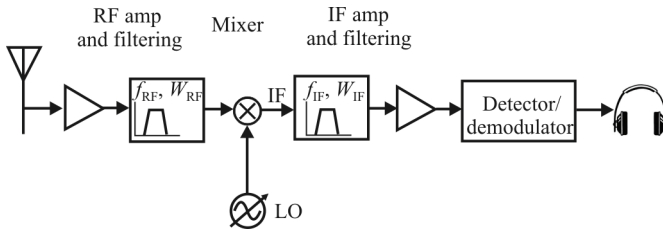
**Figure 1.6** Fundamental concept of the superheterodyne receiver.

process and tuned automatically to where signal energy is detected. The signals thus received are recorded in the receiving subsystem, which could be analog tape recorders or, more recently, digitally recorded onto computer disk storage. The operators in this case would process the recorded signals rather than the signals directly from the receivers.

We concentrate here on the receiver functions in Figures 1.4 and 1.5. For a description of the other elements shown, the reader is referred to [3–8].

## 1.5 Monitor Receivers

Monitor receivers are used in ES systems to receive signals on a more or less constant basis. That is, they are not generally used to search for *signals of interest* (SOIs). We introduce the most common receiver architecture here, the superheterodyne configuration.

### 1.5.1 Concept of the Superheterodyne Receiver

A flow diagram of the superheterodyne (superhet) receiver is shown in Figure 1.6. RF signals entering the receiver from the antenna are first amplified and filtered. They are then mixed (multiplied) with the *local oscillator* (LO) signal in the mixer to convert them to a (usually lower) frequency. Signals at all frequencies are converted to the common IF for further amplification and filtering so the LO must be variable in order to provide the correct mixing frequency. This concept is based on the trigonometric relationship describing the product of two sine waves:

$$\sin A \sin B = \frac{1}{2}[\cos(A-B) - \cos(A+B)] \tag{1.1}$$

One of terms on the *right hand side* (rhs) of (1.1) is removed by subsequent filtering (either can be used—the other eliminated). The IF signal is then amplified and further filtered (narrowband) to remove the unwanted term in (1.1) as well as

Figure showing the superhet mixing process block diagram:

Input signal at 6 MHz → Mixer (⊗) → Resulting signal at 1 MHZ and 11 MHz → 1 MHZ IF amplifier and filter ($f_{IF}$, $W_{IF}$)

Local oscillator → Oscillator signal at 5 MHz

$f_{IF} = 1$ MHZ
$W_{IF} = 100$ kHz
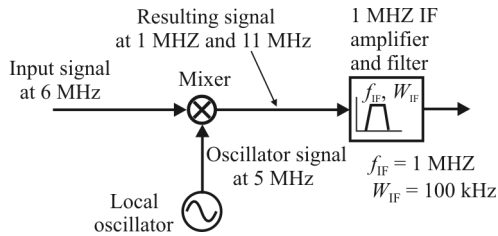
**Figure 1.7** Example of the superhet mixing process.

other unwanted signals. The IF signal is then detected, depending on the type of modulation. If the resulting signal is audio, it then drives headphones or other audio device, such as a tape recorder. If the resulting signal is digital, further digital processing is performed to extract information.

In the superhet radio, the received signal enters one input of the mixer. A locally generated signal (LO signal) is fed into the other. The result is that replicas of the RF signal are generated at new frequencies. These are applied to a fixed frequency IF amplifier and filter. Any signals that are converted down and then fall within the passband of the IF amplifier will be amplified and passed on to the next stages. Those that fall outside the passband of the IF are rejected. Mixing two sinewave signals together in this way produces a signal with components at the sum and difference frequencies according to (1.1).

In the example shown in Figure 1.7, signals will appear at the mixer output at 1MHz and 11 MHz. Tuning is accomplished simply by varying the frequency of the LO. The advantage of this process is that very selective fixed frequency filters can be used and these far outperform any variable frequency ones. They are also normally at a lower frequency than the incoming signal and again this enables their performance to be better and less costly. The spectrum is shown in Figure 1.8.

To see how this operates take the example of two signals, one at 6 MHz and another at 6.1 MHz. Also take the example of an IF situated at 1MHz. If the local oscillator is set to 5 MHz, then the two signals generated by the mixer as a result of the 6 MHz signal fall at 1 MHz and 11 MHz. If the IF filter bandwidth is

Frequency spectrum diagram with Magnitude on the vertical axis and $f$ (MHz) on the horizontal axis. Markers labeled "Original signals", "Resultant" at 1, "LO" at 5, "RF" at 6, and "Resultant" at 11.
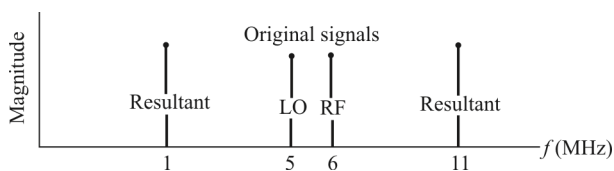
**Figure 1.8** Superhet example frequency spectrum. The signals generated by mixing or multiplying two signals together.

narrow enough, the 11 MHz signal is rejected, but the one at 1 MHz passes through the IF stages. The signal at 6.1 MHz produces a signal at 1.1 MHz (and 11.1 MHz), and this falls outside the bandwidth of the IF (±50 kHz) so the only signal to pass through the IF is that from the signal on 6 MHz.

If the LO frequency is moved up by 0.1 MHz to 5.1 MHz, then the signal at 6.1 MHz will give rise to a signal at 1 MHz and this will pass through the IF. The signal at 6 MHz will give rise to a signal of 0.9 MHz at the IF and will be rejected. In this way the receiver acts as a variable frequency filter, and tuning is accomplished.

The superhet receiver is by far the most common form of EW receiver in use. It is the best performing narrowband receiver architecture, and components are readily available for satisfying even the most demanding requirements. We discuss the superhet further in Chapter 5, and introduce some other forms of narrowband receivers.

# 1.6 Search Receiver Architectures

There are several configurations of receivers that can serve as search receivers. We will introduce three topologies and give their basic operation principles here. Those architectures are:

- Scanning narrowband receiver
- Digital transform receiver
- Compressive receiver (CxRx)

## 1.6.1 Scanning Narrowband Receiver

The simplest type of search receiver is probably the scanning superheterodyne receiver, which is simply a superheterodyne receiver whose frequency is linearly changed with time.

Most modern tuned superheterodyne receivers are digitally controlled for maximum flexibility. They can be controlled directly with an RCU or via computer as required. These receivers actually dwell on a frequency channel as opposed to scanning as in an analog equivalent.

The frequency resolution achievable with a digitally tuned narrowband receiver is inversely proportional to dwell time. For example, if the receiver dwells at a frequency for 10 ms and the instantaneous bandwidth of the receiver is 200 kHz, then the maximum channelization possible is to divide the 200 kHz bandwidth into 200 1 kHz cells.

Conventional EW receivers cannot readily detect the transmission of *frequency hopped spread spectrum* (FHSS) or short-duration signals, however. It

is necessary to search a wide frequency band and detect signals over a large dynamic range very rapidly with a high probability of success. This is only possible, considering the expected threat signals, if the sweep rate versus resolution restrictions inherent in standard superheterodyne receivers are overcome.

Figure 1.9 is a time-frequency diagram for a scanning superheterodyne receiver. The revisit time as a function of dwell time is shown in Figure 1.10. Revisit time is the time required to scan from a given frequency through the scan bandwidth, $W_s$, and back to the same frequency. Dwell time is the time a signal must exist within the analysis bandwidth, $W_B$. This constraint on dwell time is due to the finite time (approximately $2/W_B$) required to achieve essentially 100% response to a CW signal. The corresponding constraint on sweep rate is that the receiver sweep no faster than $W_B$ Hz in $2/W_B$ seconds, or $0.5W_B^2$ Hz/sec. If, for example, an analysis bandwidth of 25 kHz is to be used, the corresponding sweep rate possible is 0.313mHz/ms, hardly a sweep rate that could be used to follow even a slow frequency hopping target over the VHF band. Figure 1.10 shows the minimum cell width required.

While the superheterodyne receiver remains a valuable analysis tool, other wideband receiver techniques are promising candidates to handle the rapid signal acquisition needs in the communications frequency bands. Two wideband possibilities are the compressive receiver and digital transform receivers. Performance considerations will follow a brief description of each of the receiver types.

## 1.6.2 Compressive Receiver

A compressive receiver flow diagram is shown in Figure 1.11. The RF subsystem converts the RF input band to the compressive IF processor input frequency range. The logarithm of the amplified time-compressed IF processor output is computed to reduce the required dynamic measurement range. The logarithm of the signal is passed to the signal sorting processor, which develops the threat signal information for the jamming system controller (if the ES receiver is feeding a jammer). Information transfer is by way of the receiver controller. The heart of the CxRx is the compressive IF processor. Figure 1.12 is a conceptual block diagram of the IF processor. The input signal bandwidth is restricted by the *bandpass filter* (BPF) to the width of the *dispersive delay line* (DDL). The BPF output is then converted to the final IF, which is swept through the DDL band by the linear *swept local oscillator* (SLO). The swept IF signal generated is the complex conjugate of the DDL impulse response. The sweep occurs every receiver scan period and sweeps the processor through a frequency range that ensures complete correlation of all signals within the passband of the input BPF.

The IF processor develops an output for each scan that represents the spectral energy distribution present at its input during that scan period. A *continuous wave*

$$\mu = W_B/T_a$$
$$T_a = (W_B/W_s)T_s$$
$$W_s = \mu T_s$$

$W_s$ = Scan (search) bandwidth
$T_s$ = Scan time
$W_B$ = Analysis bandwidth
$T_a$ = Analysis time
$f_1$ = Lower scan frequency limit
$f_c$ = Intercepted center frequency
$f_2$ = Upper scan frequency limit
$\mu$ = Scan speed
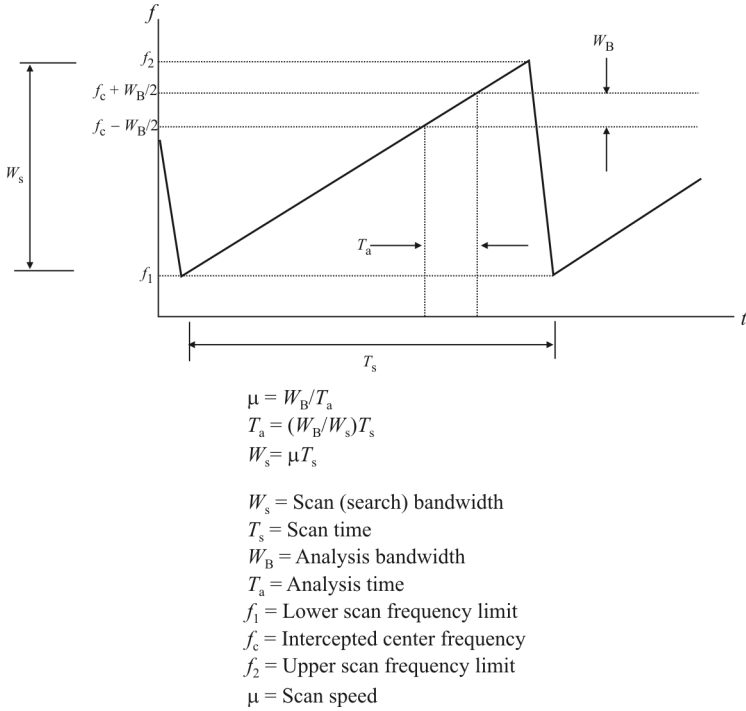
**Figure 1.9** Frequency versus time for the scanning superheterodyne receiver.
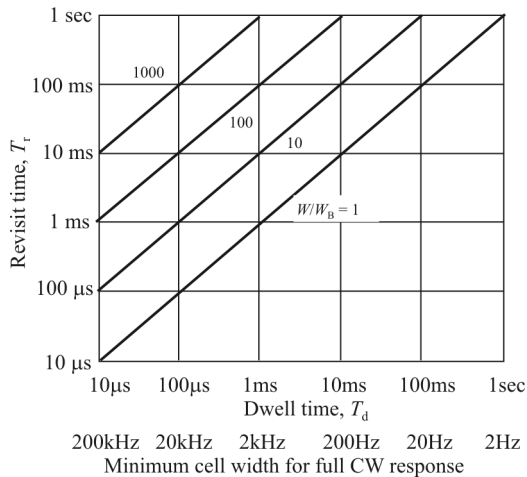


**Figure 1.10** Minimum cell width of the scanning superheterodyne receiver. $W$ is the RF search range and $W_B$ is the analysis bandwidth.
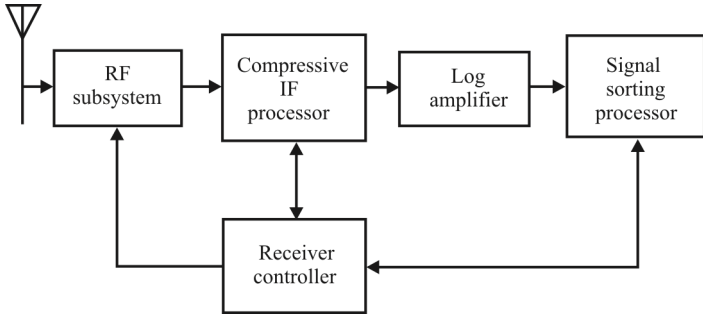
**Figure 1.11** Compressive receiver flow diagram.
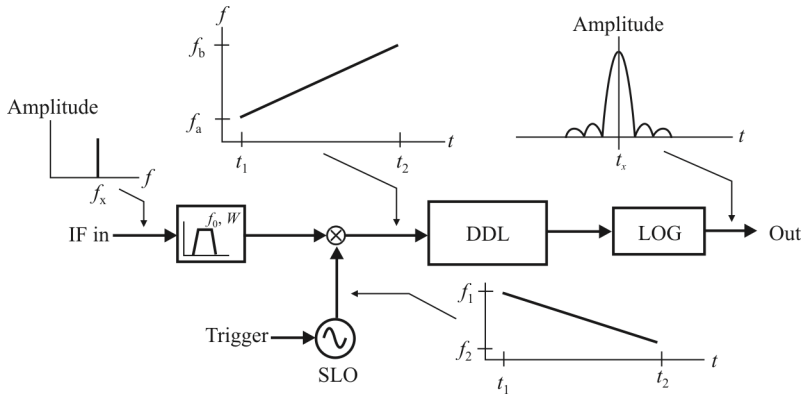


**Figure 1.12** Operation of the CxRx IF processor.
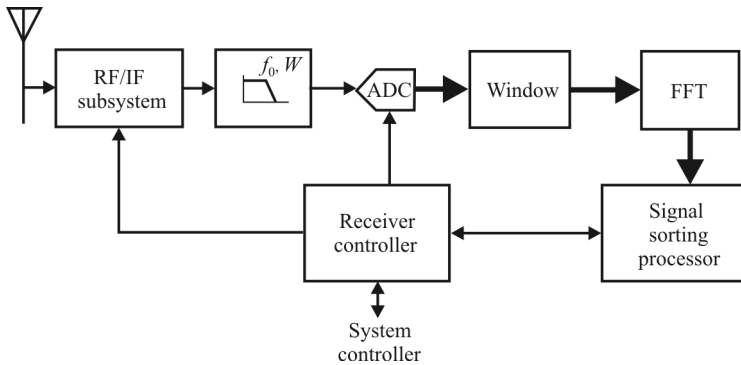
**Figure 1.13** Digital FFT receiver.

(CW) input will develop a representative output pulse once per scan at a position in time that corresponds to its frequency; that is, it maps the spectral components at its input into time domain outputs, which amounts to performing a continuous Fourier transform for each signal occurring within its input bandwidth. The output pulse results because the frequency dependent delay of the DDL is such that the beginning of an output pulse is delayed a length of time equal to the input pulse duration. Intermediate portions of the pulse are proportionately delayed a lesser time. Consequently, all signal energy tends to emerge from the DDL output at one instant of time. Because the tendency toward instantaneous response is bandlimited, the output pulse is of finite duration and is approximately the reciprocal of the DDL bandwidth. It should be noted that the output pulse amplitude is a measure of the received signal strength.

For communication systems the requirement is that the compressive IF offer modest bandwidth with long processing time to provide a frequency resolution that is compatible with typical communications frequency spacing. A broad RF band can be covered by stepping the RF subsystem LO in increments the size of the DDL bandwidth.

## 1.6.3 Digital Transform Receiver

A digital *fast Fourier transform* (FFT) receiver is shown in Figure 1.13. The RF/IF subsystem converts the RF input band to a signal at or near baseband. A *lowpass filter* (LPF) is used to limit the frequency band to be sampled by the *analog-to-digital converter* (ADC). A window function is used ahead of the FFT processor to shape the processor output response. The FFT output is passed to the signal sorting processor, which develops threat signal information.

The digital transform receiver calculates the discrete Fourier transform of the downconverted RF input band by use of an FFT algorithm. The instantaneous

processing bandwidth is basically a function of the sampling rate of the ADC and the shape factor the anti-aliasing LPF uses ahead of the ADC. As in the case of the CxRx, the RF input band converted can be extended by incrementing the RF/IF subsystem LO in frequency steps the size of the basic processor instantaneous bandwidth.

## 1.6.4 Receiver Considerations

The two candidate communication receiver approaches considered here for fast signal acquisition are the CxRx and the FFT receiver. Each of these receiver approaches has advantages as well as disadvantages that must be weighed against the given application, and the available tradeoffs associated with approaches, in terms of the desired objectives, must be evaluated. Among the tradeoffs involved are those related to size, complexity, cost, probability of specific signal intercept, speed, compatibility with overall system requirements, and the risk associated with the development of technology for a given approach. Compressive receivers and digital transform receivers are well established, low-risk techniques.

Selection of an approach is strongly influenced by the requirement imposed on the system for *probability of intercept* (POI) of a particular target signal. When the receiver will be operational only for  a fraction of the time, because of look-through requirements, the POI problem can be especially severe.

If a receiver repetitively sweeps a frequency band in a time that is less than the on-time of an in-band target signal, or otherwise constantly looks at a frequency band, the target signal will always be intercepted. But if the receiver looks through periodically, the look-through period may not coincide with the signal on-time and interception will not occur. In order to ensure interception during each look-through, the look-through period must be at least as long as the signal pulse repetition interval, assuming a simple pulse-type representation of the signal. However, the actual signal statistics will be such that a number of look-throughs will be necessary to ensure a high POI. The appropriate operational strategy must be developed through analysis of the anticipated threat signal environment and, to a large extent, will for the basis of the receiver approach selection.

Instantaneous bandwidth and frequency resolution are also important receiver concerns that help guide the choice of receiver approach. All receiver approaches have constraints on frequency resolution in common. These constraints are a consequence of the time that a target signal is availabe for processing.

After establishing the receiver requirements that are based on parameters discussed to this point, a number of additional performance parameters must be specified for a given application. Among the parameters that will be considered are dynamic range, frequency accuracy, and sensitivity.

# 1.7 Key System Performance Parameters

While there are many interrelated EW receiving system parameters to be considered, the most important for characterizing the performance of a receiving system are:

- Noise figure
- Sensitivity
- Selectivity
- Dynamic range

**1.7.1 Noise Figure**

Noise is always present in any electronic equipment, and EW receivers are no exception. Noise is the nemesis of all communication systems. It is the challenge that must be addressed for adequate performance. Noise in an EW receiver system can be categorized as external or internal.

1.7.1.1 External Noise Sources

External noise sources include thermal (sky) noise, atmospheric noise, and man-made noise. This thermal noise is caused by viewing the sky with an antenna that has a non-zero temperature.

Thermal noise is caused by agitated electrons (temperature above absolute zero). Some of this energy is viewed by the receiving antenna, and if it has directionality, more energy is absorbed in the direction of maximum gain than in other directions. Bright noise sources (such as the sun) emit considerably more energy than the background sky that an antenna absorbs.

Atmospheric noise is predominant in the frequency region up to about 100 MHz. It is caused by lightning discharges and is broadband. Such noise energy can travel for considerable distances, especially in the lower HF frequency range.

There are many types of man-made noise sources. Man-made noise sources are any noise generator produced by manufacturing and would not exist in nature if it weren't for being artificially produced. Examples are fluorescent lights and welders. See [9] for more details on external noise sources.

1.7.1.2 Internal Noise

Internal noise sources include thermal noise and LO noise. The latter will be discussed at length in Chapter 5.

Internally generated thermal noise arises for the same reason that external thermal noise does—agitated electrons emit broadband energy. The ratio of the

*signal-to-noise ratio* (SNR) at the output of a system to that at its input (which is always greater than one since noise is generated in the system that is reflected at the output but is not present at the input) is known as the *noise factor*. The noise factor expressed in dB is known as the *noise figure* (NF).

### 1.7.2 Sensitivity

Sensitivity refers to how weak a signal can be and still be used to extract information in an ES system. It is closely related to the noise level present, both internal and external to the ES system. It is often specified in terms of an SNR level below which some system parameter, such as output SNR, cannot be effectively accomplished. In the VHF frequency range, for example, a typical sensitivity value is −105 dBm with a 15 dB RF SNR in a 25 kHz bandwidth. Another example is 20 dB RF SNR for a $10^{-3}$ *bit error rate* (BER) for a digital signal.

### 1.7.3 Selectivity

Selectivity specifies how closely signals can be located in the frequency spectrum and still be separated. It is primarily determined by the shape of the filters in the IF portion of the receiver.

Signals in adjacent channels in the RF spectrum can and do leak into each other's channel. This energy spillover may be caused by the transmissions themselves or may be caused by the receiver if the filtering is not adequate. Sharp filter rolloff is often required to minimize this interference.

### 1.7.4 Dynamic Range

The dynamic range is the total range of signal power that can be processed by a receiving system. There is an instantaneous dynamic range and a total dynamic range. The former refers to the total range of signals that can be collected without inserting some form of attenuation in the signal path to avoid overload of subsequent processing steps. The total dynamic range is the totality of the signal power levels that the receiving system can cope with, including the use of attenuators in the signal path.

### 1.7.5 Other Significant Parameters

1.7.5.1 Signal Bandwidth

The bandwidth of signals is an important parameter since the processing of signals with narrow bandwidths is typically quite different from those with a wide bandwidth. These are relative terms, however.

In a crowded RF environment, typical for many EW system applications, measuring the bandwidth can be problematical. When (almost) every channel is occupied, much of the time it can be difficult to determine where one signal leaves off and the next begins.

*Narrow Bandwidth*: Signals with narrow bandwidth include traditional VHF and UHF analog FM and digital signals as well as HF voice and data signals.

*Wide Bandwidth*: Signals with a relatively wide bandwidth include several forms of multichannel formats. Multicarrier *public switched telephone network* (PSTN) signals are of this variety and might include *frequency division multiplexed* (FDM) as well as *time division multiplexed* (TDM) arrangements.

FDM signals carry two or more information-bearing signals that are separated in baseband frequency but are transmitted on a single RF carrier. All users in an FDM system have access to the RF channel all the time. The RF carrier is typically FM modulated with the composite baseband signal.

TDM signals are comprised of two or more baseband signals that share the RF spectrum on the basis of time. During one time interval, one user has access to the channel while during the next time interval, another user has that access. The modulation used for TDM is normally, but need not be, FM.

1.7.5.2 Baud Rate

The baud rate is the signaling speed of digital signals. It is the rate at which information is exchanged over the channel. It is sometimes confused with the bit rate, which is a fundamentally different parameter. It can sometimes be used to identify a particular type of signal.

1.7.5.3 Bit Rate

The bit rate is the instantaneous speed of digital signaling. If the digital signaling is continuous, the baud rate and the bit rate are equivalent. If there are interruptions in the digital signaling when the bit rate is zero, then the baud rate is slower than the bit rate.

# 1.8 Spread Spectrum

A *spread spectrum* (SS) signal is one whose RF bandwidth is much larger than the bandwidth of the underlying information signal. (This is a loose definition since wideband FM modulation falls under this categorization yet is not normally associated with SS formats.)

SS signals can be categorized as *low probability of detection* (LPD), *low probability of intercept* (LPI), and *low probability of exploitation* (LPE). LPD implies that even the presence of the signals is difficult to determine. LPI means that the presence of the signals can be readily detected but difficult to intercept, for a variety of reasons. LPE means that the signals can be detected and intercepted but exploitation is difficult. Encryption is an LPE technique, but is not limited to spread spectrum signals.

There are three predominant forms of SS signals: (1) FHSS, (2) *direct sequence spread spectrum* (DSSS), and (3) *time hopped spread spectrum* (THSS). Each has its own characteristics that are quite different from the others.

## 1.8.1 FHSS

When the frequency of the signals is changed on a relatively fast basis, the signal is categorized as FHSS. If the hopping code is changed many times for a single information bit, it is referred to as *fast frequency hopping* (FFH). When there are several information bits sent on a single frequency, it is called *slow frequency hopping* (SFH).

Early forms of FHSS sometimes used analog formats for the instantaneous modulation (AM or FM), but they have since gone by the wayside. All modern forms of FHSS employ digital signaling, typically *frequency shift keying* (FSK).

FHSS is an LPI technique. Such signals are fairly easy to detect since they are implemented by rapidly varying the carrier frequency, but at each frequency the signals are detectable.

## 1.8.2 DSSS

The energy in an information-bearing signal can be instantaneously spread over a wide bandwidth by multiplying that signal with another specially coded digital signal with a substantially higher data rate. This is referred to as DSSS. *Code division multiple access* (CDMA) is a form of DSSS signaling, where access to the RF channels is shared among several users and each user has a unique code so the correct information-bearing signal can be extracted at the CDMA receiver.

DSSS is an LPD technique since the modulated RF carriers are normally at or below the noise floor of the spectrum. There are techniques for detecting such signals but generally suspicion of the presence of the signals is required a priori to efficiently use the methods.

## 1.8.3 THSS

When the time of transmission of a bit is varied randomly according to a specified code, THSS ensues. The most popular form of THSS is *ultrawideband* (UWB) signaling. Pulses as short as several picoseconds are used to send the information

with *pulse-position modulation* (PPM), so the corresponding RF bandwidth can be very wide.

THSS is an LPD method because the spectrum of the modulated signals is quite wide (several gigahertz).


# 1.9 Collection Management

The functioning of ES systems, like all other battlefield sensors, is determined by the commander's information requirements. To satisfy those requirements the process referred to as *collection management* (CM) is used to determine which assets can best satisfy which requirement.

We briefly describe the collection management process here to provide a sense of the steps necessary to task, in particular, ES systems.

### 1.9.1 The Collection Management Process[1]

CM is the process of establishing what needs to be accomplished with information collectors in order to satisfy a commander's information needs. It goes far beyond just what can be collected with intercept systems. It includes all forms of methods for information collection: ES, *human intelligence* (HUMINT), *measurement and signature intelligence* (MASINT), and so forth. Our focus is on the ES function. For a more in-depth examination of information warfare and how receiving systems fit into the *information operations* (IO) process, [8] is recommended.

The CM process is summarized in Figure 1.14. It is cyclic in nature—as we use the process to satisfy some information requirements, we simultaneously use it to generate new requirements or reprioritize existing ones. As shown in Figure 1.14, each step of the CM process consists of a series of judgment decisions. The process is based on *specific operational requirements* (SORs) and *specific information requirements* (SIRs).

The same procedural thought process shown in Figure 1.14 is used regardless of echelon, type of operation, or time available. However, circumstances will dictate the nature and amount of detail able to be developed in the resulting products. For example, a CM section of the G2 at the corps level might take several days to execute all the procedures to produce

- An intelligence synchronization matrix
- A number of asset evaluation worksheets
- A detailed collection plan reflecting several hundred SORs

---

[1] Portions of this section are extracted from US Army field manual FM 34-2, *The Collection Management Process*.

1. Develop requirements
   a. Participate in staff wargaming
   b. Analyze requirements
      -Record
      -Validate
      -Consolidate
      -Prioritize
   c. Develop SIR sets

6. Update collection planning
   a. Eliminate satisfied requirements
   b. Redirect assets to unsatisfied requirements
   c. Cue assets to collection opportunities
   d. Maintain synchronization
   e. Add new requirements

2. Develop collection plan
   a. Evaluate resources
   b. Develop collection strategy
      -Select resources
      -Synchronize collection to requirements
   c. Develop SOR sets
   d. Prioritize SORs for collection assets

Mission management

Resource management

5. Evaluate reporting
   a. Monitor and maintain synchronization
   b. Correlate reports to requirements
   c. Screen reports
   d. Provide feedback to collectors and exploiters

Asset management

3. Task or request collection
   a. Determine tasking or request mechanism
   b. Execute and implement
   c. Collect and exploit

4. Disseminate
   a. Arrange direct dissemination
   b. Determine perishability
   c. Determine how much to disseminate
   d. Identify media for dissemination
   e. Disseminate

**Figure 1.14** The collection management process. (Source: [10].)

(Examples of the first two of these are given in the appendix to this chapter.) During an accelerated staff planning process, an experienced battalion S2 may take 5 minutes to execute exactly the same set of procedures. He then hands the event template and a simple *reconnaissance and surveillance* (R&S) tasking matrix to his scout platoon leader. He also asks for a copy of the platoon leader's plan to incorporate into the battalion R&S overlay.

Every step is always executed. The time required to conduct these steps depends on the tools available. Actually constructing asset evaluation worksheets may not be necessary if familiarity of the capabilities of the assets is available; this speeds up the process. The capabilities of the assets against the collection target must be considered before selecting them as part of the collection strategy.

> **Definition 1.2:** CM is the identification, prioritization, and refinement of uncertainties concerning the threat and the battlefield environment that a command must resolve to accomplish its mission.

The end result of CM processing is a prioritized list of exactly what needs to be collected, precisely where it needs to be collected, and when it needs to be collected and reported in order for a unit to conduct. In particular the ES system tasking is identified in terms of what, who, where, when, and how.

*Named areas of interest* (NAIs) are identified that indicate where certain types and kinds of information can be obtained. *Targeted areas of interest* (TAIs) are specific regions within which specific targets are expected and, if found there, provide specific evidence of adversarial activities.

Intelligence requirements are synchronized with the command's COA, and these provide the underlying guidance for CM. As collectors report, analysts receive the information they need to develop intelligence that drives the commander's decisions.

# 1.10 Concluding Remarks

We have shown in this introductory chapter basic architectures of ES systems and for what they are used. There are a great many variations possible for such systems and we illustrated only a few. They all perform the same basic tasks, however, irrespective of their specific implementations. All these ES systems are used to noncooperatively intercept battlefield transmissions for the purpose of collecting combat information and intelligence information.

We also illustrated how the tasking for ES systems is established. CM plans are derived to guide the specific tasks for these systems, along with all other collection assets available to satisfy the commander's intelligence requirements.

# Appendix 1.A Collection Management Process Output Products

We provide examples of two of the products of the CM process in this appendix. Specifically we show an asset evaluation worksheet (Figure 1.A.1) and an intelligence synchronization matrix (Figure 1.A.2).

## 1.A.1 Asset Evaluation Worksheet

The asset evaluation worksheets are used to evaluate the relevance of particular collection assets to a specified intelligence requirement. The example worksheet shown in Figure 1.A.1 applies to SIR 9.3: Are the HETs stationary in TAI 999? The imagery assets available consist of JSTARS, ASARS, and UAV. The ELINT collector is GRCS as is the COMINT collector. The HUMINT collector consists of an ACR and there are no MASINT collectors available. The entries indicate how well that asset applies to the capability and environmental factors listed across the top of the form. A plus sign indicates a good match, a zero indicates a marginal/moderate match, and a minus sign indicates a bad match.

To satisfy this particular SIR, U-2 ASARS, UAV, GRCS (ELINT), U-2 SENIOR SPEAR, and GRCS (COMINT) are the best available sensor assets. If not committed to a higher priority collection requirement during the time interval over which SIR 9.3 applies, these would be the best assets to select from for tasking.

## 1.A.2 Intelligence Synchronization Matrix

The intelligence synchronization matrix is a graphical depiction of the activities necessary to satisfy the commander's information requirements. It illustrates what assets are to be applied to which tasks and when. We show an example of such a matrix in Figure 1.A.2. The lines indicate processing time both before and after each collection period. The rectangles indicate the actual times of collection of information. The dark squares show the latest times that tasking can occur while the arrowheads indicate the latest time that the information collected is of use. Also indicated on the matrix are the SIRs to which the collection tasks apply.

Shown across the top is the timeline to which the matrix applies. The times indicated are in H-hours, which is the time after which the activities start ($H = 0$ is the beginning). The PIRs correspond to decision points (DPs) that have been established.

SIR 9.3: Are the HETs stationary in TAI 999?

| ASSETS | | Capability Factors | | | Environmental Factors | | | Capable | Remarks |
|---|---|---|---|---|---|---|---|---|---|
| | | Range | Timeliness | Technical Characteristics | Weather | Threat | Terrain | | |
| IMINT | U-2 ASARS | + | + | + | + | + | + | + | Cueing improves technical capability; excellent targeting accuracy |
| | JSTARS | + | + | 0 | + | + | + | 0 | MTI/FTI; cue ASARS/UAV |
| | UAV | + | + | + | + | + | + | + | |
| | | | | | | | | | |
| ELINT | U-2 SENIOR RUBY | + | 0 | + | + | + | + | 0 | Likely ADA activity |
| | GRCS | + | + | + | + | + | + | + | Likely ADA activity; Mission SA; Track N70 |
| | | | | | | | | | |
| COMINT | U-2 SENIOR SPEAR | + | + (CTT) | + | + | + | + | + | Convoy C2 sites; Cue ASARS |
| | GRCS | + | + | + | + | + | + | + | Convoy C2 sites; Mission SA; Track N70 |
| | GBCS | 0 | + | + | + | + | + | 0 | |
| HUMINT | IPW | + | 0 | 0 | + | + | + | 0 | As available |
| | CI | + | 0 | 0 | + | + | + | 0 | |
| | ACR | + | + | + | + | 0 | + | 0 | |
| MASINT | NA | | | | | | | | |
| | | | | | | | | | |
| | | | | | | | | | |
| Assets Selected: IMINT: JSTARS, ASARS, UAV<br>ELINT: GRCS<br>COMINT: GRCS<br>HUMINT: ACR<br>MASINT: NA | | | | | + Good<br>0 Marginal<br>– Poor | | | | |

**Figure 1.A.1** Asset evaluation worksheet. (Source: [10].)
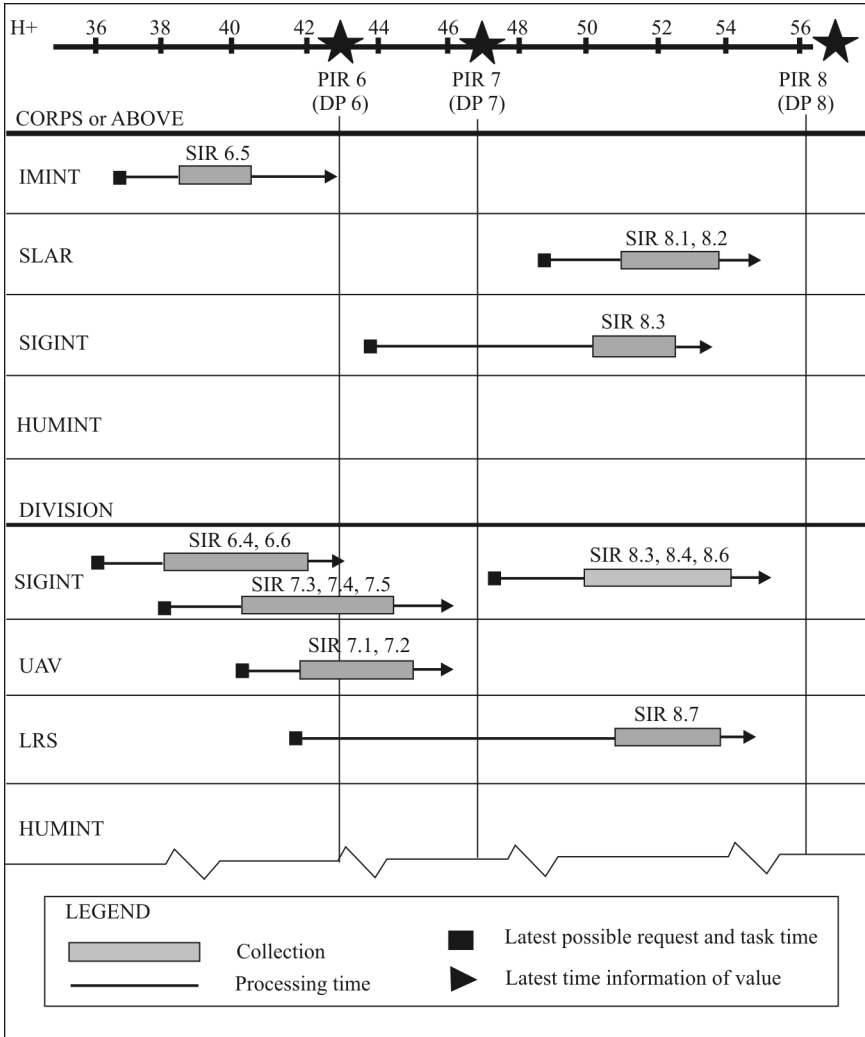
**Figure 1.A.2** Intelligence synchronization matrix. (Source: [10].)

# References

[1]    Marks, J. B., "Command and Control," *Journal of Electronic Defense*, June 1985.

[2]    Poisel, R. A., *Introduction to Communication Electronic Warfare Systems*, Norwood, MA: Artech House, 2002, p. 456.

[3]    Poisel, R. A., *Introduction to Communication Electronic Warfare Systems*, 2nd Ed., Norwood, MA: Artech House, 2008.

[4]    Poisel, R. A., *Modern Communications Jamming Principles and Techniques*, 2nd Ed., Norwood, MA: Artech House, 2011.

[5]    Poisel, R. A., *Electronic Warfare Target Location Methods*, 2nd Ed., Norwood, MA: Artech House, 2011.

[6]    Poisel, R. A., *Target Acquisition in Communication Electronic Warfare Systems*, Norwood, MA: Artech House, 2004.

[7]    Poisel, R. A., *Antenna Systems and Electronic Warfare Applications*, Norwood, MA: Artech House, 2011.

[8]    Poisel, R. A., *Information Warfare and Electronic Warfare Systems*, Norwood, MA: Artech House, 2013.

[9]    Poisel, R. A., *Modern Communications Jamming Principles and Techniques*, 2nd Ed., Norwood, MA: Artech House, 2011, Ch. 2.

[10]   *FM 34-2*, Department of the Army, Washington, DC, March 1994.

# Chapter 2

# Signals and Modulation Systems

## 2.1 Introduction

A carrier is modulated with an information signal in order to convey the information contained in that signal to a second (or more) location. The carrier is (usually) higher in frequency than the information signal for practical reasons, such as properties of the medium over which the signal must propagate. In this chapter we cover the foundations of modulations used for modern communication systems. We introduce the basic concepts of complex signals and systems in this chapter.

We begin the chapter with the notions surrounding representing signals and then discuss complex modulation and systems. The important Hilbert transform is introduced in this section. Next the modern modulation techniques are discussed including analog and digital modulations. Most of the extensive literature of modulation of communication signals assumes that the signals are deterministic. Random signals require a somewhat different treatment, and the theory of such signals is sparser. We discuss some of the concepts of random signals next. Then we review the various methods of access to communication channels. We conclude the chapter with a discussion of pulse shaping filters.

Notation: Matrices are denoted with a bold capital letter, e.g., $\mathbf{A}$ denotes a matrix. Vectors are denoted with a small letter with an arrow over-stroke, for example, $\vec{a}$ denotes a vector. Random variables are denoted with a capitalized italicized letter. A particular manifestation of a random variable is denoted as a small italicized letter. Random process variables are denoted with a bold small letter—for example, $\mathbf{a}$ denotes a random process.
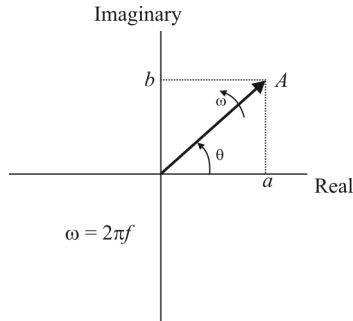
Figure 2.1 Phasor notation.

## 2.2 Representing Signals

Signals can be represented in many different ways. From Fourier's theory, we know that we can represent any real-world signal by the combination of one or more sinusoids. As such, characteristics of sinusoidal signals are important to understand.

In the complex domain, we can think of a fundamental signal as a rotating phasor. A phasor is a rotating vector in the complex plane with magnitude $A$ and rotational speed $\omega$ radians per second as illustrated in Figure 2.1. At time $t$

$$x(t) = a + jb$$

where

$$A = \sqrt{a^2 + b^2}$$
$$\theta = \omega t = \tan^{-1} \frac{b}{a}$$

We can also express the phasor in polar format as

$$x(t) = Ae^{j\omega t}$$
$$= A(\cos \omega t + j \sin \omega t)$$

A complex exponential can be represented as (Euler's formulas): since

$$e^{j\omega t} = \cos \omega t + j \sin \omega t$$
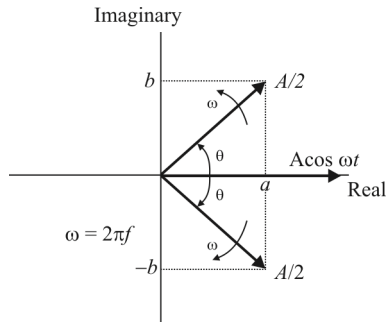
**Figure 2.2** Conjugate pair of phasors that are counter-rotating.

then

$$\cos \omega t = \frac{e^{j\omega t} + e^{-j\omega t}}{2}$$

$$\sin \omega t = \frac{e^{j\omega t} - e^{-j\omega t}}{2j}$$

A cosinusoid can be represented by a counter-rotating conjugate pair of phasors with a purely real result, since the imaginary components cancel, as shown in Figure 2.2. Similarly, a sinusoid is represented by a counter-rotating conjugate pair of phasors with a purely imaginary result.

Phasors rotate in two directions and have the following characteristics. Positively rotating phasors rotate counterclockwise and represent positive frequencies, while negatively rotating phasors rotate clockwise and represent negative frequencies. Referring to the Fourier transform, this just splits the signals up into the fundamental phasors, or complex exponential components.

## 2.3 Complex Signals and Systems

### 2.3.1 Introduction

All physical signals and waveforms are real-valued so why bother to consider complex-valued signals and systems? The original complex signal concepts can be traced back to the introduction of lowpass equivalent notation—that is, analysis of bandpass signals and systems using their lowpass/baseband equivalents. In general, a real-valued bandpass signal/system has a complex-valued lowpass equivalent. For example, linear *I/Q* modulation and demodulation principles are based on these ideas. Also all advanced frequency translation techniques and thus

the related receiver architectures (low-IF, direct-conversion, and so forth) utilize complex signals. Sampling and efficient multirate processing of bandpass signals is another good example.

### 2.3.2 Basic Concepts and Definitions

By definition, the time domain waveform or sequence $x(t)$ of a complex signal is complex-valued: $x(t) = x_I(t) + jx_Q(t)$. In practice, this is nothing more than a pair of two real-valued signals $x_I(t)$ and $x_Q(t)$ carrying the real and imaginary parts. Similarly, a complex system is defined as a system with complex-valued impulse response denoted by $h(t)$.

#### Property 2.1: Symmetric Amplitude Spectra

In the frequency domain, real-valued signals always have symmetric amplitude spectrums. Complex signals do not (need to) have any symmetry properties in general. The spectral support region (region of non-zero amplitude spectrum) can basically be anything.

#### Property 2.2: Complex Conjugation

If the spectrum of $x(t)$ is denoted by $X(f)$, then the spectrum of its conjugate, $x*(t)$, is $X*(-f)$.

This simple-looking result is surprisingly useful when interpreting some properties of complex signals. An immediate consequence is that if you consider the real part of $x(t)$, that is,

$$y(t) = \mathrm{Re}\{x(t)\} = \frac{x(t) + x^*(t)}{2} \qquad (2.1)$$

its spectrum is

$$Y(f) = \frac{X(f) + X^*(f)}{2} \qquad (2.2)$$

If $X(f)$ and $X*(-f)$ are not overlapping, $y(t) = \mathrm{Re}\{x(t)\}$ contains all the information about $x(t)$. This result finds good use, for example, in understanding frequency translations.

**Property 2.3: Convolution**

Another key operation related to linear systems in general is *convolution.* In the general complex case, the convolution of $x(t)$ and $h(t)$ can be written as

$$x(t) * h(t) = [x_I(t) + jx_Q(t)] * [h_I(t) + jh_Q(t)]$$
$$= x_I(t) * h_I(t) - x_Q(t)h_Q(t) + j[x_I(t) * h_Q(t) + x_Q(t) * h_I(t)] \qquad (2.3)$$

We can see that four real convolutions are needed in general. Obvious simplifications occur if either the filter input, $x(t)$, or the filter, $h(t)$, is real valued. In these cases, only two real convolutions need to be calculated.

### 2.3.3 Analytic Signals and Hilbert Transforms

A Hilbert transformer is generally defined as an allpass linear filter that shifts the phase of its input signal by 90 degrees.

**Property 2.4: Hilbert Transform**

The (anticausal) impulse and frequency responses of the Hilbert transformer can be formulated as

continuous-time

$$h_{HT}(t) = \frac{1}{\pi t}$$

$$H_{HT}(f) = \begin{cases} -j, & f \geq 0 \\ +j, & f < 0 \end{cases}$$

discrete-time

$$h_{HT}(n) = \begin{cases} 0, & n \text{ even} \\ \dfrac{2}{n\pi}, & n \text{ odd} \end{cases}$$

$$H_{HT}(e^{j\omega}) = \begin{cases} -j, & 0 \leq \omega < \pi \\ +j, & -\pi \leq \omega < 0 \end{cases}$$

In practice this behavior can be well approximated over a finite bandwidth. The input and output spectrums of the Hilbert transformer are illustrated in Figure 2.3.

One fascinating property related to Hilbert filters/transformers is that they can be used to construct signals with only positive frequency content. This kind of
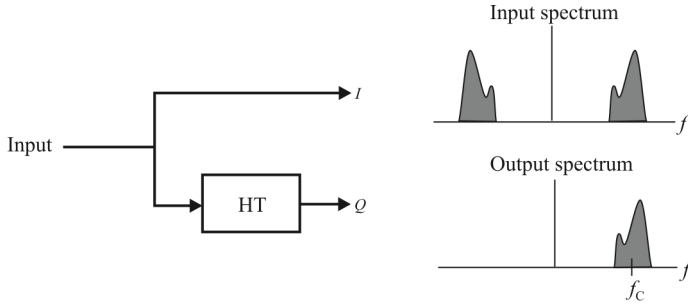
**Figure 2.3** Hilbert transformer implementation, input spectrum, and resulting output spectrum.

signal is generally termed *analytic* and is always complex. The simplest example is to take a cosine wave $A\cos(2\pi f_1 t)$ whose Hilbert transform is $A\sin 2\pi f_1 t$ (just a 90 degree phase shift!). These together when interpreted as $I$ and $Q$ components of a complex signal, result in $A\cos 2\pi f_1 t + jA\sin 2\pi f_1 t = A\exp(j2\pi f_1 t)$, whose spectrum has an impulse at $f_1$ but nothing on the other side of the spectrum.

The "elimination" of the negative frequencies can more generally be formulated as follows. Starting from an arbitrary signal $x(t)$ we form a complex signal $x(t) + jx_{\mathrm{HT}}(t)$ where $x_{\mathrm{HT}}(t)$ denotes the Hilbert transform of $x(t)$. Then the spectrum of the complex signal is $X(f)[1 + jH_{\mathrm{HT}}(f)]$ where

$$\text{continuous-time}$$

$$1 + jH_{\mathrm{HT}}(f) = \begin{cases} 1 + j\times(-j), & f \geq 0 \\ 1 + j\times j, & f < 0 \end{cases} = \begin{cases} 2, & f \geq 0 \\ 0, & f < 0 \end{cases}$$

which shows the elimination of the original negative frequency content. Similar concepts carry over to discrete-time and we can write

$$\text{discrete-time}$$

$$1 + jH_{\mathrm{HT}}(e^{j\omega}) = \begin{cases} 1 + j\times(-j), & 0 \leq \omega < \pi \\ 1 + j\times j, & -\pi \leq \omega < 0 \end{cases} = \begin{cases} 2, & 0 \leq \omega < \pi \\ 0, & -\pi \leq \omega < 0 \end{cases}$$

This idea of using the Hilbert transform to generate analytic signals is further illustrated graphically in Figure 2.3.

In practice, the Hilbert filtering causes a delay, and a corresponding delay needs to be included also in the upper (I) branch.
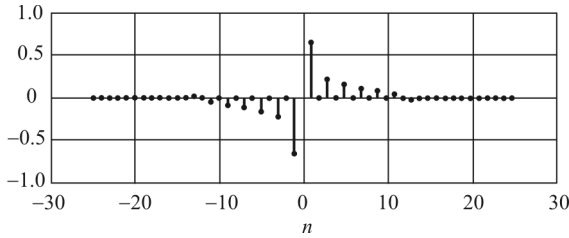
**Figure 2.4** Hilbert transformer example time response.

An example time response of a Hilbert transformer is shown in Figure 2.4 while the corresponding frequency response is shown in Figure 2.5, both amplitude and phase.

> **Example 2.1:** Consider a Hilbert transformer of order 50 with bandwidth $0.1\pi,\dots,0.9\pi$ ($\pi$ denotes half the sampling frequency). This results in about 87 dB attenuation for the negative frequencies (with respect to the corresponding positive band). The resulting frequency response is shown in Figure 2.6.

## 2.3.4 Frequency Translations and Mixing

One key operation in communications signal processing is the shifting of a signal spectrum from one center frequency to another. Conversions between baseband and bandpass representations are special cases of this.
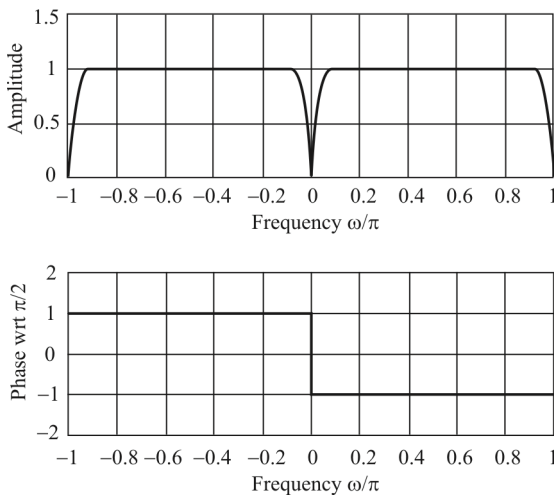


**Figure 2.5** Hilbert transformer example frequency spectrum corresponding to Figure 2.4.
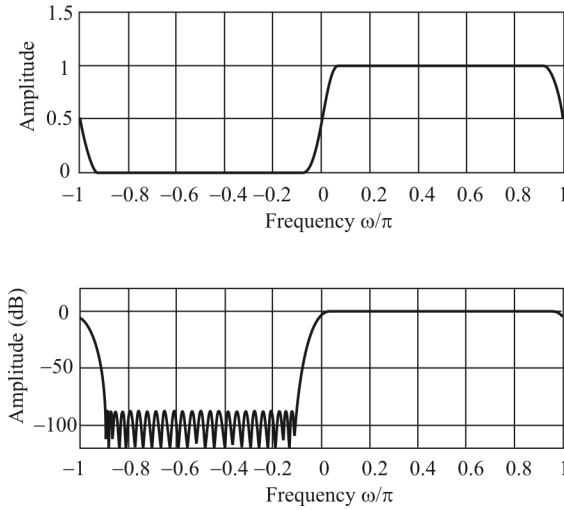
**Figure 2.6** Complex $1 + jH_{HT}$ frequency response.

2.3.4.1 Complex Translation

The basis of all frequency translations lies in multiplying a signal with a complex exponential, generally referred to as *complex* or *I/Q mixing*. This will cause a pure frequency shift; that is,

$$y(t) = x(t)e^{j\omega_{LO}t} \quad \Leftrightarrow \quad Y(f) = X(f - f_{LO}) \tag{2.4}$$

which forms the basis for all the linear modulations. This is illustrated in the frequency domain in Figure 2.7. In general, four real mixers are needed to implement a complex mixer as

$$x(t)e^{j\omega_{LO}t} = [x_I(t) + jx_Q(t)][\cos(\omega_{LO}t) + j\sin(\omega_{LO}t)]$$
$$= x_I(t)\cos(\omega_{LO}t) - x_Q(t)\sin(\omega_{LO}t) + j[x_Q(t)\cos(\omega_{LO}t) + x_I(t)\sin(\omega_{LO}t)] \tag{2.5}$$

Of course, in the special case of a real input, only two mixers are needed.

Real mixing is obviously a special case of the previous complex one and results in two frequency translations:

$$y(t) = x(t)\cos(\omega_{LO}t)$$
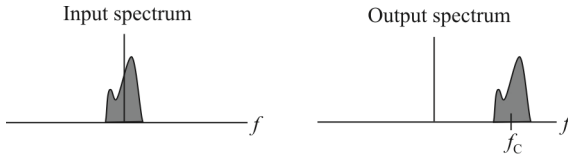
**Figure 2.7** *I/Q* mixing input and output spectra.

$$= x(t)\frac{1}{2}(e^{j\omega_{LO}t} + e^{-j\omega_{LO}t}) \quad \Leftrightarrow Y(f) = \frac{1}{2}X(f - f_{LO}) + \frac{1}{2}X(f + f_{LO}) \quad (2.6)$$

Here, the original spectral component appears twice in the mixer output, the two replicas being separated by $2f_{LO}$ in frequency. In receivers, this results in the so-called image signal problem since the signals from both $f_c + f_{LO}$ and $f_c - f_{LO}$ will appear at $f_c$ after the real mixing stage (see Figure 2.8). If real mixing is used, the image signal needs to be attenuated before the mixer stage. We will discuss this further when we present details on mixers in Chapter 4.

Linear *I/Q* modulation methods are just a special case of complex mixing. Given a complex message signal $x(t) = x_I(t) + jx_Q(t)$, it is first modulated as $x(t)\exp(j\omega_c t)$, after which only the real part is actually transmitted

$$y(t) = \text{Re}\{x(t)e^{-j\omega_c t}\} = x_I(t)\cos(\omega_c t) - x_Q(t)\sin(\omega_c t)$$
$$= \frac{1}{2}x(t)e^{j\omega_c t} + \frac{1}{2}x*(t)e^{-j\omega_c t} \quad (2.7)$$
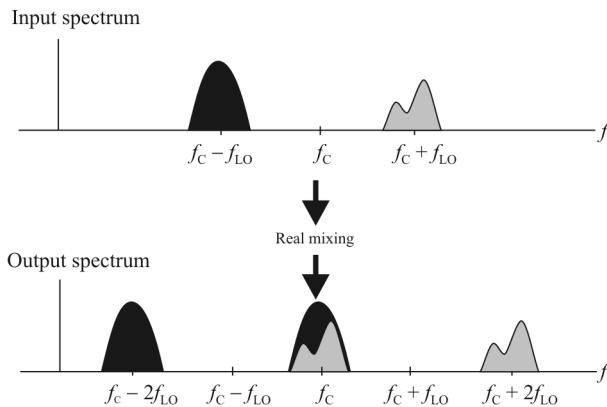


**Figure 2.8** Real mixing input and output spectra.
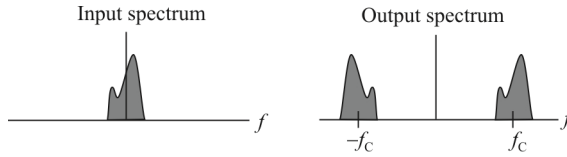
**Figure 2.9** Lowpass-to-bandpass transformation input and output spectra.

This result can be interpreted in two (equivalent) ways:

*Interpretation 1*: $x_I(t)$ and $x_Q(t)$ are modulated onto two orthogonal (cosine and sine) carriers, which is nice from the implementation point of view.

*Interpretation 2*: $x(t)$ and $x^*(t)$ are modulated onto two complex exponentials $\exp(j\omega_c t)$ and $\exp(-j\omega_c t)$. This is key in building a general understanding and recovering $x(t)$ back from $y(t)$.

Note that both terms/spectral components (at $+f_c$ and $-f_c$) contain all the original information [i.e., $x(t)$]. This process, also termed lowpass-to-bandpass transformation, is pictured in Figure 2.9.

2.3.4.2 *I/Q* Demodulation

In the receiver, the goal is to recover the original message $x(t)$ from the modulated signal $y(t)$. Based on the previous discussion, it is easy to understand that either of the signal components at $+f_c$ or $-f_c$ can be used for that purpose, while the other one should be rejected. Since

$$y(t)e^{-j\omega_c t} = \left[\frac{1}{2}x(t)e^{j\omega_c t} + \frac{1}{2}x^*(t)e^{-j\omega_c t}\right]e^{-j\omega_c t} = \frac{1}{2}x(t) + \frac{1}{2}x^*(t)e^{-j\omega_c t} \quad (2.8)$$

the message can be fully recovered by simply lowpass filtering the complex receiver mixer output. Formal flow diagrams for the modulator and demodulator in terms of complex signals are presented in Figure 2.10.

A realistic implementation of the demodulator shown in Figure 2.10 is shown in Figure 2.11.

**2.3.5 Complex Signals and Sampling**

In periodic sampling (at sample rate $f_S$) the resulting discrete-time signal has a periodic spectrum where the original continuous-time spectrum is replicated
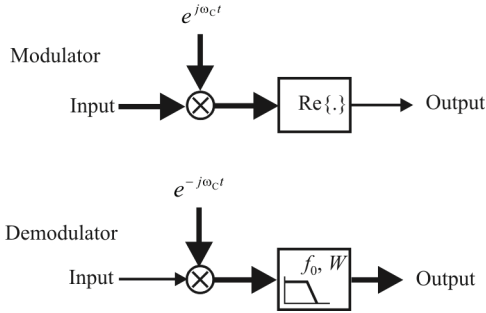
**Figure 2.10** Modulator and demodulator with complex signals.
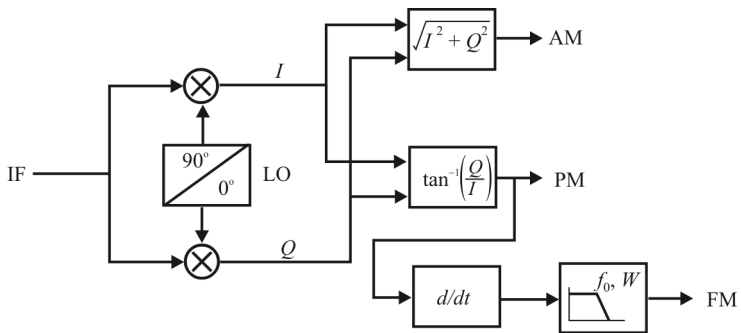


**Figure 2.11** Realistic *I/Q* demodulator.
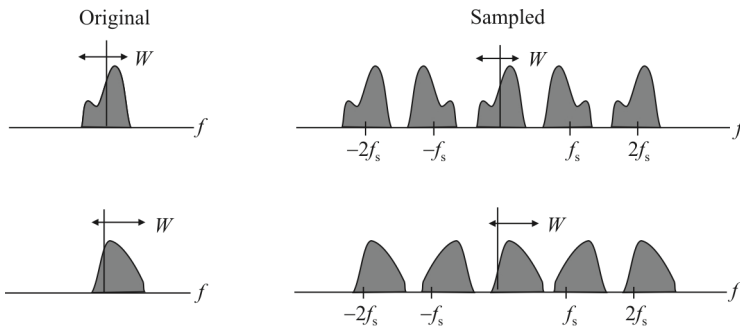
**Figure 2.12** Spectra resulting from sampling.

around the integer multiples of the sampling frequency. Interestingly, any of these spectral replicas (or "images") can be considered as the useful part and thus be used for further processing. Consequently, sampling (and multirate operations in general) can also be used, in addition to mixing techniques, in performing frequency translations.

Let $W$ denote the double-sided bandwidth of a complex-valued baseband signal (i.e., the spectrum is nonzero only for $-W_{neg} \leq f \leq W_{pos}$, $W = W_{neg} + W_{pos}$). To avoid aliasing, the sampling frequency $f_S$ must be high enough such that the spectral images do not overlap; that is,

$$f_S - W_{neg} \geq W_{pos} \quad \Leftrightarrow \quad f_S \geq W_{neg} + W_{pos} \quad \Leftrightarrow \quad f_S \geq W \qquad (2.9)$$

This is the classic *Nyquist sampling theorem*.

Naturally, since the signal to be sampled is complex-valued, there exist two real-valued sample streams ($I$ and $Q$) both at rate $f_s$. If the signal to be sampled consists of multiple frequency channels, sampling rates below $f_s = W$ are possible if only some of the channels are of interest. The sampling frequency should simply be selected in such a manner that aliasing is avoided on top of those interesting frequency bands.

Example spectra that both have the same lower limit $f_S \ll W$ for the sampling frequency are depicted in Figure 2.12.

## 2.3.6 Summary

It does not matter whether the signal is real or complex or whether it is located "symmetrically" with respect to the origin. The minimum sampling rate is always $f_S = W$. So, in general, we can conclude that the traditional statement "the signal should be sampled at least at a rate two times its highest frequency component" is inaccurate. What really matters is the double-sided bandwidth. A good example is the sampling of a real-valued lowpass signal, say $x(t)$, with spectral support

$-W...W$. When sampled directly, the minimum sampling rate is $f_S = 2W$. As an alternative, we can form an analytic signal $x(t) + jx_{HT}(t)$, where $x_{HT}(t)$ denotes the Hilbert transform of $x(t)$, for which the minimum sampling rate is only $f_S = W$ (even though the highest frequency component present in both signals is $W$).

## 2.4 System Definition

Dynamical systems can be characterized in a number of ways. They can be modeled with partial and ordinary differential equations, they can be represented with transfer functions, or if they are time variant, they can be analyzed with *stochastic differential equations* (SDE) [1], as three possibilities. In this section we will focus on the second of these [2, 3].

**Definition 2.1: System.** A *system* is defined by a mapping

$$y(t) = \mathcal{H}[x(t)]$$

from the input $x(t)$ into the output $y(t)$.

**Definition 2.2: Linear System.** A system $\mathcal{H}$ is *linear* if

$$\mathcal{H}(ax_1 + bx_2) = a\mathcal{H}(x_1) + b\mathcal{H}(x_2)$$

**Definition 2.3: Time-Invariant System.** A system is *time-invariant* if $\mathcal{H}[x(t+\tau)] = \mathcal{H}(x)(t+\tau)$. A system is time-invariant when $h(t, u) = h(t - u)$.

**Definition 2.4: Impulse Response.** The *impulse response* of a linear system is given by

$$h(t,u) = \mathcal{H}[\delta(t-u)].$$

For an arbitrary input $x(t)$, the system output is given by

$$y(t) = \mathcal{H}[x(t)] = \int_{-\infty}^{\infty} x(z)h(t,z)dz \tag{2.10}$$

If the input to a *linear, time-invariant* (LTI) system is a complex exponential at frequency $f$, given by $x(t) = \exp(j2\pi ft)$, then the output is

$$y(t) = H[x(t)] = H(f)\exp(j2\pi ft) \tag{2.11}$$

where $H(f)$ is the Fourier transform of the impulse response $h(t)$

$$H(f) = \int_{-\infty}^{\infty} h(t-z)\exp[-j2\pi f(t-z)]dz \tag{2.12}$$

and is called the *system transfer function*. For an arbitrary input with Fourier transform $X(f) = \mathcal{F}\{x(t)\}$, the output is

$$y(t) = H[x(t)] = \int_{-\infty}^{\infty} H(f)X(f)\exp(j2\pi ft)df \tag{2.13}$$

with the Fourier transform

$$Y(f) = \mathcal{F}\{H[x(t)]\} = H(f)X(f) \tag{2.14}$$

The system transfer function $H(t, f)$ for a *linear time-variant* (LTV) system is given by

$$H(t, f) = \int_{-\infty}^{\infty} h(t,z)\exp[-j2\pi f(t-z)]dz \tag{2.15}$$

Note that $H(t, f)$ in (2.15) is a function of both $f$ and $t$. If the input to an LTV system $\mathcal{H}$ is $x(t) = \exp(j2\pi ft)$, then the output is

$$y(t) = \mathcal{H}[x(t)] = H(t, f)\exp(j2\pi ft) \tag{2.16}$$

which is a generalization of (2.12) to LTV systems. For an arbitrary input with $X(f) = \mathcal{F}\{x(t)\}$, the output is

$$y(t) = H(x)(t) = \int_{-\infty}^{\infty} H(t, f)X(\omega)\exp(j2\pi t)df \tag{2.17}$$

A linear system is *linear periodically time-variant* (LPTV) if the impulse response is periodic in $t$

$$h(t+\tau,t) = h(t+T+\tau,t+T) \tag{2.18}$$

with Fourier series for the impulse response and the transfer function given by

$$h(t+\tau,t) = \sum_{n=-\infty}^{\infty} h_n(\tau)\exp(j2\pi nf_c t) \tag{2.19}$$

$$H(t,f) = \sum_{n=-\infty}^{\infty} H_n(f+nf_c)\exp(j2\pi nf_c t) \tag{2.20}$$

where $H_n(f) = \mathcal{F}\{h_n(z)\}$ are the harmonic transfer functions. If the input to an LPTV system $\mathcal{H}$ is $x(t) = \exp(j2\pi ft)$, then the output is

$$y(t) = H[x(t)] = \sum_{n=-\infty}^{\infty} H_n(f+nf_c)\exp[j2\pi(f+nf_c)t] \tag{2.21}$$

The Fourier transform of the output of an LPTV system is

$$Y(f) = \sum_{n=-\infty}^{\infty} H_n(f)X(f+nf_c),$$

where $X(f)$ is the Fourier transform of the input.

If a single complex exponential at frequency $f$ is input to an LTI system, the output is also a single complex exponential at frequency $f$ with a scaled amplitude and a phase offset, where the scaling and offset are determined by the transfer function $H(f)$. For an LTV system, the output for a single complex exponential input, in general, contains a *continuum* of frequencies. For LPTV systems, from (2.21) the output corresponding to a single complex exponential at frequency $f$ is a summation of complex exponentials at frequencies $f + nf_c$, where $f_c$ is the fundamental frequency. An LPTV system can be used to model a mixer as a single-input (RF) single-output (IF) system considering the LO as part of the mixer itself. Such a model captures frequency translation, which is the basic functionality of a mixer. On the other hand, an LPTV model cannot capture nonlinearities of the signal path. The system transfer function concept can be generalized to *nonlinear* time-invariant or (periodically) time-varying systems to capture signal path nonlinearities. For a nonlinear periodically time-varying system, the output corresponding to a single complex exponential at frequency $f$ is a summation of complex exponentials at frequencies $kf + nf_c$, $k = 1,\ldots,\infty, n = -\infty,\ldots,\infty,$ where $f_c$ is the fundamental frequency.

# 2.5 Modulations

A carrier can be modulated in three basic ways: (1) by varying its amplitude, known as *amplitude modulation* (AM); (2) by varying its frequency, known as *frequency modulation* (FM); and (3) by varying its phase, known as *phase modulation* (PM). More sophisticated methods combine two or more of these variations to improve spectral efficiency. These basic modulation forms are still used today with both analog and digital signals [4].

## 2.5.1 Analog Modulations

In analog modulations the basic principle is to superimpose the message signal in analog form onto a carrier that is a sinusoid of the form

$$A \cos(2\pi f_c t + \phi)$$

2.5.1.1 Amplitude Modulation

In AM, the carrier signal

$$A(t) \cos 2\pi f_c t$$

has its amplitude $A(t)$ *modulated* in proportion to the message-bearing signal $m(t)$ to give

$$A[1 + m(t)] \cos 2\pi f_c t$$

The magnitude of $m(t)$ is chosen to be less than or equal to 1, from reasons having to do with demodulation; that is, recovery of the signal $m(t)$ from the received signal. The modulation index is then defined to be

$$\beta_{AM} = \max_t m(t)$$

Figures 2.13 and 2.14 are depictions of what the modulated signal looks like for

$$m(t) = \beta_{AM} \sin 2\pi f_m t$$

for $\beta_{AM} = 0.2$ and 0.4, respectively.

The frequency of the *modulating signal, $f_m$*, is chosen to be much smaller than that of the carrier signal, $f_c$. If the modulation index were larger than one,
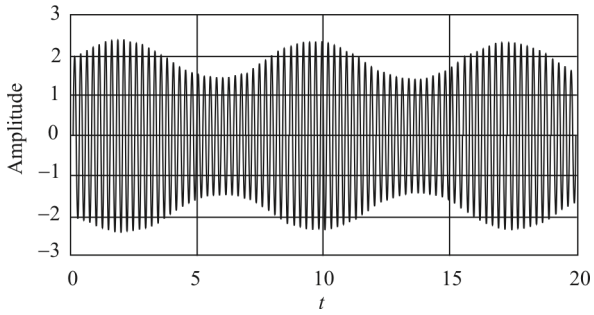
**Figure 2.13** Amplitude modulation waveform when $A = 2$ and $\beta_{AM} = 0.2$.
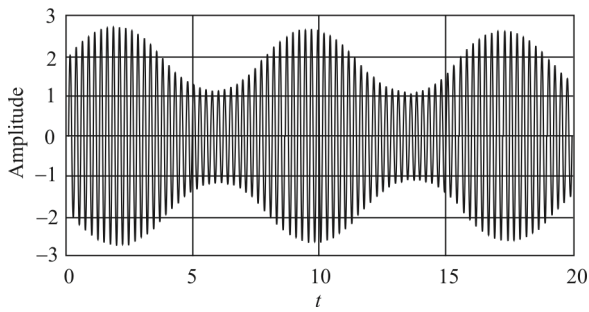


**Figure 2.14** Amplitude modulation waveform when $A = 2$ and $\beta_{AM} = 0.4$.

overmodulation ensues and the signal gets distorted. Accurate demodulation is then not possible.

Note that the AM signal is of the form

$$A(1+\beta_{\text{AM}}\sin 2\pi f_{\text{m}}t)\cos 2\pi f_{\text{c}}t$$

$$= A\cos 2\pi f_{\text{c}}t + \frac{A\beta_{\text{AM}}}{2}[\cos 2\pi(f_{\text{c}}+f_{\text{m}})t + \cos 2\pi(f_{\text{c}}-f_{\text{m}})t]$$

which has frequency components at frequencies

$$f_{\text{c}}, f_{\text{c}}+f_{\text{m}}, f_{\text{c}}-f_{\text{m}}$$

The version of AM that we described is called *AM double sideband* or AM DSB, since we send the modulating signal at both

$$f_{\text{c}}-f_{\text{m}}$$

and at

$$f_{\text{c}}+f_{\text{m}}$$

Note that the same signal is sent at these two frequencies, thus wasting spectrum. It is more efficient to transmit only one of the sidebands, which is called *AM single sideband* (AM SSB). This can be further refined to be *AM upper sideband* (AM USB) and *AM lower sideband* (AM LSB).

The spectrum of AM DSB is given by

$$X_{\text{AM}}(t) \leftrightarrow \frac{1}{2}[M(f+f_{\text{c}})+M(f-f_{\text{c}})]+\pi A[\delta(f+f_{\text{c}})+\delta(f-f_{\text{c}})] \quad (2.22)$$

which is illustrated in Figure 2.15. Both of the sidebands are apparent in this figure. The second term on the rhs of (2.22) are the carrier components shown in Figure 2.15. When these terms are suppressed, the resulting modulation method is referred to as *AM DSB suppressed carrier* (AM DSB SC).

2.5.1.2 Angle Modulations

The two forms of angle modulations are phase modulation and frequency modulation. In FM the instantaneous frequency of the carrier is modulated to impress the modulating signal $m(t)$ onto the carrier. Thus the signal that is transmitted is of the form
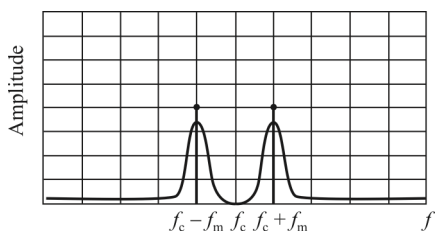
**Figure 2.15** Spectrum of AM DSB. $M(f)$ is represented by the non-zero bandwidth spectrum at $f_c - f_m$ and $f_c + f_m$.

$$x(t) = A\cos[2\pi f_c t + 2\pi\Delta f \int_0^t m(t)dt]$$

Here the signal $m(t)$ is assumed to be normalized so that the maximum of the integral is 1 and $\Delta f$ is called the frequency deviation of the modulation scheme.

To understand the concept of frequency variation, it is necessary to define the instantaneous frequency. We define a generalized sinusoidal signal

$$x(t) = A\cos\theta(t) \tag{2.23}$$

Here $\theta$ is the angle of the sinusoidal signal and is a function of $t$. For an ordinary fixed frequency signal,

$$x(t) = A\cos(2\pi f_c t + \theta_0) \tag{2.24}$$

Hence

$$\theta(t) = 2\pi f_c t + \theta_0$$

and

$$f_c = \frac{1}{2\pi}\frac{d\theta}{dt} \tag{2.25}$$

The frequency $f_c$ here is a constant, proportional to the derivative of the angle $\theta(t)$. In general, this derivative may not be a constant. We now define $d\theta/dt$ as the instantaneous frequency $f_i$, which may vary with time. Thus

$$f_i = \frac{1}{2\pi}\frac{d\theta}{dt}$$

$$\theta = 2\pi\int f_i dt \tag{2.26}$$

It is now easy to appreciate the possibility of transmission of information in $x(t)$ by varying the angle $\theta$ of a carrier.

If the angle $\theta(t)$ is varied linearly with $m(t)$, then

$$\theta(t) = 2\pi f_c t + \theta_0 + k_{PM} m(t) \tag{2.27}$$

where $k_{PM}$ is a constant, and the resulting form is PM. Thus a signal $A\cos[2\pi f_c t + \theta_0 + k_{PM} m(t)]$ represents a phase-modulated carrier. Note that the instantaneous frequency $f_i$ for a phase-modulated carrier is given by

$$f_i = \frac{d\theta}{dt} = f_c + \frac{1}{2\pi} k_{PM} \frac{dm(t)}{dt} \tag{2.28}$$

Hence, in PM the instantaneous frequency varies linearly with the derivative of the modulating signal. FM ensues, however, when we vary the instantaneous frequency directly with the modulating signal. Thus for a frequency-modulated carrier, the instantaneous frequency $f_i$ is given by

$$f_i = f_c + \frac{1}{2\pi} k_{FM} m(t) \tag{2.29}$$

and

$$\theta(t) = 2\pi\int f_i dt$$
$$= 2\pi f_c t + k_{FM}\int m(t)dt + \theta_0 \tag{2.30}$$

and the signal

$$A\cos[2\pi f_c t + \theta_0 + k_{FM}\int m(t)dt]$$

represents a frequency-modulated carrier.

We can see that although PM and FM are different forms of angle modulation, they are similar in many respects. In PM, the angle is varied linearly with the modulating signal, whereas in FM the angle varies linearly with the integral of the

modulating signal. Indeed, if we integrate the modulating signal $m(t)$ first and then allow it to phase-modulate the carrier, we obtain a frequency-modulated wave. Similarly, if we differentiate $m(t)$ first and use it to frequency-modulate a carrier, the result is a phase-modulated wave. Note that for (strictly) angle modulation the amplitude is always constant.

If the PM and FM signals are denoted by $x_{PM}(t)$ and $x_{FM}(t)$, respectively, then

$$x_{PM}(t) = A\cos[2\pi f_c t + k_{PM} m(t)]$$
$$x_{FM}(t) = A\cos\left(2\pi f_c t + k_{FM} \int m(t)dt\right)$$

$$(2.31)$$

where $m(t)$ is the message signal. In (2.31) the initial phase $\theta_0$ is assumed to be zero without loss of generality.

We express the sinusoidal signal, (2.23), by its exponential counterpart:

$$A\cos\theta(t) \sim Ae^{j\theta(t)}$$

where it is understood that we always imply the real part of the exponential signals thus represented.

$$A\cos\theta(t) = \text{Re}\{Ae^{j\theta(t)}\}$$

We use the notation $\tilde{x}(t)$ for the exponential representation of $x(t)$. Thus if

$$x(t) = A\cos\theta(t)$$

then

$$\tilde{x}(t) = Ae^{j\theta(t)}$$

and since

$$\tilde{x}(t) = A[\cos\theta(t) + j\sin\theta(t)]$$

then

$$x(t) = \text{Re}\{\tilde{x}(t)\}$$

With this notation, the PM and FM carriers in (2.31) can be expressed as

$$\tilde{x}_{PM}(t) = Ae^{j[2\pi f_c t + k_{PM} m(t)]}$$

$$\tilde{x}_{FM}(t) = Ae^{j[2\pi f_c t + k_{FM} \int m(t) dt]}$$

(2.32)

For convenience let

$$g(t) = \int m(t) dt$$

This gives

$$\tilde{x}_{FM}(t) = Ae^{j[2\pi f_c t + k_{FM} g(t)]}$$

(2.33)

*Narrowband FM*

The general expression for the FM carrier is given by (2.33). The instantaneous frequency $f_i$ is given by

$$f_i = \frac{1}{2\pi}\frac{d\theta}{dt} = f_c + \frac{1}{2\pi}k_{FM}\frac{dg}{dt} = f_c + \frac{1}{2\pi}k_{FM}m(t)$$

which is obviously proportional to the message signal $m(t)$. The term $k_{FM}(t)/2\pi$ represents the deviation of the carrier frequency from its quiescent value $f_c$. The constant $k_{FM}$ therefore controls the deviation of the carrier frequency. For small values of $k_{FM}$ the frequency deviation is small, and the spectrum of the FM signal occupies a narrow band. If $k_{FM}$ is large the bandwidth is correspondingly larger.

Let us first consider the narrowband case. If $k_{FM}$ is small so that $k_{FM}g(t) << 1$ for all $t$, then

$$e^{jk_{FM}g(t)} \approx 1 + jk_{FM}g(t)$$

and

$$\tilde{x}_{FM}(t) \approx A[1 + jk_{FM}g(t)]e^{j2\pi f_c t}$$

and

$$x_{FM}(t) = \text{Re}\{\tilde{x}_{FM}(t)\} = \underbrace{A\cos 2\pi f_c t}_{\text{carrier}} - \underbrace{Ak_{FM}g(t)\sin 2\pi f_c t}_{\text{sideband}}$$

(2.34)

We observe that the AM carrier can be expressed as

$$x_{AM}(t) = \underbrace{A\cos 2\pi f_c t}_{\text{carrier}} + \underbrace{m(t)\cos 2\pi f_c t}_{\text{sideband}} \qquad (2.35)$$

where the narrowband FM carrier is given by (2.34). Similarly, the narrowband PM carrier is given by

$$x_{PM}(t) = A\cos 2\pi f_c t - Ak_{PM}\,m(t)\sin 2\pi f_c t \qquad (2.36)$$

Each signal has a carrier term and the sidebands that are centered at $\pm f_c$. If

$$x(t) \leftrightarrow X(f)$$

and

$$g(t) \leftrightarrow G(f)$$

then since

$$g(t) = \int m(t)dt$$

it follows from the time integration property of Fourier transforms given by

$$\int_{-\infty}^{t} f(u)du \leftrightarrow \frac{1}{j2\pi f}F(f)$$

that

$$g(t) \leftrightarrow \frac{1}{j2\pi f}M(f) \qquad (2.37)$$

Hence

$$G(f) = \frac{1}{j2\pi f}M(f) \qquad (2.38)$$

and we can see that if $M(f)$ is bandlimited to $f_m$, then $G(f)$ is also bandlimited to $f_m$.

The frequency spectrum of $x_{FM}(t)$ of the FM carrier in (2.34) can be found by using the frequency shift property of the Fourier transform given by

$$f(t)\sin 2\pi f_0 t \leftrightarrow \frac{j}{2}[F(f+f_0)-F(f-f_0)]$$

Thus if

$$x_{FM}(t) \leftrightarrow X_{FM}(f)$$

then

$$X_{FM}(f) = \pi A[\delta(f-f_c)+\delta(f+f_c)] + \frac{j\pi Ak_{FM}}{2}[G(f-f_c)-G(f+f_c)] \quad (2.39)$$

Comparison of the spectrum of FM (2.39) with that of AM in (2.22) shown in Figures 2.13 and 2.14 brings out clearly the similarities and differences between the two types of modulations. In both types there is a carrier term and sideband component centered at $\pm f_c$. The sideband spectrum for FM, however, has a phase shift of $\pi/2$ with respect to the carrier, whereas that of AM is in phase with the carrier. The spectrum $F(f) = (1/j2\pi f)M(f)$ and hence if $M(f)$ is bandlimited to $f_m$, $G(f)$ is also bandlimited to $f_m$. Thus, a narrowband FM (and narrowband PM) signal occupies the same bandwidth $(2f_m)$ as that occupied by an AM signal.

*Wideband FM*

If the deviations in the carrier frequency are made large enough; that is, if the constant $k_{FM}$ is chosen large enough so that the condition $k_{FM}g(t) \ll 1$ is not satisfied the characteristics of FM signals presented in the last section do not apply and becomes very involved for a general modulating signal $m(t)$. Derivation of a precise expression for the bandwidth of a wideband FM carrier for a general modulating signal $m(t)$ is not possible because FM is a nonlinear modulation.
Suppose the modulating signal is a sinusoid

$$m(t) = a\cos 2\pi f_m t$$

The modulated signal is illustrated in Figure 2.16. We assume that the signal $m(t)$ is switched on at $t = 0$ and hence

$$g(t) = \int m(t)dt = a\int_0 \cos 2\pi f_m t dt$$
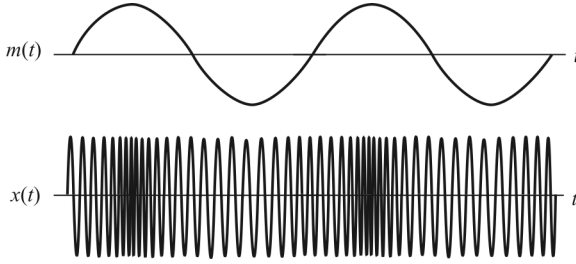
**Figure 2.16** FM modulated carrier, where $m(t)$ is the modulating signal and $x(t)$ is the modulated carrier time waveform.

$$= \frac{a}{2\pi f_{\mathrm{m}}} \sin 2\pi f_{\mathrm{m}} t \qquad (2.40)$$

Since the instantaneous frequency $f_{\mathrm{i}}$ is given by (2.29)

$$f_{\mathrm{i}} = f_{\mathrm{c}} + \frac{1}{2\pi} k_{\mathrm{FM}} f_{\mathrm{m}}(t) = f_{\mathrm{c}} + \frac{1}{2\pi} a k_{\mathrm{FM}} \cos 2\pi f_{\mathrm{m}} t \qquad (2.41)$$

it is evident from (2.41) that the maximum deviation of the carrier frequency is $a k_{\mathrm{FM}} / 2\pi$ Hz and

$$\tilde{x}_{\mathrm{FM}}(t) = A e^{j[2\pi f_{\mathrm{c}} + (\Delta f / f_m) \sin 2\pi f_m t]}$$

The quantity $\Delta f / f_{\mathrm{m}}$ is the ratio of the maximum deviation of the carrier frequency to the modulating signal frequency $f_{\mathrm{m}}$ and is called the *modulation index* and denoted $\beta_{\mathrm{FM}}$. Thus

$$\beta_{\mathrm{FM}} \triangleq \frac{\Delta f}{f_m} = \frac{a k_{\mathrm{FM}}}{2\pi f_{\mathrm{m}}} \qquad (2.42)$$

and

$$\tilde{x}_{\mathrm{FM}}(t) = A e^{j(2\pi f_{\mathrm{c}} + \beta_{\mathrm{FM}} \sin 2\pi f_m t)}$$
$$= A e^{j\beta_{\mathrm{FM}} \sin 2\pi f_m t} e^{j 2\pi f_{\mathrm{c}} t} \qquad (2.43)$$

The first exponential in (2.43) is obviously a periodic function of period $1 / f_{\mathrm{m}}$ and can be expanded with a Fourier series as

$$e^{j\beta_{FM}\sin 2\pi f_m t} = \sum_{n=-\infty}^{\infty} c_n e^{jn2\pi f_m t}$$

where

$$c_n = f_m \int_{-1/2 f_m}^{1/2 f_m} e^{j\beta_{FM}\sin 2\pi f_m t} e^{-jn2\pi f_m t} dt$$

Letting $2\pi f_m t = y$, we get

$$c_n = f_m \int_{-\pi}^{\pi} e^{j(m_f \sin y - ny)} dy \tag{2.44}$$

The integral on the right in (2.44) cannot be evaluated in closed form and must be numerically integrated.

This integral is denoted by $J_n(m_f)$ and has been extensively tabulated. It is called the Bessel function of the first kind and $n$th order [5]. These functions are plotted in Figure 2.17. Thus

$$e^{j\beta_{FM}\sin 2\pi f_m t} = \sum_{n=-\infty}^{\infty} J_n(\beta_{FM}) e^{jn2\pi f_m t} \tag{2.45}$$

We can show that

$$\begin{aligned} J_n(\beta_{FM}) &= J_{-n}(\beta_{FM}), &\qquad n \text{ even} \\ J_n(\beta_{FM}) &= -J_{-n}(\beta_{FM}), &\qquad n \text{ odd} \end{aligned} \tag{2.46}$$

Substituting (2.45) into (2.43), we get

$$x_{FM}(t) = A e^{j2\pi f_c t} \sum_{n=-\infty}^{\infty} J_n(\beta_{FM}) e^{jn2\pi f_m t}$$

and

$$x_{FM}(t) = A \sum_{n=-\infty}^{\infty} J_n(\beta_{FM}) \cos(2\pi f_c + n2\pi f_m) \tag{2.47}$$

Using (2.46), we can express (2.47) as
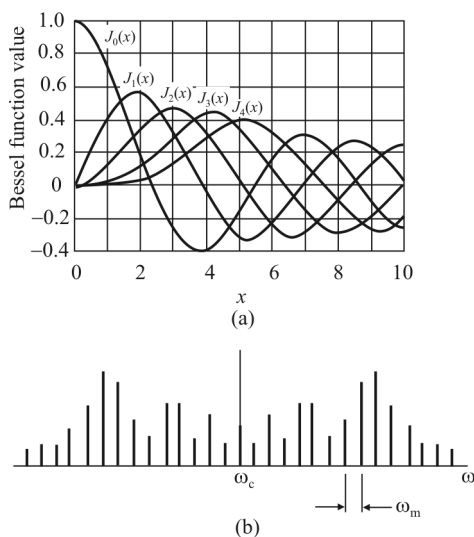
**Figure 2.17** Bessel functions: (a) the functions and (b) the spectrum of a tone FM modulated carrier.

$$x_{FM}(t) = A\{J_0(\beta_{FM})\cos 2\pi f_c t + J_1(\beta_{FM})[\cos 2\pi(f_c + f_m)t - \cos 2\pi(f_c - f_m)t]$$
$$+ J_2(\beta_{FM})[\cos 2\pi(f_c + 2f_m)t + \cos 2\pi(f_c - 2f_m)t]$$
$$+ J_3(\beta_{FM})[\cos 2\pi(f_c + 3f_m)t + \cos 2\pi(f_c - 3f_m)t] \tag{2.48}$$
$$+ \ldots\}$$

We can see from (2.48) that the modulating signal $m(t)$ of frequency $f_m$ gives rise to energy at sideband frequencies $(f_c \pm f_m), (f_c \pm 2f_m), (f_c \pm 3f_m), \ldots$, as shown in Figure 2.17(b). The general FM carrier therefore contains components of infinite frequencies and has an infinite bandwidth. In practice, however, the amplitudes of the spectral components of higher frequencies become negligible, yielding a finite bandwidth for almost all of the energy, which is obvious from Figure 2.17(a). For $\beta_{FM} \ll 1$, only $J_0(\beta_{FM})$ and $J_1(\beta_{FM})$ have any significant magnitudes. All of the higher functions, $J_2(\beta_{FM})$, $J_3(\beta_{FM})$, ..., are negligible in this case, and only the carrier and the first-order sidebands are of significance. This is, of course, the narrowband FM discussed in the previous section.

For $\beta_{FM} = 2$, the functions $J_5(\beta_{FM})$, $J_6(\beta_{FM})$, ..., have negligible amplitudes. Hence the significant spectral components of an FM carrier for $\beta_{FM} = 2$ are $f_c$, $f_c \pm f_m, f_c \pm 2f_m, f_c \pm 3f_m$, and $f_c \pm 4f_m$. In this case, the bandwidth of the significant sidebands is $8f_m$. As $\beta_{FM}$ is increased further, higher-order sidebands become more significant. The significant sidebands can be considered as those that have an amplitude of at least 1% of that of the unmodulated carrier; that is, those

for which $J_n(\beta_{FM}) > 0.01$. The number of significant sidebands for different values of $\beta_{FM}$ can be found from the plot of the Bessel functions. We can see from Figure 2.17(a) that $J_n(\beta_{FM})$ diminishes rapidly for $n > \beta_{FM}$. This is particularly true for values of $\beta_{FM} \gg 1$. Thus, for wideband FM where the number of significant sidebands may be considered to be the integer closest to $\beta_{FM}$, $\beta_{FM} = n$. The total bandwidth $W$ of the FM carrier is given by

$$W \approx 4n\pi f_m \approx 4\beta_{FM} f_m \ \text{Hz}$$

but

$$\beta_{FM} \triangleq \frac{\Delta f}{f_m} = \frac{ak_f}{2\pi f_m}$$

Hence

$$W \approx 4\pi\beta_{FM} f_m \approx 4\pi\Delta f \ \text{Hz} \qquad (2.49)$$

Actually, it can be shown that $W = 4\pi(\Delta f + 2f_m)$ is a more accurate expression than $4\pi\Delta f$. Hence we have

$$W \approx 4\pi(\Delta f + 2f_m) \qquad (2.50)$$

This rule gives a fairly good estimate for wideband FM.

The frequency deviation of the carrier as a function of $\beta_{FM}$ is shown in Figure 2.18. It is evident from this figure that for $\beta_{FM} \gg 1$, the bandwidth $W$ is approximately twice the frequency deviation of the carrier.

## 2.5.2 Modern Digital Modulations

### 2.5.2.1 Introduction

While the preceding sections discussed analog modulations, most modern modulation schemes are digital. The only significant analog modulations remaining are commercial broadcast radio (AM and FM bands). Even these are being replaced with digital formats (e.g., commercial satellite radio).

The main goal of modulation is to squeeze as much data into the least amount of spectrum possible. That objective, known *as spectral efficiency*, measures how quickly data can be transmitted in an assigned bandwidth. The unit of
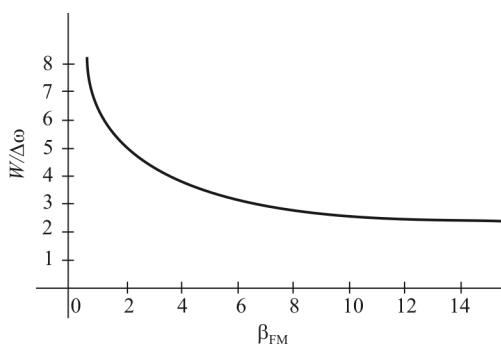
**Figure 2.18** Normalized FM bandwidth as a function of $\beta_{FM}$.

measurement is bits per second per Hertz (bps/Hz). Multiple techniques have emerged to achieve and improve spectral efficiency.

This section provides an introduction to digital modulation methods. A more mathematical treatment is contained in [6], which can be consulted by the interested reader.

### 2.5.2.2 Data Rate and Baud Rate

The maximum theoretical data rate, otherwise known as the *channel capacity* ($C$) in bits/s (bps), is a function of the channel bandwidth ($W$) channel in Hz and the SNR, denoted by γ:

$$C = W \log_2 (1 + \gamma) \tag{2.51}$$

This is called the *Shannon-Hartley law*. The maximum data rate is directly proportional to the bandwidth and logarithmically proportional the SNR. Noise greatly diminishes the data rate for a given BER.

Another key factor is the baud rate, or the number of modulation symbols transmitted per second. The term *symbol* in modulation refers to one specific state of a sine carrier signal. It can be an amplitude, a frequency, a phase, or some combination of them. Basic binary transmission uses one bit per symbol.

In ASK, a binary 0 is one amplitude and a binary 1 is another amplitude. In FSK, a binary 0 is one carrier frequency and a binary 1 is another frequency. BPSK uses a 0° shift for a binary 0 and a 180° shift for a binary 1. In each of these cases there is one bit per symbol.

Data rate in bps is calculated as the reciprocal of the *bit time* ($T_b$):

$$\text{Data Rate} = 1 / T_b \text{ bps} \tag{2.52}$$
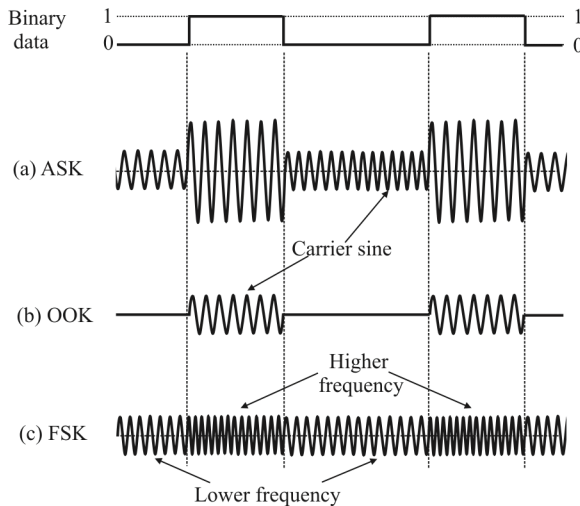
**Figure 2.19** Three basic digital modulation formats are still very popular with low-data-rate short-range wireless applications: (a) amplitude shift keying, (b) on-off keying, and (c) frequency shift keying. These waveforms are coherent as the binary state change occurs at carrier zero crossing points.

With one symbol per bit, the baud rate is the same as the bit rate. However, if we transmit more bits per symbol, the baud rate is slower than the bit rate by a factor equal to the number of bits per symbol. For example, if 2 bits per symbol are transmitted, the baud rate is the bit rate divided by 2. For instance, with QPSK a 70 Mb/sec data stream is transmitted at a baud rate of 35 Msymbols/sec.

### 2.5.2.3 Amplitude Shift Keying and Frequency Shift Keying

Figure 2.19 shows a serial digital signal of binary zeros and ones to be transmitted and the corresponding AM and FM signals resulting from modulation. There are two types of AM signals: *on-off keying* (OOK) and ASK (the former is actually a form of the latter). In Figure 2.19(a), the carrier amplitude is shifted between two amplitude levels to produce ASK. In Figure 2.19(b), the binary signal turns the carrier off and on to create OOK or ASK where one of the amplitudes is zero.

AM produces sidebands above and below the carrier offset by the highest frequency content of the modulating signal. The bandwidth required is two times this highest frequency content including any harmonics for binary pulse modulating signals.

*Frequency shift keying* (FSK) shifts the carrier between two (or more) different frequencies. For BFSK these are called the mark and space frequencies, or $f_m$ and $f_s$ [Figure 2.19(c)]. FM produces multiple sideband frequencies above and below the carrier frequency. The bandwidth produced is a function of the
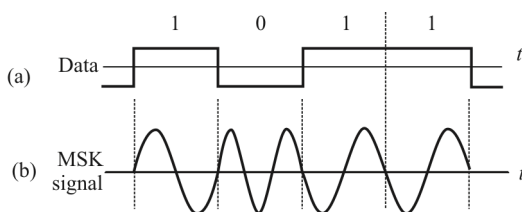
**Figure 2.20** MSK carrier (b) modulated by the data signal in (a).

highest modulating frequency including harmonics and the modulation index, which is given by

$$\beta_{FM} = \Delta f T_b \tag{2.53}$$

where $\Delta f$ is the frequency deviation or shift between the mark and space frequencies:

$$\Delta f = f_s - f_m$$

and $T_b$ is the bit time interval of the data or the reciprocal of the data rate (1/bps).

Smaller values of $\beta_{FM}$ produce fewer sidebands. A popular version of FSK, called *minimum shift keying* (MSK), ensues when $\beta_{FM} = 0.5$. Smaller values are also used such as $\beta_{FM} = 0.2$.

Binary data consists of sharp transitions between "one" and "zero" states and vice versa, potentially creating signals that have sidebands extending out a considerable distance from the carrier. This is sometimes called *spectral splatter* and creates problems for most radio communications systems, as any sidebands outside the allowed bandwidth cause interference to adjacent channels and any communication links that may be using them.

*Minimum Shift Keying*

MSK is a type of continuous-phase FSK that is used in a number of applications. MSK is illustrated in Figure 2.20. MSK modulation is a form of OQPSK in which the symbol pulse shape is a half-cycle sinusoid rather than the usual rectangular pulse. With its constant-envelope property, the power amplifier may work at saturation without significantly distorting the modulated signals. This allows the use of higher efficiency power amplifiers in the system transmitters.

Figure 2.20 shows that when using MSK modulation there are no phase discontinuities because the modulating data signal changes the frequency of the signal in a continuous fashion precluding them. This arises as a result of the unique characteristic of MSK that the frequency difference between the logical

one and logical zero states is always equal to half the data rate, which is when $\beta_{FM}$ = 0.5.

*GMSK*

A variant of MSK modulation, known as *Gaussian filtered minimum shift keying* (GMSK) is used for a number of radio communications applications including the GSM cellular telecommunications system. In GMSK the data signal is first filtered by a Gaussian filter before modulating the carrier.

   The spectral splatter problem can be overcome in part by filtering the signal as in GMSK, but the transitions in the data become progressively less sharp as the level of filtering is increased and the bandwidth reduced. The advantage of MSK is its continuous phase transitions. Here there are no phase discontinuities because the frequency changes occur at the carrier zero crossing points.

   The GMSK modulation scheme reduces signal sidelobe power level and mainlobe width by filtering the rectangular pulses before modulation using a baseband Gaussian-shaped filter. This controlled amount of *inter-symbol interference* (ISI) further reduces the carrier's phase discontinuities. This approach can satisfy an adjacent-channel interference requirement of 60dB or more. (The ratio of spurious content in the adjacent channel to that of the desired channel is 60dB).

   The spectrum of MSK and GMSK (when $WT = 0.5$) is compared in Figure 2.21.

*ASK and FSK Spectral Efficiency*

There are several ways to improve the spectral efficiency for both ASK and FSK. The data rates, carrier frequencies, and shift frequencies can be selected so there are no discontinuities in the sine carrier when changing from one binary state to
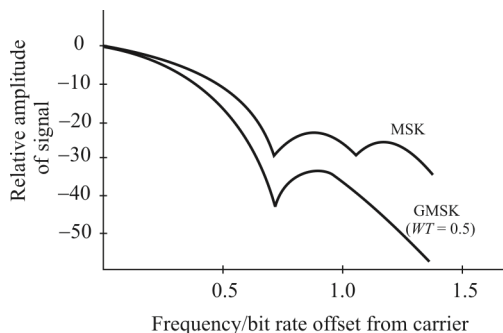


**Figure 2.21** Spectral density of MSK and GMSK signals as a function of the offset from the carrier.
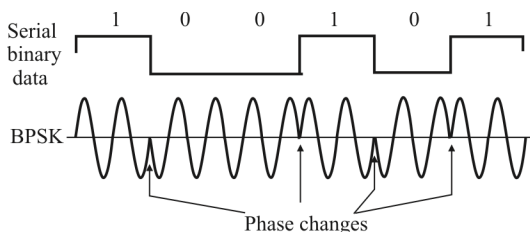
**Figure 2.22** In binary phase shift keying, note how a binary 0 is 0° while a binary 1 is 180°. The phase changes when the binary state switches so the signal is coherent.

another. These discontinuities produce glitches that increase the harmonic content and the bandwidth.

The stop and start times of the binary data are synchronized with the sine carrier so that transitions in amplitude or frequency occur at the zero crossing points. This is called *continuous phase* or *coherent* modulation. Both coherent ASK/OOK and coherent FSK have fewer harmonics and a narrower bandwidth than non-coherent signals.

A second technique is to shape the digital signal with a filter prior to modulation. This rounds the signal off, lengthens the rise and fall times, and reduces the harmonic content. Special Gaussian and raised cosine lowpass filters are used for this purpose. GSM cell phones using GMSK allow a data rate of 270 kbps in a 200kHz channel.

2.5.2.4 Binary Phase Shift Keying

A very popular digital modulation scheme, *binary phase shift keying* (BPSK), shifts the carrier sine wave 180° for each change in binary state (see Figure 2.22). BPSK is coherent as the phase transitions occur at the zero crossing points. The proper demodulation of BPSK requires the signal to be compared to a sine carrier of the same phase. This requires carrier recovery (particularly the carrier phase) and other complex circuitry.

A simpler version is differential BPSK or DPSK, where the received bit phase is compared to the phase of the previous bit. In this sense it is sometimes considered a coherent form of modulation. BPSK is very spectrally efficient in that we can transmit at a data rate equal to the bandwidth or 1 bit/Hz.

2.5.2.5 Quadrature Phase Shift Keying

A variation of BPSK is *quadrature PSK* (QPSK). The modulator produces two sine carriers 90° apart (see Figure 2.23). The binary data modulates each phase, producing four unique sine signals shifted by 45° from one another. The two
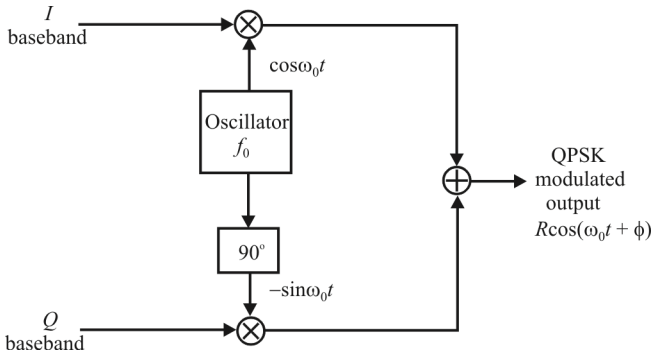
**Figure 2.23** QPSK modulator.

phases are added together to produce the final signal. Each unique pair of bits generates a carrier with a different phase (Table 2.1).

Figure 2.24(a) displays QPSK with a phasor diagram where the phasor represents the carrier sine amplitude peak and its position indicates the phase. The constellation diagram in Figure 2.24(b) shows the same information. QPSK is very spectrally efficient since each carrier phase represents two bits of data. The spectral efficiency is 2 bits/Hz, meaning twice the data rate can be achieved in the same bandwidth as BPSK.

## 2.5.2.6 Multiple Phase Shift Keying

QPSK produces two bits per symbol, making it very spectrally efficient. QPSK can be referred to as 4PSK because there are four amplitude-phase combinations. By using smaller phase shifts, more bits can be transmitted per symbol. Some popular variations are 8PSK and 16PSK. Such modulations are referred to as *multiple phase shift keying* (MPSK). 8PSK uses eight symbols with constant carrier amplitude with 45° shifts between them, enabling three bits ($8 = 2^3$) to be transmitted for each symbol. 16PSK uses 22.5° shifts of constant amplitude carrier signals. This arrangement results in a transmission of 4 bits per symbol ($16 = 2^4$). This can continue for much higher rates, and orders of 256 ($= 2^8$) are not uncommon when the noise level allows it.

**Table 2.1** Carrier Phase Shift for Each Pair of Bits Represented

| Bit Pairs | Phase (degrees) |
|-----------|-----------------|
| 00        | 45              |
| 01        | 135             |
| 11        | 225             |
| 10        | 315             |
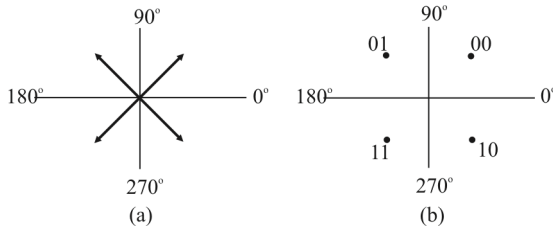
**Figure 2.24** Modulation can be represented without time domain waveforms. For example, QPSK can be represented with a phasor diagram (a) or a constellation diagram (b), both of which indicate phase and amplitude magnitudes.

While MPSK is much more spectrally efficient, the greater the number of smaller phase shifts, the more difficult the signal is to demodulate in the presence of noise. The principal benefit of MPSK is that the constant carrier amplitude means that more efficient nonlinear *power amplifiers* (PAs) can be used in the transmission scheme.

## 2.5.2.7 Quadrature Amplitude Modulation

The creation of symbols that are some combination of amplitude and phase can carry the concept of transmitting more bits per symbol further. This method is called *quadrature amplitude modulation* (QAM). For example, 8QAM uses four carrier phases plus two amplitude levels to transmit 3 bits per symbol. Other popular variations are 16QAM, 64QAM, and 256QAM, which transmit 4, 6, and 8 bits per symbol, respectively (see Figure 2.25).

While QAM is very spectrally efficient, it is more difficult to demodulate in
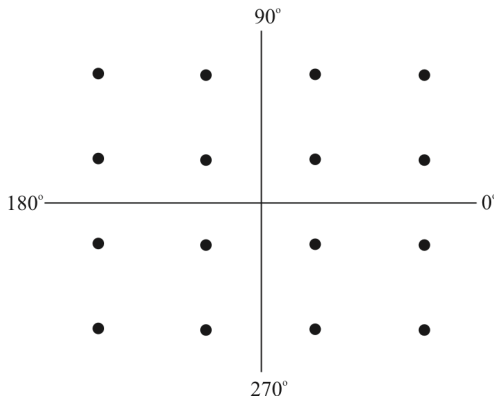


**Figure 2.25** 16QAM uses a mix of amplitudes and phases to achieve 4 bits/Hz. In this example, there are three amplitudes and 12 phase shifts.
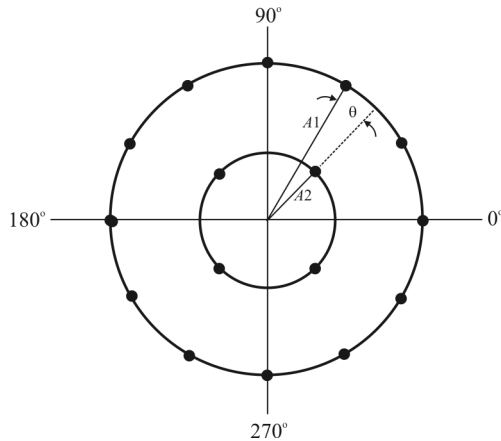
**Figure 2.26** 16APSK uses two amplitude levels, *A*1 and *A*2, plus 16 different phase positions with an offset of $\theta$. This technique is widely used in satellite communications.

the presence of noise, which in most cases is random amplitude variations. Linear power amplification is also required so spectrally efficient nonlinear transmitter PAs cannot be used. QAM is very widely used in cable TV, Wi-Fi wireless local-area networks (LANs), satellites, and cellular telephone systems to produce maximum data rate in limited bandwidths.

## 2.5.2.8 Amplitude Phase Shift Keying

*Amplitude phase shift keying* (APSK), a variation of both MPSK and QAM, was created in response to the need for an improved QAM. Higher levels of QAM such as 16QAM and above have many different amplitude levels as well as phase shifts. These amplitude levels are more susceptible to noise since the higher the order the less distance there is between levels.

Furthermore, these multiple levels require linear PAs that are less efficient than nonlinear (e.g., class C). The fewer the number of amplitude levels or the larger the difference between the amplitude levels, the greater the chance to operate in the nonlinear region of the PA to boost power level.

APSK uses fewer amplitude levels than ASK alone. It essentially arranges the symbols into two or more concentric rings with a constant phase offset $\theta$. For example, 16APSK uses a double-ring PSK format as illustrated in Figure 2.26. This is called 4-12 16APSK with four symbols in the center ring and 12 in the outer ring. Two close amplitude levels allow the amplifier to operate closer to the nonlinear region, improving efficiency as well as power output. APSK is used primarily in satellites since it is a good fit with the popular *traveling wave tube* (TWT) PAs.
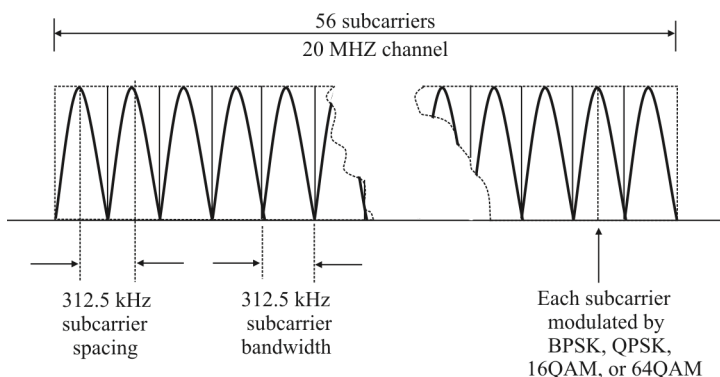
**Figure 2.27** In the OFDM signal for the IEEE 802.11n Wi-Fi standard, 56 subcarriers are spaced 312.5 kHz in a 20 MHz channel. Data rates to 300 Mbits/s can be achieved with 64QAM.

## 2.5.2.9 Orthogonal Frequency Division Multiplexing

*Orthogonal frequency division multiplexing* (OFDM) combines modulation and multiplexing techniques to improve spectral efficiency. A transmission channel is divided into many smaller subchannels or subcarriers (see Figure 2.27). The subcarrier frequencies and spacings are chosen so they are orthogonal to one another. Their spectra will not interfere with one another, then, so no guard bands are required.

The serial digital data to be transmitted is subdivided into parallel slower data rate channels. These lower data rate signals are then used to modulate each subcarrier. The most common forms of modulation are BPSK, QPSK, and several levels of QAM. BPSK, QPSK, 16QAM, and 64QAM are defined with 802.11n. Data rates up to about 300 Mbps are possible with 64QAM. Bear in mind, however, that the larger the number of states, the more susceptible to noise the signals become, so generally higher SNRs are required.

The complex modulation process is produced by DSP techniques. An inverse fast Fourier transform (IFFT) generates the signal to be transmitted. An FFT process recovers the signal at the receiver.

OFDM is very spectrally efficient. That efficiency level depends on the number of subcarriers and the type of modulation used on the subcarriers, but it can be as high as 30 bps/Hz. Because of the wide bandwidth it usually occupies and the large number of subcarriers, it also is less prone to signal loss due to fading, multipath reflections, and similar effects common in UHF and microwave radio signal propagation.

OFDM is a very popular form of digital modulation due to its spectral efficiency. It is used in Wi-Fi LANs, WiMAX broadband wireless, Long Term

**Table 2.2** Spectral Efficiency for Popular Digital Modulation Methods

| Type of Modulation | Spectral Efficiency (bps/Hz) |
|---|---|
| FSK | <1 (depends on modulation index) |
| GMSK | 1.35 |
| BPSK | 1 |
| QPSK | 2 |
| 8PSK | 3 |
| 16QAM | 4 |
| 64QAM | 6 |
| OFDM | >10 (depends on the type of modulation and the number of subcarriers) |

Evolution (LTE) 4G cellular systems, *digital subscriber line* (DSL) systems, and in most *power-line communications* (PLC) applications.

2.5.2.10 Determining Spectral Efficiency

Spectral efficiency is a measure of how quickly data can be transmitted in an assigned bandwidth, and the unit of measurement is bps/Hz. Each type of modulation has a maximum theoretical spectral efficiency measure. Table 2.2 indicates this spectral efficiency for several techniques.

SNR is another important factor that influences spectral efficiency. It also can be expressed as the *carrier-to-noise power ratio* (CNR). The measure is the BER for a given CNR value. BER is the percentage of errors that occur in a given number of bits transmitted. As the noise becomes larger compared to the signal level, the SNR and CNR decrease and more errors occur.

Some modulation methods are more immune to noise than others. Amplitude modulation methods like ASK/OOK and QAM are far more susceptible to noise so they have a higher BER for a given SNR. This is because most noise affects the amplitude of signals as opposed to their frequency or phase (LO phase noise is an exception to this). Phase and frequency modulation (BPSK, FSK, etc.) fare better in a noisy environment so they require less signal power for a given SNR. Figure 2.28 compares the BER for several types of common digital modulations.

*Out-of-Band Power*

Each type of digital modulation produces energy in channels adjacent to and close by the designated channel. This energy interferes with whatever communication that is transpiring in the adjacent channels. The undesired energy is treated as
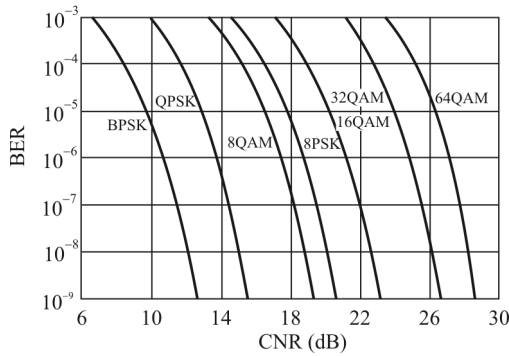
**Figure 2.28** Comparison of several popular modulation methods and their spectral efficiency expressed in terms of BER versus CNR. Note that for a given BER, a greater CNR is needed for the higher QAM levels.

noise so it produces interference that lowers the SNR in those channels. The amount of this spectral leakage is dependent on the modulation technique; some methods produce less than others.

The fractional out-of-band power for four popular forms of digital modulations are compared in Figure 2.29 [7]. We see that the energy leakage for MSK is significantly better than the other forms displayed. Since GMSK leaks even less than MSK, as illustrated in Figure 2.21, its corresponding performance curve in Figure 2.29 is below that for MSK.
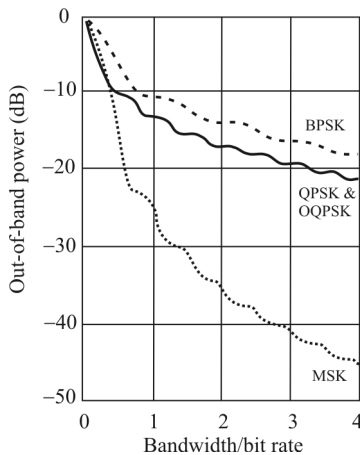


**Figure 2.29** Fractional out-of-band power as a function of the normalized bandwidth. (Source: [7], © Artech House, 2011. Reprinted with permission.)

*Other Factors Affecting Spectral Efficiency*

While modulation plays a key role in the spectral efficiency, other factors influence it as well. For example, the use of *forward error correction* (FEC) techniques can greatly improve the BER. Such coding methods add extra bits so errors can be detected and corrected at the receiver. These extra coding bits add overhead to the signal, reducing the net bit rate of the data, but that is usually an acceptable tradeoff for the single-digit decibel improvement in CNR. Such coding gain is common to almost all modern wireless systems.

Source digital compression (otherwise known as source coding) is another technique. The digital data to be sent is subjected to a compression algorithm that greatly reduces the amount of redundant information in the source data stream. This allows digital signals to be reduced in content so they can be transmitted as shorter, slower data streams.

Spectral efficiency can also be improved by the use of *multiple-input multiple-output* (MIMO) schemes, which is the use of multiple antennas and transceivers to transmit two or more bit streams [8]. A single high-rate stream is divided into two or more parallel streams and transmitted in the same bandwidth simultaneously. By coding the streams and their unique path characteristics, the receiver can identify and demodulate each stream and reassemble it into the original stream. MIMO, therefore, improves data rate, noise performance, and spectral efficiency. Newer wireless LAN (WLAN) standards like 802.11n and 802.11ac/ad and cellular standards like LTE and WiMAX use MIMO.

Severe shortages exist in the cellular and *land mobile radio* (LMR) frequency regions, inhibiting the expansion of services such as high data speeds as well as the addition of new subscribers. One approach to the problem is to improve the efficiency of usage by squeezing more users into the same or less spectrum and achieving higher data rates.

One of the most crowded areas of spectrum is the LMR and *private mobile radio* (PMR) spectrum used by the federal government, state governments, and local public safety agencies like fire and police departments. Currently they're assigned spectrum by FCC license in the 150 to 174 MHz VHF spectrum and the 421- to 512-MHz UHF spectrum (in the United States; other countries may use somewhat different spectrum for these functions).

Historically, most of these radio systems and mobile handsets use FM analog modulation that occupies a 25 kHz channel. Recently the FCC has required all such radios to change to 12.5 kHz channels. This conversion, known as *narrowbanding*, obviously doubles the number of available channels. It means that more radios can be added to the system. This conversion was required to take place before January 1, 2012.

In the future, the FCC is expected to mandate a further change from the 12.5 kHz channels to 6.25 kHz channels, again doubling capacity without increasing the amount of spectrum assigned. The new equipment can use either analog or

digital modulation. It is possible to put standard analog FM in a 12.5 kHz channel by adjusting the modulation index and using other bandwidth-narrowing techniques. However, analog FM in a 6.25 kHz channel is unworkable, so a digital technique must be used.

2.5.2.11 Implementing Modulation and Demodulation

In the past, unique circuits implemented the modulation and demodulation functions. Most modern radios are *software-defined radios* (SDR) where functions like modulation and demodulation are performed in software. This is manifest in cellular phones, for example, in the power required [a *digital signal processor* (DSP), especially a fast DSP, requires significantly more power than its analog counterpart].

The modulation process begins with the data to be transmitted being fed to a DSP device that generates two digital outputs, which are needed to define the amplitude and phase information required at the receiver to recover the data. The DSP produces two baseband streams that are sent to *digital-to-analog converters* (DACs) that produce the analog equivalents.

These modulation signals feed the mixers along with the carrier. There is a 90° shift between the carrier signals to the mixers. The resulting quadrature output signals from the mixers are summed to produce the signal to be transmitted. If the carrier signal is at the final transmission frequency, the composite signal is then amplified and sent to the antenna. This is called *direct conversion*. Alternately, the carrier signal may be at a lower IF. The IF signal is upconverted to the final carrier frequency by another mixer before being applied to the transmitter PA.

At the receiver, the signal from the antenna is amplified and downconverted to IF or directly to the original baseband signals. The amplified signal from the antenna is applied to mixers along with locally generated carrier signals. Again, there is a 90° shift between the carrier signals applied to the mixers. The mixers produce the original baseband analog signals, which are then digitized in a pair of *analog-to-digital converters* (ADCs) and sent to the DSP module where demodulation algorithms recover the original digital data.

If the modulation is QPSK or QAM, to faithfully reproduce the amplitude and phase information, the PA in the transmitter needs to be a linear amplifier. For constant modulus modulations such as FSK and BPSK, a more efficient nonlinear PA may be used.

# 2.6 Random Modulation

So far we have considered the case when the signals involved are deterministic. When the modulating signal is random, a somewhat different viewpoint is required. We will examine some of those cases in this section. We begin with a
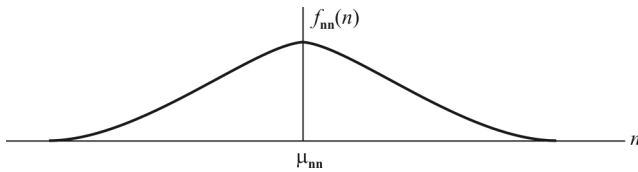
**Figure 2.30** Normal curve with mean expressed as $\mu_{nn}$.

short discussion of random variables and random processes (also known as *stochastic processes*). Such processes are characterized by their statistical properties [9, 10].

## 2.6.1 Stationary Processes

Consider an experiment where we flip a fair coin a number of times, recording the results at each flip as heads or tails. Such a sequence of results describes a (discrete) random sequence or random process and we denote it by **x**. In this case, each instance of a result could be a head (H) or tail (T) so there are two possible outcomes at each instant. We can index these instances with a variable; we'll refer to it as *t* for time. At each *t*, we have a random variable that we denote by $X(t)$. For discrete processes, $t = nT$ when the time between events is a constant *T*.

This example describes a discrete random process. Any given experimental outcome is a discrete sequence of heads or tails. The values of the random variable are also discrete in this case, but they need not be. Random processes can also be continuous and the same concepts apply. In this case, however, *t* is continuous, not discrete, and/or the values can be discrete or continuous.

Another example of a (discrete) random process is the rolling of a die. On any given roll of the die, there are six possible outcomes $X(t) = \{1, 2, 3, 4, 5, 6\}$. Again, the particular rolls are defined by a time index, *t*, and the value at *t* is discrete, selected from the set $X(t)$.

An example of a continuous random variable is the value of thermal noise at a particular time *t*. It is well known that the statistics of thermal noise behave according to Gaussian processes that are described by a normal curve, an example of which is illustrated in Figure 2.30. $\mu_{xx}$ is the mean value of the thermal noise and is usually equal to zero.

> **Definition 2.5: Mean Value.** The *mean* of the random process **x**(*t*) is the mean of random variable $X(t)$ at time instant *t*.

$$\mathcal{E}\{X(t)\} = \mu_{xx}(t) \tag{2.54}$$

where $\mathcal{E}\{\bullet\}$ denotes expected value. Let $p_{xx}(x)$ denote the pdf of $X(t)$ at time instant $t$. Then

$$\mathcal{E}\{X(t)\} = \int_{-\infty}^{\infty} x p_{xx}(x) dx \tag{2.55}$$

**Definition 2.6: Autocorrelation Function.** The *autocorrelation function* of $X(t)$ is a function of two variables $t_1 = t$ and $t_2 = t + \tau$, and is given by

$$R_{xx}(t, t + \tau) = \mathcal{E}\{X(t)X(t + \tau)\} \tag{2.56}$$

which is a measure of the degree to which two time samples of the same random process are related.

**Definition 2.7: Wide-Sense Stationary Process.** A random process $\mathbf{x}(t)$ is *wide-sense stationary* (wss) if

$$\mu_{xx}(t) = \mathcal{E}\{X(t)\} = \text{constant} \tag{2.57}$$

and

$$R_{xx}(t, t + \tau) = \mathcal{E}\{X(t)X(t + \tau)\} = R_{xx}(\tau) \tag{2.58}$$

In other words, a random process $\mathbf{x}(t)$ is wss if its first two statistics, its mean and autocorrelation, do not vary with a shift in the time origin.

**Example 2.2:** Consider the random process $X(t)$ given by

$$X(t) = A\cos(2\pi f_c t + \theta)$$

where $\theta$ is uniformly distributed over $[0, 2\pi]$. That is, the pdf of $\theta$ is given by

$$p_{\theta\theta}(\theta) = \begin{cases} \dfrac{1}{2\pi}, & 0 \leq \theta \leq 2\pi \\ 0, & \text{otherwise} \end{cases}$$

The expected value of $X(t)$ is

$$\mathcal{E}\{X(t)\} = \int\limits_0^{2\pi} \cos(2\pi f_c t + \theta)\frac{1}{2\pi}d\theta$$

$$= 0$$

while the autocorrelation function is

$$R_{xx}(t, t+\tau) = \mathcal{E}_\theta \{A\cos(2\pi f_c t + \theta)A\cos[2\pi f_c(t+\tau)+\theta]\}$$

$$= A^2\mathcal{E}_\theta \left\{\frac{1}{2}\cos(2\pi f_c t) + \frac{1}{2}\cos[2\pi f_c(2t+\tau)+2\theta]\right\}$$

$$= \frac{A^2}{2}\cos 2\pi f_c \tau$$

Since the mean and autocorrelation of $X(t)$ do not depend on time $t$, then $X(t)$ is a wss process.

**Definition 2.8: Strict-Sense Stationary Process**. A *strict-sense stationary* (sss) process is a stochastic process whose joint probability distribution does not change when shifted in time. Consequently, parameters such as the mean and variance also do not change over time.

2.6.1.1 Properties of the Autocorrelation Function

For the wss process $\mathbf{x}(t)$

- $R_{xx}(\tau) = R_{xx}(-\tau)$ : the autocorrelation process is symmetric in $\tau$ about zero.
- $|R_{xx}(\tau)| \le R_{xx}(0)$ for all $\tau$: the maximum value of the autocorrelation function occurs at the origin.
- $R_{xx}(0) = \mathcal{E}\{X^2(t)\}$ : the value of the autocorrelation function at the origin is equal to the average power in the signal.
- The *power spectral density* (psd) of $\mathbf{x}(t)$ is the Fourier transform of its autocorrelation. That is

$$S_{xx}(f) = \mathcal{F}\{R_{xx}(\tau)\} = \int\limits_{-\infty}^{\infty} R_{xx}(\tau)e^{-j2\pi f\tau}d\tau \qquad (2.59)$$

$$R_{xx}(\tau) = \mathcal{F}^{-1}\{S_{xx}(f)\} = \int\limits_{-\infty}^{\infty} S_{xx}(f)e^{j2\pi f\tau}df \qquad (2.60)$$
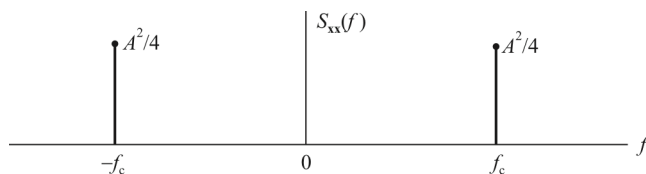
**Figure 2.31** Psd of cosine function.

**Example 2.2 (continued)** For the random process in Example 2.1, we have

$$R_{xx}(\tau) = \frac{A^2}{2}\cos(2\pi f_c \tau)$$

Hence, the psd of $x(t)$ is the Fourier transform of the autocorrelation of $X(t)$ given by

$$S_{xx}(f) = \frac{A^2}{4}[\delta(f - f_c) + \delta(f + f_c)]$$

This function is shown in Figure 2.31.

**Example 2.3** Let

$$Y(t) = X(t)\cos(2\pi f_c t + \theta)$$

where $X(t)$ is a wss process with psd $S_{xx}(f)$, $\theta$ is uniformly distributed over $[0, 2\pi]$, and $X(t)$ is independent of $\theta$ and $\cos(2\pi f_c t + \theta)$. The psd of $Y(t)$ is found as follows. First the mean is given by

$$\begin{aligned}
\mu_{yy}(t) &= \mathcal{E}\{Y(t)\} \\
&= \mathcal{E}\{X(t)\cos(2\pi f_c + \theta)\} \\
&= \mathcal{E}\{X(t)\}\mathcal{E}\{\cos(2\pi f_c t + \theta)\}
\end{aligned}$$

(because of the independence property). So

$$\mu_{yy}(t) = \mu_{xx}(t) \cdot 0$$
$$= 0$$

The autocorrelation of $Y(t)$ is

$$
\begin{aligned}
R_{yy}(t, t+\tau) &= \mathcal{E}\{Y(t)Y(t+\tau)\} \\
&= \mathcal{E}\{X(t)\cos(2\pi f_c t + \boldsymbol{\theta})X(t+\tau)\cos[2\pi f_c(t+\tau) + \boldsymbol{\theta}]\} \\
&= \underbrace{\mathcal{E}\{X(t)X(t+\tau)\}}_{R_{XX}(\tau)}\underbrace{\mathcal{E}\{\cos(2\pi f_c t + \boldsymbol{\theta})\cos[2\pi f_c(t+\tau) + \boldsymbol{\theta}]\}}_{\frac{1}{2}\cos(2\pi f_c \tau)}
\end{aligned}
$$

$$= R_{xx}(\tau)\frac{1}{2}\cos(2\pi f_c \tau) = R_{yy}(\tau)$$

Therefore $\mathbf{y}(t)$ is wss and

$$S_{yy}(f) = \mathcal{F}\{R_{yy}(\tau)\} = \frac{1}{4}\mathcal{F}\{R_{xx}(\tau)(e^{j2\pi f_c \tau} + e^{-j2\pi f_c \tau})\}$$

$$= \frac{1}{4}[S_{xx}(f - f_c) + S_{xx}(f + f_c)]$$

2.6.1.2 Properties of the psd

- $S_{xx}(f) \geq 0$: the psd is always real valued and never negative.
- $S_{xx}(f) = S_{xx}(-f)$: the psd is symmetric around $f = 0$ for $X(t)$ real valued.
- $S_{xx}(f) \leftrightarrow R_{xx}(\tau)$: the psd and autocorrelation function are a Fourier transform pair.
- $P = R_{xx}(0) = \int_{-\infty}^{\infty} S_{xx}(f)df$: relationship between the average power and the psd.

2.6.1.3 Transmission over LTI Systems

The response of LTI system to a random input $X(t)$ is given by (Figure 2.32):

$$Y(t) = X(t) * h(t)$$

$$= \int_{-\infty}^{\infty} x(t - \tau)h(\tau)d\tau$$

Properties of the output:
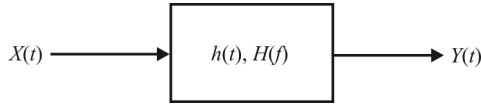


**Figure 2.32** Depiction of an LTI system.

- If $X(t)$ is wss, so is $Y(t)$.
- The mean of $Y(t)$ is

$$\mu_{YY} = \mu_{XX} H(0)$$

- The autocorrelation of $Y(t)$ is

$$R_{yy}(\tau) = R_{xx}(\tau) * h(\tau) * h(-\tau)$$

- The psd of $Y(t)$ is

$$S_{yy}(f) = S_{xx}(f)|H(f)|^2$$

## 2.6.1.4 Cross-Correlation Function

The cross-correlation function between two random processes $\mathbf{x}(t)$ and $\mathbf{y}(t)$ is defined as

$$R_{xy}(t_1, t_2) = \mathcal{E}\{x(t_1)y(t_2)\} = \mathcal{E}\{x(t)y(t+\tau)\} \tag{2.61}$$

when $t_1 = t$ and $t_2 = t + \tau$. If $\mathbf{x}(t)$ and $\mathbf{y}(t)$ are both wss, then

$$R_{xy}(t_1, t_2) = R_{xy}(\tau) \tag{2.62}$$

Like the autocorrelation function, the cross-correlation function is a measure of the similarity of the two processes $\mathbf{x}(t)$ and $\mathbf{y}(t)$ as a function of their time offset.

### 2.6.2 Random Modulation

Papoulis reviewed the notions involved with random modulation processes [11]. We summarize some of those concepts in this section.

2.6.2.1 Basic Concepts

We consider the complex process

$$
\begin{aligned}
\mathbf{z}(t) &= [\mathbf{a}(t) + j\mathbf{b}(t)]e^{j2\pi f_c t} \\
&= [\mathbf{a}(t) + j\mathbf{b}(t)][\cos 2\pi f_c t + j\sin 2\pi f_c t] \\
&= \mathbf{a}(t)\cos 2\pi f_c t + j\mathbf{b}(t)\cos 2\pi f_c t + j\mathbf{a}(t)\sin 2\pi f_c t - \mathbf{b}(t)\sin 2\pi f_c t \\
&= \mathbf{x}(t) + j\mathbf{y}(t)
\end{aligned}
\tag{2.63}
$$

where $\mathbf{a}(t)$ and $\mathbf{b}(t)$ are two real random processes and $f_c$ is a constant. From (2.63) we see that

$$
\begin{aligned}
\mathbf{x}(t) &= \mathbf{a}(t)\cos 2\pi f_c t - \mathbf{b}(t)\sin 2\pi f_c t \\
\mathbf{y}(t) &= \mathbf{b}(t)\cos 2\pi f_c t + \mathbf{a}(t)\sin 2\pi f_c t
\end{aligned}
\tag{2.64}
$$

The polar form of $\mathbf{z}(t)$ is

$$
\mathbf{z}(t) = \mathbf{w}(t)e^{j2\pi f_c t} = \mathbf{r}(t)e^{j[2\pi f_c t + \varphi(t)]}
\tag{2.65}
$$

where, from (2.63)

$$
\mathbf{w}(t) = \mathbf{a}(t) + j\mathbf{b}(t) = \mathbf{r}(t)e^{j\varphi(t)}
\tag{2.66}
$$

$$
\mathbf{r}(t) = \sqrt{\mathbf{a}^2(t) + \mathbf{b}^2(t)} \qquad \tan\varphi(t) = \mathbf{b}(t)/\mathbf{a}(t)
\tag{2.67}
$$

Therefore,

$$
\mathbf{x}(t) = \mathrm{Re}\{\mathbf{w}(t)e^{j2\pi f_c t}\} = \mathbf{r}(t)\cos[2\pi f_c t + \varphi(t)]
\tag{2.68}
$$

Thus $\mathbf{x}(t)$ is a modulated signal with *real envelope* $\mathbf{r}(t)$, *complex envelope* $\mathbf{w}(t)$, and instantaneous frequency[1]

$$
f_i(t) = f_c + \frac{1}{2\pi}\varphi'(t)
\tag{2.69}
$$

---

[1]  $\mathbf{x}'(t)$ denotes differentiation of $\mathbf{x}(t)$ with respect to time.

2.6.2.2 Frequency Modulation

We can write an FM signal as

$$\mathbf{x}(t) = \cos[2\pi f_c t + \beta_{FM}\boldsymbol{\varphi}(t) + \boldsymbol{\varphi}_0] = \operatorname{Re}\{\mathbf{z}(t)\} \qquad (2.70)$$

where

$$\boldsymbol{\varphi}(t) = \int_0^t \mathbf{c}(\alpha)d\alpha \qquad (2.71)$$

In (2.70), $\beta_{FM}\boldsymbol{\varphi}(t) + \boldsymbol{\varphi}_0$ is the phase, $2\pi f_c + \lambda\mathbf{c}(t)$ the instantaneous frequency, and $\beta_{FM}$ the modulation index of $\mathbf{x}(t)$.

We can show that

$$R_{zz}(\tau) = \mathcal{E}\{z(t+\tau)z*(t)\} = e^{j2\pi f_c \tau}\mathcal{E}\left\{e^{j\beta_{FM}\int_t^{t+\tau}\mathbf{c}(\alpha)d\alpha}\right\}$$

$$= e^{j2\pi f_c \tau}\mathcal{E}\left\{e^{j\beta_{FM}\int_0^T \mathbf{c}(\alpha)d\alpha}\right\} \qquad (2.72)$$

and that

$$R_{xx}(\tau) = \frac{1}{2}\operatorname{Re}\{R_{zz}(\tau)\} \qquad (2.73)$$

so for the determination of the spectral properties of the real bandpass process $\mathbf{x}(t)$, it suffices to find the mean

$$\mathcal{E}\{\mathbf{w}(t)\} = \mathcal{E}\left\{e^{j\beta_{FM}\boldsymbol{\varphi}(t)}\right\} = \mathcal{E}\left\{e^{j\beta_{FM}\int_0^t \mathbf{c}(\alpha)d\alpha}\right\} \qquad (2.74)$$

of the complex lowpass process

$$\mathbf{w}(t) = e^{j\beta_{FM}\boldsymbol{\varphi}(t)}$$

$\mathbf{w}(t)$ has the property that the mean and autocorrelation are equal

$$R_{\mathbf{ww}}(\tau) = \mathcal{E}\{e^{j\beta_{FM}\int_0^{\tau} c(\alpha)d\alpha}\} = \mathcal{E}\{\mathbf{w}(\tau)\} \tag{2.75}$$

We can define phase and frequency modulation as follows:

> **Definition 2.9:** A process $\mathbf{x}(t)$ is *phase modulated* if the statistics of $\boldsymbol{\varphi}(t)$ are known. In this case, $R_{\mathbf{ww}}(\tau)$ is obtained directly and it is only necessary to determine its transform.

> **Definition 2.10:** A process $\mathbf{x}(t)$ is *frequency modulated* if the available information is expressed in terms of the instantaneous frequency of $\mathbf{x}(t)$. The resulting problem is no longer simple because there is, in general, no simple relationship between the characteristic function of $\boldsymbol{\varphi}(t)$ and the statistics of $\mathbf{c}(t)$. As we show next, however, the normal case is an exception.

*Woodward's Theorem.* Woodward's theorem [12, 13] expresses the approximate power spectrum of $\mathbf{x}(t)$ under large modulation index conditions.

> **Property 2.5: Woodward's Theorem.** If $\mathbf{c}(t)$ is a real sss process, then the power spectrum of $\mathbf{x}(t)$ can be approximated by

$$S_{\mathbf{xx}}(f) \approx \frac{\pi}{\beta_{FM}}\left[p_c\left(\frac{f_c+f}{\beta_{FM}}\right) + p_c\left(\frac{f_c-f}{\beta_{FM}}\right)\right] \tag{2.76}$$

> where $p_c(c)$ is the pdf of $\mathbf{c}(t)$.

Thus the pdf of $p_c(c)$ is translated up and down in frequency by $f_c$ when the modulation index is sufficiently large.

Equation (2.76) applies for any FM signal of the form of (2.70) under the condition that the modulation index is sufficiently large. (It may be interesting to note that commercial FM satisfies the "sufficiently large" criterion while tactical analog bandlimited FM voice transmissions do not.) Under these conditions and assuming that the characteristic function of $\mathbf{c}(t)$ is approximately zero when $|\mu| > \mu_0$, then the relationship between the autocorrelation function and the characteristic function of $\mathbf{c}(t)$ is as illustrated in Figure 2.33.

*Normal Processes*

When $\mathbf{c}(t)$ is a normal process with zero mean, then $\boldsymbol{\varphi}(t)$ is also normal with variance
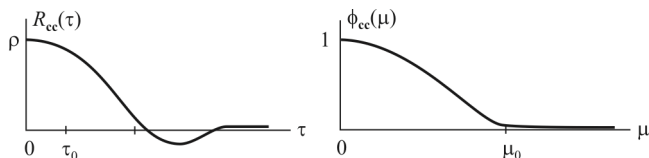
**Figure 2.33** Correlation and characteristic function of stochastic FM.

$$\sigma^2_{\varphi\varphi} = 2\int_0^t R_{cc}(\alpha)(t-\alpha)d\alpha, \qquad t > 0 \qquad (2.77)$$

Thus we get

$$R_{ww}(\tau) = \Phi_{\varphi\varphi}(\beta_{FM};\tau) = e^{-\beta^2_{FM}\sigma^2_{\varphi\varphi}(\tau)/2} \qquad (2.78)$$

In general, the transform of (2.78), $S_{ww}(f)$, is not available in closed form and can only be determined numerically. However, we can get specific results in some limiting cases.

We determine the form of $S_{ww}(f)$ for wideband (large $\beta_{FM}$) signals and narrowband (small $\beta_{FM}$). The time constant

$$\tau_{cc} = \int_0^\infty R_{cc}(\tau)d\tau/\rho, \qquad \rho = R_{cc}(0) = \sigma^2_{cc}$$

is an approximation to the duration of $R_{cc}(\tau)$, and its inverse gives a measure of the bandwidth of the frequency $\mathbf{c}(t)$.

Two additional parameters, $\tau_0$ and $\tau_1$, are defined as (Figure 2.34)

$$R_{cc}(\tau) \approx 0 \qquad \text{for } |\tau| > \tau_1 \gg \tau_{cc}$$
$$R_{cc}(\tau) \approx \rho \qquad \text{for } |\tau| < \tau_0 \ll \tau_{cc} \qquad (2.79)$$
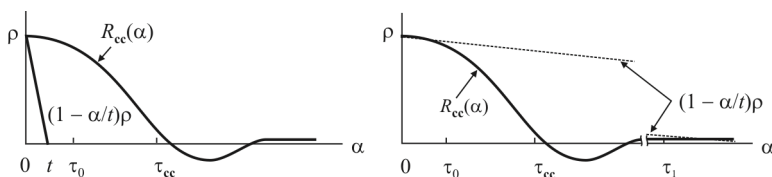


**Figure 2.34** Definition of time constants.
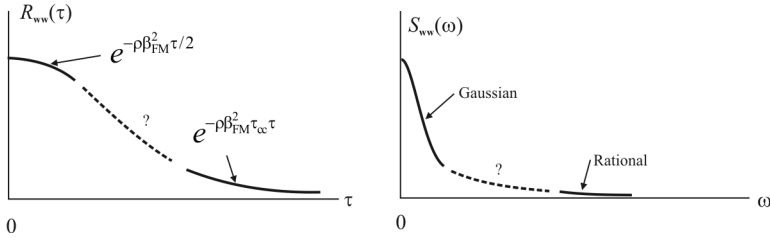
**Figure 2.35** Asymptotic forms of the correlation function and its psd.

Inserting (2.79) into (2.77), we get

$$
\begin{aligned}
\sigma_{\varphi\varphi}^2 &\approx \rho t^2, & |\tau| < \tau_0 \\
\sigma_{\varphi\varphi}^2 &\approx 2\rho t \tau_{cc}, & t > \tau_1
\end{aligned}
\tag{2.80}
$$

which yield

$$
\begin{aligned}
R_{ww}(\tau) &\approx e^{-\rho\beta_{FM}^2 \tau^2/2}, & 0 < \tau < \tau_0 \\
R_{ww}(\tau) &\approx e^{-\rho\beta_{FM}^2 \tau_{cc}\tau}, & \tau > \tau_1
\end{aligned}
\tag{2.81}
$$

The behavior of $S_{ww}(f)$ for large (small) $f$ is determined by the behavior of $R_{ww}(\tau)$ for small (large) $\tau$. Since (see Figure 2.35)

$$
e^{-\rho\beta_{FM}^2 \tau^2/2} \leftrightarrow \frac{1}{\beta_{FM}} \sqrt{\frac{2\pi}{\rho}} e^{-\frac{\omega^2}{2\rho\beta_{FM}^2}}
\tag{2.82}
$$

$$
e^{-\rho\beta_{FM}^2 \tau_{cc}|\tau|} \leftrightarrow \frac{2\rho\tau_{cc}\beta_{FM}^2}{\omega^2 + \rho^2\tau_{cc}^2\beta_{FM}^4}
\tag{2.83}
$$

From (2.82) and (2.83) we can see that $S_{ww}(f)$ is normal near the origin and approaches a first-order rational curve as $f \to \infty$.

*Wideband FM.* If $\beta_{FM}$ is sufficiently large, from (2.78)

$$
R_{ww}(\tau) \approx 0 \qquad \text{for } |\tau| > \tau_0
$$
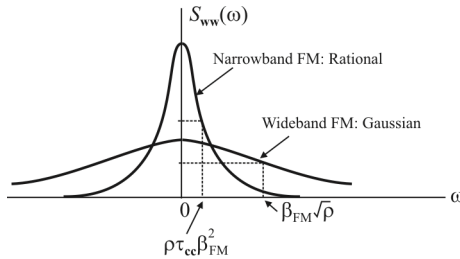
**Figure 2.36** Normal spectra for narrowband FM and wideband FM.

and if $\rho\beta_{FM}^2 \tau_0^2 \gg 1,$ the first approximation in (2.81) applies. Hence, $S_{ww}(f)$ is approximated by the normal curve in (2.82) and its bandwidth is on the order of $\beta_{FM}\sqrt{\rho}$ (Figure 2.36).

We note that in this case

$$S_{ww}(f) \approx \frac{2\pi}{\beta_{FM}} p_c\left(\frac{2\pi f}{\beta_{FM}}\right)$$

because $c(t)$ is a normal random variable with zero mean, variance $\rho$, and pdf

$$p_c(c) = \frac{1}{\sqrt{2\pi\rho}} e^{-c^2/2\rho}$$

*Narrowband FM.* If $\beta_{FM}$ is sufficiently small, then, from (2.78)

$$R_{ww}(\tau) \approx R_{ww}(0) = 1$$

From this it follows that, if $\rho\beta_{FM}^2 \tau_1\tau_{cc} \ll 1,$ then the second approximation in (2.81) applies. Hence, $S_{ww}(\omega)$ is approximated by the rational spectrum in (2.83) and its bandwidth is on the order of $\rho\tau_{cc}\beta_{FM}^2$.

2.6.2.3 Frequency Shift Keying

Suppose now that the instantaneous frequency $c(t)$ is given by

$$c(t) = b(t - \theta)$$

where
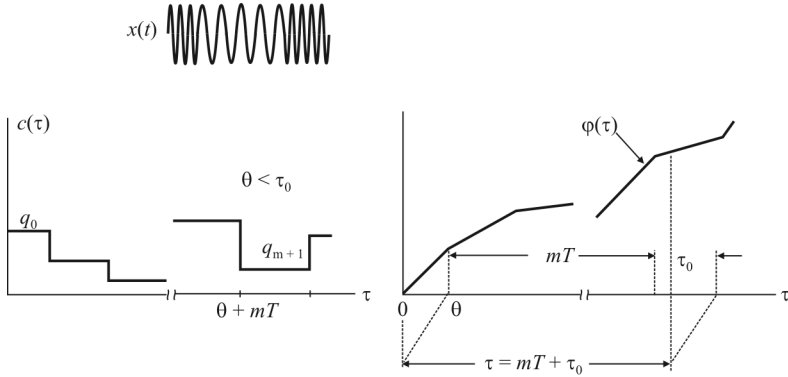
**Figure 2.37** Continuous phase FSK.

$$\mathbf{b}(t) = \sum_{n=-\infty}^{\infty} \mathbf{q}_n h(t - nT) \tag{2.84}$$

$h(t)$ is an arbitrary function, and $\mathbf{q}_n$ is a stationary discrete-time process with autocorrelation

$$R_m = \mathcal{E}\{\mathbf{q}_{n+m}, \mathbf{q}_n\}$$

We assume the random variables $\mathbf{q}_n$ are independent and we denote their characteristic function by $\Phi(u)$:

$$\Phi(u) = \mathcal{E}\{e^{ju\mathbf{q}_n}\} \tag{2.85}$$

As we see from (2.75), to determine the spectrum of the process $\mathbf{x}(t)$, it suffices to find the mean

$$\mathcal{E}\{\mathbf{w}(t)\} = \mathcal{E}\{\mathcal{E}\{\mathbf{w}(t)|\boldsymbol{\theta}\}\} = \frac{1}{T}\int_0^T \mathcal{E}\{\mathbf{w}(t)|\boldsymbol{\theta}\}d\theta \tag{2.86}$$

of $\mathbf{w}(t)$.

In the following we consider some special cases. For convenience we write the variable $\tau$ in the form

$$\tau = mT + \tau_0 \qquad 0 \le \tau_0 < T \qquad m : \text{integer}$$

and we assume that $\tau > 0$.

*Continuous-Phase FSK.* Suppose that $h(t)$ is a rectangular pulse of duration $T$ as in Figure 2.37. In this case

$$\mathbf{b}(t) = \mathbf{q}_n \qquad \text{for } (n-1)T < t < nT$$

hence, the phase

$$\varphi(t) = \int_0^t \mathbf{c}(\alpha)d\alpha = \int_0^t \mathbf{b}(\alpha - \theta)d\alpha$$

is continuous and consists of line segments with slope $\mathbf{q}_n$. Furthermore, if $\tau > T$, then

$$\varphi(\tau) = \begin{cases} \theta\mathbf{q}_0 + (\tau_0 - \theta)\mathbf{q}_{m+1} + \sum_{k=1}^m T\mathbf{q}_k, & \theta < \tau_0 \\ \theta\mathbf{q}_0 + (T + \tau_0 - \theta)\mathbf{q}_m + \sum_{k=1}^{m-1} T\mathbf{q}_k, & \theta > \tau_0 \end{cases}$$

and if $0 \le \tau \le T$

$$\varphi(\tau) = \begin{cases} \theta\mathbf{q}_0 + (\tau - \theta)\mathbf{q}_1, & \theta < \tau \\ \tau\mathbf{q}_0, & \theta > \tau \end{cases}$$

Thus we have:

If $\tau > T$, then

$$\mathcal{E}\{\mathbf{w}(\tau|\theta)\} = \begin{cases} \Phi(\theta)\Phi^m(T)\Phi(\tau_0 - \theta), & \theta < \tau_0 \\ \Phi(\theta)\Phi^{m-1}(T)\Phi(T + \tau_0 - \theta), & \theta > \tau_0 \end{cases}$$

where $\Phi(\theta)$ is given by (2.85).

if $0 \le \tau < T$, then

$$\mathcal{E}\{\mathbf{w}(\tau|\theta)\} = \begin{cases} \Phi(\theta)\Phi(\tau - \theta), & \theta < \tau \\ \Phi(\tau), & \theta > \tau \end{cases}$$
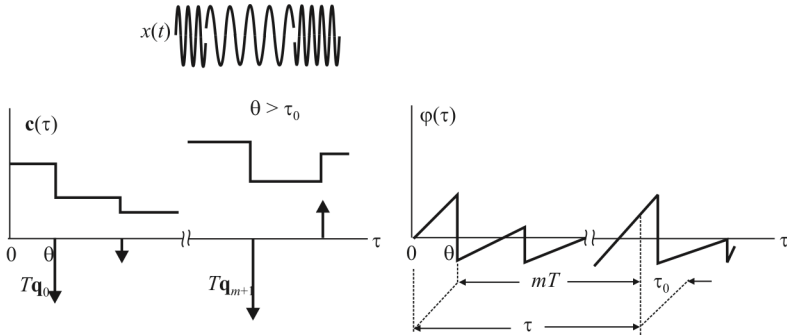
**Figure 2.38** Discontinuous phase FSK.

Inserting these results into (2.86), we obtain

$$
\mathcal{E}\{\mathbf{w}(\tau)\} =
\begin{cases}
\dfrac{1}{T}\Phi^m(T)\displaystyle\int_0^{\tau_0}\Phi(\theta)\Phi(\tau_0-\theta)d\theta \\[2ex]
\qquad +\dfrac{1}{T}\Phi^{m-1}(\tau)\displaystyle\int_{\tau_0}^{\tau}\Phi(\theta)\Phi(T-\tau_0-\theta)d\theta, & \tau > T \\[3ex]
\dfrac{1}{T}\displaystyle\int_0^{\tau}\Phi(\theta)\Phi(\tau-\theta)d\theta+\dfrac{T-\tau}{T}\Phi(\tau), & \tau < T
\end{cases}
$$

*Discontinuous-Phase FSK.* If $\varphi(t)$ consists again of line segments but is discontinuous at the points $t = nT + \theta$ with jumps equal to $T\mathbf{q}_n$, then $\mathbf{c}(t)$ contains impulses at these points. As we see from Figure 2.38

$$
\varphi(\tau) =
\begin{cases}
-(T-\theta)\mathbf{q}_0+(\tau_0-\theta)\mathbf{q}_{m+1}, & \theta < \tau_0 \\[1.5ex]
-(T-\theta)\mathbf{q}_0+(T+\tau_0-\theta)\mathbf{q}_m, & \theta > \tau_0
\end{cases}
$$

Hence, as in the previous case,

$$
\mathcal{E}\{\mathbf{w}(\tau)\} =
\begin{cases}
\dfrac{1}{T}\displaystyle\int_0^{\tau_0}\Phi(\theta-T)\Phi(\tau_0-\theta)d\theta+\dfrac{1}{T}\displaystyle\int_{\tau_0}^{T}\Phi(\theta-T)\Phi(T+\tau_0-\theta)d\theta, & \tau > T \\[3ex]
\dfrac{1}{T}\displaystyle\int_0^{\tau}\Phi(\theta-T)\Phi(\tau-\theta)d\theta+\dfrac{T-\tau}{T}\Phi(\tau), & \tau < T
\end{cases}
$$
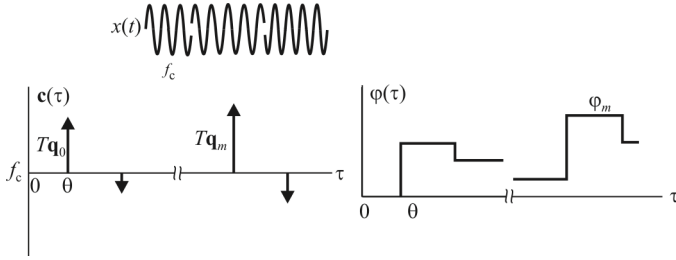
**Figure 2.39** DPSK.

This model would apply, for example, with modern SFH BFSK communication systems.

*Differential Phase-Shift Keying.* Suppose that $\boldsymbol{\varphi}(t)$ is a staircase function (DPSK) as in Figure 2.39, where

$$\boldsymbol{\varphi}(\tau) = \begin{cases} \displaystyle\sum_{k=0}^{m} T\mathbf{q}_k = \boldsymbol{\varphi}_m, & \theta < \tau_0 \\ 0, & \theta > \tau_0 = \tau \\ \displaystyle\sum_{k=0}^{m-1} T\mathbf{q}_k = \boldsymbol{\varphi}_{m-1}, & \theta > \tau_0 \neq \tau \end{cases}$$

Hence [see Figure 2.40(a)]

$$\mathcal{E}\{\mathbf{w}(\tau)\} = \Phi^{m+1}(T) + \Phi^m(T)\left(1 - \frac{\tau_0}{T}\right)$$

*Phase-Shift Keying.* In the above, $\mathbf{q}_n$ is a sequence of independent random variables, but the random variables $\boldsymbol{\varphi}_n$ are not independent. If the sequence $\boldsymbol{\varphi}_n$ is specified directly and consists of independent random variables with characteristic function

$$\Phi(u) = \mathcal{E}\{e^{ju\varphi_n}\}$$

then

$$\mathcal{E}\{e^{j\varphi(\tau)} | \theta\} = \begin{cases} 1, & \tau < \theta \\ \Phi(1), & \tau > \theta \end{cases}$$
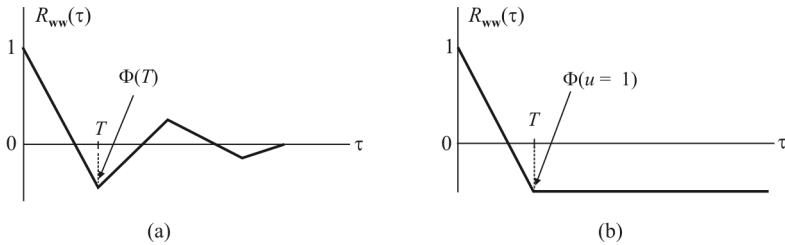
**Figure 2.40** (a) Correlation of DPSK and (b) correlation of PSK.

Hence

$$\mathcal{E}\{\mathbf{w}(\tau)\} = \begin{cases} \boldsymbol{\Phi}(1)\dfrac{\tau}{T} + \left(1 - \dfrac{\tau}{T}\right), & \tau < T \\[2ex] \boldsymbol{\Phi}(1), & \tau > T \end{cases}$$

as in Figure 2.40(b).

### 2.6.3 Summary

In this section we have provided some basic characteristics of random modulations. Their features are fundamentally different from deterministic modulating signals, and calculation of their properties follows different paths from their deterministic counterparts. We showed some of the features of specific random modulation types.

## 2.7 Access Methods

Access refers to the method whereby a communication system utilizes the communication media, in the sense of sharing the media with other systems. We cover the basic forms of access in this section.

A single-duplex system allows transmission and reception in one direction at a time. A full-duplex system allows simultaneous transmission and reception in both directions. In wireless systems, multiple-access techniques allow parallel transmissions in both directions.

Multiple-access methods are based on one or more of four domains:

- Spatial
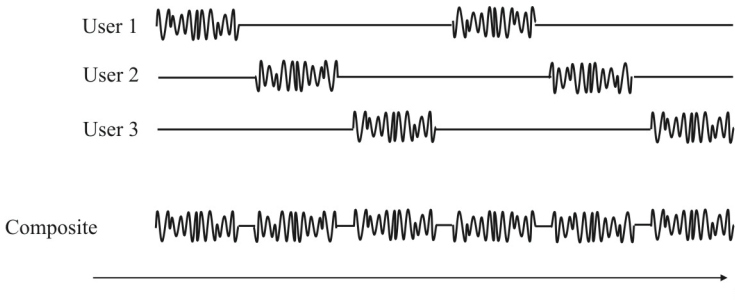
**Figure 2.41** User time slots for TDMA and the resulting composite time waveform.

- Frequency
- Time
- Code

In time division multiple access, different signals are multiplexed in non-overlapping time slots and are differentiated by their time slots at the receiver. This is known as *time division multiple access* (TDMA). Signals can also occupy separate frequency bands and transmit at the same time; that is, *frequency division multiple access* (FDMA). Antenna arrays can focus beams in one direction over others; that is known as *spatial division multiple access* (SDMA). Finally, in the code domain, signals can have little cross-correlation even though they might be transmitted at the same time and within the same frequency channel. Correlators are used to separate the uniquely coded signals. The access scheme is known as *code division multiple access* (CDMA).

## 2.7.1 TDMA

In TDMA the available radio spectrum is divided into time slots. Users can either transmit or receive in the time slots allocated to them. Time slots for $N$ number of users are collected into a periodic frame, with $N$ time slots per frame. Because TDMA data is transmitted in bursts, transmissions for a given user are not continuous. Temporal synchronization between a TDMA transmitter and receiver using time gating permits reception of a specific user's time-slot data, essentially turning the receiver on and off at the appropriate times. Figure 2.41 shows an example three-user TDMA system. The composite signal indicates that the channel is in use for the complete length of time (with short time guard bands between transmissions).

TDMA is often combined with *time division duplex* (TDD) or *frequency division duplex* (FDD). With TDD, a portion (half?) of the frame's time slots is used for transmission and the remaining portion (half?) is used for reception. With
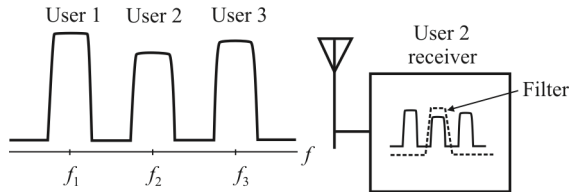
**Figure 2.42** Frequency channels for FDMA.

FDD, different carrier frequencies are used for TDMA transmission and reception, even though similar time slots may be used for both functions.

TDMA systems using FDD usually add several time slots of delay to separate a particular user's transmission and reception time slots and to synchronize transmitters and receivers. The guard time between transmissions can be designed as small as the system's synchronization permits. (Guard times of 30 to 50 msec between time slots are common in practical TDMA systems.) All units must be synchronized to a common reference to within a fraction of the guard time.

Narrowband TDMA is used in the Global System for Mobile Communications (GSM). The IS-136 TDMA standard employs 30 kHz FDMA channels subdivided into three time slots (six time slots for ½ rate) with one time slot required for each call made.

Efficiency in a TDMA system is measured by the percentage of transmitted data containing information versus overhead. The frame efficiency is the percentage of bits per frame that contain transmitted data. The transmitted data may contain source and channel coding bits, so that the end-user efficiency of the system is usually less than the frame efficiency.

## 2.7.2 FDMA

FDMA systems divide the frequency spectrum into narrow bandwidth channels where each user is assigned a specific frequency or frequencies for transmission and reception. The receiver demodulates information from the desired channel and rejects other signals nearby, usually by employing appropriate filters. Figure 2.42 shows three users of an allocated frequency band where the receiver for User 2 is shown. The channel, $f_2$, is demodulated while rejecting channels $f_1$ and $f_3$ with a filter.

## 2.7.3 CDMA

CDMA systems employ DSSS, which uses orthogonal or uncorrelated *pseudorandom-noise* (PN) codes to differentiate signals that overlap in both frequency and time; FHSS, in which signals are randomly hopped with PN codes
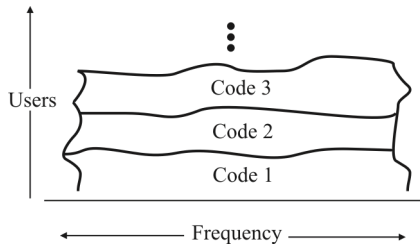
**Figure 2.43** CDMA spectrum.

about different portions of an available spectrum; or THSS, in which the time of transmitting a bit of information is randomly changed according to the PN code.

In DSSS CDMA, a narrowband message signal is multiplied by a very large-bandwidth PN spreading signal with a chip rate that is orders of magnitude larger than the data rate of the message signal. (The chip period is the inverse of the spreading rate.) A large spreading rate produces a broadband RF spectrum and can minimize the effects of multipath distortion, such as channel signal fading. Each user has a unique pseudorandom code. Due to the orthogonality of the codes, all other codes appear as noise to a given user. A matched filter extracts a specific user's signal, with little or no output signals resulting from other users. With knowledge of the proper code for that user, a CDMA receiver can effectively extract a user's signals from a channel with multiple signals at the same relative amplitude level. The spectrum of CDMA spread spectrum is illustrated in Figure 2.43.

For a cellular CDMA system to work effectively, the power levels of mobile units seen by the base-station receiver must be approximately equal. CDMA achieves this leveling using dynamic power control techniques. The total power of multiple users at a receiver determines a CDMA system's noise floor after decorrelation. Unless the power of each user within a cell is controlled so that it is approximately equal at the base-station receiver, the strongest received mobile signal can dominate the base-station's demodulator. Furthermore, the mobile units cannot necessarily hear one another, so coordination among mobile units is not feasible.

Signals rising above the level of the other signals increase the noise level at the base-station receiver. Higher-level signals decrease the probability that a desired signal will be received and decorrelated properly. As a result, CDMA systems employ power control at each base station to control the signal level of the transmitter at each mobile unit, making them all received approximately equally. In this way, a mobile unit close to the base station will not overpower the base station for a user much farther away.

Power control is implemented by rapidly sampling the *received signal strength indicator* (RSSI) level from each mobile unit and then sending a power

change command over the forward radio link to each unit. Unfortunately, out-of-cell mobile units can still provide interference for the base station since their transmitter power is not controlled by that base station.

On the uplink (from a mobile unit to the base station), power control must be accurate to within 1 dB and fast enough to compensate for channel fading (which can be on the order of milliseconds). Given a vehicle traveling at 55 mph, the Doppler bandwidth or rate is about 100 Hz (the channel changes characteristics 100 times each second). This requires power-control bits of about 10 b/Hz or about 1 kbps of control data. The power-control data must accommodate a dynamic range of about 80 dB.

CDMA enjoys a soft capacity limit; that is, an increase in the number of subscribers raises the noise floor in a linear manner. As a result, the number of users in a CDMA system is not absolutely limited. The system performance gradually degrades as the number of users increases and improves as the number of users decreases. As mentioned, large spreading rates can negate the effects of multipath distortion. RAKE receivers, where several receivers are used for the same signal, are often used in CDMA systems to improve reception by collecting several time-delayed versions of the desired signal.

Self-jamming can be a problem in a CDMA system because the spreading sequences of different users are not of infinite length and therefore are not exactly orthogonal, causing despreading for a particular PN code. In addition, power control can be difficult to implement when undesired subscribers (such as from adjacent cells) are not rejected, and their signal levels add to the system's total noise floor. PCS systems that employ CDMA, for example, update the power emitted by the mobile units at kilohertz rates in order to minimize interference.

CDMA cellular or PCS system capacity is determined by a number of factors, including the processing gain, the effective *bit energy-to-noise ratio* ($E_b/N_0$), frequency reuse, and the number of sectors in a cell. Because many subscribers operate within the same CDMA channels, frequency reuse efficiency is increased by improving the SNR.

## 2.7.4 SDMA

Multiple antennas in an array are combined so the region around an antenna is divided into focused beams in SDMA (Figure 2.44). Figure 2.45 illustrates this focusing in two dimensions (looking down from the top of the antenna array). The region around the base station is thus divided into segments. SDMA allows several users to simultaneously use the same frequency band and time slots with minimum interference with one another. The base station antennas are effectively "pointed" toward the mobile units.
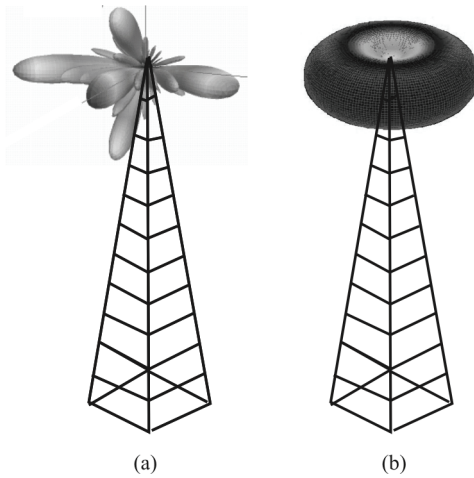
**Figure 2.44** Depiction of antenna patterns. Antennas implementing SDMA are shown in (a) while (b) shows omnidirectional coverage from the same antenna system.
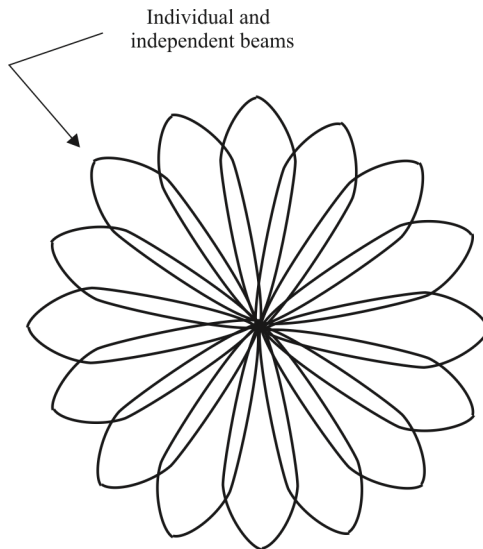


**Figure 2.45** In the horizontal plane, the (ideal) focused beams in SDMA would look like this figure shows.
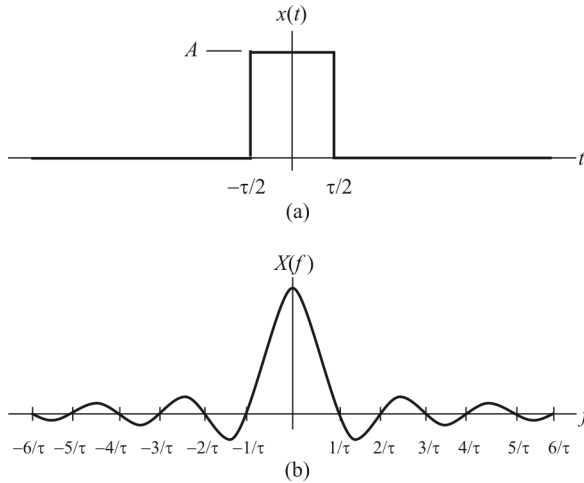
**Figure 2.46** (a) Single rectangular pulse and (b) its Fourier transform.

# 2.8 Pulse-Shaping Filters

In modern data transmission systems, bits or groups of bits (symbols) are typically transmitted in the form of individual pulses of energy. A rectangular pulse, as illustrated in Figure 2.46(a), is the most fundamental. The Fourier transform of the pulse yields its spectral characteristics, which is shown in Figure 2.46(b). Note that a pulse of width $\tau$ has the bulk of its energy contained in the main lobe, which spans a one-sided bandwidth of $1/\tau$ Hz. This would imply that the frequency span of a data transmission channel must be at least $2/\tau$ Hz wide.

Figure 2.46 shows that a pulse of a given width, $\tau$, spans a bandwidth that is inversely related to $\tau$. If a data rate of $1/\tau$ bps is chosen, then each bit occupies one pulse width (namely, $\tau$ seconds). If we wish to send bits at a faster rate, then the value of $\tau$ must be made smaller. Unfortunately, this forces the bandwidth to increase proportionally [see Figure 2.46(b)].

Such data-rate/bandwidth relationships pose a problem for bandlimited systems. This is mainly because most transmission systems have band limitations imposed by either the natural bandwidth of the transmission medium (copper wire, coaxial cable, optical fiber) or by governmental or regulatory conditions. Thus, the principal challenge in data transmission systems is to obtain the highest possible data rate in the bandwidth allotted with the least number of errors.

It is important to recognize that pulses are sent by the transmitter and ultimately detected by the receiver in any data transmission system. At the receiver, the goal is to sample the received signal at an optimal point in the pulse interval to maximize the probability of an accurate binary decision. This implies

that the fundamental shapes of the pulses be such that the interference between pulses (ISI) is minimized at the optimal sampling point.

There are two criteria that ensure noninterference:

- Criterion one is that the pulse shape exhibits a zero crossing at the sampling point of all pulse intervals except its own. Otherwise, the ISI caused by other pulses will introduce errors into the decisions made.
- Criterion two is that the shape of the pulses be such that the amplitude decays rapidly outside of the pulse interval.

This is important because any real system contains timing jitter, and the actual sampling point of the receiver will not always be optimal for every pulse. So, even if the pulse shape provides a zero crossing at the optimal sampling point of other pulse intervals, timing jitter in the receiver could cause the sampling instant to move, thereby missing the zero crossing point. This, too, introduces error into the decision-making process. Thus, the quicker a pulse decays outside of its pulse interval, the less likely it is to allow timing jitter to introduce ISI when sampling adjacent pulses. In addition to the noninterference criteria, there is the ever-present need to limit the pulse bandwidth.

## 2.8.1 Rectangular Pulse

The rectangular pulse, by definition, meets criterion number one because it is zero at all points outside of the present pulse interval. It clearly cannot cause interference during the sampling time of other pulses. The trouble with the rectangular pulse, however, as we see in Figure 2.46(b), is that it has significant energy over a fairly large bandwidth. In fact, because the spectrum of the pulse is given by the familiar $\sin(\pi x)/\pi x$ (sinc) response, its bandwidth actually extends to infinity. The unbounded frequency response of the rectangular pulse renders it unsuitable for modern transmission systems. This is where pulse shaping filters come into play.

## 2.8.2 Shaped Pulses

There are two popular forms of filters used for pulse shaping: the Gaussian filter and the raised cosine filter. We will present their predominant characteristics in this section.

### 2.8.2.1 Gaussian Filters

The Gaussian filter is the filter type that results in the most gradual passband roll-off and the lowest group delay (Figure 2.47). They are frequently used with FSK modulations and, in particular, MSK. The step response of the Gaussian filter
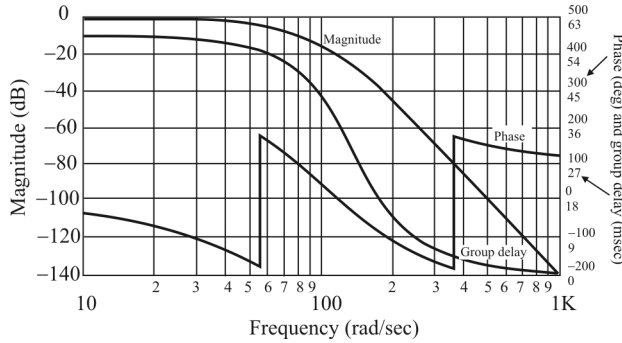
**Figure 2.47** Seventh-order lowpass Gaussian filter spectrum with 100 Hz cutoff.

never overshoots the steady-state value (see Figure 2.48). As the name implies, the Gaussian filter is derived from the same basic equations used to derive the Gaussian distribution. The most significant characteristic of the Gaussian filter is that the step response contains no overshoot at all.

The impulse response of the 1D Gaussian filter is given by:

$$h(x) = \frac{1}{\sqrt{2\pi}\sigma} e^{-\frac{x^2}{2\sigma^2}} \tag{2.87}$$

The Fourier transform of the impulse response is itself a Gaussian function given by

$$H(f) = e^{-\frac{f^2}{2\sigma_f^2}} \tag{2.88}$$
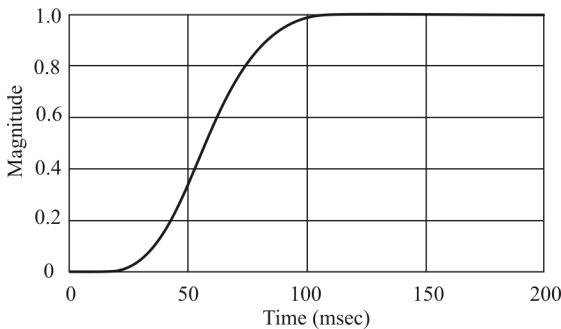


**Figure 2.48** Gaussian filter step response. Seventh order lowpass, 100 Hz cutoff.

We can see that the width of the spectrum increases as σ increases. Furthermore, the two standard deviations [σ (sec) and $\sigma_f$ (Hz)] are inversely related:

$$\sigma\sigma_f = \frac{1}{2\pi} \tag{2.89}$$

so the bandwidth of the filter is inversely related to σ.

2.8.2.2 Raised Cosine Filter

Another effective filtering technique is raised cosine filtering. The ideal raised cosine filter frequency response consists of unity gain at low frequencies, a raised cosine function in the middle, and total attenuation at high frequencies. The width of the middle frequencies is defined by the roll-off factor constant α, $(0 \le \alpha \le 1)$. The passband frequency is usually defined as the 50% signal attenuation point. The group delay must remain constant at least out to 15 to 20dB of attenuation.

Setting the passband frequency of a raised cosine filter to half the data rate, then Nyquist's first criterion is satisfied in that the impulse response is zero for $T = NT_s$, where $N$ is an integer and $T_s$ is the data period. The higher the order of the filter, the greater the raised cosine approximation. High-order raised cosine filters also produce longer time delays. The lower alpha values use less bandwidth, but they also produce more ISI due to element value errors and design imperfections.

When τ is the pulse width of the digital data, the frequency response of the raised cosine pulse is given by

$$P(f) = \begin{cases} \tau, & 0 \le f < \dfrac{\pi(1-\alpha)}{2\pi\tau} \\[2mm] \dfrac{\tau}{2}\left\{1 - \sin\left[\left(\dfrac{\tau}{2\alpha}\right)\left(2\pi f - \dfrac{\pi}{\tau}\right)\right]\right\}, & \dfrac{\pi(1-\alpha)}{2\pi\tau} \le f \le \dfrac{\pi(1+\alpha)}{2\pi\tau} \\[2mm] 0, & f > \dfrac{\pi(1+\alpha)}{2\pi\tau} \end{cases} \tag{2.90}$$

The ideal raised cosine filter frequency response is shown in Figure 2.49.

The ideal impulse response of the raised cosine filter is given by the inverse FT of (2.90):
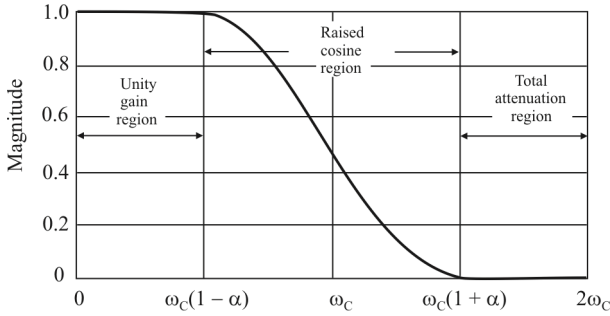
**Figure 2.49** Raised cosine frequency response. $\alpha = 0.5$.

$$p(t) = \frac{\left(\mathrm{sinc}\,\dfrac{t}{\tau}\right)\left(\cos\dfrac{\alpha\pi t}{\tau}\right)}{1 - \left(\dfrac{2\alpha t}{\tau}\right)^2} \tag{2.91}$$

The ideal cosine filter impulse response is shown in Figure 2.50.

Unlike the rectangular pulse, the raised cosine pulse takes on the shape of a sinc pulse, as indicated by the leftmost term of $p(t)$. The name "raised cosine" refers to the pulse's frequency spectrum, $P(\omega)$, not to its time domain shape, $p(t)$. The precise shape of the raised cosine spectrum is determined by the parameter $\alpha$.

Specifically, $\alpha$ governs the bandwidth occupied by the pulse and the rate at which the tails of the pulse decay. A value of $\alpha = 0$ offers the narrowest bandwidth but the slowest rate of decay in the time domain. When $\alpha = 1$, the bandwidth is $1/\tau$, but the time domain tails decay rapidly. It is interesting to note that the $\alpha = 1$ case offers a double-sided bandwidth of $2/\tau$. This exactly matches the bandwidth of the main lobe of a rectangular pulse, but with the added benefit of rapidly decaying
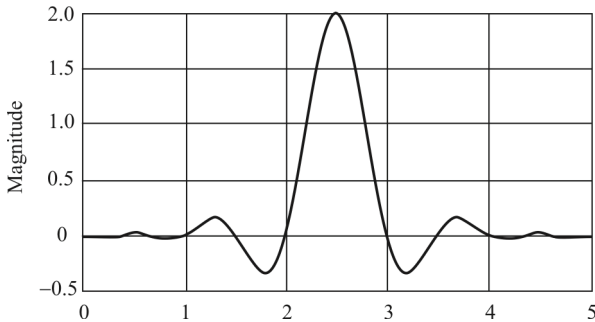


**Figure 2.50** Raised cosine impulse response.
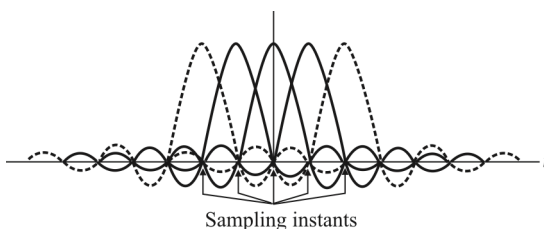
**Figure 2.51** Interaction of raised cosine pulses when the time between pulses coincides with the data rate.

time-domain tails. Conversely, when $\alpha = 0$, the bandwidth is reduced to $1/\tau$, implying a factor-of-two increase in data rate for the same bandwidth occupied by a rectangular pulse. However, this comes at the cost of a much slower rate of decay in the tails of the pulse. Thus, the parameter $\alpha$ provides a tradeoff between increased data rate and time-domain tail suppression. The latter is of prime importance for systems with relatively high timing jitter at the receiver.

Figure 2.51 shows how a train of raised cosine pulses interacts when the time between pulses coincides with the data rate. Note how the zero crossings are coincident with the pulse centers (the sampling point) as desired.

We should point out that the raised cosine pulse is not a cure-all. Its application is restricted to energy pulses that are real and even (i.e., symmetric about $t = 0$). A different form of pulse shaping is required for pulses that are not real and even. However, regardless of the necessary pulse shape, once it is expressible in either the time or frequency domain, the process of designing a pulse-shaping filter remains the same.

A variant of the raised cosine pulse is often used in modern systems—the root-raised cosine response. The frequency response is expressed simply as the square root of $P(\omega)$ [and square root of $p(t)$ in the time domain]. This shape is used when it is desirable to share the pulse-shaping load between the transmitter and receiver.

# 2.9 Concluding Remarks

The important properties of signals and modulation systems were introduced in this chapter. Complex signals were considered including the Hilbert transform. I/Q mixing was discussed for implementation of complex mixing. Real mixing was introduced as well. The impacts of sampling on the signal spectra were considered. The notion of system and its mathematical representations were discussed.

Deterministic modern modulations were introduced and their properties discussed. The properties of random modulation are fundamentally different from their deterministic counterparts, and we discussed these properties.

Techniques to access propagating media were then introduced, consisting of FDMA, TDMA, CDMA, and SDMA. The last of these is the newest of the access methods and is widely used in modern cellular phone systems.

Last we discussed the properties of pulse shaping filters and how they can be employed to improve spectral efficiency.

## References

[1]     Oksendal, B., *Stochastic Differential Equations*, Oslo: Springer, 2005.
[2]     Lynch, W. A., and J. G. Truxal, *Introductory System Analysis*, New York: McGraw-Hill, 1961.
[3]     Cooper, G. R., and C. D. McGillem, *Methods of Signal and System Analysis*, New York: Holt, Rinehardt, and Winston, 1967.
[4]     Gagliardi, R. M., *Introduction to Communications Engineering*, New York: Wiley, 1988.
[5]     Abramowitz, M., and I. A. Stegun, *Handbook of Mathematical Functions*, New York: Dover, 1972, Chapter 9.
[6]     Poisel, R. A., *Modern Communications Jamming Principles and Techniques,* 2nd Ed., Norwood, MA: Artech House, 2011.
[7]     Poisel, R. A., *Modern Communications Jamming Principles and Techniques,* 2nd Ed., Norwood, MA: Artech House, 2011, Fig. 2.15.
[8]     Poisel, R. A., *Information Warfare and Electronic Warfare Systems,* Norwood, MA: Artech House, 2013, Chapter 9.
[9]     Papoulis, A., *Probability, Random Variables, and Stochastic Processes,* New York: McGraw-Hill, 1965.
[10]    Gardner, W. A., *Introduction to Random Processes*, New York: Macmillan, 1986.
[11]    Papoulis, A., "Random Modulation: A Review," *IEEE Transactions on Acoustics, Speech, and Signal Processing,* Vol. ASSP-31, No. 1, February 1983, pp. 96–105.
[12]    Woodward, P. M., "The Spectrum of Random Frequency Modulation," Telecommunications Research Establishment, Great Malvern, Worcester, England, Memo 666, December 1962.
[13]    Blachman, N. M., and G. A. McAlphine, "The Spectrum of a High-Index FM Waveform: Woodward's Theorem Revisited," *IEEE Transactions on Communication Technology,* Vol. COM-17, No. 4, April 1969.

# Chapter 3

## RF Stage

### 3.1 Introduction

The ultimate performance of a receiver is largely determined by the first stages or front end. At the front end the signal levels are at their lowest and even very small amounts of noise can be comparable in size with the incoming signal. At later stages in the receiver the signal will have been amplified and will be much larger. The same levels of noise as are present at the front end will be much smaller in proportion to the signal and will not have the same effect. Accordingly it is important that the performance of the front end is optimized for its noise performance.

Figure 3.1 displays the typical power levels involved in EW receiver performance investigations. Typical input power levels are −130dBm, and the noise levels can be quite high. The SNR determines the ultimate performance so low signal levels or high noise levels are quite detrimental to performance.

For our purposes, the RF stage is defined collectively as those elements after the antenna and before the first mixer stage. This would typically include preselection filters, a *low noise amplifier* (LNA), and image rejection filters.

Receiver sensitivity is one of the vital specifications of any receiver. The key factor in determining the sensitivity performance of the whole receiver is the RF amplifier. By optimizing its performance, the figures for the whole of the receiver can be improved. In this way the specifications for SNR, *signal-to-interference-and-distortion ratio* (SINAD), or NF can be brought to the required level.

Noise is a limiting factor for sensitive reception. In communication receivers, noise, along with many external factors, including intermodulation, reciprocal mixing, and spurious response, may disturb the sensitive reception of the desired signal. Thus, much consideration for the noise and other factors that disturb the signal reception and their analysis is required to keep the SNR of the received signal above a desired level for the reconstruction of the signal.

Power    −174 dBm    −130 dBm    −80 dBm                                                    +10 dBm

         $4{\times}10^{-21}$ W    $10^{-16}$ W    $10^{-11}$ W                              $10^{-2}$ W

Volts
(RMS)    0.6 nV    0.1 μV    32 μV                                                          1 V
in 50Ω

         Thermal noise    MDS for         MDS for                                          Strong local
         of resistor in   good comm       cell phone                                       signal at input
         1 Hz BW          receiver in                                                      of receiver
                          3 kHz BW
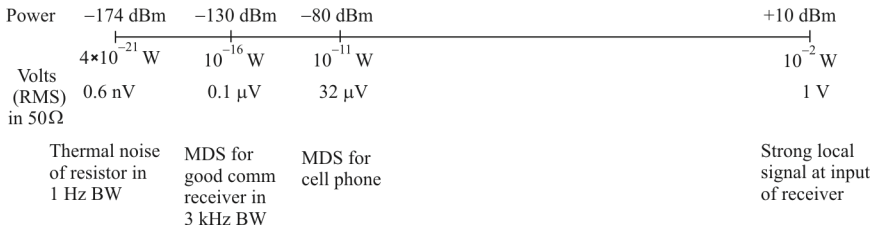
**Figure 3.1** EW receiver input power range.

In this chapter, as elsewhere, we follow the convention that capitalized margin parameters are in units of dB whereas uncapitalized margin parameters refer to their numerical values.

We begin this chapter with a discussion on noise and its sources in receiver applications. The noise figure is introduced next. In-depth discussions on low noise amplifiers follow that, as this element is critical in receiver applications. A technique for lowering the noise levels is presented next that involves using transformers at the input to the low noise amplifier. The chapter concludes with discussions of filtering at the front end to reduce the levels of interfering signals.

# 3.2 Normalized Input Referred Added Noise

The noise characteristics of a receiver are usually expressed in terms of an equivalent input noise power. Figure 3.2 shows how a noisy system may be represented by a noiseless system and an equivalent input referred noise source.

Denoting SNR by $\gamma$, a system's noise factor is given by

$$f = \frac{S_{in}/N_{in}}{S_{out}/N_{out}} = \frac{\gamma_{in}}{\gamma_{out}} \tag{3.1}$$

(we discuss noise factor extensively shortly). To understand the relation between a system's noise factor and the added noise by the system at the output, consider the system in Figure 3.3, with a gain $G$ and a noise factor $f$. When the signal with power $S_{in}$ and the noise with power $N_{0,in}$ are applied at the input, the output signal power will be $S_o$ and the output noise power will be $N_o$, where

$$S_o = GS_{in} \tag{3.2}$$
$$N_o = GN_{0,in} + N_a \tag{3.3}$$

where $N_a$ is the noise added by the system. The noise factor $f$ is
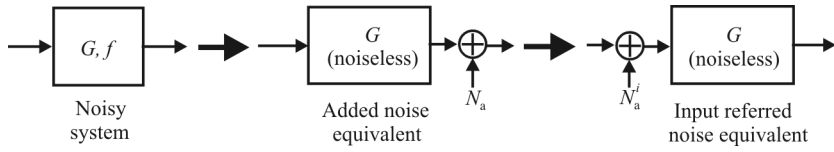
**Figure 3.2** Input referred noise equivalent of a system.
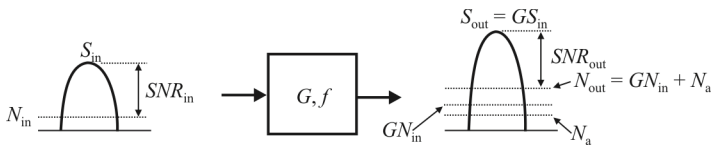


**Figure 3.3** Signals in a noisy system with gain $G$ and noise factor $f$.

$$f = \frac{\gamma_{in}}{\gamma_{out}} = \frac{S_{in}/N_{0,in}}{GS_{in}/(GN_{0,in}+N_a)} = 1 + \frac{N_a}{GN_{0,in}} \qquad (3.4)$$

The system NF, denoted by $F$, is $f$ expressed in decibels, viz,

$$F = 10\log_{10} f \qquad (3.5)$$

With the noise factor $f$, the added noise $N_a$ is represented as

$$N_a = GN_{0,in}(f-1) \qquad (3.6)$$

From (3.6), the input referred added noise $N_a^i$ is given by

$$N_a^i = \frac{N_a}{G} = N_{0,in}(f-1) \qquad (3.7)$$

By dividing both sides of (3.7) by $N_{0,in}$ and defining a new parameter, the normalized input referred added noise, $n_a^i$, we obtain

$$n_a^i = \frac{N_a^i}{N_{0,in}} = f-1 \qquad (3.8)$$

For lossy systems like filters characterized by loss $L$, the system's gain is $1/L$ and the noise factor is $L$. Thus the added noise $N_a$ for a lossy system may be represented as

$$N_a = \frac{1}{L} N_{0,in}(L-1) = \left(1-\frac{1}{L}\right)N_{0,in} \qquad (3.9)$$

Equation (3.8) can be adapted for passive systems with some modifications. In passive systems, the loss $L$ and the noise factor $f$ have the same value. Thus, the input referred added noise $N_a^i$ and the normalized input referred added noise $n_a^i$ are, respectively,

$$N_a^i = \frac{N_a}{1/L} = N_{0,in}(L-1) \qquad (3.10)$$

$$n_a^i = \frac{N_a^i}{N_{0,\text{in}}} = L - 1 \qquad (3.11)$$

To consider additive noise, several SNR degrading factors (excluding NF), such as intermodulation products, reciprocal mixing products, and spurious responses, must be included. These factors cannot be distinguished from the desired signal when they occur in the desired signal band, and they are independent from one another. Thus, in a general sense, they can be treated as noise.

## 3.3 Noise Factor/Figure

For any two-port network, amplifiers included, the NF gives a measure of the amount of noise added to a signal transmitted through the network. For any practical circuit, the SNR at its output will be worse (smaller) than at its input. Normally, the noise contribution of each two-port network can be minimized through a judicious choice of operating point and source resistance. For any two-port network there exists an optimum NF.

The noise factor of an active device, over the bandwidth of interest, represents the contribution by the device itself to thermal noise at its output. Typical noise figures range from 0.5 dB for very low noise devices, to 4 to 8 dB or higher. In some systems,—for example, heterodyne systems—total output noise power includes noise from other than thermal sources, such as spurious contributions from image-frequency transformation, but noise from these sources is not considered in determining the NF. The NF is determined only with respect to that noise that appears in the output via the principal frequency transformation of the system and excludes noise that appears via the image frequency transformation.

In (3.1), the input noise power $N_{\text{in}}$ is the available noise power at the conjugate matched input impedance, at an ambient temperature of 290 K. Typically the input impedance of the receiver for wireless communication is 50Ω with negligible reactance. With the assumption of negligible reactance, the input noise power $N_{\text{in}}$ may be written as

$$N_{\text{in}} = k_B TW - 174 + 10\log_{10} W_N \qquad \text{dBm} \qquad (3.12)$$

where

$k_B$ is Boltzmann's constant $= 1.38 \times 10^{-23}$ J/K
$T$ is the absolute temperature (K)
$W_N$ is the noise bandwidth (Hz)
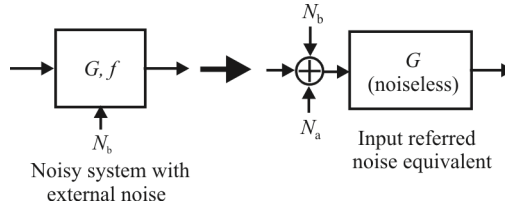
**Figure 3.4** Input referred noise equivalent for a system with two noise sources.

To distinguish this fundamental input thermal noise from others, it will have the notation $N_{0,in}$.

When considering more than two SNR degrading factors, the input referred noise equivalent model with multiple noise sources must be used. Figure 3.4 shows the input referred equivalent of a system with two different noise sources. $\gamma_{out}$ of this system is

$$\gamma_{out} = \frac{S_{out}}{N_{out}} = \frac{GS_{in}}{GN_{0,in} + N_a + N_b} \tag{3.13}$$

Since $\gamma_{in}$ is $S_{in}/N_{in,0}$,

$$\frac{\gamma_{in}}{\gamma_{out}} = 1 + \frac{N_a^i}{N_{0,in}} + \frac{N_b^i}{N_{0,in}} = 1 + n_a^i + n_b^i \tag{3.14}$$

Equation (3.14) represents the SNR degradation in the system by two noise sources. When there are $M$ noise sources, (3.14) becomes

$$\frac{\gamma_{in}}{\gamma_{out}} = 1 + n_{a1}^i + n_{a2}^i + \cdots + n_{aM}^i \tag{3.15}$$

Naturally, one of the noise sources is the thermal noise, which is characterized by a noise factor. If each noise source can be identified and the allowable SNR degradation is known, the receiver's performance using this receiver noise equation can be easily determined.

Using (3.4), $f$ of a cascaded system can be easily derived. Let the gain and noise factor of each stage be $G_1, f_1$, and $G_2, f_2$ (Figure 3.5). At the output of the first stage, the signal and noise powers are:

$$S_1 = G_1 S_{in} \tag{3.16}$$

$$N_1 = G_1 N_{in,0} + N_{a1} = G_1 N_{in,0} + G_1 N_{0,in}(f_1 - 1) = G_1 f_1 N_{0,in} \tag{3.17}$$
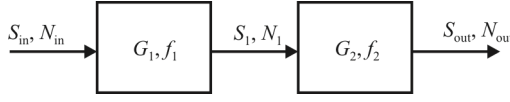
**Figure 3.5** Cascaded noisy system.

and at the output of the second stage

$$S_{\text{out}} = G_2 S_1 = G_1 G_2 S_{\text{in}} \tag{3.18}$$

$$N_{\text{out}} = G_2 N_{a1} + N_{a2} = G_1 G_2 f_1 N_{0,\text{in}} + G_2 N_{0,\text{in}} (f_2 - 1) \tag{3.19}$$

$$= G_1 G_2 \left( f_1 + \frac{f_2 - 1}{G_1} \right) N_{0,\text{in}} \tag{3.20}$$

Thus, the noise factor of the cascaded system is

$$f_{\text{total}} = \frac{S_{\text{in}} / N_{\text{in}}}{S_{\text{out}} / N_{\text{out}}} = f_1 + \frac{f_2 - 1}{G_1} \tag{3.21}$$

Extending (3.21) to an *M*-stage system, the well-known Friis' equation ensues. The Friis' equation is used to calculate the overall noise factor of a receiver, which is in turn composed of a number of stages, each with its own noise factor and gain. It is given by

$$f = f_1 + \frac{f_2 - 1}{G_1} + \frac{f_3 - 1}{G_1 G_2} + \cdots + \frac{f_i - 1}{G_1 G_2 \cdots G_{i-1}} + \cdots + \frac{f_M - 1}{G_1 G_2 \cdots G_{M-1}} \tag{3.22}$$

where $f_i$ and $G_i$ are the noise factor and gain, respectively, of the $i^{\text{th}}$ stage.

In the case of a receiver with the first stage being an LNA,

$$f = \frac{1}{G_{\text{LNA}}} (f_{\text{rest}} - 1) + f_{\text{LNA}} \tag{3.23}$$

where $f_{\text{rest}}$ is the overall noise factor of the subsequent stages. According to (3.23), the LNA can reduce the overall noise figure of the receiver but only if the gain is sufficiently high.

The sensitivity is expressed in terms of the noise figure as

$$\text{Sensitivity} = \underbrace{\text{Noise floor (dBm)}}_{-174\text{dBm}+10\log W_{\text{N}}} + \gamma_{\text{req}} + F_{\text{tot}} \quad \text{dBm} \tag{3.24}$$
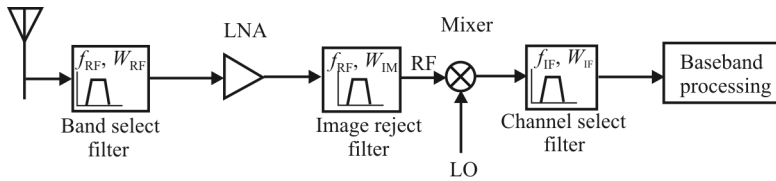
**Figure 3.6** Simplified block diagram of superhet receiver.

$\gamma_{req}$ is the SNR required to adequately process the modulated signal being considered (typically 10–15 dB for analog signals while the acceptable BER is used to establish adequate levels for digital signals, e.g., 20 dB for a $10^{-3}$ BER for BPSK).

# 3.4 Low Noise Amplifiers

### 3.4.1 Introduction

The design of the front end of EW systems is critical to their performance. It is at this stage that the fundamental detection performance is established, at least the portion that can be controlled (i.e., not external noise limited). Losses early in the RF chain increase the system NF. It is therefore desirable to minimize these losses as much as possible. Consequently, as soon in the receiving chain as possible an LNA is included so that the effects on the NF of these losses as well as the effects of noise generated in subsequent stages is minimized.

LNAs are used at the input stage of virtually every communication receiver to include those in communication EW systems. The NF of the first stage determines, to a large extent, the sensitivity of the receiver. At lower frequencies, say below 100 MHz, the external noise is the dominant source of noise. Above 100 MHz or so, however, the internal noise sources dominate, with the first one or two receiving stages being the most important.

We provide a discussion of architectures in this section for typical *bipolar junction transistor* (BJT) and *metal-oxide-semiconductor field-effect-transistor* (MOSFET) LNAs. Both are used in practice for LNA implementations. There are, of course, many more devices that can be, and are, used for LNAs, each with its own noise models. This, however, is not intended to be a thorough treatise on devices and their noise characteristics. For those interested in a more thorough treatment of noise models, [1] is a good source.

A superheterodyne receiver is illustrated in Figure 3.6 showing the typical placement of an LNA. The principal function of the LNA is to provide enough gain to overcome the noise of subsequent stages (the mixer in particular) while adding as little noise itself as possible. Also, it should accommodate large signals
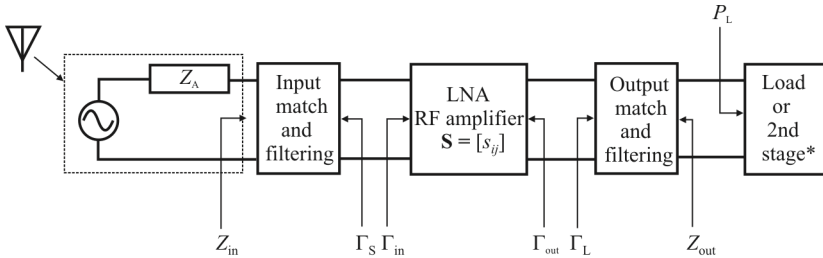
* Frequently a mixer stage

**Figure 3.7** Receiver front end. Preselection and image reject filtering are included in the input and output filtering, respectively.

without distortion and must present a specific and constant input impedance (such as 50Ω or 75Ω) to terminate an unknown length of transmission line, which delivers the signal from the antenna to the amplifier. A good input impedance match is more critical if a preselect filter precedes the LNA since the transfer characteristics of many filters are sensitive to the quality of the termination. The additional requirement is the low power consumption that is especially important for man-portable EW systems. Achieving high gain and low noise while being limited in power consumption is difficult. Both linearity specifications and input impedance matching to maximize the power transfer from the antenna are also required.

LNAs have historically been difficult to integrate because they require high $Q$ inductors and high $f_T$ transistors. In addition, to avoid oscillations, the parasitic couplings must be minimized.

For an amplifier to have a minimum NF the bias point and source resistance that produce the minimum NF for that device must be determined. With due considerations for gain and stability, the source impedance can be matched to look like that optimum value.

An LNA used at the input to a receiving system is depicted in Figure 3.7, that is, it is normally placed at the immediate output of the antenna (possibly with some preceding band-select filtering). Typical LNA characteristics are:

- Gain (10–20 dB typical)
  - To amplify the received signal
  - To reduce the input referred noise of the subsequent stages
- Good linearity
  - To handle large undesired signals with as little distortion as possible
- Low noise
  - For high sensitivity
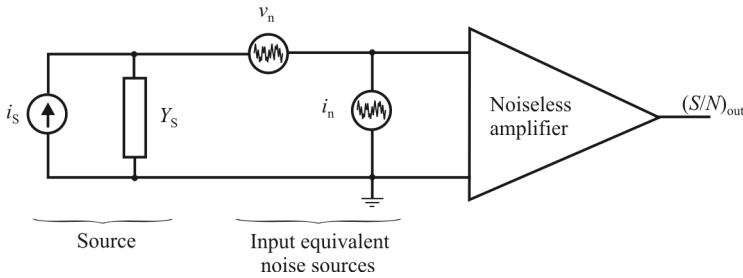
Figure 3.8 LNA model with the noise sources reflected to the input leaving a noiseless amplifier.

- Input matching
    - For maximum power gain
    - Preceding filters require 50Ω termination for proper operation
    - Can route the LNA to the antenna, which is located an unknown distance away, without worrying about the length of the transmission line

### 3.4.2 Minimum Noise Factor

As indicated, the noise factor of the first stage, $f_1$, dominates the overall noise performance if $G_1$ is sufficiently high. We will see that normally the maximum gain and minimum noise cannot be obtained at the same time. Noise performance is controlled by $\Gamma_S$, so the LNA topology usually winds up being a compromise between gain and noise [2].

An LNA with the noise reflected to the input is shown in Figure 3.8. We will determine the optimum source admittance $Y_S$ that when presented to the input of the amplifier leads to the minimum degradation of the SNR. The total output noise power is proportional to $\overline{i_{sc}^2}$, the mean-square input port short circuit current. The noise factor can be expressed as

$$f = \frac{\overline{i_{sc}^2}}{\overline{i_S^2}} = \frac{\text{noise power due to source and amp}}{\text{noise power of source alone}}$$

Now

$$i_{sc} = -i_S + i_n + v_n Y_S$$

$$\overline{i_{sc}^2} = \overline{i_S^2} + \overline{\left(i_n + v_n Y_S\right)^2} - 2\underbrace{\overline{i_S\left(i_n v_n Y_S\right)}}_{\substack{=0 \text{ since } \overline{i_S} \text{ is not} \\ \text{correlated with } \overline{i_n} \text{ or } \overline{v_n}}}$$

so

$$f = 1 + \frac{\overline{(i_n + v_n Y_S)^2}}{\overline{i_S^2}} \tag{3.25}$$

where

$\overline{i_S^2} = 4kT_0 G_S W_N$   $G_S$ is the source conductance

$\overline{v_n^2} = 4kT_0 R_N W_N$   $R_N$ is a fictitious equivalent noise resistance that represents $\overline{v_n^2}$

$i_n$ can be represented by a correlated (with $v_n$) and uncorrelated part as

$i_n = i_{nu} + i_{nc}$

where

$i_{nc} = Y_c v_n$         $Y_c$ is a fictitious correlation admittance

$i_{nu} = 4kT_0 G_u W_N$   $G_u$ is a fictitious equivalent noise conductance

Our goal is to minimize $f$. These equations with (3.25) lead to

$$f = f_{min} + \frac{R_N}{G_S} \left[ (G_S - G_{opt})^2 + (B_S - B_{opt})^2 \right] \tag{3.26}$$

where

$$Y_S = G_S + jB_S$$
$$Y_{opt} = G_{opt} + jB_{opt}$$

and

$f_{min}$ is the lowest possible noise factor
$Y_{opt}$ is the optimum source admittance for minimum noise

Manipulating (3.26) we get

$$f_a = f_{a,min} + \frac{R_N}{G_S} \left| Y_S - Y_{opt} \right|^2 \tag{3.27}$$

Normalizing everything to $Z_0$ leads to

$$f = f_{min} + \frac{r_N}{g_S}\left|y_S - y_{opt}\right|^2 \qquad (3.28)$$

Using reflection coefficients given by

$$y_S = \frac{1-\Gamma_S}{1+\Gamma_S} \qquad y_o = \frac{1-\Gamma_{opt}}{1+\Gamma_{opt}}$$

we get

$$f = f_{min} + \frac{4r_N\left|\Gamma_S - \Gamma_{opt}\right|^2}{\left(1-\left|\Gamma_S\right|^2\right)\left(1+\Gamma_{opt}\right)^2} \qquad (3.29)$$

$f_{min}$, $r_N$, and $\Gamma_{opt}$ are noise parameters of the device.

Thus we see that there is a minimum noise factor possible for a device, $f_{min}$, that is achieved only when a particular reflection coefficient, $\Gamma_{opt}$, is presented to the input. So, $\Gamma_S = \Gamma_{opt}$ leads to the minimum NF for the amplifier.

### 3.4.3 LNA Gain

In terms of the *s*-parameters, the LNA is characterized by the following scattering matrix

$$\mathbf{S} = \begin{bmatrix} s_{11} & s_{12} \\ s_{21} & s_{22} \end{bmatrix} \qquad (3.30)$$

Referring to Figure 3.7, the source reflection coefficient is given by $\Gamma_S$, and the load reflection coefficient is given by $\Gamma_L$. Then the amplifier input reflection coefficient is given by [3]

$$\Gamma_{in} = s_{11} + \frac{s_{12}s_{21}\Gamma_L}{1-s_{22}\Gamma_L} \qquad (3.31)$$

The amplifier output reflection coefficient is given by [4]

$$\Gamma_{\text{out}} = s_{22} + \frac{s_{12}s_{21}\Gamma_S}{1 - s_{11}\Gamma_S} \tag{3.32}$$

The gain specifies the small signal amplification capability of an LNA. For IC implementation, the LNA input is interfaced off-chip and usually matched to a specific impedance ($50\Omega$ or $75\Omega$ typically). Its output is not necessarily matched if the amplifier directly drives an on-chip block such as a mixer. This is characterized by voltage gain or transducer power gain by knowing the load impedance level. The transducer power gain is the power delivered to the load divided by the power available from the source, that is, for a unilateral device (so that $s_{12} = 0$)

$$G_T = \frac{1 - |\Gamma_S|^2}{|1 - s_{11}\Gamma_S|^2} |s_{21}|^2 \frac{1 - |\Gamma_L|^2}{|1 - s_{22}\Gamma_L|^2} \tag{3.33}$$

### 3.4.4 BJT LNA

The hybrid $\pi$ noise model of the BJT amplifier shown in Figure 3.9(a) is shown in Figure 3.9(b). We exclude feedback elements $R_\mu$ and $C_\mu$ from consideration so the model is limited to frequencies less than $f_T / \sqrt{\beta_0}$. Typical hybrid-$\pi$ model values for a small-signal, high-frequency transistor are:

$$
\begin{aligned}
r_\pi &= 100\,\text{k}\Omega & r_o &= 1.6\,\text{M}\Omega \\
r_x &= 300\,\Omega & r_\mu &= 15\,\text{M}\Omega \\
g_m &= 0.004\,S & C_\mu &= 5\,\text{pF} \\
\beta_0 &= 350 & C_\pi &= 25\,\text{pF}
\end{aligned}
$$

at $I_C = 0.1\,\text{mA}$ and $V_{CE} = 5\,\text{V}$.

The thermal noise of the base spreading resistance, $r_x$, of the BJT is represented by the $v_x$ noise generator while the shot noise of the base current, a characteristic of the BJT, is represented by the noise current generator $i_{nb}$. $i_{nc}$ represents the shot noise of the collector current. Typical noise characteristics of these noise sources are shown in Figure 3.10. The noise sources are

$$\overline{v_x^2} = 4k_B T r_x \tag{3.34}$$

$$\overline{i_{nb}^2} = 2qI_B \tag{3.35}$$

(a)



(b)
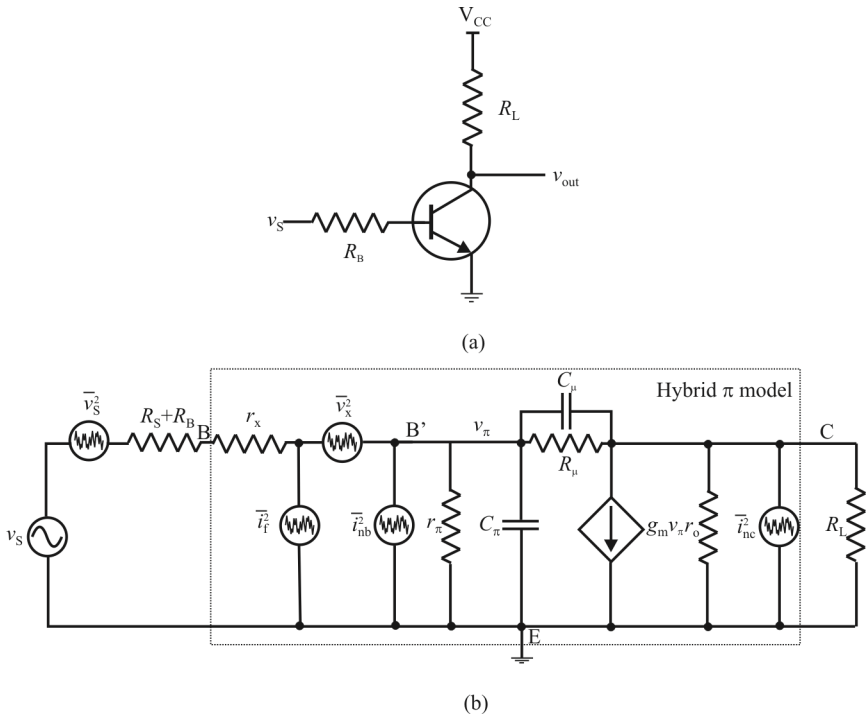
**Figure 3.9** BJT amplifier: (a) amplifier circuit and (b) noise equivalent using hybrid-$\pi$ model for the BJT.
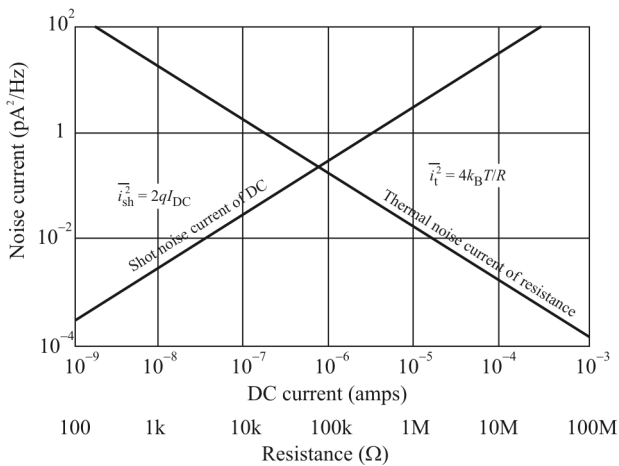


**Figure 3.10** Shot noise characteristics of a BJT.

$$\overline{i_{nc}^2} = 2qI_C \tag{3.36}$$

where $T$ is the ambient temperature, $r_x$ is the base spreading resistance, $q$ is the electron charge $(1.6\times10^{-19}\text{C})$, $I_B$ is the DC bias current in the base, and $I_C$ is the DC bias current at the collector. The thermal noise of the source resistance is

$$\overline{v_S^2} = 4k_B T R_S \tag{3.37}$$

Flicker ($1/f$) noise is represented by the generator labeled $\overline{i_f}^2$. The psd of this source is given by

$$i_f^2 = \frac{2qf_L I_B^\zeta}{f} \tag{3.38}$$

where $f_L$ is a representation of the noise corner frequency and is a constant depending on the device. $\zeta$ is a constant between 1 and 2 but most of the time is equal to 1. These constants are normally determined by measurement. The noise voltage associated with this current source is

$$\overline{v_f^2} = \frac{2qf_L I_B^\zeta r_x^2}{f} \tag{3.39}$$

3.4.4.1 Minimum Noise Factor

At room temperature, the minimum noise factor for the BJT LNA is given by [1]

$$f_{opt} = 1 + \sqrt{\frac{2r_x g_m}{\beta_0 r_e} + \frac{1}{\beta_0}} \tag{3.40}$$

Typical variation of the NF with the input matching resistance is depicted in Figure 3.11 [1]. The minimum is achieved when $R_S = R_{opt}$, with $R_{opt}$ the optimum source resistance. As $R_S$ deviates from the optimum value, the NF becomes substantially worse.

This optimum source resistance in terms of the BJT parameters is

$$R_{opt} = \sqrt{\frac{0.05\beta_0 r_x}{I_C} + \frac{(0.025)^2 \beta_0}{I_C^2}} \tag{3.41}$$
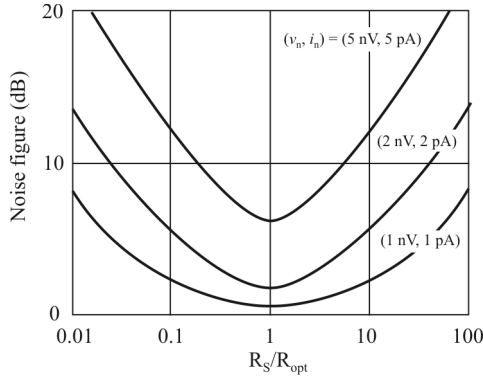
**Figure 3.11** BJT input resistance variation.

## 3.4.5 MOSFET LNA

The noise model of the MOS amplifier in Figure 3.12(a) is shown in Figure 3.12(b). The current gain of the amplifier is given by

$$i_{\mathrm{o}} = g_{\mathrm{m}} v_{\mathrm{gs}} = g_{\mathrm{m}} \frac{v_{\mathrm{S}}}{R_{\mathrm{S}} + R_{\mathrm{g}} + \dfrac{1}{j2\pi f C_{\mathrm{gs}}}}$$

$$= v_{\mathrm{S}} \frac{g_{\mathrm{m}}}{1 + j2\pi f C_{\mathrm{gs}}(R_{\mathrm{S}} + R_{\mathrm{g}})} \approx v_{\mathrm{S}} \frac{g_{\mathrm{m}}}{j2\pi f C_{\mathrm{gs}}(R_{\mathrm{S}} + R_{\mathrm{g}})} \qquad (3.42)$$

and

$$f_{\mathrm{T}} = \frac{1}{2\pi} \frac{g_{\mathrm{m}}}{C_{\mathrm{gs}}} \qquad (3.43)$$

Now

$$i_{\mathrm{o}} = G_{\mathrm{m}}(f) v_{\mathrm{S}} \qquad (3.44)$$

where

$$G_{\mathrm{m}}(f) = -j \frac{f_{\mathrm{T}}}{f} \frac{1}{R_{\mathrm{S}} + R_{\mathrm{g}}} \qquad (3.45)$$
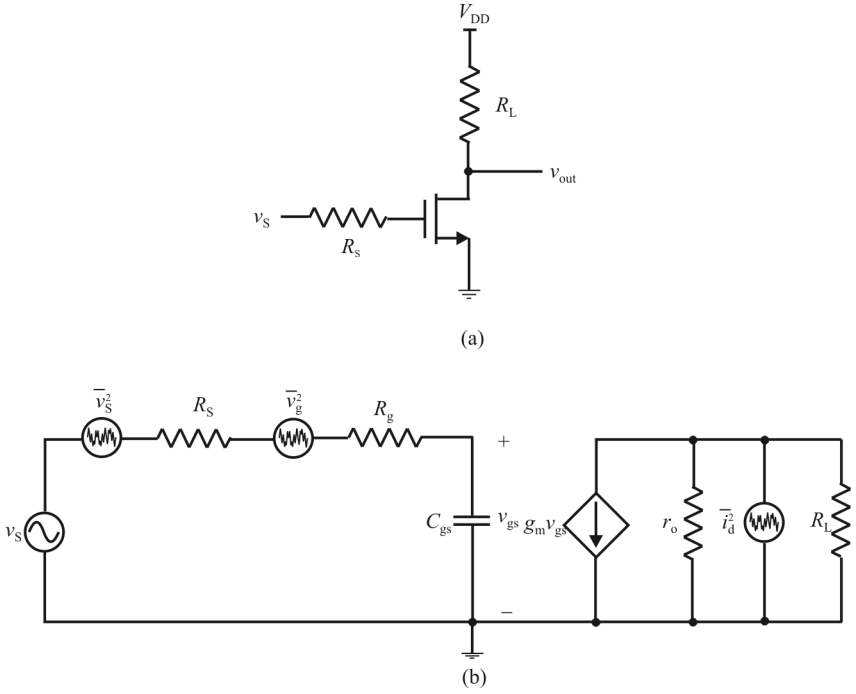
Figure 3.12 MOS amplifier: (a) amplifier circuit and (b) noise equivalent model.

The total output noise current is given by

$$\overline{i_{o,T}^2} = G_m^2 \left( \overline{v_S^2} + \overline{v_g^2} \right) + \overline{i_d^2} \tag{3.46}$$

and the noise factor can be computed as

$$f = \frac{\overline{i_{o,T}^2}}{\overline{i_o^2}} = \frac{\overline{i_{o,T}^2}}{G_m^2 \overline{v_S^2}} = 1 + \frac{\overline{v_g^2}}{\overline{v_S^2}} + \frac{\overline{i_d^2}}{G_m^2 \overline{v_S^2}} \tag{3.47}$$

where

$$\overline{v_g^2} = 4k_BTR_g, \qquad \overline{v_S^2} = 4k_BTR_S, \qquad \overline{i_d^2} = 4k_BT\frac{\zeta}{\alpha}g_m$$

Here $\alpha = g_m / g_{d0}$, where $g_{d0}$ is $g_{dS}$ evaluated at $V_{DS} = 0$, and $\zeta$ is unity in triode and 2/3 in saturation, at least in the long-channel limit.

The MOSFET LNA model has two sources arising from thermal fluctuations of channel charge. First, there is a drain noise current source:

$$\overline{i_{nd}^2} = 4k_B T \delta g_{d0} \Delta f \tag{3.48}$$

Some older references use $g_m$ but $g_{d0}$ is better related to channel charge in short-channel devices. Second, a gate noise current also flows from channel potential fluctuations coupled capacitively into the gate terminal:

$$\overline{i_{ng}^2} = 4k_B T \delta g_g \Delta f \tag{3.49}$$

where $\delta = 2\zeta$ in long devices, and

$$g_g = \frac{(2\pi f)^2 C_{gs}^2}{5 g_{d0}} \tag{3.50}$$

Substitution of the various noise sources into (3.47) leads to

$$f = 1 + \frac{R_g}{R_S} + \frac{\dfrac{\zeta}{\alpha} g_m}{R_S} \left(\frac{f}{f_T}\right)^2 (R_S + R_g)^2$$

$$\approx 1 + \frac{R_g}{R_S} + \frac{\zeta}{\alpha}\left(\frac{f}{f_T}\right)^2 g_m R_S \tag{3.51}$$

This expression contains both the channel noise and the gate-induced noise. A good approximation is

$$R_g = R_{poly} + \frac{1}{5 g_m}$$

A representative value of the gate and drain noise currents correlation coefficient, $c$, is $j0.395$ for long-channel devices. This would indicate that they are $90^\circ$ out of phase.
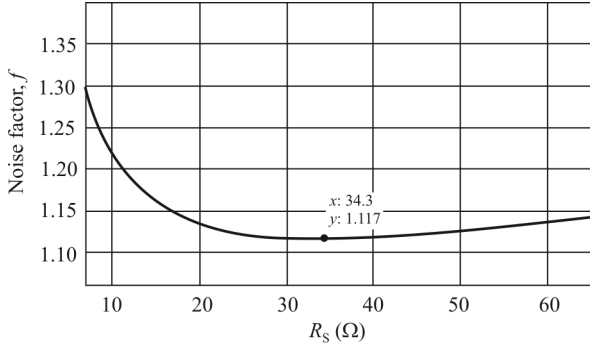
**Figure 3.13** Minimum noise factor, $f_{min}$.

## 3.4.5.1 Minimum Noise for MOS Amplifier

The optimal value of $R_S$ is found from (3.51) as

$$\frac{\partial f}{\partial R_S} = 0 = -\frac{R_g}{R_S^2} + \frac{\zeta}{\alpha} g_m \left(\frac{f}{f_T}\right)^2$$

so that

$$R_{S,opt} = \frac{f}{f_T} \sqrt{\frac{R_g}{\frac{\zeta}{\alpha} g_m}} \tag{3.52}$$

Using this value for $R_S$, the minimum noise factor is

$$f_{min} = 1 + 2\frac{f}{f_T} \sqrt{\frac{\zeta}{\alpha} g_m R_g} \tag{3.53}$$

**Example 3.1: MOSFET LNA 1.** A plot of (3.51) where the operating frequency is 3.2 GHz, $R_g = 2\Omega$, $\zeta = 3$, $\alpha = 0.75$, $f_T = 56$ GHz, and $g_m = 50$ mA/V is shown in Figure 3.13.

**Example 3.2: MOSFET LNA 2.** Assume $f_T = 75$ GHz, $f_{op} = 5$ GHz, $\zeta/\alpha = 2$, $R_{poly}$ is minimized by proper layout, and the intrinsic gate resistance is given by

$$R_{\mathrm{g}} = R_{\mathrm{poly}} + \frac{1}{5g_{\mathrm{m}}} \approx \frac{1}{5g_{\mathrm{m}}}$$

To make the noise contribution from this term equal to 0.1:

$$\frac{R_{\mathrm{g}}}{R_{\mathrm{S}}} = 0.1 \Rightarrow g_{\mathrm{m}} = \frac{10}{5R_{\mathrm{S}}} = 40\,\mathrm{mS} \Rightarrow R_{\mathrm{S,opt}} \approx 119\Omega, f_{\mathrm{min}} = 1.08$$

In practice, it is difficult to get such a low noise factor and get useful gain with the simple common source due to the bad power match. There is a conflict of the minimum noise and the optimum matching. This illustrates the need for input matching for the LNA.

### 3.4.6 Input Matching

Matching the antenna to the LNA is investigated in this section. We begin with an analysis from Weiner [5] that provides some insight as to why such matching is required in EW receiving systems by examining the effects of an arbitrary antenna/transmission line/LNA mismatch. We then discuss some common matching topologies.

3.4.6.1  Effects of Arbitrary Antenna Impedance Mismatch

In most cases the system noise factor of a receiving system whose antenna is impedance matched to the transmission line connecting the antenna to the receiver is limited by the receiver noise factor at frequencies above 100–300 MHz and by the antenna external noise factor at frequencies below this range [6, 7]. However, when there are large impedance mismatches, the noise factors of the transmission line [8] and receiver [9, 10] can be significantly increased. In such cases, the system noise factor can be limited by the transmission line or receiver noise factor. This case is of particular interest to VHF and HF receiving systems with electrically short antennas, a typical situation for tactical EW receiving systems.

As in any linear two-port network, the noise factor of the receiver increases with increasing difference of its source impedance from the design source impedance (usually 50Ω or 75Ω if fed by a transmission line with 50Ω or 75Ω characteristic impedances). As discussed previously, any noisy two-port network with internally generated noise can have the noise reflected to its input, with such noise represented by a complex noise current generator and a complex noise voltage generator in parallel and series, respectively, with the input to the noise-free two-port (Figure 3.14). Thus, a large impedance mismatch at the antenna/transmission line interface may cause the source impedance of the
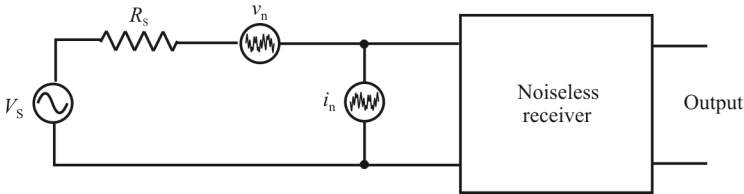
**Figure 3.14** Noise generators at the input to a noiseless receiver.

receiver to be substantially different from 50Ω or 75Ω and consequently may cause an appreciably increased noise factor of the receiver.

The system noise power $N$ referred to the output terminals of the equivalent lossless receiving antenna is the time-averaged power contributed by all noise sources, both internal and external to the receiving system, that would be delivered by the lossless antenna to a load if the load impedance were set equal to the conjugate output impedance of the lossless antenna. External noise sources are the atmosphere, stars, man-made noise (power lines, automobile ignition systems, etc.), and jammers both hostile and friendly. Internal noise sources are any passive component with a resistance and all active components such as the receiver, antenna matching network, and transmission line of the receiving system.

With reference to Figure 3.15, when all the operating temperatures are equal to the reference temperature, the system noise factor $f$ is given by

$$f = f_a - 1 - L_c L_m L_n f_r \qquad (3.54)$$

where $f_a$ is the receiving antenna external noise factor integrated over the antenna pattern function (numeric); $L_c$, $L_m$, $L_n$ are the loss factors of the receiving antenna, matching network, and transmission line, respectively (numeric), and $f_r$ is the receiver noise factor. In keeping with the transmission line literature, $\gamma_X = \alpha_X + j\beta_X$ in Figure 3.15 is the propagation constant of the transmission line.

The external noise that is incident on the receiving antenna within a differential solid angle $d\theta d\phi$ at an elevation angle $\theta$ and azimuthal angle $\phi$ (see Figure 3.15) must be integrated over the entire sphere of the gain pattern of the antenna, which is probably directional, to obtain the total external noise at the output terminals of the equivalent lossless antenna. All external noise sources in the field of the view or the antenna contribute to this noise. Accordingly, the external noise factor $f_a$ is given by

$$f_a = \int_0^{2\pi} \int_{-\pi/2}^{\pi/2} f_a(\phi,\theta) D_r(\phi,\theta) \sin\theta \, d\theta \, d\phi \qquad (3.55)$$
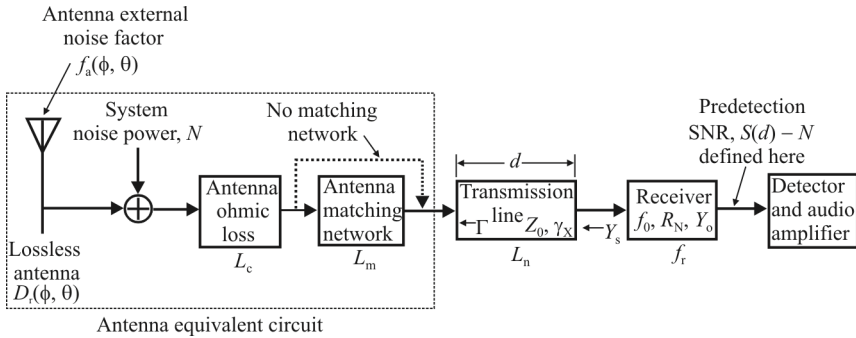
**Figure 3.15** EW receiving system.

where $D_r(\phi, \theta)$ is the receiver directive gain in the azimuth and elevation directions, $\phi$ and $\theta$, respectively (numeric) and $f_a(\phi, \theta)$ is the antenna noise factor in the azimuth and elevation directions $\phi$ and $\theta$, respectively. The factor $\sin\theta$ is included in the integrand because the integration is in spherical coordinates.

*Loss Factors*

The system loss factors $L_c$, $L_m$, $L_n$ of the antenna, matching network, and transmission line, respectively, are given by [8]

$$L_c = 1 + \frac{R_c}{R_a} \tag{3.56}$$

$$L_m = 1 + \frac{R_m + R_s}{R_a + R_c} \tag{3.57}$$

$$L_n = \frac{e^{2\alpha_X d}\left\{1 - |\Gamma|^2\, e^{-4\alpha_X d} - 2\dfrac{\mathrm{Im}\{Z_0\}}{\mathrm{Re}\{Z_0\}}\,\mathrm{Im}\left[\Gamma e^{-2\gamma_X d}\right]\right\}}{1 - |\Gamma|^2 - 2\dfrac{\mathrm{Im}\{Z_0\}}{\mathrm{Re}\{Z_0\}}\,\mathrm{Im}\{\Gamma\}} \tag{3.58}$$

where $R_a$, $R_c$, $R_m$, $R_s$, $Z_0$, $\gamma_X = \alpha_X + j\beta_X$, $d$, $\Gamma$, and $Z$ are circuit parameters defined in Figure 3.16 of the impedance equivalent circuit of the receiving system.
    The voltage reflection coefficient $\Gamma$ is given by

$$\Gamma = \frac{Z - Z_0}{Z + Z_0} \tag{3.59}$$
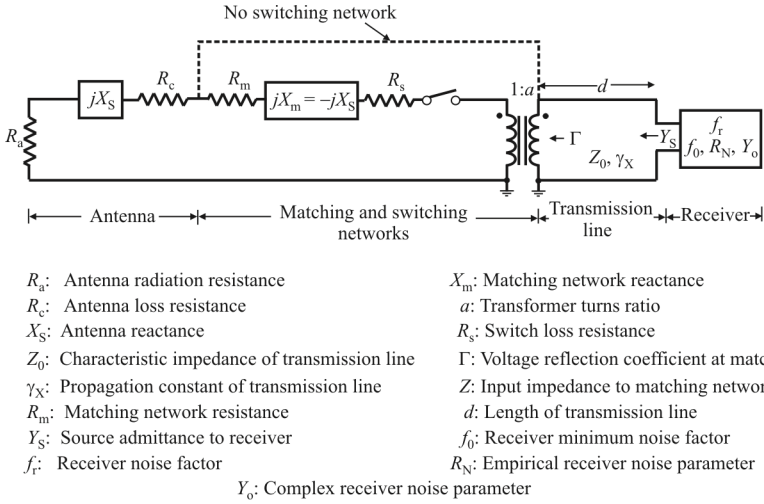
**Figure 3.16** EW receiving system impedance equivalent circuit.

$R_a$: Antenna radiation resistance

$R_c$: Antenna loss resistance

$X_S$: Antenna reactance

$Z_0$: Characteristic impedance of transmission line

$\gamma_X$: Propagation constant of transmission line

$R_m$: Matching network resistance

$Y_S$: Source admittance to receiver

$f_r$: Receiver noise factor

$X_m$: Matching network reactance

$a$: Transformer turns ratio

$R_s$: Switch loss resistance

$\Gamma$: Voltage reflection coefficient at matching network

$Z$: Input impedance to matching network

$d$: Length of transmission line

$f_0$: Receiver minimum noise factor

$R_N$: Empirical receiver noise parameter

$Y_0$: Complex receiver noise parameter

The input impedance $Z$ to the antenna, including the matching network, is given by

$$Z = a^2 \left[ R_a + R_c + R_m + R_s + j(X_a + X_m) \right]$$

$$= \begin{cases} Z_0, & \text{antenna conjugate matched to transmission line} \\ R_a + R_c + jX_a, & \text{no matching network} \end{cases} \quad (3.60)$$

When the antenna is conjugate impedance matched $(\Gamma = 0)$ to the transmission line by the matching network, then the matching network parameters $X_m$ and $a$ are given by

$$X_m = -X_a + \frac{1}{a^2} \operatorname{Im}\{Z_0\} \quad (3.61)$$

$$a = \sqrt{\frac{\operatorname{Re}\{Z_0\}}{R_a + R_c + R_m + R_S}} \quad (3.62)$$

In the absence of any matching network

$$X_m = X_m = R_S = 0 \quad (3.63)$$

$$a = 1 \tag{3.64}$$

*Receiver Noise Factor*

The receiver noise factor $f_r$ is a function of the source admittance $Y_S$ seen by the receiver looking back at the transmission line (see Figure 3.15) and consequently is a function of antenna input impedance. The receiver source admittance $Y_S$ is given by

$$Y_S = \frac{1}{Z_0} \frac{1 - \Gamma e^{-2\gamma_X d}}{1 + \Gamma e^{-2\gamma_X d}} \tag{3.65}$$

The receiver noise factor $f_r$, for an arbitrary source admittance $Y_S$ at an ambient temperature equal to the reference temperature, $T_{\text{ref}}$, is given by

$$f_r = f_{\min} + \frac{R_N}{\text{Re}\{Y_S\}} |Y_S - Y_o|^2 \tag{3.66}$$

where $f_{\min}$ is the minimum noise factor of the receiver. $Y_o = G_o + jB_o$ is the complex receiver noise parameter with the dimensions of admittance (ohms), and $R_N$ is the receiver noise parameter with the dimensions of resistance, which accounts for the sensitivity of the receiver noise factor-to-receiver source impedance (ohms).

The receiver noise factor $f_r$ has a minimum value of $f_{\min}$ for a source admittance $Y_S = Y_o$. Most well-designed receivers have a minimum noise factor $f_{\min}$ for a source admittance $Y_S = 1/Z_0$. For such a condition, the receiver input impedance is generally not matched to the characteristic impedance of the transmission line, and the receiver noise factor $f_r$ increases with increasing impedance mismatch of the antenna to the transmission line. For $|\Gamma| = 1$, $f_{\min} \leq f_r < \infty$, in particular for the case $|\Gamma| = 1$, the receiver noise factor is a minimum, whereas the transmission line noise factor is a maximum.

> **Example 3.3: VHF EW Receiving System.** The effect of antenna impedance mismatch on the operating noise figure of a radio receiving system is numerically evaluated for the case of a VHF EW receiver with an electrically short monopole antenna. For such a case, in the absence of a matching network, the real part of the antenna input impedance is typically on the order of $1\Omega$ or less, and the imaginary part is on the order of several hundred ohms or more. Therefore, the antenna presents a large

**Table 3.1** Noise Factors

| With or Without Matching Network | Frequency (MHz) | Man-Made Noise Location | Noise Factor | | | Loss Factors | | | Voltage Reflection Coefficient |
|---|---|---|---|---|---|---|---|---|---|
| | | | System $f$ | Antenna External $f_e$ | Receiver $f_r$ | Antenna Ohmic | Matching Network $l_m$ | Transmission Line $L_t$ | $\|\Gamma\|$ |
| Without | 30 | Business | 209,400 | 41,860 | 22.71 | 1.004 | 1.0 | 7,348 | |
| | | Residential | 176,600 | 9,106 | 22.71 | 1.004 | 1.0 | 7,348 | 0.9991 |
| | | Rural | 168,600 | 1,096 | 22.71 | 1.004 | 1.0 | 7,348 | |
| | 50 | Business | 42,990 | 20,560 | 13.81 | 1.002 | 1.0 | 1,257 | |
| | | Residential | 24,920 | 2,488 | 13.81 | 1.002 | 1.0 | 1,257 | 0.9986 |
| | | Rural | 22,600 | 1,720 | 13.81 | 1.002 | 1.0 | 1,257 | |
| | 88 | Business | 5,016 | 2,551 | 3.44 | 1.001 | 1.0 | 183 | |
| | | Residential | 2,831 | 366 | 3.44 | 1.001 | 1.0 | 183 | 0.9966 |
| | | Rural | 2,515 | 50 | 3.44 | 1.001 | 1.0 | 183 | |
| With | 30 | Business | 41,940 | 41,860 | 3.03 | 1.004 | 12.88 | 1.208 | |
| | | Residential | 9,184 | 9,106 | 3.03 | 1.004 | 12.88 | 1.208 | 0 |
| | | Rural | 1,174 | 1,096 | 3.03 | 1.004 | 12.88 | 1.208 | |
| | 50 | Business | 20,580 | 20,560 | 3.03 | 1.002 | 3.18 | 1.278 | |
| | | Residential | 2,507 | 2,488 | 3.03 | 1.002 | 3.18 | 1.278 | 0 |
| | | Rural | 1,915 | 1,720 | 3.03 | 1.002 | 3.18 | 1.278 | |
| | 88 | Business | 2,559 | 2,551 | 3.03 | 1.001 | 1.367 | 1.39 | |
| | | Residential | 375 | 366 | 3.03 | 1.001 | 1.367 | 1.39 | 0 |
| | | Rural | 58 | 50 | 3.03 | 1.001 | 1.367 | 1.39 | |

Antenna: 10" monopole, 1.4" diameter
Matching network: Coil, 0.5" diameter, single layer, 1.5" long
Switch: PIN diode, 0.25Ω
Transmission line: RG-58/U coaxial cable, 10 m long
Receiver: $f_0 = 5$, $R_N = 100Ω$
Source: [5].

impedance mismatch to a 50Ω or 75Ω transmission line. When matched, in the low VHF range (100–300 MHz and lower) the receiving system is generally limited by external environmental noise, which may be two or three orders of magnitude (20 to 30 dB) larger than the receiver noise [11].

We consider matching effects at 30, 50, and 88 MHz (low to high range for the tactical military frequency band) and man-made environmental noise in rural, residential, and business area locations. The antenna is a monopole of 10" length and 1.4" diameter, a matching network inductor with 1.5" length and 0.5" diameter, a PIN diode switch with 0.25Ω series resistance, a 10m length of RG-58/U coaxial transmission line, and a receiver with noise parameters of $f_{min} = 5$ and $r_n = 100Ω$.

The receiving system noise and loss factors are summarized in Table 3.1. The modulus $|\Gamma|$ of the voltage reflection coefficient, at the transmission line/antenna interface looking in the direction to the antenna, is $|\Gamma| = 0.9966 - 0.9991$ without a matching network and $|\Gamma| = 0$ with a matching network over the frequency range under consideration. In the presence of a

Antenna impedance: $0.26-j1,000\Omega$
Transmission line: RG-58/U
Receiver: $f_0 = 6$, $r_n = 100\Omega$
Frequency: 30MHZ

(a) Transmission line
(b) Receiver
(c) Transmission line and receiver
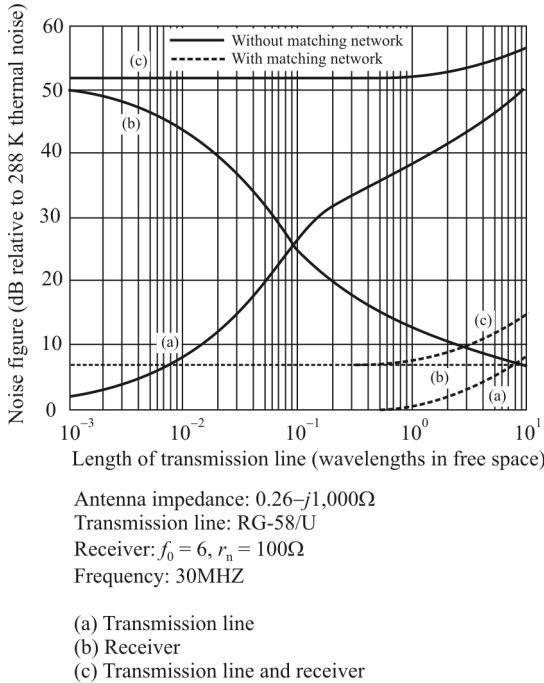
**Figure 3.17** Noise figures for Example 3.3.

matching network, the system noise factor $f$ is approximately equal to the antenna external noise factor $f_a$. However, in the absence of a matching network, the system noise factor is appreciably larger than the antenna external noise because $f_r L_n \gg f_a$.

For a large mismatch of the antenna impedance to the transmission line, the combined NF of the transmission line and receiver remains large regardless of line length (see Figure 3.17). Smaller line lengths result in smaller transmission line NF because of less ohmic loss, but a larger receiver NF because of less padding by the transmission line of the antenna impedance mismatch. When the antenna impedance is matched to the transmission line, the transmission line NF is limited to that resulting from the ordinary exponential attenuation loss of the transmission line. For arbitrary values of the receiver noise parameter $R_n$, there exists a line length for which the combined noise figure of the transmission line and receiver is minimized. In Figure 3.17, for $R_n = 100\Omega$, the combined NF is
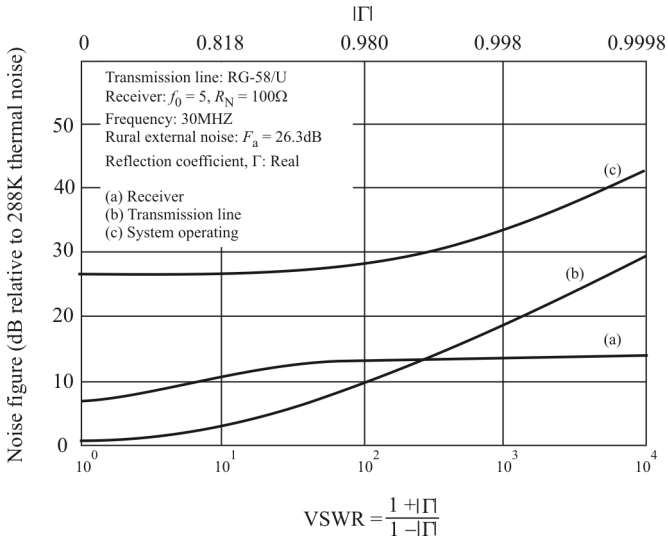
**Figure 3.18** Effects of the reflection coefficient on the noise figure.

approximately independent of line length for line lengths less than 0.1 wavelength.

*Summary*

We have shown that a significant impedance mismatch at the antenna/transmission line interface of a radio receiving system can cause a significant increase in the system internal noise figure (more than a 50 dB increase for a voltage reflection coefficient of 0.999). In the absence of a matching network, the limiting noise of a VHF EW receiving system is generated within the system (by the transmission line and receiver) and can be more than 20 dB larger than the external noise. With a matching network, the limiting noise of the system is external noise.

Antenna impedance mismatch significantly affects the transmission line NF and to a lesser extent the receiver NF when the voltage reflection coefficient $|\Gamma| \geq 0.5$ as illustrated in Figure 3.18 for $\text{Im}\{\Gamma\} = 0$ and a transmission line length of 10 m at 30 MHz.[1] However, for an antenna external NF of 26 dB, the system noise figure is not significantly affected by antenna impedance mismatch until the voltage reflection coefficient $|\Gamma| \geq 0.98$. Consequently, VHF and HF receiving

---

[1] The transmission line noise figure for $|\Gamma| = 0.9991$ is approximately 22 dB and 39 dB in Figures 3.18 and 3.17(a), respectively, because $\text{Im}\{\Gamma\} = 0$ in Figure 3.18 whereas $\text{Im}\{\Gamma\} = -j0.09965$ in Figure 3.17.

systems with electrically small antennas require some impedance matching, but only a modest amount.

3.4.6.2 LNA Input Matching Topologies

The input of a common source amplifier is primarily capacitive and provides very poor power match. Of course, maximum power transfer occurs when $Z_{in} = Z_S^*$ :

$$P_{in\_LNA\_max} = \frac{v_1^2}{|Z_{in}|} = \frac{v_S^2 |Z_{in}|}{|Z_{in} + Z_S|^2} = \frac{v_S^2}{2 \operatorname{Re}\{Z_S\}} = \frac{P_{in}}{2}$$

The very low noise requirement mandates the use of only one active device at the input of the LNA. Moreover, input matching and stability requirements limit acceptable LNA topologies to only a few. By observing MOSFET two-port four noise parameters, the source impedance that yields minimum noise factor is inductive in character and generally unrelated to the conditions that maximize power transfer. Moreover, since MOSFET input impedance is inherently capacitive, it is difficult to provide a good match to 50Ω source impedance without degrading the noise performance.

*Wideband LNA*

For wideband LNAs we consider three topologies that can be used for input matching: (1) resistive termination, (2) a common gate amplifier configuration, and (3) resistive shunt-feedback. We discuss each of these in this section.

*Resistive Termination*

We can terminate the input of a common source MOS amplifier with a resistor $R_m = R_S$ to match the input (at low frequencies anyway) since the input is primarily capacitive. A resistive termination at the amplifier input is illustrated in Figure 3.19. This configuration can be used in both narrowband and wideband applications, but its high NF (usually > 6 dB) characteristic limits its application.

The noise equivalent circuit for this LNA is illustrated in Figure 3.20. The output noise due to source resistance $R_S$ is

$$\overline{v_{n,S}^2} = k_B T R_S A_V^2 = k_B T R_S (g_{M1} R_D)^2$$

where $A_V \approx g_{M1} R_D$ and $R_D \ll Z_{out}$. The output noise due to the matching resistor $R_m = R_S$ is given by
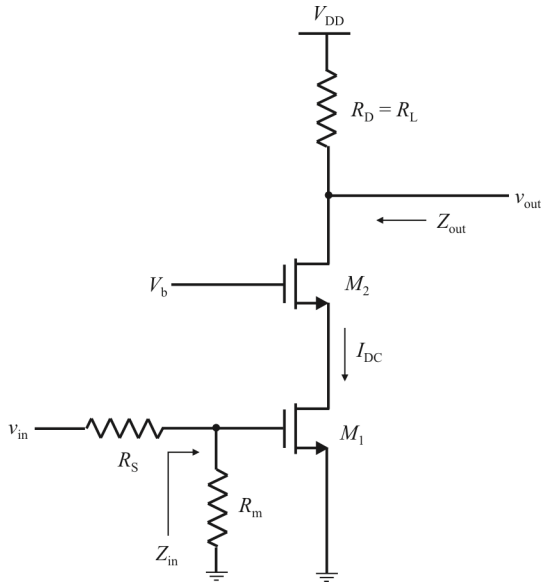
**Figure 3.19** Resistive termination at the input to an MOS amplifier.
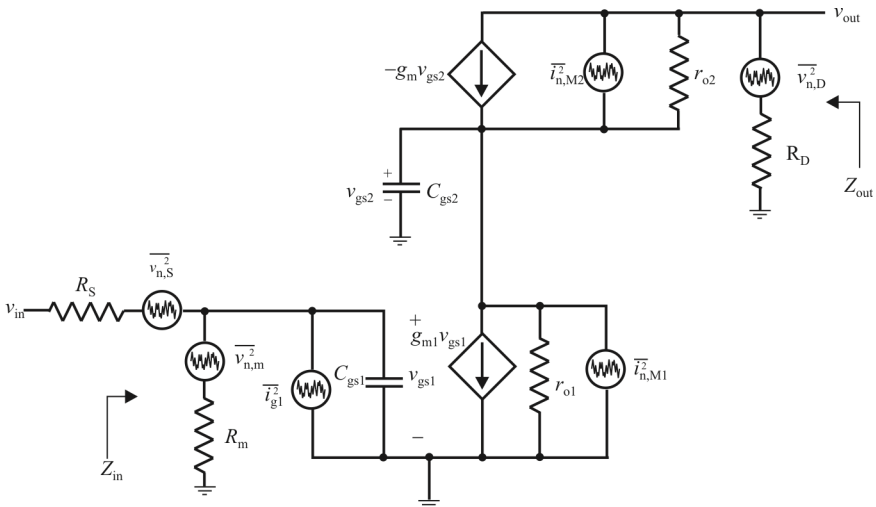


**Figure 3.20** LNA noise equivalent circuit with resistive termination at the input to an MOS amplifier.

$$\overline{v_{n,m}^2} = k_B T R_S (g_{M1} R_D)^2$$

while the output noise due to thermal noise from $M_1$ is given by

$$\overline{i_{n,M1}^2} = 4k_B T \frac{\zeta}{\alpha} g_{M1} \tag{3.67}$$

The output noise due to the load resistor, $R_D$, is given by

$$\overline{v_{n,D}^2} = k_B T R_D$$

and the output noise due to thermal noise from $M_2$ is

$$\overline{i_{n,M2}^2} = 4k_B T \frac{\zeta}{\alpha} g_{M2} \left( \frac{sC_{gs2}}{g_{M2} + sC_{gs2}} \right)^2 = \overline{i_{n,M1}^2} \frac{g_{M2}}{g_{M1}} \left( \frac{sC_{gs2}}{g_{M2} + sC_{gs2}} \right)^2$$

Now the noise factor of the LNA is given by

$$f = \frac{\text{total output noise}}{\text{noise due to the source resistor}} = \frac{\overline{v_{n,S}^2} + \overline{v_{n,m}^2} + \overline{v_{n,M1}^2} + \overline{v_{n,D}^2} + \overline{v_{n,M2}^2}}{\overline{v_{n,S}^2}}$$

The noise from $R_D$ is attenuated by the LNA gain. The noise transfer function of $M_2$ is smaller due to source degeneration. Both are ignored here for simplicity and we get

$$f \approx 1 + \frac{R_m^2}{R_S^2} + \frac{4\zeta}{\alpha g_{M1} R_S} = 2 + \frac{4\zeta}{\alpha g_{M1} R_S} \tag{3.68}$$

Therefore, even when $g_m R_S \gg 4\gamma$, $f_{min} > 2$ ($F > 3\,\text{dB}$).

Resistive termination provides a good match for maximum power transfer but greatly degrades the NF. This is because the terminating resistor adds its own noise while it drops the gain by 6 dB (compared to the common source amplifier with no termination). As a result, the input referred noise of the device and those of the following stages increase by the same factor.
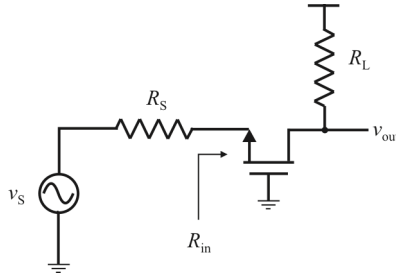
**Figure 3.21** Common gate LNA.

*Common Gate* (*CG*) *LNA*

A common gate LNA configuration is shown in Figure 3.21. The input impedance is given by

$$Z_{in} = \frac{1}{g_m + j2\pi f C_{gs}} \tag{3.69}$$

If $\omega C_{gs} \ll g_m$ then $\omega \ll g_m / C_{gs}$, $f \ll f_T$, and $Z_{in} \approx 1/g_m$.

The noise model for the configuration shown in Figure 3.21 is shown in Figure 3.22. Ignoring gate resistance, gate noise, and $r_o$, the output current is

$$\overline{i_{no}^2} = \overline{i_{no,ind}^2} + \overline{i_{no,R_S}^2}$$
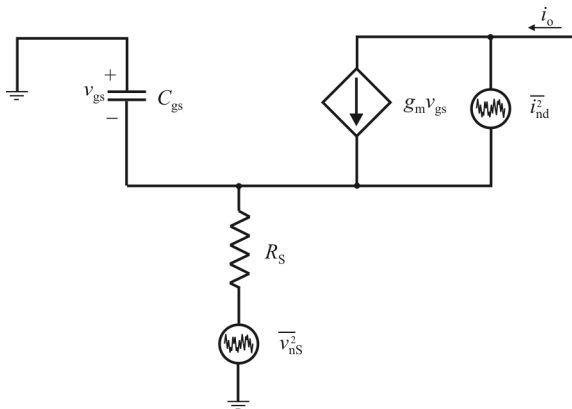


**Figure 3.22** Common gate amplifier noise model.

where

$\overline{i^2_{no,ind}}$ is the drain current noise

$\overline{i^2_{no,R_S}}$ is the output noise current due to source resistance given by

$$\overline{i^2_{no,R_S}} = \frac{\overline{v^2_{nS}}}{(R_S + R_{in})^2} = \left(\frac{g_m}{1 + g_m R_S}\right)^2 \overline{v^2_{nS}}$$

In accordance with Figure 3.22

$$i_o = i_{nd} + g_m v_{gs}$$
$$v_{gs} = -(i_{nd} + g_m v_{gs} + j\omega C_{gs} v_{gs})R_S$$

so

$$v_{gs} = -\frac{i_{nd} R_S}{1 + g_m v_{gs} + j\omega C_{gs} v_{gs}}$$

then

$$i_o = i_{nd} \frac{1 + j\omega C_{gs} R_S}{1 + g_m v_{gs} + j\omega C_{gs} R_S} \approx i_{nd} \frac{1}{1 + g_m R_S}$$

where we have assumed that $\omega C_{gs} R_S \ll 1$. Notice that if $g_m = 1/R_S$ (power match) then only half of the drain current goes to the output.

The noise factor for the common gate amplifier can be expressed as

$$f = 1 + \frac{\overline{i^2_{nd}}\left(\dfrac{1}{1 + g_m R_S}\right)}{\overline{e^2_{nS}}\left(\dfrac{g_m}{1 + g_m R_S}\right)^2} = 1 + \frac{\zeta g_{d0}}{g_m^2 R_S}$$

under the input matching conditions $R_S = 1/g_m$, and we have
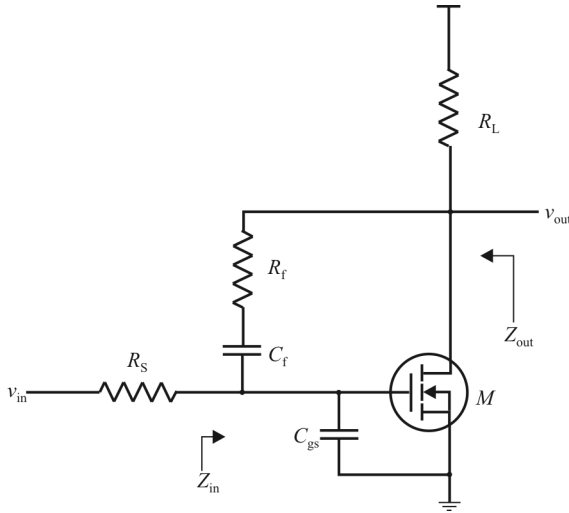
**Figure 3.23** Resistive shunt feedback LNA.

$$f = 1 + \zeta \frac{g_{d0}}{g_m} = 1 + \frac{\zeta}{\alpha} = \begin{cases} \dfrac{5}{3} \; (2.2 \, \text{dB}), & \text{Long channel} \\ \geq 3 \,(4.8 \, \text{dB}), & \text{Short channel} \end{cases}$$

*Resistive Shunt-Feedback LNA*

Recall that the output of a common source amplifier is $180^{\circ}$ out of phase with the input. Therefore, we would think that with the appropriate feedback, some amount of the input noise can be canceled by feedback from the output to the input, thereby reducing the noise factor. This is indeed the case as we will show in this section [12].

The negative feedback network is used to implement the input matching (Figure 3.23). The input impedance is determined by open loop gain and the resistor values ($R_f$, $R_L$), which are easily controlled. The resistors are noisy components and the LNA has moderate noise performance.

Voltage gain:

$$A_V = \frac{R_L (1 - g_m R_f)}{R_f + R_L}$$

Input impedance:

$$Z_{in} = \frac{R_f + R_L}{1 + g_m R_L} \parallel \frac{1}{sC_{gs}}$$

Output impedance:

$$Z_{out} = R_L \parallel \frac{R_S + R_f}{1 + g_m R_S}$$

The noise factor for the resistive shunt feedback LNA is given by:

$$f = 1 + \frac{R_f}{R_S}\left(\frac{1 + g_m R_S}{1 - g_m R_f}\right)^2 + \frac{1}{R_S R_L}\left(\frac{R_f + R_S}{1 - g_m R_f}\right)^2 + \frac{\zeta}{\alpha}\frac{g_m}{R_S}\left(\frac{R_f + R_S}{1 - g_m R_f}\right)^2$$

We discuss resistive shunt feedback more in Chapter 4 where we consider methods to extend the bandwidth of LNAs.

*Narrowband LNA*

The two topologies we consider for narrowband LNAs are (1) inductive degeneration and (2) resistive termination. The resistive terminated matching network for the narrowband case is the same as for the wideband case discussed above. On the other hand, inductive degenerated matching places an inductor in the source path and naturally leads to narrowband characteristics.

*Inductive Degeneration*

The most commonly used input-matching network for MOSFETs employs inductive source degeneration as shown in Figure 3.24. The purpose is to get real impedance without using resistors. To simplify the analysis, consider a device model that is given in Figure 3.25. The impedance looking into the gate of this circuit is given by

$$Z_{in}(s) = s(L_s + L_g) + \frac{1}{sC_{gs}} + 2\pi f_T L_s \tag{3.70}$$

If the input circuit is designed to work at resonance (i.e., narrowband),

$$Z_{in} = 2\pi f_T L_s = 50\Omega \tag{3.71}$$

Then the inductive source degenerated–narrowband LNA will have near minimum
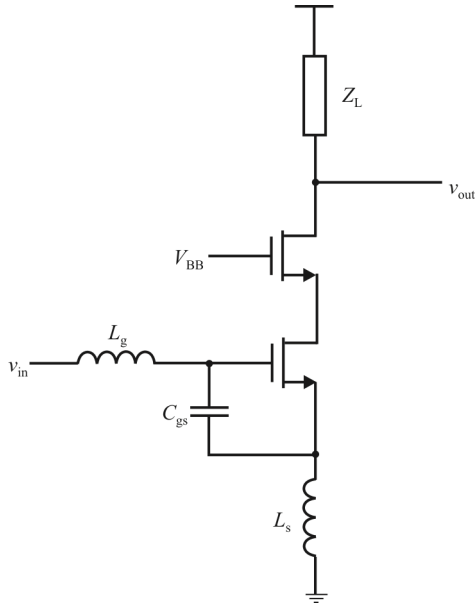
**Figure 3.24** Inductive degeneration.
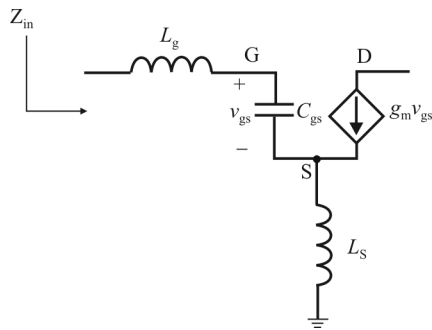


**Figure 3.25** Inductive degeneration model.

noise figure, excellent impedance match, and good power gain, all within a power budget that man-portable EW systems require. Unfortunately, except for some special cases, the LNAs in EW systems must have broad bandwidth. Therefore this type of inductive degeneration is precluded for all but those applications.

Using (3.27) and since

$$Y_s = \frac{1}{Z_0}\frac{1-\Gamma_s}{1+\Gamma_s} \qquad\qquad Y_{opt} = \frac{1}{Z_0}\frac{1-\Gamma_{opt}}{1+\Gamma_{opt}} \qquad (3.72)$$

then

$$
\begin{aligned}
\left|Y_s - Y_{opt}\right|^2 &= \frac{1}{Z_0^2}\left|\frac{1-\Gamma_s}{1+\Gamma_s} - \frac{1-\Gamma_{opt}}{1+\Gamma_{opt}}\right|^2 \\
&= \frac{1}{Z_0^2}\left|\frac{1-\Gamma_s + -\Gamma_s\Gamma_{opt} - 1 - \Gamma_s + \Gamma_{opt} + \Gamma_s\Gamma_{opt}}{(1+\Gamma_s)(1+\Gamma_{opt})}\right|^2 \\
&= \frac{1}{Z_0^2}\left|\frac{-2\Gamma_s + 2\Gamma_{opt}}{(1+\Gamma_s)(1+\Gamma_{opt})}\right|^2 \\
&= \frac{4}{Z_0^2}\left|\frac{\Gamma_s - \Gamma_{opt}}{(1+\Gamma_s)(1+\Gamma_{opt})}\right|^2 \qquad (3.73)
\end{aligned}
$$

$$
\begin{aligned}
G_s &= \mathrm{Re}\{Y_s\} = \frac{1}{2}(Y_s + Y_s^*) \\
&= \frac{1}{2Z_0}\left[\frac{1-\Gamma_s}{1+\Gamma_s} + \frac{1-\Gamma_s^*}{1+\Gamma_s^*}\right] \\
&= \frac{1}{2Z_0}\left[\frac{1-\Gamma_s + \Gamma_s^* - |\Gamma_s|^2 + 1 + \Gamma_s - \Gamma_s^* - |\Gamma_s|^2}{|1+\Gamma_s|^2}\right] \\
&= \frac{1}{Z_0}\left[\frac{1-|\Gamma_s|^2}{|1+\Gamma_s|^2}\right] \qquad (3.74)
\end{aligned}
$$

So, the noise factor becomes

$$f = f_{min} + R_N Z_0 \frac{1-|\Gamma_s|^2}{|1+\Gamma_s|^2}\frac{4}{Z_0^2}\left|\frac{\Gamma_s - \Gamma_{opt}}{(1+\Gamma_s)(1+\Gamma_{opt})}\right|$$

$$= f_{\min} + \frac{4R_N}{Z_0} \frac{\left|\Gamma_s - \Gamma_{opt}\right|^2}{(1 - \left|\Gamma_s\right|^2)\left|1 + \Gamma_{opt}\right|^2} \tag{3.75}$$

Now, what we would like is to determine the values of $\Gamma_s$ to give a fixed noise factor. To do this, we first define the noise factor parameter $N$, which consists of all the terms that do not depend on $\Gamma_s$:

$$N = \frac{\left|\Gamma_s - \Gamma_{opt}\right|^2}{1 - \left|\Gamma_s\right|^2} = \frac{f - f_{\min}}{4R_N / Z_0}\left|1 + \Gamma_{opt}\right|^2 \tag{3.76}$$

We do this to isolate the terms containing $\Gamma_s$, and lump the rest into $N$. Therefore,

$$(\Gamma_s - \Gamma_{opt})(\Gamma_s^* - \Gamma_{opt}^*) = N(1 - \Gamma_s\Gamma_s^*)$$

$$\left|\Gamma_s\right|^2 - \Gamma_s\Gamma_{opt}^* - \Gamma_s^*\Gamma_{opt} + \left|\Gamma_{opt}\right|^2 = N(1 - \left|\Gamma_s\right|^2)$$

$$\left|\Gamma_s\right|^2 - \Gamma_s\frac{\Gamma_{opt}^*}{1 + N} - \Gamma_s^*\frac{\Gamma_{opt}}{1 + N} = \frac{N - \left|\Gamma_{opt}\right|^2}{1 + N} \tag{3.77}$$

We see this is a circle with center and radius

$$C_f = \frac{\Gamma_{opt}}{N + 1} \tag{3.78}$$

$$r_f = \frac{\sqrt{N\left(N + 1 - \left|\Gamma_{opt}^2\right|\right)}}{N + 1} \tag{3.79}$$

Using these expressions, we can draw gain, stability, and noise factor circles on the $\Gamma_s$ Smith chart and pick a value of $\Gamma_s$ to achieve multiple specifications [13].

Considering Figure 3.24, the input impedance behaves like a series RLC circuit, and gate inductor $L_g$ is added to tune the resonant frequency to align with the operating frequency:

$$Z_{in} = s(L_g + L_S) + \frac{1}{sC_{gs}} + \frac{g_m L_S}{C_{gs}}$$

Matching occurs when $Z_{in}(jf_0) = R_S$

$$f_0^2 = \frac{1}{(2\pi)^2} \frac{1}{(L_g + L_s)C_{gs}}$$

and

$$R_S = \frac{g_m L_s}{C_{gs}} = 2\pi f_T L_s$$

$L_s$ can be selected by $L_s = R_S / 2\pi f_T$. If this value is too small to be practical, a capacitor can be inserted in shunt with $C_{gs}$ to artificially reduce $f_T$.

*Noise Factor*

We first ignore the correlation of the gate noise and drain current noise. The noise factor for the inductively degenerated LNA is given by

$$f = 1 + \frac{R_g}{R_S} + \frac{\zeta}{\alpha} g_m R_S \left(\frac{f_0}{f_T}\right)^2 \qquad (3.80)$$

Note that the noise factor at resonance is the same as the CS amplifier without inductive degeneration. Inductive degeneration did not raise $f_{min}$ but matched the input.

    We now consider the correlation of the gate noise and drain current noise. We can show that

$$f = 1 + \frac{R_g}{R_S} + \frac{\zeta}{\alpha} \chi g_m R_S \left(\frac{f_0}{f_T}\right)^2 \qquad (3.81)$$

where

$$\chi = 1 + 2|c|Q_L \sqrt{\frac{\delta\alpha^2}{5\zeta}} + \frac{\delta\alpha^2}{5\zeta}(1 + Q_L^2)$$

$$Q_L = Q_{C_{gs}} = \frac{1}{2\pi f_0 R_S C_{gs}} = \frac{2\pi f_0 (L_g + L_s)}{R_S}$$

and $c$ is the noise correlation coefficient. The optimal noise figure occurs for a particular $Q_L$; it is possible to obtain both a noise and power match in this case.

### 3.4.7 LNA Stability

Instability in an amplifier is when the amplifier breaks into oscillation, either permanently or temporarily. Stability is defined as the lack of instability. Instability can be caused by several reasons but they all result from feedback from the output to the input of some form.

Post presented an insightful discussion on how adding resistances to the input and output of an amplifier can enhance its stability [14, 15]. That analysis is summarized here for illustrative purposes.

Most high-performance active devices for implementing amplifiers in the RF and microwave regions are potentially unstable. However, resistive loading at the input and/or output of the amplifier can prevent oscillation at the frequency of interest for all passive source and load terminations. Adding resistances to an amplifier normally decreases its efficiency and gain.

Figure 3.26 illustrates an amplifier stage, where the first and last two-ports in the network each represent either a series or parallel resistor, or a through connection, while the center two-port represents the active device [15]. The stability as expressed by [16]

$$\mu = \frac{1 - |s_{11}|^2}{|s_{22} - s_{11}^* \Delta| + |s_{21} s_{12}|} \tag{3.82}$$

where $\Delta = s_{11} s_{22} - s_{12} s_{21}$. The condition $\mu > 1$ is necessary and sufficient for unconditional amplifier stability.

The stability of an overall network of this type can be found by cascading the transmission parameters, converting from transmission to scattering parameters, and then applying (3.82) to determine the value of $\mu$ for the overall configuration. Eight different input/output combinations are examined with this technique depending upon whether resistors are connected in series or parallel to one or both of the active device's ports. These combinations are listed in Table 3.2.

Once an amplifier is unconditionally stable, it is possible to determine the maximum transducer power gain, given as $G_{Tmax}$ in Table 3.2. Parameter $G_{Tmax}$ is defined as the ratio of the power delivered to the load by the amplifier to the power available from the source under the condition that the amplifier's input and output impedances are conjugate matched, usually through the appropriate design of input and output matching networks, which do not include the resistances shown in Figure 3.26. The table shows values for $G_{Tmax}$ for the eight resistor combinations computed at 2 GHz.

Figure 3.27 shows $\mu$ as a function of frequency from 0.10 to 30 GHz for the nine cases in the table. Curves 6 through 9 in Figure 3.27 indicate unconditional stability for all the frequencies considered.
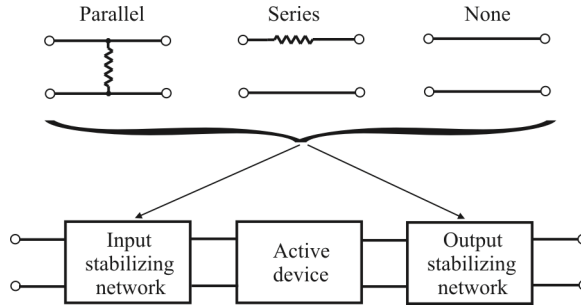
**Figure 3.26** Resistive stabilization at the input and output of an active device.

**Table 3.2** Stability of an LNA

|  | Input Resistance ($\Omega$) | | Output Resistance ($\Omega$) | | Calculated Parameters (2 GHz) | | | |
|---|---|---|---|---|---|---|---|---|
| Curve | Series | Parallel | Series | Parallel | $\mu$ | $G_{Tmax}$ (dB) | $G_T$ (dB) | $F_{total}$ (dB) |
| 1 | - | - | - | - | 0.17054 | - | - | - |
| 2 | 90.2 | - | - | - | 1.00064 | 21.70 | 19.05 | 2.16 |
| 3 | - | 670.0 | - | - | 1.00005 | 21.71 | 13.86 | 2.59 |
| 4 | - | - | 400 | - | 1.00016 | 21.70 | 13.22 | 0.46 |
| 5 | - | - | - | 13.7 | 1.00032 | 21.70 | 3.20 | 0.55 |
| 6 | 1,450 | 116 | - | - | 1.00545 | 21.10 | 13.00 | 1.54 |
| 7 | 151 | - | - | 3.0 | 1.40675 | 3.80 | 3.09 | 3.56 |
| 8 | - | 5,285 | - | 50 | 1.00046 | 21.73 | 13.45 | 0.76 |
| 9 | 281 | - | 480 | - | 1.18144 | 3.24 | 3.91 | 3.00 |

Source: [15].
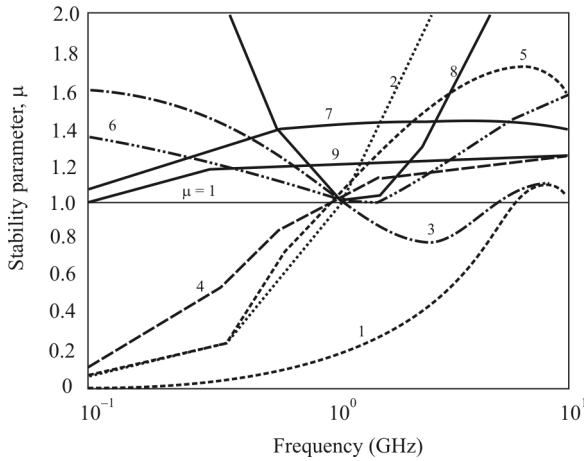
**Figure 3.27** Stability parameter μ as a function of frequency for the combinations given in Table 3.2.

Increasing the stability factor beyond unity reduces the maximum transducer power gain, $G_{\text{Tmax}}$. For the other six cases equal stability factors lead to equal power gains. The values of the resistances in Table 3.2 are determined by systematically searching the combinations. The search algorithm used to generate the results in Table 3.2 was designed to identify resistor combinations that stabilize the transistor at all frequencies while providing a stability factor as close to unity at 2 GHz as possible (curves 6 through 9 of Figure 3.27).

Adding resistance to amplifiers inevitably increases the noise figure, which decreases the output SNR. The particular configuration can have significantly different effects on noise performance, however. The noise performance of active devices can be described in terms of system reflection coefficients. This is illustrated by Figure 3.26, where resistors are represented as lossy, mismatched two-ports in a cascade network. Amplifier noise is increased by the resistive two-ports as a result of signal attenuation and the impedance mismatch between the cascade-connected ports.

In Figure 3.28 the input matching network transforms the source impedance $Z_g$ into the appropriate source reflection coefficient $\Gamma_S$ while an output matching
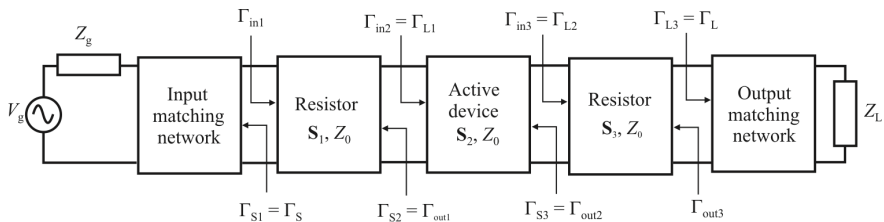


**Figure 3.28** Cascaded network.

network transforms the load impedance $Z_L$ into the appropriate load reflection coefficient $\Gamma_L$ for the active device. These matching networks are designed to provide the appropriate impedance transformations necessary to achieve maximum transducer gain, minimum noise figure, or any other amplifier specifications.

The input and output reflection coefficients for a two-port, $\Gamma_{in}$ and $\Gamma_{out}$, are given by [17]

$$\Gamma_{in} = s_{11} + \frac{s_{12}s_{21}\Gamma_L}{1 - s_{22}\Gamma_L} \tag{3.83}$$

and

$$\Gamma_{out} = s_{22} + \frac{s_{12}s_{21}\Gamma_S}{1 - s_{11}\Gamma_S} \tag{3.84}$$

where, as indicated in Figure 3.28,

$\Gamma_S$ is the reflection coefficient looking toward the two-port network's source
$\Gamma_L$ is the reflection coefficient looking toward the two-port network's load.

Referring to Figure 3.28, sequentially applying (3.83) from right to left beginning with $\Gamma_L$ and scattering parameters $\mathbf{S}_3$ allows calculation of the input reflection coefficient $\Gamma_{inm}$ for the $m^{th}$ two-port network, where $m = 1$ to 3. Similarly, sequentially applying (3.84) from left to right in Figure 3.28, beginning with $\Gamma_S$ and the scattering parameters $\mathbf{S}_1$, determines the output reflection coefficient $\Gamma_{outm}$ for the $m^{th}$ two-port network, where $m = 1$ to 3. Thus, sequential application of (3.83) and (3.84) specifies all input and output reflection coefficients for the overall network.

For active devices, the quantities $f_{min}$, $R_N$, and $\Gamma_{opt}$ are noise parameters that are characteristic of a particular device, while the quantity $Z_0$ is the system impedance, normally 50Ω. The noise factor of a transistor is

$$f_2 = f_{min} + \frac{4R_N}{Z_0} \frac{\left|\Gamma_{S2} - \Gamma_{opt}\right|^2}{\left(1 - \left|\Gamma_{S2}\right|^2\right)\left|1 + \Gamma_{opt}\right|^2} \tag{3.85}$$

where

$f_{min}$ is the minimum noise factor of the device
$R_N$ is the equivalent noise resistance of the device

$\Gamma_{opt}$ is the value of the optimum source reflection coefficient for the transistor $\Gamma_{S2}$ (in Figure 3.28) that results in a minimum device noise factor.

The available power gain for a two-port network is given by [18]

$$G_A = \frac{|s_{21}|^2 \left(1 - |\Gamma_S|^2\right)}{|1 - s_{11}\Gamma_S|^2 \left(1 - |\Gamma_{out}|^2\right)}$$ (3.86)

The noise factor of a lossy two-port network characterized at an operating temperature $T$ is given by

$$f = 1 + \frac{1 - G_A}{G_A} \frac{T}{T_0}$$ (3.87)

where

$T_0 = 290\text{K}$
$G_A$ is the available power gain

We see that at room temperature ($T = T_0$) the noise factor is equal to the power loss factor of the network, $L_A$, or

$$f = \frac{1}{G_A} = L_A$$ (3.88)

so that if the two-port network contains a lossy element, such as a series or parallel connected resistor, the noise factor of the device equals its loss. Thus, it is possible to either increase or reduce the available power gain, (3.86), and the resulting NF, (3.87), depending on the impedance mismatch at the network's ports.

Once the noise factors of the individual two-port networks are available, the overall stabilized amplifier noise factor is found by applying the expression for cascaded two-ports (3.54), which for the purposes here has three terms in it, each term corresponding to one of the two-ports shown in Figure 3.28,

$$f_a = f_1 + \frac{f_2 - 1}{G_{A1}} + \frac{f_3 - 1}{G_{A1}G_{A2}}$$ (3.89)

In (3.89), subscripts 1, 2, and 3 refer to the two-ports in Figure 3.28. Additionally, in (3.89), subscripts 1 and 3 refer to the noise factors and available gain of the

lossy two-ports that precede and follow the transistor, while subscript 2 refers to the noise factor and available gain of the transistor itself. Specifically, $f_1$ is the noise factor found from (3.87) with $G_{A1}$ from (3.86) for the first resistive network with scattering parameters $\mathbf{S}_1$ and reflection coefficients $\Gamma_{S1}$ and $\Gamma_{out1}$. Noise factor $f_3$ is also found from (3.87) with $G_{A3}$ from (3.86) for the last resistive network with scattering parameters $\mathbf{S}_3$ and reflection coefficients $\Gamma_{S3}$ and $\Gamma_{out3}$. Finally, noise factor $f_2$ for the transistor itself is found from (3.85) where $G_{A2}$ is the transistor's available gain, (3.86), with scattering parameters $\mathbf{S}_2$ and reflection coefficients $\Gamma_{S2}$ and $\Gamma_{out2}$.

The final two columns in Table 3.1, $G_T$ and $F_{total}$, predict the transducer power gain and overall noise figure when the matching network is such that the BJT's input reflection coefficient, $\Gamma_{S2}$, equals the optimum reflection coefficient $\Gamma_{opt}$.

Of special interest in these results is that the series output only (case 4) provides more than 2 dB additional gain and almost 0.1dB better noise figure performance compared with the parallel output only case (case 5). The parallel input/parallel output configuration (case 8) is unconditionally stable across the entire frequency range and improves the gain by 1.23 dB while suffering only a 0.30dB degradation of the noise figure compared to the series output-only case. These comparisons illustrate the possible choices of a stabilizing network for the amplifier that provides alternative compromises among gain, noise, and stability for a given application.

The results in the preceding paragraph can be understood from the Friis expression (3.89). For example, cases 4, 5, and 8 result in the lowest noise contribution, with cases 4 and 5 lower than case 3. This is because the attenuator follows the transistor, and as (3.89) shows, the effect of the noise contribution from the final two-port network is reduced by the relatively large amplifier gains. In the example of case 8, the overall noise figure is slightly worse than for cases 4 and 5 because the attenuation is applied at the amplifier input, and as (3.89) shows, the full noise contribution of this two-port network appears in the overall noise factor, $f_a$. This attenuator is relatively ineffective in adding noise, however, because the attenuation and mismatch produced by the parallel connected 5 k$\Omega$ resistor is very small compared with the other cases shown. Thus, attenuators at the input and the output do not contribute equally to the degradation of the overall amplifier noise factor, $f_a$, but the degree of degradation also depends upon the attenuation and mismatch of a specific attenuator, in addition to its location.

### 3.4.8 LNA Nonlinearity Model

An LNA is inherently a nonlinear device, as is any amplifier, when driven to its limits. A nonlinear system output up to the third order is given by

$$y(t) = a_0 + a_1 x(t) + a_2 x^2(t) + a_3 x^3(t) \tag{3.90}$$
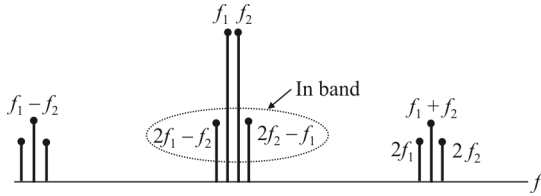
**Figure 3.29** Output signal spectrum of a nonlinear device.

Given a two-tone input signal into this nonlinearity

$$x(t) = A\cos(\omega_1 t) + A\cos(\omega_2 t) \qquad (3.91)$$

we wind up with signals at $nf_1 \pm mf_2$ and $nf_2 \pm mf_1$, a few of which are shown in Figure 3.29. Usually the distortion term represented by $2f_1 - f_2$ and $2f_2 - f_1$ fall in band as we see in Figure 3.29. This is the characteristic of a third-order nonlinearity. A large in-band blocking signal (called a blocker) can desensitize the circuit. It is measured by the 1dB compression point.

> **Definition 3.1: 1dB Compression Point.** The 1dB compression point is where the transfer characteristic deviates from linear by 1dB. It is a measure of the gain compression for large input signals (Figure 3.30).

The ideal transfer characteristic of any device is linear. The output of an ideal LNA is an exact replica of the input amplified by the gain of the amplifier. Such behavior is only approximate and there are input levels that, when reached, cause
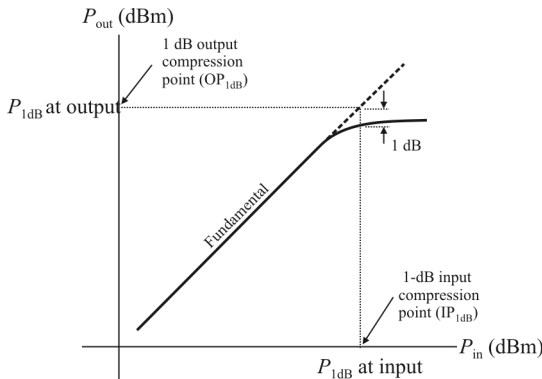


**Figure 3.30** Definition of the 1 dB compression point.

the output to no longer be replicates of the input. These levels are defined by the intercept points.

> **Definition 3.2: Input Second-Order Intercept Point.** The *input second-order intercept point* (IIP2) is the point where the linear transfer characteristic and the second-order intermodulation curve intersect (see Figure 3.31).

> **Definition 3.3: Input Third-Order Intercept Point.** The *input third-order intercept point* (IIP3) is a similar concept using the IM3 transfer characteristic, as shown in Figure 3.31.

IIP2 and IIP3 are measures of intermodulation behavior. The output intercept points (OIP2 and OIP3) are the corresponding outputs on the transfer characteristic.

As indicated in Figure 3.29, nonlinear behavior of the LNA produces extraneous signals at the output. These unwanted signals are referred to as *spurs*. The range of input signal levels over which these spurs do not appear is referred to as the spur-free dynamic range.

> **Definition 3.4: Spur-Free Dynamic Range.** The *spur-free dynamic range* (SFDR) is the range of input levels for which there are no undesired spurs created in the output (Figure 3.32). It is the input range over which the output signal is a faithful reproduction (amplified) of the input signal.

More will be considered about these parameters in subsequent chapters when specific areas of application are discussed.

# 3.5 Noise Reduction with an Input Transformer

A transformer at the input of an amplifier may improve its noise performance. Figure 3.33(a) shows a signal source connected to an amplifier through a transformer with a turns ratio 1:n. Resistors $R_1$ and $R_2$ represent the primary and the secondary winding resistances, respectively. Figure 3.33(b) shows the equivalent circuit seen by the amplifier input with all noise sources shown. The source $v_{t_1}$ represents the thermal noise generated by the effective source resistance $n^2(R_S + R_1) + R_2$. Analysis of this circuit reveals that the instantaneous amplifier output voltage is given by
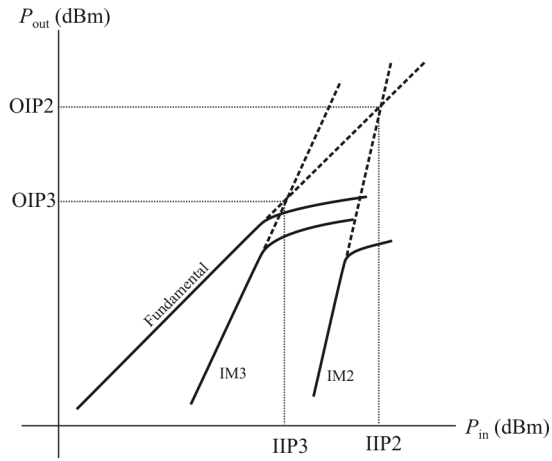
**Figure 3.31** Definition of intercept points.
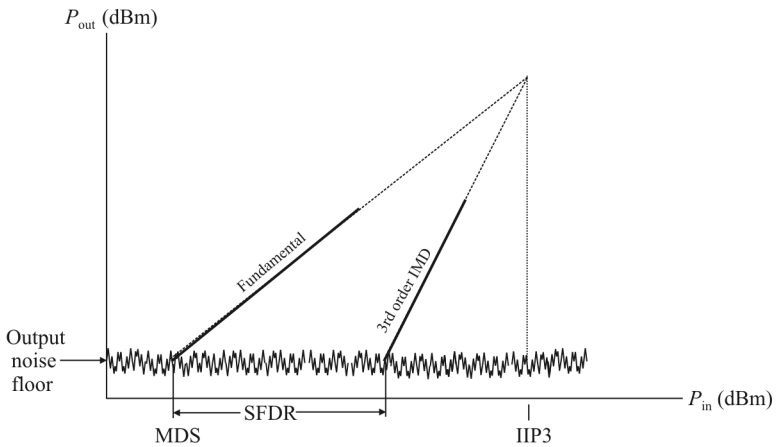


**Figure 3.32** Definition of spur-free dynamic range (SFDR).

(a)

(b)
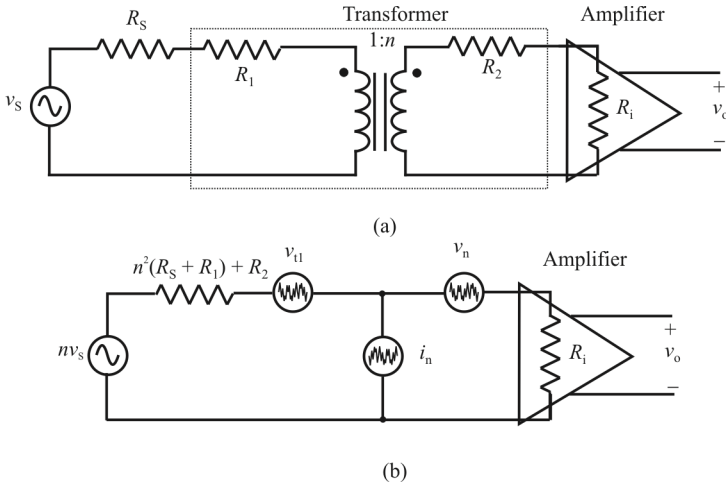
**Figure 3.33** Signal source coupled to an amplifier: (a) coupled to amplifier through an ideal transformer and (b) amplifier with equivalent input circuit.

$$v_o = \frac{AR_i}{n^2(R_S+R_1)+R_2+R_i}\{nv_S+v_{t_1}+v_n+i_n[n^2(R_S+R_1)+R_2]\} \quad (3.92)$$

The equivalent noise input voltage referred to the source is obtained by factoring the turns ratio from the brackets in (3.92) and retaining all terms except the $v_S$ term. The expression obtained can be converted into a root-square sum to obtain

$$V_{nis} = \left[ 4k_BT\left(R_S+R_1+\frac{R_2}{n^2}\right)\Delta f + \frac{V_n^2}{n^2} + 2\rho v_n i_n\left(R_S+R_1+\frac{R_2}{n^2}\right) \right.$$
$$\left. +i_n^2\left(n(R_S+R_1)+\frac{R_2}{n}\right)^2 \right]^{1/2} \quad (3.93)$$

where $\rho$ is the correlation coefficient between $v_n$ and $i_n$.

Since the series resistance of a transformer winding is proportional to the number of turns in the winding, it follows that $R_2/R_1 \propto n$. This makes it difficult to specify the value of $n$ which minimizes $V_{nis}$. In the case that $R_S \gg R_1 + R_2/n^2$, the expression for $v_{nis}$ is given approximately by

$$v_{nis} \approx \sqrt{4k_BTR_S\Delta f + \frac{1}{n^2}v_n^2 + 2\rho v_n i_n R_S + i_n^2 n^2 R_S^2} \quad (3.94)$$
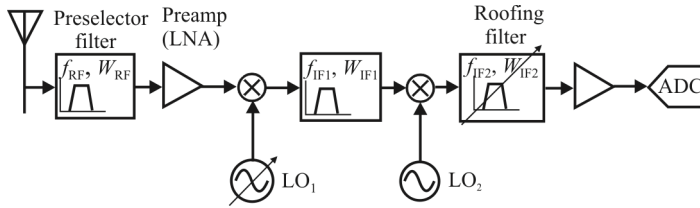
**Figure 3.34** EW receiver block diagram.

This is minimized when $n$ is given by

$$n = \sqrt{\frac{v_n}{i_n R_S}} \qquad (3.95)$$

In this case, the effective source resistance seen by the amplifier is $n^2 R_S = v_n / i_n$. This is the optimum source resistance that minimizes the NF. Thus, the NF is minimized and the SNR is maximized simultaneously by the transformer.

The transformer winding resistance can be a significant contributor to the thermal noise at the amplifier input, especially if the source resistance is small. For this reason, a transformer can result in a decreased SNR compared to the case without the transformer. With a BJT input stage the noise can be minimized by biasing the input stage at a particular current. When this is done, a transformer cannot be used to further decrease the noise.

# 3.6 Band Select Filtering/Preselector Filters

*Preselection filtering* is often included in the receiver front end. This filtering selects large portions of the frequency spectrum to be filtered for passing on to the rest of the receiver. Its purpose is to reject those portions of the spectrum that are not of current interest. Preselection filters also contribute to the rejection of images (discussed next). *Roofing filters* are inserted into the lower frequency IF chain to provide for fine-grain filtering unattainable by preselection filtering.

Figure 3.34 shows where these additional elements are added to the basic receiver structure. The preselector filter can either be a bank of fixed tuned suboctave filters or a tunable filter (typically with bandwidth 8–10% of tuned frequency). In either case, the bandwidths of the filters should be less than one octave in order to effectively block harmonics of strong interfering signals. In Figure 3.35, the *signal of interest* (SOI) is located at $f_2$. The preselector filter tunes to allow $f_2$ to pass. If a large amplitude interfering signal located at a frequency of
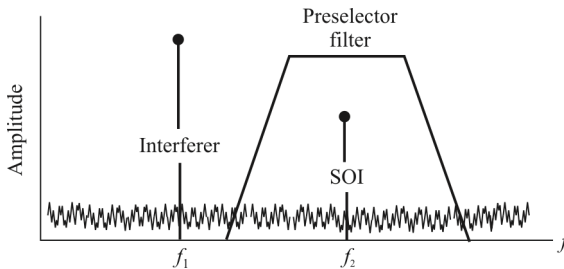
**Figure 3.35** Preselector filter blocks interfering signals.

$f_1$, such that $f_1 = f_2/2$, is present, the preselector filter prevents the receiver's first mixer from generating second harmonic distortion that would potentially mask this SOI.

The location of the preamplifier is crucial. It is purposely located after the preselector filter. Preamplifiers require large gain and low noise figures to overcome the noise figure of the downstream receiver. By locating the preamplifier after the preselector filter, large-amplitude interfering signals are attenuated before they reach the preamplifier. The results are both good distortion and a good noise figure for the receiver. For this reason, noise performance does not need to be traded off for distortion performance in EW receivers.

## 3.6.1 Roofing Filters

At RF frequencies, the low quality factor ($Q$) of the preselector filters prevents sufficiently narrow bandwidth to block all interfering signals. If the signal of interest is located at a frequency close to the interfering signal, both signals can progress through the receiver chain. The roofing filters, located at one of the IF stages (usually the first), provide further suppression of interfering signals before they can reach the final IF stages or the ADC. These analog filters are a set of fixed frequency bandpass filters whose bandwidths are variable. These filters can either be configured as a bank of filters or a single filter with tunable bandwidth.

Figure 3.36 shows how the roofing filter is used in the EW system. In this figure, two large-amplitude signals are close enough in frequency that the preselector filter at the RF input cannot remove both tones. The roofing filter, due to operating at a lower frequency, has a $Q$ sufficiently large to allow for narrow bandwidths. Roofing filters are effective when an SOI is located at a frequency that would fall near an *intermodulation distortion* (IMD) product generated by the two large interfering signals. When measuring the weaker SOI, the large-amplitude interfering signals fall outside the roofing filter bandwidth. With the interfering tones attenuated by the roofing filter, the amplifier stages that follow the roofing filters no longer create significant distortion, which allows the gain of these final stages to be increased. Two important results occur: one is that the
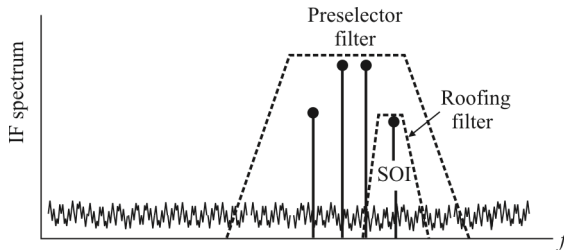
**Figure 3.36** Roofing filter suppresses distortion in final IF stages.

increased gain helps overcome the noise figure of the ADC, and the other is that the higher signal level at the ADC input improves the ADC's SFDR performance.

More details on signal filters are considered in Chapter 6 where we discuss IF filters and RF filters in general.

# 3.7 Concluding Remarks

The RF stage, which consists of all elements between the antenna and the mixer in a receiver, was introduced in this chapter. Normally these elements include preselection filters, an LNA, and image reject filters.

The LNA typically establishes the sensitivity of a receiver through its NF. The NF essentially sets the noise floor, and the components farther down the receive chain have a diminishing effect on that level if the gain of the LNA is sufficiently high. Any losses before the LNA due to passive devices, such as preselection filters, directly add to the NF of the receiver. Therefore such filters should be as high quality (low loss) as possible.

The preselection filters perform the function of RF band selection and are normally suboctave or tuned filters. They eliminate strong out-of-band signals from desensitizing the receiver. The image reject filters (which are discussed at length in Chapter 4) cause signals at the image frequencies generated in the mixer to be attenuated so the IF chain only amplifies the SOI.

## References

[1]     Motchenbacher, A. C., and J. A. Connelly, *Low-Noise Electronic System Design*, New York: Wiley, 1993.
[2]     Long, S., "Design of Low Noise Amplifiers," Course Notes ECE145A/ECE218A, February 2007.
[3]     White, J. F., *High Frequency Techniques*, Hoboken, NJ: Wiley, 2004, p. 413.
[4]     White, J. F., *High Frequency Techniques*, Hoboken, NJ: Wiley, 2004, p. 414.

[5]     Weiner, M. M., "Noise Factor of Receiving System with Arbitrary Antenna Impedance Mismatch," *IEEE Transactions on Aerospace and Electronic Systems*, Vol. 24, No. 2, March 1988, pp. 133–140.

[6]     Report 258-3, International Radio Consultive Committee, International Telecommunications Union, Geneva, Switzerland, 1980.

[7]     Spaulding, A. D., and R. T. Disney, "Man-Made Radio Noise Part I: Estimate for Business, Residential, and Rural Areas," Report 74-28, Office of Transportation, Department of Commerce, Boulder, Colorado, June 1974.

[8]     Weiner, M. M., "Effects of Antenna Impedance Mismatch on the Signal-To-Noise Ratio of a Radio Receiving System," ESD-TR-85-136, The MITRE Corporation, Bedford, MA, National Technical Information Service, Astia Document A159070m, July 1985.

[9]     Haus, H. A., et al., "The IRE Standards on Methods of Measuring Noise in Linear Two-Ports," *Proceedings of the Institute of Radio Engineers*, Vol. 48, January 1960, pp. 6–68.

[10]    Haus, H. A., et al., "Representation of Noise in Linear Two-Ports," *Proceedings of the Institute of Radio Engineers*, Vol. 48, January 1960, pp. 69–74.

[11]    Poisel, R. A., *Modern Communications Jamming Principles and Techniques*, 2nd Ed., Norwood, MA: Artech House, 2011, Ch. 2.

[12]    Zhang, H., "Low Noise Amplifiers," ECEN 665 Course Notes.

[13]    Poisel, R. A., *Antenna Systems and Electronic Warfare Applications*, Norwood, MA: Artech House, 2012, Section 20.3.

[14]    Edwards, M. L., and J. H. Sinsky, "A New Criterion for Linear 2-Port Stability Using a Single Geometrically Derived Parameter," *IEEE Transactions on Microwave Theory and Techniques*, Vol. 40, No. 12, December 1992, pp. 2302–2311.

[15]    Post, J. E., "Resistive Loading Enhances LNA Stability," *Microwaves and RF*, December 2003.

[16]    Pozer, D. M., *Microwave Engineering*, 3rd Ed., New York: Wiley, 2005, p. 645.

[17]    Pozer, D. M., *Microwave Engineering*, 3rd Ed., New York: Wiley, 2005, p. 192.

[18]    Vendelin, G. D., J. C. Pedro, and P. M. Cabrat, "Amplifier and Transistor Gains Revisited," *Microwave Journal*, April 6, 2005.

# Chapter 4

## Bandwidth Expansion for Small Signal Amplifiers

### 4.1 Introduction

Over the past few decades, many techniques have been developed to improve the bandwidth of amplifiers [1, 2]. As we attempt to quantify below, an improvement in the bandwidth of the amplifier is often accompanied by a corresponding drop in its low-frequency voltage gain and other effects. As such, the *gain-bandwidth* (GBW) product serves as a useful figure of merit for an amplifier topology in a given device technology [3]. For the purposes of this discussion, the bandwidth is defined as the lowest frequency at which the voltage gain drops by 3dB.[1] Accordingly, this bandwidth is often called the 3*dB bandwidth*.

One of the requirements for an RF stage amplifier in an EW system in most cases is that it must be broadband.[2] As discussed in Pozar [4], there are various ways to achieve broader bandwidths than otherwise, but like other practices in engineering, they all inevitably lead to tradeoffs of some kind.

Some popular methods of achieving broadband operation are:

1.  Shunt peaking
2.  Input and output matching to compensate for the $|s_{21}|$ falloff, but this is generally accompanied by a mismatch of input and output impedances, which, in turn, lead to poor power transfer between stages

---

[1] Note that this definition of bandwidth works here because small signal amplifiers are being discussed. This loss is unacceptable for power amplifiers.

[2] In the most general case, broadband refers to a filter response that is nominally the same, ideally flat, over a band of frequencies rather than at a single frequency. For our purposes, we embrace this definition but the band of frequencies is normally quite large—several hundreds of MHz is not atypical.
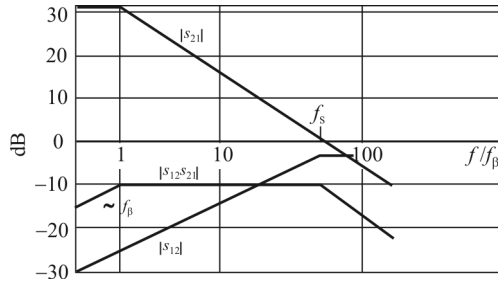
**Figure 4.1** Typical *s*-parameter performance versus frequency. $f_\beta$ is the beta cutoff frequency and, $f_S$ is the transducer cutoff frequency.

3. Resistive matching networks, where good impedance matching can be provided with an attendant decrease in gain and/or noise figure. This is sometimes referred to as *lossy matching* [5]
4. Negative feedback. Again gain and noise figure suffer, but wide bandwidths are possible
5. Balanced amplifiers
6. Distributed amplifiers.

We discuss these methods of bandwidth enhancement in this chapter.

Typically the *s*-parameters of an unstabilized and untuned amplifier have the characteristics illustrated in Figure 4.1. $|s_{21}|$ is constant for frequencies below the beta cutoff frequency ($f_\beta$) and falls off at 6dB per octave after that point. The transducer cutoff frequency ($f_S$) is the frequency where $|s_{21}|$ falls to 0dB.

## 4.2 Shunt Peaking

Shunt peaking is one of the earliest and perhaps the simplest technique for bandwidth expansion. Consider the simple common source amplifier illustrated in Figure 4.2(a) [6]. We assume that the frequency at which this amplifier is to operate is governed by a single dominant pole, which is determined solely by the output load resistance and the load capacitance shown in the FET amplifier model shown in Figure 4.2(b). The voltage gain of this stage is given by

$$G_V = \frac{V_{out}(\omega)}{V_{in}(\omega)} = \frac{g_m R}{1 + j\omega RC} \tag{4.1}$$
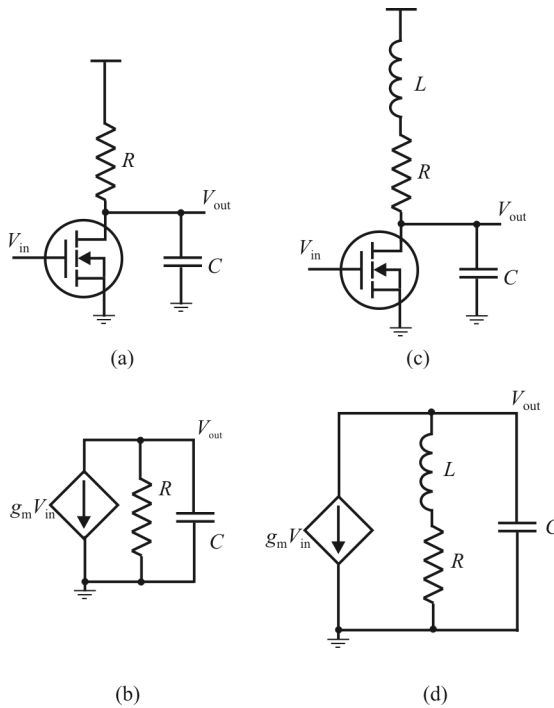
**Figure 4.2** Shunt peaking a common source amplifier. (a) Simple common source amplifier and (b) its equivalent small signal model. (c) Common source amplifier with shunt peaking and (d) its equivalent small signal model.

which illustrates the single dominant pole [6].

The introduction of an inductance in series with the load resistance as shown in Figure 4.2(c) alters the frequency response of the amplifier. This technique, referred to as *shunt peaking*, enhances the bandwidth of the amplifier by transforming the frequency response from that of a single pole to one with two poles and a zero as in Figure 4.2(d). The gain of the amplifier stage is now

$$G_V = \frac{V_{out}(\omega)}{V_{in}(\omega)} = \frac{g_m(R + j\omega L)}{1 + j\omega RC - \omega^2 LC} \qquad (4.2)$$

While the poles may not be complex, they usually are when the networks are used for bandwidth extension. The zero is determined solely by the time constant and is primarily responsible for the bandwidth enhancement.
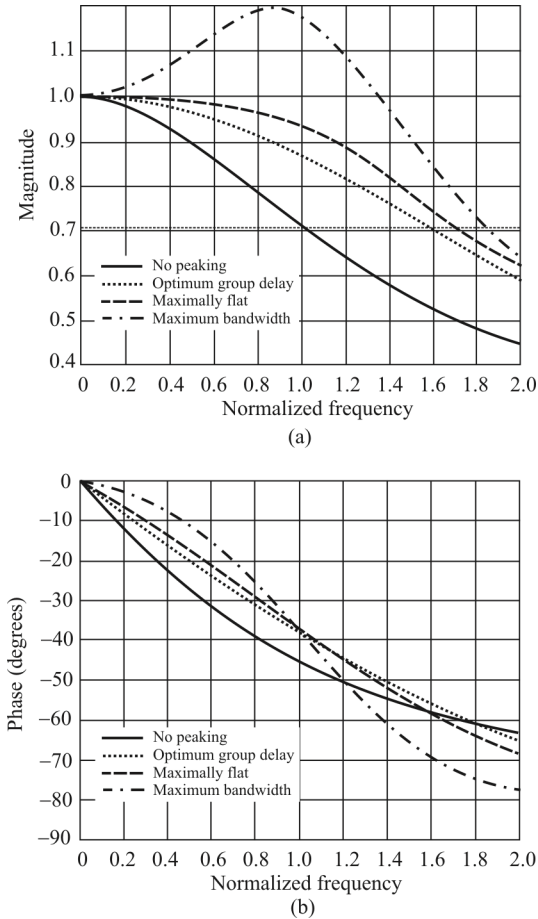
**Figure 4.3** Frequency response of shunt peaked cases in Table 4.1: (a) magnitude responses and (b) phase responses.

The frequency response of this shunt peaked amplifier is characterized by the ratio of the L/R and RC time constants. We denote this ratio by *m* so that $L = mR^2C$. Figure 4.3 [6] illustrates the shunt-peaking effects on the frequency response of the amplifier for the values of *m* delineated in Table 4.1. The case with no shunt peaking is used as the reference so that its low-frequency gain and its 3dB bandwidth are equal to one ($RC = 1$ and $g_mR = 1$).

Table 4.1 Performance Metrics for Shunt Peaking

| *m* | Normalized $\omega_{3dB}$ | Response |
|-----|---------------------------|----------|
| 0 | 1.00 | No shunt peaking |
| 0.32 | 1.60 | Optimum group delay |
| 0.41 | 1.72 | Maximally flat |
| 0.71 | 1.85 | Maximum bandwidth |

Source: [6].

As seen, the 3dB bandwidth increases as *m* increases. An 85% improvement in bandwidth occurs when *m* = 0.71, which is the maximum bandwidth obtained with two poles and a single zero. However, this comes at the cost of significant magnitude peaking. A maximally flat response is obtained for *m* = 0.41 with a bandwidth improvement of 72%.

A linear phase response up to the 3dB bandwidth occurs when *m* = 0.32, which is 60% higher than the case without shunt peaking. This is called the *optimum group delay case* and is desirable for optimizing pulse fidelity in broadband systems that receive digital signals. Deviations from linearity, however, are tolerable with this approach for the other values of *m* considered.

# 4.3 Input and Output Matching

It is not uncommon that at small signal levels, as applicable to the discussions in this chapter, concerns other than maximum power transfer between stages are important, such as maximizing usable bandwidth in this case. Therefore, it is not necessarily a bad characteristic if the interstage matching is not retained.

### 4.3.1 Bandwidth Enhancement for Transimpedance Amplifiers

The parasitic capacitances of the active devices used for amplification are the main cause of limited bandwidth in wideband amplifiers. As just seen, adding an inductor in series with the output load to increase the effective load impedance as the capacitive reactance drops at high frequencies is one way to implement first-order shunt peaking, thereby significantly enhancing the bandwidth.

The approach to bandwidth extension presented in [7] turns the entire amplifier into a lowpass filter with a well-defined passband characteristic and cutoff frequency. The parasitic capacitances of the active devices are absorbed as part of the lowpass filter, and hence, the bandwidth of the amplifier can be controlled. Theoretical limits of the gain-bandwidth product of lumped amplifiers have been known for over half a century [8]. Broadband filter synthesis techniques for bandwidth enhancement have been used for wideband amplifier [9, 10] and interconnect [11] design. Applying proper matching networks between amplifier stages to approach those limits is the key step in improving wideband amplifier

(a)



(b)
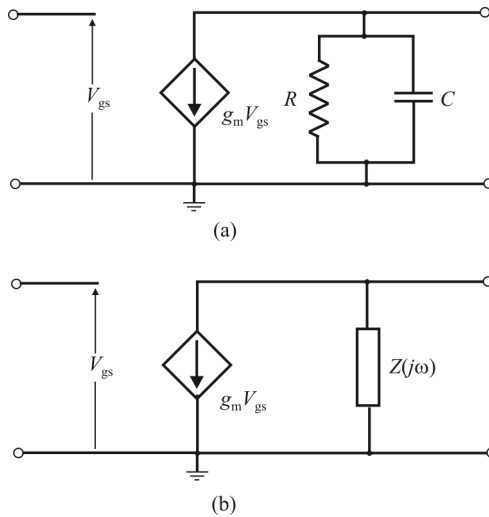
**Figure 4.4** Single-stage amplifier. (a) First-order load. (b) General passive impedance load.

bandwidth with this method.

## 4.3.2 Limits to Bandwidth Enhancement

The ideal characteristics of an EW broadband amplifier include maintaining constant gain and linear phase over its designed passband. It has already been mentioned several times that the bandwidth requirements for EW systems are quite large due to the unknown target environment such systems must be prepared to address. While evolving semiconductor technologies continue to provide transistors with higher cutoff frequencies, achieving the widest possible bandwidth with any given technology is still a desirable goal for several reasons. First, a design must at some point be frozen so that it can be constructed and used. That dictates some form of available technology and the bandwidth with that technology must be as wide as possible. Second, the wider the bandwidth of a given amplifier the fewer the required amplifiers, which, in turn, means lower cost, lower heat dissipation requirements, smaller size, etc.

### 4.3.2.1 Single-Stage Amplifiers

*One-Port Load Network*

Figure 4.4(a) shows a simple, low- to mid-frequency model for a linear single-stage transimpedance amplifier, where $R$ and $C$ are the aggregate parasitic

resistance and capacitance of the transistor and the input of the following stage, respectively. This load is a single-port network. The GBW product of this amplifier is given by

$$GBW = \frac{g_m}{2\pi C} \tag{4.3}$$

The parasitic capacitance limits the bandwidth according to (4.3) by reducing the output impedance of the amplifier as the frequency increases, while the resistance has no first-order effect on GBW. Hence, maintaining uniform output impedance by somehow countering the effects of the capacitance over a wider frequency range will increase the GBW. Inserting a more elaborate passive load network than a simple RC network is one way to accomplish this. Figure 4.4(b) shows the generic load network, $Z(j\omega)$, that should look like a constant resistance over the frequency range of interest.

   The Bode-Fano limit is a theoretical limit on the GBW that can be attained by inserting $Z(j\omega)$. For the amplifier in Figure 4.4(b) it is [12]

$$GBW_{max} = \frac{g_m}{\pi \overline{C}} \tag{4.4}$$

where $\overline{C}$ is defined as

$$\overline{C} = \lim_{\omega \to \infty} \left( \frac{1}{j\omega Z} \right) \tag{4.5}$$

and $Z(j\omega)$ is an impedance function.[3] $Z(j\omega)$ includes the aggregated output capacitance $C$, shown in Figure 4.4(a). $\overline{C}$ is greater than or equal to $C$ for a one-port load network. Thus, according to (4.4), any one-port passive network added in parallel to $C$ can improve the GBW product by at most a factor of two over that of the amplifier in Figure 4.4(a). As a result, the maximum achievable *bandwidth enhancement ratio* (BWER) for a one-port load is two. Shunt peaking is an example of this. Shunt peaking results in BWERs of 1.6 and 1.72 when designed for optimum group delay or maximally flat responses, respectively.

---

[3] An *impedance function* is a rational function (ratio of two polynomials with real coefficients) of frequency with no right half-plane poles. In addition, the numerator polynomial is of at most one degree higher than the denominator.

(a)



(b)



(c)
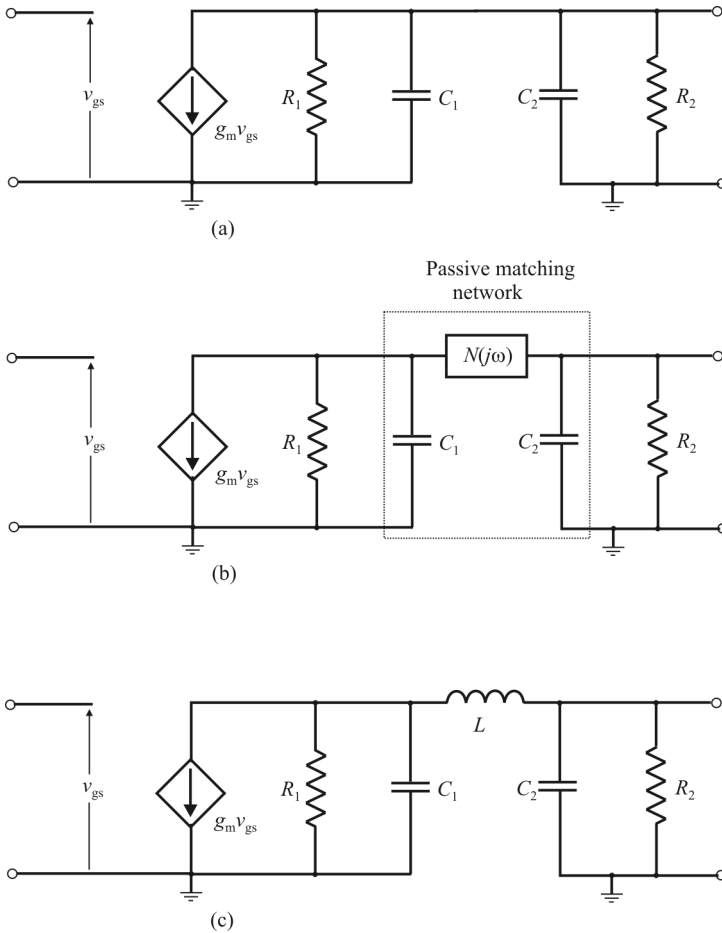
**Figure 4.5** (a) Small signal model of an amplifier with the loading effect of the next stage amplifier. (b) The inserted passive network isolates the amplifier parasites and the load. (c) Additional inductor forms a third-order passive network at the output.

*Two-Port Matching Network*

Consider the single-stage transimpedance amplifier shown in Figure 4.5(a). The intrinsic output resistance and capacitance of the transistor, i.e., $R_1$ and $C_1$, are separated from those of the load—namely, $C_2$ and $R_2$. The combination of capacitors limits the bandwidth of the amplifier; that is,

$$\text{GBW} = \frac{g_\text{m}}{2\pi(C_1 + C_2)} \tag{4.6}$$

A passive two-port network can be inserted between the transistor's intrinsic components ($R_1$ and $C_1$) and load ($C_2$ and $R_2$) to increase the bandwidth, as shown in Figure 4.5(b) [7]. This two-port passive network can maintain the impedance seen at the output of the amplification stage constant over a wider frequency range than if it were not there, as it separates and isolates $C_1$ from $C_2$. Therefore, $C_1$ is the only capacitor that affects GBW at the input port of the network (output of the amplification stage).

As above, the maximum GBW product at the input port of $N(j\omega)$ is

$$\text{GBW}_\text{max} = \frac{g_\text{m}}{\pi C_1} \tag{4.7}$$

Bode has shown that, for $C_1 = C_2 = C/2$ it is possible to design $N(j\omega)$ in such a way that the GBW product at the output port is the same as that of the input. Thus, for a single-stage amplifier with a two-port passive reactive load network, we have

$$\text{GBW}_\text{max} = \frac{2g_\text{m}}{\pi C_1} \tag{4.8}$$

One such configuration for $N(j\omega)$ is a constant-$k$ LC-ladder filter [13] terminated in its image impedance.[4] Compared to (4.6) with $C_1 = C_2 = C/2$, (4.8) is four times larger than the GBW product of a single-stage amplifier without the additional coupling network. As a result, for equal low-frequency gain, the maximum achievable BWER for a two-port load is four.

It is typically computationally difficult to determine the component values for the optimizing two-port network directly. Even for the case of the third-order system in Figure 4.5(c), with only an additional inductor between the device and the load, the value of the inductor that maximizes the bandwidth is quite difficult to find. Instead, graphical or simulation methods can be used. Figure 4.6 [7] shows the normalized gain of a single-stage amplifier with a passive network load consisting of a single inductor similar to Figure 4.5(c), where the inductor isolates $C_1$ and $C_2$. The component values are normalized to achieve 0dB gain at low frequency and a 1 rps 3dB bandwidth when the output impedance of the amplifier is equal to the load ($R_1 = R_2 = 1\Omega$ and $C_1 = C_2 = 1$F). (Methods to denormalize

---

[4] A constant-$k$ LC-ladder filter that is terminated in its image impedance has a constant transfer function over the frequencies less than its cutoff frequency ($f_c$).
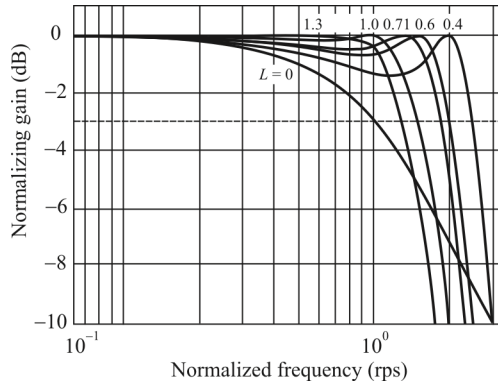
**Figure 4.6** Normalized gain of the amplifier with third-order network load and different inductor values. $R_1 = R_2 = 1\Omega$, $C_1 = C_2 = 1F$.

these values to more realistic ranges are covered in Chapter 5.)

Values for the BWER, defined as the ratio of the 3dB bandwidth of the amplifier to the 3dB bandwidth when $L = 0$, are summarized in Table 4.2. Even with the simple third-order $\pi$-section passive network, the BWER is significant compared to its theoretical limit. Bandwidth optimization assumes no gain peaking constraints.

## 4.3.2.2 Multistage Amplifiers

It is frequently difficult to achieve a desirable GBW product with a single stage of amplification. Every technology yields active devices that are inherently limited in some way. To overcome this difficulty, several stages of amplification are typically cascaded, with the total gain being the product of the gain of each stage. However, the overall bandwidth is less than the bandwidth of each stage, because the gain drop in the passband of each amplifier will accumulate. In fact, there is an

**Table 4.2** BWER for the Third-Order Passive Network in Figure 4.6

| L (H) | BWER |
|-------|------|
| 0     | 1    |
| 0.2   | 1.44 |
| 0.4   | 2.46 |
| 0.5   | 2.2  |
| 0.6   | 2.0  |
| 0.707 | 1.83 |
| 1.0   | 1.52 |
| 1.3   | 1.31 |

optimum value for the gain of each stage in a multistage arrangement that maximizes the overall bandwidth.
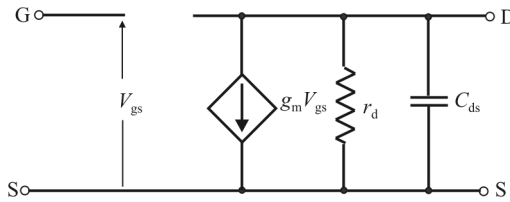
**Figure 4.7** FET (MOSFET and JFET) HF model.

Consider the simple model shown in Figure 4.7 for a CMOS amplification stage. The transfer function for a cascade of $N$ such stages is given by the product of the transfer function of each stage:

$$G(s) = \left( \frac{G_0}{1 + s / \omega_p} \right)^N \tag{4.9}$$

where $G_0$ and $\omega_p$ are the gain and 3 dB bandwidth of a single stage, respectively. The 3dB frequency for the overall network, denoted here by $\omega_h$, can be found with

$$\frac{|G(s)|^2}{G_0^{2N}} = \frac{1}{\left[ 1 + \left( \frac{\omega_h}{\omega_p} \right)^2 \right]^N} = \frac{1}{2}$$

which yields

$$r = \frac{\omega_h}{\omega_p} = \sqrt{2^{1/N} - 1} \tag{4.10}$$

This function is plotted in Figure 4.8. Even cascading two stages to provide gain reduces the bandwidth by over 25%. Now

$$\omega_p = \frac{g_{m2}}{C_{total}} = \frac{g_{m2}}{\dfrac{g_{m1}}{\omega_T} + \dfrac{g_{m2}}{\omega_T}} = \frac{\omega_T}{G_0 + 1}$$

The total gain is the product of the individual gains, viz
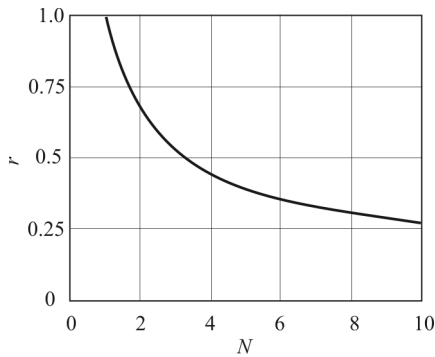
**Figure 4.8** Bandwidth degradation with multiple stages of amplification and filtering.

$$G_{\text{total}} = NG_0 \tag{4.11}$$

Substituting these into (4.10) yields

$$\frac{\omega_h}{\omega_T} = \frac{\sqrt{2^{1/N} - 1}}{G_{\text{total}}^{1/N} + 1} \tag{4.12}$$

Expression (4.12) has a maximum that is independent of $G_{\text{total}}$. Assume that $N$ is large ($N > 4$). Then

$$\omega_h = \omega_p \sqrt{2^{1/N} - 1} \approx \omega_p \frac{0.83}{\sqrt{N}} \tag{4.13}$$

In addition, assume that the capacitance of the load conductance can be neglected as we do in Figure 4.7, $g_{m1} / \omega_T \gg g_{m2} / \omega_T$. Then

$$\omega_p \approx \omega_T \frac{g_{m1}}{g_{m2}} = \frac{\omega_T}{G_0} = \frac{\omega_T}{G_{\text{total}}^{1/N}} \tag{4.14}$$

Combining (4.14) with (4.13) yields

$$\frac{\omega_h}{\omega_T} = \frac{0.83}{G_{\text{total}}^{1/N} \sqrt{N}} \tag{4.15}$$

Note that

$$GBW = G_{\text{total}}^{N}\omega_{\text{h}} \tag{4.16}$$

Comparing to the single-stage GBW product, $G_{\text{V}}\omega_{\text{p}}$, there is a gain-bandwidth improvement of

$$\frac{GBW_{\text{multistage}}}{GBW_{\text{one-stage}}} = G_{\text{total}}^{N-1}\sqrt{2^{1/N}-1} \tag{4.17}$$

for instance, that corresponds to a factor of 4.4 improvement in GBW. For larger $G_{\text{total}}$, GBW will increase dramatically by introducing additional single stages at the price of increasing overall power consumption, cost, etc. In practice, each stage has a loading effect on its previous stage, which reduces its bandwidth, hence reducing the overall bandwidth. The matching networks can reduce the loading effect by separating the output of an amplifier from the input of its next stage. One disadvantage of multistage amplifiers, in general, and multistage amplifiers with two-port matching networks between each stage in particular, is excessive phase shift that each amplifier stage or each network adds to the signal path [14], which can result in instability in feedback amplifiers.

# 4.4 Lossy Matching

The application of dissipative gain compensation in interstate matching networks [15] and amplifier stabilization by means of resistive-loaded shunt networks [5] have been known for many years. In this section we consider the electrical behavior of lossy match amplifiers and examine the influence of the individual circuit elements on the amplifier's performance characteristics such as NF, gain, and reflection coefficients. Formulas that express the important tradeoffs that exist between gain and reflection coefficients are discussed. Furthermore, formulas for the amplifier's NF and minimum NF are presented. Finally, the experimental and theoretical results of a two-stage lossy match amplifier are compared.

### 4.4.1 Performance Parameters

The schematic of a multistage lossy match amplifier is shown in Figure 4.9 [5]. The basic circuit functions of this amplifier are three: input matching, amplification, and interstage matching. The topology of the basic lossy match amplifier block containing dissipative circuit elements across its input and output terminals may be represented by *y*-parameters as shown in Figure 4.10. The two-port between these two resistive shunt elements consists of the transistor and any
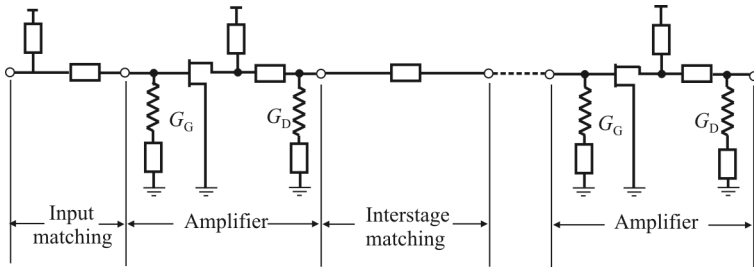
**Figure 4.9** Circuit topology of a multistage lossy match amplifier.
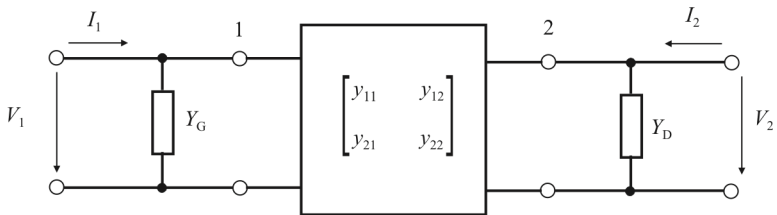


**Figure 4.10** Block diagram of the basic lossy match amplifier.
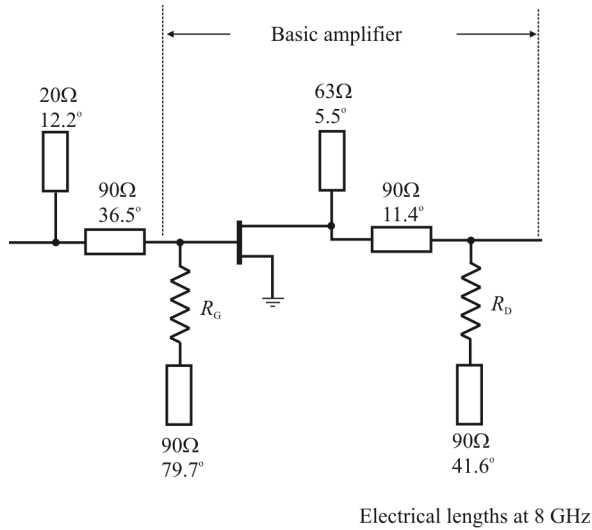
**Figure 4.11** Circuit topology of a single-stage lossy match amplifier and equivalent circuit elements of the GaAs MESFET.

additional elements that may be required for desired performance. In the case of the basic amplifier block in Figure 4.11, an open circuit shunt stub cascaded with a 90Ω transmission line at the transistor's drain terminal serves this purpose.

Using the admittance representation of Figure 4.10, the scattering parameters of this network can be determined, yielding

$$s_{21} = -\frac{Y_o}{y_{12}}\left[\sqrt{1+\frac{y_{21}y_{12}}{Y_o^2(1+s_{11})(1+s_{22})}} - 1\right] \tag{4.18}$$

This expression leads to the calculation of the impact of any improvement of the reflection coefficients

$$s_{11} = \frac{[Y_0 - (y_{11} + Y_G)][Y_0 + (y_{22} + Y_D)] + y_{12}y_{21}}{[Y_0 + (y_{11} + Y_G)][Y_0 + (y_{22} + Y_D)] - y_{12}y_{21}} \tag{4.19}$$

$$s_{22} = -\frac{[Y_0 + (y_{11} + Y_G)][Y_0 - (y_{22} + Y_D)] + y_{12}y_{21}}{[Y_0 + (y_{11} + Y_G)][Y_0 + (y_{22} + Y_D)] - y_{12}y_{21}} \tag{4.20}$$

by means of the admittances $Y_G$ and $Y_D$ on the unit's gain $|s_{21}|^2$. $Y_0$ is the characteristic admittance.

When

$$\left| \frac{y_{21}y_{12}}{Y_0^2}(1 + s_{11})(1 + s_{22}) \right| \ll 1 \tag{4.21}$$

is satisfied (which is normally true), applying the binomial theorem to (4.18) yields

$$s_{21} \approx -\frac{y_{21}}{2Y_0}(1 + s_{11})(1 + s_{22}) \tag{4.22}$$

A close examination of (4.19) and (4.20) reveals that the input and output reflection coefficients $s_{11}$ and $s_{22}$ can only be made zero by means of the lossy shunt elements $Y_G$ and $Y_D$ as long as

$$G_{in} \le Y_0 \tag{4.23}$$
$$G_{out} \le Y_0 \tag{4.24}$$

where $G_{in}$ and $G_{out}$ are the conductance of the input and output admittances

$$Y_{in} = G_{in} + jB_{in} = y_{11} + Y_G - \frac{y_{12}y_{21}}{Y_0 + y_{22} + Y_D} \tag{4.25}$$

$$Y_{out} = G_{out} + jB_{out} = y_{22} + Y_D - \frac{y_{12}y_{21}}{Y_0 + y_{11} + Y_G} \tag{4.26}$$

However, even if conditions (4.23) and (4.24) are not met, input and output matches may be improved by the reactive components of $Y_G$ and $Y_D$.

In most practical cases of lossy match *gallium-arsenide* (GaAs) *metal-semiconductor FET* (MESFET) amplifiers, (4.23) and (4.24) are satisfied over most or at least over the lower portion of the frequency band. In order to improve

the matches over the upper portion of the band, conventional matching techniques may be added by employing transmission line elements and open-circuit shunt stubs outside of the basic lossy match amplifier of Figure 4.10. This may be accomplished in form of the input and interstage matching networks shown in Figure 4.9.

The insertion gain of the basic amplifier derived from (4.19) and (4.20) is

$$\text{Gain} = \left|\frac{Y_0}{y_{12}}\right|^2 \left|\sqrt{1 + \frac{y_{21}y_{12}}{Y_0^2}(1+s_{11})(1+s_{22})} - 1\right|^2 \tag{4.27}$$

At frequencies where (4.21) is satisfied, the exact formula for gain (4.27) can be approximated with

$$\text{Gain} = \frac{1}{4}\left|\frac{y_{21}}{Y_0}\right|^2 |1+s_{11}|^2 |1+s_{22}|^2 \tag{4.28}$$

The error when using (4.28) in case of the basic amplifier contained in Figure 4.11(a) for $R_G = R_D = 100\Omega$ does not exceed 0.25dB up to frequencies of 5 GHz.

While (4.27) expresses the tradeoffs between gain and reflection coefficients in their exact form, they can most easily be demonstrated on the basic amplifier's low-frequency model. The reactive elements of the transistor model listed in Figure 4.11(b) have relatively little influence on the magnitude of the amplifier's gain and reflection coefficients for frequencies up to 1 GHz. Thus, the transistor can be represented by its low-frequency model and the amplifier circuit can be reduced to the simple network at the inset in Figure 4.12. For this idealized model, the scattering parameters are

$$s_{11} = \frac{1 - G_G Z_0}{1 + G_G Z_0} \tag{4.29}$$

and

$$s_{12} = 0 \tag{4.30}$$

$$s_{21} = -\frac{2g_m Z_0}{[1 + G_G Z_0][1 + (G_{ds} + G_D)Z_0]} \tag{4.31}$$

$$s_{22} = \frac{1 - (G_{ds} + G_D)Z_0}{1 + (G_{ds} + G_D)Z_0} \tag{4.32}$$
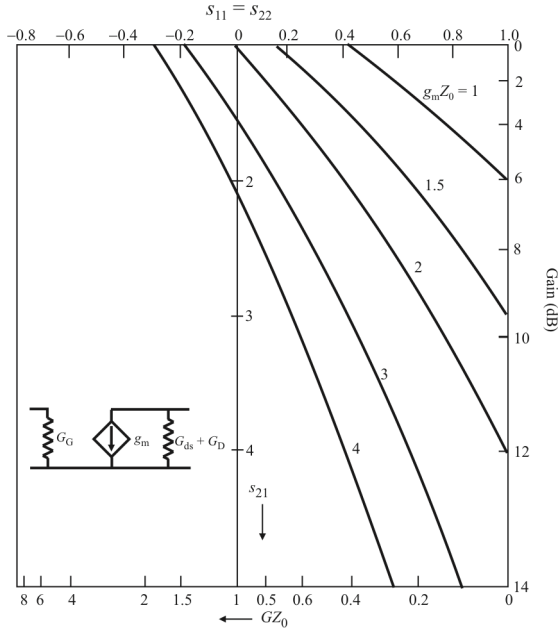
**Figure 4.12** Gain and reflection coefficients of a symmetric module ($s_{11} = s_{22}$) at low frequencies as a function of $GZ_0 = G_G Z_0 = (G_{ds} + G_D)Z_0$.

where $Z_0$ is the characteristic impedance. Furthermore, substituting $Y_{21} = g_m$ and $Y_{12} = 0$ into (4.18), where $g_m$ is the transconductance, results in

$$s_{21} = -\frac{g_m Z_0}{2}(1 + s_{11})(1 + s_{22}) \tag{4.33}$$

At low frequencies, $s_{11}$ and $s_{22}$ have negligible imaginary components, and the gain can be expressed as

$$\text{Gain} = |s_{21}|^2 = \left[\frac{g_m Z_0}{2}(1 + s_{11})(1 + s_{22})\right]^2 \tag{4.34}$$

which clearly expresses the tradeoffs between the gain and the reflection coefficients. This relationship is presented in graphical form in Figure 4.12 for a lossy match amplifier with identical input and output conductance; that is, $G_G = G_{ds} + G_D = G$, resulting in $s_{11} = s_{22}$.

Electrical length at 8 GHz
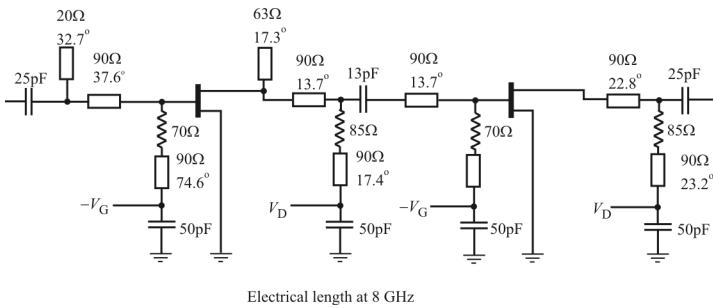
**Figure 4.13** Circuit topology of the optimized two-stage amplifier with the shunt resistors $R_G = 70\Omega$ and $R_D = 85\Omega$.

### 4.4.2 Practical Considerations

When cascading realistic lossy match amplifier modules, some of the unit's circuit elements require values somewhat different from those of the schematic in Figure 4.11(a). This is due to the fact that the inputs and outputs of individual stages are no longer terminated by 50Ω impedances.

The topology of an optimized two-stage amplifier is given in Figure 4.13. The lossy match resistors $R_G = 70\Omega$ and $R_D = 85\Omega$ were not subjected to optimization but rather determined experimentally by trying to achieve flat gain performance over the 2- to 8-GHz band. The measured and computed NFs, gains, and reflection coefficients for this two-stage amplifier are compared in Figure 4.14.

### 4.4.3 Summary

The NF, gain, and reflection coefficients of the lossy match amplifier have been examined and formulas to calculate these parameters developed. Based on the theoretical results, a two-stage amplifier was designed and tested. The unit's computed performance was compared with actual test data over the design frequency band of 2- to 8-GHz. The comparison demonstrates good agreement between the measured and computed results. These results show the enormous bandwidth potential of the lossy match amplifier achievable in an extremely compact size.

## 4.5 Feedback

### 4.5.1 Shunt-Series Feedback

The shunt-series feedback amplifier configurations are shown in Figure 4.15 for the three types of active devices considered here. Shunt feedback is provided by $R_2$
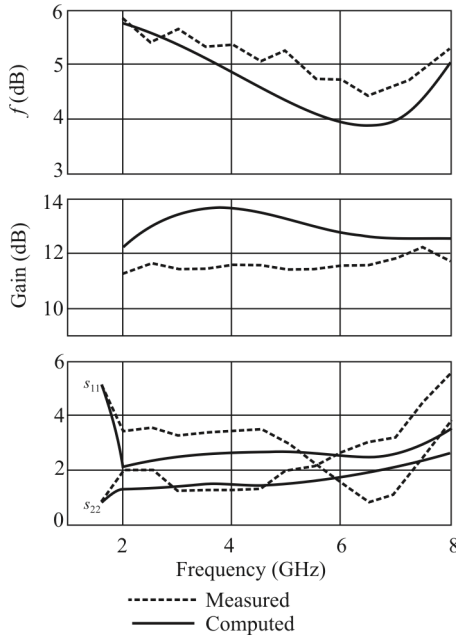
**Figure 4.14** Comparison or the computed and measured performance characteristics of the amplifier shown in Figure 4.13.

because the small signal model for the FET puts $R_2$ in a shunt role, while the series feedback is provided by $R_1$. The current flowing from the drain to the source causes a voltage drop across $R_1$, effectively causing $v_\pi$ to be smaller, producing a negative feedback path.

The input currents and voltages are related by the admittance matrix, which for the circuit shown in Figure 4.16 is given by

$$
\begin{bmatrix} I_1 \\ I_2 \end{bmatrix} = \begin{bmatrix} 1/r_g & -1/r_g \\ \dfrac{g_m}{1+g_m R_1} - \dfrac{1}{r_g} & 1/r_g \end{bmatrix} \begin{bmatrix} V_1 \\ V_2 \end{bmatrix}
\tag{4.35}
$$

This admittance matrix can be converted to the scattering matrix yielding
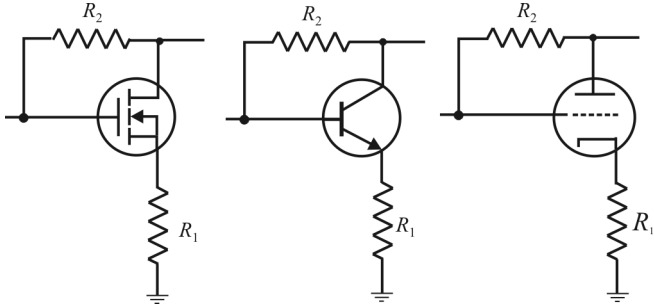
**Figure 4.15** Shunt-series negative feedback.
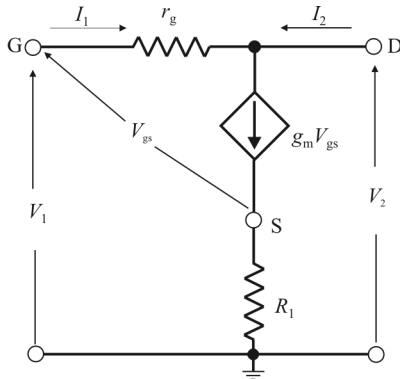


**Figure 4.16** Low-frequency equivalent circuit of GaAs FET amplifier.

$$S = \begin{bmatrix} \dfrac{1}{d}\left[1 - \dfrac{g_m Z_0^2}{r_g(1+g_m R_1)}\right] & \dfrac{2Z_0}{d r_g} \\[4ex] \dfrac{1}{d}\left(-\dfrac{2g_m Z_0}{1+g_m R_1} + \dfrac{2Z_0}{r_g}\right) & \dfrac{1}{d}\left[1 - \dfrac{g_m Z_0^2}{r_g(1+g_m R_1)}\right] \end{bmatrix}$$                (4.36)

where

$$d = 1 + \frac{2Z_0}{r_g} + \frac{g_m Z_0^2}{r_g(1+g_m R_1)}$$

To make $s_{11} = s_{22} = 0$

$$1 + g_m R_1 = \frac{g_m Z_0^2}{r_g}$$                (4.37)

or

$$R_1 = \frac{Z_0^2}{r_g} - \frac{1}{g_m}$$                (4.38)

Then $s_{21}$ and $s_{12}$ of the feedback amplifier are

$$s_{21} = \frac{Z_0 - r_g}{Z_0}$$                (4.39)

and

$$s_{12} = \frac{Z_0}{r_g + Z_0}$$                (4.40)

Thus, we can see that the transistor $s_{ij}$ are not frequency dependent.

### 4.5.2 Shunt Feedback

From (4.39),

$$r_g = Z_0(1 - s_{21})$$ (4.41)

Shunt only feedback is provided when $R_1 = 0$, so from (4.38)

$$R_1 = \frac{Z_0^2}{r_g} - \frac{1}{g_m} = 0$$ (4.42)

So $g_m$ for $s_{ii} = 0$ is

$$g_m = \frac{r_g}{Z_0^2}$$ (4.43)

so if the device $g_m$ is different from that specified by (4.43) then $s_{ii}$ will not be zero. Furthermore, if $g_m$ has a high value, $\min(VSWR)_{\text{in,out}}$ can be obtained when $R_1 r_g \sim Z_0^2$.

> **Example 4.1:** Suppose we need flat gain (loss) of 10dB in a 50Ω system. Since

$$G_p = |s_{21}|^2$$

then $s_{21} = -\sqrt{10} = -3.16$, so from (4.41)

$$r_g = 50(1 + 3.16) = 208\,\Omega.$$ (4.44)

The required value of $g_m$ for the transistor is given by (4.43)

$$g_m = \frac{208^2}{50^2} = 83\,\text{mS}$$ (4.45)

### 4.5.3 Bandwidth Extension

Consider an amplifier whose high-frequency response is characterized by a single pole. Its gain at mid- and high frequencies is given by

$$\alpha(s) = \frac{\alpha_M}{1 + s / \omega_H}$$ (4.46)
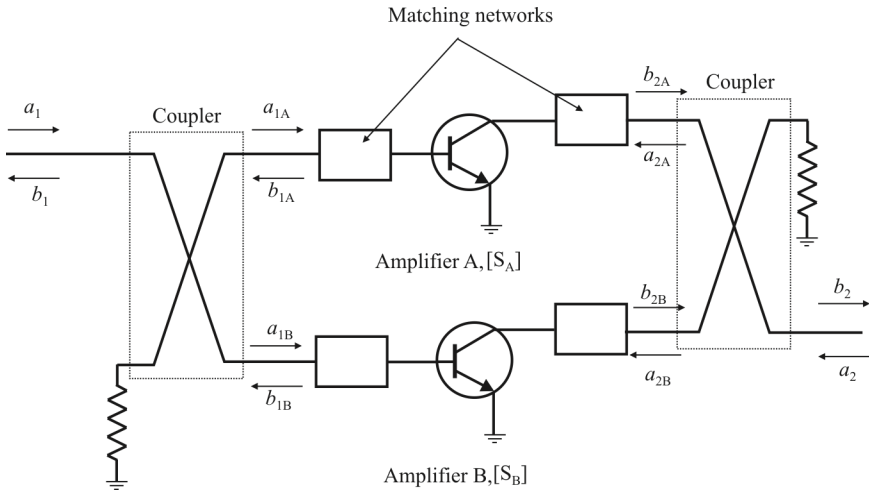
**Figure 4.17** Balanced amplifier.

where $\alpha_M$ denotes the mid-band gain and $\omega_H$ is the upper 3dB frequency. Application of negative feedback, $\beta$, results in a closed-loop gain of

$$\alpha_f(s) = \frac{\alpha(s)}{1+\beta\alpha(s)} = \frac{\alpha_M/(1+\alpha_M\beta)}{1+s/\omega_H(1+\alpha_M\beta)} \qquad (4.47)$$

Thus the feedback amplifier will have a mid-band gain of $\alpha_M/(1+\alpha_M\beta)$ and an upper frequency of $\omega_{Hf} = \omega_H(1+\alpha_M\beta)$. The mid-band gain has been reduced by the amount of feedback, $(1+\alpha\beta)$, while the upper 3 dB frequency has been increased by this same amount. Similarly a lower 3 dB frequency is $\omega_{Lf} = \omega_L/(1+\alpha_M\beta)$.

# 4.6 Balanced Amplifiers

A *balanced amplifier*, also known as a *quadrature combined amplifier*, implements two separate amplification chains as illustrated in Figure 4.17. The inputs to the amplifiers are derived from the input signal by passing the input signal through a 90° hybrid, which separates one path with no phase shift from the other, which has a 90° phase shift. After amplification, the output signals are
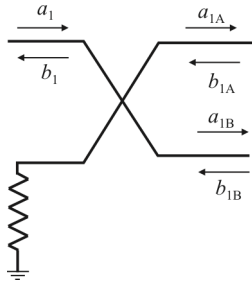
**Figure 4.18** Input 90° hybrid coupler.

passed through another 90° hybrid, in this case in a combiner role, which effectively removes the 90° shift [4].

The advantages of the balanced amplifier is that the input and output impedances can be well matched and broad bandwidth can be achieved—up to and surpassing a decade.

The *s*-parameters for the two amplifiers are given by

$$\begin{bmatrix} s_{11} & s_{12} \\ s_{21} & s_{22} \end{bmatrix} = \frac{1}{2} \begin{bmatrix} s_{11A} - s_{11B} & -j(s_{12A} + s_{12B}) \\ -j(s_{21A} + s_{21B}) & -(s_{22A} - s_{22B}) \end{bmatrix} \tag{4.48}$$

The *s*-parameters for the entire network are derived below. The 90° hybrids are also known as 3dB *Lange couplers*. Based on the input hybrid shown in Figure 4.18, since one port of the hybrid is terminated in the characteristic impedance, the waves on the input side in Figure 4.17 are related by

$$\begin{bmatrix} b_1 \\ a_{1A} \\ a_{1B} \end{bmatrix} = \begin{bmatrix} 0 & \dfrac{1}{\sqrt{2}} & -\dfrac{j}{\sqrt{2}} \\ \dfrac{1}{\sqrt{2}} & 0 & 0 \\ -\dfrac{j}{\sqrt{2}} & 0 & 0 \end{bmatrix} \begin{bmatrix} a_1 \\ b_{1A} \\ b_{1B} \end{bmatrix} \tag{4.49}$$

The *s*-parameter matrices for the two amplifiers are given by

$$\begin{bmatrix} b_{1A,B} \\ b_{2A,B} \end{bmatrix} = \begin{bmatrix} s_{11A,B} & s_{12A,B} \\ s_{21A,B} & s_{22A,B} \end{bmatrix} \begin{bmatrix} a_{1A,B} \\ a_{2A,B} \end{bmatrix} \tag{4.50}$$

while the waves on the output hybrid coupler shown in Figure 4.19 are given by
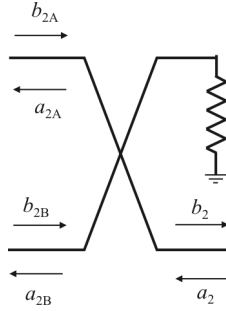
**Figure 4.19** Output 90° hybrid coupler.

$$
\begin{bmatrix} a_{2A} \\ a_{2B} \\ b_2 \end{bmatrix} =
\begin{bmatrix}
0 & 0 & -\dfrac{j}{\sqrt{2}} \\
0 & 0 & \dfrac{1}{\sqrt{2}} \\
-\dfrac{j}{\sqrt{2}} & \dfrac{1}{\sqrt{2}} & 0
\end{bmatrix}
\begin{bmatrix} b_{2A} \\ b_{2B} \\ a_2 \end{bmatrix}
\tag{4.51}
$$

Therefore

$$
b_1 = \frac{1}{\sqrt{2}} b_{1A} + \frac{-j}{\sqrt{2}} b_{1B}
$$

$$
= \frac{1}{\sqrt{2}}(s_{11A}a_{1A} + s_{12A}a_{2A}) + \frac{-j}{\sqrt{2}}(s_{11B}a_{1B} + s_{12B}a_{2B})
$$

$$
= \frac{1}{\sqrt{2}}\left( s_{11A}\frac{1}{\sqrt{2}}a_1 + s_{12A}\frac{-j}{\sqrt{2}}a_2 \right) + \frac{-j}{\sqrt{2}}\left( s_{11B}\frac{-j}{\sqrt{2}}a_1 + s_{12B}\frac{1}{\sqrt{2}}a_2 \right)
$$

$$
= \frac{1}{2}(s_{11A} - s_{11B})a_1 + \frac{-j}{2}(s_{12A} + s_{12B})a_2
\tag{4.52}
$$

$$
b_2 = \frac{-j}{\sqrt{2}} b_{2A} + \frac{1}{\sqrt{2}} b_{2B}
$$

$$
= \frac{-j}{\sqrt{2}}(s_{21A}a_{1A} + s_{22A}a_{2A}) + \frac{1}{\sqrt{2}}(s_{21B}a_{1B} + s_{22B}a_{2B})
$$

$$
= \frac{-j}{\sqrt{2}}\left( s_{21A}\frac{1}{\sqrt{2}}a_1 + s_{22A}\frac{-j}{\sqrt{2}}a_2 \right) + \frac{1}{\sqrt{2}}\left( s_{21B}\frac{-j}{\sqrt{2}}a_1 + s_{22B}\frac{1}{\sqrt{2}}a_2 \right)
$$

$$= \frac{-j}{2}(s_{21A} - s_{21B})a_1 + \frac{-1}{2}(s_{22A} + s_{22B})a_2 \qquad (4.53)$$

and

$$\begin{bmatrix} b_1 \\ b_2 \end{bmatrix} = \begin{bmatrix} \frac{1}{2}(s_{11A} - s_{11B}) & \frac{-j}{2}(s_{12A} + s_{12B}) \\ \frac{-j}{2}(s_{21A} - s_{21B}) & \frac{-1}{2}(s_{22A} + s_{22B}) \end{bmatrix} \begin{bmatrix} a_1 \\ a_2 \end{bmatrix} \qquad (4.54)$$

There are a number of advantages to this amplifier architecture. When the amplifiers and the hybrids are well matched, then the balanced amplifier has good stability. In addition, there are fewer components in the amplifier than some other topologies, leading to higher reliability, fewer tuning requirements, and lower cost. The input and output matching are accomplished by the two hybrids, and any mismatch reflections are absorbed by the two resistors. If one of the amplifiers fails, the gain decreases by 6dB, but total failure is avoided so the failure is not catastrophic. Last, the bandwidth of the balanced amplifier is determined by the two hybrids and can be an octave or more [4].

We will examine three types of couplers for the balanced amplifier: the branch-line coupler, in both discrete form and microstrip form, the Wilkinson combiner, and the TLT coupler.

### 4.6.1 Coupling

4.6.1.1 Branch-Line Coupler

Consider the coupler shown in Figure 4.20. With input power applied to port 1 and ports 2, 3, and 4, terminated at $50\Omega$, with $a_1$ at port 1, then

$$b_2 = \frac{a_1}{\sqrt{2}} e^{-j\pi/2} \qquad (4.55)$$

$$b_3 = \frac{a_1}{\sqrt{2}} e^{-j\pi} \qquad (4.56)$$

$$b_4 = 0 \qquad (4.57)$$

Then

$$b_1 = \frac{a_2}{\sqrt{2}} e^{-j\pi/2} + \frac{a_3}{\sqrt{2}} e^{-j\pi} \qquad (4.58)$$
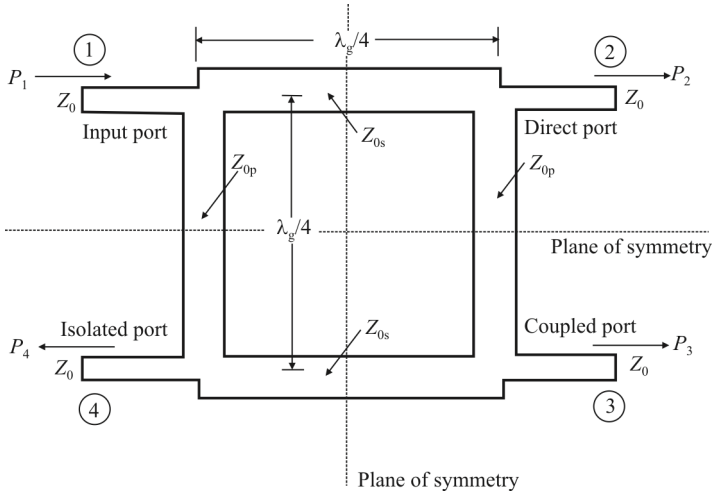
**Figure 4.20** $\lambda/2$ Branch-line coupler.

$$b_2 = \frac{a_1}{\sqrt{2}} e^{-j\pi/2} + \frac{a_4}{\sqrt{2}} e^{-j\pi} \tag{4.59}$$

The *s*-parameters for the 4-port network are

$$\mathbf{S} = \begin{bmatrix} 0 & \frac{1}{\sqrt{2}} e^{-j\pi/2} & \frac{1}{\sqrt{2}} e^{-j\pi} & 0 \\ \frac{1}{\sqrt{2}} e^{-j\pi/2} & 0 & 0 & \frac{1}{\sqrt{2}} e^{-j\pi} \\ \frac{1}{\sqrt{2}} e^{-j\pi} & 0 & 0 & \frac{1}{\sqrt{2}} e^{-j\pi/2} \\ 0 & \frac{1}{\sqrt{2}} e^{-j\pi} & \frac{1}{\sqrt{2}} e^{-j\pi/2} & 0 \end{bmatrix} \tag{4.60}$$

When port 4 is terminated in $Z_0 = 50\Omega$, then the coupler becomes a 3-port divider/combiner with scattering matrix

$$\mathbf{S} = \begin{bmatrix} 0 & \dfrac{1}{\sqrt{2}}e^{-j\pi/2} & \dfrac{1}{\sqrt{2}}e^{-j\pi} \\[3ex] \dfrac{1}{\sqrt{2}}e^{-j\pi/2} & 0 & 0 \\[3ex] \dfrac{1}{\sqrt{2}}e^{-j\pi} & 0 & 0 \end{bmatrix} \tag{4.61}$$

*Divider*

For a divider, $a_1 = a_1$, $a_2 = 0$, and $a_3 = 0$. In that case

$$b_1 = 0 \tag{4.62}$$

$$b_2 = \frac{a_1}{\sqrt{2}}e^{-j\pi/2} \tag{4.63}$$

$$b_3 = \frac{a_1}{\sqrt{2}}e^{-j\pi} \tag{4.64}$$

*Combiner*

For a combiner, $a_1 = 0$, $a_2 = a_2$, $a_3 = a_2 e^{j\pi/2}$. Then

$$b_1 = \frac{1}{\sqrt{2}}\left(a_2 + a_3 e^{-j\pi/2}\right) = \frac{2a_2}{\sqrt{2}}e^{-j\pi/2} \tag{4.65}$$

For the balanced amplifier with branch-line couplers, when port 1 is excited, port 4 is terminated in $Z_0 = 50\Omega$, and ports 2 and 3 are connected to amplifiers, the waves reflected back to the coupler are

$$a_2 = a_1 \frac{e^{-j\pi/2}}{\sqrt{2}} s_{11A} \tag{4.66}$$

$$a_3 = a_1 \frac{e^{-j\pi}}{\sqrt{2}} s_{11B} \tag{4.67}$$

$$b_1 = a_1 \frac{e^{-j\pi}}{2} s_{11A} + \frac{a_1}{2} s_{11B} = a_1 \frac{e^{-j\pi}}{2}(s_{11A} - s_{11B}) \tag{4.68}$$

The *s*-parameters for the balanced amplifier are
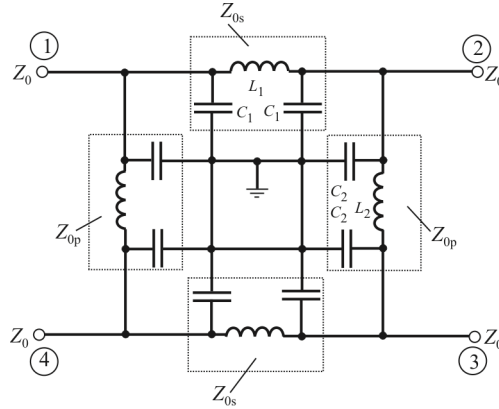
**Figure 4.21** Lumped element branch-line coupler.

$$s_{11} = \frac{e^{-j\pi}}{2}(s_{11A} - s_{11B}) \tag{4.69}$$

$$s_{21} = \frac{e^{-j\pi/2}}{2}(s_{21A} + s_{21B}) \tag{4.70}$$

$$s_{12} = \frac{e^{-j\pi/2}}{2}(s_{12A} + s_{12B}) \tag{4.71}$$

$$s_{22} = \frac{e^{-j\pi}}{2}(s_{22A} - s_{22B}) \tag{4.72}$$

Hence

$$|s_{11}| = 0.5|s_{11A} - s_{11B}| \tag{4.73}$$

$$|s_{21}| = 0.5|s_{21A} + s_{21B}| \tag{4.74}$$

$$|s_{12}| = 0.5|s_{12A} + s_{12B}| \tag{4.75}$$

$$|s_{22}| = 0.5|s_{22A} - s_{22B}| \tag{4.76}$$

A balanced amplifier implemented with lumped element branch-line couplers is illustrated in Figure 4.21. The ABCD matrix of an inductor with two shunt capacitances at both ends is

$$\begin{bmatrix} A & B \\ C & D \end{bmatrix} = \begin{bmatrix} 1 & 0 \\ j\omega C & 1 \end{bmatrix} \begin{bmatrix} 1 & j\omega L \\ 0 & 1 \end{bmatrix} \begin{bmatrix} 1 & 0 \\ j\omega C & 1 \end{bmatrix} \tag{4.77}$$

**Table 4.3** Advantages and Disadvantages of Balanced Amplifiers with Branch-Line Couplers

| Advantages | Disadvantages |
|---|---|
| No VSWR problems with individual amplifiers | More DC power required |
| High stability | Some insertion loss |
| 3 dB higher output power | If one of the amplifiers fails, power gain decreases by 6 dB |
| Easy to cascade | Large area on MMIC substrate |
| BW is limited by the couplers | |

By equating the matrix elements

$$L_1 = \frac{Z_{0s}}{\omega_0} \tag{4.78}$$

$$C_1 = \frac{1}{Z_{0s}\omega_0} \tag{4.79}$$

$$L_2 = \frac{Z_{0p}}{\omega_0} \tag{4.80}$$

$$C_2 = \frac{1}{Z_{0p}\omega_0} \tag{4.81}$$

Typical values for a 900 MHz coupler are $L_1 = 6.3$ nH, $L_2 = 4.8$ nH, $C_t = C_1 + C_2 = 4.5$ pF.

Some advantages and disadvantages of balanced amplifiers using branch-line couplers are listed in Table 4.3.

## 4.6.1.2 Modified Branch-Line Coupler

The size of the branches in a branch-line coupler can be reduced. Consider the coupler shown in Figure 4.22. The ABCD matrix of a $\lambda/4$ transmission line of $Z_0$ is given by

$$\begin{bmatrix} A & B \\ C & D \end{bmatrix} = \begin{bmatrix} 0 & jZ_c \\ j/Z_c & 0 \end{bmatrix} \tag{4.82}$$

The ABCD matrix of a $\theta$ transmission line of $Z$ with two shunt capacitances at each end is given by
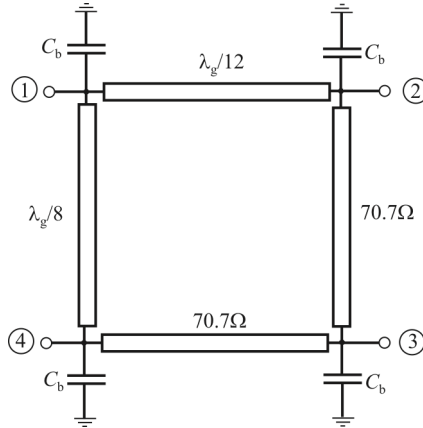
**Figure 4.22** Modified branch-line coupler.

$$\begin{bmatrix} A & B \\ C & D \end{bmatrix} = \begin{bmatrix} 1 & 0 \\ j\omega C & 1 \end{bmatrix} \begin{bmatrix} \cos\theta & jZ\sin\theta \\ j\sin\theta/Z & \cos\theta \end{bmatrix} \begin{bmatrix} 1 & 0 \\ j\omega C & 1 \end{bmatrix} \tag{4.83}$$

By equating the matrix elements we get

$$Z = \frac{Z_c}{\sin\theta} \tag{4.84}$$

$$\omega C = \frac{\cos\theta}{Z_c} \tag{4.85}$$

If $Z > Z_c$, the main lines and shunt branches become less than $\lambda/4$. With

$$y = \frac{Z_0}{Z} \tag{4.86}$$

the lengths of the main lines ($\theta_1$) and shunt branches ($\theta_2$) are

$$\theta_1 = \sin^{-1} y \tag{4.87}$$

$$\theta_2 = \sin^{-1}\frac{y}{\sqrt{2}} \tag{4.88}$$

$$\omega_0 C_b Z_0 = \sqrt{1-y^2} + \sqrt{2-y^2} \tag{4.89}$$
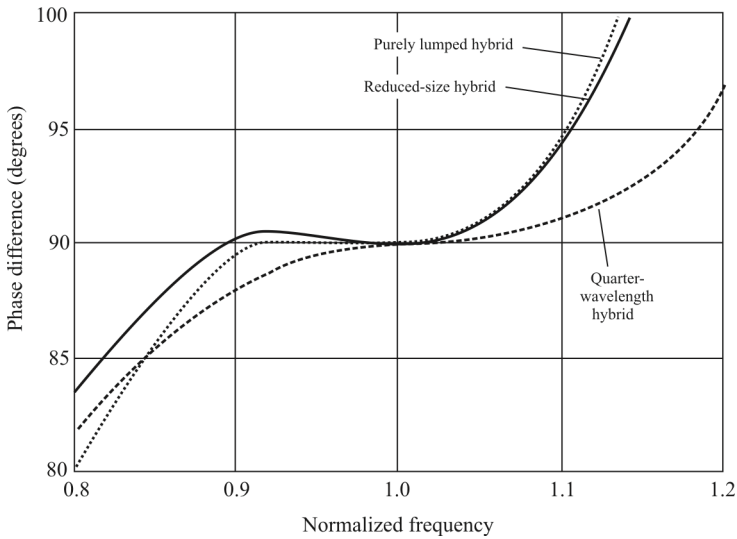
**Figure 4.23** Comparison of the three branch-line couplers.

A comparison of the three branch-line couplers is provided in Figure 4.23. The quarter wave coupler provides the best performance while the performance of the modified coupler and lumped element coupler is similar.

### 4.6.1.3 Transmission Line Transformer Coupler

One implementation of the balanced amplifier using *transmission line transformers* (TLTs) is illustrated in Figure 4.24. The hybrid for the input splitter is formed with $T_2$ and $R_1$, while the hybrid output combiner is formed with $T_3$ and
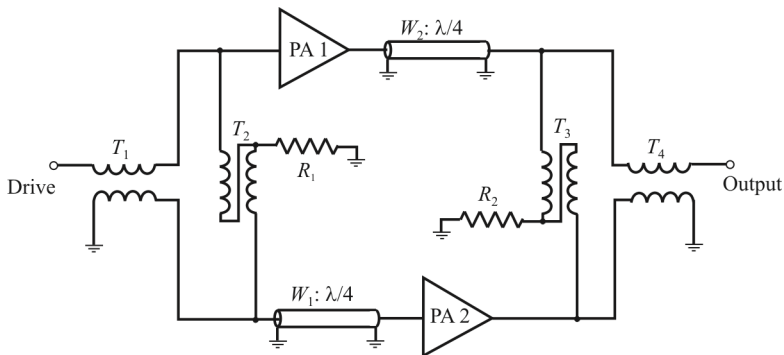


**Figure 4.24** Balanced amplifier implementation with TLT couplers.

(a)



(b)
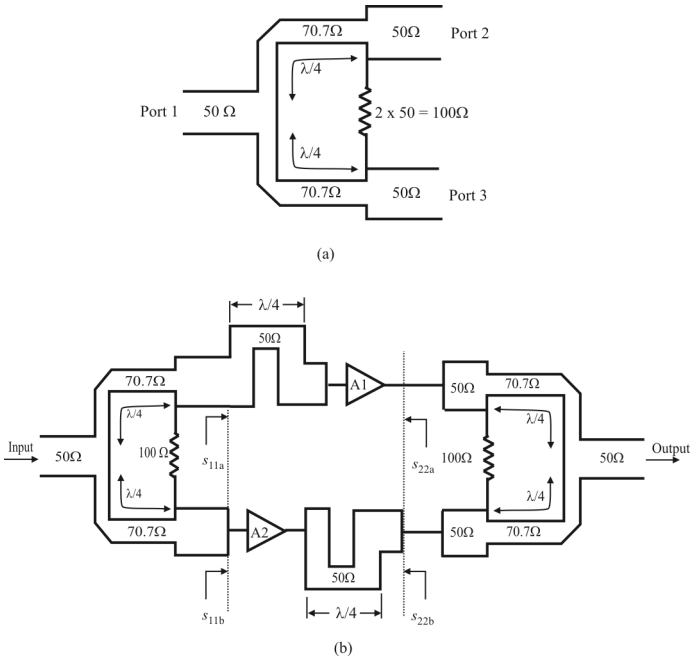
**Figure 4.25** (a) 3dB Wilkinson combiner. (b) Balanced amplifier implemented with the 3dB Wilkinson combiner. Purely lumped hybrid.

$R_2$. $T_1$ and $T_4$ are baluns that allow one side to be grounded. The required 90° phase shifts on the input and output are provided by the $\lambda/4$ transmission lines, $W_1$ and $W_2$, respectively. The transmission lines as shown are particularly applicable at microwave frequencies. For lower VHF and UHF frequency applications, lumped element T or π networks would be more applicable due to the required length for the transmission lines.

## 4.6.1.4 Wilkinson Combiners

A balanced amplifier implemented with Wilkinson combiners is illustrated in Figure 4.25. This implementation is particularly oriented toward microstrip implementations of the coupler as well as the matching networks. The scattering matrix for the Wilkinson combiner is
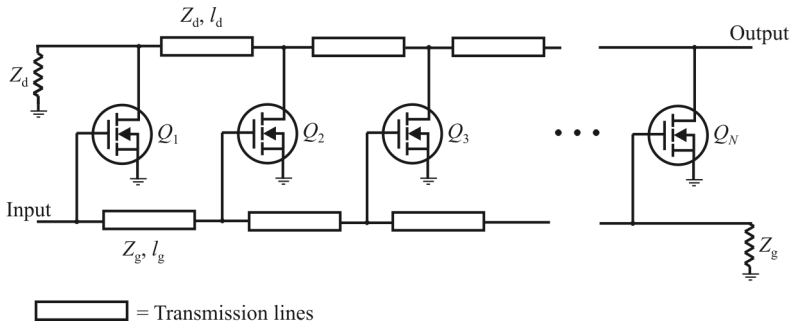
**Figure 4.26** Distributed amplifier.

$$\mathbf{S} = \begin{bmatrix} 0 & \dfrac{e^{-j\pi/2}}{\sqrt{2}} & \dfrac{e^{-j\pi/2}}{\sqrt{2}} \\ \dfrac{e^{-j\pi/2}}{\sqrt{2}} & 0 & 0 \\ \dfrac{e^{-j\pi/2}}{\sqrt{2}} & 0 & 0 \end{bmatrix} \qquad (4.90)$$

## 4.7 Distributed Amplifier

We briefly describe the concept of distributed amplification in this section. It is one of the best known methods for creating wideband amplifiers. For an in-depth coverage of the topic, the reader is referred to [16]. There are also a considerable number of technical papers on the subject [5, 17–20].

A method to solving the bandwidth limitation problem was proposed by Ginzton et al. [21] using distributed amplification. In a distributed amplifier, the gain stages are separated with transmission lines, as illustrated in Figure 4.26. Although the gain contributions of several stages are added together, the artificial transmission line isolates the parasitic capacitors of several stages. In the absence of loss, we can improve the GBW product without limit by increasing the number of stages. In practice, the improvement is limited by the loss of the transmission line. Hence, the design of distributed amplifiers requires careful electromagnetic simulations and very accurate modeling of transistor parasitics.

The term "distributed amplifier" was first coined in a paper by Ginzton et al. in 1948 [21] although the concept was actually introduced 8 years earlier in a UK patent of Percival [22].

It is well known that cascading identical amplifier stages to achieve a desired power level in the signal reduces the bandwidth of the resultant cascaded chain. As discussed above, the resultant bandwidth is given by

$$\omega_{\text{overall}} = \omega_0 \sqrt{2^{1/N} - 1} \qquad (4.91)$$

where $\omega_0$ is the bandwidth of a single stage and $N$ is the number of stages. This bandwidth reduction is due to the fact that the GBW product remains constant, so if the gain is increased, the bandwidth must be reduced. The reduction is due to the interaction of the reactances between stages (in particular, capacitive reactances). If these reactances could be isolated from one another, then the bandwidth would not be reduced. That is the principle behind the distributed amplifier. Elements (could be discrete but distributed is more common) are placed between stages that are properly phased with each other so that the desired reactance isolation occurs. This is illustrated in Figure 4.26 where transmission lines are used. It is the inductive reactance properties of the transmission lines that primarily are used to isolate the capacitive reactances of each successive stage.

The distributed amplifier shown in Figure 4.27(b) [20] consists of two transmission lines on the input and the output, and multiple transistors providing gain through multiple signal paths. The forward wave (to the right) on the input line is amplified by each transistor. The incident wave on the output line travels forward in synchronization with the traveling wave on the input line. Each transistor adds power in phase to the signal at each tap point on the output line. The forward traveling wave on the gate line and the backward wave (traveling to the left) on the drain line are absorbed by terminations matched to loaded characteristic impedance of the input line, $Z_{\text{in}}$, and output line, $Z_{\text{out}}$, respectively, to avoid reflections.

For input and output lines with equal characteristic impedances, the (voltage) gain of the distributed amplifier can be approximated by

$$A_{\text{V}} = \frac{N}{2} g_{\text{m}} Z_0 L \qquad (4.92)$$

where $N$ is the number of amplifier stages, $g_{\text{m}}$ is the transconductance of each transistor, $Z_0$ is the characteristic impedances of the input and output lines, and $L$ is the end-to-end loss of the effective transmission lines. As we see, in the absence of loss the gain can be increased by addition of extra transistor sections without a penalty on the bandwidth and hence improving the GBW product without a limit.

The transmission lines may be replaced with lumped inductors, as shown in Figure 4.27(a). These inductors together with the parasitic capacitors of the transistors form LC ladder lowpass filters at the input and output.

(a)



(b)
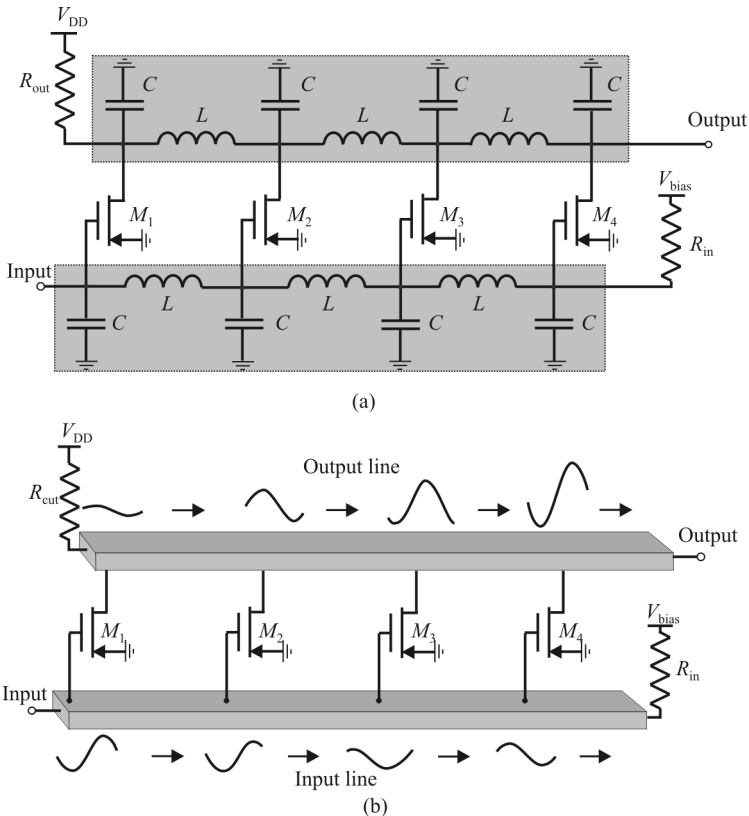
**Figure 4.27** Distributed amplifier concept: (a) lumped element and (b) transmission line.

# 4.8 Concluding Remarks

We examined some methods of enhancing the bandwidth of small-signal amplifiers in this chapter. Broadband amplifiers are required for the LNA function in the RF stage of receivers. The broader the bandwidth of these amplifiers, the fewer the number is required. Most EW receivers cover broad bandwidth since the target coverage of the systems in which they are installed is frequently not a priori known. Keeping the number of LNAs to a minimum both decreases the cost of implementation and lowers the amount of power required of the receiver.

Increasing the bandwidth invariably causes tradeoffs to be made. The principal tradeoff of concern for LNAs is the effects on the NF. Some of the methods discussed here effectively increase the NF, although the effects are not

the same for the methods discussed. As always occurs, lowering the $Q$ of tuned circuits broadens their bandwidth. This lowering almost always involves inserting loss (resistance) into the circuits. Such is the case with the lossy matching method considered. Shunt peaking does not add loss, so the effects on the NF are minimized.

# References

[1]     Lee, T. H., *The Design of CMOS Radio-Frequency Integrated Circuits*, Cambridge, U.K.: Cambridge Univ. Press, 1994.

[2]     Ahn, H. T., and D. J. Allstot, "A 0.5–4.5GHz Fully Differential CMOS Distributed Amplifier," *IEEE Journal on Solid-State Circuits*, Vol. 37, pp. 985–993, August 2002.

[3]     Hansen, W., "On Maximum Gain-Bandwidth Product in Amplifiers," *Journal of Applied Physics*, Vol. 16, 1945, pp. 528–534.

[4]     Pozar, D. M., *Microwave Engineering*, 3rd Edition, New York: Wiley, 2005, pp. 561–572.

[5]     Niclas, K. B., "On Design and Performance of Lossy Match GaAs MESFET Amplifiers," *IEEE Transactions on Microwave Theory and Techniques*, Vol. 30, No. 11, November 1982, pp. 1900–1904.

[6]     Mohan, S. S., M. dM. Hershenson, S. P. Boyud, and T. H. Lee, "Bandwidth Extension in CMOS with Optimized On-Chip Inductors," *IEEE Journal of Solid-State Circuits*, Vol. 15, No. 3, March 2000, pp. 346–355.

[7]     Analui, B., and A. Hajimiri, "Bandwidth Enhancement for Transimpedance Amplifiers," *IEEE Journal of Solid State Circuits,* Vol. 39, No. 8, August 2004, pp. 1263–1270.

[8]     Ku, W., and W. Petersen, "Optimum Gain-Bandwidth Limitations of Transistor Amplifiers as Reactively Constrained Active Two-Port Networks," *IEEE Transactions on Circuits and Systems*, Vol. CAS-22, June 1975, pp. 523–533.

[9]     Kim, H. H., S. Chandrasekhar, C. A. Burrus Jr., and J. Bauman, "A Si BiCMOS Trans-Impedance Amplifier for 10 Gb/s SONET Receiver," *IEEE Journal on Solid-State Circuits*, Vol. 36, May 2001, pp. 769–776.

[10]    Rooney, J. P., R. Parry, I. Hunter, and R. D. Pollard, "A Filter Synthesis Technique Applied to the Design of Multistage Broadband Microwave Amplifiers," *IEEE Transactions on Microwave Theory and Techniques,* Vol. 50, No. 12, December 2002, pp. 2947–2953.

[11]    Budka, T. P., "Wide-Bandwidth Millimeter-Wave Bond-Wire Interconnects," *IEEE Transactions on Microwave Theory Technology*, Part 1, Vol. 49, April 2001, pp. 715–718.

[12]    Wong, T., *Fundamentals of Distributed Amplification*, 1st Ed., Boston: Artech House, 1993.

[13]    D. M. Pozar, *Microwave Engineering*, New York: Wiley, 1994.

[14]    Bode, H., *Network Analysis and Feedback Amplifier Design*, Princeton, NJ: Van Nostrand, 1945.

[15]    Marshaf, N., "Optimizing Multistage Amplifiers for Low-Noise," *Microwaves*, April 1974, pp. 62–64; May 1974, pp. 60–64.

[16]    Wong, T. T. Y., *Fundamentals of Distributed Amplification*, Norwood, MA: Artech House, 1993.

[17]    Payne, D. V., "Distributed Amplifier Theory," *IEEE Transactions on Microwave Theory and Techniques,* Vol. MTT-31, No. 6, June 1983, pp. 759–762.

[18]    Horton, W. H., "Distributed Amplifiers: Practical Considerations and Experimental Results," *Proceedings of the IRE*, July 1950, pp. 748–754.

[19]    Jutzi, W., "Uniform Distributed Amplifier Analysis with Fast and Slow Waves," *Proceedings of the IEEE*, January 1968, pp. 66–67.

[20]    Hajimiri, A., "Distributed Integrated Circuits: An Alternative Approach to High-Frequency Design," *IEEE Communications Magazine*, February 2002, pp. 2–4.

[21]     Ginzton, E. L., W. R. Hewlett, J. H. Jasberg, and J. D. Noe, "Distributed Amplification,"
         *Proceedings of the IRE,* August 1948, pp. 956–969.
[22]     Percival, W. S., British Patent No. 460,562, July 24, 1934.

# Chapter 5

# RF Mixers and Mixing

## 5.1 Introduction

Mixers are used in EW receivers for frequency conversion, signal detection, and phase detection. Often, it is the performance of the mixer that establishes limits for the intercept point of a receiving system.  We will initially focus on the frequency conversion here since that is, by far, the most common use for mixers. Using a mixer as a phase detection device is addressed later in the chapter when oscillators are considered.

The superheterodyne receiver architecture, by far the most prolific receiver configuration in use, often has several frequency translation stages (IF frequencies) to optimize image rejection, selectivity, and dynamic range. Direct conversion receiver architectures use mixers at the input to both downconvert and demodulate the digital information. Mixers are thus widely used in the analog/RF sections of receivers. In these applications, often the mixer must be designed to handle a very wide dynamic range of signal powers at the input.

The mixer can be used for demodulation, although the trend is to digitize following a low IF frequency and implement the demodulation function digitally. They can also be used as analog multipliers to provide gain control. In this application, one input is a DC or slowly varying RSSI signal, which, when multiplied by the RF/IF signal, will control the degree of gain or attenuation.

While the nonlinearities in most electronic devices are troublesome and their elimination is fervently sought, mixers are nonlinear devices by their very nature. The process of mixing to translate signals in frequency depends heavily on the nonlinearities in mixers. It is also their greatest nemesis since such mixing generates superfluous signals that must be eliminated or at least reduced.

This chapter is structured as follows. We begin with a discussion of the RF mixing process, and the resulting signals generated. Some of these signals are desired while others are interference. We discuss some methods for dealing with these unwanted signals, including filtering and phase compensation. That is followed by a presentation on local oscillators and, in particular, phase locked
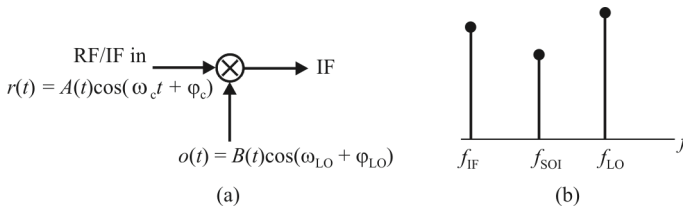
**Figure 5.1** Mixer: (a) circuit symbol and (b) spectrum. One input to the mixer comes from the RF stage [$r(t)$] and the other from the LO [$o(t)$]. The mixer multiplies them together and produces the IF signal.

loops and digital synthesizers. We conclude the chapter with some comments on phase noise generated in the oscillator and oscillator stability.

# 5.2 RF Mixers

### 5.2.1 Introduction

Mixers are used in receivers to move signals from one frequency to another. In Figure 5.1, one input from the RF stage [$r(t)$] is multiplied from the signal from the LO [$o(t)$] to produce the output IF signal. The process of multiplication generates the IF signal at the frequency desired for further processing. As we will see, other signals are generated as well, and, since the mixer is a nonlinear device unwanted spurious signals (spurs) are generated that must be eliminated or minimized.

There are two types of mixers, passive and active. Generally passive types have higher conversion losses and hence higher noise figures than active mixers, although they have better *third-order intermodulation distortion* (IMD3) performance.

Another categorization for mixers is whether they are single balanced mixers or double balanced mixers, both of which can be passive or active. Single balanced mixers are much less complex but have inferior performance in terms of RF to IF and LO to IF rejection, compared to double balanced mixers.

Some of the more important advantages and disadvantages of double balanced mixers are as follows:

*Advantages*

- Both LO and RF are balanced, providing both LO and RF rejection at the IF output.
- All ports of the mixer are inherently isolated from each other.
- Linearity is increased compared to singly balanced.

- Suppression of spurious products is improved (all even order products of the LO and/or the RF are suppressed).
- Intercept points are higher.
- Lower susceptibility to supply voltage noise due to the differential topography.

*Disadvantages*

- A higher LO drive level is required.
- Two baluns are required (although the mixer will usually be connected to differential amplifiers).
- The ports are highly sensitive to reactive terminations.

The most popular active, double balanced mixer architecture in *radio frequency integrated circuit* (RFIC) design is the Gilbert cell mixer. This type of mixer exploits symmetry to remove the unwanted RF and LO output signals from the IF by cancellation. We will explore Gilbert cell mixers later.

High-performance RF mixers use nonlinear characteristics to generate the multiplication. Thus, they also generate many undesired output frequencies. Three techniques have proven to be effective in the implementation of mixers with high dynamic range:

- Use a device that has a known and controlled nonlinearity.
- Switch the RF signal path on and off at the LO frequency.
- Sample the RF signal with a sample-hold function at the LO frequency.

## 5.2.2 Nonlinear Mixers

The nonlinear mixer can be applicable at any frequency where the device presents a known nonlinearity. It is the only approach available at the upper millimeter wave frequencies. When frequencies are low enough that good switches can be constructed, the switching mixer mode is preferred because it generates fewer spurs. In some cases, sampling has been substituted for switching.

We see that our output may contain a DC term, RF and LO feedthrough, and terms at all harmonics of the RF and LO frequencies. Only the second-order product term produces the desired output. In addition, when $r(t)$ consists of multiple carriers, the power series will also produce cross-products that make the desired output products dependent on the amplitude of other inputs. Spurious output signal strengths can be decreased when devices that are primarily square-law, such as FETs with longer gate lengths, are used in place of diodes or BJTs.

An architecture for a nonlinear mixer is shown in Figure 5.2. In this case the two signal sources are connected in series. The IF output is labeled $v_o(t)$ across the
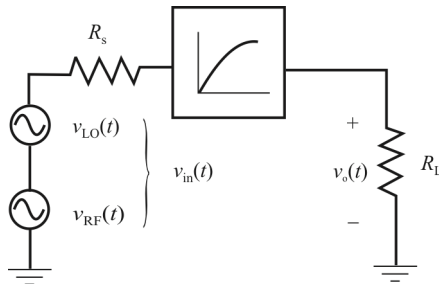
**Figure 5.2** Nonlinear mixer operation.

load $R_L$. Several devices can be used as the nonlinearity; a diode is a popular choice as we will see.

### 5.2.3 Analog Mixing

As indicated previously, analog mixing implements the following trigonometric identity:

$$2\cos(\omega_1 t)\cos(\omega_2 t) = \cos[(\omega_1 + \omega_2)t] + \cos[(\omega_1 - \omega_2)t]$$

The mixer output is comprised of two frequencies, which are the sum and difference of the two input frequencies. In a practical system, the two inputs (the SOI and a local oscillator) are sufficiently separated in frequency to allow one or the other of the output frequencies to be selected by filtering. In an ideal system, the selected output is an exact replica of the SOI, shifted up or down in frequency by an amount equal to the local oscillator frequency.

It is easy to understand how any deviation from perfect linearity will result in unwanted signals at the output. Nonlinearities can generate harmonics of the input signals, which are also multiplied, with sum and difference frequencies appearing at the output. If the input is modulated, harmonics of the modulation sidebands create further spurious signals at the output. Like the desired modulation sidebands, these spurious products of modulation are adjacent to the desired frequency, so they cannot be removed by filtering.

High-linearity analog circuits require class A bias to handle sufficient amplitude for the expected range of signal levels. With predictable signal levels, linear mixers are practical and easily implemented as typical RFICs. Integration also offers the advantages of active baluns and on-chip buffers. However, to achieve high dynamic range, these circuits consume considerable power relative to the signal levels, since high-level signal handling can be achieved only with high quiescent current. This may result in unacceptably high power consumption and heat dissipation.
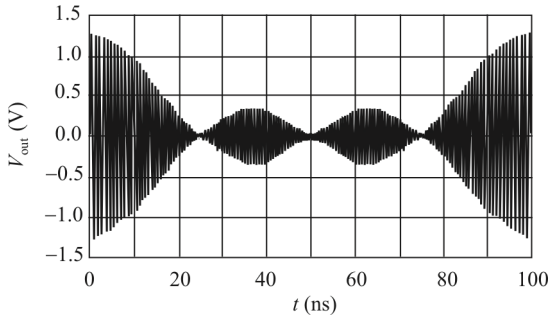
**Figure 5.3** Large signal mixer performance. Four sources at $P = 0$dBm, in phase at $t = 0$, $W = 10$ MHz. Peak signal voltage, not average power, dictates when distortion becomes excessive.

## 5.2.4 Large Signal Mixer Performance

In EW receiver applications, a mixer is often exposed to several signals within its preselected input bandwidth. It is important to understand that it is the peak signal voltage, not average signal power, that dictates when distortion becomes excessive in an amplifier or mixer. In the simulated example shown in Figure 5.3, carriers, each with 0 dBm average power, are applied to the input. Each signal is separated by 10 MHz and all four are in phase at $t = 0$. As we see, these signals will appear in phase periodically, with 4 times the peak signal voltage of a single carrier. While expressing the large-signal performance in terms of an input power in dBm is common, we must remember that the time domain instantaneous signal peaks are what stress the system. Real signals are likely to be much more complex than this, so the probability of having a large peak like this is less likely in a real application. But even infrequent overdrive and distortion generation can degrade bit error rates.

### 5.2.4.1 Gain Compression

As given in Definition 3.1, gain compression is a useful index of distortion generation. It is specified in terms of an input power level (or peak voltage) at which the small signal conversion gain falls by 1dB. When referring to the input power at this point it is denoted $IP_{1\,dB}$. When referring to the output power at this point it is denoted by $OP_{1\,dB}$. Assuming that a simple cubic function represents the nonlinearity of the signal path with

$$v_{in}(t) = V_R \sin(\omega_{RF} t) \tag{5.1}$$

we have

$$v_{RF}(t) = v_{in} - a_3 v_{in}^3 \tag{5.2}$$

$$= V_R \left(1 - \underbrace{\frac{3a_3 V_R^2}{4}}_{\substack{\text{Gain} \\ \text{compression}}}\right) \sin(\omega_{RF} t) + \underbrace{\frac{1}{4} a_3 V_R^3 \sin(3\omega_{RF} t)}_{\substack{\text{Third-order} \\ \text{distortion}}} \tag{5.3}$$

Using trig identities, we see a term that produces gain compression

$$1 - \frac{3a_3 V_R^2}{4} \tag{5.4}$$

If we know the coefficient $a_3$, we can predict the 1dB compression input voltage.

This is typically obtained by measurement of gain versus input voltage. The reduced amplitude output voltage then gets mixed down to the IF frequency. We also see a cubic term that represents the *third-order harmonic distortion* (HD3) that also is caused by the nonlinearity of the signal path. Harmonic distortion is easily removed by filtering; it is the IMD that results from multiple signals that is more troublesome to deal with. Note that in this simple example, the fundamental is proportional to $V_R$ whereas the HD3 is proportional to $V_R^3$. Thus, if $P_{out}$ versus $P_{in}$ were plotted on a decibel scale, the HD3 power will increase at three times the rate that the fundamental power increases with input power.

A typical mixer (or amplifier) transfer characteristic is illustrated in Figure 5.4. We see the output 1dB compression point, $OP_{1\,dB}$ and input 1dB compression point, $IP_{1dB}$. Unless otherwise specified, the output point is referred to. The fundamental refers to the linear transfer characteristic. Also shown are the second-order and third-order responses producing the second- and third-order intercept points. The larger these values, the better performance the mixer has.

## 5.2.4.2 Intermodulation Distortion

The gain compression power characterization provides a good indication of the signal amplitude that the mixer will tolerate before really bad distortion is generated. We should stay well below the $P_{1\,dB}$, input level. Another indicator of large-signal capability is the IMD. IMD occurs when two or more signals are present at the RF input to the mixer. The LO input is provided as before. These two signals can interact with the nonlinearities in the mixer signal path (RF to IF) to generate unwanted IMD products (distortion) that then get mixed down to IF.
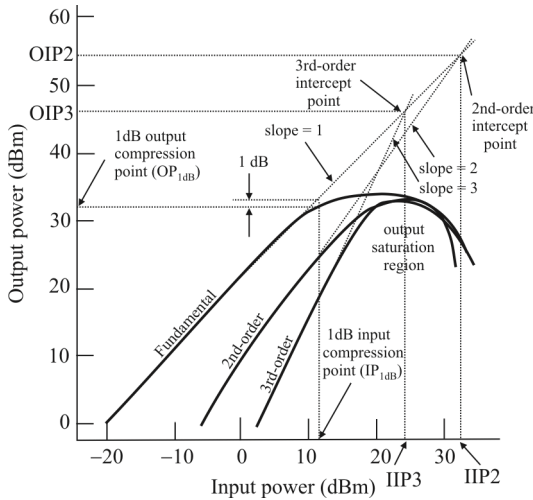
**Figure 5.4** Mixer transfer characteristic. In this case $G = 20$dB.

Let us consider the third-order nonlinearity $a_3 v_{in}^3$. Also assume that there are two signals in the RF signal $v_{in} = V_1 \sin(\omega_1 t) + V_2 \sin(\omega_2 t)$. Then

$$V_{out3} = a_3 [V_1^3 \sin^3(\omega_1 t) + V_2^3 \sin^3(\omega_2 t) \\ + 3V_1^2 V_2 \sin^2(\omega_1 t)\sin(\omega_2 t) + 3V_1 V_2^2 \sin(\omega_1 t)\sin^2(\omega_2 t)] \tag{5.5}$$

The third term on the right can be expressed as

$$\frac{3V_1^2 V_2 a_3}{2} \left\{ \underbrace{\sin(\omega_2 t)}_{\text{cross modulaton}} - \frac{1}{2}\underbrace{[\sin(2\omega_1 - \omega_2)t - \sin(2\omega_1 + \omega_2)t]}_{\text{third-order IMD}} \right\} \tag{5.6}$$

When two inputs at $\omega_1$ and $\omega_2$ are applied simultaneously to the RF input of the mixer, the cubing produces many terms, some at the harmonics and some at the IMD frequency pairs. The trigonometric identities show us the origin of these nonidealities [1].

A widely used figure of merit for IMD is the third-order intercept point (Definition 3.3). This is a fictitious signal level at which the extrapolated fundamental and extrapolated third-order product terms intersect. The input level where this intersection occurs is denoted IIP3, and the output level is denoted OIP3 (Figure 3.31).
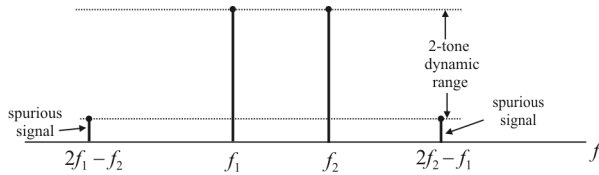
**Figure 5.5** Two-tone dynamic range. IMD3 products at $2f_1 - f_2$ and $2f_2 - f_1$ will be present in the IF output.

We typically are mainly concerned with IMD3. This is especially troublesome since it can occur at frequencies within the IF bandwidth. For example, suppose we have two input frequencies at 895.990 and 900.010 MHz. Third-order products at $2f_1 - f_2$ and $2f_2 - f_1$ will be generated at 895.980 and 900.020 MHz. Once multiplied with the LO frequency, these IMD3 products may fall within the filter bandwidth of the IF filter and thus cause interference to an SOI. IMD3 power, just as HD3 power, will have a slope of 3 on a decibel transfer characteristic graph. We show one example of this in Figure 5.5.

In addition, the cross-modulation effect can also be seen. The amplitude of one signal (say $\omega_1$) influences the amplitude of the SOI at $\omega_2$ through the coefficient $3V_1^2 V_2 a_3 / 2$ in (5.5). A slowly varying modulation envelope on $V_1$ will cause the envelope of the SOI output at $\omega_2$ to vary as well since this fundamental term created by the cubic nonlinearity will add to the linear fundamental term. This cross-modulation can have error-generating effects at the IF output. Other higher odd-order IMD products, such as fifth and seventh, are also of interest but normally are much smaller.

Note that the third-order ($m_3$) and fifth-order ($m_5$) products are quite close in frequency to the SOI ($m_1$). This means that they are often impossible to remove by filtering. The two IMD sidebands are approximately of equal power. In reality, the intercept power is 10 to 15 dB higher than the $P_{1dB}$ gain compression power, so the circuit does not amplify or operate correctly at the IIP3 input level. The third-order intercept point is indicated in Figure 5.5 and the IIP3 is indicated in Figure 5.6. The higher the IIP3, the better the large signal capability of the mixer.

It is common practice to extrapolate or calculate the intercept point from data taken at least 10 dB below $P_{1dB}$. We should check the slopes to verify that the data obeys the expected slope = 1 or slope = 3 behavior. In this example, we can see that this is true only at lower signal power levels.

5.2.4.3 Spur-Free Dynamic Range

Any real mixer or amplifier will degrade the SNR because noise is added to the signal. Therefore, $\gamma_{out} < \gamma_{in}$ so the noise factor $f_a > 0$. The *minimum detectable signal* (MDS) power is determined by noise and corresponds to a signal whose
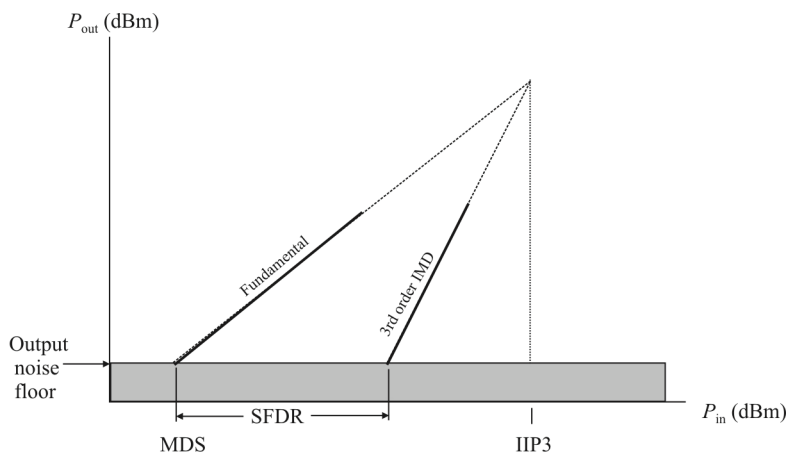
**Figure 5.6** Spur-free dynamic range.

strength just equals the noise (see Figure 5.6). The thermal noise power in bandwidth $W_n$ is $10\log_{10}(k_B T W_n)$, where $k_B$ is Boltzmann's constant and $T$ is absolute temperature (Kelvins). Thus, MDS (dBm) $= 10\log_{10}(k_B T W_n) + F_a$ since the system-generated noise adds to the ambient thermal noise. The maximum signal power is limited by distortion, which we describe by IIP3.

The *two-tone dynamic range* (also called the spur-free dynamic range, SFDR, Definition 3.4) is a measure of the mixer performance. One depiction of this parameter is illustrated in Figure 5.5. Another depiction is shown in Figure 5.6; these two concepts are equivalent. Mathematically the SFDR is given by

$$SFDR = \frac{2}{3}\left[IIP3 - MDS\right] \quad dB \qquad (5.7)$$

If the signal power is increased beyond the point where the IMD rises above the noise floor, then the SINAD dominates and degrades by 3dB for every 1dB increase in signal power. If we are concerned with the third-order distortion, the SFDR is calculated from the geometric 2/3 relationship between the input intercept and the IMD3 (5.7). It is important to remember that the SFDR depends directly on the bandwidth $W_n$. It has no meaning without specifying bandwidth.

### 5.2.5 Switching or Sampling Mixers

5.2.5.1 Mixing with Switches

A *switching mixer* (also known as a *sampling mixer*) is illustrated in Figure 5.7. This simple switch, in series with the RF source, is operated by the LO. If the LO
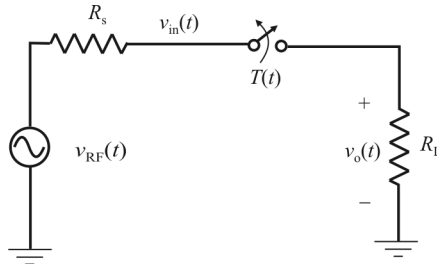
$$T(t) = \frac{1}{2} + \frac{2}{\pi}\left[\sin(\omega_{LO}t) + \frac{1}{3}\sin(3\omega_{LO}t) + \frac{1}{5}\sin(5\omega_{LO}t) + \Lambda\right]$$

No even order harmonics
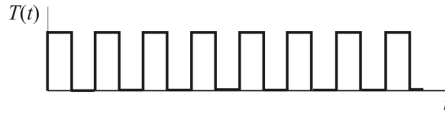


**Figure 5.7** Switching or sampling mixer.

is a square wave with 50% duty cycle, it is easily represented by its Fourier series. The symmetry causes the even-order harmonics to drop out of the LO spectrum. When multiplied by a single frequency cosine at $\omega_{RF}$, the desired sum and difference outputs will be obtained as follows. Let

$$v_{RF}(t) = A\cos(\omega_{RF}t)$$

Then

$$
\begin{aligned}
T(t)&v_{RF}(t) \\
&= AT(t)\cos(\omega_{RF}t) \\
&= \frac{A}{2}\cos(\omega_{RF}t) + \frac{2A}{\pi}\left[\begin{array}{l}\sin(\omega_{LO}t)\cos(\omega_{RF}t) + \dfrac{1}{3}\sin(3\omega_{LO}t)\cos(\omega_{RF}t) \\[2mm] +\dfrac{1}{5}\sin(5\omega_{LO}t)\cos(\omega_{RF}t) + \cdots\end{array}\right] \\
&= \frac{A}{2}\cos(\omega_{RF}t) + \frac{2A}{\pi}\left[\begin{array}{l}\dfrac{1}{2}\{\sin[(\omega_{LO} + \omega_{RF})]t] \\[2mm] + \sin[(\omega_{LO} - \omega_{RF})]t]\} + \text{higher order terms}\end{array}\right]
\end{aligned} \qquad (5.8)
$$
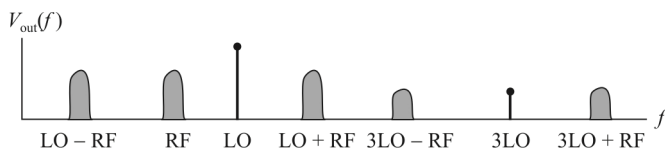
**Figure 5.8** Sampling mixer output spectrum.

When the lower frequency is the RF signal of interest ($\omega_{IF} = \omega_{RF} - \omega_{LO}$), a low-pass filter can be used to eliminate the higher order terms as well as the $\omega_{RF}$ term.

Note that everything is single-ended; there is no balancing required. There will be harmonics of the LO present at $3\omega_{LO}$, $5\omega_{LO}$, etc. that will also mix to output spurs (see Figure 5.8) as

$$\frac{A}{2}\underbrace{\cos(\omega_{RF}t)}_{\text{RF feedthrough}} + \frac{2A}{\pi}\left[\begin{array}{c}\underbrace{\sin(\omega_{LO}t)\cos(\omega_{RF}t)}_{2^{nd}\text{-order product}} + \underbrace{\frac{1}{3}\sin(3\omega_{LO}t)\cos(\omega_{RF}t)}_{4^{th}\text{-order spur}} \\ + \underbrace{\frac{1}{5}\sin(5\omega_{LO}t)\cos(\omega_{RF}t)}_{6^{th}\text{-order spur}} + \cdots\end{array}\right]$$

These harmonics also convert broadband noise that is generated internal to the mixer (or that is allowed into the mixer input in the absence of preselection and image reject filters) into the IF output band.

With an ideal switch, the ON state will be linear, passing the input directly to the output (see Figure 5.9). In the OFF state, no signal is present and, thus, no distortion products can be present. With fast ON-OFF and OFF-ON transition periods, low on-resistance in the switches, and minimal nonlinearities in other components, very high performance can be achieved.

Figure 5.9 is the equivalent circuit of a switching mixer, using the common ring topology and showing the active devices as ideal switches plus their associated on and off resistances, $R_{on}$ and $R_{off}$. The diode ring version was analyzed in 1967 by Walker [2], and the FET switch version was described in 1986 by Oxner [3].

For a switching mixer with ideal elements, the optimum conversion loss in decibels is [3]

$$L_C = 10\log_{10}\frac{4}{\pi^2} = 3.92\,\text{dB} \tag{5.9}$$

The total loss consists of (a) the result of the fundamental being split into the sum and difference frequency outputs (3dB); and (b) the sum of the mixing
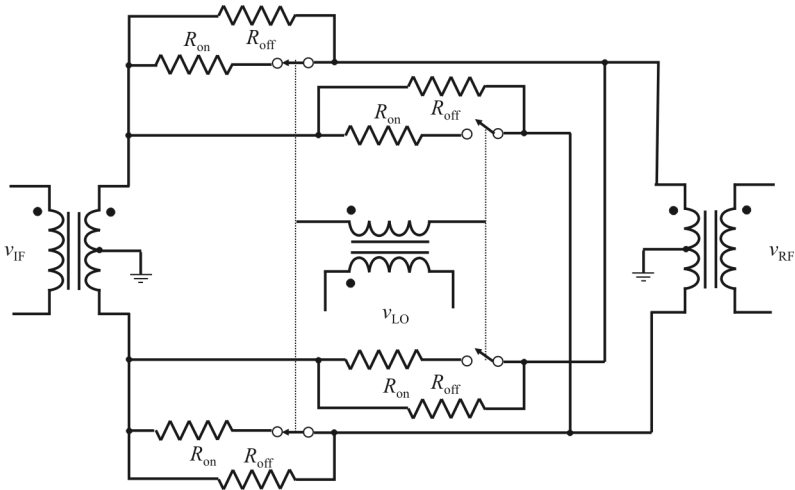
**Figure 5.9** Circuit diagram of a ring mixer, showing the switching components and their associated finite on and off resistances.

products resulting from the harmonics of the local oscillator switching frequency. Of course, a practical mixer has nonideal components, and the conversion loss is greater.

### 5.2.5.2 Balanced Switching Mixer

Digital signal processing has shortened the RF/microwave path between the front end and baseband in modern receivers. Sometimes that path includes little more than a bandpass filter followed by two mixer/detectors that deliver $I$ and $Q$ signals to the baseband processor. Without the usual IF filter to provide additional selectivity, the performance of the mixer has an even greater effect on the receiver's ability to reject unwanted signals.

*Single Balanced Mixer*

A single balanced mixer is shown in Figure 5.10. The RF feedthrough can be eliminated by using a differential IF output and a polarity reversing LO switch. The amplifier here is a transconductance amplifier, characterized by $I_{out} = g_m V_{in}$; that is, the amplifier does a voltage-to-current conversion. The load resistors perform a linear current-to-voltage conversion. The switch reverses the polarity of the RF current.
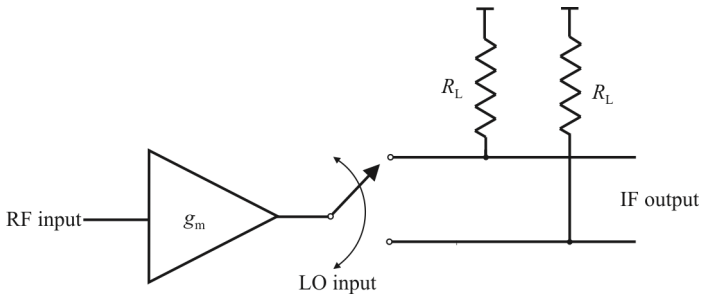
**Figure 5.10** Single balanced mixer.

*Double Balanced Mixer*

The RF feedthrough can be eliminated by using a differential IF output and a polarity reversing LO switch as shown in Figure 5.11. The polarity reversing LO switching function is

$$T(t) = T_1(t) + T_2(t)$$

where

$$T_1(t) = \frac{1}{2} + \frac{2}{\pi}\left[\sin(\omega_{LO}t) + \frac{1}{3}\sin(3\omega_{LO}t) + \cdots\right]$$
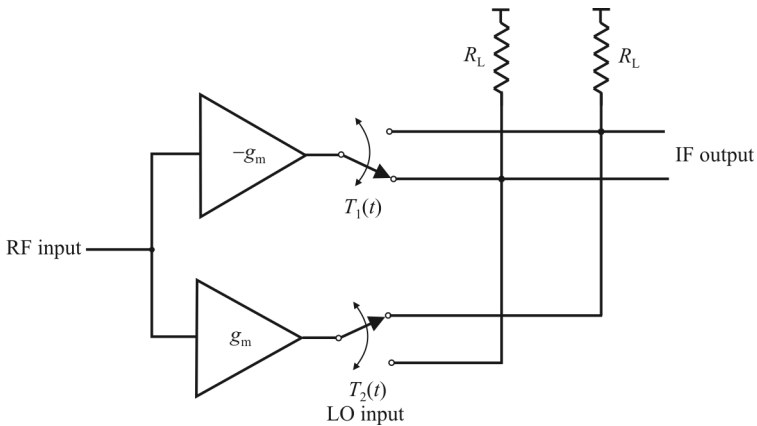


**Figure 5.11** Double balanced mixer.
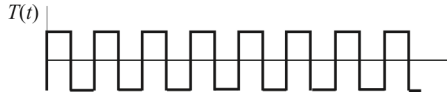
**Figure 5.12** Balanced switching mixer LO.

$$T_2(t) = -\frac{1}{2} + \frac{2}{\pi}\left[\sin(\omega_{LO}t) + \frac{1}{3}\sin(3\omega_{LO}t) + \cdots\right]$$

*T*(*t*) is shown in Figure 5.12.

When added together, the DC terms (1/2 and −1/2) cancel. The DC term was responsible for the RF feedthrough in the unbalanced mixer since the $\cos(\omega_{RF}t)$ term was only multiplied by $T_1(t)$. The IF signal is now

$$v_{IF}(t) = g_m R_L V_R \cos(\omega_{RF}t)\frac{4}{\pi}\left[\sin(\omega_{L0}t) + \frac{1}{3}\sin(3\omega_{LO}t) + \frac{1}{5}\sin(5\omega_{LO}t) + \cdots\right] \qquad (5.10)$$

with a second-order term

$$\frac{2g_m R_L V_R}{\pi}\left[\sin(\omega_{RF} + \omega_{LO})t + \sin(\omega_{RF} - \omega_{LO})t\right] \qquad (5.11)$$

Here we see that the ideal conversion gain $(v_{IF}/v_{RF})^2 = (2/\pi)^2$ is 6dB greater than for the unbalanced topology. But, we can still get LO feedthrough if there is a DC current in the signal path. This is often the case since the output of the transconductance amplifier will have a DC current component. This current shows up as a differential output.

An ideal double balanced mixer consists of a switch driven by the LO that reverses the polarity of the RF input at the LO frequency [4] and a differential transconductance amplifier stage. The polarity reversing switch and differential IF cancels any output at the RF input frequency since the DC term cancels as was the case for the single balanced topology. The double LO switch cancels out any LO frequency component, even with currents in the RF to IF path, since we are taking the IF output as a differential signal and the LO shows up now as common mode. Therefore, to take full advantage of this approach, an IF balun, either active (a differential amplifier) or passive (a transformer or hybrid), is required. The LO is typically suppressed by 50-or 60-dB if the components are well matched and balanced. To get the highest performance from the mixer, we must make the RF to IF path as linear as possible and minimize the switching time of the LO switch. The ideal mixer above would not be troubled by noise (at the low end of the dynamic range) or IMD at the high end since the transconductors and resistors are linear and the switches are ideal.
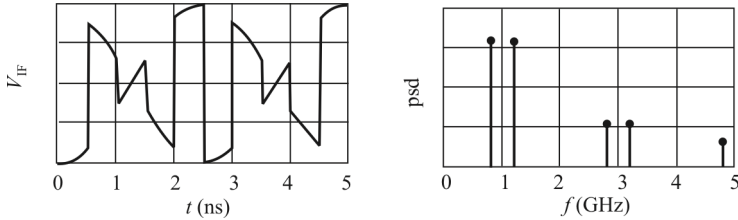
**Figure 5.13** Double balanced mixer output $f_{RF}$ = 200 MHz, $f_{LO}$ = 1.0 GHz, $f_{IF}$ at 800 and 1,200 MHz.

The IF signal expanded, while keeping only the first- and second-order terms, is

$$v_{IF}(t) = \frac{4R_L}{\pi}\left\{I_{DC}\sin(\omega_{LO}t) + \frac{1}{2}g_m V_{RF}[\sin(\omega_{RF}+\omega_{LO})t + \sin(\omega_{RF}-\omega_{LO})t]\right\} \qquad (5.12)$$

so we see that we can still get LO feedthrough if we use a single-ended output or there is a DC current in the signal path. That is due to the $[4R_L I_{DC}\sin(\omega_{LO}t)]/\pi$ term in (5.12). There is often DC present since the output of the transconductance amplifier will have a DC current component. This current shows up as a differential output.

*Output Spectrum*

Simulation results of an example differential output voltage and spectrum are shown in Figure 5.13.

In real mixers, there is always some imbalance. Transistors and baluns are never perfectly matched or balanced. These nonidealities will produce some LO to IF and/or RF to IF feedthrough. This is usually specified in terms of a power ratio relative to the desired IF output power denoted as dBc.

Since the RF to IF path is not perfectly linear, this will lead to IMD. Odd-order distortion (typically the third and fifth orders are most significant) will cause spurs within the IF bandwidth or cross-modulation when strong signals are present. Also, the LO switches are not perfectly linear, especially while in the transition region. This can add more distortion to the IF output and will increase loss due to the resistance of the switches.

Some performance specifications relate to the mixer's ability to process very weak and very strong signals. We would like to maximize mixer performance by:

- Maximizing linearity in the signal path
- Ideal switching: high slew rates
- Minimizing noise contributions

5.2.5.3 Intermodulation Distortion

The causes of IMD are the various non-linearities that occur when nonideal components are used in practical circuit. For a switching mixer, these include [5]:

- Improper termination of the ports, which causes signals reflecting back into the mixer
- Discontinuity in switching action at zero crossings due to the voltage drop in diodes and gate voltage threshold of FET switches
- Modulation of $R_{on}$ in the switching devices by high signal levels
- Finite rise and fall times, which can create discontinuities and imbalance

Also, in a balanced mixer, any deviation in the component values will unbalance the circuit, allowing even-order products to appear at the output. Because switching mixers rely on fast rise and fall times, the following expression can predict the improvement in the relative intermodulation performance (in decibels) as a function of LO rise/fall time:

$$\text{Relative IMD} = 20\log_{10}\left[\left(T_r \omega_{LO} \frac{V_{RF}}{V_{LO}}\right)^2 / 8\right] \tag{5.13}$$

where $T_r$ is the rise/fall time of $v_{LO}$, $\omega_{LO}$ is the local oscillator frequency, $V_{RF}$ is the peak signal voltage, and $V_{LO}$ is the peak-to-peak local oscillator voltage.

This expression illustrates that IMD improvements occur if the signal voltage is reduced, the LO voltage is increased, the LO frequency is lower (low-side injection) and if the rise/fall time is reduced. In practice, each of these factors has its limitations. Lower $V_{RF}$ degrades the SNR, higher $V_{LO}$ increases power consumption, and the LO frequency often cannot be changed. Depending on the frequency of operation and the devices being used, rise and fall time may be improved.

5.2.5.4 Summary

This section has presented basic information on mixers as switching circuits. This type of analysis can lead to very high-dynamic-range implementations, and there are volumes of information on the development and application of high performance switching mixers.
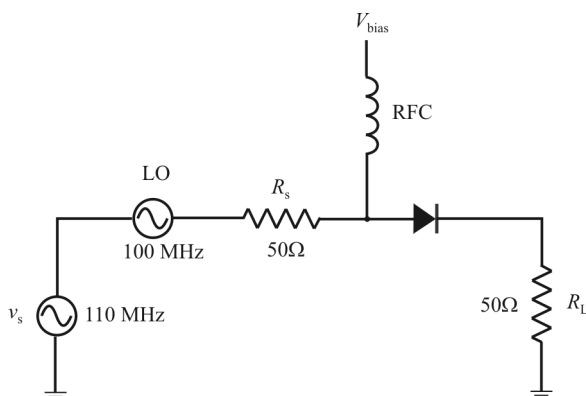
**Figure 5.14** Unbalanced diode mixer.

## 5.2.6 Some Passive Mixers

Passive mixers are widely used because of their relative simplicity, wide bandwidth, and good IMD performance. The transformers or baluns generally limit the bandwidth. They must introduce some loss into the signal path, however, which can be of some concern for the NF. As discussed in Chapter 3, an LNA can be introduced ahead of the mixer, usually with some degradation in IMD performance.

Active mixers are preferred for RFIC implementation. They can be configured to provide conversion gain and can use differential amplifiers for active baluns. Because of the need for additional amplifier stages in the RF and IF paths with fully integrated versions, it is often difficult to obtain high third-order intercepts and 1dB compression points with active mixers.

### 5.2.6.1 Diode Mixers

An unbalanced diode mixer is illustrated in Figure 5.14. The two signal sources, $v_s$ and LO, are connected in series. The diode is forward biased through the *RF choke* (RFC) so that its operating point is in its nonlinear region (Figure 5.15). The IF output across $R_L$ is shown in Figure 5.16. In Figure 5.16 we can see that there are many spurious outputs generated. Ideally, we would like to see outputs only at 10 MHz and 210 MHz. So, we prefer the switching-type mixer when the RF and LO frequencies are low enough that we can make high-performance switches. This extends into the millimeter wave spectrum.

### 5.2.6.2 Diode Doubly Balanced Mixer

A diode doubly balanced mixer is shown in Figure 5.17. The diode double-balanced quad mixer is very popular and available in a wide variety of frequency
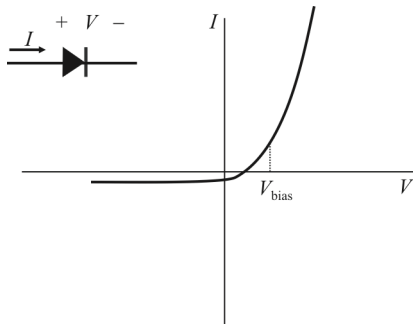
**Figure 5.15** Diode characteristic.
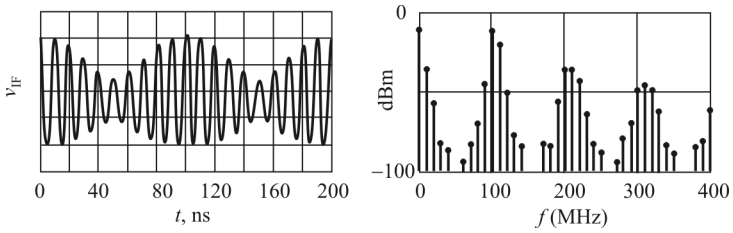


**Figure 5.16** Unbalanced diode mixer output.
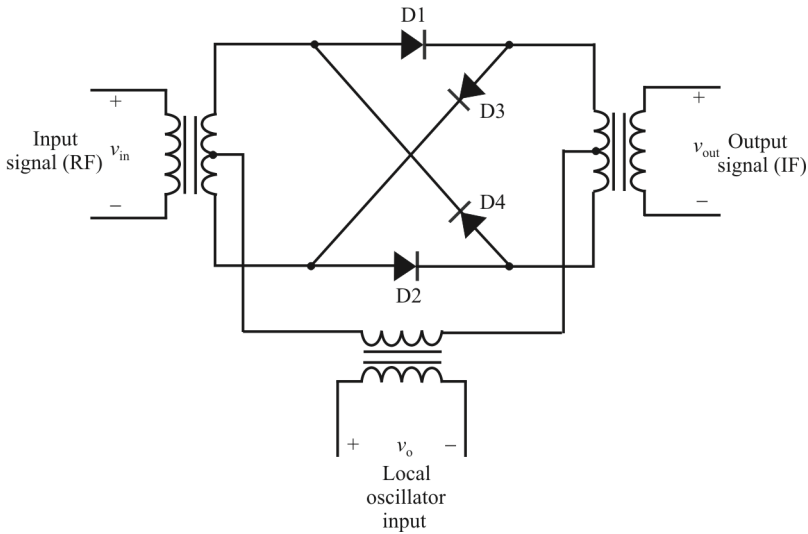
**Figure 5.17** Diode doubly balanced mixer.

bandwidths and distortion specifications. The diodes act as polarity reversing switches. When the left of the LO transformer is positive, D1 and D2 conduct, while D3 and D4 are reverse biased. When the right side is positive, D3 and D4 conduct while D1 and D2 are reverse biased, and the polarity is reversed. Both LO and RF feedthrough are suppressed by the symmetry and balancing provided by the transformers. The LO signal at the RF and IF ports appears to be a virtual ground for either LO polarity.

Since the LO signal must switch the diodes on and off, a large LO power is required, typically 7dBm when one diode is placed in each leg, and 17dBm with two diodes per path. With this considerable LO power; even with good isolation, there may still be significant LO in the IF output. When the diodes are conducting with LO current much greater than the RF current, the mixer should behave linearly. At large RF signal powers, the RF voltage modulates the diode conduction, so significant distortion will result. The diodes are also sensitive to RF modulation when they are biased close to their threshold current ($I_T$)/voltage ($V_T$)[1]. For both reasons, we prefer high LO drive with a fast transition (high slew rate—a square wave LO is better than sine wave) between on and off. The IMD performance is very poor with small LO power.

---

[1] The threshold voltage is the voltage at which a forward biased diode will start conducting current. $V_T \approx 0.7$ V for silicon and $V_T \approx 0.3$ V for germanium.
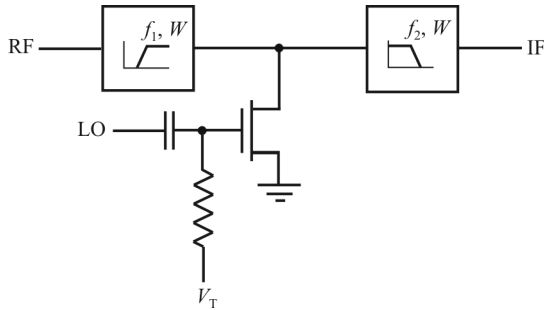
**Figure 5.18** Low IMD FET mixer.

## 5.2.6.3 Simple FET Mixer

Another popular mixer utilizes only one FET in its simplest form as seen in Figure 5.18. The LO signal switches the FET on and off. The gate is biased close to threshold. The channel resistance of the FET therefore becomes time dependent and provides a switching mixer behavior. The RF input and IF outputs are separated by highpass (HPF) and lowpass (LPF) filters, respectively. The surprising thing about this design is the high $P_{1\ dB}$ and IIP3 that it can deliver. On the down side, we must do some balancing to get rid of significant LO to IF feedthrough.

The mixer RF to IF path will be quite linear if the total drain voltage ($V_{DS}$) remains small. As illustrated in Figure 5.19, the MOSFET exhibits quite linear channel resistance up to at least a $V_{DS}$ of ±250mV. The device width and LO voltage can be optimized for performance.

There is one significant problem with this mixer design, however. There is a very large LO feedthrough to the IF port due to the large $C_{GD}$ of the MOSFET. We can reduce this by designing a better HPF or inserting a resonant LO trap in the output. Probably a better way is to use double balancing, although this will require 4 FETs and some transformers.
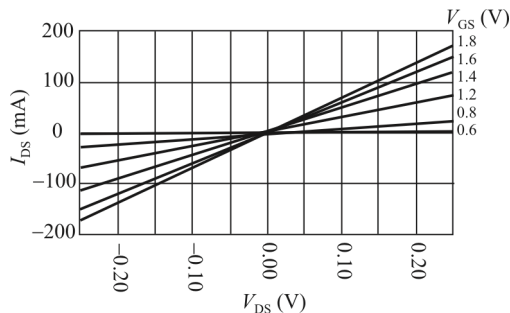


**Figure 5.19** FET channel resistance. The slope of each line is $1/R_{DS}$ at the indicated values of $V_{GS}$.

$V_{GG}$

LO in

RF in

IF out
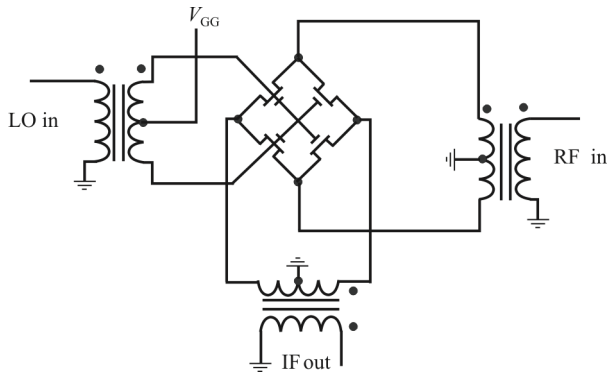
**Figure 5.20** MOSFET ring mixer.

OIP3 is reasonably high for this simple mixer.

### 5.2.6.4 MOSFET Ring Mixer

A MOSFET ring mixer is illustrated in Figure 5.20. Operation of this mixer is similar to the diode balanced mixer discussed previously.

The channel resistance of a large FET when in its triode region (below saturation) can be quite low and is not as current dependent as the diode. Therefore, switching configurations using FETs can be more linear in the RF to IF path than diode switching mixers.

The conversion loss is similar to the diode mixer. However, large LO drive voltage is needed (1 to 5V).

With the FET ring mixer, devices alternate polarity between the RF input and IF output. If the devices were ideal switches, then the input and output would be directly connected. Thus, transformers with identical turns ratios should be used. The impedance level at the FET ring should be much higher than the series resistance of the FETs in order to reduce conversion losses. This may also help with linearity. If the impedance is too high, however, LO feedthrough may be higher and frequency response more limited. So some optimization is needed.

The RF and LO impedances at the diode ring theoretically should be determined and matched at all of the relevant harmonics [6]. For most designs, optimizing the transformer ratios with the IF port connected to 50Ω should be sufficient, since we cannot select impedances at each frequency independently, and this approach would not be possible for a broadband design such as this.

*Passive Mixer Output Loading*

Since these passive diode switch mixers are bilateral—that is, the IF and RF ports can be reversed, the performance of the mixer is very sensitive to the termination
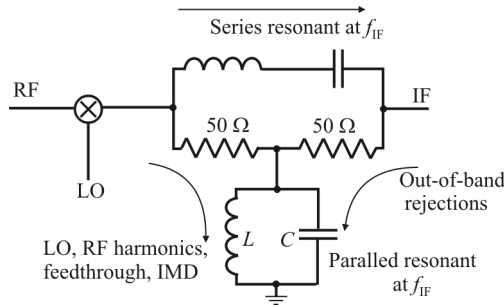
**Figure 5.21** Passive diplexer.

impedances at all ports. A wideband resistive termination is needed to absorb not only the desired IF output but also any images, harmonics, and IMD signals. If these signals are reflected back into the mixer, they will remix and show up at the RF port and again at the IF port. The phase shifts associated with the multiple replicas of the same signals can seriously deteriorate the IMD performance of the mixer.

The passive diplexer shown in Figure 5.21 provides a low-loss forward path through the series resonant branch. At $f_{IF}$, the parallel resonant branch has high impedance and does not load the IF. Outside of the IF band the series resonant branch presents high impedance and the parallel resonant branch low reactive impedance. At these frequencies, above (through $C$) and below $f_{IF}$ (through $L$), the resistors terminate the output. The farther away from $f_{IF}$, the better the match.

An active wideband termination is illustrated in Figure 5.22. When the maximum frequency at the input is well below the $f_T$ of the transistor, this common base stage provides wideband resistive impedance. The bias current can be set to provide a 50Ω input impedance. Alternatively, the BJT can be biased at higher current levels and a series resistor added at the input. Of course, this degrades noise but will improve IMD performance. The amplifier must be capable of handling the power levels of the mixer without distortion.
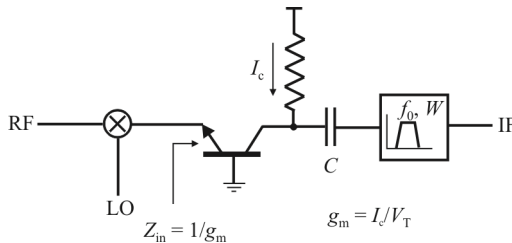


**Figure 5.22** Active wideband termination.
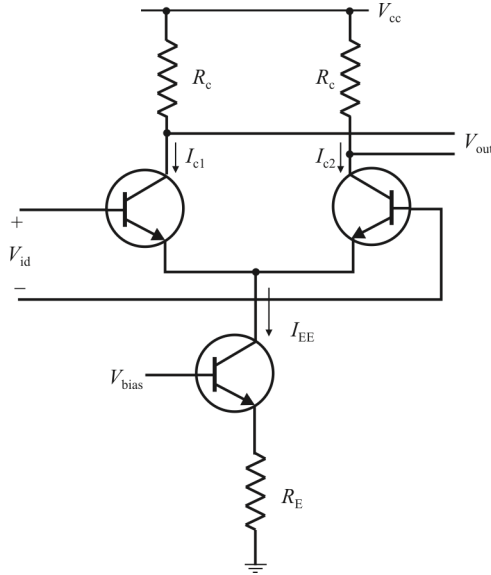
**Figure 5.23** Differential pair as a mixer.

### 5.2.7 Some Active Mixers

A differential pair is the basis for active mixers (Figure 5.23). The emitter-coupled pair can be used to provide multiplication if the input range limitations are observed. Here we have a differential transconductance stage with voltage $V_{id}$ as input and $\Delta I_c$ as output. If $V_{id} \ll 2V_T$, then

$$\Delta I_c \approx I_{EE}(V_{id} / 2V_T) = g_m V_{id}$$

Since the transconductance $g_m = I_{EE} / 2V_T$ can be varied with $I_{EE}$, a second input can be added that will produce 2 quadrant multiplication. Let

$$\Delta I_c = I_{c1} - I_{c2} = I_{EE} \tanh(V_{id} / 2V_T)$$

where

$$V_{id} = V_{in+} - V_{in-}$$

Let $u = V_{id}/2V_T$. $\tanh(u)$ is plotted in Figure 5.24.
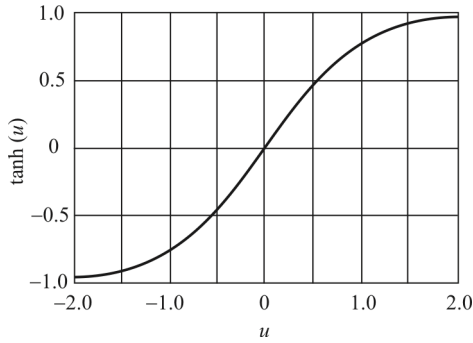
**Figure 5.24** Differential pair characteristics.

## 5.2.7.1 Single Balanced Active Mixer

A single balanced active mixer is shown in Figure 5.25. For this network

$$I_{EE} = \frac{V_{i2} - V_{BE}}{R_B}$$

and

$$\Delta I_c \approx \left( \frac{V_{i2} - V_{BE}}{R_B} \right) \left( \frac{V_{id}}{2V_T} \right)$$
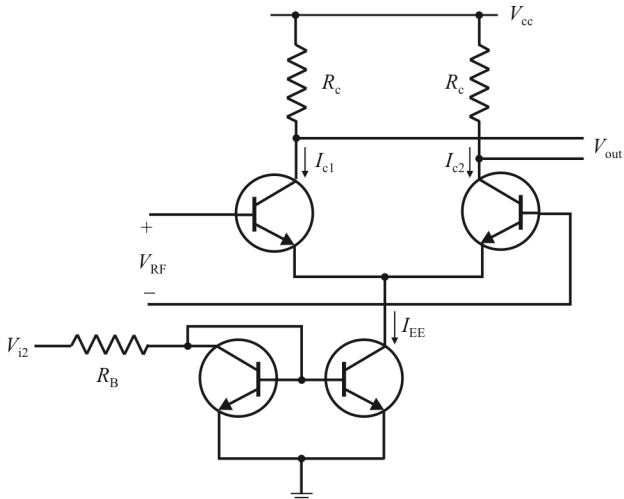


**Figure 5.25** Single balanced active mixer.

But $V_{i2} > V_{BE}$ and $V_{id}$ must be small, much less than $V_T$. For these reasons, there is rather limited use. So, we really should go one step further and use a doubly balanced mixer to suppress the LO feedthrough. That leads us to the Gilbert cell mixer.

5.2.7.2 Gilbert Cell Mixer

This double-balanced active mixer was first described in the 1960s by Barrie Gilbert, who was awarded the patent. Figure 5.26 shows a BJT implementation of the Gilbert cell. However, other active devices can be used as well (such as MOSFETs). Some observations on this circuit:

- $Q_1$–$Q_4$ provide a fully balanced, phase reversing switch. When $V_{RF} = 0$, $I_{OUT}$ is also 0 regardless of the status of $V_{LO}$. This is because $I_{C1-3}$ and $I_{C2-4}$ each will add up to $I_{EE}/2$ in this condition. When $V_{LO} \neq 0$, the same condition applies. Therefore, there is never any LO component in the output differential current. The upper tier of BJTs only provides the phase reversal of the RF signal as controlled by the LO voltage.
- The mixer can provide conversion gain—depending on the load impedance presented to the collectors and $I_{EE}$.
- The signal handling capability is still limited below $V_T$, but with emitter degeneration the linearity is improved.
- The distortion is entirely odd-order for perfectly matched transistors.

Other features of the Gilbert cell mixers are:

- They are easily integrated with other circuits.
- They exhibit better isolation than the double balanced diode or FET mixers.
- They require less LO power than the passive mixers.
- They are less fussy about IF termination impedance than the passive mixers due to the better isolation.
- Their main liability is large signal handling capability. They cannot handle as much signal as the passive mixers.

The Gilbert cell mixer shown in Figure 5.26 is a very popular method of mixing signals. It is a compact approach to combining a differential amplifier with a phase reversing switch mixer and is efficiently implemented as an integrated circuit, thus its modern popularity. One of its more significant virtues is that it can multiply in all four quadrants. Another is that frequently the differential amplifier
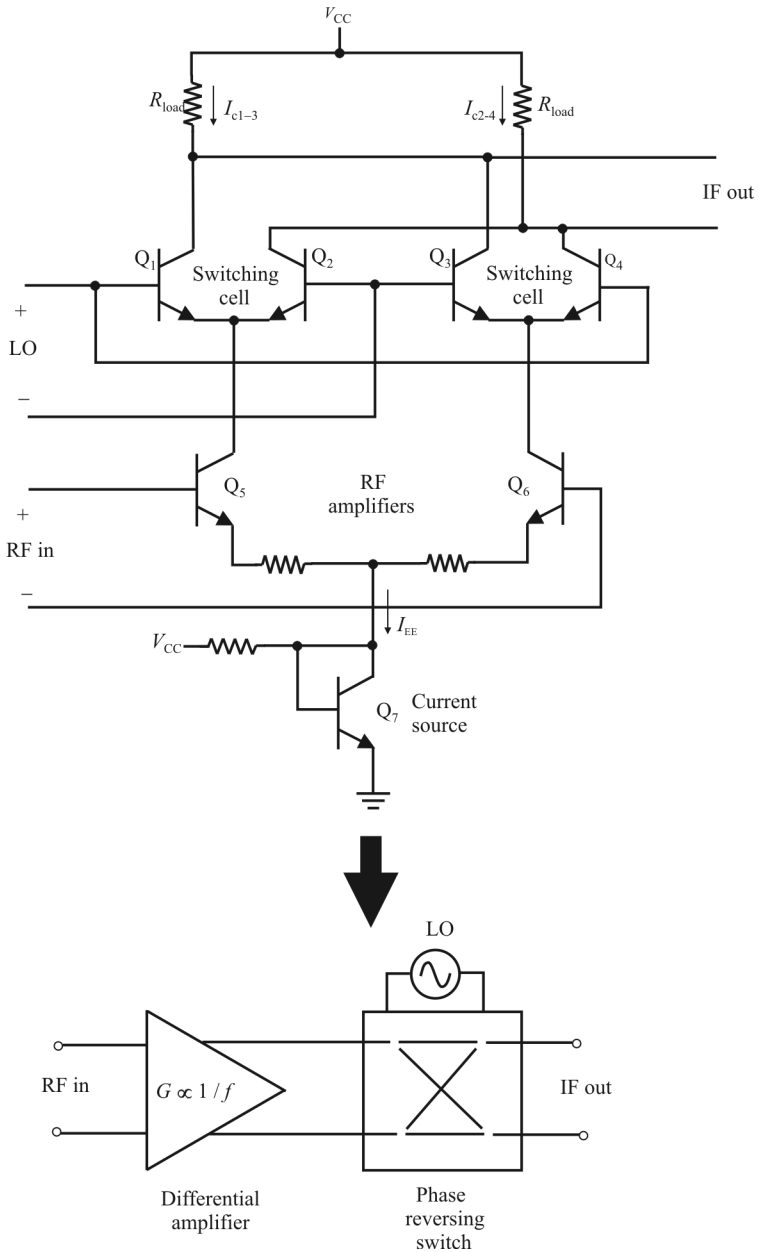
**Figure 5.26** Gilbert cell mixer.

provides unbalanced to balanced transformation. The switching transistors can also operate with an unbalanced input. However, the best even-order distortion performance and LO to IF isolation are obtained with balanced inputs.

With no filter between the differential amplifier and the switching cell, the gain of the mixer has the $1/f$ slope of the amplifier. Shunt resistors across the RF input will improve the flatness, provide an input match, and add noise. The lack of an image frequency filter between the RF amplifier and the mixer degrades the NF by more than 3dB, if the LO is above the RF frequency. If two such mixers are used in an image reject configuration, the image noise from the differential RF amplifiers will not be rejected. This is a severe disadvantage compared with a passive mixer followed by an IF amplifier of modest gain.

For best NF and IIP3 performance the LO voltage drives the switching cell transistors rapidly through the crossover, or phase reversing, region.

*Mixer Operation*

The RF signal is applied to the transistors $Q_5$ and $Q_6$, which perform a voltage-to-current conversion. For correct operation these devices should not be driven into saturation, and therefore, signals considerably less than the 1dB compression point should be used. The resistors in the emitter paths provide for expanded dynamic range by adding degeneration.

$Q_1$ through $Q_4$ form a multiplication function, multiplying the linear RF signal current from $Q_5$ and $Q_6$ with the LO signal applied across $Q_1$ to $Q_4$, which provide the switching function. $Q_5$ and $Q_6$ provide $\pm$RF current and $Q_1$ and $Q_4$ switch between them to provide the RF signal or the inverted RF signal to the left load. $Q_3$ and $Q_4$ switch between them for the right load. The two load resistors, $R_{load}$, form a current to voltage transformation giving a differential output IF.

*Linearity of RF–IF path*

We have seen that the RF input differential pair converts the input voltage into a differential current. We want the RF–IF path to be very linear. We can analyze the transfer function for linearity and distortion with

$$\Delta I = I_{EE} \tanh(V_{LO} / 2V_T) \tanh(V_{RF} / 2V_T)$$

The LO input is intentionally overdriven so that it is just acting as a polarity switch. So we only need to investigate the behavior of the RF port. Let us normalize as $u = V_{RF}/2V_T$. Then the gain is proportional to the derivative of tanh $u$:

$$\text{gain} = I_{EE} \text{sech}^2 u$$
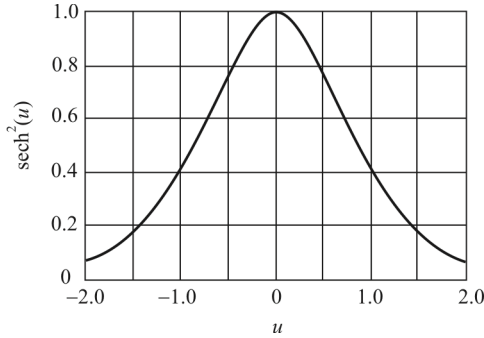
**Figure 5.27** Gilbert gain for RF input.

We must remember that it is the instantaneous peak voltage at the input that drives the stage into nonlinearity, not the average voltage. From the graph in Figure 5.27, we can see that the $\text{sech}^2$ function is not very linear.

The incremental gain predicted by the $\text{sech}^2 u$ function is down by 10% for inputs with a peak-to-peak voltage as small as $u = 0.66$ or 34mV. This is very close to the 1dB gain compression input power, $IP_{1dB}$. The $50\Omega$ referred input power that corresponds to this is $-15.7$dBm, not a very high $IP_{1dB}$.

The $\tanh u$ is not very linear either. To predict third-order harmonic or IMD produced by the tanh function, we use a Taylor series approximation. This series is given by

$$\tanh u = u - \frac{1}{3}u^3 + \frac{2}{15}u^5 - \cdots \tag{5.14}$$

We use the first two terms in (5.14), which is accurate to 1% to $u = 0.6$:

$$\tanh u \approx u - \frac{1}{3}u^3 \tag{5.15}$$

Figure 5.28 shows the difference between $\tanh u$ and (5.15).

Let $u = U \sin \omega t$, then

$$\tanh(U \sin \omega t) \approx U \sin \omega t - \frac{1}{3}(U \sin \omega t)^3$$

$$= U \sin \omega t - \frac{1}{12}U^3[3\sin \omega t - \sin(3\omega t)]$$
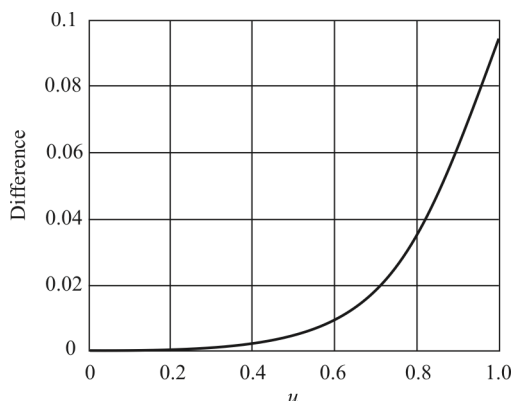
**Figure 5.28** Difference between tanh $u$ and (5.15).

$$= U\left(1 - \frac{U^2}{4}\right)\sin \omega t + \frac{1}{12}U^3 \sin(3\omega t)$$

Now choose some small single frequency value for $U$. We can calculate the fundamental and third harmonic amplitudes from the series terms and predict the harmonic distortion.

Let $U = 0.01$. This corresponds to an amplitude of $U \times 52\text{mV}$ or a power $P_{IN}$ (in $50\Omega$) of $V^2/2R = 2.7$ nW or $-55.7$dBm. Then, the fundamental term

$$U\left(1 - \frac{U^2}{4}\right) = 0.00999$$

which is negligible gain compression. Therefore $P_{OUT}$ is $-55.7$dBm and the third harmonic is

$$\frac{1}{12}U^3 = 8.33 \times 10^{-8}$$

for a $P_3$ of $-157$dBm.
    Now

$$P_{3OI} = P_{IN} + \frac{P_{OUT} - P_3}{2} = -5\,\text{dBm} = \text{IIP3}$$

Note that the calculation can be reversed to predict what input $U$ is required for a
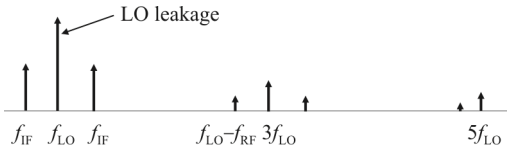
**Figure 5.29** Switching mixer output spectrum.

known HD3 level (dBc) as predicted by $P_{3OI}$. The HD3 level is specified by decibels relative to the carrier (dBc), $P_{OUT} - P_3$ (dB below the fundamental power "carrier" = c).

### 5.2.8 Isolation

Isolation can be quite important for certain mixer applications. For example, LO to RF leakage can be quite serious in direct conversion receiver architectures because it will remix with the RF and produce a DC offset at the IF output. Large LO to IF leakage can degrade the performance of a mixer postamplifier if it is located prior to IF filtering. LO leakage is depicted in Figure 5.29.

### 5.2.9 Conversion Gain

*Conversion gain* is defined as the ratio of the IF output power to the available RF source power. If the source and load impedances are different, the power gain must account for this as (Figure 5.30).

$$\text{Conversion Gain} = \frac{\text{Output power at } f_{IF}}{\text{RF available input power}} = \frac{4R_S v_{IF}^2 / R_L}{v_{RF}^2} \qquad (5.16)$$

Active or passive implementations can be used for the mixer. Each has its advantages and disadvantages. The passive implementations using diodes as nonlinear elements or switches or FETs as passive switches always exhibit conversion loss rather than gain. This can impact the overall system noise
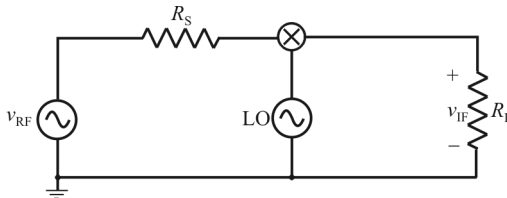


**Figure 5.30** Conversion gain.

performance, so if noise is critical, as it usually is for EW receivers, an LNA is usually added before the mixer as we considered in Chapter 3.

We see that the simple switching mixer has low conversion gain because the voltage gain $A_V$ is only $1/\pi$. Also, the RF feedthrough problem and, in most instances, an LO feedthrough problem exist. All of these deficiencies can be improved by the use of balanced topologies, which provide some cancellation of RF and LO signals as well as increasing conversion gain.

## 5.2.10 Mixer Noise

Noise power in the RF and image bands mixes with the LO and translates to the IF frequency whether RF and image signals are present or not as shown in Figure 5.31. A mixer's noise characterization is performed using one of two methods:

- Single-sideband (SSB)
- Double-sideband (DSB)

For SSB, output noise power is assumed to originate at the input from the RF frequency band. DSB assumes that output noise power originates from both the RF and image frequency bands. Under either assumption, the mixer has both an image response and an RF response. Both responses usually have nearly the same conversion efficiency. When image and RF conversions are equivalent, the DSB noise temperature is half the SSB noise temperature; thus, the SSB NF is 3dB greater than the DSB NF.
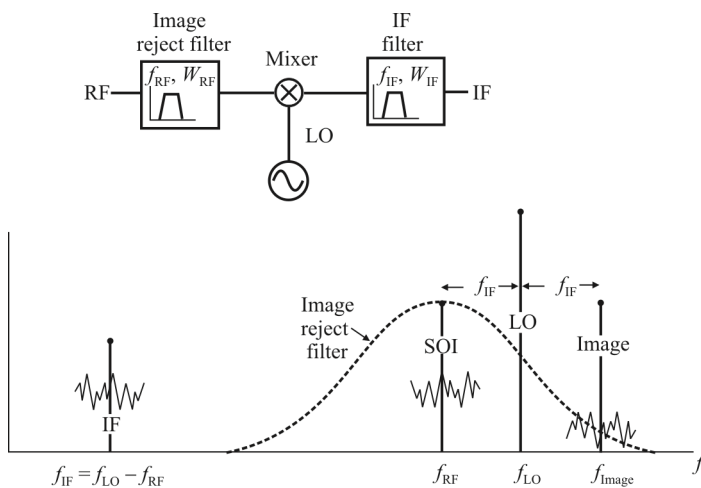


**Figure 5.31** Mixer conversion noise.
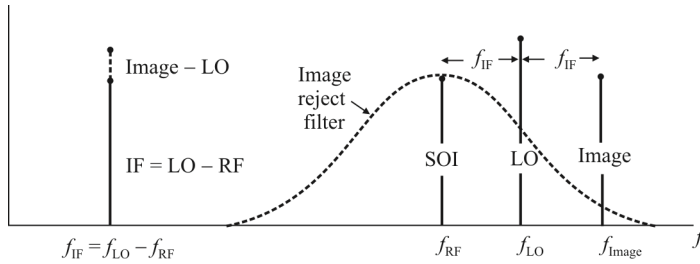
**Figure 5.32** High side injection example.

## 5.2.11 Image Reject Filtering

The basic concept of the superhet receiver means that it is possible for two signals to enter the IF amplifier chain where most of the gain in superheterodyne receivers occurs. Often filtering of the images generated by the mixing process in superheterodyne receivers is provided by filtering just prior to the mixer. We discuss this technique in this section.

### 5.2.11.1 Image Generation

As is well established by now, heterodyne receivers use mixers to move received signals in frequency. This is accomplished by using the mixer as a multiplier where the incoming signal is multiplied by a locally generated LO signal. This multiplication results in signals at the sum and difference frequencies of the two signals. If the input signal is given by $r(t) = \cos(2\pi f_c t)$ and the LO signal is given by $o(t) = \cos(2\pi f_{LO} t)$, then

$$r(t)o(t) = \cos(2\pi f_c t)\cos(2\pi f_{LO} t) \tag{5.17}$$

$$= \cos[2\pi(f_c + f_{LO})t] + \cos[2\pi(f_c - f_{LO})t] \tag{5.18}$$

(neglecting amplitudes for the moment). Generally, we want to further process one of these signals and reject the other. The unwanted signal is referred to as the *image* (actually it is some undesired signal that is located at the frequency of the image that is unwanted, not the image itself).

Two cases for downconversion are possible. High side injection has the LO frequency above the desired RF signal, as depicted in Figure 5.32. Low side injection has the LO frequency below the desired RF signal. $f_{IF}$ is the frequency difference between the RF and LO frequencies:

$$f_{IF} = f_{LO} \pm f_{RF} \tag{5.19}$$

where

$f_{IF}$ is the intermediate frequency output at the IF port
$f_{RF}$ is the frequency of any RF signal available at the RF port
$f_{LO}$ is the frequency of the local oscillator signal injected into the mixer LO port

However,

$$f_{IF} = f_{Image} - f_{LO} \tag{5.20}$$

as well. The effect is illustrated in Figure 5.31.

Because the mixer circuit is a nonlinear device, spurs are possible. *Spurious responses* are caused by undesired signals reaching the mixer's RF input port and producing a response at the IF frequency. The effect is exactly the same as that portrayed for nonlinear LNAs in Section 3.5.5. The undesired signal at the RF port does not have to fall within the RF passband to cause interference. When a receiver is subjected to spurious response signals, interference with the desired signal is possible. The frequencies of mixer spurious responses are given by:

$$f_{spur} = mf_{RF} + nf_{LO} \tag{5.21}$$

where:

$m = \pm 1, \pm 2, \pm 3 \dots$ and $n = \pm 1, \pm 2, \pm 3 \dots$

The integers $m$ and $n$ are harmonics of the RF and LO frequencies, respectively.

The most common spurious responses are the half-IF, image, and LO spurs. The RF, LO, and IF frequencies are carefully selected to avoid spurious responses.

*Image Response*

The image is a spurious response with integers $m$ and $n$ equal to unity. Figure 5.32 shows a high side injection example with the desired RF frequency $f_{RF} = f_{SOI}$ below $f_{LO}$. If the SOI had been at $f_U$ with low side injection, then $f_{RF}$ would be the image frequency. The RF and image signals are presented to the RF port. The IF signal at $f_{IF}$ is available from the IF port. The SOI at $f_{RF}$ mixes with the LO signal to produce a difference term at the IF frequency. The undesired signal called the image frequency $f_U$ also mixes with the LO signal to produce an IF frequency. The image frequency interferes with the reception of the SOI at $f_{RF}$. For protection from this spur, the image frequency must be filtered before it reaches the mixer. This filtering is usually performed by an image-reject RF filter prior to the mixer. Alternately, an image-reject mixer protects from the image frequency as well.
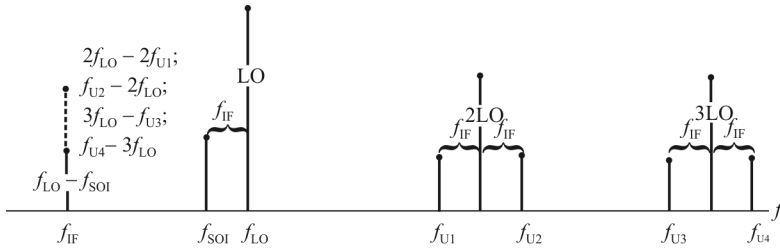
**Figure 5.33** Frequency spectrum of RF and LO.

## *LO Spurious Responses*

Additional unwanted IF responses result from mixing the LO's harmonics with RF signals spaced one IF away. The interfering RF signals that produce the unwanted IF responses are known as LO spurious responses. Figure 5.33 shows the frequency spectrum for the RF and LO frequencies. The LO signal and its harmonics are injected into the mixer LO port. The mixer also internally generates LO harmonics. The SOI at $f_{SOI}$ and all undesired signals $f_{U1}$, $f_{U2}$, $f_{U3}$, and $f_{U4}$ are available at the RF input port as shown.

Each signal at the RF port is shown to have equal signal level, and thus an opportunity for downconversion to $f_{IF}$. The undesired responses are spaced an IF frequency away above and below each LO harmonic. Each mixes down directly to the IF frequency to interfere with the SOI. LO and RF filters protect from LO spurs. Proper selection of the IF also determines whether or not filtering in the RF path is effective against LO spurs.

## *Half-IF Spurious Response*

The half-IF spur is a fourth-order response where both the $m$ and $n$ integers equal two. The half-IF response is an interfering signal occurring halfway between the SOI and the LO signal, as shown in Figure 5.34.
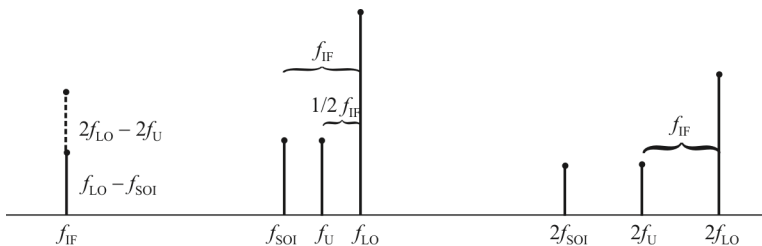


**Figure 5.34** Half-IF spur.
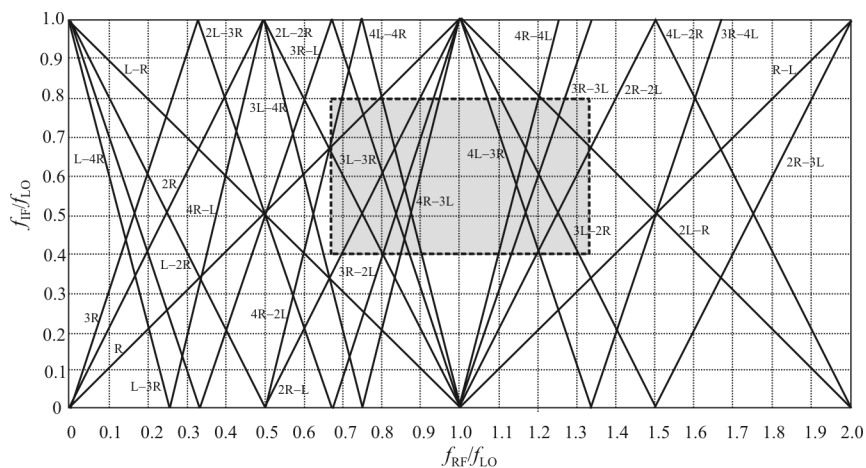
**Figure 5.35** Spur chart. Example 5.1 is shown in dashed lines.

Figure 5.34 shows a high side injection example with the SOI at $f_{\text{SOI}}$ below the LO injection frequency. The SOI mixes with the LO signal to produce an IF signal at $f_{\text{IF}}$. The undesired signal's second harmonic, $2f_{\text{U}}$, called the *half-IF spur*, mixes with the LO signal's second harmonic to produce an IF $2f_{\text{LO}} - 2f_{\text{U}}$, shown by the dotted spectral line. This half-IF frequency interferes with the reception of the SOI at $f_{\text{SOI}}$. The interfering signal, $2f_{\text{U}}$, is also attenuated by the RF image-reject filter prior to reaching the mixer.

Because the spur is a fourth-order response, the mixer's conversion efficiency is not as good as for the SOI frequency conversion. Thus, some natural protection against the half-IF spur is provided. Proper IF frequency selection is crucial to determine if filtering is possible. Selecting a low IF frequency moves the spur frequency close to the RF frequency, making filtering difficult if not impossible.

## 5.2.11.2 Spur Chart

A chart of spurious responses generated by the mixing process is provided in Figure 5.35. To read this chart, the abscissa is the ratio of $f_{\text{RF}}/f_{\text{LO}}$ while the ordinate is $f_{\text{IF}}/f_{\text{LO}}$. Construct a rectangle in the chart where the corners are defined by dividing the RF upper and lower frequencies by the LO frequency and dividing the IF upper and lower frequencies by the LO frequency. Spur lines that pass through the area represent inband spurs at the IF output.

Similar charts are available for larger ratios of the parameters, as well as larger ratios for $f_{\text{IF}}/f_{\text{LO}}$ above 1. Also Figure 5.35 shows only the difference frequencies. A similar chart is available that corresponds to the sum frequencies.

**Table 5.1** Spurs for Example 5,1 $f_{LO}$ = 75 MHz, $f_{IF}$ = 60 MHz

| 4L – 3R = 60:R = 240 MHz | 3L– 2R = 60:R = 82.5 MHz |
|---|---|
| 4L – 2R = 60:R = 120 MHz | 3R – 3L = 60:R = 285 MHz |
| 2L – R = 60:R = 90 MHz | 2R – 2L = 60:R = 105 MHz |
| 3L – 3R = 60: R = 165 MHz | 4R – 3L = 60:R = 285 MHz |
| 3R – 2L = 60:R = 70 MHz | 2R – L = 60: R = 105 MHz |
| 4R – 2L = 60:R = 52.5 MHz | 4R – 4L = 60:R = 90 MHz |
| 4L – 4R = 60:R = 60 MHz | |

**Example 5.1: Spurious Responses.** If $f_{RF,max}$ = 100 MHz and $f_{LO}$ = 75 MHz, then $f_{RF,max}/f_{LO}$ = 1.33. If $f_{RF,min}$ = 50 MHz, then $f_{RF,min}/f_{LO}$ = 0.65. If $f_{IF,max}$ = 80 MHz, then $f_{IF,max}/f_{LO}$ = 0.8 and if $f_{IF,min}$ = 30 MHz, then $f_{IF,min}/f_{LO}$ = 0.40. The spurs corresponding box is shown in Figure 5.35. The spurs' corresponding to Figure 5.35 for the frequency parameters shown are indicated in Table 5.1.

## 5.2.11.3 Image Rejection

There are many ways to remove (actually suppress) this image signal. The three most popular are:

- Filtering
- Phasing: Weaver method
- Phasing: Hartley method

Filters protect against RF signals outside the RF passband that cause an IF response. Some mixer designs protect against certain spurious responses. Image reject mixers protect against the image frequency. Balanced mixers reject some if not all spurious responses where *m* or *n* is even. LO filters also protect against certain types of spurious responses.

The image rejection specification compares the levels of signals of equal strength on the SOI and image frequencies, quoting the level of rejection of the unwanted signal. The image rejection of a receiver will be specified as the ratio between the SOI and image signals expressed in decibels at a certain operating frequency. For example, it may be 60 dB at 30 MHz. This means that if signals of the same strength were present on the SOI frequency and the image frequency, then the image signal would be 60 dB lower than the SOI—that is, it would be $1/10^3$ lower in terms of voltage or $1/10^6$ lower in terms of power.

*The Filter Method of Image Rejection*

A *bandpass image rejection filter* (a notch filter can also be used) is often used immediately ahead of the mixer to suppress the image signal (Figure 5.36). The IF
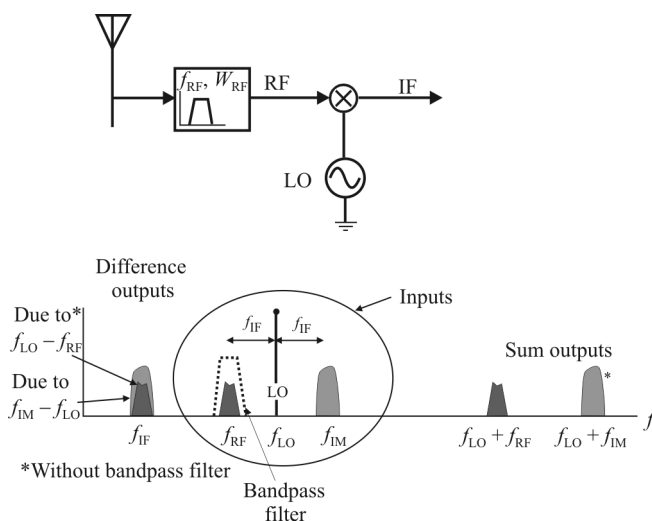
**Figure 5.36** Image reject bandpass filtering. We see that a lowpass notch image-reject filter to suppress $f_{IM}$ prior to the mixer would work as well. The preselection filtering and LNA are not shown.

and LO frequencies must be carefully selected to avoid image frequencies that are too close to the SOI RF frequency to be effectively filtered. In a receiver front end, out-of-band inputs at the image frequency could cause interference when mixed to the same IF frequency. Also, the noise present at the image is translated to the IF band, degrading the SNR. Alternatively, an *image-rejection mixer* can be designed that suppresses one of the input sidebands by phase and amplitude cancellation. This approach requires two mixers and some phase-shifting networks.

A typical commercial AM band superheterodyne receiver uses an $f_{IF}$ of 455 kHz (Figure 5.37). If an AM station is transmitting on 1490 kHz, then the LO must be tuned to 1490 + 455 kHz, or 1945 kHz, in order to convert the station frequency of 1490 kHz to the IF frequency of 455 kHz. However, a station transmitting on the image frequency of 2400 kHz will also be converted to the IF frequency of 455 kHz unless a preselection filter is used to prevent the 2400 kHz signal from reaching the input of the mixer.

Traditionally, a tuned filter is used at the input of the mixer to reject the image frequency (Figure 5.37). In AM and FM receivers, the front end tuned filter is designed to track the LO by a constant difference of 455 kHz (10.7 MHz or 21.4 MHz in VHF receivers, higher frequencies for higher frequency receivers). In an analog receiver, this is usually done by a specially designed double ganged variable capacitor that sets both the frequency of the LO and the passband frequency of the image reject filter simultaneously. In a receiver where the LO is a *numerically controlled oscillator* (NCO) or a *direct digital synthesizer* (DDS), the digital control word is changed to match the required LO frequency.
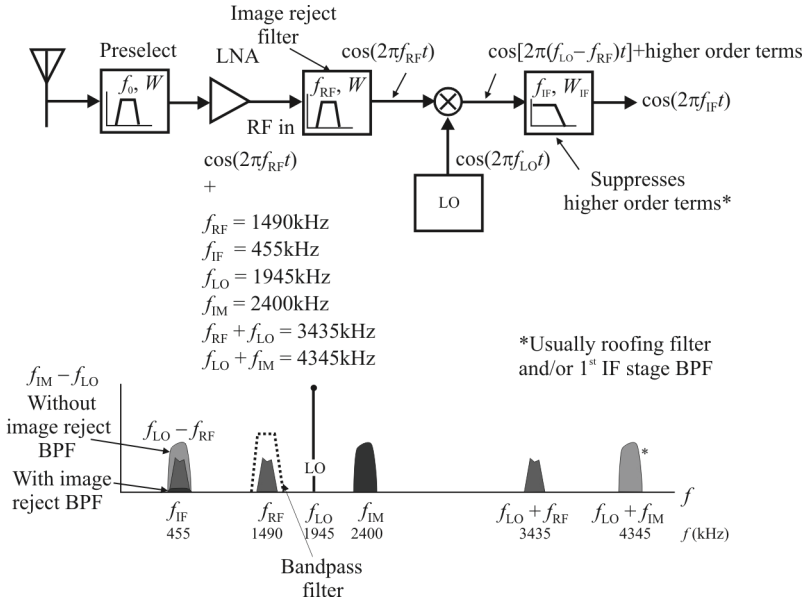
**Figure 5.37** Filter method of image rejection. The antenna, preselector (to a large extent), and LNA are not directly involved in the image rejection process but are shown here to show where the image filter sits in the receive chain.

## Image-Reject Mixers

A widely used alternative to filtering to remove image signals is to employ phase cancellation to reject images. To the extent that accurate phase and amplitude matching can be obtained, very high image-reject ratios can be obtained. The image rejection process is incorporated into the mixer through the use of in-phase and quadrature signals.

## The Phasing Method of Image Rejection

In the analysis of the phasing method in Figure 5.38, $v_1(t)$ consists of a $\cos(\omega_{IF}t)$ term from the upper image and a $\cos(\omega_{IF}t)$ from the lower image. $v_2(t)$ consists of a $\cos(\omega_{IF}t - 90°)$ term from the upper image and a $\cos(-\omega_{IF}t - 90°)$ term from the lower image. A property of the Hilbert transform is that it shifts all positive frequencies by $+90°$ and all negative frequencies by $-90°$. Therefore, the two terms, after the Hilbert transform, become $\cos(\omega_1 t)$ from the upper image, and $\cos(-\omega_{IF}t - 180°)$ for the lower image. Since $\cos(A) = \cos(-A)$, the $\cos(-\omega_{IF}t - 180°)$ term is the
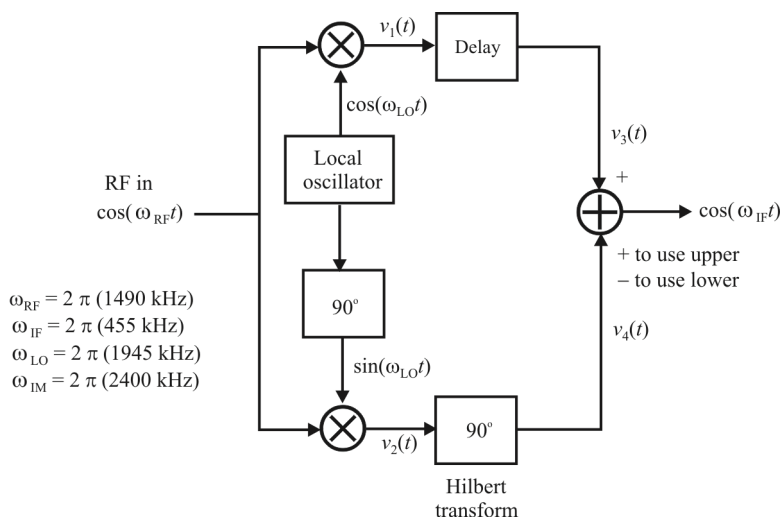
**Figure 5.38** Phasing method of image rejection.

same as $\cos(\omega_{IF}t + 180°)$. Adding or subtracting in the adder can then select whether the IF frequency, $\omega_{IF}$, is derived from the upper or the lower RF image.

*Hartley Architecture.* Another phasing technique for image rejection is provided by the Hartley architecture shown in Figure 5.39. The incoming RF signal is mixed with quadrature outputs of the local oscillator signal—namely, $\sin(\omega_{LO}t)$ and $\cos(\omega_{LO}t)$ and fed through filters. The signal at node A, as illustrated in Figure 5.40, is then shifted by 90° by a RC-CR network and added with the signal at node D. We see that the sum of B and D results in cancellation of the image and leaves only the desired signal.

The principal drawback of the Hartley architecture is its sensitivity to mismatches. If the gain and phase of the two signal paths are not perfectly balanced, the image is only partially cancelled. Sources of mismatch include *I/Q* generation errors and the inaccuracy of *R* and *C* parameters.

*Weaver Architecture.* To alleviate the mismatch problem associated with the 90° shift network in the Hartley architecture, the network can be replaced with a second quadrature mixing stage. The resulting topology is called the Weaver architecture and is illustrated in Figure 5.41.

The Fourier representations of the signals at nodes A to D are shown in Figure 5.42. It can be seen that the second-stage quadrature mixers produce outputs whose difference cancels the image, while maintaining the desired signal.
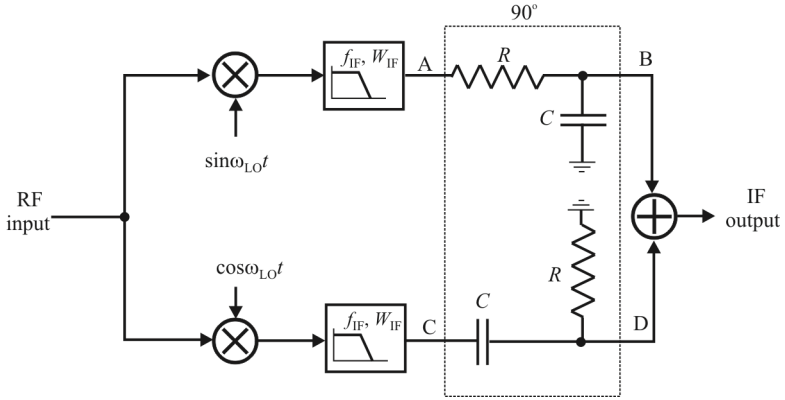
**Figure 5.39** Hartley architecture.
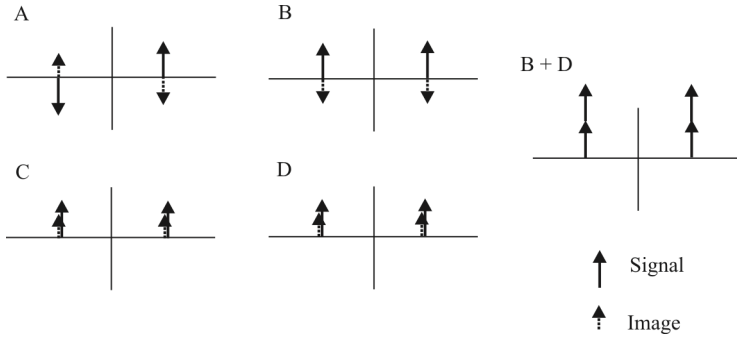


**Figure 5.40** Hartley signals.
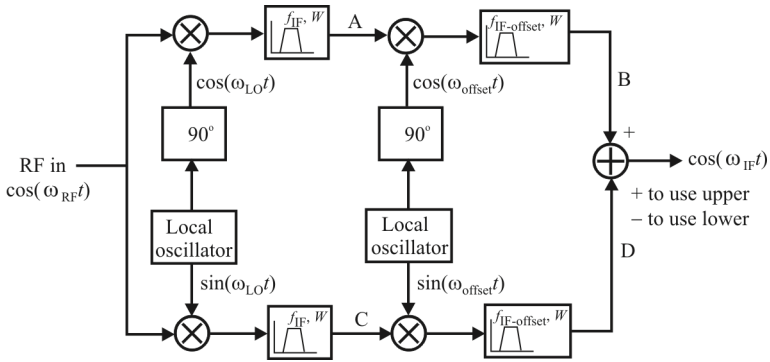
**Figure 5.41** The Weaver method of image rejection.
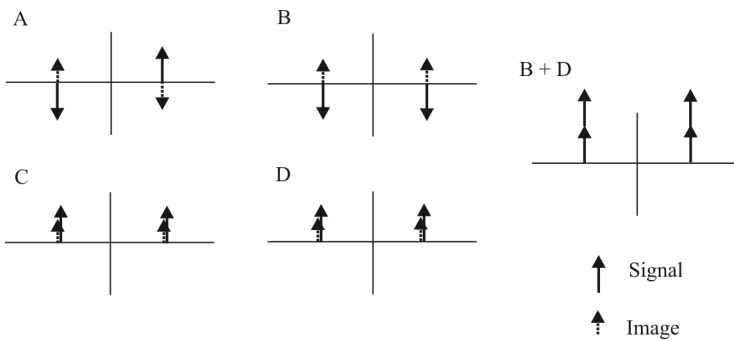


**Figure 5.42** Weaver signals.

By avoiding the RC-CR network, the Weaver architecture achieves greater image rejection. However, because the circuit still depends on the precise cancellation of the image-tone through subtraction, gain and phase mismatches between the signal paths are still a critical problem.

The Hartley and Weaver architectures eliminate the need for an explicit image-reject filter, but their performance degrades considerably in the presence of gain and phase mismatches. (This will be quantified shortly.)

Image Reject Mixer Considerations and Performance

There are a number of considerations to be taken into account when using an image-reject mixer.

- *Conversion loss:*  The conversion loss of an image rejection mixer will be higher than that of a standard mixer as the overall loss will need to include that of the quadrature hybrids, power splitters, etc. The additional loss introduced by these components will need to be added into the overall equation. However, the level of loss is still normally acceptable; typical figures expected may be around 8–10dB.
- *Level of image rejection levels:*  Typical levels of image rejection will vary according to the product. However, typical levels of image rejection that may be achieved are often in the region of 25–35dB.
- *Frequency dependence:*  The level of image rejection obtained with an image-reject mixer is largely determined by the amplitude and phase balance within the image rejection mixer circuitry. These parameters are frequency dependent to a degree, and therefore the performance of an imager-reject mixer will also be frequency dependent.
- *Usage:* Image rejection mixers are not nearly as widely used as straight mixers. However, they can provide significant advantages in some applications, saving considerable complexity and costs.

Effect of Poor Image Rejection

A receiver with a poor level of image rejection will suffer from much higher levels of interference than one with a high level of image rejection. In view of this, EW receivers need to have a good image rejection performance.

When a receiver has a poor image rejection, signals that should not be received will pass through the IF stages along with the SOI. This means that unwanted signals are received along with the wanted ones and that the levels of interference will be higher than those with a high level of image rejection.

In addition to this, the image signals will tune in the opposite direction to the wanted ones. When they interfere, heterodyne notes will be heard, and as the receiver is tuned, the pitch of the signals will change. In view of this, it is very

important to reduce the image response to acceptable levels, particularly for the exacting EW receiver applications.

Effects of Mismatch

The degree to which an image is rejected is given by the *image rejection ratio* (IRR). IRR is defined as:

$$IRR(\text{dB}) = 10 \log_{10} \frac{P_{\text{Image}}}{P_{\text{RF}}} \qquad (5.22)$$

The IRR mixer technique requires accurate phase and amplitude matching to achieve high levels of image rejection. With $\Delta A / A$ expressed in decibels and $\theta$ expressed in radians, when $\Delta A / A \ll 1\,\text{dB}$ and $\Delta\theta \ll 1$ radian

$$IRR = \frac{P_{\text{RF}}}{P_{\text{Image}}} \approx \frac{4}{\left(\dfrac{\Delta A}{A}\right)^2 + (\Delta\theta)^2}$$

IRR is charted in Figure 5.43 versus the gain error and in Figure 5.44 versus phase error.

In addition, all realistic realizations of quadrature phase shift networks are also frequency dependent. This limits the IRR bandwidth.

Basic Hartley and Weaver architectures typically have image rejection ratios in the range of 30–35dB. This is far below the 60dB typical specification. As a result, considerable effort has gone into minimizing mismatches in the signal paths.

### 5.2.12 Summary

We presented an introduction to mixers in this section. Both active and passive mixers were discussed as were single and double balanced topologies. We showed that most of the time the double balanced architectures outperformed their single balanced counterparts.

## 5.3 Local Oscillators

An LO is used in heterodyne EW receivers to drive one input to the mixer for the purpose of relocating the received signal to a different portion of the frequency spectrum. In this section we present the basic properties of such local oscillators.
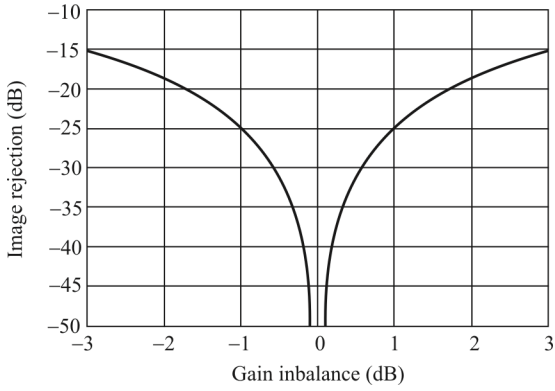
**Figure 5.43** IRR versus gain error. $\Delta\theta = 0$.
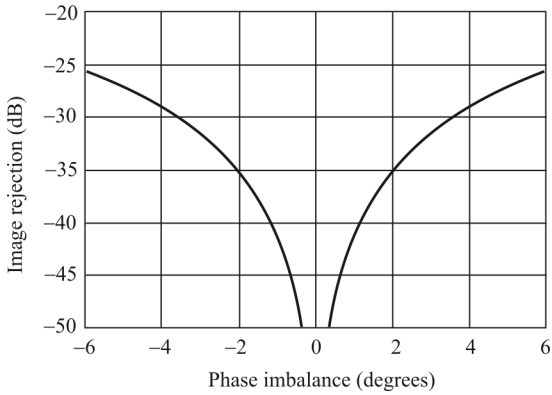


**Figure 5.44** IRR versus phase error. $\Delta A / A = 0$.
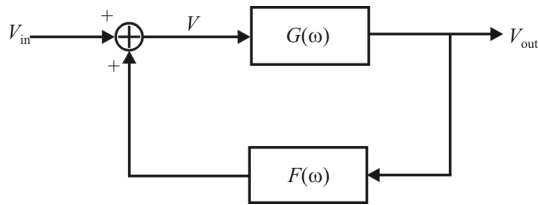
**Figure 5.45** Oscillator block diagram.

## 5.3.1 Characteristics of Feedback

Oscillators are amplifiers with a feedback path that contains a resonator in that feedback path, *resonator* being a term describing a network of inductors, capacitors, and resistors usually tuned to a specific frequency. The resonator can take many forms: crystal, *surface acoustic wave* (SAW), *inductive/capacitive* (LC), distributed line, or *microelectromechanical* (MEM), to mention some. With sufficient gain, noise will be amplified enough to eventually stabilize the amplitude and create an output signal that consists of narrowband noise.

It was long thought that oscillation occurs because the device must be initially powered and this must create a transient that jump starts oscillations, but this is inaccurate. The transient obviously exists, but oscillations are maintained due to initial and continuous noise in the system from passive or active devices. An oscillator is a device with very high gain (and $Q$) that continuously amplifies noise.

At turn on, when power is first applied, random noise is generated within the active device and then amplified. This noise is fed back positively through frequency selective circuits to the input where it is amplified again and so on. Ultimately a state of equilibrium is reached where the losses in the circuit are compensated by consuming power from the power supply and the frequency of oscillation is determined by the external components, be they inductors and capacitors (LC) or a crystal. The amount of positive feedback to sustain oscillation is also determined by external components.

The resonator in the oscillator with a high $Q$ dictates that the noise spectrum that gets amplified is narrowband. ($Q$ is defined as the ratio of radiated-to-stored energy.) In the limit, narrowband noise with zero bandwidth of necessity is a sinusoid. Therefore, the oscillator generates sinusoidal-like signals. The noise spectrum is centered on an average $\omega_0$ (called the *center frequency*). A general block diagram of an oscillator is shown in Figure 5.45.

The advantage of using a high-$Q$ filter is illustrated in Figure 5.46 [7]. Low-$Q$ resonators are possible with LC elements. High-$Q$ resonators are possible by implementation with crystals or MEM devices.
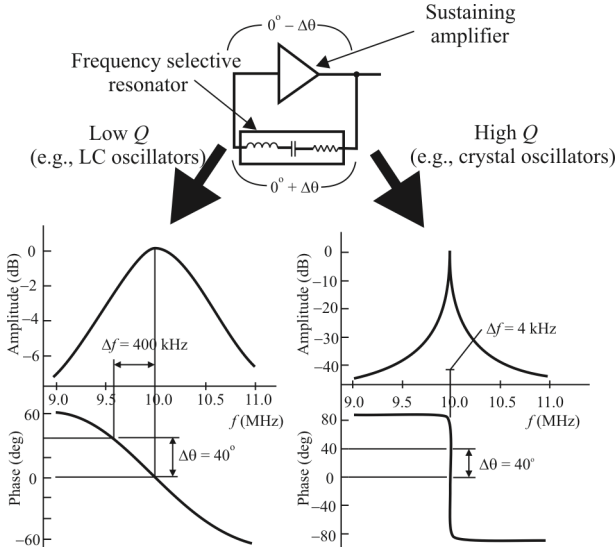
**Figure 5.46** Comparing high-$Q$ resonator feedback versus low-$Q$.

Let $G(\omega)$ denote the transfer function of the amplifier. For our purposes it can be assumed that $G(\omega)$ is flat around $\omega_0$ with amplitude $A$ and phase shift $\phi(\omega)$:

$$G(\omega) = Ae^{j\phi(\omega)} \tag{5.23}$$

When oscillating, the signal is narrowband in comparison to amplifier bandwidth and group delay (phase shift rate). The feedback, $F(\omega)$, is a narrowband (high-$Q$) LC resonator.

The transfer function of the system is obtained as follows.

$$V = V_{in} + F(\omega)V_{out}$$

but

$$V_{out} = G(\omega)V$$

so

$$V_{out} = G(\omega)[V_{in} + F(\omega)V_{out}]$$

and

$$V_{out}[1 - G(\omega)F(\omega)] = G(\omega)V_{in}$$

So the transfer function of the system is

$$H(\omega) = \frac{V_{out}}{V_{in}} = \frac{G(\omega)}{1 - G(\omega)F(\omega)} \qquad (5.24)$$

With the aforementioned assumptions, since this is a feedback system and linearity is assumed, the closed-loop transfer function is

$$H(\omega) \approx \frac{Ae^{j\phi(\omega)}}{1 - AF(\omega)e^{j\phi(\omega)}} \qquad (5.25)$$

In our case the input voltage, $V_{in}$, is noise from one or several internal sources.

Oscillations occur when the denominator approaches zero. This happens when $|AF(j\omega_0)| \rightarrow 1$ and the phase goes to 0 radians (or $2\pi$ radians, depending on total phase shift around the circuit, which must be zero). To begin oscillation, the circuit must satisfy the following *Barkhausen criteria*:

(1) The loop gain exceeds unity at the resonant frequency.
(2) The phase shift around the loop is $n2\pi$ radians (where $n$ is an integer).

It should be remembered that the output signal from the device is actually amplified noise, not a sinusoid. In addition, the open-loop gain should peak at the same frequency that the group delay peaks (maximum resonator phase rate). Otherwise, additional AM noise will be converted to phase noise. The resonator amplitude and phase components contribute to the phase noise. The local minimum in Figure 5.47 is at $f_0$, where $dA(f)/df = 0$, $L_2$ is the $d\phi/df$ term, and $L_1$ is the $dA/df$ term.

The active, energy-restoring device in oscillators act as an amplifier with immense gain resulting in very high Q, amplifying the tiny $k_B T$ to a signal in the milliwatt levels, with the SNR floor dynamic range in the 150- to 160-dB range or more. The active devices can also contribute flicker noise (especially the BJT), which is a dominant term in practical oscillator design.

An example of an oscillator using an npn BJT as the energy restorer is illustrated in Figure 5.48. In this case the oscillator is one of the most common types called a Colpitts oscillator. Note that the BJT as an energy restorer is not noiseless. When modeling, however, the noise sources in the active devices can be
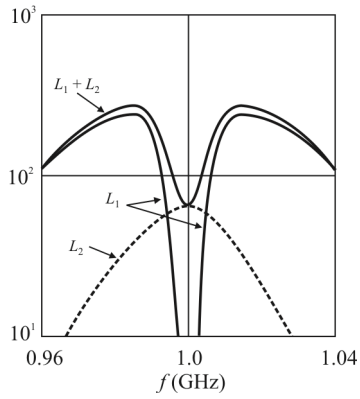
**Figure 5.47** Resonator amplitude and phase components for a 1 GHz oscillator. $L_2$ is the $d\phi/df$ term, and $L_1$ is the $dA/df$ term.
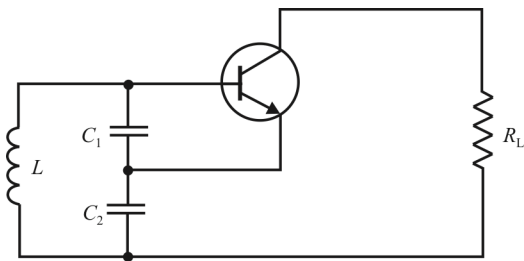


**Figure 5.48** Colpitts oscillator implemented with a BJT.
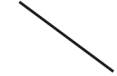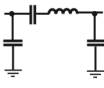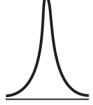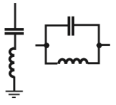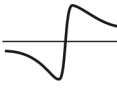
| Type | Circuit | Phase Response | Phase Derivative | Amplitude Response |
|---|---|---|---|---|
| **All-Pass Transmission Line** | | | | |
| **Bandpass Resonator** | | | | |
| **Band-Stop Resonator** | | | | |

**Figure 5.49** Basic types of resonators.

included in the resistances shown. The capacitor and inductor determine the frequency of oscillation.

There are three basic types of resonators that are normally used in oscillators. Characteristics of these resonators are illustrated in Figure 5.49.

Operation of an oscillator is generally broken up into two phases: startup and steady-state operation. An oscillator must start itself with no external stimulus. When the power is first applied, voltage changes in the bias network result in voltage changes in the filter network. These voltage changes excite the natural frequency of the filter network, and signal buildup begins and the signal developed in the filter network is small. Positive feedback and excess gain in the amplifier continuously increase the signal until the nonlinearity of the amplifier limits the loop gain to unity. At this point, the oscillator enters steady-state operation; the time from power on to steady-state operation is the oscillator start-up time.

Every oscillator has at least one active device, be it a transistor or even the old vacuum tube. This active device serves as an amplifier. For this first part of the discussion, we will confine ourselves to LC oscillators; we'll cover crystal oscillators subsequently.

An oscillator's steady-state operation is governed by the amplifier and the tuned circuit of the filter block. Loop gain steadies at unity due to the nonlinearity of the amplifier. The tuned circuit reactance will adjust itself to match the Barkhausen phase requirement of $2\pi$ radians. During steady-state operation, the main concerns are the power output and loading of the tuned circuit. The amplifier circuit is typically implemented with a BJT or MOSFET. The linear characteristics of the transistor determine the starting conditions of the oscillation while the nonlinear characteristics determine an oscillator's operating point.
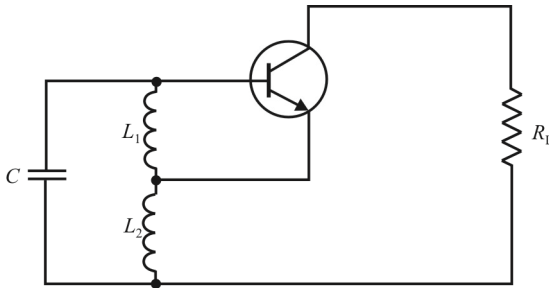
**Figure 5.50** Hartley oscillator implemented with a BJT.

The filter block sets the frequency at which the oscillator will operate, which is accomplished by using an LC tuned circuit or crystal. Since an inverting amplifier is being used, the filter block must provide a $\pi$ radian phase shift to satisfy the second Barkhausen criteria.

## 5.3.2 Fundamental Oscillator Types

There is an unlimited number of circuit combinations for oscillators. Numerous circuits take on the name of their inventors (i.e., Butler, Clapp, Colpitts, Hartley, Meacham, Miller, Seiler, and Pierce), and, in turn, many of these circuits are derivatives of one another. No one circuit is universally suitable for all applications and the choice of oscillator circuit depends on device requirements.

### 5.3.2.1 Hartley Oscillator

The simplified circuit diagram for a Hartley oscillator is shown in Figure 5.50. In the Hartley oscillator, the tuned circuit consists of a single capacitor in parallel with two inductors in series (or a single tapped inductor), and the feedback signal needed for oscillation is taken from the center connection of the two inductors. The oscillation frequency is given by

$$f_0 = \frac{1}{2\pi\sqrt{(L_1 + L_2)C}}$$  (5.26)

### 5.3.2.2 Colpitts Oscillator

The Colpitts oscillator is similar to the Hartley oscillator except the roles of the inductors and capacitors are reversed. The Colpitts oscillator employs two capacitors in series, with the feedback point where the two capacitors join, as shown in Figure 5.51. Considering that positive feedback is applied to compensate
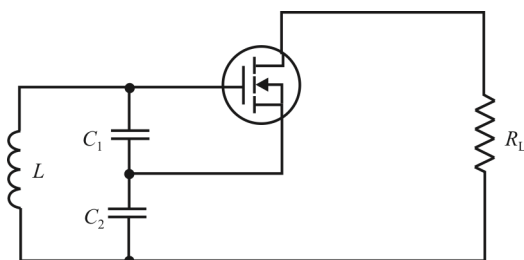
**Figure 5.51** A Colpitts oscillator architecture implemented with a MOSFET.

for the losses in the tuned circuit, the amplifier and feedback circuit create a negative resistor. When $Z_1$ and $Z_2$ are capacitive we can show that the input impedance is a negative resistor in series with $C_1$ and $C_2$. The oscillation frequency is given by

$$f_0 = \frac{1}{2\pi\sqrt{\dfrac{LC_1C_2}{C_1 + C_2}}} \tag{5.27}$$

## 5.3.2.3 Pierce Oscillator

The simplified structure for a Pierce oscillator is shown in Figure 5.52. Pierce topologies are popular for integrated circuit implementation. They have many desirable characteristics, including the capability of operating over a wide range of frequencies with very good short-term stability. Although inductors and capacitors are convenient for use in oscillator-tuned circuits, the primary disadvantage of this type of oscillator is the tendency to drift with changes in temperature, power-supply voltage, or mechanical vibrations. Setting the frequency of an LC oscillator requires precise manual tuning.

Another feature of the Pierce oscillator topology is the use of capacitors that have one terminal grounded. Floating capacitors on IC substrates are more difficult to manufacture than those with one end grounded.
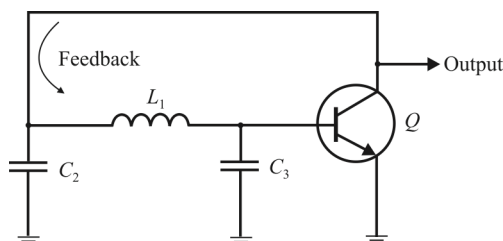


**Figure 5.52** Pierce oscillator architecture.
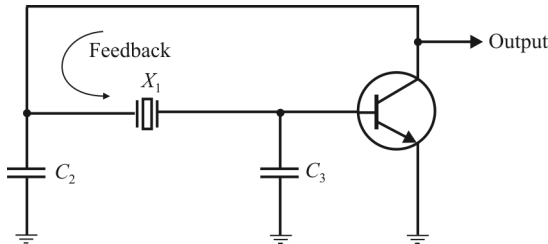
**Figure 5.53** Pierce crystal oscillator.

### 5.3.3 Crystal Oscillators

Crystals are used in many oscillator circuits due their inherent frequency stability over temperature and time compared with RLC components. We provide a basic explanation of crystal resonators and crystal oscillators in this section [8].

Reduced to its simplest components, a crystal oscillator consists of an amplifier and a filter operating in a positive feedback loop. A Pierce configuration is provided in Figure 5.53. Intuitively, we see that the amplifier provides the gain for the first Barkhausen criterion. The amplifier is inverting, causing a $\pi$ radian phase shift to meet the requirements of the second criterion. The filter block provides an additional $\pi$ radian phase shift for a total of $2\pi$ radians around the entire loop. By design, the filter block inherently provides the phase shift in addition to providing a coupling network to and from the amplifier. The filter block also sets the frequency of oscillation, using a crystal.

Quartz crystals have very desirable characteristics for use in tuned oscillator circuits, since their natural oscillation frequencies are very stable. In addition, the resonance has a very high $Q$, ranging from 10,000 to several hundred thousand. In some cases, $Q$ values of two million have been achieved. Ultimately, however, $Q$ values and stability are the principal limitations of crystal-based oscillators.

The practical frequency range for fundamental-mode AT-cut quartz crystals is up to about 30 MHz. Crystals for fundamental frequencies higher than 30- to 40-MHz are very thin and fragile. Higher-frequency operation is achieved by utilization of overtones of the fundamental frequency. Ninth-overtone crystals are used up to approximately 200 MHz, the practical upper limit of crystal oscillators.

Quartz is a piezoelectric material and when it is placed in an electric field a physical displacement occurs. The schematic symbol for a quartz crystal is shown in Figure 5.54(a) and the equivalent circuit for a quartz crystal near fundamental resonance is shown in Figure 5.54(b). The equivalent circuit is an electrical representation of the quartz crystal's mechanical and electrical behavior, and it does not represent actual circuit components. The crystal is, after all, a mechanically vibrating piece of quartz. The circuit elements $C_1$, $L_1$, and $R_1$ are
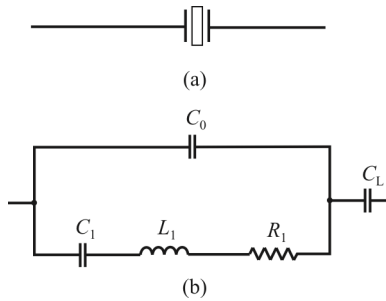
**Figure 5.54** Crystal equivalent circuit: (a) schematic symbol and (b) equivalent circuit near fundamental resonance.

known as the motional arm and represent the mechanical behavior of the crystal element, while capacitor $C_0$ represents the electrical behavior of the crystal element and its holder.

The equivalent circuit in Figure 5.54(b) represents the fundamental oscillation mode. A more complex model can represent a crystal through as many overtones as desired. For the sake of simplicity, this simple model is usually employed and different values are used to model fundamental or overtone modes. Spurious resonances occur at frequencies near the desired resonance. In high-quality crystals, the motional resistance of spurious modes is at least two or three times the primary resonance resistance and the spurious modes may be ignored.

Table 5.2 displays typical crystal specifications. Shunt capacitance $C_0$ is typically listed as a maximum value and not as an absolute value. Notice also that motional parameters $C_1$, $L_1$, and $R_1$ are not typically provided in the crystal data sheet. They can generally be obtained from a crystal manufacturer or from measurements. Table 5.3 shows equivalent circuit values for an example crystal. In Table 5.3, shunt capacitance is provided as an absolute value. However, shunt capacitance can be measured with a capacitance meter at a frequency much less than the fundamental frequency.

A crystal has two resonant frequencies characterized by a zero phase shift. The first is the series resonant frequency, $f_s$, which can be found from:

**Table 5.2** Example of Crystal Specifications

| Parameter | Value |
|---|---|
| Frequency ($f_{XTAL}$) | 8.0 MHz |
| Load Capacitance ($C_L$) | 13 pF |
| Mode of Operation | Fundamental |
| Shunt Capacitance ($C_0$) | 7 pF (maximum) |
| Equivalent Series Resistance (ESR) | 100Ω (maximum) |

**Table 5.3** Equivalent Circuit Crystal Values

| Equivalent Component | Value |
|---|---|
| $C_0$ | 5.5 pF |
| $C_1$ | 0.018 pF |
| $L_1$ | 22 mH |
| $R_1$ | 30$\Omega$ |

$$f_s = \frac{1}{2\pi\sqrt{L_1 C_1}} \tag{5.28}$$

This is the basic equation for the resonant frequency of an inductor and capacitor in series. Recall that series resonance is that particular frequency, which the inductive and capacitive reactances are equal and cancel: $X_{L1} = X_{C1}$. When the crystal is operating at its series resonant frequency, the impedance will be at a minimum and current flow will be at a maximum. The reactance of the shunt capacitance, $X_{C0}$, is in parallel with the resistance $R_1$. At resonance, $X_{C0} << R_1$, and as a result, the crystal appears resistive in the circuit at a value very near $R_1$. Solving for the example crystal, we can see that $f_s = 7,997,835.8$ Hz.

The second resonant frequency is the anti-resonant frequency, $f_a$, which is given by

$$f_a = \frac{1}{2\pi\sqrt{L_1 \dfrac{C_1 C_0}{C_1 + C_0}}} \tag{5.29}$$

This equation combines the parallel capacitance of $C_0$ and $C_1$. When a crystal is operating at its antiresonant frequency, the impedance will be at its maximum and current flow will be at its minimum. Solving for the example crystal, we get $f_a = 8,013,85.5$ Hz. Note that $f_s$ is less than $f_a$ and that the specified crystal frequency is between $f_s$ and $f_a$ so that $f_s < f_{XTAL} < f_a$. This region of frequencies between $f_s$ and $f_a$ is known as the area of *parallel resonance*. The crystal has resistive and reactive components and therefore complex impedances. The complex impedances are in parallel and are given by:

$$Z_0 = \frac{-j}{2\pi f C_0} \tag{5.30}$$
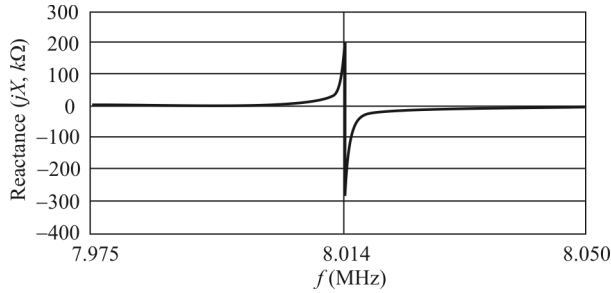
**Figure 5.55** Crystal reactance versus frequency.

$$Z_1 = R_1 + j\left(\frac{2\pi fL_1 - 1}{2\pi fC_1}\right) \tag{5.31}$$

Combining $Z_0$ and $Z_1$ in parallel yields:

$$Z_p = \frac{Z_0 Z_1}{Z_0 + Z_1} \tag{5.32}$$

Using the values in Table 5.3, this reactance versus frequency plot can be created (Figure 5.55). This plot shows where the crystal is inductive ($X > 0$) or capacitive ($X < 0$) in the circuit. Between the frequencies $f_s$ and $f_a$, the impedance of the crystal is inductive, and at frequencies less than $f_s$ and frequencies greater than $f_a$, the crystal is capacitive.

There is no difference in the construction of a series resonant crystal and a parallel resonant crystal, as they are manufactured exactly alike. The only difference between them is that the desired operating frequency of the parallel resonant crystal is set 100 ppm or so above the series resonant frequency. Parallel resonance means that a small capacitance, known as load capacitance ($C_L$), of 12 to 32 pF (depending on the crystal) should be placed across the crystal terminals to obtain the desired operating frequency. Figure 5.54 depicts load capacitance in series with the crystal equivalent circuit.

A quartz crystal is a tuned circuit with a very high-$Q$, which, along with many other desirable attributes, makes the crystal an excellent component choice for oscillators. Crystal oscillators are recognizable from their LC oscillator counterparts. For the Pierce oscillator, the crystal replaces the inductor in the corresponding LC-tuned circuit oscillators, and not surprisingly, the crystal appears inductive in the circuit.
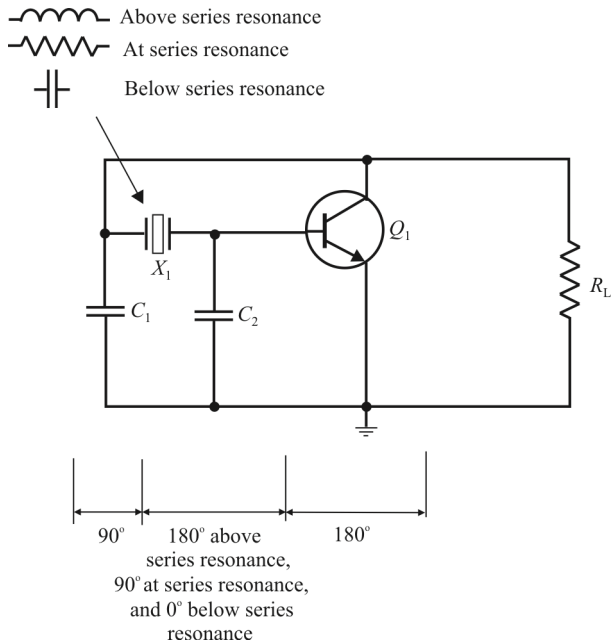
**Figure 5.56** Pierce ideal operation.

Upon startup, the amplitude of oscillation builds up to the point where nonlinearities in the amplifier decrease the loop gain to unity. During steady-state operation, the crystal, which has a large reactance-frequency slope (Figure 5.55), is located in the feedback network at a point where it has the maximum influence on the frequency of oscillation. A crystal oscillator is unique in that the impedance of the crystal changes so rapidly with frequency that all other circuit components can be considered to be of constant reactance, this reactance being calculated at the nominal frequency of the crystal. The frequency of oscillation will adjust itself so that the crystal presents a reactance to the circuit, which will satisfy the Barkhausen phase requirement.

At series resonance, the crystal appears resistive in the circuit (Figure 5.56), and the phase shift around the circuit is $2\pi$ radians. If the frequency of the circuit shifts above or below the series resonant frequency of the crystal, it increases or decreases the phase shift so that the total is no longer equal to $2\pi$ radians, thereby maintaining the steady-state operation at the crystal frequency. However, this only happens in an ideal circuit. Under actual circuit operation (Figure 5.57), the phase shift through the transistor is typically more than $\pi$ radians due to increased delay, and the tuned circuit typically falls short of $\pi$ radians. Therefore, the crystal must
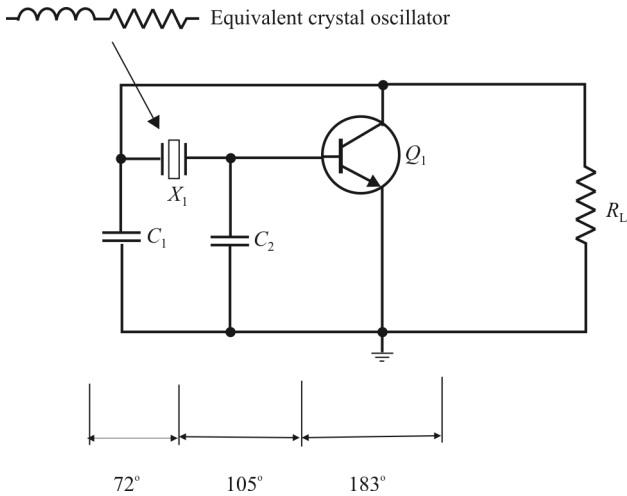
**Figure 5.57** Pierce actual operation.

appear inductive to provide the phase shift needed in the circuit to sustain oscillation.

Thus, the output frequency of the Pierce crystal oscillator is not at the crystal-series resonant frequency. Typically, a parallel resonant crystal is specified by frequency and load capacitance, $C_L$. Capacitance $C_L$ is the circuit capacitance required by the crystal for operation at the desired frequency. The circuit-load capacitance is determined by external capacitors $C_2$ and $C_3$, transistor internal capacitance, and stray capacitance, $C_S$. The values of capacitors $C_2$ and $C_3$ to match the crystal $C_L$ are determined by:

$$C_L = \frac{C_2 C_3}{C_2 + C_3} + C_S \tag{5.33}$$

## 5.3.4 Microelectromechanical Oscillators

MEMS are small integrated devices or systems that combine electrical and mechanical components. They range in size from the sub-micrometer level to the millimeter level, and there can be any number, from a few to millions, in a particular system. MEMS extend the fabrication techniques developed for the integrated circuit industry to add mechanical elements such as beams, gears, diaphragms, and springs to devices.
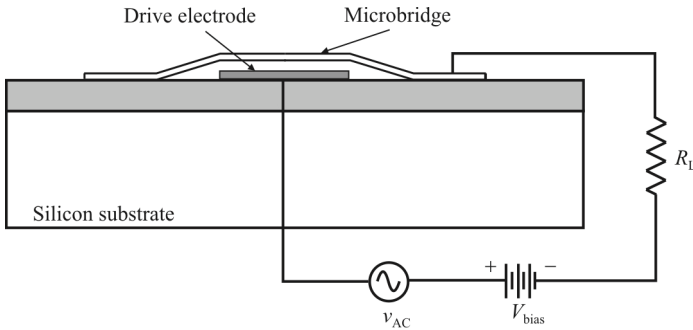
 **Figure 5.58** MEMS cantilever beam.

A basic cantilever beam is illustrated in Figure 5.58. If an AC signal is applied to a cantilever beam, its response is to vibrate. This is the fundamental operating principle of MEMS devices. One of the primary applications of such devices is resonators. These resonators can be used in filters and oscillators.

Mechanical resonators such as these devices are better than passive electronic resonators. The frequency of resonance and other properties are determined by the material and structural properties as opposed to their electronic counterparts. The characteristics of the latter are determined by IC manufacturing techniques that are harder to control. $Q$'s in the range of 10,000 in air have been demonstrated with such MEMS resonators. Ease of integration onto silicon substrates is one of the primary advantages of MEMS devices.

MEMS resonators have an additional characteristic that they operate with very low power consumption (in the microwatt region).

Although the operation of MEMS resonators extends to the GHz range, the structure shown in Figure 5.58 exhibits characteristics (impedances too high) that preclude its use at RF frequencies (Figure 5.59). A structure that is usable at RF is shown in Figure 5.60. This topology is referred to as the wine glass resonator, and it operates by oscillating as shown in the bottom pane. This type of resonator, with a radius of 26.5 μm, has been demonstrated to have a $Q$ of 8600 in air at 73.4 MHz [9].

Another topology shown in Figure 5.61 is known as the contour-mode disk resonator. With a radius of 17 μm, this resonator has demonstrated a $Q$ of 9400 at 156.23 MHz [10].

## 5.3.5 Phase Locked Loops

### 5.3.5.1 Introduction

The *phase locked loop* (PLL) forms the basis of most modern oscillator topologies. The technique aims to get a high-quality (good phase noise), high-frequency
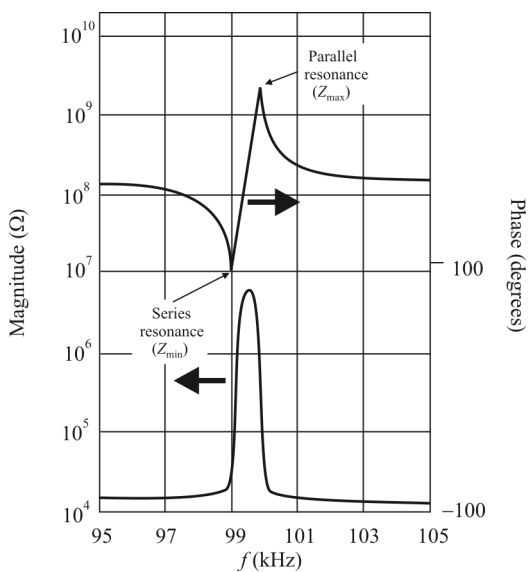
**Figure 5.59** MEMS beam characteristics.
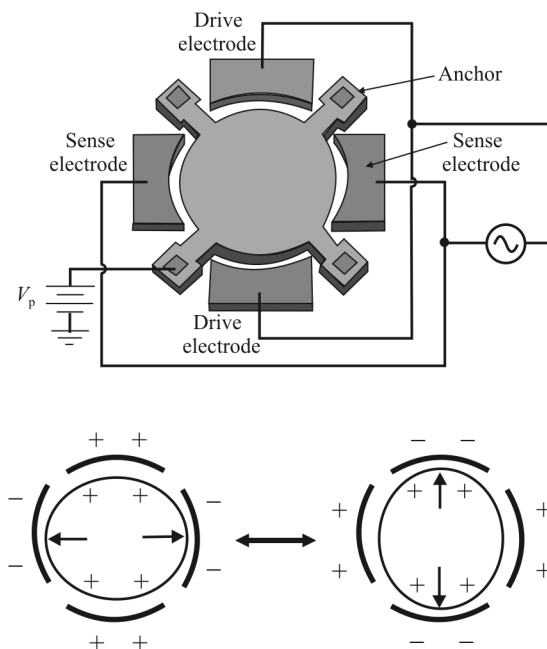


**Figure 5.60** MEMS wine glass resonator.

(a)



(b)
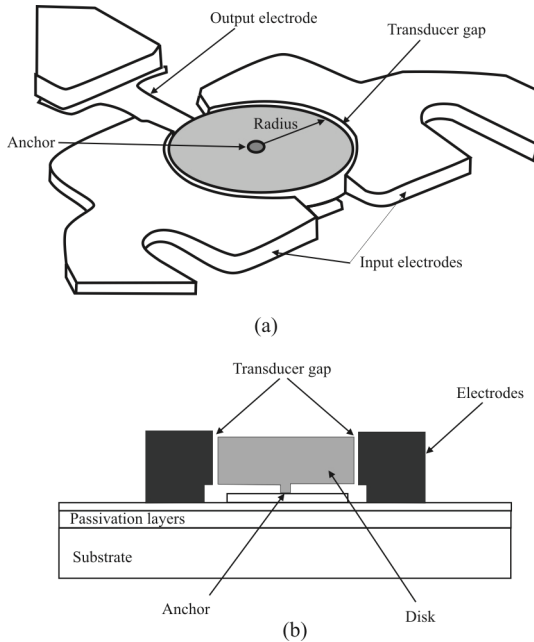
**Figure 5.61** MEMS contour-mode disk resonator.

oscillator to be locked to a stable, low-level, low-cost (often crystal derived) source.

The simplest form of PLL synthesizer contains a *voltage-controlled oscillator* (VCO) operating at the required carrier frequency (e.g., a resonator), a frequency divider (a digital divider circuit), a phase comparison circuit, and a loop filter. The circuit acts to lock the reference frequency ($f_R$) to $f_{VCO}/N$, resulting in an output frequency of $Nf_R$. The architecture is illustrated in Figure 5.62. By adding a further divider, $M$, between the reference frequency source and the PLL, it is possible to synthesize a whole range of output frequencies with value $Nf_R/M$.

The components in Figure 5.62 that every PLL must have are:

- A *phase detector* (PD): This is a nonlinear device whose output contains the phase difference between the two oscillating input signals.
- A *VCO*: This is another nonlinear device that produces an oscillation whose frequency is controlled by a lower frequency input voltage.
- A *loop filter* (LF): While this can be omitted, resulting in what is known as a first order PLL, it is always conceptually there since PLLs depend on some sort of lowpass filtering in order to function properly.
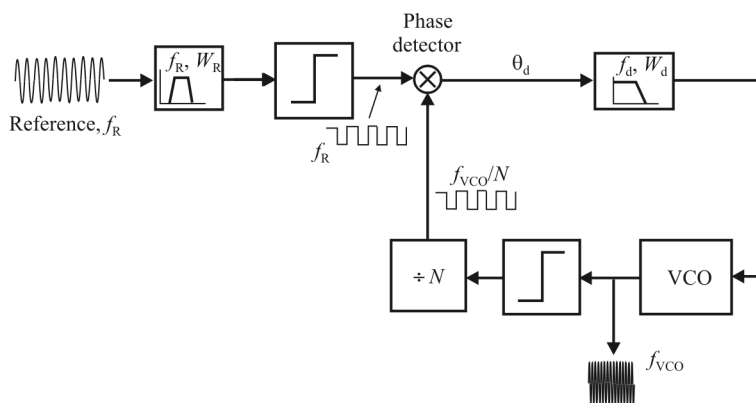
**Figure 5.62** Phase-locked loop.

- A *feedback interconnection*: Namely, the phase detector takes as its input the reference signal and the output of the VCO. The output of the phase detector, the phase error, is used as the control voltage for the VCO. The phase error may or may not be filtered.

The basic idea of a phase-locked loop is that if we inject a signal into the reference input, the internal oscillator in the loop will lock to the signal in such a way that the frequency and phase differences between the reference signal and the internal sinusoid will be driven to some constant value or 0 (depending on the system type). The internal sinusoid then represents a filtered or smoothed version of the reference signal.

Realization of the classic mixing phase-locked loop may include a lowpass filter at the output of the mixer. This filter eliminates the double frequency term arising due to the mixing. It also limits the input noise with minimal impact on the loop dynamics. In addition, typically a bandpass filter would be placed in front of the mixer also to minimize the amount of spurious signals input to the PLL.

A sinusoidal signal at the reference input of a PLL as shown in Figure 5.63 can be written as:
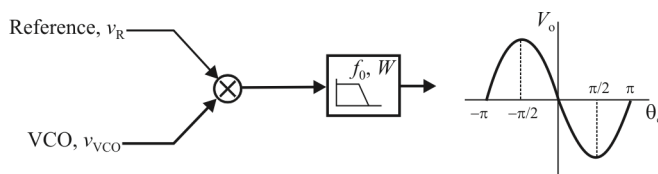


**Figure 5.63** Mixing phase detector.
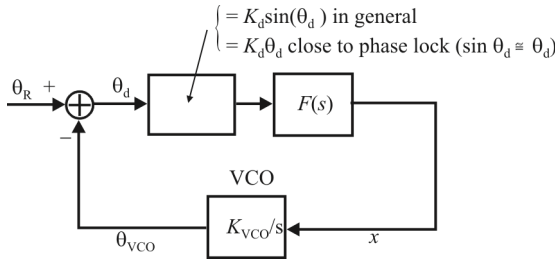
**Figure 5.64** Conceptual block diagram of PLL with sine detector. This is a transition stage in the analysis of the classical mixing loop. This model represents the effect of the multiplying detector once the high-frequency component has been attenuated. In general the detector block transfer function is equal to $K_d \sin(\theta_d)$ but close to lock where $\sin(\theta_d) \approx \theta_d$, the transfer function simply equals $\theta_d$. The latter case is the one mostly used for analysis of PLL performance.

$$v_R = A \sin(\omega_R t + \theta_R) \tag{5.34}$$

Without loss of generality, we can assume that the output signal from the VCO into the mixer is given by

$$v_{VCO} = \cos(\omega_{VCO} t + \theta_{VCO}) \tag{5.35}$$

The output of the mixer in Figure 5.63 is then given by

$$v_d = \frac{K}{2} \sin(\omega_R t + \theta_R) \cos(\omega_{VCO} t + \theta_{VCO}) \tag{5.36}$$

where $K$ includes any gain from the mixer. Now applying the elementary trigonometric identity:

$$2\sin(\omega_R t + \theta_R)\cos(\omega_{VCO} t + \theta_{VCO})$$
$$= \sin[(\omega_R + \omega_{VCO})t + \theta_R + \theta_{VCO}] + \sin[(\omega_R - \omega_{VCO})t + \theta_R - \theta_{VCO}] \tag{5.37}$$

Let $\theta_d = \theta_R - \theta_{VCO}$ and $\omega_d = \omega_R - \omega_{VCO}$. Then assume that:

- the first term in (5.37) is attenuated by the lowpass filter in Figure 5.63 and by the lowpass nature of the PLL itself.
- $\omega_R \approx \omega_{VCO}$, so that the difference can be incorporated into $\theta_d$. This means that the VCO can be modeled as an integrator.

Making these assumptions leads to the PLL model shown in Figure 5.64 when the loop is close to lock. The problem is that this is still a nonlinear system and as such is in general difficult to analyze. The typical methods of analysis include:

- *Linearization*: For $\theta_d$ small and slowly varying $\omega_d$, $\sin\theta_d \approx \theta_d$, $\cos\theta_d \approx 1$, and $\theta_d \approx 0$. While this is useful for studying loops that are near lock, it does not help for analyzing the loop when $\theta_d$ is large.
- *Phase plane graphs*: This method is a classical graphical method of analyzing the behavior of low-order nonlinear systems about a singular point. The disadvantage to this is that phase plane trajectories can only completely describe first- and second-order systems (since the graph axis each displays a single phase variable).

The linearized model is shown in Figure 5.64. This is derived from the sine detector loop by assuming that the phase error is small and thus $\sin\theta_d \approx \theta_d$. This is the model with which most analyses of phase-locked loops are done.

Typically the lowpass filter shown in Figure 5.63 is omitted. This is important because this filter is highly useful in attenuating the effects of the double-frequency signal. The PLL is inherently lowpass anyway, and the loop filter itself is optimized for the stability and performance of the baseband (phase).

As seen in (5.36), the amplitude of the phase error is dependent upon *A*, the input signal amplitude. The linearized model has a loop gain that is dependent on the loop components. Thus, the input effects of the amplitude on the loop must be anticipated.

The mixing phase detector shown in Figure 5.63 has superior noise performance to many of the other detectors.

5.3.5.2 Linear Analysis Methods for Classical PLLs

The PLL model in Figure 5.64 is a closed-loop feedback system. The transfer function from reference phase input to VCO phase output, $T(s)$, can be obtained as

$$T(s) = \frac{\Theta_{\text{VCO}}(s)}{\Theta_R(s)} = \frac{K_d F(s) K_{\text{VCO}}/s}{1 + K_d F(s) K_{\text{VCO}}/s}$$
$$= \frac{K_d K_{\text{VCO}} F(s)}{s + K_d K_{\text{VCO}} F(s)} \tag{5.38}$$

Similarly, the transfer function from the reference phase input to the phase error, $S(s)$, is
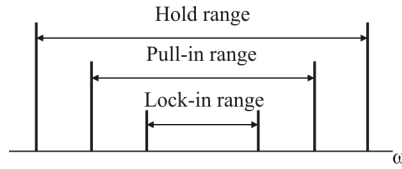
**Figure 5.65** PLL ranges.

$$S(s) = \frac{\Theta_d(s)}{\Theta_R(s)} = \frac{1}{1 + K_d F(s) K_{VCO}/s}$$

$$= \frac{s}{s + K_d K_{VCO} F(s)} \tag{5.39}$$

Among the basic properties of interest in this transfer function are the loop stability, order, and system type. The order of the PLL system is obvious from the denominator of (5.38). The stability of the system can be determined by a variety of classical methods including root locus, Bode plots, Nyquist plots, and Nichols charts.

### 5.3.5.3 PLL Operational Frequency Ranges

PLLs operate over a limited region of frequencies. These are specified by: (1) hold range, (2) lock range, and (3) pull-in/pull-out range. These ranges are indicated in Figure 5.65.

*Hold Range*

The hold range, $\Delta\omega_H$, is defined as that frequency range at which the PLL is able to statically maintain phase tracking. It is determined by calculating the frequency offset at the reference input that causes the phase error to be beyond the range of linear analysis. For a multiplying or XOR phase detector, this phase error is $\pi/2$.

For sequential detectors, it will be larger. Since loops will be permanently out of lock if the frequency offset at the input is greater than the hold range, this quantity is more of an academic matter than a practical one, but it can be calculated for a classical PLL (sinusoidal phase detector) as

$$\Delta\omega_H = K_o K_d F(0) \tag{5.40}$$

*Lock-In Range*

The lock-in range, $\Delta\omega_L$, is defined as that frequency range within which the PLL locks within one single-beat note between the reference frequency and output frequency. The lock range must be calculated from a nonlinear equation, but there

are several useful approximations that can be made. In particular, if the relative order of numerator and denominator of the PLL is 1, then the loop behaves like a first-order loop at higher frequencies, and thus the lock range can be estimated as

$$\Delta\omega_L \approx \pm K_o K_d F(\infty) \tag{5.41}$$

*Pull-In and Pull-Out Range*

The pull-in range, $\Delta\omega_P$, is defined as the frequency range in which the PLL will always become locked. The pull-out range, $\Delta\omega_{PO}$, is defined as the limit of dynamic stability for the PLL. Unfortunately, there are no simple relationships for these.

### 5.3.5.4 The Steady-State Error

Steady-state errors of PLLs are obtained from the linear analysis using the final value theorem [11]:

$$\lim_{t\to\infty}\theta_d(t) = \lim_{s\to 0}s\Theta_d(s)$$
$$= \lim_{s\to 0}s\Theta_R(s)S(s) \tag{5.42}$$

As seen from (5.39), the presence of a VCO makes every PLL at least a Type 1 system, achieving zero steady-state error to a phase step at $\theta_R$. For a phase ramp or (equivalently) a frequency step, there must be another integrator in the forward path, and the natural place for this is the LF, $F(s)$.

### 5.3.5.5 Voltage-Controlled Oscillators

The actual clock generated by a PLL comes from the VCO. The VCO is a nonlinear device that generates a periodic oscillation. The frequency of this oscillation can be controlled by modulating some control voltage (hence the name). In a PLL, the control voltage corresponds to a filtered form of the phase error. In response to this, the VCO adjusts its frequency. As the VCO frequency is slewed by the control voltage, the phase error is driven toward 0. This frequency adjustment to achieve phase lock results in the model of a VCO as an integrator.

A common form of VCO is the resonant oscillator. Consider the second-order bandpass filter in the feedback path:
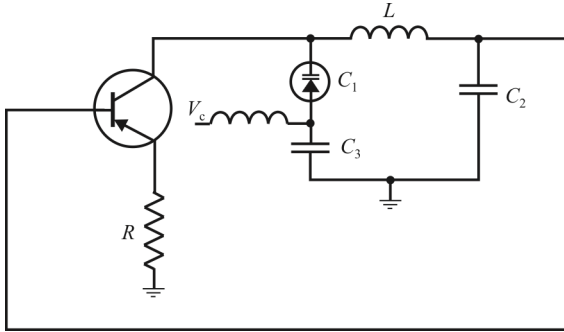
**Figure 5.66** A VCO implemented through a $\pi$ network. The frequency is adjusted by adjusting the reverse bias on the varactor diode, $C_1$.

$$F(s) = \frac{2\zeta\omega_0 s}{s^2 + 2\zeta\omega_0 s + \omega_0^2} \tag{5.43}$$

and $G(s) = K < 1.$ Then

$$\text{VCO}(s) = \frac{G(s)}{1 - G(s)F(s)} = K\frac{s^2 + 2\zeta\omega_0 s + \omega_0^2}{s^2 + 2\zeta_1\omega_0 s + \omega_0^2} \tag{5.44}$$

where $\zeta_1 = (1 - K)\zeta$. Lowering the damping ratio is called "$Q$ amplification" ($Q = 1/2\zeta$) and moves the poles even closer to the $j\omega$ axis. (In the case of the $\pi$ network, there is a complex pair of poles and one pole on the negative real axis. The dominant effect, $Q$ amplification, takes place on the complex pair.) The frequency is controlled by altering the capacitance of the resonator, typically by using a varactor diode as a capacitor. A simple circuit diagram for a resonant circuit VCO is shown in Figure 5.66. The control voltage, $V_c$, is applied to the anode terminal of a varactor diode in this case.

For the all-digital and software PLLs, the VCO is replaced by a digitally or numerically controlled oscillator (DCO/NCO). In this case, the input voltage is replaced by some digital value. The output is a digital oscillating waveform.

*Varactor Diode*

The varactor diode symbol is shown in Figure 5.67 with a diagram representation. When a reverse voltage is applied to a PN junction, the holes in the P-region are attracted to the anode terminal, and electrons in the N-region are attracted to the cathode terminal, creating a region where there is little current. This region, the

(a)                                    (b)
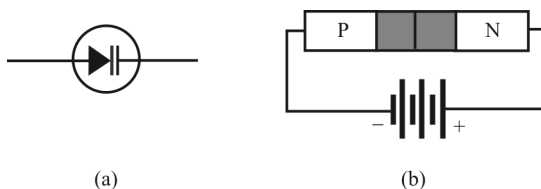
**Figure 5.67** Varactor diode: (a) circuit symbol and (b) physical construction.

*depletion region*, is essentially devoid of carriers and behaves as the dielectric of a capacitor.

The depletion region increases as reverse voltage across it increases, and since capacitance varies inversely as dielectric thickness, the junction capacitance will decrease as the voltage across the PN junction increases. So by varying the reverse voltage across a PN junction, the junction capacitance can be varied. This is shown in the typical varactor voltage-capacitance curve in Figure 5.68. Notice the nonlinear increase in capacitance as the reverse voltage is decreased. This nonlinearity allows the varactor to be used as a harmonic generator as well.

Major varactor considerations are:

- Capacitance value
- Voltage
- Variation in capacitance with voltage
- Maximum working voltage
- Leakage current

### 5.3.6 Frequency Synthesizers

The design of digital frequency synthesizers, also known as NCOs or DDS, is challenging for receivers because of the requirements for:
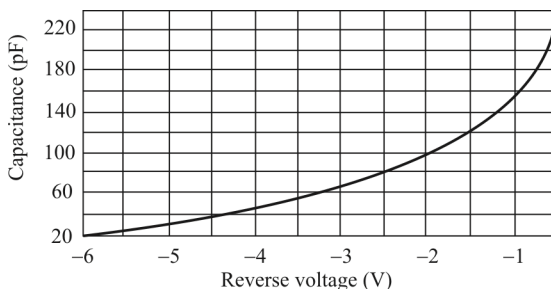


**Figure 5.68** Varactor characteristics.

- *Spectral purity*: The more the synthesized signal deviates from a pure tone, the more phase noise gets added to subsequent RF processing, causing the SNR to decrease.
- *Frequency range*: Frequently the frequency range requirements are quite large at least for one of the NCOs in an EW receiver.
- *Fast tuning*: To change the operating frequency of an EW receiver, the NCO is commanded to the new center frequency. In many (most?) applications, the faster this is accomplished the better spectrum coverage ensues.
- *Power consumption*: In many EW applications, such as man-portable equipment, the power available is extremely limited.

DDS as the name suggests creates the source frequency from digitally generated samples of the output waveform, which are then passed through a D/A converter. With sufficient processing speed and word length in the device, it is practical to achieve very fine resolution of the output frequency (millihertz accuracy and millihertz resolution) with incredibly fast switching times (microseconds).

By using DDS in conjunction with conventional PLL-based synthesis, it is possible to get the benefits of each method, but with a cost: power consumption and size penalty combine to make them much more suited to fixed site or large platform (e.g., truck, fixed-wing manned aircraft) applications than low-power EW systems.

5.3.6.1 Frequency Synthesis

To generate exciter signals at arbitrary frequencies, it is desirable to have a clock that is phase locked with an input signal of some different frequency. This can be accomplished by synthesizing a frequency from an input signal at a different (often lower) frequency. The appellation *harmonic locking loop* is applied to this configuration of a PLL, where the VCO frequency is at some multiple of the input signal frequency, as shown in Figure 5.62. The output of the divide by $N$ operation is at the same frequency as the input signal, and thus the phase detector can provide an error signal. For this to happen, however, the VCO must run at a frequency $N$ times the input frequency. It is also possible to have values of $N$ that are not integers. The reference signal is often from a very stable source, such as a crystal oscillator, so the exciter frequency can be set very precisely.

5.3.6.2 Synthesizer Architecture

The architecture of the digital synthesizer we discuss here is shown in Figure 5.69. It is based on an architecture described by Valkama [12], which, without the
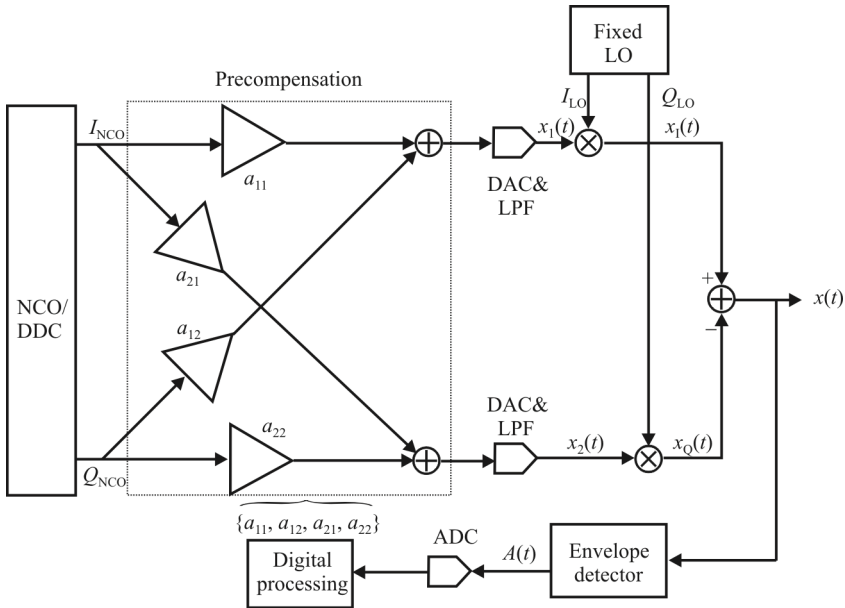
**Figure 5.69** Synthesizer architecture where digital precompensation is used to compensate for the nonidealities of the analog part.

precompensation components, represents the standard topology for a synthesizer. Digital and analog approaches to implementing a synthesizer are combined in this approach. The NCO output employs precompensation to account for the unavoidable mismatches between the amplitudes and phases of the $I$ and $Q$ branches that result in imperfect sideband rejection that degrades the spectral purity of the synthesized signal.

The signals from the NCO are given by

$$I_{NCO}(t) = \cos(\omega_{NCO}t) \qquad Q_{NCO}(t) = \sin(\omega_{NCO}t)$$

while the signals from the LO are given by

$$I_{LO}(t) = \cos(\omega_{LO}t) \qquad \qquad Q_{LO}(t) = g\sin(\omega_{LO}t + \varphi)$$

where $g$ and $\varphi$ denote the gain and phase imbalances of the mixing stage. Furthermore, let $\theta_1$ and $\theta_2$ denote the relative phase shifts due to the DACs and branch filters.

We can show that the synthesizer output signal $x(t)$ is of the form $x(t) = \text{Re}[x_{LP}(t)\exp(j\omega_{LO}t)]$, where the lowpass equivalent $x_{LP}(t)$ is given by

$$x_{LP}(t) = \alpha e^{j\omega_{NCO}t} + \beta e^{-j\omega_{NCO}t} \tag{5.45}$$

Thus, the synthesizer output consists of two spectral components: the desired tone at $\omega_{LO} + \omega_{NCO}$ and the image tone at $\omega_{LO} - \omega_{NCO}$ whose relative strengths $|\alpha|^2$ and $|\beta|^2$ depend on $g$, $\varphi$, and $\theta = \theta_2 - \theta_1$, as well as on the compensation parameters $a_{ij}$.

With practical analog electronics, the image tone attenuation defined here as

$$L = \frac{|\alpha|^2}{|\beta|^2} \tag{5.46}$$

is only 20–40dB if no compensation is used (i.e., $a_{11} = a_{22} = 1$ and $a_{12} = a_{21} = 0$). These levels of synthesizer spurious tones can result in severe interchannel interference (ICI). In general, for EW receiver applications, image tone attenuations in the order of 50–80dB or more are needed. This image tone at the synthesizer output can, however, be canceled with proper precompensation parameters $a_{ij}$. In fact, setting $\beta = 0$ and $\alpha = \exp(j\theta_1)$ will force the output to be a pure sinusoidal (with relative phase $\theta_1$).

These optimum parameters $a_{ij}$ can be shown to be of the form

$$a_{11} = 1, \ a_{12} = \tan\phi, \ a_{21} = -\frac{\sin\theta}{g\cos\theta}, \ a_{22} = \frac{\cos\theta}{g\cos\phi} \tag{5.47}$$

If the only motivation is really just to cancel the image tone (i.e., to set $\beta = 0$), a simpler solution is available. Using the notation $\psi = \varphi - \theta$, the solution can be formulated as

$$a_{11} = 1, a_{12} = \tan\psi, a_{21} = 0, a_{22} = \frac{1}{g\cos\psi} \tag{5.48}$$

for which also $\alpha \approx \exp(j\theta_1)$ with practical imbalance values. From (5.48) we see that only two actual compensation parameters, $a_{12}$ and $a_{22}$, need to be implemented. We can note that only the phase error difference $\psi = \varphi - \theta$ and the gain mismatch $g$ are actually contributing to the image tone and, therefore, to the ideal compensation parameters.

*Practical Compensator Update*

The imbalances $g$, $\varphi$, and $\theta$ needed to calculate these coefficients are unknown and need to be estimated somehow. The approach taken here is to carry out the estimation using only the envelope of the synthesizer output:

$$A(t) = \left| x_{\text{LP}}(t) \right| = \left| \alpha e^{j\omega_{\text{NCO}}t} + \beta e^{-j\omega_{\text{NCO}}t} \right| = \sqrt{\left|\alpha\right|^2 + \left|\beta\right|^2 + 2\,\text{Re}\{\alpha\beta * e^{j2\omega_{\text{NCO}}t}\}} \quad (5.49)$$

The envelope is flat only if the image tone is completely attenuated ($\beta = 0$). Thus, instead of estimating $g$ and $\psi$, a simpler approach is to directly adapt $a_{12}$ and $a_{22}$ to minimize the envelope variation.

One possibility is to consider the envelope peak-to-peak (PP) value

$$d_{\text{A}} = \max\{A(t)\} - \min\{A(t)\} \quad (5.50)$$

Given that $|\alpha| > |\beta|$, which is always the case with practical imbalance values, the above peak-to-peak value can also be expressed as

$$d_{\text{A}} = 2|\beta| = \sqrt{1 + g2a_{22}^2 + a_{12}^2 - 2ga_{22}(\cos\psi + a_{12}\sin\psi)} \quad (5.51)$$

Though not strictly parabolic, the $d_{\text{A}}$-surface having a unique minimum lends itself well to iterative minimization. The true gradient of $d_{\text{A}}$ (derivative with respect to $a_{12}$ and $a_{22}$) depends, however, on $g$ and $\psi$, which are unknown.

A possible approach is to adapt only one parameter (either $a_{12}$ or $a_{22}$) at a time. The direction (sign) of the needed one-dimensional gradient at each iteration can be determined based on observing the behavior of $d_{\text{A}}$ between two previous adaptations of the corresponding parameter. Assuming that $a_{12}$ and $a_{22}$ are updated at odd and even adaptation instants, respectively, this leads to the following update rule

$$\hat{a}_{12}(n) = \hat{a}_{12}(n-2) + K_{12}(n)\lambda_1 \frac{d_{\text{A}}(n)}{\lambda_2 + d_{\text{A}}(n)} \quad (5.52)$$

$$\hat{a}_{22}(n) = \hat{a}_{22}(n-1) \quad (5.53)$$

for $n$ odd with $K_{12} \in \{+1,-1\}$ and

$$\hat{a}_{12}(n) = \hat{a}_{12}(n-1) \quad (5.54)$$

$$\hat{a}_{22}(n) = \hat{a}_{22}(n-2) + K_{22}(n)\lambda_1 \frac{d_{\text{A}}(n)}{\lambda_2 + d_{\text{A}}(n)} \quad (5.55)$$

for $n$ even with $K_{22} \in \{+1,-1\}$.

In the above adaptation scheme, $K_{12}(n) = K_{12}(n-2)$ if $d_{\text{A}}(n-1) \leq d_{\text{A}}(n-2)$ and $K_{12}(n) = -K_{12}(n-2)$ if $d_{\text{A}}(n-1) > d_{\text{A}}(n-2)$ with similar reasoning for $K_{22}$. Step-size parameters $\lambda_1 > 0$ and $\lambda_2 \geq 0$ are used to control the adaptation speed and
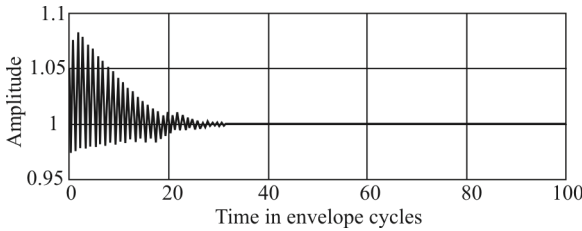
**Figure 5.70** Envelope of synthesizer output signal during the adaptation ($g = 1.05$ and $\psi = 5°$).

steady-state accuracy. Notice that the magnitude of the update term is always between zero and $\lambda_1$, depending on the value of $d_A$.

*Example Simulations*

An example of the proposed technique for coefficient determination is provided in the reference [12]. In that simulation, imbalance values of $g = 1.05$, $\phi = 6°$, and $\theta = 1°$ ($\psi = \phi - \theta = 5°$) were used, corresponding to an image tone attenuation of approximately 26dB. Updating was carried out once per envelope cycle and step-size values of $\lambda_1 = 0.01$ and $\lambda_2 = 0.02$ were used.

The output envelope is depicted in Figure 5.70. With these imbalance and step-size values, the steady-state operation is reached in approximately 50 iterations and the steady-state image attenuation is in the order of 100–150.

*Summary*

In this section, frequency synthesizer design for EW receivers was considered. To achieve fast switching capabilities with high operating frequencies and reasonable power consumption, the approach was to use I/Q modulation of digitally tunable low frequency tones. The practical imbalance problem with analog I/Q signal processing was then considered and analyzed.

Based on this analysis, a digital precompensation structure was presented together with some simple yet efficient approaches to determine the compensator coefficients.

## 5.3.7 Oscillator Phase Noise

### 5.3.7.1 Frequency Source

Probably the two most crucial factors affecting an LO signal source are frequency stability and phase noise. Phase noise affects not only the received signal's jitter, SNR, and BER but also can have adverse effect on adjacent channels.
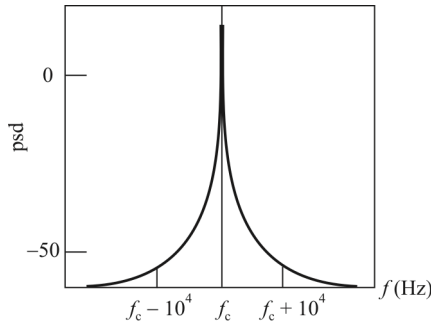
**Figure 5.71** LO phase noise.

The oscillator phase noise (also called *phase jitter*) results in a nonzero bandwidth of the carrier that could also cause energy to spill over into adjacent channels (Figure 5.71). In addition, if the phase noise is too high, the demodulated signal can be corrupted if any of the phase modulations are used. This can limit adjacent channel selectivity due to reciprocal mixing.

Real signals are accurately given by $A(t)\sin[\phi(t)]$, where $A(t)$ is a fluctuating amplitude with AM noise and $\phi(t)$ describes phase fluctuation noise with an average derivative that is called the *center frequency*. Normally, AM noise is very low in comparison, so the first approximation describes the signal as $A\sin[\phi(t)]$. We see that real signal energy is not concentrated in one frequency (delta function); rather it has a noisy spectrum. The more concentrated (spiky) this spectrum, the better the signal quality.

Real signals can only be described in statistical terms. Their phase, $\phi(t) = \omega_0 t + \theta(t)$, has a carrier angular frequency $(d\phi/dt)$ with an average of $\omega_0$. Note that $\omega_0$ is an average; its instantaneous value changes over time. Phase noise is the standard deviation of the phase fluctuation and can be described either in degrees rms (integrated number) or in detail as the signal's spectrum. The lower this value, the better the signal quality. Note that this noise (spectrum) is part of the signal itself. The corrupted signal is modeled as $\sin(\omega_0 t + m\sin\omega_m t)$, where the first term represents an ideal phase and the second term models phase fluctuations. If $m$ is small (it is usually assumed that the synthesizer noise is low and $m$ is the modulation index of a general FM signal), then $m \ll 1$. This signal is periodic. Therefore, its Fourier series [actually expressed as Bessel functions of the various orders where the center frequency value is $J_0(m)$, the first term $J_1(m)$, and so forth] can be approximated as

$$\sin\omega_0 t + \frac{m}{2}\sin(\omega_0 + \omega_m)t - \frac{m}{2}\sin(\omega_0 - \omega_m)t + \text{other terms are negligible}$$

(For $m \ll 1$, Bessel coefficients $J_0 = 1$ and $J_1 = m/2$; others are negligible.) Thus, the model reflects a perfect carrier with two sidebands, each with a peak amplitude value $m/2$. These sidebands represent the noise perturbation in the model as displayed in the time representation of the phase and signal's spectral density. The phase deviation has rms power given by $\mathcal{E}\{(m \sin \omega_m t)^2\} = m^2/2 \, \text{radians}^2$. The spectral energy of the sidebands has a relative power of $m^2/4$ each for a total of $m^2/2$. It can be summarized that the phase noise in radians$^2$ is equal to the relative power of the sidebands. The extension of this analysis from $\sin \omega_m t$ modulating the carrier to noise modulation is readily accomplished. We can summarize that for real LO signals with reasonably good spectral purity ($m \ll 1$), the phase jitter in radians$^2$ is equivalent to the noise spectrum's power.

Most LO signal sources have a monotonically declining phase noise spectrum (see Figure 5.71). Close to the carrier, the noise indicates slow fluctuations (sometimes crystal drift in temperature or time) and flicker noise of active devices. These slowly varying noise components usually can be tracked by the receiver. As we move away from the center frequency, noise components become faster and contribute to the ever-present additive noise.

The spectrum of the signal is usually defined by the function $\mathcal{L}(f_m)$, which indicates the SSB noise distribution in a 1 Hz bandwidth relative to total power at an offset $f_m$ from the center frequency. $\mathcal{L}(f_m)$ is usually specified in decibels below the carrier power level (dBc/Hz). Thus, a 1 GHz synthesized signal having an $\mathcal{L}(f_m)$ of $-90$dBc/Hz at an offset of 10 kHz from the carrier means that at an offset of $\pm 10$ kHz from 1 GHz, the signal's SSB power in a 1 Hz bandwidth is 90dB below the total signal's power. If this signal has a power level of $-10$dBm, then its spectral components at 10 kHz offset are at a level of $-80$dBm/Hz.

To determine the contribution of this noise, the frequency range of interest must be defined. When this range is given by $(f_1, f_2)$, then the phase noise is given by

$$\phi_j^2 = 2 \int_{f_1}^{f_2} \mathcal{L}(f_m) df \qquad \text{rad}^2 \qquad (5.56)$$

The 2 multiplier is because $\mathcal{L}(f_m)$ is SSB. The time jitter caused by this phase noise is given by

$$\tau_j = \frac{\phi_j}{\omega_0} \qquad (5.57)$$

Once a given noise profile is obtained, (5.56) can be evaluated, typically numerically. For example, for an LO signal with the phase noise characteristics

**Table 5.4** Leeson Phase Noise Characteristics

| Offset from Carrier (Hz) | $\mathcal{L}(f_m)$ (dB/Hz) |
|:---:|:---:|
| 1 | −25 |
| 10 | −45 |
| 100 | −62 |
| 1k | −72 |
| 10k | −90 |
| 100k | −115 |
| 1M | −135 |

listed in Table 5.4, the phase jitter from 10 Hz to 100 kHz is calculated to be 2° rms. This result means that in a perfect channel with no noise, the LO signal's noise will contribute 2° of noise. In eight-phase modulated signaling, the phase difference between states is 45° and a phase offset of 22.5° causes errors. Such a signal presents a maximum achievable SNR (all other sources of noise are not included) of $(22.5/2)^2 \Rightarrow 20$dB.

Spurious signals add phase jitter as random noise. For example, an ideal signal with a single spur that is –40dB below the carrier will cause a phase jitter that is $\phi_{j,dB}^2 = -40\,dB \Rightarrow 0.0001$. Thus $\phi_j = 0.01$ radian (0.57°). Noise and spurious add incoherently so the total contribution caused by phase noise and spurious is given by their sum: $\phi_j^2 = \phi_j^2\big|_{noise} + \phi_j^2\big|_{spurs}$.

### 5.3.7.2 Leeson Model

The generally accepted engineering model for phase noise is the one developed by Leeson [13]. The model is expressed as

$$\mathcal{L}(f_m) = 10\log\left\{\frac{2k_B T\Phi}{P_s}\left(1 + \frac{f_{1/f^3}}{f_m}\right)\left[1 + \left(\frac{f_0}{2Qf_m}\right)^2\right]\right\} \tag{5.58}$$

where

$T$ is the temperature (K)
$\Phi$ is a constant that accounts for the increased noise in the $1/f^2$ region
$f_{1/f^3}$ is the breakpoint frequency between the –2 and –3 exponents

$f_0$ is the center frequency of the oscillator
$Q$ is the quality factor of the resonator

A graph of this function is shown in Figure 5.72.
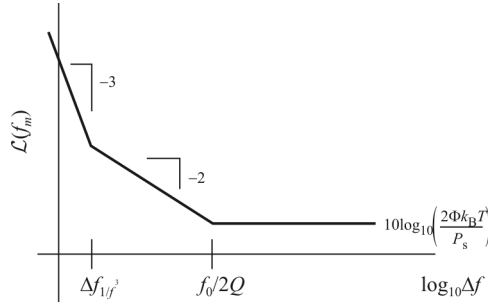
**Figure 5.72** Leeson model.

This model includes a factor ($\Phi$) to account for the increased noise in the $1/(\Delta\omega)^2$ region, an additive factor of unity (inside the braces) to account for the noise floor, and a multiplicative factor (the term in the second set of parentheses) to provide a $1/|\Delta\omega|^3$ behavior at sufficiently small offset frequencies.

A typical measured oscillator noise profile at 1 GHz with $Q = 50$ is shown in Figure 5.73 where $f_m = 10$ Hz to 5 MHz. Eventually, the noise will reach a floor (in this case close to $-160$dBc/Hz). We immediately see that across a 10 Hz to 5 MHz offset the noise profile covers a 130- to 140-dB dynamic range. Oscillator noise is usually highly dependent on $Q$. The lower the tuning/modulation sensitivity of a VCO, the better the phase noise.

It is important to note that the factor $\Phi$ is an empirical fitting parameter and therefore must be determined from measurements, diminishing the predictive power of the phase noise equation. Furthermore, the model asserts that $\Delta f_{1/f^3}$, the
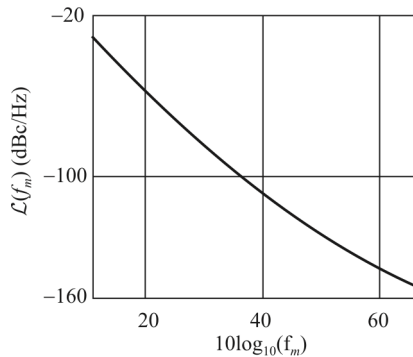


**Figure 5.73** Oscillator phase noise profile for a 1 GHz oscillator.

boundary between the $1/(\Delta f)^2$ and $1/|\Delta f|^3$ regions, is precisely equal to the $1/f$ corner of device noise. However, measurements frequently show no such equality, and $1/|\Delta f|^3$ must be treated as an empirical fitting parameter as well. Also, it is not clear what the corner frequency will be in the presence of more than one noise source with $1/f$ noise contribution. Last, the frequency at which the noise flattens out is not always equal to half the resonator bandwidth, $\omega_0/2Q$.

The units are thus proportional to the log of a density. Specifically, they are commonly expressed as "decibels below the carrier per hertz," or dBc/Hz, specified at a particular offset frequency from the carrier frequency. For example, we might speak of a 2 GHz oscillator's phase noise as "−110dBc/Hz at a 100 kHz offset." It is important to note that the "per Hz" actually applies to the argument of the log, not to the log itself; doubling the measurement bandwidth does not double the decibel quantity. As lacking in rigor as " dBc/Hz" is, it is common usage.

## 5.3.7.3 Reducing Phase Noise

Some good practices for minimizing the phase noise in LOs are:

- Maximize the $Q$ of the resonator.
- Maximize reactive energy by means of a high RF voltage across the resonator. Use a low LC ratio.
- Avoid device saturation and try to use antiparallel (back-to-back) tuning diodes.
- Choose an active device with the lowest NF.
- Choose a device with low flicker noise. This can be reduced by RF feedback. A bipolar transistor with an unbypassed emitter resistor of 10 to 30Ω can improve flicker noise by as much as 40dB.
- The output circuits should be isolated from the oscillator circuit and take as little power as possible.

The Leeson equation presents certain characteristics.

- Close to the carrier the phase noise monotonically declines at 30dB/decade; it then changes to 20dB/decade until it hits a noise floor.
- The equation predicts that when $f_0$ doubles, the loss in the phase noise per the same $Q$ is in the 6 dB range. In reality, going from 1 to 2 GHz causes a loss of ~6dB. Going from 1 to 5 GHz is predicted to cause only a 14dB loss. However, in reality, the number is significantly higher. In that regard, the best solution for high-frequency sources is to oscillate at the 1 GHz range and use multipliers (multipliers lose only a 20log multiplication ratio).

- Intuitively, the more power drawn from the device, the better the SNR (hence, $P_s$ in the denominator). On the other hand, bleeding more energy from the resonator reduces $Q$.
- Seemingly, no relationship exists between phase noise performance and VCO constant ($K_v$= MHz/V). In practice, lower $K_v$ allows lower coupling of the resonator, hence higher $Q$ and better phase noise.

The VCO must run in nonlinear mode because its closed-loop gain must be one (or nearly so) for oscillations to occur. Still, because the device (bipolar or field-effect transistor) has nonlinear output characteristics, it can be expected that as the gain drive level increases, a related rise in output will follow. Therefore, linear analysis is practically (and theoretically) justified.

5.3.7.4 MEMS Microresonator Noise

*Short-Term Frequency Stability*

Many phenomena contribute to phase noise in oscillators. The most common phenomenon is superposed electronic noise from the sustaining amplifier. With MEMS resonators, however, noise due to Brownian motion and mass loading has increased influence and may actually dominate among mechanisms that cause phase noise.

*Electronic Noise*

The phase noise power due to electronic noise from the sustaining amplifier may be predicted theoretically. Assuming a linear series resonant oscillator, the expression for the relative oscillator phase noise power density $N_{op}$ to carrier $C$ power ratio at a deviation $f_m$ from carrier frequency $f_0$ is

$$\frac{N_{op}}{C} = \frac{f k_B T}{C} \frac{1}{8Q^2} \frac{G^2 R_L}{(R_L + R_{in})^2 R_{in}} \left(\frac{f_0}{f_m}\right)^2 \tag{5.59}$$

where $f$ is the amplifier noise factor, $Q$ is the loaded quality factor of the resonator, $G$ is the gain of the transresistance sustaining amplifier, $R_{in}$ is the input resistance of the sustaining amplifier, and $R_L$ is the combination of the amplifier output resistance and the series motional resistance $R_m$ of the resonator.

*Mass Loading Noise*

In addition to superposed electronic noise, any physical phenomenon that causes instantaneous frequency deviations of the resonator will contribute to the total

phase noise power. Given the typical mass of a mechanical resonator, mass loading noise is expected to make a sizable contribution.

Pressure Dependence

The phase noise of a MEMS resonator is dependent on ambient pressure. There is a strong dependence on the contaminant activation energy. On-chip vacuum encapsulation techniques have been investigated that provide vacuums with low pressures.

Temperature Dependence

In addition to a dependence upon pressure, mass loading noise depends upon temperature as well. This dependence arises mainly from the temperature dependence of the rates of adsorption of contaminants. The effect of mass loading on the short-term frequency stability of a resonator should taper off as temperatures increase. This suggests that a low-power microoven could be used to substantially reduce phase noise contributions due to mass loading.

*Oscillator Noise Reduction Techniques*

Traditional oscillator design has involved maximizing the $Q$ of the resonant element, selecting a low noise sustaining-stage amplifier and matching circuit elements for optimum performance. Leeson's model (5.58) is invaluable for free-running oscillator design, where oscillator phase noise is determined by active device phase noise $S_\phi^{amp}$, resonator loaded quality factor $Q_L$, and resonator residual noise $S_\phi^{res}$ :

$$S_\phi^{osc}(\text{free running}) = S_\phi^{res} + S_\phi^{amp}\left[1 + \left(\frac{f_{0.5}}{f_m}\right)^2\right] \qquad (5.60)$$

where $f_{0.5} = f_0/2$ and $f_0$ is the operating frequency. Once the components of an oscillator have been optimized to practical limits, noise reduction may be employed to further lower the noise.

Table 5.5 summarizes the performance of feedforward and feedback noise reduction systems. The conclusion on which technique is preferred is application dependent where particular system requirements may place emphasis on different performance aspects.

<div align="center">

**Table 5.5** Summary of Feedforward and Feedback Noise Reduction Performance

</div>

|  | **Feedforward** | **Feedback** |
|---|---|---|
| Noise Floor | Excellent—close to thermal limit. Set by achievable carrier cancellation in first loop. | Set generally by noise floor of phase detector. Close to thermal limit for carrier suppressed systems. |
| PM Reduction | Depends on balance of both loops. | Set by noise floor and available gain. Often proportional to input power. |
| AM Reduction | Inherent, as with PM. | Often requires a complementary control system. |
| System Complexity | Open loop configuration reasonable. Two amps required. Long-term operation requires sophisticated control. | Simple for standard mixer-based systems. Carrier suppression systems similar to feedforward but control simpler. |
| Bandwidth/Operating Frequency Range | Wideband noise reduction. Operating frequency range depends on delay matching in both loops. | Limited by controller bandwidth. Operating frequency range set by delay matching. |
| Stability | Unconditionally stable, but addition of loop control may compromise. | Conditionally stable. Stability criteria compromise noise reduction bandwidth/loop gain limit. |

## 5.3.7.5 PLL Noise

Since a PLL locks to the phase of the input signal, one of the key measures of the performance of the loop is the phase noise in the output, $\theta_o$. Figure 5.74 shows the linear PLL model with noise at both the reference input, $\theta_{in}$, and the VCO, $\theta_{VCO}$. In particular the loop can be made to minimize $\theta_o$ or to have $\theta_o$ track $\theta_{in}$ precisely. As with a standard linear feedback loop,

$$\theta_o = T(s)\theta_{in} + S(s)\theta_{VCO} \tag{5.61}$$

where $T(s)$ and $S(s)$ are obtained from (5.38) and (5.39), respectively. We can assume that the psds of $\theta_{in}$ and $\theta_{vco}$ are independent, and the psd of the output phase can be expressed as

$$G_o(j\omega) = |T(j\omega)|^2 \, G_{in}(j\omega) + |S(j\omega)|^2 \, G_{VCO}(j\omega) \tag{5.62}$$

As with most feedback systems, we normally have some control over the effect of $\theta_{in}$ on $\theta_o$ through the shaping of the loop, but beyond the loop bandwidth, $\theta_o$ is dominated by $\theta_{VCO}$.
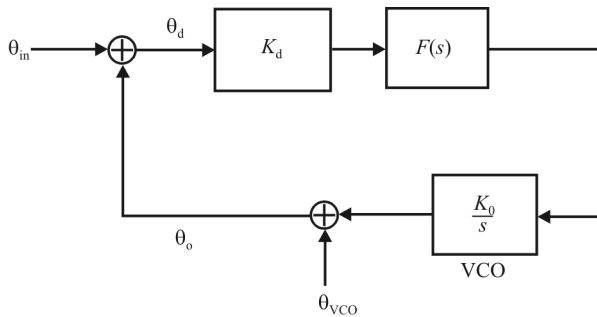
**Figure 5.74** Linear model of input and VCO noise passing through a PLL.

We have touched on two noise sources, but every component of a PLL is a potential source of phase noise, from the phase detector to the resistors in the filter.

### 5.3.8 Oscillator Stability

Frequency stability refers to the drift (or lack of it) of the LO signal's frequency with temperature, aging, and mechanical factors such as vibration and shock. In EW receivers the frequency stability determines how well signals can be intercepted while avoiding interference from adjacent signals.

A stable oscillator requires a stable tuned element in the feedback path. A simple LC stabilized oscillator is generally not adequate. Using a transmission line in place of the LC circuit usually exhibits less drift with temperature. A ceramic resonator, widely used as a clock source for microprocessor applications, has a frequency tolerance of only approximately 3000 ppm and hence is not adequate for most EW receiver applications. Coaxial resonators (often ceramic based) can provide very high-$Q$ elements and hence have excellent phase noise. Their temperature stability is, however, poor and on their own they are not sufficient to act as the LO. [Locking a coaxial resonator to a stable (e.g., crystal) source is, however, a viable and widely used synthesis process.] SAW devices can provide the accuracy needed for wideband operation, giving typically $\pm 300$ ppm stability over $-40°C$ to $+60°C$ for frequencies up to 1 GHz or beyond. They usually have an initial tolerance of approximately $\pm 50$ kHz which can be tuned on manufacture. Because they provide a low-cost, on-frequency source, SAW-based oscillators are very popular for wideband low-power receiver applications.

A crystal oscillator is the most widely used stable frequency source, relying on the natural vibration frequency of the quartz crystal. Depending on the quality of the crystal and the type and tolerance of the cut, accurate temperature-stabilized devices can be fabricated. For a very cheap crystal, a temperature tolerance of

$\pm15$ ppm  is typical, whereas for a *temperature compensated crystal oscillator* (TCXO), a  $\pm3$ ppm  tolerance or better is possible. The major drawback with crystal-based oscillators compared with SAW devices is that the oscillation frequency is typically below 30 MHz for a fundamental mode design, and possibly up to 100  MHz using a fifth overtone design.

Short-term frequency stability is of utmost importance for LOs in EW receivers. Short-term stability is typically measured in terms of close to carrier phase noise power density, which is directly related to frequency noise power.

Frequency or phase stability of an oscillator is customarily considered in the long-term stability case where frequency changes are measured over minutes, hours, days, and even years. Of interest here are the effects of the component changes, with ambient conditions, on the frequency of oscillation. These might be caused by changes in the input voltage, variations in temperature, humidity, and aging of components.

## 5.3.8.1 Minimizing Frequency Drift

Some guidelines for minimizing the frequency drift in LOs are as follows:

- Isolate the oscillator from succeeding stages with a buffer stage followed by a stage of amplification. Large signals can often then be reduced by a 3- or 6-dB attenuator which also has the benefit of presenting a well-defined load impedance to the amplifier. If the stage is feeding a mixer, as is most often the case, then another benefit is the mixer also sees a source impedance of 50Ω.
- Ensure the mechanical stability of the oscillator is such that mechanical vibration can have no effect on components, especially the frequency determining components.
- Supply the oscillator with a clean well-regulated supply. If using varactor tuning, doubly ensure the tuning DC voltage is as clean as possible; a few hundred microvolts of noise can be imposed on the oscillator signal. Use back-to-back diodes for the variable element. Air variables are hard to come by although they offer far superior $Q$ figures. DC tuning tends to be more versatile.
- Minimize circuit changes from ambient variations by using NPO capacitors. Polystyrene is excellent.
- The inductor should be air wound on a coil form with a configuration to maximize $Q$. If a toroid must be used, where possible use the 6 type as it offers the best $Q$. Sometimes, for other reasons, a slug tuned form must be used.

- Parallel a number of smaller value NPO capacitors rather than using one large one in frequency determining components. For trimmers use an air variable.
- Bipolar or FETs for active devices seem to be a matter of personal preference. Consensus seems to come down in favor of FETs.

# 5.4 Concluding Remarks

The mixing process was considered in this chapter. The principal components involved are the mixer and LO.

The mixer takes in the RF and LO signals and generates the IF signal. The IF signal is at a constant frequency irrespective of the RF input frequency. This is accomplished by provided tuning in the LO. The IF is always a constant offset from the RF signal and is given by $f_{RF} \pm f_{LO}$. Whether the sum or difference is used is determined by the particular design; in both cases the signal at the other frequency is eliminated or substantially reduced, normally by filtering.

Mixing generates signals at image frequencies. These images can be numerous and some method is normally required to minimize their impact. There are two techniques that are typically used for dealing with such images. The first is to place a filter in the RF signal path prior to the mixer tuned to the frequency of the image. The other method is to employ phase cancellation techniques in the mixer itself. We discussed both of these methods in this chapter.

Last we considered the configurations of LOs that are used in receivers. We discussed the most common LO topologies and provided some of the pros and cons of each. Oscillator noise was also addressed, with the most common type of detrimental noise provided by the LO being phase noise, which is manifest in variations of the phase of the LO signal. While amplitude noise is also present on the LO signal, it is usually negligible compared to the phase noise.

## References

[1]     Hayward, W., *Introduction to Radio Frequency Design*, Newington, CT: American Radio Relay League, 1994, Ch. 6.
[2]     Walker, H. P., "Sources of Intermodulation in Diode-Ring Mixers," *The Radio and Electronic Engineer*, Vol. 46, No. 5, May 1965.
[3]     Oxner, E., "A Commutation Double Balanced Mixer of High Dynamic Range," *RF Design*, February 1985.
[4]     Gray, P. R., and R. G. Meyer, *Design of Analog Integrated Circuits*, 3rd Ed., New York: Wiley, 1993, Ch. 10.
[5]     Breed, G., "Understanding Mixers from a Switching Perspective," *High Frequency Electronics*, April 2006, pp. 48–51.
[6]     Maas, S., "The Diode Ring Mixer," *RF Design*, November 1993, pp. 54–62.

[7]     Nguyen, C.T.–C., L.P. B. Katehi, and G. M. Rebeiz, "Micromachined Devices for Wireless
        Communications," *Proceedings of the IEEE*, Vol. 86, No. 8, August 1998, pp. 1756–1768.
[8]     Matthys, R. J., *Crystal Oscillator Circuits*, Malabar, FL: Krieger Publishing, 1992.
[9]     De Los Santos, H. J., *Introduction to Microelectromechanical Microwave Systems*,
        Norwood, MA: Artech House, 2004, p. 108.
[10]    De Los Santos, H. J., *Introduction to Microelectromechanical Microwave Systems*,
        Norwood, MA: Artech House, 2004, p. 103.
[11]    Dorf, R. C., *Modern Control Systems*, Reading, MA: Addison-Wesley, 1965.
[12]    Valkama, M., and M. Renfors*, "*Advanced I/Q Signal Processing for Communication
        Systems," *Proceedings SDR-03 Technical Conference*, Orlando, Florida, November 2003.
[13]    Leeson, D. B., "A Simple Model of Feedback Oscillator Noise Spectrum," *Proceedings of
        the IEEE*, Vol. 54, No. 2, February 1966, pp. 329–330.

# Chapter 6

## IF Amplifiers

### 6.1 Introduction

IF stages in communications EW receivers are comprised of amplifiers for boosting the levels of signals and relatively narrowband filters for improving the selectivity of the receiver. Selectivity refers to the rejection or suppression of signals in adjacent RF channels to prevent or minimize interference to the SOI channel. The filters are normally placed between the stages of amplification and are used for matching the stages as well as filtration [1].

In this chapter we examine the basic parameters of RF amplifiers. We defer the discussion of the IF filters to Chapter 7.

The bulk of the signal amplification occurs in the IF stages in a receiver. Signals with power in the –130dBm range must be amplified to be in about the 10dBm range or more, implying total amplification in a receiver to be 140dB or more. The IF amplifiers are responsible for most of this amplification.

### 6.2 Amplifier Input and Output Impedances and Gain

Recall that the gain of a stage is calculated by using the input and output signals. Consider the voltage gain of the circuit shown in Figure 6.1. The capacitors $C_1$ and $C_3$ are coupling capacitors to isolate the bias levels of this stage from the stages before and after this one, respectively. The filters in this network consist of $R$, $L$, and $C$ components. As such, $R_1$ and filter $F_1$ form a voltage divider at the input to the transistor. With the input level and $R_1$ fixed, as the impedance of filter $F_1$ increases in value, the voltage on the base of the transistor increases, which causes the output voltage on the collector to decrease. Likewise, $R_2$ and filter $F_2$ form a voltage divider on the output. With all else held constant, as the impedance of filter $F_2$ increases, the voltage on the collector increases in magnitude. Therefore, if we incorporate impedances that vary with frequency, we can make an amplifier stage that amplifies signals only at a certain frequency as determined by these impedances (a range of frequencies really). In the shunt configuration shown in
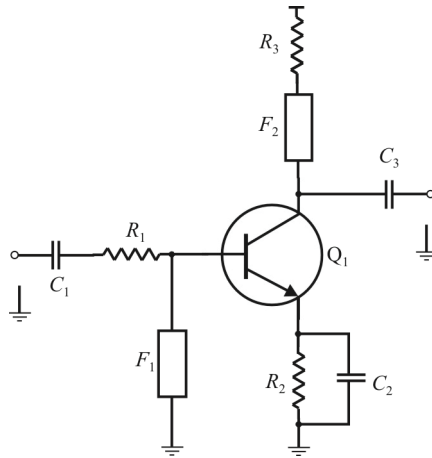
**Figure 6.1** Input and output filters.

Figure 6.2, these impedances would have their maximum values at the desired frequency of operation. It is not necessary to have the impedances of both filters vary; one will typically do.

The variable impedances could also be inserted in series with the input and output rather than shunt. In that case the networks would exhibit minimum impedances at the resonant (desired) frequency. This configuration is illustrated in Figure 6.3.

The reactance of an inductor and a capacitor varies as frequency changes. As frequency increases, inductive reactance increases, and capacitive reactance
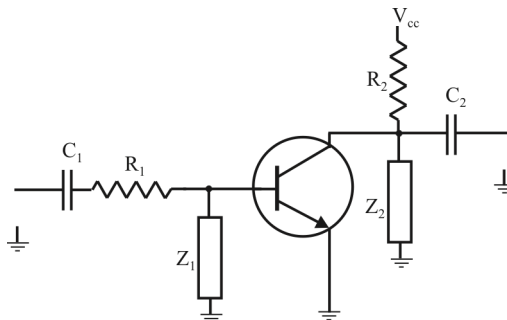


**Figure 6.2** BJT input and output shunt filters.
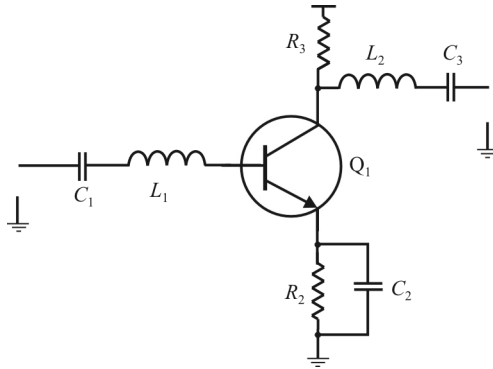
**Figure 6.3** Amplifier stage with series tuned filters.

decreases. At some frequency, inductive and capacitive reactance will be equal. When the inductor and capacitor are connected as a parallel LC circuit, a tuned circuit is formed. This circuit is tuned to give the proper response at the desired frequency by selecting the proper values of inductance and capacitance. A circuit using this principle is shown in Figure 6.4, which shows an RF amplifier with parallel LC circuits used as filter networks. This RF amplifier will only be effective in amplifying the frequency determined by the parallel LC circuits.

The impedance characteristic of the parallel tuned circuits is shown in Figure 6.5. Around the resonant frequency given by $f_0 = 1/\sqrt{LC}$, the impedance rises sharply where elsewhere the impedance is relatively small. The small impedance shorts the signal to ground at the input and to the power supply (AC ground) at the output. Therefore the stage will only amplify signals close to resonance.

A similar result would be expected with the series resonant circuits shown in Figure 6.3. The impedance characteristic for the series filter is illustrated in Figure 6.6. In this case the impedance is a minimum at resonance, and connected in series as illustrated in Figure 6.3, will only pass signals that are close to resonance (not all the bias elements are shown). Signals at other frequencies are blocked. The input and output capacitors with the series filter double in function as the bias isolating elements between stages.

The $Q$-factors displayed in Figures 6.5 and 6.6 are a measure of the quality (sharpness) of the filter. Mathematically, they are given by the ratio of the impedance to the resistance in the circuit (all realistic circuits have some resistance). The sharper the $Q$, as is obvious from these figures, the narrower is the passband of the stage. This is a detriment to EW systems when broadband amplifiers are required such as in LNAs but is desirable for IF amplifiers due to the increase in selectivity facilitated by such filter characteristics.
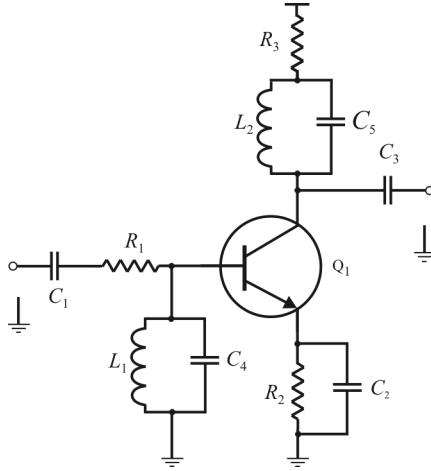
**Figure 6.4** Shunt parallel tuned input and output.
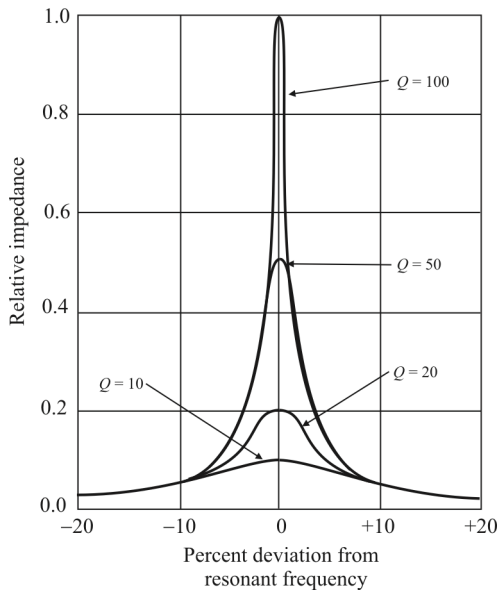


**Figure 6.5** Relative impedance of the shunt parallel tuned circuit as the filter.
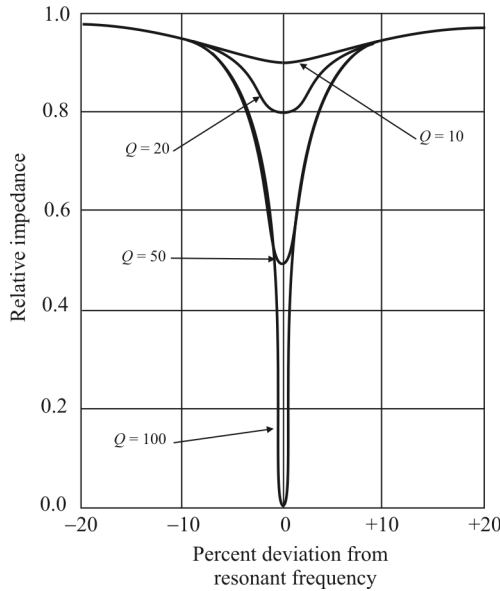
**Figure 6.6** Relative impedance characteristic of the series tuned filter.

# 6.3 RF Amplifiers

We consider RF amplifiers used in IF applications in this section. Since intermediate frequencies are usually set at a single value with relatively (relative to the intermediate frequency) narrow bandwidths, we consider narrowband amplifiers. This is as opposed to the LNA wideband amplifiers we examined in the RF section chapter. Although any frequency can be used, typical intermediate frequencies are 455 kHz for receivers in the HF (3–30 MHz), 21.4 MHz in the VHF (30–300 MHz), and 70 MHz in the UHF (300–3000 MHz) ranges. Typical bandwidths are 3 kHz and 10 kHz in the HF range; 10 kHz, 25 kHz, and 250 kHz in the VHF range; and 25 kHz, 100 kHz, 300 kHz, and 500 kHz in the UHF range.

There are several possible configurations for active devices in amplifiers. We will focus on class A topologies since that is the most popular for linear amplification but it should be remembered that there are other possibilities. Most of the discussion in this chapter applies to the narrowband RF preselection amplifiers in the RF stage as well.

## 6.3.1 EW RF Amplifier Analysis

A simplified configuration for a common source MOSFET class A biased amplifier stage is shown in Figure 6.7. For purposes of AC analysis, the power
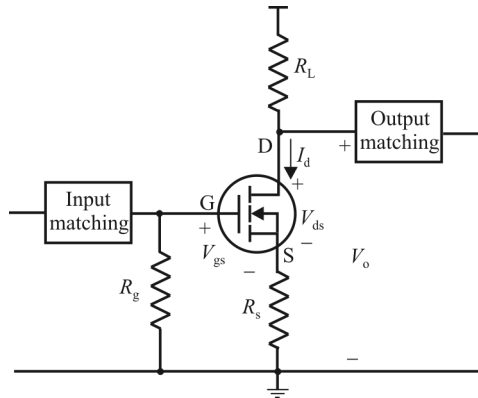
**Figure 6.7** Common source MOSFET class A amplifier.

supply voltage is at ground potential, so the upper end of the load resistor is grounded. The output matching circuit is attached to the junction of the load resistor and the FET. Matching is used at the input and output for optimum signal transfer purposes, and the stability considerations are incorporated into these networks. We will not delve into the details of matching and stability here. (See [2] for a discussion of matching and Section 3.4.7 for a discussion of stability in amplifiers.) The IF filters are incorporated at the input and output of amplifier stages such as this.

The s-parameters of the active device are normally used to analyze EW RF amplifier architectures when the frequency of operation includes regions above the VHF range (generally greater than 300 MHz). The active device could be a BJT, an FET, a thermionic vacuum tube, or any other device whose s-parameters indicate gain may be obtained. These s-parameters are a function of the device geometry, the materials used in its manufacture, the quality of the manufacturing process, and the semiconductor physics of the material used. They are normally determined by measurement. The s-parameters are used to design the bias circuitry as well as to determine the AC amplification characteristics.

As described above, the bias point is where, on the input and output characteristic curves, the active device voltages and currents are established when there is no RF signal present. This is referred to as the Q-point. It is determined by adding resistors between appropriate points in the circuit. These points are normally a DC voltage source, ground, and the terminals of the active device. The RF signals are assumed to be small relative to the values of the bias levels so that operation of the amplifier is nominally in a small region around the quiescent point.

The active device is a two-port network described by a range of S-parameters that have been measured over a specified frequency range. Usually this range is

**Table 6.1** *s*-Parameters for Example Transistor. In this case $V_{CE}$ = 3 V and $I_C$ = 5 mA

| $f$ (GHz) | $s_{11}$ | | $s_{21}$ | | $s_{12}$ | | $s_{22}$ | |
|---|---|---|---|---|---|---|---|---|
| | $\lvert s_{11} \rvert$ | $\angle s_{11}$ | $\lvert s_{21} \rvert$ | $\angle s_{21}$ | $\lvert s_{12} \rvert$ | $\angle s_{12}$ | $\lvert s_{22} \rvert$ | $\angle s_{22}$ |
| 0.1 | 0.88 | −13 | 16.38 | 170 | 0.01 | 83 | 0.98 | −6 |
| 0.5 | 0.75 | −59 | 12.59 | 134 | 0.03 | 61 | 0.85 | −22 |
| 0.9 | 0.60 | −94 | 9.43 | 111 | 0.05 | 49 | 0.70 | −33 |
| 1.0 | 0.56 | −102 | 8.78 | 106 | 0.05 | 47 | 0.69 | −34 |
| 1.5 | 0.46 | −134 | 6.31 | 88 | 0.06 | 39 | 0.53 | −42 |
| 1.9 | 0.42 | −158 | 6.29 | 75 | 0.06 | 36 | 0.53 | −42 |
| 2.0 | 0.42 | −161 | 6.03 | 72 | 0.06 | 36 | 0.53 | −43 |
| 2.4 | 0.41 | −178 | 4.30 | 62 | 0.07 | 34 | 0.49 | −47 |
| 3.0 | 0.42 | 160 | 3.51 | 48 | 0.08 | 30 | 0.43 | −54 |
| 3.5 | 0.42 | 143 | 3.01 | 37 | 0.09 | 26 | 0.43 | −58 |
| 4.0 | 0.44 | 129 | 2.63 | 27 | 0.09 | 23 | 0.42 | −63 |
| 4.5 | 0.45 | 116 | 2.40 | 17 | 0.10 | 19 | 0.39 | −67 |
| 6.0 | 0.47 | 104 | 2.18 | 7 | 0.11 | 15 | 0.37 | −72 |

Source: Freescale.

the region for which it has useful gain. First the bias and heat removal needs of the transistor are addressed. After that the RF design is determined using the *s*-parameters.

We will demonstrate a simplified design procedure here by way of example. Suppose an amplifier is required that is to operate at 1 GHz with 50Ω source and load impedances. For other reasons, if suitable, the transistor of choice is characterized by the table of S-parameters shown in Table 6.1. The table shows the S-parameters in standard format where frequency is shown on the left and the parameter across the rows in magnitude/angle format.

Recall that when the source and load impedances are the same as those used to determine the S-parameters, the magnitude of $s_{21}$ is the ratio of the outgoing wave at the output port, $b_2$, to the incoming wave at the amplifier RF input, $a_1$. Hence, it is equivalent to the voltage or current gain of the amplifier. Similarly, the square of the magnitude of $s_{21}$ is equal to the power gain. The magnitude of $s_{21}$ is 8.78 at 1 GHz. The basic gain, without tuning, in a 50Ω system is:

$$G = 10\log \lvert s_{21} \rvert^2 = 20\log 8.78$$
$$= 18.9 \text{ dB} \tag{6.1}$$
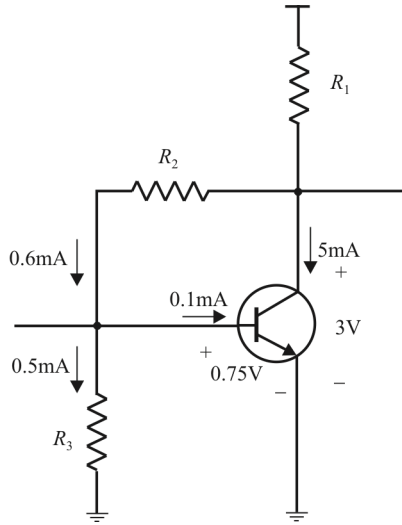
**Figure 6.8** RF BJT CE RF amplifier biasing.

If this gain is acceptable we can move on to design the bias circuitry. If it is too low, then a different device or different values of $V_{ce}$ and/or $I_c$ can be selected. If it is too high, then perhaps different values for $V_{ce}$ and/or $I_c$ could be tried or a different, less expensive, device may make more sense. We'll assume here that it is adequate and proceed to determine the bias element configuration.

The DC source needs to be larger than 3V because the data in the table is for when $V_{ce} = 3V$. Suppose a 5 V source is used. The performance was obtained with $V_{ce} = 3V$ and $I_c = 5$ mA. The DC current gain, $\beta = I_c / I_b$, although not listed in this table, is normally also included in the specification sheet. Assume that at this $\beta = 50$. Figure 6.8 shows a standard biasing network for a CE amplifier configuration.

The bias resistor values are calculated as follows. The base current is 0.1 mA (5 mA/50). However, a shunt path to carry about five times this value, say 0.5 mA, is desirable so that when the 5V level falls, the base current will fall nearly proportionately. Since we are assuming that the transistor is a silicon npn, the base-emitter junction will have a voltage drop at turn-on of about 0.75V. The emitter-base shunting resistor can be calculated as:

$$R_3 = \frac{0.75\,\text{V}}{0.5\,\text{mA}} = 1500\,\Omega \tag{6.2}$$

$$R_2 = \frac{(3-0.75)\,\text{V}}{(0.5+0.1)\,\text{mA}} = 3750\,\Omega \tag{6.3}$$
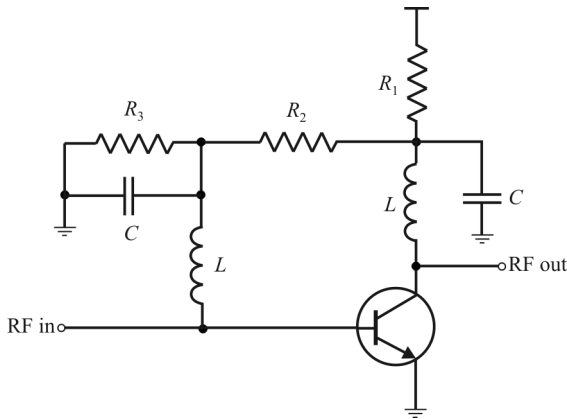
**Figure 6.9** RF bias isolation.

$$R_1 = \frac{(5-3)\,\text{V}}{(0.6+5)\,\text{mA}} = 357\,\Omega \tag{6.4}$$

Practically, of course, the closest values of standard resistors are used. This standard bias circuit tends to self-compensate with temperature. As the temperature increases, the base current increases for a given $V_{be}$. However, this causes an increase in $I_c$, resulting in a larger voltage drop in $R_1$ and thereby reducing $V_{be}$.

The bias resistors are large compared to the $50\Omega$ RF impedance level at the input. However, their parasitic components at the frequency of operation may cause them to place an excessive load on the RF circuit. Furthermore, it is undesirable to have RF signals present in the bias circuit, since this may cause undesired RF radiation. RF isolation from the bias resistors is therefore normally employed. One method to do this with discrete components is illustrated in Figure 6.9. This isolation could be accomplished with quarter- and half-wave transmission line impedance converters as well.

High RF impedances are created by the bias isolation circuitry. Figure 6.10 shows one way of doing this with discrete components. For this 1 GHz, $50\Omega$ amplifier example, isolating elements of $L = 100$ nH and $C = 100$ pF are typical values. When space permits, the isolating elements can be "printed" as distributed transmission lines along with the RF circuit. These transmission lines are $\lambda/4$ long at the amplifier's RF center frequency, which equates to $l = 6.5$ cm at 1 GHz.
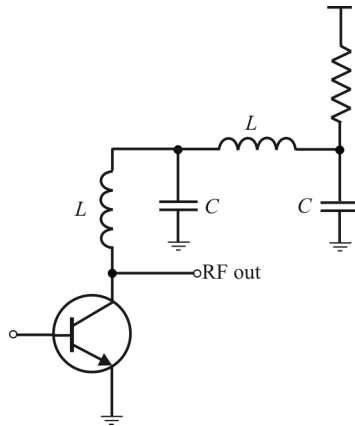
**Figure 6.10** RF bias multistage isolation.

Bias isolating networks are critically important in RF amplifiers. Transistors typically have gain at frequencies well above the design bandwidth. As seen in Table 6.1, the transistor has significant gain above the design frequency of 1 GHz. It also has the potential of breaking into oscillation at any frequency for which it has gain, which will be discussed in a later section.

The bias circuits shown in Figure 6.9 have only single high-impedance and low-impedance elements for isolation in each of the input and output bias circuits. Single stages such as this are not adequate for all applications, and multiple stages are preferred when possible, as illustrated in Figure 6.10.

An amplifier designed in the way indicated here should undergo computer simulation to verify its performance and determine its stability characteristics. Many *computer-aided engineering* (CAE) simulators are available for this purpose.

Ignoring the issues of matching and stability, the electronic portion of the amplifier design is complete. However, the input and output reflection coefficients, $s_{11}$ and $s_{22}$, respectively, in Table 6.1 at 1 GHz, there is a considerable amount of power lost to reflection at the input and mismatch at the output. Specifically

$$|s_{11}| = 0.56$$

$$\text{Input Mismatch Loss} = 1 - |s_{11}|^2 = 1 - 0.56^2 = 0.69 = -1.6 \text{ dB}$$

$$|s_{22}| = 0.69$$

$$\text{Output Mismatch Loss} = 1 - |s_{22}|^2 = 1 - 0.69^2 = 0.79 = -1.0 \text{ dB}$$
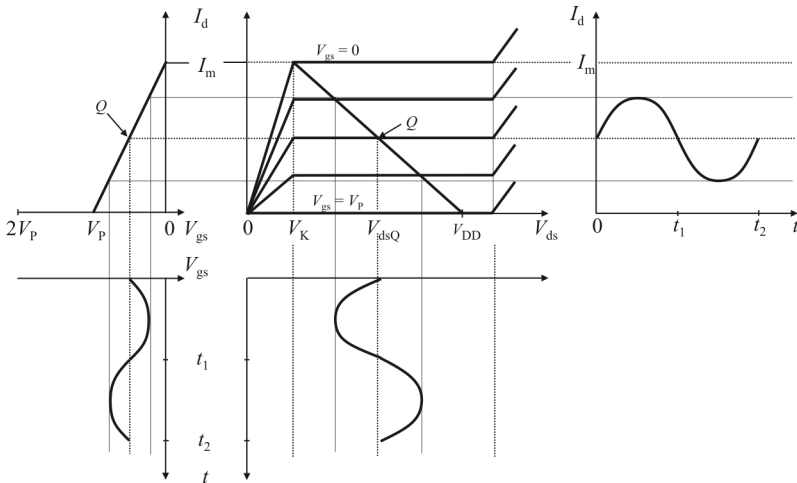
**Figure 6.11** MOSFET class A characteristics.

These mismatch losses correspond to 44% power loss at the input and 21% power loss at the output. Therefore, by matching input and output, as much as 2.6dB gain can be recovered, which is a non-trivial fraction of the 16.9dB.

The typical transfer and output characteristics of the class A biased MOSFET shown in Figure 6.7 are shown in Figure 6.11. The input voltage, after the input matching circuit, is impressed on the gate (G) and is labeled $V_{gs}$, which is the abscissa for the transfer characteristic in Figure 6.11. This voltage causes current to flow from the drain (D) to the source, labeled $I_d$, and therefore through the load. The amount of drain current caused by $V_{gs}$ is determined by the transconductance parameter $g_m$, which is the slope of the transfer characteristic curve. $I_d$ is the ordinate for both the transfer characteristic as well as the output characteristic in Figure 6.11. The particular curve on the output characteristic where the device is currently (instantaneously) operating is determined by the $V_{gs}$ labels on the output.

The load resistor imposes a load line on the output curve—the current and voltage in the FET/load must satisfy both the FET output characteristic as well as the load resistor. The load line shows up as a line that has a downward slope from left to right and the slope $m = 1/R_L$.

Note that within the normal operating range of the FET, the output characteristic shown in Figure 6.11 dictates that irrespective of the output voltage, $V_{ds}$ (the abscissa for the output characteristic on the right), the same current flows through the load. This is the output characteristic of a current source.

If the active device in Figure 6.7 were a BJT, then typical transfer and output characteristics are as illustrated in Figure 6.12, where the parameters are defined in Figure 6.13. A BJT configured in a *common emitter* (CE) architecture as in Figure
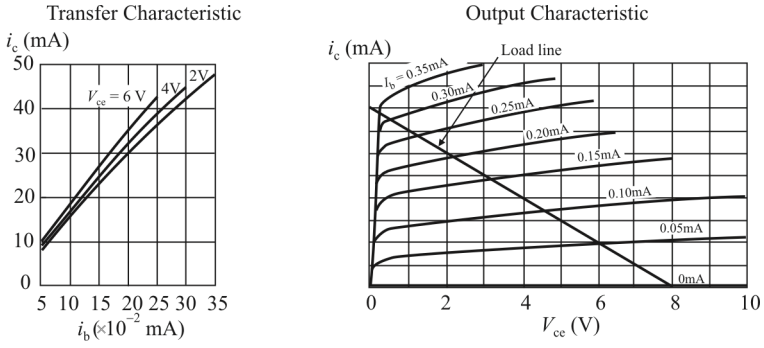
**Figure 6.12** BJT class A characteristics.
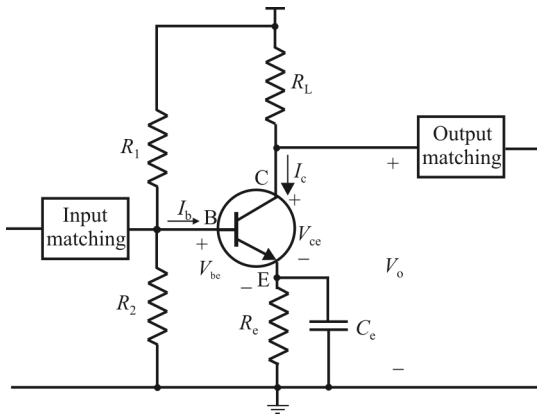
**Figure 6.13** BJT class A amplifier.
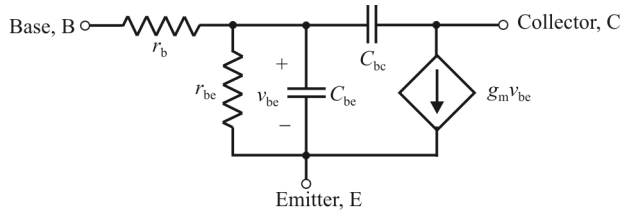
**Figure 6.14** Simplified CE BJT model useful for RF.

6.13 is normally considered a current amplifying device and the output (collector) current is controlled by the input (base) current. Therefore the transfer characteristic on the left in Figure 6.12 has $i_b$ as the abscissa and $i_c$ as the ordinate. Note that the particular transfer curve selected is a moderate function of the collector-emitter voltage, $V_{ce}$. As the base current increases, it causes an increase in the collector current and therefore an increase in the current through the load resistor. A small amount of base current (say, 0.12 mA) will cause a relatively larger amount of collector current (say 20 mA when $V_{ce} = 4V$), which means that the current gain is 20/0.12 = 167 (22dB) at this operating point.

Note that the output current for a BJT is (approximately) independent of $V_{ce}$, a characteristic similar to the FET. Thus the BJT amplifier is also considered as an approximation to a current source.

### 6.3.2 BJT IF Amplifiers

A simplified CE BJT model that is useful at high frequencies is illustrated in Figure 6.14. This model is directly applicable to BJTs that are in chip form—that is, not packaged. If the BJT is packaged, however, the parasitic packaging impedances must be included. One such model is shown in Figure 6.15 [3].
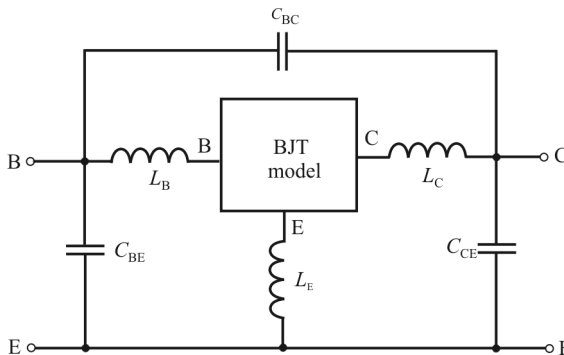


**Figure 6.15** Packaged BJT model.
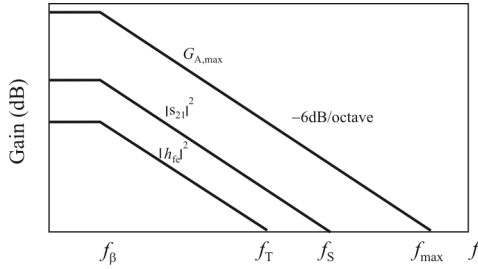
**Figure 6.16** Gain parameters.

Typical values for these parasitic impedances are 0.2 nH to 1 nH and 0.01 pF to 0.05 pF [3].

Based on the model in Figure 6.14, the gain-bandwidth frequency, $f_T$, the frequency where the magnitude of the forward current gain, $|h_{fe}|$, is unity, is given approximately by

$$f_T = \frac{g_m}{2\pi C_{be}} \tag{6.5}$$

and maximum frequency of operation, $f_{max}$, which is the frequency where the maximum available power gain from the transistor, given by [4]

$$f_{max} = \sqrt{\frac{f_T}{8\pi r_{be} C_{be}}} \tag{6.6}$$

is unity. Another figure of merit for BJTs is the beta cutoff frequency, $f_\beta$, given approximately by

$$f_\beta \approx \frac{1}{2\pi r_{be} C_{be}} \tag{6.7}$$

These parameters are illustrated in Figure 6.16 [5].

### 6.3.3 MOSFET High-Frequency Amplifiers

The high-frequency model for FET amplifiers [both MOSFET and *junction FET* (JFET)] is illustrated in Figure 6.17. The frequency-dependent components are:
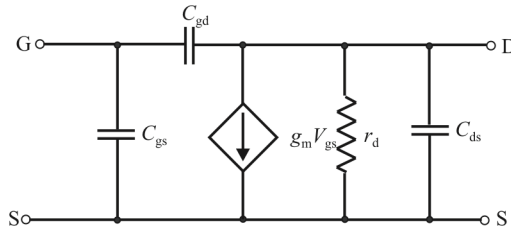
**Figure 6.17** FET (MOSFET and JFET) HF model.

$C_{gs}$ : gate-to-source capacitance
$C_{gd}$ : gate-to-drain capacitance (sometimes called the overlap capacitance)
$C_{ds}$ : drain-to-source capacitance

Since $C_{gs} \gg C_{ds}$, $C_{ds}$ can usually be ignored. The capacitances in the high-frequency small-signal model of the MOSFET are relatively constant over the frequency range.

The maximum operating frequency, $\omega_T$, is the frequency at which the FET no longer amplifies the input signal—that is, the dependent current source $g_m v_{gs}$ is equal to the input current. It is approximated by

$$\omega_T = \frac{g_m}{C_{gs} + C_{ds}} \tag{6.8}$$

In general, BJTs have higher maximum operating frequencies than FETs. Two factors are responsible for the lower frequency performance of FETs compared to BJTs:

- For a given area and operating current, the $g_m$ of silicon FETs is less than half that of silicon BJTs.
- In MOSFET structures, considerable capacitance is observed at the input due to the oxide layer. In JFETs, semiconductor properties and physical dimensions of the device result in long channel lengths that reduce high-frequency performance.

## 6.3.4 Frequency Response of RF Amplifiers

All amplifiers have limited frequency range. This is due to interstage tuned circuits as well as the inherent frequency limitations of the active devices themselves. The tuned circuits are used to control transients.

Tuned circuits must be retunable in EW amplifiers. If an amplifier uses tuned circuits between stages that are retuned as the frequency of operation changes, that
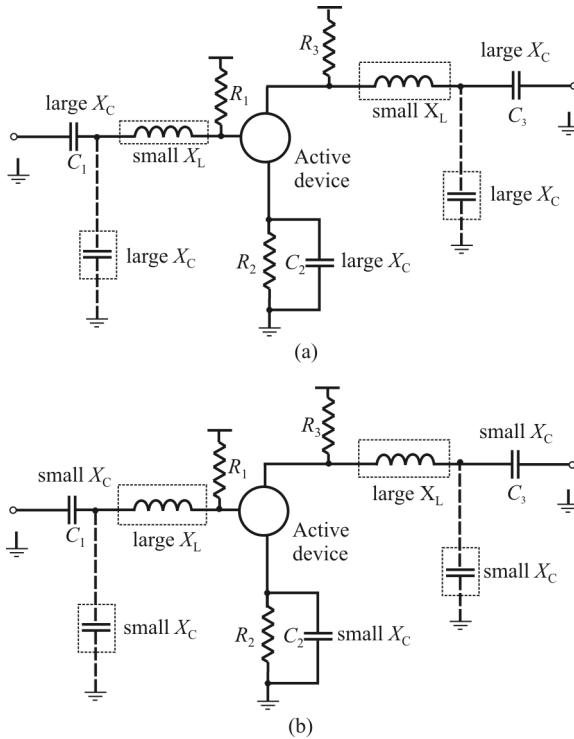
**Figure 6.18** Amplifier stage: (a) low-frequency input and (b) high-frequency input. The parasitic reactances are shown dashed.

amplifier chain can only be used at a single frequency at a time. While this is one mode of operation of an amplifier, it is also possible to use amplifiers that amplify multiple signals (multiple frequencies) simultaneously, which is precluded with interstage retuning.

The frequency response of any AC circuit, including RF amplifiers, is determined for the most part by the reactive elements (capacitance and inductance), including those associated with the active devices. This is because the impedances of these components vary with the frequency. In addition to the reactance of other components in the circuit, most amplifier stages are coupled using RC components. Capacitors are sometimes used to isolate the bias voltages associated with each stage—capacitors block DC current. The other normal method of coupling that also retains bias isolation between stages is to use transformers; this discussion has its own dedicated section later. However, they are highpass components—their impedance increases as the frequency is decreased. There is also some amount of capacitance and inductance in the wiring of the circuit. The end result is that all RF amplifiers have a gain response that varies with frequency.

Figure 6.18 illustrates an amplifier stage including the reactive components just mentioned (the parasitic inductances and capacitances associated with the active device are not shown). In Figure 6.18(a) it is assumed that the input signal has a relatively low frequency (low is relative to the purpose for which the amplifier is used—in general, it does not necessarily imply any specific frequency). Likewise in Figure 6.18(b) the frequency is relatively higher. At low frequencies the reactances of the capacitors are large while the reactances of the inductors are small. At higher frequencies these switch, with the capacitive reactance becoming small and the inductive reactance large. Since the impedances of these inductors and capacitors vary with frequency, they impose a filtering effect.

The circuit components are $C_1$, $C_2$, $C_3$, $R_1$, $R_2$, $R_3$, and the active device that could be a BJT, FET, or vacuum tube. The circuit components are there for a specific purpose. $C_1$ is used to isolate the bias levels of this amplifier from whatever provides the input. $R_1$ is used to provide a bias current, as does $R_2$. $R_2$ is also used to provide stability. $C_2$ connects the bottom active device terminal to ground at high frequency. $R_3$ provides bias current for the active device and $C_3$ couples the output signal to the following stage while isolating the bias levels for this stage. The active device, of course, provides the gain. The parasitic reactive components provide undesired effects but are ever present and must be taken into consideration, especially as the operating frequency increases. Since the formulas for capacitive reactance and inductive reactance are

$$X_C = \frac{1}{j\omega C} \qquad\qquad X_L = j\omega L \qquad\qquad (6.9)$$

at lower frequencies $X_C$ will be larger than at higher frequencies and vice versa for inductors—at low frequencies $X_L$ will be lower than at higher frequencies. Therefore the reactances will tend to be as illustrated in Figure 6.18. Ignoring the parasitic capacitances and inductances of resistors, they have the same values at low and high frequencies.

In addition to the other circuit components, an amplifying device (transistor or vacuum tube), itself, has parasitic reactances present which, cause it to react differently to high frequencies than it does to low frequencies. In most cases these parasitic reactances tend to be best modeled as capacitive. Figure 6.19 shows a portion of the interelectrode capacitance of a transistor and the way in which this affects high- and low-frequency signals.

The transistor is shown with interelectrode capacitances. $C_{eb}$ represents the emitter-base capacitance while $C_{bc}$ represents the base-collector capacitance. Figure 6.19(a) shows the reactance as high when there is a low-frequency input signal. For a low-frequency signal, the high reactances cause very little effect on the amplifier stage. The transistor amplifies the input signal as shown. However, when a high-frequency input signal is applied to the transistor, as in Figure

$C_{bc}$
($X_C$ large)

$C_{bc}$
($X_C$ small)

$C_{eb}$
($X_C$ large)

$C_{eb}$
($X_C$ small)

(a)                                    (b)
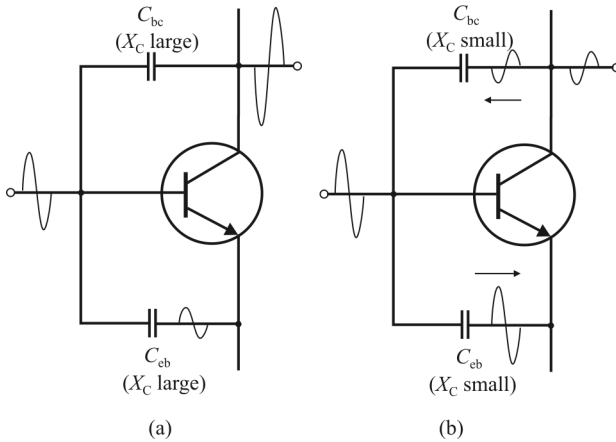
**Figure 6.19** BJT junction capacitance: (a) low-frequency input and (b) high-frequency input.

6.19(b), the capacitive reactances are low. As the voltage on the base of the transistor starts to go positive during the first half of the input signal, a significant amount of this positive voltage is felt on the emitter through $C_{eb}$. If both the base and the emitter go positive at the same time, there is minimal change in emitter–base voltage, and the conduction of the transistor will not change significantly. As the output signal is developed on the collector, part of this signal is fed back to the base through $C_{cb}$, which represents a small $X_C$. Since the signal on the collector is 180° out of phase with the base signal, this tends to drive the base in a negative direction. The effect of this is to further reduce the emitter–base voltage and the conduction of the transistor. During the second half of the input signal, the same effect occurs with the polarity reversed. The net effect is a reduction in the gain of the transistor as indicated by the small output signal.

This decrease in the amplifier output at higher frequencies is caused by the interelectrode capacitance. This is referred to as a *degenerative feedback* effect since as the frequency increases the reactances caused by the interelectrode capacitances shown decrease in value, causing more (negative) feedback than desired.

### 6.3.5 Microwave Tubes

The triode interelectrode capacitances illustrated in Figure 6.20 and transit-time delays of standard vacuum tubes preclude them from use above about 1 GHz. Alternate tube construction methods have been devised to deal with these challenges, however. Most current-day uses of microwave tubes are in high-power applications, and that is the case in EW systems as well. As the material in this
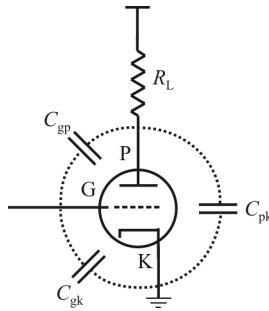
**Figure 6.20** Parasitic capacitance in a triode.

chapter concerns low-power applications, no further discussion of tube amplifiers is included.

# 6.4 Transformer Coupling

The amplifier stage shown in Figure 6.18 uses capacitive coupling to connect one stage with the next. This is only one way to connect stages. Another way is by using transformers. One such stage is illustrated in Figure 6.21. As seen, the transformers isolate the bias of the individual stages just as the capacitors did in the capacitively coupled amplifier. Transformer coupling has many advantages over RC coupling for RF amplifiers; for example, voltage gain (not power) can be
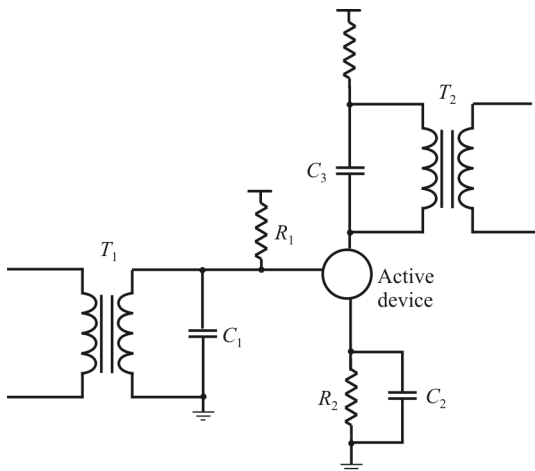


**Figure 6.21** Transformer-coupled RF amplifier.
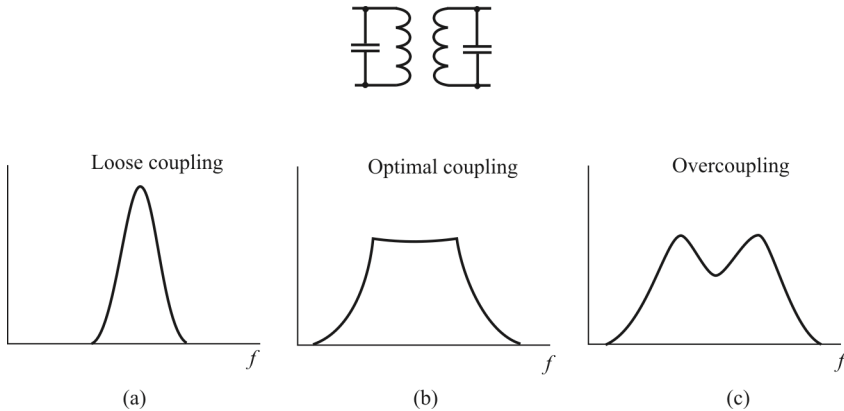
**Figure 6.22** Transformer coupling: (a) loose coupling; (b) optimal coupling; and (c) overcoupling.

provided by using a step-up transformer at the output. Likewise, if current gain is required, a step-down transformer can be used. In Figure 6.21, the secondary of $T_1$ and capacitor $C_1$ form a tuned circuit. Likewise, the primary of $T_2$ and capacitor $C_2$ are a tuned circuit which acts as the load for the active device.

Transformers are particularly effective at transforming from one impedance level to another. Since the input and output impedances of amplifier stages are typically different, transformers are frequently used to match these impedances. Depending on the configuration of the amplifier, the input could be low impedance while the output is at a high impedance, or vice versa.

The tuned circuits formed by the transformers and capacitors may not have the bandwidth required for the amplifier. EW amplifiers are typically quite broadband. In other words, the bandwidth of the tuned circuit may be too "narrow" for the requirements of the amplifier. One way of increasing the bandwidth of a tuned circuit is to use a resistor. A resistor connected in parallel with the tuned circuit decreases the $Q$ of the tuned circuit, thereby causing a much broader bandpass.

Alternately, the amount of coupling in the transformer can be varied to increase the bandwidth. Transformer coupling is the amount of flux established by the primary that gets coupled into the secondary. A transformer can be *loosely coupled* where little energy is transferred from the primary to the secondary, *optimally coupled* where the maximum amount of energy is transferred, or *overcoupled*. Figure 6.22 shows the effect of coupling on frequency response when parallel LC circuits are made from the primary and secondary windings of transformers.

When loosely coupled, the frequency response curve exhibits a relatively narrow bandwidth as illustrated in Figure 6.22(a). For optimum coupling, in Figure 6.22(b), the bandwidth is wider and the middle of the curve is relatively

flat. When overcoupled, the frequency response curve exhibits a broad bandpass, but the curve dips in the middle. The bandpass available from optimum coupling may not be wide enough. In these cases, a resistor can be added to decrease the $Q$. If still inadequate bandwidth ensues, another amplifier may be required.

The frequencies at which EW RF amplifiers operate can be quite high, causing some problems. One of these problems is losses in the transformers, which are due to three causes. First there is loss due to the resistance of the wire. This type of power loss is called copper loss or $I^2R$ loss. This loss tends not to be a function of frequency as it is simple resistive loss.

The second source of loss is due to eddy currents. The core of a transformer is usually constructed of some type of ferromagnetic material because it is a good conductor of magnetic lines of flux. Whenever the primary of an iron-core transformer is energized by an AC source, a fluctuating magnetic field is produced. This magnetic field cuts the conducting core material and induces a voltage into it. The induced voltage causes random currents to flow through the core, which dissipates power in the form of heat. These undesirable currents are called *eddy currents*. Eddy current losses in a transformer do not exhibit a strong dependence on frequency.

The third phenomenon that causes losses in transformers is called *hysteresis loss*. When a magnetic field is passed through a core, the core material becomes magnetized and the domains within the core must align themselves with the external field. If the direction of the field is reversed, the domains must turn so that their poles are aligned with the new direction of the external field.

Each tiny domain must realign itself twice during each cycle. The energy used to turn each domain is dissipated as heat within the iron core. This is hysteresis loss and can be thought of as resulting from molecular friction. Hysteresis loss can be held to a small value by proper choice of core materials. It is, however, frequency dependent, increasing as the frequency increases. This increase in hysteresis loss causes the efficiency of the transformer and the amplifier to decrease. The energy that goes into hysteresis loss is taken away from energy that could go into the signal. RF transformers, specially designed for use at higher frequencies, are used to correct the problem of excessive hysteresis loss in the transformer of an RF amplifier. The windings of RF transformers are wound onto a tube of nonmagnetic material and the core is either powdered iron or air. These types of cores also reduce eddy current loss.

# 6.5 Automatic Gain Control

### 6.5.1 Introduction

Most communication EW receivers must handle signals over a wide range of amplitudes. Near transmitters are received with considerable amplitude while
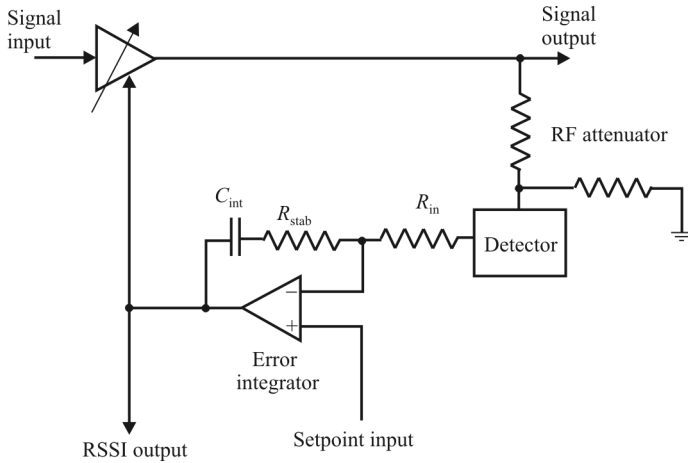
**Figure 6.23** VGA-based AGC loop block diagram.

those farther away are relatively weak. To keep from overdriving the receiver amplifier and other active circuits, *automatic gain control* (AGC) is typically employed. This is a mechanism for adjusting the gain of some of the front-end amplifiers so that the weak signals can be intercepted as well as the strong ones.

This section introduces the use of *variable gain amplifiers* (VGAs) in AGC applications. Figure 6.23 is a general block diagram for an AGC loop. The input signal passes through the VGA to produce the output level to be stabilized. The detector's output is compared against a reference voltage to produce an error signal, which is then integrated to produce the gain control voltage. This is applied to the control input of the VGA. The RF attenuator shown between the VGA and the detector is used to align the maximum output level of the VGA with the maximum input level of the detector.

In this section we will examine several key issues in AGC applications of VGAs, including VGA types, loop dynamics, detector types, the operating level of VGA, and the operating level of the detector.

## 6.5.2 VGA Types

There are two major classes of VGAs. The first is called IVGA (input VGA), which consists of a passive variable attenuator followed by a fixed-gain amplifier (Figure 6.24). The second type is the output VGA (OVGA), which is a fixed-gain amplifier followed by a passive variable attenuator (Figure 6.25). An IVGA is the preferred choice for a receive AGC system because the available output level at low distortion is relatively independent of the gain setting. This is the desired trait for an AGC system, where the objective is to maintain a constant output in the
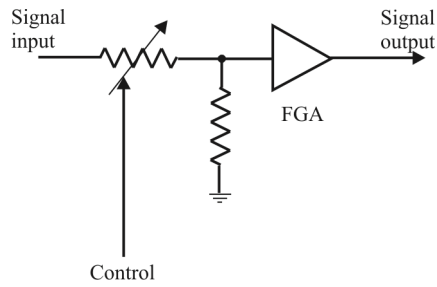
**Figure 6.24** IVGA schematic.
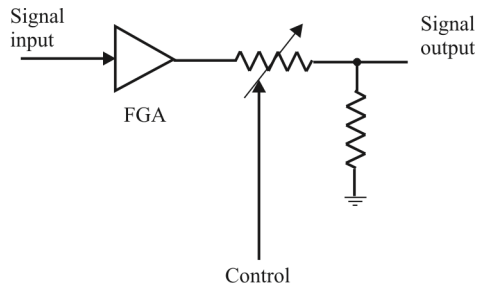


**Figure 6.25** OVGA schematic.

face of varying input signal amplitude. The OVGA is generally ill suited to AGC applications because of its reduced output signal handling capability at low gain settings. We will not discuss this configuration further here.

When a single IVGA is used in a situation in which the VGA sets the system noise floor, the output SNR is essentially independent of the input signal; it does not improve as is often preferred. Occasionally, it is desirable to cascade two VGAs in order to ameliorate this behavior or simply to obtain more gain control range. Doing so requires proper coordination of the gain control inputs of the two devices. If the gain control of only the second stage VGA is manipulated in the weak signal regime, the signal level to the first stage VGA's amplifier increases with increasing input level, so the output SNR improves with increasing input level. It is necessary to hand off the gain control from the second stage to the first stage only when overload of the first stage's amplifier is imminent and detected.

Alternatively, the two gain control inputs may simply be driven in parallel, in which case the output SNR (expressed in dB) improves at half the rate at which the input level (also expressed in dB) rises. In cases where the VGAs used have residual ripple in their gain control functions, an additional benefit of this approach can be obtained if the two gain control input signals are intentionally offset by half the period of the ripple. This can considerably reduce the ripple.

One of the benefits of using an IVGA in an AGC loop is that the VGA's gain control voltage bears an accurate logarithmic relationship to the input signal level when the loop is in equilibrium. This means that the gain control voltage may also be used as an excellent RSSI, as illustrated in Figure 6.23.

### 6.5.3 Loop Dynamics

Response time is an important issue with any AGC loop. There is usually a compromise between having the loop respond to undesired input level fluctuations as rapidly as we would like and having it impose undesirable AM on the signal. Additionally, large and/or abrupt changes in the input level may lead to unacceptable recovery behavior, causing further adjustments of the response time.

The issue of excessive loop bandwidth deserves a bit more explanation. If the loop responds too quickly, it will introduce undesired gain modulation arising from the loop's efforts to stabilize the output level of a signal containing legitimate AM. This is referred to as *gain pumping*. In the context of digital modulation, the presence of appreciable gain pumping can result in significant modulation errors and perhaps even noticeable spectral re-growth in extreme cases. A tolerable value of gain pumping would generally be only a fairly small fraction of 1 dB.

### 6.5.4 Detector Types

One convenient aspect of an AGC loop is that the detector need not necessarily have a very wide dynamic range over which it obeys any particular law. This is

because the detector operates at a constant average level when the AGC loop is in equilibrium; thus, the detector should only need to cope accurately with the level range associated with a modulated signal. However, as mentioned earlier, the detector's response law (i.e., linear, log, square law, etc.) can play a significant role in determining the loop's dynamic response during large, abrupt changes in signal level. Perhaps more importantly, the detector's response law influences the dependency of the loop's equilibrium level on the input's waveform or crest factor.

Four detector types will be considered here: envelope detector, square law detector, true-RMS detector, and log detector.

## 6.5.4.1 Envelope Detector (Rectifier)

The output voltage of the envelope detector is proportional to the magnitude of the instantaneous RF input voltage. Assuming that sufficient lowpass filtering is applied at its output to eliminate RF ripple, this detector produces a voltage proportional to the envelope amplitude of the RF signal. Assuming that the loop's bandwidth is sufficiently small so as to avoid significant gain pumping, the effect of the loop using an envelope detector is to stabilize the average rectified voltage of the signal. The resulting power is therefore dependent on the RF signal's envelope waveform.

Such a loop acting on a constant-envelope signal such as GSM will produce an average output power that is different from that for a heavily AM signal, such as CDMA or 64QAM. The output of the envelope detector cannot go negative no matter how weak the input signal but may reach extreme positive values in response to very strong signals. Starting with the AGC loop in equilibrium, a sudden large increase in input amplitude causes a very large initial increase in detector output, which very rapidly drives the loop toward lower gain.

On the other hand, an abrupt reduction of the input signal level (no matter by how many decibels) cannot reduce the detector output below zero, and the loop's best response is to slew toward equilibrium at a fairly low rate until the detector output begins to change by a significant fraction of the reference voltage, at which point the recovery trends toward an exponential decay. In the slew rate-limited region, the gain of the signal path is varying at a constant number of decibels per second.

Figure 6.26 shows the behavior of such a loop for a large input level step (note that curves for all four detector types are superimposed on this plot). These results were obtained from simulations in which the VGA has representative limits on the gain range and on the maximum output level. The detectors contrived for these simulations have no particular limits, on the grounds that in most practical situations the designer will scale the circuit so that the detector does not limit appreciably before the VGA does.
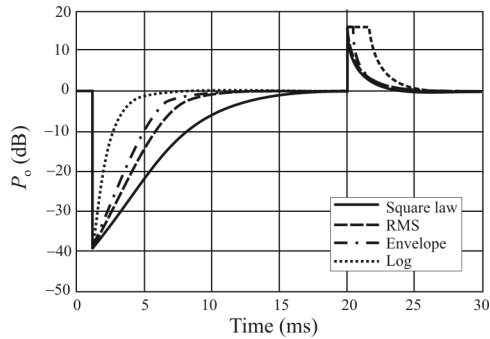
**Figure 6.26** AGC loop responses to large amplitude steps for various detectors.

## 6.5.4.2 Square Law Detector

This type of detector has an instantaneous output, which is proportional to the square of the instantaneous RF input voltage, which is equivalent to saying that its output is proportional to input power. This behavior, when incorporated into an AGC loop of sensible bandwidth, makes the loop's equilibrium average output power independent of the input waveform. As with the envelope detector, the output can never go negative, resulting in the loop having a similar tendency toward slew rate-limited behavior when reacting to abrupt decreases in input amplitude.

The response to large abrupt increases in input amplitude can be even more striking, however, because the square law detector characteristic exaggerates the effect of the input increase. The extent to which this happens depends on the clipping level of either the VGA or the detector, whichever is smaller.

## 6.5.4.3 True-RMS Detector

This detector comprises a square law detector followed by a lowpass filter followed by a square root function. The lowpass filter performs the "mean" operation associated with the root-mean-square (RMS) function, and it should have a sufficiently long time constant to smooth the output variations of the squaring detector that would otherwise arise from the legitimate modulation of the signal. Because of the square root element in this detector, the average output is proportional to the signal voltage, not power, so the loop's response to small abrupt decreases or increases of signal level should essentially be the same as that for an envelope detector, provided that the added filter pole within the RMS detector is correctly compensated for elsewhere in the loop. The fact that the added pole is located in a region of the signal path that is square law brings forth the possibility of the large step response being different from that of the simple

envelope detector, which can indeed be seen in the figure. Note that the RMS detector has a slightly slower recovery from a large downward amplitude step than does the standard envelope detector but a slightly faster recovery (and a bit of overshoot) from a step up in input amplitude. In common with the square law detector, the true-RMS detector will make the AGC loop's equilibrium point independent of the RF signal waveform.

It should be noted that the presence of the long time-constant lowpass filter in this detector may have a marked influence on loop dynamics; indeed, this filter may even provide the dominant pole in some designs. This time constant must therefore be coordinated with the remainder of the loop design.

6.5.4.4 Log Detector

This type of detector produces an output proportional to the logarithm of the RF input voltage. Because this behavior is complementary to that of the linear-in-dB VGA in the loop, the resulting loop dynamics are those of a linear system, assuming that signal level fluctuations during transients remain within the measurement range of the log detector. Subject to that assumption, the AGC loop's response to abrupt large changes in input level will not be slew rate-limited and will often be faster to recover from amplitude decreases.

As with the envelope detector, the equilibrium point of an AGC loop using the log detector will depend on the RF input waveform.

6.5.4.5 Comparison of Responses with Different Detectors

The AGC loops whose simulation results are shown were designed so that the small-signal response speeds are identical. The results show that the loop's large-step transient response is markedly dependent on the type of detector. At one extreme, the log detector gives the fastest response to large abrupt decreases in input level because the logarithmic curve has a very steep slope for low inputs, which exaggerates the loop's response. However, the log detector has a shallow slope for high-input levels, resulting in a diminished response rate to sudden increases in signal level. At the other extreme, the square law detector's small slope near zero input level gives it a very sluggish response to large decreases in input amplitude. Conversely, the square law detector exaggerates the response to large signals, giving the fastest response to increasing signals. The envelope and RMS detectors, having intermediate characteristics, give response speeds in between.

**6.5.5 Operating Level of Detector**

Ideally the operating level of the detector should be set as high as possible in order to minimize the error due to residual DC offsets. However, other considerations

often rule. For signals with amplitude modulation, the peak input to the detector when the loop is in equilibrium must be no higher than what the detector will support, and so the average must be lower. Even for constant-envelope signals, the average level must be reasonably lower than the maximum, so that there is room for the detector level to increase if the system input level increases; otherwise, there could be little or no error signal to drive the loop back toward equilibrium. Note that there will generally be unequal amounts of room for the detector output to swing up or down from the design equilibrium level, which will make the apparent attack and decay speeds of the loop differ.


# 6.6 Concluding Remarks

The basic operating principles of small-signal RF amplifiers as they are used as IF amplifiers in EW receiving systems were presented in this chapter. All of this material also applies to the RF LNA in the RF stage, except that IF amplifiers are typically narrowband and need only amplify a narrow portion of the spectrum (relative to their center frequency).

Only the common emitter BJT and common source MOSFET amplifier configurations were introduced. There are many other amplifier configurations that can be used for amplification of RF signals [6–9]. Our intent here was to provide a basic introduction to establish common terminology and a fundamental understanding of RF amplifiers and, in particular, their use as IF amplifiers in EW receivers. The CE and CS amplifiers are, by far, the two most common topologies in use for this application.

## References

[1]     White, J. F., "Applying S-Parameters to Amplifier Design," *Microwaves and RF*, July 2004.
[2]     Poisel, R. A., *Antenna Systems and Electronic Warfare Applications*, Norwood, MA: Artech House, 2012, Ch. 20.
[3]     Gonzolez, G., *Microwave Transistor Amplifiers Analysis and Design*, Upper Saddle River, NJ: Prentice Hall, 1997, p. 76.
[4]     Gonzolez, G., *Microwave Transistor Amplifiers Analysis and Design*, Upper Saddle River, NJ: Prentice Hall, 1997, p. 84.
[5]     Gonzolez, G., *Microwave Transistor Amplifiers Analysis and Design*, Upper Saddle River, NJ: Prentice Hall, 1997, p. 81.
[6]     Razavi, B., *RF Microelectronics*, Upper Saddle River, NJ: Prentice Hall, 1998.
[7]     Pozar, D. M., *Microwave Engineering*, 3rd Ed., New York: Wiley, 2006.
[8]     Krauss, H. L., C. W. Bostian, and F. H. Raab, *Solid State Radio Engineering*, New York: Wiley, 1980.
[9]     White, J. F., *High Frequency Techniques*, New York: Wiley, 2004.

# Chapter 7

# IF Filters

## 7.1 Introduction

IF stages in communication EW receivers are comprised of amplifiers for boosting the levels of signals and relatively narrowband filters for improving the selectivity of the receiver. Selectivity refers to the rejection or suppression of signals in adjacent RF channels to prevent or minimize interference to the SOI channel. The filters are normally placed between the stages of amplification and are used for matching the stages as well as filtration. In this chapter, we examine the basic parameters of RF amplifiers and filters.

Signal filtering is often central to the design of many communication EW subsystems. The isolation or elimination of information contained in frequency ranges is of critical importance. In simple AM receivers, for example, the user selects one radio station using bandpass filter techniques. Other radio stations occupying frequencies close to the selected radio station are eliminated.

This chapter is intended to serve as a basic introduction to some of the fundamental concepts and terms associated with filters. It will not turn a novice into a filter designer, but it can serve as a starting point for those wishing to learn more about filter design. Enough information is provided to understand the majority of the application of filtering in communication EW receivers and other components in the receiving chain (such as diplexers and multicouplers).

We include passive filters only, even though filters implemented with active devices can serve well in many applications. The reason for this is that active filters were devised originally to address the large inductor problems associated with low-frequency (primarily audio) signals. Compact and efficient filters can be constructed using active devices with resistors and capacitors while leaving out inductors altogether. As operating frequencies increase, the inductors involved with passive RLC networks become reasonably small, leaving the advantage of active filters behind in the process. The biggest reason for implementing active filters in the RF range is to incorporate gain greater than one into the topology.
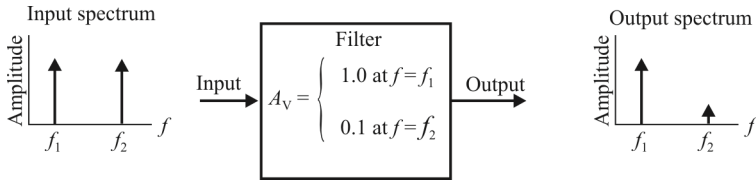
**Figure 7.1** Using a filter to reduce the effect of an undesired signal at $f_2$ while retaining the desired signal at $f_1$.

This can also be accomplished with passive RLC networks and amplifiers before and/or after the filter, so the advantages are minimal in so doing. Therefore, we only address passive filter networks in our discussion in this chapter.

Another reason for active filter implementation is for integrated *systems on silicon* (SoS) applications, such as with cellular telephones. We do not address such applications in our discussions of EW receivers, as there is generally little motivation for such receiver implementations (such as production volume, cost, etc.).

# 7.2 Filters and Signals

A filter is an electrical network that alters the amplitude and/or phase characteristics of a signal with respect to frequency. Ideally, a filter will not add new frequencies to the input signal, nor will it change the component frequencies of that signal, but it will change the relative amplitudes of the various frequency components and/or their phase relationships. Filters are often used in electronic systems to emphasize signals in certain frequency ranges and reject signals in other frequency ranges. Such a filter has a gain that is dependent on signal frequency. As an example, consider a situation where a useful signal at frequency $f_1$ has been contaminated with an unwanted signal at $f_2$. If the contaminated signal is passed through a circuit (Figure 7.1) that has very low gain at $f_2$ compared to $f_1$, the undesired signal can be removed, and the useful signal will remain. Note that in the case of this simple example, we are not concerned with the gain of the filter at any frequency other than $f_1$ and $f_2$. As long as $f_2$ is sufficiently attenuated relative to $f_1$, the performance of this filter will be satisfactory. In general, however, a filter's gain may be specified at several different frequencies or over a band of frequencies.

The two types of frequency selective circuit configurations most commonly used in EW systems are the passive *LC* filter (lowpass, highpass, bandpass, and bandstop responses) and the tuned amplifier (bandpass response). LC ladder networks are commonly used as building blocks for passive filters at RF. The
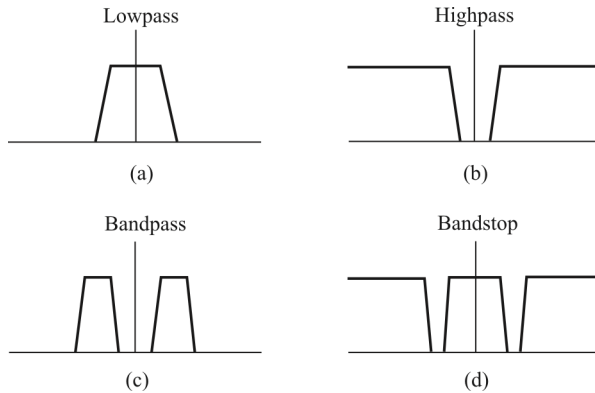
**Figure 7.2** The basic four ideal frequency responses.

values of the inductors and capacitors are varied depending on the type of filter, frequency specifications, and terminations. We examine some other types of passive filtering techniques, mostly bandpass, as well.

Since filters are defined by their frequency domain effects on signals, it makes sense that the most useful analytical and graphical descriptions of filters also fall into the frequency domain. Thus, curves of gain versus frequency and phase versus frequency are commonly used to illustrate filter characteristics, and the most widely used mathematical tools are based in the frequency domain.

# 7.3 Basic Filter Types

Although we concentrate mostly on bandpass IF filters here, in addition to the lowpass frequency response, other basic ideal responses are often needed in practice. The ideal highpass filter rejects signals with frequencies below a certain value and passes those with frequencies above that value. The ideal bandpass filter passes only a band of frequencies, and the ideal bandstop filter completely rejects a band of frequencies. These ideal frequency responses are illustrated in Figure 7.2. There is an additional basic type of filter we consider that is called the all-pass. This filter ideally has no impact on the amplitude but changes the phase of the signals.

## 7.3.1 Transfer Functions

The frequency domain behavior of a filter is described mathematically in terms of its transfer function or network function. This is the ratio of the Laplace

transforms of its output and input signals. The voltage transfer function $H(s)$ of a filter can therefore be written as

$$H(s) = \frac{V_{out}(s)}{V_{in}(s)} \qquad (7.1)$$

where $V_{in}(s)$ and $V_{out}(s)$ are the input and output signal voltages and $s = \sigma + j\omega$ is the complex frequency variable. The transfer function defines the filter's response to any arbitrary input signal, but we are most often concerned with its effect on continuous sine waves. There are two principal reasons for this. First, sine waves are commonly encountered in practice. Many modulation techniques assume that the carrier is a sine wave. Second, all periodic signals can be expressed in terms of a Fourier series expansion, which uses sine waves as its basis functions. All such signals then can be represented as a (infinite) sum of weighted sine waves—thus the importance of sine wave analysis for filtering investigations.

Especially important is the magnitude of the transfer function as a function of frequency, which indicates the effect of the filter on the amplitudes of sinusoidal signals at various frequencies. Knowing the transfer function magnitude (or gain) at each frequency allows us to determine how well the filter can distinguish between signals at different frequencies. The transfer function magnitude versus frequency is called the *frequency response*.

Similarly, the phase response of the filter gives the amount of phase shift introduced in sinusoidal signals as a function of frequency. Since a change in phase of a signal also represents a change in time, the phase characteristics of a filter become especially important when dealing with complex signals where the time relationships between signal components at different frequencies are critical.

By replacing the variable $s$ in (7.1) with $j\omega$, where $\omega$ is the radian frequency ($\omega = 2\pi f$), we can find the filter's effect on the magnitude and phase of the input signal. The magnitude is found by taking the absolute value of the result of doing so

$$|H(j\omega)| = \left| \frac{V_{out}(j\omega)}{V_{in}(j\omega)} \right| \qquad (7.2)$$

and the phase is

$$\arg H(j\omega) = \arg \frac{V_{out}(j\omega)}{V_{in}(j\omega)} \qquad (7.3)$$
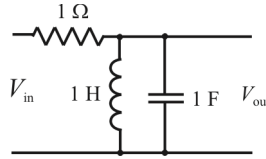
**Figure 7.3** Filter network.

As an example, the network of Figure 7.3 has the transfer function

$$H_{BP}(s) = \frac{s}{s^2 + s + 1} \tag{7.4}$$

This is a second-order system. The order of a filter is the highest power of the variable $s$ in its transfer function. The order of a filter is also usually equal to the total number of capacitors and inductors in the circuit. Higher order filters will obviously be more expensive to build, since they use more components, and they will also be more complicated to design. However, higher order filters can more effectively discriminate between signals at different frequencies.

Before actually calculating the amplitude response of the network, we can see that as $s \to 0$, that is, at very low frequencies, the numerator also approaches zero, as do the first two terms of the denominator. Thus, as $s \to 0$, the numerator approaches zero, the denominator approaches one, and $H(s)$ approaches zero. Similarly, as $s \to \infty$, $H(s)$ also becomes progressively smaller, because the denominator increases with the square of frequency while the numerator increases linearly with frequency. Therefore, $H(s)$ will have its maximum value at some frequency between zero and infinity and will decrease at frequencies above and below that peak.

To find the magnitude of the transfer function, replace $s$ with $j\omega$ to yield

$$A(\omega) = \left| H(s) \right|_{s=j\omega} = \left| \frac{j\omega}{-\omega^2 + j\omega + 1} \right| \tag{7.5}$$

$$= \frac{\omega}{\sqrt{\omega^2 + (1-\omega^2)^2}} \tag{7.6}$$

The phase is

$$\theta(\omega) = \arg H(s)_{s=j\omega} = 90° - \tan^{-1}\frac{\omega^2}{1-\omega^2} \tag{7.7}$$
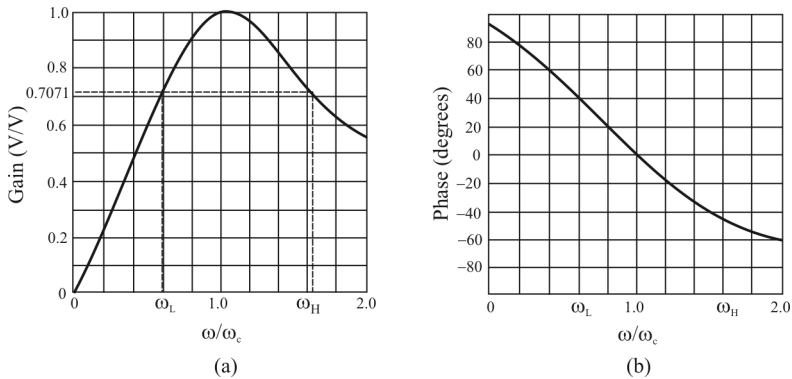
**Figure 7.4** Filter transfer characteristic: (a) gain and (b) phase shift.

The above relations are expressed in terms of the radian frequency $\omega$, in units of radians/second (rps). Plots of magnitude and phase versus radian frequency are shown in Figure 7.4.

Figure 7.4(a) shows that, as we predicted, the magnitude of the transfer function has a maximum value at a specific frequency ($\omega_0$) between 0 and infinity, and falls off on either side of that frequency.[1] A filter with this general shape is known as a bandpass filter because it passes signals falling within a relatively narrow band of frequencies and attenuates signals outside of that band. The range of frequencies passed by a filter is known as the filter's passband. Since the amplitude response curve of this filter is fairly smooth, there are no obvious boundaries for the passband. Often, the passband limits will be defined by system requirements. A system may require, for example, that the gain variation between 400 Hz and 1.5 kHz be less than 1dB. This specification would effectively define the passband as 400 Hz to 1.5 kHz. In other cases, though, we may be presented with a transfer function with no passband limits specified. In this case, and in any other case with no explicit passband limits, the passband limits are usually assumed to be the frequencies where the gain has dropped by 3dB (to $\sqrt{2}/2$ or 0.507 of its maximum voltage gain). These frequencies are therefore called the −3dB frequencies or the cutoff frequencies. However, if a passband gain variation (i.e., 1dB) is specified, the cutoff frequencies will be the frequencies at which the maximum gain variation specification is exceeded.

The precise shape of a bandpass filter's amplitude response curve will depend on the particular network, but any second-order bandpass response will have a

---

[1] Where possible, we use the symbol $\omega_0$ to represent the center frequency of a bandpass or bandstop filter and $\omega_c$ to represent the corner frequency of a lowpass or highpass filter. When discussing an arbitrary frequency value, we use $\omega_0$.

peak value at the filter's center frequency. The center frequency is equal to the geometric mean of the –3 dB frequencies given by

$$f_c = \sqrt{f_L f_H} \qquad (7.8)$$

where $f_c$ is the center frequency
$f_L$ is the lower –3dB frequency
$f_H$ is the higher –3dB frequency

The $Q$ of a bandpass filter is the ratio of the center frequency to the difference between the two –3dB frequencies (also known as the 3 dB bandwidth). Therefore

$$Q = \frac{f_0}{f_H - f_L} \qquad (7.9)$$

This is a measure of the "sharpness" of the amplitude response.

When evaluating the performance of a filter, we are usually interested in its performance over ratios of frequencies. Thus we might want to know how much attenuation occurs at twice the center frequency and at half the center frequency. (In the case of the second-order bandpass above, the attenuation would be the same at both points.) It is also usually desirable to have amplitude and phase response curves that cover a wide range of frequencies. It is difficult to obtain a useful response curve with a linear frequency scale if the desire is to observe gain and phase over wide frequency ratios. For example, if $f_0 = 1$ kHz, and we wish to look at the response to 10 kHz, the amplitude response peak will be close to the left-hand side of the frequency scale. Thus, it would be very difficult to observe the gain at 100 Hz, since this would represent only 1% of the frequency axis. A logarithmic frequency scale is very useful in such cases, as it gives equal weight to equal ratios of frequencies.

Since the range of amplitudes may also be large, the amplitude scale is usually expressed in decibels $(20 \log_{10} |H(j\omega)|$ when $H(j\omega)$ is a ratio of voltages). Figure 7.5 shows the curves of Figure 7.4 with logarithmic frequency scales and a decibel amplitude scale. Note the improved symmetry in the curves of Figure 7.5 relative to those of Figure 7.4.

Second-order filters are characterized by four basic properties: the filter type (highpass, bandpass, etc.), the passband gain, the center frequency (1 rps in the above examples), and the filter $Q$. All the filters discussed so far have unity gain in the passband, but in general filters can be built with any gain. $Q$ was mentioned earlier in connection with bandpass and notch filters, but in second-order filters it is also a useful quantity for describing the behavior of the other types as well. The $Q$ of a second-order filter of a given type will determine the relative shape of the
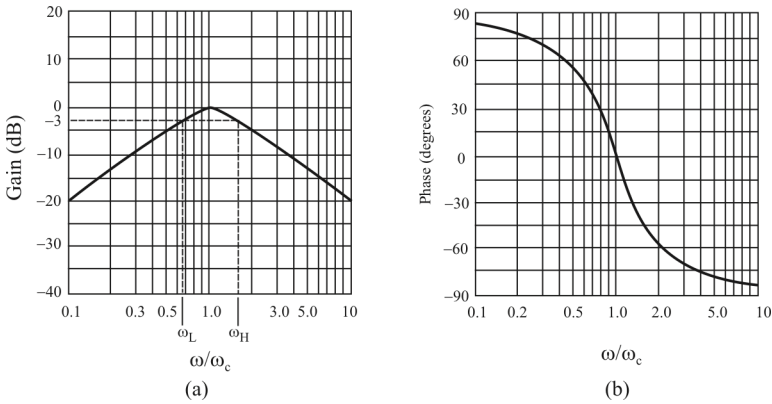
**Figure 7.5** Filter transfer characteristic with gain in decibels: (a) gain and (b) phase shift.

amplitude response. $Q$ can be found from the denominator of the transfer function if it is written in the form

$$d(s) = s^2 + \frac{\omega_0}{Q} s + \omega_0^2 \qquad (7.10)$$

Again, the $Q$ relates to the sharpness of the amplitude response curve. As $Q$ increases, so does the sharpness of the response. Lowpass and highpass filters exhibit peaks in their response curves when $Q$ becomes large. Figure 7.6 shows amplitude response curves for second-order bandpass, notch, lowpass, and highpass and the phase characteristics of all-pass filters with various values of $Q$.

There is a great deal of symmetry inherent in the transfer functions we have considered here, which is evident when the amplitude response curves are plotted on a logarithmic frequency scale. For instance, bandpass and notch amplitude response curves are symmetrical about $f_0$ (with log frequency scales). This means that their gains at $2f_0$ will be the same as their gains at $f_0/2$, their gains at $10f_0$ will be the same as their gains at $f_0/10$, and so on.

The lowpass and highpass amplitude response curves also exhibit symmetry but with each other rather than with themselves. They are effectively mirror images of each other about $f_c$. Thus, the highpass gain at $2f_c$ will equal the lowpass gain at $f_c/2$ and so on. The similarities between the various filter functions prove to be quite helpful when designing complex filters.

As the curves for the different filter types imply, the number of possible filter response curves that can be generated is infinite. The differences between different filter responses within one filter type (e.g., lowpass) can include, among others, characteristic frequencies, filter order, roll-off slope, and flatness of the passband
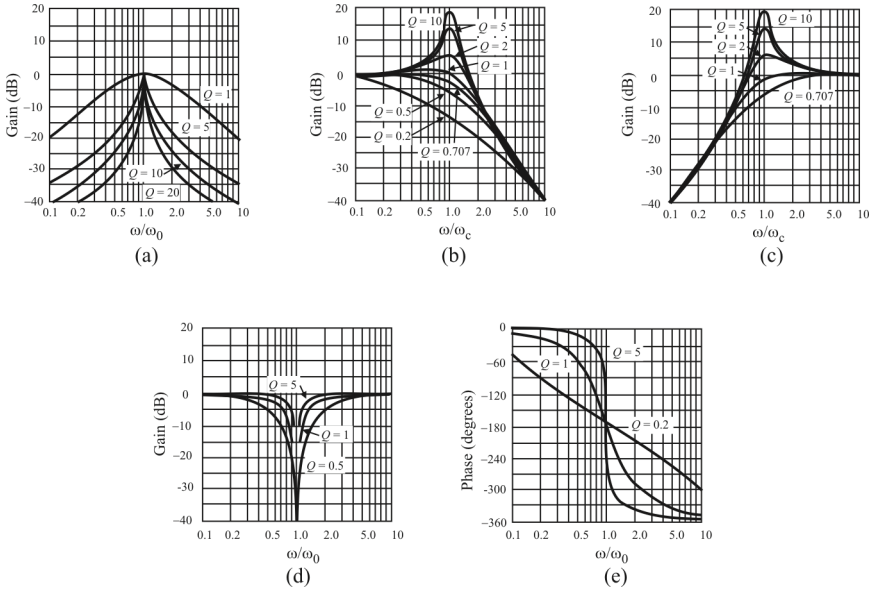
**Figure 7.6** Responses of various second-order filters as a function of $Q$: (a) bandpass, (b) lowpass, (c) highpass, (d) notch, and (e) all-pass.

and stopband regions. The transfer function ultimately chosen for a given application will often be the result of a tradeoff between the above characteristics.

## 7.3.2 Brick-Wall Filter

The brick-wall filter in Figure 7.7 is valuable from a theoretical standpoint because it serves as the standard for filter approximations. However, we can never actually build this brick-wall filter for one simple reason: its magnitude response is zero over an infinite band of frequencies. Aside from the fact that the phase is undefined for a band of zero frequencies, the finite bandwidth of the filter makes it noncausal, that is, it has a response without any input. Indeed, the impulse response of the brick-wall filter is the $\sin x/x$ function, which extends for all time.
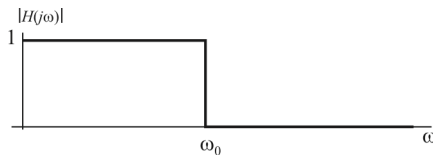


**Figure 7.7** Ideal brick-wall filter. We cannot actually build this ideal filter because the magnitude response is zero over an infinite band of frequencies.
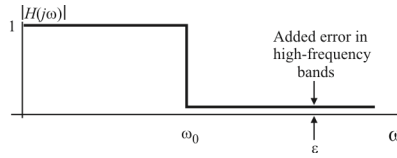
**Figure 7.8** Realizable brick-wall filter.

On the other hand the brick-wall filter shown in Figure 7.8 is realizable because some error is added to the transfer function in the frequency range above the cutoff frequency.

### 7.3.3 Bandpass

The number of possible bandpass response characteristics is infinite, but they all share the same basic form. Several examples of bandpass amplitude response curves are shown in Figure 7.9. The curve in 7.9(a) is called an "ideal" bandpass response, with absolutely constant gain within the passband, zero gain outside the passband, and an abrupt boundary between the two. As mentioned, this response characteristic is impossible to realize in practice, but it can be approximated to varying degrees of accuracy by real filters. Curves (b) through (d) are examples of a few bandpass amplitude response curves that approximate the ideal curves with varying degrees of accuracy. Note that while some bandpass responses are very smooth, other have ripple (gain variations in their passbands). Other have ripple in their stopbands as well. The stopband is the range of frequencies over which unwanted signals are attenuated. Bandpass filters have two stopbands, one above and one below the passband.

Just as it is difficult to determine by observation exactly where the passband ends, the boundary of the stopband is also seldom obvious. Consequently, the
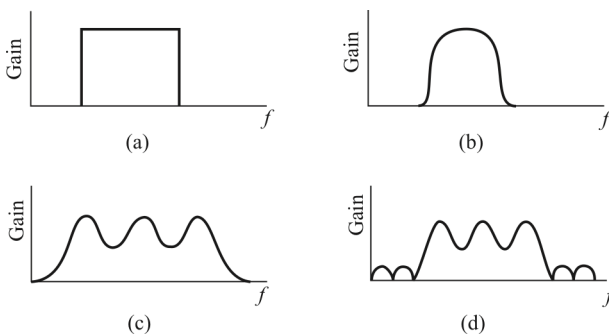


**Figure 7.9** Bandpass filter amplitude response: (a) ideal, (b) no ripple, (c) passband ripple only, and (d) passband and stopband ripple.
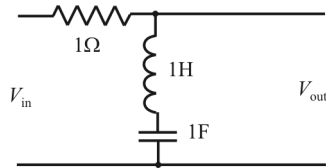
**Figure 7.10** Notch filter.

frequency at which a stopband begins is usually defined by the requirements of a given system. For example, a system specification might require that the signal must be attenuated at least 35dB at 30 MHz. This would define the beginning of a stopband at 30 MHz. The rate of change of attenuation between the passband and the stopband also differs from one filter to the next. The slope of the curve in this region depends strongly on the order of the filter, with higher-order filters having steeper cutoff slopes. The attenuation slope is usually expressed in dB/octave (an octave is a factor of 2 in frequency) or dB/decade (a decade is a factor of 10 in frequency).

Bandpass filters are used in electronic systems to separate a signal at one frequency or within a band of frequencies from signals at other frequencies. In Figure 7.1 an example was given of a filter whose purpose was to pass a desired signal at frequency $f_1$, while attenuating as much as possible an unwanted signal at frequency $f_2$. This function could be performed by an appropriate bandpass filter with center frequency $f_1$. Such a filter could also reject unwanted signals at other frequencies outside of the passband, so it could be useful in situations where the signal of interest has been contaminated by signals at a number of different frequencies.

### 7.3.4 Notch or Bandstop

A filter with effectively the opposite function of the bandpass is the bandstop or notch filter. As an example, the components in the network of Figure 7.3 can be rearranged to form the notch filter of Figure 7.10, which has the transfer function

$$H_N(s) = \frac{s^2 + 1}{s^2 + s + 1} \tag{7.11}$$

The amplitude and phase curves for this circuit are shown in Figure 7.11. A number of notch filter amplitude response curves are shown in Figure 7.12. As in Figure 7.9, curve (a) shows an ideal notch response, while the other curves show various approximations to the ideal characteristic.
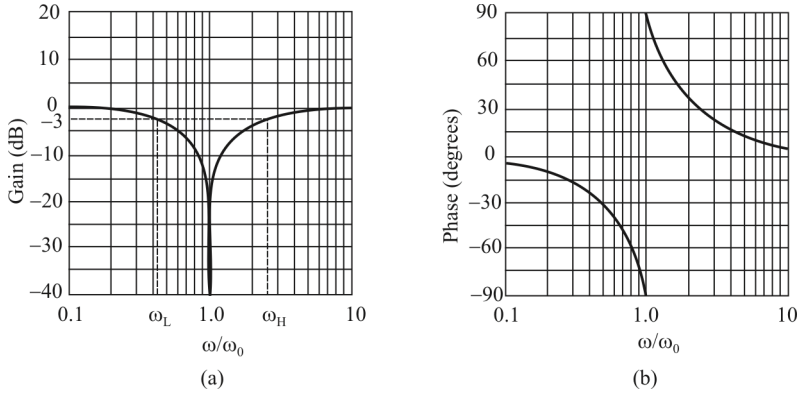
**Figure 7.11** Notch filter: (a) magnitude response and (b) phase response.
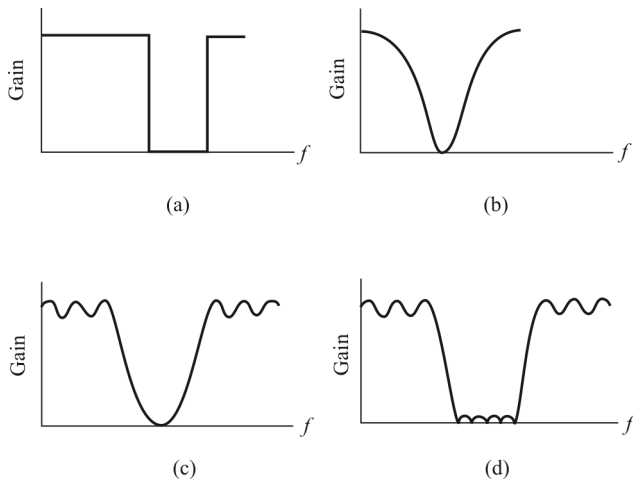


**Figure 7.12** Bandstop filters: (a) ideal, (b) no ripple, (c) bandpass ripple, and (d) bandpass and bandstop ripple.
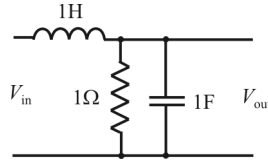
**Figure 7.13** Lowpass filter.

Notch filters are used to remove an unwanted frequency from a signal, while affecting all other frequencies as little as possible. An example of the use of a notch filter is with an audio program that has been contaminated by 60 Hz powerline hum. A notch filter with a center frequency of 60 Hz can remove the hum while having little effect on the audio signals.

### 7.3.5 Lowpass

A lowpass filter passes low frequency signals and suppresses signals at frequencies above the filter's cutoff frequency. The transfer function of the lowpass filter in Figure 7.13 is

$$H_{\mathrm{LP}}(s) = \frac{1}{s^2 + s + 1} \tag{7.12}$$

By inspection this transfer function has more gain at low frequencies than at high frequencies: as $s \to 0$, $H_{\mathrm{LP}}$ approaches 1 (0dB); as $s \to \infty$, $H_{\mathrm{LP}}$ approaches 0 ($-\infty$dB).
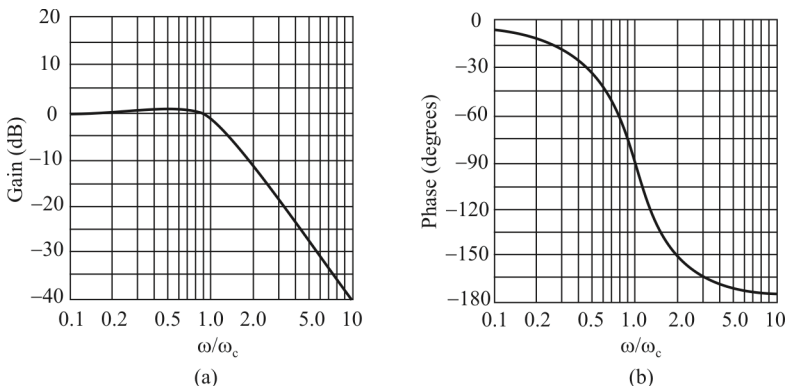


**Figure 7.14** Amplitude (a) and phase (b) response curves for lowpass filter.
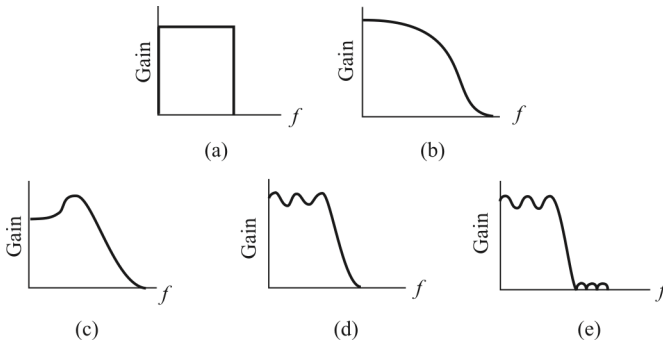
**Figure 7.15** Lowpass filters: (a) ideal, (b) no ripple, (c) shunt peaked, (d) passband ripple, and (d) passband and stopband ripple.

Amplitude and phase response curves are shown in Figure 7.14 for a lowpass filter, and several possible amplitude response curves are shown in Figure 7.15. The various approximations to the unrealizable ideal lowpass amplitude characteristics in Figure 7.15(a) take different forms, some being monotonic, always having a negative slope, and others having ripple in the passband and/or stopband.

### 7.3.6 Highpass

The highpass filter suppresses signals below its cutoff frequency. An example of a highpass filter is shown in Figure 7.16. The transfer function for this filter is

$$H_{HP}(s) = \frac{s^2}{s^2 + s + 1} \tag{7.13}$$

and the amplitude and phase curves are shown in Figure 7.17. Again, by inspection we can see that as $s \to 0$, $H_{HP}$ approaches 0, and as $s \to \infty$, $H_{HP}$ approaches 1. We can also see that the amplitude response of the highpass is a mirror image of the lowpass response. Further examples of highpass filter responses are shown in Figure 7.18, with the unrealizable, ideal response in Figure
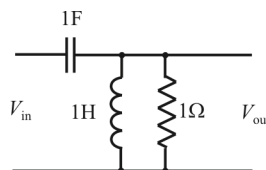


**Figure 7.16** Highpass filter.
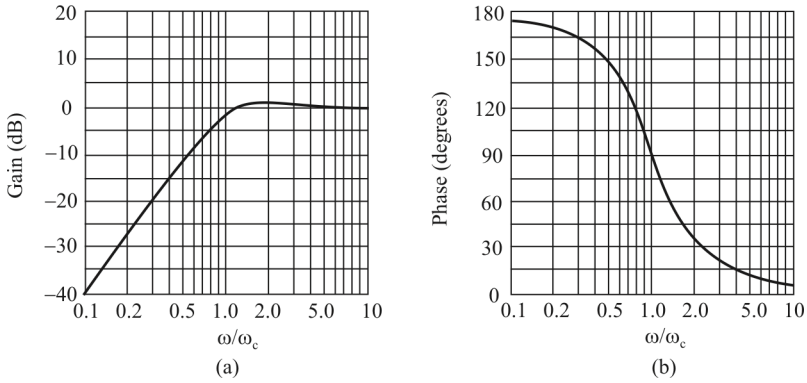
**Figure 7.17** Highpass filter.: (a) amplitude response and (b) phase response.

7.18(a) and various approximations to the ideal shown in Figure 7.18(b) through (e).

### 7.3.7 All-Pass or Phase-Shift

The fifth and final filter response type has no effect on the amplitude of the signal at different frequencies. Instead, its function is to change the phase of the signal without affecting its amplitude. This type of filter is called an all-pass or phase-shift filter. The effect of a shift in phase is illustrated in Figure 7.19. Two sinusoidal waveforms, one drawn in dashed lines, the other a solid line, are shown. The curves are identical except that the peaks and zero crossings of the dashed curve occur at later times than those of the solid curve. Thus, we can say that the dashed curve has undergone a time delay relative to the solid curve.
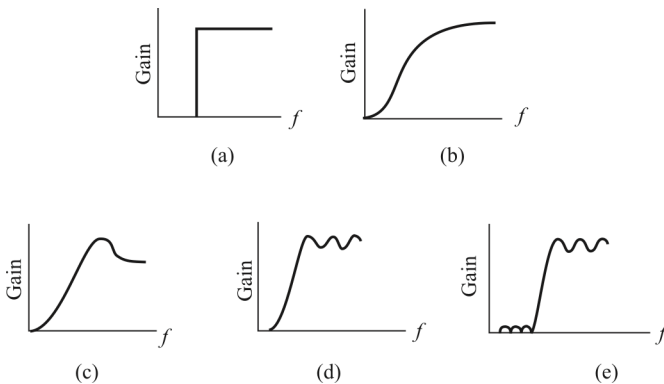


**Figure 7.18** Highpass (a) ideal, (b) no ripple, (c) shunt peaked, (d) passband ripple, and (c) passband and stopband ripple.
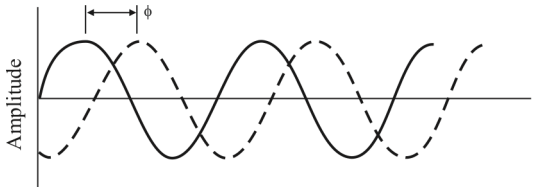
**Figure 7.19** Sinusoids. The phase delay $\phi$ (rads) is equivalent to a time delay of $\phi/\omega$ (sec), $\omega$ in rps.

Since we are dealing here with periodic waveforms, time and phase can be interchanged—the time delay can also be interpreted as a phase shift of the dashed curve relative to the solid curve. The phase shift here is equal to $\phi$ radians. The relation between time delay and phase shift is $t_d = \phi/\omega$, so if the phase shift is constant with frequency, time delay will decrease as frequency increases. All-pass filters are typically used to introduce phase shifts into signals in order to cancel or partially cancel any unwanted phase shifts previously imposed upon the signals by other circuitry or transmission media.

Figure 7.20 shows a curve of phase versus frequency for an all-pass filter with the transfer function

$$H_{AP}(s) = \frac{s^2 - s + 1}{s^2 + s + 1} \tag{7.14}$$

The absolute value of the gain is equal to unity at all frequencies, but the phase changes as a function of frequency.

### 7.3.8 Higher-Order Filters

Note that all of the transfer functions we have considered so far share the same denominator. Also note that all of the numerators are made up of terms found in
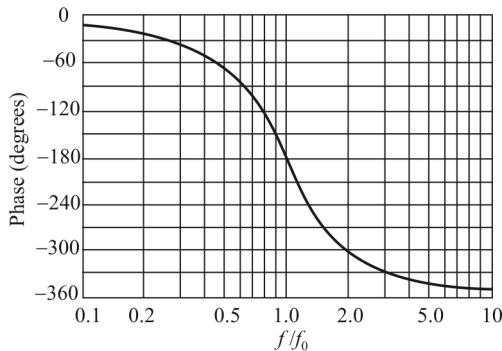


**Figure 7.20** Phase response curve for second-order all-pass filter.

the denominator: the highpass numerator is the first term ($s^2$) in the denominator, the bandpass numerator is the second term ($s$), the lowpass numerator is the third term (1), and the notch numerator is the sum of the denominator's first and third terms ($s^2 + 1$). The numerator for the all-pass transfer function is a little different in that it includes all of the denominator terms, but one of the terms has a negative sign.

In Sections 7.3.3–7.3.7 above, a few simple passive filters were described and their transfer functions were shown. Since the filters were only second-order networks, the expressions associated with them were not very difficult to analyze. When the filter in question becomes more complicated than a simple second-order network, however, it helps to have a general mathematical method of describing its characteristics. This allows us to use standard terms in describing filter characteristics and also simplifies the application of computers to filter design problems. The transfer functions we will be dealing with consist of a numerator divided by a denominator, each of which is a function of $s$, so they have the form

$$H(s) = \frac{n(s)}{d(s)} \tag{7.15}$$

Thus, for the second-order bandpass example described in (7.4), we would have $n(s) = s$, and $d(s) = s^2 + s + 1$.

The numerator and denominator can always be written as polynomials in $s$, as in the example above. A transfer function for an $n$th-order network (one with $n$ energy storage elements, that is, capacitors and inductors) can be expressed as

$$H(s) = H_0 \frac{s^n + b_{n-1}s^{n-1} + \cdots + b_1 s + b_0}{s^n + a_{n-1}s^{n-1} + \cdots + a_1 s + a_0} \tag{7.16}$$

Any filter transfer function (including the second-order bandpass of the examples) will have the general form of (7.16), with the values of the coefficients $a_i$ and $b_i$ depending on the particular filter.

The values of the coefficients completely determine the characteristics of the filter. As an example of the effect of changing just one coefficient, refer again to Figure 7.6(a), which shows the amplitude and phase response for second-order bandpass filters with different values of $Q$. The $Q$ of a second-order bandpass filter is changed simply by changing the coefficient $a_1$, so the curves reflect the influence of that coefficient on the filter response.

Note that if the coefficients are known, we do not even have to write the whole transfer function, because the expression can be reconstructed from the coefficients. In fact, in the interest of brevity, many filters are described in filter design tables solely in terms of their coefficients. Using this approach, the second-

order bandpass of Figure 7.3 could be sufficiently specified by $a_0 = a_1 = a_2 = b_1 = 1$, with all other coefficients equal to zero.

Any polynomial such as the numerator or denominator in (7.16) can be factored. Thus the transfer function also can be expressed as

$$H(s) = H_0 \frac{(s - z_0)(s - z_1) \cdots (s - z_n)}{(s - p_0)(s - p_1) \cdots (s - p_n)} \qquad (7.17)$$

The roots of the numerator, $z_0, z_1, z_2, \ldots, z_n$ are known as *zeros* and the roots of the denominator, $p_0, p_1, \ldots, p_n$, are called *poles*. The zeros and poles are in general complex numbers. Zeros are where the transfer function is zero; that is when $s = z_1$, for example, $n(s) = 0$ and there is no energy transferred from the input to the output of the filter. Likewise, when $s = p_1$, $d(s) = 0$ and $H(s) \to \infty$. All of the poles and zeros will either be real roots (with no imaginary part) or appear in complex conjugate pairs. For example, the second-order bandpass network function of (7.4) can be factored to give

$$H(s) = \frac{s}{\left(s + 0.5 + j\dfrac{\sqrt{3}}{2}\right)\left(s + 0.5 - j\dfrac{\sqrt{3}}{2}\right)} \qquad (7.18)$$

$H(s)$ has a pole at

$$s = -0.5 - j\sqrt{3}/2$$

and one at

$$s = -0.5 + j\sqrt{3}/2$$

It also has a zero at $s = 0$.

The factored form of a network function can be depicted graphically in a *pole-zero diagram* (also called an *Argand diagram*). Such a diagram corresponding to (7.18) is shown in Figure 7.21. The diagram shows the zero at the origin (O) and the two conjugate poles (×).

Certain aspects of filters can be ascertained directly from the pole-zero diagram. A pole anywhere to the right of the imaginary axis indicates instability. If the pole is located on the positive real axis, the network output will be an increasing exponential function in response to an impulse input. A positive pole not located on the real axis will give an exponentially increasing sinusoidal output.
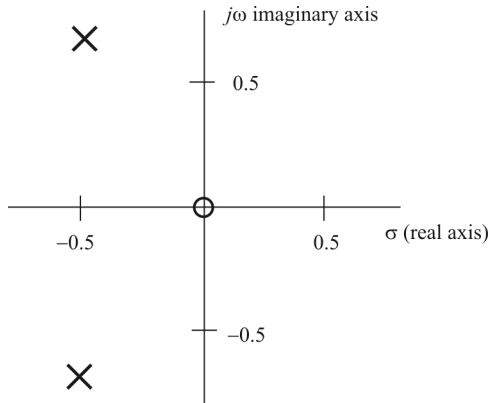
**Figure 7.21** Pole-zero (Argand) diagram corresponding to (7.18).

Stable networks will have their poles located on or to the left of the imaginary axis. Poles on the imaginary axis indicate an undamped sinusoidal output (in other words, oscillators), while poles on the left real axis indicate damped exponential response, and complex poles in the negative half-plane indicate damped sinusoidal response.

# 7.4 Filter Approximations

## 7.4.1 Introduction

In Section 7.3 we saw several examples of amplitude response curves for various filter types. These always included an ideal curve with a rectangular shape, indicating that the boundary between the passband and the stopband was abrupt and that the roll-off slope was infinitely steep. This type of response would be ideal because it would allow us to completely separate signals at different frequencies from one another. Unfortunately, such an amplitude response curve is not physically realizable. We will have to settle for the best approximation that will still meet our requirements for a given application. Deciding on the best approximation involves making a compromise between various properties of the filter's transfer function. The important properties are considered in this section.

*Filter Order.* The order of a filter is important for several reasons. It is directly related to the number of components in the filter and therefore to its cost, its physical size, and the complexity of the design task. Therefore, higher order filters are more expensive, take up more space, and are more difficult to design. The

primary advantage of a higher order filter is that it will have a steeper roll-off slope than a similar lower order filter.

*Ultimate Roll-off Rate.* This is usually expressed as the amount of attenuation in decibels for a given ratio of frequencies. The most common units are dB/octave and dB/decade. While the ultimate roll-off rate will be 20dB/decade for every filter pole in the case of a lowpass or highpass filter and 20dB/decade for every pair of poles for a bandpass filter, some filters will have steeper attenuation slopes near the cutoff frequency than others of the same order.

*Attenuation Rate Near the Cutoff Frequency.* If a filter is intended to reject a signal very close in frequency to a signal that must be passed, a sharp cutoff characteristic is desirable between those two frequencies. This is typically the case for IF filters in EW receivers. Note that this steep slope may not continue to frequency extremes.

*Transient Response.* Curves of amplitude response show how a filter reacts to steady-state sinusoidal input signals. Since a real filter will have far more complex signals applied to its input terminals, it is often of interest to know how it will behave under transient conditions. An input signal consisting of a step function provides a good indication of this. Figure 7.22 shows the responses of two lowpass filters to a step input. Curve (b) has a smooth reaction to the input step, while curve (a) exhibits some ringing. As a rule of thumb, filters with sharper cutoff characteristics or higher $Q$ will have more pronounced ringing.

*Monotonicity.* A filter has a monotonic amplitude response if its gain slope never changes sign; in other words, if the gain always increases with increasing frequency or always decreases with increasing frequency. Obviously, this can happen only in the case of a lowpass or highpass filter. A bandpass or notch filter can be monotonic on either side of the center frequency, however. Figures 7.15(b) and (c) and 7.18(b) and (c) are examples of monotonic transfer functions.
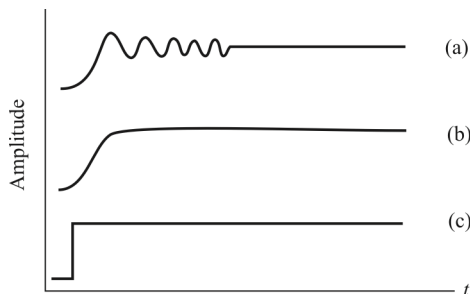


**Figure 7.22** Filter responses to a step function (c): (a) excessive ringing and (b) no ringing.
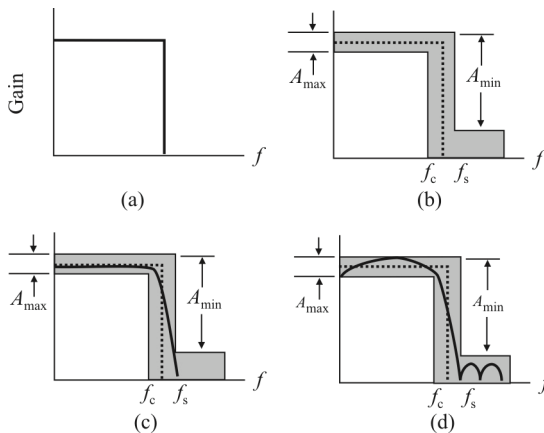
**Figure 7.23** (a) Ideal lowpass response, (b) amplitude response limits for a practical filter, (c) one characteristic curve that meets the specification, and (d) a second type of response that also meets the specification. $A_{max}$ is the maximum peak-to-peak passband ripple while $A_{min}$ is the minimum stopband attenuation.

*Passband Ripple.* If a filter is not monotonic within its passband, the transfer function within the passband will exhibit one or more bumps. These bumps are known as ripple. Some systems do not necessarily require monotonicity, but do require that the passband ripple be limited to some maximum value (usually 1dB or less). Examples of passband ripple can be found in Figures 7.9(c) and 18(d). Although bandpass and notch filters do not have monotonic transfer functions, they can be free of ripple within their passbands.

*Stopband Ripple.* Some filter responses also have ripple in the stopbands. Examples are shown in Figures 7.9(e) and 7.18(e). We are normally unconcerned about the amount of ripple in the stopband, as long as the signal to be rejected is sufficiently attenuated.

Given that the ideal filter amplitude response curves are not physically realizable, we must choose an acceptable approximation to the ideal response. The word *acceptable* may have different meanings in different contexts.

The acceptability of a filter design will depend on many interrelated factors, including the amplitude response characteristics, transient response, the physical size of the circuit, and the cost of implementing the design. The ideal lowpass amplitude response is shown again in Figure 7.23(a). If we are willing to accept some deviations from this ideal in order to build a practical filter, we might end up with a curve like the one in Figure 7.23(b), which allows ripple in the passband, a finite attenuation rate, and stopband gain greater than zero. Four parameters are of concern in the figure:

- $A_{max}$ is the maximum allowable change in gain within the passband. This quantity is also often called the *maximum passband ripple*, but the word ripple implies non-monotonic behavior, while $A_{max}$ can obviously apply to monotonic response curves as well.
- $A_{min}$ is the minimum allowable attenuation (referred to the maximum passband gain) within the stopband.
- $f_c$ is the cutoff frequency or passband limit.
- $f_s$ is the frequency at which the stopband begins.

If we can define our filter requirements in terms of these parameters, we will be able to design an acceptable filter using standard cookbook design methods. It should be apparent that an unlimited number of different amplitude response curves could fit within the boundaries determined by these parameters, as illustrated in Figure 7.23(c) and (d). Filters with acceptable amplitude response curves may differ in terms of such characteristics as transient response, passband and stopband flatness, and complexity. How do we choose the best filter from the infinity of possible transfer functions?

Fortunately, a great deal of work has already been done in this area, and a number of standard filter characteristics have already been defined. These usually provide sufficient flexibility to solve the majority of filtering problems.

The classic filter functions were developed by mathematicians (most bear their inventors' names), and each was designed to optimize some filter property. The most widely used of these are discussed below. No attempt is made here to show the mathematical derivations of these functions, as they are covered in detail in numerous texts on filter theory. Nor is there an attempt to cover all the possible available filter types.

## 7.4.2 Butterworth

The first, and probably best known, filter approximation is the *Butterworth* or *maximally-flat response*. It exhibits a nearly flat passband with no ripple. The roll-off is smooth and monotonic, with a lowpass or highpass roll-off rate of 20dB/decade (6dB/octave) for every pole. Thus, a fifth-order Butterworth lowpass filter would have an attenuation rate of 100dB for every factor of ten increase in frequency beyond the cutoff frequency.

The general equation for a Butterworth filter's amplitude response is

$$\left| H_{BU}(\omega) \right| = \frac{1}{1 + \left( \dfrac{\omega}{\omega_c} \right)^{2n}} \tag{7.19}$$
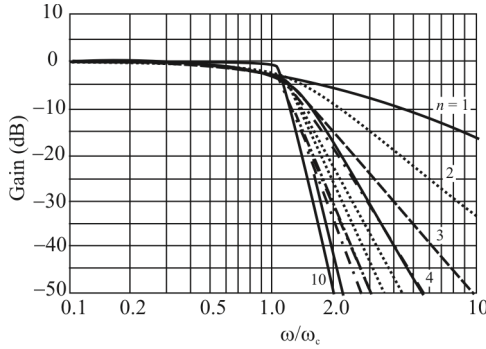
**Figure 7.24** Amplitude response for Butterworth filters.

where *n* is the order of the filter, and can be any positive whole number (1, 2, 3, ...), and $\omega_c$ is the −3dB frequency of the filter.

Figure 7.24 shows the amplitude response curves for Butterworth lowpass filters of various orders. The frequency scale is normalized to $\omega/\omega_{-3\mathrm{dB}}$ so that all of the curves show −3dB attenuation for $\omega/\omega_{-3\mathrm{dB}} = 1.0$.

The coefficients for the denominators of Butterworth filters of various orders are shown in Table 7.1. Table 7.2 shows the denominators factored in terms of second-order polynomials. Again, all of the coefficients correspond to a corner frequency of 1 rps (finding the coefficients for a different cutoff frequency will be covered later). As an example, the tables show that a fifth-order Butterworth lowpass filter's transfer function can be written:

$$H(s) = \frac{1}{s^5 + 3.236s^4 + 5.236s^3 + 5.236s^2 + 3.236s + 1} \tag{7.20}$$

$$= \frac{1}{(s+1)(s^2 + 0.8180s + 1)(s^2 + 1.6180s + 1)} \tag{7.21}$$

This is the product of one first-order and two second-order transfer functions. Note that neither of the second-order transfer functions alone is a Butterworth transfer function, but that they both have the same center frequency. Figure 7.25 shows the step response of Butterworth lowpass filters of various orders. Note that the amplitude and duration of the ringing increase as *n* increases.

### 7.4.3 Chebyshev

Another approximation to the ideal filter is the *Chebyshev filter*, also known as the *equal ripple response* filter. There are two types of Chebyshev filters: type I and

**Table 7.1** Butterworth Polynomials

| Denominator coefficients for polynomials of the form $s^n + a_{n-1}s^{n-1} + ... + a_1s + a_0$ | | | | | | | | | | |
|---|---|---|---|---|---|---|---|---|---|---|
| $n$ | $a_0$ | $a_1$ | $a_2$ | $a_3$ | $a_4$ | $a_5$ | $a_6$ | $a_7$ | $a_8$ | $a_9$ |
| 1 | 1 | | | | | | | | | |
| 2 | 1 | 1.414 | | | | | | | | |
| 3 | 1 | 2.000 | 2.000 | | | | | | | |
| 4 | 1 | 2.613 | 3.414 | 2.613 | | | | | | |
| 5 | 1 | 3.236 | 7.236 | 7.236 | 3.236 | | | | | |
| 6 | 1 | 3.684 | 7.464 | 9.142 | 7.464 | 3.864 | | | | |
| 7 | 1 | 4.494 | 7.098 | 14.592 | 14.592 | 7.098 | 4.494 | | | |
| 8 | 1 | 7.126 | 13.137 | 21.846 | 27.688 | 21.846 | 13.137 | 7.126 | | |
| 9 | 1 | 7.559 | 17.582 | 31.163 | 41.986 | 42.966 | 31.163 | 17.582 | 7.559 | |
| 10 | 1 | 7.392 | 20.432 | 42.802 | 64.882 | 74.233 | 64.882 | 42.802 | 20.432 | 7.392 |

**Table 7.2** Butterworth Quadratic Factors

| $n$ | |
|---|---|
| 1 | $(s + 1)$ |
| 2 | $(s^2 + 1.4142s + 1)$ |
| 3 | $(s + 1)(s^2 + s + 1)$ |
| 4 | $(s^2 + 0.5654s + 1)(s^2 + 1.8478s + 1)$ |
| 5 | $(s + 1)(s^2 + 0.6180s + 1)(s^2 + 1.6180s + 1)$ |
| 6 | $(s^2 + 0.5176s + 1)(s^2 + 1.4142s + 1)(s^2 + 1.9319)$ |
| 7 | $(s + 1)(s^2 + 0.4450s + 1)(s^2 + 1.2470s + 1)(s^2 + 1.8019s + 1)$ |
| 8 | $(s^2 + 0.3902s + 1)(s^2 + 1.1111s + 1)(s^2 + 1.6629s + 1)(s^2 + 1.9619s + 1)$ |
| 9 | $(s + 1)(s^2 + 0.3473s + 1)(s^2 + 1.0000s + 1))(s^2 + 1.5321s + 1)(s^2 + 1.8794s + 1)$ |
| 10 | $(s^2 + 0.3129s + 1)(s^2 + 0.9080s + 1)(s^2 + 1.4142s + 1)(s^2 + 1.5820s + 1)(s^2 + 1.9754s + 1)$ |
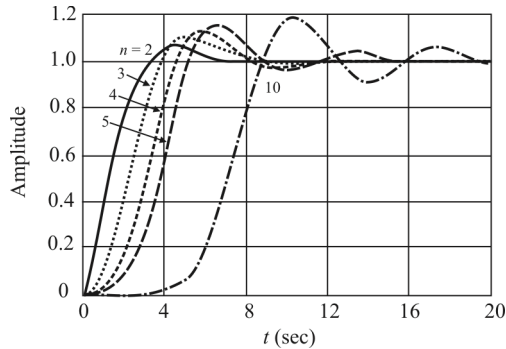
**Figure 7.25** Butterworth step response.

type II. As the latter name implies, this sort of filter will have ripple in either the passband (type I) or stopband (type II) amplitude response. The amount of ripple is one of the parameters used in specifying a Chebyshev filter. The roll-off is steeper near the cutoff frequency compared to the Butterworth, but at the expense of monotonicity in the passband (type I) or stopband (type II), and poorer transient response. A few different type I Chebyshev filter responses are shown in Figure 7.26. The filter responses in the figure have 0.1dB and 0.5dB ripple in the passband, which is small, compared to the amplitude scale in Figure 7.26(a) and (b), so it is shown expanded in Figure 7.26(c).

Note that a Chebyshev filter of order $n$ will have $n - 1$ peaks or dips in its passband response. Note also that the nominal gain of the filter (unity in the case of the responses in Figure 7.26) is equal to the filter's maximum passband gain. An odd-order Chebyshev will have a DC gain (in the lowpass case) equal to the nominal gain, with dips in the amplitude response curve equal to the ripple value. An even-order Chebyshev lowpass will have its DC gain equal to the nominal filter gain minus the ripple value; the nominal gain for an even-order Chebyshev occurs at the peaks of the passband ripple. Therefore, if we are considering a fourth-order Chebyshev lowpass filter with 0.5 dB ripple and we want it to have unity gain at DC, we will have to design for a nominal gain of 0.5dB.

The cutoff frequency of a Chebyshev filter is not assumed to be the –3dB frequency as in the case of a Butterworth filter. Instead, the Chebyshev cutoff frequency is normally the frequency at which the ripple (or $A_{max}$) specification is exceeded. The addition of passband ripple as a parameter makes the specification process for a Chebyshev filter a bit more complicated than for a Butterworth filter but also increases flexibility.

Figure 7.27 shows the step response of 0.1 dB ripple Chebyshev filters of various orders. As with the Butterworth filters, the higher order filters ring more.
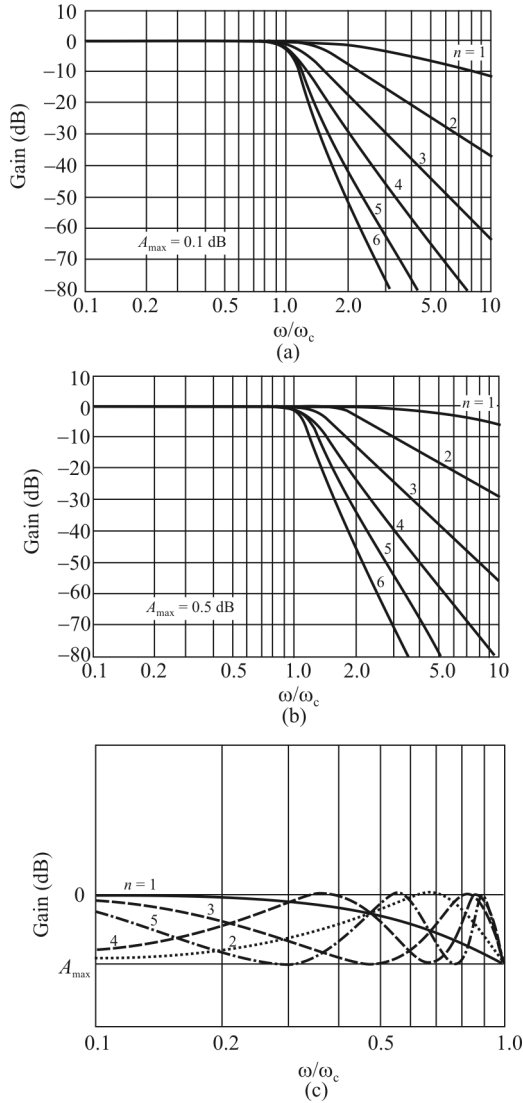
**Figure 7.26** (a) Chebychev amplitude response. $A_{max} = 0.1$dB, (b) $A_{max} = 0.5$dB, and (c) Chebyshev amplitude response.
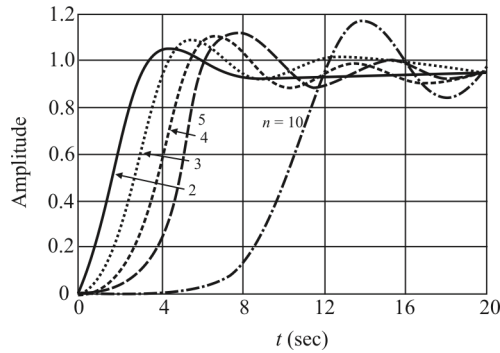
**Figure 7.27** Step response for Chebyshev lowpass filters. In each case, $\omega_0 = 1$, ripple $= 0.1$dB, and the step amplitude is 1.0.

## 7.4.4 Bessel

All filters exhibit phase shift that varies with frequency. This is an expected and normal characteristic of filters, but in certain instances it can present problems. If the phase increases linearly with frequency, its effect is simply to delay the output signal by a constant time period. However, if the phase shift is not directly proportional to frequency, components of the input signal at one frequency will appear at the output shifted in phase (or time) with respect to other frequencies. The overall effect is to distort nonsinusoidal waveshapes, as illustrated in Figure 7.28 for a square wave passed through a Butterworth lowpass filter. The resulting waveform exhibits ringing and overshoot because the square wave's component frequencies are shifted in time with respect to each other so that the resulting waveform is very different from the input square wave.

When ringing and overshoot are undesirable, a Bessel or Thompson filter may be used. The Bessel characteristic exhibits approximately linear phase shift with frequency, so within the passband it approximates a delay line with a lowpass characteristic. The higher the filter order, the more linear the Bessel's phase
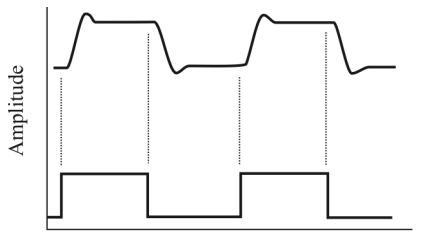


**Figure 7.28** Response of a fourth-order Butterworth lowpass (upper curve) to a square wave input (lower curve). The ringing in the response shows that the nonlinear phase shift distorts the filter wave shape.
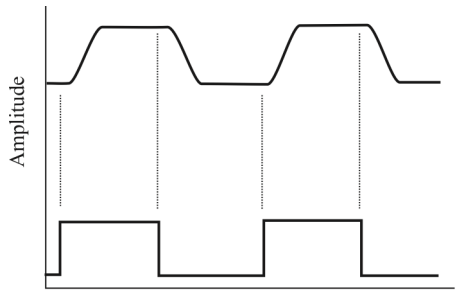
**Figure 7.29** Response of fourth-order Bessel lowpass (upper curve) to a square wave input (lower curve). Note the lack of ringing in the response. Except for the rounding of the corners due to the reduction of high-frequency components, the response is a relatively undistorted version of the input square wave.

response. Figure 7.29 shows the square wave response of a Bessel lowpass filter. Note the lack of ringing and overshoot. Except for the rounding off of the square wave due to the attenuation of high-frequency harmonics, the wave shape is preserved.

The amplitude response of the Bessel filter is monotonic and smooth, but the Bessel filter's cutoff characteristic is quite gradual compared to either the Butterworth or Chebyshev, as can be seen from the Bessel lowpass amplitude response curves in Figure 7.30. Bessel step responses are plotted in Figure 7.31 for orders ranging from 2 to 7. The poles of Bessel filters for orders ranging from 1 to 10 are shown in Table 7.3.

The Bessel filters are Gaussian filters. A Gaussian filter is a filter whose impulse response is a Gaussian function. Gaussian filters are designed to give no overshoot to a step function input while minimizing the rise and fall times. This behavior is closely connected to the fact that the Gaussian filter has the minimum
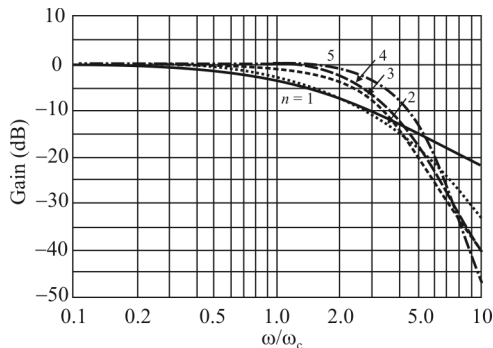


**Figure 7.30** Amplitude response curves for Bessel filters of various orders. The nominal delay of each filter is 1 second.
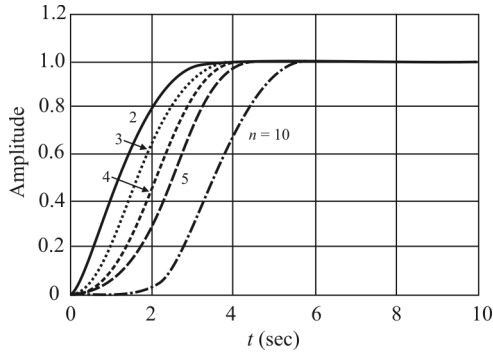
**Figure 7.31** Step responses for Bessel lowpass filters. In each case, $\omega_0 = 1$ and the input step amplitude is 1.0.

**Table 7.3** Poles of Bessel Filters

| Order ($n$) | Real Part ($-\sigma$) | Imaginary Part ($\pm j\omega$) |
|---|---|---|
| 1 | 1.0000 | |
| 2 | 1.1050 | 0.6368 |
| 3 | 1.0509 | 1.0025 |
| | 1.3270 | |
| 4 | 1.3596 | 0.4071 |
| | 0.9877 | 1.2756 |
| 5 | 1.3851 | 0.7201 |
| | 0.9606 | 1.4756 |
| | 1.5069 | |
| 6 | 1.5735 | 0.3213 |
| | 1.3836 | 0.9727 |
| | 0.9318 | 1.6640 |
| 7 | 1.6130 | 0.5896 |
| | 1.3797 | 1.1923 |
| | 0.9104 | 1.8375 |
| | 1.6853 | |
| 8 | 1.7627 | 0.2737 |
| | 0.8955 | 2.0044 |
| | 1.3780 | 1.3926 |
| | 1.6419 | 0.8256 |
| 9 | 1.8081 | 0.5126 |
| | 1.6532 | 1.0319 |
| | 1.3683 | 1.5685 |
| | 0.8788 | 2.1509 |
| | 1.8575 | |
| 10 | 1.9335 | 0.2451 |
| | 1.8467 | 0.7335 |
| | 1.6661 | 1.2246 |
| | 1.3648 | 1.7395 |
| | 0.8686 | 2.2994 |

**Table 7.4** Normalized Component Values for Bessel Prototype Filter

| Order (n) | C1 | L2 | C3 | L4 | C5 | L6 | C7 | L8 | C9 | L10 |
|---|---|---|---|---|---|---|---|---|---|---|
| 1 | 2.000 | | | | | | | | | |
| 2 | 0.5760 | 2.148 | | | | | | | | |
| 3 | 0.3374 | 0.9705 | 2.2034 | | | | | | | |
| 4 | 0.2334 | 0.6725 | 1.0815 | 2.2404 | | | | | | |
| 5 | 0.1743 | 0.5072 | 0.8040 | 1.1110 | 2.2582 | | | | | |
| 6 | 0.1365 | 0.4002 | 0.6392 | 0.8538 | 1.1126 | 2.2645 | | | | |
| 7 | 0.1106 | 0.3259 | 0.5249 | 0.5020 | 0.8690 | 1.1052 | 2.2659 | | | |
| 8 | 0.0919 | 0.2719 | 0.4409 | 0.5936 | 0.5303 | 0.8695 | 1.0956 | 2.2656 | | |
| 9 | 0.0780 | 0.2313 | 0.3770 | 0.5108 | 0.6306 | 0.5407 | 0.8639 | 1.0863 | 2.2649 | |
| 10 | 0.0672 | 0.1998 | 0.3270 | 0.4454 | 0.5528 | 0.6493 | 0.5420 | 0.8561 | 1.0781 | 2.2641 |
| Order (n) | L1 | C2 | L3 | C4 | L5 | C6 | L7 | C8 | L9 | C10 |

possible group delay. Mathematically, a Gaussian filter modifies the input signal by convolution with a Gaussian function; this transformation is also known as the *Weierstrass transformation*.

Table 7.4 lists prototype element values for the normalized lowpass function, which assumes a cutoff frequency of 1 rps and source and load impedances of $1\Omega$.

Either an input capacitor (top reference line in Table 7.4) or an inductor (bottom line in Table 7.4) can be used; see Figure 7.32.

### 7.4.5 Elliptic (Cauer)

The cutoff slope of an elliptic filter is steeper than that of a Butterworth, Chebyshev, or Bessel, but the amplitude response has ripple in both the passband and the stopband, and the phase response is very nonlinear. However, if the primary concern is to pass frequencies falling within a certain frequency band and



(a)

(b)
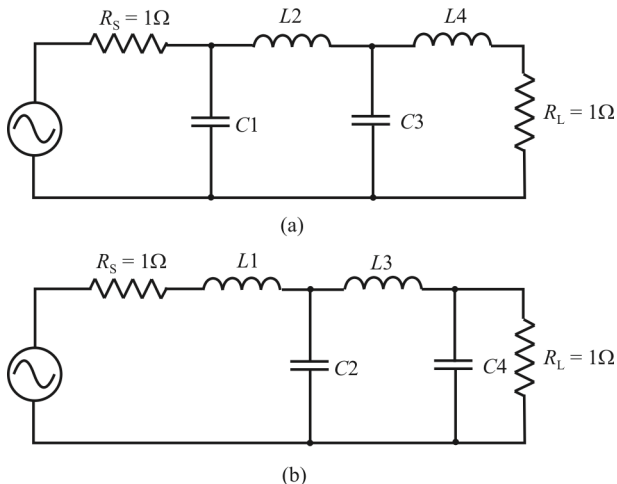
**Figure 7.32** Bessel filter prototypes: (a) capacitor input and (b) inductor input.
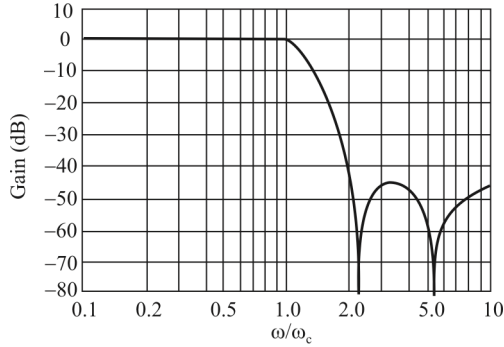
**Figure 7.33** Example of an elliptic lowpass amplitude response. This particular filter is fourth-order with $A_{max} = 0.5$dB and $f_s/f_c = 2$. The passband ripple is similar in form to the Chebyshev ripple shown in Figure 7.26(c).

reject frequencies outside that band, regardless of phase shifts or ringing, the elliptic response will perform that function with the lowest order filter. The elliptic function gives a sharp cutoff by adding notches in the stopband. These cause the transfer function to drop to zero at one or more frequencies in the stopband. Ripple is also introduced in the passband (see Figure 7.33). An elliptic filter function can be specified by three parameters (again excluding gain and cutoff frequency): passband ripple, stopband attenuation, and filter order $n$. Because of the greater complexity of the elliptic filter, a computer is normally applied to determine the coefficients.

# 7.5 Approaches to Implementing Filters

There are several varieties of filter techniques available. We have discussed LC filters extensively so far. We will discuss some of the other more common passive ones here, including SAW filters, ceramic resonators, and MEMS resonators.

Filters using active components are also possible but are normally implemented for low-frequency application. Low-frequency filters require fairly large passive components so active filters are attractive alternatives. At higher frequencies the passive components are not large so passive implementations are normally less costly, both financially as well as in real estate. Another area where active filters are starting to dominate is in monolithic implementations of filters where inductors are difficult to construct. There, a 2-port gyrator can transform a capacitor at port 2 into an inductor at port 1, so theoretically no inductors are needed. We will not discuss active filter implementations further here.

Transmission lines can implement filters as well but we do not cover that here. For that discussion see [1].

### 7.5.1 Passive Filters

All of the filters used for the earlier examples were made up of passive components: resistors, capacitors, and inductors, so they are referred to as passive filters. A passive filter is simply a filter that uses no amplifying elements (transistors, operational amplifiers, etc.).

In most cases, the only resistors in the filter are the source and load impedances. These resistors might exist in the circuit as separate resistor components, or they might be an inherent feature of the amplifier that provides the signal and the amplifier that receives the output of the filter. In the section on filter polynomials, we show how to arrive at a polynomial function of frequency that best matches the requirements. Passive filters implement these polynomial frequency responses with capacitors and inductors that interact with the source and load impedances.

Passive filters are the simplest (in terms of the number of necessary components) implementation of a given transfer function. Passive filters have other advantages as well. Because they have no active components, passive filters require no power supplies. Since they are not restricted by the bandwidth limitations of op-amps, they can work well at very high frequencies. They can be used in applications involving larger current or voltage levels than can be handled by active devices. Passive filters also generate little noise when compared with circuits using active gain elements. The noise that they produce is simply the thermal noise from the resistive and capacitive components, and, with careful design, the amplitude of this noise can be very low.

Passive filters have some important disadvantages in certain applications, however. Since they use no active elements, they cannot provide signal gain. Input impedances can be lower than desirable, and output impedances can be higher than optimum for some applications, so buffer amplifiers may be needed. Inductors are necessary for the synthesis of most useful passive filter characteristics, and these can be prohibitively expensive if high accuracy (1% or 2%), small physical size, or large values are required. Standard values of inductors are not very closely spaced, and it is difficult to find an off-the-shelf unit within 10% of any arbitrary value, so adjustable inductors are often used. Tuning these to the required values is time consuming and expensive when producing large quantities of filters.

A classic passive filter takes the form of a sideways ladder, in which the bottom rail is a signal ground, and the top rail is a series of inductors or a series of capacitors. It will be inductors in a lowpass filter and capacitors in a highpass filter. The steps of the ladder (if the ladder were vertical they would be the steps) are capacitors in a lowpass filter and inductors in a highpass filter. The total number of capacitors and inductors in the ladder is equal to the highest power of
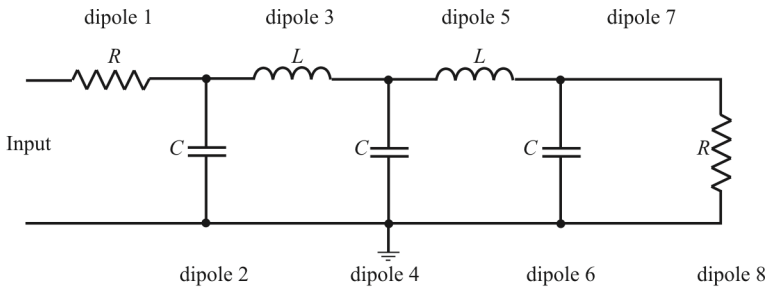
DIPOLE 1
R1 = 50

DIPOLE 2
C2 = 196.63293pF

DIPOLE 3
L3 = 1.287µH

DIPOLE 4
C4 = 636.31752pF

DIPOLE 5
L5 = 1.287µH

DIPOLE 6
C6 = 196.63293pF

DIPOLE 8
R8 = 50

**Figure 7.34** Butterworth schematic.

frequency in the frequency polynomial and gives us the order of the filter. The ladder is the favored structure for passive filters because the method of continued fractions allows us to convert a polynomial frequency function into a ladder circuit with comparative ease.

As an example, consider the fifth-order Butterworth lowpass filter schematic shown in Figure 7.34. This filter was extracted from AADE®.[2] We see the series inductors along the top and the shunt capacitors. In this case this is a shunt configuration. The Bode gain plot for this filter is shown in Figure 7.35.

Given that the filter is a ladder, another thing that needs to be specified for a passive filter is whether it is a "shunt" or "series" filter. A shunt filter is one in which the first element connects to signal ground. A series filter is one in which the first element connects to the second element, and the second element connects to ground (see Figure 7.36).

If the source impedance is zero, a shunt filter does not make sense, because no component to ground can affect a signal with zero source impedance. But zero source impedance is in any case impractical when driving a passive filter. The

---

[2] AADE = Almost All Digital Electronics, www.aade.com.
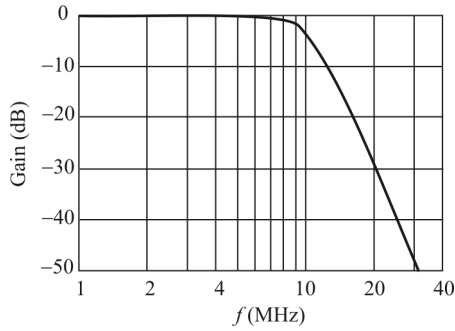
**Figure 7.35** Butterworth Bode plot.
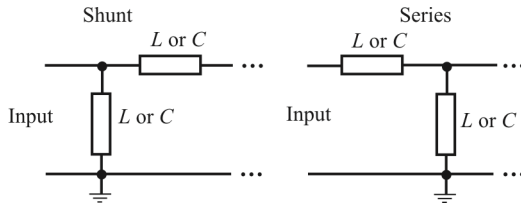


**Figure 7.36** Shunt and series.

impedance of the filter, as seen by the source, tends to drop dramatically near the cutoff frequency, regardless of whether it is a shunt or series arrangement. When the filter impedance drops, the current drawn from the source will increase dramatically until the source can no longer maintain the appearance of zero source impedance, and the input signal becomes severely distorted. Thus the performance of the filter is compromised in practice when we design for zero source impedance. A finite source impedance reduces the current the filter must draw, at the expense of losing some signal amplitude. But we assume that this amplitude can be made up later with an amplifier.

Infinite load impedance turns out to be impractical also, because it requires infinite-valued inductors and infinitesimal capacitors. Indeed, any time the ratio of source to load impedance is greater than 10, the filter is going to be hard to implement with standard parts.

Keep in mind that a voltage source, $V$, in series with a resistor, $R$, is equivalent to a current source $I = V/R$ in parallel with the same resistance, $R$. If the signal source is the collector of an npn transistor driving a $50\Omega$ load, the collector is equivalent to a voltage source in series with this resistor. The output can be shunt to ground through a capacitor to start a lowpass filter, or we can put an inductor is series with it. On the other hand, we cannot shunt it to ground with an inductor to start a highpass filter because we will ruin the DC bias of the transistor. But we could start with a large series capacitance, whose impedance is negligible compared to the source impedance, to isolate the transistor from the filter at DC, and then begin the highpass filter with an inductance shunt to ground.

In all cases, and throughout the filter, we find that the impedances of each individual capacitor and inductor are of the same order as the source and load impedances at the desired highpass or lowpass cutoff frequency. If the source impedance is $50\Omega$ and the load impedance is $500\Omega$, the impedance of the components will increase through the circuit so that those closest to the source are of order $50\Omega$ and those closest to the load are of order $500\Omega$.

We are likely to be using active filters in the cases where the source and load are high impedances or mismatched impedances. Our most likely application for a passive filter will be in RF circuits where amplifiers have $50\Omega$ output and input impedance. But there are other times when a passive filter is the simplest and most compact solution.

## 7.5.1.1 Ladder LC RF Filters

Two common lowpass LC filter configurations are shown in Figure 7.37. Each section consists of an LC pair, with each section corresponding to the order of the filter. Two section (or second-order) filters are shown in Figure 7.37. Note that the values of the capacitors and inductors change with varying input and output resistances. Tabulated normalized values for the inductors and capacitors for
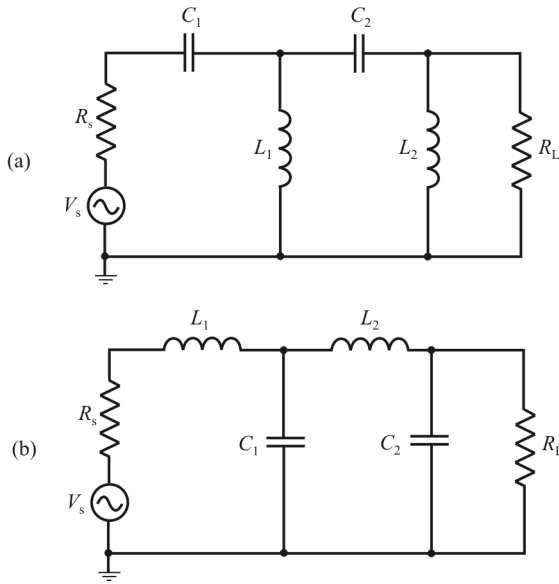
**Figure 7.37** Two ladder network configurations for LC filters: (a) has a leading capacitor while (b) has a leading inductor.

varying termination ratios are available.[3]  The component values in the tables are normalized with respect to the termination ratio and cutoff frequency. Generic representations of the *LC* lowpass filter are shown in Figure 7.38.

*Filter Polynomials*

The Butterworth polynomials provide maximally flat amplitude response in the passband. The ratio of the output amplitude to the input amplitude is $(1 + \omega^{2n} / \omega_c^{2n})^{-1/2}$, where $n$ is the number of poles in the filter, $\omega$ is the frequency of the input in rps, and $\omega_c$ is the cutoff frequency in rps. This amplitude relation defines the Butterworth polynomials.

The transfer function in the Laplace domain is

$$G(s) = \frac{Y(s)}{X(s)} = \frac{1}{s^2 + \sqrt{2}s + 1} \tag{7.22}$$

---

[3] Alternately, there is an excellent filter design software package available from Almost All Digital Electronics® (http://www.aade.com) called AADE[3].

(a)



(b)
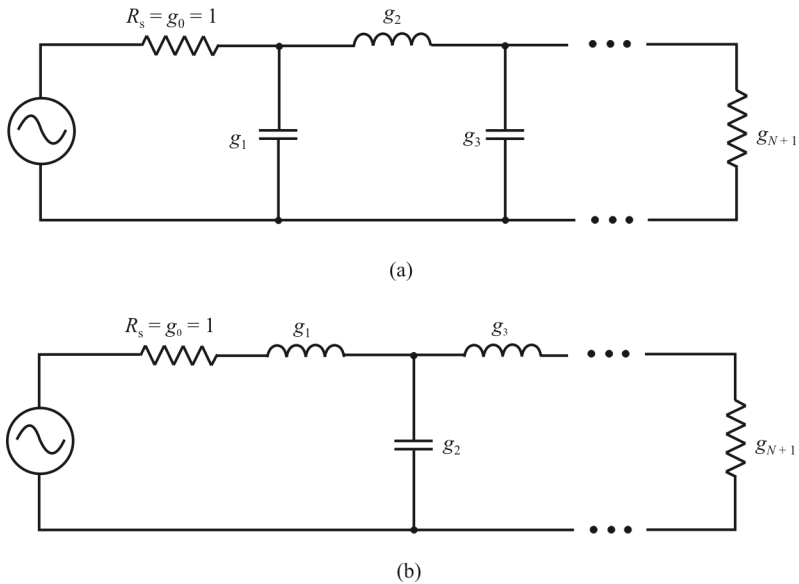
**Figure 7.38** Two LC topologies: (a) has a leading shunt capacitor while (b) has a leading series inductor.

which has the normalized second-order Butterworth polynomial in the denominator. The normalized polynomial is the polynomial for $\omega_c = 1$ rps. The poles of this normalized second-order polynomial are the poles we give in row two of Table 7.5. Let $s = j\omega$ in (7.22) to obtain the complex gain for sinusoidal inputs of the form $x = e^{j\omega t}$. Then

**Table 7.5** Poles of Lowpass Butterworth Filters with Cutoff Frequency 1 rps

| Order | Poles |
|---|---|
| 1 | $-1 \pm j0$ |
| 2 | $-0.507 \pm j0.507$ |
| 3 | $-1 \pm j0, -0.5 \pm j0.866$ |
| 4 | $-0.924 \pm j0.383, -0.383 \pm j0.924$ |
| 5 | $-1 \pm j0, -0.809 \pm j0.588, -0.309 \pm j0.951$ |
| 6 | $-0.966 \pm j0.259, -0.507 \pm j0.507, -0.259 \pm j0.966$ |
| 7 | $-1 \pm j0, -0.901 \pm j0.434, -0.624 \pm j0.582, -0.222 \pm j0.975$ |
| 8 | $-0.981 \pm j0.195, -0.832 \pm j0.556, -0.556 \pm j0.832, -0.195 \pm j0.981$ |

**Table 7.6** Normalized Chebyshev Polynomials for 3dB Passband Ripple

| Filter-Order | Chebyshev Polynomials |
|:---:|:---|
| 1 | $1.00s + 1$ |
| 2 | $1.41s^2 + 0.911s + 1$ |
| 3 | $3.98s^3 + 2.38s^2 + 3.50s + 1$ |
| 4 | $7.65s^4 + 3.29s^3 + 7.60s^2 + 2.29s + 1$ |
| 5 | $17.9s^5 + 9.11s^4 + 22.5s^3 + 7.51s^2 + 7.48s + 1$ |

$$G(\omega) = \frac{1}{-\omega^2 + \sqrt{2}\omega j + 1}$$

so

$$\begin{aligned} |G(\omega)| &= \frac{1}{\sqrt{(1-\omega)^2 + (\sqrt{2}\omega)^2}} \\ &= \frac{1}{\sqrt{1+\omega^4}} \end{aligned}$$

which is the maximally flat second-order response. The general form of $|G(\omega)|$ for $n^{\text{th}}$-order and cutoff frequency $\omega_c$ is

$$|G(\omega)| = \frac{1}{\sqrt{1+(\omega/\omega_c)^{2n}}} \tag{7.23}$$

The Chebyshev polynomials provide us with the Chebyschev poles. The Chebyshev polynomials allow variation in the passband amplitude response in exchange for sharper cutoff just outside the passband. The normalized second-order Butterworth amplitude response reduces to $(1+\omega^4)^{-1/2}$. There is no term in $\omega^2$. Because there are no terms in $\omega^2$, the amplitude response is always decreasing as frequency increases and contains no ripples. But if we can accept some ripples in the passband amplitude response, then we can add a $\omega^2$ term that cooperates with the $\omega^4$ term to drop the response more sharply above $\omega_c$.

The Chebyshev polynomials are given in Table 7.6. All the polynomials in Table 7.6 have value 1 for $s = 0$. If our transfer function has the polynomial in its denominator, its gain for $\omega = 0$ rps will be 1. At $\omega = 1$ rps, all the polynomials produce a gain that is 3dB less than the maximum gain for $\omega \leq 1$ rps. The maximum gain of the Butterworth filter is 1 and occurs at $\omega = 0$ rps, but the

maximum gain of the 3 dB Chebyshev filter is $\sqrt{2}$, or 3dB greater than unity, and occurs at one or more values of $\omega$ between 0 rps and 1 rps. The gain of the Chebyshev filter at $\omega = 1$ rps is 1.

By comparing the Chebyshev and Butterworth polynomials, we can see why the Chebyshev provides a sharper cutoff outside its passband. The $s^5$ term in the fifth-order Chebyshev polynomial has coefficient 17.9, while the $s^5$ term in the Butterworth polynomial has coefficient 1. For frequencies less than $\omega_c$, the fifth-order Chebyshev polynomial balances its large $s^5$ term with large $s^4$, $s^3$, $s^2$, and $s$ terms. This balancing is done in such a way that we produce the minimum amount of ripple in the passband response for the maximum coefficient in $s^7$. Once $\omega$ rises above $\omega_c$, the $s^5$ term overtakes all other terms rapidly and gives a sudden drop in response. Not only does the Chebyshev filter always give us a sharper cutoff than the Butterworth filter, but the advantage grows with the order of the filter.

## 7.5.1.2 Frequency Normalization and Denormalization in LC Filters

Filter coefficients that appear in tables such as Table 7.6 are normalized for cutoff frequencies of $\omega_c = 1$ rps. Therefore, if these coefficients are used to generate a filter transfer function, the cutoff (or center) frequency of the transfer function will be at $\omega_c = 1$ rps. This is a convenient way to standardize filter coefficients and transfer functions. If this were not done, we would need to produce a different set of coefficients for every possible center frequency. Instead, we use coefficients that are normalized for $\omega_c = 1$ rps because it is simple to rescale the frequency behavior of a 1 rps filter. In order to denormalize a transfer function, we merely replace each $s$ term in the transfer function with $s/\omega_0$, where $\omega_0$ is the desired cutoff frequency. Thus the second-order Butterworth lowpass function

$$H(s) = \frac{1}{s^2 + \sqrt{2}s + 1} \tag{7.24}$$

could be denormalized to have a cutoff frequency of 1000 Hz by replacing $s$ with $s/2000\pi$ as

$$H(s) = \frac{1}{\dfrac{s^2}{4 \times 10^6 \pi^2} + \dfrac{\sqrt{2}s}{2000\pi} + 1}$$

$$= \frac{4 \times 10^6 \pi^2}{s^2 + 2828.4s + 4 \times 10^6 \pi^2}$$

$$= \frac{3.948 \times 10^7}{s^2 + 8885.8s + 3.948 \times 10^7}$$

If it is necessary to normalize a transfer function, the opposite procedure can be performed by replacing each $s$ in the transfer function with $\omega_0 s$.

The subscript a will be used to denote the actual value of a parameter, and the subscript n will be used to denote its normalized value. When the impedance level is maintained constant while the frequency is normalized, the following ensue:

$$L_a = \left( \frac{\omega_n}{\omega_a} \right) L_n \qquad\qquad (7.25)$$

$$C_a = \left( \frac{\omega_n}{\omega_a} \right) C_n \qquad\qquad (7.26)$$

Equations (7.25) and (7.26) follow from the fact that the products $\omega L$ and $\omega C$ must remain constant if the impedance level remains constant. Multiplication of (7.25) and (7.26) yields

$$L_a C_a = \left( \frac{\omega_n^2}{\omega_a^2} \right) L_n C_n \qquad\qquad (7.27)$$

Equation (7.27) is an identity that holds for all values of the variables.

When the frequency is unaltered but the impedance level is normalized, the inductance is directly proportional to the impedance ratio whereas the capacitance is inversely proportional to the impedance ratio. This follows from the fact that inductive reactance is directly proportional to frequency whereas capacitive reactance is inversely proportional to frequency. Therefore, when the frequency is unaltered while the impedance is normalized, the actual values of inductance and capacitance are given by

$$L_a = \left( \frac{Z_a}{Z_n} \right) L_n \qquad\qquad (7.28)$$

$$C_a = \left( \frac{Z_n}{Z_a} \right) C_n \qquad\qquad (7.29)$$

Multiplication of (7.28) and (7.29) yields

$$L_a C_a = L_n C_n \qquad\qquad (7.30)$$
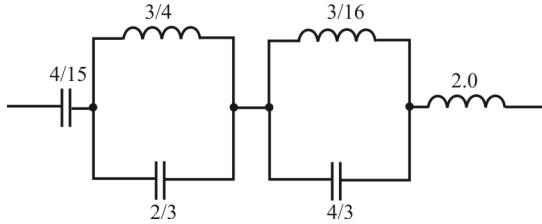
**Figure 7.39** Filter with normalized components.

It follows from (7.30) that $\omega_a = \omega_n$, showing that the frequency remains unchanged.

When both the frequency and the impedance are normalized in order to simplify the calculation, it follows from (7.25), (7.26), (7.28), and (7.29) that the actual parameters are given in terms of normalized parameters by

$$L_a = \left(\frac{\omega_n}{\omega_a}\right)\left(\frac{Z_a}{Z_n}\right)L_n \tag{7.31}$$

$$C_a = \left(\frac{\omega_n}{\omega_a}\right)\left(\frac{Z_n}{Z_a}\right)C_n \tag{7.32}$$

To illustrate the application of normalization, assume the network shown in Figure 7.39 was derived to satisfy the transfer function

$$Z(s) = 2\left[\frac{(s^2+1)(s^2+3)(s^2+5)}{s(s^2+2)(s^2+4)}\right] \tag{7.33}$$

and the frequency ratio is

$$\frac{\omega_n}{\omega_a} = 10^{-6}$$

Further assume that the impedance ratio is

$$\frac{Z_n}{Z_a} = 10^{-3}$$

It follows from (7.31) and (7.32) that
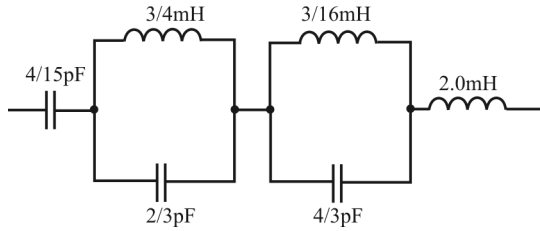
**Figure 7.40** Actual network implementation of the normlized network shown in Figure 7.39.

$$L_a = 10^{-6} \times \left( \frac{1}{10^{-3}} \right) L_n = 10^{-3} L_n \qquad (7.34)$$

$$C_a = 10^{-6} \times 10^{-3} C_n = 10^{-9} C_n \qquad (7.35)$$

Hence, the actual impedance is found by dividing the normalized impedance by $10^3$, and the actual capacitance is found by dividing the normalized capacitance by $10^9$. Figure 7.40 shows the actual (denormalized) network.

### 7.5.1.3 Filter Type Transformations

The various types of filters can be obtained with a procedure that first determines a lowpass prototype and then applies frequency transformations to implement the other types. When used on the four classical approximations (e.g., Butterworth, Chebyshev, Bessel, and elliptic function), the optimality is preserved.

*Change the Band-Edge*

The classical filters have all been developed for a band-edge of $\omega_0 = 1$. That is where the Butterworth filter has a magnitude squared of one half: $|H| = 0.5$, or the Chebyshev filter has its passband edge, or the Bessel has its stopband edge, or the elliptic filter has its passband edge. To scale the band-edge, simply replace $s$ by $Ks$ or $s \to Ks$, where $K$ is the reciprocal of the new desired band-edge. What happened to the prototype filter at $\omega = 1$ will now happen at $\omega = 1/K$. It is simply a linear scaling of the $\omega$ axis. This change can be done before the conversions below or after.

*Highpass Filter*

The frequency response illustrated in Figure 7.2(b) can be obtained from that in Figure 7.2(a) by replacing the complex frequency variable $s$ in the transfer function by $1/s$. This change of variable maps zero frequency to infinity, unity into

unity, and infinity to zero. It turns the complex s-plane inside out and leaves the unit circle alone.

In the design procedure, the desired band-edge $\omega_0$ for the highpass filter is mapped by $1/\omega_0$ to give the band-edge for the prototype lowpass filter. This lowpass filter is next designed by one of the procedures already covered and then converted to a highpass transfer function by replacing $s$ by $1/s$. If an elliptic-function filter approximation is used, both the passband edge $\omega_p$ and the stop-bandedge $\omega_s$ are transformed. Because most lowpass design procedures give the designed transfer function in factored form from explicit formulas for the poles and zeros, the transformation can be performed on each pole and zero to give the highpass transfer function in factored form.

*Bandpass Filter*

In order to convert the lowpass filter of Figure 7.2(a) into that of Figure 7.2(c), a more complicated frequency transformation is required. In order to reduce confusion, the complex frequency variable for the prototype analog filter transfer function will be denoted by $p$ and that for the transformed analog filter by $s$. The transformation is given by

$$p = \frac{s^2 + \omega_0^2}{s} \tag{7.36}$$

This change of variables doubles the order of the filter, maps the origin of the s-plane to both plus and minus $j\omega_0$, and maps minus and plus infinity to zero and infinity. The entire $\omega$ axis of the prototype response is mapped between zero and plus infinity on the transformed responses. It is also mapped onto the left-half axis between minus infinity and zero. This is illustrated in Figure 7.41.

In order that the transformation give $-\omega_p = (\omega_2^2 - \omega_0^2)/\omega_2$ and $\omega_p = (\omega_3^2 - \omega_0^2)/\omega_3$, the "center" frequency $\omega_0$ must be

$$\omega_0 = \sqrt{\omega_2 \omega_3} \tag{7.37}$$

However, because $-\omega_s = (\omega_1^2 - \omega_0^2)/\omega_1$, and $\omega_s = (\omega_4^2 - \omega_0^2)/\omega_4$, the center frequency must also be

$$\omega_0 = \sqrt{\omega_1 \omega_4} \tag{7.38}$$
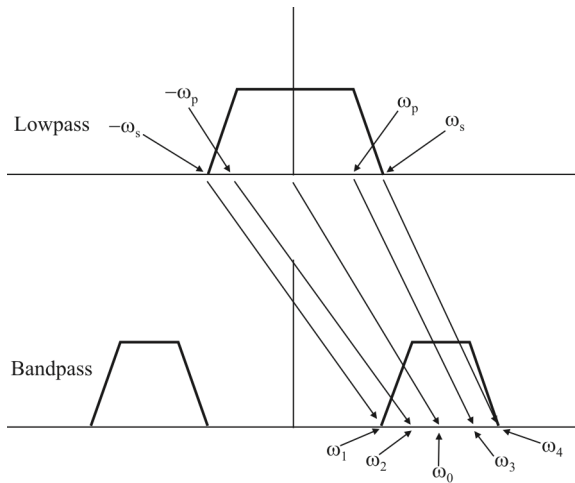
**Figure 7.41** Lowpass prototype to bandpass transformation.

This means that only three of the four band-edge frequencies $\omega_1$, $\omega_2$, $\omega_3$, and $\omega_4$ can be independently specified. Normally, $\omega_0$ is determined by $\omega_2$ and $\omega_3$, which then specifies the prototype passband edge by

$$\omega_p = \frac{\omega_3^2 - \omega_0^2}{\omega_3} \qquad (7.39)$$

and, using the same $\omega_0$, the stopband edge is set by either $\omega_1$ or $\omega_4$, whichever gives the smaller $\omega_s$:

$$\omega_s = \frac{\omega_4^2 - \omega_0^2}{\omega_4} \qquad \text{or} \qquad \omega_s = \frac{\omega_0^2 - \omega_1^2}{\omega_1} \qquad (7.40)$$

The final bandpass filter will meet both passband edges and one transition band width, but the other will be narrower than originally specified. This is not a problem with the Butterworth or either of the Chebyshev approximations because they only have passband edges or stopband edges but not both. The elliptic function has both.

After the band-edges for the prototype lowpass filter $\omega_p$ and/or $\omega_s$ are calculated, the filter is designed by one of the approximation methods discussed above. Because most of these methods give the pole and zero locations directly, they can be individually transformed to give the bandpass filter transfer function in

factored form. This is accomplished by solving $s^2 - ps + \omega_0^2$ from the original transformation to give the root locations

$$s = \frac{p \pm \sqrt{p^2 - 4\omega_0^2}}{2} \tag{7.41}$$

This gives two transformed roots for each prototype root, which doubles the order as expected.

*Bandstop Filter*

To design a filter that will reject a band of frequencies, a frequency transformation of the form

$$p = \frac{s}{s^2 + \omega_0^2} \tag{7.42}$$

is used on the prototype lowpass filter. This transforms the origin of the $p$-plane into both the origin and infinity of the $s$-plane. It maps infinity in the $p$-plane into $j\omega_0$ in the $s$-plane.

Similar to the bandpass case, the transformation must give $-\omega_p = \omega_4 / (\omega_0^2 - \omega_4^2)$ and $\omega_p = \omega_1 / (\omega_0^2 - \omega_1^2)$. A similar relation of $\omega_s$ to $\omega_2$ and $\omega_3$ requires that the center frequency $\omega_0$ must be
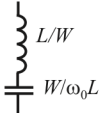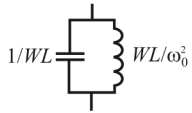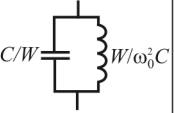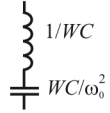
$$\omega_0 = \sqrt{\omega_1 \omega_4} = \sqrt{\omega_2 \omega_3} \tag{7.43}$$

As before, only three of the four band-edge frequencies can be independently specified. Normally, $\omega_0$ is determined by $\omega_1$ and $\omega_4$, which then specify the prototype passband edge by

$$\omega_p = \frac{\omega_1}{\omega_0^2 - \omega_1^2} \tag{7.44}$$

and, using the same $\omega_0$, the stopband edge is set by either $\omega_2$ or $\omega_3$, whichever gives the smaller $\omega_s$.

$$\omega_s = \frac{\omega_2}{\omega_0^2 - \omega_2^2} \quad \text{or} \quad \omega_s = \frac{\omega_3}{\omega_3^2 - \omega_0^2} \tag{7.45}$$

| Prototype Lowpass | Lowpass | Highpass | Bandpass | Bandstop |
|---|---|---|---|---|
| $L = g_k$ | $L/\omega_c$ | $1/\omega_c L$ | $L/W$ <br> $W/\omega_0 L$ | $1/WL$  $WL/\omega_0^2$ |
| $C = g_k$ | $C/\omega_c$ | $1/\omega_c C$ | $C/W$  $W/\omega_0^2 C$ | $1/WC$ <br> $WC/\omega_0^2$ |

$\Delta = (\omega_U - \omega_L)/\omega_0,\ \omega_0 = \sqrt{\omega_U \omega_L}$

**Figure 7.42** Filter type transformations. $\omega_c$ is the cutoff frequency, $\omega_0$ is the center frequency, and $W$ is the bandwidth.

The final bandpass filter will meet both passband edges and one transition band width, but the other will be narrower than originally specified. This does not occur with the Butterworth or either Chebyshev approximation, only with the elliptic function.

After the band-edges for the prototype lowpass filter $\omega_p$ and/or $\omega_s$ are calculated, the filter is designed. The poles and zeros of this filter are individually transformed to give the bandstop filter transfer function in factored form. This is carried out by solving $s^2 - (1/p)s + \omega_0^2$ to give for the root locations

$$ s = \frac{1/p \pm \sqrt{(1/p)^2 - 4\omega_0^2}}{2} \tag{7.46} $$

A more complicated set of transformations could be developed by using a general map of $s = f(s)$ with a higher order. Several pass- or stopbands could be specified, but the calculations become fairly complicated.

Although this method of transformation is a powerful and simple way for designing bandpass and bandstop filters, it does impose certain restrictions. A Chebyshev bandpass filter will be equal ripple in the passband and maximally flat at both zero and infinity, but the transformation forces the degree of flatness at zero and infinity to be equal. The elliptic function bandpass filter will have the same number of ripples in both stopbands even if they are of very different widths. These restrictions are usually considered mild when compared with the complexity of alternative design methods.

The impedance and frequency transformations between lowpass and other types of filters, including highpass, are summarized in tabular form in Figure 7.42 [2, 3]. As is shown in Figure 7.42 for highpass filter design, the capacitors and
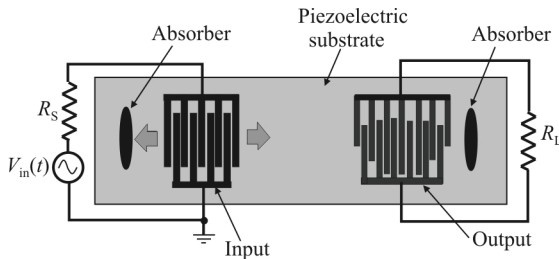
**Figure 7.43** SAW filters have one or more terminals (here we show two). The absorber could also be a reflector that reverses the path of the surface wave that comes at it.

inductors are interchanged, and a transformation is applied to the values of the components. The transformed value takes into account the cutoff frequency.

## 7.5.2 Surface Acoustic Wave Filters

SAW technology is used in many areas of electronics to provide resonators for oscillators, filters, and transformers. One of the major uses of these devices is as SAW filters, which find widespread use in communication EW applications. These SAW filters provide good performance filtering while offering a cost-effective solution.

SAW filters are widely used in EW applications for filtering. Here they provide considerable advantages in terms of cost and size, in an environment where these two aspects are of considerable importance. Additionally, their importance in the cellular industry has meant that considerable research and development has been undertaken on SAW filters in recent years, and their performance has improved considerably as a result.

A SAW filter is a small, passive device made out of piezoelectric crystal. Most SAW filters are bandpass filters. Imagine a thin, rectangular piece of piezoelectric crystal. The crystal expands and contracts with applied electric field. If we tap the crystal, it will shiver for a short time, like a crystal wine glass, but at a frequency too high for us to hear. As the crystal shivers, it develops a voltage across its surfaces that matches the frequency and amplitude of the shiver. If we put electrodes on the top and bottom surfaces, the crystal will resonate when we apply a sinusoidal voltage of the correct frequency. Crystal oscillators use this resonance to create a frequency that is as accurate as the dimensions and flatness of the crystal.

A typical SAW filter is illustrated in Figure 7.43. The device is an electroacoustic bandpass filter that operates via delay paths that conduct (passband) and cancel (stopband) frequencies. An RF signal applied to the electrodes generates surface waves on the piezoelectric ceramic material. The amplitude and phase of the surface waves are functions of the distance between

and overlap of the electrodes. The input to the filter is through the *inter-digital transducer* (IDT), which generates a SAW in the piezoelectric substrate. This wave travels to the output IDT and produces an output voltage across the load resistor. Damping material forms absorbers at each end that direct and prevent scattering of the wave.

SAW filters exhibit higher insertion loss than do LC filters, so we need to provide more gain in a given circuit to compensate for the loss. The prime features of a SAW filter are its flat passband characteristic (low ripple), a constant group delay (low phase distortion), and steep skirts.

A SAW filter does not use bulk resonance of the crystal. It uses surface acoustic waves. Instead of electrodes on opposite faces of the crystal, the SAW filter has two interlocking combs of electrodes on one end of the crystal surface and another two such combs at the opposite end but on the same crystal surface. We connect our input across these combs as seen in Figure 7.43.

The combs set up electric fields along the surface of the crystal instead of within the bulk of the crystal. The electric fields cause the surface of the crystal to expand and contract. If we apply a sinusoidal voltage across the input electrodes of just the right frequency, we will create a surface wave that propagates across the crystal, where it creates a voltage across the output electrodes, which are also interlocking combs. We can see that only frequencies with a whole number of wavelengths between the teeth of each comb will be reinforced as they propagate across the comb fingers. The result is a filter: only frequencies that match the combs at both ends will be transformed from electrical signals into surface wave signals and back to electrical signals again.

Waves travel along the surface of the crystal at a velocity dictated by the crystal's Young's modulus, which is on the order of 4000 m/s for piezoelectric crystals. The wavelength of a 950 MHz wave propagating at this speed is 4.2 μm. At such high frequencies, SAW filters tend to use harmonics of the fundamental resonant frequency of its combs. They do this by starting with a comb designed for an integer fraction of the desired bandpass frequency, and then inserting cuts in the comb fingers that make the combs inefficient at the fundamental frequency, but efficient at the desired bandpass frequency.

If we imagine that the SAW filter is a combination of a highpass filter at the low end of its passband and a lowpass filter at the high end, then we can compare its response at the high end to that of a polynomial lowpass filter. We see that within 10 MHz of the cutoff frequency, the SAW filter's virtual lowpass filter response drops by 30dB. Suppose we were to try to build a polynomial lowpass filter with the same response. A 10-pole 3dB Chebyshev filter response drops by 30 dB after a 10% change in frequency. In other words, the SAW filter cutoff at both ends of its passband is 10 times sharper than that of a 10-pole 3dB ripple Chebyshev filter. Perhaps we could match the SAW filter response with a 100-pole filter made with 0.1% tolerant inductors and capacitors. The result would cost hundreds of dollars and take up a hundred square centimeters of board space.
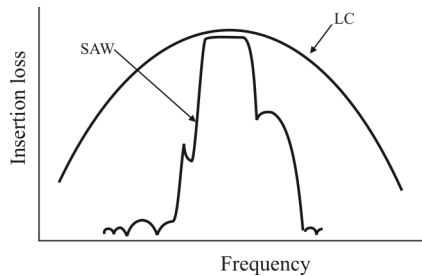
**Figure 7.44** A SAW bandpass filter has much steeper skirts than an LC filter.

The frequency roll-off characteristics for SAW filters are much sharper than those of LC filters. A comparison of typical characteristics is illustrated in Figure 7.44. The roll-off characteristics of a SAW filter are not necessarily monotonic and exhibit some unusual behavior, but this property is of little consequence in most applications. Note that both types exhibit virtually no amplitude ripple in the passband. The insertion loss of a SAW filter is greater than that of the LC filters as shown. Again, this loss has little impact in most applications as the loss can generally be overcome with additional amplification both before and after the SAW device.

A SAW filter is a small and thin filter using SAWs excited on a piezoelectric substrate. They use waves propagated on the surface of an elastic solid for signal processing. A typical SAW filter uses a transducer to convert electromagnetic signal waves, which travel close to the speed of light, to acoustic signal waves, that propagate along the surface between 1600 and 3200 m/s, depending on the material.

The basic structure of a SAW filter consists of one input and one output IDTs deposited on a piezoelectric substrate. These IDTs function as a transmitter and receiver for the surface acoustic waves. By adjusting the geometry of the IDTs the characteristics of the SAW device can be manipulated, providing various characteristics and functions, the filtering function being among the most important. An IDT includes electrode bus bars and electrode fingers extending from each electrode bus bar in an inter-digital configuration. The input and output transducers typically include inter-digital electrodes formed on the top surface of the substrate. The shape and spacing of the electrodes determine the center frequency and the band shape of the acoustic waves produced by the input transducer. The amplitude of the SAWs at a particular frequency is determined by the constructive interference of the acoustic waves generated by the transducers. The geometry of the IDTs (beamwidth, pitch, number of fingers) on the piezoelectric substrate plays a significant role in the frequency response characteristics of a SAW device. The choice and cut of piezoelectric substrate

material from which the SAW filter is constructed and the electrode shape, spacing, and location influence the characteristics of the SAW filter.

There are various types of SAW filters. A transversal SAW filter has an IDT deposited on a surface of a piezoelectric member for selecting a frequency component based on an interaction between a surface acoustic wave propagated through the surface of the piezoelectric member. Transversal filters utilizing a SAW device are generally modeled as an input signal that passes through a series of delays. Transversally coupled multimode resonator-type SAW filters are widely used as the IF filters of EW receivers because they are small, low loss, and have fewer narrow-band passband characteristics with sharp skirts and also fewer out-of-band unwanted modes.

When it is required to have a relatively broad bandwidth and flat phase characteristics in the passband as with IF filters in EW receivers, SAW filters of the transversal type are often used. Reflective SAW filters generally have at least one input transducer, one output transducer, and one reflector formed on a piezoelectric substrate. The reflector is typically a reflective grating including spaced apart grid lines defining gaps between. The acoustic waves received by the reflector from the input transducer are reflected by the grid lines within the grating so that the reflected waves constructively and destructively interfere with each other as the wave path is unfolded. The constructively interfered waves are reflected back to the output transducer having a particular phase. Reflective SAW filters are therefore smaller in size and have high frequency selectivity and thus are desirable for RF applications.

A SAW resonator filter has a resonator including an IDT provided on a piezoelectric substrate. In an edge reflection-type SAW resonator filter, the resonator is provided between two opposite edges of the piezoelectric substrate, and the edges are used to reflect the *shear horizontal* (SH) waves. Since reflectors are not needed, a compact filter can be realized. SAW filters used in an RF stage comprise two types: a longitudinally coupled type and a ladder type. The ladder SAW filter has lower loss than a vertical mode SAW filter. The ladder model is formed of a plurality of SAW resonators coupled to each other in a ladder form. The sophistication of the SAW filter depends on the sophistication of each one of the SAW resonators.

The SAW filter is described mathematically similarly to digital FIR filters, and they can be designed using the same methodologies [4].

### 7.5.3 Crystal Filters

The equivalent circuit of a crystal along with its reactance characteristic with frequency is illustrated in Figure 7.45. Below the series resonant frequency ($f_s$) the impedance is capacitive and between the series resonant frequency and the parallel resonant frequency ($f_p$) it is inductive. At the parallel resonant frequency the impedance quickly changes from inductive back to capacitive.

$$f_s = \frac{1}{2\pi\sqrt{L_s C_s}}$$

$$f_p = f_s\sqrt{1 + \frac{C_s}{C_0}}$$

$$Q_s = \frac{2\pi f_s L_s}{R_s}$$
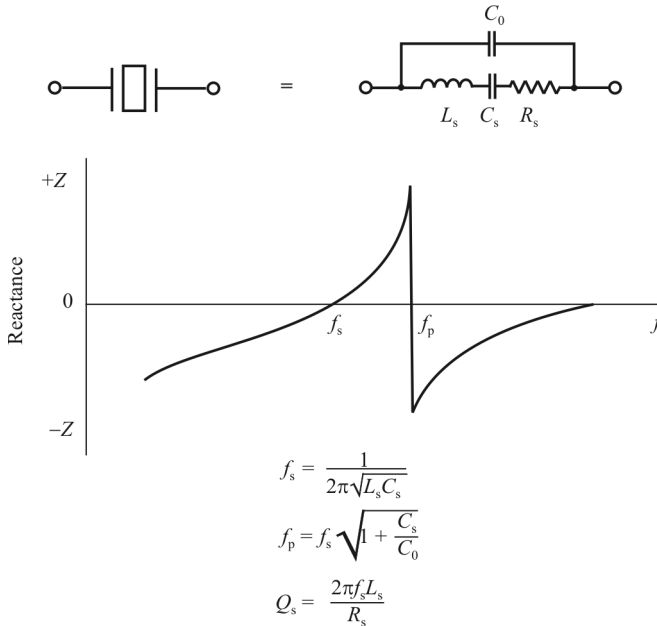
**Figure 7.45** Crystal response.

The closest approximation to a brick wall filter (which does not exist in practice) is a Nyquist filter (raised cosine) with $\alpha = 0.0$. Simpler filters, such as the 2-pole crystal filter seen in Figure 7.46, yield crude approximations. A series resonant crystal at the top in Figure 7.46(a), labeled $X_1$, is shunted by a parallel resonant crystal $X_2$. The two operate at slightly different frequencies to yield the frequency response in Figure 7.46(b). The phase shift from edge to edge is 180°, so there is a resemblance to the ideal filter. The group delay is calculated as

$$T_g = \frac{\Delta\phi}{2\pi\Delta f} \tag{7.47}$$

The bandpass is determined by the $Q$ of the crystals.

## 7.5.3.1 Operating Region

Crystal filters can be built at center frequencies from less than 1 kHz up to several hundred megahertz. Figure 7.47 shows the more common regions where they are usually built. There are several areas within the main one where the most practical
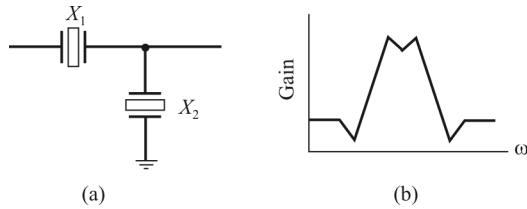
**Figure 7.46** Crude crystal filter: (a) configuration and (b) frequency response.

and cost-effective filters are built. The center frequencies range from around 5 MHz up to 40 MHz with bandwidths ranging from 0.05 to 1.5%.

The narrowest bandwidth that can be achieved is controlled by two factors: the available $Q$ of the crystal resonators and their temperature stability. For example, a filter can be made with a bandwidth of 10 Hz at a center frequency of 1 MHz. However, if the temperature range extends from –55 to +85°C, the crystals could drift ±20 ppm (or more) and so the center frequency would drift ±20 Hz, or twice as much as the bandwidth.

Figure 7.48 shows the frequency-temperature characteristics for AT cut resonators. The family of curves are for crystals cut out of the quartz crystal at slightly different angles. Each adjacent curve is separated by 2 minutes of arc from the preceding one. The designer selects the angle that will give the least change in frequency over the specified temperature range. The normal manufacturing angular spread for practical crystals will be about ±3 degrees of arc. This controls the temperature stability that can be achieved. Tighter control can be obtained but only at the added expense of 100% screening.
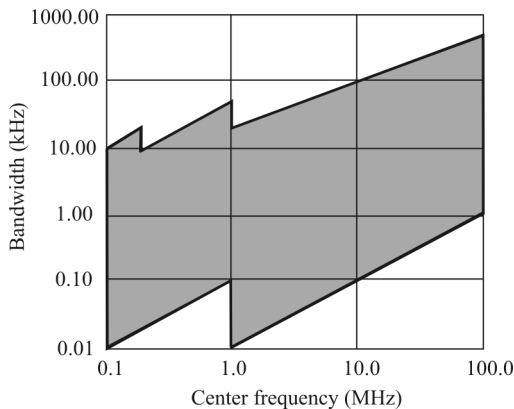


**Figure 7.47** Crystal operating region.
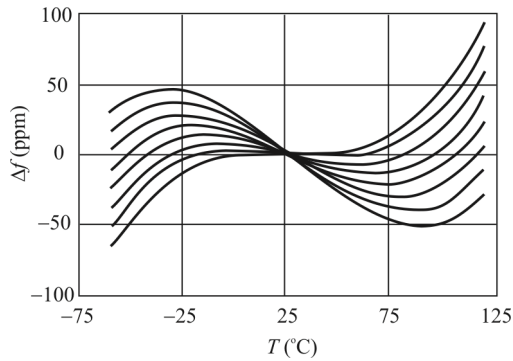
**Figure 7.48** Temperature characteristics for AT-cut quartz crystal.

## 7.5.3.2 Crystal Lattice Filters

The topology of a lattice filter is illustrated in Figure 7.49 [5]. This structure was first developed by W. P. Mason in 1929 and is still one of the major crystal filter architectures in use.

## 7.5.3.3 Crystal Bandpass Filters

The very high $Q$ makes the quartz crystal resonators ideal for use as the primary bandpass RF filter in high-performance EW communication receivers. As a result of this there are a number of circuits that have been used to provide the required level of selectivity and performance over the years. These include the single crystal filter, the half lattice crystal filter, and the ladder filter.
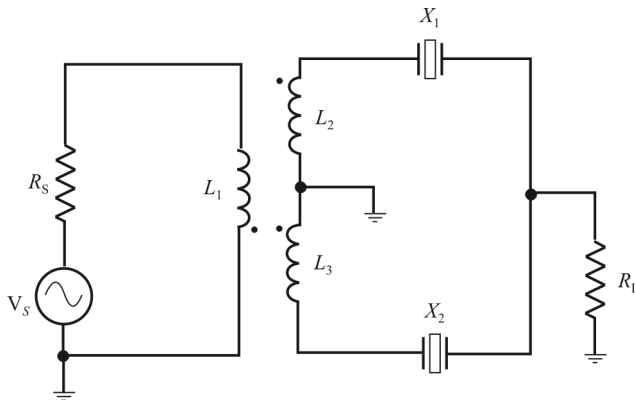


**Figure 7.49** Crystal lattice filter.
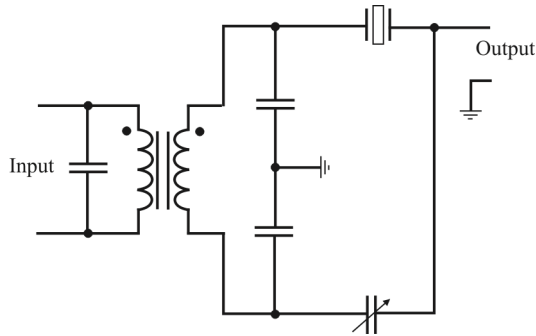
**Figure 7.50** Diagram of filter using a single quartz crystal.

*Single Crystal Filter*

The simplest crystal filter employs a single crystal (Figure 7.50). This type of RF filter was developed in the 1930s and was used in early receivers dating from before the 1960s but is rarely used today. Although it employs the very high $Q$ of the crystal, its response is asymmetric and it is too narrow for most applications, having a bandwidth of 100 Hz or less.

In the circuit there is a variable capacitor that is used to compensate for the parasitic capacitance in the crystal. This capacitor was normally included as a front panel control.

*Half Lattice Crystal Filter*

This form of bandpass RF filter provided a significant improvement in performance over the single crystal filter. In this configuration the parasitic capacitances of each of the crystals cancel each other out and enable the circuit to operate satisfactorily. By adopting a slightly different frequency for the crystals, a wider bandwidth is obtained. However, the slope response outside the required passband falls away quickly, enabling high levels of out-of-band rejection to be obtained. Typically, the parallel resonant frequency of one crystal is designed to be equal to the series resonant frequency of the other (Figure 7.51). The gain characteristics for the filter in Figure 7.51 are shown in Figure 7.52 when the crystals use a slightly different frequency.

Despite the fact that the half lattice crystal filter can offer a much flatter in-band response, there is still some ripple. This results from the fact that the two crystals have different resonant frequencies. The response has a small peak at either side of the center frequency and a small dip in the middle. As a rough rule of thumb it is found that the 3dB bandwidth of the RF filter is about 1.5 times the
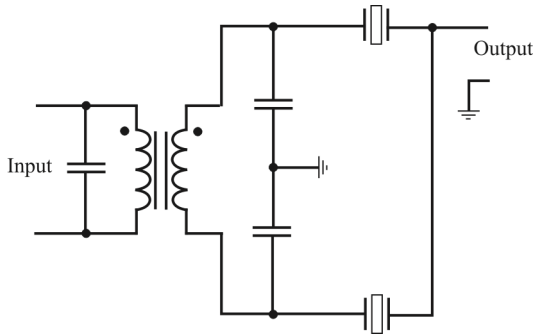
**Figure 7.51** Circuit diagram of a half lattice crystal filter.

frequency difference between the two resonant frequencies. It is also found that for optimum performance the matching of the filter is very important. To achieve this, matching resistors are often placed on the input and output. If the filter is not properly matched then there is more in-band ripple and the ultimate rejection may not be as good.

A 2-pole filter (i.e., one with two crystals) is not normally adequate to meet many requirements. The shape factor can be greatly improved by adding further sections. Typically ultimate rejections of 70dB and more are required in an EW receiver. As a rough guide a 2-pole filter will generally give a rejection of around 20dB; a 4-pole filter, 5 dB; a 6-pole filter, 70dB; and an 8-pole one, 90dB.

### 7.5.3.4 Crystal Filter Design Parameters

When a quartz crystal filter is designed, factors such as the input and output impedance as well as bandwidth, crystal $Q$, and many other factors need to be taken into account.

Some of the chief factors are obviously the bandwidth, shape factor, and ultimate cutoff. Although it is very much a simplification, these factors are dependent upon the number of poles (equivalent to the number of crystals), their $Q$ value, and their individual frequencies.
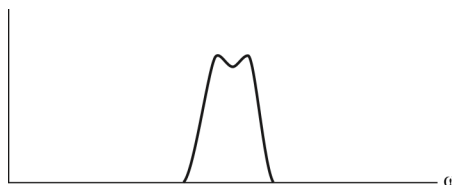


**Figure 7.52** Half lattice crystal filter gain.

Further factors such as the maximum bandwidth that can be achieved is controlled by the filter impedance and also the spurious responses that are present in the individual quartz crystal elements. The location of the important responses for quartz crystal filters can be controlled by the size of the plates deposited onto the crystals. By making them smaller, the responses also become less critical. The down side of this is that the impedance of the overall quartz crystal filter rises. This means that the quartz crystal filter will need impedance transformers at the input and the output. This obviously needs to be avoided if at all possible, but for wideband filters it is often the only option.

Crystal filters are widely used in many communication EW receiver applications. Here these filters are able to provide very high levels of performance and at a cost that is very reasonable for the performance that is given. These RF filters may be made in a variety of formats according to the applications and the performance needed. While these RF filters can be made from discrete components, ready manufactured crystal filters are normally bought, either off the shelf, or made to a given specification.

### 7.5.4 Ceramic RF and IF Filters

Ceramic filters are also constructed with piezoelectric crystals. While their performance characteristics are similar to those of crystal filters, they are less expensive and have somewhat poorer performance in most other areas. Ceramic filters are widely used in IF and RF bandpass filter applications for EW receivers.

### 7.5.4.1 RF and IF Ceramic Filter Basics

As the name implies, RF and IF ceramic bandpass filters are manufactured from ceramics that exhibit the piezoelectric effect. These filters were initially available for lower frequencies, with center frequencies typically being within the range of a few kilohertz up to frequencies of 7.5 MHz, which is a standard IF for VHF receivers. However, significant investment in the development of these filters enabled much higher frequencies and specification levels to be achieved. Frequencies up to UHF and beyond are now available.

Having a lower $Q$ than quartz, these ceramic RF and IF filters have bandwidths that are typically measured between 0.05 and 20% of the operating frequency. Often the $Q$ levels range between around 500 up to 10,000 or possibly more as the technology improves.

### 7.5.4.2 Ceramic Resonator Outline

The elemental format for the ceramic filter is a simple ceramic resonator that has electrodes plated onto either side. This behaves in much the same way as a single quartz crystal, although with a lower level of performance. Also the separation
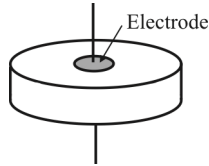
**Figure 7.53** Ceramic resonator used as the basis for the ceramic bandpass filter.

between the parallel and series resonant frequencies is greater. A sketch of a ceramic resonator used to make ceramic bandpass filters is shown in Figure 7.53.

The ceramic bandpass filter has a similar equivalent circuit diagram to that of a quartz crystal; it is illustrated in Figure 7.54. From this we can see that there are two ways in which the circuit can become resonant—one being a parallel resonance and the other a series resonance. The impedance characteristics are illustrated in Figure 7.55.

### 7.5.4.3 Ceramic Bandpass Filter Overview

It is possible to make a complete bandpass filter using a ceramic resonator by splitting and separating one of the electrodes. This gives a common connection—the single electrode—and input and output connections as shown in the equivalent circuit shown in Figure 7.56.

### 7.5.4.4 Ceramic RF and IF Bandpass Filter Circuit Symbol

The circuit symbol for the ceramic filter shown in Figure 7.57 gives a representation for the ceramic resonator together with the common electrode at the bottom and the input and output electrodes separated at a distance across the ceramic resonator element itself.
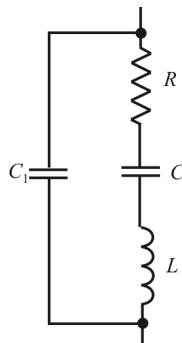


**Figure 7.54** Ceramic resonator equivalent circuit.
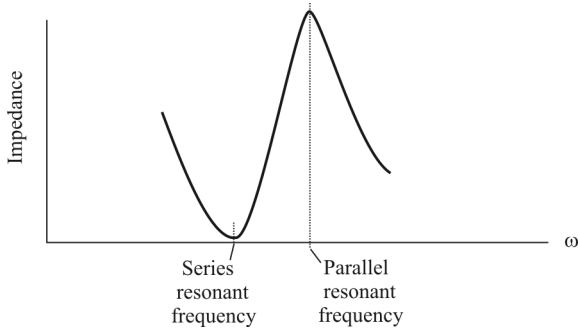
**Figure 7.55** Ceramic resonator response curve.
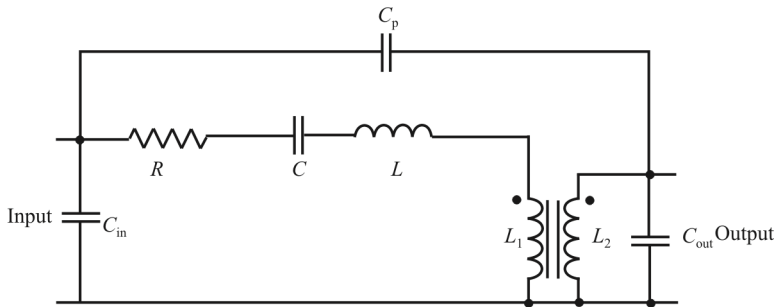


**Figure 7.56** Ceramic bandpass filter equivalent circuit.
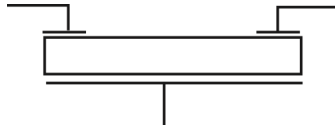
**Figure 7.57** Ceramic bandpass filter circuit symbol.

Depending on your point of view whether it is a good or bad characteristic, we must remember that, unlike a transformer-style LC filter used for inter-stage coupling and tuning, there is no DC path within the ceramic filter—it is an insulator. Therefore, any circuit using ceramic filters must take account of this, providing all the bias and source current from outside the filter. A transistor circuit of the format shown in Figure 7.58 would work, although many IF amplifier or complete receiver ICs have ports specifically to use ceramic filters and will incorporate the correct current and bias paths outside the ceramic filter.

### 7.5.5 MEMS RF Filters

Very small tunable capacitors and inductors can be made with MEMS technology [6, 7]. In particular:

> In the contour-mode disk resonator shown in Figure 7.59 the vibrations occur along the disk radius. The disk is anchored at a single point at its center. One of the key advantages of this mode of vibration is that a given frequency may be achieved with
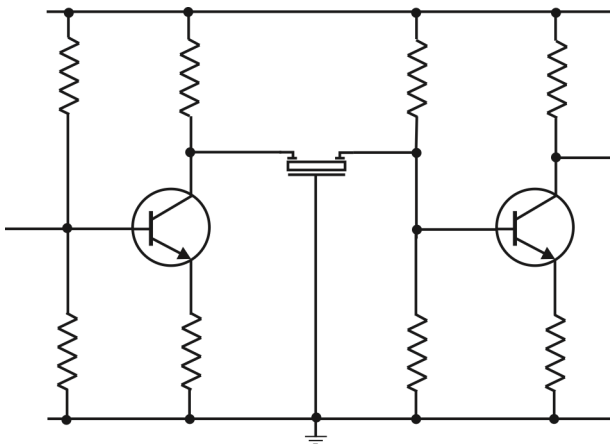


**Figure 7.58** Ceramic bandpass filter circuit using transistors and showing DC arrangements.

(a)



(b)
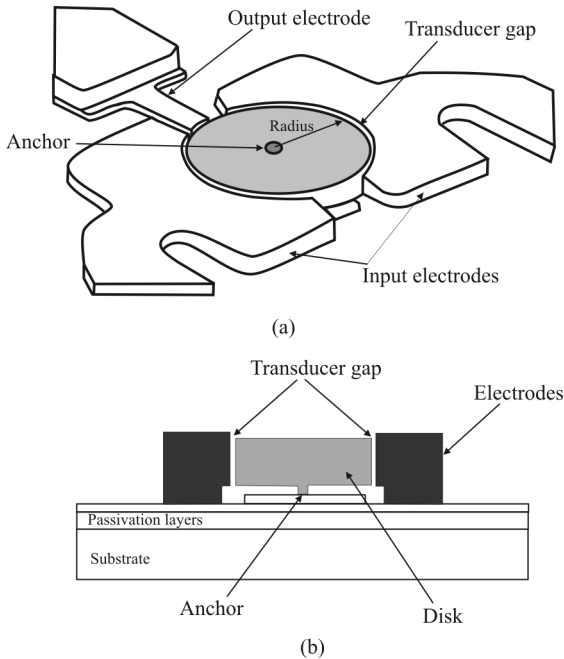
**Figure 7.59** MEMS disk resonator: (a) physical layout, and (b) cross section.

larger dimensions than would be necessary with a beam. For
example, a disk resonator with a radius of 17 μm, a thickness of
2 μm, a drive electrode-resonator gap of 1000 Å, and a
polarization voltage of 35V, exhibited a resonance frequency of
157.23 MHz and a $Q$ of 9400 [8].

Unfortunately, the motional resistance of this disk resonator is too high for
efficient coupling at RF (several hundred ohms), so interfacing the traditional 50Ω
circuits is difficult. Nevertheless it does point out the tremendous possibilities for
MEMS technology.

Another type of MEMS resonator called *the wine-glass resonator* is shown in
Figure 7.60. While normally a circle, the perimeter of this device elongates in
orthogonal directions when excitation is applied as seen in the lower pane. This
type of resonator with disc radius $R = 27.5$ μm, thickness $b = 1.5$ μm, and gap $d =$
1000 Å demonstrated a resonant frequency of 73.4 MHz with atmospheric $Q$ of
8600 [9].

Characteristics of a resonator with multiple devices coupled together are
illustrated in Figure 7.61. In this example, the IF is at 455 kHz. We can see the
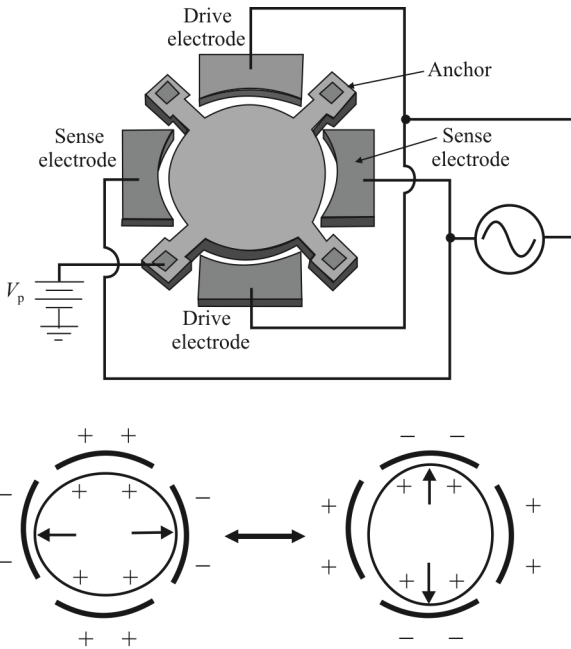
**Figure 7.60** MEMS resonator.
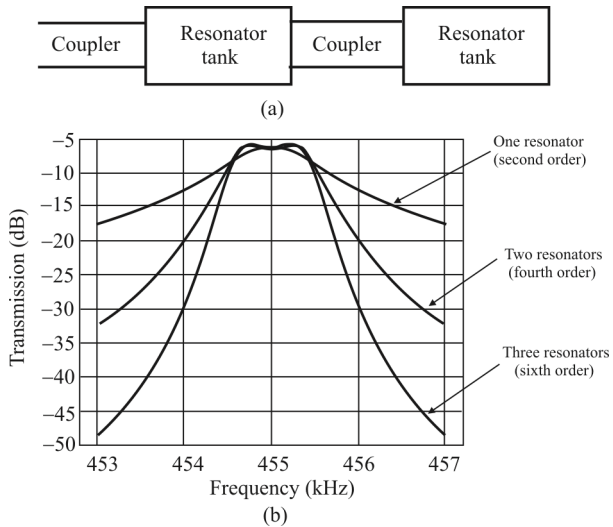


**Figure 7.61** MEMS IF filter: (a)Topology of a bandpass filter, and (b) filter response simulations showing sharper passband-to-stopband roll-offs as the number of resonators increases.

sharp skirts possible with multiple filters. This is a result of the high $Q$s of each individual MEMS filter.

7.5.5.1 Projections and Conclusions

RF MEMS is a powerful technology with various advantages. Besides the low-loss/high-isolation switching, the separation of control and RF ports and the degree of freedom with the mechanical design to realize mechanical filter behavior are attractive features. The maximum number of switching times is a less critical parameter if RF MEMS is used for reconfiguration purposes.

# 7.6 Concluding Remarks

We reviewed the basic types of filter topologies used for IF and RF filters in this chapter. LC filters have been the most prolific primarily due to their flexibility and ease of construction. SAW filters are also used especially at the higher frequencies. MEMS filters are the newest form.

MEMS offer perhaps the best performance for IF filter applications because of their high $Q$, providing excellent selectivity for EW receivers. Such selectivity is required in high-density RF environments. SAW filters also provide good performance as do crystal filters. Ceramic filters have poorer performance than crystal filters but better than LC filters. LC filters have been around the longest and for medium performance applications provide acceptable performance.

## References

[1]     Poisel, R. A., *Antenna Systems and Electronic Warfare Applications*, Norwood, MA: Artech House, 2012, Ch. 20.
[2]     Pozar, D. M., *Microwave Engineering,* 3rd Ed., New York: Wiley, 2005, Section 7.4.
[3]     White, J. F., *High Frequency Techniques,* New York: Wiley, 2004, pp. 336–351.
[4]     Feldmann, M., and J. Henaff, *Surface Acoustic Waves for Signal Processing*, Norwood, MA: Artech, 1986, Chapter 7.
[5]     Kinsman, R. G., "A History of Crystal Filters," *Proceedings of the International Frequency Control Symposium*, 27–29 May 1998, pp. 563–570.
[6]     De Los Santos, H.  J., G. Fischer, H. A. C. Tilmans, and J. T.M. van Beek, "RF MEMS for Ubiquitous Wireless Connectivity, Part 2," *IEEE Microwave Magazine,* December 2004, pp. 50–67.
[7]     De Los Santos, *Introduction to Microelectromechanical Microwave Systems,* Norwood, MA: Artech House, 2004, Chapter 7.
[8]     De Los Santos, *Introduction to Microelectromechanical Microwave Systems,* Norwood, MA: Artech House, 2004, p. 103.
[9]     De Los Santos, *Introduction to Microelectromechanical Microwave Systems,* Norwood, MA: Artech House, 2004, p. 107.

# Chapter 8

## Narrowband Receivers

### 8.1 Introduction

Narrowband communication EW receivers are used for monitoring communication traffic [1]. For signal searching, narrowband receivers can be manually tuned, looking for signals of interest. This was the method for signal search with older, analog receivers. If they are digitally tuned, then they can sweep or step through a segment of the spectrum measuring energy at each channel. If energy is present, then further action can be undertaken depending on the operational requirements.

We discuss the basic types of narrowband receivers in this chapter. The most popular by an overwhelming margin is the superheterodyne receiver architecture introduced in Chapter 4 when discussing filtering image signals [2, 3].

Optimizing the performance of a communications receiver is inherently a process of compromise, which makes such "optimization" in fact, non-optimized. The best that can be hoped for is a receiver that meets the operational requirements in the application of concern. Noise limits the smallest signals that a receiver system is capable of processing. The largest signal is limited by distortions arising from nonlinearities of receiver circuits. The smallest and largest signals define the dynamic range of the receiver system.

Large interfering signals also hinder the reception of small desired signals. The nonlinearities in the receiver networks generate distortion products that fall within the receiver passband. These distortion products prohibit or reduce message reliability. An optimal noise topology typically yields less than optimal large signal performance, and vice versa: the best large signal performance suffers from higher noise degradation, which in turn limits the weak signal reception.

EW receivers are particularly subject to these tradeoffs. Large close-in but not SOIs can be expected. These signals are caused by friendly forces that are closer to the receiver system than the SOIs. However, the SOI population is often considerably farther away than these larger signals. Such weaker signals can easily
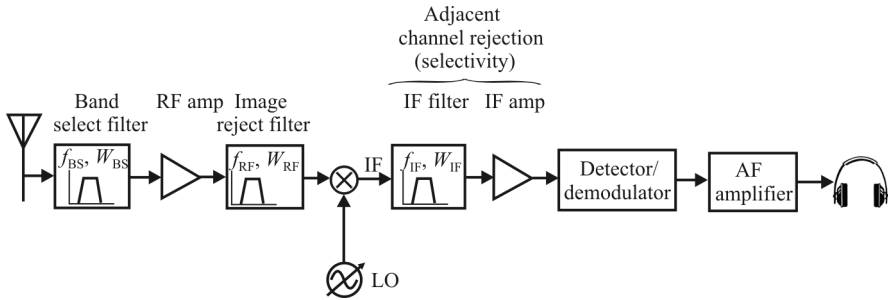
**Figure 8.1** Block diagram of a basic superheterodyne radio receiver.

fall below the noise floor when actions are taken (such as turning up the AGC) to limit the large signal effects.

For example, a superheterodyne receiver may require filtering between the antenna and front-end mixer to prevent interference or compression from unwanted signals. But a narrowband filter introduces signal losses equivalent to a rise in the receiver noise figure. Adding a low-noise preamplifier to compensate for the filter's losses can lower the NF. But the preamplifier also introduces *intermodulation* (IM) products and raises signal levels to the mixer, possibly degrading mixer spurious performance. However, it is still possible to optimize key receiver performance parameters, such as sensitivity and dynamic range, without compromising other considerations, such as complexity, size, and cost.

## 8.2 Superheterodyne Receivers

A heterodyne receiver translates the desired RF frequency to one or more intermediate frequencies before demodulation. Modulation information is recovered from the last IF frequency. Figure 8.1 shows a single-conversion superheterodyne receiver. A mixer translates the RF signal to the IF frequency. The LO signal tuned to a particular spacing above or below the RF signal is injected into the mixer. The RF and LO signals mix to produce a difference frequency known as the IF frequency. The result is a single-conversion receiver, described as such because of the one down conversion mixer.

The advantages that a heterodyne receiver has over a zero-IF receiver (described later in this chapter) include better immunity from interfering signals and better selectivity.

Narrow-bandwidth passive IF filtering is typically employed using crystal, ceramic, or SAW filters. These filters offer good protection against signals close to the SOI because passive filters are not degraded by the compression resulting from large signals. That is, they provide for good selectivity. Active filters do not

provide such protection. However, the price for improved protection is larger physical size and required printed circuit board real estate.

Undesired signals that cause a response at the IF frequency in addition to the desired signal are known as *spurious responses*. Spurious responses must be filtered out before reaching mixer stages in the heterodyne receiver. One spurious response is known as an *image frequency*. An RF filter (known as an *image-reject filter*) is required prior to the mixer for protection against the image unless an image-reject mixer or some other image-rejecting method is used.

The superheterodyne receiver is one of the most popular forms of receivers in use today in a variety of applications, including EW. Although other forms of radio receivers are used, the superheterodyne receiver is one of the most widely used forms. Initially developed in the early days of radio technology, the superhet receiver offers significant advantages in EW. Naturally, the basic concept has been developed since its early days, and more complicated and sophisticated versions are used, but the basic concept remains the same.

**8.2.1 Superheterodyne Receiver History**

The superhet receiver is based around the idea of mixing signals in a nonlinear fashion. This idea was first noticed when beats were detected between two signals. R. A. Fessenden patented the idea in 1901.[1]

The approach was not pursued for several years as most receivers consisted of detectors and tuned circuits. The diode thermionic valve or vacuum tube was invented by Ambrose Fleming in 1904, and then a third grid was added by Lee de Forest. Early tubes were very unstable, however, and it was difficult to elicit much useful performance from them.

Edwin Armstrong started to utilize the characteristics of the thermionic valve, inventing the regenerative receiver around 1910. This provided a considerable increase in useful gain over what had been previously attained.

It was WW I in 1914 that gave new emphasis to radio receiver design. Sensitive radio receivers were required for a variety of tasks. The first major step was taken by a Frenchman named Lucien Levy. At the time the performance of valves was limited to around 100 kHz or so, and he developed a method for reducing the frequency of the incoming signal. He used a system of beats—the RF signal could then be tuned and amplified more effectively at a lower frequency.

At that time Armstrong developed the superheterodyne receiver with the architecture we still use today with a fixed frequency IF filter and amplification and a variable LO. His idea was developed in 1918, at the end of the war, so it was not widely used. As a result, Edwin Armstrong was credited with the invention.

---

[1] One of the major advances made by Fessenden was the development of the heterodyne principle. He undertook experiments with this in 1901, but in view of the state of wireless technology, it was well ahead of its time and was not used for over 10 years afterward. It required the generation of stable continuous-wave signals, and these were not practicable until the vacuum tube became available.

The superheterodyne receiver was not extensively used initially for economic reasons. Many valves were required in a receiver and valves were expensive. However, as the number of broadcast stations increased and selectivity became an issue (to separate signals), along with the falling cost of thermionic valves, use of the superhet receiver started to grow in the late 1920s and early 1930s. It has been in widespread use ever since.

## 8.2.2 Mixing and the Superhet Receiver

The idea of the superheterodyne receiver revolves around the process of mixing described in Chapter 4. RF mixers are used to multiply two signals together. When two signals are multiplied together the output is the product of the instantaneous level of the signal at one input and the instantaneous level of the signal at the other input. New signals are developed at frequencies that are the sum and difference of the two input signals; that is, if the two input frequencies are $f_1$ and $f_2$, then new signals are seen at frequencies of $f_1 + f_2$ and $f_1 - f_2$. To take an example, if two signals, one at a frequency of 5 MHz and another at a frequency of 6 MHz, are mixed together, then new signals with components at frequencies of 11 MHz and 1 MHz are generated.

## 8.2.3 Images in the Superhet Receiver

Even though the selectivity of the superhet is very good, there is a fundamental problem with superhet receivers in that there are two signals that can enter the IF. With the LO set to 5 MHz we have already seen that a signal at 6 MHz mixes with the LO to produce a signal at 1 MHz that will pass through the IF filter. However, if a signal at 4 MHz enters the mixer it produces two mixing products, one at the sum frequency of 10 MHz, while the difference frequency appears at 1 MHz; two input signals on different frequencies can enter the IF. The signal at the unwanted frequency is known as the *image*. Fortunately, it is possible to place a tuned circuit before the mixer to prevent the image from entering the mixer or, more correctly, to reduce its level to an acceptable value. See Figure 8.2.

Fortunately, this tuned circuit does not need to have sharp skirts. It does not need to reject signals on adjacent channels, but instead it needs to reject signals on the image frequency. These will be separated from the wanted channel by a frequency equal to twice the IF. In other words, with an IF at 1 MHz, the image will be 2 MHz away from the SOI frequency.

## 8.2.4 IF Frequencies

The selection of specific IF frequencies depends on the application and range of input and output frequencies that are desired. Each mixer in the system is, by design, a nonlinear device that results in distortion of the original RF signal. One
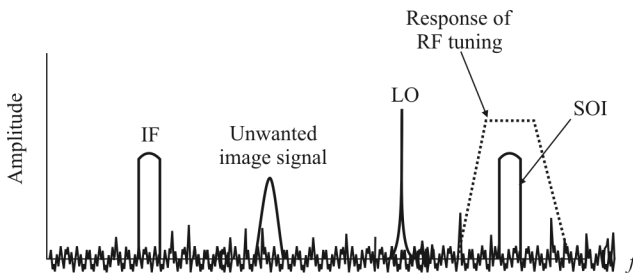
**Figure 8.2** Using a tuned circuit to remove the image signal.

way this can happen is through *reciprocal mixing*. A mixer cannot distinguish between a desired signal and an undesired signal so it mixes noise and undesired signals just as well as the desired signal. The effect of this is a mixing of not only the desired signal and the LO but also of any noise in the LO against any undesired signals, desired signals against each other, etc. The end result of having a receiver with multiple IF stages is a gradual mixing of undesired noise that gets spread around the reception bandwidth of the receiver.

These undesired mixing products can cover or distort weak signals. In addition, superheterodyne receivers require a filter after the mixer to remove signals that are mixed resulting in signals outside of the desired band. These signals, if not eliminated, can make the reciprocal mixing problem even worse. The typical solution to the problem is to employ the use of a crystal filter. Unfortunately, crystal filters also have nonlinearities in them that tend to occur at the worst possible moment—when there are strong adjacent signals that vary in amplitude that cause varying drive levels on the crystal filter. Crystal filters after the mixer and before the IF, also known as *roofing filters*, can mean the difference in hearing and not hearing a weak signal—a strong signal can de-sense the receiver (force the AGC to lower the gain, removing the gain from a weak signal and causing it to disappear in the receiver), and elimination of this signal with a roofing filter allows the reception of the weak signal.

The very narrow RF/IF crystals also introduce group delay distortion, where slightly different frequencies encounter different time delays, manifesting as differential phase shifts. While not directly perceived or audible by the human ear, this phase distortion causes operator hearing fatigue during long sessions of listening or operating. They can also affect the automated processing of signals.

In EW receivers, the system can be designed such that the receive signal strength of the SOI is of sufficient level to overcome any of these distortions and render them unimportant. While not a major problem in commercial receivers, reciprocal mixing in EW receivers where intercepting signals at or just 10–20 dB above the noise level when there are other large signals near is a frequent occurrence, and can be a significant issue. EW receivers therefore require a high-dynamic range communications medium since there are both large and small

signals present at the same time and the receiver must demodulate both in the presence of the other.

## 8.2.5 Superhet Receiver Block Diagram

A simplified block diagram of a superhet receiver is shown in Figure 8.1. The superheterodyne block diagram is relatively straightforward and builds on the basic functional block used to convert the incoming frequency down to a fixed IF stage.

While there may be some simplified versions for a superheterodyne block diagram, each receiver will be different as a result of the differing requirements for each receiver. However, the basic principles are the same, and many superheterodyne block diagrams are very similar.

### 8.2.5.1 Basic Superhet Block Diagram and Functionality

Signals enter the front end circuitry from the antenna. The front end often contains a broadband filter and associated amplifier to select the frequency band of operation. This is called a *band-select* filter and is often called *preselection*. The front end also contains the image-reject filter for the superhet to remove the image signal and often includes an RF amplifier to amplify the signals before they enter the mixer. The level of this amplification is carefully calculated so that it does not overload the mixer when strong signals are present but enables the signals to be amplified sufficiently to ensure a good SNR is achieved.

As we considered in Chapter 3, the first components encountered by arriving signals establish the majority of the noise that subsequent stages must handle. Therefore these band-select components must be carefully chosen to generate low noise.

The tuned and amplified signal then enters one port of the mixer. The LO signal enters the other port. The LO may consist of a variable frequency oscillator that can be tuned by altering the setting on a variable capacitor. Alternatively, it may be, and often is, a frequency synthesizer that enables greater levels of stability and setting accuracy.

For dynamic range reasons mixers tend to require fairly high-level signals to operate properly. This requirement primarily applies to the LO level, which often requires turning diodes or other semiconductor devices on and off. These levels therefore are on the order of volts, whereas the incoming RF signals are on the order of microvolts (see Figure 3.1).

Once the signals leave the mixer they enter the IF stages. These stages contain most of the amplification in the receiver as well as the filtering that enables signals on one frequency to be separated from those on the next. Filters may consist simply of LC tuned transformers providing inter-stage coupling, or they may be

much higher performance ceramic or crystal filters, or perhaps MEMS filters, depending on what is required.

EW receivers often must operate in high signal-density environments, and therefore selectivity requirements are normally quite stringent. If not, signals from adjacent and nearby channels will interfere with the SOI, making processing very difficult.

Once the signals have passed through the IF stages of the superheterodyne receiver, they need to be demodulated. Different demodulators are required for different types of transmissions, and as a result some receivers may have a variety of demodulators that can be switched in order to accommodate the different types of transmissions that are to be encountered. The output from the demodulator is the recovered audio or perhaps digital baseband signals. If audio, it is passed into the audio stages where they are amplified and presented to the headphones or loudspeaker or perhaps recorded. If digital, the bits are passed to DSPs for subsequent processing.

In some newer superhet receivers, conversion to digital form is performed much earlier in the receiver, at the RF or, more often, at the IF. This allows for much or most of the processing in the receiver to be done digitally, permitting much more flexibility in the architecture. This is the basis for the SDR.

8.2.5.2 Other Topologies for Superhet Receivers

The diagram shown in Figure 8.1 is a very basic version of the superhet receiver. Many modern receivers are far more complicated. Some superhet radios have more than one frequency conversion and other areas of additional circuitry to provide the required levels of performance. However the basic superhet concept remains the same, using the idea of mixing the incoming signal with a locally generated oscillator signal to convert the signals to a new frequency. (See [4] for an example of a complete receiver.)

Double Conversion Superheterodyne Receiver

Although the basic idea for the superhet receiver works very well, to ensure the optimum performance under a number of situations, an extension of the principle, known as the *double conversion superhet radio receiver*, may be used. A block diagram of such a receiver is shown in Figure 8.3.

The double superheterodyne radio receiver improves the performance in a number of areas including LO stability (although synthesizers have largely overcome this problem), image rejection, and adjacent channel filter performance.

The double superheterodyne radio receiver is still widely used, especially at high frequencies where factors such as image rejection and filter performance are important.
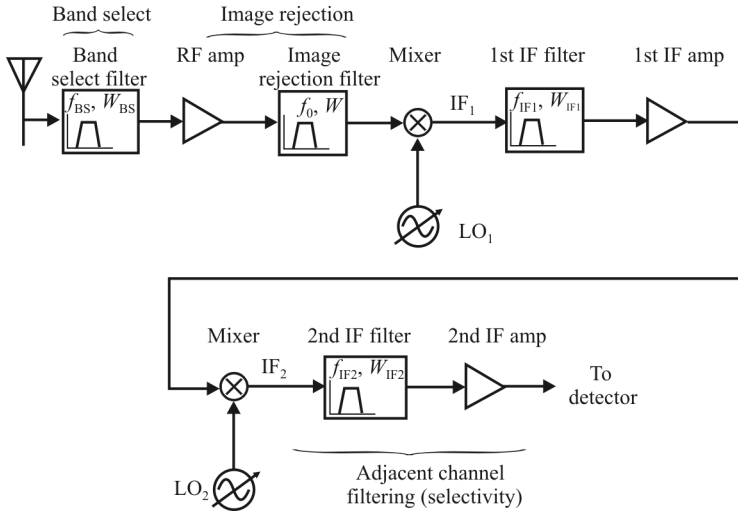
**Figure 8.3** Basic double conversion superheterodyne receiver concept.

*Advantages of Double Conversion Superhet Receiver*

When choosing the IF for a superhet receiver there is a trade-off to be made between the advantages of using a low- or high-frequency IF:

- *High-frequency IF*: The use of a high-frequency IF means that the difference between the wanted frequency and the unwanted image is much greater and it is easier to achieve high levels of image rejection performance because the front end filtering is able to provide high levels of rejection.
- *Low-frequency IF*: The advantage of choosing a lower frequency IF is that the filters that provide the adjacent channel rejection are lower in frequency. This means the filter skirts can be sharper, which enables the performance to be high while keeping the cost low.

Accordingly there are two conflicting requirements that cannot be easily satisfied using a single IF. The solution is to use a double conversion superhet topology to provide a means of satisfying both requirements.

*Double Conversion Superheterodyne Receiver Concept*

The basic concept behind the double conversion superheterodyne radio receiver is the use of a high IF to achieve the high levels of image rejection that are required

and a further low IF to provide the levels of performance required for the adjacent channel selectivity.

Typically the receiver will convert the incoming signal to a relatively high first IF stage. This enables the high levels of image rejection to be achieved. As the image frequency lies at a frequency twice that of the IF away from the SOI, the higher the IF, the farther away the image is and the easier it is to reject at the front end.

As we see in Figure 8.3, once the signal has passed through the first IF at the higher frequency, it is then passed through a second mixer to convert it down to a lower IF where the narrowband filtering is accomplished so that the adjacent channel signals can be removed. At the lower frequency, filters are cheaper and the performance can be higher due to steeper filter skirts.

*Double Conversion Superheterodyne Architectures*

While the basic concept for the double conversion superhet radio receiver involving two stages of frequency conversion may remain the same, there are a number of different topologies that can be adopted:

- *Tuned first oscillator*: This is the most usual form of double conversion superhet receiver. The first conversion uses a variable frequency oscillator that converts the signal to the first IF. See Figure 8.3.
- *Fixed frequency first oscillator*: This style of double conversion superhet receiver was popular before the days of frequency synthesizers and other very stable LOs. To ensure the frequency stability, a crystal oscillator was used to provide the LO for the first conversion. Crystal oscillators typically are not tunable. A bandpass filter would be used to provide selectivity and allow a band of frequencies to be passed. The second local oscillator would allow tuning over the range allowed by the bandpass filter. When further coverage was required, the first, crystal controlled oscillator, would need to be switched to the next crystal (Figure 8.4). In this way continuous broad coverage could be obtained, albeit with a number of crystals.

    Apart from providing high levels of image rejection, this concept gave considerably improved levels of frequency stability for receivers of the time. Modern frequency synthesizers rarely need or use this topology.

Although little selectivity is generally provided in the first IF, as mentioned, a roofing filter may often  be used to provide some adjacent channel filtering. This prevents very strong adjacent channel signals from overloading the later stages of the IF. However, the main selectivity is still provided in the lower frequency IF stages. Whatever the style of double conversion superheterodyne receiver, the basic concept of providing two frequency conversion stages applies.
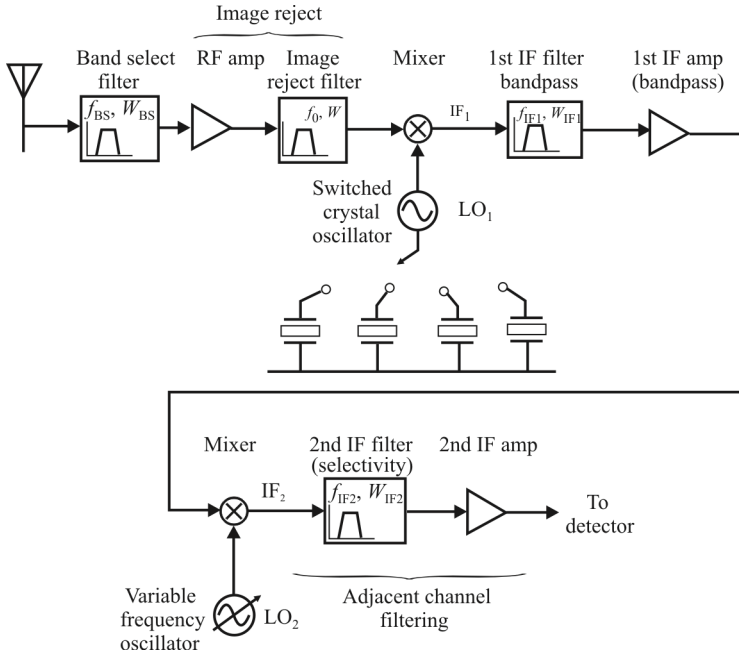
**Figure 8.4** Double conversion superheterodyne receiver with fixed frequency first LO.

## 8.2.5.3 Triple Conversion Superheterodyne Receiver

For some designs, particularly those at microwave frequencies, there may be advantages in using three conversions. While these receivers are less common, they are still found on some occasions. Their design provides for high levels of adjacent channel selectivity while still achieving adequate levels of image rejection. For EW applications both specifications are particularly important, so this may only be achieved by using a number of conversion processes. In cases like these, triple conversion superheterodyne receivers may be needed, although costs are naturally high in view of the additional circuitry required. EW receivers are typically not as cost sensitive as commercial receivers, so this is not a fundamental problem if sufficient performance improvement is attained.

The double superheterodyne radio receiver is normally found where high levels of performance are required. The additional circuitry needed adds cost, and to minimize the occurrence of spurious signals within the receiver, the design must be undertaken with care. However, it is possible to achieve very high levels of performance with a double superheterodyne or where particularly needed, a triple superheterodyne radio receiver.

# 8.3 Homodyne (Zero-IF) Receiver

A homodyne, direct conversion (DCR), or zero-IF (zero intermediate frequency) receiver translates the desired RF frequency directly to baseband for information recovery [5]. Baseband is the range of frequencies occupied by the signal before modulation or after demodulation. Baseband signals are typically at frequencies substantially below the carrier frequencies.

### 8.3.1 Concept of the DCR

The desired RF spectrum is converted directly to DC using an LO frequency exactly equal to the RF. The simplicity of this architecture affords two major advantages over the heterodyne approach. First, because the IF is zero, the image to the desired RF signal is the desired signal itself, which means DCRs do not face conventional image problems. Therefore, bulky, off-chip, front-end image-reject filters, which are required in heterodyne topologies, are unnecessary in a DCR. Second, with the desired spectrum downconverted directly to baseband, channel selection can be performed either with a simple analog lowpass filter or by converting to the digital domain with an ADC and digitally performing channel selection with  digital signal processing. The latter approach raises the possibility of having a universal RF front-end where any type of wireless standard can be received with the same analog blocks and decoded using digital methods (assuming the front end has sufficient bandwidth and sensitivity).

On the low end of baseband, signals may approach or include DC. The upper frequency limit of baseband depends on the data rate, or speed, at which information is sent and whether or not special signals called subcarriers are utilized. Figure 8.5 shows an example flow diagram of a zero-IF receiver architecture. A mixer translates the RF frequency directly to baseband. The LO signal, tuned to the same frequency as the desired RF signal, is injected into the mixer. The RF and LO signals mix to produce the baseband frequency. Some receivers employ an I/Q mixer to recover baseband information.

When translating directly from RF to baseband, a DC component (along with the band-limited information signal) is realized at the output of the mixer. The DC component (or DC-offset) must be removed to prevent large DC pulses from de-sensitizing the baseband demodulator, which creates a problem if the SOI contains significant information at DC. The system can either be AC-coupled or incorporate some form of DC notch filtering after the mixer.

The zero-IF receiver can provide narrow baseband filtering with integrated lowpass filters. Often, the filters are active op-amp-based filters known as *gyrators* [6, 7]. The gyrators provide protection from most undesired signals. The gyrator filters eliminate the need for expensive crystal and ceramic IF filters, which take more space on a printed circuit board. The gyrator in a two-port network
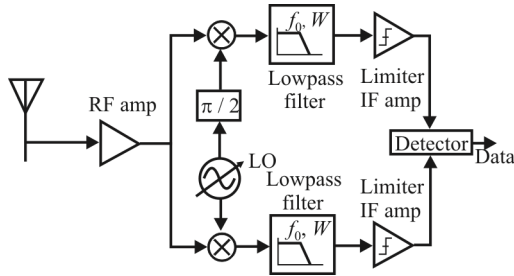
**Figure 8.5** Zero-IF receiver.

effectively makes an inductor at one of its ports look like a capacitor at the other. So an inductor/gyrator configuration can replace a large capacitor.

The zero-IF topology offers the only fully integrated receiver currently possible. This fully integrated receiver architecture minimizes the board real estate required, the number of components, receiver complexity, and cost. As mentioned, most zero-IF receiver architectures also do not require image-reject filters, thus reducing cost, size, and weight.

Zero-IF receiver limitations require tighter frequency centering of the LO and RF frequencies. Significant offsets in the RF or LO frequencies degrade the BER. When the desired signal is above the VHF range, the zero-IF design becomes more complex, partially due to these frequency offset problems. One solution for higher frequency zero-IF topologies is to add *automatic frequency control* (AFC). AFC prevents the centering problem by adjusting the frequency of the LO automatically.

Performance is typically limited in a zero-IF architecture in several ways. Sensitivity and rejection to some undesired signals, such as IMD, can be difficult to achieve. The active gyrator filters compress with large undesired signals. Once the gyrator is compressed, filter rejection is reduced, thus limiting protection. Zero-IF receivers typically require an AGC circuit to protect against large signal interference that compresses the gyrator filters. We should note, however, that well-designed superhet receivers normally also incorporate AGC.

Because the LO is tuned to the RF frequency, self-reception may also be an issue. Self-reception can be reduced by running the LO at twice the RF frequency and then dividing-by-two before injecting into the mixer. Because the zero-IF LO is tuned to RF frequencies, the receiver LO may also interfere with other nearby receivers tuned to the same frequency. The RF amplifier reverse isolation, however, prevents most LO leakage to the receiver antenna.

The direct-conversion architecture is highly attractive for integrated RF receivers. The elimination of off-chip filters simplifies interstage matching, since the need to match to the input and output impedances of the off-chip filter is eliminated. By filtering at baseband frequencies, device parasitics are less severe,

and less current is needed for amplification; thus, DCRs also offer lower power consumption. However, DCRs have a number of unique issues that make their actual implementation less than straightforward. For example, translating the RF spectrum to 0 Hz means that quadrature (*I/Q*) downconversion is required to properly handle the negative frequency portion of the spectrum (although if *I/Q* demodulation is mandated by the communications modulation format anyway, this is not really an issue). DCRs are also susceptible to dynamic range limitations, primarily due to: second-order distortion, $1/f$ noise, *I/Q* mismatch, and DC offsets [8]. We now examine these DC offsets.

## 8.3.2 Overview of DC Offsets in DCRs

### 8.3.2.1 Self-Mixing

RF band selection (preselection) is typically the only filtering performed in the receive chain of a DCR prior to the signal being downconverted directly to baseband. Therefore, a strong nearby signal, including the receiver's own LO, can mix with itself down to zero-IF. This is called *self-mixing*, and generates a DC level that appears as interference at the center of the desired band. Three potential self-mixing mechanisms that can lead to DC offsets in DCR applications are shown in Figure 8.6.

Self-mixing due to the finite isolation typical of silicon-based ICs between the LO and RF ports of a mixer is shown in Figure 8.6(a). In these mixers, port-to-port isolation is limited by low-resistivity substrate coupling, bond wire radiation, and capacitive and magnetic coupling [8]. In order to provide sufficient drive for the mixer switches (e.g., diodes), the LO is typically a strong signal. It can leak with sufficiently high amplitude through these unintended paths back to the front end LNA. There, the LO signal can reflect off the LNA output back into the mixer RF input and mix with itself, thereby generating a static DC level (LO self-mixing); the situation is exacerbated if the LO signal leaks back to the LNA input and is amplified before reaching the mixer input. The LO signal can also be reradiated by the antenna; reflect off obstructions, such as a building or moving vehicle; and be recaptured by the front end [Figure 8.6(b)]. With fading and multipath propagation, the received power level can, therefore, vary rapidly, which results in a time-varying or dynamic DC offset.

The reradiation of the LO can also cause problems for other nearby receivers operating in the same band. Since the LO is at the same frequency as the RF, the LO signal appears in the passbands of the RF band select filters of other receivers. Thus, as shown in Figure 8.6(c), a strong nearby interferer, such as another receiver's LO, can also generate DC offsets by finding a path to the mixer LO port and mixing with itself (interferer self-mixing).
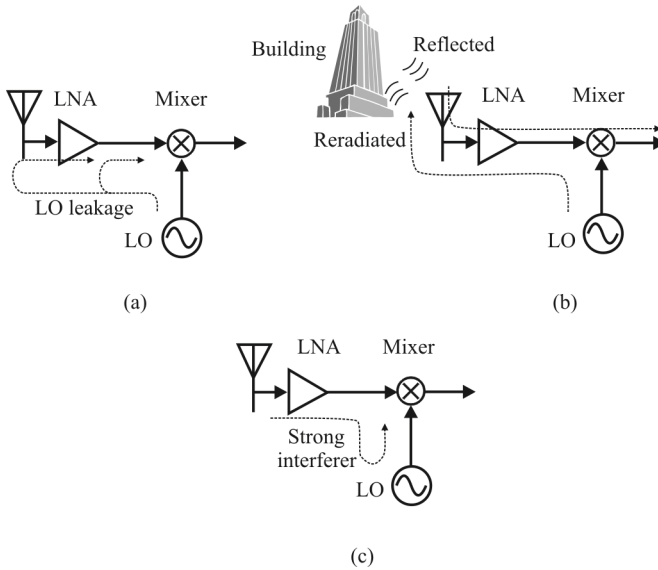
**Figure 8.6** DC offset mechanisms, self-mixing: (a) LO leakage, (b) LO reradiation, (c) strong in-band interferer.

## 8.3.2.2 Nonlinearities

Second-order nonlinearities can also create DC offsets by the interaction of an interfering signal and these nonlinearities. For example, if the nonlinear response of a circuit is approximated by the standard power series:

$$y(t) = k_1 x(t) + k_2 x^2(t) + k_3 x^3(t) + \ldots \tag{8.1}$$

and a single-tone input signal, $x(t) = A\cos \omega t$, is applied to the circuit, then the resulting output signal (up to second order) is given by

$$y(t) = k_1 A \cos \omega t + k_2 A^2 \cos^2 \omega t$$

$$= k_1 A \cos \omega t + \frac{1}{2} k_2 A^2 [1 + \cos(2\omega t)]$$

$$= \frac{1}{2} k_2 A^2 + k_1 A \cos \omega t + \frac{1}{2} k_2 A^2 \cos(2\omega t) \tag{8.2}$$

The first term in (8.2) is a DC component related to the second-order nonlinearity of the circuit $k_2$ and is magnified by the square of the input signal amplitude. Therefore, any large signal within the passband of a DCR can generate a large DC

offset if the even-order performance of the receiver is poor (i.e., $k_2$ is relatively large).

8.3.2.3 Offset Removal

The simplest solution for removing DC offsets is to highpass filter the spectrum with a series AC coupling capacitor; however, this method is not always feasible. The corner frequency of the highpass filter has to be extremely low, on the order of tens of hertz, which, at these frequencies, makes the required on-chip area for series capacitors prohibitively large. Large size capacitors also tend to react slowly to dynamically changing DC levels. Therefore, other methods, or combinations of methods, must be employed to mitigate unwanted DC levels, including

- *Sub- or Super-Harmonic Mixing*: with an LO at some integer multiple or sub-multiple of the RF, DC offsets due to LO self-mixing can be significantly suppressed [9]
- *Offset Calibration Techniques*: digital sample-and-hold feedback, offset estimation with corrective feedback at baseband, and servo loops can be used to track the DC offset and remove it from the desired spectrum [8]

## 8.3.3 Noise in Direct Conversion Receivers

Direct conversion receivers avoid the cumulative nonlinear effects that plague superheterodyne receivers used in high-dynamic-range EW systems. First, because there is no IF stage where gain in the form of AGC can be employed, there can be a wide range of signals on the output of the conversion stage. Since the ultimate output of a direct conversion stage is baseband, the output corresponds to the same frequencies in use for audio. To mitigate this problem, very high-dynamic-range ADCs are available that can discern both large and weak signals at the same time—in other words, the ADCs have a very high dynamic range—ADCs are available that have dynamic ranges of 120 dB or more at low frequencies. With this dynamic range, roofing filters are no longer required in the system and so with their departure also goes the nonlinearities that come with them.

Another problem that was difficult to overcome was the rejection of images. Remember that, along with the $f_1 - f_2$ signals that we receive from a conversion stage or mixer, we also receive an $f_1 + f_2$ term. In the case of a superheterodyne receiver, these signals are generally many megahertz away since $f_1 - f_2$ is, itself, large. In the case of a direct conversion receiver, $f_2$ is picked to be the same or very near the frequency we are trying to receive. This means that $f_1 + f_2$ and $f_1 - f_2$ can both be in the same receive bandwidth. These images must be suppressed.

Since there is only a single downconversion or downmixing process from the RF band of interest direct to baseband, there is only a single opportunity for phase noise to enter the analog signal processing. If phase noise at this point is properly
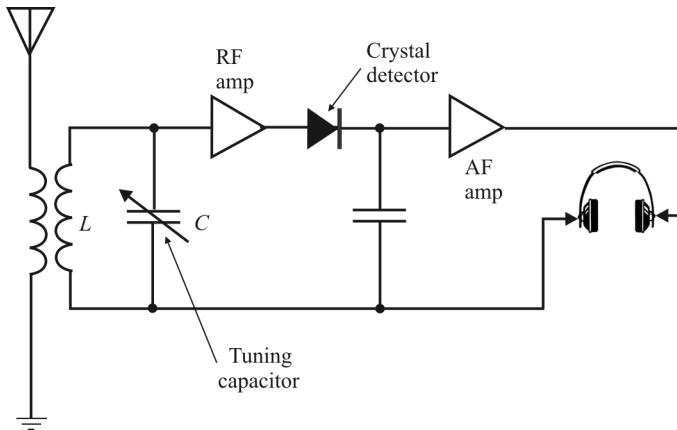
**Figure 8.7** TRF receiver.

controlled, it sets the phase noise performance of the entire receiver, unlike the multiple downconversions and multiple LOs in a traditional superhet. Providing excellent phase noise performance is inherently easier in a direct conversion receiver.

By moving all of the narrowband filtering, traditionally provided by the low IF in a superhet radio into the realm of DSP, which are, or can be, pure mathematic processes, the digitized baseband signals can be processed, filtered, and demodulated with whatever desired dynamic range and linearity level is desired, and the DSP backend can therefore be designed not to add perceptible further distortion or noise beyond what exists in the analog signal entering the digitizer. With minimal analog processing in the form of a single direct conversion front end, the end result is a system with fewer opportunities and points of noise and distortion contribution.

## 8.4 Tuned Radio Frequency Receivers

A *tuned radio frequency* (TRF) receiver is one of the simplest radio types in existence. It is characterized by a low component count, reasonable sensitivity, and easy operation (it has only tuning and volume controls). The receiver consists of one (or several) stages of RF filtering and amplification, a detector, and an audio amplifier (Figure 8.7).

Most of the receiver's sensitivity is due to RF amplification within the passband of a tuned LC circuit as illustrated in Figure 8.7. The filter usually consists of an inductor and capacitor connected in parallel. The inductor ($L$) is a

fixed component, and the capacitor is usually a ganged variable capacitor. The resonant frequency of the filter is given by

$$f_0 = \frac{1}{2\pi\sqrt{LC}} \qquad (8.3)$$

The RF amplifier also amplifies the noise produced in this stage. The noise produced is a result of the bandwidth of the resonant circuit (higher bandwidth means more noise) and the circuit design characteristics. Typically, the active component in this stage would be a BJT, FET, or op amp. A low noise amplifier should always be specified.

The SNR along with the frequency range of the receiver provides the performance specifications for this type of receiver. Receiver selectivity is also governed by the tuned circuit in the RF amplifier stage. This is limited by the quality factor ($Q$) of the resonant circuit, which is given by

$$Q = \frac{|X_L|}{R_L} \qquad (8.4)$$

where

$X_L$ = inductive reactance of the coil = $j\omega L$
$R_L$ = coil resistance

Unfortunately, the receiver bandwidth changes with the resonant frequency of the LC tuned circuit because

$$W = \frac{f_0}{Q} \qquad (8.5)$$

and $Q$ is a constant. As the resonant frequency of the tuned circuit changes, so must the bandwidth. What this means is that the receiver selectivity changes with the tuned frequency of the receiver. This is an undesirable characteristic. Selectivity is a measurement of the receiver's ability to reject unwanted signals.

Having the receiver's selectivity change with frequency is eliminated by providing fixed bandpass characteristics in the RF amplifier circuit of more advanced receiver designs (such as in a superheterodyne receiver).

# 8.5 Concluding Remarks

The common forms of narrowband receivers were introduced in this chapter. These are the superheterodyne receiver, the direct conversion receiver, and the tuned frequency receiver. The last of these is not common for high-quality receivers used in EW applications. The DCR architecture is popular for small, lightweight applications. It is quite common for the commercial applications in cellular phones. It can, however, be applied to EW problems where its architecture can be put to effective use.

The superheterodyne topology is by far the most common architecture for narrowband applications. It exhibits superb sensitivity and selectivity. Its architecture is flexible and can effectively be used to cover broad frequency ranges, a requirement of most EW receivers.

## References

[1]  Rohde, U. L., and T. T. N. Bucher, *Communication Receivers Principles and Design*, New York: McGraw-Hill, 1988.
[2]  Vaccaro, D. D., *Electronic Warfare Receiving Systems*, Norwood, MA: Artech House, 1993.
[3]  Erst, S. J., *Receiving Systems Design*, Norwood, MA: Artech House, 1984, Section 4.1.
[4]  Drentea, C., *Modern Communications Receiver Design and Technology*, Norwood, MA: Artech House, 2010.
[5]  Erst, S. J., *Receiving Systems Design*, Norwood, MA: Artech House, 1984, Section 4.2.
[6]  *Handbook of Operational Amplifier Active RC Networks*, Tucson: Burr-Brown Research Corporation, 1966, Ch. 6.
[7]  Huelsman, L. P., *Theory and Design of Active RC Circuits*, New York: McGraw-Hill, 1968, Ch. 8.
[8]  Mashhour, A., W. Domino, and N. Beamish, "On the Direct Conversion Receiver—A Tutorial," *Microwave Journal*, Vol. 44, No. 6, June 2001, pp. 114–128.
[9]  Matinpour, B., and J. Laskar, "A Compact Direct-Conversion Receiver for C-band Wireless Applications," *IEEE RFIC Symposium Digest 1999*, pp. 25–28.

# Chapter 9

# Compressive Receivers

## 9.1 Introduction

Many EW applications require wideband receivers to handle modern threat environments. These environments typically contain a variety of signal types and an even larger variety of modulation formats. The compressive receiver is one such receiver that satisfies many of the requirements of wideband EW receivers.

A CxRx determines the real-time Fourier transform on signals present at its input. Typically, hundreds of megahertz are scanned in several microseconds so the signal acquisition process is very rapid. A scanning superheterodyne receiver would require hundreds of milliseconds to scan the same frequency range with equivalent resolution. This speed makes them very good at intercepting FHSS signals [1]. They also provide a very efficient method for the detection of DSSS signals [2].

Another outstanding feature of the CxRx is its ability to retain the amplitude and phase of the signal being analyzed. This allows the direct application of multiple channel antenna arrays to determine the direction of arrival of the signal at the intercept system.

Table 9.1 lists representative principal characteristics of a CxRx used for communication EW intercept applications.

We describe the salient characteristics of compressive receivers useful for intercepting communication and other types of signals in this chapter. We begin by presenting an overview of their operation. That is followed by a detailed mathematical analysis of the CxRx operation.

## 9.2 Compressive Receiver Configurations

The compressive receiver implements the chirp-Z transform [3]. It is an RF processing device that rapidly scans a frequency range and provides time-

| Parameter | Value |
|---|---|
| Input Bandwidth | 500 MHz |
| Sweep Rate | 1 MHz/μs |
| Resolution | 25 kHz |
| Delay Line | 60 MHz × 60 μs |
| Processing Gain | 36dB |
| Tangential Sensitivity | −110 dBm |
| Spurious Signal Level | Below −120 dBm |

separated outputs for each signal present at its RF input. These output samples are processed to generate RF pulse descriptors or queuing information for other receivers. The CxRx is a Fourier transform device and can have nearly 100% POI.

The basic CxRx consists of the compressive network consisting of one or more DDLs followed by an envelope detector device and parameter encoder. The compressive network performs the signal power compression over frequency and time as well as output sample time separation. The envelope detector provides a video signal for each RF sample. The parameter encoder measures frequency, amplitude, phase difference, and other signal characteristics, such as pulse width and time of arrival.

An RF signal appearing at the input to the CxRx is multiplied by an LO that is linear-sweeping (see Figure 9.1). This signal is applied to a DDL with an equal but opposite time-frequency slope. All spectral energy that falls within the bandwidth of the DDL will appear in a narrow time slot at the output of the delay line. Time
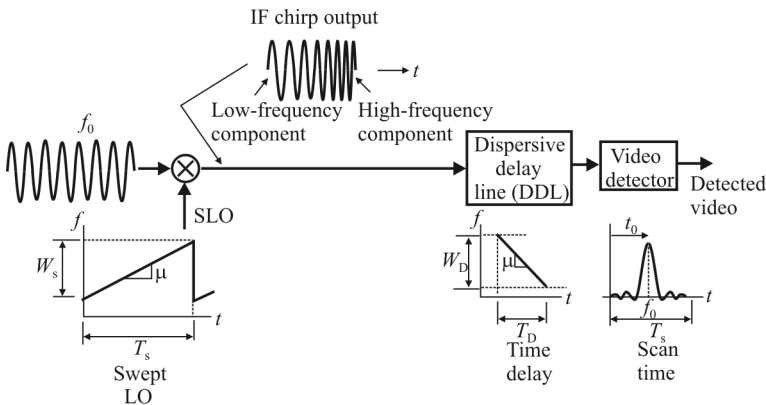


**Figure 9.1** CxRx block diagram.
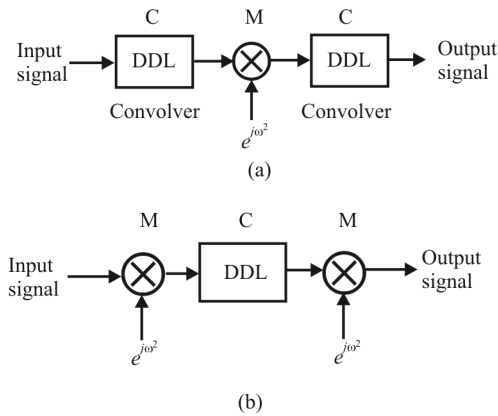
**Figure 9.2** Analog approaches to CxRx: (a) convolve-multiply-convolve, and (b) multiply-convolve-multiply.

separation between output signals, due to input signals with different RF frequencies, will cause the IF sweeps to be offset in frequency from each other. The time separation at the output between different input signals permits parameter measurements of simultaneously received signals.

### 9.2.1 C-M-C and M-C-M Configurations

The finite length of actual chirp signals and filters leads to two possible implementable full chirp transforms, the convolve-multiply-convolve, C(s)-M(l)-C(s), and the multiply-convolve-multiply, M(s)-C(l)-M(s), where l stands for long and s means short. These are shown in Figure 9.2(a) and (b). Typically, the long chirp is twice the length and bandwidth of the short chirp. If only frequency, amplitude, and *relative* phase between two channels is important (as it often is), the final M of the M-C-M or the first C of the C-M-C can be dropped. Absolute phase information requires a full M-C-M or C-M-C implementation. The complex exponential inputs to the mixers represent chirp waveforms (linearly increasing or decreasing as a function of time). Both configurations are functionally identical in that they can produce the same outputs. Provided a chirp with sufficient *time-bandwidth* (*TW*) product can be produced, the C-M-C configuration generally offers the best overall performance for *command, control, communication, and intelligence* (C3I) applications.

In a C-M configuration, the first convolver linearly time-skews the frequency components of wideband signals to counter the time-skewing that occurs in the second convolver. This nulling effect minimizes phase distortion in the compressed output signal. If phase information is not important, then the first convolver can be eliminated for reduced cost and complexity.

We present the details of CxRx operation in the following sections based on the M-C-M topology.

## 9.3 Fundamentals of CxRx Operation

The chirp-transform algorithm can be derived from the Fourier transform relationship [4–6]

$$F(\omega) = \int_{-\infty}^{\infty} f(t) e^{-j\omega t} dt \qquad (9.1)$$

by a substitution of the form

$$-2\omega t = (t - \omega)^2 - t^2 - \omega^2 \qquad (9.2)$$

Assuming a linear relationship of frequency and time, (9.2) yields

$$F(\omega) = F(\mu t) = e^{-j\frac{1}{2}\mu t^2} \int_{-\infty}^{\infty} [f(u) e^{-j\frac{1}{2}\mu u^2}] e^{j\frac{1}{2}\mu(t-u)^2} du \qquad (9.3)$$

So we see that premultiplication of an input signal $f(t)$ with a chirp waveform $\exp\{-j\mu u^2 / 2\}$ followed by convolution in a chirp filter (given by the integral and $\exp\{j\mu(t-u)^2 / 2\}$) and subsequent postmultiplication with another chirp waveform $\exp\{-j\mu t^2 / 2\}$ will yield the Fourier transform $F(\omega)$. It also has been shown that the inverse Fourier transform can be obtained with a similar configuration of chirp filters.

In the M(l)-C(s) arrangement, the postmultiplication does not yield the expected Fourier transform components, and this scheme can only be used for the power spectrum analysis of signals whose spectral components remain constant for the duration of the premultiplier chirp interval. It is the M(s)-C(l)-M arrangement of filters that is best suited for a Fourier transform processor.

In the all-SAW implementation of the M-C-M chirp transform (Figure 9.3) the chirp waveforms used for signal multiplication are assumed to be generated by impulsing physically realizable SAW chirp filters. The convolution filter is also assumed to be such a SAW chirp filter. The impulse response of the premultiplying chirp $c_1(t)$, the postmultiplying chirp $c_2(t)$, and the convolution filter $h_0(t)$ (Figure 9.3) are all of the form
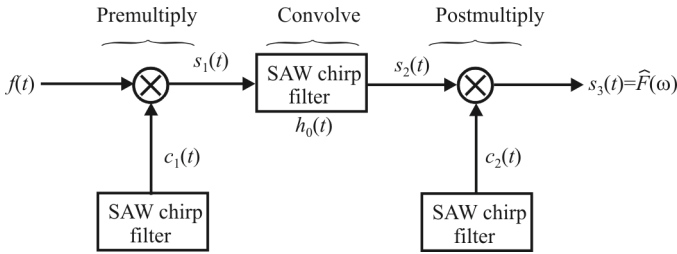
**Figure 9.3** M-C-M chirp transform processor arrangement.

$$c_i(t) = \Pi\left\{\frac{t-t_i}{T_i}\right\} w_i(t) \cos\left\{\omega_i t - \frac{1}{2}\mu t^2 + \phi_i\right\} \tag{9.4}$$

where $\Pi\{(t-t_i)/T_i\}$ denotes a rectangular gating function of duration $t_i$ centered on time $t = T_i$. The delay between the applied impulse and commencement of the response has been neglected. $w_i(t)$ is a weighting function and $\phi_i$ is a phase term that will be assigned the values of 0 or $\pi/2$ later. The factor $\mu$ is defined as the magnitude of the rate of change of instantaneous angular frequency and corresponds to the dispersive slope of the chirp filter.

### 9.3.1 The M(s)-C(l)-M Arrangement

The processor cycle takes its time origin from the impulse signal used to generate the premultiplying chirp waveform $c_1(t)$. The real input signal, $f(t)$, appears at the input to the SAW processor and, after premultiplication by $c_1(t)$ and passage through the filter $h_0(t)$ (Figure 9.3), the output is given by the convolution integral

$$s_2(t) = \int_{-\infty}^{\infty} f(u)\Pi\left\{\frac{u-\frac{1}{2}T_1}{T_1}\right\} c_1(u)\Pi\left\{\frac{t-u-\frac{1}{2}T_0}{T_0}\right\} h_0(t-u)du \tag{9.5}$$

Equation (9.5) can be written as

$$s_2(t) = \Pi\left\{\frac{t-t'}{T'}\right\} \text{Re}\left\{\hat{F}(\omega)e^{j(\omega_0 t + \frac{1}{2}\mu t^2 + \phi_0 + \phi_1)}\right\} \tag{9.6}$$

where

$$\hat{F}(\omega) = \hat{F}(\omega_0 - \omega_1 + \mu t)$$

is the Fourier transform of $\hat{f}(t)$, where

$$\hat{f}(t) = f(t)\Pi\left\{\frac{t - T_1/2}{T_1}\right\} \tag{9.7}$$

is the truncated form of $f(t)$.

Rewriting $\hat{F}(\omega)$ in terms of its modulus and argument

$$\hat{F}(\omega) = \left|\hat{F}(\omega)\right| \angle \Phi(\omega)$$

(9.6) becomes

$$s_2(t) = \Pi\left\{\frac{t - t'}{T'}\right\}\left|\hat{F}(\omega)\right| \cos\left[\omega_0 t + \frac{1}{2}\mu t^2 + \phi_0 + \phi_1 + \Phi(\omega)\right] \tag{9.8}$$

From (9.8) we see that the envelope of the signal $s_2(t)$, present at the output of the filter, yields the amplitude spectrum of the (truncated) signal $f(t)$ over the frequency range

$$\omega_0 - \omega_1 + \mu T_1 \le \omega \le \omega_0 - \omega_1 + \mu T_0 \tag{9.9}$$

Thus the output is centered at frequency

$$2\pi f_{c0} = \omega_0 - \omega_1 + \frac{1}{2}\mu(T_0 + T_1) \tag{9.10}$$

and, once squared, displays the power spectrum over a bandwidth

$$2\pi W = \mu(T_0 - T_1) \tag{9.11}$$

($W$ in Hertz).

We see that the phase information $\Phi(\omega)$ is also present in (9.8). This can be recovered by postmultiplication by $c_2(t)$ in the appropriate time interval as defined as

$$t' = (T_1 + T_0)/2 \qquad\qquad T' = T_0 - T_1 \tag{9.12}$$

Premultiply     Convolve     Postmultiply

$f(t)$
Real input

$g(t)$
Imaginary input

$s_1(t)$

SAW chirp filter
$h_0(t)$

$s_2(t)$

$f_0, W$   $\widehat{F}_R(\omega) - \widehat{G}_I(\omega)$
Real output

$f_0, W$   $\widehat{F}_R(\omega) + \widehat{G}_I(\omega)$
Imaginary output

$0 \quad \pi/2$
Quadrature hybrid
$c_1(t)$
SAW chirp filter

$0 \quad \pi/2$
Quadrature hybrid
$c_2(t)$
SAW chirp filter

Input: $x(t) = f(t) + jg(t)$
Output: $\widehat{X}(\omega) = \widehat{F}_R(\omega) - \widehat{G}_I(\omega)$
$+j[\widehat{F}_R(\omega) + \widehat{G}_I(\omega)]$
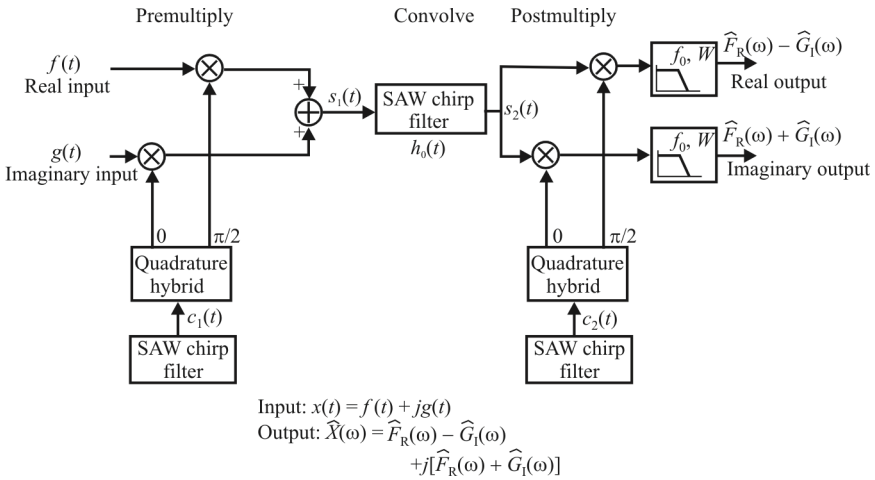
**Figure 9.4** SAW chirp transform topology for baseband operation.

to yield

$$s_3(t) = \Pi\left\{\frac{t-t'}{T'}\right\}\cos[(\omega_0 - \omega_1)t + \phi_0 + \phi_1 - \phi_2 + \Phi(\omega)] \tag{9.13}$$

where the sum term in $\omega_0 + \omega_2$ is removed by filtering and $w_2(t)$ is set to unity. Thus, in (9.13), the phase spectrum is a phase modulation on $s_3(t)$ and may be recovered by demodulation with a frequency $(\omega_0 - \omega_2)/2\pi$ with appropriate selection of phase terms $\phi_n$.

Figure 9.3 shows the M(s)-C(l)-M chirp transform arrangement when the input $f(t)$ is a complex modulation on a carrier of frequency $f_{c0}$ and the output transform is obtained on a carrier of $(\omega_0 - \omega_2)/2\pi$. When the input consists of baseband channels with separate real and imaginary components of a complex signal, the topology shown Figure 9.4 emerges as one possibility. Quadrature premultiplication by $c_1(t)$ is required, as is quadrature postmultiplication by $c_2(t)$ to achieve the required phase relationships in (9.13). Selection of $\omega_0 = \omega_2$ and lowpass filtering yields the transform outputs directly at baseband.

# 9.4 Dispersive Delay Lines

A DDL has the characteristic that the time delay of a signal through the device depends on the frequency of the signal at the input [Figure 9.5(a)] [7]. So if a signal at frequency $f_1$ is input to the DDL, it will arrive at the output $\tau_1$ seconds
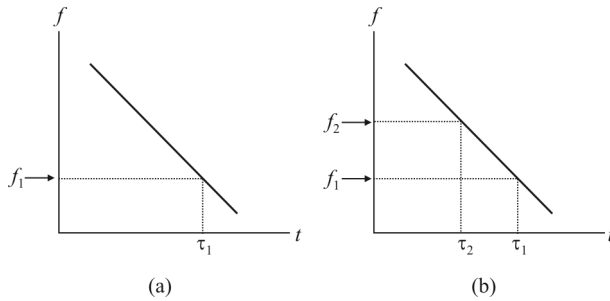
**Figure 9.5** DDL: (a) a single signal at the input, and (b) two signals at the input.

later. A DDL provides a delay to RF signals that either linearly increases or decreases with frequency. DDLs are commonly rated by the *TW* product, which represents the processing gain of the device. The bandwidth (*W*) is the operational bandwidth of the device and time (*T*) is the differential delay between the band edges, called the *dispersion*.

If the input to the DDL has a linearly changing frequency that goes from $f_1$ to $f_2$ [Figure 9.5(b)], then the signal input at the time $f_1$ is input reaches the output at $\tau_1$, while the signal at all the intermediate frequencies arrives at time delays between $\tau_2$ and $\tau_1$. Since the  DDL has a linear characteristic, all of these signal components arrive at the output at the same time. That time delay is determined by the slowest propagating component—the one at $f_1$. Thus there is a unique time delay, $\tau_1$, corresponding to the sweeping input that starts at $f_1$ and goes to $f_2$.

The process obviously works just as well if the slope of the DDL characteristic is opposite those shown in Figure 9.5 as long as the sweeping input signal sweeps in the opposite direction.

SAW technology has made the CxRx a practical IF processing tool for a range of applications. SAW delay line fabrication, utilizing direct-write electron beam technology, has made it possible to extend the frequency operating range of DDLs to 2GHz. Current DDL implementation, utilizing SAW technology, achieves bandwidth delay products of up to 10,000. As bandwidth increases, the achievable delay decreases. Figure 9.6 shows the possible bandwidths and dispersive delays currently possible. The long dispersive delays (>1 μsec) are constructed as SAW reflective array compressor DDLs, while short dispersive delays (<μsec), are realized as slanted arrays with interdigital transducers.
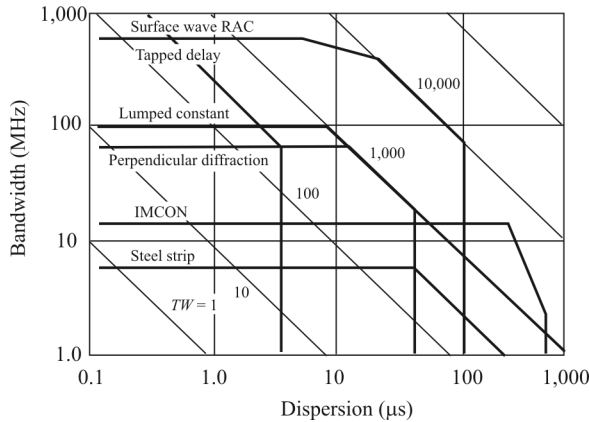
**Figure 9.6** SAW characteristics circa 2009.

There are several types of lines to choose from, including SAW technology. SAW DDLs are fabricated on a piezoelectric substrate such as quartz or lithium niobate. The input electrical signal is converted into an acoustic wave via an input transducer, processed in the SAW DDL, and then converted back into an electrical signal at the output. Because of the slow velocity of surface waves, SAW delay lines are orders of magnitude smaller than some other types of DDLs. *TW* products of 10,000 have been achieved. Depending on the configuration, SAW DDLs can operate from a few megahertz to a few gigahertz with from 15- to 50-dB insertion loss. In general, the wider the bandwidth, the greater will be the loss.

### 9.4.1 Limitations of Practical SAW Devices

The SAW Fourier transform processor configured in the M(s)-C(*l*)-M arrangement displays frequency components over a maximum bandwidth, as defined in (9.11)

$$2\pi W_{max} = \mu(T_0 - T_1)$$

**Table 9.2** Comparison of the Characteristics of Metalized IDT and Grooved RAC SAW Chirp Filters

| Parameter | IDT | RAC |
|---|---|---|
| Center Frequency (MHz) | 10–1500 | 60–2000 |
| Bandwidth (MHz) | 1–750 | 1–1000 |
| Time Dispersion (µs) | 0.1–80 | 0.5–120 |
| TW Product | 4–2000 | 10–50 k |
| Amplitude Ripple (dB p-p) | 0.1 | 0.5 |
| Phase Error (deg RMS) | 0.2 | 0.5 |
| Sidelobe Suppression (dB) | −50 | −45 |

and the maximum signal duration on which the processor can operate is $T_1$. Using the ratio $c = T_1/T_0$, the maximum processor time-bandwidth product is given by

$$2\pi W_{max} T_1 = \mu T_0^2 c(c-1) \tag{9.14}$$

which is a maximum for $c = 0.5$ corresponding to a maximum operating time bandwidth product of $W_1 T_1 = W_0 T_0 / 4$. Thus, it is obvious that for processors with large numbers of transform points, say 1024, large time-bandwidth product *reflector array compressor* (RAC) filters are essential. Table 9.2 lists typical characteristics of the IDT and RAC devices.

## 9.5 M-C CxRx Operation

The M-C (M-C-M without the final multiply) CxRx can be implemented in one of two basic configurations as shown in Figure 9.7, typically designated as M(l)-C(s) and M(s)-C(l), but here simplified to *long multiplier* (LM) and *long convolver* (LC), respectively. In the LC topology, the received signal is multiplied by a short linear frequency chirp and processed by a long DDL. In the LM architecture, the input signal is first multiplied by an LO scan that is twice the receiver's
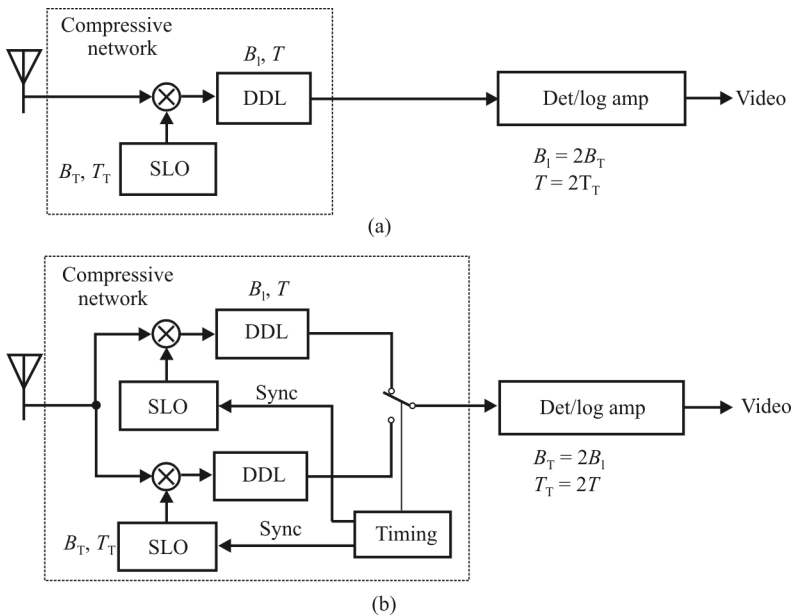


**Figure 9.7** M-C CxRx configurations: (a) M(s)-C(l) long convolver configuration, and (b) M(l)-C(s) long multiplier configuration. In (a) the POI is ~50% while it is ~100% in (b).

bandwidth. The result is processed by the DDL with the same bandwidth as the receiver's frequency coverage. We discuss the LM and LC configurations of M-C CxRx receivers in this section.

Consider the LC configuration shown in Figure 9.8(a). The RF input bandwidth is denoted by $W_R$, and this bandwidth is presented to the RF input for a time at least twice the frame time, $T_T$. The SLO has a bandwidth denoted by $W_T$, and it completes its negative-sloped sweep in $T_T$.

Multiplying signal $S_1$ and $S_2$ at frequencies $f_1$ and $f_2$, respectively (we assume here that $f_1 < f_2$), by the SLO signal causes the IF frequencies corresponding to $S_1$ to linearly increase as seen on the left in Figure 9.8(a). Applying these changing frequencies to the DDL that has a matched but opposite slope as the SLO, and whose characteristics are shown on the right in Figure 9.8(a), causes impulses to appear at the DDL output at time delays corresponding to the frequencies of the input signals. $S_2$, being at a higher frequency than $S_1$, has a shorter time delay within the DDL so it emerges first corresponding to the short delay. $S_1$ appears somewhat later, corresponding to a longer time delay within the DDL. The DDL compresses all the energy in $S_2$ so that its output at $T_2$ contains all the energy in $S_2$. Similarly for $S_1$. ($T_2$ and $T_1$ are measured from the beginning of the scan.) In this way, the signals are output of the DDL in a time sequence corresponding to the input frequencies, highest frequency first.

Now consider the LM topology shown in Figure 9.8(b). In this case there is only one sweep of the LO in $T_T$ seconds. $S_1$ and $S_2$ get multiplied as before and then input to the DDL, but only a portion of their sweep range is processed by the DDL over time $T$ and bandwidth $W_1$. The DDL delays the frequency components as for the LC configuration so that the output of the DDL is a time-separated sequence of pulses corresponding to the input signals.

Consider now the case where the duration $T_1$ of the chirp premultiplier $c_1(t)$ is greater than the duration $T_0$ of the impulse response of the convolution filter $h_0(t)$. This is the LM configuration. We show that this is not a wholly satisfactory arrangement for Fourier transform processors.

The M(l)-C(s) configuration does not produce a true replica of the FT of the input signal. Consider (9.5), which describes the output, $s_2(t)$, from the chirp filter, for which the condition $T_1 > T_0$ and we have

$$s_2(t) = \Pi\left\{\frac{t-t''}{T''}\right\} \int_{-\infty}^{\infty} f(u)\Pi\left\{\frac{u-t-\frac{1}{2}T_0}{T''}\right\} c_1(u)h_0(t-u)du \qquad (9.15)$$

where

$$t'' = \frac{1}{2}(T_0 + T_1) \qquad\qquad T'' = T_1 - T_0 \qquad (9.16)$$
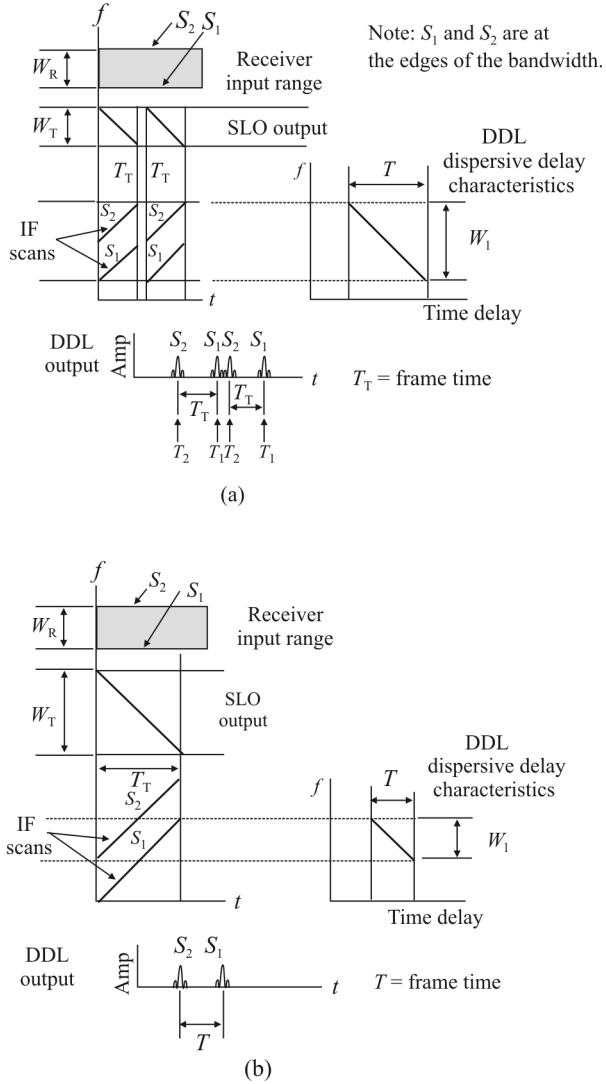
**Figure 9.8** M-C CxRx signal relationships: (a) M(s)-C(l), long convolver, and (b) M(l)-C(s), long multiplier.

Here when $w_1(t)$ and $w_0(t)$ are set to unity, the Fourier transform of the function

$$f(u)\Pi\left\{\frac{t-u-\dfrac{1}{2}T_0}{T_0}\right\}$$

can be determined, as previously shown. We can see here that the gating function on $f(t)$ is itself a function of time. As a consequence the FT computation is not using a fixed gate function, $\hat{f}(t)$, as defined in (9.7), but the gating function is sliding across $f(t)$, covering different sections of this function while at the same time performing Fourier transformations.

The effect of this sliding gating function produces distortions in the output transform when the input signal is limited in duration. These distortions can be determined and we conclude that the sliding M(l)-C(s) transform arrangement has application only in the power spectrum analysis of stationary signals for which the spectral components are invariant over the time duration of the (long) premultiplier. Although the M(l)-C(s) arrangement cannot be used directly for general Fourier transform processor realizations, the distortion present in this arrangement can be overcome. One method is to pregate (time filter) the input $f(t)$ such that the truncated input signal duration is less than $T_0$. This is simply the M(s)-C(l)-M scheme but here, by repetitively reading delayed versions of the input waveform, the full bandwidth of the M(l)-C(s)-M arrangement can be utilized. Another approach is to filter the input signal $f(t)$ in a SAW chirp filter, thereby realizing the C-M-C chirp transform arrangement.

### 9.5.1 Swept Local Oscillator

The CxRx operation and performance depend on the design and performance of the SLO. The SLO waveform can be generated by generating the waveform using direct digital synthesis, by sweeping a VCO, or by exciting a DDL matched to a compression DDL with an impulse. These three basic techniques are shown in Figure 9.9. The choice depends on the sweep speeds, frequency range, and linearity required. The selected SLO technique and the performance limits of associated components determine the overall performance of the CxRx, much as the performance of the LO in narrowband receivers to a large extent dictate their performance.

The classic method of generating the chirped signal (SLO) is by impulsing a DDL that has a *TW* product directly related to that of the convolving DDL. The DDL spreads the spectrum of the impulse in time, producing a linear frequency
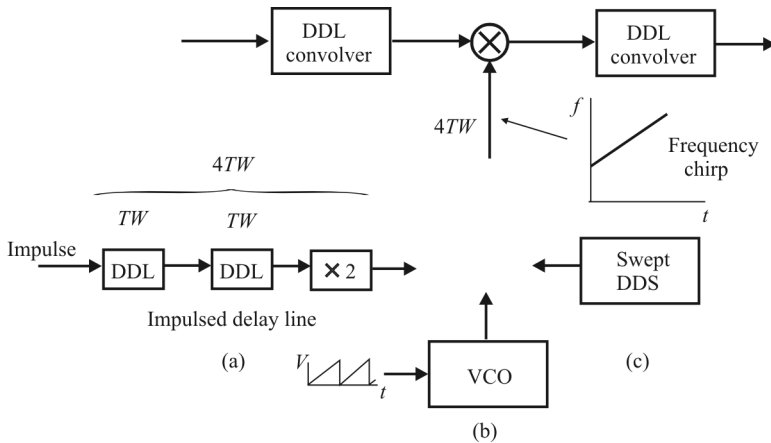
**Figure 9.9** C-M-C Fourier transformer: (a) impulse delay line, (b) VCO with ramp control voltage, and (c) swept DDS. In all cases a frequency chirp with a $4TW$ characteristic ensues.

sweep as a function of time. For the C-M-C configuration, the $TW$ product of the frequency chirped SLO signal must be four times that of the convolver and the magnitude of the frequency versus time slopes must be identical.

The impulse LO uses two DDLs in series followed by a frequency doubler to produce a constant amplitude frequency chirped LO signals with a $4TW = 2T2W$ characteristic. For very fast (>200 MHz/μs) applications, as in radar, the impulse DDL technique is the only practical means of generating chirps. The chirps, however, have fairly high noise due to DDL losses and will not perfectly match the slope of the convolver. This limits receiver dynamic range to 40 to 50 dB and decreases frequency resolution.

The VCO implementation driven by a linearly changing ramp voltage is a straightforward method of generating a SLO and is identical to such an arrangement for the scanning superheterodyne discussed in Chapter 5. The major problem here is matching the ramp characteristics of the sweep waveform driving the VCO with the ramp characteristics of the DDL, a problem not shared with the superheterodyne receiver.

The swept DDS is an active chirp generation technique. It provides very linear long or short duration sweeps over moderate bandwidths (to 250 MHz). Sweep rates up to 200 MHz/μs are possible. Noise outputs are low and the sweep slope can be finely adjusted for a near perfect match to the DDL convolver. Although the output is discretely stepped, steps can be sufficiently fine to allow good resolution in the receiver. Wideband applications (>100 MHz) require the use of GaAs logic and GaAs DACs. The main advantages of the swept DDS chirp generator are small size, low recurring cost, high sweep rate capability, reproducibility, and independence from environmental factors.
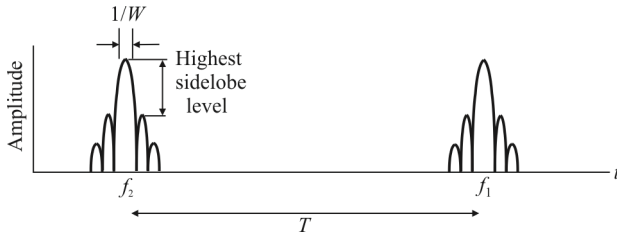
**Figure 9.10** CxRx time response. (Source: [8], © Artech House, 2002. Reprinted with permission.)

## 9.5.2 Frequency Resolution

Frequency resolution $(\Delta f_0)$ establishes the limits on the ability to resolve multiple simultaneous signals with different carrier frequencies. For a CxRx it is usually equated to the reciprocal of the compression time. The sampling that the CxRx performs in the time domain causes sidelobes to be produced in the frequency domain. This is seen in Figure 9.10. The cause of this sidelobe generation is illustrated in Figure 9.11. Multiplication in the time domain causes convolution in the frequency domain. The Fourier transform of the time gate is a sinc $x$ form as seen in Figure 9.11(b). Convolving sinc $x$ with the two impulses, which are the Fourier transform of the cosine wave, generates sinc $x$ transforms centered at $\pm f_0$.

When two of the sinc $x$ transforms are too close together, then smearing in the frequency domain can occur. Thus two such responses can be separated according to the frequency resolution. This is illustrated in Figure 9.12. This definition of resolution is when one response is 3 dB down from that of the adjacent response.
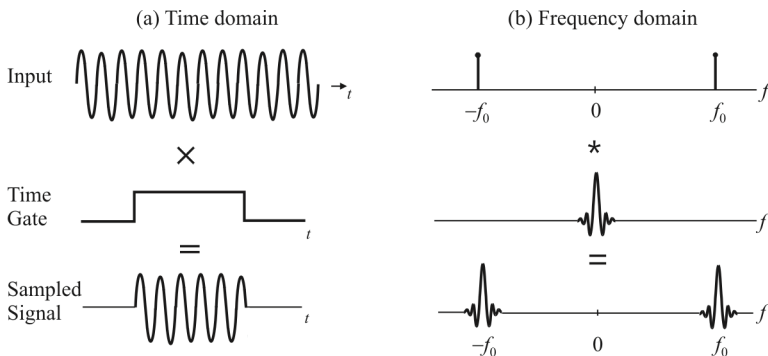


**Figure 9.11** CxRx sidelobes. (Source: [8], © Artech House, 2002. Reprinted with permission.)
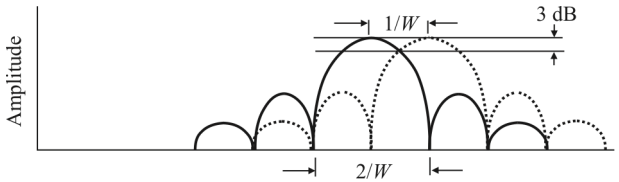
**Figure 9.12** CxRx frequency resolution. (Source: [8], © Artech House, 2002. Reprinted with permission.)

The tradeoff between frequency coverage and compression time is governed by the bandwidth and dispersive delay limitations of DDLs as illustrated in Figure 9.9. The limits shown are approximate, since frequency resolution depends on device characteristics. It also is assumed that the difference in signal strength of two adjacent signals is less than 30dB. For greater than 30dB, the resolution degrades by 20 to 30%. A different view of frequency resolution is shown in Figure 9.13, where the minimum frequency separation is plotted versus bandwidth when the signals have equal amplitudes. Theoretically, the resolving capability is not a function of bandwidth but is a constant depending only on the scan time. For real devices this is only an approximation as shown. This shows that for a wideband CxRx, the ability to resolve two adjacent signals is affected by component limitations. As the bandwidth increases, the compressed pulse width decreases. For receiver bandwidths above 100 MHz, the compressed output-pulse
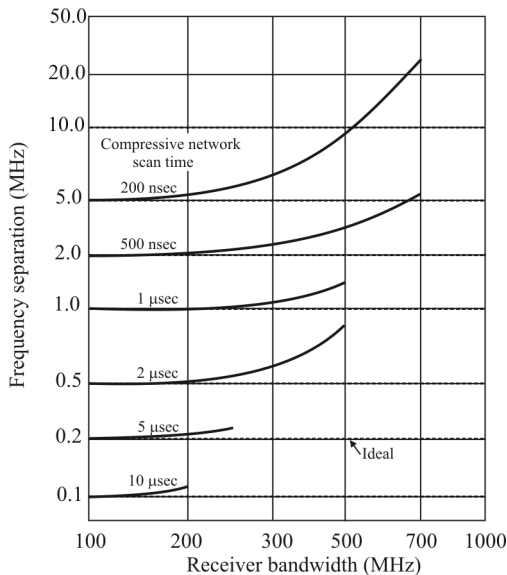


**Figure 9.13** Minimum frequency separation between two signals with equal amplitude.
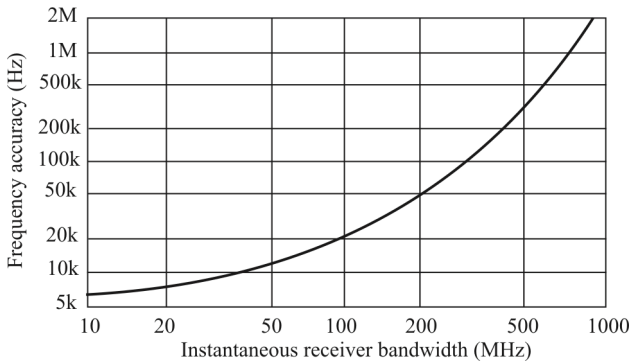
**Figure 9.14** CxRx frequency accuracy.

envelope is not reproduced faithfully by the detection circuit. The detection circuit's rise and fall time will increase the resulting video output pulse width and, thereby, decrease the frequency resolution capability of the receiver.

### 9.5.3 Frequency Accuracy

The CxRx measures the frequency of a carrier by measuring the time between the frame start and the compressive network output pulse. The frequency accuracy of each input signal depends on the instantaneous frequency range of the receiver, the compression rate, the frame time, the clock rate, and the number of bits in the frequency measuring circuit. Figure 9.14 shows a curve of typical frequency accuracy versus instantaneous bandwidth.

The accuracy of the frequency estimate determines, inter alia, the bandwidth requirements for the monitor receivers. The signal must appear within the bandwidth of these receivers when they are tuned according to the CxRx output.

### 9.5.4 Sensitivity and Compression Time

In the CxRx, signal power is integrated during each compression period of the receiver. This provides sensitivity improvement over other types of receivers and, in particular, the SHR receiver. The receiver sensitivity is directly proportional to the compression time, as long as the input signal is present throughout the entire compression period. If the input signal is only partially present during a compression period, the RF output power, and therefore the sensitivity, becomes a function of the input signal duration. This occurs when the duration of the RF input is less than twice the compression period. For this condition we cannot accurately establish system sensitivity. Because an input signal will appear asynchronous with respect to the compression rate, the sensitivity prediction can only be made statistically.
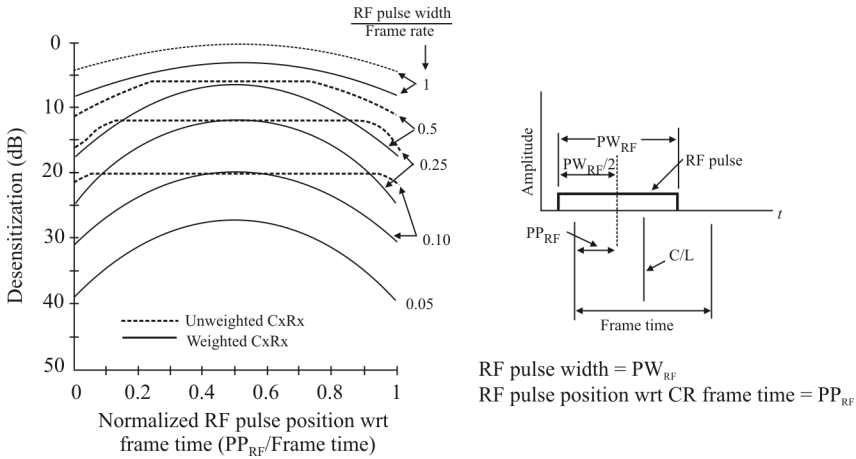
**Figure 9.15** CxRx desensitization.

The optimum compression time depends on the application. For simultaneous interception of long and short RF signals, a compromise must be made. The compression time should be less than half the length of the shortest expected signal length and have adequate compression gain to provide the desired sensitivity for RF pulses or CW. In some applications these two conditions cannot be simultaneously satisfied. The curves shown in Figure 9.15 are based on an LM design with the scan time of the SLO equal to twice the dispersive delay of the DDL. An alternate approach is to utilize two compressive channels, one optimized for signals with long durations, or CW, and one for short signals.

The choice of the scan time will depend on sensitivity required for long pulses and the shortest expected pulse. The tradeoff is based on

$$\text{Sensitivity} = 10\log_{10}(k_\text{B} T \times 10^6) + 10\log_{10} W_\text{in} - 10\log_{10}(W\tau) \qquad (9.17)$$

where

$W_\text{in}$ is the input bandwidth in MHz

$W$ is the spectral width of the compressed pulse

$\tau$ is the temporal width of IF input to DDL

We can see that the sensitivity is proportional to $W$ and $\tau$, which, in turn, are a function of the duration of the applied signal and when it arrived with respect to the start of the scan. Signals arrive randomly and, therefore, will be asynchronous with the scanning periods. This causes the sampled energy to be split between two
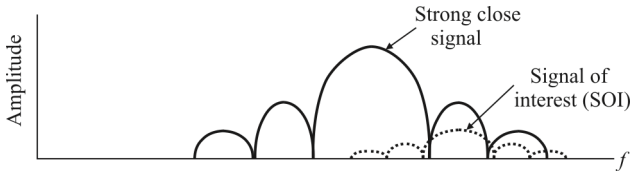
**Figure 9.16** CxRx masking. (Source: [8], © Artech House, 2002. Reprinted with permission.)

scans for short pulses, thus resulting in degraded sensitivity. The effect on sensitivity of this latter phenomenon is shown in Figure 9.15. As we see, sensitivity to short signals is considerably worse if bandpass weighting is used.

### 9.5.5 Simultaneous Signal Detection

One of the most significant features of the CxRx is its ability to detect and process simultaneous signals. The number of signals $N_S$ that can be encoded during each frame period is a function of the practical frequency resolution $(\Delta f_0)$ of the receiver, $N_S = W_R / \Delta f_0$. The output can be selectively blocked to reduce the output data rate. Blanking may be implemented by frequency, *angle of arrival* (AoA), amplitude, or some other parameter.

### 9.5.6 CxRx Response

9.5.6.1 SOI Masking

The sidelobes of the CxRx response can cause masking of a possible SOI. This is illustrated in Figure 9.16. Often, the SOIs of EW receivers are farther away than friendly, close networks. The closer networks generate more powerful signals at the receiver as shown. This necessitates the application of weighting in the CxRx response.

9.5.6.2 DDL Response Weighting

The impulse response of the DDL is typically weighted to reduce energy that otherwise spills into the nearby channels in the CxRx. This effect is illustrated in Figures 9.16 and 9.17. This windowing has two effects on the DDL response: first the width of the impulse response widens. That is, the bandwidth increases. Second, sidelobes are decreased. These two affects can be seen in Figure 9.17. The rectangular (brick-wall) filter response is shown as the solid line. We see relatively high sidelobes in the near adjacent channels. In fact, significant energy slips out a considerable distance. The Hanning window response is shown as a dotted line and we can see that the lobe width has widened relative to the rectangular response
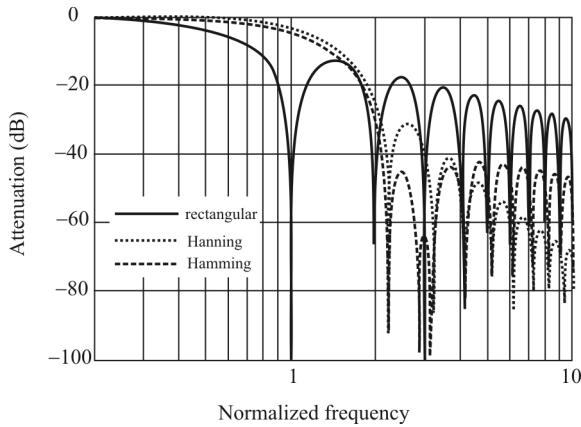
**Figure 9.17** Window functions. The responses are truncated at a normalized frequency of 10, but of course they continue on to infinity.

and the sidelobe levels are reduced. The same can be said for the Hamming window response shown as the broken line.

The characteristics of the normal window functions that are typically used to weight the impulse response are indicated in Table 9.3. Harris [9] contains a much more extensive list and their characteristics. The last two windows in Table 9.3 are not common, but do achieve the highly desirable sidelobe level of –60dB or more. These window functions are derived from the autocorrelation function of the Hamming window and is a two-parameter $(p, \gamma)$ set of functions given by [10]

**Table 9.3** Window Functions

| Window | Peak Sidelobe (dB) | Relative Bandwidth | Sidelobe Roll-Off (dB/octave) |
|--------|--------------------|--------------------|-------------------------------|
| Rectangular | −13 | 1.0 | 6 |
| Bartlett | −25 | 1.43 | 12 |
| Hanning | −31 | 1.65 | 18 |
| Taylor | −40 | 1.41 | 6 |
| Hamming | −43 | 1.50 | 6 |
| Blackman | −57 | 3.0 | 18 |
| AH (.7, 2.6) | −64 | 1.88 | 9 |
| AH (1, 2.6) | −86 | 2.12 | 12 |
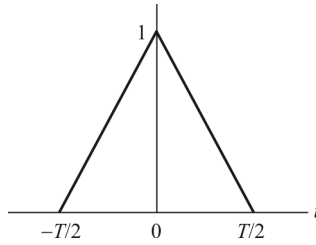
**Figure 9.18** Triangle function.

$$
\text{AH}(t) = \left\{ \frac{tr(t)\left[1 + \dfrac{1}{2}\left(\dfrac{\gamma^2 - 1}{\gamma^2}\right)^2 \cos\left(\dfrac{4\pi t}{T}\right)\right] + \dfrac{\gamma^2 - 1}{\pi\gamma^2}\left(1 - \dfrac{\gamma^2 - 1}{4\gamma^2}\right)\sin\left(\dfrac{4\pi |t|}{T}\right)}{1 + \dfrac{1}{2}\left(\dfrac{\gamma^2 - 1}{\gamma^2}\right)^2} \right\}^p
\tag{9.18}
$$

$tr(t)$ is the triangle function shown in Figure 9.18, for $-T/2 \leq t \leq T/2$. Equation (9.18) is shown in Figure 9.19 for $\gamma = 2.6$ and $p = 1.0$. The normalized Fourier transform of AH($t$) is the waveform of interest and is given by (for $p = 1.0$)

$$
\mathcal{F}\{\text{AH}(t)\} = \left[\frac{\sin(\pi f T / 2)}{\pi f} \frac{\dfrac{2}{T\gamma^2}\left(f - \dfrac{2\gamma}{T}\right)\left(f + \dfrac{2\gamma}{T}\right)}{(f - 2/T)(f + 2/T)}\right]^2
\tag{9.19}
$$
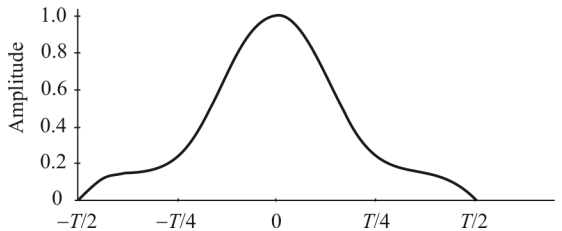


**Figure 9.19** AH(1, 2.6) time window.
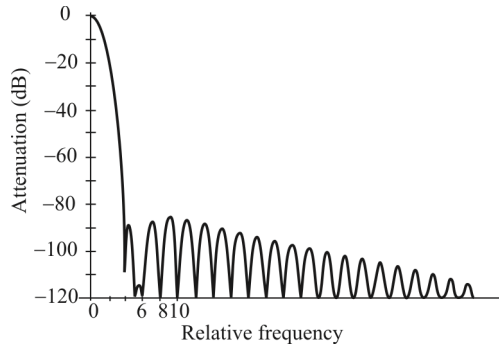
**Figure 9.20** Spectrum of AH(1, 2.6).

and is shown in Figure 9.20. Note the −85 dB sidelobes. Both the bandwidth and sidelobe levels change with $\gamma$ and $p$. This behavior is shown in Figures 9.21 and 9.22 for $\gamma$ variations and in Table 9.4 for several values of $p$ with $\gamma$ fixed at 2.9.

### 9.5.6.3 Spurious Outputs

The most serious problem with the M(s)-C(l) configuration is that it has spurious outputs caused by out-of-band signals [11]. This is illustrated in Figure 9.23. For example, a signal 50 MHz outside the receiver frequency range would appear as an in-band signal 50 MHz within the selected receiver bandwidth. The out-of-band signal would be considerably rejected by placing a bandpass filter before the compressive network. But this rejection at 50 MHz from the band would be 40dB, at best, with typical filter designs. The loss of compressive network conversion gain is only 1dB. As a result this signal (50 MHz from the band edge) would be attenuated by only 1dB. At the input level of −30dBm, there would be an in-band spurious output of −71 dBm. On the other hand, the two-channel M(l)-C(s) configuration achieves a rejection greater than 60dB by selecting the output alternately from the two channels.

### 9.5.6.4 Triple-Transient Response

The other dynamic-range limitation of the M(s)-C(l) configuration is demonstrated in Figure 9.24. Any SAW DDL will have a triple-transit response. Typical DDLs have a desired signal loss of 30dB. The compressive gain is 27dB. The desired-signal ouput, therefore, will be 3dB down from the input level. The resulting difference beween SOI output and triple-transit output is only 47dB. As seen in Figure 9.24, the triple transit output in the M(s)-C(l) configuration appears four scans after the SOI was seen. There is no additional rejection possible in the
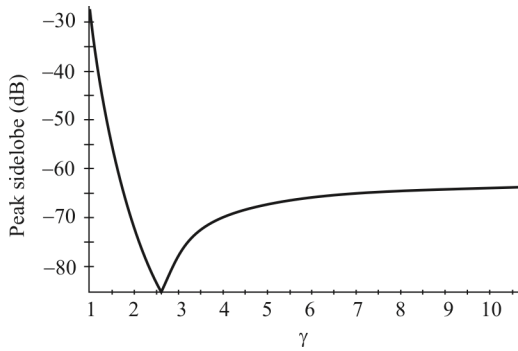
**Figure 9.21** Peak sidelobes of AH($p$, $\gamma$). $p = 1$.
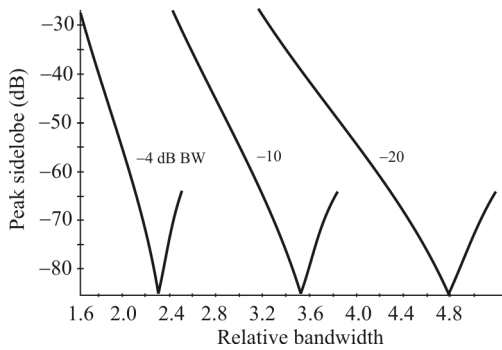


**Figure 9.22** Peak sidelobes versus relative bandwidth. BW parameters indicate where the width of the bandwidth occurs.

**Table 9.4** Bandwidth and Sidelobe Levels ($\gamma = 2.6$)

| $p$ | Relative Bandwidth | Peak Sidelobe (dB) |
|------|--------------------|--------------------|
| 1.0  | 2.12               | −85                |
| 0.7  | 1.88               | −64                |
| 0.5  | 1.62               | −43                |
| 0.25 | 1.37               | −25                |

Frequency

Out-of-band
signal

IF
input
range

SLO
sweep
range

① ② ③

DDL
characteristics

Frequency

Time

Due to
out-of-band
signal

DDL
passband

① ② ③

Due to
in-band
signals

Spurious signal due
to out-of-band signal

Output
amplitude

Any out-of-band
signal producing an IF
sweep within shaded
region will show up
as spurious output signals.

① ② ③

Scan periods

Loss of compression gain $=$  1  dB
Bandpass filter rejection $= 40$ dB
                                                     $= 41$ dB

This out-of-band signal would appear as a spurious signal only 41 dB
down from an in-band signal at the same input level.

**Figure 9.23** Spurious signals.

configuration, since the detectors monitor the outputs of the DDL 100% of the
time.

In the M(l)-C(s) configuration, the output detector is switched to the alternate
channel when the triple transit occurs. The rejection, therefore, is a function of the
switch isolation and is typically greater than 110dB. This is demonstrated in
Figure 9.24. The output of channel A is monitored by the detector only during
scans 1, 3, 5, 7, etc., but the triple transit occurs during scans 4, 6, 8, etc. The
M(l)-C(s) configuraition is the only technique that eliminates triple-transit outputs
so as not to degrade the CxRx dynamic range.

## 9.5.6.5 LM and LC Comparison

The LM has the potential for wider receiver bandwidth, since the LC compressive
network has a DDL covering twice the receiver bandwidth. Bandwidth constraints
in the LM topology are primarily in the SLO, which does not necessarily have its
sweep range determined by a single DDL (Figure 9.9).
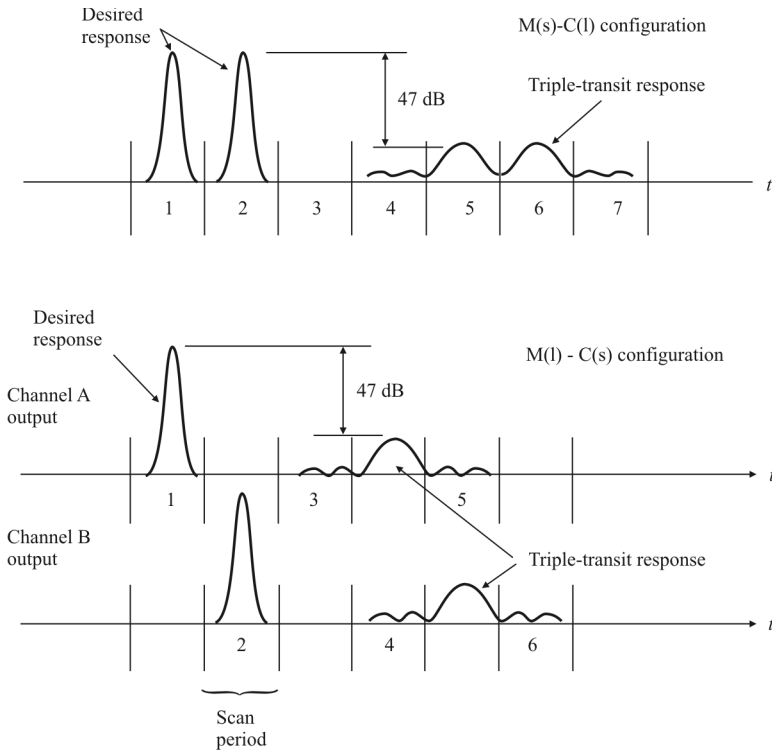
**Figure 9.24** Triple-transit response.

The LC is smaller and less complex because it requires fewer components. Only a single DDL in the compressive network is needed. This is particularly attractive for high compression gain receivers with long integration time and, therefore, long dispersive delay where the DDL is inherently large ($t > 20$ μsec). Matching DDL is problematic, especially maintaining that matching over time and temperature, which also makes the LC approach appealing.

Without two compressive channels operating in parallel and used alternately as shown in Figure 9.7(b), the LM has only a 50% duty cycle and, therefore, less than a 50% POI for RF signals, which is less than the compression time of the receiver. With the addition of a parallel channel, the POI is similar to the LC, nearly 100%.

The LC configuration could experience spurious outputs due to out-of-band signals if designed as shown in Figure 9.7(a). This may be reduced by implementing a complete chirp-z transform, M(s)-C(l)-M(s), by multiplying the DDL output with a replica of the first multiplying chirp. The LM inherently places

out-of-band signals outside the frame time. Again, implementing the postmultiply chirp filter to match that of the input can be problematical.

As we discussed, the triple-transient response of SAW DDLs can generate spurious signal outputs that can degrade the dynamic range. The level of these spurious signals is a function of the DDL characteristics. A good approximation for SAW DDLs for the ratio of spurious signal level relative to the desired output is the DDL insertion loss ($L_{DDL}$) plus 17dB. For example, a DDL with $W_1 = 10$ MHz and $T = 50$ μsec will have a typical $L_{DDL}$ of 45dB. The expected spurious signals level relative to the desired output is therefore 62dB. On the other hand a wideband DDL with $W_1 = 500$ MHz and $T = 0.5$ μsec will have a typical $L_{DDL}$ of 30dB and produce a spurious signal level of 47dB. Since the dynamic range requirements of EW receivers is a minimum of 50- to 60-dB, the spurious signals need to be reduced in the latter example. The dual channel LM design with a correct choice of offset delay in the DDL will reduce the triple-transit signal responses and allow the receiver to have a wider multiple signal dynamic range than the LC approach.

# 9.6 The C-M-C Chirp Transform Arrangement

The operational equations for the C-M-C scheme can be derived from those of the M-C-M arrangement by interchanging the operations of multiplication and convolution. Thus the (time-gated) input signal is first convolved in a chirp filter, then multiplied by a (long) chirp of equal but opposite dispersive slope, and finally convolved in another chirp filter. The dualized nature of convolutions and multiplication in the time domain and frequency domain makes it possible to analyze the operation of the C-M-C arrangement using the theory presented earlier (Figure 9.25). Reference [4] explains this dualism.

In hardware terms, the C-M-C arrangement offers one distinct advantage over the equivalent M(s)-C(l)-M arrangement. With the C-M-C arrangement, the largest time bandwidth product chirp waveform is used only as a multiplying signal and, as a consequence, techniques such as frequency doubling and double chirp expansion may be used to achieve the required waveform parameters from SAW chirp filters of modest *TW* product. Thus, in terms of ultimate processor frequency resolution and bandwidth, the C-M-C configuration is the optimum choice. Further, for a given set of processor parameters, the convolution filters required in the C-M-C arrangement are of lower TW product and hence of lower insertion loss, which leads to superior SNR and dynamic range in the processor.

The biggest disadvantage of the C-M-C arrangement is that three SAW devices are always required even for power spectrum analysis, in comparison to the two devices required in the M-C-M arrangement. Since matching and maintaining that match over the life of the SAW devices is difficult, the advantage of using only two of them is significant.

M-C-M

$(W_0:T_0)$

(Figure: M-C-M block diagram)

$(W_S:T_S)$ → ⊗ → SAW chirp filter $h_0(t)$ → ⊗ →

$c_1(t)$

SAW chirp filter $(W_1:T_1)$

$c_2(t)$

SAW chirp filter $(W_2:T_2)$
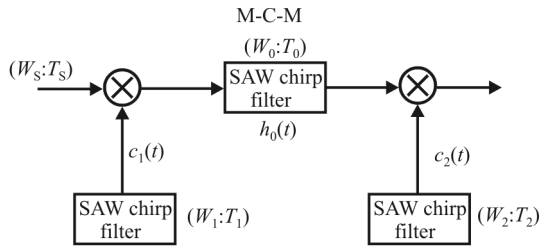
Maximum signal duration: $T_1$
Maximum signal bandwidth: $W_2 = W_0 - W_1$
For $W_2 > W_0 - W_1$: truncation of transform output
For $T_S > T_1$: truncation of input signal

C-M-C

$(W_1:T_1)$ SAW chirp filter $c_1(t)$ → ⊗ → $(W_2:T_2)$ SAW chirp filter $c_2(t)$ →

$h_1(t)$

SAW chirp filter $(W_0:T_0)$
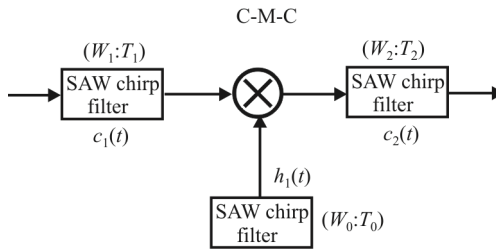
Maximum signal bandwidth: $W_1$
Maximum duration: $T_2 = T_0 - T_1$
For $T_S > T_0 - T_1$: truncation of input signal
For $W_S > W_1$: truncation of output transform

**Figure 9.25** Dualism.

# 9.7 Concluding Remarks

The compressive receiver is a useful device for wideband EW applications. Its fast scanning capability is virtually unmatched for many uses. Its primary shortcoming, which incidentally is shared by most wideband receivers, is its high first sidelobe response. Relatively weak signals of interest can be masked by stronger, closer, signals. It recovers from this masking rapidly, however. The sidelobes can be reduced by weighting at the expense of broadening of the width of the main lobe response in some cases.

For some applications, a true Fourier transform may not be required. The final chirp multiplication does not change the amplitude characteristics of the signal that emerges from the DDL, but it can be used to create a baseband waveform that is easily weighted with a lowpass filter for sidelobe reduction. The relative phase

between channels in multichannel receivers is maintained without the final multiplication as well, which is useful in some applications such as direction finding. If absolute phase in a channel is important, then the final multiplication is required.

# References

[1]     Snelling, W. E., and E. Geraniotis, "Analysis of Compressive Receivers for the Optimal Interception of Frequency-Hopped Waveforms," *IEEE Transactions on Communications*, Vol. 42, No. 1, January 1994, pp. 127–139.

[2]     Li, K. H., and L. D. Milstein, "On the Use of a Compressive Receiver for Signal Detection," *IEEE Transactions on Communications*, Vol. 39, No. 4, April 1991, pp. 557–569.

[3]     Breuer, K. D., J. S. Levy, and H. C. Paczkowski, "The Compressive Receiver: A Versatile Tool for EW Systems," *Microwave Journal,* October 1989, pp. 81–99.

[4]     Jack, M. A., P. M. Grant, and J. H. Colling, "Theory, Design, and Applications of Surface Acoustic Wave Fourier-Transform Processors," *Proceedings of the IEEE*, Vol. 68, No. 4, April 1980, pp. 450–469.

[5]     Daniels, W. D., M. Churchman, R. Kyle, and W. Skudera, "Compressive Receiver Technology," *Microwave Journal*, April 1986, pp. 175–185.

[6]     Snelling, W. E., and E. A. Geraniotis, "The Optimal Interception of Frequency-Hopped Waveforms via a Compressive Receiver," *Proceedings MILCOM 1990*, pp. 817–824.

[7]     Luther, R. A., and W. J. Tanis, "Advanced Compressive Receiver Techniques," *Journal of Electronic Defense*, July 1990, pp. 59–69.

[8]     Poisel, R. A., *Introduction to Communications Electronic Warfare Systems*, Norwood, MA: Artech House, 2002.

[9]     Harris, F. J., "On the Use of Windows for Harmonic Analysis with the Discrete Fourier Transform," *Proceedings of the IEEE*, Vol. 66, No. 1, January 1978, pp. 51–83.

[10]    Ready, P. J., "Adaptive Compressive Receiver Study," Pacific-Sierra Research Corporation, Final Technical Report RADC-TR-80-159, July 1980.

[11]    Breuer, K. D., J. J. Whelehan, and K. Russ, "Compressive Receivers Applied to ESM System Design," *Microwave System News*, October 1986, pp. 66–75.

# Chapter 10

## Digital Receivers Overview

## 10.1 Introduction

The increasing processing speed of ADC technology as well as the speed and flexibility of DSPs and corresponding digital signal processing has produced the architectures for digital EW receivers. There are many desirable features that ensue with digital processing of analog radio signals as we discuss in this and the next two chapters. The definition of a digital or software receiver is general and encompasses numerous architectures with various types of analog RF stages.

Technology has advanced to the point where (almost) all-digital radio receivers are possible. A digital receiver processes RF signals (analog or digital) in the digital domain. The signals are converted into digital form as early in the receive path as possible and all subsequent processing is done digitally [1].

In the modern parlance of signal processing, digital signal processing fits within the general framework of sampled-data signal processing, or discrete time signal processing [2]. In this category, time is divided into discrete steps and calculations are performed on signals at discrete time intervals while the signal amplitudes are sampled but analog. The amplitude samples correspond to the signal amplitude at the time of sampling. It is a further, and independent, step to include discrete-ized signal amplitudes, although when discussing digital signal processing in modern parlance, that is what is intended. That is our framework here—we will only include in our discussions cases when both time and amplitude are represented by discrete levels. It is important to remember, however, that sampled-data signal processing is a discussion topic all to its own.

Digital circuitry is more producible, reliable, and accurate than the analog counterparts. The latter tends to change its operating characteristics with time and temperature, while digital implementations do not. In addition, as technology advances, digital circuitry becomes very low cost. Also, digital logic can be programmable—the receiver can be reconfigured with software. No hardware changes are required.

One of the most attractive features of a digital receiver is its ability to perform signal processing that is difficult or impossible to do with conventional analog circuitry. As an example, digital circuitry can synthesize filters that have linear phase, extremely steep symmetrical skirts, and identical passbands.

The ideal receiver would be entirely digital. The ADC would be connected to the output of the antenna. In practice, this architecture would not work acceptably. At a minimum, an analog preselection filter is required at the input to the ADC; otherwise, interference results. Nevertheless, getting the ADC as close to the antenna as possible is the goal of modern digital receivers.

This chapter presents some of the aspects of digital receivers for use in EW systems. It is organized as follows. We begin with an introduction to digital receiver architectures. That is followed by a discussion on the technology drivers associated with digital receivers and then an introduction of digital RF/IF processing. Special aspects of digital receivers for EW applications are then considered. ADCs are introduced next followed by a discussion on gain and phase imbalances in receivers. The last topic covered in this chapter is aspects of *I*/*Q* sampling.

# 10.2 Digital Receiver Architectures

Digital receivers perform the functions of signal reception with much of the required processing accomplished in the digital domain. Digital architectures allow for considerably more flexibility both in receiver design and operation. They also are substantially more stable in operation over time due to the lack of component characteristic drift with time and temperature.

There are three fundamental architectures that are normally addressed when discussing digital receivers. These are narrowband implementations and digital RF/IF structures. The topologies of the latter include direct RF sampling, RF subsampling, IF sampling, and IF subsampling. The RF architecture converts the received signal as far forward in the receiver chain as possible (ideally at the antenna). A block diagram for the baseband implementation is shown in Figure 10.1. The block diagram of an RF sampling or subsampling receiver is shown in Figure 10.2, and the block diagram of an IF sampling or subsampling receiver is shown in Figure 10.3.

## 10.2.1 Narrowband Digital Receiver

The receiver in Figure 10.1 is an architecture for a narrowband implementation of a digital receiver and is simply the digital version of the analog superheterodyne architecture discussed in Chapter 5. This particular example converts IF
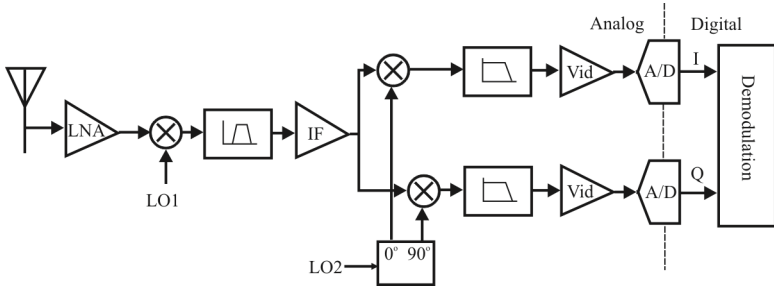
**Figure 10.1** Baseband digital receiver architecture.
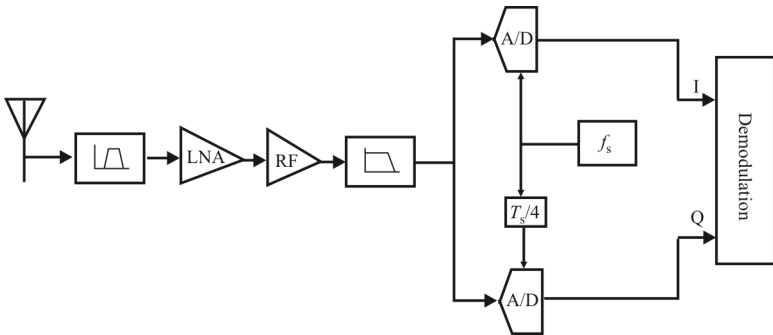


**Figure 10.2** RF digital sampling or subsampling receiver architecture.

frequencies twice, first with LO1 and then with LO2. Multiple conversion architectures are popular because multiple spurious signals can be avoided by proper selection of the IF frequencies. Detection of narrowband AM signals, for example, can be accomplished with this architecture using

$$\text{Envelope } s(t) = AM = \sqrt{\text{Re}^2[s(t)] + \text{Im}^2[s(t)]} \qquad (10.1)$$

while detection of FM uses

$$\text{Instantaneous frequency } s(t) = FM = \frac{d}{dt}\tan^{-1}\frac{Q(t)}{I(t)} \qquad (10.2)$$

and

$$\text{Phase } s(t) = \tan^{-1}\frac{Q(t)}{I(t)} \qquad (10.3)$$

## 10.2.2 Digital RF Architecture

A simplified flow diagram of a receiver with an RF topology is shown in Figure 10.2. Usually preselector filters are placed before the LNA as shown. The LNA brings all the attributes discussed in Chapter 3, principally establishing the noise floor (sensitivity) of the receiver. That may (or may not) be followed by additional RF amplification since ADCs sometimes require larger signals than are normally provided by an LNA. That signal is then sent to $I$ and $Q$ channels where it is converted into quadrature components by ADCs sampled with two clocks whose sample times are separated by $T_s/4$ seconds. After that, further processing is performed in the digital domain. This processing can include filtering into narrower channels, demodulation, and so forth.

## 10.2.3 IF Sampling Topology

A flow diagram for a practical IF sampling digital receiver is shown in Figure 10.3. Again a preselector, block frequency converter, and amplification are placed ahead of the ADC. Digital processing is performed at an IF. This configuration allows lower speed, high-dynamic-range ADCs to be used—a cost saving. Additional frequency conversion, filtering, and detection are performed in the digital domain.
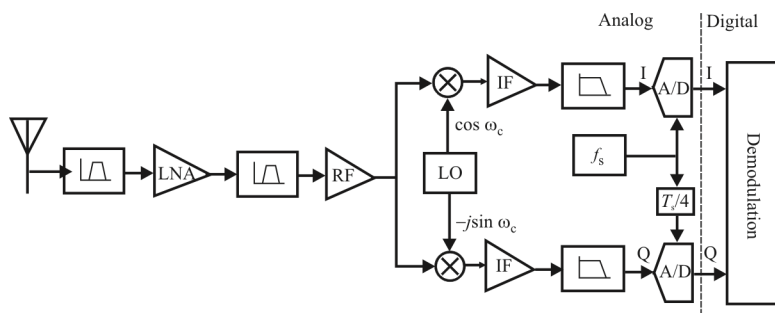
**Figure 10.3** IF digital sampling or subsampling receiver architecture.

The major difference between this architecture and the RF digital receiver is that the ADCs operate at (typically) a lower frequency than the RF receiver. Separation into quadrature channels follows the same principal as for the RF receiver.

IF sampling architectures currently demonstrate better performance than RF sampling architectures due to their lower susceptibility to aperture jitter and the fact that anti-aliasing filters and ADCs can be implemented with improved performance at lower frequencies. RF sampling receivers offer potential advantages in circuit complexity and area, power consumption, and re-configurability, but their use is currently limited to lower performance applications where the effects of aperture jitter and the limited performance of ADCs and anti-aliasing filters at RF frequencies can be tolerated.

## 10.2.4 Electronic Warfare Digital Receiver

EW receivers monitor a wide frequency band to detect and intercept hostile signals. They are required to insure a high probability of signal intercept. To accomplish this, a channelized receiver architecture is desired. Fortunately, a digital channelized receiver is easy to implement and produces excellent performance. Figure 10.4 contains a block diagram of a digital channelized receiver. The total RF coverage typically required of EW receivers dictates that an IF sampling architecture would be required. If wide bandwidth is not required, then an RF sampling topology may be possible.

The DFT shown in Figure 10.4 basically forms a filter bank and can be realized by the FFT algorithm. The FFT transforms the digitized time sequence from the ADC into a digitized frequency sequence representing the output of a filter bank.
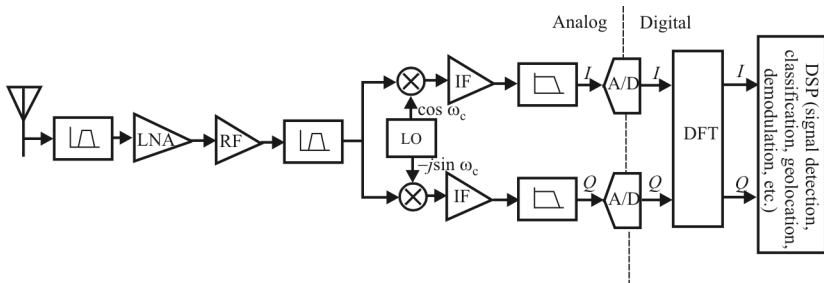
**Figure 10.4** EW digital receiver architecture.

# 10.3 Digital Receiver Technology Drivers

### 10.3.1 Analog-to-Digital Converter

One of the most critical digital receiver subsystems is the ADC. The ADC sets the receiver's maximum bandwidth, SNR, and instantaneous dynamic range. The maximum bandwidth is equal to a percentage of the ADC's sampling rate. With a sinusoidal (narrowband) signal, the maximum SNR realized by an ideal ADC is

$$\gamma = 1.76 + 6.02b \quad \text{dB} \tag{10.4}$$

where $b$ is the number of ADC quantization bits

As an example, an 8 bit ADC will produce a maximum SNR of 49.9dB. The ADC's instantaneous dynamic range is more complicated. The dynamic range is not only a function of the ADC's discrete quantization; it also depends upon the ADC's static and dynamic nonlinearities. The ADC's *effective bit* specification is related to its dynamic range. Its effective bits are always less than its actual bits. In addition, dynamic nonlinearities cause the ADC's effective bits to decrease as the signal frequency increases. The bandwidth is equal to the sampling rate when quadrature sampling is used with two ADCs.

We discuss ADC performance at length in Chapter 8.

### 10.3.2 Digital Signal Processor

After the signal is digitized by the ADC, it must be frequency converted, filtered, and detected, and probably subjected to other specific processing, depending on the signal type and threat environment. A DSP performs these tasks in the digital domain. For narrow bandwidth applications, the DSP can be a single chip microprocessor. In wide bandwidth applications, the DSP would consist of several circuit boards that contain high-performance, digital integrated circuits. In all
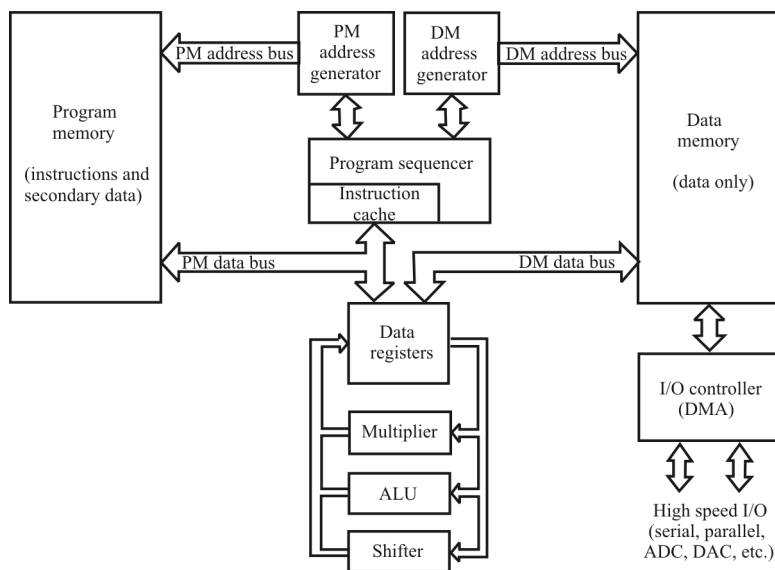
**Figure 10.5** Typical DSP architecture. Digital signal processors are designed to implement tasks in parallel.

cases, the DSP must process data at a rate commensurate with the ADC. It makes little sense to implement a high-sampling-rate ADC and a low-speed DSP (or vice versa).

A block diagram of a typical DSP is illustrated in Figure 10.5. The program memory holds only the program instructions while the data is all stored in the data memory. The program sequencer steps through the instructions in order. The data registers hold temporary data values while the multiplier, *arithmetic/logic unit* (ALU), and shifter perform mathematical and logical operations on the data in the registers. Data is normally input to the DSP through *direct memory access* (DMA) channels for speed.

# 10.4 Elementary Introduction to RF/IF Digital Signal Processing

In this section we present a very basic introduction to sampling and its effects on continuous analog RF/IF signals. For those comfortable with the DSP notation and sampling properties, this section can be skipped. For those readers who would like to refresh their background in DSP, including spectra replication and negative frequencies, this review might be helpful.
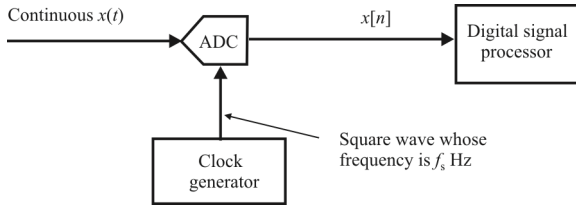
**Figure 10.6**  Digitization with periodic sampling.

## 10.4.1 Frequency Domain Ambiguity

The process of converting an analog signal to a digital one is illustrated in Figure 10.6. The ADC perfoms this function.  This process samples the continuous $x(t)$ signal to produce the $x[n]$ sequence of binary words stored in the DSP for follow-on processing. (Variable $n$ is a dimensionless integer used as the independent time-domain index in DSP, just as the letter $t$ is used in continuous-time equations.) The $x[n]$ sequence represents the voltage of $x(t)$ at periodically spaced instants in time. This process is called *periodic sampling*. The time period between samples is designated as $T_s$. It will be measured in seconds and defined as the reciprocal of the sampling frequency $f_s$, i.e., $T_s = 1/f_s$.

Consider the example in Figure 10.10. The effect of sampling a 400 Hz sinusoidal $x(t)$ waveform at a sampling frequency $f_s = 1$ kHz is shown in Figure 10.7(a). The $x[n]$ discrete-time samples from the ADC are plotted as the dots, and they are separated in time by 1 millisecond ($1/f_s$). The first three samples of the $x[n]$ sequence are $x[0] = 0$, $x[1] = 0.59$, and $x[2] = -0.95$.

The frequency domain ambiguity is illustrated in Figure 10.7(b), where the $x[n]$ samples would be unchanged if the ADC input $x(t)$ were a 1400 Hz continuous sinusoid. Another case is shown in Figure 10.7(c), where the continuous $x(t)$ is a −600 Hz sinusoid, again resulting in identical $x[n]$ samples. This means that, given the $x[n]$ samples alone, it cannot be determined whether the frequency of the continuous $x(t)$ sine wave is 400 Hz, 1400 Hz, or −600 Hz. That uncertainty is the frequency domain ambiguity. (The concept of negative
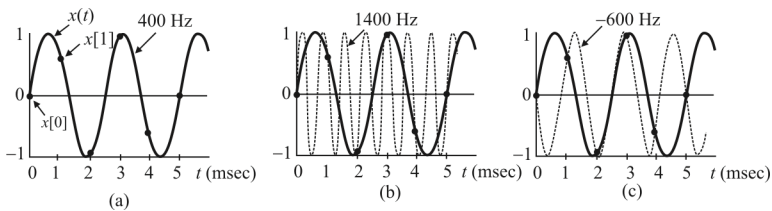


**Figure 10.7** Frequency domain ambiguity: (a) $x(t)$ at 400 Hz, (b) 1400 Hz dashed curve, and (c) −600 Hz dashed curve.

| k | $f_r(k)$ |
|---|---|
| ... | ... |
| −2 | −1000 Hz |
| −1 | −600 Hz |
| 0 | 400 Hz |
| 1 | 1400 Hz |
| 2 | 2400 Hz |
| ... | ... |

(a)                                    (b)
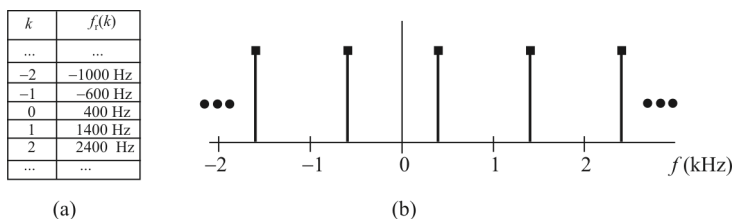
**Figure 10.8** Examples of replicated frequencies of 400 Hz when $f_s$ is 1 kHz: (a) a few examples, and (b) one possible frequency domain depiction.

frequency will be addressed shortly. For now, the definition of the −600 Hz sine wave is one whose phase is shifted by 180° relative to a +600 Hz sine wave.)

Thus we see that it is reasonable to assume that there are an infinite number of other frequencies that a sinusoidal $x(t)$ could have and still result in the same $x[n]$ samples of Figure 10.10. Those other frequencies, defined as images with frequencies $f_i(k)$, can be identified by:

$$f_i(k) = 400 + kf_s \quad \text{Hz} \tag{10.5}$$

where $k$ is an integer, and the $i$ subscript means image. Equation (10.5) indicates that any continuous sine wave whose frequency differs from 400 Hz by an integer multiple of $f_s$ is indistinguishable from a 400 Hz sine wave in the domain of discrete samples. A few of the replications of 400 Hz, when $f_s = 1$ kHz are listed in Figure 10.8(a). One reasonable frequency-domain depiction of this situation is shown in Figure 10.8(b), where it can be said that the spectrum of our discrete $x[n]$ sequence is an infinite set of spectral impulses periodically spaced in the frequency domain.

Three issues should be noted:

- First, the notion that the spectrum of the discrete $x[n]$ sequence is an infinite set of spectral impulses does not imply that $x[n]$ has infinite energy. Those multiple impulses in Figure 10.8(b) merely indicate that $x[n]$ could be a sampled (discrete-time) version of any one of infinitely many continuous sine waves.
- Second, resist the temptation to call those spectral impulses harmonics. The word *harmonic* has a specific meaning in the analog domain—related to spurious tones generated by nonlinear hardware components—that is not implied by Figure 10.8(b). For now, define those frequency domain impulses as spectral replications.
- Third, notice that the spacing between the spectral replications is the sampling rate $f_s$.
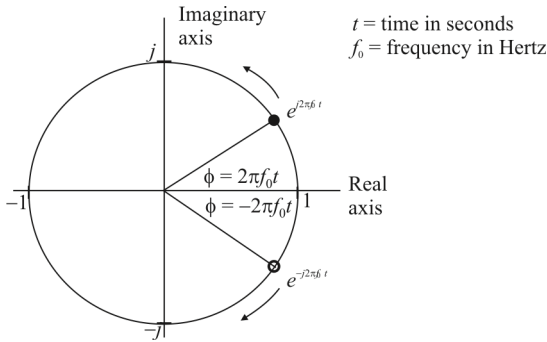
**Figure 10.9** A snapshot in time of two complex numbers whose exponents, and thus their phase angles, change with time.

## 10.4.2 Quadrature Signals

Next we address the concepts of complex (quadrature) signals and negative frequency. This is critical because so much of DSP deals with complex numbers such as the complex-valued (magnitude and phase) spectra of discrete time-domain sequences and the complex-valued frequency responses of digital filters.

Recall that a single complex number can be represented by a point on the two-dimensional complex plane with its two axes (real and imaginary) orthogonal to one another. This means there is a 90° difference in the axes' orientations. Another appellation for this two dimensional figure is an *Argand diagram* [Argand (1806) is generally credited with the discovery].

Consider a complex number whose magnitude is one and whose phase angle increases with time. That complex number is the $e^{j2\pi f_0 t}$ point shown on the complex plane in Figure 10.10. (Here the $2\pi f_0$ term is frequency in rps, and it corresponds to a frequency of $f_0$ Hz.) As time $t$ increases, the complex number's phase angle $\phi = 2\pi f_0 t$ increases and the number orbits the origin of the complex plane in a counterclockwise direction. Figure 10.9 shows that number, represented by the solid dot, frozen at some arbitrary instant in time. (That rotating $e^{j2\pi f_0 t}$ complex number goes by two names in DSP literature: it's often called a *complex exponential*, and it's also referred to as a *quadrature signal*.) If the frequency $f_0 = 2$ Hz, then the solid dot rotates around the circle two times, or two cycles per second.

Because complex numbers can be represented in both polar and rectangular notation, the polar $e^{j2\pi f_0 t}$ quadrature signal in rectangular coordinates is

$$e^{j2\pi f_0 t} = \cos(2\pi f_0 t) + j\sin(2\pi f_0 t) \qquad (10.6)$$
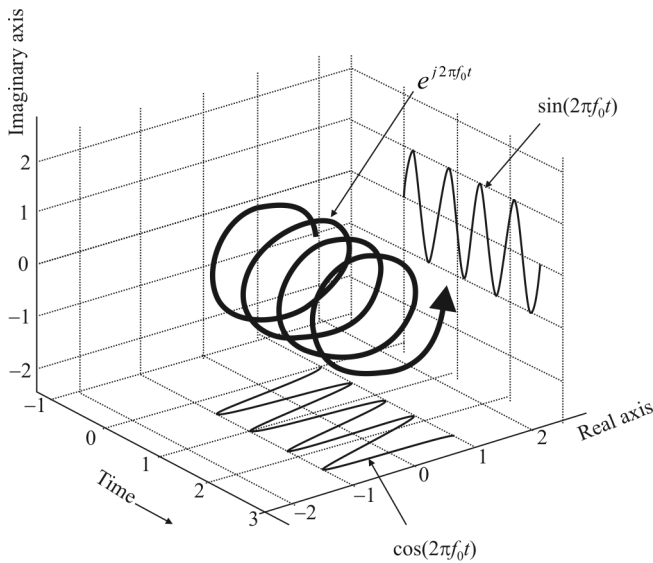
**Figure 10.10** Value of the complex exponential function (exp) over time.

Equation (10.6) indicates that as $e^{j2\pi f_0 t}$ rotates around the origin, its real part, the *x*-distance from the origin, varies as a cosine wave. Its imaginary part, the *y*-distance from the origin, varies as a sine wave.

The attributes of our two-dimensional $e^{j2\pi f_0 t}$ complex exponential are best illustrated with a three-dimensional time domain (see Figure 10.10). Notice how the $e^{j2\pi f_0 t}$ signal spirals along the time axis with its real part being a cosine wave and its imaginary part being a sine wave. At time $t = 0$ the signal has a value of $1 + j0$ as we would expect. [Equation (10.6) allows the representation of a single complex exponential as the orthogonal sum of real cosine and real sine functions.]

The concept of negative frequency is sometimes confusing. Referring again to Figure 10.9, there is a complex exponential, $e^{-j2\pi f_0 t}$, the open dot, orbiting in a clockwise direction. This occurs because its phase angle, $\phi = -2\pi f_0 t$, gets more negative as time increases. Again, if the frequency $f_0 = 2$ Hz, then the open dot would rotate around the circle two times, or two cycles, per second in the clockwise direction.

When the two exponentials are algebraically added, we get

$$e^{j2\pi f_0 t} + e^{-j2\pi f_0 t} = \cos(2\pi f_0 t) + j\sin(2\pi f_0 t) + \cos(2\pi f_0 t) - j\sin(2\pi f_0 t)$$
$$= 2\cos(2\pi f_0 t) \tag{10.7}$$
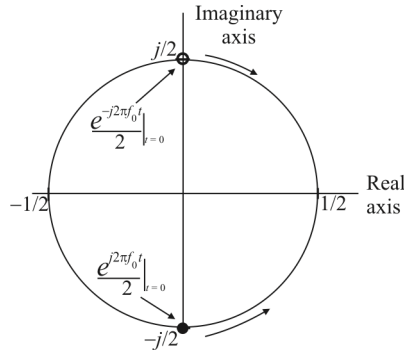
**Figure 10.11** Complex exponentials at zero.

which is a real signal—its imaginary part is always zero. That real-only sum is a cosine wave whose peak amplitude is 2. If the magnitudes of the complex exponentials in Figure 10.9 had been 0.5 instead of 1, from (10.7) we get:

$$\cos(2\pi f_0 t) = \frac{e^{j2\pi f_0 t} + e^{-j2\pi f_0 t}}{2} \tag{10.8}$$

Equation (10.8) provides the ability to represent a real cosine wave as the sum of positive-frequency and negative-frequency complex exponentials. By previous definitions, a positive-frequency complex exponential's exponent is positive, and a negative-frequency complex exponential is one whose exponent is negative.

In a similar manner we can derive the other Euler identity, which gives the relationship of a real sine wave as the sum of positive-frequency and negative-frequency complex exponentials

$$\sin(2\pi f_0 t) = \frac{e^{j2\pi f_0 t} - e^{-j2\pi f_0 t}}{2j} \tag{10.9}$$

The $j$-operators in (10.9) merely explain the relative phase of the complex exponentials at time $t = 0$ as illustrated in Figure 10.11. At time $t = 0$, (10.9) becomes:

$$\sin(2\pi f_0 t)\big|_{t=0} = \frac{e^{j2\pi f_0 t}\big|_{t=0} - e^{-j2\pi f_0 t}\big|_{t=0}}{2j} = \frac{e^{j0} - e^{-j0}}{2j} = \frac{1-1}{2j} = 0 \tag{10.10}$$

Consider Figure 10.12, which is the complex spectra of a few simple sinusoids. The time-domain waveform and the complex spectra of a sine wave
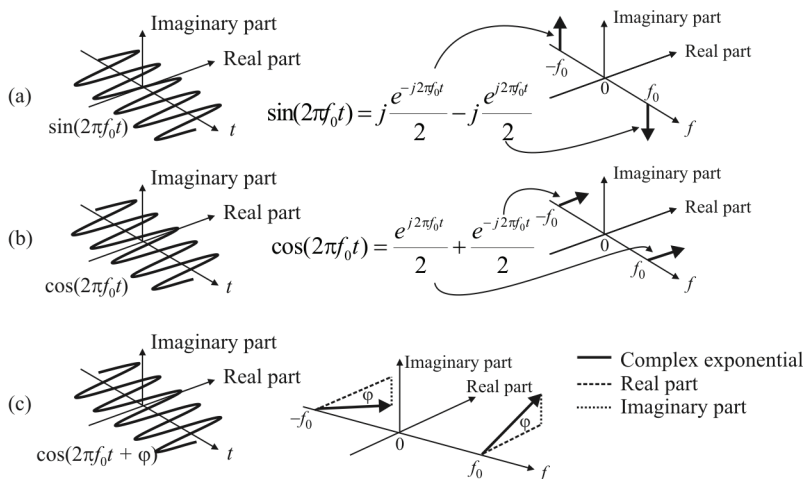
**Figure 10.12** Three sinusoids: (a) $\sin(2\pi f_0 t)$, (b) $\cos(2\pi f_0 t)$, and (c) $\cos(2\pi f_0 t + \varphi)$.

defined by $\sin(2\pi f_0 t)$ is shown in Figure 10.12(a). Shifting that sine wave in time by 90° develops the cosine wave shown in Figure 10.12(b). Another shift in time by $\varphi$ results in the arbitrary-phase cosine wave of Figure 10.12(c).

Remember now, the positive and negative-frequency spectral components of the sine wave rotated counterclockwise and clockwise, respectively, by 90° in going from Figure 10.12(a) to Figure 10.12(b). If those cosine waves' spectral components continued their rotation by $\varphi°$, the result would be the situation shown in Figure 10.12(c). These three-dimensional frequency domain spectra are shown replete with phase information because, in the world of digital signal processing, the spectral phase relationships are important. The FFT algorithm is used to measure spectral magnitude and phase. Note that Figure 10.12 illustrates an important signal processing principle. A time-domain shift of a periodic signal results only in phase shifts in the frequency domain; spectral magnitudes do not change.

Figure 10.12(a) illustrates (10.9) and Figure 10.12(b) is a graphical description of (10.8). Figure 10.12 is a reminder that one legitimate, and useful, way to show the spectrum of a real cosine wave is to include both positive- and negative-frequency spectral components.

With this thought in mind, refer to the drawing of the spectral magnitude (ignoring any phase information) of a continuous 400 Hz sinusoid as shown in Figure 10.13(a). This figure shows the inherent spectral symmetry about 0 Hz when representing real signal spectra with complex exponentials. In this case, *real signal* is defined by an $x(t)$ signal having a non-zero real part but whose imaginary part is always zero. (We treat all signals as complex and regard real signals as a special case of complex signals.) Figure 10.12(a) is another graphical representation of Euler's identity in (10.9).
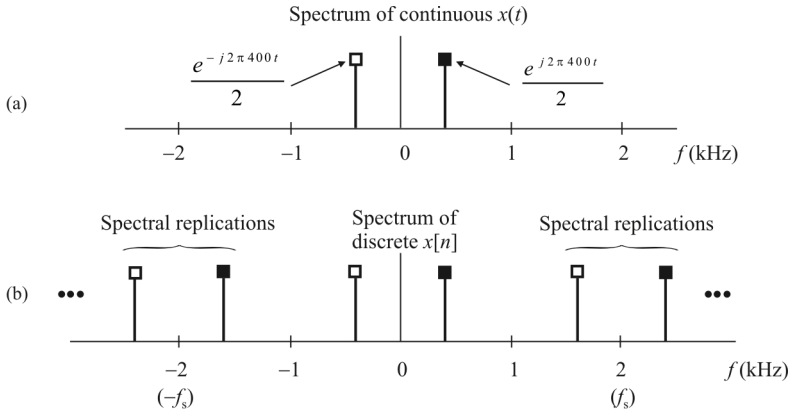
**Figure 10.13** The spectral magnitude plot of (a) a 400 Hz continuous sinusoid, and (b) a discrete sequence of a 400 Hz sinusoid sampled at a 2 kHz sample rate.

Applying this convention of "spectral replications due to periodic sampling" to this analysis illustrates the spectral magnitude of discrete samples of a 400 Hz sinusoid, sampled at an $f_s = 2$ kHz sampling rate, as that of Figure 10.13(b).

Finally, Figure 10.13(b) is typical of the spectral magnitude representations used in the digital signal processing literature. It combines the spectral replications (centered about integer multiples of $f_s$) due to periodic sampling, as well as the use of negative frequency components resulting from representing real signals in complex notation.

Figure 10.14(a) shows the spectral magnitude of a continuous $x(t)$ signal having four components in the range of 100 Hz to 700 Hz. Dark and light squares distinguish the positive- and negative-frequency spectral components. Figure 10.14(b) shows the spectral replication for a discrete $x[n]$ sequence that's $x(t)$ sampled at 2 kHz.

Thus we see that Figure 10.14(b) represents the spectrum of discrete samples of a real sinusoid in the complex-valued world of digital signal processing. This figure is a reminder of the following important properties: continuous real signals have spectral symmetry of about 0 Hz, and discrete real signals have spectral symmetry of about 0 Hz and $f_s/2$ Hz.

Figure 10.14 illustrates the reason that the Nyquist criterion for lowpass signals—signals whose spectral components are centered about 0 Hz—states that the $f_s$ sampling rate must be equal to or greater than twice the highest spectral component of $x(t)$. Because $x(t)$'s highest spectral component is 700 Hz, the $f_s$ sampling rate must be no less than 1.4 kHz. If $f_s$ were 1.3k Hz, as in Figure 10.14(c), the spectral replications would be too close together and spectral overlap would occur. It can be seen that the spectrum in the range of −1 kHz to +1 kHz in Figure 10.14(c) does not correctly represent the original spectrum in Figure 10.14(a).
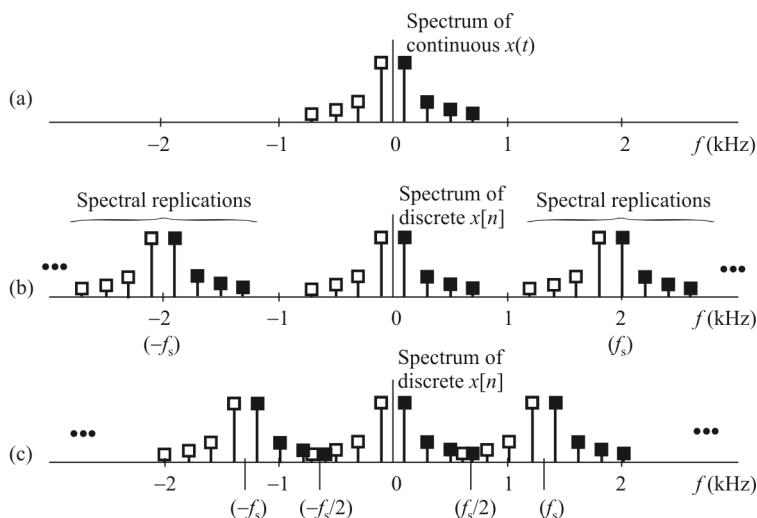
**Figure 10.14** Spectrum of a signal with four components in the range of 100 Hz to 700 Hz: (a) spectral magnitude of the continuous signal, (b) spectrum of a sampled sequence when $f_s = 2$ kHz, and (c) spectrum when $f_s = 1.3$ kHz.

This situation is called *aliasing*, and it results in $x[n]$ sample values that contain amplitude errors. Unfortunately, for meaningful information-carrying signals, there is no way to correct for those errors.

We see that the spectral overlap is centered about $f_s/2$ and that this particular frequency is important enough to have its own nomenclature. It is sometimes called the *folding frequency*, but more often it's called the *Nyquist frequency*. Because of this anomaly, the following important statement relating continuous and discrete signals can be made:

> **Property 10.1:** Only continuous frequency components as high as the Nyquist frequency ($f_s/2$) can be unambiguously represented by a discrete sequence obtained at an $f_s$ sampling rate.

Figure 10.14(c) also presents another fundamental connection between the worlds of continuous and discrete signals. All of the continuous $x(t)$ spectral energy shows up in the discrete $x[n]$ sequence's spectral frequency range of $-f_s/2$ to $+f_s/2$.

Figure 10.14 provides a straightforward explanation for the effects of overlapped spectra due to aliasing. Drawing replicated spectra is useful in illustrating the spectral translation that takes place in bandpass sampling and describing the result of frequency translation operations such as digital down-conversion, both of which are discussed in the next chapter.

### 10.4.3 Summary

This discussion has reviewed the graphical depictions and terminology of digital signal processing to explain the differences between continuous (analog) and discrete spectrum analysis with regard to spectral replications and the idea of negative frequency. The use of spectral replications in digital signal processing diagrams is a way of accounting for the inherent frequency domain ambiguity when performing periodic sampling of a continuous signal. These replications provided a consistent explanation for errors due to aliasing. The use of Euler's identities relating real-only signals and complex exponentials leads to a definition of negative frequency that allows the representation of all signals in complex notation.

## 10.5 Digital EW Receivers

### 10.5.1 Introduction

Many advances in radio design and architecture are allowing for changes in the way radio receivers are implemented. These changes allow reduction of size, cost, and complexity and improve manufacturability by using digital components to replace unreliable and inaccurate analog components. Many advances in semiconductor design and fabrication have come to fruition over the past few years. Some of these advances include better integrated mixers, LNA, improved SAW filters, lower cost high-performance ADCs, and programmable digital processors. In this section we summarize an analysis approach for digital receivers. Each of the topics introduced here is discussed in depth in other chapters.

The purpose of the receiver is first to downconvert and filter the signal at the antenna and then convert it to digital form. The second purpose is to provide a DSP that extracts the desired information from the intercepted signal. A digital receiver can be used to receive any type of modulation including any of the analog or digital modulations. Furthermore, the DSP allows many aspects of the entire radio receiver to be controlled through software. As such, these DSPs can be reprogrammed with upgrades or new features based on new/unexpected threat environments or new required functionality.
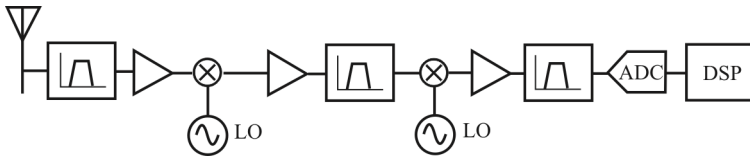
**Figure 10.15** Single-signal receiver.

Our focus here is the receiver and how to predict performance. We focus on the processing chain in this chapter and those to follow up to and including the ADC. The functionality of the DSP following the ADC depends on the particular application. Such functionality could include channel selection (filtering, selectivity), signal detection, signal demodulation, direction finding, and so forth. We will consider some of this functionality in the chapters to follow. There are many books that cover that topic in depth [3–6].

We discuss the following topics:

- Available Noise Power
- Cascaded Noise Figure
- Noise Figure and ADCs
- Conversion Gain and Sensitivity
- ADC Spurious Signals and Dither
- Third-Order Intercept Point
- ADC Clock Jitter
- Phase Noise
- IP3 in the RF section

### 10.5.2 Single-Signal versus Multisignal

We consider two basic types of receivers. The first is called a *single-signal* and the second a *multisignal* receiver. (These appellations in the communication system domain are *single-carrier* and *multicarrier*. We will use both.) Their names imply the obvious, but their function may not be fully clear. The single-signal receiver is a traditional radio receiver deriving selectivity in the analog filters of the IF stages (Figure 10.15). The multisignal receiver processes all signals within the band with a single RF/IF analog strip and derives selectivity within the digital filters that follow the ADC (Figure 10.16). The benefit of such a receiver is that in applications with multiple receivers tuned to different frequencies within the same band, smaller system designs and reduced cost due to eliminated redundant circuits can be achieved.

EW receivers can be of either variety. In multioperator applications, the multisignal variety would typically be chosen with each operator intercepting a different signal. ("Operator" here does not necessarily refer to a person. It could be
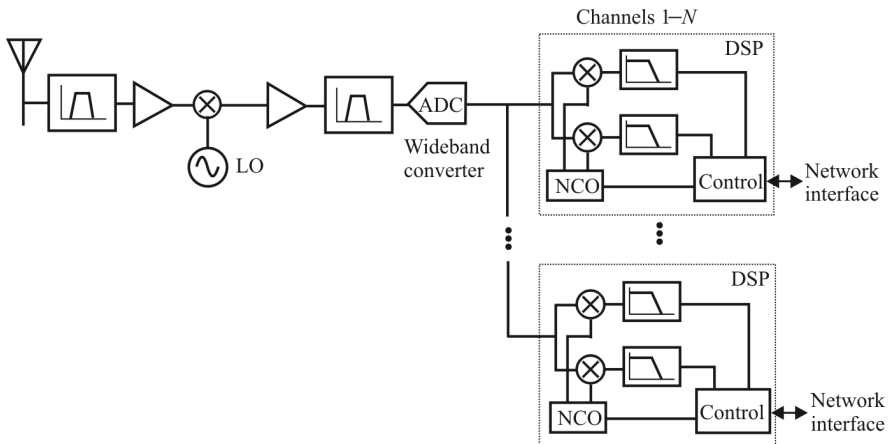
**Figure 10.16**  Multisignal receiver.

some automated intercept process.) For single-operator systems, the single-signal configuration may be acceptable and cheaper.

### 10.5.3 Benefits of Implementing a Digital Receiver

Before the details of the analysis of a digital receiver are discussed, we discuss some of the technical benefits. These include oversampling, processing gain, undersampling, and frequency planning/spur placement. Many of these provide technical advantages not otherwise achievable with a traditional receiver design.

10.5.3.1 Oversampling and Process Gain

The Nyquist criterion compactly determines the sampling rate required for any given signal. Many times, the Nyquist rate is quoted as the sample rate that is twice that of the highest frequency component. This implies that for an IF sampling application at 70 MHz, a sample rate of 140 Msps would be required. If our signal only occupies 5 MHz around 70 MHz, then sampling at 140 Msps entails significant waste of resources. Instead, Nyquist requires that the signal be sampled twice the *bandwidth* of the signal. Therefore, if our signal bandwidth is 5 MHz, then sampling at 10 MHz is adequate. Anything beyond this carries the appellation *oversampling*. As we will show, oversampling allows for an effective gain of received SNR in the digital domain.

The antithesis of oversampling is undersampling. *Undersampling* is sampling at a frequency much less than the half of the actual signal frequency. It is possible to be oversampling and undersampling simultaneously since one is defined with respect to bandwidth and the other at the frequency of the SOI.

In any digitization process, the faster the signal is sampled, the lower the noise floor because noise is spread out over more frequencies. The total integrated noise remains constant but is now spread out over a wider spectrum. The SNR is given by

$$\gamma = 6.02b + 1.76 + 10\log_{10}(f_s / 2W) \qquad (10.11)$$

where

$b$ is the number of ADC bits
$f_s$ is the sample frequency
$W$ is the SOI bandwidth

This equation reflects the level of the quantization noise within the converter and shows the relationship between SNR and the sample rate $f_s$. For fixed SOI bandwidth $W$, each time the sample rate is doubled, the SNR improves by 3dB.

Digital filtering has the effect of removing all unwanted noise and spurious signals, leaving only the desired signal as shown in Figures 10.17 and 10.18. The SNR of the ADC may be greatly improved as shown in these figures. This SNR improvement is because of the third term in (10.11) and is due to the significant oversampling. As we see in (10.11), the greater the ratio between sample rate and signal bandwidth, the higher the process gain. In fact, gains as high as 30dB are achievable.

10.5.3.2 Undersampling and Frequency Translation

Undersampling is when the sampling frequency is less than half of the actual signal frequency. For example, a 70 MHz signal sampled at 13 Msps is undersampled. Undersampling can serve a function very similar to mixing. When a signal is undersampled, the frequencies are aliased into the first Nyquist band. For example, the 5 MHz bandwidth signal at 70 MHz when sampled at 13 Msps would appear at 5 MHz. This can mathematically be described by:

$$f_{\text{signal}} \bmod f_s$$

This equation provides the resulting frequency in the first and second Nyquist zones. Since the ADC aliases all information to the first Nyquist zone, results generated by this equation must be checked to see if they are above $f_s / 2$. If they are, then the frequency must be folded back into the first Nyquist zone by subtracting the result from $f_s$.

Table 10.1 shows how signals can be aliased into baseband and their spectral orientation. Although the process of sampling (aliasing) is different from mixing
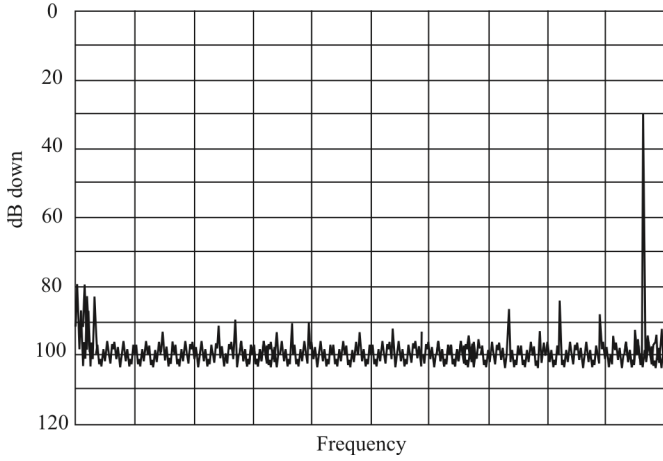
**Figure 10.17**  ADC spectrum before filtering.
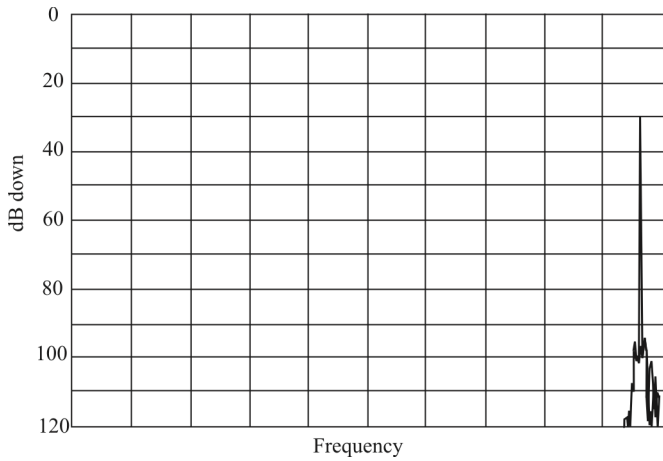


**Figure 10.18** ADC spectrum after filtering.

**Table 10.1** Frequency Planning and Spur Placement

| Input Signal | Frequency Range | Frequency Shift | Spectral Sense |
|---|---|---|---|
| 1st Nyquist Zone | $DC - f_s/2$ | Input | Normal |
| 2nd Nyquist Zone | $f_s/2 - f_s$ | $f_s -$ Input | Reversed |
| 3rd Nyquist Zone | $f_s - 3f_s/2$ | Input $- f_s$ | Normal |
| 4th Nyquist Zone | $3f_s/2 - 2f_s$ | $2f_s -$ Input | Reversed |
| 5th Nyquist Zone | $2f_s - 5f_s/2$ | Input $- 2f_s$ | Normal |

(multiplication), the results are quite similar, but sampling is periodic about the sample rate. Another phenomenon is that of spectral reversal. As in mixers, certain products become reversed in the sampling process, such as upper and lower sideband reversal. Table 10.1 also shows which cases cause spectral reversal.

One of the biggest challenges for a receiver architecture is that of IF frequency placement. Compounding this problem is that amplifiers and ADCs tend to generate unwanted harmonics that show up in the digital spectrum of the data conversion, appearing as false signals. Whether the application is wideband or not, careful selection of sample rates and IF frequencies can place these spurs at locations that render them harmless when used with digital tuners/filters that can select the SOI and reject all others. By carefully selecting input frequency range and sample rate, the amplifier and ADC harmonics can be placed out-of-band. Oversampling only simplifies matters by providing more spectrum within which the harmonics will fall.

An example of frequency planning can be found in undersampling. If the analog input signal range is from DC to $f_s/2$, then the amplifier and filter combination must perform to the specification required. However, if the signal is placed in the third Nyquist zone ($f_s$ to $3f_s/2$; see Figure 10.19), the amplifier is no longer required to meet the harmonic performance required by the system specifications since all harmonics would fall outside the passband filter. For example, the passband filter would range from $f_s$ to $3f_s/2$. The second harmonic would span from $2f_s$ to $3f_s$, well outside the passband filters range. The burden then has been passed off to the filter design provided that the ADC meets the basic specifications at the frequency of interest. In many applications, this is a worthwhile tradeoff since many complex filters can easily be realized using SAW and LCR techniques alike at these relatively high IF frequencies. Although harmonic performance of the amplifier is relaxed by this technique, intermodulation performance cannot be sacrificed.

Using this technique to cause harmonics to fall outside the Nyquist zone of interest allows them to be easily filtered, as shown in Figure 10.19. However, if the ADC still generates harmonics of its own, the technique previously discussed can be used to carefully select sample rate and analog frequency so that harmonics fall into unused sections of bandwidth and are digitally filtered.
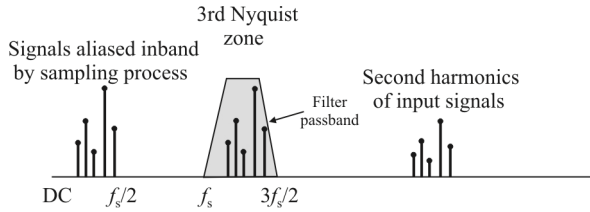
**Figure 10.19** Third Nyquist zone.

## 10.5.4 Receiver Performance Expectations

We use the generic receiver shown in Figure 10.20 for our performance analysis. This discussion begins with the antenna and ends with the digital tuner/filter (DSP) at the end. The specific processing within the DSP is outside the scope of this discussion; some of these are covered in subsequent chapters.

Analysis starts with several assumptions (that can be removed or modified as the analysis proceeds if necessary). First, it is assumed that the receiver is noise limited—that is, that no spurs exist in-band that would otherwise limit performance. It is reasonable to assume that LO and IF choices can be made such that this is true. Additionally, we will show later that spurs generated within the ADC are generally not a problem as they can often be eliminated with the application of dither or through judicious use of oversampling and signal placement. In some instances, these may not be realistic assumptions, but they do provide a starting point with which performance limits can be benchmarked.

The second assumption is that the bandwidth of the receiver front end is our Nyquist bandwidth. Although our actual allocated bandwidth may only be 5 MHz, using the Nyquist bandwidth will simplify computations along the way. Therefore, a sample rate of 65 Msps would give a Nyquist bandwidth of 32.5 MHz.

## 10.5.5 Available Noise Power

First, the noise at the antenna/RF stage interface must be considered. Since a properly matched antenna is resistive, we can use
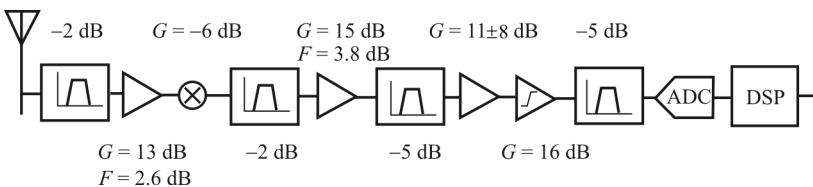


**Figure 10.20** Flow diagram of a generic receiver.

$$V_n^2 = 4k_B TRW \qquad (10.12)$$

where

$k_B$ is Boltzmann's constant $1.38 \times 10^{-23}$ J/K
$T$ is temperature in K
$R$ is resistance
$W$ is bandwidth

to determine the noise voltage across the matched input terminals. Available power from the source, in this case the antenna, is thus:

$$P_a = \frac{V_n^2}{4R}$$

from which we get

$$P_a = k_B TW \qquad (10.13)$$

Thus in reality, the available noise power from the source in this case is independent of impedance for non-zero and finite resistance values.

   This is the reference point to which our receiver will be compared. It is often stated when dealing with the NF of a stage, that it exhibits "$x$ dB" above "$k_B T$" noise. This is the source of this expression.

   With each progressive stage through the receiver, this noise is degraded by the NF of the stage as discussed below. Finally, when the channel is tuned and filtered, much of the noise is removed, leaving only that which lies within the channel of interest.

## 10.5.6 Cascaded Noise Figure

As we discussed in Chapter 3, NF is a figure of merit used to describe how much noise is added to a signal in the receive chain of a receiver. Usually, it is specified in decibels although in the computation of NF, the noise factor (non-log) is used. The noise factor is usually denoted as $f$, where it is defined by (3.1).

   Once an NF is assigned to each of the stages, it can be used to determine the cascaded performances. The total noise factor referenced to the antenna/RF stage interface can be computed with the Friis equation (3.22).

   The $f$'s in (3.22) are the noise factors for each of the serial stages while the $G$'s are the gains of the stages. Neither the noise factor nor the gains are in log form at this point. When this equation is applied, it reflects all component noise to

the antenna port. Thus, the available noise from the previous section can be incorporated directly using the NF

$$P_{total} = P_a + F + G \qquad (10.14)$$

For example, if the available noise is −100dBm, the NF is 10dB, and the conversion gain is 20 dB, then the total equivalent noise at the output is −70 dBm. There are several points to consider when applying these equations. First, for passive components, $F$ is equal to their loss, $L$. Second, passive components in series can be summed before the equation is applied. For example if two lowpass filters are in series, each with an insertion loss of 3 dB, they may be combined and the loss of the consolidated element is 6 dB. Finally, mixers often do not have a NF assigned to them by the manufacturer. If not specified, the insertion loss may be used; however, if an NF is supplied with the device, it should be used.

## 10.5.7 Noise Figures and ADCs

Although an NF could be assigned to the ADC, it is often easier to analyze the ADC performance in a different manner. ADCs are voltage devices, whereas the NF is a noise power parameter. Therefore, it is easier to analyze the RF/IF sections in terms of NF and then convert to voltage at the ADC. Then, the noise from the RF/IF sections and ADC can be summed at the ADC input to find the total effective noise.

For specificity we will assume the ADC has 12 bits and can sample at 65 Msps, a rate suitable for entire cellular bands. This is more than adequate for GSM and CDMA applications. We will further assume that the ADC SNR is 68dB. Therefore, the next step is to figure the noise degradation within the receiver due to ADC noises. If the ADC has a 2V peak-to-peak input range (1V peak, 0.707V RMS), the squared RMS input voltage is

$$V^2_{noise} = (0.707 \times 10^{-SNR/20})^2 \approx 79 \times 10^{-9} \qquad V^2$$

This voltage represents all noises within the ADC: thermal and quantization. The full-scale range of the ADC is 0.707Vs RMS.

With the ADC equivalent input noise computed, the next computation is the noise generated from the RF/IF sections. Since we are assuming that the receiver bandwidth is the Nyquist bandwidth, a sample rate of 65 Msps produces a bandwidth of 32.5 MHz. From the available noise power equations, noise power from the RF/IF sections is $134.6 \times 10^{-15}$ W or −98.7 dBm. This is the noise present at the antenna/RF stage interface, which is amplified by the conversion gain and degraded by the NF. The conversion gain in Figure 10.20 is 25dB and the NF is 5dB, and so the noise presented to the ADC input is

$$-98.7\,\mathrm{dBm} + 25\,\mathrm{dB} + 5\,\mathrm{dB} = -68.7\,\mathrm{dBm}$$

$(134.9 \times 10^{-12}\,\mathrm{W})$. Since the ADC has an input impedance of about $1000\Omega$, we must either match the standard $50\Omega$ IF impedance to this or pad the ADC impedance down. A reasonable compromise is to pad the range down to $200\Omega$ with a parallel resistor and then use a 1:4 transformer to match the rest. The transformer also serves to convert the unbalanced input to the balanced signal required for the ADC as well as provide some voltage gain. Since there is a 1:4 impedance step up, there is also a voltage gain of 2 in the process. Also

$$V^2 = PR \qquad (10.15)$$

so the voltage squared into $50\Omega$ is $6.75 \times 10^{-9}$ or into $200\Omega$ is $26.9 \times 10^{-9}$.

Now that we know the noise from the ADC and the RF stage (including the IF stage noise reflected to the input), the total noise in the system can be computed by the square root of the sum of the squares. The total voltage is thus $325.9\mu\mathrm{V}$. This is now the total noise present at the ADC due to both RF/IF noise and ADC noise, including quantization noise.

### 10.5.8 Conversion Gain and Sensitivity

The noise voltage contribution to the ADC performance is to reduce the SNR. Assume that only one RF signal is present in the receiver bandwidth. The (maximum) SNR would then be:

$$\gamma = 20\log_{10}(S/N) = 20\log_{10}(0.707/325.9\times10^{-9}) = 66.7\,\mathrm{dB}$$

Since this is an oversampling application and the actual signal bandwidth is much less than the sample rate, noise will be greatly reduced once digitally filtered as dictated by (10.11). Since the front end bandwidth is the same as our ADC bandwidth, both ADC noise and RF/IF noise will improve at the same rate. We assume, for example, that the SOI channel width is 30 kHz, producing a gain of 33.4dB from process gain. Therefore, our original SNR of 66.7 dB is now 100.1 dB. Remember that SNR increased because excess noise was filtered, which is the source of process gain.

If this is a multisignal receiver, the ADC dynamic range must be shared with other RF carriers. For example, if there are eight carriers of equal power (Figure 10.21), each signal should be no larger than 1/8 the total range if peak-to-peak signals are considered. However, since normally the signals are not in phase with one another in a receiver (because the targets are not phase locked), the signals
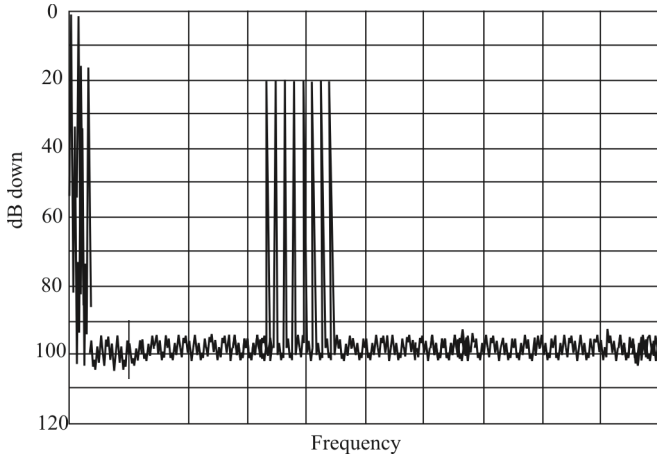
**Figure 10.21** Eight equal power carriers.
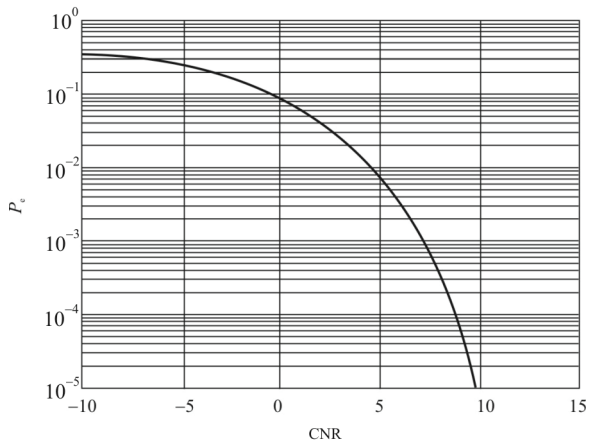


**Figure 10.22** BER BPSK.

will rarely if ever align. Therefore, much less than the required 18dB is needed. Since in reality, only no more than 2 signals will align at any one time and because they are modulated signals, only 3dB will be reserved for the purpose of head room. In the event that signals do align and cause the converter to clip, it will occur for only a small fraction of a second before the overdrive condition is cleared. In the case of a single carrier radio, no head room is required.

Depending on the modulation scheme, a minimum CNR is required for adequate demodulation. If the scheme is digital, then the BER must be considered as shown in Figure 10.22. Assuming a minimum CNR of 10dB is required, our input signal level cannot be so small that the remaining SNR is less than 10dB. Thus, our signal level may fall 90.1dB from its present level. Since the ADC has a full-scale range of +4dBm (200Ω), the signal level at the ADC input is then –86.1dBm. If there were 25 dB of gain in the RF/IF path, then receiver sensitivity at the antenna would be –86.1 minus 25 dB or –111.1dBm. If more sensitivity is required, then more gain is placed in the RF/IF stages. However, the NF is not independent of gain and an increase in the gain may also have an adverse effect on noise performance from additional gain stages.

## 10.5.9 ADC Spurious Signals and Dither

A noise limited example does not adequately describe the true limitations in a receiver. Other limitations such as SFDR can be more restrictive than SNR and noise. Assume that the ADC has an SFDR specification of –80dBFS or –76dBm (full-scale = +4dBm). Also assume that a tolerable *carrier to interferer* (*C/I*, different from *C/N*) ratio is 18dB. This means that the minimum signal level is –62dBFS (–80 plus 18) or –58dBm. At the antenna, this is –83dBm. Therefore, as can be seen, the SFDR (single or multitone) would limit receiver performance long before the actual noise limitation is reached.

However, a technique known as *dithering* can greatly improve SFDR. The addition of out-of-band noise can improve SFDR well into the noise floor. Although the amount of dither is ADC specific, the technique applies to all ADCs as long as static DNL is the performance limitation and not AC problems such as slew rate. As shown in Figures 10.23 and 10.24, the plots both before and after dither provide insight into the potential for improvement. In simple terms, dither works by taking the coherent spurious signals generated within the ADC and randomizes them. Since the energy of the spurs must be conserved, dither simply causes them to appear as additional noise at the floor of the converter. This can be observed in the before and after plots of dither as a slight increase in the average noise floor of the converter. Thus, the tradeoff made through the use of out-of-band dither is that literally all internally generated spurious signals can be removed. However, there is a slight hit in the overall SNR of the converter which in practical terms amounts to less than 1 dB of sensitivity loss compared to the
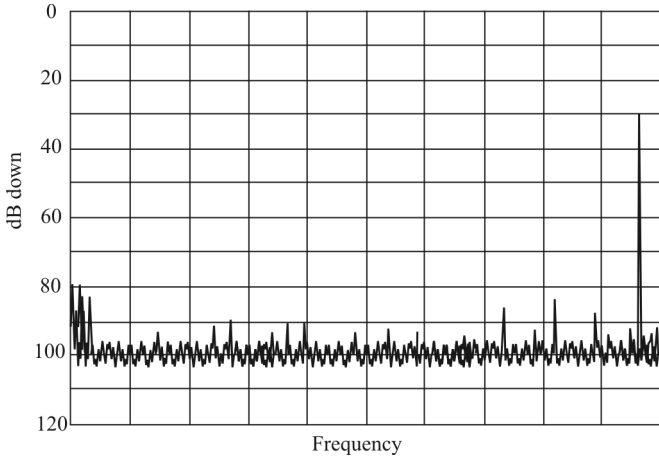
**Figure 10.23** ADC without dither.
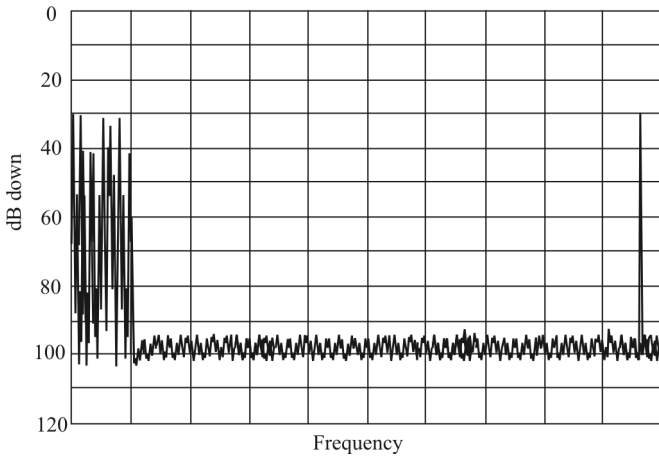


**Figure 10.24** ADC with dither.
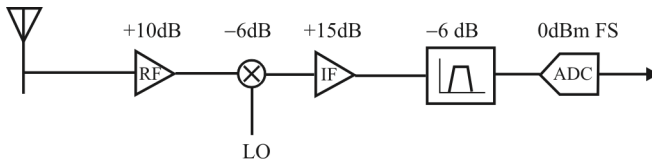
**Figure 10.25** Third-order intercept.

noise limited example and much better than the SFDR-limited example shown earlier.

Two important points need to be mentioned about dither. First, in a multi-signal receiver, none of the channels can be expected to be correlated. If this is true, then often the multiple signals will serve as self-dither for the receiver channel. While this is true some of the time, there will be times when additional dither will need to be added when signal strengths are weak, the typical case for EW receivers.

Second, the noise contributed from the analog front end alone is insufficient to dither the ADC. From the example above, −32.5dBm of dither was added to yield an optimum improvement in SFDR. In comparison, the analog front end only provides −68 dBm of noise power, far from what is needed to provide optimum performance.

## 10.5.10 Third-Order Intercept Point

Besides converter SFDR, the RF/IF sections contribute to the spurious performance of the receiver. These spurs are unaffected by techniques such as dither and must be addressed to prevent degradation of receiver performance. To determine what level of performance is required of wideband RF/IF components, we will use as an example the cellular GSM specification, perhaps the most demanding of commercial receiver applications.

A GSM receiver must be able to recover a signal with a power level between −13dBm and −104dBm. Assume also that the full scale of the ADC is 0dBm and that losses through the receiver filters and mixer are 12dB. Also, since multiple signals are to be processed simultaneously, an AGC should not be employed. This would reduce RF sensitivity and cause weaker signals to be dropped. Using these valuesm the RF/IF gain is determined to be $g = 25$dB ($0 = -13 - 6 - 6 + g$).

The 25dB gain of the RF/IF chain is distributed as shown in Figure 10.25. Although a complete system would have additional components, this simplified signal flow diagram will serve for this discussion. From this, with a GSM signal at −13dBm, ADC input will be 0dBm. However, with a minimal GSM signal of −104dBm, the signal at the ADC would be −91dBm. From this point, the discussion above can be used to determine the suitability of the ADC in terms of noise performance and spurious performance. Now with these signals and the

system gains required, the amplifier and mixer specifications can be examined when driven by the full scale signal of −13dBm. Solving for the third-order products in terms of signal full-scale we use

$$IIP3 = \frac{3}{2}\left(Sig - \frac{OIP3}{3}\right)$$                (10.16)

where *Sig* is the full scale input level of the ADC in dBm and OIP3 is the required third-order product level.

Assuming that overall spurious performance must be greater than 100dB, solving this equation for the front end amplifier shows that an amplifier with IIP3 >+37 dBm is required. At the mixer, the signal level has been increased by 10dB, and the new signal level is −3dBm. However, since mixers are specified at their output, this level is reduced by at least 6dB to −9dBm. Therefore for the mixer, an OIP3 > +41dBm is required. At the final gain stage, the signal will be attenuated to −9dBm (same as the mixer output). For the IF amplifier, the IIP3 > +41 dBm.

## 10.5.11 ADC Clock Jitter

ADC clock jitter is one of the critical issues with digital receivers. Although low jitter is important for acceptable baseband performance, its effect is magnified when sampling higher frequency signals (higher slew rate) such as is found in undersampling applications. The overall effect of a poor jitter performance is a reduction in SNR as input frequencies increase.

Aperture jitter is the sample-to-sample variation in the conversion process. It has three residual effects: the first is an increase in system noise, the second is uncertainty in the actual phase of the sampled signal itself, and third is ISI. Aperture uncertainty of less than 1 ps is required when IF sampling in order to achieve tolerable noise performance. In terms of phase accuracy and ISI, the effects of aperture uncertainty are small. In a worst case scenario of 1 ps RMS, at an IF of 250 MHz, the phase uncertainty or error is 0.09 degrees RMS. Therefore the focus of this analysis will be on overall noise contribution due to aperture uncertainty.

In a sine wave, the maximum slew rate is at the zero crossing (Figure 10.26). At this point, the slew rate is defined by the first derivative of the sine function evaluated at $t = 0$:

$$v(t) = A\sin(2\pi ft)$$

$$\frac{dv(t)}{dt} = A2\pi f \cos(2\pi ft)$$                (10.17)

evaluated at $t = 0$. The cosine function evaluates to 1 and (10.17) reduces to
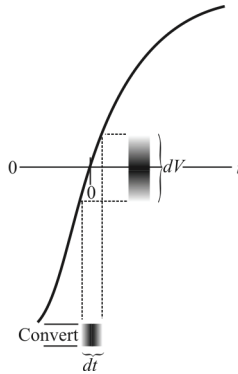
**Figure 10.26**  Noise generation at the zero crossing.

$$\left.\frac{dv(t)}{dt}\right|_{t=0} = A2\pi f$$

The units of slew rate are volts per second and yields how fast the signal is slewing through the zero crossing of the input signal.

In a sampling system, a reference clock is used to sample the input signal. If the sample clock has aperture uncertainty, then an error voltage is generated. This error voltage can be determined by multiplying the input slew rate by the jitter, viz.,

$$v_{\text{error}} = \text{slew rate} \times t_{\text{jitter}} \tag{10.18}$$

We see that this yields unit of volts. When aperture uncertainty is expressed in seconds RMS, the error voltage is in volts RMS. We also see that as the SOI frequency increases, the RMS error voltage also increases in direct proportion to the aperture uncertainty.

In IF sampling converters, clock purity is of extreme importance. As with the mixing process, the input signal is multiplied by a local oscillator or, in this case, a sampling clock. Since multiplication in time is convolution in the frequency domain, the spectrum of the sample clock is convolved with the spectrum of the input signal. Since aperture uncertainty is wideband noise on the clock, it shows up as wideband noise in the sampled spectrum as well. And since an ADC is a sampling system, the spectrum is periodic and repeated around the sample rate. This wideband noise therefore degrades the noise floor performance of the ADC. The theoretical SNR for an ADC as limited by aperture uncertainty is given by

$$\gamma = -20\log_{10}\left(2\pi f t_{j_{\text{RMS}}}\right) \tag{10.19}$$

If this equation is evaluated for a frequency of 201 MHz and 0.7 ps RMS jitter, the theoretical SNR is limited to 61dB. It should be noted that this is the same requirement as would have been demanded had another mixer stage been used. Therefore, systems that require high dynamic range and high input frequencies also require a very low jitter clock source. When using standard TTL/CMOS clock oscillators modules, 0.7 ps RMS has been verified for both the ADC and the oscillator. Better performance can be achieved with low noise modules.

When considering overall system performance, a more generalized equation may be used. This equation builds on the previous equation but includes the effects of thermal noise and *differential nonlinearity* (DNL)

$$\gamma = -20\log_{10}\left[\left(2\pi f t_{j_{\text{RMS}}}\right)^2 + \left(\frac{1+\varepsilon}{2^b}\right)^2 + \left(\frac{v_{\text{noise}_{\text{RMS}}}}{2^b}\right)^2\right]^{1/2} \tag{10.20}$$

where

$f$ is the frequency of the SOI

$t_{j_{\text{RMS}}}$ is the aperture uncertainty

$\varepsilon$ is the average dnl of the ADC [~0.4 *least significant bit* (lsb) typically]

$v_{\text{noise}_{\text{RMS}}}$ is the thermal noise in lsb units

$b$ is the number of ADC bits

## 10.5.12 Phase Noise

Although synthesizer phase noise is similar to jitter on the encode clock, it has slightly different effects on the receiver, but in the end, the effects are very similar. The primary difference between jitter and phase noise is that jitter is a wideband problem with uniform density around the sample clock and phase noise is a non-uniform distribution around a local oscillator that usually gets better the farther away from the tone. As with jitter, the less phase noise the better.

Since the LO is mixed with incoming signal, noise on the LO will affect the SOI. The frequency domain process of the mixer is convolution (the time domain process of the mixer is multiplication). As a result of mixing, phase noise from the LO causes energy from adjacent (and active) channels to be integrated into the desired channel, which causes an increase in the noise floor. This is called *reciprocal mixing*.

**Example 10.1: Phase Noise.** For this example we assume that a VHF signal is the SOI and the channel spacing is 20 kHz. The phase noise can be expressed as

$$Noise = \int_{f=-0.0125}^{0.0125} X(f)P(f)df \tag{10.21}$$

where *Noise* is the noise in the SOI channel caused by phase noise, $X(f)$ is the phase noise expressed in non-log format, and $P(f)$ is the spectral density function for the SOI. For this example, we assume that the SOI signal power is –13dBm. Also, we assume that the LO has a phase noise that is constant across the channel (typically the phase noise reduces with carrier offset). Since $X(f)$ is assumed to be constant (PN—phase noise) and the integrated power of a full-scale SOI channel is –13dBm, the noise is given by

$$Noise = PN \times Signal_{\text{adjacent}}$$

or, in log form

$$Noise = PM_{\text{log}} + Signal_{\text{log}}$$
$$= PN + (-13\,\text{dBm})$$
$$PN_{\text{required}} = Noise - (-13\,\text{dBm})$$

Our goal is to require that phase noise be lower than thermal noise. Assuming that noise at the mixer is the same as at the antenna, –131dBm (noise in 20 kHz at the antenna $P_a = k_B TW$) can be used. Thus, the phase noise from the LO must be lower than –118dBm with an offset of 20 kHz.

## 10.5.13 Summary

In this section we have provided a simplified analysis of the primary performance issues associated with the RF and IF sections of a digital receiver, up through and including the ADC.

The material presented here is intended to be an introduction to these topics, with more detail provided in earlier and later chapters.
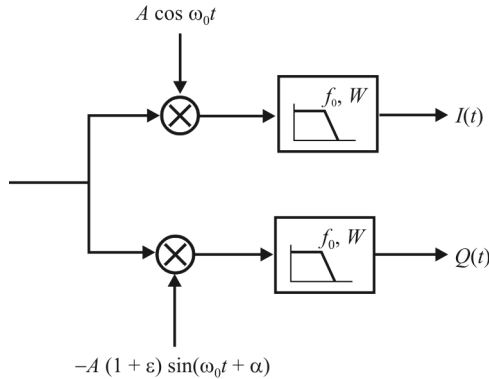
**Figure 10.27** Quadrature downconverter with gain and phase imbalance.

# 10.6 Gain and Phase Imbalance

We have mentioned the inphase and quadrature signal paths in receivers on several occasions in the above discussions. Generating these signal paths in a receiver is a standard way of processing all forms of analog and digital signals in digital receivers. However, separating the processing paths this way raises balancing issues with the analog components involved (digital processing does not have balance problems). We briefly discuss this balancing issue in this section.

Gain and phase imbalance between the *I* and *Q* paths are the cause of crosstalk between the in-phase and quadrature (*I/Q*) components [6]. This, in turn, can result in coupling between the many narrowband channels in an *N*-channel receiver. This spectral coupling can be described compactly by examining the model shown in Figure 10.27. Here, the composite *I/Q* gain and phase imbalances have been assigned to the quadrature term as the amplitude and phase shift of the sinusoid.

We can examine the unbalanced complex sinusoid presented to the mixer pair and compare its spectrum to that of the balanced spectrum. The complex sinusoid

$$g(t) = A[\cos \omega_0 t - j(1+\varepsilon)\sin(\omega_0 t + \alpha)] \qquad (10.22)$$

can be expanded as

$$g(t) = \left\{ \left[ \frac{A}{2} - \frac{A}{2}(1+\varepsilon)\cos\alpha \right] - j\left[ \frac{A}{2}(1+\varepsilon)\sin\alpha \right] \right\} e^{j\omega_0 t}$$

$$+ \left\{ \left[ \frac{A}{2} + \frac{A}{2}(1+\varepsilon)\cos\alpha \right] - j\left[ \frac{A}{2}(1+\varepsilon)\sin\alpha \right] \right\} e^{-j\omega_0 t} \qquad (10.23)$$
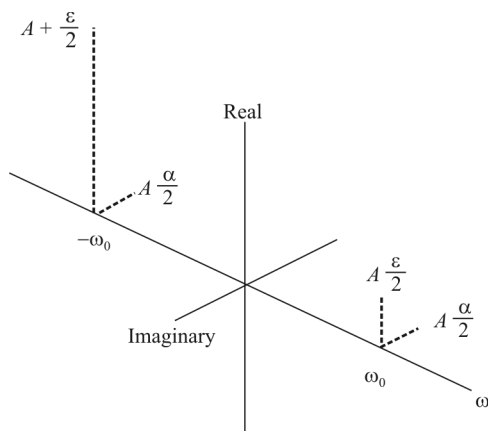
**Figure 10.28** Spectral components of unbalanced complex sinusoid.

to explicitly show the positive and negative frequency components. We can use the small-signal approximation to obtain a simple estimate of the effects of gain and phase imbalance on the positive and negative frequency components of the quadrature mixer signal as

$$g(t) \approx A\left[\frac{\varepsilon}{2} - j\frac{\alpha}{2}\right]e^{j\omega_0 t} + A\left[\left(1 + \frac{\varepsilon}{2} - j\frac{\alpha}{2}\right)\right]e^{-j\omega_0 t} \tag{10.24}$$

Figure 10.28 presents a graphical visualization of these same spectral components.

Besides the obvious coupling between the quadrature components at the same frequency due to phase imbalance, we see a coupling between positive and negative frequencies due to both amplitude and phase imbalance. To achieve an imbalance related spectral image 40 dB below the desired spectral term, each imbalance term must be less than 1% of the desired term. It is difficult to sustain, over time and temperature, gain and phase balance of analog components to better than 1%. The need to achieve extreme levels of *I/Q* balance motivates us to perform the complex conversion process in the digital domain.

# 10.7 Concluding Remarks

Digital receivers are perhaps the most flexible receiver architectures for EW applications. This flexibility is manifest both in design phases as well as after the design is finalized and implemented. EW systems are frequently expected to adapt

to changing target environments unforeseen when originally conceived. Digital topologies can be changed to adjust to these conditions without total redesign of the receiver and frequency simply by software reprogramming.

Digital implementations of receiver functions provide for stability over time, temperature, and other environmental variations, as opposed to their analog counterparts. Their significant shortfall is power consumption that typically is considerably higher than analog architectures.

# References

[1]     Tsui, J., *Digital Techniques for Wideband Receivers*, Norwood, MA: Artech, 1995.

[2]     Tretter, S. A., *Introduction to Discrete-Time Signal Processing,* New York: Wiley, 1976.

[3]     Proakis, J. G., and D. K. Manolakis, *Digital Signal Processing,* 4th Ed., Englewood Cliffs, NJ: Prentice Hall, 2006.

[4]     Oppenheim, A. V., and R. W. Schafer, *Digital Signal Processing*, Englewood Cliffs, NJ: Prentice Hall, 1975.

[5]     Lyons, R. G., *Understanding Digital Signal Processing,* 3rd Ed., Upper Saddle River, NJ: Pearson Education, Inc., 2010.

[6]     Harris, F. J., "On Measuring the Gain and Phase Imbalance and DC Offsets of Quadrature A-to-D Converters with an Adaptive Canceling Filter," *Proceedings 21st Annual Asilomar Conference on Signals, Systems, and Computers*, Pacific Grove, CA, Nov. 2–4, 1981.

# Chapter 11

## Sampling and Analog-to-Digital Converters

## 11.1 Introduction

Rapid advances in the hardware development of ADCs have paved the way for the development of radio receivers using digitization at the IF and, in some cases, at the RF. The constraints placed on these receivers due to the hardware limitations of these devices are discussed in this chapter.

As advances in technology provide increasingly faster and less expensive digital hardware, more of the traditional analog functions of a radio receiver are replaced with software or digital hardware. The ultimate goal in radio receiver design is to directly digitize the RF signal at the output of the receive antenna and hence implement all receiver functions in either digital hardware or software. Trends in receiver design have evolved toward this goal by incorporating digitization more closely to the receive antenna for systems at increasingly higher frequencies and wider bandwidths. As a typical EW system has a requirement to cover broad frequency ranges with wide instantaneous bandwidths, they are a natural application of this technology.

The ADC is a key component in these radio receivers. ADCs most often used for wideband digitization at the RF or IF are organized as shown in Figure 11.1. Key parameters of ADCs are affected by specific ADC circuit elements. For example, accuracy and linearity are primarily determined by the sample-and-hold circuitry, while jitter in the sampling clock can introduce noise in the desired output of the ADC. The quantizer establishes the resolution of the ADC. For a given burst rate, the buffers limit the sustainable throughput.

We begin the discussion in this chapter with the topic of sampling, as that is the function that an ADC is to perform. Analog signals, and all RF signals begin as analog signals even if the underlying modulation is digital, are converted into a digital form by the ADC via sampling the analog signal. This sampling imposes
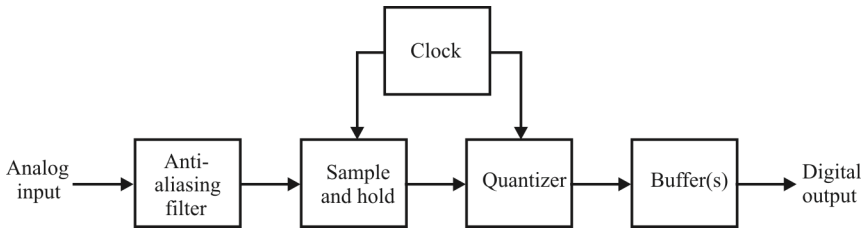
**Figure 11.1** Elements of ADC used for wideband digitization at the RF or IF.

some characteristics onto the digital representations of the signal, such as periodic *power spectral densities* (psds). There are limitations that this sampling must conform to in order to properly represent the analog counterpart.

ADCs and their characteristics, in particular noise performance *and spur-free dynamic range* (SFDR), are discussed in the second part of the chapter.

# 11.2 Wideband Receivers[1]

Wideband receivers are normally used for searching the RF spectrum for energy. Whereas a wideband receiver can stare at a portion of the spectrum indefinitely, in most cases further processing of the signals received is required. This further processing normally deals with only a portion of the signals, dividing the time scale into segments. What happens to the time signals when this is done is illustrated in Figure 11.2. In this case an input signal in the form of a cosine wave at frequency $f_0$ is illustrated; however, Fourier analysis shows that any deterministic periodic signal can be described in terms of sine and cosine functions, so the conclusions are general in nature. Of course, stochastic signals are not deterministic so a different approach is required in that case. Shown at the top of Figure 11.2(b) is the frequency representation of the cosine wave.

The cosine signal is effectively multiplied by a time gate that defines the segment of the signal that is to be processed. For example, an ADC may change this analog signal into digital words over only this time segment for further digital processing. The frequency representation of the time gate is a sinc function shown in the middle of Figure 11.2(b). Since multiplication in the time domain is equivalent to convolution in the frequency domain, the two frequency representations at the top and middle of Figure 11.2(b) are convolved (denoted by *), resulting in the frequency representation of the gated cosine waveform shown at the bottom of Figure 11.2(b). Two sinc regions emerge, located at $\pm f_0$.

---

[1] Much of this section is from [1]. Reprinted with permission.
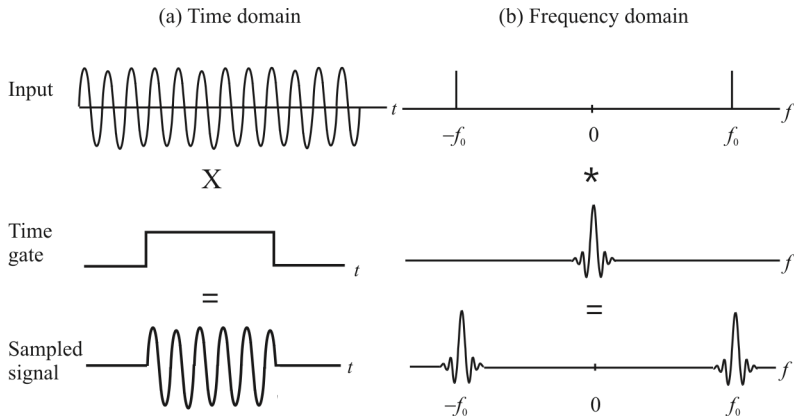
**Figure 11.2** The effects on a signal that is sampled in (a) the time domain are to add sidelobes in (b) the frequency domain. (Source: [1], © Artech House, 2002. Reprinted with permission.)

This illustration is ideal, assuming that the time gate includes an integer number of complete periods of the incoming signal. This would not normally be the case for a searching wideband receiver. The more normal case is illustrated in Figure 11.3, where the input waveform has been expanded for clarity. Only portions of the first and last period are included within the time gate that causes
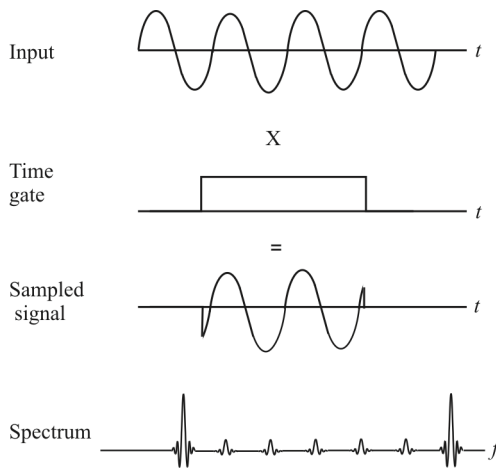


**Figure 11.3** Effects of misalignment of time sampling. (Source: [1], © Artech House, 2002. Reprinted with permission.)
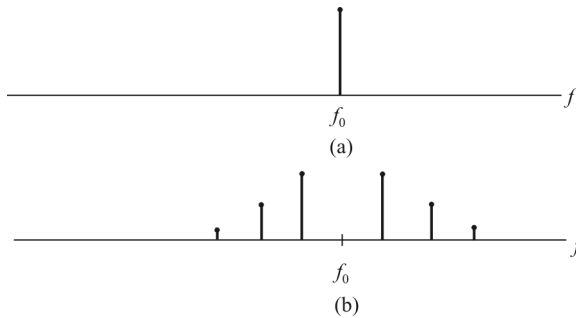
**Figure 11.4** Effects of not sampling the input signal at the proper frequency: (a) spectrum of input signal and (b) its spectrum from incorrect sampling frequency. (Source: [1], © Artech House, 2002. Reprinted with permission.)

portions of the spectrum of the signal to appear at other places in the frequency spectrum.

### 11.2.1 Channelized

Channelized receivers are essentially a bank of fixed tuned (normally narrowband) receivers. The RF spectrum is divided into channels, the bandwidth of which depends on the signal types of interest. For VHF communication channels, the bandwidth is typically 25 kHz, although that is getting narrower.

The implementation of channelized receivers can be in a variety of forms. The TRF receivers described in Chapter 5 can be configured into banks, where each one of the banks covers one channel. Alternately, a digital receiver can be used where one or more Fourier transform points cover each channel.

When the channelized receiver is implemented by taking the Fourier transform, unless the frequency point is precisely at the frequency of the input signal, splitting of the energy in the signal to several points occurs. This is illustrated in Figure 11.4.

## 11.3 Sampling Methods and Analog Filtering

The sampling process is of critical importance in radio receivers using digitization at the RF or IF. The content of the resulting sampled signal waveform is highly dependent on the relationship between the sampling rate employed and the minimum and maximum frequency components of the analog input signal. Some common sampling techniques that utilize a uniform spacing between the samples include Nyquist sampling, oversampling, quadrature sampling, and bandpass
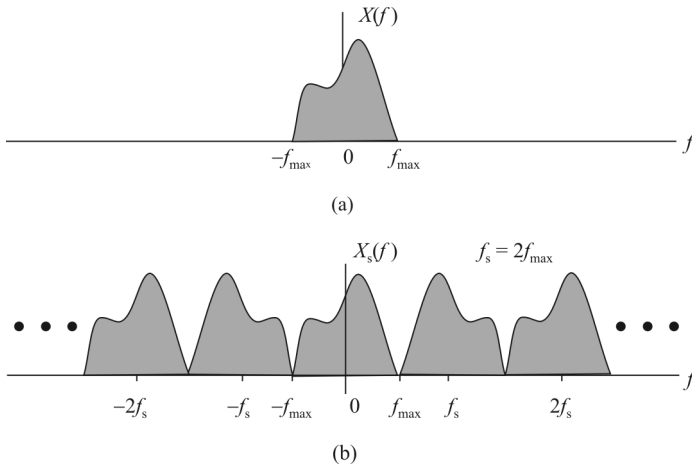
**Figure 11.5** Spectrum of (a) a band-limited continuous analog signal, and (b) the signal sampled at $f_s = 2f_{max}$.

sampling (also called *downsampling* or *direct downconversion*). Sampling techniques with nonuniform spacing between the samples do exist, but they are not widely used and therefore are not considered here. Sampling theory is much more developed for uniform sampling than nonuniform sampling.

Any time a continuous-time analog signal is uniformly sampled, the psd of the original signal is repeated at integer multiples of the sampling frequency (i.e., the psd becomes periodic). This is an inherent effect of sampling and cannot be avoided. This phenomenon is shown graphically in Figure 11.5 (there is a spectral reversal that happens as well). Figure 11.5(a) shows the spectrum of the original analog signal $X(f)$. Figure 11.5(b) shows the spectrum of the sampled signal $X_s(f)$ using a sampling rate of $f_s = 2f_{max}$.

## 11.3.1 Nyquist Sampling

The ability to reconstruct a sampled signal from its samples is dictated by the sampling theorem.

> **Property 11.1: Sampling Theorem (Nyquist).** The general sampling theorem for sampling a band-limited analog signal (a signal having no frequency components above a certain frequency $f_{max}$) requires that the sampling rate be at least two times the highest frequency component of the analog signal $2f_{max}$.
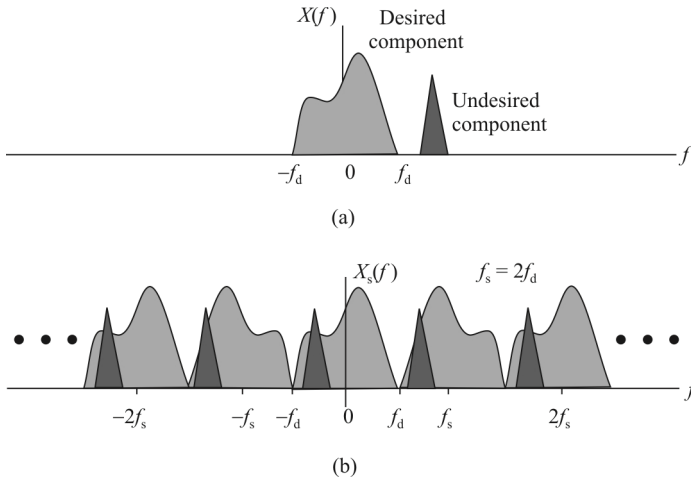
**Figure 11.6** Spectrum of (a) a continuous-time analog signal with a desired and undesired component, and (b) the signal sampled at $f_s = 2f_{max}$.

A sampling rate of two times the highest frequency component of the analog signal is called the *Nyquist sampling rate*. Figure 11.5(b) shows an example of sampling a band-limited signal with a maximum frequency of $f_{max}$ at the Nyquist rate ($f_s = 2f_{max}$). Note that the copies of the spectrum of the analog signal $X(f)$ that are present in the spectrum of the sampled signal $X_s(f)$ do not overlap.

As the sampling rate is increased beyond the Nyquist rate, the copies of the spectrum of the analog signal $X(f)$ that are present in the spectrum of the sampled signal $X_s(f)$ are spread even farther apart. Sampling a band-limited signal at rates equal to or greater than the Nyquist rate guarantees that spectrum overlap (often called *aliasing*) does not occur and that the original analog signal can be reconstructed exactly [2, 3].

### 11.3.1.1 Out-of-Band Energy

Two practical problems arise when sampling at the Nyquist rate: defining what a band-limited signal truly is in a practical sense and analog filtering before the ADC. A theoretically defined analog band-limited signal is a signal with no frequency components above a certain frequency. When considering real signals such as an RF signal at the input of a receiver, however, signals of all frequencies are always present. It is the amplitude of these frequencies that is important. In particular, the relative amplitude of the undesired signal to the SOI determines whether the undesired signal significantly interferes with the SOI. When digitizing an RF or IF signal at the Nyquist rate in a receiver, undesired signals (above one half the sampling rate) of a sufficient amplitude can create spectrum overlap and

distort the SOI, as illustrated in Figure 11.6. Figure 11.6(a) shows the spectrum of the analog input signal with its desired and undesired components. If this signal is sampled at two times the highest frequency in the SOI, the resulting spectrum of the sampled signal $X_s(f)$ is as shown in Figure 11.6(b). Note that spectrum overlap has occurred here (i.e., the spectrum of the undesired signal appears within the spectrum of the SOI). This causes distortion in the reconstructed SOI.

This effect raises an important question: What is the relative amplitude of the signals occurring above one half of the sampling rate at which distortion of the SOI due to spectrum overlap begins to dominate the distortion due to ADC nonlinearities? Nonlinearities in the ADC cause spurious responses in the ADC output spectrum. Distortion due to spectrum overlap dominates distortion due to ADC nonlinearities when the undesired signals appearing in the first Nyquist band[2] due to spectrum overlap exceed the largest spurious response of the ADC due to nonlinearities. Therefore, undesired signals appearing in the first Nyquist band due to spectrum overlap must be lower in power than the largest spurious response of the ADC. This can be quite a stringent requirement.

Whether the undesired signal interferes too much with the SOI depends on many variables, but the fundamental issue is the type of signal. Distortion of analog communication signals (AM, FM, and so forth) can frequently be tolerated better than digital signals [4]. Digital signal quality requirements are often dictated by the tolerable BER, which, in turn, is normally controlled by the SNR of the signal.

## 11.3.1.2 Realizable Anti-Aliasing Filters

Analog filtering before the ADC stage is intimately related to the definition of band limiting. Where the definition of band limiting deals with the content of the signals that may be present, analog filtering before the ADC represents a signal processing stage where certain frequencies can be attenuated. It is important to know both the signals that can be present before filtering and the amount of attenuation that the filter offers for different frequencies. With knowledge of both of these, the true spectrum of the signal to be digitized can be determined.

Sampling at the Nyquist rate presents a large and often impractical demand on the filter used before digitization (the anti-aliasing filter). Ideally, an anti-aliasing filter placed before an ADC would pass all of the desired frequencies up to some cutoff frequency and provide infinite attenuation for frequencies above the cutoff frequency. Then sampling at the Nyquist rate would be two times the cutoff frequency and no spectrum overlap would occur. Unfortunately, practically realizable filters cannot provide this type of brick-wall response. The attenuation of real filters increases more gradually from the cutoff frequency to the stopband.

---

[2] The "first" Nyquist band is from DC to $f_s/2$. The other bands will be discussed in the section on bandpass sampling.
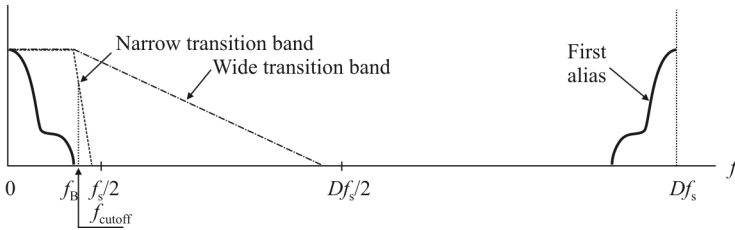
**Figure 11.7** Oversampling and anti-aliasing filters.

Therefore, for a given cutoff frequency on a real filter, sampling at two times this cutoff frequency will produce some spectrum overlap. The steeper the transition from the passband to the stopband and the more attenuation in the stopband, the less the sampled signal will be distorted by spectrum overlap. In general, more complicated filters are required to achieve steeper transitions and higher attenuation in the stopband. Therefore, more complicated filters are required to reduce the distortion in the sampled signal due to spectrum overlap for a given sampling rate. Limitations on the practical implementation of analog filters make high-order, steep-rolloff filters difficult to realize. Also, as the steepness of the rolloff is increased, the phase response tends to become more nonlinear. This can create distortion of the SOI since different frequencies within a signal can be delayed in time by different amounts (i.e., phase shifted by amounts not proportional to frequency).

## 11.3.1.3 Oversampling Eases Requirements on the Anti-Aliasing Filter

Sampling at rates greater than the Nyquist sampling rate is called *oversampling*. One of the benefits of oversampling is that the copies of the spectrum of the analog signal $x(t)$ that are present in the spectrum of the sampled signal $x[n]$ become increasingly separated as the sampling rate is increased beyond the Nyquist rate. For an analog signal with a given frequency content and a given anti-aliasing filter with a cutoff frequency of $f_{cutoff}$, sampling at the Nyquist rate (two times the cutoff frequency) produces a certain amount of distortion due to spectrum overlap. When sampling at a higher rate, a simpler anti-aliasing filter with a more gradual transition from passband to stopband and less stopband attenuation can be used without any increase in the distortion due to spectrum overlap (Figure 11.7). Therefore, oversampling can lower the requirements of the anti-aliasing filter. The tradeoff, of course, is that increasingly faster ADCs are required to digitize relatively low-frequency signals.

11.3.1.4 Quadrature Sampling Reduces Required Sampling Rate

In quadrature sampling the signal to be digitized is split into two signals. One of these signals is multiplied by a sinusoid to downconvert it to a zero center frequency and form the in-phase component of the original signal. The other signal is multiplied by a 90° phase-shifted sinusoid to downconvert it to a zero center frequency and form the quadrature phase component of the original signal. Each of these components occupies only one half of the bandwidth of the original signal and can be sampled at one half the sampling rate required for the original signal. Therefore, quadrature sampling reduces the required sampling rate by a factor of two at the expense of using two phase-locked ADCs instead of one.

**11.3.2 Bandpass Sampling**

Sampling at rates lower than $2f_{max}$ can still allow for an exact reconstruction of the information content of the analog signal if the signal is a bandpass signal. An ideal bandpass signal has no frequency components below a certain frequency $f_L$ and above a certain frequency $f_U$. For a bandpass signal the minimum requirements on the sampling rate to allow for exact reconstruction are that the sampling rate be at least two times the bandwidth, $W$, of the signal.

When using uniform sampling, which is normally the case, the signal can be correctly reconstructed as long as the bandpass property is satisfied.

> **Property 11.2: Bandpass Sampling.** The classical bandpass property for uniform sampling states that a signal can be reconstructed if the sampling rate is at least $f_s^{min} = 2f_U / n$, where $n$ is the largest integer within $f_U/W$, denoted by[3] $n = \lfloor f_U / W \rfloor$.

To ensure that spectrum overlap does not occur, when sampling rates are between two times the bandwidth of the bandpass signal and two times the highest frequency in the bandpass signal, the sampling frequency $f_s$ must satisfy

$$\frac{2f_U}{k} \le f_s \le \frac{2f_L}{k-1}$$

where $k$ is restricted to integer values that satisfy [3]

---

[3] $\lfloor \cdot \rfloor$ is known as the *floor function*.
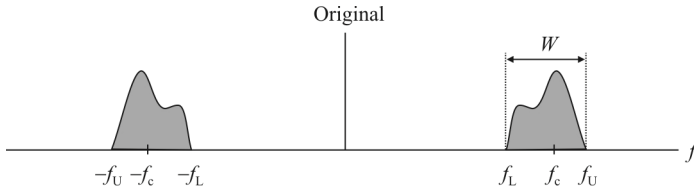
**Figure 11.8** Baseband real spectrum.

$$2 \leq k \leq \frac{f_U}{f_U - f_L}$$

and

$$f_U - f_L \leq f_L$$

Bandpass sampling can be used to downconvert a signal from a bandpass signal at an RF or IF to a bandpass signal at a lower IF. Since the bandpass signal is repeated at integer multiples of the sampling frequency, selecting the appropriate spectral replica of the original bandpass signal provides the down-conversion function.

Bandpass sampling holds promise for receivers that digitize directly at the RF or IF, since the desired input signals to receivers are normally bandpass signals. Theoretically, bandpass sampling allows sampling rates to be much lower than those required by sampling at two or more times the highest frequency content of the bandpass signal. This means that ADCs with slower sampling rates (and therefore higher performance, lower power consumption, or lower cost) may be used. An important practical limitation, however, is that the ADC must still be able to effectively operate on the highest frequency component in the signal. This specification is usually given as the analog input bandwidth for the ADC. Conventional ADCs are designed to operate on signals having maximum frequencies of one half the sampling rate. Performance of the ADC typically degrades with increasing input frequency. When using ADCs for bandpass sampling applications, the specifications of the converter must be examined to determine the behavior at higher frequency inputs. In addition, when bandpass sampling, stringent requirements on analog bandpass filters (steep rolloffs) are needed to prevent distortion of the SOI from strong adjacent channel signals.

We consider two cases; starting from a real-valued bandpass analog signal, the resulting sample stream is either real-valued or complex-valued.

## 11.3.2.1 Real Subsampling

Consider the real-valued bandpass signal, bandwidth $W$, center frequency $f_c$, upper band-edge $f_U = f_c + W/2$, and lower band-dge $f_L = f_c - W/2$, as shown in Figure
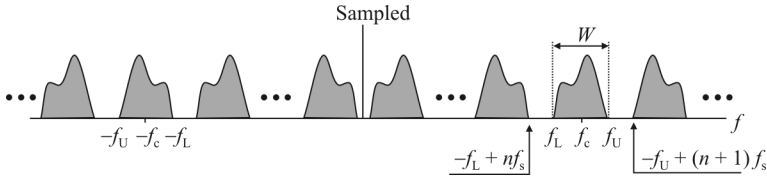
**Figure 11.9** Sampled spectra.

11.8. Sampling this signal at some rate $f_s$ results in a signal where the previous spectrum is replicated at integer multiples of the sampling rate. With $f_s < 2f_U$, aliasing will take place but as long as the aliasing components don't fall on top of each other, distortion is avoided.

So an example spectrum of the sampled signal could look like Figure 11.9 when there is no harmful aliasing and yet $f_s < 2f_U$. From Figure 11.9 we can see the regions of allowable sampling rates. These are in general of the form

$$\frac{2f_c + W}{n+1} \le f_s \le \frac{2f_c - W}{n+1} \tag{11.1}$$

where

$$0 \le n \le \left\lfloor \frac{2f_c - W}{2W} \right\rfloor \tag{11.2}$$

As we see, the possible values of the sampling rate depend on both the bandwidth $W$ and the center frequency $f_c$. For $n = 0$, we get $f_s \ge 2f_c + W = 2(f_c + W) = 2f_U$, which is the traditional Nyquist sampling property (the upper limit becomes infinity). For $n > 0$ we are really sampling at a lower frequency than given by the traditional Nyquist theorem. For $n > 0$, aliasing does occur but with given values of $f_s$, not on top of the SOI band (no harmful aliasing). The lowest possible sampling rate is in general given by

$$f_s \ge \frac{f_c + W}{n_{max} + 1} = \frac{2f_c + W}{\left\lfloor \dfrac{2f_c - W}{2W} \right\rfloor + 1} = \frac{2f_c + W}{\left\lfloor \dfrac{2f_c - W}{2W} + 1 \right\rfloor} = \frac{2f_c + W}{\left\lfloor \dfrac{2f_c + W}{2W} \right\rfloor} \tag{11.3}$$

The ultimate sampling rate $f_s = 2W$ is utilizable if and only if $(2f_c + W)/2W$ is an integer because then and only then $\lfloor (2f_c + W)/2W \rfloor = (2f_c + W)/2W$.
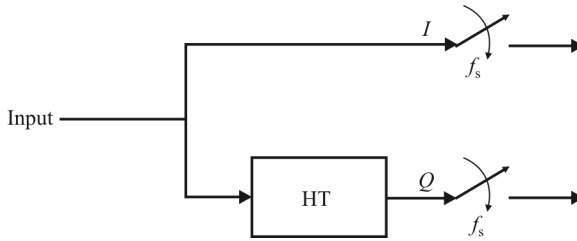
**Figure 11.10** Hilbert transformer for complex sampling.

> **Example 11.1:** $f_c = 20$ kHz and $W = 10$ kHz, so
>
> $$0 \le n \le \lfloor (40-10)/20 \rfloor = \lfloor 1.5 \rfloor = 1$$

and the possible values for $f_s$ are

$$n = 0: \qquad 50 \text{ kHz} \le f_s \le \infty$$
$$n = 1: \qquad 25 \text{ kHz} \le f_s \le 30 \text{ kHz.}$$

## 11.3.2.2 Complex Subsampling

As we saw in Chapter 2, instead of sampling the real-valued signal directly, we can sample the corresponding analytic signal. So, based on Figure 2.3, the sampling structure looks like that in Figure 11.10. (HT denotes the Hilbert transformer.) Now since the analytic signal is free from negative frequency components, sampling frequency of $f_s = W$ (or any rate above that) is always (independent of the center frequency $f_c$) sufficient to avoid harmful aliasing.

Some example spectra with the same input signal as in the previous subsection are shown in Figure 11.11. In Figure 11.11(a) $f_s = W$, in 11.11(b) $f_s > W$, and in 11.11(c) $f_s < W$. In the first two cases the signal can be flawlessly recovered (theoretically), while in the third case the spectra overlap. There is no hope to recover the original signal in that case.

It is important to note that if the center frequency $f_c$ is an integer multiple of the sample rate $f_s$ (i.e., $f_s = f_c / k$) as depicted in Figure 11.11, the center frequency of the $k$th spectral replica will coincide with zero frequency and a direct bandpass-to-lowpass transformation is obtained. This is easy to understand based on spectral interpretations but can also be seen as follows. The real bandpass input, say $x(t)$, can be written in terms of its baseband equivalent $z(t)$ as

$$x(t) = \text{Re}\left\{ z(t) e^{j\omega_c t} \right\} = \frac{1}{2} z(t) e^{j\omega_c t} + \frac{1}{2} z^*(t) e^{-j\omega_c t} \tag{11.4}$$
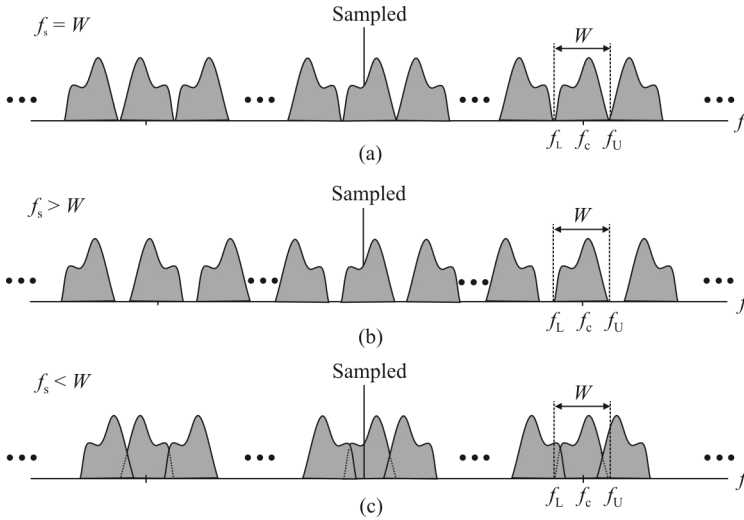
**Figure 11.11** Sampled spectra. The center frequency $f_c$ is an integer multiple of the sample rate $f_s$ (i.e., $f_s = f_c / k$) so the center frequency of the $k$th spectral replica coincides with zero frequency and a direct bandpass-to-lowpass transformation is obtained. (a) $f_s = W$, (b) $f_s > W$, and (c) $f_s < W$.

Then the corresponding analytic signal is of the form

$$x(t) + j x_{\text{HT}}(t) = \frac{1}{2} z(t) e^{j\omega_c t} + \frac{1}{2} z^*(t) e^{-j\omega_c t} + j\left[ -j\frac{1}{2} z(t) e^{j\omega_c t} + j\frac{1}{2} z^*(t) e^{-j\omega_c t} \right] \quad (11.5)$$

Thus, sampling at $f_s = f_c / k$ (with $k$ integer) results in

$$x[nT_s] + j x_{\text{HT}}[nT_s] = z[nT_s] e^{j\omega_c n T_s} = z[nT_s] e^{j2\pi f_c n T_s} = z[nT_s] e^{j2\pi n k} = z[nT_s] \quad (11.6)$$

which are indeed just the samples of the baseband equivalent.

### 11.3.2.3 Guard Bands

It is typical to implement guard bands on each side of a bandpass filter to minimize aliasing. The requirements on these guard-bands are briefly discussed here [5].

 The relative precision required of the sampling oscillator is depicted in Figure 11.12 as the line marked with minimum guard band and the relative precision is proportional to $W / f_U$. The positions of a typical crystal and RC oscillator are
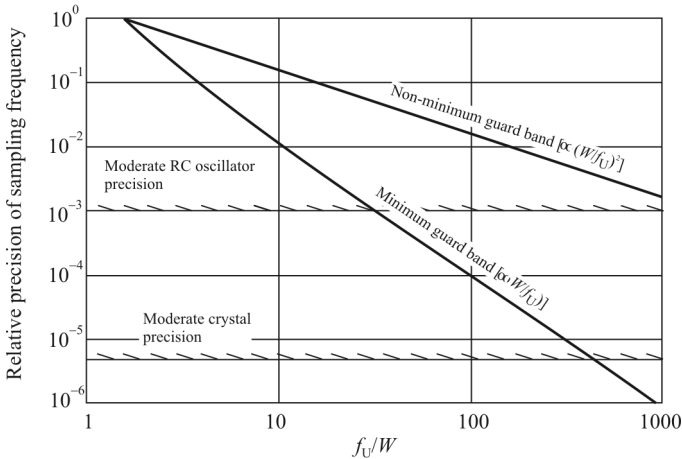
**Figure 11.12** Relative precision of the sampling frequency.

indicated to give a feel for practical requirements. With the inclusion of larger guard bands, the line marked nonminimum guard band is proportional to $(W / f_{U})^2$ and it runs above the minimum guard band line.

The lower line represents operating with the minimum allowed set of sampling rates and the maximum available guard-band. The guard band width decreases with increasing $n$, where $n$ is the largest integer within $f_{U}/W$. and the line is $\sim O(1/n)$. If the relative guard band is now held at a constant size, then the relative precision of the sampling rate becomes $\Delta f_s / 2W \approx W_{GT} / W \times 1 / n.$ This demonstrates the tradeoff between the precision required of the sampling rate and the guard band size. For practical situations, a modest increase in the sampling rate permits a realizable precision requirement.

In addressing sampling rate variation, it must be borne in mind that so far the discussion has been limited to avoiding aliasing in the sampling process. Exact (re)construction of the bandpass analog waveform requires exact implementation of the sampling parameters.

# 11.4 Effects of Quantization Noise, Distortion, and Receiver Noise

## 11.4.1 Introduction

The performance of the ADC has a considerable impact on the performance of a digital receiver that uses direct IF sampling. The error sources of the ADC can be
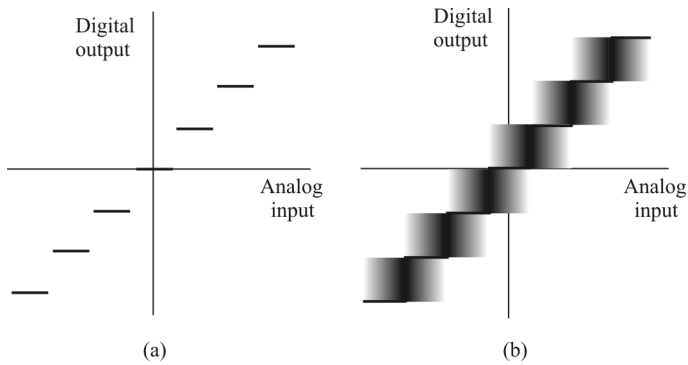
**Figure 11.13** ADC transfer function: (a) ideal ADC transfer function and (b) realistic ADC transfer function. Code-transition noise (input-referred noise) and its effect on ADC transfer function.

divided into the categories of static and dynamic. In this section the quantization noise, jitter noise, and spurious component of ADCs are introduced, and their effects on dynamic range of the digital receiver are considered. The methods to improve the performance of digital receivers are discussed.

## 11.4.2 ADC Transfer Function

The transfer function of an ideal ADC is shown in Figure 11.13(a). As the analog input voltage is increased, the ADC maintains a constant output code until a transition region is reached, at which point it instantly jumps to the next value, remaining there until the next transition region is reached [shown in Figure 11.13(a)]. A theoretically perfect ADC has zero *code-transition noise* and a transition region width equal to zero [6].

## 11.4.3 Input-Referred Noise

Practical ADCs deviate from ideal ADCs in many ways. Input-referred noise (a.k.a. code-transition noise) is certainly a departure from the ideal, and its effect on the overall ADC transfer function is shown in Figure 11.13(b). A practical ADC has a certain amount of code transition noise and therefore a finite transition region width. Figure 11.13(b) shows a situation where the width of the code transition noise is approximately one lsb peak-to-peak.

Internally, all ADCs produce a certain amount of noise due to resistance and $k_B T/C$ noise.[4] This noise, present even for DC input signals, accounts for the code-

---

[4]  $k_B T/C$ noise is noise caused by capacitors in a network. $k_B$ is Boltzmann's constant, $k_B = 1.38 \times 10^{-23}$.

transition noise, generally referred to as input-referred noise, similar to the concept
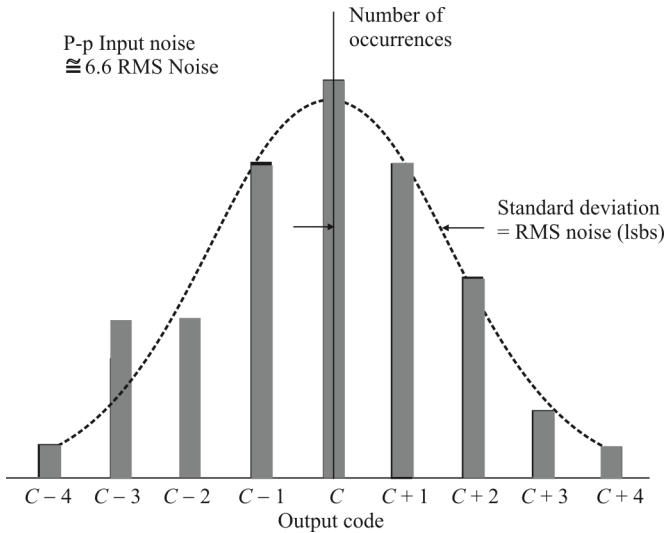


**Figure 11.14** ADC noise distribution.

associated with LNAs discussed in Chapter 3, where the noise is reflected to the input and the amplifier is considered noise free. Input-referred noise is most often characterized by examining the histogram of a number of output samples, while the input to the ADC is held constant at a DC value (typically zero volts). The output of most high-speed or high-resolution ADCs is a distribution of codes, typically centered around the nominal value of the DC input. This is illustrated in Figure 11.14.

## 11.4.4 Theoretical Signal-to-Noise Ratio

For receiver applications where the amplitude of the SOI falls within the ADC's *full scale range* (FSR), and the bandwidth of the SOI is equal to the Nyquist bandwidth, the SNR of an ADC can be calculated [7]. The theoretical SNR of ADCs is generally thought of as $6b$ (dB), where $b$ is the number of bits of resolution of the ADC. A more precise expression providing the maximum possible theoretical SNR can be derived based on some assumptions about the noise and the input signal.

First, it is assumed that the noise present is due to quantization error only. The amplitude of this quantization noise is assumed to be a random variable uniformly distributed over one quantization step. Assuming a sinusoidal input with an amplitude equal to the FSR of the ADC, the maximum possible theoretical SNR is given by (7.11) [8, 9]. The commonly stated theoretical SNR of $6b$ (dB) is an

approximation to this equation when $f_s = 2f_{max}$ and the 1.76dB is neglected. From this equation, note that as the sampling frequency is increased beyond the Nyquist rate of $2f_{max}$, the SNR increases. This occurs because the quantization noise power, which is fixed and independent of bandwidth, is spread out over an increasingly wider band as the sampling frequency is increased. This lessens the amount of the quantization noise that falls within the first Nyquist band (DC to $f_s/2$). Consequently, this means that oversampling increases the maximum possible SNR. Such oversampling is sometimes used to realize a greater maximum SNR than at first appears possible. An 8$b$ ADC, with a sampling rate of 20 Msps, for example, can provide 68 dB rather than 48dB of maximum SNR for 100 kHz signals in the passband if appropriate digital filtering is used to recover the 100 kHz signal.

### 11.4.5 Practical Specifications for Real ADCs

The SNR in a real ADC can be determined by measuring the residual error. Residual error is the combination of quantization noise, random noise, and nonlinear distortion (i.e., all undesired components of the output signal from the ADC). The residual error for an ADC is found by using a sinusoidal input into the ADC. An estimate of the input signal is subtracted from the output of the ADC, and the remaining signal is the residual error. The mean squared power of the residual error is then computed. The SNR is then found by dividing the mean squared (MS) power of the input signal by the MS power of the residual error.

A specification sometimes used for real ADCs instead of the SNR is the effective number of bits. This specification is defined as the number of bits required in an ideal ADC so that the MS noise power in the ideal ADC equals the MS power of the residual error in the real ADC.

### 11.4.6 ADC Noises

The ADC noises impact negatively on the performance of receiver systems. We describe the quantization noise and jitter noise in analog-to-digital conversion and the limitations of these noises on the SNR of a digital receiver in this section.

#### 11.4.6.1 Quantization Noise

Quantization is a process to divide a signal into a set of discrete levels (as opposed to discretization, which divides the time into discrete values and has different noise error called *jitter*). This process will introduce a quantization error $\varepsilon$, the difference between the signal level and the nearest quantization level. In practical applications, the amplitude range of the input signal is much wider than the quantization step $q$, and thus error may be assumed to have uniform distribution. If the ADC's input signal is periodic, the quantization error is also periodic. This

error results in harmonic distortion. To reduce this harmonic distortion the technique called *dithering* is used. For a periodic input signal, dither added to the ADC spreads the energy in the harmonic bins into random noise, thus smoothing the spurious components. The MS quantization noise power of an ideal uniform quantizer may be calculated as

$$\overline{\varepsilon}^2 = \frac{1}{q} \int_{-q/2}^{q/2} x^2 dx = \frac{q^2}{12} \tag{11.7}$$

From (10.11), we know that for a given signal with bandwidth $W$, increasing the oversampling ratio results in a uniform spreading of the quantization noise power over the wider first Nyquist zone (which has width of $f_s/2$). A digital filter may be employed subsequent to the ADC to filter out all noises that fall outside the filter bandwidth $W$, thereby reducing the noise power of quantization and any other noise source falling outside of the bandwidth $W$, resulting in an improvement of SNR. The SNR improvement or processing gain due to oversampling and subsequent filtering may be computed as $10\log_{10}\left(f_s/2W\right)$, which is the source of the third term on the rhs of (10.11). We can see that if the sampling frequency is doubled, a 3dB processing gain will be realized. The dynamic range of the receiver with digital signal processing will increase 3dB.

11.4.6.2 Jitter Noise

Besides being limited by the quantization step size (resolution), the SNR of the ADC is also limited by aperture jitter [10]. *Aperture jitter* is the variation in time of the exact sampling instant. Aperture jitter can be caused externally by jitter in the sampling clock or internally since the sampling switch does not open at precise times. Aperture jitter causes a phase modulation of the sampled signal and thus results in an additional noise component in the sampled signal [11]. The maximum analog input frequency of the ADC is limited by this aperture jitter since the SNR due to aperture jitter degrades as the input frequency increases. To achieve required noise performance, aperture jitter on the sub-picosecond level is often required when performing RF/IF sampling. The predominant mechanism limiting high SNR at very high-input frequencies in sampled systems is the aperture jitter.

There are two sources that generate jitter: one is the variance of the aperture delay—that is, aperture jitter—and the other is the sampling clock jitter. The *aperture jitter* is the random fluctuations in the ADC aperture time about the nominal ADC aperture time. *Clock jitter* means random fluctuations in the clock period about the nominal clock period. The compete jitter contribution may be represented as

$$\sigma_{\text{jitter}_{\text{RMS}}} = \sqrt{\sigma_{\text{ja}}^2 + \sigma_{\text{jclk}}^2} \tag{11.8}$$
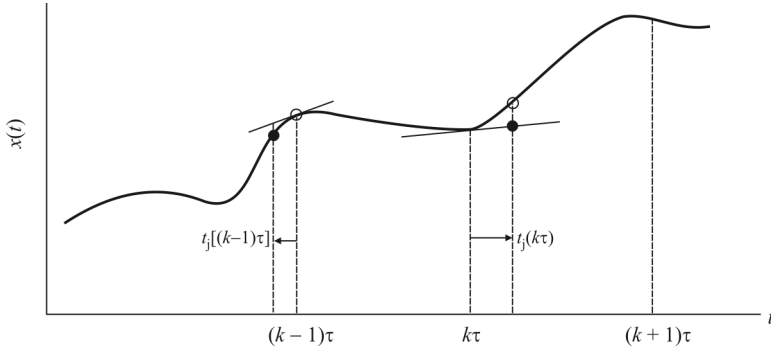


**Figure 11.15** ADC linear approximations.

where

$\sigma_{\text{aj}}$ is the aperture jitter standard deviation

$\sigma_{\text{jclk}}$ is the sampling clock jitter standard deviation

To derive the expression for the SNR, the autocorrelation function of the sampled signal $y$ is calculated using the linear approximation illustrated in Figure 11.15. The sampling instants for an ideal clock of period $T_s$ are indicated with $(k - 1)T_s$, $kT_s$, and $(k + 1)T_s$. Note that we assume $t_j$ to be a time-discrete random variable, so that every sampling instant has its own $t_j(kT_s)$, two of which are included in Figure 11.15. The values of this random variable can be positive or negative as illustrated. The linear approximation used here is the first-order Taylor expansion, which results in replacing the real sampled values (open circles) with the values lying on the tangent to $x(mT_s)$, $m = k - 1$, $k$ at the time instant $(k - 1)T_s - t_j[(k - 1)T_s]$, and $kT_s + t_j(kT_s)$, (filled circles), respectively. This is a feasible approximation if the input signal $x(t)$ is assumed to be smooth enough to admit a local derivative and $t_j \ll 1/f_{\text{max}}$, where $f_{\text{max}}$ is the maximum frequency component of the input signal $x(t)$. These conditions are usually very well satisfied in practical applications.

Calculation of the autocorrelation function of $x$, denoted by $r_x(T_s)$, yields the expression for the SNR due to clock jitter of [10]

$$\gamma = 10 \log_{10}\left( -\frac{r_x(0)}{r_x''(0)r_{t_j}(0)} \right) \text{ dB} \tag{11.9}$$

where $r_x''(0)$ is the second time derivative of $r_x(\tau)$ evaluated at $\tau = 0$.

Therefore, we can determine the SNR of the A/D conversion and the consequent requirements on the jitter of the sampling clock by simply determining the autocorrelation $r_x$, by applying an inverse Fourier transform to the input signal spectrum, and then using this result in (11.9).

From (11.9) we can see that, with the linear approximation, the SNR due to the jitter of the sampling clock depends on the variance of the timing jitter $t_j$ [if $t_j$ has zero mean, then $r_{t_j}(0) = \sigma_{t_j}^2$] and on the second time derivative of the autocorrelation function of the input signal. Expression (11.9) quantifies the intuitive fact that the sampling of slowly varying signals is less affected by the jitter of the sampling clock. Indeed in statistical terms, the autocorrelation function of those signals is somewhat flat around the zero value, thus decreasing the denominator of (11.9) and increasing the SNR.

We can conclude that in the time domain, the SNR is independent of the autocorrelation function of the jitter, as long as $r_{t_j}(0)$ stays constant. In the frequency domain this means that the SNR is independent of the spectral distribution of the jitter, as long as the total energy of the spectrum $r_{t_j}(0)$ is constant. A sinusoidal signal with frequency equal to 0.1 sampled with a clock having period 1 affected first by white noise jitter and then by a jitter sinusoidally modulated at different frequencies (from 0 to the Nyquist value 0.5) was simulated. In both cases, the value $r_{tj}(0)$ was the same. The SNR is illustrated in Figure 11.16; the dashed line corresponds to the white noise jitter, and the solid line to the sinusoidal jitter at various frequencies. As we can see, there is no difference in the SNR due to the different spectral distribution of the jitter.

**Example 11.2: Sinusoidal Input.** The autocorrelation function for $x(t) = A\sin(\omega t)$ is

$$r_x(mT_s) = \frac{A^2}{2}\cos(\omega m T_s) \tag{11.10}$$

and the second derivative is

$$r_x''(mT_s) = -\frac{\omega^2 A^2}{2}\cos(\omega m T_s) \tag{11.11}$$

By substitution in (11.9), we find the well-known formula for the aperture jitter SNR in sampling sinusoidal signals
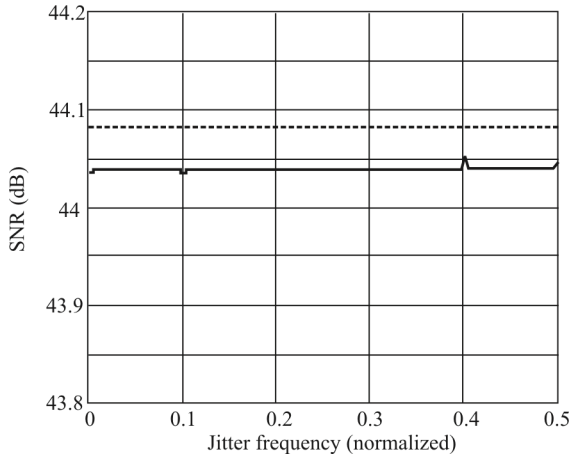
**Figure 11.16** SNR due to jitter with different power spectra: white noise jitter (dashed line), sinusoidal jitter at various frequencies (solid line). The frequency of the sampled sinusoid is 0.1, the sampling frequency is 1.

$$\gamma = 20 \log_{10} \left( \frac{1}{\omega \sigma_{\text{jitter}_{\text{RMS}}}} \right) \quad \text{dB} \tag{11.12}$$

The following example, while describing a useful case, is particularly illustrative of these points.

> **Example 11.3: Random Signal with Rectangular Power Spectrum.** Suppose that $x$ is an arbitrary random signal with the only restriction that its psd is uniform on $(-f_c, f_c)$ (Figure 11.17). The power spectrum can be written as
>
> $$S_x(f) = \text{rect}\left( \frac{f}{2f_c} \right) \tag{11.13}$$
>
> Then, by inverse Fourier transform of (11.13), the autocorrelation $r_x(t)$ and then its second time derivative $r_X''(0)$ can be found. The inverse Fourier transform of (11.13) is given by
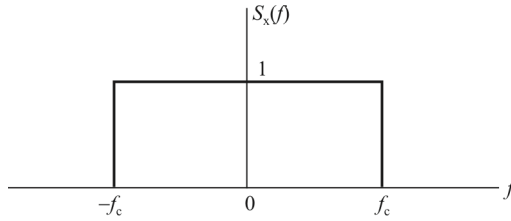
**Figure 11.17** Rectangular power spectrum for Example 11.3.

$$r_x(t) = 2f_c \frac{\sin(\omega_c t)}{\omega_c t} \tag{11.14}$$

so that

$$r_x''(t) = -\frac{\sin(\omega_c t)(\omega_c^2 t^2 - 2) + 2\omega_c t \cos(\omega_c t)}{\pi t^3} \tag{11.15}$$

Using limit principles, (11.15) can be evaluated at $t = 0$ as can the indeterminate form that results from (11.14). Substituting those result into (11.9) yields

$$\gamma = 10 \log_{10}\left(\frac{3}{\omega_c^2 r_{rj}(0)}\right) = 20 \log_{10}\left(\frac{\sqrt{3}}{\omega_c \sigma_{jitter_{RMS}}}\right) \tag{11.16}$$

11.4.6.3 Phase Noise

It is well known that phase noise in oscillators and clocks becomes one of the limiting degradations in modern receiving systems.

*Phase Jitter in Sampled Data Systems*

The easiest way to calculate the SNR degradations incurred by phase noise in a sampled data system is to convert phase noise to phase jitter. This is most easily accomplished by recognizing that a time delay is the same as a phase delay at a given frequency. Extending this concept and writing it in terms of noise power yields

$$\sigma_\theta^2 = \omega_{clk}^2 \sigma_\tau^2 \tag{11.17}$$
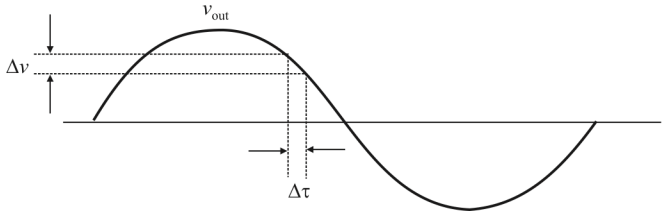
**Figure 11.18** Noisy clock.

where

$\sigma_\theta$ is the phase noise in RMS radians

$\sigma_\tau$ is the phase jitter in RMS seconds

$\omega_{clk}$ is the clock frequency in rps

For a given jitter error, a higher frequency signal will have more phase error. The term $\sigma_\theta$ is the total integrated phase noise of the clock and defines the clock SNR by

$$\gamma_{clk} = -10\log_{10}\sigma_\theta^2 \qquad (11.18)$$

Thus, (11.17) relates the total integrated phase noise, or clock SNR, to the total jitter in the clock. Phase noise and clock jitter are two different ways to look at the same phenomenon.

We use Figure 11.18 as an aid to determine how noise on a clock generates an error in the sampled data. From this it is seen that

$$\Delta v(t) = \Delta t v'_{out}(t) \qquad (11.19)$$
$$\mathcal{E}\{\Delta v^2(t)\} = \mathcal{E}\{\Delta t^2 v'^2_{out}(t)\} \qquad (11.20)$$

If we assume that $\Delta v$ and $\Delta t$ have zero means and are independent, then

$$\sigma_{err}^2 = \sigma_t^2 \mathcal{E}\{v'^2_{out}\} \qquad (11.21)$$

where $\sigma_t^2$ is in (RMS seconds)$^2$. From this we see that the noise power is a function of the jitter power and the power in the signal derivative.

The SNR of a signal sampled with a jittery clock is defined as

$$\gamma = \frac{\text{power in signal}}{\text{power in noise}} = \frac{\sigma_{\text{out}}^2}{\sigma_{\text{err}}^2} = \frac{1}{\sigma_t^2} \frac{\mathcal{E}\{v_{\text{out}}^2(t)\}}{\mathcal{E}\{v_{\text{out}}'^2(t)\}} \tag{11.22}$$

**Example 11.4: Single Signal Receiver.** For a single sine wave,

$$v_{\text{out}}(t) = A \sin \omega_0 t \tag{11.23}$$

$$v_{\text{out}}'(t) = A \omega_0 \cos \omega_0 t \tag{11.24}$$

Therefore,

$$\mathcal{E}\{v_{\text{out}}^2(t)\} = \text{power in } v_{\text{out}}(t) = \frac{A^2}{2} \tag{11.25}$$

$$\mathcal{E}\{v_{\text{out}}'^2(t)\} = \text{power in } v_{\text{out}}'(t) = \frac{\omega_0^2 A^2}{2} \tag{11.26}$$

Using (11.22),

$$\gamma = \frac{1}{\sigma_t^2} \frac{A^2/2}{\omega_0^2 A^2/2} = \frac{1}{\sigma_t^2} \frac{1}{\omega_0^2} \tag{11.27}$$

$$\gamma = \frac{1}{4\pi^2 f_0^2 \sigma_t^2}, \qquad \text{for a single-signal system} \tag{11.28}$$

This is the standard SNR equation for a single sine wave sampled by a clock with jitter and can be found in many publications.

Intuitively what is happening is that higher frequency signals have larger slew rates. This results in larger voltage changes as the sample time changes. It should be remembered that quantization noise and thermal noise must also be added to this to obtain the total noise out of a data converter.

**Example 11.5: Multisignal Receivers.** Extending this to a multisignal case is a simple matter. Using the same procedure as before with $v_{\text{out}}$ defined as a summation of $n$ equal amplitude sine waves,

$$\mathcal{E}\{v_{\text{out}}^2(t)\} = \frac{nA^2}{2} \tag{11.29}$$

$$\mathcal{E}\{v'^2_{\text{out}}(t)\} = \frac{A^2(\omega_1^2 + \omega_2^2 + \cdots + \omega_n^2)}{2} \tag{11.30}$$

$$\gamma = \frac{1}{\sigma_t^2} \frac{nA^2/2}{A^2(\omega_1^2 + \omega_2^2 + \cdots + \omega_n^2)/2} = \frac{1}{\sigma_t^2} \frac{n}{\omega_1^2 + \omega_2^2 + \cdots + \omega_n^2} \tag{11.31}$$

$$= \frac{n}{4\pi^2 \sigma_t^2 \sum\limits_n f_i^2} \tag{11.32}$$

This is relative to the entire signal, $v_{\text{out}}$. When referenced to only one of the signals, the SNR becomes

$$\gamma = \frac{1}{4\pi^2 \sigma_t^2 \sum\limits_n f_i^2} \quad \text{for a single signal in a multisignal system} \tag{11.33}$$

*Phase Noise in Sampled Data Systems*

Nowhere in the preceding discussion did the spectrum of the clock phase noise come into play. All that was considered was the total jitter (in RMS seconds), which was calculated from the total integrated phase noise using (11.17). To see how the phase noise spectrum of the clock affects the sampled data spectrum, use a single sinewave signal. Combining (11.17) with (11.28) yields

$$\gamma = \frac{1}{\sigma_\theta^2} \left(\frac{f_{\text{clk}}}{f_{\text{sig}}}\right)^2 \tag{11.34}$$

The SNR of the resulting sampled signal is the same as the SNR of the clock but scaled by the clock and signal frequency ratio. As the signal frequency gets higher, the SNR degrades in a 20log fashion. This illustrates why undersampled systems (i.e., one in which the signal frequency occupies one of the higher Nyquist bands) require clocks with much better phase jitter than baseband systems. In fact, performance in IF-sampling digital receiver architectures is often limited by clock phase noise, not data converter performance.

Although not apparent from (11.34), the spectral shape of the clock phase noise is superimposed on the sampled data, as illustrated in Figure 11.19. This can intuitively be seen by modeling the sampling process with a mixer. As shown in Figure 11.20, when a clock with phase noise $\theta(f)$ is applied to a mixer, the output contains two mixing products, each of which contains the full phase noise $\theta(f)$ of the clock. Although this simplistic model does not show the scaling factor
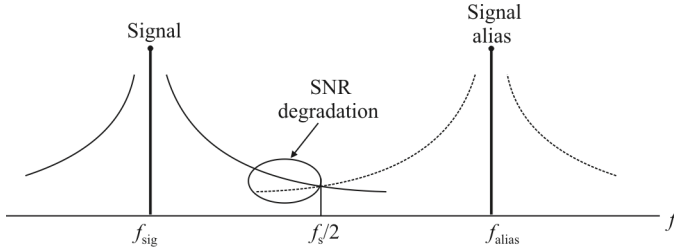
**Figure 11.19** Aliasing may cause clock phase noise to degrade SNR more than what is predicted by the equations.



$$V_{out} = RV \sin[2\pi(f_{clk} + f_{sig})t + \theta(f)]$$
$$+ RV \sin[2\pi(f_{clk} - f_{sig})t + \theta(f)]$$

$$R\cos(2\pi f_{sig}t)$$
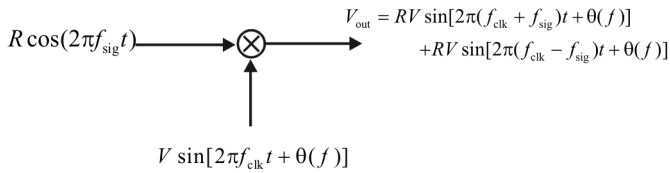
$$V \sin[2\pi f_{clk}t + \theta(f)]$$

**Figure 11.20** Sampling modeled as a mixer.

described in (11.34), it is useful to show how the phase spectrum of the clock shows up on the resulting signal.

It is important to remember that phase noise is always measured by the residual noise:

$$\phi_j^2 = 2\int_{f_1}^{f_2} \mathcal{L}(f_m) df_m \qquad \text{or} \qquad \gamma = 10\log_{10} \phi_j^2 \qquad (11.35)$$

*Aperture Distortion*

At the sampling instant, the transition of control signals from track to hold causes distortion in the sampled signal. The distortion can occur through a number of mechanisms that are dependent on the clock signal transition time, the signal characteristics, the sampling circuit architecture, the device geometries, and the fabrication technology. The distortion increases with input frequency, imposing stricter requirements on sampling switches and clock generation circuits as the frequency being sampled increases.

The increase in distortion with frequency being sampled is difficult to quantify because it depends on multiple factors but several authors have quantified the total harmonic distortion caused by sample and hold settling time for specific sampling architectures. Required clock transition times are also dependent on the specific sampling architecture used, the maximum input frequency, and the required ADC resolution.

*Effective Number of Bits*

From (10.4), the *effective number of bits* (ENOB) for an ADC is limited by the SINAD and is given by

$$\text{ENOB} = \frac{\text{SINAD} - 1.76\,\text{dB}}{6.02} \qquad (11.36)$$

Using (11.36) and (11.12), the maximum achievable ADC resolution for an ideal ADC where SNR is limited only by aperture jitter can be plotted versus input frequency for several clock jitter values as shown in Figure 11.21. Aperture jitter can cause additional performance degradation in subsampling systems. Jitter affects frequencies in the sampled signal spectrum that are aliased to the frequency band of interest but this effect can be mitigated by adequate anti-aliasing filtering (see Figure 11.19).

The jitter requirements imposed by the subsampling process become more stringent as the frequency being sampled increases but are independent of the jitter requirements imposed by the required ADC resolution. Despite the SNR
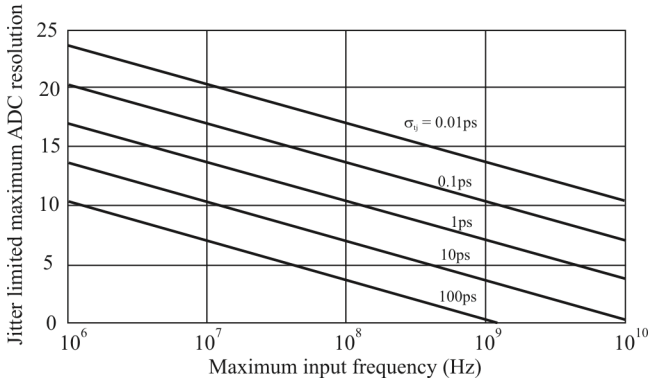
**Figure 11.21** Number of ADC bits versus aperture jitter and maximum input frequency.

degradation caused by clock jitter in both direct RF sampling and RF sub-sampling and the jitter requirements imposed by the sampling frequency limitations in RF subsampling, receivers using both types of RF sampling have been implemented for applications that do not require very high ADC resolution.

## 11.4.7 Spurious-Free Dynamic Range

The SFDR of an ADC is determined by considering all error sources within the Nyquist band including harmonics of the input signal and the nonlinearities with that ADC. One definition of the SFDR, and the one we use here, assumes a sinusoidal input to the ADC. It is defined as the ratio of the RMS signal amplitude to the RMS value of the largest harmonic or spurious spectral component at the output and within the entire first Nyquist zone, DC to $f_s/2$ as

$$\text{SFDR} = 20\log_{10}\frac{\left|X_{\text{sig}}(f)\right|}{\max\left\{\left|X_{\text{h}}(f)\right|,\left|X_{\text{spur}}(f)\right|\right\}} \tag{11.37}$$

where

$X_{\text{sig}}(f)$ is the spectrum of input signal at ADC output
$X_{\text{h}}(f)$ is the spectrum of harmonic at ADC output
$X_{\text{spur}}(f)$ is the spectrum of spurious component at ADC output

The SFDR limits the receiver performance more restrictively than the SNR. The impact of the SFDR on the spectrum of the output of an ADC is illustrated in Figure 11.22. In this figure the SOI is at 10 MHz, and all the rest of the signals, spurs, are caused by the nonlinearity of the ADC reacting to the SOI. The largest
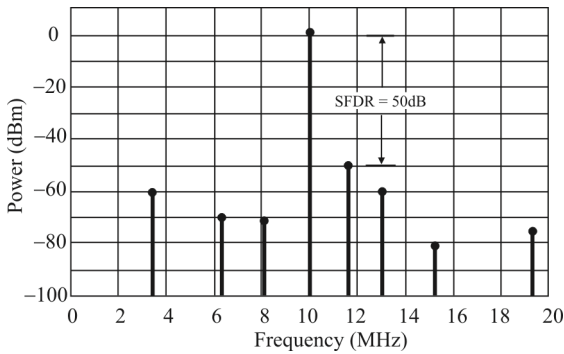
**Figure 11.22** Spur-free dynamic range of an ADC.

of these undesired signals has a power of −50dB relative to the SOI so the SFDR = 50dB.

The SFDR allows us to assess how well an ADC can simultaneously detect a very small signal in the presence of a very large signal. Hence, it is an important specification for ADCs used in EW receiver applications, since in many cases the EW receiver is tasked with detection of distant, weak signals in the presence of close-by interferers.

The SFDR specification is useful for applications when the SOI bandwidth is smaller than $f_s/2$. In this case, a wide band of frequencies is digitized and results in a given SNR. The SOI is then obtained by using a narrowband digital bandpass filter on this entire band of frequencies. The SNR is improved by this digital filtering process since the power of the residual error is decreased by filtering. The SFDR specification for the ADC becomes very important since a spurious component may still fall within the bandwidth of the digital filter, and hence the SFDR, unlike the SNR, does not necessarily improve by the digital filtering process. However, several techniques are available to improve the SFDR. Dithering improves the SFDR of ADCs. Additionally, post-digitization processing techniques such as phase-plane compensation [12], state variable compensation [13], and projection filtering [14] have been used to improve SFDR.

For an ideal ADC, the maximum SFDR occurs at a full-scale input level. In practical ADCs, the maximum SFDR occurs at input levels at least several decibels below the full-scale input level. This occurs because as the input levels approach full scale, the response of the ADC becomes more nonlinear and more distortion is exhibited. Additionally, due to random fluctuations in the amplitude of real input signals, as the input signal level approaches the FSR of the ADC, the probability of the signal amplitude exceeding the FSR increases. This causes additional distortion from clipping. Therefore, it is extremely important to avoid input signal levels that closely approach the full-scale level in ADCs. Prediction of
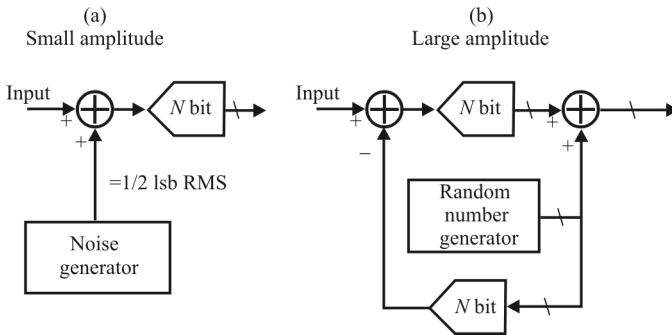
**Figure 11.23**  Using dither to randomize the ADC transfer function.

the SFDR for practical ADCs is difficult; therefore measurements are usually required to characterize the SFDR of the ADC.

In the preceding discussion on SFDR, a sinusoidal ADC input signal was assumed. However, IMD due to multitone inputs is important in ADCs used for wideband EW receiver applications. To characterize this IMD due to multi-tone inputs, another definition of the SFDR could be used. In this case, the SFDR is the ratio of the combined signal power of all of the multi-tone inputs to the peak power of the largest spurious signal in the ADC output spectrum.

11.4.7.1 Using Noise Dither to Increase an ADC's Spurious-Free Dynamic Range

Two fundamental limitations to maximizing the SFDR in a high-speed ADC are the distortion produced by the front-end amplifier and the sample-and-hold circuit and that produced by nonlinearity in the transfer function of the encoder portion of the ADC. The key to achieving high SFDR is to minimize both sources of nonlinearity.

Nothing can be done externally to the ADC to significantly reduce the inherent distortion caused by the receiver RF/IF stages. However, the differential nonlinearity in the ADC's encoder transfer function can be reduced by the proper use of dither (external noise that is intentionally summed with the analog input signal).

Dithering can be used to improve the SFDR of an ADC under certain conditions [7, 15–17]. For example, even in a perfect ADC, some correlation exists between the quantization noise and the input signal. This correlation can reduce the SFDR of the ADC, especially if the input signal is an exact sub-multiple of the sampling frequency. Summing about ½ LSB RMS of broadband noise with the input signal tends to randomize the quantization noise and minimize this effect [Figure 11.23(a)]. In most systems, however, the noise already riding on top of the signal (including the input-referred noise of the ADC) obviates the need
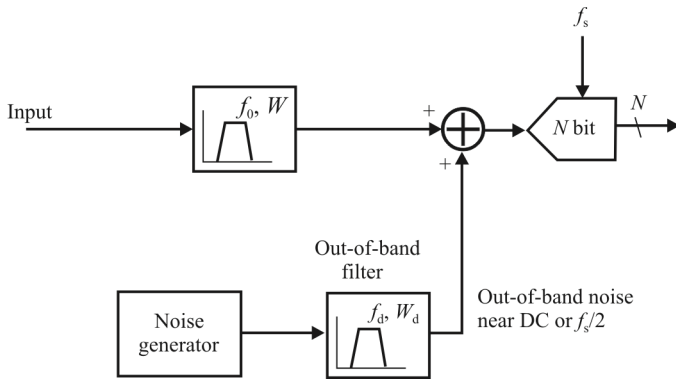
**Figure 11.24** Injecting out-of-band dither to improve ADC SFDR.

for additional dither noise. Increasing the wideband RMS noise level beyond approximately 1 lsb will proportionally reduce the SNR and result in no additional improvement.

Other schemes have been developed using larger amounts of dither noise to randomize the transfer function of the ADC. Figure 11.23(b) shows a dither-noise source comprising a pseudo-random-number generator driving a DAC. This signal is subtracted from the ADC input signal and then digitally added to the ADC output, thereby causing no significant degradation in the SNR. An inherent disadvantage of this technique, however, is that the input signal swing must be reduced to prevent overdriving the ADC as the amplitude of the dither signal is increased. Note that although this scheme improves distortion produced by the ADC's encoder nonlinearity, it does not significantly improve distortion created by the RF/IF stages.

Another method, one that is easier to implement—especially in wideband receivers—is to inject a narrowband dither signal outside the signal band of interest, as shown in Figure 11.24. Usually, no signal components are located in the frequency range near DC, so this low-frequency region is often used for such a dither signal. Another possible location for the dither signal is slightly below $f_s/2$. The dither signal occupies only a small bandwidth relative to the signal bandwidth (usually a bandwidth of a few hundred kHz is sufficient), so no significant degradation in SNR occurs—as it would if the dither were broadband.

## 11.4.8 Noise Power Ratio

The *noise power ratio* (NPR) is a useful parameter in EW receiver applications, where the spectrum of a signal to be digitized consists of many narrowband
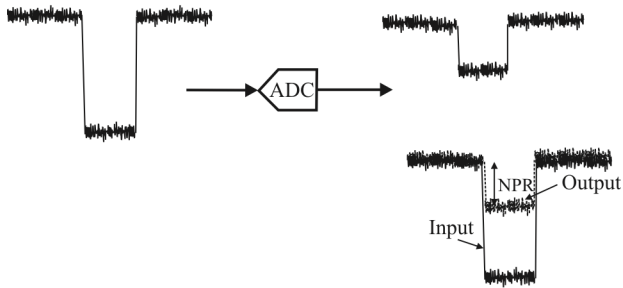
**Figure 11.25** Noise power ratio.

channels and where adjacent channel interference can degrade system performance. In particular, the NPR provides information on how well an ADC can limit crosstalk between channels.

The NPR is measured by using a noise input signal into the ADC. This noise signal has a flat spectrum that is band limited to a frequency that is less than one half the sampling frequency. Additionally, a narrow band of frequencies is removed from the noise signal using a notch filter. This noise spectrum is used as the input signal to the ADC. The frequency spectrum of the output of the ADC is then determined. The NPR is then computed by dividing the power spectral density of the noise outside the frequency band of the notch filter by the power spectral density of the noise inside the frequency band of the notch filter. The concept is illustrated in Figure 11.25.

When using an ADC in a bandpass sampling application where the maximum input frequency into the ADC is actually higher than one half the sampling frequency, the full-power analog input bandwidth is an important consideration. A common definition of full-power analog input bandwidth (although not universal) is the range from DC to the frequency where the amplitude of the output of the ADC falls to 3dB below the maximum output level. This assumes a full-scale input signal to the ADC. Typically, the ADC is operated at input frequencies below this bandwidth. Aside from full-power analog input bandwidth, it is important to examine the behavior of the other characteristics such as SNR, SFDR, and NPR at the desired operating frequencies since these specifications may vary with frequency.

# 11.5 Flash ADC

*Flash analog-to-digital converters*, also known as *parallel ADCs*, are the fastest way to convert an analog signal to a digital signal. Flash ADCs are required for applications requiring very large bandwidths. However, they consume considerable power, have relatively low resolution, and can be quite expensive
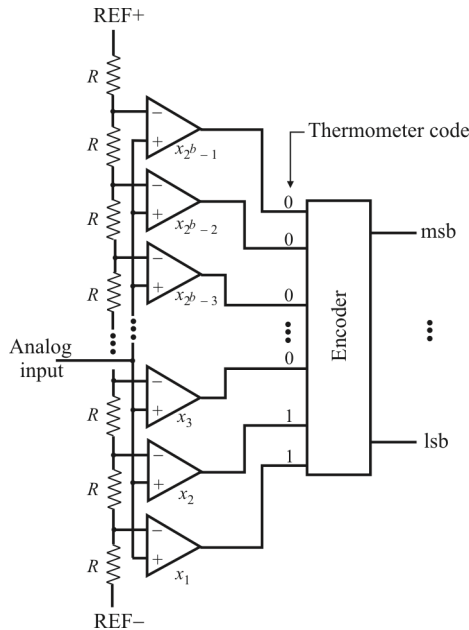
**Figure 11.26** Flash ADC topology. As shown, ideally, if the analog input is between $V_{x_2}$ and $V_{x_3}$, comparators, $x_1$ and $x_2$ produce 1s and the remaining comparators produce 0s.

(which normally is not a first-order concern for cost-insensitive applications such as EW receivers). This limits them to high-frequency applications that typically cannot be addressed any other way. There is a converter for every value of output. So for a 6 bit ADC there are 63 converters included.

## 11.5.1 Flash ADC Architecture

Flash ADCs are constructed by cascading high-speed comparators. See Figure 11.26. For a $b$-bit converter, $2^b - 1$ comparators are employed. A resistive-divider with $2^b$ resistors provides the reference voltages for each of the comparators. The reference voltage for each comparator is 1 lsb greater than the reference voltage for the comparator immediately preceding it. Each comparator produces a 1 when its analog input voltage is higher than its reference voltage. Otherwise, the comparator output is 0. Thus, if the analog input is between $V_{x_2}$ and $V_{x_3}$, comparators $x_1$ and $x_2$ produce 1s and the remaining comparators produce 0s. The point where the code changes from ones to zeros is the point at which the input signal becomes smaller than the respective comparator reference-voltage levels.

This topology is known as *thermometer code encoding* because the encoding is similar to a mercury thermometer, in which the mercury column always rises to the appropriate temperature and no mercury is present above that temperature. The thermometer code is then encoded to the appropriate digital output code (typically 2's complement binary, or a Gray code).

The comparators are normally wideband low-gain stages. They are low gain because at high frequencies it is difficult to obtain both wide bandwidth and high gain. The comparators are designed for low-voltage offset, so that the input offset of each comparator is smaller than an lsb of the ADC. Otherwise, the comparator's offset could falsely trip the comparator, resulting in a digital output code that is not representative of a thermometer code. A regenerative latch at each comparator output stores the result. The latch has positive feedback, so that the end state is forced to either a 1 or a 0.

### 11.5.2 Sparkle Codes

When operating properly, the comparator outputs will be a thermometer code, such as 00011111. Errors can cause an output like 00010111, meaning that there is a spurious zero in the result (or a spurious 1). This out-of-sequence 0 is called a *sparkle*, which is caused by imperfect input settling or comparator timing mismatch. The magnitude of the error can be quite large. Modern high quality ADCs usually employ an input *track-and-hold* (T/H), also known as *sample-and-hold* (S/H) in front of the ADC along with an encoding technique that suppresses sparkle codes.

### 11.5.3 Metastability

A comparator output that is ambiguous (neither a 1 nor a 0) is called *metastable*. Metastability can be reduced by allowing more time for regeneration. Metastability can be greatly improved upon by the application of Gray code encoding, which allows only 1 bit in the output to change at a time. Thus, the comparator outputs are first converted to Gray code encoding and then later encoded to binary, if required.

Another problem can occur when a metastable output drives two distinct circuits. It is possible for one circuit to declare the input a 1, while the other circuit thinks that it is a 0. Obviously, this can create major errors. Using only one circuit to sense a potentially mestatable output can minimize this problem.

### 11.5.4 Input Signal Frequency Dependence

When the input signal changes before all the comparators have settled, the ADC's performance is adversely impacted. The most serious impact is a dropoff in SINAD as the frequency of the analog input frequency increases.
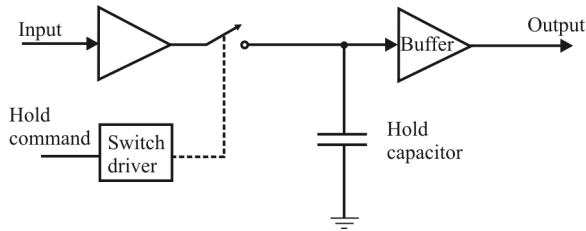
**Figure 11.27** For a sample and hold, the switch is normally open and is closed when a sample is to be taken. In a track and hold, the switch is normally closed and is opened when a sample is to be held. The net effect is the same. The buffer normally has a high input impedance so as not to unduly load the hold capacitor.

The SFDR is another good parameter to evaluate converter performance. The effective bits achieved by the ADC is a function of input frequency; it can be improved by adding a T/H circuit in front of the ADC. A typical T/H configuration is shown in Figure 11.27. The T/H circuit allows dramatic improvement, especially when input frequencies approach the Nyquist frequency, as shown in Figure 11.28. Converters without T/H show a significant dropoff in SFDR.

# 11.6 Sigma-Delta ADCs

## 11.6.1 Introduction

*Sigma-delta analog-digital converters* ($\Sigma$-$\Delta$ ADCs) have been known for over thirty years, but only recently has the technology high-density digital *very large*



**Figure 11.28** Spurious free dynamic range of a flash ADC as a function of input frequency. The ADC in this example is 8 bits for a ~60 dB dynamic range.

**Figure 11.29** First-order Σ-Δ ADC topology.

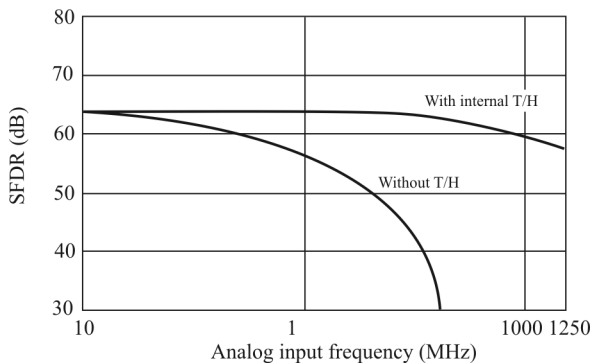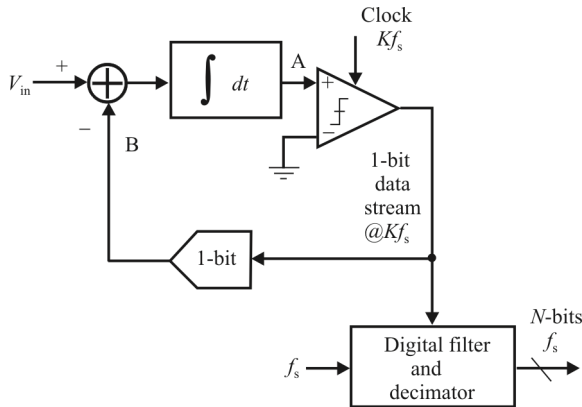*scale integrated* (VLSI) circuits existed to manufacture them as inexpensive monolithic integrated circuits. They are now used in many applications where a low-cost, low-bandwidth, low-power, high-resolution ADC is required.

A Σ-Δ ADC contains very simple analog electronics (a comparator, voltage reference, a switch, one or more integrators, and analog summing circuits), and quite complex digital computational circuitry. This circuitry consists of a DSP that acts as a filter (generally, but not invariably, a lowpass filter). It is not necessary to know precisely how the filter works to appreciate what it does. We delve into the operation of digital filters in the next chapter.

If we consider a 1 bit ADC (generally known as a *comparator*), drive it with the output of an integrator, and feed the integrator with an input signal summed with the output of a 1-bit DAC fed from the ADC output, we have a first-order Σ-Δ modulator as shown in Figure 11.29. Add a digital lowpass filter and decimator at the digital output, and we have a Σ-Δ ADC—the Σ-Δ modulator shapes the quantization noise so that it lies above the passband of the digital output filter, and the ENOB is therefore much larger than would otherwise be expected from the oversampling ratio.

### 11.6.2 Σ-Δ ADC Operation

Let us consider the technique of oversampling with an analysis in the frequency domain. A sampled data system has quantization noise where a DC conversion has a quantization error of up to ½ LSB. As mentioned above, a perfect classical *b*-bit sampling ADC has an RMS quantization noise of $q/\sqrt{12}$ uniformly distributed within the first Nyquist band of DC to $f_s/2$ (where $q$ is the value of the lsb) as shown in Figure 11.30(a). Therefore, its SNR with a full-scale sine wave input will be $(6.02b + 1.76)$ dB (without oversampling). If the ADC is less than perfect, and
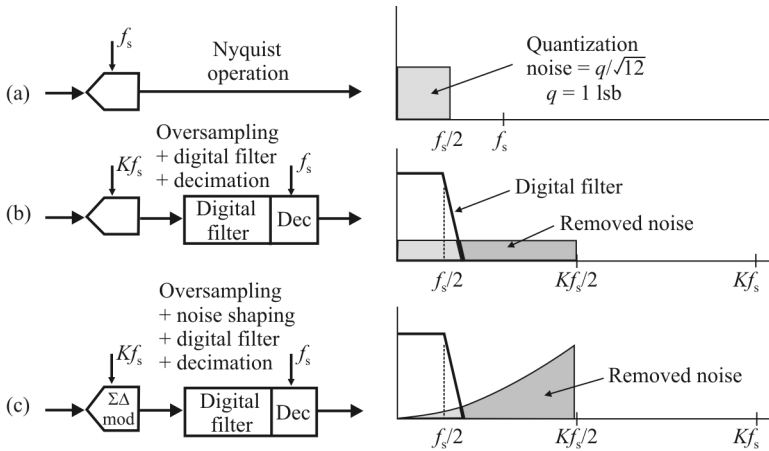
**Figure 11.30** (a) Minimum sampling rate, (b) oversampling, digital filtering, and decimation, and (c) noise shaping by oversampling, filtering, and subsequent decimation.

its noise is greater than its theoretical minimum quantization noise, then its effective resolution will be less than $b$-bits. Its actual resolution is given by the ENOB (11.36).

If we choose a much higher sampling rate, $Kf_s$ (see Figure 11.30), the RMS quantization noise remains $q/\sqrt{12}$, but the noise is now distributed over a wider bandwidth DC to $Kf_s/2$. If we then apply a lowpass filter to the output we remove much of the quantization noise, but do not affect the wanted signal—so the ENOB is improved. We have accomplished a high-resolution A/D conversion with a low-resolution ADC. The factor $K$ is generally referred to as the *oversampling ratio*. As noted previously, oversampling has an added benefit in that it relaxes the requirements on the analog anti-aliasing filter.

As previously indicated, since the bandwidth is reduced by the digital output filter, the output data rate may be lower than the original sampling rate ($Kf_s$) and still satisfy the Nyquist criterion. This may be achieved by passing every $M$th result to the output and discarding the remainder. The process is known as *decimation* by a factor of $M$. Despite the origins of the term (*decem* is Latin for ten), $M$ can have any integer value, provided that the output data rate is more than twice the signal bandwidth. Decimation does not cause any loss of information [Figure 11.30(b)].

If we simply use oversampling to improve resolution, we must oversample by a factor of $2^{2N}$ to obtain an $N$-bit increase in resolution. The $\Sigma$-$\Delta$ converter does not need such a high oversampling ratio because it not only limits the signal passband but also shapes the quantization noise so that most of it falls outside this passband as shown in Figure 11.30.
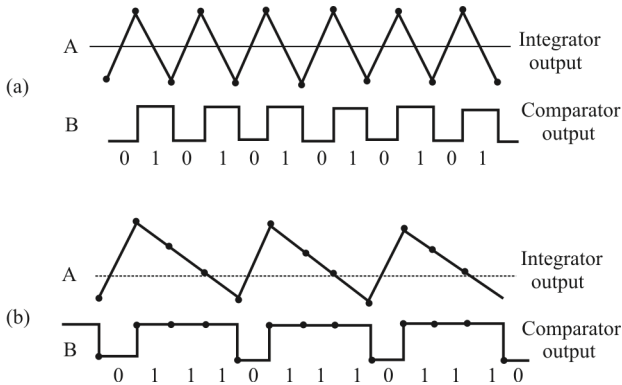
**Figure 11.31** Sigma delta waveforms: (a) $V_{in} = 0V = 2/4 = 4/8$ and (b) $V_{in} = V_{ref}/2 = 3/4 = 6/11$.

Intuitively, a Σ-Δ ADC operates as follows (Figure 11.29). Assume a DC input at $V_{in}$. The integrator is constantly ramping up or down at node A. The output of the comparator is fed back through a 1-bit DAC to the summing input at node B. The negative feedback loop from the comparator output through the 1-bit DAC back to the summing point will force the average DC voltage at node B to be equal to $V_{in}$. This implies that the average DAC output voltage must equal the input voltage $V_{in}$. The average DAC output voltage is controlled by the *ones-density* in the 1-bit data stream from the comparator output. As the input signal increases toward $+V_{ref}$, the number of 1s in the serial bit stream increases, and the number of 0s decreases. Similarly, as the signal goes negative towards $-V_{ref}$, the number of 1s in the serial bit stream decreases, and the number of 0s increases. From a very simplistic standpoint, this analysis shows that the average value of the input voltage is contained in the serial bit stream out of the comparator. The digital filter and decimator process the serial bit stream and produce the final output data.

For any given input value in a single sampling interval, the data from the 1-bit ADC is virtually meaningless. Only when a large number of samples are averaged will a meaningful value result. The Σ-Δ modulator is very difficult to analyze in the time domain because of this apparent randomness of the single-bit data output. If the input signal is near positive full-scale, it is clear that there will be more 1s than 0s in the bit stream. Likewise, for signals near negative full-scale, there will be more 0s than 1s in the bit stream. For signals near midscale, there will be approximately an equal number of 1s and 0s in the bit stream. Figure 11.31 shows the output of the integrator for two input conditions. The first is for an input of zero (midscale). To decode the output, pass the output samples through a simple digital lowpass filter that averages every four samples. The output of the filter is 2/4. This value represents bipolar zero. If more samples are averaged, more dynamic range is achieved. For example, averaging four samples gives two bits of resolution, while
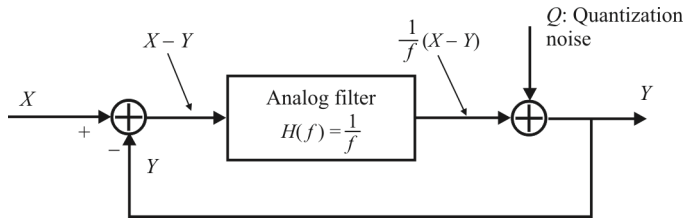
**Figure 11.32** Linearized sigma-delta ADC topology.

averaging eight samples yields 4/8, or three bits of resolution. In the bottom waveform of Figure 11.31, the average obtained for four samples is 3/4, and the average for eight samples is 6/11.

We explain the concept of noise shaping in the frequency domain by considering the simple Σ-Δ modulator model in Figure 11.32. The integrator in the modulator is represented as an analog low-pass filter with a transfer function of $H(f) = 1/f$, which has an amplitude response that is inversely proportional to the input frequency. The 1 bit quantizer generates quantization noise, $Q$, which is injected into the output summing block. If we let the input signal be $X$, and the output $Y$, the signal coming out of the input summer is $X - Y$. This is multiplied by the filter transfer function, $1/f$, and the result goes to one input to the output summer. By inspection, we can then write the expression for the output voltage $Y$ as

$$Y = \frac{1}{f}(X - Y) + Q \tag{11.38}$$

It is trivial to rearrange this expression to solve for $Y$ in terms of $X$, $f$, and $Q$:

$$Y = \underbrace{\frac{X}{f+1}}_{\text{Signal term}} + \underbrace{\frac{Qf}{f+1}}_{\text{Noise term}} \tag{11.39}$$

Note that as the frequency $f$ approaches zero, the output voltage $Y$ approaches $X$ with no noise component. At higher frequencies, the amplitude of the signal component approaches zero, and the noise component approaches $Q$. At high frequency, the output consists primarily of quantization noise. In essence, the analog filter has a lowpass effect on the signal and a highpass effect on the quantization noise. Thus the analog filter performs the noise shaping function in the Σ-Δ modulator model.

For a given input frequency, higher order analog filters offer more attenuation. The same is true of Σ-Δ modulators, provided certain precautions are
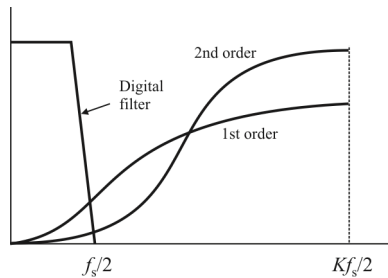
**Figure 11.33** Shaped quantization noise.

taken. By using more than one integration and summing stage in the Σ-Δ modulator, we can achieve higher orders of quantization noise shaping and even better ENOB for a given oversampling ratio as is shown in Figure 11.33 for both a first- and second-order Σ-Δ modulator.

## 11.6.3 Higher Order Loop Considerations

The flow diagram for the second-order Σ-Δ modulator is shown in Figure 11.34. Third- and higher-order Σ-Δ ADCs were once thought to be potentially unstable at some values of input—recent analyses using finite rather than infinite gains in the comparator have shown that this is not necessarily so, but even if instability does start to occur, it is not important, since the DSP in the digital filter and decimator can be made to recognize incipient instability and react to prevent it.

Figure 11.35 shows the relationship between the order of the Σ-Δ modulator and the amount of oversampling necessary to achieve a particular SNR. For instance, if the oversampling ratio is 64, an ideal second-order system is capable of providing an SNR of about 80 dB. This implies approximately 13 ENOB.

Although the filtering done by the digital filter and decimator can be done to any degree of precision desirable, it would be pointless to carry more than 13 binary bits to the outside world. Additional bits would carry no useful signal information and would be buried in the quantization noise unless post-filtering techniques were employed. Additional resolution can be obtained by increasing the oversampling ratio and/or by using a higher order modulator.

The simple linear models previously discussed are no longer fully accurate, however. The instability in higher order loops arises because the comparator is a nonlinear element whose effective gain varies inversely with the input level. This mechanism for instability causes the following behavior: if the loop is operating normally, and a large signal is applied to the input that overloads the loop, the average gain of the comparator is reduced. The reduction in comparator gain in the linear model causes loop instability. This causes instability even when the signal that caused it is removed. In actual practice, such a circuit would normally oscillate on power-up due to initial conditions caused by turn-on transients.
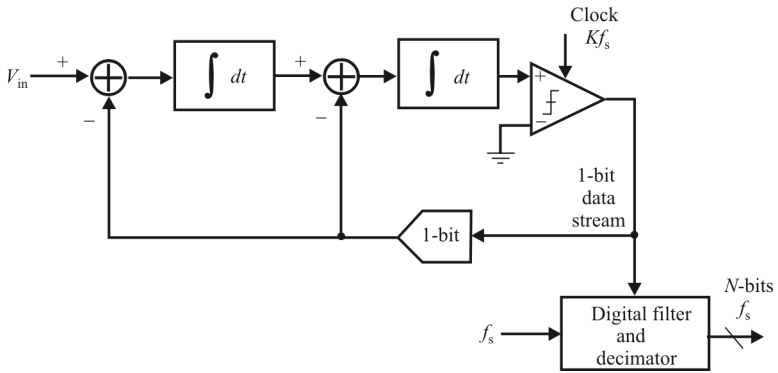
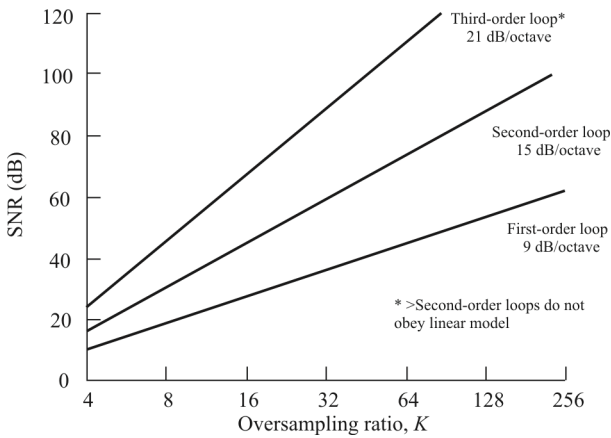**Figure 11.34** Second-order $\Sigma$-$\Delta$ ADC architecture.



**Figure 11.35** SNR versus oversampling ratio for first-, second-, and third-order loops.
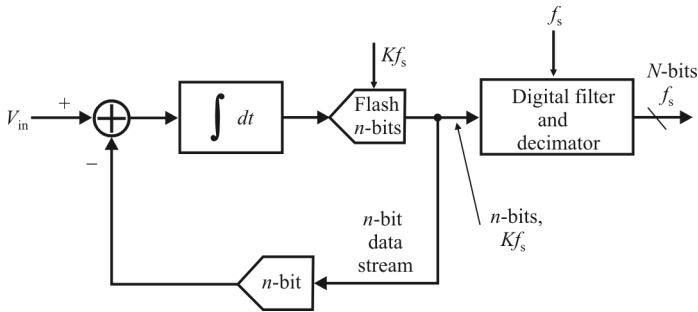
**Figure 11.36** Multibit Σ-Δ ADC.

## 11.6.4 Multibit Sigma-Delta Converters

So far we have considered only Σ-Δ converters which contain a single-bit ADC (comparator) and a single-bit DAC (switch). The flow diagram of Figure 11.36 shows a multibit Σ-Δ ADC that uses an $n$-bit flash ADC and an $n$-bit DAC. Obviously, this architecture will give a higher dynamic range for a given oversampling ratio and order of loop filter. Stabilization is easier, since second-order loops can generally be used. Idling patterns tend to be more random, thereby minimizing tonal effects.

The disadvantage of this technique is that the linearity depends on the DAC linearity, and thin film laser trimming is required to approach 16-bit performance levels. This makes the multibit architecture impractical to implement on mixed-signal ICs using traditional binary DAC techniques.

## 11.6.5 Bandpass Sigma-Delta Converters

The Σ-Δ ADCs that we have described so far contain integrators, which are in essence lowpass filters, whose pass band extends from DC. Thus, their quantization noise is pushed up in frequency. Most commercially available Σ-Δ ADCs are of this type, although some contain bandpass rather than lowpass digital filters to eliminate any system DC offsets. But there is no particular reason why the filters of the Σ-Δ modulator should be LPFs, except that traditionally ADCs have been thought of as being baseband devices, and that integrators are somewhat easier to construct than bandpass filters. If we replace the integrators in a Σ-Δ ADC with bandpass filters as shown in Figure 11.37, the quantization noise is moved up and down in frequency to leave a virtually noise-free region in the passband (see [18–20]). If the digital filter has its passband in this region, we have a Σ-Δ ADC with a bandpass, rather than a lowpass characteristic. Such devices are useful in direct IF-to-digital conversion digital receivers.
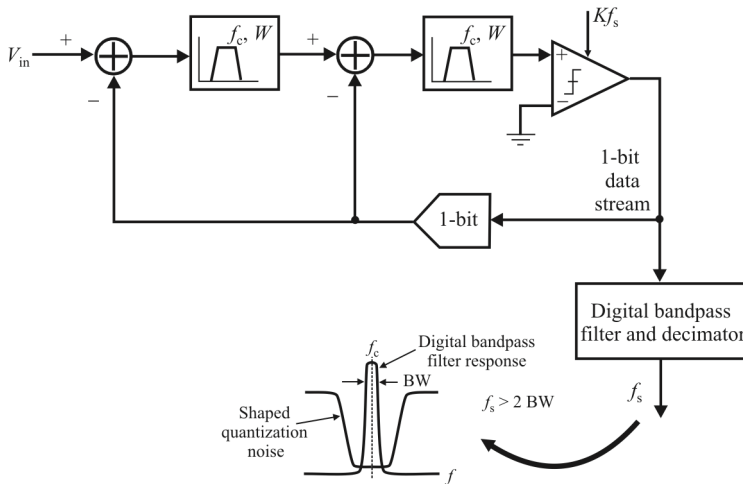
**Figure 11.37** Bandpass Σ-Δ ADC.

In an undersampling application of a bandpass Σ-Δ ADC, the minimum sampling frequency must still be at least twice the signal bandwidth, $W$. The signal is centered around a carrier frequency, $f_c$. A typical digital receiver application uses a 455 kHz center frequency and a signal bandwidth of 10 kHz. An oversampling frequency $Kf_s$ = 2 Msps and an output rate $f_s$ = 20 ksps yields a dynamic range of 70 dB within the signal bandwidth.

Another example of a bandpass topology is an IF digitizing receiver having a nominal oversampling frequency of 18 Msps, a center frequency of 2.25 MHz, and a bandwidth of 10 kHz to 150 kHz.

# 11.7 Flash ADC versus Other ADC Architectures

## 11.7.1 Flash versus SAR ADCs

In a SAR converter, shown in Figure 11.38, a single high-speed, high-accuracy comparator determines the bits, one bit at a time (from the msb down to the lsb). The negative analog input to the comparator is from the DAC whose output is updated by previously decided bits is compared to the signal sample from the *sample and hold* (S/H). Thus, the digital estimate successively approximates the analog input. This serial nature of the SAR limits its speed to no more than a few tens of samples per second, while flash ADCs exceed giga-samples-per-second conversion rates.

SAR converters are available in resolutions up to 16 bits. Flash ADCs are typically limited to around 8 bits. The slower speed also allows the SAR ADC to

 **Figure 11.38** SAR ADC.

consume much less power. The SAR architecture is also less expensive. Package sizes are larger for flash converters. In ad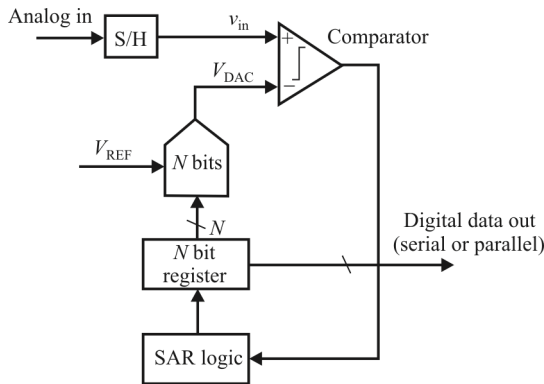dition to a larger die size requiring a larger package, the package needs to dissipate considerable power and needs many pins for power and ground signal integrity.

## 11.7.2 Flash versus Pipelined ADCs

A pipelined ADC employs a parallel structure in which each stage works on one to a few bits of successive samples concurrently (Figure 11.39). This design improves speed at the expense of power and latency, but each pipelined stage is much slower than a flash section. The pipelined ADC requires accurate amplification in the DACs and interstage amplifiers, and these stages have to settle to the desired linearity level. By contrast, in a flash ADC the comparator only needs to be low offset and to resolve its inputs to a digital level; there is no linear settling time involved. Some flash converters require preamplifers to drive the comparators. Gain linearity needs to be carefully controlled.

Pipelined ADCs are perhaps the most popular type, satisfying the majority of the requirements where their capabilities are adequate. They provide a compromise between the slower SAR ADCs and the more power hungry and expensive flash ADCs. Pipelined converters convert at speeds of a few hundred Msps with 8- to 14-bit resolutions. For a given resolution, pipelined ADCs are around 10 times slower than flash converters of similar resolution. Pipelined converters are possibly the optimal architecture for ADCs that need to sample at rates up to around 100 Msps with resolution at 10 bits and above. For resolutions up to 10 bits and conversion rates above a few hundred Msps, flash ADCs dominate.
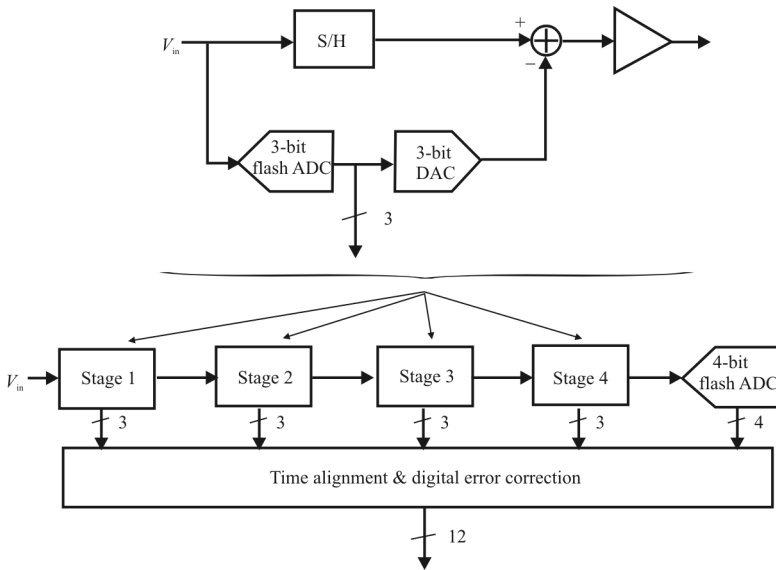
**Figure 11.39** Pipelined ADC.

## 11.7.3 Flash versus Integrating ADCs

Single, dual, and multislope ADCs achieve high resolutions of 16 bits or more, are relatively inexpensive, and dissipate materially less power. See Figure 11.40 for a single slope ADC. These devices support very low conversion rates, typically less than a few hundred samples per second.

In Figure 11.40(a), the counter keeps counting until the comparator toggles. At that point the digital output is available. These ADCs are simple, inherently monotonic, but very slow $(2^b T_{clk}$ per sample). The relevant operation is shown in Figure 11.40(b). A precision capacitor and current source are required. Errors arise due to current source output impedance and leakage current. The comparator must handle large common-mode inputs.

This architecture competes with Σ-Δ converters.

## 11.7.4 Flash versus Sigma-Delta ADCs

Flash ADCs do not compete with a Σ-Δ architecture because currently the achievable conversion rates differ by up to two orders of magnitude. The Σ-Δ architecture is suitable for applications with much lower bandwidth, typically less than 1 MHz, and with resolutions in the 12- to 24-bit range. Σ-Δ converters are capable of the highest resolution possible in ADCs, and therefore they are at the

(a)



$$V_{in} = \frac{I}{C} t_1 \qquad D_o = \frac{t_1}{T_{clk}}$$

$$\Rightarrow D_o = \frac{C}{I T_{clk}} V_{in}$$

(b)
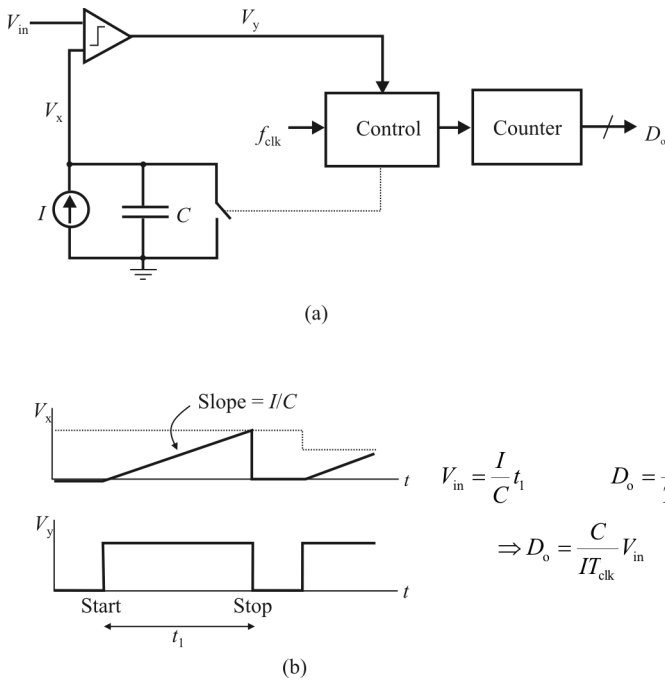
**Figure 11.40** Integrating ADC.

other end of the resolution/speed spectrum than flash converters. They require simpler anti-alias filters (if needed) to band-limit the signal prior to conversion. A flow diagram of a Σ-Δ ADC is shown in Figure 11.29.

Σ-Δ ADCs trade speed for resolution by oversampling, followed by filtering to reduce noise. However, these devices are not always efficient for multichannel applications. This architecture can be implemented by using sampled data filters, also known as modulators, or continuous-time filters. Another interesting use of a flash ADC is as a building block inside a Σ-Δ circuit to increase the conversion rate of the ADC, as illustrated previously.

## 11.7.5 Flash ADC Architectural Tradeoffs

Flash ADCs can be implemented by employing a variety of architectures. The principal tradeoffs among these alternatives are discussed here.

### 11.7.5.1 Conversion Time

The conversion time does not change materially with increased resolution for flash converters. The conversion time for SAR or pipelined converters, however,

increases approximately linearly with an increase in resolution [Figure 11.41(a)]. The conversion time doubles with every bit increase in resolution for integrating ADCs.

11.7.5.2 Component Matching

Flash ADC component matching requirements typically limit resolution to around 8 bits. Calibration and trimming are sometimes used to improve the matching available on chip. Component matching requirements double for every bit increase in resolution. While this pattern applies to flash, successive approximation, or pipelined converters, it does not apply to integrating converters. For integrating converters, component matching does not materially increase with an increase in resolution [Figure 11.41(b)].

11.7.5.3 Die Size, Cost, and Power

For flash converters, every bit increase in resolution almost doubles the size of the ADC core circuitry. This essentially doubles the power as well. In contrast, a SAR, pipelined, or $\Sigma$-$\Delta$ ADC die size will increase linearly with an increase in resolution; an integrating converter core die size will not materially change with an increase in resolution [Figure 11.41(c)]. Finally, it is well known that an increase in die size increases cost.

**11.7.6 Flash Converter Characteristics**

From the above discussion we can summarize some of the salient characteristics of flash converters. First, they are very fast—the fastest architecture available. There is only 1 clock cycle per conversion: ½ clock cycle for $v_{in}$ and $V_{DAC}$ comparison and ½ clock cycle for the $2^b - 1$ to $b$ encoding. Second, they are high complexity, requiring $2^b - 1$ comparators. Third, the input capacitance of $2^b - 1$ comparators connected to the input node is quite high.

**11.7.7 Summary**

For applications requiring modest resolutions, typically up to 8 bits, at sampling frequencies in the high hundreds of MHz, the flash architecture may be the only viable alternative. A low-jitter clock must be used to ensure good ADC performance. For applications with high-analog input frequencies, the ADC should have an internal T/H.
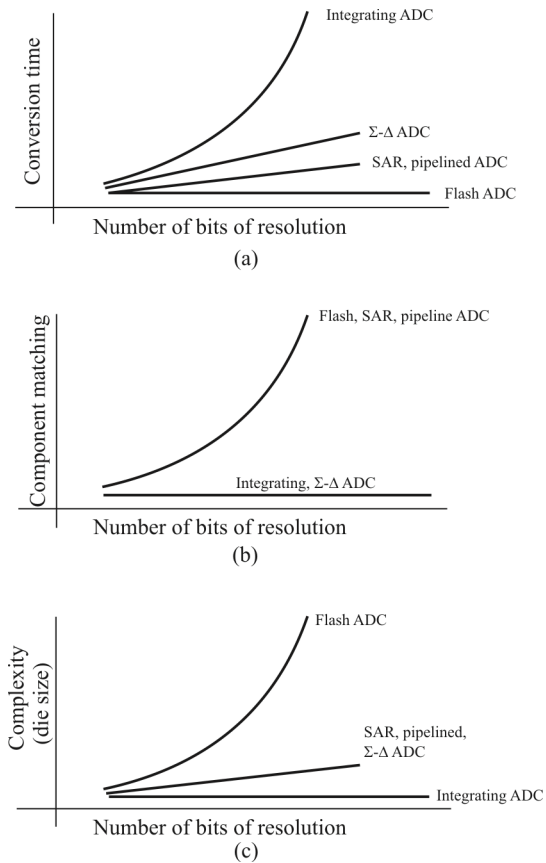
**Figure 11.41** ADC comparisons: (a) conversion time, (b) component matching requirements, and (c) complexity, all versus the number of bits of resolution.

# 11.8 Other Sampling and ADC Considerations

### 11.8.1 Ease of ADC Implementation

Speed limitations in ADCs make it difficult to perform A/D conversion at RF frequencies, especially at high resolutions. These speed limitations are due to the inherent speed limitations of the transistors used to design the ADCs and to the increase in power and area that is needed to achieve high resolution at high frequencies. Therefore, in the case of an RF sampling receiver where A/D conversion with sufficient resolution cannot be done at the RF frequency, discrete time filtering and decimation are done prior to A/D conversion.

### 11.8.2 Linearity

In addition to the usual second- and third-order intermodulation products that cause distortion in receivers, RF and IF sampling receivers are sensitive to distortion due to aliasing. Aliasing causes distortion products in the sampler input spectrum to appear in the Nyquist spectrum and is especially difficult to mitigate in the case of subsampling where the number of frequencies that alias to the first Nyquist band is significantly increased. Due to the effects of aliasing, subsampling receivers generally have poorer linearity and more stringent anti-aliasing filter requirements than Nyquist sampling receivers, but this degradation in linearity may be difficult to capture using figures of merit such as IP3, which are geared to receiver front ends that do not perform sampling.

RF sampling and subsampling receivers may suffer from distortion problems because all the gain is realized at the RF frequency and high gain with good linearity is generally more difficult to achieve at high frequency due to the increased effect of parasitics and the lower intrinsic gain of transistors at high frequencies. IF sampling and sub-sampling receivers may have degraded distortion performance compared to RF sampling receivers due to the use of a mixer, which may introduce additional distortion products.

### 11.8.3 Power Consumption, Circuit Complexity, Chip Area, and Reconfigurability

The analog receiver front end power consumption, circuit complexity, and chip area of an RF sampling receiver are generally less than those of an IF sampling receiver because fewer circuit blocks are used. However, different filter implementations at RF and IF frequencies may require very different amounts of chip area and consume different amounts of current so the comparison depends strongly on the design of the circuit blocks comprising the receivers. The power consumption of a complete RF sampling receiver including the digital base band may be higher than that of an IF sampling receiver due to the high power

consumption of very high-frequency digital signal processing. This problem may be mitigated by discrete time filtering and decimating the sampled RF signal before A/D conversion, but this adds circuit complexity.

RF sampling receivers are generally more reconfigurable for multipurpose use than IF sampling receivers because they contain a smaller number of analog circuit blocks, which are typically less reconfigurable than digital circuits.

## 11.9 Concluding Remarks

We have discussed some of the important factors that must be considered when using ADCs in EW receiver applications. These factors include the choice of sampling method, the amount and effects of out-of-band energy, the analog filtering required, the effects of quantization noise, receiver noise, and distortion, and the critical ADC specifications for EW receiver applications. The differences between Nyquist sampling, oversampling, and bandpass sampling were discussed. It was shown that sampling at the Nyquist rate presents a large and often impractical demand on the anti-aliasing filter. Oversampling eases the requirements on the anti-aliasing filter. A very steep rolloff bandpass filter is required for bandpass sampling when there are strong signals present in adjacent channels. Quadrature sampling was shown to reduce the required sampling rate by a factor of two at the expense of using two phase-locked ADCs instead of one. It was also shown that, in general, some sort of gain control is required for proper digitization of signals at the RF or IF in a receiver. ADC specifications of particular importance to receiver applications such as SNR, SFDR, full-power bandwidth, and NPR were examined, and some examples of high speed, state-of-the-art ADCs were given. As ADC performance continues to improve, digitization at the RF and IF in radio receivers, at increasingly higher frequencies, will be used in an increasingly broad range of applications.

## References

[1]     Poisel, R. A., *Introduction to Communication Electronic Warfare Systems*, Norwood, MA: Artech House, 2002.

[2]     Stremler, F. G., *Introduction to Communication Systems*, Reading, MA: Addison-Wesley, 1977, pp. 112–120.

[3]     Brigham, E. O., *The Fast Fourier Transform and Its Applications*, Englewood Cliffs, NJ: Prentice Hall, 1988, pp. 83–86 and 320–337.

[4]     Poisel, R. A., *Introduction to Communication Electronic Warfare Systems*, 2nd Ed., Norwood, MA: Artech House, 2011.

[5]     Vaughn, R. G., N. L. Scott, and D. R. White, "The Theory of Bandpass Sampling," *IEEE Transactions on Signal Processing*, Vol. 39, No. 9, September 1991, pp. 1973–1984.

[6]     Kester, W., "Add Noise Dither to Blow Out ADCs' Dynamic Range," *Electronic Design*, Analog Applications Supplement, November 22, 1999, pp. 20–26.

[7]     Wepman, J. A., and H. R. Hoffman, *RF and IF Digitization in Radio Receivers*, NTIA Report 96-328, U.S. Department of Commerce, March 1996.

[8]     Lober, R. M., "A DSP-Based Approach to HF Receiver Design. Higher Performance at a Lower Cost,*" RF Design*, Vol. 16, No. 8, 1993, pp. 92–100.

[9]     Amarandos, M., and S. Andrezyk, "Considerations in the Development of a Low Cost, High Performance Receiver Based on DSP Techniques," *DSP Applications,* Vol. 2, No. 12, December 1993, pp. 1–11.

[10]    Da Dalt, N., M. Harteneck, C. Sander, and A. Wiesbauer, "On the Jitter Requirements of the Sampling Clock for Analog-to-Digital Converters, *IEEE Transactions on Circuits and Systems–1: Fundamental Theory and Applications*, Vol. 49, No. 9, September 2002, pp. 1354–1360.

[11]    Groshong, R., and S. Ruscak, "Undersampling Techniques Digital Radio," *Electronic Design*, Vol. 39, No. 10, May 1991, pp. 67–71.

[12]    Spencer, N. W., "Comparison of State-of-the-Art Analog-to-Digital Converters," Massachusetts Institute of Technology, Lincoln Laboratory, Lexington, MA, Project Report AST-4, March, 1981.

[13]    Irons, F. H., and T. A. Rebold, "Characterization of High-Frequency Analog-to-Digital Converters for Spectral Analysis Applications," Massachusetts Institute of Technology, Lincoln Laboratory, Lexington, MA, Project Report AST-2, November 1986.

[14]    Thao, N. T., and M. Vetterli, "Optimal MSE Signal Reconstruction in Oversampled A/D Conversion Using Convexity," *Proceedings ICASSP "*92, 1992, Vol. 4, pp. 165–168.

[15]    Brannon, B., "Overcoming Converter Nonlinearities with Dither," Application Note AN-410, Norwood, MA: Analog Devices, 1995.

[16]    Jung, W., *Op Amp Applications*, Norwood, MA: Analog Devices, 2002, ISBN 0-916550-26-5, p. 6.165, "A Simple Wideband Noise Generator." Also available as *Op Amp Applications Handbook*, Newnes, 2005, ISBN 0-7506-7844-5, p. 5611.

[17]    Jung, W., "Wideband Noise Generator," *Electronic Design*, October 1, 1996.

[18]    Gailus, P. H., W. J. Turney, and F. R. Yester, Jr., "Method and Arrangement for a Sigma Delta Converter for Band-Pass Signals," U.S. Patent 4,857,928, August 15, 1988.

[19]    Jantzi, S. A., M. Snelgrove, and P. F. Ferguson Jr., "A 4th-Order Band-Pass Sigma-Delta Modulator," *IEEE Journal of Solid State Circuits*, Vol. 38, No. 3, March 1993, pp. 282–291.

[20]    Hendriks, P., R. Schreier, and J. DiPilato, "High Performance Narrowband Receiver Design Simplified by IF Digitizing Subsystem in LQFP," *Analog Dialogue*, Vol. 35-3, June–July 2001.

# Chapter 12

## Digital Filtering

### 12.1 Introduction

In signal processing, the function of a filter is to remove unwanted parts of the signal, such as random noise, or to extract useful parts of the signal, such as the components lying within a certain frequency range. Figure 12.1 illustrates the basic idea [1–4].

There are two main kinds of filters, analog and digital. They are quite different in their physical makeup and in how they work. An analog filter uses analog electronic circuits made up from components such as resistors, capacitors, and operational amplifiers (op amps) to produce the required filtering effect. Such filter circuits are widely used in many areas, such as noise reduction, video signal enhancement, and graphic equalizers. There are well-established standard techniques for designing an analog filter circuit for a given requirement. At all stages, the signal being filtered is an electrical voltage or current, which is the direct analog of the physical quantity (e.g., a sound or video signal or transducer output) involved. A digital filter uses a digital processor to perform numerical calculations on sampled values of the signal. The processor may be a general-purpose computer such as a PC or a specialized DSP chip.

There are many reasons why we process these analog signals in the digital domain, but these can all be reduced to three primary reasons:

- *Cost*:  DSP systems are almost always cheaper than analog
- *Functionality*: DSP systems can perform many operations that are impossible in the analog world
- *Programmability*: DSP systems can be reprogrammed to perform different functions. Analog systems must be redesigned for this functionality
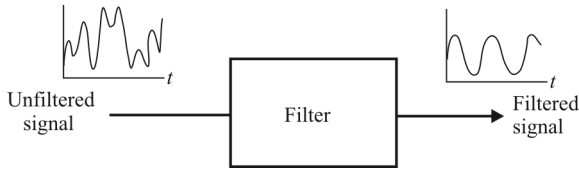
**Figure 12.1** Filtering concept.

The frequency characteristics of filters, be they analog or digital, are the primary way to specify their operations. Figure 12.2 shows such a typical frequency response.

For digital signal processing, an analog input signal must first be sampled and digitized using an ADC if the original signal is not already in digital form. The resulting binary numbers, representing successive sampled values of the input signal, are transferred to the processor, which carries out numerical calculations on them. These calculations typically involve multiplying the input values by constants and adding the products together. If necessary, the results of these calculations, which now represent sampled values of the filtered signal, are output through a DAC (*digital-to-analog-converter*) to convert the signal back to analog form. Note that in a digital filter, the signal is represented by a sequence of numbers rather than a voltage or current. The flow process diagram shown in Figure 12.3 illustrates the basic operation of such a system.

## 12.1.1 Advantages of Using Digital Filters

There are several advantages of implementing filtering digitally rather than with the analog counterparts. Among these are the following:
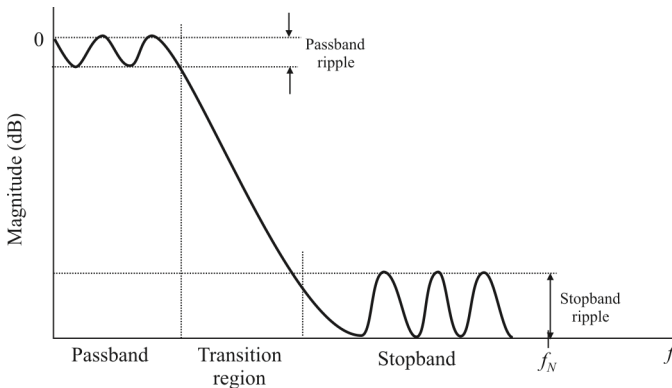


**Figure 12.2** Typical filter frequency characteristics.

- A digital filter's operation is determined by a program stored in the processor's memory, that is, they are programmable. This means the characteristics of the digital filter can easily be changed without affecting the circuitry (hardware). The functioning of an analog filter, on the other hand, can only be changed by redesigning the filter circuit.
- Extensive software exists so that digital filters are easily designed, tested, and implemented on general-purpose workstations. Debugging can occur where the economic impacts on design mistakes and errors are the least.
- The characteristics of analog filter circuits (particularly those containing active components) are subject to drift and are dependent on temperature. Digital filters do not suffer from these problems; they are absolutely stable with respect both to time and temperature.
- Unlike their analog counterparts, digital filters can handle low-frequency signals accurately. Also, as the speed of DSP technology continues to increase, digital filters are being applied to the RF domain, which in the past was the exclusive preserve of analog technology.
- Digital filters are very much more versatile in their ability to process signals in a variety of ways; this includes the ability of some types of digital filters to adapt to changes in the characteristics of the signal. Closely related to their reprogrammability, the characteristics of digital filters can be changed simply by downloading a different set of filter coefficients to perform completely different functions.
- Fast DSPs can handle complex combinations of filters in parallel or series, making the hardware requirements relatively simple and compact in comparison with the equivalent analog circuitry.

## 12.1.2 Disadvantages of Digital Filters

- Digital filters in general consume more power than their analog counterparts. This is particularly bothersome as their speed increases, facilitating filtering of RF signal, since the faster a digital filter operates, the more power it requires. Power consumption is a significant concern in many (most? all?) portable applications.
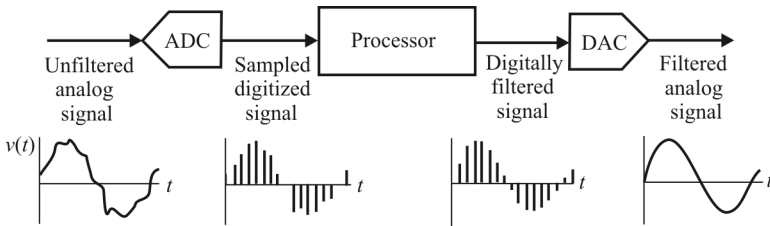
**Figure 12.3** Digital signal processing.

- Digitization is an approximate process, in that filtering occurs on samples of signals. When properly designed, this normally does not create serious problems. Nevertheless, there is always a maximum speed at which digital filters can operate.
- Analog filters can operate at higher frequency ranges.

This chapter is structured as follows. After this introduction we discuss the fundamental concepts of digital filtering. Then we present some very simple digital filters. The differences between recursive and nonrecursive filters are considered next. Then we discuss the filter transfer function in general. Multirate filters are presented next. The chapter concludes with a discussion of digital Hilbert transformers used as filters and how they compare with a simple delay for the same purpose.

## 12.2 Operation of Digital Filters

Suppose the raw signal that is to be digitally filtered is in the form of a voltage waveform (Figure 12.3) described by the function

$$x(t) = v(t) \tag{12.1}$$

where $t$ is time. This signal is sampled at time intervals $T_s$ (the sampling interval). The sampled value at time $t = iT_s$ is

$$x[i] = x(iT_s) \tag{12.2}$$

Thus, the digital values transferred from the ADC to the processor can be represented by the sequence

$$x[0], x[1], x[2], x[3], \ldots$$

corresponding to the values of the signal waveform at

$$t = 0, T_s, 2T_s, 3T_s, \ldots$$

and $t = 0$ is the instant at which sampling begins. At time $t = nT_s$ (where $n$ is some positive integer), the values available to the processor, stored in memory, are

$$x[0], x[1], x[2], \ldots, x[n]$$

Note that the sampled values $x[n + 1]$, $[n + 2]$ etc. are not available, as they haven't happened yet. The digital output from the processor to the DAC consists of the sequence of values

$$y[0], y[1], y[2], \ldots, y[n]$$

In general, the value of $y_n$ is calculated from the values $x[0]$, $x[1]$, $x[2]$, $x[3]$,..., $x[n]$. The way in which the $y$s are calculated from the $x$s determines the filtering action of the digital filter.

## 12.3 Simple Digital Filters

The following examples illustrate the essential features of digital filters.

*Unity gain filter*

$$y[n] = x[n]$$

Each output value $y_n$ is exactly the same as the corresponding input value $x_n$:

$$y[0] = x[0]$$
$$y[1] = x[1]$$
$$\ldots$$

This is a trivial case in which the filter has no effect on the signal.

*Simple gain filter*

$$y[n] = Kx[n] \tag{12.3}$$

where $K$ = constant. This simply applies a gain factor $K$ to each input value. $K > 1$ makes the filter an amplifier, while $0 < K < 1$ makes it an attenuator. $K < 0$ corresponds to an inverting amplifier.

*Single delay filter*

$$y[n] = x[n-1] \qquad (12.4)$$

The output value at time $t = nT_s$ is simply the input at time $t = (n-1)T_s$, that is, the signal is delayed by time $T_s$

$y[0] = x[-1]$
$y[1] = x[0]$
$y[2] = x[1]$
…

Since sampling is assumed to commence at $t = 0$, the input value $x[-1]$ at $t = -T_s$ is undefined. It is usual to take this (and any other values of $x$ prior to $t = 0$) as zero.

*Two-term difference filter*

$$y[n] = x[n] - x[n-1] \qquad (12.5)$$

The output value at $t = nT_s$ is equal to the difference between the current input $x[n]$ and the previous input $x[n-1]$:

$y[0] = x[0] - x[-1]$
$y[1] = x[1] - x[0]$
$y[2] = x[2] - x[1]$
…

That is, the output is the *change* in the input over the most recent sampling interval $T_s$. The effect of this filter is similar to that of an analog differentiator circuit and is the discrete time equivalent of it. As above, the value of $x[-1]$ is assumed to be zero.

*Two-term average filter*

$$y[n] = \frac{x[n] + x[n-1]}{2} \qquad (12.6)$$

The output is the average (arithmetic mean) of the current and previous input. This is a simple type of lowpass filter as it tends to smooth out high-frequency variations in a signal.

*Three-term average filter*

$$y[n] = \frac{x[n] + x[n-1] + x[n-1]}{3} \tag{12.7}$$

This is similar to the previous example, with the average being taken of the current and two previous inputs.

*Central difference filter*

$$y[n] = \frac{x[n] - x[n-2]}{2} \tag{12.8}$$

This is similar in its effect to (12.6). The output is equal to half the change in the input signal over the previous two sampling intervals.

### 12.3.1 Order of a Digital Filter

> **Definition 12.1:** The *order* of a digital filter is the number of *previous* inputs (stored in the processor's memory) used to calculate the current output.

Thus:

- Equation (12.3) above is a zero-order filter, as the current output $y[n]$ depends only on the current input $x[n]$ and not on any previous inputs.
- In (12.7) and (12.8), two previous inputs ($x[n-1]$ and $x[n-2]$) are needed, so these are second-order filters.

Filters may be of any order from zero upward.

### 12.3.2 Digital Filter Coefficients

All of the digital filter examples given above can be written in the following general forms:

**Table 12.1** Example Filter Coefficients

| Example | Order | $a_0$ | $a_1$ | $a_2$ |
|---------|-------|-------|-------|-------|
| 1 | 0 | 1 | - | - |
| 2 | 0 | $K$ | 0 | - |
| 3 | 0 | 0 | 1 | - |
| 4 | 1 | 1 | −1 | - |
| 5 | 1 | 1/2 | 1/2 | - |
| 6 | 1 | 1/3 | 1/3 | 1/3 |
| 7 | 2 | 1/2 | 0 | −1/2 |

Zero order: $\quad y[n] = a_0 x[n]$

First order: $\quad y[n] = a_0 x[n] + a_1 x[n-1]$

Second order: $\quad y[n] = a_0 x[n] + a_1 x[n-1] + a_2 x[n-2]$

or, in general,

$$k\text{th order:} \qquad y[n] = \sum_{i=0}^{k} a_i x[n-i]$$

The constants $a_0$, $a_1$, $a_2$, ..., appearing in these expressions are called the *filter coefficients*. It is the values of these coefficients that determine the characteristics of a particular filter.

**Example 12.1:** Order $a_0$ $a_1$ $a_2$. See Table 12.1.

There are many computer tools for designing the coefficients and with most of these packages the user specifies the desired filter performance, and the tools will generate best fit coefficients for a specified filter length. The criteria include:

The passband cutoff frequency (in Hz)
Stopband cutoff frequency (in Hz)
The passband ripple (in dB)
The stopband attenuation (in dB)

The number of coefficients is dependent on the steepness of the roll-off between the passband and the stopband and also the magnitudes of the ripple and the attenuation in the appropriate bands. The basic rule of digital filters is the more stringent the requirements, the more CPU cycles will be required.
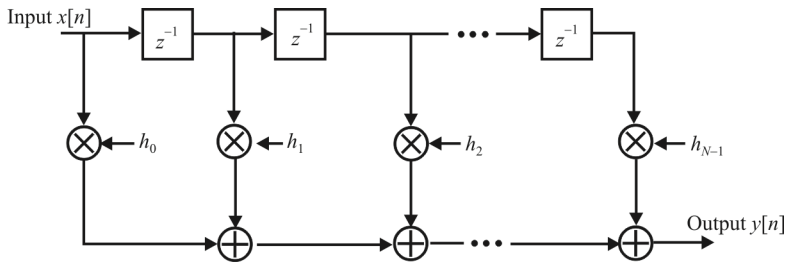
**Figure 12.4** Multiplier and accumulator.

# 12.4 Recursive and Non-Recursive Filters

### 12.4.1 Impulse Response

The impulse response of a digital filter is the output sequence from the filter when a *unit impulse* is applied at its input. A unit impulse is a very simple input sequence consisting of a single value of 1 at time $t = 0$, followed by zeros at all subsequent sampling instants. An FIR filter is one whose impulse response is of finite duration. An IIR filter is one whose impulse response theoretically continues forever because the recursive terms feed back energy into the filter input and keep it going.

One of the most important algorithms for processing signals is the convolution operator, which is also known as the *finite impulse response* (FIR) filter, also referred to as *non-recursive filters*. All of the filters considered so far are FIR filters. Filters reduce (or attenuate) certain frequency bands within a signal and they are typically classified into four types: lowpass, highpass, bandpass, and bandstop (notch).

The fundamental operations for the convolution operation are the *multiplication and accumulation* (MAC), and these are the fundamental operations for all DSP operations. The operation is described mathematically by

$$y[m] = \sum_{n=0}^{N-1} h_n x[m-n] \qquad\qquad 0 \le m \le N-1 \qquad\qquad (12.9)$$

This is equivalent to the flow diagram shown in Figure 12.4, which is also a functional filter block diagram.

This flow diagram shows more clearly how the MAC operations are used together to produce the output. The digital input values are placed into the filter in the top left-hand corner where they are multiplied by the first coefficient $h_0$ and then all of the products (between data and coefficient values) are added together (accumulated) to generate the output. On subsequent sample periods the samples
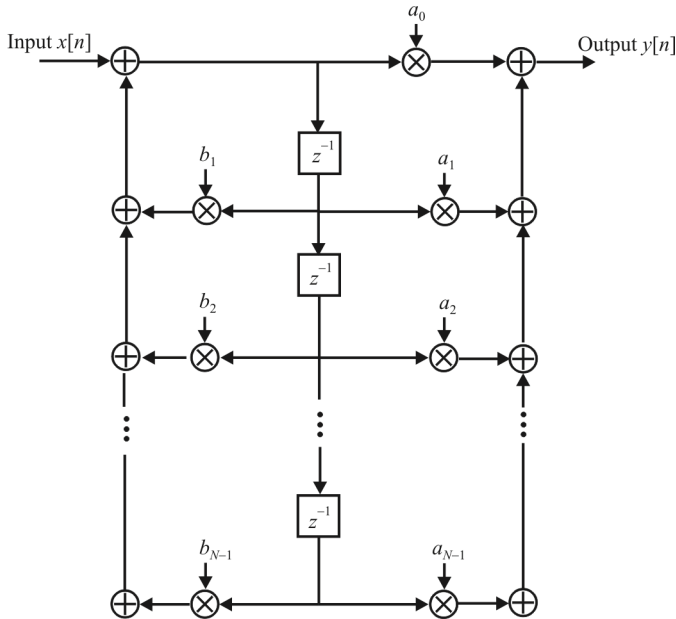
**Figure 12.5** Infinite impulse response digital filter.

move down the delay line from left to right, and then the next sequence of MACs is performed. The blocks shown as $z^{-1}$ delay each sample by one sample period so the overall delay is equal to the number of delay operators.

The structure in Figure 12.4 uses a feedforward arrangement. It is also possible to implement a similar structure with both feedforward and feedback data paths. When the filter includes feedback—then it is referred to as an *infinite impulse response* (IIR) filter, that is, even with the most basic input signal, the system will reverberate forever. Another name for the IIR filter is a *recursive filter*. The end result of using feedback is that the output is dependent on all previous input values, whereas the output of an FIR filter is only dependent on $N$ coefficients, where $N$ is the number of coefficients in the filter.

The processing flow diagram of an IIR filter is shown in Figure 12.5. The governing equation for this IIR filter is

$$y[n] = \sum_{k=1}^{N} b_k y[n-k] + \sum_{k=0}^{M} a_k x[n-k] \qquad (12.10)$$

Comparing FIR filters to IIR filters, we see that FIR filters can have linear phase (in real-time), which means that all of the frequencies in a signal are delayed by a

**Table 12.2** Lowpass FIR Filter Coefficients

| $h_0 =$ | $h_{20} =$ | −0.0324800 |
|---|---|---|
| $h_1 =$ | $h_{19} =$ | 0.0381875 |
| $h_2 =$ | $h_{18} =$ | 0.0288168 |
| $h_3 =$ | $h_{17} =$ | −0.0476191 |
| $h_4 =$ | $h_{16} =$ | −0.0264265 |
| $h_5 =$ | $h_{15} =$ | 0.0651707 |
| $h_6 =$ | $h_{14} =$ | 0.0249165 |
| $h_7 =$ | $h_{13} =$ | −0.1070000 |
| $h_8 =$ | $h_{12} =$ | −0.0240785 |
| $h_9 =$ | $h_{11} =$ | 0.3186069 |
| $h_{10} = 0.5238096$ | | |

fixed number of cycles. Nonlinear phase in feedback filters means that different frequencies are delayed by different amounts, which can cause problems in certain applications. FIR filters also have low noise levels because the feedback in IIR filters will also feed back any quantization noise, which leads to IIR filters potentially being unstable. The primary benefit of IIR filters is that, due to the effects of feedback, they typically provide sharper transition between the pass-band and stopband and they can also provider higher levels of attenuation in the stopband for a given number of MAC cycles.

## 12.4.2 Lowpass FIR Filter

The transfer function for an ideal lowpass FIR filter is illustrated in Figure 12.6(a). This transfer function has a passband extending from $\omega = 0$ to $\omega = \omega_l$ and a stopband extending from $\omega = \omega_l$ up to the Nyquist frequency of $\omega = \pi$ as we see in the figure. In some cases there is a region between the passband and the stop-band where neither the desired nor the undesired signals exist. Or the region can be defined as a transition region, with the ideal response having a transition function that more smoothly connects the passband and stopband responses and allows a better total approximation [see Figure 12.6(b)]. The third possibility shown in Figure 12.6(c) does not define the approximation over the transition region and is called a *transition band*. All three cases are considered by the different design criteria and methods.

There are numerous computer programs that solve for the FIR filter coefficients. Using such a program we have the following example of filter design.

**Example 12.2: Length 21 Lowpass Filter by Frequency Sampling.** Suppose we are to design an odd-length 21, linear phase, lowpass filter where the desired frequency response has a passband that is half of the maximum frequency as illustrated in
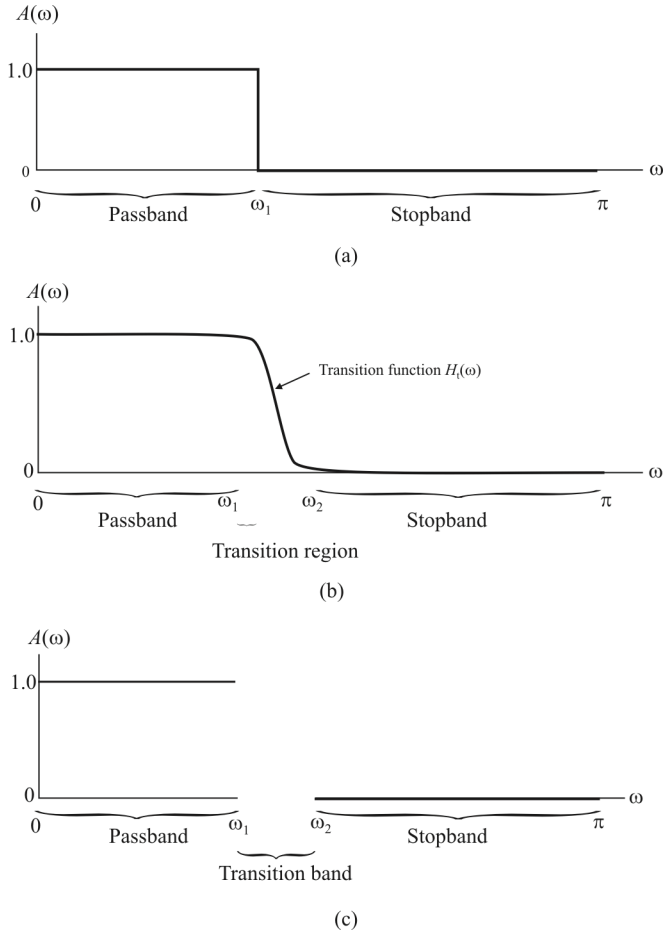
**Figure 12.6** Lowpass filter characteristics: (a) idea, (b) realistic, and (c) without a specified transition band characteristic.
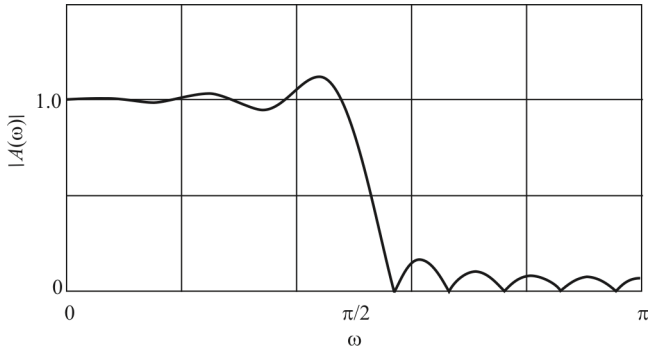
**Figure 12.7** Length 21 lowpass filter amplitude response.

Figure 12.6(a). Thus the band-edge is $f_p = 0.25$ Hz for a sampling frequency of one sample per second. The odd-length formula given by [5] is

$$h_n = \frac{1}{N}\left[A_0 + \sum_{k=1}^{M} 2A_k \cos\left(\frac{2\pi(n-M)k}{N}\right)\right]$$ (12.11)

The resulting filter coefficients are given in Table 12.2. The frequency response is shown in Figure 12.7. Note the ripple in the passband and the stopband near the band edge and the exact interpolation of the sample points in the passband and the stopband. The locations of the zeros in the transfer function are shown in Figure 12.8.

## 12.4.3 Order of an IIR Digital Filter

The order of a digital filter was defined earlier as the number of previous inputs that have to be stored in order to generate a given output. This definition is
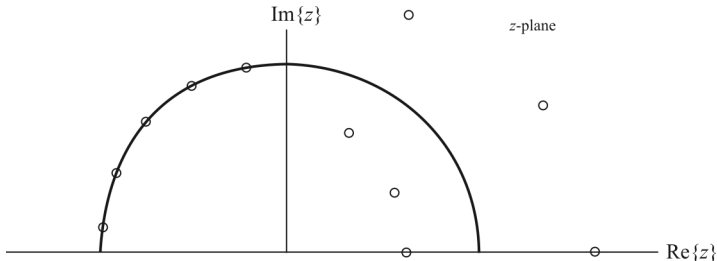


**Figure 12.8** Length 21 lowpass filter zeros.

appropriate for FIR filters, which use only the current and previous inputs to compute the current output. In the case of recursive filters, the definition can be extended as follows:

> **Definition 12.2:** The *order* of a recursive filter is the larger of the number of previous input or output values required to compute the current output.

Thus

$$k\text{th order: } y[n] = \sum_{i=0}^{N} a_i x[n-i] + \sum_{i=1}^{M} b_i y[n-i], \ k \text{ is the larger of } N, M \qquad (12.12)$$

We can see that this definition is quite general: it applies both to FIR and IIR filters. For example, the recursive filter discussed above, given by the expression

$$y[n] = x[n] + y[n-1] \qquad (12.13)$$

is first order, because it uses one previous output value ($y[n-1]$), even though no previous inputs are required.

In practice, recursive filters usually require the *same number of previous inputs and outputs*. Thus, a first-order recursive filter generally requires one previous input ($x[n-1]$) and one previous output ($y[n-1]$), while a second-order recursive filter makes use of two previous inputs ($x[n-1]$ and $x[n-2]$) and two previous outputs ($y[n-1]$ and $y[n-2]$); and so on, for higher orders.

### 12.4.4 Example of a Recursive Filter

A simple example of a recursive digital filter is given by

$$y[n] = x[n] + y[n-1]$$

In   words, this filter determines the current output ($y[n]$) by adding the current input ($x[n]$) to the previous output ($y[n-1]$). Note that $y[-1]$ (like $x[-1]$) is undefined and is usually taken to be zero. The flow diagram for this filter is shown in Figure 12.9.

Let us consider the effect of this filter in more detail. If in each of the expressions we substitute for $y[n-1]$ the value given by the previous expression, we get the following:
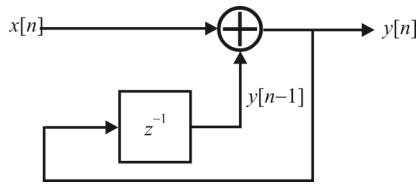
$$y[0] = x[0] + y[-1] = x[0]$$

**Figure 12.9** Flow diagram of a simple recursive filter. This filter is an integrator (see text).

$$y[1] = x[1] + y[0] = x[1] + x[0]$$
$$y[2] = x[2] + y[1] = x[2] + x[1] + x[0]$$
$$y[3] = x[3] + y[2] = x[3] + x[2] + x[1] + x[0]$$
$$\ldots$$

Thus, we can see that $y[n]$, the output at $t = nT_s$, is equal to the sum of the current input $x[n]$ and all the previous inputs. This filter therefore sums, or *integrates*, the input values, and so has a similar effect to an analog integrator. This example demonstrates an important and useful feature of recursive filters: the economy with which the output values are calculated, as compared with the equivalent non-recursive filter. In this example, each output is determined simply by adding two numbers together. For instance, to calculate the output at time $t = 10T_s$, the recursive filter uses the expression

$$y[10] = x[10] + y[9]$$

## 12.4.5 Coefficients of IIR Digital Filters

From the above discussion, we can see that a recursive filter is basically like a non-recursive filter, with the addition of extra terms involving previous inputs ($y[n-1]$, $y[n-2]$ etc.). A first-order recursive filter can be written in the general form

$$y[n] = \frac{a_0 x[n] + a_1 x[n-1] - b_1 y[n-1]}{b_0} \tag{12.14}$$

Note the minus sign in front of the recursive term $b_1 y[n-1]$ and the factor $(1/b_0)$ applied to all the coefficients. The reason for expressing the filter in this way is that it allows us to rewrite the expression in the following symmetrical form:

$$b_0 y[n] + b_1 y[n-1] = a_0 x[n] + a_1 x[n-1]$$

In the case of a second-order filter, the general form is

$$y[n] = \frac{a_0 x[n] + a_1 x[n-1] + a_2 x[n-2] - b_1 y[n-1] - b_2 y[n-2]}{b_0}$$

The alternative symmetrical form of this expression is

$$b_0 y[n] + b_1 y[n-1] + b_2 y[n-2] = a_0 x[n] + a_1 x[n-1] + a_2 x[n-2] \qquad (12.15)$$

Note the common convention is that the coefficients of the inputs (the $x$s) are denoted by $a$s, while the coefficients of the outputs (the $y$s) are denoted by $b$s.

## 12.5 The Transfer Function of a Digital Filter

In the last section, we used two different ways of expressing the functioning of a digital filter: a form giving the output $y[n]$ directly, and a symmetrical form with all the output terms on one side and all the input terms on the other. In this section, we introduce what is called the *transfer function* of a digital filter. This is obtained from the symmetrical form of the filter expression, and it allows us to describe a filter by means of a convenient, compact expression. We can also use the transfer function of a filter to determine its frequency response.

First of all, we must introduce the *delay operator*, denoted by the symbol $z^{-1}$. When applied to a sequence of digital values, this operator gives the previous value in the sequence. It therefore in effect introduces a delay of one sampling interval. Applying the operator $z^{-1}$ to an input value (say $x[n]$) gives the previous input ($x[n-1]$):

$$z^{-1} x[n] = x[n-1] \qquad (12.16)$$

Note that $z^{-1} x[0]$ would be $x[-1]$, which is unspecified (and usually taken to be zero). Similarly, applying the $z^{-1}$ operator to an output gives the previous output

$$z^{-1} y[n] = y[n-1]$$

Applying the delay operator $z^{-1}$ twice produces a delay of two sampling intervals

$$z^{-1}(z^{-1} x[n]) = z^{-1} x[n-1] = x[n-2]$$

Thus

$$z^{-1}z^{-1} = z^{-2}$$

That is, the operator $z^{-2}$ represents a delay of two sampling intervals

$$z^{-2}x[n] = x[n-2]$$

This notation can be extended to delays of three or more sampling intervals, the appropriate power of $z^{-1}$ being used.

Let us now use this notation in the description of a recursive digital filter. Consider, for example, a general second-order filter, given in its symmetrical form by (12.15). We will make use of the following identities:

$$y[n-1] = z^{-1}y[n]$$
$$y[n-2] = z^{-2}y[n]$$
$$x[n-1] = z^{-1}x[n]$$
$$x[n-2] = z^{-2}x[n]$$

Substituting these expressions into (12.15) gives

$$(b_0 + b_1 z^{-1} + b_2 z^{-2})y[n] = (a_0 + a_1 z^{-1} + a_2 z^{-2})x[n]$$

Rearranging this to give a direct relationship between the output and input for the filter, we get

$$H(z) = \frac{y[n]}{x[n]} = \frac{a_0 + a_1 z^{-1} + a_2 z^{-2}}{b_0 + b_1 z^{-1} + b_2 z^{-2}} \tag{12.17}$$

This is the general form of the transfer function for a second-order IIR filter.

For a first-order filter, the terms in $z^{-2}$ are omitted in (12.17). For filters of order higher than 2, further terms involving higher powers of $z^{-1}$ are added to both the numerator and denominator of the transfer function.

A nonrecursive (FIR) filter has a simpler transfer function that does not contain any denominator terms. The coefficient $b_0$ is usually taken to be equal to 1, and all the other $b$ coefficients are zero. The transfer function of a second-order FIR filter can therefore be expressed in the general form

$$H(z) = \frac{y[n]}{x[n]} = a_0 + a_1 z^{-1} + a_2 z^{-2} \tag{12.18}$$

For example, the three-term average filter, defined by (12.7), can be written using the $z^{-1}$ operator notation as

$$y[n] = \frac{x[n] + z^{-1}x[n] + z^{-2}x[n]}{3} = \frac{(1 + z^{-1} + z^{-2})x[n]}{3}$$

The transfer function for the filter is therefore

$$H(z) = \frac{y[n]}{x[n]} = \frac{1 + z^{-1} + z^{-2}}{3}$$

The general form of the transfer function for a first-order recursive filter can be written

$$H(z) = \frac{y[n]}{x[n]} = \frac{a_0 + a_1 z^{-1}}{b_0 + b_1 z^{-1}} \tag{12.19}$$

**Example 12.3:** Consider the simple first-order recursive filter given by (12.13). To derive the transfer function for this filter, we rewrite the filter expression using the $z^{-1}$ operator:

$$(1 - z^{-1})y[n] = x[n]$$

Rearranging gives the filter transfer function as

$$H(z) = \frac{y[n]}{x[n]} = \frac{1}{1 - z^{-1}}$$

**Example 12.4:** Consider the second-order IIR filter

$$y[n] = x[n] + 2x[n-1] + x[n-2] - 2y[n-1] + y[n-2]$$

Collecting output terms on the left and input terms on the right to give the symmetrical form of the filter expression, we get

$$y[n] + 2y[n-1] - y[n-2] = x[n] + 2x[n-1] + x[n-2]$$

Expressing this in terms of the $z^{-1}$ operator gives

$$(1+2z^{-1}-z^{-2})y[n]=(1+2z^{-1}+z^{-2})x[n]$$

and so the transfer function is

$$H(z)=\frac{y[n]}{x[n]}=\frac{1+2z^{-1}+z^{-2}}{1+2z^{-1}-z^{-2}}$$

## 12.5.1 The Frequency Response of Digital Filters

The $z$-transform of a discrete time (sampled) $f(n\tau)$ is defined as

$$F(z)=\sum_{n=-\infty}^{\infty}f(n\tau)z^{-n} \tag{12.20}$$

If we substitute $z=e^{s\tau}$ into (12.20) we see that

$$F(s)=F(z)\big|_{z=e^{s\tau}} \tag{12.21}$$

Equation (12.21) is the Laplace transform of the sampled sequence $f(nT_\mathrm{s})$. Then if the region of convergence for $F(z)$ includes the unit circle, $|z|=1$, then

$$F(j\omega)=\left|F(z)\right|_{z=e^{j\omega\tau}} \tag{12.22}$$

It turns out that the filter transfer functions we have discussed so far are the $z$-transforms of the filter impulse response. So we see that the transfer function can be represented in the complex plane as

$$H(j\omega)=H(z)\big|_{z=j\omega} \tag{12.23}$$

So the frequency response of the digital filter can be obtained by using (12.23).

Equation (12.23) generally leads to a complex function that has magnitude and phase components:

$$H(z)\big|_{z=j\omega}=\left|H(j\omega)\right|e^{j\Theta(\omega)} \tag{12.24}$$

and, of course,

$$|H(j\omega)| = \sqrt{\text{Re}^2\{H(j\omega)\} + \text{Im}^2\{H(j\omega)\}}$$

$$\Theta(j\omega) = \tan^{-1}\frac{\text{Im}\{H(j\omega)\}}{\text{Re}\{H(j\omega)\}}$$

**Example 12.5** Consider Example 12.4. By multiplying the numerator and denominator by $z$, $H(z)$ can be written as

$$H(z) = \frac{z}{z-1}$$

leading to

$$H(j\omega) = H(z)\big|_{z=j\omega} = \frac{j\omega}{j\omega - 1}$$

that, after some trivial manipulations, yields

$$H(j\omega) = \frac{\omega^2}{1+\omega^2} - j\frac{\omega}{1+\omega^2} \tag{12.25}$$

with

$$|H(j\omega)| = \sqrt{\text{Re}^2\{H(j\omega)\} + \text{Im}^2\{H(j\omega)\}}$$

$$= \sqrt{\left(\frac{\omega^2}{1+\omega^2}\right)^2 + \left(\frac{\omega}{1+\omega^2}\right)^2}$$

$$= \frac{\omega}{\sqrt{1+\omega^2}}$$

and

$$\text{Arg}\{H(j\omega)\} = \tan^{-1}\frac{\text{Im}\{H(j\omega)\}}{\text{Re}\{H(j\omega)\}}$$

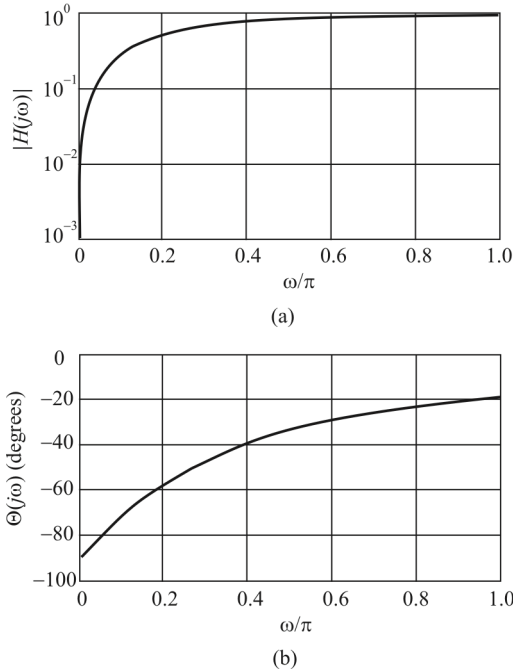$$= \tan^{-1}\frac{\dfrac{-\omega}{1+\omega^2}}{\dfrac{\omega^2}{1+\omega^2}}$$

**Figure 12.10** Frequency response of Example 12.5: (a) is the magnitude, while (b) is the phase of the transfer function.

$$= \tan^{-1} \frac{-1}{\omega} = -\tan^{-1} \frac{1}{\omega}$$

The amplitude and phase of $H(j\omega)$ based on (12.25) are shown in Figure 12.10.

# 12.6 Multirate Processing of Bandpass and *I/Q* Signals

Multirate processing of digitized signals allows for considerable flexibility in processing such signals. The two fundamental multirate operations, decimation/downsampling and interpolation/upsampling, enable the sample rate to be altered digitally. In addition to this, they also offer an interesting alternative to mixing in performing frequency translations [6].

### 12.6.1 Decimation or Downsampling with Complex Signals

The flow diagram to reduce the sample rate by an integer factor $L$ is presented in Figure 12.11, with $f_s$ denoting the original sample rate. In the downsampling ($\downarrow L$), every $L$th sample of the input sequence is selected to form the output sequence and the new sample rate becomes $f_s /L$. As a consequence, all the frequency bands located at the integer multiples of $f_s /L$ (within $-f_s/2 \dots f_s/2$ of course) are aliased down to baseband. Thus, if the (generally complex) input signal is of lowpass type (passband $-W_{neg} \dots W_{pos}$), the decimation filter $H(z)$ should attenuate all the frequency bands of width $W = W_{neg} + W_{pos}$ located correspondingly at the previous critical frequencies. Naturally, the bandwidth $W = W_{neg} + W_{pos}$ needs to be smaller than $f_s /L$ but there's no restriction such that, for example, $W_{pos}$ should be smaller than $(f_s /L)/2$. As long as $f_s /L \geq W$, the downsampled signal is free from aliasing.

On the other hand, if the desired signal is originally a bandpass signal (with a generally complex-valued baseband equivalent), the inherent aliasing can be exploited to change the signal center frequency. Now, the decimation filter $H(z)$ is a bandpass filter selecting the desired frequency band, and aliasing can be used to bring the signal closer to baseband. As a special case of this, if the signal is centered at any multiple of the output sample frequency $f_s /L$, an analytic bandpass filter and decimation will result in a direct bandpass-to-lowpass transformation. This basically represents a digital equivalent of the complex ($I/Q$) subsampling scheme of the previous section. Two example cases are shown in Figures 12.11 and 12.12.

### 12.6.2 Interpolation or Upsampling with Complex Signals

The basic flow diagram to increase the sample rate by an integer factor $L$ is presented in Figure 12.13, with $f_s$ again denoting the original sample rate. The output sequence of the upsampler ($\uparrow L$) is formed by adding $L - 1$ zeros between each original input sample. As a consequence, all the spectral images (within $-Lf_s/2 \dots Lf_s/2$) of the input spectrum appear now at the output signal at the multiples of the input sample rate $f_s$. Traditionally, the interpolation filter $H(z)$ attenuates these extra images, retaining only the original spectral component. This is, however, not the only possibility. More precisely, any of the spectral images within $-Lf_s/2 \dots Lf_s/2$ can be considered to be the desired one. As an example, the original lowpass signal can be transformed into a bandpass signal by simply using a proper bandpass filter as the interpolation filter $H(z)$. This filter now retains the spectral image at the desired center frequency and attenuates the others.

### 12.6.3 Efficient Polyphase Structures

Polyphase filtering represents one interesting approach to implement decimation or interpolation in a flexible yet computationally efficient way. In the traditional
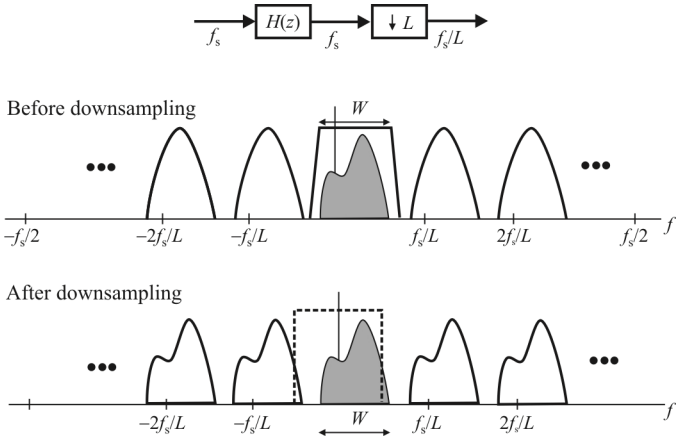
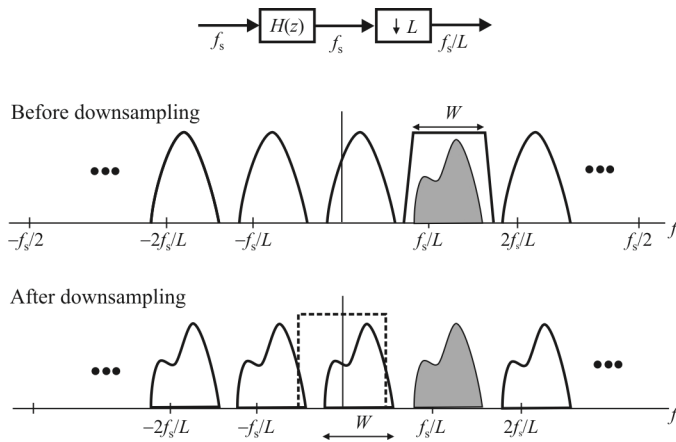**Figure 12.11** Downsampling example.



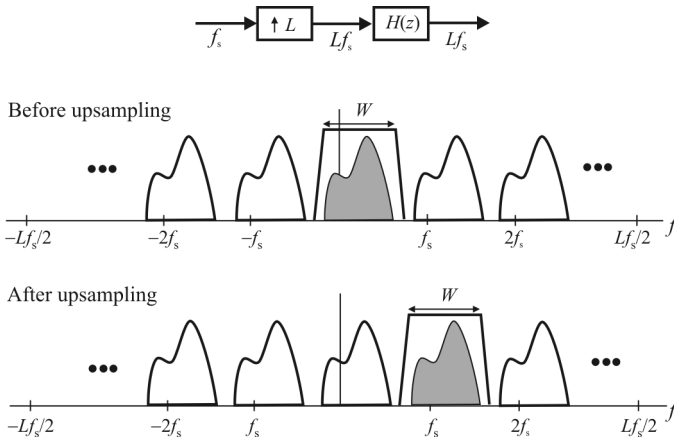**Figure 12.12** A second downsampling example.

Figure 12.13 Upsampling example.

approaches, the decimation/interpolation filters operate at the higher sampling rate, either before downsampling or after upsampling. Given that the down/up sampling ratio is $L$, the idea in the polyphase structures is to split the related filtering into $L$ parallel stages operating at the lower sampling rate. In applications requiring very high operation speeds such as frequently encountered in digital EW receivers, this can be a crucial benefit. Furthermore, the polyphase structures are quite flexible if used, for example, in channelization applications. These aspects will be explained in more detail in the following.

### 12.6.3.1 Polyphase Decomposition of FIR Filters

The so-called polyphase decomposition of a finite length filter $H(z)$ is usually formulated as

$$H(z) = \sum_{l=0}^{L-1} z^{-l} H_l(z^L) \tag{12.26}$$

In words, the output of any FIR filter in general can be constructed as a sum of the outputs of the filters $H_0(z^L)$, $H_1(z^L)$, …, $H_{L-1}(z^L)$ whose input signals are delayed by $z^0$, $z^{-1}$, …, $z^{-(L-1)}$. Given that the impulse response of $H(z)$ is $h[n]$, the impulse responses of $H_0(z)$, $H_1(z)$, …, $H_{L-1}(z)$ are simply

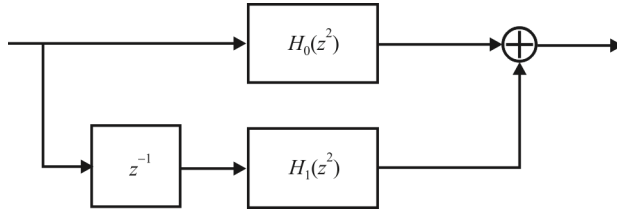**Figure 12.14** Polyphase FIR.

$$h_0[n] = \{h[0], h[L], \ldots\}$$
$$h_1[n] = \{h[1], h[L+1], \ldots\}$$
$$\vdots$$
$$h_{L-1}[n] = \{h[L-1], h[2L-1], \ldots\}$$

(12.27)

**Example 12.6:** Two-phase decomposition of $H(z) = h[0] + h[1]$ $z^1 + \ldots + h\,[14]z^{-14}$ is

$$H(z) = h[0] + h[2]z^{-2} + h[4]z^{-4} + h[6]z^{-6} + h[8]z^{-8}$$
$$+ h[10]z^{-10} + h[12]z^{-12} + h[14]z^{-14} + h[1]z^{-1} + h[3]z^{-3}$$
$$+ h[5]z^{-5} + h[7]z^{-7} + h[9]z^{-9} + h[11]z^{-11} + h[13]z^{-13}$$
$$= H_0(z^2) + z^{-1}H_1(z^2)$$

(12.28)

where

$$h_0[n] = \{h[0], h[2], h[4], h[6], h[8], h[10], h[12], h[14]\}$$
$$h_1[n] = \{h[1], h[3], h[5], h[7], h[9], h[11], h[13]\}$$

The resulting polyphase architecture is shown in Figure 12.14. The spectra of the two branches as well as their sums are shown in Figure 12.15.

12.6.3.2 Basic Polyphase Decimators and Interpolators

In decimation applications, the downsampler that traditionally operates on the filter output can now be transferred to the front of the branch filters given that the $L$ time delays in the filters $H_0(z^L)$ and $H_1(z^L)$ are replaced by ordinary unit delays. This operation is intuitively clear and theoretically justified by the famous *noble*
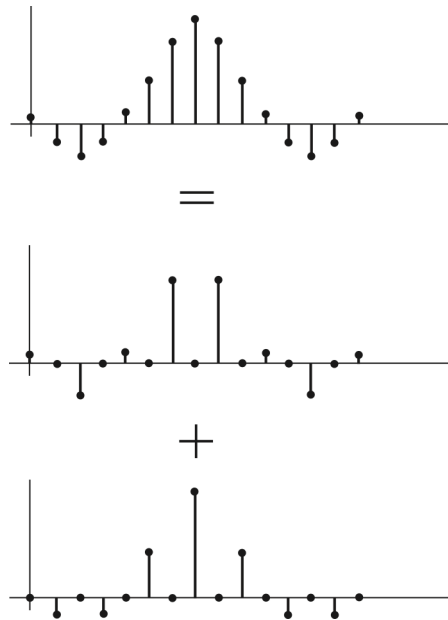
**Figure 12.15** Polyphase FIR spectra.

*identity* of multirate signal processing. This identity is illustrated in Figure 12.16. So in the $i$th branch, the input signal is delayed by $z^{-i}$, downsampled by $L$, and filtered using $H_i(z)$. Finally, the outputs of the $L$ branches are summed to form the final decimated output signal. Note that all the branch filters operate at the lower sampling rate. This is illustrated in the following example.

> **Example 12.6 (continued):** Downsampling by $L = 2$. See Figure 12.17.

Since in general the delay $z^{-i}$ is different in every branch and the down-samplers operate synchronously, the low-rate data sequences entering the branch filters are all disjoint. Thus, the front-end delays and downsamplers can actually be discarded by simply feeding every $L$th sample (with a proper time shift) to the polyphase branches using a commutative switch. This final structure is depicted in Figure 12.18.

Similar reasoning can also be used in the interpolation case. The traditional approach based on zero-padding and filtering maps into a polyphase structure where the input signal to be interpolated is fed directly into the branch filters $H_0(z)$, $H_1(z)$, …, $H_{L-1}(z)$. The outputs of these filters are then upsampled and delayed, the delay being $z^{-1}$ in the $i$th branch, and finally summed to form the
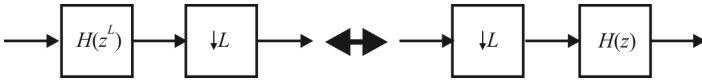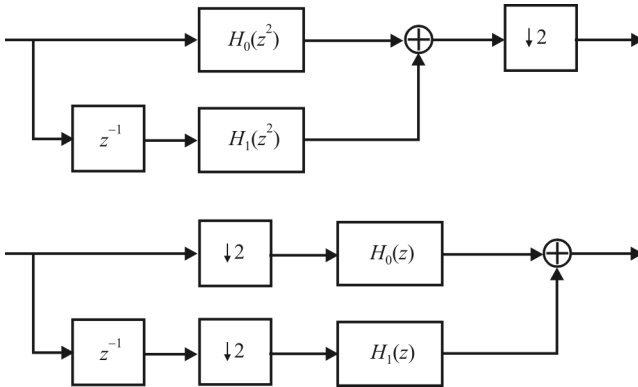
**Figure 12.16** Noble identity.



**Figure 12.17** Another polyphase FIR.

(a)                                        (b)

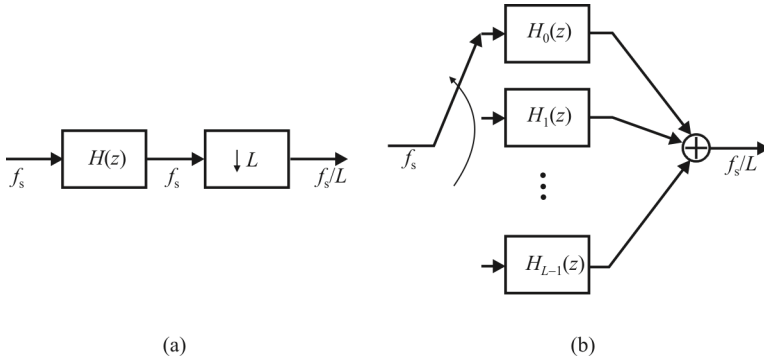**Figure 12.18**  (a) The basic decimation (downsampling) scheme. (b) The corresponding polyphase implementation.

interpolator output. Due to zero-packing and different branch delays, only one branch filter output actually contributes to the final output (with other outputs being zero) at any given time instant.  Thus, as in the decimation case, the final structure can be implemented by simply multiplexing the branch filter outputs using a commutator. This approach is illustrated in Figure 12.19.

One interesting interpretation of the previous polyphase structures is related to aliasing and the amplitude and phase characteristics of the polyphase filters. As an example, consider the decimation case. Since the input signal is directly down-sampled in each polyphase branch, all the bands located at the integer multiples of the final output sampling rate alias to baseband. However, due to the relative delays of the different branches as well as different phase characteristics of the
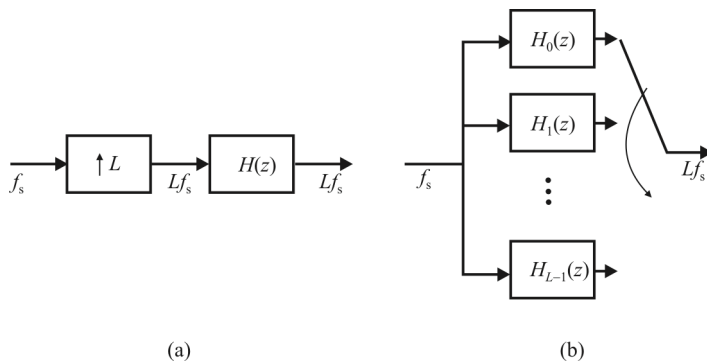


(a)                                        (b)

**Figure 12.19**    (a) The basic interpolation (upsampling) scheme. (b) The corresponding polyphase implementation.

polyphase filters, only the information within the passband of the prototype filter $H(z)$ will appear in the final decimator output. To be more specific, all the polyphase branch filters are actually all-pass filters [4] whose amplitude response is ideally constant. Furthermore, the phase delays of the different filters differ by $1/L$, with $H_0(z)$ having the largest delay. This is easy to see even intuitively when considering how the polyphase filters are obtained from the "prototype" $H(z)$.

### 12.6.3.3 Bandpass Polyphase Structures

The previous discussion is valid for both lowpass and bandpass decimator/ interpolator structures. The only difference is, of course, related to the characteristics and design of the filter $H(z)$. A straightforward way to handle the lowpass and bandpass cases is to consider them separately. However, the full flexibility of the polyphase structures can only be capitalized by treating them together.

To illustrate the basic idea, assume the filter $H(z)$ is designed for a specific lowpass decimation scenario (passband $W_{\text{neg}} - W_{\text{pos}}$ in general). Now, suppose we wish to change the structure to process a bandpass signal located around a center-frequency $f_c$, which is an integer multiple of the output rate $f_s /L$. In terms of the normalized frequency variable $\omega = 2\pi f/f_s$, this means that $\omega_c$ is an integer multiple of $2\pi/L$. In general, an analytic filter $G(z)$ to extract the interesting band can be obtained simply by frequency translating the corresponding lowpass prototype filter $H(z)$ as $g[n] = h[n]\exp(j\omega Cn)$. The impulse responses of the corresponding polyphase implementation of $g[n]$ are then obtained as presented before, that is, $g_0[n] = \{g[0], g[L],\ldots\}$, $g_1[n] = \{g[1], g[L+1],\ldots\}$, etc.

However, after some manipulations, the polyphase impulse responses for the analytic filter $G(z)$ can be written simply as

$$
\begin{aligned}
g_0[n] &= h_0[n] \\
g_1[n] &= h_1[n]\exp(jk2\pi / L) \\
g_2[n] &= h_2[n]\exp(jk2\pi 2 / L) \\
&\;\;\vdots \\
g_{L-1}[n] &= h_{L-1}[n]\exp(jk2\pi(L-1)/ L)
\end{aligned}
\tag{12.29}
$$

where the integer $k$ is the channel index—that is, $\omega_c = k(2\pi/L)$. This is the same polyphase representation as in the lowpass case except for the constant complex multipliers $\exp[jk(2\pi)i/L]$.

**Example 12.7:** Bandpass downsampling by $L = 4$ with $\omega_c = \pi/2$ (i.e., $f_c = f_s / 4$), $g[n] = h[n]\exp(j(\pi/2)n)$
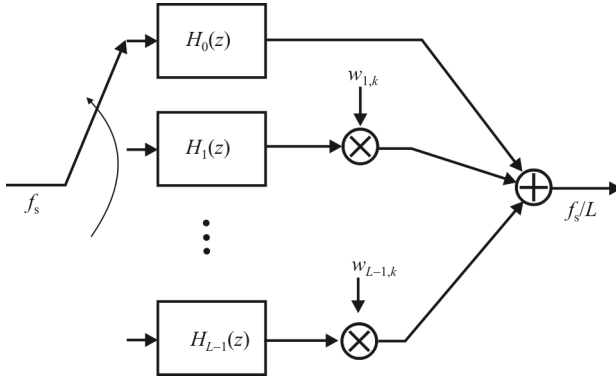
**Figure 12.20** General polyphase decimator.

$$g_0[n] = \{h[0]e^{j\frac{\pi}{2}0}, h[4]e^{j\frac{\pi}{2}4}, h[8]e^{j\frac{\pi}{2}8}, \ldots\} = \{h[0], h[4], h[8], \ldots\}$$

$$g_1[n] = \{h(1)e^{j\frac{\pi}{2}1}, h(5)e^{j\frac{\pi}{2}5}, h(9)e^{j\frac{\pi}{2}9}, \ldots\} = \{h(1), h(5), h(9), \ldots\}e^{j\frac{\pi}{2}}$$

$$g_2[n] = \{h[2]e^{j\frac{\pi}{2}2}, h[6]e^{j\frac{\pi}{2}6}, h[10]e^{j\frac{\pi}{2}10}, \ldots\} = \{h[2], h[6], h[10], \ldots\}e^{j\pi}$$

$$g_3[n] = \{h[3]e^{j\frac{\pi}{2}3}, h[7]e^{j\frac{\pi}{2}7}, h[11]e^{j\frac{\pi}{2}11}, \ldots\} = \{h[3], h[7], h[11], \ldots\}e^{j\frac{3\pi}{2}}$$

So as stated before, the modulating exponentials in the polyphase filters reduce to constant multipliers $w_{i,k} = \exp(jk2\pi i / L), i = 1, 2, \ldots, L-1$. This effect, in turn, can be implemented by simply multiplying the outputs of the lowpass polyphase filters by the constants $w_{i,k}$. As a consequence, the same polyphase front end (the same filters) can be used to extract any channel located at the multiple of the output rate. This general polyphase decimator structure is illustrated in Figure 12.20.

Similar reasoning can again be used also in the interpolation (upsampling) case.


# 12.7 Hilbert Transform and Delay

Consider the complex (*I/Q*) sampling of bandpass signals. A Hilbert transformer is shown in Figure 12.21 whose transfer characteristic is shown in Figure 12.22(a). We are attempting to approximate the needed 90 degree phase shift of the Hilbert transformer using a simple time delay of one quarter of the carrier cycle as
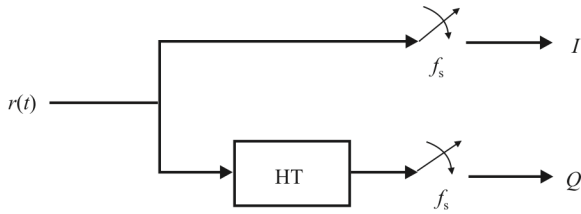
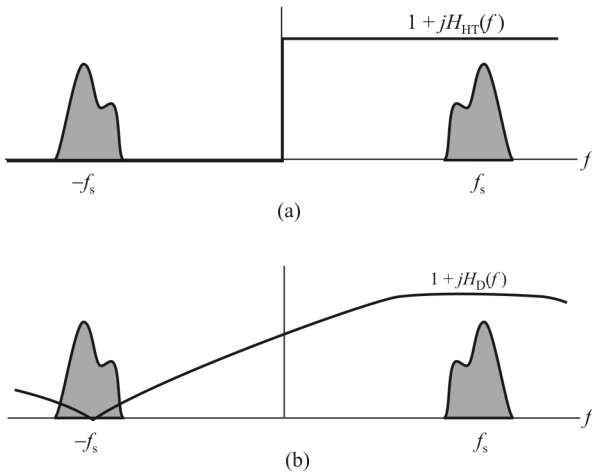**Figure 12.21** Hilbert transformer.



**Figure 12.22** Amplitude response of Hilbert transform and delay: (a) with Hilbert transformer, and (b) with delay.
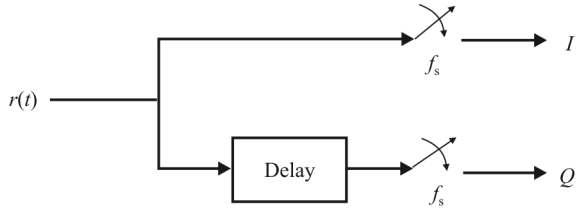
**Figure 12.23** Delay.

illustrated in Figure 12.23. The time delay transfer characteristic is also shown in Figure 12.22. The time delay of $\Delta T = 1/(4f_c)$ corresponds to a frequency-dependent phase shift of

$$-2\pi f \Delta T = -\frac{\pi}{2}\frac{f}{f_c} \tag{12.30}$$

where $f_c$ is the carrier frequency. Thus the ideal Hilbert filtering is achieved only at the carrier frequency $\pm f_c$. As a result, the suppression of the negative frequency content (image components) is generally imperfect.

### 12.7.1 Filtering Effect of the Delay Processing

We write the input bandpass signal $r(t)$ in terms of its baseband equivalent signal $y(t) = y_I(t) + jy_Q(t)$ as (scaling by 2 is irrelevant and can be ignored)

$$r(t) = 2\,\text{Re}\left\{y(t)e^{j2\pi f_c t}\right\} = y(t)e^{j2\pi f_c t} + y*(t)e^{-j2\pi f_c t}$$

Then the complex signal, say $x(t)$, entering the sampler(s) is generally of the form $x(t) = r(t) + jr(t - \Delta T)$, where $\Delta T = 1/(4 f_s)$. The spectrum of this signal can be written as

$$X(f) = [1 + jH_D(f)]R(f) \tag{12.31}$$

where

$$H_D(f) = e^{-j2\pi f \Delta T}$$

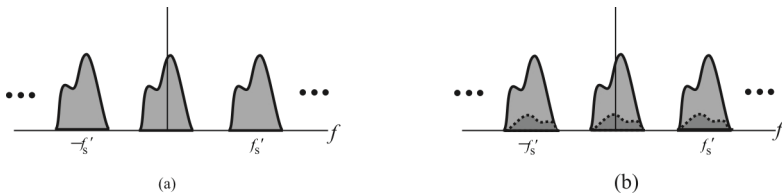This effect is illustrated in the frequency domain in Figure 12.22.

**Figure 12.24** Spectrum overlap: (a) with Hilbert transformer, and (b) with delay.

Now suppose that we use a subharmonic sampling frequency $f_s' = f_s / r$, where the integer $r \geq 1$ denotes the subsampling ratio. As a result, the signal is aliased directly to baseband. In the case of delay processing, the component from negative frequencies falls directly on top of the desired component (Figure 12.24). This is a kind of self-interference. The impact depends on the structure of the signal. In the case of a single-frequency channel (as shown in Figure 12.24), this interference is not really problematic, especially with low-order modulations; but how about in the wideband/multichannel case?

When applied to multichannel signals, the image band signal can be much more powerful than the desired channel. This creates an obvious problem. We will provide quantitative measures shortly, but the problem is illustrated in Figure 12.25.

12.7.1.1 Image Attenuation Analysis

After some manipulations, the sampled complex signal with $f_s' = f_s / r$, where the integer $r \geq 1$ can be written as
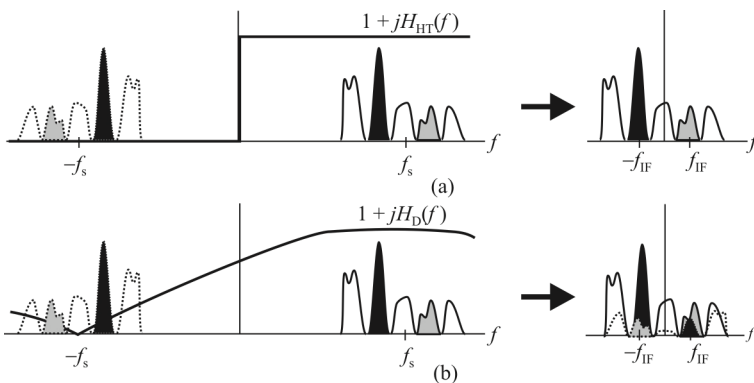


**Figure 12.25** Wideband image channels: (a) with Hilbert transformer, and (b) with delay.

$$x(nT_S) = r(nT_S) + jr(nT_S - \Delta T)$$
$$= 2y_I(nT_S) + j2y_Q(nT_S - \Delta T)$$
$$= I'[n] + jQ'[n] \qquad (12.32)$$

Thus we see that the front-end delay maps directly into a corresponding delay of the baseband observation. We can consider that the discrete time signal is obtained by sampling the corresponding continuous time baseband signal

$$y'(t) = 2y_I(t) + j2y_Q(t - \Delta T) \qquad (12.33)$$

Equation (12.33) can be written in a more informative form as

$$y'(t) = y(t) + y(t - \Delta T) + y*(t) + y*(t - \Delta T) \qquad (12.34)$$

The part including $y(t)$ and $y(t - \Delta T)$ corresponds to the signal component originating from positive frequencies, while the part including $y*(t)$ and $y*(t - \Delta T)$ corresponds to the signal component originating from negative frequencies.

To get the exact image attenuation, we write the Fourier transform of $y'(t)$ as

$$Y'(f) = \left(1 + e^{-j2\pi f \Delta T}\right) Y(f) + \left(1 - e^{-j2\pi f \Delta T}\right) Y*(-f) \qquad (12.35)$$

Then, the image attenuation $L_2(f)$ provided by the second-order sampling is given by

$$L_2(f) = \frac{\left|1 + e^{-j2\pi f \Delta T}\right|^2}{\left|1 - e^{-j2\pi f \Delta T}\right|^2} = \left|\frac{1 + \cos(2\pi f \Delta T)}{\sin(2\pi f \Delta T)}\right|^2 \qquad (12.36)$$

To illustrate, if the center frequency $f_s$ = 100 MHz and the bandwidth $W$ = 25 MHz, the image attenuation $L_2(f)$ at the band-edge is only around 20dB. In the case of multichannel downconversion, the power difference of the individual channel signals can be even 50–100dB. It is clear then that the image attenuation $L_2(f)$ and therefore the basic second-order sampling scheme are not sufficient as such for wideband multichannel receivers.

## 12.7.1.2 Second-Order Sampling and Enhanced Image Rejection

As we saw above, in narrowband single channel receivers, the image signal is inherently a self-image and the attenuation of the basic second-order sampling scheme as such can be adequate. Also, in multichannel receivers, the image band
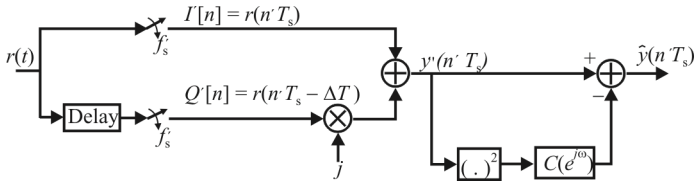
**Figure 12.26** Interference canceller.

signal can be up to 50–100 dB stronger than the desired channel signal, and the image attenuation of the basic second-order scheme alone is clearly insufficient.

We now present two alternative methods to enhance this image attenuation. For simplicity, the following compensation methods are analyzed in the continuous time domain.

*Interference Cancellation*

To enhance the obtainable image attenuation and, thus, to reproduce an accurate baseband observation of the multichannel signal $y(t)$, the interference canceller type of compensation structure shown in Figure 12.26 can be used. As illustrated, the idea is to use a fixed compensation filter $C(f)$ together with the complex conjugate of $y'(t)$ as a reference signal to estimate and subtract the image signal interference. Based on the previous signal model for $Y'(f)$ and on the proposed compensation strategy, the frequency response of $y'(t)$ can be written as

$$\hat{Y}(f) = Y'(f) - C(f)Y'^*(-f)$$
$$= G_{1,\text{IC}}(f)Y(f) + G_{2,\text{IC}}(f)Y^*(-f) \qquad (12.37)$$

where

$$G_{1,\text{IC}}(f) = 1 + e^{-j2\pi f \Delta T} - C(f)(1 - e^{-j2\pi f \Delta T})$$
$$G_{2,\text{IC}}(f) = 1 - e^{-j2\pi f \Delta T} - C(f)(1 + e^{-j2\pi f \Delta T})$$

As a result, the image signal components of $y'(t)$ are attenuated with respect to the desired signal components by

$$L_{\text{IC}}(f) = \frac{\left|G_{1,\text{IC}}(f)\right|^2}{\left|G_{2,\text{IC}}(f)\right|^2} \qquad (12.38)$$

Then, to completely cancel the image signal components, the compensator frequency response $C(f)$ should be selected such that $G_{2,\text{IC}}(f) = 0$.

In this approach, referred to as the *zero forcing* solution, $C_{\text{ZF}}(f)$ is given by

$$C_{\text{ZF}}(f) = \frac{1 - e^{-j2\pi f \Delta T}}{1 + e^{-j2\pi f \Delta T}} \qquad (12.39)$$

After some manipulation, this can be written as

$$C_{\text{ZF}}(f) = \frac{j\sin(2\pi f \Delta T)}{1 + \cos(2\pi f \Delta T)} \qquad (12.40)$$

Equation (12.40) can be well approximated using a real-valued impulse response with odd symmetry. Therefore, no cross-filtering between the $I$ and $Q$ components of the input signal $y'(t)$ is needed.

Using this optimum compensator, the gain $G_{1,\text{ZF}}(f)$ of the desired signal components can be easily shown to be of the form

$$G_{1,\text{ZF}}(f) = 1 + e^{-j2\pi f \Delta T} - C_{\text{ZF}}(f)(1 - e^{-j2\pi f \Delta T}) = \frac{e^{-j2\pi f \Delta T}}{1 + e^{-j2\pi f \Delta T}} \qquad (12.41)$$

With reasonable bandwidth-to-center frequency ratios ($W/f_\text{s}$), this describes practically a constant gain, linear phase frequency response. As a consequence, the effect of image components $Y^*(-f)$ can be successfully compensated without causing any notable distortion to the desired components $Y(f)$.

Thus, an accurate reproduction of $y(t)$ is obtained: $\hat{y}(t) \approx y(t)$ (up to a delay and multiplication by a constant). In the actual digital implementation, $C_{\text{ZF}}(f)$ gives the desired response that should be approximated using a finite-order discrete time FIR/IIR filter. This can be done, for example, using a type III FIR filter (odd symmetry). A design example is given below:

> **Example 12.8:** Suppose $f_\text{s}$ = 100 MHz, $W$ = 25 MHz, $f_\text{s}' = 50$ MHz. A type III FIR filter, length 9, LS and minimax approximations of the given optimum response is shown in Figure 12.27.

*Fractional-Delay Filtering*

Motivated by the original signal model, the image attenuation of the basic second-order sampling scheme can also be enhanced by properly delaying the $I$ branch
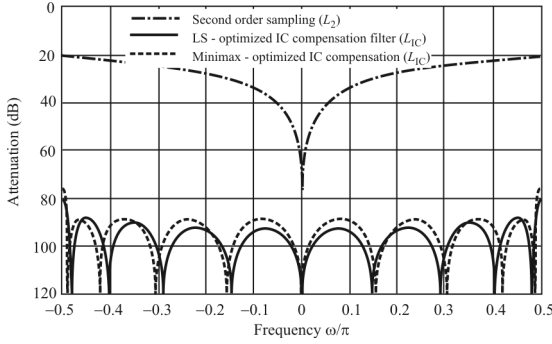
**Figure 12.27** Interference canceller for Example 12.8.

signal $r(nT'_s)$ relative to the $Q$ branch signal $r(nT''_s - \Delta T)$. Using a sampling frequency $f'_s = f_s / r$, the needed delay $\Delta T = T'_s / (4r)$ is only a fraction of the sampling interval $T'_s$. Therefore, a digital fractional delay filter $D(y)$ is a natural choice for the delay implementation.

The flow diagram of the modified second-order sampling based quadrature demodulator utilizing this idea is presented in Figure 12.28. To analyze the image attenuation of the complete structure, we proceed as follows (in continuous time domain for simplicity).

First, let $D(f)$ denote the frequency response of the fractional delay compensation filter. Then, the Fourier transform of the compensated signal $y'(t)$ is given by

$$\hat{Y}(f) = 2Y_I(f)D(f) + j2Y_Q(f)e^{-j2\pi f \Delta T} \tag{12.42}$$

After some manipulations, this can be written in a more convenient form as

$$\hat{Y}(f) = G_{1,\text{FD}}(f)Y(f) + G_{2,\text{FD}}(f)Y^*(-f) \tag{12.43}$$
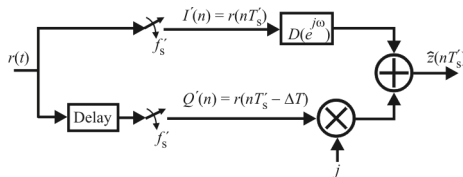
where



**Figure 12.28** Fractional delay.

$$G_{1,\text{FD}}(f) = D(f) + e^{-j2\pi f \Delta T}$$
$$G_{2,\text{FD}}(f) = D(f) - e^{-j2\pi f \Delta T}$$

As a result, the enhanced image attenuation $L_{\text{FD}}(f)$ of fractional delay processing is given by

$$L_{\text{FD}}(f) = \frac{\left|G_{1,\text{FD}}(f)\right|^2}{\left|G_{2,\text{FD}}(f)\right|^2} = \frac{\left|D(f) + e^{-j2\pi f \Delta T}\right|^2}{\left|D(f) - e^{-j2\pi f \Delta T}\right|^2} \qquad (12.44)$$

Naturally, the ideal frequency response of the needed fractional delay filter is, indeed, $e^{-j2\pi f \Delta T}$, for which $L_{\text{FD}} \to \infty$. Based on the previous analysis, this would result in a perfect (up to a delay and multiplication by a constant) reconstruction of the desired baseband equivalent signal as $\hat{y}(t) = 2y(t - \Delta T)$.

Considering the actual digital implementation, let $\mu = \Delta T / T_s' = 1/(4r)$ denote the normalized fractional delay. Then, the frequency response of the ideal digital FD filter is given by

$$D_{\text{OPT}}(e^{j\omega}, \mu) = e^{-j\omega\mu} \ \text{ for } |\omega| \leq \pi W / f_S \qquad (12.45)$$

where $\omega = 2\pi f / f_s'$. Again, the task is to approximate this ideal response using a finite-order FIR/IIR filter.

### 12.7.1.3 General Conclusion

Based on the design examples presented, image attenuations in the order of 80–100 dB can be easily achieved (at least theoretically) using either of the techniques presented (IC/FD).

## 12.8 Concluding Remarks

We considered the basic functioning of digital filtering in this chapter. We started with an examination of what digital sampling and basic filtering entails. FIR and IIR filters were considered and their transfer functions discussed. Multirate filters were introduced as efficient ways to filter complex signals. The chapter concluded with a comparison of the digital Hilbert transform versus a simple delay as filters.

# References

[1]     *Signal Processing Techniques*, Interstate Electronics Corporation, 1979.

[2]     Parks, T. W., and C. S. Burrus, *Digital Filter Design*, New York: Wiley, 1987.

[3]     Oppenheimm, A. V., and R. W. Schafer, *Digital Signal Processing*, Englewood Cliffs, NJ: Prentice-Hall, 1975.

[4]     Rabiner, L. R., and B. Gold, *Theory and Application of Digital Signal Processing*, Englewood Cliffs, NJ: Prentice-Hall, 1975.

[5]     Parks, T. W., and C. S. Burrus, *Digital Filter Design*, New York: Wiley, 1987, p. 38.

[6]     Vaidyanathan, P. P., *Multirate Systems and Filter Banks*, Upper Saddle River, NJ: Prentice Hall, 1993.

# Chapter 13

# Digital Demodulation

## 13.1 Introduction

To retrieve the information conveyed in a communiqué, some form of demodulation is always required. Information is modulated onto a carrier at the transmitter. The function of an EW receiver is to noncooperatively retrieve that information or as much of it as possible. In this chapter we consider how this demodulation is accomplished with digital signal processing.

This chapter is structured as follows. We begin with a description of a way to generate digital samples of the *I* and *Q* components of the IF signal. That is followed by a description of the methods of extracting the AM, PM, or FM carried on these signals. The last topic discussed is a way to compensate for the *I* and *Q* channel imbalance mentioned in Chapter 7.

## 13.2 Digital *I/Q* Demodulation

### 13.2.1 Introduction

The premise of a digital direct IF sampled receiver is relatively simple [1]. Either the IF or baseband signal may be sampled directly by a high-performance ADC. The sampled signal is then processed in real time while it is in digital form. By applying a combination of algorithms, the information contained within the signal is extracted [2, 3].

A conventional *I/Q* demodulator is shown in Figure 13.1. It consists of splitting the received signal into two paths and multiplying each arm by an LO signal and its 90° shifted version. This provides *I* and *Q* components after lowpass filtering and quantization. However, a number of errors can corrupt the conventional approach shown in Figure 13.1, mainly because the two paths must
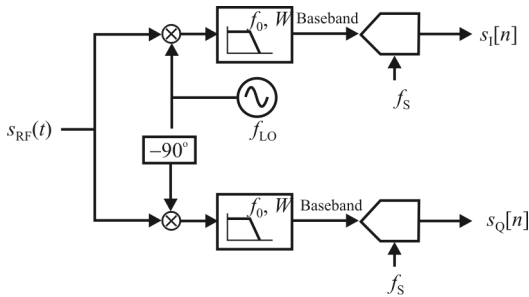
**Figure 13.1** Conventional *I/Q* demodulator.

be closely matched for correct demodulation—for example, gain balance, quadrature-phase balance, or DC offsets (we consider *I* and *Q* mismatch later). Recent advances in ADC technology allow IF sampling strategies to be realized and the *I/Q* demodulator to be implemented digitally, overcoming some of these error sources [4]. The analog components of the RF/IF chain still have to be carefully designed, however [5].

### 13.2.2 *I/Q* Demodulation

A complex baseband signal $x(t)$, which has a bandwidth of $W$ Hz, is transmitted at RF. We denote $x_I(t)$ and $x_Q(t)$ as the in-phase and quadrature components of $x(t)$, respectively. After downconversion to an intermediate frequency, $f_{IF}$, the signal is bandpass filtered at the receiver to avoid aliasing and to remove high-frequency components. At the output of the RF chain, the received real signal consists of the desired IF signal corrupted by noise:

$$s_{IF}(t) = aV(t)\cos[2\pi f_{IF}t + \theta(t)] + n(t) \tag{13.1}$$

where $a$ is the amplitude of the signal and $n(t)$ is additive noise. $V(t)$ and $\theta(t)$ are the envelope and the phase of $x(t) = x_I(t) + jx_Q(t)$, respectively. The IF signal feeds an ADC, which samples the signal at a sampling rate of $f_s = 1/T_s$. Hence, the sampled version of the IF signal can be expressed as

$$s_{IF}[n] = aV[n]\cos(2\pi f_{IF}nT_s + \theta[n]) + n[n] \tag{13.2}$$

As considered in Chapter 7, with digital IF sampling, we undersample the IF signal in order to obtain a replica of the signal at baseband, without requiring an additional downconversion. We can do this by properly choosing $f_{IF}$ and $f_s$. In general, we require that
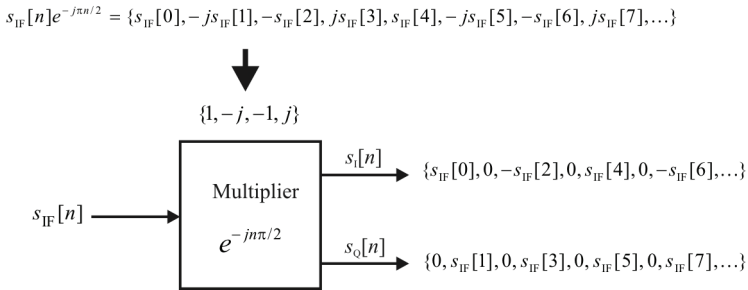
$$s_{\mathrm{IF}}[n]e^{-j\pi n/2} = \{s_{\mathrm{IF}}[0], -js_{\mathrm{IF}}[1], -s_{\mathrm{IF}}[2], js_{\mathrm{IF}}[3], s_{\mathrm{IF}}[4], -js_{\mathrm{IF}}[5], -s_{\mathrm{IF}}[6], js_{\mathrm{IF}}[7], \ldots\}$$

$$\{1, -j, -1, j\}$$

Multiplier

$e^{-jn\pi/2}$

$s_{\mathrm{IF}}[n]$

$s_{\mathrm{I}}[n]$ → $\{s_{\mathrm{IF}}[0], 0, -s_{\mathrm{IF}}[2], 0, s_{\mathrm{IF}}[4], 0, -s_{\mathrm{IF}}[6], \ldots\}$

$s_{\mathrm{Q}}[n]$ → $\{0, s_{\mathrm{IF}}[1], 0, s_{\mathrm{IF}}[3], 0, s_{\mathrm{IF}}[5], 0, s_{\mathrm{IF}}[7], \ldots\}$

**Figure 13.2** After frequency-shift, I&Q components are obtained.

$$f_{\mathrm{IF}} = kf_{\mathrm{s}} \pm \frac{f_{\mathrm{s}}}{4}, \qquad \forall k \in \mathbb{Z} \,|\, k \geq 1$$

$$f_{\mathrm{s}} \geq 4W \tag{13.3}$$

to ensure that a non-overlapped alias will appear centered at $f_{\mathrm{s}}$ = 4. Then one of the replicas at $\pm f_{\mathrm{s}}/4$ can be downconverted to baseband using the frequency-shifting property of the Fourier transform of a signal—that is, $Z(f \pm f_0) \leftrightarrow z[n]e^{\mp j2\pi f_0 nT_s}$. With $f_0 = f_{\mathrm{s}}/4$, we must multiply the IF signal by $e^{-j\pi n/2}$ to shift the spectrum to the left. However, the sequence of cyclic values of $e^{-j\pi n/2}$ is $\{1, -j, -1, j\}$, where $j^2 = -1$, which simplifies the process. As shown in Figure 13.2, this provides the *I* and *Q* components of the desired signal.

Figure 13.3 shows the spectra of the signals involved. $S_{\mathrm{IF}}(f)$ is the psd of the received IF signal in (13.1). Setting $f_{\mathrm{IF}} = 3f_{\mathrm{s}}/4$, i.e., $k = 1$, and sampling $s_{\mathrm{IF}}(t)$ according to (13.3), we see in Figure 13.3 that aliasing appears without overlapping in its spectrum $S_{\mathrm{IF}}^{\mathrm{ADC}}(\omega)$ since we have assumed a band-limited signal $V[n]$. After the frequency shift, we obtain a baseband replica of the desired signal in $S(\omega) = S_{\mathrm{IF}}^{\mathrm{ADC}}(\omega - \omega_{\mathrm{s}}/4)$.

Notice that the psd $S_{\mathrm{IF}}^{\mathrm{ADC}}(\omega)$ shown in Figure 13.3 is obtained for any chosen $k$ in (13.3). Thus, the selection of $k$ is an implementation issue—that is, to select a suitable $f_{\mathrm{IF}}$ for the application under consideration. The restriction on $f_{\mathrm{s}}$ to be a minimum of twice the Nyquist frequency arises in order to avoid overlapping in $S_{\mathrm{IF}}^{\mathrm{ADC}}(\omega)$. After lowpass filtering $S(\omega)$ we can decimate the signal up to a factor that depends on the chosen sampling frequency.
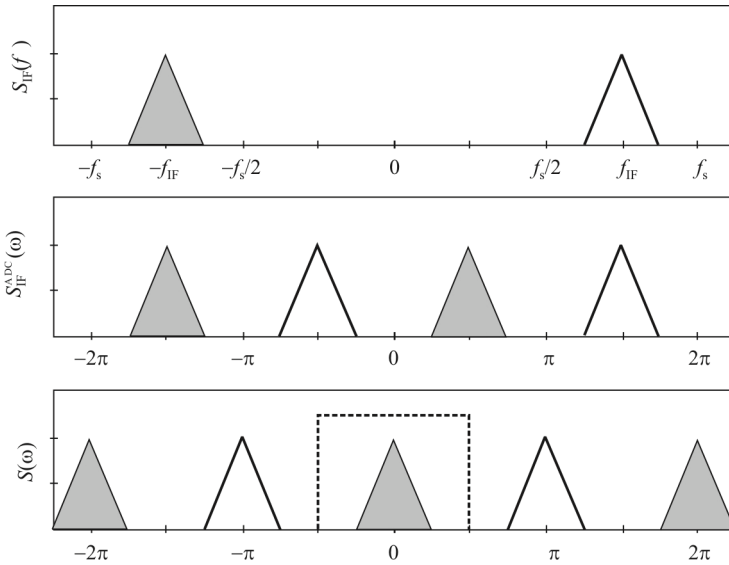
**Figure 13.3** Spectral densities of $s_{IF}(t)$, $s_{IF}[n]$, and $s[n] = s_{IF}[n]e^{-j\pi n/2}$.

# 13.3 Direct IF Digital Demodulator

Demodulation refers to the means whereby the information is extracted or recovered from the radio carrier. The original information (commonly termed *baseband*) may be either in analog or digital format. Demodulation can be accomplished by analog or digital processing. Typical analog FM demodulation methods include

- Quadrature detector
- PLL detector
- Frequency discriminator

There are also several analog techniques for demodulating phase such as those typically used in the modulation of digital information. Digital modulation need not be limited to phase-coherent methods. Phase-coherent simply means that the RF/IF phase is known. MFSK is one example of a non-coherent method. QPSK is an example of a phase-coherent type.

## 13.3.1 Digital Signal Processing without the Digital Signal Processor

A typical architecture of a direct IF receiver includes a DSP IC as a core processor (see [6] as an example). The DSP performs tasks such as IF sample to quadrature
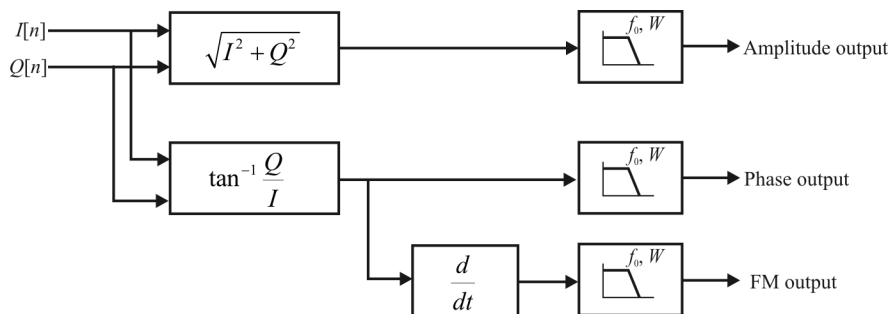
**Figure 13.4** Direct IF digital demodulation flow diagram.

vector conversion, decimation filtering, lowpass filtering, and trigonometric functions required for phase demodulation. The flow diagram shown in Figure 13.4 represents the typical flow of processing in such a DSP implementation.

It is also possible to consider dedicated hardware for these tasks in order to eliminate the DSP, since the functions of a direct IF demodulator are well understood. Figure 13.4 also represents a block diagram of the direct IF system architecture. Carrier phase information is recovered from the in-phase and quadrature ($I$ and $Q$) components of the signal after a trigonometric transform is applied. Taking the derivative of the phase difference with respect to time can extract FM. Amplitude information can be calculated from the magnitude of the IQ vector. All three of these are illustrated in Figure 13.4.

Quadrature baseband signals $I$ and $Q$ are conventional representations of the modulus of the in-phase–$I$ axis, chosen arbitrarily, and the quadrature–$Q$ component, which lags the in-phase component of the carrier by 90°. Note that any type of modulation is possible with this expression: phase, frequency, and amplitude. For a linear system, the reciprocal case is also true: demodulation of any modulation type is possible simply by recovering the quadrature baseband components.

## 13.3.2 *I/Q* Sampling

### 13.3.2.1 RF Vector Representation

Any sinusoidal RF signal can be represented as a phasor as illustrated in Figure 13.5. If

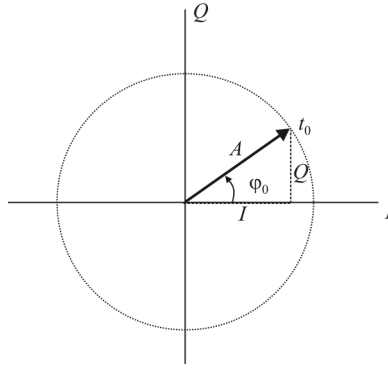$$y(t) = A\sin(\omega t + \varphi_0) \tag{13.4}$$

**Figure 13.5** Phasor notation.

then, according to Figure 13.5

$$y(t) = \underbrace{A\cos\varphi_0}_{\triangleq I} \sin\omega t + \underbrace{A\sin\varphi_0}_{\triangleq Q} \cos\omega t \qquad (13.5)$$

where

$I$ is the in-phase component
$Q$ is the quadrature phase component

so that

$$y(t) = I\sin\omega t + Q\cos\omega t \qquad (13.6)$$

where

$$I = A\cos\varphi_0 \qquad\qquad A = \sqrt{I^2 + Q^2}$$
$$\qquad\qquad\qquad\qquad\qquad\qquad\qquad (13.7)$$
$$Q = A\sin\varphi_0 \qquad\qquad \varphi_0 = \tan^{-1}\frac{Q}{I}$$

We assume positive frequencies so that the phasor is rotating counterclockwise.

13.3.2.2 *I/Q* Sampling

In *I/Q* sampling we want to monitor the amplitude and phase ($A$ and $\varphi_0$) variations of the incoming RF/IF signal. We process sampled *I/Q* values for comparison. The
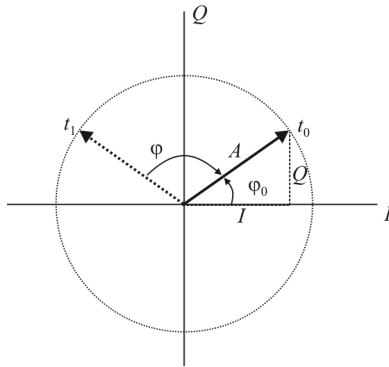
**Figure 13.6** *I/Q* sampling.

phasor can be rotated back to the reference phasor if the phase advance between sampling is known. See Figure 13.6.

When the sampling frequency and RF/IF frequency have the relationship

$$f_s = 4f$$

there is a 90° phase shift between two samples (Figure 13.7).

We can see in Figure 13.8 how the samples correspond to the *I* and *Q* samples. We can obtain the values of *I* and *Q* from (13.6) by sampling $y(t)$ at the correct times as
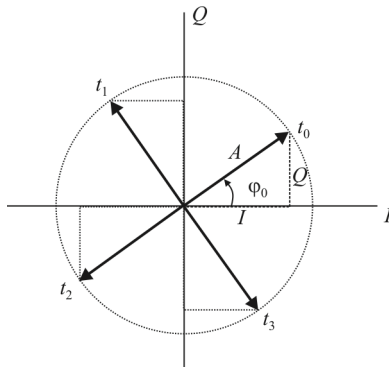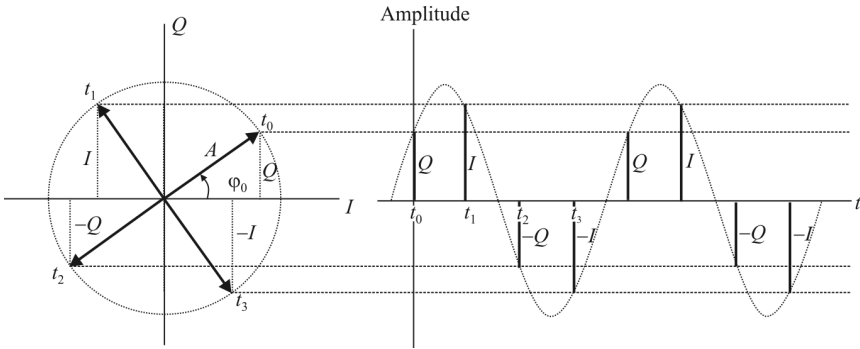


**Figure 13.7** *I/Q* sampling phase shifted by 90°.

**Figure 13.8** *I/Q* sampling at four time instants.

$$\omega t_0 = 0 \qquad y(t_0) = Q$$
$$\omega t_1 = \pi/2 \qquad y(t_1) = I$$
$$\omega t_2 = \pi \qquad y(t_2) = -Q$$
$$\omega t_3 = 3\pi/2 \qquad y(t_3) = -I$$

We can build up *I/Q* vectors based on two successive samples (Figure 13.9). Then we rotate the corresponding *I/Q* vector by –90°, –180°, and 270° in order to compare initial *I/Q* values. Since

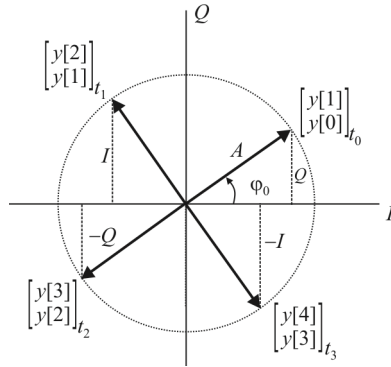$$y[0] = y(t_0) = Q$$
$$y[1] = y(t_1) = I$$

**Figure 13.9** *I/Q* sampling vectors based on two successive samples.
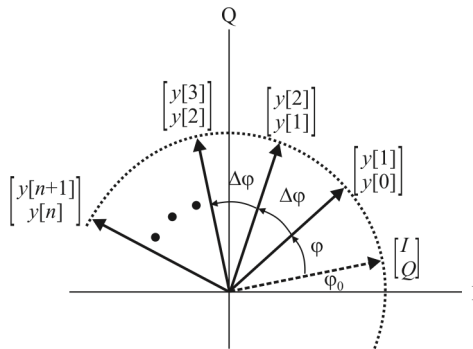
$$y[2] = y(t_2) = -Q$$



**Figure 13.10** *I/Q* sampling phase advance between consecutive samples.

$$y[3] = y(t_3) = -I$$

The rotation matrix with angle $\Delta\varphi$ is

$$\mathbf{R} = \begin{bmatrix} \cos\Delta\varphi & -\sin\Delta\varphi \\ \sin\Delta\varphi & \cos\Delta\varphi \end{bmatrix}$$

and we have

$$t_0 : \mathbf{R}\vec{y} = \begin{bmatrix} \cos 0 & -\sin 0 \\ \sin 0 & \cos 0 \end{bmatrix} = \begin{bmatrix} 1 & 0 \\ 0 & 1 \end{bmatrix} \begin{bmatrix} y[1] \\ y[0] \end{bmatrix} = \begin{bmatrix} y[1] \\ y[0] \end{bmatrix} = \begin{bmatrix} I \\ Q \end{bmatrix}_{t_0}$$

$$t_1 : \mathbf{R}\vec{y} = \begin{bmatrix} \cos(-\pi/2) & -\sin(-\pi/2) \\ \sin(-\pi/2) & \cos(-\pi/2) \end{bmatrix} = \begin{bmatrix} 0 & 1 \\ -1 & 0 \end{bmatrix} \begin{bmatrix} y[2] \\ y[1] \end{bmatrix} = \begin{bmatrix} y[1] \\ -y[2] \end{bmatrix} = \begin{bmatrix} I \\ Q \end{bmatrix}_{t_1}$$

$$t_2 : \mathbf{R}\vec{y} = \begin{bmatrix} \cos(-\pi) & -\sin(-\pi) \\ \sin(-\pi) & \cos(-\pi) \end{bmatrix} = \begin{bmatrix} -1 & 0 \\ 0 & -1 \end{bmatrix} \begin{bmatrix} y[3] \\ y[2] \end{bmatrix} = \begin{bmatrix} -y[3] \\ -y[2] \end{bmatrix} = \begin{bmatrix} I \\ Q \end{bmatrix}_{t_2}$$

$$t_3 : \mathbf{R}\vec{y} = \begin{bmatrix} \cos(-3\pi/2) & -\sin(-3\pi/2) \\ \sin(-3\pi/2) & \cos(-3\pi/2) \end{bmatrix} = \begin{bmatrix} 0 & -1 \\ 1 & 0 \end{bmatrix} \begin{bmatrix} y[4] \\ y[3] \end{bmatrix} = \begin{bmatrix} -y[3] \\ y[4] \end{bmatrix} = \begin{bmatrix} I \\ Q \end{bmatrix}_{t_3}$$

In general

$$f_s / f_{IF} = m, \qquad m \text{ integer}$$

The phase advance between consecutive samples (Figure 13.10) is

$$\Delta\varphi = \frac{2\pi}{m}$$

The relation between measured amplitudes and $I/Q$ is

$$\begin{bmatrix} I[n] \\ Q[n] \end{bmatrix} = \frac{1}{\sin \Delta\varphi} \begin{bmatrix} 1 & -\cos \Delta\varphi \\ 0 & \sin \Delta\varphi \end{bmatrix} \begin{bmatrix} y[n+1] \\ y[n] \end{bmatrix} \tag{13.8}$$

The rotation of $\begin{pmatrix} I[n] \\ Q[n] \end{pmatrix}$ to $\begin{bmatrix} I[0] \\ Q[0] \end{bmatrix} = \begin{bmatrix} y[1] \\ y[0] \end{bmatrix}$ with angle $-n\Delta\varphi$ is given by

$$\begin{bmatrix} I[0] \\ Q[0] \end{bmatrix} = \frac{1}{\sin \Delta\varphi} \begin{bmatrix} \cos n\Delta\varphi & -\cos(n+1)\Delta\varphi \\ -\sin n\Delta\varphi & \sin(n+1)\Delta\varphi \end{bmatrix} \begin{bmatrix} y[n+1] \\ y[n] \end{bmatrix}$$

The rotation of $\begin{pmatrix} I[0] \\ Q[0] \end{pmatrix}$ to $\begin{pmatrix} I \\ Q \end{pmatrix}$ with angle $-\varphi$ is given by

$$\begin{bmatrix} I \\ Q \end{bmatrix} = \frac{1}{\sin \Delta\varphi} \begin{bmatrix} \cos[\varphi + n\Delta\varphi] & -\cos[\varphi + (n+1)\Delta\varphi] \\ -\sin[\varphi + n\Delta\varphi] & \sin[\varphi + (n+1)\Delta\varphi] \end{bmatrix} \begin{bmatrix} y[n+1] \\ y[n] \end{bmatrix}$$

13.3.2.3 Potential Problems with $I/Q$ Sampling

*Nonuniform Sampling*

The samples are not exactly $90^\circ$ apart, for example, due to ADC clock jitter. This produces a ripple on *I/Q* values with the frequency of carrier, for example, at $f_{\text{IF}}$. The effect is illustrated in Figure 13.11. These errors are easily detectable in *I/Q* demodulation.

*Large Phase Advances*

Choosing phase advances "far away" from $90^\circ$ can worsen the SNR

$$\begin{bmatrix} I[0] \\ Q[0] \end{bmatrix} = \underbrace{\frac{1}{\sin \Delta\varphi}}_{\text{worsens SNR}} \begin{bmatrix} \cos n\Delta\varphi & -\cos(n+1)\Delta\varphi \\ -\sin n\Delta\varphi & \sin(n+1)\Delta\varphi \end{bmatrix} \begin{bmatrix} y[n+1] \\ y[n] \end{bmatrix}$$
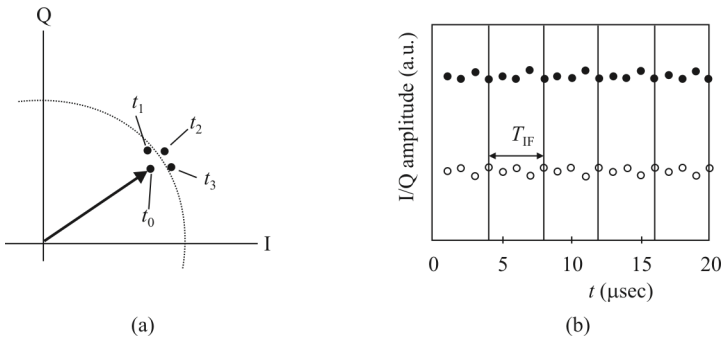
(a)                             (b)

**Figure 13.11** Samples not 90° apart: (a) rotated vector and (b) amplitude ripple.

*Nonlinearities of Mixers*

These generate high harmonics of the input carrier. Odd harmonics of the carrier frequency are not distinguishable from the carrier by I/Q detection (Figure 13.12). These errors are difficult to detect in *I/Q* demodulation.

> **Example 13.1:** IF fundamental with 20% of third harmonic component is shown in Figure 13.13.

If the input phase and amplitude change, the distortion changes and can corrupt the measurement.
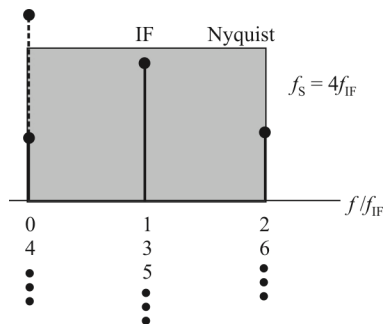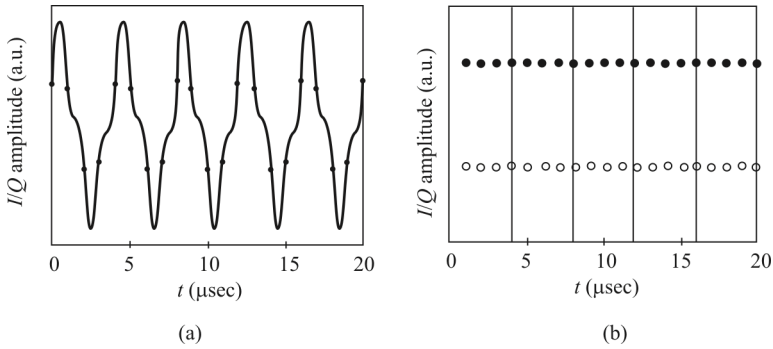


**Figure 13.12** Nonlinear mixer.

(a)  (b)

**Figure 13.13** *I*/*Q* sampling example when harmonics are present.

### 13.3.3 Vector Representation

The digital sampling demodulator shown in Figure 13.8 is capable of recovering the baseband *I* and *Q* components. Applying convolution theory and assuming an equivalent zero-order hold for the sampling detector yield

$$s(t) \leftrightarrow S(\omega) = \sum I\left(\omega + \frac{n}{T_s}\right) + Q\left(\omega + \frac{n}{T_s}\right) \tag{13.9}$$

where $T_s$ is the sampling period and the *n*th component in the frequency domain occurs at the *n*th multiple of the sampling frequency**.**

### 13.3.4 Undersampling

The digital demodulator shown in Figure 13.8 does not necessarily require sampling beyond the Nyquist rate for the IF, provided the IF bandwidth is sufficiently narrow. Figure 13.14 illustrates the undersampling artifacts in the frequency domain that occur as a result of sampling the IF at a rate of $1/T_s$.

## 13.4 Direct IF Processing Elements

The direct digital demodulator processing elements as outlined in Figure 13.4 are as follows:

- A/D converter/IF Sampler
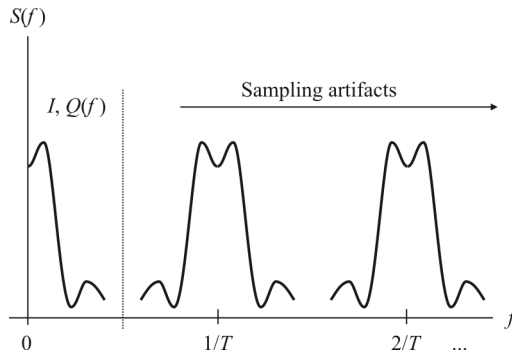- Digital IF sample to *I*/*Q* vector conversion

**Figure 13.14** Undersampling artifacts.

- *I/Q* vector-to-phase conversion
- Phase differentiator for FM detection
- Vector magnitude function for AM detection

We briefly discuss these elements in this section.

### 13.4.1 A/D Converter/IF Sampler

Quantization and sampling effects must be considered. A good digital IF processor will include some capability for features such as dynamic bandwidth adjustment, amplitude demodulation, AM rejection for FM and PM detection, and dynamic AGC (automatic gain control) of the IF amplifier. The converter must also have sufficient bandwidth to pass the IF frequency without appreciable amplitude or group delay distortion across the IF bandwidth. A reasonable guideline is for the signal level to occupy one third of the dynamic range, leaving two thirds of the total as dynamic headroom.

### 13.4.2 Digital IF Sample to *I/Q* Vector Conversion

The I&Q demodulator example of Figure 13.8 samples the IF at $\pi/2$ radian intervals. This is also known as orthogonal sampling. There are significant drawbacks to the orthogonal sampling technique. A $\pi/2$ period requires a sampling rate of $4\times$ the IF, or $4\times$ a sub-multiple of the IF as in the case with an under-sampled system. The sampling system (e.g., the ADC and ADC clock generator) both generate currents within the system at the sampling rate. Because the sample clock harmonics fall directly at the IF, it can be tricky to suppress them and they may cause interference with the IF. Orthogonal sampling is also sensitive to signal distortion because of the correlated nature of the sample timing.
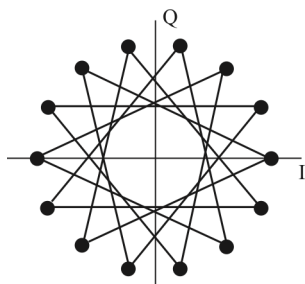
**Figure 13.15** 9π/7 non-orthogonal sampling.

A better approach to *I/Q* vector conversion is to use a non-orthogonal technique. Figure 13.15 illustrates the vector constellation of a 9π/7 sampling rate. Using this technique, sample clock interference is reduced and effective dynamic range is improved. The SNR of the recovered I&Q digital baseband information can be calculated for both orthogonal and non-orthogonal cases as a function of ADC effective resolution, IF noise floor, and bandwidth as

$$\gamma = 20 \log_{10} \left[ \frac{\sum P_n A_d}{\dfrac{1}{2^N} + V_{nf} \sqrt{W}} \right] \tag{13.10}$$

where

$P_n$ is the $n$th *I/Q* 9π/7 or π/2 normalization coefficient
$A_d$ is the fraction of usable dynamic range
$N$ is the ADC effective binary resolution
$V_{nf}$ is the IF noise floor voltage
$W$ is the bandwidth

Normalization coefficients are calculated using

$$P_{I,n} = \cos\left(\frac{1}{nT_s}\right) \tag{13.11}$$

and

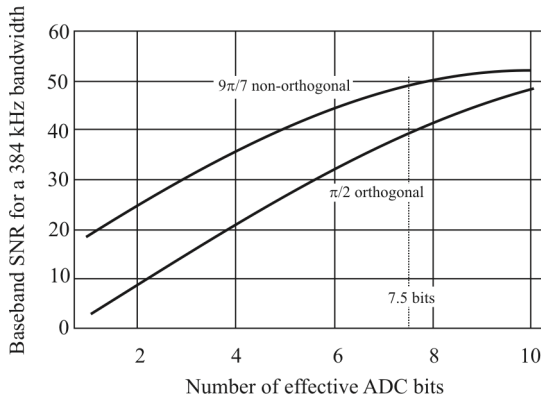$$P_{Q,n} = \sin\left(\frac{1}{nT_s}\right) \tag{13.12}$$

**Figure 13.16** SNR of *I/Q* versus ADC resolution.

Figure 13.16 shows the SNR of the digitally recovered baseband information as a function of ADC resolution for both orthogonal and non-orthogonal sampling methods, as calculated by the formulas (13.10)–(13.12). The dynamic range, $A_d$, is one third. The bandwidth of the recovered data is 384 kHz and the IF noise floor is $-120\,\text{dBc}/\sqrt{\text{Hz}}$. At the 7.5 bits of A/D resolution indicated, the non-orthogonal method yields a 10dB improvement in baseband SNR over the quadrature sampling method. In practice, an even better improvement is found due to the correlated aspects of the distortion and noise on the IF signal. If amplitude demodulation is not required, or if strong AM rejection is unimportant, then the $A_d$ coefficient may be increased by as much as $2\times$, yielding equivalent performance for one less bit of ADC resolution.

### 13.4.3 *I/Q* Vector to Phase Conversion

Binary *I/Q* to phase vector mapping can be simplified by applying the symmetry of the *I/Q* vector space. Figure 13.17 shows the circle divided into octants, with the resultant first three corresponding bits arbitrarily assigned. Note that the angle wraps through the zero point from 111 back to 000. First, the circle is divided into quadrants, simply by using the sign of the *I/Q* vectors to determine the first two bits. Then the quadrants are bisected by comparing absolute magnitudes of *I* and *Q*. Within the octant, the final result must be determined by estimating the arctangent of *I/Q*.

13.4.3.1 Phase Differentiator for FM Detection

Once accurate binary phase has been determined, FM calculation merely requires differentiation with respect to time. If the phase detector output sample rate is
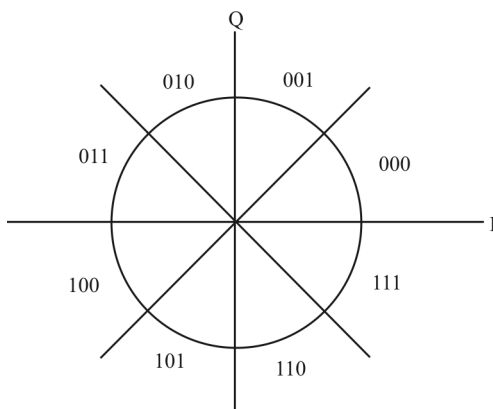
**Figure 13.17** *I/Q* symmetry and phase demodulation.

384 kHz, for example, FM baseband information can be extracted by lowpass filtering the phase difference at each sample interval. The best case SNR for strong signal reception can be calculated by

$$\gamma = 20 \log_{10} \left( \gamma_{bb} \frac{W_{IF}}{2W_{FM}} \right)$$

(13.13)

For the example, using a 7.5 bit ADC for the IF sampling, in the nonorthogonal case, and limiting the recovered demodulated bandwidth to approximately 17 kHz, $\gamma = 67$dB.

### 13.4.4 Vector Magnitude: AM Detection

Absolute magnitude of the *I/Q* vector sum can be calculated by the sum of squares method. As in the FM case, lowpass filtering is required and the SNR is dependent upon recovered bandwidth.

### 13.4.5 Summary

A digital demodulator can be implemented in dedicated hardware to realize all of the performance benefits of a soft DSP system but at a fraction of the cost. The integrated system described herein is ideal for mobile (tactical) applications requiring high performance.
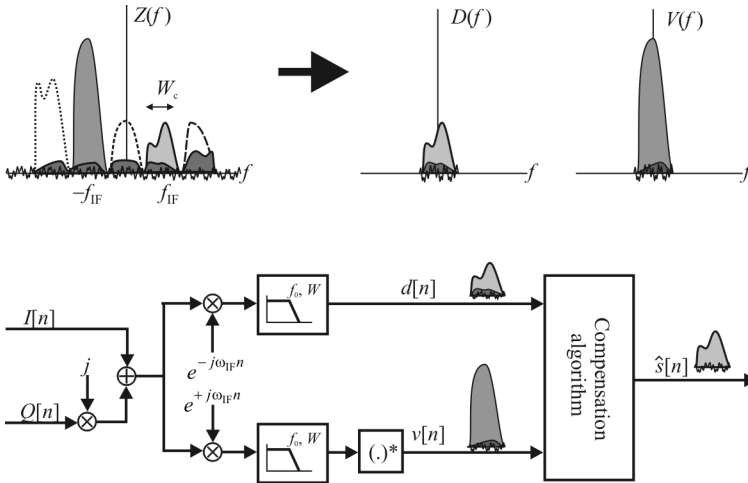
**Figure 13.18** I/Q imbalance compensation algorithm.

# 13.5 *I/Q* Imbalance Compensation

We discussed in Chapter 7, and again mentioned above, that *I/Q* channel imbalance degrades reception in analog receivers. We present in this section a method for compensating for this imbalance in digital receivers [7].

### 13.5.1 Baseband Signal Model for Digital Imbalance Compensation

The purpose of imbalance compensation is to enhance the finite image attenuation $L(f)$ of the analog processing. More precisely, the goal is to obtain an image-free channel (referred to as the *desired channel*) signal located at non-zero IF after the initial wideband downconversion.

The traditional approach is to try to estimate the imbalance parameters and use them in some kind of a correction network. Here we directly estimate the final quantity of interest: the desired signal.

In this section the desired channel (light gray in Figure 13.18) baseband equivalent signal is denoted by $s(t)$. The image channel (medium grey) baseband equivalent signal is denoted by $i(t)$. Cochannel interference is represented with dark gray. In general, we denote the power in signal $x(t)$ as $P_x = \mathcal{E}\left\{|x(t)|^2\right\}$.

As in the ideal (perfect matching) case, the unbalanced multichannel signal $Z(f)$ contains a desired signal component around $+f_{IF}$ and an image component

around $-f_{IF}$. Due to unbalances, $Z(f)$ also has a destructive image signal component around $+f_{IF}$ and a desired signal component around $-f_{IF}$. Motivated by this, we generate two baseband observations, $d(t)$ and $v(t)$:

- $d(t)$ is the baseband observation of the combined signal around $+f_{IF}$
- $v(t)$ is the mirrored (complex-conjugated) baseband observation of the combined signal around $-f_{IF}$

This observation generation is illustrated in Figure 13.18. The desired signal $s(t)$ is then estimated as

$$\hat{s}(t) = L\{d(t), d(t-1), d(t-2), \ldots, v(t), v(t-1), v(t-2), \ldots\} \qquad (13.14)$$

where $L\{\cdot\}$ is yet to be determined.

After some manipulation, the frequency domain expression for these observations can be written using a matrix formulation as

$$\mathbf{X}(f) = \mathbf{A}(f)\mathbf{S}(f) \qquad (13.15)$$

where $\mathbf{X}(f) = [D(f)\ V(f)]^{\mathrm{T}}$, $\mathbf{S}(f) = [S(f)\ I^*(-f)]^{\mathrm{T}}$, and $s(t)$ and $i(t)$ denote the baseband equivalents of the desired and image signals, respectively.

The matrix $\mathbf{A}(f)$ is given by

$$\mathbf{A}(f) = \begin{bmatrix} G_1(f + f_{IF}) & G_2(f + f_{IF}) \\ G_2^*(-f - f_{IF}) & G_1^*(-f - f_{IF}) \end{bmatrix} \mathbf{P}(f, W_c) \qquad (13.16)$$

where $W_c$ denotes the individual channel bandwidth and $\mathbf{P}(f, W_c) = \mathrm{diag}[\Pi(f, W_c), \Pi(f, W_c)]$ with

$$\Pi(f, W_c) = \begin{cases} 1, & |f| \leq W_c / 2 \\ 0, & \text{otherwise} \end{cases}$$

If $H_I(f) = H_Q(f)$, where these represent the transfer functions of the LP filters in the *I*-path and *Q*-path, respectively, the general model reduces to an instantaneous mixture model

$$\begin{bmatrix} d(t) \\ v(t) \end{bmatrix} = \begin{bmatrix} K_1\sqrt{P_s} & K_2\sqrt{P_s} \\ K_2^*\sqrt{P_s} & K_1^*\sqrt{P_s} \end{bmatrix} \qquad (13.17)$$

where $s_1(t) = s(t)/\sqrt{P_s}$, $s_2(t) = i*(t)/\sqrt{P_i}$, and $P_s = \mathcal{E}\left\{|s(t)|^2\right\}$.

This is a valid model if the *I/Q* demodulator is the main source of imbalance. Notice that compensation is actually needed only if the image signal is more powerful than the desired signal—that is, $\hat{s}(t) = d(t)$ is a good estimator if $P_s \gg P_i$.

Also note that even though the baseband model was given here in the continuous time domain, the observations can in practice be generated digitally (after ADC) where excess imbalance effects are avoided. Consequently, discrete time notations $d[n]$, $v([n]$, $s[n]$, and $i(n)$ are used hereafter.

In general, the observations $x_1[n] = d[n]$ and $x_2[n] = v[n]$ appear as convoluted mixtures of the effective source sequences $s_1[n] = s[n]$ and $s_2[n] = i*[n]$. The instantaneous mixture model is a special case of this.

## 13.5.2 Adaptive Interference Cancellation (IC)-Based Compensation

If the desired channel signal is more powerful than the image signal ($P_s \gg P_i$), the image attenuation of analog processing is sufficient. In that case the desired channel observation $d[n]$ can be used directly as an estimate of $s[n]$. On the other hand, in the difficult case of a strong image signal ($P_i \gg P_s$), the attenuation of analog processing is insufficient. $v[n]$ is highly correlated with the interfering signal component but only weakly correlated with the desired signal component of $d[n]$.

Motivated by this, adaptive interference cancelling can be used to estimate $s[n]$ as

$$\hat{s}_{IC}[n] = d[n] - \sum_{k=0}^{N_{IC}} w_k[n]v[n-k] \qquad (13.18)$$

The filter coefficients $w_k[n]$, $k = \{0, ..., N_{IC}\}$, can be adapted with any practical algorithm, such as the well-known *least-mean-square* (LMS) or *recursive least-squares* (RLS) algorithms.

## 13.5.3 Summary

In general, the IC-based compensator is only utilizable if the image signal is more powerful than the desired channel signal. Consequently, some kind of power estimation of the different channel signals is needed to decide when to switch the IC structure on and off.
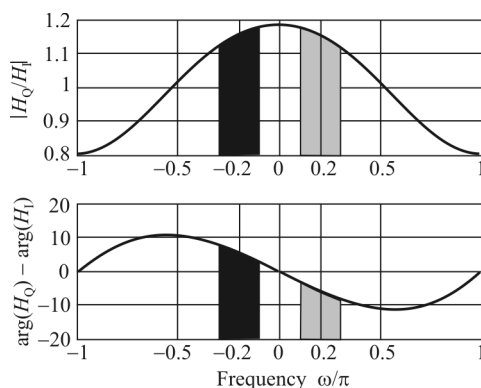
**Figure 13.19** Relative amplitude and phase mismatches of branch components.

The IC method is insensitive to the effects of additive noise and symbol timing errors, and, especially, to different interferer types. It is a blind technique, as no training signals are needed. It can cope with frequency-selective mismatches and it can tolerate time-variant mismatch effects due to its inherent adaptive nature.

### 13.5.4 Verification and Validation

We present in this section the simulation example of the technique presented in [8]. The received signal consists of the SOI and image channels of bandwidth $0.2\pi$ located originally around $0.7\pi$ and $0.3\pi$, respectively. The SOI and image signals are QPSK- and 8PSK-modulated, respectively, with raised-cosine pulse shapes (roll-off 0.35). The relative power difference is $-40$dB. In translating the SOI channel signal to an IF of $0.2\pi$, imbalance values of $g = 1.02$ and $\varphi = -2°$ are assumed for the quadrature demodulator. The branch mismatches are modeled as $H_I(z) = 0.01 + z^{-1} + 0.01z^{-2}$ and $H_Q(z) = 0.01 + z^{-1} + 0.2z^{-2}$. Finally, the symbol rate baseband observations $d[n]$ and $v[n]$ are generated by proper frequency translations of $\pm 0.2\pi$, lowpass filtering, and decimation.

The standard RLS algorithm with a forgetting factor of 0.999 is used to adapt the IC filter of length 5 ($N_{IC} = 4$). The total number of samples is 2000 to ensure steady-state operation.

Front-end imbalance properties used in the simulations are illustrated in Figure 13.19 and Figure 13.20. Single realizations of the absolute value of the center tap $w_2[n]$ are presented in Figure 13.21 to illustrate the convergence properties. Convergence in this case occurs after about five iterations.

The symbol constellation after convergence is shown in Figure 13.22 for the SOI. Recall that this signal has QPSK modulation (same as QAM) and is 40dB

less in amplitude than the image signal. We see that the image is almost totally suppressed.
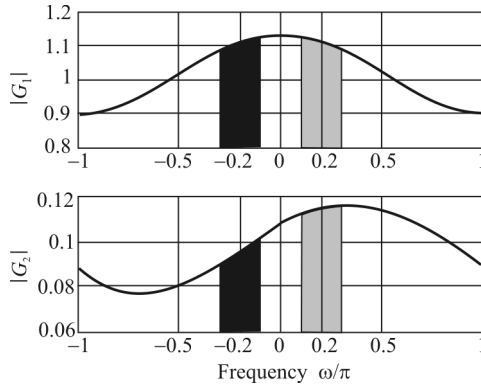


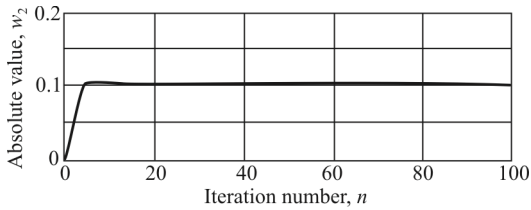**Figure 13.20** General imbalance coefficients $G_1$ and $G_2$.



**Figure 13.21** Center tap value $w_2[n]$; forgetting factor = 0.999, $N_{IC}$ = 4.
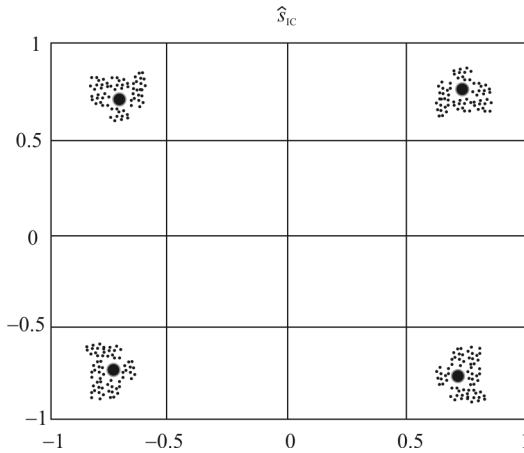
$$\hat{s}_{1C}$$



**Figure 13.22** Compensated output samples.

# 13.6 Concluding Remarks

Demodulating signals digitally is not functionally different from demodulating them in the analog domain. However, if the signals are already digital, due to IF or RF digitization, for example, then they need not be converted back to analog form for demodulation. We covered the basics of such demodulation in this chapter as well as provided a technique for demodulation without resorting to a DSP for that purpose.

A method was offered for compensating for the inevitable phase and gain imbalances in *I/Q* processing. The technique is applied once the signals have been converted to digital form. These imbalances are due to the analog components in the RF stage as well as the IF chain prior to the A/D conversion.

## References

[1]      Bernal, D., P. Closas, and J. A. Fernandez-Rubio, "Digital I&Q Demodulation in Array Processing: Theory and Implementation," *Proceedings 16th European Signal Processing Conference*, Lausanne, Switzerland, August 25–29, 2008.

[2]      Ziemer, R. E., and R. L. Peterson, *Introduction to Digital Communication*, 2nd Ed., Upper Saddle River, NJ: Prentice Hall, 2001, Ch. 4.

[3]      Simon, M. K., S. M. Hinedi, and W. C. Lindsey, *Digital Communication Techniques Signal Design and Detection*, Upper Saddle River, NJ: Prentice Hall, 1995.

[4]      Tsui, J., *Digital Techniques for Wideband Receivers*, 2nd Ed., Norwood, MA: Artech House, 2001.

[5]      Walden, R. H., "Analog-to-Digital Converter Survey and Analysis," *IEEE Journal on Selected Areas in Communications*, Vol. 17, No. 4, April 1999, pp. 539–550.

[6]      Schwarzinger, A., *Digital Signal Processing in Modern Communication Systems*, 2013.

[7]	Jessup, M., and J. Reyland, "PC-Based Implementation of a Flexible FSK Demodulator," USA CECOM Center for Signals Warfare Technical Report No. USACCSW-RT 90003(U), October 1989.

[8]	Valkama, M., and M. Renfors, "Advanced I/Q Signal Processing for Communication Systems," *Proceedings SDR-03 Technical Conference*, Orlando, Florida, November 2003.

# Chapter 14

## Digital-to-Analog Converters

## 14.1 Introduction

A *digital-to-analog converter* (DAC or D/A converter) is a device for converting a digital (usually binary) code to an analog signal (current, voltage, or charges). DACs are the interface between the digital signal processing domain and the analog domain. Simple switches, a network of resistors, current sources, or capacitors may implement this conversion. A DAC inputs a binary number and outputs an analog voltage or current signal. The block diagram symbol for a DAC is shown in Figure 14.1 [1–7].

A modern DAC today typically has the converter itself and a collection of support circuitry built into a single chip. The first DACs were board level designs, built from discrete components, including vacuum tubes as the switching elements. Monolithic DACs began to appear in the early 1970s along with other monolithic circuits. These early examples were actually sub-blocks of the DAC. As progress in monolithic integrated circuits advanced, these functions were integrated on the same die, and additional digital circuitry, specifically latches to store the digital input, were added. The input bank of latches could also be a shift register, which would allow a serial interface.

Since the output of the DAC is often a current, an op amp is often added to perform the current-to-voltage (I/V) conversion. We have more on this later. On the input a voltage reference is usually added.

Process limitations did not allow the integration of all these sub-blocks to occur at once. Initially, the processes used to make the various sub-blocks were not compatible. The process that made the best switches was typically not the best for the amplifier and the reference. As the processes became more advanced these limitations decreased in importance. Today CMOS process technology can make acceptable amplifiers and processes combining bipolar and CMOS together.
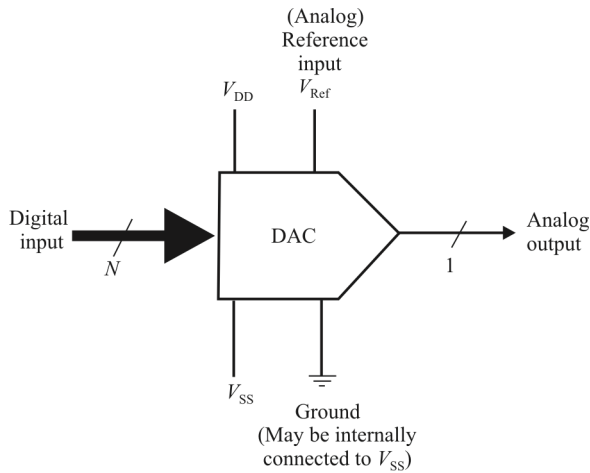
**Figure 14.1** DAC symbol.

This chapter is structured as follows. First, several DAC topologies are introduced. Each of these has its own properties and we discuss some of them. DAC error sources, both static and dynamic, are discussed next. The outputs of DACs are not smooth analog waveforms but sequences of discrete levels. This output must be filtered in order to remove the discontinuities. Reconstruction filters are used for this purpose, and they are discussed next.

The switches and current sources shown in this chapter are most often implemented with semiconductor devices (BJT, MOSFET, CMOS, etc.) in modern DACs. Consequently, we conclude the chapter with an appendix that considers using MOSFETs as switches and current sources.

# 14.2 Digital-to-Analog Converter Architectures

## 14.2.1 DAC Transfer Function

The DAC analog output is shown in Figure 14.2 for $N = 3$. In the ideal case, the analog output is a liner function of the input code because the input digital code word is infinitely long, and there is no quantization of the output. In a practical realization, where the input code does not consist of an infinite length digital word, the output is represented as a fraction of the reference as
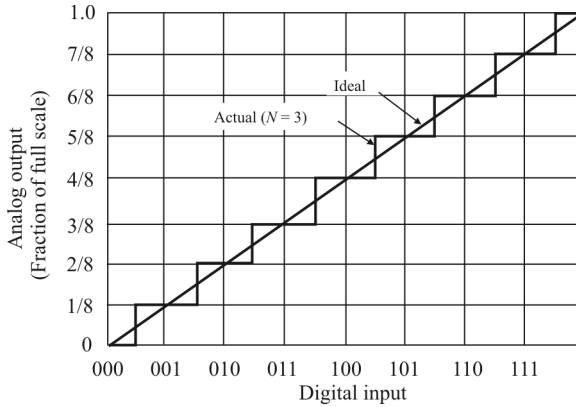
**Figure 14.2** DAC transfer function, 8-bit example.

$$V_o = \frac{D_i}{2^N} V_{Ref} \tag{14.1}$$

where:

$V_o$ is the analog output
$D_i$ is the digital input code
$N$ is the number of digital input bits (resolution)
$V_{Ref}$ is the reference voltage (full-scale)

Next we will examine some DAC architectures. When we refer to DACs here, we are referring to the basic converter rather than a complete system.

### 14.2.2 String DAC

14.2.2.1 Voltage Reference Divider

Perhaps the simplest structure of all to understand is the voltage reference divider DAC shown in Figure 14.3. An *N*-bit version of this DAC simply consists of $2^N$ equal resistors in series and $2^N$ switches (usually CMOS), one between each node of the chain and the output. One switch at a time in Figure 14.3 is closed, depending on the 3-bit digital input word. The decoding logic driving this DAC is shown in Table 14.1, where *V* corresponds to the unit voltge associated with the drop across each of the resistors. Obviously, this becomes quite complex as the number of bits rises above 8 or so, especially considering that often the resistors
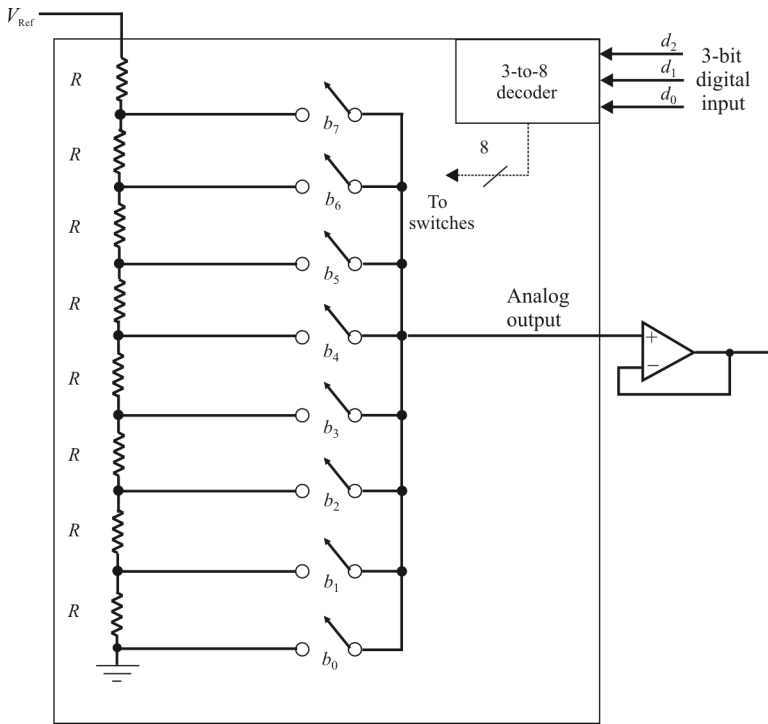
**Figure 14.3** Voltage reference divider DAC. 3-bit converter in this case (eight possible levels). Virtually no current flows through switches.

must be precisely trimmed for acceptable operation. The current flows through the switches so impedance characteristics of the switches must be taken into consideration.

The output is taken from the appropriate tap by closing just one of the switches, while leaving the rest open (there is some slight digital complexity involved in decoding to 1 of $2^N$ switches from $N$-bit data). This architecture is simple, has a voltage output, and is inherently monotonic—even if a resistor is accidentally short-circuited, output $n$ cannot exceed output $n + 1$. It is linear if all the resistors are equal but may be made nonlinear if a nonlinear DAC is required. The output is a voltage but it has the disadvantage of having relatively large output impedance. This output impedance is also code dependent (the impedance changes with changes to the digital input). In many cases it is beneficial to follow the output of the DAC with an amplifier, as shown in Figure 14.3, to buffer this output impedance and present a low-impedance source to the following stage [8].

**Table 14.1** Decoding Logic for the Voltage Divider in Figure 14.3

| $d_2$ | $d_1$ | $d_0$ | | $b_0$ | $b_1$ | $b_2$ | $b_3$ | $b_4$ | $b_5$ | $b_6$ | $b_7$ | $V_{out}$ |
|---|---|---|---|---|---|---|---|---|---|---|---|---|
| 0 | 0 | 0 | | ON | OFF | OFF | OFF | OFF | OFF | OFF | OFF | 0 |
| 0 | 0 | 1 | | OFF | ON | OFF | OFF | OFF | OFF | OFF | OFF | $V$ |
| 0 | 1 | 0 | | OFF | OFF | ON | OFF | OFF | OFF | OFF | OFF | $2V$ |
| 0 | 1 | 1 | | OFF | OFF | OFF | ON | OFF | OFF | OFF | OFF | $3V$ |
| 1 | 0 | 0 | | OFF | OFF | OFF | OFF | ON | OFF | OFF | OFF | $4V$ |
| 1 | 0 | 1 | | OFF | OFF | OFF | OFF | OFF | ON | OFF | OFF | $5V$ |
| 1 | 1 | 0 | | OFF | OFF | OFF | OFF | OFF | OFF | ON | OFF | $6V$ |
| 1 | 1 | 1 | | OFF | OFF | OFF | OFF | OFF | OFF | OFF | ON | $7V$ |

Since only two switches operate during any transition, it is a low-glitch topology (the concept of glitch will be examined in Section 14.3.2). Also, the switching glitch is not code-dependent, making it ideal for low-distortion applications. Because the glitch is constant regardless of the code transition, the frequency content of the glitch is at the DAC update rate and its harmonics—not at the harmonics of the DAC output signal frequency.

The major drawback of the string DAC is the large number of resistors and switches required for high resolution. There are $2^N$ resistors required, so a 10-bit DAC would require 1024 switches and resistors, and as a result it was not commonly used as a simple DAC architecture until the advent of very small IC feature sizes made it practical for low and medium DAC resolution (typically up to 10 bits).

The output of a DAC for an all 1s code is 1 lsb below the reference, so a string divider DAC intended for use as a general-purpose DAC has a resistor between the reference terminal and the first switch as shown in Figure 14.3.

## 14.2.2.2 Segmented String DACs

A variation of the voltage reference divider DAC is the segmented string DAC. Here we reduce the number of resistors required by segmenting. Figure 14.4 shows a segmented voltage-output DAC. Since there are buffers between the first and second stages, the second string DAC does not load the first, and the resistors in the second string do not need to have the same value as the resistors in the first. For linearity, however, all the resistors in each string do need to be equal to each other. The example shown has 3-bit first and second stages but for the sake of generality, let us refer to the first (msb) stage resolution as $M$-bits and the second (lsb) as $K$-bits for a total of $N = M + K$ bits. The msb DAC has a string of $2^M$ equal resistors and a string of $2^K$ equal resistors making up the lsb DAC. As an example, if we make a 10-bit string DAC out of two 5-bit sections, each segment would have 32 resistors, for a total of 64, as opposed to the 1024 required for a standard string divider. This is an obvious huge advantage. The decoding for all switches
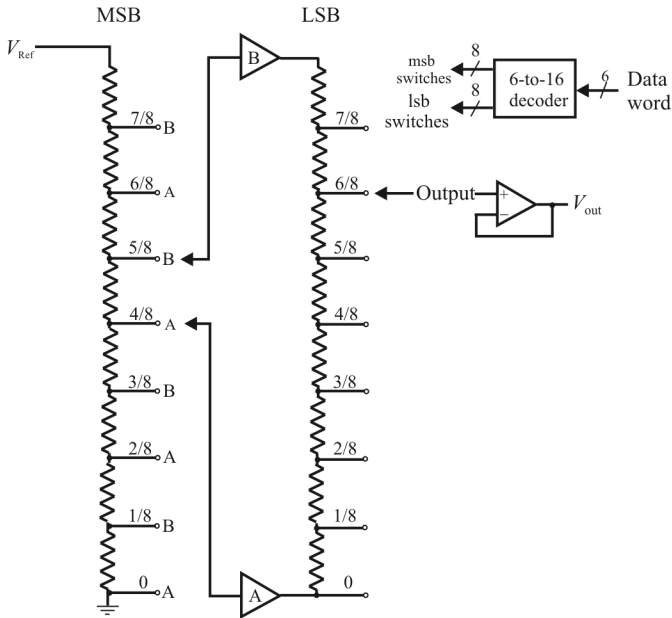
**Figure 14.4** Segmented voltage-output DAC.

occurs in parallel, however, so there is no delay disadvantage of this architecture compared to the single string topology.

For the switch settings in Figure 14.4, we have msb = 100 (4/8) and lsb = 110 (6/8) corresponding to the data word 100110.

Buffer amplifiers can have offset, of course, and this can cause nonmonotonicity in a buffered segmented string DAC. In the configuration of a buffered segmented string divider buffer shown in Figure 14.4, buffer A is always at a lower potential than buffer B, and an extra tap labeled "8/8" on the lsb string DAC is not necessary. The data decoding is just two priority encoders. But if the decoding of the msb string DAC is made more complex so that buffer A can only be connected to the taps labeled "A" in the msb string DAC and buffer B to the taps labeled "B" (this is normally the case), then it is not possible for buffer offsets to cause nonmonotonicity. Of course, the lsb string DAC decoding must change direction each time one buffer leapfrogs the other, and taps 0 and 8/8 on the lsb string DAC are alternately not used—but this involves a fairly trivial increase in logic complexity and is justified by the increased performance.

Little current flows through the msb switches because of the high input impedance of the buffer amplifiers. The same cannot be said for the lsb switches, and the output impedance will be data word dependent. Therefore, an amplifier is
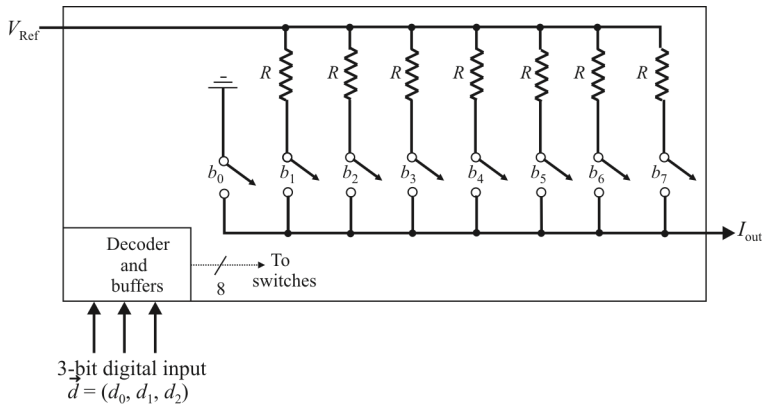
**Figure 14.5** Resistor current ladder. The simplest current-output fully decoded DAC.

often placed at the output as shown. This places a high impedance load to the LSB resistors, minimizing the loading effects as well as the current through the switches.

### 14.2.3 Fully Decoded DACs

The current-output DAC architecture analogous to a string DAC consists of $2^N - 1$ switchable current sources (which may be resistors and a voltage reference or may be active current sources) connected to an output terminal. This output level must be at, or close to, ground potential; therefore the loading of the following stage must have very low impedance. Figure 14.5 shows a fully decoded DAC that uses resistors connected to a reference voltage to generate the currents.

If active current sources are used as shown in Figure 14.6, the output may have more compliance (the allowable voltage on the output pin that still guarantees performance), and a resistive load is typically used to develop an output voltage.[1] The load resistance must be chosen so that at maximum output current the output terminal remains within its rated compliance voltage.

Once a current in a fully decoded DAC is switched into the circuit by increasing the digital code, any further increases do not switch it out again. The structure is thus inherently monotonic, irrespective of inaccuracies in the currents. Again, like the string divider, only the advent of high-density IC processes has made this architecture practical for general-purpose medium-resolution DACs.

The decoding logic for these current ladders is displayed in Table 14.2.

---

[1] We discuss using transistors as current sources in the appendix to this chapter.
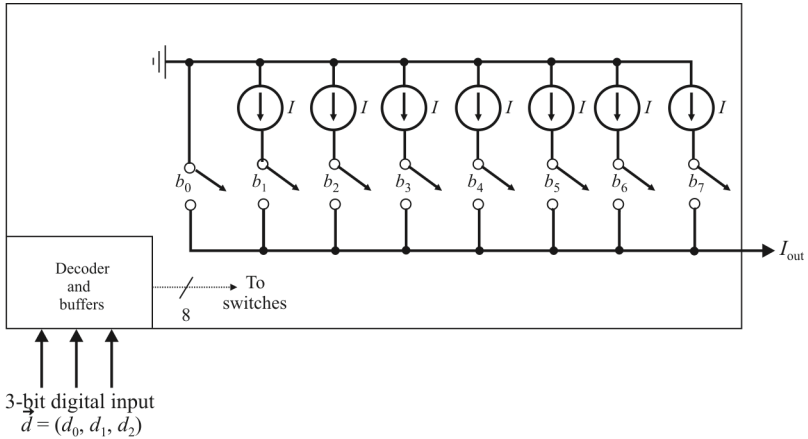
**Figure 14.6** Current sources improve the basic current-output fully decoded DAC.

**Table 14.2** Decoding Logic for the Current Ladders in Figures 14.5, 14.6, and 14.7

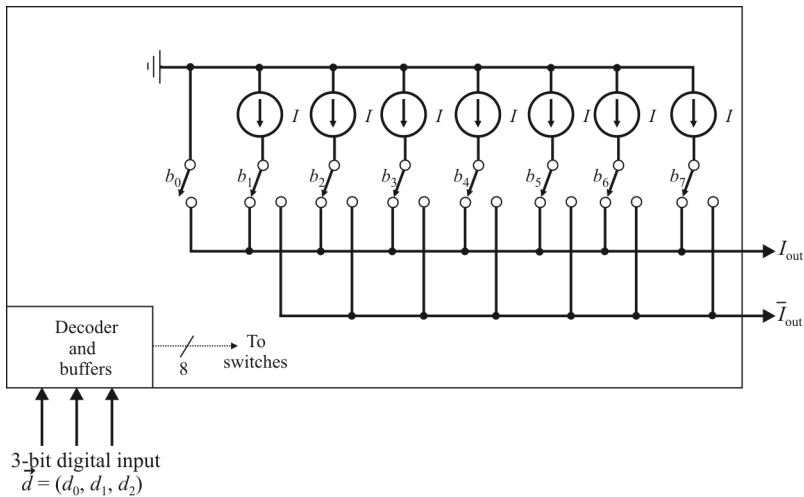| $d_2$ | $d_1$ | $d_0$ |  | $b_0$ | $b_1$ | $b_2$ | $b_3$ | $b_4$ | $b_5$ | $b_6$ | $b_7$ | $I_{out}$ |
|---|---|---|---|---|---|---|---|---|---|---|---|---|
| 0 | 0 | 0 |  | ON | OFF | OFF | OFF | OFF | OFF | OFF | OFF | 0 |
| 0 | 0 | 1 |  | OFF | ON | OFF | OFF | OFF | OFF | OFF | OFF | $I$ |
| 0 | 1 | 0 |  | OFF | ON | ON | OFF | OFF | OFF | OFF | OFF | $2I$ |
| 0 | 1 | 1 |  | OFF | ON | ON | ON | OFF | OFF | OFF | OFF | $3I$ |
| 1 | 0 | 0 |  | OFF | ON | ON | ON | ON | OFF | OFF | OFF | $4I$ |
| 1 | 0 | 1 |  | OFF | ON | ON | ON | ON | ON | OFF | OFF | $5I$ |
| 1 | 1 | 0 |  | OFF | ON | ON | ON | ON | ON | ON | OFF | $6I$ |
| 1 | 1 | 1 |  | OFF | ON | ON | ON | ON | ON | ON | ON | $7I$ |

**Figure 14.7** Current ladder with complementary current outputs.

## 14.2.3.1 Binary Weighted Ladder

The binary weighted ladder shown in Figure 14.5 contains one resistor or current source for each bit of the DAC connected to a summing point. These precise voltages or currents sum to the correct output value. This is one of the fastest conversion methods but suffers from poor accuracy because of the high precision required for each individual voltage or current. Such high-precision resistors and current sources are expensive, so this type of converter is usually limited to 8-bit resolution or less.

The DAC where the currents are switched between two output lines—one of which is often grounded, but may, in the more general case, be used as the inverted output—is more suitable for high-speed applications because switching a current between two outputs is far less disruptive and so causes a far lower glitch than simply switching a current on and off. This architecture is shown in Figure 14.7.

But the settling time of this DAC still varies with initial and final code, giving rise to *intersymbol distortion* [also known as *intersymbol interference* (ISI) in the communication literature]. This can be addressed with even more complex switching where the output current is returned to zero before going to its next value. Note that although the current in the output is returned to zero it is not turned off—the current is dumped to ground when it is not being used rather than being switched on and off.
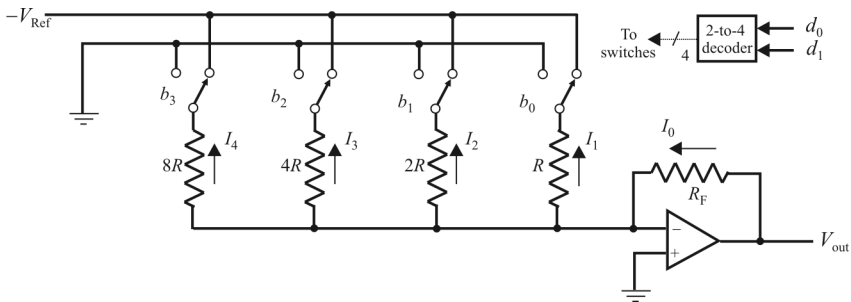
**Figure 14.8** Binary-weighted resistor ladder.

In the normal (linear) version of this DAC, all the currents are nominally equal. Where it is used for high-speed applications, its linearity can also be improved by dynamically changing the order in which the currents are switched by ascending code. Instead of code 001 always turning on current A, code 010 always turning on currents A and B, code 011 always turning on currents A, B, and C, etc., the order of turn-on relative to ascending code changes for each new data point. This can be done quite easily with a little extra logic in the decoder. The simplest way of achieving it is with a counter that increments with each clock cycle so that the order advances: ABCDEFG, BCDEFGA, CDEFGAB, etc., but this algorithm may give rise to spurious tones in the DAC output. A better approach is to set a new pseudo-random order on each clock cycle—this requires a little more logic, but even complex logic is now very cheap and easily implemented on CMOS processes. There are other, even more complex, techniques that involve using the data itself to select bits and thus turn current mismatch into shaped noise.

### 14.2.3.2 Binary-Weighted Current Source

The voltage-mode binary-weighted resistor DAC shown in Figure 14.8 is a simple example of a DAC. However, this DAC is not inherently monotonic and is actually quite hard to manufacture successfully at high resolutions due to the large spread in component (resistor) values. In addition, the output impedance of the voltage mode binary DAC changes with the input code.

Current-mode binary-weighted DACs are shown in Figure 14.9(a) (resistor-based) and Figure 14.9(b) (current source-based) [9]. An $N$-bit DAC of this type consists of $N$-weighted current sources (which may simply be resistors and a voltage reference) in the ratio $1:2:4:8:,\ldots,:2^N$. The lsb switches the $2^N$ current, the msb the 1 current, etc. The theory is simple but the practical problems of manufacturing an IC of an economical size with current or resistor ratios of even 128:1 for an 8-bit DAC are enormous, especially as they must have matched temperature coefficients. This architecture is virtually never used on its own in
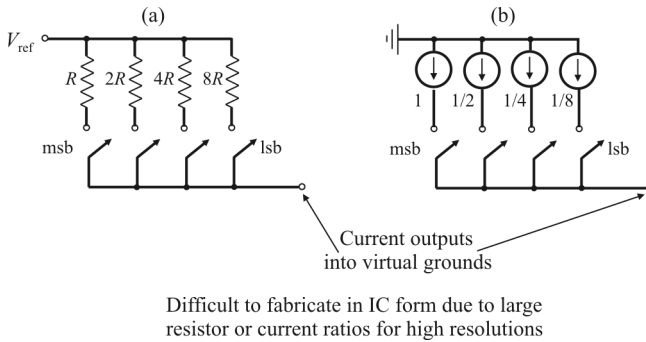
Figure 14.9 Current mode binary-weighted DACs: (a) resistor, and (b) current source.

integrated circuit DACs, although, again, 3 bit or 4 bit versions have been used as components in more complex structures.

### 14.2.3.3 R/2R Ladder

A simpler circuit is the R/2R ladder, which uses $3N + 2$ resistors [10–12]. This is shown in Figure 14.10. The R/2R ladder DAC is a binary-weighted DAC that creates each value with a repeating structure of two resistor values, $R$ and $2R$. This improves DAC precision due to the ease of producing many equal matched values of resistors or current sources but lowers conversion speed due to parasitic capacitance. Also, there are relatively few resistors to trim.

The operating principles of the R/2R ladder can be explained with the aid of Figure 14.11. We want to generate currents $I_0$, $2I_0$, $4I_0$,.... Two 2R resistors in parallel means that the $2I_0$ current will split equally parallel as in Figure 14.11(a). The two Thévenin resistances of the two branches at $V_1$ in Figure 14.11(b) both equal $2R$ so the current into this node splits evenly. We already know that the
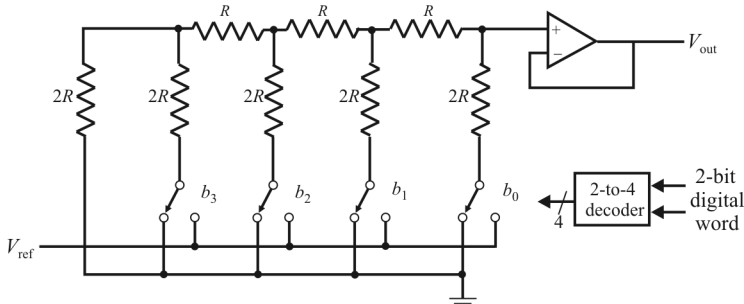


Figure 14.10 R/2R ladder; 2 bit converter in this case. Current flows through switches so $R_{on}$ is a consideration.
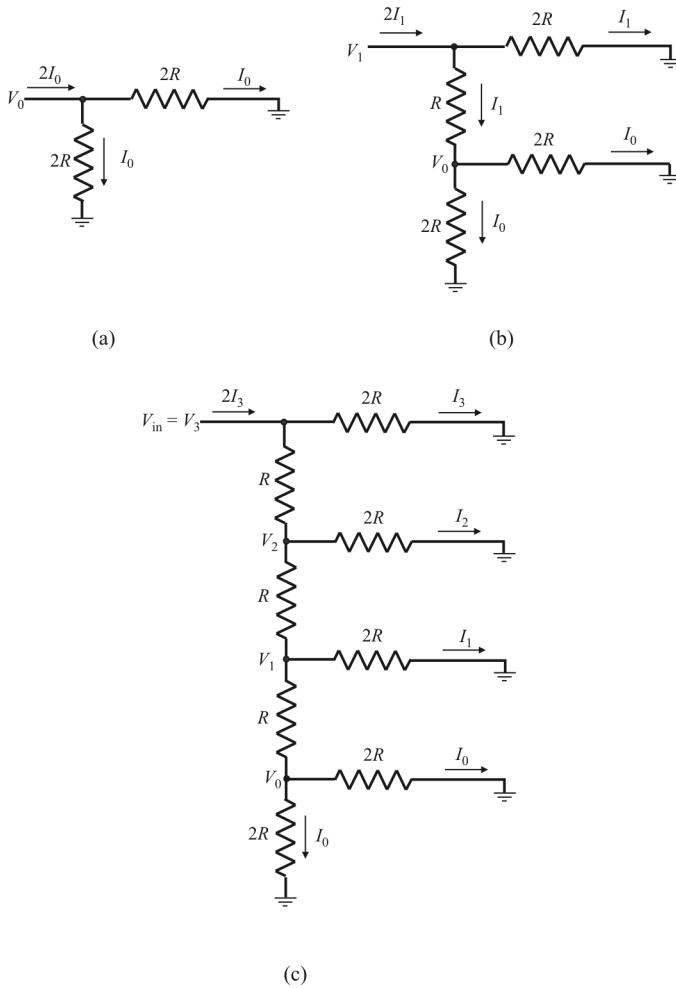
(a)

(b)

(c)

**Figure 14.11** R/2R ladder current flows: (a) two $2R$ resistors in parallel split the $2I_0$ current equally, (b) the current into the node splits evenly, and (c) the process in (b) repeated.
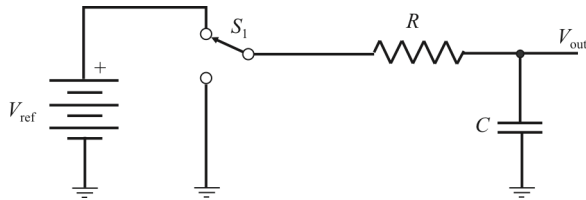
**Figure 14.12** Pulse width demodulator.

current into node $V_0$ is $2I_0$, so it follows that $I_1 = 2I_0$. We can repeat this process indefinitely and, using only two resistor values, can generate a whole series of currents, where $I_n = 2^n I_0$ as we see in Figure 14.11(c). From the voltage drop across the horizontal resistors, we see that $V_n = 2RI_n = 2^{n+1}RI_0$. For an $N$-bit ladder the input voltage is therefore $V_{in} = 2^N RI_0$ so that $I_0 = 2^{-N}V_{in}/R$. This is the basis for the $R/2R$ ladder DAC.

Note that $R_{on}$ of the switches is in series with the $2R$ leg, so $R_{on}$ should be significantly less than $2R$.

## 14.2.4 Time Reference Divider

The time reference divider segregates time into widths proportionally to the voltage at the input. This is illustrated in Figure 14.12. The time that $S_1$ is in the on position is controlled by the digital word input to the DAC. In principle, the longer $S_1$ is on, the larger the output voltage. The shorter $S_1$ is on, the lower the output voltage. This is illustrated in Figure 14.13. The voltage out of the switch is lowpass filtered and sent to the output. This is referred to as *pulse width modulation* (actually pulse width demodulation, since modulation is reverse of this process). What is actually shown is a 1-bit DAC, where the input bit determines the direction, or slope, of the output waveform. The input bits are fed into the DAC serially, one bit at a time.

In Figure 14.13(a) we see the input serial stream of bits. Notice that in regions marked "A," there are about the same number of 1s as 0s and the output waveform
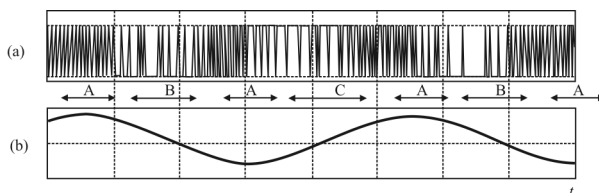


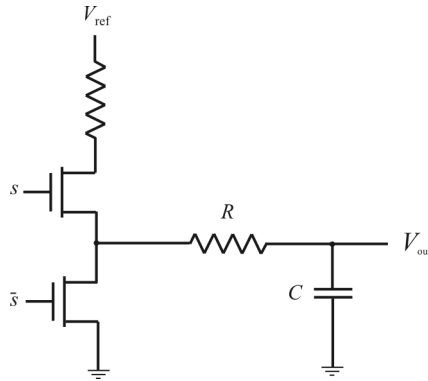**Figure 14.13** Pulse width demodulator waveforms: (a) input, and (b) demodulated output.

**Figure 14.14** DAC demodulator. One possible pulse width demodulator.

in Figure 14.13(b) is approximately flat, or the derivative is around zero. In the regions marked B there are more 0s than 1s and the slope is negative, forcing the output waveform to decrease toward its minimum value. In the regions marked C, there are more 1s than 0s and the output waveform has a positive trajectory, heading toward its maximum value.

One possible circuit to implement this demodulation function is shown in Figure 14.14.

## 14.2.5 Oversampling DACs

The concept of oversampling can be applied to high-speed DACs just as it was for ADCs in Chapter 8 and for the same reasons. Oversampling relaxes the requirements on the output filter as well as increase the SNR due to process gain. Consider a traditional DAC driven at an input word rate of 30 Msps [Figure 14.15(a)]. Assume the DAC output frequency is 10 MHz. Then the image frequency component at 30 MHz – 10 MHz = 20 MHz must be attenuated by the analog reconstruction filter, and the transition band of the filter is therefore 10 MHz to 20 MHz.

If the image frequency must be attenuated by 60dB, the filter must go from a passband of 10 MHz to 60dB stopband attenuation over the transition band lying between 10 MHz and 20 MHz (one octave). Filters provide 6dB attenuation per octave for each pole. Therefore, a minimum of 10 poles is required to provide the required attenuation. This is a fairly aggressive filter and would involve high $Q$ sections that would be difficult to manufacture and align and to keep aligned. Filters become even more complex as the transition band becomes narrower. When we increase the DAC update rate to 60 Msps and insert a zero between each original data sample, the parallel data stream rate becomes 60 Msps, but we must now determine the value of the zero-value data points. This is done by passing the
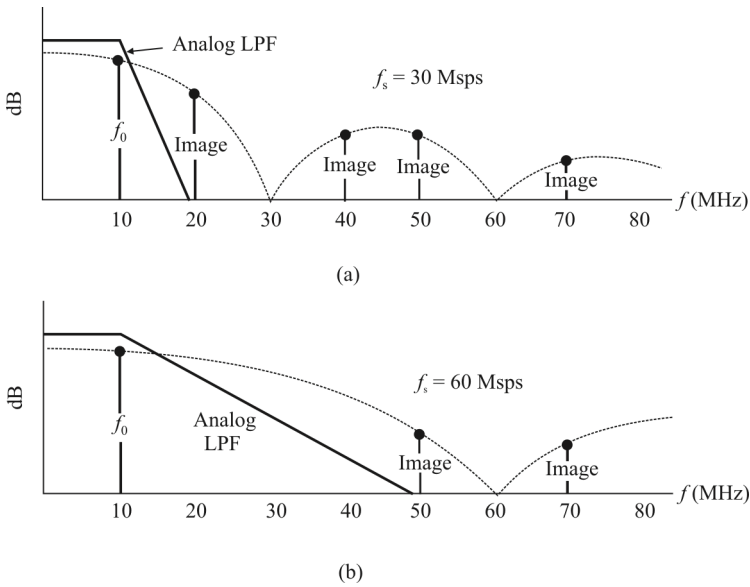
**Figure 14.15** Analog filter requirements for $f_0 = 10$ MHz: (a) $f_s = 30$ Msps, and (b) $f_s = 60$ Msps.

60 Msps data stream with the added zeros through a digital interpolation filter that computes the additional data points. The response of the digital filter relative to the 2× oversampling frequency is shown in Figure 14.15(b). The analog antialiasing filter transition zone is now 10 MHz to 50 MHz (the first image occurs at $2f_s - f_0 = 60 - 10 = 50$ MHz). This transition zone is a little greater than 2 octaves, implying that a 5-pole or 6-pole Butterworth filter is adequate.

## 14.2.6 Sigma-Delta DACs

Oversampling DACs such as the Σ-Δ DAC use a pulse density conversion technique. The oversampling technique allows for the use of a lower resolution DAC internally. A simple 1 bit DAC is often chosen, as it is inherently linear. The DAC is driven with a pulse density modulated signal, created through negative feedback. The negative feedback acts as a highpass filter for the quantization (signal processing) noise, thus pushing this noise out of the passband. Most very high-resolution DACs (greater than 16 bits) are of this type due to their high linearity and low cost. Speeds of greater than 10 Msps and resolutions of 24 bits are attainable with Σ-Δ DACs. Simple first-order Σ-Δ modulators or higher order topologies such as *multistage noise shaping* can be used to generate the pulse
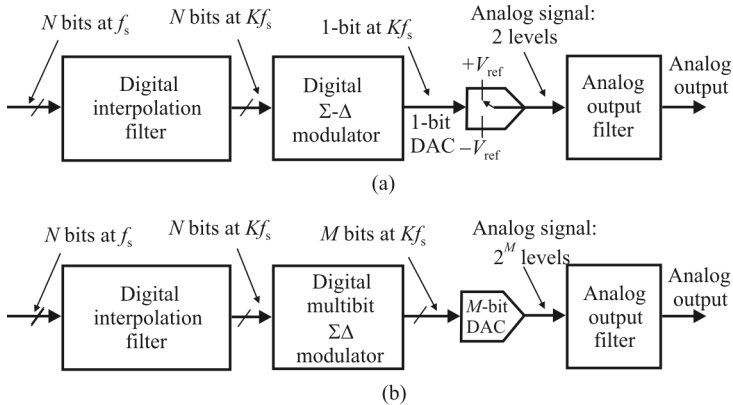
**Figure 14.16** Sigma delta DACs: (a) single bit, and (b) multibit.

density signal. Higher oversampling rates relax the specifications of the output lowpass filter and enable further suppression of quantization noise.

$\Sigma$-$\Delta$ DACs operate very similarly to $\Sigma$-$\Delta$ ADCs. However, in a $\Sigma$-$\Delta$ DAC, the noise-shaping function is accomplished with a digital modulator rather than an analog one.

A $\Sigma$-$\Delta$ DAC, unlike the $\Sigma$-$\Delta$ ADC, is mostly digital [Figure 14.16(a)]. It consists of an *interpolation filter* (a digital circuit that accepts data at a low rate, inserts zeros at a high rate, and then applies a digital filter algorithm and outputs data at a high rate), a $\Sigma$-$\Delta$ modulator (which effectively acts as a lowpass filter to the signal but as a highpass filter to the quantization noise and converts the resulting data to a high-speed bit stream), and a 1 bit DAC whose output switches between equal positive and negative reference voltages. The output is filtered in an external analog LPF. Because of the high oversampling frequency, the complexity of the LPF is much less than the case of traditional Nyquist operation [13].

It is possible to use more than one bit in the $\Sigma$-$\Delta$ DAC, and this leads to the *multibit* architecture shown in Figure 14.16(b). The concept is similar to that of interpolating DACs previously discussed, with the addition of the digital $\Sigma$-$\Delta$ modulator. In the past, multibit DACs have been difficult to design because of the accuracy requirement on the *n*-bit internal DAC (this DAC, although only *n* bits, must have the linearity of the final number of bits, *N*).

## 14.2.7 Current-to-Voltage Converters

IC DACs provide either voltage or current outputs. Figure 14.17 shows three fundamental configurations, all of which use an op amp to develop a buffered output voltage.
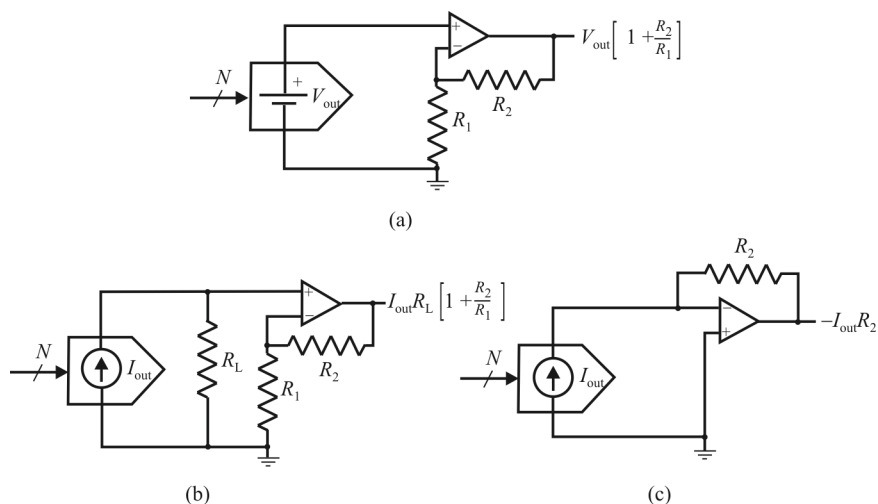
**Figure 14.17** Buffering DAC outputs with op amps: (a) buffered voltage output, (b) voltage developed across $R_L$, and (c) current-to-voltage direct method.

Figure 14.17(a) shows a buffered voltage output DAC. In many cases, the DAC output can be used directly, without additional buffering. This is largely determined by the loading on the output. If an additional op amp is needed, it is usually configured in a noninverting mode, with gain determined by $R_1$ and $R_2$.

There are two basic methods for dealing with a current output DAC. A direct method to convert the output current into a voltage is shown in Figure 14.17(c). This circuit is usually called a current-to-voltage converter, or I/V. In this circuit, the DAC output drives the inverting input of an op amp, with the output voltage developed across the $R_2$ feedback resistor. In this approach the DAC output always operates at virtual ground [which may give a linearity improvement vis-à-vis Figure 14.17(b)].

In Figure 14.17(b), a voltage is simply developed across external load resistor, $R_L$. This is typically done with high-speed op amps. An external op amp can be used to buffer and/or amplify this voltage if required. The output current is dumped into a resistor instead of into an op amp directly since the fast edges may exceed the slew rate of the amplifier and cause distortion. Many DACs supply full-scale currents of 20 mA or more, thereby allowing reasonable voltages to be developed across fairly low value load resistors. For instance, fast settling video DACs typically supply nearly 30 mA full-scale current, allowing 1V to be developed across a source and load terminated 75Ω coaxial cable (representing a DC load of 37.5Ω to the DAC output).

The general selection process for an op amp used as a DAC buffer is that the performance of the op amp should not compromise the performance of the DAC.

The basic specifications of interest are DC accuracy, noise, settling time, bandwidth, distortion, etc.

# 14.3 Error Sources in DACs

The error sources inherent to DACs can be categorized as either static or dynamic. Static error sources are inherent to the DAC in question and are independent of the particular signal being converted. On the other hand, the effects of dynamic errors are signal dependent.

## 14.3.1 Static Error Sources

14.3.1.1 Nonlinearity

An *integral nonlinearity* (INL) is the maximum deviation of the analog output from the ideal straight line passing through the end points. Such a nonlinearity is illustrated in Figure 14.18.

A differential nonlinearity is the maximum deviation of the difference in the analog output between two adjacent codes from the ideal step size.

14.3.1.2 Offset Error

Offset error is a constant offset of the analog output irrespective of the input symbol. See Figure 14.19.

14.3.1.3 Gain Error

When the output is linear but has the wrong conversion gain, as indicated by an incorrect slope in the transfer function, gain error is exhibited. This error source is also illustrated in Figure 14.19.

14.3.1.4 Non-Monotonicity

A DAC is monotonic if the output either increases or remains constant as the input code increases by one lsb anywhere in the transfer function. If the output decreases when the input symbol is increased by 1 lsb then non-monotonicity is manifest. The DAC corresponding to the transfer function shown in Figure 14.20 is monotonic.
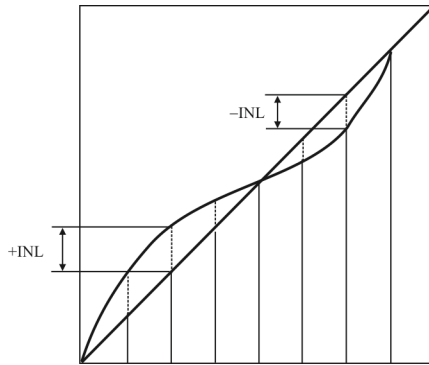
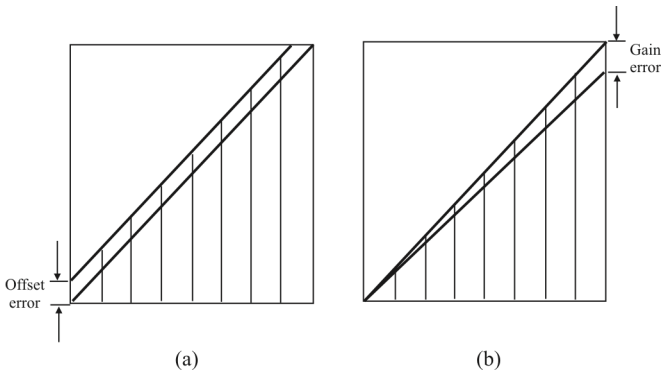**Figure 14.18** Integral nonlinearity.



(a)  (b)

**Figure 14.19** Static nonidealities: (a) offset error, and (b) gain error.
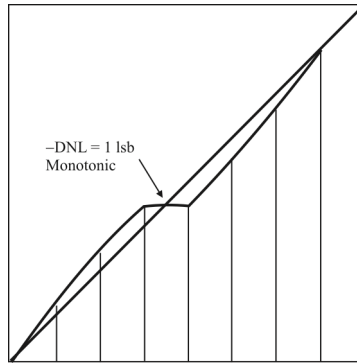
**Figure 14.20** Monotonic transfer function.

14.3.1.5 Quantization Noise Error

The digital input cannot precisely represent a continuous analog output. This is referred to as quantization noise, as we discussed in Chapter 8 for ADCs. The noise power due to quantization is

$$\varepsilon^2 = q^2 / 12$$

where

$q$ is 1 lsb
1 lsb = Full-scale/$2^N$

The SNR is then given by (7.4), which is the quantization noise limit on the SNR. Quantization noise is illustrated in Figure 14.21 for $N = 3$.

**14.3.2 Dynamic Error Sources**

The dynamic specifications that are most important with DACs are *settling time*, *glitch impulse area*, *distortion*, and SFDR [14].

14.3.2.1 Settling Time

The settling time of a DAC is the time from a change of digital code to when the output comes within and remains within some error band as shown in Figure 14.22. With amplifiers, it is hard to make comparisons of settling time, since their
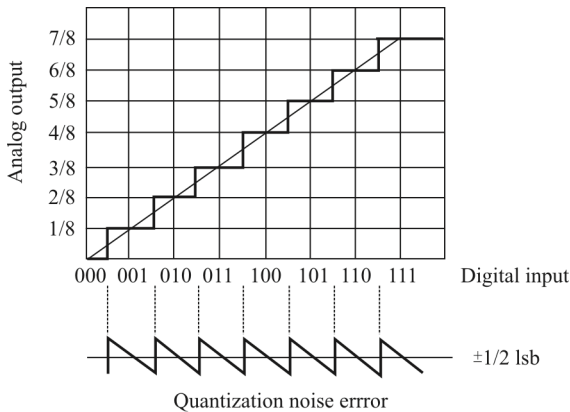
**Figure 14.21** DAC quantization noise for $N = 3$.

error bands may differ from amplifier to amplifier, but with DACs the error band will almost invariably be ±1 or ±½ LSB.

The settling time of a DAC is made up of four different time periods (see Figure 14.22): the *switching time* or *dead time* (during which the digital switching, but not the output, is changing), the *slewing time* (during which the rate of change of output is limited by the slew rate of the DAC output), the *recovery time* (when the DAC is recovering from its fast slew and may overshoot), and the *linear settling time* (when the DAC output approaches its final value in an exponential or near exponential manner). If the slew time is short compared to the other three (as is usually the case with current output DACs), then the settling time will be largely independent of the output step size. On the other hand, if the slew time is a significant part of the total, then the larger the step, the longer the settling time.
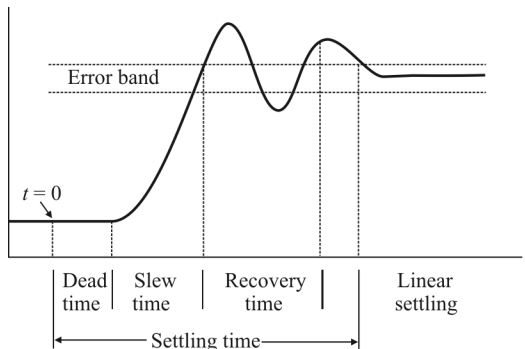
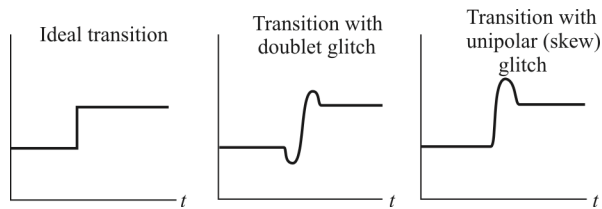

**Figure 14.22** DAC settling time.

**Figure 14.23** DAC transitions (showing glitch).

## 14.3.2.2 Glitch Impulse Area

Ideally, when a DAC output changes it should move from one value to its new one monotonically. In practice, the output is likely to overshoot, undershoot, or both (Figure 14.23). This uncontrolled movement of the DAC output during a transition is known as a *glitch*. It can arise from two mechanisms: capacitive coupling of digital transitions to the analog output and the effects of some switches in the DAC operating more quickly than others and producing temporary spurious outputs.

Capacitive coupling frequently produces roughly equal positive and negative spikes (sometimes called a *doublet* glitch) that more or less cancel in the longer term. The glitch produced by switch timing differences is generally unipolar, much larger, and of greater concern.

Glitches can be characterized by measuring the *glitch impulse area*, sometimes inaccurately called glitch energy. The term *glitch energy* is a misnomer, since the unit for glitch impulse area is volt-seconds (or more probably µV-sec or pV-sec). The *peak glitch area* is the area of the largest of the positive or negative glitch areas. The glitch impulse area is the net area under the voltage-versus-time curve and can be estimated by approximating the waveforms by triangles, computing the areas, and subtracting the negative area from the positive area as shown in Figure 14.24.

The mid-scale glitch produced by the transition between the codes 0114...111 and 1000...000 is usually the worst glitch since typically all the switches try to change state at the same time. Glitches at other code transition points (such as ¼ and ¾ full-scale) are generally less. Figure 14.25 shows the mid-scale glitch for a fast low-glitch DAC. The peak and net glitch areas are estimated using triangles as described above. Settling time is measured from the time the waveform leaves the initial 1-lsb error band until it enters and remains within the final 1-lsb error band. The step size between the transition regions is also 1lsb.

## 14.3.2.3 SFDR and SNR

If we consider the spectrum of a waveform reconstructed by a DAC from digital data, we find that, in addition to the expected spectrum (which will contain one or

$$\text{Peak glitch impulse area} = A1 \approx \frac{V_1 t_1}{2}$$

$$\text{Net glitch impulse area} = A1 - A2 \approx \frac{V_1 t_1}{2} - \frac{V_2 t_2}{2}$$
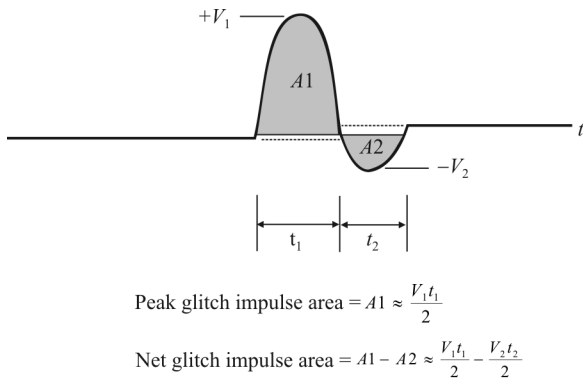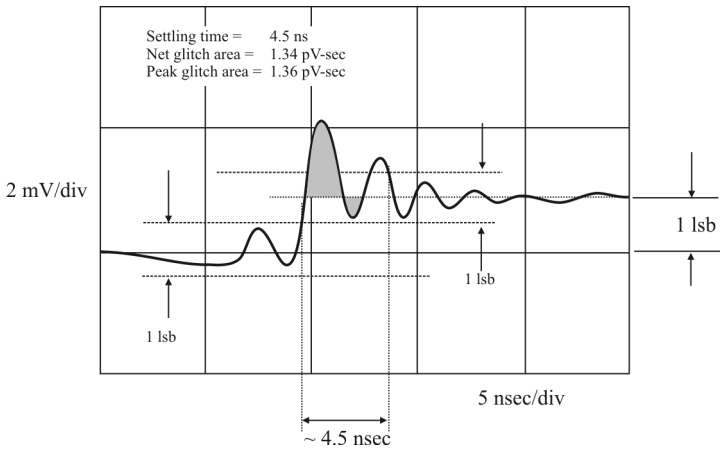
**Figure 14.24** Calculating net glitch areas.



**Figure 14.25** DAC mid-scale glitch shows 1.34 pV-sec net impulse area and settling time of 4.5 nsec.
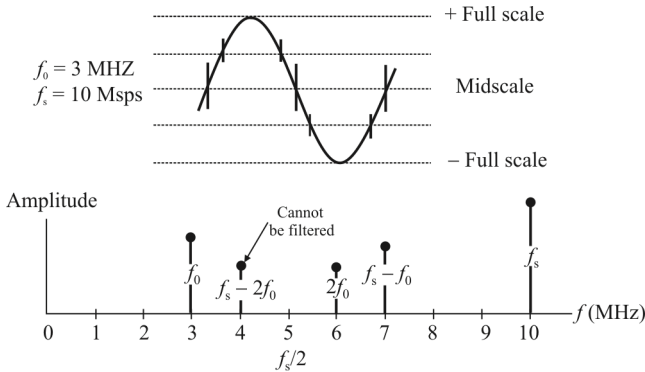
**Figure 14.26** Effect of code-dependent glitches on spectral output.

more frequencies, depending on the nature of the reconstructed waveform), there will also be noise and distortion products [15, 16]. Distortion may be specified in terms of harmonic distortion, SFDR, intermodulation distortion, or all of these. Harmonic distortion is defined as the ratio of harmonics to fundamental when a (theoretically) pure sine wave is reconstructed and is the most common specification.

SFDR is the ratio of the worst spur (usually, but not necessarily, always a harmonic of the fundamental) to the fundamental. Code-dependent glitches will produce both out-of-band and in-band harmonics when the DAC is reconstructing a digitally generated sine wave as in a DDS system. The mid-scale glitch occurs twice during a single cycle of a reconstructed sine wave (at each mid-scale crossing) and will therefore produce a second harmonic of the sine wave, as shown in Figure 14.26. Note that the higher order harmonics of the sine wave, which alias back into the first Nyquist bandwidth (DC to $f_s/2$), cannot be filtered.

It is difficult to predict the harmonic distortion or SFDR from the glitch area specification alone. Other factors, such as the overall linearity of the DAC, also contribute to distortion. In addition, certain ratios between the DAC output frequency and the sampling clock cause the quantization noise to concentrate at harmonics of the fundamental, thereby increasing the distortion at these points. It is therefore usually necessary to determine some parameters through testing.

There are nearly an infinite combination of possible clock and output frequencies for a low distortion DAC, and SFDR is generally specified for a limited number of selected combinations [17].

### 14.3.2.4 Other Dynamic Considerations

Again, some specifications may be encountered that are less common and are listed below.

*Automatic Zero*: To achieve zero stability in many integrating-type converters, a time interval is provided during each conversion cycle to allow the circuitry to compensate for drift errors. The drift error in such converters is essentially zero.

*Channel-to-Channel Isolation*: In multiple DACs, the proportion of analog input signal from one DAC's reference input that appears at the output of the other DAC, expressed logarithmically in decibels. See also *crosstalk*.

*Crosstalk*: Leakage of signals, usually via capacitance between circuits or channels of a multichannel system or device, such as a multiplexer, multiple op amp, or multiple DAC. Crosstalk is usually determined by the impedance parameters of the physical circuit, and actual values are frequency-dependent. See also *channel-to-channel isolation*. Multiple DACs have a *digital crosstalk* specification: the spike (sometimes called a glitch) impulse appearing at the output of one converter due to a change in the digital input code of another of the converters. It is specified in nanovolt- or picovolt-seconds and measured at $V_{Ref} = 0$ V.

*Feedthrough*: Undesirable signal coupling around switches or other devices that are supposed to be turned off or provide isolation—for example, *feedthrough error* in a sample-and-hold, multiplexer, or multiplying DAC. Feedthrough is variously specified in percent, decibels, parts per million, fractions of 1 lsb, or fractions of 1 volt, with a given set of inputs, at a specified frequency.

# 14.4 Reconstruction Filters

The output of a DAC is not a continuously varying waveform but instead a series of DC levels. This output must be passed through a filter to remove the high-frequency components and smooth the waveform into a more truly analog waveform. The concept of digital filtering was discussed in more detail in Chapter 9. In general, to preserve spectral purity, the images of the DAC output must be attenuated below the resolution of the DAC. To use the example cited above, we assume that the DAC output passband is 10 MHz. The sample rate is 30 MHz. Therefore, the image of the passband that must be attenuated is 30 MHz – 10 MHz = 20 MHz. This is the sample rate minus the passband frequency. The DAC in this example is a 10 bit device, which would indicate a distortion level of −60dB. So a reconstruction filter should reduce the image by 60dB while not attenuating the fundamental at all. Since a filter attenuates at 6 dB/pole, this would indicate that a tenth-order filter would be required.

There are several other considerations that must be taken into account. First is that most filter cutoffs are measured at the −3 dBpoint. Therefore, if we do not want the fundamental attenuated, some margin in the filter is required. The graphs
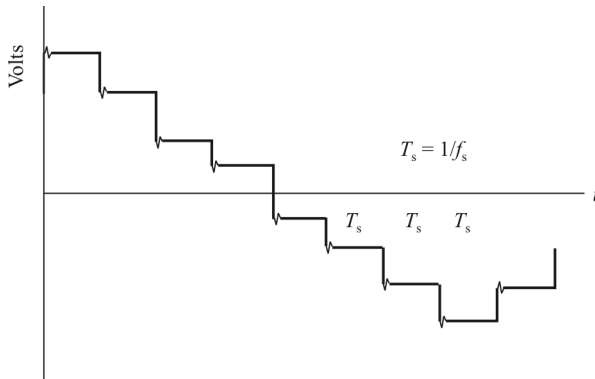
**Figure 14.27** DAC output.

in the filter section will help illustrate this point. This will cause the transition band to become narrower and thus the order of the filter to increase.

Second, since the output of a DAC is not a continuously varying waveform; instead, a series of DC level, the DAC puts out a DC level until it is told to put out a new level. This is illustrated in Figure 14.27. The width of the pulses is $1/f_s$. The spectrum of each pulse is represented by the sinc function shown in Figure 14.28. This response is added to the response of the reconstruction filter to provide the overall response of the converter. This will cause an amplitude error as the output frequency approaches the Nyquist frequency ($f_s/2$). Some high-speed DACs incorporate an inverse filter (in the digital domain) to compensate for this rolloff.

# 14.5 Concluding Remarks

We covered several DAC architectures and discussed some of the advantages and disadvantages of each of them in this chapter. The speed and resolution (determined by the number of bits) of DACs are regularly improving and
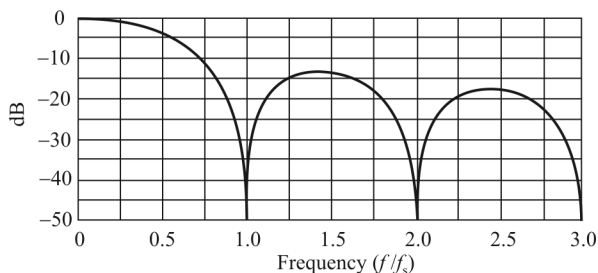


**Figure 14.28** Sinc function (normalized to $f_s$).

performance into the Gsps range with 80dB SFDR is available.

We also discussed the primary sources of errors in DACs, both static and dynamic errors. An example of the former is a nonlinear transfer function while timing glitches are an example of the latter.

# Appendix 14.A Semiconductor Current Sources and Switches

## 14.A.1 Semiconductor Current Sources

The ideal current source has its output supply current independent of its output voltage. We illustrate in Figure 14.A.1 the output characteristics of an NMOS device as well as that of an ideal current source, and we can see that such a device closely resembles that of an ideal current source. The particular curve followed by the output characteristic is determined by the control parameter $V_{GS}$ [18].

As a related point of interest, the output characteristics shown in Figure 14.29 also indicate a resistive region at lower levels of output voltage. The device acts as a voltage-controlled variable resistor in this region because the current through the channel is a (relatively) linear function of the voltage across it.

The output conductance of a semiconductor source such as that shown in Figure 14.29 is given by

$$G_s = \frac{\Delta I_S}{\Delta V_{DS}}$$

For the example shown

$$G_s \approx \frac{(28-26)\times10^{-6}}{1.8-0.4} = 1.4\times10^{-6}$$



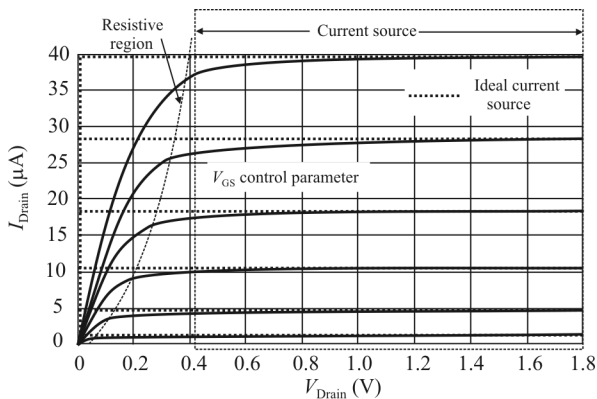**Figure 14.A.1** NMOS as current source. NMOS enhancement mode in this case.
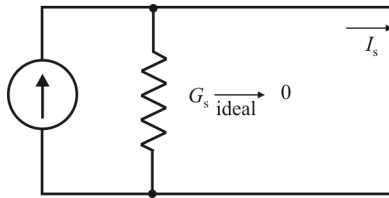
**Figure 14.A.2** Current source.

Of course, the output resistance of an ideal current source is infinite, since the current source can be modeled as illustrated in Figure 14.A.2.

### 14.A.2 Semiconductor Switches

MOS and BJT devices can be configured as electronic switches. These can be voltage switches or current switches as required for the particular architecture being considered. We show in Figure 14.A.3 the configuration as well as the output characteristic curves for an NMOS device configured as a current switch, but we must keep in mind that the active device can be almost any form of semiconductor 3-terminal device: BJT, NMOSFET, PMOSFET, as well as any of several other forms of MOS devices (e.g., JFETs).

The on-resistance of the switch shown in Figure 14.A.3 is given by the slope of the characteristic curve at $V_{DS} = 1.8V$ and, in the case of the example given in Figure 14.A.3

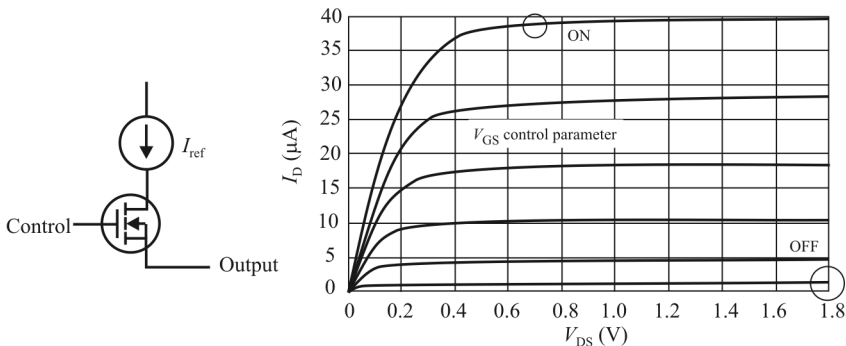$$R_{on} \approx \frac{0.2}{(33-26)\times10^{-6}} = 28\,k\Omega$$



**Figure 14.A.3** MOSFET as current switch. NMOS enhancement mode in this case.
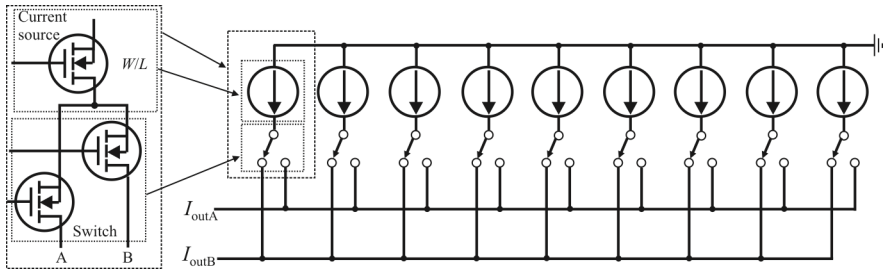
**Figure 14.A.4** DAC MOSFET as a current source and switch.

On the other hand, when the switch is OFF, ideally $G_s = 0$. We see from Figure 14.A.3 that

$$G_s\big|_{OFF} \approx \frac{0}{0.2} = 0$$

## 14.A.3 Transistors as Current Source and Switch

Both MOS and BJT transistors can be configured into current sources with integrated switches as illustrated in Figure 14.A.4. For weighted unit currents (equal or binary weighted) the MOS matching is a function of gate area and gate voltage, $V_{GS} - V_t$. Statistical averaging across a large collection of smaller devices results in improved matching performance.

## References

[1]     Mercer, D., et al., "12-b 125 MSPS CMOS D/A Designed For Spectral Performance," *ISLPED 1996 Digest of Technical Papers*, 1996, pp. 243–246.
[2]     Lin, C. H., et al., "A 10-b 500-MSample/s CMOS DAC in 0.6 mm²," *IEEE Journal of Solid-State Circuits*, Vol. 33, No. 12, December 1998, pp. 1948–1958.
[3]     Cong, Y., et al., "A 1.5V 14-bit 100 MSPS Self-calibrated DAC," *IEEE Journal of Solid-State Circuits*, Vol. 38, No. 12, December 2003, pp. 2051–2060.
[4]     Tiilikainen, M., "A 14-bit 1.8-V 20-mW 1-mm² CMOS DAC," *IEEE Journal of Solid-State Circuits*, Vol. 36, No. 7, July 2001, pp. 1144–1147.
[5]     Tesch, B., et al., "A 14-b, 125 MSPS Digital to Analog Converter and Bandgap Voltage Reference in 0.5 μm CMOS," *ISCAS 1999 Digest of Technical Papers*, pp. II-452–455.
[6]     Bugeja, A. R., et al., "A 14-b, 100-MS/s CMOS DAC Designed for Spectral Performance," *IEEE Journal of Solid-State Circuits*, Vol. 34, No .12, December 1999, pp. 1719–1732.
[7]     Schofield, W., et al., "A 16-b 400 MS/s DAC with < –80dBc IMD to 300 MHz and < –160dBm/Hz Noise Power Spectral Density," *ISSCC Digest of Technical Papers*, February 9, 2003, pp. 126–127.
[8]     Luschas, S., et al., "Output Impedance Requirements for DACs," *Proceedings of the 2003 ISCAS*, Vol. 1, May 25–28, 2003, pp. I-861–I-864.

[9]     Deveugele, J., et al., "A 10b 250MS/s Binary-Weighted Current- Steering DAC," *IEEE Journal of Solid-State Circuits*, Vol. 41, No. 2, February 2006, pp. 320-329.

[10]    Horowitz, P. and W. Hill, *The Art of Electronics*, Cambridge: Cambridge University Press, 1980.

[11]    Tocci, R. J., *Digital Systems*, 5th Ed, Prentice-Hall, 1991.

[12]    Simpson, R. E., *Introductory Electronics for Scientists and Engineers*, 2nd Ed., Allyn and Bacon, 1987.

[13]    Schreier, R., and G. C. Temes, *Understanding Delta-Sigma Data Converters*, IEEE Press, 2005.

[14]    Mercer, D., "A Study Of Error Sources In Current Steering Digital-to-Analog Converters," *CICC 2004 Conference Proceedings*, pp. 185-190.

[15]    Van den Bosch, A., et al., "SFDR-Bandwidth Limitations for High-Speed High-Resolution Current-Steering CMOS D/A Converters," *Proceedings IEEE International Conference on Electronics, Circuits, and Systems*, 1999, pp. 1193-1196.

[16]    Mercer, D., "A 16b D/A Converter with Increased Spurious Free Dynamic Range*," IEEE Journal of Solid-State Circuits*, Vol. 29, No. 10, October 1994, pp. 1180–1185.

[17]    Gonzalez, J. L., et al. ; "Clock-Jitter Induced Distortion In High Speed CMOS Switched-Current Segmented Digital-to-analog Converters," *ISCAS 2001 Digest of Technical Papers*, May 2001, pp. I-512–515.

[18]    Pelgrom, M. J. M., et al., "Matching Properties of MOS Transistors," *IEEE Journal of Solid-State Circuits*, Vol. 24, No. 5, October 1989, pp. 1433 – 1435.

# Chapter 15

## Direct Digital Converters

### 15.1 Introduction

In this chapter we investigate techniques for extracting narrowband signals from wideband signals. The latter may be comprised of several such narrowband signals. An example of such a wideband signal could be a multicarrier signal and another is FDM.

This chapter is arranged as follows. In the first part we address narrowband signal extraction by demodulation with the $I$ and $Q$ channels of the wideband signal. In the second part we discuss *direct digital converters* (DDCs), also known as *digital drop receivers* (DDRs).

### 15.2 Digital Receivers

Digital receivers accept digitized samples of IF or RF signals typically derived from the antenna. They utilize digital signal-processing techniques to translate a desired signal at a certain frequency down to DC and then remove all other signals by lowpass filtering.

The three essential elements of a digital receiver are the LO, the mixer, and the filter terms appropriately derived from their discrete analog circuitry counterparts in a traditional superhet radio (Figure 15.1). The LO consists of a phase accumulator (an adder and a register) and a *lookup table* (LUT) to generate digital quadrature sine and cosine signals. The accumulator is clocked at the ADC sample clock frequency so that the LO output sample rate matches the ADC sample rate. Frequency control is achieved by programming the phase increment for each clock.

The complex mixer consists of two digital multipliers that accept digital samples from the ADC and the LO. They produce a complex representation of the input signal, which has been translated down by the frequency setting of the local
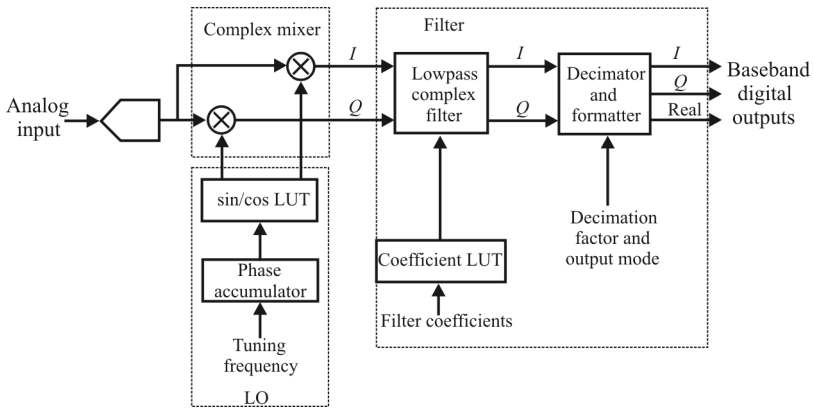
**Figure 15.1** Basic elements of a digital receiver include the LO, complex mixer, and lowpass filter. The LO consists of a phase accumulator and LUT to generate digital quadrature sine and cosine signals. The complex mixer has two digital multipliers that receive digital samples from the ADC and the LO, producing a complex representation of the input signal. The complex FIR lowpass filter accepts *I* and *Q* samples from the mixer and at the output the decimator drops all but one of every *N* samples.

oscillator. By appropriately tuning the LO, any frequency band of interest can be centered on 0 Hz.

The complex FIR lowpass filter accepts *I* and *Q* samples from the mixer. By judicious choices for coefficient values and the number of taps, it can implement a wide range of transfer functions, each with specific passband flatness, shape factors, and stopband attenuation to reject unwanted signals outside the band of interest.

At the filter output, a decimation stage drops all but one of every *N* samples, consistent with the bandwidth reduction of the filter. This produces a complex baseband output suitable for subsequent signal-processing tasks such as demodulation, decoding, or storage. By suitable reordering and sign changing of the *I* and *Q* output components, a real representation of the signal is also available. A useful definition of the decimation factor is the ratio between the input sampling rate and output bandwidth.

Digital receivers are divided into two classes appropriately named for the relative range of output signal bandwidths: wideband and narrowband. Digital receivers with minimum decimation ranges of 32 or more generally fall into the narrowband category and are extremely appropriate for extracting voice signals with bandwidths of several kilohertz from digitized input signals with bandwidths of several tens of megahertz. In these applications decimation factors can be 10,000 or higher.

Because the complexity of the FIR lowpass filter is proportional to the decimation factor (and inversely proportional to the bandwidth), *application-*
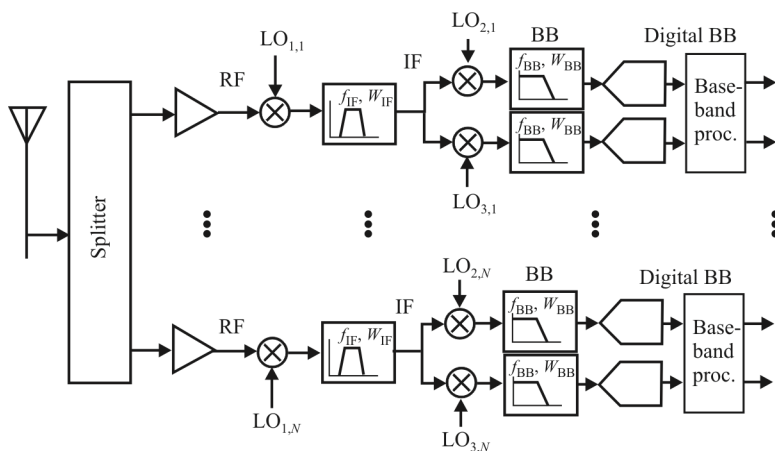
**Figure 15.2** First-generation RF architecture of *N*-channel receiver. A/D conversion is accomplished at baseband in this receiver.

*specific integrated circuit* (ASIC) implementations of narrowband receivers usually rely on an initial *cascaded integrated comb* (CIC) filter stage to perform high decimation factors without requiring hardware multipliers. We discuss CIC filters at length shortly. Since the CIC filter produces a sloping frequency response in its passband, its output is delivered to a *compensating FIR* (CFIR) filter, which restores an overall flat passband response. Finally, a PFIR (programmable FIR) filter is used to achieve the desired final frequency response.

EW receivers are an example of radio systems that must simultaneously downconvert and demodulate multiple narrowband RF channels. For example, recent FCC regulations in the United States dictate that as of January 1, 2013, the spectrum channelization in the private land mobile VHF frequency range (150–174 MHz) and UHF frequency ranges (450–470 MHz) be reduced from 25 kHz to at least half that, to 12.5 kHz, with eventual reduction to 6.25 kHz. The traditional architecture of a radio receiver that performs this task is shown in Figure 15.2. This architecture contains sets of dual-conversion sub-receivers. Each receiver amplifies and downconverts a selected RF channel to an IF filter that performs initial bandwidth limiting [1–3]. Harris et al. describe an architecture for EW receivers that utilizes polyphase filtering to perform the receiving task much more efficiently than that shown in Figure 15.2 [4].

In Figure 15.2, the output of each IF filter is again downconverted to baseband by matched quadrature mixers that are followed by matched baseband filters that perform final bandwidth control. Each quadrature downconverted signal is then converted to their digital representation by a pair of matched ADCs. The outputs of the ADCs are processed by DSP engines that perform the required synchronization, equalization, demodulation, detection, and channel decoding.
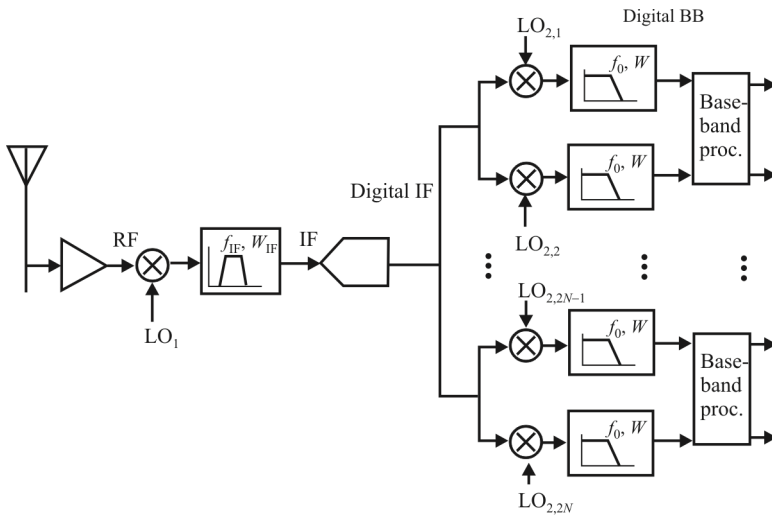
**Figure 15.3** Second-generation RF architecture of *N*-channel receiver. Digitization is performed at IF in this receiver.

Figure 15.3 presents a block diagram of a second-generation multichannel receiver in which the conversion from analog to digital occurs at IF rather than at baseband. Examining the receiver, we see that the downconversion of the separate channels is performed by a set of digital downconverters and digital lowpass filters. The digital process can realize arbitrarily small levels of *I/Q* imbalance by controlling the number of bits involved in the arithmetic operations [5]. Precision of coefficients used in the filtering process sets an upper bound to spectral artifact levels at 5dB/bit so that 12 bit arithmetic can achieve image levels below 60dB. Thus, the DSP-based complex downconversion does not introduce significant imbalance-related spectral terms. The rule-of-thumb here is that the levels of spectral images are controlled to be below the quantizing noise floor of the ADC involved in the conversion process. A second advantage of the digital translation process is that the digital filters following or preceding the mixers are designed to have linear phase characteristics, a characteristic trivially simple to realize in digital nonrecursive (FIR) filters [6 and Chapter 9].

The dynamic range and conversion speed of the ADC and DAC become the limiting factors in the application of the architectures shown in Figure 15.3. The dynamic range of the converter is determined to first order by the number of bits in the converter with each bit contributing 6dB [7]. The Nyquist criterion [8] establishes the minimum sample rate to obtain an alias-free representation of the sampled signal. The Nyquist criterion directs us to select the sample rate to exceed the two-sided bandwidth of the signal. Converters have the property that the product of sample rate and number of conversion levels is a constant [9]. This relationship is
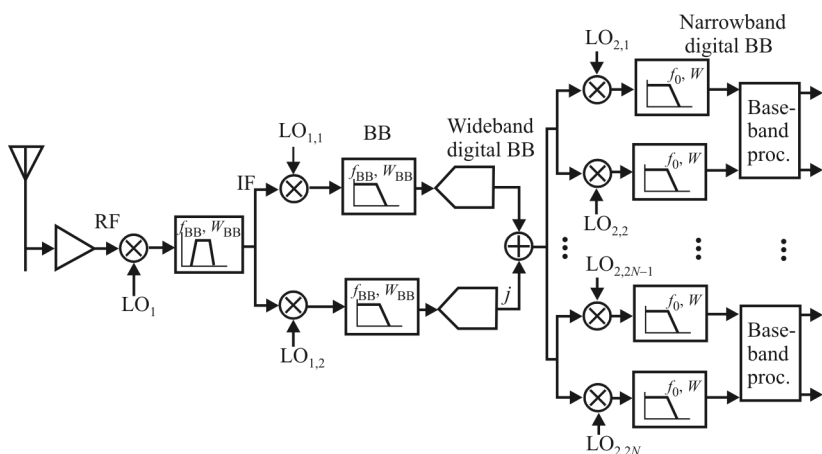
**Figure 15.4** Second-generation hybrid RF digital *N*-channel receiver.

$$\log_2(2^b f_{\text{sample}}) = k \tag{15.1}$$

or

$$b = \log_2 k - \log_2 f_{\text{sample}} \tag{15.2}$$

where *b* is the number of bits in the converter. Equation (15.2) shows how the number of bits varies inversely with the sample rate.

The spurious terms generated by converter nonlinearities often exceed the quantizing noise levels described by the 6dB-per-bit rule. The true performance measure of the ADC is the full-bandwidth SFDR [10].

The limited dynamic range available from high-speed ADCs restricts the range of applications for the architecture presented in Figure 15.3 to IF center frequencies to the low to mid-100s of megahertz. To extend the application range of digital *N*-channel receivers, a hybrid scheme is often used, illustrated in Figure 15.4, where the initial complex downconversion is performed with analog *I/Q* mixers and the channelization is performed digitally after the ADC. The first conversion can be considered a block conversion to baseband that delivers the frequency band of interest to the DSP arena for subsequent channelization. DSP techniques are applied to the digitized *I/Q* data to balance the gain and phase offsets in the analog ADC and DAC. DSP-based *I/Q* balance correction is a standard signal conditioning task.
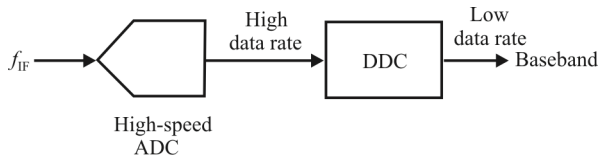
**Figure 15.5** DDC.

# 15.3 Digital Downconverters

## 15.3.1 Introduction

The purpose of digital downconverters (sometimes referred to as DDRs) is to shift the digitized band-limited RF or IF signal from its carrier down to baseband. A DDC is illustrated in Figure 15.5. As an example, suppose that $f_{IF}$ = 40 MHz and sample rate $f_s$ = 100 MHz. When the signal bandwidth is 1 MHz, an output sample rate of 2.5 MHz is acceptable. Therefore, we are oversampling with a decimation of 100/2.5 = 40.

We want to reduce the amount of required subsequent processing of the signal without loss of any of the information carried by the IF signal.

There are two classes of DDCs:

- Narrowband, where the decimation $R \geq 32$, yielding the CIC filter
- Wideband, where the decimation $R < 32$, yielding the FIR and multirate FIR filters

We will examine both of these architectures.

In the last section, we described the process of sampling an analog IF signal or complex analog baseband signal containing the set of FDM channels to be further processed or channelized by the DSP. We consider the input signal to be composed of many equal-bandwidth equally spaced FDM channels, as shown in Figure 15.6. These many channels are digitally downconverted to baseband, bandwidth constrained by digital filters, and subjected to a sample rate reduction commensurate with the bandwidth reduction.
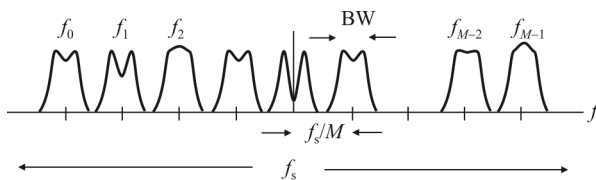


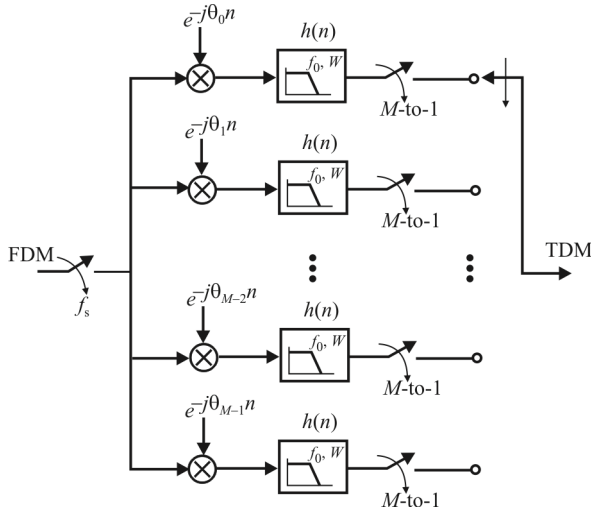**Figure 15.6** Input spectrum of FDM.

**Figure 15.7** Conventional channelizer as a replica of analog prototype: downconverters, baseband filters, and resamplers.

The signal processing task can be performed as a replica of the analog prototype technique by a DSP-based set of independent downconversion processes, as indicated in Figure 15.7. The digital frequency denoted by the angle $\theta_k$ is derived from analog frequency $f_k$. A complex sinusoid of frequency $2\pi f_k$ is represented as

$$g(t) = \exp(j2\pi f_k t) \tag{15.3}$$

Frequency is the time derivative of the phase angle and has units of radians/second. The sampled data sinusoid is obtained by replacing the time variable $t$ with the sampled time variable $nT_s$, as

$$g[n] = g(t)\big|_{t=nT_s} = \exp(j2\pi f_k n T_s) \tag{15.4}$$

The units of the sample time variable are samples and seconds/sample, respectively. The angle formed by the product $2\pi f_k$ and $T_s$ or by the equivalent term $2\pi f_k / f_s$, where $f_s = 1/T_s$, as shown in

$$g[n] = \exp\left(j2\pi \frac{f_k}{f_s} n\right) = \exp(j\theta_k n) \tag{15.5}$$
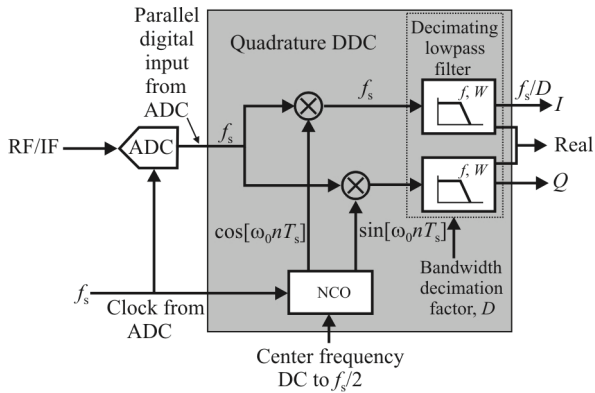
**Figure 15.8** A DDC consists of three main components: an LO, as represented by the NCO, two digital mixers (multipliers), and two decimating lowpass (digital) filters.

Here, the product term $2\pi f_k T_s$, denoted by $\theta_k$, has units of radians/second multiplied by seconds/sample or radians/sample.

## 15.3.2 Digital Downconverters

There are three major sections to a DDC (see Figure 15.8):

- Local oscillator (typically an NCO). The NCO is normally implemented with sine and cosine LUTs
- Mixers (digital). These are ideal multipliers
- Decimating lowpass filter (often implemented as a CIC and FIR)

15.3.2.1 Numerically Controlled Oscillator

The components of an NCO are illustrated in Figure 15.9. The phase accumulator calculates the new phase at $f_s$ with phase advance determined by the tuning word $M$. The NCO is clocked at the sample rate $f_s$. The phase is converted to amplitude values with the phase to amplitude conversion block. This is often accomplished in ROM-based sine LUTs; either one full sine wave is stored or only a quarter with some math on the pointer increment. With phase accumulator overflow, wraparound is accomplished in a circular LUT.

The advantages of an NCO include that the tuning word is programmable and frequencies up to nearly $f_s/2$ (Nyquist) are possible. The frequency changing speed is extremely fast (Figure 15.10). The phase continuous frequency hops with no over/undershoot or analog-related settling time anomalies.

The time it takes to retune the LO is simply the time it takes to load a new digital frequency word (32-bit binary number) into a register, usually well below 1
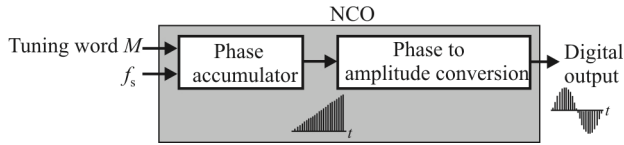
**Figure 15.9** NCO.

microcsecond. As we saw in Chapter 6, some digital receivers require an LO with a chirp function. This is a fast, programmable, and precise frequency sweep. A sweeping LO is easily implemented with an NCO simply by linearly incrementing the tuning word.

The NCO described here forms the basis for the digitally controlled synthesizer, used in many analog applications of digitally controlled oscillators. The fundamentals of *direct digital synthesis* (DDS) are described in the Appendix.

The oscillator generates digital samples of two sine waves precisely offset by $90^o$ in phase, creating sine and cosine signals. It uses a digital phase accumulator and sine/cosine lookup tables. Note that the ADC clock is fed into the LO. The digital samples out of the LO are generated at a sampling frequency exactly equal to the ADC sample clock frequency, $f_s$.

It is important to understand that the output sampling rate is always fixed at $f_s$, regardless of the frequency setting. The sine/cosine output frequency is changed by programming the amount of phase advance per sample. A small phase advance per sample corresponds to a low frequency and a large advance to a high frequency. The phase advance per sample is directly proportional to the output frequency and is programmable from DC to $f_s/2$ with up to 32 bits of resolution. This allows the LO to perform FSK and very finely resolved sweeps. Transients and settling normally associated with other types of LOs, such as a PLL synthesizer, are eliminated.

## 15.3.2.2 Mixer

The mixer in a DDC consists of two digital multipliers. Digital input samples from the ADC are mathematically multiplied by the digital sine and cosine samples from the LO.
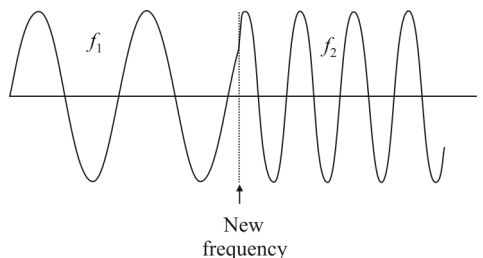


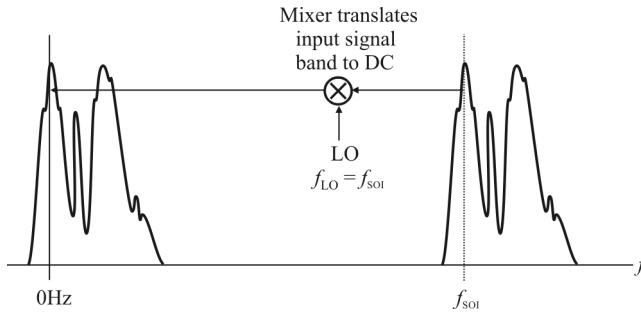**Figure 15.10** NCO changing frequencies.

**Figure 15.11** Digital receiver mixer translation.

Note that the input ADC data samples and the sine and cosine samples from the LO are being generated at the same rate—namely, once every ADC sample clock. Since the data rates into both inputs of the mixers are the ADC sampling rate $f_s$, the multipliers also operate at that same rate and produce multiplied output product samples at $f_s$.

The sine and cosine inputs from the LO create in-phase (I) and quadrature (Q) outputs that are important for maintaining phase information contained in the input signal. From a signal standpoint, the mixing produces a single-sideband complex translation of the real input.

Unlike analog mixers, which also generate many unwanted mixer products, the digital mixer is nearly ideal and produces only two outputs: the sum and difference frequency signals.

Consider the difference mixer product in the frequency domain as shown in Figure 15.11. At the output of the mixer, the high-frequency wideband signals in the ADC input have been translated down to DC with a shift or offset equal to the LO frequency.

This is similar to the analog receiver mixer except that the analog receiver mixes the RF input down to an IF. In the digital receiver, the precision afforded by the digital signal processing allows us to mix down to baseband (or 0 Hz). Overlapping mixer images, difficult to reduce with analog mixers, are strongly rejected by the accuracy of the sine and cosine LO samples and the mathematical precision of the multipliers in the digital mixer.

By tuning the LO over its frequency range, any portion of the RF input signal can be translated down to DC. In effect, the wideband RF signal spectrum can be shifted around 0 Hz, left and right, simply by changing the LO frequency. The objective is to tune the LO to center the signal of interest around 0 Hz so that the lowpass filter that follows can pass only the SOI.

## 15.3.2.3 Decimating Lowpass Filter

Once the RF signal has been translated, it is ready for filtering. The decimating lowpass filter accepts input samples from the mixer output at the full ADC
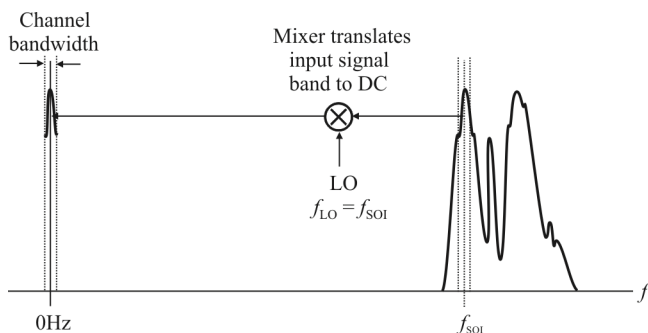
**Figure 15.12** Band-limiting decimating filter.

sampling frequency $f_s$. It utilizes digital signal processing to implement an FIR filter transfer function. The filter passes all signals from 0 Hz up to a programmable cutoff frequency or bandwidth and rejects all signals above that cutoff frequency. This digital filter is a complex filter that processes both $I$ and $Q$ signals from the mixer. At the output, either $I$ and $Q$ (complex) values or just real values can be selected, depending on system architecture.

Figure 15.12 shows a representation of the action of the filter in the frequency domain. The filter passes only signals from 0 Hz up to the filter bandwidth. All higher frequencies have been removed. Remember, the wideband input signal was translated down to DC by the mixer and positioned around 0 Hz by the tuning frequency of the LO.

Now, at the filter output we have effectively selected a narrow slice of the RF input signal and translated it to DC. Note that we have blocked all other signals above and below the band of interest. The band-limiting action of the filter is analogous to the action of the IF stage in the analog receiver, except that the decimating lowpass filter operates around DC instead of being centered at an IF.

*Filter Bandwidth*

In order to set the bandwidth of the filter, a parameter called the *decimation factor*, $D$, is used (see Figure 15.8). Since the output bandwidth and the output sampling rate are directly related in the DDC, the decimation factor also sets the output sampling rate. $D$ determines the ratio between input and output sampling rates and also the ratio between input and output bandwidths. Note that the output sampling rate for real outputs is twice that for complex outputs.

The DDC parameters depend on the decimation rate as follows:

$$\text{Output bandwidth} = \frac{\text{Input sample rate}}{D} \qquad (15.6)$$

$$\text{Complex output sample rate} = \frac{\text{Input sample rate}}{D} \qquad (15.7)$$

$$\text{Real output sample rate} = \frac{2 \times \text{Input sample rate}}{D} \qquad (15.8)$$

As mentioned, digital receivers can be divided into two classes, narrowband and wideband, distinguished by the programmable range of decimation factors. Narrowband receivers typically have a range of decimation factors from 32 or 64 to 65,536 or 131,072, depending on the chip manufacturer. Wideband receivers typically have a range of decimation factors from 2 to 64.

Because everything inside the decimating lowpass filter is performed with digital circuitry and DSP techniques, there are no undesirable effects normally associated with conventional analog filters. There are no initial component tolerance or temperature variations or aging characteristics. No calibration or preventive maintenance is required. This provides excellent channel-to-channel matching for applications where phase variation among channels is important, such as direction finding.  The FIR digital filters used have linear phase for well-behaved transient responses. The filter bandwidth is programmable over a wide range (1000 to 1), with absolutely predictable and uniform response. Last, the signal is tailored precisely for DSP processing by preselecting only the signal of interest through band-limiting and providing it to the DSP at the optimum sampling rate.

*Cascaded Integrated Comb Filter (CIC)*

The CIC is a computationally efficient implementation of a narrowband lowpass filter that requires no multipliers. They are multirate filters as discussed in Chapter 9.

A basic integrator is shown in Figure 15.13. In this configuration we have

$$y[n] = y[n-1] + x[n]$$

with a transfer function

$$H_1(z) = \frac{1}{1 - z^{-1}}$$

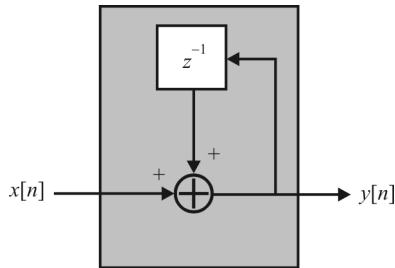The basic comb is shown in Figure 15.14. The output of this block is

**Figure 15.13** Basic integrator.

$$y[n] = x[n] - x[n-D]$$

with a transfer function

$$H_{\mathrm{C}}(z) = 1 - z^{-D}$$

The filter structure for a decimating CIC is shown in Figure 15.15. The structure for an interpolating CIC is shown in Figure 15.16. In these figures, $\Delta$ is the differential delay. The reference sampling rate for the transfer functions is always a higher frequency. The basic comb filter (referenced to the high-input sample rate) is

$$H_{\mathrm{C}}(z) = 1 - z^{-R\Delta}$$

The overall transfer function is

$$H(z) = (H_{\mathrm{I}})^M (H_{\mathrm{C}})^M = \frac{(1 - z^{-R\Delta})^M}{(1 - z^{-1})^M} = \left( \sum_{k=0}^{R\Delta - 1} z^{-k} \right)^M$$
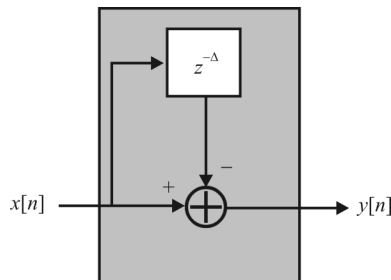


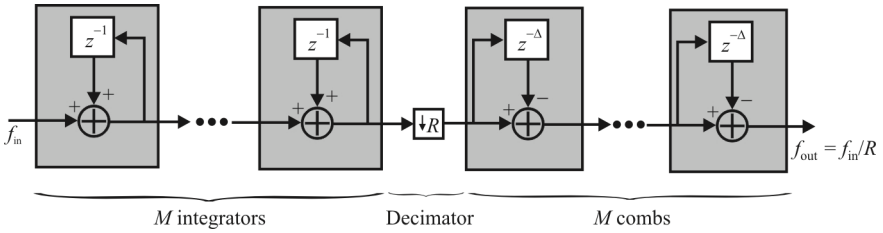**Figure 15.14** Basic comb.

**Figure 15.15** Decimating CIC.
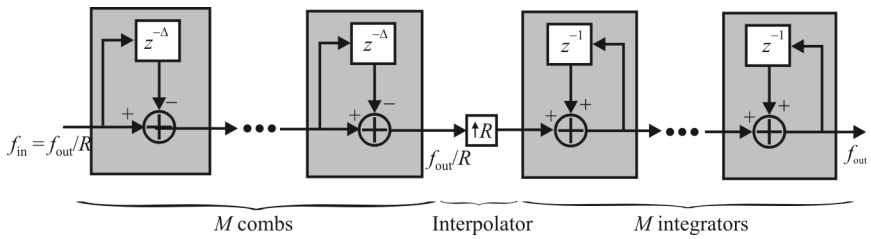


**Figure 15.16** Interpolating CIC.
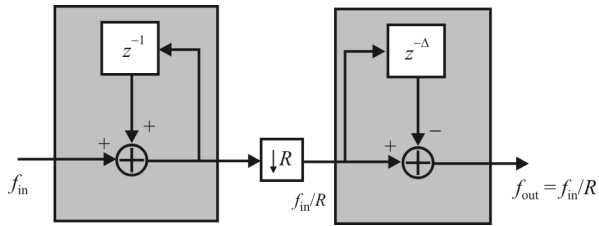
**Figure 15.17** First-order CIC.

which is the transfer function of a FIR filter and therefore stable.

> **Example 15.1:** Decimating first order CIC with integer decimation factor $R$. Implementation is as shown in Figure 15.17.

The concept of the CIC originated with the notion of a recursive running-sum filter, which is an efficient form of a non-recursive moving average filter. The moving average filter of length $N$ is illustrated in Figure 15.18. The output of this filter is given by

$$y[n] = \frac{1}{N}(x[n] + x[n-1] + \cdots + x[n-N+1])$$

while the transfer function is given by

$$H(z) = \frac{1}{N}\left(1 + z^{-1} + \cdots + z^{-(N-1)}\right) = \frac{1}{N}\underbrace{\sum_{k=0}^{N-1}z^{-k}}_{\text{geometric sum}} = \frac{1}{N}\frac{1-z^{-N}}{1-z^{-1}}$$
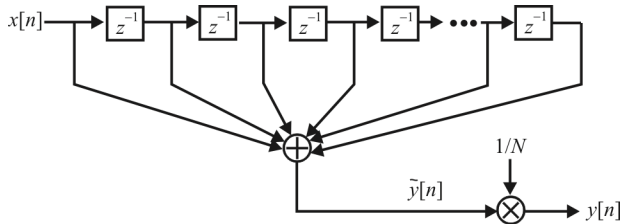


**Figure 15.18** Moving average filter. Note that the transfer function for this filter has all zeros (no poles).
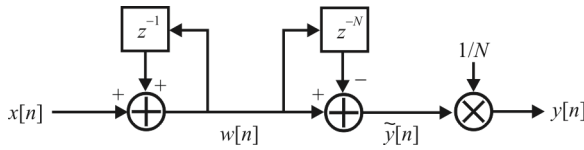
**Figure 15.19** Recursive running sum.

The recursive running sum

$$y[n] = y[n-1] + \frac{1}{N}(x[n] - x[n-N])$$

has the flow diagram shown in Figure 15.19. If we let

$$w[n] = z^{-1}w[n] + x[n]$$

then

$$y[n] = \frac{1}{N}\left(w[n] + x^{-N}w[n]\right)$$

The transfer function of the running sum is therefore

$$H(z) = \frac{1}{N}\frac{1-z^{-N}}{1-z^{-1}}$$

In many applications, the moving average filter is followed by decimation by $R = N$ as illustrated in Figure 15.20. In this case, the transfer function is given by

$$H(z) = \frac{1}{N}\frac{1-z^{-R\Delta}}{1-z^{-1}}$$



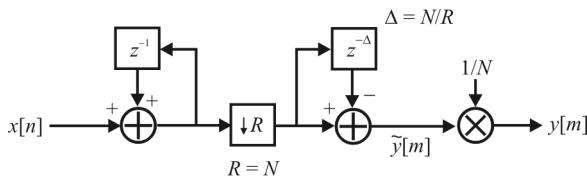**Figure 15.20** Moving average filter followed by decimation. Note that the transfer function for this filter has all zeros (no poles), which is a property of all moving average filters.

Compare this with the first order CIC whose transfer function is

$$H(z) = \frac{1 - z^{-R\Delta}}{1 - z^{-1}}$$

We can therefore see that the recursive running-sum filters have the same transfer function as a first-order CIC (except for the $1/N$ gain and general differential delay $\Delta$).

*CIC Properties*

The applications of CICs include anti-aliasing filtering prior to decimation. They are typically employed in applications that have a large excess sample rate. This is when the system sample rate is much larger than the bandwidth occupied by the signal (remember the example $f_{IF} = 40$ MHz, $f_s = 100$ MHz, and $W = 1$ MHz).

The frequency response of the CIC $H(z)$ can be evaluated at $z = e^{j\omega T_s} = e^{j2\pi f / f_s}$ as

$$\left| H(e^{j\omega T_s}) \right| = \left| \frac{\sin(\pi R \Delta f / f_s)}{\sin(\pi f / f_s)} \right|^M$$

The frequency response with respect to the output frequency $f_0 = f_s/R$ is

$$|H(f)| = \left| \frac{\sin(\pi \Delta f / f_0)}{\sin([\pi / R][f / f_0])} \right|^M$$

$\Delta$ determines the location of the zeros as

$$f = k f_0 / \Delta \qquad k \text{ integer}$$

*DC Gain.* The DC gain of the CIC is $(RD)^M$. This is because

$$\lim_{f \to 0} |H(f)| = (R\Delta)^M$$

*Frequency Response.* Examples of the frequency response of the CIC are shown in Figure 15.21. Note that the shape of the filter response changes very little as a function of the decimation ratio $R$.
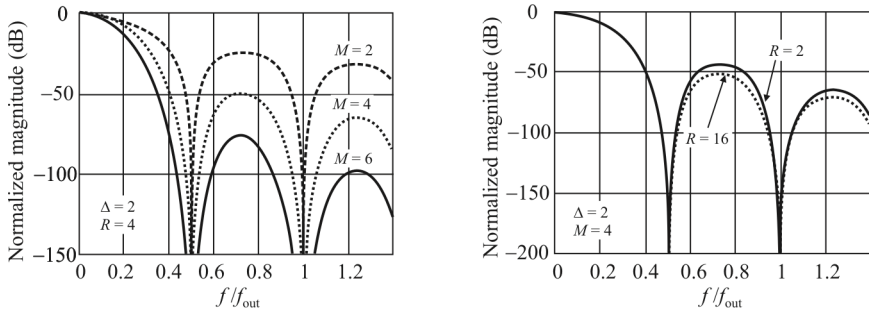
**Figure 15.21** CIC example frequency responses.

# 15.4 Polyphase Filter Banks

### 15.4.1 Introduction

The polyphase *N*-path filter bank [11] is an alternate implementation that performs the channelization as a single merged process, as shown in Figure 15.22. The polyphase filter bank partition offers a number of significant advantages relative to the set of individual downconversion receivers. The primary advantage is reduced cost due to major reduction in system resources required to perform the equivalent multichannel processing. This equates to reduced numbers of required computations for each frame that, in turn, equates, ceteris paribus, to fewer DSP engines required.

To illustrate the advantages of polyphase filters we make a comparison of the conventional mixer downconverter and the resampled polyphase downconverter. The input to either process can be real or complex. In the mixer downconverter in Figure 15.7, a separate mixer pair and filter pair is assigned to each channel of the



**Figure 15.22** Polyphase channelizer: resampler, all-pass partition, and FFT phase shifters.

channelizer, and these mixers must all operate at the high-input data rate, prior to downsampling. In the polyphase filter, there is only one lowpass filter required to service all the channels of the channelizer, and this single filter accommodates all the channels as co-occupying alias contributors of the baseband bandwidth. This means that all the processing performed in the polyphase channeliz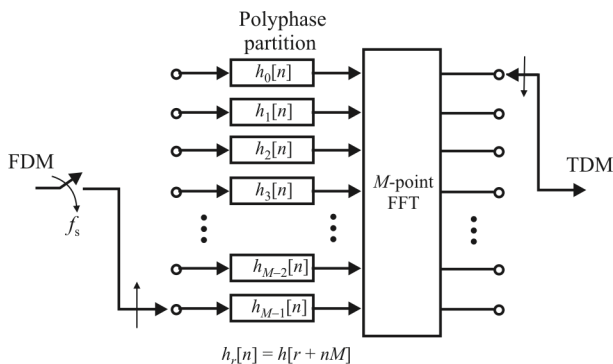er occurs at the low-output sample rate. When the input signal is real, there is another significant difference between the two processes. In the mixer downconverter, the signal is made complex by the input mixers as we enter the process, which means that the lowpass filtering task requires two filters, one for each of the quadrature components, while in the polyphase channelizer, the signal is made complex by the phase rotators as we leave the process; consequently, we require only one partitioned lowpass filter to process the real input signal.

The partitioned *M*-path filter performs the task of aligning the time origins of the offset sampled data sequences delivered by the input commutator to a single common output time origin. This is accomplished by the allpass characteristics of the *M*-path filter sections that apply the required differential time delay to the individual input time series. The DFT performs the equivalent of a beam-forming operation: the coherent summation of the time-aligned signals at each output port with selected phase profiles. The phase coherent summation of the outputs of the *M*-path filters separate the various aliases residing in each path by constructively summing the selected aliased frequency components located in each path while simultaneously destructively canceling the remaining aliased spectral components.

## 15.4.2 Polyphase Bandwidth, Spectral Spacing, and Output Sample Rates

We now address the interaction and coupling, or lack of them, between the parameters that define the polyphase filter bank [12]. The DFT performs the task of separating the channels after the polyphase filter so the transform size is locked to the number of channels. Also the filter bandwidth is determined by the weights of the lowpass prototype and this bandwidth and spectral shape are common to all the channels.

When a channelizer is used to separate adjacent communication channels, which are characterized by known center frequencies and known controlled nonoverlapping bandwidths, the channelizer must preserve separation of the channel outputs. Such is normally the case for EW receivers, where most target environment characteristics are generally known ahead of time. This characterization is developed with extensive *intelligence preparation of the battlefield* (IPB) that transpires continually. Inadequate adjacent channel separation can result in adjacent channel interference. Typical spectral responses for channel bandwidths corresponding to the communication EW scenario are shown in Figure 15.23.

The polyphase filter channelizer uses the input *M*-to-1 resampling to alias the spectral terms residing at multiples of the output sample rate to baseband. This
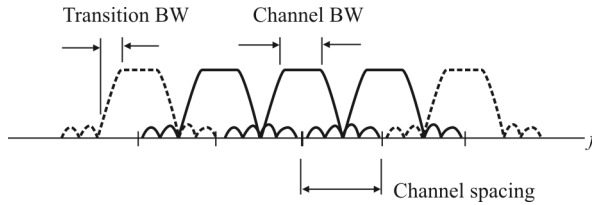
**Figure 15.23** Spectral characteristics of two channelizers with same channel spacing, one for spectral analysis and one for FDM channel separation.

means that, for the standard polyphase channelizer, the output sample rate is the same as the channel spacing. Operating at this rate satisfies the Nyquist criterion, permitting the separation of the channels with an output rate that avoids band-edge aliasing.

The conventional way we use the $M$-path polyphase filter bank is to deliver $M$-input samples to the $M$-paths and then compute outputs from each channel at the rate $f_s / M$. Increasing the output sample rate of the polyphase channel bank by a factor of two makes subsequent interpolation tasks less expensive since the spectra of the output signals would already be oversampled by a factor of two with increased spectral separation. Operation in this mode would also permit channelization of overlapped channels without aliasing of the spectral transition bands. The alias-free partition is handy in applications requiring perfect reconstruction of the original time series from spectrally partitioned subchannels, a requirement sometimes imposed in receivers used for EW applications. A polyphase filter bank can be operated with an output sample rate of any rational ratio times the input sample rate. With minor modifications, the filter can be operated with totally arbitrary ratios between input and output sample rates. This is true for the sample rate reduction imbedded in a polyphase receiver.

## 15.4.3 Computational Complexity

In this section we compare the computational workload required to implement a channelizer as a bank of conventional downconverters with that required to implement the polyphase filter approach. We assume a 50-channel channelizer to supply actual numbers. We first determine the length of the FIR prototype filter required to satisfy the filter specifications. We note that the filter designed to operate at an input rate of 15.288 MHz has its specifications controlled by its output rate of 256 kHz. This is because the filter must satisfy the Nyquist sampling criterion after spectral folding as a result of the downsampling operation. The length of any FIR filter is controlled by the ratio of input sample rate to filter transition bandwidth and the required out-of-band attenuation, as well as level of in-band ripple. The specifications of the filter used here are shown in Figure 15.24.
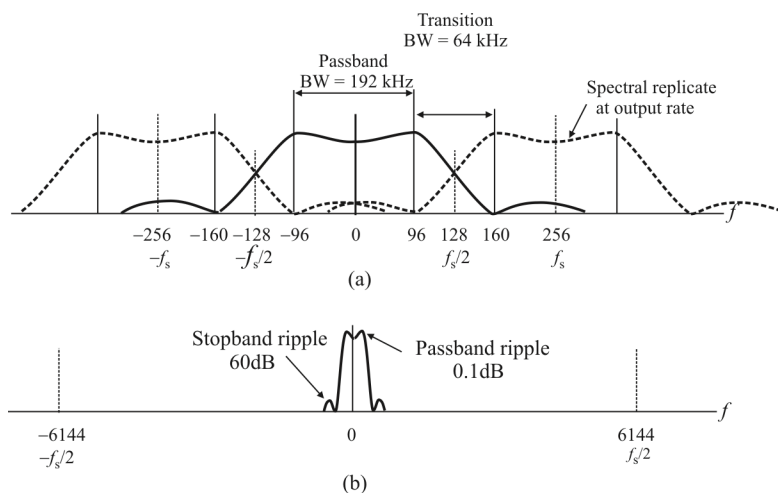
**Figure 15.24** Spectral characteristics of prototype filter at output and input sample rates: (a) filter spectrum at output sample rate (256 kHz), and (b) filter spectrum at input sample rate (12,288 MHz).

Standard design rules determine the filter length from the filter specification, and for those indicated in Figure 15.24, the filter length was found to be 512 samples and the Remez algorithm [13, 14] was used to supply the filter impulse response.

An important consideration and perspective for filters that have different input and output sample rates is the ratio of filter length (with units of operations/output) to resample ratio (with units of inputs/outputs) to obtain the filter workload (with units of operations/inputs). A useful comparison of two processes is the number of multiplies and adds per input point. We count a multiply and add with their requisite data and coefficient fetch cycles as a single processor operation and use the shorthand notation of ops per input (see Figure 10.5 for an example of a DSP that performs these operations).

A single channel of a standard downconverter channelizer requires one complex multiply per input point for the input heterodyne and computes one complex output from the pair of 512 tap filters after collecting 48 inputs from the heterodyne. The four real ops per input for the mixer and the two (512/48) ops per input for the filter result in a per channel workload of 26 ops per input, which occur at the input sample rate. The polyphase version of the downconverter collects 48 input samples from the input commutator, performs 1024 ops in the pair of 512 tap filters, and then performs a 64-point FFT with its upper bound workload of real ops. The total workload of 1024 ops for the filter and 768 ops for the FFT results in 1792 ops performed once per 48 inputs for an input workload of 38 real ops/input. The higher workload per input is the consequence of forming 64 output channels in the FFT but preserving only 50 of them.

The workload per input sample for the standard  channelizer was found to be 26 ops and, for the polyphase channelizer, was found to be 38 ops. However, the polyphase 38 ops per input built all 50 channels, and the standard downconverter's 26 ops per input built only one channel and had to be repeated 50 times.

When we compare hardware resources, we observe that the standard channelizer must build and apply 50 complex sinusoids as input heterodynes to the input data at the high input sample rate and further must store the 50 sets of downconverted data for the filtering operations. On the other hand, the polyphase filter bank only stores one set of input data because the complex phase rotators are applied after the filter rather than before and the phase rotators are applied at the filter output rate, as opposed to the filter input rate.

When the FDM signal is a collection of independent signals, as is the normal case confronting an EW receiving system, the many signals do not share a common time reference or a common carrier frequency reference. The channels likely differ in small carrier and timing offsets that must be resolved in subsequent processing. For this situation it is appropriate for the channelizer to only perform the standard downconversion, bandwidth reduction, and sample rate reduction. For this application, the filter passes the selected channel bandwidths without further spectral modification.

# 15.5 Concluding Remarks

Extracting narrowband signals from wideband signals is the subject of this chapter. Wideband EW receivers often must process many signals at a time, and these signals are typically narrowband so it is important to have efficient ways to address this problem.

Digital receivers were considered in this chapter. The conventional receiver, where the digitization is at baseband; the IF-digitized receiver, where the IF signal is digitized, and the RF-digitized receiver, where the digitization is in the RF front-end stage, were the types of receivers included.

We then discussed the two forms of the DDC: the cascaded integrator comb (CIC), where the decimation factor $R \geq 32$ and the multirate FIR filter where $R < 32$.

Finally we presented the fundamental ideas surrounding polyphase filter banks and how they can be used to extract narrowband signals from wideband signals.

# Appendix 15.A Direct Digital Synthesis

*Direct digital synthesis* (DDS) is accomplished with NCOs. The output of the NCO, instead of being used directly in the digital domain, is converted into the analog domain as illustrated in Figure 15.A.1.

The DDS produces an analog waveform by generating a time-varying signal in digital form. The size of the LUT (that accomplishes the phase-to-amplitude conversion) is determined by:

- The number of table entries
- The bit width of entries (which determines the amplitude output resolution)

The output frequency is given by

$$f_{out} = M\,\frac{f_{clk}}{2^N}$$

where $M$ is the tuning word and $N$ is the length in bits of the phase accumulator. For example, if $N = 32$ bits, and $f_s = 50$ MHz, then $\Delta f = 12$ mHz. This generates $2N$ 8-bit entries, which is 4 GByte entries in the LUT.

## 15.A.1 Phase Truncation

In order to save memory in the LUT table, we can truncate the phase before the lookup table. For example, when $N = 32$ bits, we need only keep the uppermost 12 bits and truncate the lower 20 bits. The implications of this are that phase errors are introduced that are periodic in time, and amplitude errors occur due to phase-to-amplitude conversion. These are phase truncation spurs as illustrated in Figure 15.A.2. With the cost of large memories rapidly falling, using such measures to save memory space is probably not required, however.
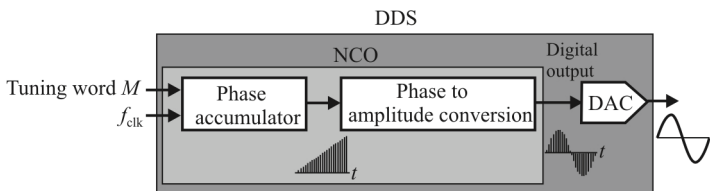


**Figure 15.A.1** DDS.
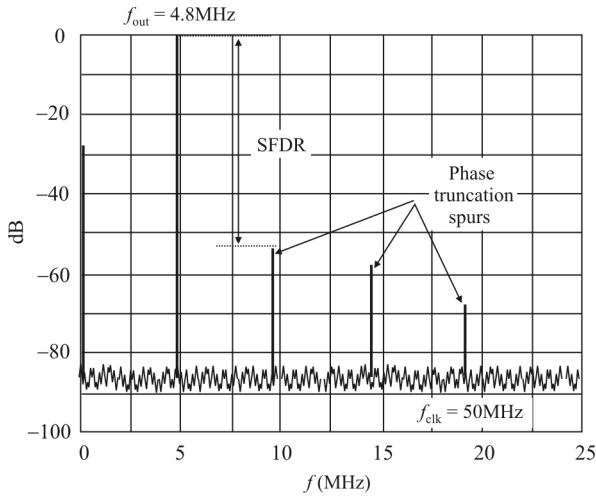
**Figure 15.A.2** Phase truncation spurs.

To deal with these problems, we can use output precompensation, which is a sin x/x rolloff response due to DAC output spectrum that is quite significant. The DAC output is precompensated with the inverse sinc filter (Figure 15.A.3).

## 15.A.2 Direct Digital Synthesis

DDS is a powerful technique used in the generation of RF signals. The technique has become far more widespread in recent years with the advances being made in
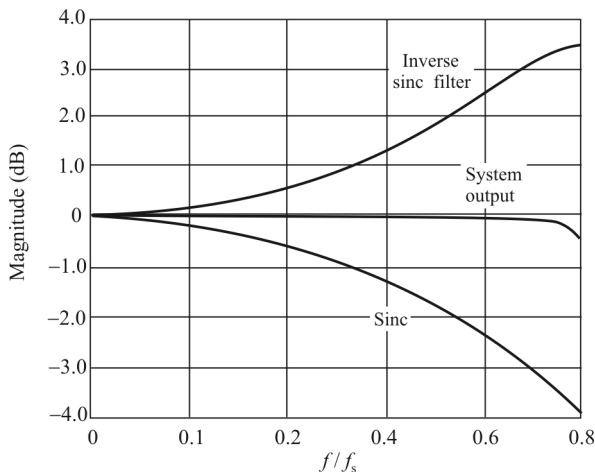


**Figure 15.A.3** Inverse sinc filter response.
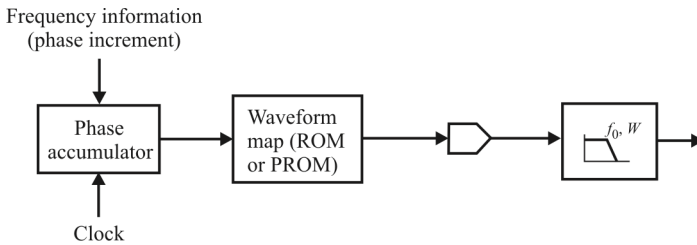
**Figure 15.A.4** Block diagram of a basic DDS.

integrated circuit technology that allow much faster speeds to be handled that in turn enable higher frequency DDS chips.

A block diagram of a DDS architecture is shown in Figure 15.A.4. The phase accumulator is just a counter, incremented each clock pulse by one. That phase accumulator provides the address to the waveform (sine wave) samples stored in *read only memory* (ROM) or *programmable read only memory* (PROM). The resulting digital word is converted into analog form in the DAC, the signal from which is lowpass filtered to form the DDS output.

Although often used on its own, DDS is often used in conjunction with indirect or phase locked loop synthesizer loops. By combining both technologies, it is possible to take advantage of the best aspects of each.

A DDS operates by storing the points of a waveform in digital format and then recalling them to generate the waveform. The rate at which the synthesizer completes one cycle then determines the frequency. The overall block diagram is shown in Figure 15.A.4.

The operation can be envisaged by looking at the way that phase progresses over the course of one cycle of the waveform. This can be envisioned as the phase progressing around a circle. As the phase advances around the circle, this corresponds to advances in the waveform.

The synthesizer operates by storing various points in the waveform in digital form and then recalling them to generate the waveform. Its operation can be
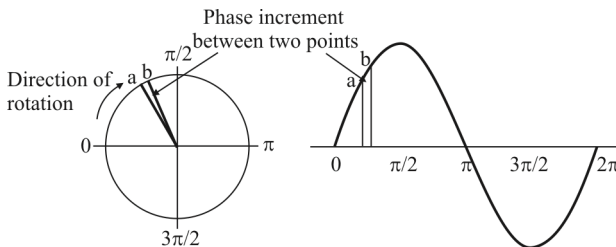


**Figure 15.A.5** Operation of the phase accumulator in a DDS.

explained in more detail by considering the phase advances around a circle as shown in Figure 15.A.5. As the phase advances around the circle, it corresponds to advances in the waveform—that is, the greater the number corresponding to the phase, the greater the point is along the waveform. By successively advancing the number corresponding to the phase, it is possible to move farther along the waveform cycle.

The digital number representing the phase is held in the phase accumulator. The number held here corresponds to the phase and is increased at regular intervals. In this way, it can be seen that the phase accumulator is basically a form of counter. When it is clocked, it adds a preset number to the one already held. When it fills up, it resets and starts counting from zero again.

Once the phase has been determined, it is necessary to convert it into a digital representation of the waveform. This is accomplished using a waveform map. This is a memory that stores a number corresponding to the voltage required for each value of phase on the waveform. In most cases the memory is either a ROM or PROM. This contains a vast number of points on the waveform, very many more than are accessed each cycle. A large number of points are required so that the phase accumulator can increment by a certain number of points to set the required frequency.

The next stage in the process is to convert the digital numbers coming from the sine LUT into an analog voltage. This is achieved using a DAC. This signal is filtered to remove any unwanted signals and amplified to give the required level as necessary.

Tuning is accomplished by increasing or decreasing the size of the step or phase increment between sample points. A larger increment at each update to the phase accumulator will mean that the phase reaches the full cycle value faster and the frequency is correspondingly high. Smaller increments to the phase accumulator value means that it takes longer to increase the full cycle value and a correspondingly low value of frequency. In this way it is possible to control the frequency. It can also be seen that frequency changes can be made instantly by simply changing the increment value. There is no settling time as in the case of phase-locked loop-based synthesizer.

From this it can be seen that there is a finite difference between one frequency and the next and that the minimum frequency difference or frequency resolution is determined by the total number of points available in the phase accumulator. A 24-bit phase accumulator provides just over 16 million points and gives a frequency resolution of about 0.25 Hz when used with a 5 MHz clock. This is more than adequate for most purposes.

These synthesizers do have some disadvantages. There are a number of spurious signals that are generated by a DDS. The most important of these are the alias signals. Here images of the signal are generated on either side of the clock frequency and its multiples. For example if the required signal had a frequency of 3 MHz and the clock were at 10 MHz, then alias signals would appear at 7 MHz

and 13 MHz as well as 17 MHz and 23 MHz, etc. These can be removed by a lowpass filter. Also, some low-level spurious signals are produced close to the required signal. These are normally acceptable in level, although for some applications they can cause problems.

# References

[1]     Vaidyanathan, P. P., *Multirate Systems and Filter Banks*, Upper Saddle River, NJ: Prentice Hall, 1993.

[2]     Vaidyanathan, P. P., "Multirate Digital Filters, Filter Banks, Polyphase Networks, and Applications: A Tutorial," *Proceedings of the IEEE*, Vol. 78, No. 1, January 1990, pp. 56–93.

[3]     Scheuermann, H., and H. Gockler, "A Comprehensive Survey of Digital Transmultiplexing Methods," *Proceedings of the IEEE*, Vol. 69, No. 11, November 1981, pp. 1219–1250.

[4]     Harris, F. J., C. Dick, and M. Rice, "Digital Receivers and Transmitters Using Polyphase for Wireless Communications," *IEEE Transactions on Microwave Theory and Techniques*, Vol. 51, No. 4, April 2003, pp. 1395–1412.

[5]     Harris, F. J., "On Measuring the Gain and Phase Imbalance and DC Offsets of Quadrature A-to-D Converters with an Adaptive Canceling Filter," *Proceedings 21st Annual Asilomar Conference on Signals, Systems, and Computers*, Pacific Grove, CA, November 2–4, 1987.

[6]     Mitra, S. K., *Digital Signal Processing: A Computer Based Approach*, 2nd Ed., New York: McGraw-Hill, 2001.

[7]     Sklar, B., *Digital Communications: Fundamentals and Applications*, 2nd Ed., Englewood Cliffs, NJ: Prentice-Hall, 2002, Sec. 15.2.

[8]     Proakis, J. G., and D. G. Manolokis, *Digital Signal Processing: Principles, Algorithms, and Applications*, 3rd Ed., Upper Saddle River, NJ: Prentice-Hall, 1996, Sec. 1.4.

[9]     Steinbrecher, D., "Broadband High Dynamic Range ADC Conversion Limitations," *Proceedings Analogue to Digital and Digital to Analogue Conversion International Conference*, Swansea, U.K., September 17–19, 1991.

[10]    "Defining and Testing Dynamic Parameters in High Speed ADC: Part I and Part II," *MAXIM Application Notes.* Available at: http://www.maxim-ic.com/appnotes.cfm/appnote_number/728, February 2001, and http://www.maxim-ic.com/appnotes.cfm/appnote_number/729, January 2001.

[11]    Ribey, M., "Exploration of Transmultiplexers in Telecommunication Networks," *IEEE Transactions on Communications*, Vol. COM-30, July 1982, pp. 1293–1297.

[12]    Harris, F. J., and C. Dick, "Performing Simultaneous Arbitrary Spectral Translation and Sample Rate Change in Polyphase Interpolating and Decimating Filters in Transmitters and Receivers," *Proceedings Software Defined Radio Technical Conference*, San Diego, CA, November 11–12, 2002.

[13]    *Signal Processing Techniques*, Annaheim, CA: Interstate Electronics Corporation, 1979, Appendix J.

[14]    Parks, T. W., and C. S. Burrus, *Digital Filter Design*, New York: Wiley, 1987, pp. 89–94.

# Chapter 16

## Spread Spectrum Techniques

### 16.1 Introduction

Many of the modern communication systems that are potential threats to be addressed by EW systems employ *spread spectrum* (SS) technology, so we provide a brief introduction to the subject in this chapter. The next three chapters are devoted to discussions of receivers for each of the varieties of SS in detail. A summary of the SS technology is provided here [1–5].

SS is employed to accomplish various levels of security. The most basic reason is for *low probability of detection* (LPD). This is attempting to avoid identifying the presence of the signal at all, trying to remain unnoticed by opposing forces' attempts at detection of signals. The next level up is *low probability of intercept* (LPI). LPI yields to allowing for detection of the presence of a signal but, when detected, minimizing the likelihood of being able to intercept the signal. Last is *low probability of exploitation* (LPE), where, again, yielding to the intercept of signals, the probability of exploitation of the signal is minimized.

Another facet of SS technology not belonging to the family of interception of signal is *anti-jamming* (AJ). SS signals occupy considerably larger bandwidths than would otherwise be required of the information bearing signals. This spreading is for the purpose of requiring any *electronic attack* (EA) attempts against the signal to occupy large bandwidths as well, which spreads jamming energy over broad segments of the spectrum. As we will demonstrate, narrowband jamming of SS signals is largely ineffective due to the decorrelation process at SS receivers. On the other hand, spreading jammer energy over broad bandwidths reduces the amount of jamming power in any single channel, increasing the likelihood of the signal to punch through any jamming attempts.

For the reader interested in more in-depth discussion of these technologies, [6] is recommended.

The two principal SS technologies are *direct sequence SS* (DSSS) and *frequency hopped SS* (FHSS). We will introduce these techniques in this chapter.

A third technique is *time-hopped SS* (THSS) that is not as prolific as the first two. We introduce this method as well. Current embodiments of THSS are actually a hybrid of techniques, employing DSSS along with the randomness of transmission times.

Combinations of DSSS and FHSS are also possible, where the word *hybrid* is used to describe the methods. While hybrids take advantage of the benefits of both of the underlying SS techniques, implementation is often quite complex, so it has not been as popular as DSSS and FHSS alone.

SS technologies were developed by the military in the latter part of the 20th century for the purposes discussed above (LPD, LPI, LPE, and AJ). DSSS has become very popular for non-military applications of wireless communications due to some of its beneficial properties for spectrum sharing. The frequency spectrum is a limited resource, and economic commercial use requires that the spectrum utilization be optimized. The principle used here is referred to as CDMA, whereas in DSSS (it also applies to a lesser extent in FHSS) the same spectrum is used by multiple users at the same time. The signals are separated by the use of unique codes for each user of the spectrum. Properly equipped receivers can respond to these unique codes to separate the signals at the receivers. We examine the key differentiators between FHSS and DSSS implementations.

# 16.2 Review of Direct Sequence Spread Spectrum

SS transmissions have been in practical use since the 1950s. They found many applications in military systems due to their suitability for covert message transmission and resistance to jamming [7]. In the early 1980s, SS technology was proposed for private and commercial use, especially in CDMA transmissions. The CDMA system has been adopted for use in commercially available WLANs [8]. Another useful feature of CDMA for indoor systems is its low power spectral density. This allows a CDMA system to coexist with licensed communications systems in environments where low levels of electromagnetic interference are desirable, such as hospital. In such environments, CDMA is ideally suited to high data rates being transmitted over hostile fading channels with the minimum of interference to sensitive equipment [9].

DSSS is a transmission technique in which a pseudo-random sequence or PN code [10], independent of the information data, is employed as a modulation waveform to spread the signal energy over a bandwidth much greater than the information signal bandwidth [11]. In practical systems, the bandwidth expansion factor, which is the ratio between the chip rate $f_c$ and the data symbol rate $f_s$, is usually an integer. The amplitude, and thus the power in the SS signal, is the same as in the information signal. Due to the increased bandwidth of the SS signal, the psd must be lower and can then be below the noise level [12]. Furthermore, the autocorrelation of a PN code has properties similar to those of white noise, so the
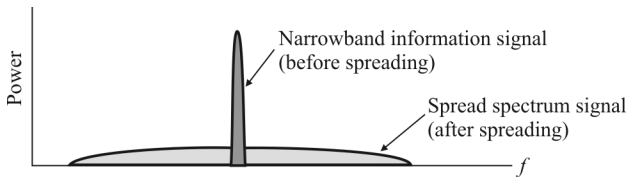
**Figure 16.1** DSSS spreading.

SS signal looks like a white noise, and hence is very difficult to intercept. At the receiver, the signal is despread using a synchronized replica of the PN sequence used at the transmitter. The optimum multiple-user CDMA receiver is based on a correlator, or a bank of sequence matched filters, each followed by *maximum likelihood sequence estimation* (MLSE) detectors. The objective of the MLSE is to find the input sequence that maximizes the conditional probability or likelihood of the given output sequence [13].

In the context of spectrum surveillance, the PN sequence used by the transmitter is unknown, as well as other transmitter parameters such as duration of the sequence, symbol frequency, and carrier frequency. Moreover, the longer the period of the PN code is, the closer the transmitted signal will be to a truly random binary wave and the harder it is to detect [14].

## 16.2.1 Fundamentals of DSSS Operation

DSSS uses wideband, noise-like signals that are hard to detect, intercept, or demodulate. Additionally, SS signals are harder to jam (interfere with) than narrowband signals. These LPI and AJ features are why the military has used SS for so many years. SS signals are intentionally made to be a much wider band than the information they are carrying to make them more noise-like.

SS transmitters use similar transmit power levels to narrowband transmitters. Because SS signals are so wide, they transmit at a much lower spectral power density, measured in watts per hertz, than narrowband transmitters. This lower transmitted power density characteristic gives SS signals a big plus. SS and narrowband signals can occupy the same band, with little or no interference. This capability is the main reason for all the interest in SS today.

The use of special PN codes in SS communications makes signals appear wideband and noise-like. It is this very characteristic that makes SS signals possess LPI. SS signals are hard to detect on narrowband equipment because the signal's energy is spread over a bandwidth of maybe 100 times the information bandwidth (Figure 16.1). The width of the main lobe in Figure 16.2 is given by $2R_c$, where $R_c$ is the bit rate of the code sequence used by the transmitter.

Multiplication of the lower rate information signal by a higher rate code bit sequence has the effect of broadening the spectrum occupied by the signal. This spreading lowers the signal energy in any single RF channel. In some cases the
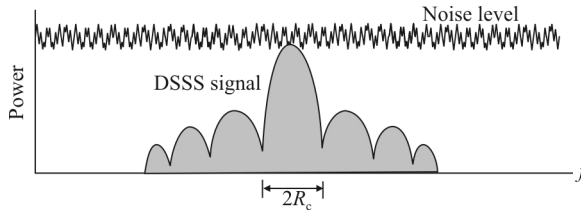
**Figure 16.2** DSSS signal below the noise floor.

magnitude of the spread signal is below the noise as illustrated in Figure 16.2. The resulting signal has a noise-like characteristic that makes it difficult to detect and demodulate unless the spreading code is known. Knowledge of the spreading code allows decorrelation at the receiver, which removes the code and recovers the information signal.

The spread of energy over a wideband, or lower psd, also makes SS signals less likely to interfere with narrowband communications. Narrowband communications, conversely, cause little to no interference to SS systems because the correlation receiver effectively integrates over a very wide bandwidth to recover an SS signal. The correlator then spreads out a narrowband interferer over the receiver's total detection bandwidth (Figure 16.3).

The total integrated signal density or SNR at the correlator's input determines whether there will be interference or not. All SS systems have a threshold or tolerance level of interference beyond which useful communication ceases. This tolerance or threshold is related to the SS processing gain, which is essentially the ratio of the RF bandwidth to the information bandwidth.

The carrier of the DSSS radio stays at a fixed frequency. Narrowband information is spread out into a much larger (at least 10 times) bandwidth by using a PN chip sequence. The generation of the DSSS (spreading) is shown in Figure 16.3.

In Figure 16.3, the narrowband signal and the SS signal both use the same amount of transmit power and carry the same information. However, the power density of the SS signal is much lower than the narrowband signal. As a result, it is more difficult to detect the presence of the SS signal. The power density is the amount of power over a certain frequency range. In the case of Figure 16.3, the narrowband signal's power density is 10 times higher than the SS signal, assuming the spread ratio is 10.

At the receiving end of a direct-sequence system, the SS signal is despread to generate the original narrowband signal. Figure 16.4 shows the despreading process. If there is an interference jammer in the same band, it will be spread out during the despreading. As a result, the jammer's impact is greatly reduced. This is

**Figure 16.3** Narrowband despreading: (a) before despreading, and (b) after despreading. Despreading decorrelates the narrowband signal and spreads the energy out over a wide spectrum while collapsing the SOI to the original narrowband signal.
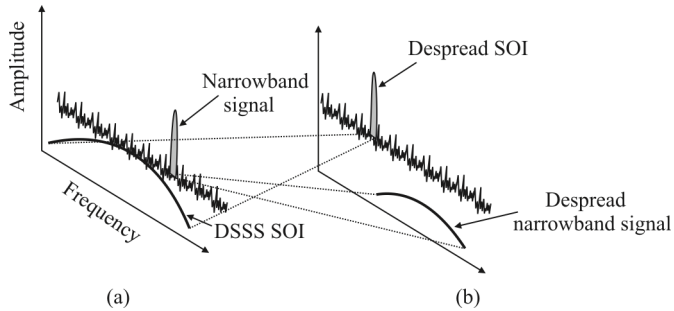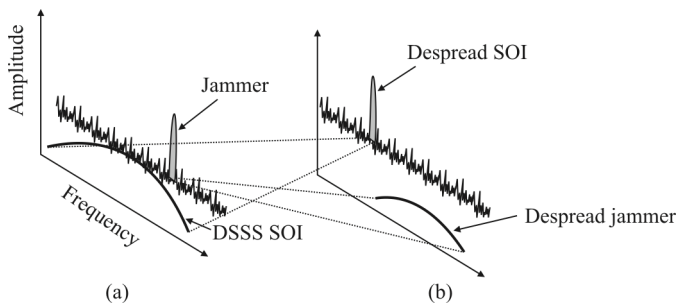


**Figure 16.4** Jammer spreading: (a) before despreading, and (b) after despreading. Despreading decorrelates the narrowband jammer and spreads the energy out over a wide spectrum while collapsing the SOI to the original narrowband signal. Direct-sequence systems combat noise problems by spreading jammers across a wide band as shown in this figure.
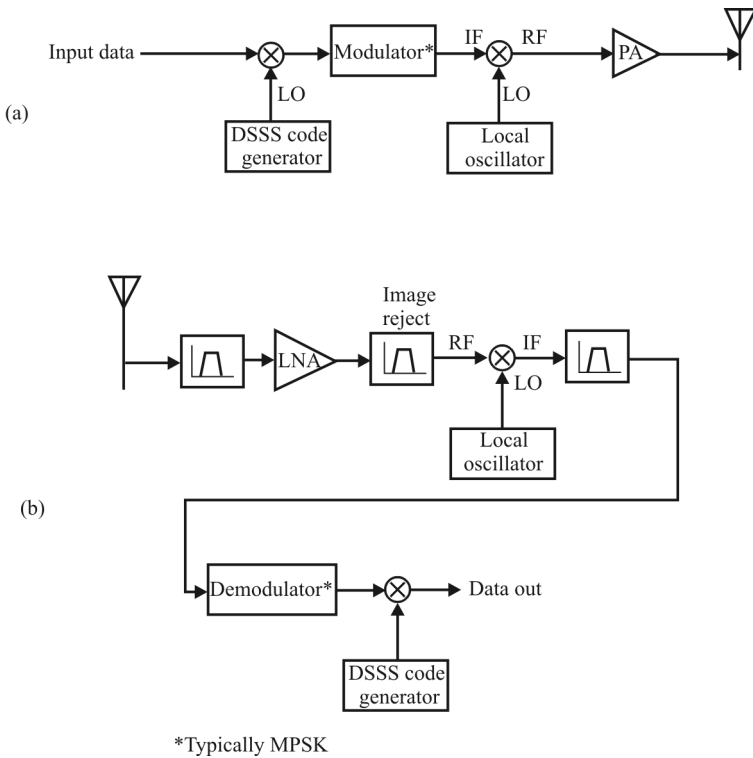
**Figure 16.5** DSSS system: (a) transmitter, and (b) receiver.

the way that the DSSS radio fights the interference. It spreads out the offending jammer by the spreading factor (Figure 16.4). Since the spreading factor is at least a factor of 10, the offending jammer's amplitude is greatly reduced by at least 90%.

When the narrowband signal is a jammer, the same decorrelation effect occurs at the receiver (Figure 16.4). This makes narrowband jamming attempts at DSSS signals largely ineffective. Broader bandwidth jammer signals are required for DSSS EA, and, as mentioned, this places less power at any individual channel increasing the probability of successful jamming punchthrough.

A simplified flow diagram of a DSSS communication system is illustrated in Figure 16.5. The information signal (assumed to be digital, as they usually are) is multiplied by the code bit sequence, which has a much higher bit rate. This sequence is then modulated by some scheme (discussed next). The resulting modulated baseband signal is then modulated onto a fixed carrier for transmission. At the receiver the signal is lowered in frequency to baseband and then demodulated. The demodulated bit stream is then multiplied by the same code

sequence that was applied at the transmitter (implying synchronization requirements between the transmitter and receiver). This multiplication (actually an exclusive OR operation) removes the code sequence yielding the information signal, which is then made available for further processing at the receiver.

## 16.2.2 Modulation and Demodulation

For DSSS systems the encoding signal is used to modulate a carrier, usually by phase-shift keying (PSK; bi-phase or quad-phase) at the code rate. FHSS systems generate their wideband by transmitting at different frequencies, hopping from one frequency to another according to the code sequence. Typically such a system may have a few thousand frequencies to choose from, and unlike direct sequence signals, it has only one output rather than symmetrically distributed outputs.

It's important to note that both DSSS and FHSS systems generate wideband signals controlled by the code sequence generator. For one the code is the direct carrier modulation (direct sequence) and the other commands the carrier frequency (frequency hopping).

There are several different modulation techniques that can be employed when developing FHSS or DSSS systems. Information modulation can be accomplished using amplitude (AM) or frequency modulation (FM) techniques. AM is normally used because it tends to be detectable when examining the spectrum. FM is more useful because it is a constant-envelope signal, but information is still readily observed. In both AM and FM, no knowledge of the code is needed to receive the transmitted information.

In DSSS, balance modulation can be used in any suppressed carrier system used to generate the transmitted signal. Balanced modulation helps to hide the signal, and there is no power wasted in transmitting a carrier that would contribute to interference rejection or information transfer. When a signal has poor balance in either code or carrier, spikes are seen in its spectrum. With these spikes, or spurs, the signal is easily detectable, since these spikes are noticed above the noise and thus provide a path for detecting the hidden signal.

Once the signal is coded, modulated, and then sent, the receiver must demodulate the signal. This is usually done in two steps. The first step entails removing the spectrum-spreading modulation. Then, the remaining information-bearing signal is demodulated by multiplying with a local reference identical in structure and synchronized with the received signal.

## 16.2.3 Coding Techniques

In order to transmit anything, codes used for data transmission have to be considered. However, this section will not discuss the coding of information (like error correction coding) but those that act as noise-like carriers for the information

being transferred. These codes are of much greater length than those for the usual areas of data transfer, since it is intended for bandwidth spreading.

Codes in an SS system are used for

- Protection against interference: Coding enables a bandwidth trade for processing gain against interfering signals.
- Provision for privacy: Coding enables protection of signals from eavesdropping, so that even the code is secure.
- Noise-effect reduction: Error-detection and -correction codes can reduce the effects of noise and interference.

Maximal sequencing is one of the more popular coding methods in an SS system. Maximal codes can be generated by a given shift register or a delay element of given length. In binary shift register sequence generators, the maximum length sequence is $2^n - 1$ chips, where $n$ is the number of stages in the shift register. The codes used for DSSS should be as orthogonal as possible. Theoretically, only infinitely long codes are truly orthogonal. The codes used in DSSS systems are usually truncated, so the code words are only approximately orthogonal.

A shift register generator consists of a shift register in conjunction with the appropriate logic, which feeds back a logical combination of the state of two or more of its stages to its input. The output, and the contents of its $n$ stages at any clock time, is its function of the outputs of the stages fed back at the proceeding sample time. Some maximal codes can be of length 7 to $2^{36} - 1$ chips or longer.

In DSSS, *error detection and correction codes* (EDACs) may not be advisable because of the effect they have on the code, increasing the apparent data transmission rate, and may increase the jamming threshold. Some demodulators can operate detecting errors at approximately the same accuracy as an EDAC, so it may not be worthwhile to include a complex coding/decoding scheme in the system.

### 16.2.4 Near-Far Problem

One issue with DSSS systems is known as the near-far problem. Since DSSS signals in general are quite weak, a receiver attempting reception of these signals must have a high sensitivity. Close-in, strong signals can overpower such receivers if adequate measures are not taken to preclude it. This indicates how susceptible DSSS systems can be to EA countermeasures (jamming) with narrowband jammers.

Modern 3G+ cellular systems that are based on CDMA principles deal with this problem by implementing power control over the mobile units. The base stations monitor the power level of signals they are receiving and adjust the transmit power of the mobiles continuously (a thousand times per second).
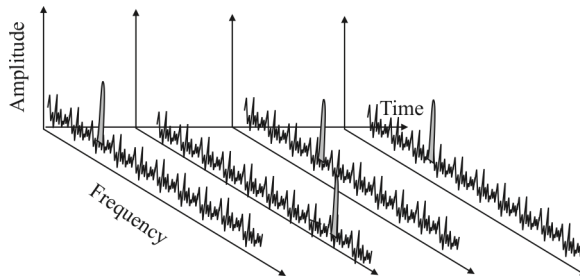
**Figure 16.6** Frequency hopping.

# 16.3 Review of Frequency Hopping Spread Spectrum

### 16.3.1 FHSS Operation

FHSS systems achieve similar results provided by direct-sequence systems by using different carrier frequency at different times. The frequency hopped system's carrier randomly hops to channels within the band to avoid a jammer as much as possible. The fewer the number of channels covered by the jammer, the better the countermeasure technique works.

A frequency hopped signal is shown in Figure 16.6. The frequency-hopping technique does not spread the signal. As a result, there is no processing gain in the same sense as DSSS. The processing gain is the increase in power density when the signal is despread and it will improve the received signal's SNR. In other words, the frequency hopper needs to put out more power in order to have the same SNR as a direct-sequence radio.

The effects of a narrowband interfering signal, jammer or otherwise, is illustrated in Figure 16.7. We can see that there is no effect on either signal caused by the other as long as the hopping signal avoids the channel occupied by the interfering signal. If overlap occurs, then both signals are affected. If the interferer is a jamming signal, jamming will only be effective when this overlap occurs, yielding narrowband jamming attempts to be ineffective for the most part. In such scenarios, jammers typically employ some form of broadband jamming. Broadband jamming may be total band jamming (*broadband noise*, BBN), where the entire communication band is jammed simultaneously, yielding very low jamming energy per channel. They can also employ *partial band noise* (PBN), jamming where a portion or portions of the spectrum are jammed, increasing the probability of the hopping signal entering the jammed portion. *Multitone* (MT) jamming is another technique employed, where the effects are similar to PBN jamming.

The frequency hopper is more difficult to synchronize than DSSS. In these architectures, the receiver and the transmitter must be synchronized in time and
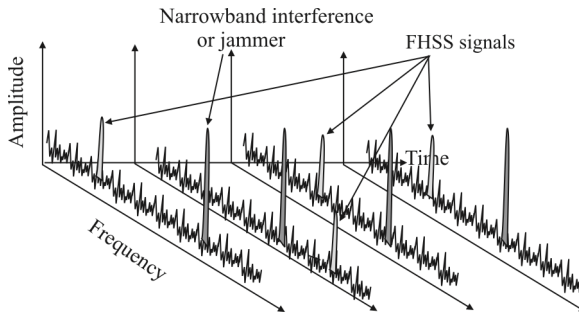
**Figure 16.7** FHSS with narrowband interference.

frequency in order to ensure proper transmission and reception of signals. In a direct-sequence radio, on the other hand, only the timing of the chips needs to be synchronized.

The frequency hopper also needs more time to search the signal and lock to it. As a result, the latency time is usually longer. A direct-sequence radio can lock in the chip sequence in just a few bits.

To make the initial synchronization possible, the frequency hopper will typically park at a fixed frequency before hopping or communication begins. If the jammer happens to locate at the same frequency as the parking frequency, the hopper will not be able to hop at all. And once it hops, it will be very difficult, if not impossible, to re-synchronize if the receiver ever loses the sync.

The frequency hopper, however, is better than the direct-sequence radio when dealing with multipath. The hopper does not stay at the same frequency and a null at one frequency is usually not a null at another frequency if it is not too close to the original frequency. So a hopper can usually deal with multipath fading issues (the fading creates the nulls at the receiver) better than direct-sequence radio.

The hopper itself, however, could suffer performance problems if it interferes with another radio. In these scenarios, the system that survives depends on which can suffer more data loss. In general, a voice system can survive an error rate as high as $10^{-2}$ while a data system must have an error rate better than $10^{-4}$. (These error rates are highly dependent on the type and amount of EDAC used.) Voice systems can tolerate more data loss because the human brain can guess between the words while a dumb processor can't.

Figure 16.8 shows simplified flow diagrams of a typical frequency hopped transmitter and receiver. In the transmitter, a pseudo-random hopping code is used to control the output frequency of a PLL-based synthesizer. The carrier is then modulated with a data signal and transmitted. An example of a hopping signal (frequency versus time) is shown in Figure 16.9. In the receiver, an identical copy of the hopping pattern plus an IF-offset is subtracted from the incoming signal in
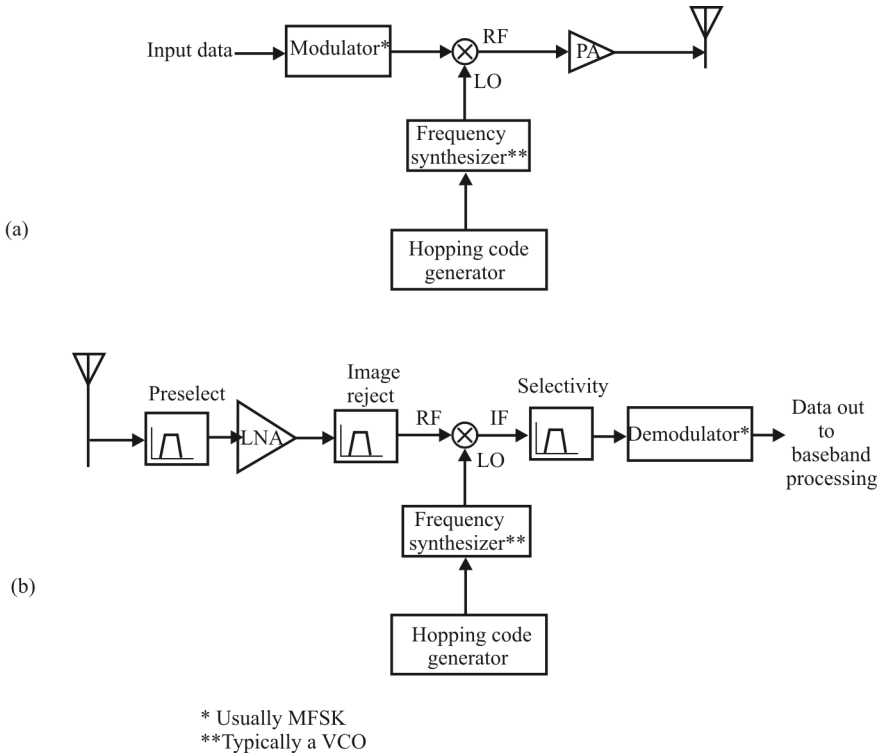
(a)

(b)

* Usually MFSK
**Typically a VCO

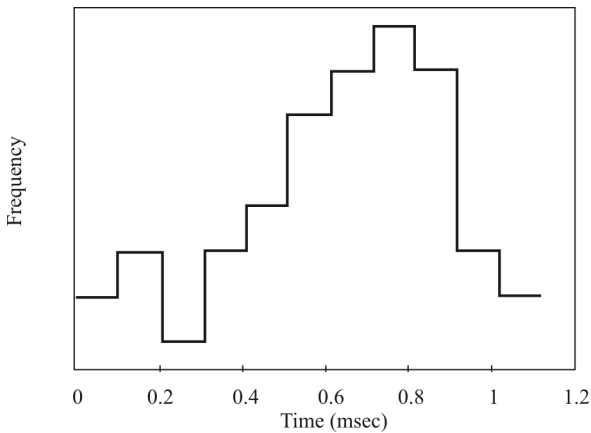**Figure 16.8** FHSS system: (a) transmitter, and (b) receiver.



**Figure 16.9** FHSS frequency versus time.

the frequency domain (i.e., by mixing). If the received signal is the desired one, and the transmitter and the receiver are properly synchronized, the result of the subtraction is the FM carrier modulated with the data and centered at the IF.

The effectiveness of a particular frequency hopped system for a given transmission channel depends on several factors, such as the hopping rate, the size of the hops, and the number of data symbols transmitted during each hop interval. If there are one or fewer data symbols transmitted during a hop interval the process is called *fast frequency hopping* (FFH). In FFH, a high level of redundancy is present because there can be several hops/data symbol. This means that even if some of the hops are not properly received, due to interference or fading, there is still enough information available by using diversity combining techniques to make a correct symbol decision.

If there is more than one data symbol transmitted on each hop interval, then the system is using *slow frequency hopping* (SFH). SFH does not enjoy the same degree of redundancy as FFH systems. If the signal is fading, several data symbols can be lost.

The number of hops taken/symbol interval is known as the *order* or *diversity* and it can be expressed as

$$L = \frac{T_{symbol}}{T_{hop}} \tag{16.1}$$

where $T_{symbol}$ is the data symbol duration and $T_{hop}$ is the hop duration. Equation (16.1) assumes that the frequency separation between any two successive hops is large enough that the channel degradations encountered by the two carriers are statistically independent.

## 16.3.2 Modulation

Most modern FHSS systems use some form of FSK to modulate the PN selected carrier signal, where $2^k$ frequency tones are used. The simplest and most popular form of FSK is binary FSK (BFSK, $k = 1$), where two frequencies are used to represent the binary digits. This is true whether the system employs FFH or SFH. An FHSS channel has the spectrum characteristic shown in Figure 16.10, where, for example, $k = 2$.

## 16.3.3 Coding

The codes used for FHSS are selected in exactly the same way they are selected for DSSS. Shift registers with maximal sequences are typically the implementation method. The codes should be as orthogonal as possible.
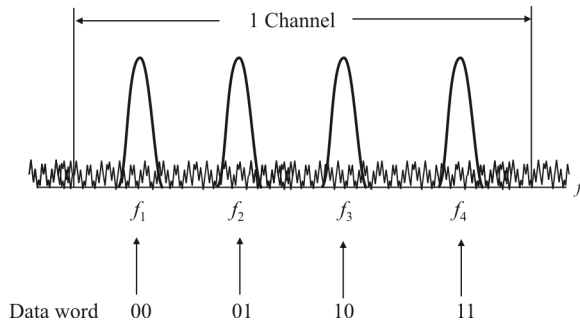
**Figure 16.10** FSK mapping. In this example $k = 2$, for $2^k = 4$ possible tones to represent length 2 digital information bits.

## 16.3.4 FHSS Issues

The two main problems encountered in PLL-based frequency hopping are spectral splatter and transient mismatch between the transmit and the receive synthesizers. During a hop transient, shown in Figure 16.11, a simple frequency hopping system has no control over the transmitted frequency spectrum, and many undesired frequency components are present in the output of the transmitter. This phenomenon is known as spectral splatter and results in a loss of useful transmitter energy during each hop, as well as adjacent channel interference. Additionally, if there is a mismatch in the hopping transient of the receive synthesizer from that of the transmit synthesizer, bursts of frequency error occur in the receiver IF at the hopping rate, producing an overall degradation in the receiver SNR.
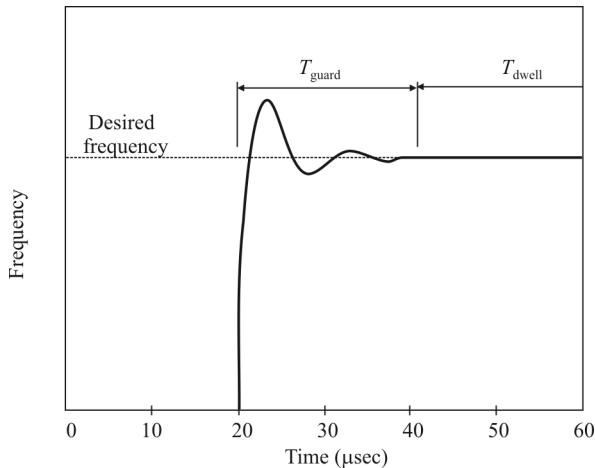


**Figure 16.11** FHSS hop transient.

### 16.3.5 Near-Far Problem

FHSS systems do not suffer from the near-far problem as DSSS systems do.

# 16.4 Time Hopped Spread Spectrum

### 16.4.1 Introduction

In this section we examine THSS communication systems.[1] Probably the only such technology available for this purpose at the time of this writing is UWB signals, so that is the technology we will focus on here. We must bear in mind that UWB is not the only technology for implementing THSS, however.

THSS systems transmit short pulses at times that are selected by a pseudo-random sequence. The optimum detector of signals in *additive white Gaussian noise* (AWGN) channels is the radiometer, which measures the energy content at a point in the RF spectrum. The longer the channel is integrated, the better the detection performance. If a short pulse is transmitted followed by a long period of silence, then much more noise is integrated than signal, and the detection performance deteriorates accordingly. This is the fundamental principle behind THSS that provides some of the LPI functionality. Another is the pseudo-random placement in time of the data pulses. This provides further LPI/LPE capabilities. Last, the very narrowband pulses transmitted by these systems spread the signal energy across a very wide bandwidth, making the psd at any one channel very small—below the noise. This makes it very difficult to detect the presence of the pulse, much as in DSSS.

### 16.4.2 Ultrawideband Systems

UWB communication technology is relatively new, and in the United States, it has been approved for use only under extremely limited conditions. Because of its potential for interference with so many existing communication services, those conditions limit its use to *personal area networks* (PANs). Such networks are for communication between devices either a person is wearing or are otherwise within very close proximity. It could be argued that such applications would probably be of limited use as EW targets. However, this is not to say that UWB communications will forever be limited to this application—a very unlikely circumstance. Therefore, we include this examination of the EW performance against such systems, especially for urban environments.

---

[1]Much of the material in this section is from [15]. Reprinted with permission.
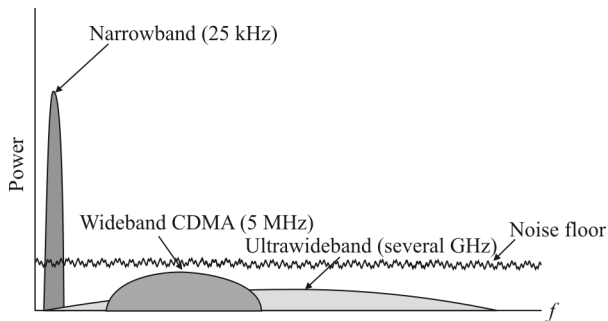
**Figure 16.12** Frequency spectrum comparison of NB, WB, and UWB.

A notional comparison of narrowband (NB), wideband (WB), and UWB signals is illustrated in Figure 16.12. NB signals, typically 25 kHz wide, are normally fairly powerful compared to the noise floor, to be effective at communication. WB signals, as typified by 3G PCS CDMA signals, are typically several megahertz in width and utilize notably less power than the NB counterparts. UWB signals can occupy several gigahertz, and their power is so low it is typically below the noise floor.

A signal is classified as UWB if its bandwidth is 500 MHz or greater or 20% or more of its center frequency. UWB communication is also called *baseband* and *carrier-free transmission*.

UWB communication systems are a relatively new concept that exhibit some very useful characteristics, including

- Extremely short-duration pulses that result in UWB signals of hundreds to thousands of megahertz
- Extremely low psd—they qualify as DSSS signals
- Center frequencies typically between 650 MHz and 5 GHz
- Multimile ranges with submicrowatt average power levels
- Excellent immunity to jamming, intentional or otherwise
- Exceptional multipath tolerance (most of the time)
- Relatively simple and are less costly to build than radios built using other SS technologies
- Consume substantially less power than conventional radios

Due to their low PSD, *impulse radios* (another appellation for UWB radios) can qualify for type acceptance in the United States under the rules of Part 15 for unlicensed applications and can share spectrum without affecting conventional radio transmissions. This means that any operator anywhere in the United States can implement her or his own cell phone system without getting the approval of the FCC or any other government agency.

The spectrum of an impulse function is a constant value and an impulse function can be approximated in practice. It sometimes consists of a few cycles of a carrier signal above 1 GHz but often is a derivative of a Gaussian function, which is easy to generate.

THSS is employed with UWB by randomly varying the pulse times. This TH tries to foil the attempts of a receiver to integrate the signal for reliable detection. As with other forms of SS technology, such THSS would be controlled by a PN sequence. Processing gain is achieved by coherently adding more than one impulse per data bit, denoted by $L$, and the processing gain is given by $G_L = 10 \log_{10} L$. Additional processing gain is achieved by the low duty cycle of the pulses relative to the frame time, $T_f$. This processing gain is then $G_T = 10 \log_{10}(T_f / T_p)$. The total processing gain is then the sum of these. Thus, if $L = 4$, $T_p = 1$ nsec, and $T_f = 1$ μs (corresponding to an uncoded data rate of 1 Mbps), then $G_T = 30$dB, $G_L = 6$dB, and $G_p = 36$dB.

By using THSS, multiple users can share the same spectrum, by the same rationale, employed for DSSS and FHSS. The coding that controls the impulse time minimizes the collisions of the pulses. In this example, if perfect coding were employed, 1000 users could share the same spectrum.

UWB communication is an LPD/LPI technique. The energy in the spectrum is spread across such wide bandwidth and the peak power is so low that the spectrum looks noise-like, much as a DSSS signal looks noise-like. UWB does not achieve such wide bandwidths by applying coding, as in DSSS and FHSS, but by taking advantage of the very narrow pulse width.

This form of SS communication achieves AJ capabilities by gating the time at which the receiver looks for the impulse, and the gate has a width of approximately the width of the impulse—that is, 1 nsec or so. This precludes jamming energy from having any impact on the receiver except during that gate. Time hopping is introduced via pseudo-random coding so that the timing of the next frame varies randomly. The PN code is known only to the transmitter and receiver.

### 16.4.3 Modulation Formats

PPM, OOK, and *pulse amplitude modulation* (PAM) are the principal modulation types used for UWB communication systems. Channel coding can be applied as well, to improve system performance. Each information bit is represented by one or more impulses. While the impulse is there, a wide spectrum signal emerges that has very low PSD. The time between pulses is typically long enough for the pulse response of the channel to die out so there is little ISI. Also, during this time there is no signal in the spectrum.
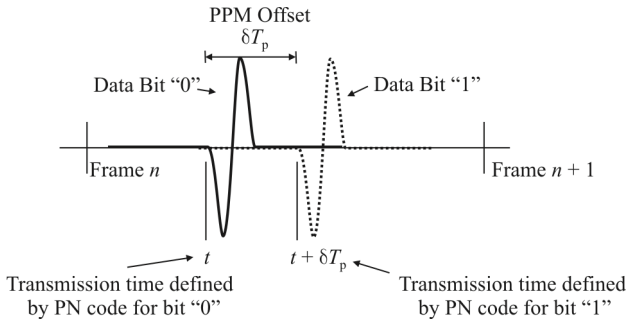
**Figure 16.13** PPM modulation with time-hopping for UWB communications.

PPM modulation with THSS is illustrated in Figure 16.13. A frame is the timeframe within which a time hopped signal occurs. If a zero is sent, the leftmost impulse is transmitted, while if a 1 is transmitted, the impulse is delayed for a duration $\delta T_p$ where $T_p$ is the impulse width.

In *binary PAM* (BPAM), an impulse is sent to represent the binary 1 and its negative is sent to represent the binary zero. In OOK, the pulse is sent to represent the binary one, and no pulse is sent to represent the binary zero. BPAM enjoys a 6dB processing advantage over *binary OOK* (BOOK).

## 16.4.4 UWB Pulse Position Modulation

There are several ways UWB communication systems can be implemented. Probably the most popular modulation scheme is PPM, but other methods of impressing the information stream onto the carrier, such as OFDM and BPSK, are certainly possible.

In UWB PPM communications, information is conveyed with narrow pulses (monocycles), so the RF and analog circuitry is reduced to a wideband low-noise amplifier, a correlator, and data converters. No up/downconversion or mixer is needed, which results in substantial reduction of transceiver size and power consumption. A comparison of a direct IF sampling transceiver and a UWB transceiver architecture is shown is Figures 16.14 and 16.15. It indicates that a UWB transceiver can be implemented with considerably fewer components than the IF sampling receiver and can be implemented as a simple chipset with very few off-chip components.

In PPM, typically ultrashort Gaussian monocycle pulses with carefully controlled pulse-to-pulse intervals are transmitted. A Gaussian monocycle is the first derivative of the Gaussian pulse shown in Figure 16.16. The transmitter sends the appropriately delayed Gaussian pulse to the antenna. The function of the transmitter antenna is to formulate the first derivative of the Gaussian pulse
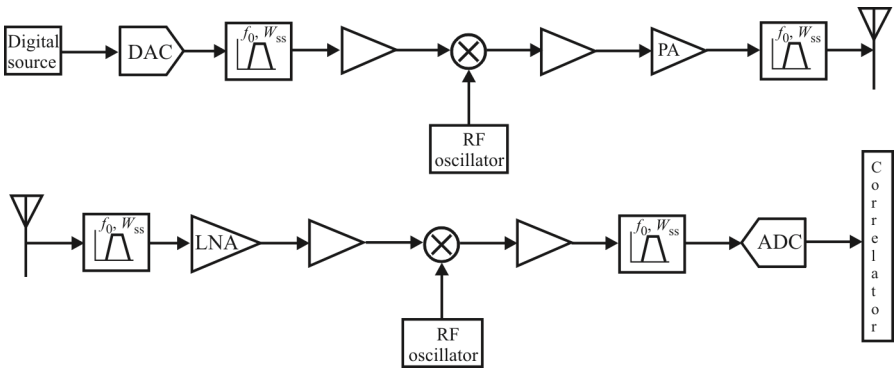
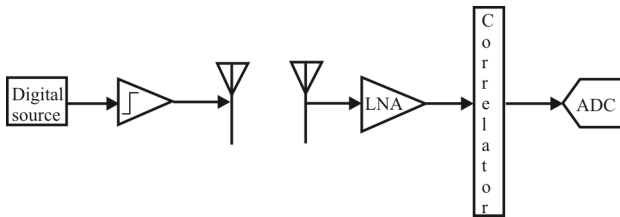**Figure 16.14** Traditional IF sampling transceiver architecture.



**Figure 16.15** UWB transceiver architecture is much simpler than a superheterodyne receiver.
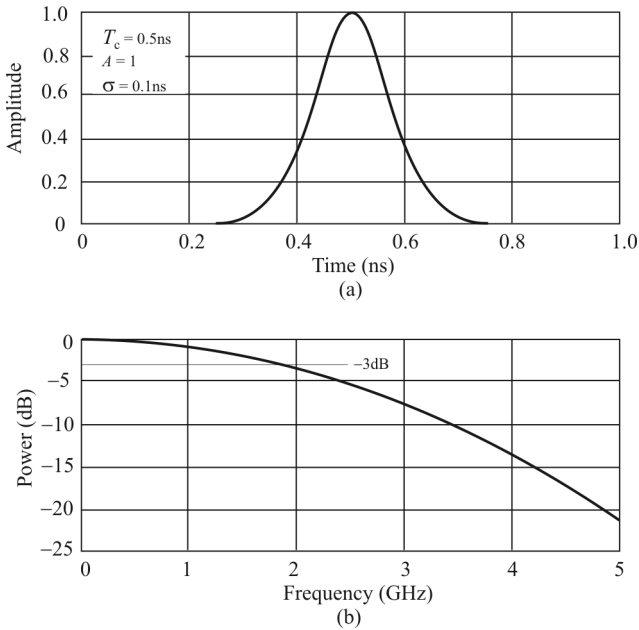
**Figure 16.16** (a) Waveform, and (b) psd of Gaussian pulse.

yielding the Gaussian monopulse[2] as the actual waveform transmitted shown in Figure 16.17. At the receive antenna, the function of the antenna is also to find the first derivative of the received signal, and that is what is sent to the receiver.

The widths of these pulses is typically in the 200 psec to 1.5 nsec range, while the time between data pulses is on the order of 100 nsec to 1 μsec. With these pulse rates, data rates on the order of 1 Mbps to 10 Mbps are possible. These short monocycle pulses are inherently wideband. For example, a pulse width of 200 psec corresponds to a bandwidth of 5 GHz. Typical time domain and the corresponding frequency domain performances are illustrated in Figure 16.18.

## 16.4.5 Jam Resistance and Processing Gain

Processing gain is a measure of the communication system's resistance to interference and UWB has a huge processing gain. One definition of processing gain is the ratio of the bandwidth of the signal to the bandwidth of the information

---

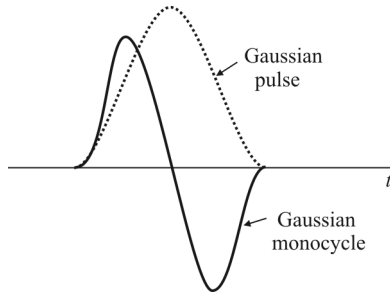[2] Also referred to as the Gaussian doublet.

**Figure 16.17** Time waveform of the Gaussian monocycle.
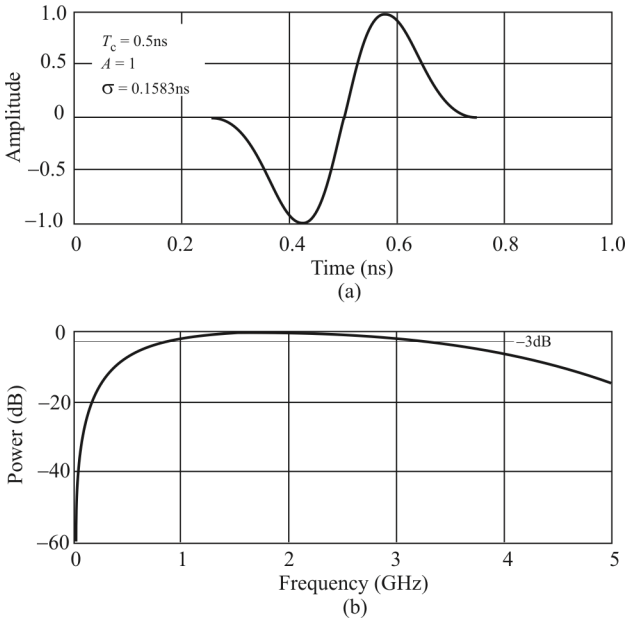


**Figure 16.18** (a) Waveform, and (b) psd of Gaussian monocycle.

signal. For example, an IS-95 SS system with 8 kHz of information bandwidth and a 1.25 MHz channel bandwidth yields a processing gain of 156 (22dB). For an impulse system transmitting the same 8 kHz information bandwidth and a 2 GHz channel bandwidth, the processing gain is 250,000 or 54dB.

Other ways of calculating the processing gain for a UWB signal are

- The duty cycle of the transmission (e.g., a 1% duty cycle yields a process gain of 20dB)
- The effect of integrating over multiple pulses to recover the information (e.g., integrating energy over 100 pulses to determine one digital bit yields a process gain of 20dB)
- The total process gain is then 40dB

Thus, a 2 GHz/10 Mpps link transmitting 8 kbps would have a process gain of 54 dB, because it has a 0.5 nsec pulse width with a 100 nsec pulse repetition interval = 0.5% duty cycle (23dB) and 10 Mpps/8000 bps = 1250 pulses per bit (another 31dB).

## 16.4.6 Multipath and Propagation

Multipath fading is less of a problem for UWB systems than for conventional communication systems. In fact, Rayleigh fading, so noticeable in cellular communication, is a continuous wave phenomenon, not an impulse communication phenomenon. In an impulse system, in order for there to be multipath effects, one of the following special conditions must exist:

- The path length traveled by the multipath pulse must be less than the pulse width times the speed of light. For a 2 GHz pulse, that equals 0.15 m or about 1/2 ft—that is, $[1/2 \text{ nsec}] \times [3 \times 10^8 \text{ meters/second}]$. This is illustrated in Figure 16.19, in the case where the pulse traveling path 1 arrives one half a pulse width after the direct path pulse.

- The multipath pulse travels a distance that equals multiples of the interval of time between pulses multiplied by the speed of light. For a 1 Mpps system, that would be equal to traveling an extra 300, 600, and 900 meters. However, because each individual pulse is subject to the pseudo-random dither, these pulses are decorrelated.

Pulses traveling between these intervals do not cause self-interference. In Figure 16.19, this is illustrated by the pulse traveling path 2, while pulses traveling grazing paths, as illustrated in Figure 16.19 by path 1, create impulse radio multipath effects. Figure 16.20 shows how easy it is to resolve multipath impulse
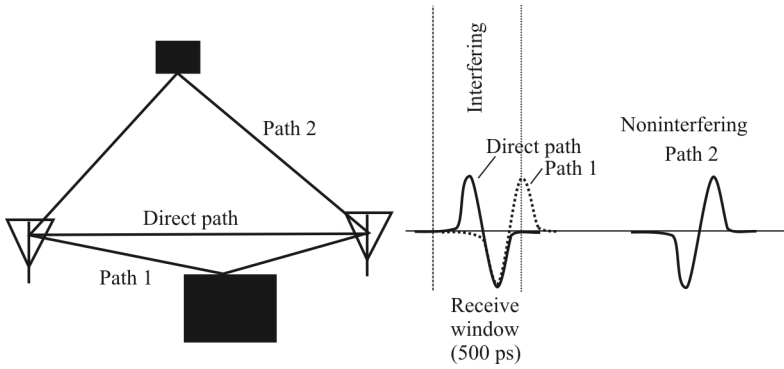
**Figure 16.19** UWB multipath. A multipath problem occurs when the reflecting path is short as in Path 1.
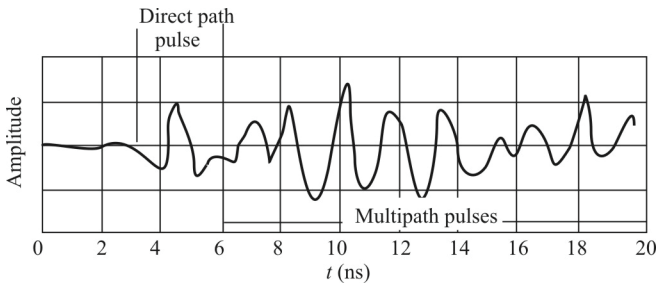


**Figure 16.20** UWB multiple multipath examples.

signals in the time domain. Note that the receive antenna's characteristics convert the Gaussian monocycle into a "W" waveform as seen in Figure 16.20. The first arriving pulse (between 3 ns and 6 ns) is of a lower amplitude because it traveled through more walls than some later arriving pulses (the pulse arriving at between 8 nsec and 11 nsec).

UWB PPM communication systems have a far superior performance in high multipath environments than narrowband systems, as well as DSSS systems. Multipath is a critical problem for most communication systems in urban environments because there are many objects that reflect RF signals. In these environments, UWB systems can operate at high data rates with lower bit error rates and with lower transmit powers.

# 16.5 Advantages of Spread Spectrum

Spread spectrum systems provide some clear advantages. We present here some benefits that ensue with SS-based systems.

- *Reduced crosstalk interference*: In SS systems, crosstalk interference is greatly attenuated by the processing gain of the SS system as described earlier. The effect of the suppressed crosstalk interference can be essentially removed with digital processing where noise below certain thresholds results in negligible bit errors. These negligible bit errors have little effect on voice transmissions.

- *Better voice quality/data integrity and less static noise*: Due to the processing gain and digital processing nature of SS technology, an SS-based system is more immune to interference and noise.

- *Lowered susceptibility to multipath fading*: Because of its inherent frequency diversity properties due to wide spectrum spread, an SS system is much less susceptible to multipath fading.

- *Inherent security*: In an SS system, a PN sequence is used to either modulate the signal in the time domain (DSSS) or select the carrier frequency (FHSS). Due to the pseudo-random nature of the PN sequence, the signal in the air has been randomized. Only the receiver having the exact same pseudo-random sequence and synchronous timing can de-spread and retrieve the original signal. Consequently, an SS system provides signal security that is not available to conventional analog wireless systems.

- *Coexistence*: An SS system is less susceptible to interference than other non-SS systems. In addition, with the proper designing of pseudo-random sequences, multiple SS systems can coexist without creating severe interference to other systems. This further increases the system capacity.

- *Hard to detect*: SS signals are much wider than conventional narrowband transmission (of the order of 20 to 254 times the bandwidth of narrowband transmissions). Since the communication band is spread, power at any given frequency is significantly reduced, lowering the detectability.

- *Hard to intercept or demodulate*: The very foundation of the spreading technique is the code use to spread the signal. Without knowing the code, it is impossible to decode the transmission.

- *Harder to jam*: The most important feature of SS is its ability to reject interference. At first glance, it may be considered that SS would be most affected by interference. However, any signal is spread in the bandwidth, and after it passes through the correlator, the bandwidth signal is equal to its original bandwidth, plus the bandwidth of the local interference. An interference signal with 2 MHz bandwidth being input into a direct-sequence receiver whose signal is 10 MHz wide gives an output from the correlator of 12 MHz. The wider the interference bandwidth, the wider the output signal. Thus, the wider the input signal, the less its effect on the system because the power density of the signal after processing is lower, and less power falls in the bandpass filter.

## 16.6 Concluding Remarks

SS communication methods were developed by the military to combat eavesdropping and to thwart jamming. They perform these functions rather well. The advantages of LPD, LPI, and LPE approaches to communications were outlined at the end of the chapter.

LPI techniques, in particular DSSS in the form of CDMA, have migrated into the commercial marketplace primarily because they can share limited spectrum efficiently—more efficiently than any other approaches to spectrum reuse. All modern cellular phone systems worldwide are migrating to CDMA for economic reasons.

We have outlined the fundamental SS techniques in this chapter. DSSS and FHSS are widely deployed, while THSS is newer and not used as much. The only

approved use for THSS so far has been for PANs since it has the characteristic of possibly interfering with many other communication services.

# References

[1]     Dixon, R. C., *Spread Spectrum Systems*, New York: Wiley, 1984.

[2]     Holmes, J. K., *Coherent Spread Spectrum Systems*, New York: Wiley, 1982.

[3]     Simon, M. K., et al., *Spread Spectrum Communications Handbook*, Revised Edition, New York: McGraw-Hill, 1994.

[4]     Torrieri, D. J., *Principles of Secure Communication Systems*, 2nd Ed., Norwood, MA: Artech House, 1992.

[5]     Peterson, R. L., R. E. Ziemer, and D. E. Borth, *Introduction to Spread Spectrum Communications*, Upper Saddle River, NJ: Prentice Hall, 1995.

[6]     Poisel, R. A., *Modern Communications Jamming Principles and Techniques*, 2nd Ed., Norwood, MA: Artech House, 2011.

[7]     Cook, C. E., and H. S. Marsh, "An Introduction to Spread Spectrum," *IEEE Communications Magazine*, March 1983, pp. 8–16.

[8]     Flikkema, P. G., "Spread-Spectrum Techniques for Wireless Communication," *IEEE Signal Processing Magazine*, May 1997, pp. 26–36.

[9]     Oppermann, I., P. Van Rooyen, and R. Kohno, "Guest Editorial Spread Spectrum for Global Communications II," *IEEE Journal on Selected Areas in Communications*, Vol. 18, No. 1, January 2000, pp. 1–5.

[10]    Sarwate, D. V., M. B. Pursley, "Crosscorrelation Properties of Pseudorandom and Related Sequences," *Proceedings of the IEEE*, Vol. 68, No. 5, May 1980, pp. 593–619.

[11]    Proakis, J. G., *Digital Communications*, 3rd Ed., New York: Mc Graw-Hill, 1995.

[12]    Pickholtz, R. L., D. L. Schilling, and L. B. Milstein, "Theory of Spread Spectrum Communications—A Tutorial," *IEEE Transactions on Communications*, Vol. COM 30, No. 5, May 1982, pp. 855–884.

[13]    Glisic, S., and B. Vucetic, *Spread Spectrum CDMA Systems for Wireless Communications*, Norwood, MA: Artech House, 1997.

[14]    Gold, R., "Optimal Binary Sequences for Spread Spectrum Multiplexing," *IEEE Transactions on Information Theory*, October 1967, pp. 619–621.

[15]    Poisel, R. A., *Modern Communications Jamming Principles and Techniques*, 2nd Ed., Norwood, MA: Artech House, 2011, Ch. 3.

# Chapter 17

## Receivers for Direct Sequence Spread Spectrum Intercept

### 17.1 Introduction

There are a myriad of ways known and some yet unknown to deal with DSSS intercept problems. We point out a few techniques in this chapter to illustrate the complexity. It is not intended to be a thorough discourse on the topic.

A *receiver* in the vernacular we are considering here is a set of processes that can be executed on signals. We do not specifically infer a particular set of hardware. These processes consist of sets of mathematical manipulations on signal samples or variables derived from these samples.

Although any of the receiver architectures discussed previously with adequate bandwidth can be used as the manifestation of the hardware for the receivers in this chapter, in most modern cases the receiver would likely be a digital receiver with bandwidth large enough to process the DSSS signal.

In this chapter, we consider eavesdropping on an adversary's communication that uses DSSS. DSSS is a covert communication technique developed by the military. The information symbols are modulated by a PN sequence prior to transmission to enable this covert property. This results in a wideband signal that is resistant to interference, jamming, interception, and multipath fading [1–3].

Due to the method of generating a DSSS signal—that is, using a PN sequence to spread the signal energy over a large bandwidth—the task of noncooperative interception becomes very difficult. The goal of the intercepting receiver is to remove the PN sequence from the signal to retrieve the underlying information.

We discuss two particular manifestations of DSSS receivers in this chapter. There are others (though not many). Both techniques rely on estimation of the sample covariance matrix. The processing on this matrix is, however, different for the two approaches. For those interested in more in-depth coverage of some

receiver designs, [4] is recommended. Also, both of the receivers we consider, which they share with most DSSS receivers, function only on short codes.[1]

The principal requirement for a DSSS receiver is to determine the spreading sequence. Without knowing that, despreading DSSS signals is not possible. Both of the receivers described in this chapter strive to determine this sequence. Once the sequence is derived, it is used in a DSSS receiver to extract the underlying information.

This chapter is structured as follows. We first provide brief overviews of the two receivers. Then the first receiver that relies on an analysis of the eigenvalues and corresponding eigenvectors of the estimated data covariance matrix is described. Next, the second receiver that also relies on the estimated covariance matrix but uses the matrix in a different way is described. Examples are provided for both methods.

# 17.2 Overview of Two Receivers

## 17.2.1 Eigenanalysis Technique

Bouder, Azou, and Burel investigated a method of determining the symbol duration, while simultaneously providing a procedure for establishing the presence of a DSSS signal [5]. A method for estimating the PN sequence without prior knowledge about the transmitter in this section was considered. The received signal is sampled and divided into temporal windows, the size of which make up the PN sequence period, which is assumed to have been estimated. The spreading waveform can be recovered from the first and second eigenvectors of the sample covariance matrix. The PN sequence used at the transmitter can be estimated from these eigenvectors. Furthermore, useful information about time offset can be extracted from the eigenvalues.

## 17.2.2 Spectral Norm Maximization

The second intercept method we consider, developed by Jo and Wu [6], proceeds by identifying the basic steps required to eavesdrop on an adversary's communication. The steps involved are

- Determine the symbol duration, which also serves as the method for determining the presence of the DSSS signal. This is done by measuring the *fluctuations* of the signal.

---

[1] A *short code* is when one or more complete periods of the spreading sequence are present in every symbol. A long code is when the spreading sequence is expanded beyond one symbol.

- Identify the start position of a data symbol in the spread signal for symbol synchronization purpose.
- Remove the PN sequence.
- Estimate the PN sequence.
- Estimate the generator polynomial to determine the correct polarity of the spreading sequence.

To identify the start position of data symbols, we will discuss a method based on the spectral norm that achieves low estimation errors. After the symbol synchronization, we remove a PN sequence from the intercepted signal by a correlation method to estimate data symbols without a priori knowledge about that PN sequence. Identification of a PN sequence is processed by a matched filter between the intercepted signal and the estimated data symbols.

One of the harder problems in eavesdropping on DSSS signals is the polarity ambiguity of the estimated spread sequence and data symbols. Erroneous reversal of polarity of each chip in the estimated PN sequence compared to the true PN sequence is a major source of the performance degradation of an EW eavesdropper. One way to mitigate this polarity problem is to estimate the code generator polynomial. The technique also reduces the memory requirement of an eavesdropper, which can run into saving hundreds or thousands of sequence bits in the memory of an eavesdropper. We discuss such a technique later in this chapter.

The probability of error performance of an eavesdropper is a function of SNR, the number of data symbols, and the length of the spread sequence of the intercepted signal. Therefore, we discuss the analytical probability of error performance of the eavesdropper with respect to these parameters. By doing so, we can efficiently predict the performance of the eavesdropper.

# 17.3 Eigenanalysis Direct Sequence Spread Spectrum Receiver

## 17.3.1 Signal Model

Let $a_k$ be a QPSK or BPSK symbol transmitted at time $lT_s$, where $T_s$ is the symbol duration.[2] This symbol is multiplied by a pseudo-random sequence of chip duration $T_c$, which spreads the signal bandwidth. This discrete signal is then filtered, sent through the communication channel, and filtered again at the receiver. A baseband representation of a DSSS signal is given by [8, 9]

---

[2] For reasons of simplicity and clarity of presentation, we focus only on the QPSK/BPSK modulation. If we adopt a blind modulation detection method (such as in [7]), these results can be applied to higher order modulation like 64QAM with little modification.

$$y(t) = \sum_{l=-\infty}^{\infty} a_l h(t - lT_s) + n(t) \qquad (17.1)$$

where

$$h(t) = \sum_{k=0}^{P-1} c_k p(t - kT_c) \qquad (17.2)$$

and $n(t)$ is the AWGN output of the receiver filter and uncorrelated with the information signal $a_l$. We assume the symbols $a_l$ are centered and uncorrelated. The effects of the transmitter filter, the reception filter, the channel response, and the pseudo-random sequence $c_k$ are represented by $h(t)$. $p(t)$ denotes the convolution of all filters of the transmission chain. $T_c$ is the chip duration and $\{c_k\}_{k=0,1,\cdots,P-1}$ is the pseudo-random sequence of length $P$, where $P = T_s/T_c$ because of the short code assumption. Further, we assume that the SNR, $\gamma$ (in dB), at the output of the receiver filter is negative—that is, the signal is hidden in the noise; all other parameters are unknown.

## 17.3.2 Estimation of the Symbol Duration

The basic principle of any intercept receiver is to take advantage of the fact that the transmitted signal statistical properties are not the same as the noise statistical properties; that is, they are independent stochastic processes. For instance, in some simple applications, the signal and noise frequencies are not the same; hence filters are sufficient to detect the presence of a signal. Here, the application is much more complex, because a DSSS signal is specially built to be similar to a noise in order to be LPI. For instance, the autocorrelation of an SS signal is close to a Dirac function, similar to the autocorrelation of white noise (this is due to the pseudo-random sequence).

The intercept receiver implements two major steps: first the presence of any DSSS transmission is detected and then the blind spreading sequence is estimated before demodulation. The first step also leads to a spreading code period estimate that is then used in the rest of the algorithm.

The first step relies on the fluctuations of autocorrelation estimators, denoted by $\rho(\tau)$, instead of on the autocorrelation itself. Although the autocorrelation of a DSSS signal is similar to the autocorrelation of noise, it is shown in [10] that the fluctuations of estimators are totally different.

In order to compute the fluctuations, the received signal $y(t)$ is divided into $M$ nonoverlapping temporal windows, each of duration $T$ large enough to contain a few symbols. Then an autocorrelation estimator is applied to each window:
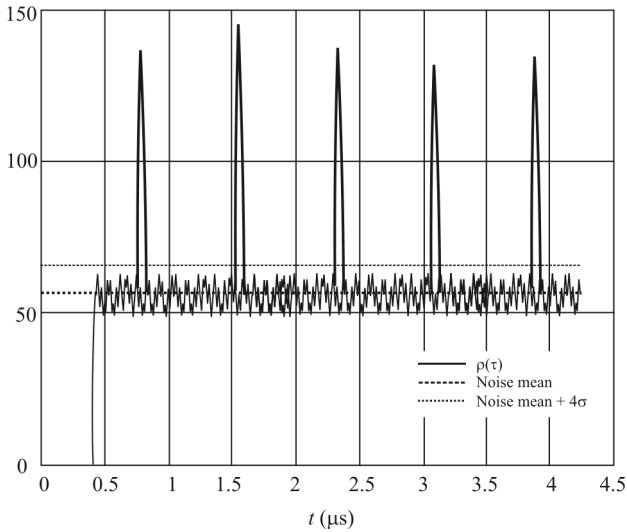
**Figure 17.1** Example of DSSS signal detector output (fluctuations) with Gold code of length 31 at a chip rate $f_C = 40$ MHz in a Gaussian channel with $\gamma = -5$dB.

$$\hat{\mathbf{R}}^m_{yy}(\tau) = \frac{1}{T} \int_{t_m}^{t_m+T} y(t) y^*(t-\tau) dt, \quad m = 1,\ldots,M \tag{17.3}$$

We can then estimate the second-order moment of this autocorrelation estimator, the fluctuations, as:

$$\rho(\tau) = \frac{1}{M} \sum_{m=1}^{M} \left| \hat{\mathbf{R}}^m_{yy}(\tau) \right|^2 \tag{17.4}$$

By comparing the theoretical fluctuations, $\rho(\tau)$, in the case of noise only to that obtained by computation from the incoming signal, we can detect the presence of a DSSS transmission.

This is illustrated in Figure 17.1 where some fluctuations $\rho(\tau)$ are plotted. The horizontal dashed line shows the theoretical average fluctuations $m_\rho^{(n)}$, and the dotted line corresponds to the theoretical average fluctuations plus 4 times the theoretical standard deviation $\sigma_\rho^{(n)}$ on the fluctuations (noise only). Large peaks that are observed, far above $m_\rho^{(n)} + 4\sigma_\rho^{(n)}$, indicate the presence of a DSSS signal. These peaks are obtained for values of $\tau$ that are multiples of the spreading code period (0.775 μsec for this example).

Since short codes are assumed for the DSSS system, the period of the spreading sequence is the same as for the symbol duration.

### 17.3.3 Blind Estimation of the Spreading Sequence

Eigenanalysis techniques are exploited to recover the spreading sequence used at the transmitter. As above, the received signal is sampled and divided into non-overlapping windows, but in this case the duration of these windows is equal to the symbol time, $T_s$. Let $\vec{y}$ denote the content of a window. The covariance matrix of $\vec{y}$ is given by

$$\mathbf{R} = \mathcal{E}\{\vec{y}\vec{y}^H\} \tag{17.5}$$

where H denotes the Hermitian transpose. Since the window duration is equal to the symbol duration, a window always contains the end of a symbol for a duration $T_s - t_0$, followed by the beginning of the next symbol for a duration $t_0$, where $t_0$, the offset between a window and a symbol, is unknown.

Hence

$$\vec{y} = a_m \vec{h}_0 + a_{m+1} \vec{h}_{-1} + \vec{n} \tag{17.6}$$

where $\vec{n}$ is the noise vector; $\vec{h}_0$ is a vector containing the end of the spreading waveform for a duration $T_s - t_0$, followed by zeros for a duration $t_0$; $\vec{h}_{-1}$ is a vector containing zeros for a duration $T_s - t_0$, followed by the beginning of the spreading waveform.

Equation (17.6) leads to

$$\mathbf{R} = \mathcal{E}\left\{|a_m|^2\right\}\vec{h}_0\vec{h}_0^H + \mathcal{E}\left\{|a_{m+1}|^2\right\}\vec{h}_{-1}\vec{h}_{-1}^H + \sigma_n^2\mathbf{I} \tag{17.7}$$

for the covariance matrix (17.5). From (17.7) it is clear that two eigenvalues will be larger than the others. The corresponding eigenvectors are given by $\vec{h}_0$ and $\vec{h}_{-1}$, up to multiplicative factors.

The eigenvalues can be expressed in decreasing order according to the symbol period, $T_s$, the SNR, $\gamma$, the sampling period, $T_e$, and the noise variance, $\sigma_n^2$, according to

$$\lambda_1 = \left(1 + \gamma\frac{T_s - t_0}{T_e}\right)\sigma_n^2 \tag{17.8}$$

$$\lambda_2 = \left(1 + \gamma \frac{t_0}{T_e}\right)\sigma_n^2 \qquad (17.9)$$

$$\lambda_i = \sigma_n^2, \ i \geq 3 \qquad (17.10)$$

The expressions for (17.8) and (17.9) must be interchanged if $t_0 > T_s / 2$. The spreading sequence can then be recovered, once the corresponding normalized eigenvectors $\vec{v}_0 = \vec{h}_0 / \|\vec{h}_0\|^2$ and $\vec{v}_{-1} = \vec{h}_{-1} / \|\vec{h}_{-1}\|^2$ are concatenated.

It can be shown that the offset time $t_0$ and the SNR, $\gamma$, can be estimated from (17.8)–(17.10)

$$\hat{\gamma} = \left(\frac{\lambda_1 + \lambda_2}{\sigma_n^2} - 2\right)\frac{T_e}{T_s} \qquad (17.11)$$

$$\hat{t}_0 = \frac{T_e}{\hat{\gamma}}\left(\frac{\lambda_2}{\sigma_n^2} - 1\right) \qquad (17.12)$$

Note that the covariance matrix (17.5) cannot be exactly determined but only estimated by the sample covariance matrix:

$$\hat{\mathbf{R}} = \frac{1}{N}\sum_{n=1}^{N} \vec{y}_n \vec{y}_n^{H} \qquad (17.13)$$

where $N$ is the number of temporal windows of duration $T_s$. The performance of the estimation of the spreading sequence will therefore depend on the number $N$ as well as the SNR. In the following we will assume that the sampling period is set to $T_e = T_c$, to make the interpretation of the results easier, but this is not a requirement. In this case, the covariance matrix is a $P \times P$ complex matrix, where $P$ is the length of the spreading sequence.

To illustrate the algorithm, computer simulations will be given in the next section to show the method can provide a good estimation of the spreading sequence, even when the received signal is far below the noise level.

## 17.3.4 Verification and Validation

In this section, we provide representative comparisons of the approach. An example also illustrates the performance in a multipath environment.
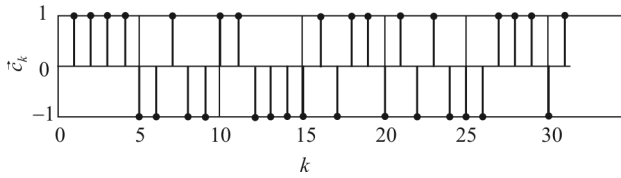
**Figure 17.2** Gold sequence.

**Example 17.1:** Eigenanalysis Receiver (no multipath). Consider an SS signal generated by spreading a QPSK modulation with a Gold sequence of length 31 (Figure 17.2). AWG noise is added to the received signal to produce $\gamma = -5$dB. We assume $N = 200$ analysis windows, and the spreading code length $P$ and the chip period $T_c$ are known.

The chip sequence is the length 31 Gold code shown in Figure 17.2. Figure 17.3 shows the received estimated sequence determined by this eigenanalysis technique when an offset time $t_0 = 8$ chips is present.

The eigenanalysis of $\hat{\mathbf{R}}$ shows there are two large eigenvalues. Once the offset time has been estimated according to the eigenvalues (17.12), it is possible to determine which eigenvector contains the beginning of the spreading sequence and which one the end. In Figure 17.3(a) the first eigenvector is shown, which contains the end of the spreading sequence during $T_s - t_0$ followed by zeros during $t_0$, where $t_0$ is equal to 8 chips, while the second eigenvector at Figure 17.3(b) contains zeros during $T_s - t_0$ followed by the beginning of the spreading code during $t_0$. The eigenvectors can then be concatenated to recover the spreading code used at the transmitter.

**Example 17.2:** Multipath Environment. A Monte Carlo simulation was conducted to evaluate the performance of the proposed method in a multipath environment. A DSSS signal is generated using a random sequence of length $P = 31$. The symbols belong to a BPSK constellation. The spreading sequence is shown in Figure 17.4. The signal is then transmitted through a multipath channel, with impulse response

$$h(t) = 1.2 - 0.8\delta(t - T_c) + 0.6\delta(t - 2T_c)$$

AWGN is added to the received signal producing $\gamma = -10$dB. Figure 17.5 shows an example of the transmitted and received sequences.
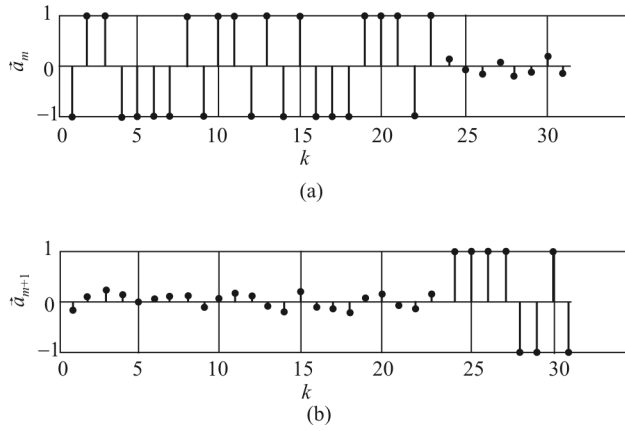
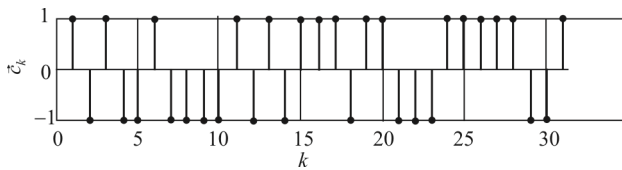**Figure 17.3** Windows: (a) $\vec{a}_m$ and (b) $\vec{a}_{m+1}$. These are also the eigenvectors.
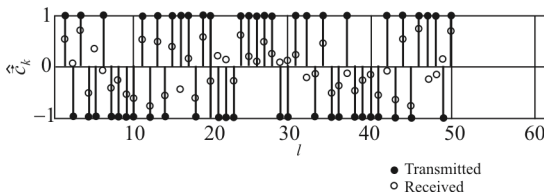


**Figure 17.4** Spreading sequence.

**Figure 17.5** Transmitted and received sequences for the multipath example. $P = 31$, $\gamma = -10$dB.

The estimated spreading sequence can then be used by a DSSS receiver in order to recover the transmitted information from the received data.

### 17.3.5 Summary

We considered a blind spreading sequence estimation approach to estimating the spreading sequence in a DSSS transmission system in this section. The algorithm requires a single eigenvalue decomposition of the received signal sample covariance matrix. The process also enables the estimation of parameters such as SNR and offset time. No assumption was made on the nature of the spreading sequence: it can be a sequence generated by pseudo-random shift registers, such as Gold sequences, but this is not a requirement. Once estimated, the sequence can be used by an SS receiver in order to retrieve the information symbols.

# 17.4 Spectral Norm Direct Sequence Spread Spectrum Receiver

We consider the second approach to estimating the spreading sequence in this section. This method was devised by Jo and Wu [6] and is based on maximizing the spectral norm of a sample covariance matrix, which achieves smaller estimation error than the method of maximizing the Frobenius norm. After synchronization, we remove the spread sequence by a cross-correlation-based method, and identify the spread sequence by a matched filter. We also discuss a searching method to identify a generator polynomial that is capable of correcting polarity errors existing in some of the previous methods.

### 17.4.1 Symbol Synchronization

The captured signal $y(t)$ in (17.1) is sampled and divided into non-overlapping windows with the eavesdropper's sampling duration $T_e$. We assume the sampling duration of an eavesdropper is the chip duration. Therefore, $P(L + 1)$ samples are available by sampling $(L + 1)T_s$ long signal with the sample duration $T_c$.

We form the matrix $\mathbf{Y}^k$ with dimensions $P \times (L+1)$, from the $P(L+1)$ samples as

$$\mathbf{Y}^k = [\vec{y}_{-1}^{\,k} \quad \cdots \quad \vec{y}_{l-1}^{\,k} \quad \vec{y}_{l}^{\,k} \quad \cdots \quad \vec{y}_{L-1}^{\,k}] \tag{17.14}$$

where the superscript $k$ represents the $kT_c$ time-delayed desynchronized signal of (17.1) for $k = 0, 1, \ldots, P-1$. $\vec{y}_{l}^{\,k}$ denotes a column of the desynchronized $\mathbf{Y}^k$. We may write $\vec{y}_{l}^{\,k}$ as follows

$$\vec{y}_{l}^{\,k} = [y_{l,k} \quad \cdots \quad y_{l,P-1} \quad y_{l+1,0} \quad \cdots \quad y_{l+1,k-1}]^{\mathrm{T}}$$

$$= \begin{bmatrix} a_l h_{l,k} + n_k \\ \vdots \\ a_l h_{l,P-1} + n_{P-1} \\ a_{l+1} h_{l+1,0} + n_0 \\ \vdots \\ a_{l+1} h_{l+1,k-1} + n_{k-1} \end{bmatrix} \tag{17.15}$$

where $\{\}^{\mathrm{T}}$ denotes the transpose, $y_{l,k}$ is the $k^{\mathrm{th}}$ entry of a column $\vec{y}_{l}^{\,k}$, and $h_{l,k}$ is the spreading sequence of $y_{l,k}$. Now, we can rewrite (17.15) as

$$\vec{y}_{l}^{\,k} = \begin{bmatrix} h_{l,k} & 0 \\ \vdots & \vdots \\ h_{l,P-1} & 0 \\ 0 & h_{l+1,0} \\ \vdots & \vdots \\ 0 & h_{l+1,k-1} \end{bmatrix} \begin{bmatrix} a_l \\ a_{l+1} \end{bmatrix} + \begin{bmatrix} n_k \\ \vdots \\ n_{P-1} \\ n_0 \\ \vdots \\ n_{k-1} \end{bmatrix}$$

$$= [\vec{h}_{l}^{\,e} \quad \vec{h}_{l+1}^{\,b}] \vec{a}_{l}^{\,k} + \vec{n}^{\,k}$$
$$= \vec{h}_{l}^{\,k} \vec{a}_{l}^{\,k} + \vec{n}^{\,k} \tag{17.16}$$

where $\vec{h}_{l}^{\,e}$ denotes a vector containing the end of the spreading waveform for a duration of $T_s - kT_c$ followed by zeros for a duration $kT_c$; $\vec{h}_{l+1}^{\,b}$ is a vector containing zeros for a duration $T_s - kT_c$ followed by the beginning of the spreading waveform for a duration $kT_c$; $\vec{a}_{l}^{\,k}$ denotes a vector containing two desynchronized

symbols $a_l$ and $a_{l+1}$; $\vec{n}^k$ stands for the noise. Therefore, it is necessary to make a column $\vec{y}_l^k$ have only one data symbol $a_l$. That is

$$\vec{y}_l^0 = [y_{l,0} \quad \cdots \quad y_{l,k-1} \quad y_{l,k} \quad \cdots \quad y_{l,P-1}]^{\mathrm{T}}$$
$$= \vec{h}_{l,0} a_l + \vec{n}^0 \tag{17.17}$$

and (17.14) becomes

$$\mathbf{Y}^0 = [\vec{y}_0^0 \quad \cdots \quad \vec{y}_{l-1}^0 \quad \vec{y}_l^0 \quad \cdots \quad \vec{y}_{L-1}^0] \tag{17.18}$$

Note that samples that belong to $a_{-1}$ and $a_L$ in (17.14) are truncated in the synchronized intercepted signal (17.18). Let $\mathbf{R}$ denote the covariance matrix of (17.16)

$$\mathbf{R} = \mathcal{E}\{\vec{y}_l^k \vec{y}_l^{k^*}\}$$
$$= \vec{h}_l^k \mathcal{E}\{\vec{a}_l^k \vec{a}_l^{k^*}\} \vec{h}_l^{k^*} + \sigma_{\mathrm{n}}^2 \mathbf{I}_{\mathrm{P}} \tag{17.19}$$

where $\cdot^*$ denotes the conjugate transpose; $\mathbf{I}_{\mathrm{P}}$ represents a $P \times P$ identity matrix, $\mathcal{E}\{\cdot\}$ denotes expectation, and $\sigma_{\mathrm{n}}^2$ is the noise variance.

To place the starting spread sequence $h_{l,0}$ in the proper position in (17.15), we search for a maximum of the spectral norm[3] of the sample covariance matrix of (17.19). Let $\|\vec{y}\|_2$ denote the spectral norm of the square covariance matrix

$$\|\vec{y}\|_2 = \sqrt{\lambda_{\max}(\mathbf{R})} \tag{17.20}$$

where $\lambda_{\max}(\mathbf{R})$ stands for the largest eigenvalue of the covariance matrix. Then the spectral norm of (17.18) is

$$\|\vec{y}_l^0\|_2 = \|\vec{h}_l^0\|^2 \mathcal{E}\{|a_l|^2\} + \sigma_{\mathrm{n}}^2 \tag{17.21}$$

However, the spectral norm of (17.19) is

---

[3] The spectral norm of matrix $\mathbf{A}$ is the square root of the largest eigenvalue of $\mathbf{A}$.
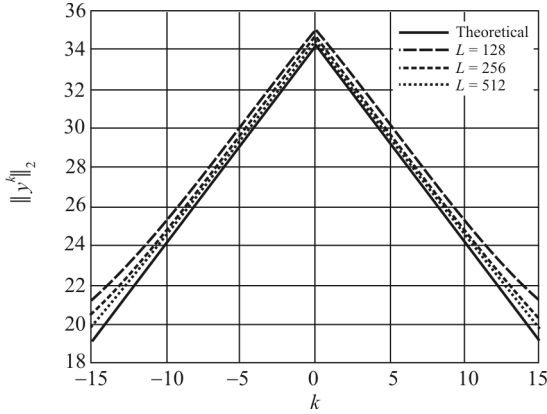
**Figure 17.6** Theoretical and simulated spectral norm, $\left\|\bar{y}^k\right\|_2$, in (17.23) with $P = 31$ and $\gamma = -5$ dB.

$$\left\|\bar{y}_l^k\right\|_2 = \begin{cases} \left\|\bar{h}_l^e\right\|^2 \mathcal{E}\{|a_l|^2\} + \sigma_n^2, & kT_c \leq T_s / 2 \\ \left\|\bar{h}_{l+1}^b\right\|^2 \mathcal{E}\{|a_{l+1}|^2\} + \sigma_n^2, & kT_c > T_s / 2 \end{cases} \tag{17.22}$$

if the singular values are expressed in decreasing order. Since $\left\|\bar{h}_l^0\right\|^2 \geq \left\|\bar{h}_l^e\right\|^2$ or $\left\|\bar{h}_l^0\right\|^2 \geq \left\|\bar{h}_{l+1}^b\right\|^2$, we can determine the synchronized version of (17.14) by maximizing the spectral norm in (17.20) with respect to $k = 0, 1, \ldots, P-1$ as follows

$$\hat{\mathbf{Y}}^0 = \arg\max_{k \in [0, P-1]} \sqrt{\lambda_{\max} \mathcal{E}\{\bar{y}^k \bar{y}^{k^*}\}} \tag{17.23}$$

Figure 17.6 shows the theoretical and simulated squared spectral norm $\|\bar{y}\|_2$ in (17.23). For the calculation, 10,000 trials are carried out and averaged together. In the simulation, we use QPSK. The PN sequence is an *m*-sequence [11–13] with the length $P = 31$ and with a generator polynomial $f(x) = 1 + x^2 + x^5$. The SNR $\gamma = -5$dB. When $k = 0$, the spectral norm has a peak. Note that the more samples, the more accurate estimation of $\hat{\mathbf{Y}}^0$ in (17.23) can be achieved.

### 17.4.2 Symbol Estimation

After symbol synchronization, we need to remove the spread sequence in (17.17) to estimate the information symbol $a_l$ from the synchronized signal $\vec{y}_l^{\,0}$ in (17.18). With the property of strong self-correlation and weak cross-correlation of spread spectrum, we use a method based on a cross-correlation between a test column, say $\vec{y}_t^{\,0}$, and a column of a data symbol $a_l$, say $\vec{y}_l^{\,0}$, of the synchronized signal in (17.18). Then we have

$$C_{\vec{y}_t^{\,0} \vec{y}_l^{\,0}}(\tau) = \vec{y}_t^{\,0} \vec{y}_l^{\,0^*}(\tau) \tag{17.24}$$

If the spread sequence is an *m*-sequence [11, 13], $\left. C_{\vec{y}_t^{\,0} \vec{y}_l^{\,0}}(\tau)\right|_{\tau=0} \geq \left. C_{\vec{y}_t^{\,0} \vec{y}_l^{\,0}}(\tau)\right|_{\tau\neq0}$. Then

$$C_{\vec{y}_t^{\,0} \vec{y}_l^{\,0}}(\tau) = \sum_{k=0}^{P-1} y_{t,k}\, y_{l,k}^* \tag{17.25}$$

Now we can estimate the symbol $a_l$ from (17.25) as follows

$$\hat{a}_l = \mathrm{sgn}\left[\mathrm{Re}\{C_{\vec{y}_t^{\,0} \vec{y}_l^{\,0}}(0)\}\right] + j\,\mathrm{sgn}\left[\mathrm{Im}\{C_{\vec{y}_t^{\,0} \vec{y}_l^{\,0}}(0)\}\right] \tag{17.26}$$

where $\mathrm{Re}\{\cdot\}$ takes the real part and $\mathrm{Im}\{\cdot\}$ takes the imaginary part of a complex number. $\mathrm{sgn}(x)$ is the sign function

$$\mathrm{sgn}(x) = \begin{cases} +1, & x > 0 \\ -1, & x < 0 \end{cases} \tag{17.27}$$

Note that the estimated symbol $\hat{a}_l$ in (17.26) is estimated up to an unknown multiplicative factor. Therefore, the sign of the symbol in (17.26) can be reversed by this multiplicative factor.

The BER of estimation of the symbol $a_l$ can be determined to be

$$P_b^a = \frac{1}{2}\,\mathrm{erfc}\left(\sqrt{\frac{P}{2\sigma_\varsigma^2}}\right) \tag{17.28}$$

where

$$\sigma_\varsigma^2 = 2\sigma^2 + \sigma^4$$

when

$$\sigma^2 = \frac{\sigma_n^2}{|c_k|^2}$$

$$c_k = h_{0,k} = h_{l,k}$$

$\sigma_n^2$ is the variance (power) of the AWGN.

### 17.4.3 Spread Sequence Estimation

To recover the PN sequence in (17.17), we use a matched filter operation between the synchronized intercepted signal $\mathbf{Y}^0$ in (17.18) (one row at a time) and the estimated data symbols $\hat{\vec{a}}$ in (17.26). That is

$$\hat{\vec{c}} = \mathrm{sgn}(< \mathbf{Y}^0, \hat{\vec{a}} >) \qquad (17.29)$$

Where $< \cdot, \cdot >$ denotes the inner product,[4] $\hat{\vec{a}} = [\hat{a}_0 \quad \cdots \quad \hat{a}_{L-1}]^T$ is a vector of the estimated symbols, and $\hat{\vec{c}} = [\hat{c}_0 \quad \cdots \quad \hat{c}_{P-1}]^T$ denotes a vector of the estimated spread sequence. The sign of the sequence in (17.29) can also be reversed by a multiplicative factor in (17.26).

To analyze the performance of the sequence estimator in (17.29), it is rewritten as follows

$$\hat{c}_k = \sum_{l=0}^{L-1} y_{l,k} \hat{a}_l$$
$$= \sum_{l=0}^{L-1} (a_l h_{l,k} + n_{l,k}) \hat{a}_l \qquad (17.30)$$

Let $w_{l,k} = y_{l,k} \hat{a}_l$ and $h_{l,k} = c_k$ for simplicity.

The probability of error $P_b^c$ in estimation of the sequence $c_k$ can be determined to be

$$P_b^c = \frac{1}{2} \mathrm{erfc}\left(\sqrt{\frac{L}{2\sigma_w^2}}\right) \qquad (17.31)$$

---

[4] The inner product of two vectors of dimension $M$, $\vec{a} = [a_1 \quad a_2 \quad \cdots \quad a_M]^T$ and $\vec{b} = [b_1 \quad b_2 \quad \cdots \quad b_M]^T$, is $< \vec{a}, \vec{b} > = \vec{a} \cdot \vec{b} = \vec{a}^T \vec{b} = a_1 b_1 + a_2 b_2 + \ldots + a_M b_M$.

where

$$\sigma_w^2 = 3\sigma^2 + 3\sigma^4 + \sigma^6$$
$$\sigma^2 = \sigma_n^2 / \varepsilon$$
$$\varepsilon = |a_l|^2.$$

Note that the probability of error in (17.28) and (17.31) does not account for the possible polarity error. We will address this problem in the next section.

### 17.4.4 Identification of Generator Polynomial

Hundreds or thousands of sequence bits, say $\hat{\vec{c}} = [\hat{c}_0 \quad \cdots \quad \hat{c}_{P-1}]^T$, must remain in the memory of the eavesdropper. This motivates us to estimate a generator polynomial of the estimated spread sequence from (17.29).

Shift registers are the practical and efficient implementation for the spread sequence. We considered a *linear feedback shift register* (LFSR) as the implementation technique for PN sequences. The correct selection of the $n$-tuple tap-weights (or $n$ feedback stages) will result in a maximal sequence of the length $N = 2^n - 1$ [13].

Let $\mathcal{F} = GF(q)$, where $q$ is a prime or a power of a prime, and $GF$ denotes a finite field;[5] $q$ is called the *order* of the field $\mathcal{F}$ [14]. If the feedback function $f(x_0, \ldots, x_{n-1})$ is a linear function—that is, if it can be expressed as

$$f(x_0, \ldots, x_{n-1}) = w_0 x_0 + \cdots + w_{n-1} x_{n-1}, \qquad w_i \in \mathcal{F} \qquad (17.32)$$

where $w_i$ denotes a tap weight of the LFSR for $i = 0, \ldots, n-1$ over $\mathcal{F}$, then sequences have the linear recursion relation

$$c_{n+k} = \sum_{i=0}^{n-1} w_i c_{k+i}, \qquad k = 0, 1, 2, \ldots \qquad (17.33)$$

If we have $2n$ successive sequence bits, we can estimate the generator polynomial of sequence $\vec{c} = (c_0, \ldots, c_{P-1})$ over $\mathcal{F} = GF(q)$. We may rewrite the recursion relation (17.33) into the following matrix representation

---

[5] Finite fields are also called Galois fields.

$$
\begin{bmatrix} c_n \\ c_{n+1} \\ \vdots \\ c_{2n-1} \end{bmatrix} = \begin{bmatrix} c_0 & c_1 & \cdots & c_{n-1} \\ c_1 & c_2 & \cdots & c_n \\ \vdots & \ddots & \ddots & \vdots \\ c_{n-1} & c_n & \cdots & c_{2n-2} \end{bmatrix} \begin{bmatrix} w_0 \\ w_1 \\ \vdots \\ w_{n-1} \end{bmatrix} \tag{17.34}
$$

We can solve the recursion relation in (17.34) over $GF(q)$ to obtain tap weights $\vec{w} = (w_0, \ldots, w_{n-1})$. The next successive sequence bit can be generated and tested with the estimated tap weights $\hat{w}$ and $n$ successive sequences using transform matrix $\mathbf{M}$ of an LFSR as follows

$$
\mathbf{M} = \begin{bmatrix} 0 & 0 & \cdots & 0 & \hat{w}_0 \\ 1 & 0 & \cdots & 0 & \hat{w}_1 \\ \vdots & \ddots & \ddots & \ddots & \vdots \\ 0 & 0 & \cdots & 1 & \hat{w}_{n-1} \end{bmatrix} \tag{17.35}
$$

and

$$
(\hat{c}_{k+1}, \hat{c}_{k+2}, \ldots, \hat{c}_{k+n}) = (\hat{c}_0, \hat{c}_1, \ldots, \hat{c}_{n-1}) \mathbf{M}^{k+1} \tag{17.36}
$$

Note that $\det(\mathbf{M}) = (-1)^n \hat{w}_0$ and thus $\mathbf{M}$ is invertible if and only if $\hat{w}_0 \neq 0$.

In [6] a procedure is presented for determining the generator polynomial primarily based on (17.34) and (17.36) from the estimated sequence $\hat{\vec{c}}$ in (17.29), and also corrects the polarity error in the estimated sequence $\hat{\vec{c}}$ and data symbol $\hat{\vec{a}}$. The resulting estimated sequence is denoted by $\hat{\vec{c}}_{\text{signcorrected}}$.

The method presented can also be applied to Gold codes. Some pairs of $m$-sequences with the same degree can be used to generate Gold codes by linearly combining two $m$-sequences with different offsets in a Galois field. If the estimated generator polynomial can be decomposed into two preferred pairs of $m$-sequences, we can decompose the estimated generator polynomial into two $m$-sequences. For example, a Gold code generator $f(x) = 1 + x + x^2 + x^3 + x^4 + x^5 + x^6$ can be factored into $f_1(x) = 1 + x + x^3$ and $f_2(x) = 1 + x^2 + x^3$.

We use a matched filter operation between the intercepted signal $\vec{y}^s$ and the sign-corrected estimated sequence $\hat{\vec{c}}_{\text{signcorrected}}$ to estimate the symbol $\hat{\vec{a}}$. That is

$$
\hat{\vec{a}}_{\text{signcorrected}} = \text{sgn}(< \vec{y}^0, \hat{\vec{c}}_{\text{signcorrected}} >) \tag{17.37}
$$

However,

$$\hat{\bar{a}}_{\text{w/osigncorrection}} = \text{sgn}(< \vec{y}^0, \hat{\bar{c}} >)$$  (17.38)

To find the probability of error of the estimator in (17.37), we first find the probability of error of the symbol detector without the estimator of (17.38). After that, the probability of the symbol detector by the estimator (17.37) is analyzed. A symbol detector of a cooperative receiver ($R_x$) can be written as follows

$$\hat{\bar{a}} = \text{sgn}(< \vec{y}, \vec{c} >) = \text{sgn}(< \vec{c}\bar{a} + \sigma\bar{\bar{n}}, \vec{c} >)$$
$$= \text{sgn}(\bar{a} < \vec{c}, \vec{c} > + \sigma < \bar{\bar{n}}, \vec{c} >)$$  (17.39)

where $\bar{\bar{n}} \sim \mathcal{N}(0,1)$. Then the SNR of the cooperative receiver, $\gamma_{R_x}$ is

$$\gamma_{R_x} = \frac{<\vec{c}, \vec{c}>^2}{\sigma^2 \|\vec{c}\|^2} = \frac{P}{\sigma^2}$$  (17.40)

Therefore, the probability of error of the cooperative receiver with the known spread sequence $\vec{c}$ is [15]

$$P^a_{b,R_x} = \frac{1}{2}\text{erfc}\left(\sqrt{\frac{P}{2\sigma^2}}\right)$$  (17.41)

However, the SNR of the eavesdropper, $\gamma_e$ is

$$\gamma_e = \frac{<\vec{c}, \hat{\bar{c}}>^2}{\sigma^2 \|\hat{\bar{c}}\|^2} = \frac{<\vec{c}, \hat{\bar{c}}>^2}{\sigma^2 P}$$  (17.42)

Let $K$ denote the number of errors in the estimation of the spread sequence $\vec{c}$ of the length $P$. Then $K \sim \mathcal{B}(P, P^c_b)$. [6] The probability of error in the estimation of symbols with the estimator $P^a_{b,\text{signcorrected}}$ is then

---

[6] If the random variable $X$ is characterized by the binomial distribution with parameters $n$ and $p$, we write $X \sim \mathcal{B}(n, p)$. The probability of getting exactly $k$ successes in $n$ trials is given by the pdf (since $X$ is discrete, this is more accurately entitled a *probability mass function*):

$$f(k; n, p) = \Pr(X = k) = \binom{n}{k} p^k (1-p)^{n-k}$$

for $k = 0, 1, 2, ..., n$, where

$$P^a_{b,\text{signcorrected}} = \sum_{k=0}^{P-1} \frac{1}{2} \operatorname{erfc}\left[ (P-2k)\sqrt{\frac{1}{2\sigma^2 P}} \right] \Pr\{K = k\}$$

$$+ \frac{1}{2} \operatorname{erfc}\left( \sqrt{\frac{P}{2\sigma^2}} \right) \Pr\{K = P\} \qquad (17.43)$$

### 17.4.5 Verification and Validation

In this section, simulation examples are presented to illustrate the performance.

> **Example 17.3:** We consider information symbols modulated by an *m*-sequence with the generator polynomial $f(x) = 1 + x^2 + x^5$ of length $N = P = 31$. The signal constellation is BPSK and the number of data symbols is $L = 128$. The received signal is corrupted by AWGN with $\gamma = -10$dB. We assume the sampling rate of an eavesdropper is the chip rate $T_c$, but this is not required.
>
> First, we need to determine a synchronized version of the intercepted signal by (17.23). Figure 17.7(a) shows a desynchronized signal $\vec{y}^{k=26}$ delayed by $26T_c$. Therefore, a sample window $\vec{y}^{k=26}_{-1}$ contains the end of a symbol $a_{-1}$ for a duration of $5T_c$ followed by the beginning of the next symbol signal $a_0$ for a duration $26T_c$. A synchronized signal $\vec{y}^{k=0}_0$ by (17.23) is shown in Figure 17.7(b). Note that the desynchronized samples that belong to $a_{-1}$ are truncated. Figure 17.7(c) shows two synchronized sample windows for the purpose of comparison.

$$\binom{n}{k} = \frac{n!}{k!(n-k)!}$$
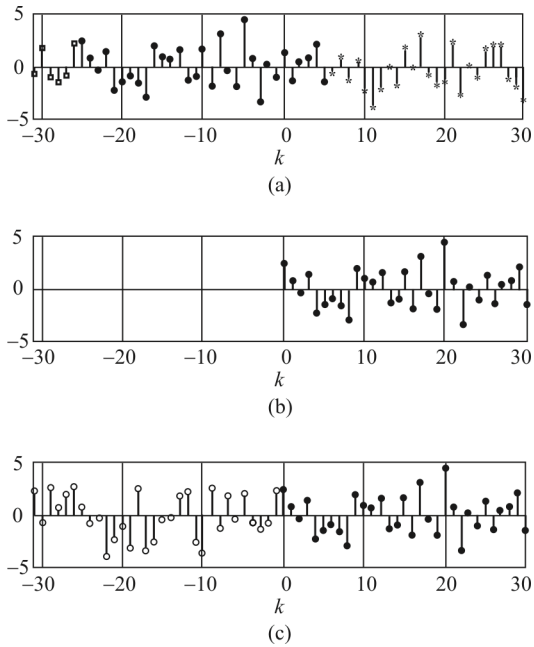
**Figure 17.7** Symbol synchronization by the spectral norm where $\epsilon$ denote $\vec{a}_{-1}$, ● denote $\vec{a}_0$, and $*$ denote $\vec{a}_1$, respectively. (a) Desynchronized signal $\vec{y}_0^{k=26}$, (b) synchronized signal $\vec{y}_0^0$, and (c) true signal $\vec{y}$.

(a)



(b)
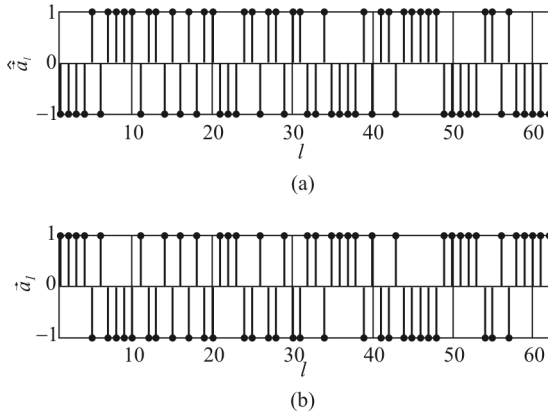
**Figure 17.8** Data symbol estimation by (17.26): (a) estimated data symbols $\hat{\bar{a}}$, and (b) true data symbols $\bar{a}$.
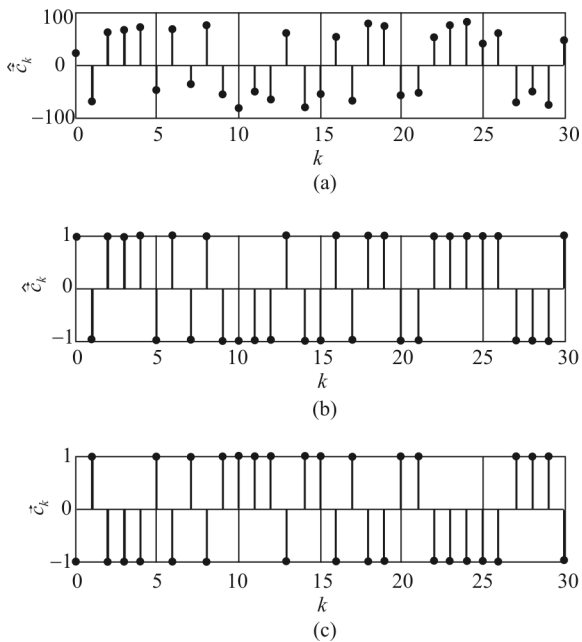


(a)



(b)



(c)

**Figure 17.9** Spread sequence estimation by (17.29): (a) noisy estimated sequence $\hat{\bar{c}}$, (b) estimated sequence $\mathrm{sgn}(\hat{\bar{c}})$, and (c) true sequence $\bar{c}$.

Second, estimations of data symbols and spread sequences are followed by the symbol synchronization. Figure 17.8 shows the first 62 estimated data symbols $\hat{a}$ by (17.26). Figure 17.9(b) shows the noisy estimated sequence $\hat{c}$ by (17.29). Note that the estimated data $\hat{a}$ in Figure 17.8(a) and the estimated sequence in Figure 17.9(b) are sign reversed versions of the true symbol $a$ and the true sequence $\vec{c}$, respectively. Therefore, $< \vec{c}, \hat{\vec{c}} > = -P$. We can correct polarity errors in the estimated data symbol $\hat{a}$ and the spread sequence $\hat{c}$ by the proposed estimator.

Third, we can correct polarity errors in the estimated data symbol $\hat{a}$ and the spread sequences $\hat{c}$ by the estimator. The estimator in Section 17.4.4 searches and tests a generator polynomial from the estimated sequence $\hat{c}$ by the recursion relation in (17.34) and the transform matrix in (17.35). Figure 17.10 shows the sign-corrected sequence $\hat{\vec{c}}_{\text{signcorrected}}$ and data symbol $\hat{a}_{\text{signccorrected}}$ by the estimator.

A simulation to evaluate the performance of the proposed estimator was performed. The generator polynomial used in this simulation is an *m*-sequence with $f(x) = 1 + x + x^{11} + x^{12} + x^{14}$ and the sequence is truncated, $P < N = 2^n - 1$ for comparison. Initial conditions were randomly seeded and randomly generated data symbols were corrupted by AWGN. The signal constellation was BPSK. Ten thousand simulation trials were carried out and averaged.

We compare $\Pr\{< \vec{c}, \hat{\vec{c}} > = P\}$ with the estimator and without the estimator. Figure 17.11 shows $\Pr\{< \vec{c}, \hat{\vec{c}} > = P\}$ with different combinations of the number of data symbols $L$ and the length of the spread sequence $P$. Note that the $\Pr\{< \vec{c}, \hat{\vec{c}} > = P\}$ corresponds to $\Pr\{K = 0\}$ without the estimator and $\Pr\{K = 0\} + \Pr\{K = P\}$ with the estimator. $\Pr\{< \vec{c}, \hat{\vec{c}} > = P\}$ increases as the number of the intercepted symbols $L$ increased and also increases as the length of the spread sequence $P$ increased. Therefore, $\Pr\{< \vec{c}, \hat{\vec{c}} > = P\}$ obtained by the estimator is almost two times greater than that without the estimator.

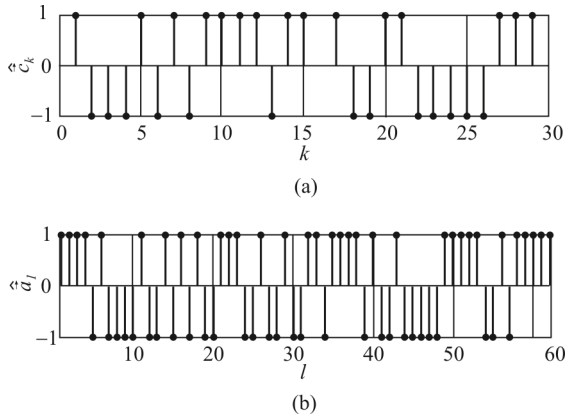**Figure 17.10** Sign corrected: (a) sign-corrected sequence $\hat{\hat{c}}$, and (b) sign-corrected data symbol $\hat{\hat{a}}$.
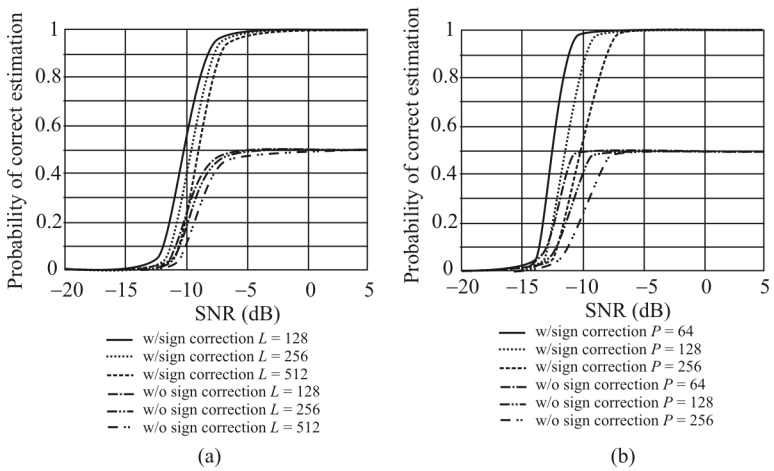


**Figure 17.11** Comparison of the probability of correct estimation of the spread sequence: (a) $P = 64$, and (b) $L = 512$.

**17.4.6 Summary**

In this section, we considered the implementation of a receiver for eavesdropping on an adversary's communication system that uses DSSS. To intercept such a system we need to

- Determine the symbol duration, which also serves as the method for detecting the presence of the DSSS signal. This is done by measuring the fluctuations of the signal.
- Identify the start position of a data symbol in the spread signal for symbol synchronization purpose.
- Remove the PN sequence.
- Estimate the PN sequence.
- Estimate the generator polynomial to determine the correct polarity of the spreading sequence.

We discussed effective methods to address these last four problems.

To identify the start position of a data symbol, a method was presented that uses the spectral norm of the sample covariance matrix. After symbol synchronization, a method based on the cross-correlation was used to estimate data symbols up to an unknown multiplicative factor. These estimated symbols were used by a matched filtering operation for identifying the PN sequence from the intercepted signal. In addition to obtaining the PN sequence and the data symbols, we considered an estimator to identify the PN code generator polynomial and to identify the polarity in the received signal.

We also analyzed the probability of error of the estimator in terms of SNR, the number of intercepted data symbols, and the length of the spread sequence. Our validation by simulation and theoretical analysis shows the effectiveness of the receiver topology.

# 17.5 Concluding Remarks

From the discussions in this chapter it is fairly obvious that blind, noncooperative interception of DSSS signals requires labor-intensive processes. The main requirement of a DSSS receiver is determining the spreading sequence of the spread signal. This is normally not known by a noncooperative EW system, so it must be estimated. We presented two methods for estimating this sequence; both begin with an estimate of the covariance matrix of the received data. Once the spreading sequence is determined, it can be used as the code in a DSSS receiver.

It should be noted that both of the techniques described in this chapter assume that the DSSS system employs short codes.

# References

[1]     Cook, C. E., and H. S. Marsh, "An Introduction to Spread Spectrum," *IEEE Communications Magazine*, March 1983, pp. 8–17.

[2]     Flikkema, P. G., "Spread-Spectrum Techniques for Wireless Communication," *IEEE Signal Processing Magazine*, May 1997, pp. 26–36.

[3]     Oppermann, I., P. Van Rooyen, and R. Kohno, "Spread Spectrum for Global Communications II," *IEEE Journal on Selected Areas in Communication*, Vol. 18, No. 1, January 2000, pp. 1–5.

[4]     Poisel, R. A., *Modern Communications Jamming Principles and Techniques*, 2nd Ed., Norwood, MA: Artech House, 2011.

[5]     Bouder, C., S. Azou, and G. Burel, "Performance Analysis of a Spreading Sequence Estimator for Spread Spectrum Transmissions," *Journal of the Franklin Institute,* Vol. 341, Issue 7, October 2004, pp. 595–617.

[6]     Jo, Y., and D. Wu, "On Cracking Direct Sequence Spread-Spectrum Systems," *Wireless Communications and Mobile Computing*, 2008, pp. 1–15.

[7]     Azzouz E. E., and A. K. Nandi, *Automatic Modulation Recognition of Communication Signl*s, Kluwer Academic Publishers: Boston, 1996.

[8]     Moulines, E., P. Duhamel, J-F. Cardoso, and S. Mayrargue, "Subspace Methods for the Blind Identification of Multichannel FIR Filters," *IEEE Transactions on Signal Processing*, Vol. 43, No. 2, February 1995, pp. 516–525.

[9]     Burel, G., and C. Bouder, "Blind Estimation of the Pseudo-Random Sequence of a Direct Sequence Spread Spectrum Signal," *Proceedings IEEE 21st Century Military Communications Conference*, IEEE MILCOM 2000, October 2000, Los Angeles.

[10]    Burel, G., "Detection of Spread Spectrum Transmissions Using Fluctuations of Correlation Estimators," *Proceedings IEEE International Symposium on Intelligent Signal Processing and Communication Systems* (ISPACS 2000), Hawaii, November 2000.

[11]    Simon, M. K., J. K. Omura, R. A. Scholtz, and B. K. Levitt, *Spread Spectrum Communications Handbook* (Revised Ed.), New York: McGraw-Hill, 1994.

[12]    Golomb, S. W., and G. Gong, *Signal Design for Good Correlation: For Wireless Communication, Cryptography, and Radar*. Cambridge University Press: New York, 2004.

[13]    Sarwarte D. V., and M. B. Pursley, *Cross-Correlation Properties of Pseudorandom and Related Sequences*, May 1980, Vol. 68, No. 5, pp. 593–619.

[14]    Poisel, R. A., *Modern Communications Jamming Principles and Techniques*, 2nd Ed., Norwood, MA: Artech House, 2011, Chapter 6.

[15]    Verdu, S., *Multiuser Detection*, Cambridge: Cambridge University Press, 1998.

# Chapter 18

## Receivers for Frequency Hopped Spread Spectrum Intercept

## 18.1 Introduction

Frequency hopping countermeasures are found in many VHF and UHF radios in use by military forces worldwide, including non-developed countries. As such, they become targets of concern for EW systems.

There are two basic needs to be fulfilled to intercept any signal successfully. First, the signal must be present within the detection band of the intercept receiver; second, the SNR must be adequate for the detection process to be successful. The first need is significant when the signal is a frequency hopper that occupies a small portion of the RF spectrum for a short time. A typical FH target may use 25 kHz of a 100 MHz band for as little as 2 msec before hopping to another frequency in the band. The hop period is normally fixed, while the sequence of hop frequencies is pseudo-random.

### 18.1.1 Signal Detection

The fundamental problem we are addressing here is the detection of the presence of an SOI and, in particular, an FHSS SOI. This is as opposed to the other detection problem in EW systems of detecting which symbol was transmitted; this is the information content problem. Detecting the presence of a signal is a signal *externals* problem. We have no interest in the content of the signal at this time.

Detecting signals in the presence of noise, and noise is always present in any realistic EW RF signal situation, can lead to erroneous decisions. Noise can occur that is of sufficient energy that it appears that a signal is present even when one is not. Likewise, the noise energy can be of a nature that it destroys the signal even when it is present (phase relationships have much to do with this). Thus, the problem is stochastic and can only realistically be dealt with in statistical terms.

Signal detection (perhaps incorrectly) occurs when the decision variable exceeds a detection threshold $\eta$. The two relevant hypotheses are given by

$$
\begin{aligned}
H_0: & \qquad r(t) = n(t) \\
H_1: & \qquad r(t) = s(t) + n(t)
\end{aligned}
\tag{18.1}
$$

When the decision variable is denoted by $R_{ij}$ (the purpose of the $i, j$ subscripts will become clear shortly), then *detection* occurs when $R_{ij} > \eta | H_1$. On the other hand, a *false alarm* results when $R_{ij} > \eta | H_0$. When $R_{ij} < \eta | H_1$ then a *missed detection* occurs. Last, when $R_{ij} < \eta | H_0$, then a correct decision is made as to no signal present.

This chapter is arranged as follows. We first present optimal architectures for implementing receivers for SFHSS targets and FFHSS targets. Being optimal, these receivers are not practical for actually constructing receivers due to their complexity. They do, however, form a basis against which other configurations can be measured. We next discuss the *filter bank combiner* (FBC) as a method for constructing FHSS receivers, including using the radiometer as the optimal detector for the FBC. Next we consider the scanning narrowband superheterodyne receiver that can be used for FHSS interception. Last, we discuss the CxRx as a fast-scanning wideband receiver. The CxRx presents a realizable, high-performance wideband receiver for FHSS intercept, both SFHSS and FFHSS. We present simulation and/or analytical results for all of the configurations considered.

# 18.2 Optimal Receivers for Frequency Hopped Spread Spectrum Interception

In the early 1990s JPL, under sponsorship of the U.S. Army, developed the architectures for receivers that optimally intercept FHSS signals [1–9].

The optimal *average likelihood ratio* (ALR) receiver for SFHSS signals is shown in Figure 18.1. In SFHSS, many $(>1)$ code symbols (typically MFSK, where $M = 2$) are transmitted on each hop of the carrier signal. These symbols can be coherent or incoherent. The ALR receiver implements a separate radiometer for each possible symbol pattern, given by $\varphi(d_l, t)$, at each possible carrier frequency as shown in Figure 18.1.

The optimal ALR receiver for receiving FFHSS signals is shown in Figure 18.2. In FFHSS, each symbol is transmitted many times $(> 1)$ on multiple carrier frequencies. Therefore the optimal MSE receiver consists of many parallel channels of radiometers, each one corresponding to each possible data sequence as
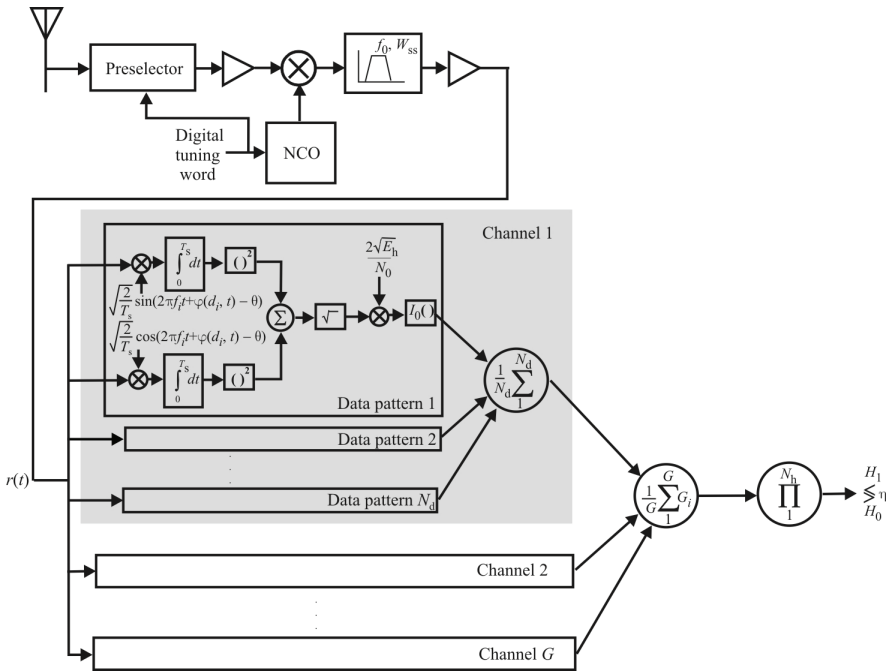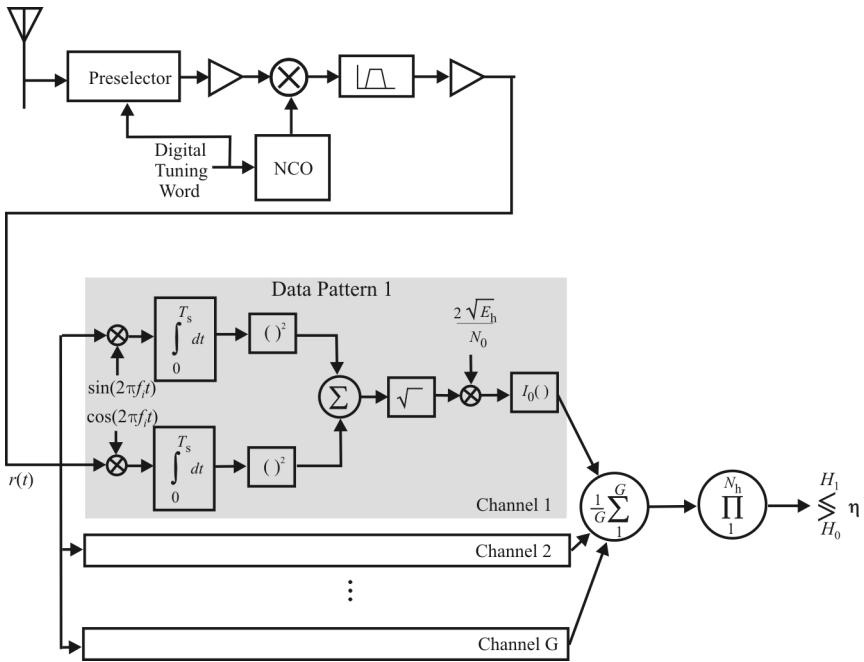
**Figure 18.1** Optimal ALR SFHSS receiver.

**Figure 18.2** Optimal ALR FFHSS receiver. $I_0$ is the modified Bessel function of first kind and 0th order.
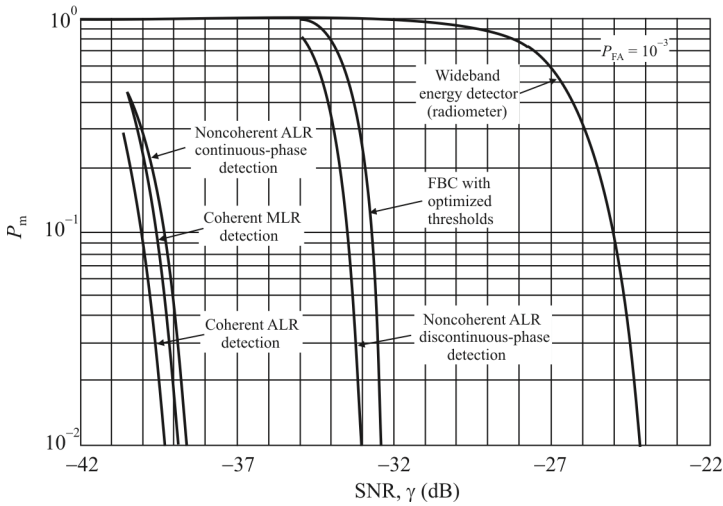
**Figure 18.3** SFH performance. $W_{ss}$ = 10 MHz, $R_h$ = 100 hps, $R_S$ = 10k sps, $T$ = 0.2 sec, $N_h$ = 20 consecutive hops, $N_S$ = 100 sph. ALR: average likelihood ratio, MLR: maximum likelihood ratio, FBC: filter bank combiner.

shown in Figure 18.2. These receivers optimally detect the presence of FHSS signals in an ALR sense.

These receiver architectures do not represent practical implementations, but rather exhibit the optimal architectures against which other realizations can be compared. The FFH architecture shown in Figure 18.2, for example, has a receive path for each possible data pattern. There are, however, suboptimal configurations based on these optimal topologies that perform almost as well and are considerably less complex (the FBC, discussed shortly, is one of these).

The performance of the optimum receivers as well as some other architectures are compared in Figure 18.3. These configurations are explained in the sections to follow. The SNR in Figure 18.3 uses the complete hopping range as the noise bandwidth. For example, if the hopping range is 10 MHz, and considering 25 kHz channels, then the narrowband (per hop) SNR corresponding to –42dB is $-42 + 10\log_{10} 10^7 - 10\log_{10} 25 \times 10^3 = -16\,\text{dB}$.

The total SS bandwidth is denoted as $W_{ss}$ (Hz), and the hop rate is specified as $R_h$ (hops per second). The hop swell time is given by $T_h = 1/R_h$. The dwell bandwidth is given by $W_m = W_{ss}/N_c$, where $N_c$ denotes the number of channels of width $W_m$ in $W_{ss}$. The detector observation window is given by $(0, T)$ and it is assumed that the observation interval contains an integral number $N_h = T/T_h$ of complete hops.
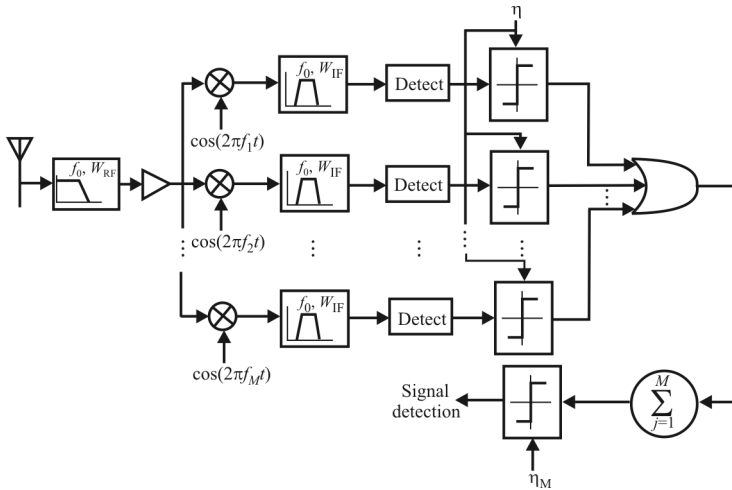
**Figure 18.4** Filter bank combiner.

## 18.3 Detection of Frequency Hopped Spread Spectrum Signals with Filter Bank Combiners

### 18.3.1 Introduction

We examine the performance of an FBC for the detection of FHSS signals in this section. The classical FBC [10, 11] uses an array of bandpass receivers to measure the received energy within each frequency channel over each hypothesized hop (referred to as a *frequency-time cell*) (Figure 18.4). The detectors can be of many varieties, two of which are shown in Figure 18.5. The radiometer is the most
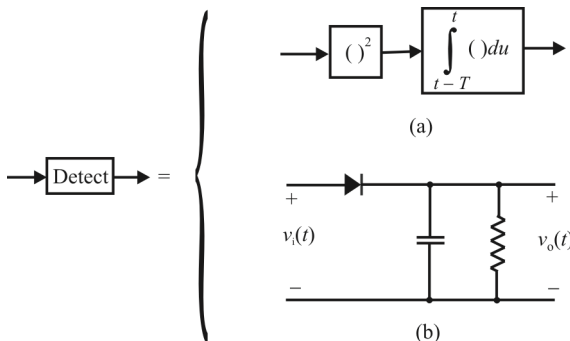


**Figure 18.5** Detectors: (a) radiometer and (b) envelope detector.
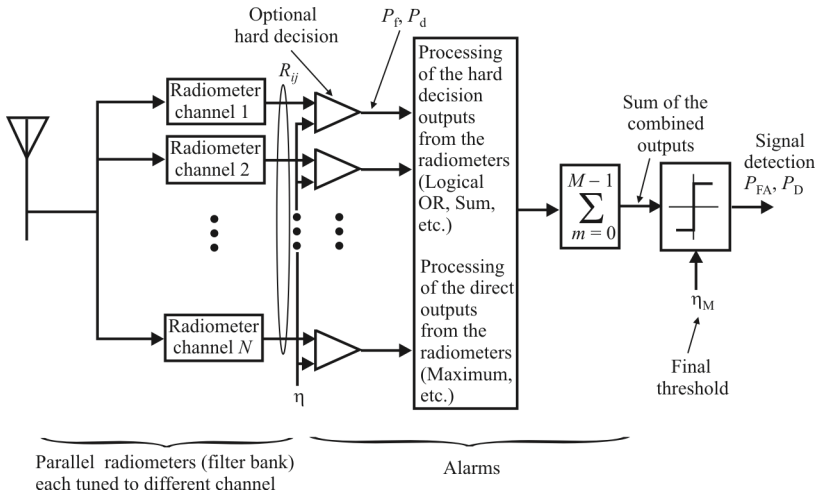
**Figure 18.6** Channelized radiometer flow diagram.

popular type of detector in common use and that's the configuration upon which we will concentrate. The FBC then compares each of these measured energies with a preselected threshold to make hard (1-bit) decisions as to whether a given frequency-time cell contains signal plus noise, logically ORs these bits over all frequency bins within each hop, and sums these outputs over all observed hops. The sum is then compared with a second threshold to decide between $H_0$ and $H_1$. The two thresholds must be jointly optimized to minimize $P_m$ for a particular $P_{FA}$ and received SNR.

The FBC is a suboptimal FH detector because it makes hard decisions within each frequency-time cell. However, it is operationally practical and performs almost as well as the optimum channelized receiver in the absence of a priori data modulation information that can be exploited for improved performance [12].

The term *channelized receivers* is frequently used to refer to the FBC. We will use both terms here, as they refer to the same topology. Also, when the FBC is implemented with radiometers, the term *channelized radiometer* is sometimes used.

The basic idea in channelized receivers is to use several parallel narrowband receivers simultaneously. The channelized radiometer uses multiple radiometers— that is, it integrates energy in many frequency bins simultaneously. It can be used, for example, for detection of an FHSS signal. Figure 18.6 shows the structure of a channelized radiometer-based detection system. The system has $N_C$ radiometers, which form a channelized radiometer, each with bandwidth $W_R$ and integration time $T_R$. The descriptions of the alarm topologies are addressed shortly. Basically, the local or preliminary decisions from the individual radiometers are combined

using, for example, a logical-OR operation. It is possible to sum several combined outputs to smooth the noise. These combined outputs from different integration intervals are summed. The output is compared with the second threshold $\eta_M$.

In a practical channelized radiometer implementation, instantaneous bandwidth may be smaller than the signal bandwidth. This may happen especially when the signal to be detected is an SS signal—for example, an FHSS signal. On the other hand, in some implementations, the number of radiometers may be limited. In systems with limited bandwidth, the simplest possibility is to use the same center (carrier) frequency at all times. Another possibility is to change the center frequency of the receiver—that is, to perform frequency sweeping. Rapid sweeping has been used for detecting SFHSS signals. Here, rapid sweeping refers to a situation where the duration that the receiver stays at a certain frequency is small relative to the time that the signal frequency is unchanged.

A radiometer is an energy (or power) measurement device, which was originally used and analyzed for (deterministic) signal detection [13]. It integrates energy (square of a voltage waveform) in a frequency band with bandwidth $W_R$ and alerts when the energy $V$ integrated over last $T_R$ seconds exceeds a threshold. When the radiometer is configured as integrate-and-dump, the radiometer output $V$ is sampled every $T_R$ seconds [14].

A channelized radiometer integrates energy in many bands simultaneously by using multiple parallel radiometers. A logical-OR function [10] to combine different radiometer outputs followed by summation of the last $M$ OR outputs is typically used for detection. This summing is sometimes referred to as *binary integration*. In block-by-block detection, summing is done over non-overlapping intervals. A final decision is made by comparing the sum value against another threshold $\eta_M$. It is also possible to use a sum instead of a logical-OR function to combine different radiometer outputs [7]. This is a good choice in a situation where multiple signals are expected to be present. If only one signal is present the system using a logical-OR has slightly better performance. In *binary moving-window* (BMW) detection, the summing is done in overlapping blocks.

In this section we examine interception and detection of SFHSS signals using a sweeping/stepping channelized radiometer. Two methods to combine the channelized radiometer outputs are analyzed: logical-OR-sum and max-sum. The first of these is a suboptimal FBC while the latter does not hard limit the radiometer decisions.

## 18.3.2 Receiver Structure

The signal to be detected is an SFHSS signal with $N_c$ non-overlapping hop channels. The hop bandwidth is $W_h$, the hop rate is $R_h$, and the hop duration is $T_h = 1/R_h$. The transmission could use, for example, BFSK modulation [2], which is a widely used type. The noise is assumed to be a white Gaussian process with two-sided psd $N_0/2$. The intercept receiver employs $N$ radiometers that form the
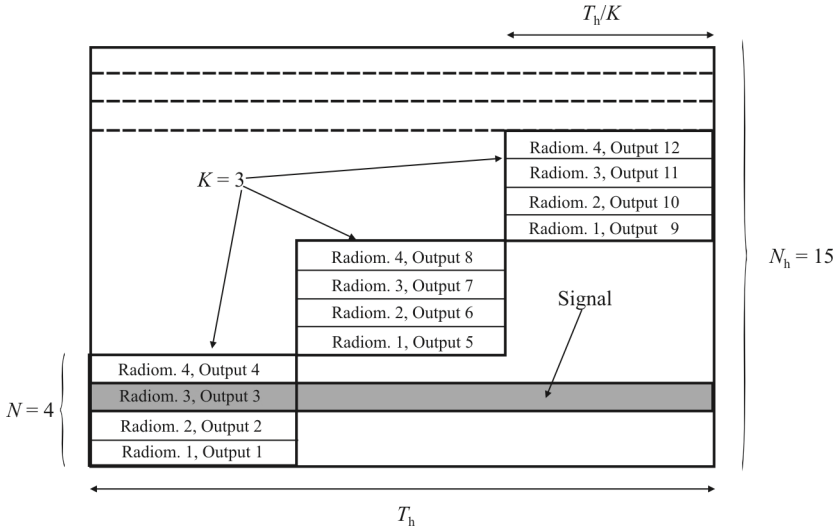
**Figure 18.7** The detection structure in the synchronous case, 15 possible hop channels, 4 radiometers, 3 detection phases, signal intercepted in the first phase by radiometer 3, $N_{\text{eff}} = 12$.

channelized radiometer, each with bandwidth matched to the SOI, $W_R = W_h$. The detector steps the received frequency band $K$ times within each hop such that the POI is increased. For example, if $R_h = 100$ hps ($T_h = 10$ ms), then the detector may be hopped in 1 ms increments corresponding to $K = 10$. For simplicity, we assume synchronization with the hop timing and that the frequency ranges of the individual radiometers match those of the hop channels. In practice, there is random splitting of the signal energy in both time and frequency. This can be approximately taken into account by adding energy loss $L_{t+f}$ (dB) to the required SNR found assuming no splitting; see [14] for a detailed analysis.

The total number of radiometer outputs within a hop duration is given by $N_{\text{eff}} = KN$. The output of a radiometer is the energy of the signal at the input within the bandwidth of the radiometer. These outputs are indexed so that in the first phase the outputs have indices $1, 2, \ldots, N$; in the second phase the outputs have indices $N + 1, N + 2, \ldots, 2N$, and so on. This detection structure is analytically equivalent to $N_{\text{eff}}$ radiometers with bandwidth $W_h$ and integration time $T_h/K$. Figure 18.7 illustrates the detection structure for the case of $K = 3$ detection phases per hop duration and $N = 4$ radiometers. Sweeping makes the instantaneous bandwidth large, but the integration time is reduced. The total number of hops observed before a decision is made is given by $M$. Since the hop position is random, the probability of intercept per hop is $p_I = N_{\text{eff}}/N_c \leq 1$. In the case shown in Figure 18.7, $p_I = 80\%$. The energy due to the signal in the time-frequency cell of the radiometer within which the signal occurs is given by $E_{ij} = E_h/K$, where $E_h$ is the

received energy per hop, $i$ is the hop index, $i \in \{1, 2, \ldots, M\}$, and $j$ is the radiometer output index, $j \in \{1, 2, \ldots, N_{\text{eff}}\}$. Thus the $i$, $j$ subscripts in the explanation after (18.1). In practice, this assumption is an approximation, since the signal may leak some energy also to adjacent radiometers. The time-frequency product of each individual radiometer is $T_R W_R = (T_h/K)W_h$ and the instantaneous bandwidth considering all radiometers is $W_h N$. In the following, it is assumed that $T_R W_R$ is an integer or that it is rounded to an integer. The normalized radiometer output is given by $R_{ij} = 2V_{ij}/N_0$, where $V_{ij}$ is the measured energy including the energy of the noise.

### 18.3.3 Radiometer Output Distribution

It is well known that under $H_0$, the distribution function of $R_{ij}$ can be approximated by the chi-square distribution with $2T_R W_R$ degrees of freedom [15, 16]. In the deterministic signal-and-noise case, the distribution can be approximated by the noncentral chi-square distribution with $2T_R W_R$ degrees of freedom and noncentrality parameter $\lambda = 2E_{ij}/N_0$.

The probability of false alarm, $P_f$, is the probability that the radiometer output exceeds a threshold when only noise is present. Individual radiometers have the probability of false alarm given by

$$P_f = \Pr\{R_{ij} > \eta | H_0\} = \int_\eta^\infty \frac{u^{T_R W_R - 1} e^{-u/2}}{2^{T_R W_R} \Gamma(T_R W_R)} du \tag{18.2}$$

where $\eta$ is the threshold and $\Gamma$ is the gamma function. Based on (18.2) we can calculate the threshold for the required probability of false alarm.

The probability of detection is the probability that threshold is exceeded under $H_1$—that is, $P_d = \Pr\{R_{ij} > \eta | H_1\}$. The probability of detection assuming a deterministic signal is

$$P_d = \Pr\{R_{ij} > \eta | H_1\} = Q_{T_R W_R}\left(\sqrt{2E_{ij}/N_0}, \sqrt{\eta}\right) \tag{18.3}$$

where $Q_L$ is the generalized Marcum's $Q$ function with parameter $L$ given by

$$Q_L(\alpha, \beta) = \frac{1}{\alpha^{L-1}} \int_\beta^\infty u^L e^{-(u^2 + \alpha^2)/2} I_{L-1}(\alpha u) du \tag{18.4}$$

where $I_N(u)$ is the modified Bessel function of the first kind. The SNR required for a given probability of detection can be approximated by

$$\frac{E_{ij}}{N_0} \approx \frac{1}{2}\left([\sqrt{\eta - (2T_R W_R - 1)/2} - Q^{-1}(P_d)]^2 - (2T_R W_R - 1)/2\right) \qquad (18.5)$$

where $Q^{-1}$ is the inverse of the tail integral of the normal distribution. This result is an accurate approximation, especially when $P_d$ is relatively high.

## 18.3.4 Channelization Techniques

An FFT can be used to approximate an ideal channelized radiometer. In such a case, an $N$-point FFT is taken every $1/W_h$ seconds so that the bin spacing corresponds to the FH channel separation [17]. There are $W_h(T_h/K)$ $N$-point FFTs per detection phase. Squared magnitudes of FFT bins corresponding to the same frequency are summed to get the channelized radiometer outputs. In this case, when only noise is present, the chi-square distribution is the exact result. If windowing is not used, there is a significant leakage—that is, narrowband signals leak energy to multiple FFT bins. If windowing is used, correlation arises between FFT bins so that there is also correlation between the final radiometer outputs, making analysis more awkward. Here the results are given for an ideal channelized radiometer.

## 18.3.5 Logical OR-SUM Channelized Radiometer

When hard 1-bit limiting is applied to the output of the radiometers, the outputs of the comparators will be a logical 0 or logical 1. A logical-OR operation can then be used to combine all $N_{eff}$ individual radiometric decisions in a hop. If any of the outputs exceeds the threshold, then its output will be a 1; all other outputs (subject to noise considerations) will be 0. If none of the radiometer outputs exceeds the threshold, then they all will be 0 (again, subject to noise considerations). The resulting probability of false alarm per hop when using logical-OR detection is

$$p_0 = 1 - (1 - P_f)^{N_{eff}} \qquad (18.6)$$

because false alarm occurs if at least one radiometer output exceeds the threshold. The probability of detection per hop is

$$p_1 = p_I\left[1 - (1 - P_d)(1 - P_f)^{N_{eff}-1}\right] + (1 - p_I)p_0 \qquad (18.7)$$

because at most one time-frequency cell (radiometer output) can have signal energy. The probability of this occurring is the probability of intercept, $p_I$. That is, $p_I$ is the a priori probability of the SOI being on any frequency in $T_h$. If the signal is not intercepted, the probability of detection is the false alarm probability. The

total probability theorem can be applied to combine these two mutually exclusive events to get the result (18.7). Since the hop positions are independent, the overall probability of false alarm is [11, 18]

$$P_{FA} = \sum_{m=\eta_M}^{M} \binom{M}{m} p_0^m (1-p_0)^{M-m} \tag{18.8}$$

where $\eta_M$ is the final threshold that is used after summing the last $M$ logical-OR outputs (see Figure 18.6). The overall probability of detection is

$$P_D = \sum_{m=\eta_M}^{M} \binom{M}{m} p_1^m (1-p_1)^{M-m} \tag{18.9}$$

### 18.3.6 MAX-SUM Channelized Radiometer

A maximum-based intercept receiver sums per hop maxima [19, 20]

$$\chi = \sum_{i=1}^{M} \chi_i \tag{18.10}$$

where $\chi_i = \max_j \{R_{ij}\}$. No threshold is applied directly at the output of the radiometers. In general, the maximum-based receiver is the best of the practical receivers considered in this section, assuming that the probability of intercept is sufficiently high. The optimal threshold does not depend on the SNR. Because the conditional pdfs under $H_1$ and $H_0$ are known [20, 21], we can calculate the corresponding raw moments.[1] Let $\mu_0^k = \mathcal{E}\{\chi_i^k\}$ denote the $k$th raw moment under $H_0$ and $\mu_1^k = \mathcal{E}\{\chi_i^k\}$ denote the $k$th raw moment under $H_1$. Under $H_0$ the mean $\kappa_1$, variance $\kappa_2$, and third central moment $\kappa_3$ of the per hop maximum are

$$\kappa_1 = \mu_0^1$$
$$\kappa_2 = \mu_0^2 - (\mu_0^1)^2$$
$$\kappa_3 = 2(\mu_0^1)^3 - 3\mu_0^1\mu_0^2 + \mu_0^3$$

---

[1] The raw moments are the moments of a stochastic variable assuming the mean is zero. The central moments of a random variable are those taken about the mean (i.e., the mean is not assumed to be zero).
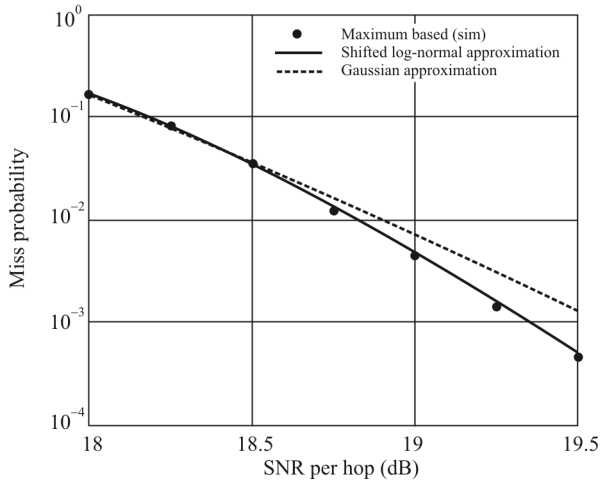
**Figure 18.8** Theoretical (Gaussian and shifted log-normal approximations) and simulated miss probabilities for the maximum-based channelized radiometer, 100 hops observed, 464 radiometers in the receiver, the signal has 2320 FH-channels, $K = 1$ (POI 20%), $P_f = 10^{-3}$, and the time-frequency product of the radiometers $T_R W_R = 250$.

The raw moments of the per hop maximum, when taking the POI per hop ($p_I$) into account, are given by $Z_0^k = p_I \mu_1^k + (1 - p_I) \mu_0^k$. The mean, variance, and third central moment can be calculated in a similar way as in the noise-only case. Now we know the mean, variance, and the third central moment of the sum (18.10) under $H_0$ and $H_1$, taking the POI into account. The shifted log-normal approximation that is matched to the first three central moments of the sum [22] was used. The shifted log-normal approximation is first used to obtain the threshold and then to obtain the probability of detection. The shifted log-normal approximation is especially useful when the number of observed hops is relatively small. Figure 18.8 shows a comparison of shifted log-normal and normal approximations.

## 18.3.7 Verification and Validation

For specificity, we assume that the target SOI has some parameters similar to those of the SINGCARS radio; namely, $W_h = 25$ kHz, $T_h = 0.01$ sec, and $N_c = 2320$ channels. Other parameters used here are $P_f = 10^{-3}$ and $N = 464$ channels in the receiver. The POI for these parameters is $p_I = KN/N_c = 0.2K$. For example, when $K = 1$, so that no sweeping is performed, $p_I = 0.2$. The other values examined are 0.4, 0.6, 0.8, and 1. We assume that the number of hops observed per decision correspond to a 3 sec transmission so that $M = 300$. The required SNR for a logical OR-sum-based channelized radiometer was calculated using procedures similar to
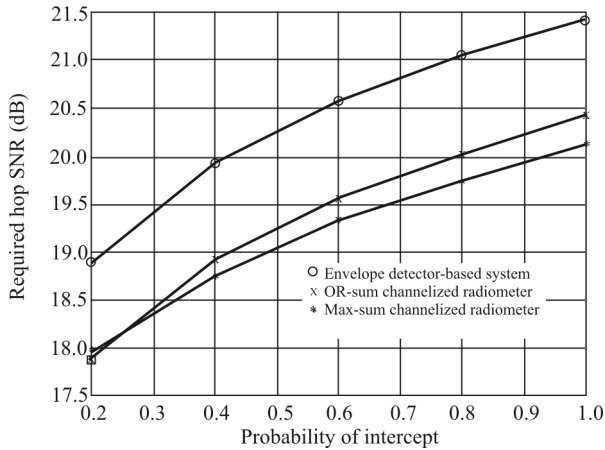
**Figure 18.9** Required hop SNR ($E_b/N_0$). $W_h = 25$ kHz, $T_h = 0.01$s, $N_c = 2320$, $M = 300$, $P_d = 0.999$,   $P_f = 10^{-3}$.

those in [18]. Optimal thresholds were found with search. The required SNR for the maximum based receiver was determined by using the shifted log-normal approximation.

For comparison purposes, the hard decision envelope detector was examined. In this case, the normal approximations were applied. After analytically solving (18.2) and (18.3) for $P_f$ and $P_d$, binomial inversion was used to obtain the required probabilities for individual envelope detector outputs. For simplicity, we assumed that each envelope detector output containing signal had equal signal components, although in practice, the strength of the signal components varies. When $p_I = 0.4$ the required SNR per FFT bin was –4.0466dB. The result is –4.05dB.

Figure 18.9 shows the required energy per hop to have $P_D = 0.999$ with an envelope detector, logical-OR-sum-based channelized radiometer, and maximum-based channelized radiometer. We observe from Figure 18.9 that the envelope detection is about 1 dB worse than the radiometer-based solutions. The maximum-based intercept receiver is the best of the receivers discussed here, except when POI is 20%. We can see that when the number of hops observed is large, sweeping does not increase the probability of detection. However, if the frequency band of the transmitter is unknown, some type of frequency sweeping (at least at the hop level) should be used. Otherwise, the POI can be vanishingly small.

## 18.3.8 Summary

In the previous sections we analyzed the logical-OR-sum channelized radiometer and max-sum channelized radiometer using frequency sweeping, so that there are multiple detection phases within each hop. The numerical results presented here,

for a slow frequency hopping signal having parameters similar to those of the SINGCARS radio, support the following conclusions:

- If the number of hops observed per decision is large, frequency sweeping decreases the performance compared to a system that does not apply frequency sweeping.
- The maximum-based intercept receiver has the best performance of the receivers discussed here unless the POI is small.

## 18.3.9 Partial-Band Detection

The implementations of wideband receivers as discussed in the previous section can be quite complex and therefore expensive for EW applications. Therefore, in practical implementations, hardware or real-time computational signal processing considerations may limit the detector bandwidth to $\rho_0 W_{ss}$, or, equivalently, $\rho_0 G$ FH channels, where $\rho_0 < 1$. Under this *partial-band detection* (PBD) limitation, only $\rho_0$ of the hops will be intercepted, assuming that all hops are equally likely. If the FH detection decision were only based on a single possible received hop, the probability of a miss, $P_m = \Pr\{H_0 | H_1\}$, could never be less than $1 - \rho_0$. However, the detector usually observes many received hops, $N_h \gg 1$, under $H_1$ so $P_m$ might still be acceptably small for a specified probability of false alarm, $P_{FA} = \Pr\{H_1 | H_0\}$. This leads us to the concept of a reduced-complexity FBC that observes only part of the SS band [23].

Consider the case when the receiver front end can be tuned so that the measured frequency band can be located anywhere within the total FH band. This allows several alternative operating modes ranging from minimum PBD to full-band detection. For example, assume that the receiver is consecutively tuned to $K$ non-overlapping bands (all within the received FH band assuming that the PBD factor or fraction of the entire SS band is covered, $\rho = K\rho_0 \leq 1$) for $1/K$ of each hop duration. If it is assumed that $\rho_0$ is an exact integer sub-multiple of 1 (i.e., $1/\rho_0$ is an integer), the possible discrete PBD factors are $\rho = \rho_0, 2\rho_0, \ldots, 1$.

The implied PBD tradeoffs can be illustrated by considering the two extreme cases. As noted earlier, in the minimum PBD mode $\rho = \rho_0$, where the FFT band remains fixed, only $\rho_0$ of the hops are intercepted. But when a hop falls into the FFT band, the detection metric can process the received signal energy over the entire hop. In particular, if hard decisions are made within each frequency-time cell as in the FBC structure, those hops that are intercepted will be detected more reliably than in the other candidate modes. However, the ultimate decisions as to whether an FH-hop signal has been received are based on an average of only $\rho_0 N_h$ intercept hops. By comparison, in PBD mode $\rho = 1$, the receiver covers the

entire FH band. An FBC type of detector makes less reliable hard decisions within each frequency-time cell since these are based on the received signal energy in only $\rho_0$ of the hop, but all $N_h$ hops are intercepted.

We consider here a modified implementation of an FBC, which is motivated by practical implementation considerations. We consider the PBD tradeoff issue in the context of hard-decision channelized receivers similar to a FBC with some significant differences. In place of the FBC array of radiometers, the channelization is achieved by an FFT preprocessor. The FFT frequency bin spacing $\Delta f$ corresponds to the FH channel separation $W_{ss}/G$, which implies that a new FFT is generated every interval $1/\Delta f$. The signal of interest is assumed to have *M-ary FSK* (MFSK) data modulation with an FFH carrier such that there is a single MFSK tone per hop in one of the $G$ possible FH channels. For hop-rate $R_h$, $N_s = \Delta f / R_h$ FFT samples are generated in each frequency band over each hop. Since this system parameter is independent of the FFT bandwidth $\rho_0 W_{ss}$, the performance would always be best at $\rho_0 = 1$. However, as argued earlier, this is not always a real-world option and it is assumed that $\rho_0$ is restricted to be an integer submultiple of 1.

Also unlike the FBC, to further reduce the computational load, the FFT amplitude samples are hard-quantized by comparing each with a threshold $\eta_1$. As in the FBC, though, hard decisions are made regarding the presence of the FH signal within each frequency-time cell. For PBD factors $\rho = K\rho_0$, these decisions are based on $N_s/K$ (more precisely, the integer part thereof) successive FFT samples. It has been shown that the asymptotically optimum classical *ALR test* (ALRT) detection metric [24] for producing these frequency-time cell hard decisions in the limit of small received SNR is to compare the Hamming weight of the sequence of $N_s/K$ FFT amplitude bits with a second threshold $\eta_2$ [25].

Some traditional idealized detector assumptions are employed to simplify the analysis. It is assumed that the FFT frequency bands coincide exactly with the possible received FFH/MFSK tones, so that when a hop is intercepted, all of the signal energy falls into a single FFT bin. It is also assumed that the receiver has perfect hop epoch timing information; that is, it knows when the received FH hop transitions occur. This allows *statistically independent* (SI) decisions to be made within each hop, which permits the performance to be determined analytically. Without this hop-timing assumption, a moving window Hamming metric has to be used in each FFT frequency bin resulting in correlated observables, the performance of which must be determined by computer simulation techniques [25].

Once hard decisions have been made in each frequency-time cell, a final decision regarding hypotheses $H_0$ and $H_1$ must be made based on the $\rho G$ observed frequency channels and $N_h$ possible received hops. ALRT analytical techniques are used to derive the asymptotically optimum detection rule for low SNRs resulting in yet a third threshold $\eta_3$. All three thresholds must be jointly optimized to yield
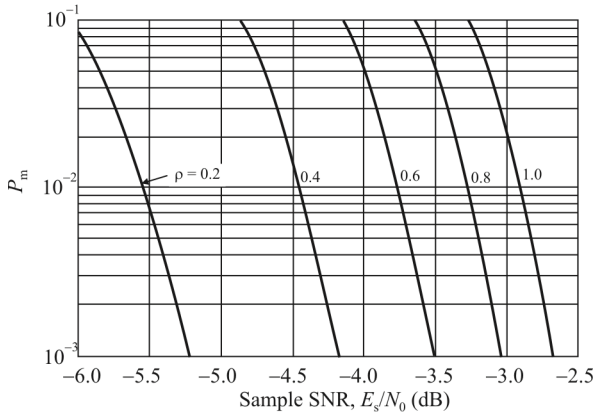
**Figure 18.10** PBD performance when $P_{FA} = 10^{-2}$.

the minimum $P_m$ for a given $P_{FA}$ and SNR. It can be shown that this approximate ALRT metric replaces the OR in the FBC by the Hamming-weighted sum of the 1-bit frequency-time cell decisions over all observed frequency channels, although this distinction may not be significant if $\eta_2$ is large enough to minimize the likelihood of exceeding this threshold in pure noise.

Finally, the detection performance is compared for all possible discrete PBD factors between $\rho_0$ and 1 to determine the optimum mode.

## 18.3.9.1 Verification and Validation

To illustrate the results of the analysis in [6], we use an example with characteristics similar to the SINCGARS system. In particular, $W_{ss} = 58$ MHz, $\Delta f = 25$ kHz, and $R_h = 100$ hps. Thus $G = 2320$ FH channels and $N_s = 250$ FFT samples/frequency bin/hop. When $\rho_0 = 0.2$, we have $\rho_0 W_{ss} = 11.6$ MHz or $\rho_0 G = 464$ frequency bins at a time. We assume that one third of each hop time is spent on each dwell, which is equivalent to examining 1392 channels at a time. When we observe a 3 second interval and must make a determination as to whether a signal is present or not, we have $N_h = 300$ hops.

We should note that the expressions for the PBD performance are a function of the SNR and the three thresholds $\eta_1$, $\eta_2$, and $\eta_3$. As noted, determining the optimum performance over all three thresholds requires that $P_m$ be jointly minimized over all three thresholds for each SNR and $P_{FA}$. It turns out that the optimum solutions are saddlepoints, meaning that they are independent of the order in which they are optimized. Furthermore, for a given choice of $\rho$, there are only minor variations in the set of optimizing thresholds over a wide range of $E_s/N_0$ and $P_{FA}$.
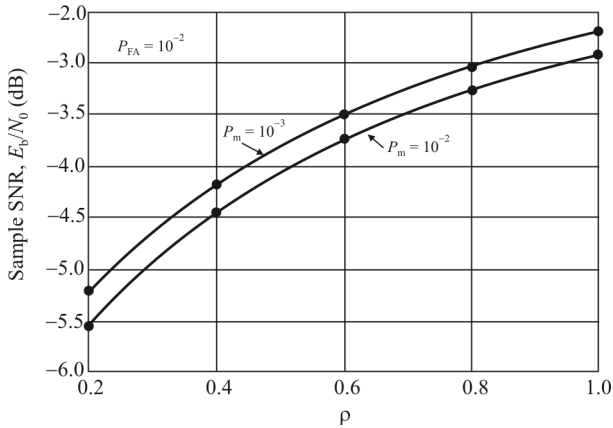
**Figure 18.11** PBD performance SNR versus $\rho$ when $P_{FA} = 10^{-2}$.

Performance results are shown in Figure 18.10 in the form of $P_m$ versus the sample SNR for various subband factors $\rho$ when $P_{FA} = 10^{-2}$. We can see that the best PBD strategy in terms of receiver sensitivity (the minimum SNR for the desired performance) is to use the minimum PBD factor, $\rho = \rho_0$. In addition, we can see that the performance is extremely sensitive to the received SNR—that is, for a given $P_{FA}$, $P_m$ changes by several orders of magnitude for a 1dB variation in $E_s/N_0$. The optimizing thresholds for a given PBD mode lie in the range $1.85 \le \eta_1 \le 1.86$, $71 \le \eta_2 \le 73$, and $3 \le \eta_3 \le 7$ for the $\rho = \rho_0 = 0.2$ curves in Figure 18.10. Similarly, for $\rho = 1$, the threshold ranges are $1.97 \le \eta_1 \le 1.99$, $\eta_2 = 19$, and $24 \le \eta_3 \le 38$.

The required sample SNR is shown in Figure 18.11 plotted versus the fractional bandwidth factor $\rho$ for two values of $P_m$ and for $P_{FA} = 10^{-2}$. The superiority of the fixed FFT band (i.e., $\rho = \rho_0$) approach is clearly evident, with SNR sensitivity advantages of approximately 1.1 to 2.6 dB over the available swept-FFT modes. Recall that the principal tradeoff between the PBD modes is the number of FFT samples and corresponding hard-decision reliability within each frequency-time cell (both highest at $\rho = \rho_0$) versus the number of hops intercepted (highest at $\rho = 1$). Therefore, we can say that for the assumed architecture in which independent hard decisions are made on each FFT sample and each frequency-time cell prior to the final asymptotically optimum ALRT decision between $H_0$ and $H_1$, it is more important to make reliable intermediated decisions on those hops that are intercepted than to try to intercept all of them.
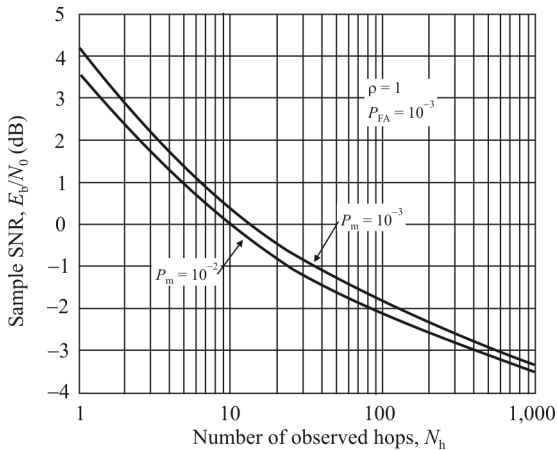
**Figure 18.12** PBD performance SNR versus number of hops when $P_{FA} = 10^{-2}$.

The sample SNR required is shown as a function of the number of observed hops, $N_h$ in Figure 18.12 for two values of $P_m$ and when $\rho = 1$ and $P_{FA} = 10^{-2}$. The case for $N_h = 1$ is particularly important for EW applications because a decision must be made on each and every hop as to the presence of a signal or not in order to apply resources (monitor receivers) to copy the transmission. Note that these monitor receivers need not necessarily be separate units, but could be digital receivers applied to the stored and delayed version of the intercepted signal in a frequency-time bin. Such architectures were explored in Chapter 7. Even in this case, however, in order to provide copy in real time, a signal-present decision must be made on each hop.

# 18.4 Scanning Superhet for Frequency Hopped Spread Spectrum Target Detection

### 18.4.1 Scanning Narrowband Receiver

The simplest automated signal search scheme is probably the scanning superheterodyne receiver, which is simply a superheterodyne receiver whose frequency is linearly changed with time. Most modern tuned superheterodyne receivers are digitally controlled for maximum flexibility. They can be controlled directly with an RCU or via computer as required. These receivers actually dwell on a frequency channel as opposed to scanning as in an analog equivalent. The scanning detector structure in this case is as illustrated in Figure 18.13 when $K = 3$.
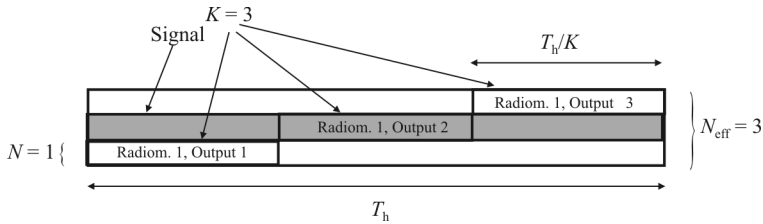
**Figure 18.13** Scanning detector structure for a single channel receiver.

This type of receiver is used for scanning the frequency spectrum, looking for energy in channels. Thus, frequencies of SOIs as well as estimates of their amplitudes can be determined. Scanning receivers of this type have long been used to implement spectrum analyzers, a common piece of RF electronic test equipment.

### 18.4.1.1 Analog Scanning Narrowband Receivers

A flow diagram of such an analog receiver is shown in Figure 18.14. The frequency of the VCO is controlled with a linearly increasing sawtooth waveform. Torrieri [26] provided a detailed analysis of this receiver.

The mixer combines the incoming RF signals with the signal from the sweeping LO. The preselector filters must also be tuned along with the LO. A narrowband signal at the input will be mixed whenever the LO tunes to the IF offset from the signal (recall that the mixer output is a constant frequency). At that point in time the AM detector will detect the peak amplitude of the signal and the peak detector will measure the amplitude. By measuring where the peak occurs in time, that time can be compared with where the scanning LO is at that time so a frequency estimate can be computed.
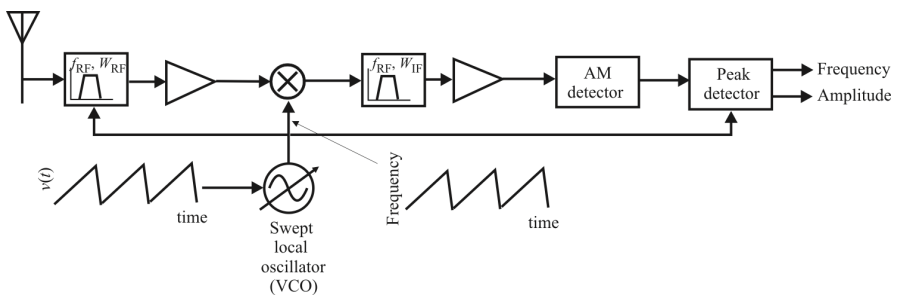


**Figure 18.14** Simplified flow diagram of a scanning analog superheterodyne receiver.
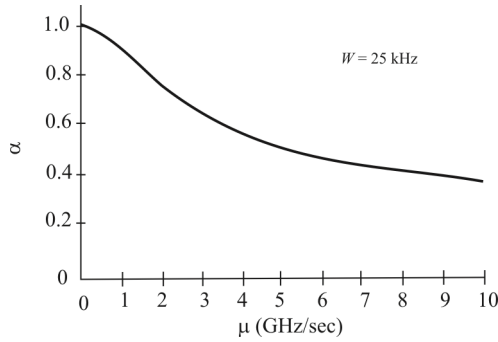
**Figure 18.15** Scanning superheterodyne receiver normalized peak value when $W = 25$ kHz.

As derived in [26], if $\mu$ represents the scanning rate of the receiver in Hertz per second and $W$ represents the 3dB bandwidth of the bandpass filter after the mixer, the normalized peak value $\alpha$ (normalized relative to the amplitude of the input signal) is given by

$$\alpha = \left( 1 + 0.195 \frac{\mu^2}{W^4} \right)^{-1/4} \tag{18.11}$$

and the frequency resolution is given by

$$\Delta = W \left( 1 + 0.195 \frac{\mu^2}{W^4} \right)^{1/2} \tag{18.12}$$

These expressions are plotted in Figures 18.15 and 18.16 when the bandpass bandwidth is 25 kHz. Thus the normalized amplitude peak value decreases as the
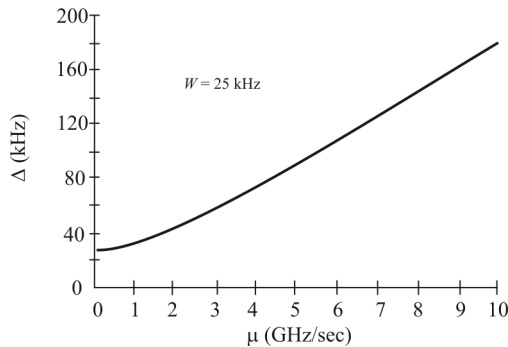


**Figure 18.16** Scanning superheterodyne receiver frequency resolution when $W = 25$ kHz.
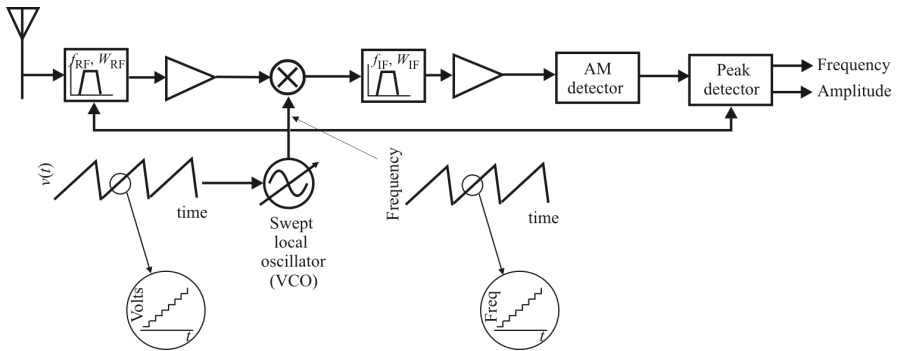
**Figure 18.17** Simplified flow diagram of a scanning digital superheterodyne receiver.

scan rate increases while the resolution increases in bandwidth (decreases in selectivity).  In a dense RF environment, a resolution bandwidth of less than 50 kHz or so is desirable in order to minimize adjacent channel interference.  Thus in the military VHF range where the signals typically have a bandwidth of 25 kHz, the scanning rage must be kept at about 3 GHz per second or less in order to maintain the required resolution.

18.4.1.2 Digital Stepping Narrowband Receivers

The frequency resolution achievable with a digitally tuned narrowband receiver is inversely proportional to dwell time. For example, if the receiver dwells at a frequency for 10 ms and the instantaneous bandwidth of the receiver is 200 kHz, then the maximum channelization possible is to divide the 200 kHz bandwidth into 200 1 kHz cells.

   The simplified flow diagram for the digital superheterodyne receiver is shown in Figure 18.17. As shown, the waveforms that control the instantaneous frequency appear to be a sawtooth. With an analog receiver, these may actually be sawtooth waveforms, but with modern, digitally controlled receivers, they are approximations to sawtooths as shown in Figure 18.17. The LO is tuned to a frequency and dwells there for a period of time before moving to the next frequency. In fact, with digitally controlled receivers, the sequence of frequencies need not be linear as implied by the sawtooth but could be anywhere in the frequency spectrum covered by the receiver.

   The receiver frequency versus time is thus shown in Figure 18.18(a). The digital stepping superheterodyne receiver measures the energy at a single frequency bin at any given time. Detection occurs if and only if there is coincidence between the scanning frequency and the frequency of the FHSS system. One of these coincidences is shown in Figure 18.18(b). The details of a coincidence are illustrated in Figure 18.18(a), where offsets in time and frequency
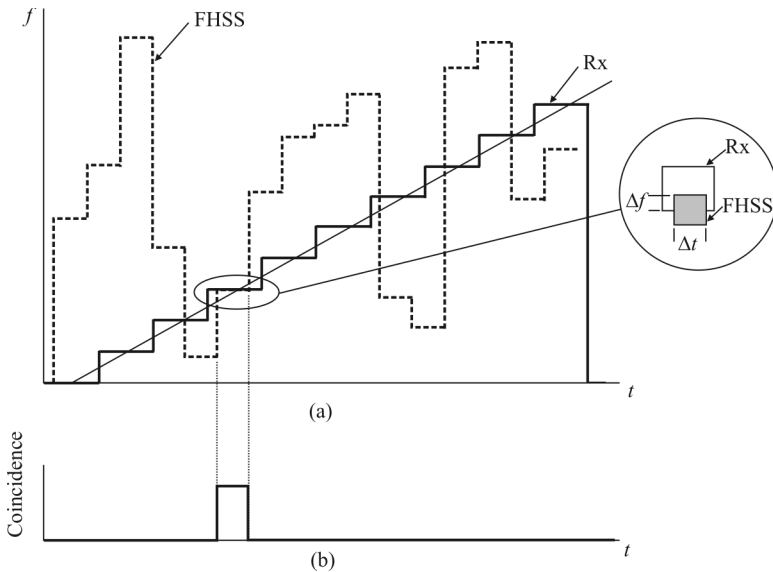
**Figure 18.18** Coincidence of pulse trains.

are illustrated. The receiver has a finite bandwidth for each dwell as does the SOI FHSS system. In addition, the timing of the receiver dwell in general is not the same as the FHSS dwell timing. It is generally assumed that these offsets are negligible in order to make analysis tractable. We assume here that the overlap of the receiver dwell and FHSS dwell are sufficient so that reliable detection results when coincidence occurs.

The biggest performance difference in the analog and digital implementation of scanning/stepping is the resolution reduction characteristics as the sweep speed increases. The characteristic for analog receivers is illustrated in Figure 18.16 while the resolution reduction for stepping digital receivers is shown in Figure 18.19. The faster the receiver steps (shorter dwell time per frequency), the frequency resolution decreases (the resolvable bandwidth increases).

There is obviously a dependence on the hop rate that is detectable with stepping superhet with a given dwell time. For example, if the dwell time is 1 ms, the frequency resolution is approximately 1 kHz, but there are 2400 25 kHz channels between 30 and 90 MHz. It would take 2.4 sec to scan this entire range at a 1 ms dwell time rate, clearly too slow to track even the slowest hopping radios.

## 18.4.2 Performance of Scanning Superhet Receivers

We will assume that the scanning/stepping superheterodyne receiver is the RF portion of the FHSS detection receiver, which is followed by a radiometer for
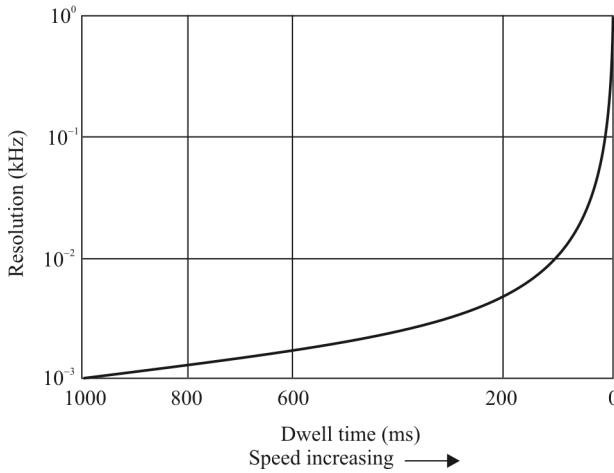
**Figure 18.19** Digital stepping superheterodyne receiver frequency resolution.

signal detection processing (Figure 18.20). The performance of such a scanning superheterodyne receiver with a radiometer measuring its predetected output is indicated by the above results for the channelized radiometer when the number of channels is equal to one, as this is the number of channels available at any instant.

As above, using the logical OR-SUM approach with $N_{eff}$ individual radiometric decisions in a hop, the probability of false alarm per hop is

$$p_0 = 1 - (1 - P_f)^{N_{eff}} \tag{18.13}$$
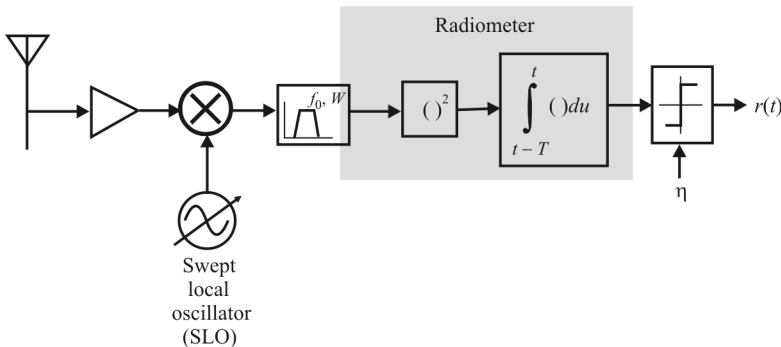


**Figure 18.20** A radiometer embedded in a stepping receiver. (Source: [29], ©Artech House, 2011. Reprinted with permission.)

The probability of detection per hop is

$$p_1 = p_I \left[ 1 - (1 - P_d)(1 - P_f)^{N_{eff} - 1} \right] + (1 - p_I) p_0 \qquad (18.14)$$

because at most one time-frequency cell (radiometer output) can have signal energy. The probability of this occurring is the probability of intercept, $p_I$. Again, the total probability theorem can be applied to combine these two mutually exclusive events to get the result (18.14). The final probability of false alarm is

$$P_{FA} = \sum_{m=\eta_M}^{M} \binom{M}{m} p_0^m (1 - p_0)^{M-m} \qquad (18.15)$$

where $\eta_M$ is the final threshold that is used after summing the last $M$ logical-OR outputs (see Figure 18.6). The final probability of detection is

$$P_D = \sum_{m=\eta_M}^{M} \binom{M}{m} p_1^m (1 - p_1)^{M-m} \qquad (18.16)$$

The results for the parameters shown in the caption of Figure 18.21 are illustrated in the figure. This example would correspond to a 1000-channel SFH (100 hps) FHSS system where the receiver dwells at each bin for 1 ms. We can see that for the parameters used, the detection probability is less than 1% for all values of $P_d$ considered. While a scanning narrowband receiver is a viable method for searching and detecting single channel communication systems, it is obvious from Figure 18.21 that it is inadequate for intercept of FHSS systems.

### 18.4.3 Sequential versus Nonsequential Scanning

It is to be noted that the strategy of linearly scanning the receiver through the frequency cells may not be the best strategy. Krasner showed that an optimum strategy based on linear programming can produce better (shorter time) detection results [27]. This is illustrated in Figure 18.22.
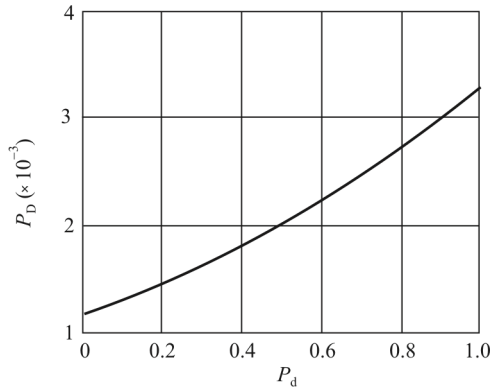
**Figure 18.21** Scanning performance when $N_c = 1000$, $M = 100$, $K = 10$, $P_f = 10^{-2}$, $N = 1$.
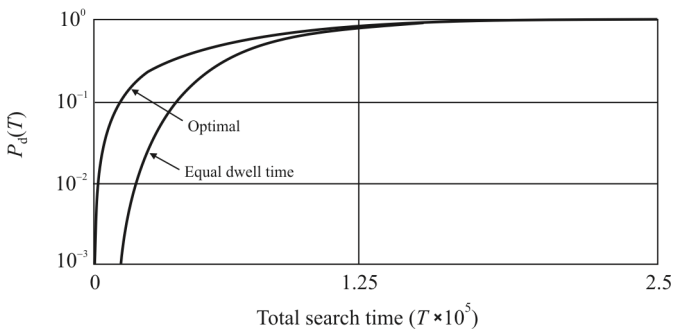


**Figure 18.22** $P_d$ for optimal dwell times and equal dwell times. Input SNR = −10 dB, a priori probability = 0.04, total search time = 250,000, $\alpha = 5$, yielding $P_{FA} = 10^{-5}$. (Source: [30]. ©Artech House, 2011. Reprinted with permission.)

# 18.5 Compressive Receivers for Frequency Hopped Spread Spectrum Interception

### 18.5.1 Compressive Receiver

A compressive receiver (CxRx) is an alternative to channelized receivers. Its use for detecting FFH signals has been examined by Snelling and Geraniotis [28] and we include their relevant characteristics here. As discussed in Chapter 6, in a CxRx, the signal is mixed with a chirp-type signal (linearly increasing or decreasing in frequency) and is filtered with a matching pulse compression filter.

Figure 9.1 is the flow diagram of a CxRx. The SLO expands the signal over a band equal to the width of the sweep. The DDL, with a delay versus frequency slope that is the inverse to the sweep ($\mu$), compresses the expanded signal, producing pulses at times and amplitudes proportional to the spectral components of the input signal. That is, the output time axis corresponds to the input frequency axis while the output amplitude axis corresponds to the input amplitude axis. A logarithmically detected display of the output appears like that of a typical spectrum analyzer display.

Using the typical signal previously described for illustration, the CxRx must sweep 100 MHz ($W_s$) in 2 msec ($T_s$) to guaranteee that the signal will appear in the CxRx no matter what the frequency is during that time.[2] This implies a sweep rate of $\mu = 50$ MHz/ms $= 2\pi \times 50 \times 10^9$ rad/s$^2$.

If we wish to distinguish each hop—it is important to recognize that a signal is a hopper—then the CxRx must have a resolution of 25 kHz or less (low VHF channelization is 25 kHz). The resolution will be determined by the DDL's dispersion and weighting functions. An unweighted line results in a resolution equal to the inverse of the dispersion time ($T_D$). Common weighting (used to reduce the sidelobe responses of the delay line that appear in nearby channels) results in approximately a 50% decrease in resolution by widening the width of the response (Table 9.3). These weighting functions are also called *window functions* and are normally applied in the time domain. Therefore, to achieve 25 kHz weighted resolution an unweighted resolution of 6.7 kHz would be needed, which results from a dispersion of 60 $\mu$sec. [Resolution $\approx 1/(60 \times 10^{-6}) \times 1.5$.]

It is necessary to calculate the bandwidth required of the DDL so that it can be determined that the line can be built and what integration gain will be realized. The DDL bandwidth ($W_D$) is the product of the sweep rate and the dispersion,

---

[2] This timing, of course, neglects any time that may be necessary to process the signal, such as for parameter extraction. When this is included the scan speed will be considerably faster. Alternately, a separate receiver module can be tuned, based on the CxRx signal detection, to extract such parameters, which reduces the speed requirements on the CxRx. The receiver module synthesizer tuning speed (and settling time) must also be included in that case.

which for our example results in a bandwidth of 3 MHz. A 3 MHz by 60 μsec line is well within the realm of producibility.

The processing gain given by $10 \log_{10}(T_D W_D)$ is

$$10 \log_{10}(60 \times 10^{-6} \times 3 \times 10^{6}) = 23\,\text{dB}$$

This probably is not acceptable, because the target receiver will have a processing gain of 36 dB on the basis of noncoherent bandwidth reduction alone $[36\,\text{dB} = 10 \log_{10}(100 \times 10^{6} / 25 \times 10^{3})]$. (This is called the FHSS *processing gain*.) This implies the eavesdropper will be at a 13dB range disadvantage. Since ground-ground signal propagation causes about 12dB/octave (doubling of distance) signal level loss, the target network will have about a $2\times$ range advantage.[3] CxRx processing gain can be increased by choosing a DDL with greater bandwidth and sweeping the DDL faster. Table 9.1 lists the typical characteristics of a CxRx that would easily fulfill the receiver requirements to intercept this signal. In fact, this receiver could intercept a signal hopping at a 2k Hz rate.

### 18.5.2 Noise and Signal

18.5.2.1 Input Signal Model

The FHSS waveforms have the form

$$s(t) = \sum_{i=1}^{N_h} v_i(t) \tag{18.17}$$

where

$$v_i(t) = \sqrt{2\overline{S}} \, \sin(\omega_k t + \theta_i) \ \text{ for } iT_h \le t \le (i+1)T_h$$

$\{w_k\}_{k=1}^{K}$  is a family of known frequencies within the SS
$\{k_i\}$     are integer valued, independent, uniformly distributed random variables ranging between 1 and $K$ inclusively
$\{\theta_i\}$     are continuous, independent, uniformly distributed random variables ranging between 0 and $2\pi$ that represent carrier phase
$\overline{S}$       is the average signal energy

---

[3] Airborne targets against ground-based interceptors, and vice versa, have about a 9dB/octave loss and air-to-air target interceptor links have about a 6dB/octave loss.
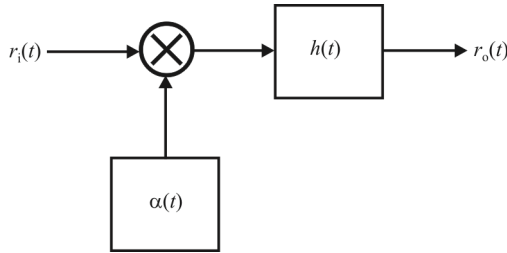
**Figure 18.23** Compressive receiver model.

$T_h$       is the epoch, or time duration, of each hop
$N_h$       is the number of hops during message transmission

As above, the signal detection problem is a composite hypothesis problem. Specifically, given the observation $r(t)$, the problem is one of choosing between $H_0$, which is the hypothesis that an FHSS waveform is not present, and $H_{\gamma'}$, which is the hypothesis that an FHSS waveform is present with SNR $\gamma'$ greater than some minimum SNR $\gamma$. The model is precisely

$$H_0: \qquad r(t) = n(t)$$

versus                                                                                            (18.18)

$$H_{\gamma'}: \qquad r(t) = s(t) + n(t), \ \ \gamma' > \gamma$$

where the frequency-hopped waveform $s(t)$ is given by (18.17) and $n(t)$ is stationary colored Gaussian noise with variance $\sigma_i^2$ and autocorrelation function $\sigma_i^2 R_i(t)$ (the subscript i means "input" as will become relevant later). The hypothesized SNR $\gamma'$ is related to the other model parameters by $\gamma' = \bar{S}T_h / \sigma_i^2$, while similarly the minimum SNR $\gamma = ST_h / \sigma_i^2$.

The signal model allows for colored noise and is, therefore, quite general. Note that the model assumes that all signal parameters (especially timing epoch), except for amplitude and hop frequency, are known.

18.5.2.2 Receiver Model

The model of the compressive receiver we use for this analysis is shown in Figure 18.23. The compressive receiver mixes the input signal $y_i(t)$ with a linearly frequency-modulated signal

$$\alpha(t) = \cos(\omega_0 t - \mu t^2), \qquad 0 \leq t \leq T_s \tag{18.19}$$

$\alpha(t)$ scans downward in frequency from $\omega_0$ to $\omega_0 - 2\mu T_s$, where $T_s$ is the scan time. The scanned waveform is input to a pulse compression filter whose impulse response, $h(t)$, is given by

$$h(t) = \cos(\omega_0 t + \mu t^2)w(t), \quad 0 \le t \le T_c \tag{18.20}$$

where $w(t)$ is a weighting function used to minimize energy spillover into adjacent and nearby RF channels [$w(t)$ is assumed piecewise continuous and of bounded variation]. The output of the compressive receiver is then given by

$$r_o(t) = \int_0^{T_c} \alpha(t-\tau)r_i(t-\tau)h(\tau)d\tau, \qquad T_c \le t \le T_s \tag{18.21}$$

$$= \begin{cases} n_o(t) & \text{under } H_0 \\ s_o(t) + n_o(t) & \text{under } H_{\gamma'} \end{cases} \tag{18.22}$$

where

$$s_o(t) \triangleq \int_0^{T_c} \alpha(t-\tau)s_i(t-\tau)h(\tau)d\tau, \qquad T_c \le t \le T_s \tag{18.23}$$

$$n_o(t) \triangleq \int_0^{T_c} \alpha(t-\tau)n_i(t-\tau)h(\tau)d\tau, \qquad T_c \le t \le T_s \tag{18.24}$$

### 18.5.2.3 Output Due to Signal

Using (18.19), (18.20), and the commuted version of (18.23), the output of the compressive receiver can be expressed as

$$s_o(t) = \int_{t-T_c}^{t} s(\tau)\cos(\omega_0 \tau - \mu \tau^2)\cos[\omega_0(t-\tau) + \mu(t-\tau)^2]w(t-\tau)d\tau \tag{18.25}$$

whenever $T_c \le t \le T_s$.

### 18.5.2.4 Output Due to Noise

If

$$\omega_0 > 2\mu T_s + \mu T_c$$

the normalized autocorrelation (normalized to $\sigma_i^2$) of the compressive receiver output when the input noise is white,[4] that is,

$$\sigma_i^2 R_i(t) = \delta(t) N_0 / 2$$

then the output noise is stationary and has autocorrelation [28]

$$R_o(d) = \frac{1}{16} \int_{|d|}^{2T_c - |d|} \cos[|d|(\omega_0 + \mu u)] \times w\left(\frac{u + |d|}{2}\right) w\left(\frac{u - |d|}{2}\right) du \qquad (18.26)$$

Furthermore, under these same conditions and if the window function $w$ is rectangular, then the output noise is stationary and has autocorrelation

$$R_o(d) = \begin{cases} \dfrac{1}{8} \dfrac{\sin[\beta|d|(T_c - |d|)]}{\mu|d|} \cos[|d|(\omega_0 + \mu T_c)], & |d| \le T_c \\ 0, & \text{otherwise} \end{cases} \qquad (18.27)$$

## 18.5.3 Low SNR Detector

The goal is to develop a detector of FHSS waveforms that is valid at low SNRs, based on a CxRx output. Since the optimal detector of FHSS waveforms integrates coherently over a single hop period, we expect that an optimally configured CxRx should integrate over a period commensurate with the hop epoch $T_h$. But we also want to avoid interhop interference. Thus, we choose $T_s = T_h$, and assume that the CxRx is synchronized to frequency-hopping epochs. This is not a realistic assumption in reality but one that leads to an optimum detector, whose performance degrades gracefully upon relaxing this assumption.

Because the interfering noise is typically of much larger bandwidth than the hop rate, the correlation between hops is negligible, and so the optimal multihop detection statistic is some kind of combination of single-hop detection statistics. We thus confine ourselves to the problem of using the CxRx to optimally detect, given an observation period of $T_s$, a sine wave of unknown amplitude and phase and whose frequency is one of the known hop frequencies.

Based on the above assumption, the detection problem is now

$$H_0 : r_i(t) = n_i(t)$$

---

[4] Since the variance of a white noise process is undefined, letting $\sigma_i^2 = N_0$, where $N_0/2$ is the two-sided density of the white noise process, makes the SNR, $\gamma$, consistent with other definitions in the literature.

versus

$$H_{\gamma'} : r_i(t) = \sqrt{2S}\,\sin(\omega_k t + \theta) + n_i(t) \tag{18.28}$$

where $S$ corresponds to the average signal energy corresponding to the minimum SNR, and $\gamma < \gamma'$ and $T_c \le t \le T_s$. The parameters $\theta$, $\gamma'$, $\omega_k$, and $n_i(t)$ are as defined in Section 18.5.2.1.

The detection problem based on the output of the compressive receiver is thus

$$H_0 : r_o(t) = n_o(t)$$

versus $\tag{18.29}$

$$H_{\gamma'} : r_o(t) = \sqrt{2\overline{S}}\,\cos\theta s_c(t,\omega_k) + \sqrt{2\overline{S}}\,\sin\theta s_s(t,\omega_k) + n_o(t)$$

For $\gamma < \gamma'$ and $T_c \le t \le T_s$, where $n_o(t)$ is stationary, colored Gaussian noise with autocorrelation function $R_o(d)$ is defined by (18.26) and

$$
\begin{aligned}
s_c(t,\omega_k) \triangleq &\frac{1}{2}\cos(\omega_0 t + \mu t^2)\int_{t-T_c}^{t}\cos(\omega_k t)\cos(2\mu t\tau)w(t-\tau)d\tau \\
&+\frac{1}{2}\sin(\omega_0 t + \mu t^2)\int_{t-T_c}^{t}\cos(\omega_k t)\sin(2\mu t\tau)w(t-\tau)d\tau
\end{aligned}
\tag{18.30}
$$

$$
\begin{aligned}
s_s(t,\omega_k) \triangleq &\frac{1}{2}\cos(\omega_0 t + \mu t^2)\int_{t-T_c}^{t}\sin(\omega_k t)\cos(2\mu t\tau)w(t-\tau)d\tau \\
&+\frac{1}{2}\sin(\omega_0 t + \mu t^2)\int_{t-T_c}^{t}\sin(\omega_k t)\sin(2\mu t\tau)w(t-\tau)d\tau
\end{aligned}
\tag{18.31}
$$

For low SNR conditions, the conditional log-likelihood function for this problem is

$$
\begin{aligned}
\ln\Lambda[s_o(t)|\omega_k,\theta,\gamma] \approx & \\
&\sqrt{\frac{2\gamma}{\sigma_i^2 T_h}}\cos\theta\int_{T_c}^{T_s}r_o(\tau)g_c(\tau,\omega_k)d\tau + \sqrt{\frac{2\gamma}{\sigma_i^2 T_h}}\sin\theta\int_{T_c}^{T_s}r_o(\tau)g_s(\tau,\omega_k)d\tau
\end{aligned}
\tag{18.32}
$$

where the functions $g_c(t,\omega_k)$ and $g_s(t,\omega_k)$ are defined by the integral equations
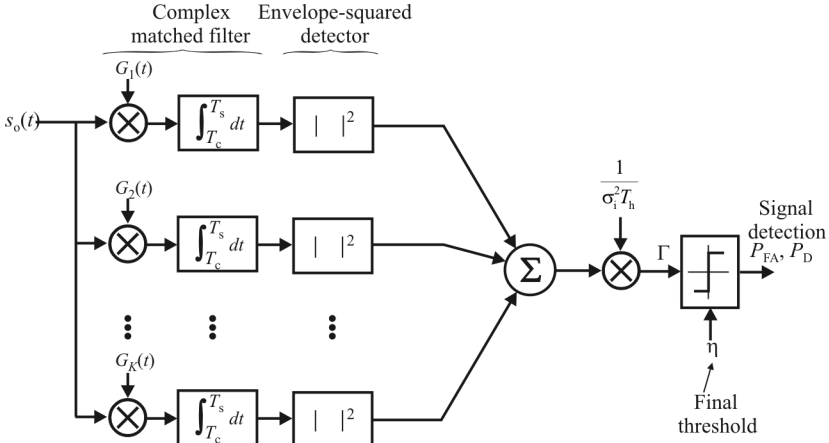
**Figure 18.24** Low SNR single-epoch detector.

$$\int_{T_c}^{T_s} R_o\left[\frac{t+\tau}{2}, \tau-t\right] g_c(\tau, \omega_k) d\tau = s_c(t, \omega_k) \qquad (18.33)$$

$$\int_{T_c}^{T_s} R_o\left[\frac{t+\tau}{2}, \tau-t\right] g_s(\tau, \omega_k) d\tau = s_s(t, \omega_k) \qquad (18.34)$$

for $T_c \leq t \leq T_s$. Averaging (18.32) over $\theta$ and $\omega_k$ yields

$$\Lambda[r_o(t)/\gamma] = \sum_{k=1}^{K} I_0\left[\sqrt{\frac{2\gamma}{\sigma_i^2 T_h}} \left|\int_{T_c}^{T_s} r_o(\tau) G_k(\tau) d\tau\right|\right] \qquad (18.35)$$

Where $I_0[\bullet]$ is the modified Bessel function of the first kind and zero order and the complex-valued function $G_k(t)$ is defined as

$$G_k(t) \triangleq g_c(t, \omega_k) + jg_s(t, \omega_k)$$

For small $\gamma$, noting that $I_0(x) \approx 1 + x^2/4$, (18.35) becomes

$$\Gamma = \frac{1}{\sigma_i^2 T_h} \sum_{k=1}^{K} \left|\int_{T_c}^{T_s} r_o(\tau) G_k(\tau) d\tau\right|^2 \qquad (18.36)$$
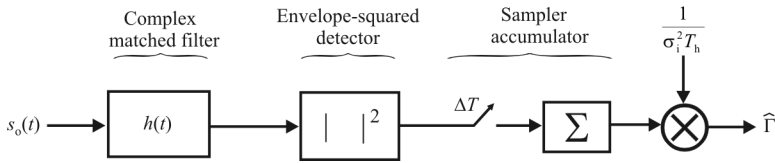
**Figure 18.25** Simple filter detector.

where the scale factor $1/\sigma_i^2 T_h$ is added for later use. Figure 18.24 shows the flow diagram for (18.36).

To complete the detector, $\Gamma$ is compared against a threshold $\eta$, whose value determines the probability of false alarm $P_{FA}$.

### 18.5.4 Simple Filter Detectors

The optimum detector derived in the previous section and shown in Figure 18.24 is quite complicated, partially negating the simplicity of the compressive receiver for the FHSS detection problem. Snelling and Geraniotis considered four types of simple detectors [28] to simplify the optimum detector derived in the previous section while attempting to maintain close to the optimum performance envelope. The general form of these detectors is shown in Figure 18.25. These detectors are: (1) the time-multiplexed detector, (2) the time-averaged detector, (3) the time-typical detector, and (4) the truncated detector. We consider the time-multiplexed detector here.

The simple filter detector is depicted in Figure 18.25. It consists of a complex filter, with impulse response $h(t)$, whose squared outputs are sampled at times $t = T_s + (k-1)\Delta T$ for $k = 1, 2,\dots, K$ and then summed and scaled by $1/\sigma_i^2 T_h$ to produce the test statistic $\hat{\Gamma}$ given by

$$\hat{\Gamma} = \frac{1}{\sigma_i^2 T_h} \sum_{k=1}^{K} \left| \int_{T_c}^{T_s} s_o(\tau) h[T_s + (k-1)\Delta T - \tau] d\tau \right|^2 \tag{18.37}$$

The matched filter with impulse response $h(t)$ is determined by $G_k(t)$ as

$$h(t) = \sum_{k=1}^{K} G_k[T_s - t + (k-1)\Delta T] \tag{18.38}$$

which, by defining

$$\hat{G}_k(t) \triangleq h[T_s - t + (k-1)\Delta T] \qquad \text{for} \qquad T_c \leq t \leq T_s \qquad (18.39)$$

yields the alternate expression

$$\hat{\Gamma} = \frac{1}{\sigma_i^2 T_h} \sum_{k=1}^{K} \left| \int_{T_c}^{T_s} s_o(\tau) \hat{G}_k(\tau) d\tau \right|^2 \qquad (18.40)$$

To find the filter response of the time-multiplexed detector as a function of the pseudo-signals $G_k(t)$, we form

$$h(t) = \sum_{j=1}^{K} G_j[T_s - t + (j-1)\Delta T] \qquad (18.41)$$

This transforms (18.39) to

$$\hat{G}_k(t) = \sum_{j=1}^{K} G_j[(j-k)\Delta T + t] \qquad (18.42)$$

which, for $\Delta T \geq T_s - T_c$ implies $\hat{G}_k(t) = G_k(t)$, since the $G_j$s are zero outside the range $T_c \leq t \leq T_s$.

### 18.5.5 Verification and Validation

The performance of the low SNR CxRx detector is shown in Figure 18.26. A performance comparison of the low SNR detector to the time-averaged detector is shown in Figure 18.27. These are simulated results where the parameters chosen are given in the caption. We can see that after only 100 ms (1000 hops at 10 khop/sec), reliable detection is possible with $P_f \sim 0.1$ even for SNRs below zero.

### 18.5.6 Summary

We have considered the use of a CxRx for the detection of FHSS signals in this section. The CxRx structure is simple, yet the optimum receiver based on the CxRx is rather complicated. We examined some simpler filter structures that are not optimum but provide slightly less performance for considerably less complexity.
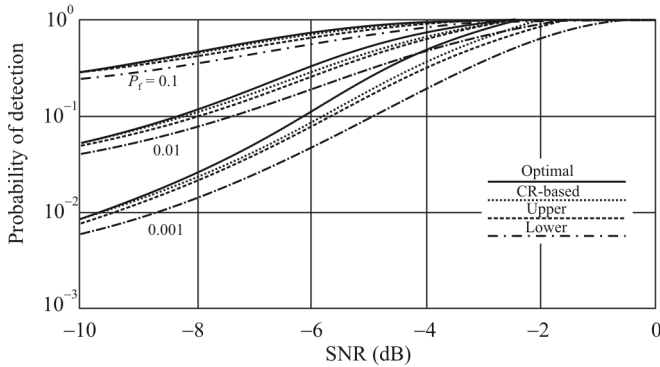
**Figure 18.26** Performance of low SNR detector. Performance of low SNR detector based on CxRx observations versus optimal, FBC based on direct observations. In this case, $T_c = 50$ μsec, $T_s = 100$ μsec, $\omega_0 = 2\pi \times 40$ MHz, 100 hop frequencies between 2.33 MHz and 4.33 MHz, 10 khops/s, with 1000 hop observations, $\Delta T = (\omega_2 - \omega_1)/2\beta$.

# 18.6 Concluding Remarks

We considered some receiver topologies for intercepting FHSS signals in this chapter. We presented two optimal configurations—one for SFHSS signals and one for FFHSS signals and indicated that these are not practical receivers due to their complexity. We then discussed the FBC with radiometric detectors and showed that this is a practical implementation for FHSS receivers, especially when FFT methods are used for implementation where many narrowband channels can
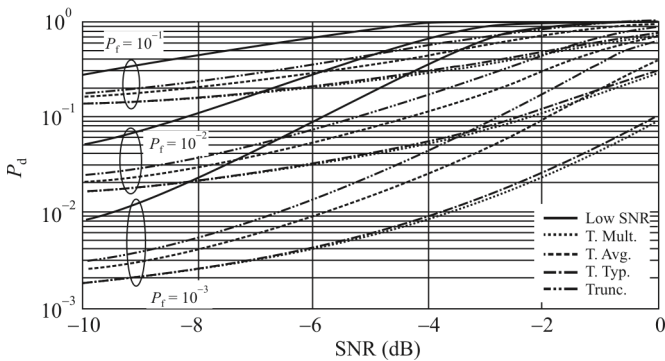


**Figure 18.27** CxRx performance comparison. Performance of low SNR detector compared to the simple filters considered. In this case, $T_c = 50$ μsec, $T_s = 100$ μsec, $\omega_0 = 2\pi \times 40$ MHz, 100 hop frequencies between 2.33 MHz and 4.33 MHz, 10 khops/s, with 1000 hop observations, $\Delta T = (\omega_2 - \omega_1)/2\beta$.

be readily accommodated. The scanning narrowband superheterodyne receiver was considered next as a candidate for an FHSS receiver and we showed that it does not lead to realistic performance against most FHSS targets.

We considered the resolution of some scanning/stepping architectures and discussed the resolution degradation that occurs when they are sped up. Note that this resolution is not the same as frequency accuracy. The latter is primarily determined by the various timing sources in the receivers such as the LOs and timing clocks in digital receivers.

Last, we discussed the CxRx as an implementable FHSS receiver. These receivers have excellent performance in many cases, especially when the target environment is not overcrowded and the high sidelobe levels can be tolerated.

# References

[1]     Levitt, B. K., and U. Cheng, "Optimum Detection of Frequency-Hopped Signals," *Proceedings of the IEEE MILCOM*, 1992.
[2]     Levitt, B. K., U. Cheng, A. Polydoros, and M. K. Simon, "Optimum Detection of Slow Frequency-Hopped Signals," *IEEE Transactions on Communications*, Vol. 42, No. 2/3/4, February/March/April 1994, pp. 1990–2000.
[3]     Chung, C. D., and A. Polydoros, "Detection and Hop-Rate Estimation of Random FH Signals via Autocorrelation Techniques," *Proceedings IEEE MILCOM,* 1991, pp. 345–349.
[4]     Levitt, B. K., and U. Cheng, "Detection of Bandlimited Signals with Deterministic/Unknown or Random Frequency and Phase," JPL Technical Memorandum, August 28, 1991.
[5]     Levitt, B. K., and A. Polydoros, "Bandwidth Occupancy for Multiple Independent Frequency Hoppers," JPL Interoffice Memorandum 331-91.2-034, June 12, 1991.
[6]     Levitt, B. K., M. K. Simon, A. Polydoros, and U. Cheng, "Partial-Band Detection of Frequency-Hopped Signals," JPL Technical Memorandum JPL D-10572, February 25, 1993.
[7]     Levitt, G. K., M. K. Simon, A. Polydoros, and U. Cheng, "Partial Band Detection of Frequency-Hopped Signals, *Proceedings IEEE Globecom*, Vol. 4, Houston, Texas, November/December 1993, pp. 70–76.
[8]     Cheng, U., M. K. Simon, A. Polydoros, and B. K. Levitt, "Statistical Models for Evaluating the Performance of Noncoherent Slow Frequency Hopped M-FSK Intercept Receivers," *IEEE Transactions  on Communications*, Vol. 43, No. 2/3/4, February/March/April 1995, pp. 1703–1712.
[9]     Simon, M. K., U. Cheng, L. Aydin, A. Polydoros, and B. K. Levitt, "Hop Timing Estimation for Noncoherent Frquency Hopped M-FSK Intercept Receivers," *IEEE Transactions on Communications*, Vol. 43, No. 2/3/4. February/March/April 1995, pp. 1144–1154.
[10]    Dillard, R. A., "Detectability of Spread-Spectrum Signal*," IEEE Transactions on Aerospace and Electronic Systems*, Vol. AES-15, No. 4, July 1979, pp. 526–537.
[11]    DiFranco, J. V., and W. L. Rubin, *Radar Detection*, Englewood Cliffs, NJ: Prentice Hall, 1968.
[12]    Cheng, U., B. K. Levitt, A. Polydoros, and M. K. Simon, "Optimum Detection of Frequency-Hopped Signals," JPL Report D-10363, 1994.
[13]    Urkowitz, H., "Energy Detection of Unknown Deterministic Signals," *Proceedings of the IEEE*, Vol. 55, No. 4, April 1967, pp. 523–531.

[14]     Dillard, R. A., and G. M. Dillard, *Detectability of Spread-Spectrum Signals*. Norwood, MA: Artech House, MA, 1989.

[15]     Simon, M. K., J. K. Omura, R. A. Scholtz, and B. K. Levitt, *Spread Spectrum Handbook*, New York: McGraw-Hill, 1994.

[16]     Poisel, R. A., *Target Acquisition in Communication Electronic Warfare Systems*, Norwood, MA: Artech House, 2004, Section 8.2.2.

[17]     Levitt, B. K., M. K. Simon, A. Polydoros, and U. Cheng, "Partial-Band Detection of Frequency-Hopped Signals," *Proceedings IEEE Globecom'93*, Vol. 4, Houston, November./December 1993, pp. 70–76.

[18]     Miller, L. E., J. S. Lee, and D. J. Torrieri, "Frequency-Hopping Signal Detection Using Partial Band Coverage," *IEEE Transactions on Aerospace and. Electronic Systems*, Vol. 29, No. 2, April 1993, pp. 540–553.

[19]     Chung, C. D., "Generalized Likelihood-Ratio Detection of Multiple-Hop Frequency-Hopping Signals," *IEE Proceedings in Communications*, Vol. 141, No. 2, April 1994, pp. 70–78.

[20]     Lehtomaki, J. J., "Maximum Based Detection of Slow Frequency Hopping Signals," *IEEE Communication Letters*, Vol. 7, No. 5, May 2003, pp. 201–203.

[21]     Chung, C. D., "Generalized Likelihood-Ratio Detection of Multiple-Hop Frequency-Hopping Signals," *IEE Proceedings in Communications*, Vol. 141, No. 2, April 1994, pp. 70–78.

[22]     Read, K. L. Q., "A Lognormal Approximation for the Collector's Problem," *The American Statistician*, Vol. 52, No. 2, May 1998, pp. 175–180.

[23]     Woodring, D. G., "Performance of Optimum and Suboptimum Detectors for Spread Spectrum Waveforms," U.S. Naval Research Laboratory, Report No. 8432, December 1980.

[24]     Van Trees, H. L., *Detection, Estimation, and Modulation Theory, Part 1*, New York: Wiley, 1968.

[25]     Levitt, B. K., U. Cheng, A. Polydoros, and M. K. Simon, "Detecting and Timing Estimation Techniques for Channelized Receivers," JPL Report D-10535, January 27, 1993.

[26]     Torrieri, D. J., *Principles of Secure Communication Systems*, Norwood, MA: Artech House, 1992.

[27]     Krasner, N. F., "Efficient Search Methods Using Energy Detectors—Maximum Probability of Detection," *IEEE Journal on Selected Areas in Communications*, Vol. SAC-4, No. 2, March 1986, pp. 273–279.

[28]     Snelling, W. E., and E. Geraniotis, "Analysis of Compressive Receivers for the Optimal Interception of Frequency-Hopped Waveforms," *IEEE Transactions on Communications*, Vol. 42, No. 1, January 1994, pp. 127–139.

[29]     Poisel, R. A., *Modern Communications Jamming Principles and Techniques*, 2nd Ed., Norwood, MA: Artech House, 2011, Figure 4.10.

[30]     Poisel, R. A., *Modern Communications Jamming Principles and Techniques*, 2nd Ed., Norwood, MA: Artech House, 2011, Figure 4.11.

# Chapter 19

## Receivers for Time-Hopped Spread Spectrum Intercept[1]

### 19.1 Introduction

Time-hopping spread spectrum systems provide covertness to transmissions by transmitting energy at pseudo-random intervals determined by properly designed codes. A noncooperative receiver dwelling at the appropriate place in the frequency spectrum will, for the most part, be observing noise. The pulses that carry information arrive very infrequently. This causes the SNRs involved to be quite low, making detection extremely difficult.

The practical THSS communications available all employ UWB signaling, as discussed in Chapter 13. Therefore, in this chapter we will scrutinize receiver topologies for UWB intercept and examine their performance.

UWB systems transmit information with very short-duration pulses rather than by modulating a carrier to move the information signal elsewhere in frequency. The large bandwidth of a UWB system is determined by the pulse shape and duration. This large system bandwidth relative to the information bandwidth allows UWB systems to operate with a (very) low power spectral density. A low power spectral density implies an inherent covertness of UWB, due to the fact that the UWB signal may be near or below the noise floor of an EW receiver, much the same as DSSS signals can be.

We investigate the detectability of UWB systems with noncooperative EW systems in this chapter. UWB signals are hard to detect because a limited amount of power is distributed across a very wide bandwidth. This is not the primary reason for a communicator to use UWB signaling, however. It is principally a technique for sharing common bandwidth among many users.

---

[1] Much of the material in this chapter is extracted from [1]. Reprinted with permission.

Since the details of the modulation process are not known to a noncooperative EW receiver, the interceptor cannot use a matched filter or a correlator and must treat the signal as a random process and base its detection on the presence or absence of energy compared to the background noise. As described in Chapter 2, the module that does this is an energy detector.

# 19.2 Detecting UWB Signals

We examine the detectability of UWB signals in this section. Two measures of detectability will be described. The first measure computes $P_D$ versus the SNR required to achieve some measure of performance, usually $P_{FA}$ and $P_D$. The second measure is the ratio of the distance an intercepting interloper must be to the distance between the target transmitter and receiver to achieve a measure of performance, again usually $P_D$ and $P_{FA}$.

## 19.2.1 Modulations

The UWB system considered here employs time hopping as an LPD/LPI technique. The signal transmitted by the $l$th user is given by

$$s^{(l)}(t) = \sum_i w\left[t - iT_f - c_i^{(l)}T_c - d_i^{(l)}\right] \tag{19.1}$$

where $t$ is the transmitter clock time. The frame time $T_f$ typically is a hundred to a thousand times the pulse width resulting in a signal with a very low duty cycle. The superscript $(l)$ represents the $l$th user, $N_s$ is the number of pulses used to represent one data symbol, $w()$ is the pulse shape with normalized energy, $c_i^{(l)}$ is a pseudo-random, repetitive time-hopping sequence, $T_c$ is the time-hop delay, and $d_i^{(l)}$ is a function of the data sequence. $n(t)$ is AWGN. $w(t)$ typically is the Gaussian monocycle.

Possible modulation schemes that have been proposed for UWB communications systems are PAM, OOK, bipolar signaling, PPM, and various combinations of these. An $M$-ary PPM scheme, bipolar signaling, and an $M$-ary combination of bipolar signaling and PPM (biorthogonal signaling) are considered here.

For the $M$-ary PPM, the data is contained in one of $M$ possible time delays, so $d_i^{(l)} = 0, 1, \ldots, M-1$. For bipolar signaling, the data is contained in the polarity of the transmitted pulses, so $d_i^{(l)} = 0$. For biorthogonal signaling, the data is contained in the polarity of the pulse and one of $M/2$ possible time delays, such that $d_i^{(l)} = 0, 1, \ldots, M/2-1$.
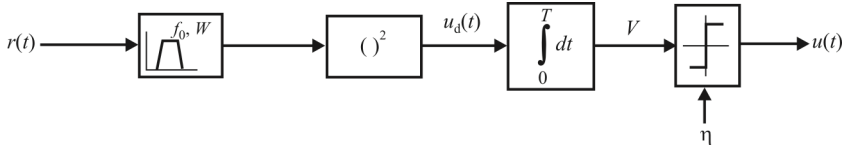
**Figure 19.1** Radiometer UWB detector.

## 19.2.2 Required SNR Measure of Effectiveness

### 19.2.2.1 Radiometer Detectors

We will use the radiometer as the architecture to examine the detectability of UWB signals. We discussed radiometers at length in Chapter 2 where, in particular, the fundamental radiometer shown in Figure 19.1 was characterized. This section describes a wideband radiometer system and introduces the multi-radiometer detector in the form of a time-channelized radiometer.

As pointed out in Chapter 13, the optimal receiver for detection of a signal in AWGN is the energy detector or the radiometer. It is easily implemented in hardware and can be used to detect SS signals. Detection is accomplished by calculating the energy of the received message and comparing with a predetermined threshold. As illustrated in Figure 19.1, it consists of a bandpass filter of bandwidth $W$, a squaring device, and an integrator with an integration time $T$ set equal to the observation time interval.

The performance of the radiometer is characterized by the probability of detection $P_D$ when the signal is present (along with the noise, of course) and the probability of false alarm $P_{FA}$ when only noise is present. The SNR psd, $S/N_0$, is usually the parameter specified to achieve the $P_D$ and $P_{FA}$ goals. We will use $S/N_0$ as a measure of the covertness of the communication system under consideration ($\gamma$ denotes the SNR).

When the signal is absent and the input to the radiometer is strictly noise, with two-sided psd $N_0/2$ the normalized random variable $Y = 2V / N_0$ has a central chi-square distribution with $v = 2TW$ degrees of freedom, where $T$ and $W$ are the observation time interval and the filter bandwidth of the radiometer, respectively, as illustrated in Figure 19.1. The PDF of $Y$ is given by [2]

$$p_n(y) = \frac{1}{2^{v/2}\Gamma\left(\dfrac{v}{2}\right)} y^{(v-2)/2} e^{-y/2}, \qquad y \geq 0 \tag{19.2}$$

When the signal is present at the input to the radiometer with energy $E$ measured over time $T$, then the random variable $Y$ has a noncentral chi-square

distribution with $v = 2TW$ degrees of freedom and noncentrality parameter $\lambda = 2E / N_0$. The pdf of $Y$ can then be written as [2]

$$p_{\text{s+n}}(y) = \frac{1}{2}\left(\frac{y}{\lambda}\right)^{(v-2)/4} e^{-(y+\lambda)/2} I_{(v-2)/2}\left(\sqrt{y\lambda}\right), \quad y \geq 0 \tag{19.3}$$

where $I_n(z)$ is the $n$th order modified Bessel function of the first kind. The $P_{\text{FA}}$ and $P_{\text{D}}$ values of the radiometer can be determined by integrating (19.2) and (19.3), respectively, as

$$P_{\text{FA}} = \int_{2\eta/N_0}^{\infty} p_{\text{n}}(y)dy \tag{19.4}$$

and

$$P_{\text{D}} = \int_{2\eta/N_0}^{\infty} p_{\text{s+n}}(y)dy \tag{19.5}$$

where $\eta$ is the detection threshold.

The threshold $\eta$ and the $S/N_0$ are determined in order to satisfy the performance criteria of the radiometer, given in (19.4) and (19.5). However, closed-form solutions for (19.4) and (19.5) are not available so they must be evaluated numerically. For large TW, the chi-square and the noncentral chi-square density functions asymptotically converge to a Gaussian by the central limit theorem.

*Probability of Error*

Assuming that $N_{\text{u}}$ users are active in the system, the received signal $r(t)$ can be expressed as [2, 3],

$$r(t) = \sum_{l=1}^{N_{\text{u}}} \alpha^{(l)} s^{(l)}[(t - \tau^{(l)}] + n(t) \tag{19.6}$$

where $\alpha^{(l)}$ is the attenuation of the signal over the channel and $\tau^{(l)}$ represents the timing mismatch between the transmitter and the receiver. Under the assumptions that the interfering signals have the same power level as that of the target and the time offsets of interfering pulses arriving at the receiver are independent and uniformly distributed random variables over the frame time $[0, T_{\text{f}})$, the total

interference can be modeled as a zero mean Gaussian random process [2, 3]. The probability of error is given as

$$P_e(N_u) = \frac{1}{\sqrt{2\pi}} \int_{\sqrt{\gamma(N_u)}}^{\infty} \exp\left(-\frac{x^2}{2}\right) dx \qquad (19.7)$$

where $\gamma(N_u)$ is the radiometer output SNR for $N_u$ users and can be expressed as

$$\gamma(N_u) = \frac{1}{\dfrac{\sigma_n^2}{(\alpha^{(1)} N_s m_p)^2} + \dfrac{1}{N_s} \dfrac{\sigma_a^2}{m_p} \sum_{l=2}^{N_u} \left(\dfrac{\alpha^{(l)}}{\alpha^{(1)}}\right)^2} \qquad (19.8)$$

where $m_p$ is the receiver correlator output for a single received pulse, $\sigma_a^2$ is the variance of the interfering users, $\sigma_n^2$ is the noise power, and $\alpha^{(l)}$ is the attenuation of the signal from the $l$th user. Without loss of generality, we let $\alpha^{(1)}$ be the amplitude for the target signal. The SNR for the single user case can be written as

$$\gamma(N_1) = \frac{(\alpha^{(1)} N_s m_p)^2}{\sigma_n^2} \qquad (19.9)$$

The power of the signal at the output of the energy detector bandpass filter, $z(t)$, is $\sigma_z^2 = N_0 W_i$ in the absence of a signal ($\hat{H}_0$) of the filter and $\sigma_z^2 + \sigma_s^2 = (N_{signal} + N_0)W_i$ in the presence of the signal ($\hat{H}_1$), where $N_{signal}$ is the psd of the signal and $N_0$ is the one-sided PSD of noise. The signal at the output of the square law device with no signal present, $u_0$, is given by

$$u_0 = n^2(t), \qquad \text{noise only} \qquad (19.10)$$

and with a signal present is

$$u_1 = [r(t) + n(t)]^2, \text{ signal and noise} \qquad (19.11)$$

The difference between the expected value of the output of the square law device, $u_d$, when no signal is present ($u_0$) and when a signal is present ($u_1$) is how the radiometer detects a signal. Assuming zero mean noise, this is given by

$$\overline{\Delta u} = \mathcal{E}\{u_1\} - \mathcal{E}\{u_0\} = N_{signal} W_i \qquad (19.12)$$

The random fluctuations of the energy output of the square law device mask the energy difference. This is due to the variance of the random processes. The signal to be detected can be expected to cause no *variation* in the output power when measured over the whole bandwidth. The variance depends on the noise psd and is given by [4]

$$\text{Var}\{u_d\} = \sigma_z^4 = (N_0 W_i)^2 \tag{19.13}$$

The integrator in the radiometer time integrates $u_d$ over the observation window $T$ in order to make the constant component $\overline{\Delta u}$ visible by smoothing the random fluctuations $\sigma_z^4$. For reliable detection, the number of statistical independent samples, $N_s \approx W_i T$, should be large.

When $N_s \gg 1$ the conditional pdf at the integrator's output is given by Edell's model [4]

$$p(V|H_i) = \frac{1}{\sqrt{2\pi N_s \sigma_n^2}} \exp\left\{\frac{(V - N_s \overline{u}_{di})^2}{2 N_s \sigma_n^4}\right\}, \quad i = 0,1 \tag{19.14}$$

yielding the probability of a false alarm

$$P_{FA} = \Pr\{\hat{E} \ge \eta | H_0\} = \int_{\eta_{th}}^{\infty} p(\hat{E}|H_0) d\hat{E} = Q\left(\frac{\eta - N_s \overline{u}_{d0}}{\sqrt{N_s} \sigma_n^2}\right) \tag{19.15}$$

and the probability of detection [4]

$$P_d = \Pr\{V \ge \eta | H_1\} = \int_{\eta_{th}}^{\infty} p(V|H_1) dV = Q\left(\frac{\eta - N_s \overline{u}_{d1}}{\sqrt{N_s} \sigma_n^2}\right) = Q\left[Q^{-1}(P_{FA}) - q_i\right] \tag{19.16}$$

where $q_i$ is given by

$$q_i = \frac{N_s \overline{\Delta u}_d}{\sqrt{N_s} \sigma_n^2} = \sqrt{W_i T} \frac{S}{W N_0} \tag{19.17}$$

$P_{FA}$ is a system parameter that is specified by the requirements of the application, and it is set in the radiometer[2] and the second term is due to the observation

---

[2] Setting the value of $P_{FA}$ is referred to as *constant false alarm rate* (CFAR) detection.
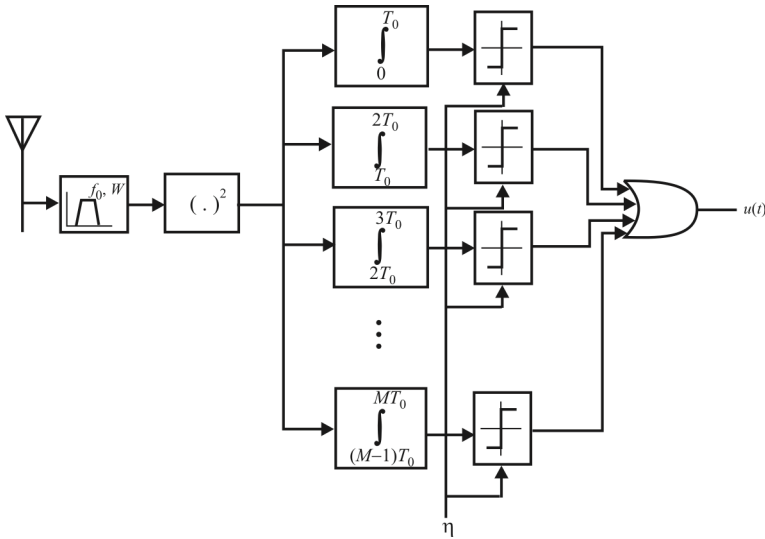
**Figure 19.2** Time-channelized radiometer.

window ($W_iT$) of the radiometer and the UWB psd. We can thus see that the probability of noncooperative detection for UWB signals is extremely low as $S/WN_0$ is very small due to the ultrawide bandwidth used and low received power $S$. $P_D$ is highest when $W_i$ is equal to $W$, and (6.13) can then be rewritten as

$$q_i = \sqrt{\frac{T}{W}} \frac{S}{N_0} \tag{19.18}$$

### 19.2.2.2 Time-Channelized Multichannel Radiometer

The radiometer described above is a wideband radiometer in which a single radiometer observes the entire bandwidth $W_i$ over time $T$. Other radiometer architectures improve the total time bandwidth product and thereby the probability of detection. One possibility is the channelized radiometer exemplified in Figure 19.2. $M$ radiometers are used in parallel and each radiometer can observe either a different portion of the spectrum or a different time window, reducing the noise measured by each radiometer [5].

The time interval for each channel of this system is on the same order as the pulse duration, $T_p$, which yields $T_0W$ approximately equal to 1. For these radiometers, Edell's model is no longer valid, but other models for a wide range of $TW$ are given in [2]. Park's [6] and Dillard's [7] models are derived from Barton's radar detector loss function [8], which is based on $TW = 1$, so we will use them. Probability of detection for each channel using Park's model can be expressed as

$$P_d = Q\left[Q^{-1}(P_f) - \sqrt{2Y}\right] \tag{19.19}$$

and probability of detection for each channel using Dillard's model can similarly be expressed as

$$P_d = Q\left[\sqrt{-2\ln(P_f)} - \sqrt{Y\left(1 + \sqrt{1 + 9.2/Y}\right)}\right] \tag{19.20}$$

where

$$Y = \frac{T_0 S_i^2}{2.3WN_0^2 + S_i N_0} \tag{19.21}$$

and where $S_i$ is the average received power in the $i$th channel during one time interval, $T_0$. Here $S_l$ is the power received by radiometer $l$ and $P_f$ is the probability of false alarm for the radiometers, assumed to be the same for all.

A time-channelized radiometer gives better detection performance for UWB signals than a frequency channelized configuration. This is due to the fact that UWB systems only transmit a short period of time. The total observation window $T$ is divided among the $M$ radiometers, each observing $T_0 = T/M$ of the window.[3] The optimum $M$ is when $T/M$ is equal to the pulse duration $T_p$ because increasing the time window beyond the pulse duration only increases the noise captured without measuring any additional signal energy.

The detectability of a UWB signal varies depending on what is a priori known about the signal. The ideal detector is a multiradiometer system that is perfectly synchronized with the received pulse and has prior knowledge of pulse width as well as the bandwidth of the SOI. For this case, the bandwidth of the input filter is set to the signal bandwidth and the observation intervals to the signal pulse width ($T_0$). When less is known about the SOI, less sensitivity ensues and the parameters of the multiradiometer system are adjusted according to what is known about the SOI.

*Single Signal*

The overall performance (i.e., the probability of detection $P_D$ and the probability of false alarm $P_{FA}$) of the intercept system is a function of the performance ($P_d$ and the $P_f$) of the individual radiometers. The radiometer analytical models require

---

[3] This configuration of radiometers can be accomplished with suitable sample-and-hold modules and a single radiometer.

that only one radiometer with a single observation and integration interval is used for detection and that there is significant signal energy present for the entire duration of the observation interval. Observation intervals of the individual radiometers larger than the pulse width result in the signal being limited to only part of the observation interval because UWB signals are (very) low duty cycle pulses. Furthermore, the Gaussian assumption for the output statistics of the radiometer is invalid because for UWB signals, $TW \sim 1$. For these reasons, the available theoretical models are not applicable, so to determine the detectability we must resort to numerical simulation.

We assume that the individual radiometers in the multiradiometer system (FBC) are identical; thus, the parameters $P_\mathrm{f}$ and $P_\mathrm{d}$ are the same for each of them. $P_\mathrm{FA}$ and the $P_\mathrm{D}$ for the overall time-channelized radiometer system can be expressed in terms of $P_\mathrm{f}$ and $P_\mathrm{d}$ as

$$P_\mathrm{D} = 1 - \left[ (1 - P_\mathrm{d})(1 - P_\mathrm{FA})^{M-1} \right] \qquad (19.22)$$

and

$$P_\mathrm{FA} = 1 - (1 - P_\mathrm{f})^{M} \qquad (19.23)$$

Equations (19.22) and (19.23) are valid for the single user case when there is a single pulse to be detected within a frame and with $M$ radiometers in the frame.

Given $P_\mathrm{FA}$ and $P_\mathrm{D}$ for the multiradiometer system, $P_\mathrm{f}$ and $P_\mathrm{d}$ can be calculated iteratively using (19.22) and (19.23). The threshold for the individual radiometers is determined by simulation to meet the $P_\mathrm{f}$ criterion and then, given this threshold value, the $S/N_0$ is found to meet the required $P_\mathrm{d}$ criterion. We will compare the results so obtained with the required $S/N_0$ for CDMA by applying the analytical models to the latter since the constraints that render the models inapplicable in UWB do not exist in wideband CDMA.

Since the bandwidth or the pulse width may not be known to the intercept receiver, we first consider the performance of the receiver unaware of the SOI specifications. The multiradiometer system for this receiver is similar in structure to the optimal receiver, but the observation interval, $T_0$, and the bandwidth of the input filter will likely not be equal to the actual pulse width or the bandwidth of the SOI. We consider the performance when the bandwidth is unknown but the pulse width is known and also the case when the pulse width is unknown but the bandwidth is known. However, for now, synchronization is assumed. We now consider these scenarios in more detail.

*Bandwidth Unknown, Pulse Width Known.* First we consider the case when the SOI bandwidth is unknown. For this case, the receiver structure is similar to the optimal receiver with the same number of radiometers, $M$, and the observation interval set equal to the pulse width. If the bandwidth of the input filter of the radiometer is set to be greater than the SOI bandwidth, then the noise power increases. For bandwidths less than the SOI bandwidth the signal power decreases. Both cases reduce the available SNR.

*Pulse Width Unknown, Bandwidth Known.* We assume in this case that the observation interval of the intercept receiver is different from the actual pulse width of the SOI while we can set the bandwidth to be that of the SOI since it is known. As before, an observation interval that is longer than the pulse width results in excess noise, while an observation interval smaller than the pulse width reduces the signal power. Again both cases reduce the available SNR. Clearly, the number of individual radiometers required to cover a frame is a function of the observation interval, $T_0$, as is obvious from Figure 19.2. Assuming the observation interval of the receiver is $T_R$, then the total number of radiometers per frame is $M' = T_f / T_R \neq M$ if $T_R \neq T_p$. In this case,

$$P_D = 1 - \left[ (1 - P_d)(1 - P_{FA})^{M'-1} \right] \qquad (19.24)$$

and

$$P_{FA} = 1 - (1 - P_f)^{M'} \qquad (19.25)$$

We have assumed the received signal to be time synchronized with the observation intervals of the individual radiometers for the cases considered above. For asynchronous signals, there is overlap into adjacent radiometer integration intervals. In the worst-case scenario, exactly half the signal overlaps onto the observation interval of the following radiometer, since the radiometers are aligned in time, thus minimizing signal power in both radiometers. In this case, the signal power input to a particular radiometer is reduced by 3dB. As a result the required $S/N_0$ to meet performance criteria increases by 3dB-Hz. The actual performance of the receiver depends on the amount of signal overlap, and the performance (required SNR) increases as $\gamma + 3\kappa$ dB-Hz where $0 < \kappa < 1$. However, since our objective is to obtain an upper bound on signal detectability, the assumption of perfect synchronism is reasonable for our purposes.

*Multiple Signals*

For $L$ active users in the environment there are $L$ pulses, which are pseudo-randomly shifted within a time frame. The multiradiometer receiver structure is still that in Figure 19.2, but because of the presence of more pulses in the system and thus more energy per frame, the performance criterion of the individual radiometers $(P_d)$ can be decreased while meeting the system performance criteria. The $L$ pulses may or may not overlap with each other and as a result two cases arise. We assume that all the pulses have equal amplitudes. We also assume that the intercepting receiver has knowledge of the bandwidth and pulse width of the SOI (the most likely case unless there is nothing known about the signal environment).

*Nonoverlapping Signals.* In this case, we are assuming that the pulses occupy different time slots within a frame. The multiradiometer system for this case is similar to that in the single user case, except that for $L$ users, $P_D$ of the overall system is related to the individual radiometer $P_d$, assumed to be equivalent for all radiometer channels, by

$$P_{\mathrm{D}} = 1 - \left[ (1 - P_{\mathrm{d}})^L (1 - P_{\mathrm{f}})^{M-L} \right] \tag{19.26}$$

The $P_f$ values of the radiometers are insensitive to the number of users since it is a parameter that is obtained assuming no signals are present. Given the performance criteria for the individual radiometers, simulation is used to obtain the $S/N_0$ required for a specific value of $P_d$.

*Overlapping Signals.* If $L$ users are active in the system and $x$ pulses overlap $(2 \leq x \leq L)$, then the amplitude increases by a factor of $x$. The probability of detection for the individual radiometers is given by (assuming complete overlap)

$$P_{\mathrm{D}} = \begin{cases} 1 - \left[ (1 - P_{\mathrm{d}})^{\alpha} (1 - P_{\mathrm{f}})^{M-\alpha} \right], & L \leq M \\ 1 - \left[ (1 - P_{\mathrm{d}})^{\beta} (1 - P_{\mathrm{f}})^{M-\beta} \right], & L > M, x \geq L/M \\ 1 - (1 - P_{\mathrm{d}})^{M}, & L > M, x < L/M \end{cases} \tag{19.27}$$

where $\alpha = L - x + 1$ and $\beta = (M/L)(L-x)+1$. Again, complete overlap of pulses is a reasonable assumption since we seek an upper bound on signal detectability.

The detectability is dependent on the number of overlapping pulses, $x$, which varies between $2 \leq x \leq L$. Define the average SNR for a given number of users $L$ as

$$\gamma_L = \sum_{x=2}^{L} \gamma_x p(x) \qquad (19.28)$$

where $\gamma_L$ is the SNR for $L$ users and $\gamma_x$ is the signal-to-noise psf ratio $S / N_0$ when $L$ users are active and $x$ pulses overlap. $p(x)$ is the probability that $x$ pulses out of $L$ pulses overlap.

Because $p(x)$ is not normally available in closed form, we use numerical simulation to evaluate (19.28). When $L$ users are active, each frame has exactly $L$ pulses, which are pseudo-randomly placed within the frame. Since a pulse can occupy any time slot in the frame with equal probability, the individual user pulses are uniformly spread within the frame. The performance for a particular frame depends on the *maximum* overlap. The average for a given number of users is calculated by averaging $S/N_0$ over the number of frames, where the maximum overlap for each frame is the maximum number of users that overlap in a single time slot in the frame. The performance for the CDMA signal is calculated by using the analytical expressions given in (19.19) or (19.20) with allowances made for multiple users resulting in decrease in performance according to

$$\gamma_L = \gamma_1 - 10 \log_{10} L \qquad (19.29)$$

*Performance*

Numerical results for the UWB signals are obtained using Monte Carlo simulation. The users are assumed to be stationary for the duration of the simulation in the peer-to-peer network topology. For simplicity we assume that all the pulses at the multiradiometer detection system have equal amplitudes.

The UWB system uses a Gaussian monocycle of center frequency $f_c = 2$ GHz and pulse width $T_p = 6 \times 10^{-10}$ s. The frame time is $T_f = 6 \times 10^{-8}$ sec, resulting in $M = 100$ for the number of time slots in one frame. The bandwidth of the pulse is $W_p = 4$ GHz.

*Ideal Multiradiometer.* In the ideal case, the multiradiometer system is assumed to have complete knowledge of the system specifications (i.e., the bandwidth and the pulse width). The performance criteria for the radiometer is assumed to be $P_D = 0.9$ and $P_{FA} = 0.01$. The filter is a fourth-order Butterworth filter with a 4 GHz cutoff. The observation interval of the radiometer is the pulse width, $T_p$.

**Table 19.1** Required SNR for $P_D = 0.9$ and $P_{FA} = 0.01$
for the Ideal Radiometer

| Target System | Required SNR (dB-Hz) |
|---------------|----------------------|
| UWB           | 107.78               |
| DSSS CDMA     | 75.12                |

Source: [9].

   The $P_f$ and the $P_d$ values for the individual radiometers are calculated iteratively for the single user case using (19.22) and (19.23). The integrator is reset after each observation interval $T_p$. The threshold is selected to meet the $P_f$ requirements of the individual radiometers. This threshold is then used to calculate the required $S/N_0$ to meet the $P_d$ criterion.

   The required SNR obtained for UWB in the single user case is compared with that for CDMA in Table 19.1. For CDMA we assume a bandwidth of $W_w = 5$ MHz and a chip rate of 3.7 Mcps. As for the UWB system, performance criteria of $P_D = 0.9$ and $P_{FA} = 0.01$ are assumed for this CDMA system. We used the Park model of the radiometer to compute these values. We see that UWB is much more difficult to detect (by more than 30 dB) than a DSSS CDMA system in the single-user case. Note that 100dB-Hz corresponds to

$$10\log_{10}\gamma = 100 \quad \text{dB-Hz}$$
$$\gamma = 10^{10}$$

so in a 4 GHz bandwidth

$$\gamma = 10\log_{10}\frac{10^{10}}{4\times10^9} = 10\log_{10}2.5 = 3.9\,\text{dB}$$

*Multiradiometer Performance with Unknown Bandwidth.* In this section, we evaluate the performance of the multiradiometer detector without prior knowledge of the UWB system bandwidth. The other parameters are the same as in the ideal case. The $P_d$ and the $P_f$ of the radiometer are unchanged from the optimal case because the observation interval is known. Figure 19.3 shows the probability of detection, $P_D$, as a function of $S/N_0$ for bandwidths of $W = 4$ GHz and 50 GHz. We can conclude that the multiradiometer performance is not very sensitive to filter bandwidth mismatch.

*Multiradiometer Performance with Unknown Pulse Width.* The parameters of the suboptimal multiradiometer system are similar to those in the ideal case, but the $P_f$ and the $P_d$ change according to (19.24) and (19.25) because the number of
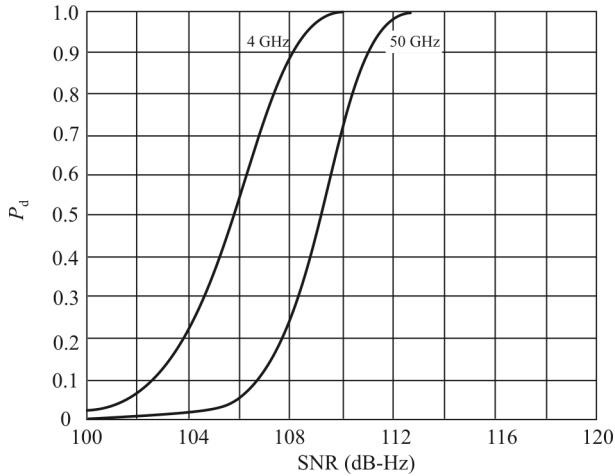
**Figure 19.3** Probability of detection versus the normalized SNR for two filter bandwidths, 4 GHz and 50 GHz.

radiometers within a single time frame vary with the observation interval. Figure 19.4 shows $P_D$ as a function of the $S/N_0$ for observation periods of the radiometer of 0.6 nsec and 60 nsec. For the second case, the observation interval is set equal to the frame time; thus a single radiometer occupies the entire frame. This represents the extreme case when maximum noise power is input to the radiometer. We see that multiradiometer receiver performance is relatively insensitive to variations of the observation interval.

*Summary*

In this section we quantitatively evaluated the UWB detection performance of a multiradiometer intercept receiver. We quantified this performance for a few variations of the radiometer parameters to evaluate how well they match the parameters of the SOI. Results showed that the detector was relatively insensitive to prior knowledge about the bandwidth and pulse width of the UWB signal. In addition it was shown that UWB signals are considerably more difficult to detect than CDMA signals.

**19.2.3 Ratio of Distances Measure of Effectiveness**

McKinstry and Bueher [10] took a somewhat different approach to evaluate the detectability of UWB systems. We briefly describe their approach and some of their results here.
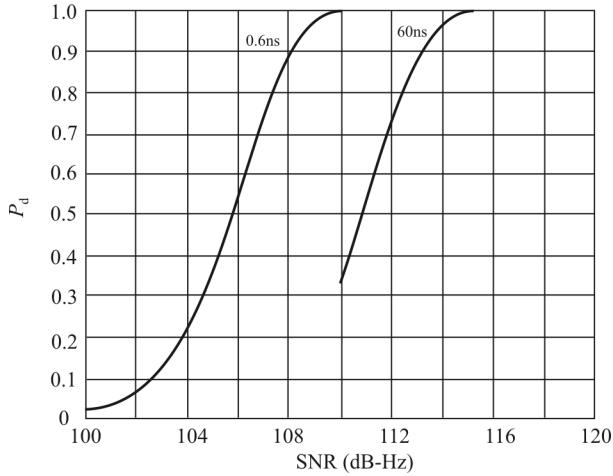
**Figure 19.4** Probability of detection as a function of normalized SNR for two observation intervals, 0.6 ns and 60 ns.

The pulse shape assumed here is the Gaussian monopulse (see Chapter 13) given by

$$w(t) = \sqrt{\frac{16}{3T_p}} \left[ 1 - 16\pi \left( \frac{t}{T_p} \right)^2 \right] \exp \left[ -8\pi \left( \frac{t}{T_p} \right)^2 \right] \tag{19.30}$$

where $T_p$ is the pulse width (approximately 99.99% of the energy in $w(t)$ is contained in the interval $-T_p/2$ to $T_p/2$).

The pulse repetition time is assumed a constant for this system. As above, the SOI is assumed to be time-hopping controlled by a pseudo-random sequence. $d_{\lfloor \ \rfloor}^{(k)}$ is set to $2T_p$ to assure orthogonality between possible PPM time shifts.

### 19.2.3.1 Detection Methods

For radiometers with a large time-bandwidth product, *TW*, many of the available models are very closely approximated by Edell's model. In that case, the probability of detection, $P_D$, is given by

$$P_D = Q \left[ Q^{-1} \left( P_{FA} \right) - \sqrt{\frac{T}{W}} \frac{S}{N_0} \right], \qquad TW \gg 1 \tag{19.31}$$
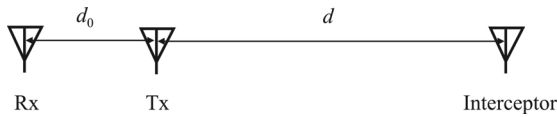
**Figure 19.5** Interceptor scenario.

where $P_{FA}$ is the probability of false alarm in noise alone, $S$ is the average signal power at the radiometer, and $N_0$ is the noise psd. This single radiometer model is used in [3] to compare the detectability of a UWB system with more traditional wideband DSSS systems. To quantitatively evaluate performance, [11] determines the probability of detection versus the relative distance between transmitter and interceptor. This assumes a scenario such as that depicted in Figure 19.5. The probability of detection can be found as a function of the ratio $d/d_0$, the ratio of the distance from the transmitter to interceptor ($d$) to the distance from the transmitter to the intended receiver ($d_0$). The interceptor in this situation is attempting to detect the presence of the transmitted signal, not demodulate it. This same metric will be used here to compare the detectability of UWB systems and also to compare different radiometer configurations.

The same time-channelized multiradiometer system as above was used, whose architecture is shown in Figure 19.2. This system consists of $M$ radiometers, each of which detects energy over an interval of $T_0$. This gives an overall observation interval of $T = MT_0$. Considered above is the case when $T$ of the radiometer system is equal to the frame time, $T_f$, of the UWB system; however, this is not a necessary condition and actually creates some limitations to the performance of the detection system. If $T$ is allowed to be greater than $T_f$, these difficulties are alleviated as will be shown.

As above, the overall desired $P_{FA}$ can be chosen by setting the probability of false alarm for each channel, $P_f$, to satisfy

$$P_{FA} = 1 - \left(1 - P_f\right)^M \tag{19.32}$$

The overall probability of detection of an impulsive UWB signal not known to be synchronized with the radiometer cannot be expressed simply, so we use numerical simulation to determine this relationship.

Simulation of UWB systems employing binary PPM, bipolar modulation, 4-ary PPM, 4-ary biorthogonal modulation, 16-ary PPM, and 16-ary biorthogonal modulation were carried out to evaluate BER performance in AWGN. Simulation of the binary PPM system using a rate 1/4, constraint length 9 convolutional code with Viterbi soft decoding was also performed.

Note that $P_{FA} \neq P_f$, where $P_{FA}$ is the false alarm for the whole receiver. $P_{FA}$ is the probability that $\kappa$ or more hop decisions result in a detection when no signal is actually present. We determine that as follows. The probability that none of the $M$

channels has a false alarm is the product of the probabilities of each cell not having a false alarm given by $(1 - P_f)^M$. If we assume that the noise in each of the channels is independent of the others, and the channel is AWGN, then the probability of a 1 at the output of the OR gate in the noise-only case will be the probability that at least one of the channels has a false alarm, expressed as

$$P_o = 1 - (1 - P_f)^M \tag{19.33}$$

From the binomial expansion theorem, the probability of this occurring exactly $n$ out of the $N$ times will be

$$\binom{N}{n} P_o^n (1 - P_o)^{N-n} \tag{19.34}$$

Thus, $P_{FA}$ will be the summation of the probabilities of all possible events exceeding the $\kappa$ threshold

$$P_{FA} = \sum_{n=\kappa}^{N} P_o^n (1 - P_o)^{N-n} \tag{19.35}$$

We can conclude from this that noncooperative detection of UWB signals has a very low probability of success and the distance required to detect a signal with a reasonable probability of detection is substantially less than the distance at which the target receiver using a matched filter and knowledge of the transmitter can receive the signal.

The above analysis assumes that the receiver knows when the pulses are to occur so it can look for them. In a noncooperative EW system, that is not the case. The issue is further compounded when the UWB systems use PN codes to randomize the pulse occurrence time. This PN code is known to the target transmitter and receiver but not to the EW system. The only known answer to this quagmire is to let a wideband radiometer integrate over a reasonably wide bandwidth.

*Single Wideband Radiometer Detector*

The performance of a single wideband radiometer (represented effectively by Edell's model) with an observation time of 100 μs against a single user employing uncoded UWB SOIs, and a binary PPM system using a rate 1/4, constraint length 9 convolutional code with Viterbi soft decoding is shown in Figure 19.6. This plot shows that higher order modulations and channel coding can negatively impact detectability.
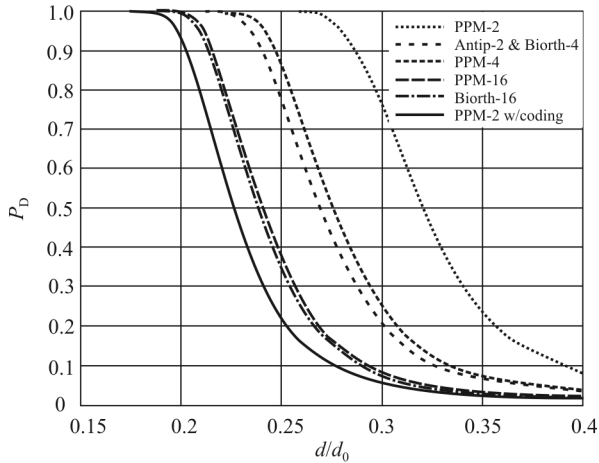
**Figure 19.6** Single radiometer UWB SOIs. Covertness of UWB systems employing different modulation schemes. (Detection is by a single radiometer using an observation window of 100 μsec, computed using a path loss coefficient of 4, a BER at intended receiver of $10^{-4}$, and a $P_{FA}$ of $10^{-2}$. The UWB signal has a bandwidth $W$ of 3.25 GHz, a pulse width of 400 psec, and a pulse repetition time of 1 μsec).

## Channelized Wideband Radiometer Detector

For the channelized radiometer system, the performance of the detector is affected by the parameters chosen. The total interval time for detection decisions was equal to the frame time of the UWB signal above. If the detector's frame is synchronized with the received UWB signal's frame, then when a signal is present, each detector frame will have a channel that overlaps with the UWB pulse transmitted during that frame. But if the detector's frame is not synchronized (e.g., exactly half a frame time off), there will be some detector frames that contain no UWB pulses (assuming the pulse in a given frame is randomly distributed due to the time-hopping code). These frames that do not overlap with a pulse will have a very low probability (= $P_{FA}$) of indicating that a signal is present. This also has a ceiling effect on the maximum achievable average probability of detection when the detector is not synchronized. The probability of detection as a function of distance for the uncoded binary PPM signal is plotted in Figure 19.7 for the cases where the detector is perfectly synchronized with the receiver, the detector is exactly half a frame and half a pulse width off from synchronization, and the detector is assumed to have a uniformly random time offset from synchronization. For this comparison the overall observation interval was set equal to the UWB frame duration ($T = T_f$), the observation interval of each channel was set equal to the pulse duration ($T_0 = T_p$), and the overall probability of false alarm was set to 0.01. All plots
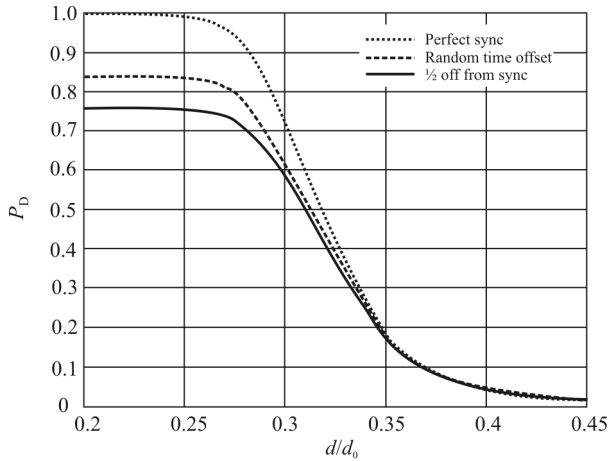
**Figure 19.7** Detectability bounds for uncoded binary PPM with a multiradiometer.

giving the results of the channelized radiometer detector are from simulations using Park's model (19.19) for each radiometer channel. The results from the simulations using Dillard's model are nearly identical and thus are not shown.

The probability of detection for the channelized radiometer can be improved by increasing the overall observation interval. A similar effect is seen in the single wideband radiometer when the observation interval is increased [3, 6]. By increasing the overall observation time to multiple frames, the ceiling effect seen in Figure 19.7 disappears and the difference due to frame synchronization is greatly minimized.

As can be seen by comparing Figures 19.6 and 19.7, the channelized radiometer is able to detect the UWB signal from a greater distance than the single radiometer (except for very small probability of detection values). It is interesting to note that the channelized radiometer detection curve has a steeper slope than the single radiometer curve. This implies that the distance between almost certain detection and almost certain failure of detection is smaller for the channelized radiometer.

The choice of the observation interval for each channel is also important to the performance of the detector. This choice may be influenced by the hardware difficulties for detecting energy over such short intervals or due to lack of information about the pulse width of the signal to be detected. Figure 19.8 compares the performance of the channelized detector for different channel observation intervals. As the channel observation interval grows larger than the pulse duration, more noise is captured relative to the energy of the pulse, resulting in a reduction of the SNR and the performance of the detector decreases. The performance of the channelized system to detect the binary PPM UWB signal with $T_0 = 25T_p$ (shown in Figure 19.8) yields roughly equivalent performance to the
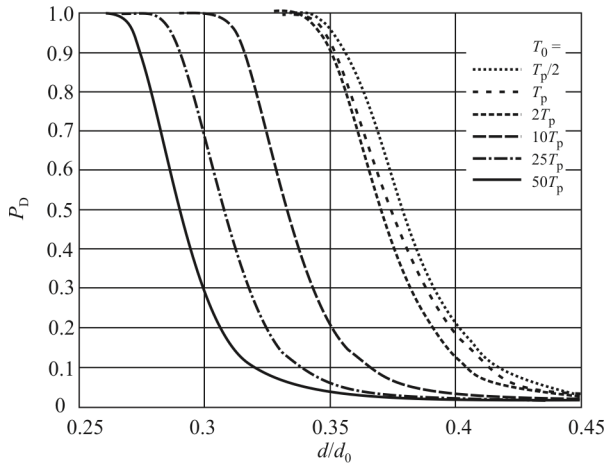
**Figure 19.8** Multiradiometer detectability with different observation times for uncoded PPM.

single wideband radiometer. The energy distribution over time of the pulse used determines the optimal value for the channel observation interval for the detector. Simulation revealed this optimum value is slightly less than $T_p$ for detecting the UWB SOI described here.

*Summary*

The performance of a channelized radiometer detector was evaluated for use in detecting UWB signals and compared to the single wideband radiometer detector. The parameters that impact the performance of such a channelized detector were evaluated and it was shown that it is possible to construct a channelized radiometer detector that improves detectability of UWB signals over a single radiometer if sufficient information about the UWB system is known.

# 19.3 Concluding Remarks

We examined the detectability of THSS signals in this chapter. The receiver considered for this purpose was the time-channelized radiometer.

## References

[1]         Poisel, R. A., *Modern Communications Jamming Principles and Techniques,* 2nd Ed., Norwood, MA: Artech House, 2011, Ch. 13.

[2]     Mills, R. F., and G. E. Prescott, "A Comparison of Various Radiometer Detection Models," *IEEE Transactions on Aerospace and Electronic Systems*, January 1996, Vol. 32, pp. 467–473.

[3]     Weeks, G. D., J. K. Townsend, and J. A. Freebersyer, "Quantifying the Covertness of UWB," *Proceedings of Ultra Wideband Conference*, Washington, DC, September 1999.

[4]     Ipatov, P. V., *Spread Spectrum and CDMA: Principles and Applications*, New York: Wiley, 2005.

[5]     Torrieri, D. J., *Principles of Spread-Spectrum Communication Systems*, Norwood, MA: Artech House, 1992.

[6]     Park, K. Y. "Performance Evaluation of Energy Detectors," *IEEE Transactions on Aerospace and Electronic Systems*, Vol. AES-14, March 1978, pp. 237–241.

[7]     Dillard, R. A. "Detectability of Spread Spectrum Signals," *IEEE Transactions on Aerospace and Electronic Systems*, Vol. AES-15, July 1979, pp. 526–537.

[8]     Barton, D. K. "Simple Procedures for Radar Detection Calculations," *IEEE Transactions on Aerospace and Electronic Systems*, Vol. AES-5, September 1969, pp. 837–846.

[9]     Bharadwaj, A., and J. K. Townsend, "Evaluation of the Covertness of Time-Hopping Impulse Radio Using a Multi-Radiometer Detection System," *Proceedings IEEE MILCOM*, 2001, Vol. 1, pp. 128–134.

[10]    McKinstry, D. R., and R. M. Buehrer, "Issues in the Performance and Covertness of UWB Communications Systems," *MWSCAS-2002, 45th Midwest Symposium on Circuits and Systems*, 2002, Vol. 3.

[11]    Weeks, G. D., J. K. Townsend, and  J. A. Freebersyer, "A Method and Metric for Quantitatively Defining Low Probability of Detection," *Proceedings IEEE MILCOM*, 1998, Vol. 3,  pp. 821–826.

# Chapter 20

## Direction Finding Receivers

### 20.1 Introduction

Determining the *direction of arrival* (DOA) of a signal impinging on an antenna array at an EW receiving system is one of the more important functions of such systems. Determining such DOA, however, sometimes imposes additional requirements on the characteristics of the receivers used for this purpose. We examine some of these requirements in this chapter.

We consider three types of *direction finding* (DF) systems in this chapter as representative samples of such systems. The degradation of the DF accuracy of these systems due to imperfections of the receiver is analyzed. The first type of system uses an amplitude comparison scheme to estimate the DOA of the signal impinging on the EW system array. We use a four-element Adcock antenna arrangement, followed by Watson-Watt signal processing for this analysis [1].

The second configuration is perhaps the simplest arrangement of components for DF. It is called pseudoDoppler and relies on the Doppler principle to estimate the DOA of signals. An array of antennas (typically circular) is sequentially sampled, with the resulting signals sent to a single receiver. Phase differences detected between the antennas as the antennas are commuted are used for the estimation.

The third type of DF system analyzed uses phase interferometry as the technique for estimating the DOA. The basic configuration for phase interferometry is to compare the phase of the signals at two antennas that form a baseline and extract the DOA information from this comparison. Such baselines then can be configured into antenna arrays of arbitrary geometry and size.

Hammerle [2] presented a rather complete exposition on the error sources for Adcock/Watson-Watt and pseudoDoppler DF systems. We present a summary of some of those results here.

The chapter is structured as follows. We begin with an examination of the types of categories of error sources that occur in receivers performing the DF
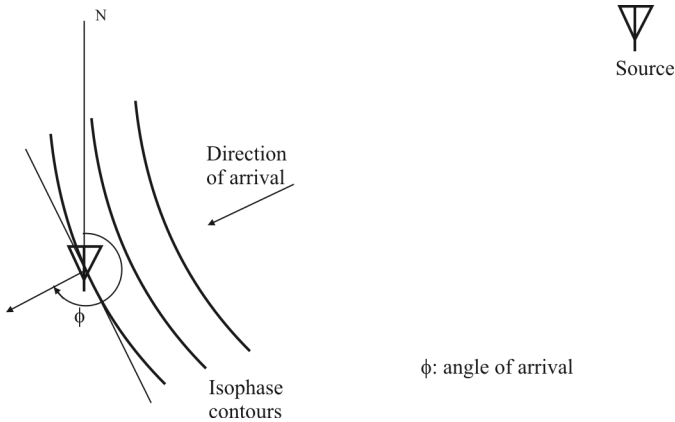
**Figure 20.1** Ideal isophase contours.

function. We follow that with brief descriptions of the types of DF systems analyzed. That is followed by sections on each of the types, with emphasis on the error sources and the impact on DF performance of the receiver error sources. The chapter concludes with a discussion of dual channel compressive receivers, useful for wideband DF applications.


# 20.2 Direction of Arrival

The DOA of a signal at a receiver is the angle (normally measured relative to magnetic or true North) at which the signal arrives. It is customarily defined to be the angle formed between North and the orthogonal to the isophase contour formed within the signal. The isophase contours shown in Figure 20.1 illustrate this concept. The contours in Figure 20.1 are relatively well behaved in the sense that they are smooth and represent a chord of a sphere (circles in two dimensions as shown here). When the antenna array is in the far-field of the target transmitter antenna, these chords are usually assumed to be rectangular planes with no curvature.

Most real situations do not support the ideal case shown in Figure 20.1. Reflections (coherent interference) and cochannel interference (incoherent interference) as well as a myriad of other noise sources tend to cause these isophase contours to take on irregular shapes. This causes the DOA to be estimated in error since the orthogonal to the tangent of the isophase contour depends on where on the isophase curve the antennas occupy in space (Figure 20.2).
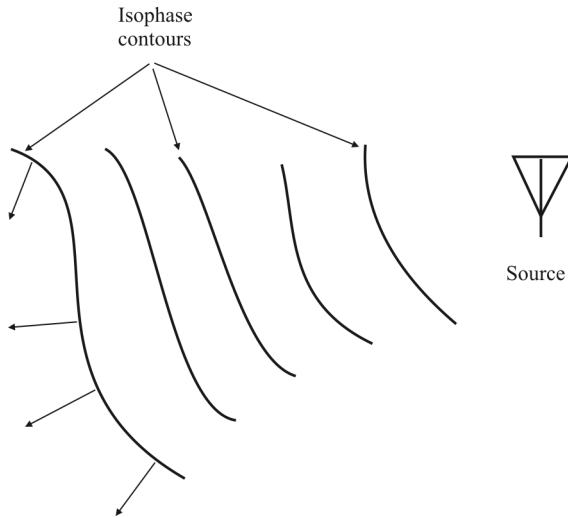
**Figure 20.2** Irregular constant-phase lines such as these are caused by interfering signals and objects in the propagation path. Defining the AOA as the orthogonal to the tangent of the isophase lines can cause errors in estimating the direction to the target.

# 20.3 Direction Finding Techniques Overview

In this section we provide an overview of three popular techniques for determining the DOA of signals at an EW system. The number of techniques for obtaining a DOA is limited only by the imagination of the system designer. Therefore, the methods presented are not exhaustive. They do, however, represent three popular techniques and are useful for examining the requirements of the corresponding receivers used in such applications. In the second part of the chapter, we examine the errors involved in each of these methods and the requirements imposed on the receivers by the applications.

## 20.3.1 The Adcock Array and the Watson-Watt System

During the Second World War, one of the most common techniques of radio direction finding employed in the signals intelligence (SIGINT) stations was based in the use of arrays of four monopoles or dipoles arranged in an orthogonal pattern. By means of rotating the array and combining the signals received in a proper way, a bidirectional radiation pattern is achieved, allowing the determination of the DOA of an SOI, especially through the nulls of the radiation pattern. This technique was patented by Lieutenant Engineer Frank Adcock, No. 3
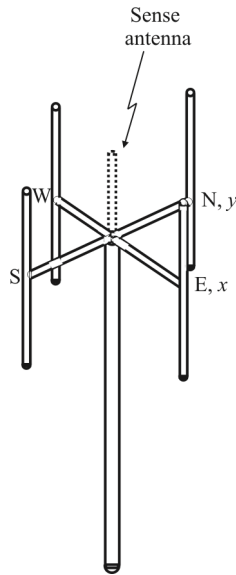
**Figure 20.3** Four-element Adcock array.

Army Wireless Observation Group, in 1920. This is therefore a method of amplitude comparison to determine the DOA of radio signals.

In 1925–26, Sir Robert Watson-Watt (one of the pioneers of the implementation of radar as an early warning system during WWII) improved the system proposed by Adcock by means of using a fifth antenna to avoid the ambiguities and using a cathode ray oscilloscope to plot the angle of arrival, allowing the antenna array to operate in a static configuration.

In an Adcock array, the four antennas are grouped in pairs, laying each pair along a reference axis. Let's suppose, for example, that one of the pairs lies in the North-South axis (Y) and the other lies in the East-West axis (X), as shown in Figure 20.3. This configuration would apply, for example, with ground-based EW systems in the VHF and above frequency range. The four RF voltages of a four-element Adcock system are combined into two differential voltages of equal phase, which feed a double-channel receiver. Originally, the IF signals were fed to the two pairs of plates of the cathode ray tube. The bearing figure drawn on the tube would be a straight line under ideal conditions, whose angle to the X-axis represents the bearing angle (DF value). Modern implementations perform most of this processing digitally, although the fundamental concepts remain the same.

The antenna arrangement in Figure 20.3 provides for two long baselines configured as North-South (N-S) dipole antennas and East-West (E-W) dipole
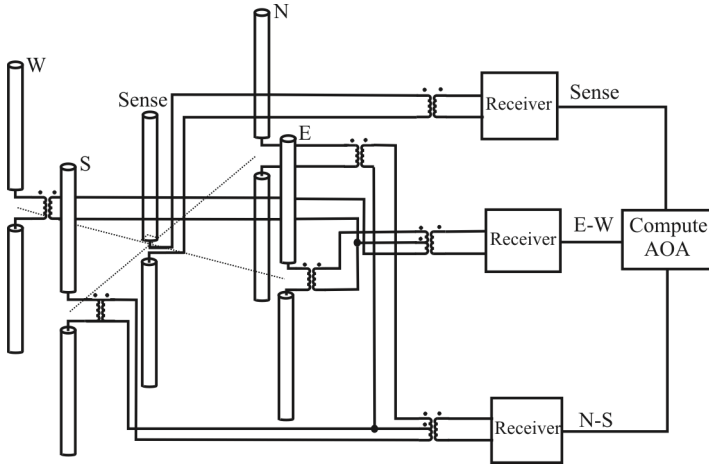
**Figure 20.4** Watson-Watt electrical configuration.

antennas. The Watson-Watt processing associated with this array is an amplitude comparison system that compares the amplitude of the signal in the E-W array response with the amplitude of the signal in the N-S array response.

The electrical configuration is shown in Figure 20.4. The 2D antenna E-field radiation patterns are illustrated in Figure 20.5. The top view of the array is illustrated in Figure 20.6. The pattern for each of the two baselines in the Adcock array configured for the Watson-Watt configuration is in the shape of a figure 8 when viewed from above, as illustrated in Figure 20.5. A signal arriving at some angle onto this array will cause voltages at the output of the antennas that depend on amplitudes of the figure 8 response. A comparison of these amplitudes provides an indication of the arrival angle. A 3D view of these antenna patterns is shown in Figure 20.7.

In two dimensions, the antenna signals in Figure 20.6 are given by

$$V_N(t) = m(t)e^{j\beta R\cos\phi} \qquad\qquad V_S(t) = m(t)e^{-j\beta R\cos\phi}$$
$$V_E(t) = m(t)e^{j\beta R\sin\phi} \qquad\qquad V_W(t) = m(t)e^{-j\beta R\sin\phi} \tag{20.1}$$

We form the difference signals in the array as

$$V_{NS}(t) = V_N(t) - V_S(t) = m(t)\left[e^{j\beta Rr\cos\phi} - e^{-j\beta R\cos\phi}\right] = 2jm(t)\sin(\beta R\cos\phi)$$
$$V_{EW}(t) = V_E(t) - V_W(t) = m(t)\left[e^{j\beta R\sin\phi} - e^{-j\beta R\sin\phi}\right] = 2jm(t)\sin(\beta R\sin\phi) \tag{20.2}$$
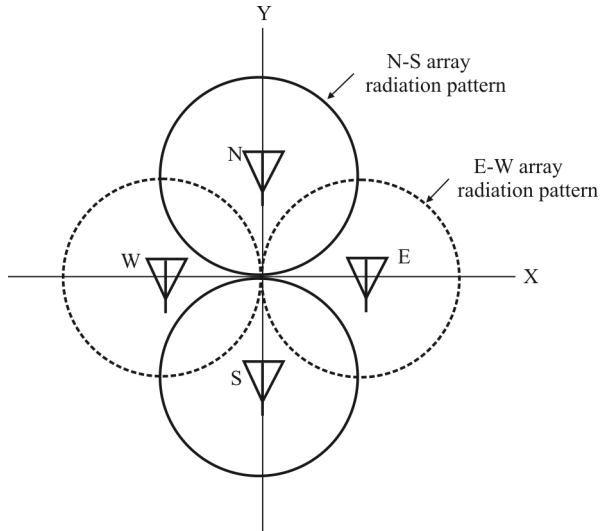
**Figure 20.5** Top view of N-S and E-W antenna patterns for an Adcock/Watson-Watt array.
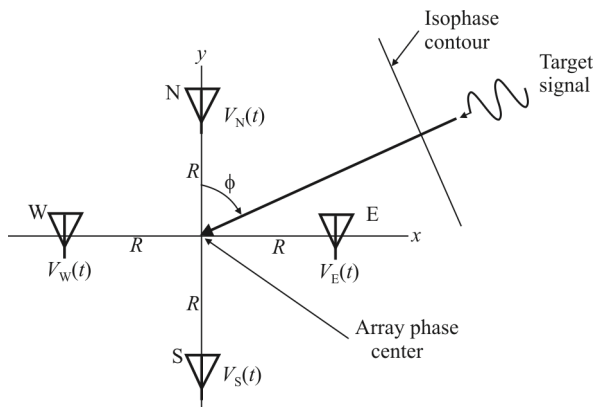


**Figure 20.6** Antenna configuration of a four-element Adcock.

(a)                                                            (b)
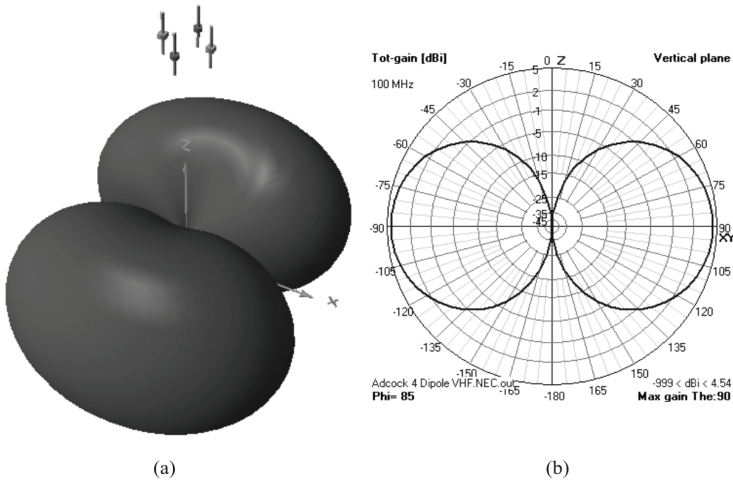
**Figure 20.7** Mast-mounted VHF Adcock baseline pattern: (a) 3-dimensional view, and (b) vertical plane.

Forming the ratio of these signals yields

$$\frac{V_{EW}(t)}{V_{NS}(t)} = \frac{2\,jm(t)\sin(\beta R \sin \phi)}{2\,jm(t)\sin(\beta R \cos \phi)} \tag{20.3}$$

Because $\beta = 2\pi/\lambda \ll 1$, we make the approximations that $\sin(\beta R \sin \phi) \approx \beta R \sin \phi$ and $\sin(\beta R \cos \phi) \approx \beta R \cos \phi$ so that

$$\frac{V_{EW}(t)}{V_{NS}(t)} \approx \frac{\beta R \sin \phi}{\beta R \cos \phi} = \tan \phi \tag{20.4}$$

and so

$$\hat{\phi} = \tan^{-1}\frac{V_{EW}(t)}{V_{NS}(t)} \approx \phi \tag{20.5}$$

In the Watson-Watt system, the two antennas at the end of the baselines are configured as counterphase and that is what creates the patterns shown in Figure 20.5. When connected so that the antennas are in phase, an omnidirectional (in azimuth) pattern emerges. This pattern, shown in Figure 20.8, is very similar to that of a single monopole [3]. When they are in phase (e.g., as is the case for some
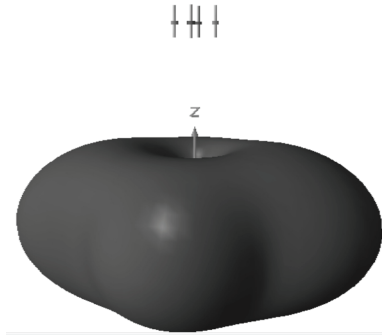
**Figure 20.8** Mast-mounted VHF Adcock four dipole omni pattern. In this configuration the N-S (Y-plane) antennas are fed in-phase producing approximately an omni pattern in the horizontal plane.

phase interferometers), the patterns approach omnidirectionality (in the horizontal plane) as we see in Figure 20.8.

The antenna patterns in Figures 20.7 and 20.8 are approximated with the antennas in free space and are shown in Figure 20.5. For this example, the antennas are $\lambda/2$ in length and the baselines are $\lambda/2$ long. The mast height is 10 m, and the effects of the metallic mast are not considered. This pattern, of course, is when the array is configured as a Watson-Watt array where the two antennas at the end of the baselines are in phase opposition (for amplitude DF configurations).

A common method of determining the antenna array response is to use NEC modeling. Such a technique was used to generate the patterns shown here. The 4NEC2 model for this mast-mounted antenna array is illustrated in Figure 20.9. The 4NEC2 code to model this antenna to produce the patterns shown is given in Figure 20.10.

The sense antenna in Figure 20.4 need not be a separate receiving path. In Figure 20.4 we show a separate antenna located at the phase center of the array feeding its own receiver. Another configuration is shown in Figure 20.11, where the four antennas at the end of the baselines are combined in phase-shifting hybrid combiners and the sense signal is generated directly from these four antennas. This configuration also has $U_{NS}$ and $U_{EW}$ generated simultaneously in these same shown in Figure 20.8.

As a second example, consider the ground-based monopole array depicted in Figure 20.12. Again, four antennas are arranged at the ends of two baselines that are equal in length. The aim is focused on the determination of the DOA of a radio signal of interest, which may be in the range between 2 MHz and 10 MHz (MF–HF), and for specificity, the example for a 5 MHz signal is considered.
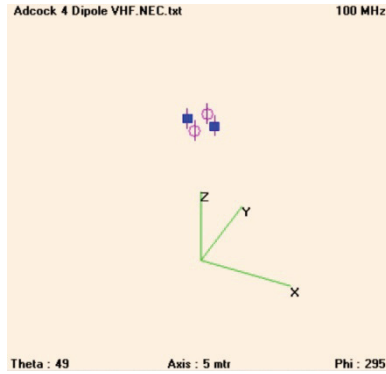
**Figure 20.9** Mast-mounted VHF Adcock four dipole geometry.

CM 100 MHz Adcock 4 Dipole Direction Finding Array

CM on 10m mast

CM Poisel 6.12.2013

CM

CE

| | | | | | | | |
|---|---|---|---|---|---|---|---|
| GW 1 25 | 0 | 0.75 | 9.25 | 0 | 0.75 | 10.75 | .02' North Dipole |
| GW 2 25 | 0.75 | 0 | 9.25 | 0.75 | 0 | 10.75 | .02' East Dipole |
| GW 3 25 | 0 | -.75 | 9.25 | 0 | -.75 | 10.75 | .02' South Dipole |
| GW 4 25 | -.75 | 0 | 9.25 | -.75 | 0 | 10.75 | .02' West Dipole |

GE 0 'Free space

FR 0 1 0 0 100 0' 100 MHz Operating Frequency

EX 0 1 12 0 1 0' North generator

EX 0 3 12 0 -1 0' South generator

LD 0 2 12 0 50 0 0' East loading

LD 0 4 12 0 50 0 0' West loading

EN

**Figure 20.10** Mast-mounted VHF Adcock four dipole NEC code.

$$RF = V_N + V_E + V_S + V_W$$
$$V_{NS} = V_N - V_S$$
$$V_{EW} = V_E - V_W$$
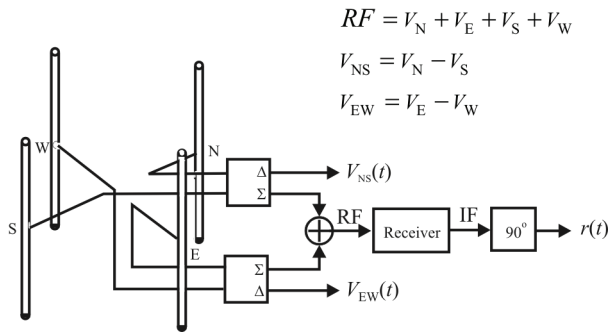
**Figure 20.11** Generation of reference signal.
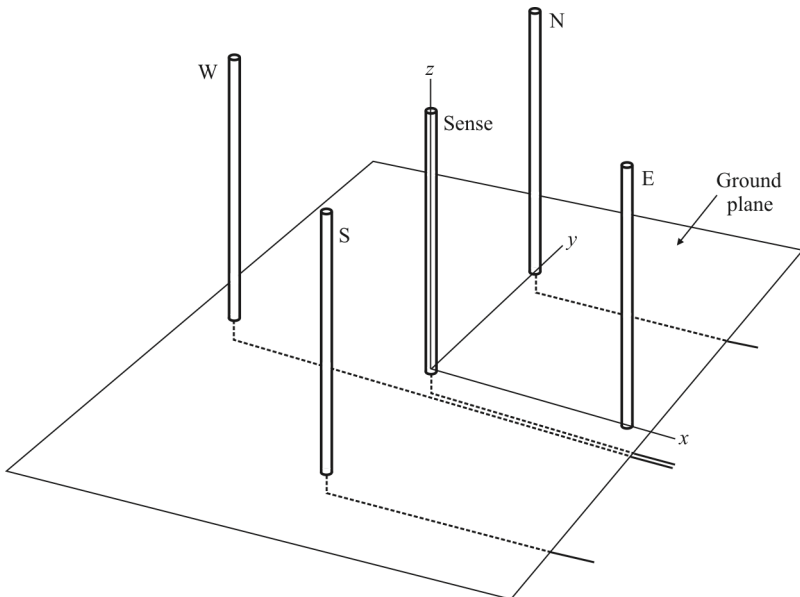


**Figure 20.12** Adcock four monopole array.

(a)  (b)
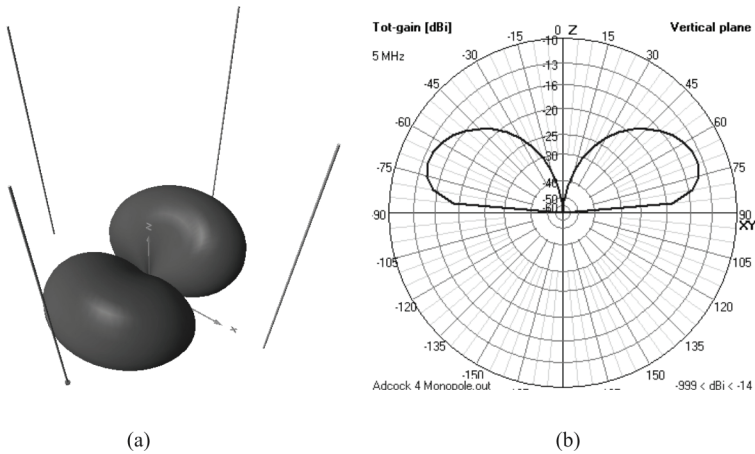
**Figure 20.13** Adcock four-monopole baseline N-S antenna array pattern: (a) 3-dimensional, and (b) vertical plane.

The receiver configuration for this monopole array is the same as for the mast-mounted array discussed previously. As such, the signal processing is the same. With ground-mounted arrays with a ground plane, the antenna patterns are truncated at the ground as illustrated in Figure 20.13, which shows the pattern for a single baseline. Combining all four antennas in phase produces an omnidirectional pattern (in the horizontal plane) as illustrated in Figure 20.14.

We consider ¼ wavelength monopoles for a working frequency of 5 MHz. That is, each monopole has a length of 15m. In order to simplify the analysis, the part relative to the antenna coupling in all the working band will be obviated, although in fact it is not necessary for the antennas to be resonant in the frequency of the SOI.

The antenna separation or baseline is another important point and must be half the wavelength of the maximum working frequency at the most, ideally around one eighth or one tenth of the working wavelength. If the separation is higher than half the wavelength, a risk of having ambiguities in the measurements exists. That's the reason why, if the bandwidth to be watched is high, it may be appropriate to have different baselines for each frequency or frequency range.

The baselines in this case are 15m long and the antenna baselines are 30m. The operating frequency is 5 MHz. The antennas in Figure 20.12 are assumed to be operating over a perfect ground plane, so the patterns reach to the ground plane undisturbed. Over a more realistic ground plane, there is a curvature of the patterns close to the ground caused by the poorer propagation constants of the ground.

The 4NEC2 code for the four-element monopole Adcock array is shown in Figure 20.15.
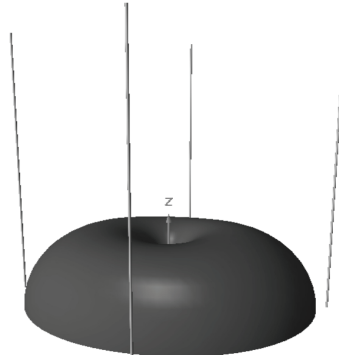
**Figure 20.14** Adcock four monopole omni pattern in the horizontal plane.

The ground-based monopole array shown in Figure 20.12 is not adequate for high-frequency radio direction finding (HF/DF) for *near vertical incidence system* (NVIS) signals, due to the fact that the radiation patterns of the monopoles employed have low gain for high takeoff angles [4]. In addition, the baseline effects disappear at high receive elevation angles so the amplitude comparison scheme fails.

The precision of an Adcock/Watson-Watt radio direction finding system in the computation of angles of arrival is estimated to be around 2–3 degrees.

## 20.3.2 PseudoDoppler DF System Overview[1]

The pseudoDoppler technique takes advantage of the effects on a received signal at an antenna that is moving. When an antenna is moving toward the source of a signal, then the frequency of the signal at the antenna is somewhat higher than if the antenna were still. When the antenna is moving away from the source of the signal, then the frequency is somewhat lower than the true frequency. These frequency differences are due to the well-known physical phenomenon called *Doppler shift*.

Doppler shift can be exploited to determine the DOA of signals impinging on an EW system. An antenna can be rotated in an EM field, as shown in Figure 20.16, and the output frequency measured. The frequency difference between the signal received at the rotating antenna and the true frequency measured at the stationary antenna determines the AOA.

Consider the diagram shown in Figure 20.17, which is a top view of Figure 20.16. The Doppler shift is given approximately by (assuming that $v \ll c$)

---

[1] Much of the material in this section is from [4]. Reprinted with permission.

```
CM 4-Monopole Adcock Array 5 MHz
CM
CE

SY monlen=15 'Monopole length
SY monsep=15 'Monopole Separation

GW  1 128    0       monsep/2 0.001    0            monsep/2    monlen    2mm'North
Monopole
GW  2 128    0       -monsep/2 0.001   0            -monsep/2   monlen    2mm'South
Monopole
GW  3 128    -monsep/2 0    0.001   -monsep/2        0          monlen    2mm'West
Monopole
GW  4 128    -monsep/2 0    0.001   monsep/2         0          monlen    2mm'East
Monopole


GE  1
GN  1
EK

EX  0    1    1    0    1    0         0    'Generator at North Monopole
EX  0    2    1    0    -1   1.22e-16  0    'Generator at South Monopole

FR  0    1    0    0    5.0  0' 5 MHz Operating Frequency

EN
```

**Figure 20.15** 4NEC2 code for four element monopole Adcock/Watson-Watt array.
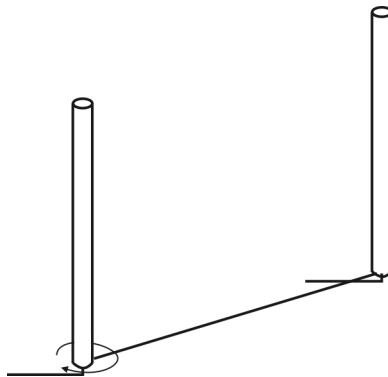


**Figure 20.16** Doppler antenna configuration.
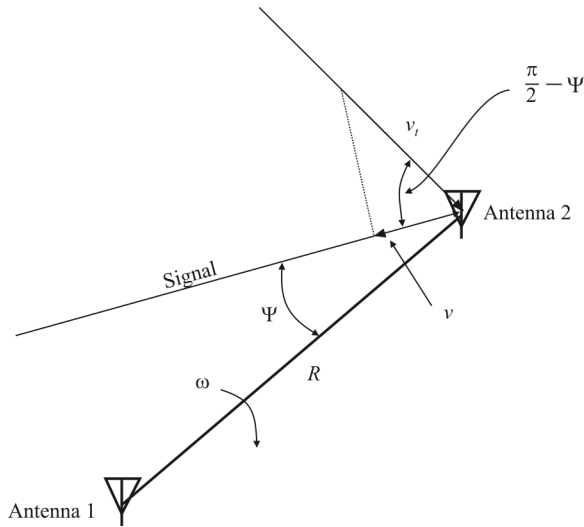
**Figure 20.17** Top view of the Doppler rotating antenna array. Antenna 1 is stationary while antenna 2 rotates around it.

$$\Delta f = \frac{v}{c} f_0 \tag{20.6}$$

where $v$ is the rotating antenna velocity in the direction of the signal, $f_0$ is the signal frequency, and $c$ is the speed of propagation. The tangential velocity, $v_t$, shown in Figure 20.17 is given by

$$v_t = R\omega \tag{20.7}$$

where $R$ is the baseline length and $\omega$ is the angular velocity of the rotating antenna. The velocity $v$ is related to the tangential velocity by

$$v = v_t \cos\left(\frac{\pi}{2} - \Psi\right) = v_t \sin \Psi \tag{20.8}$$

Therefore, the Doppler shift is given by

$$\Delta f = \frac{R\omega}{c} f_0 \sin \Psi \tag{20.9}$$
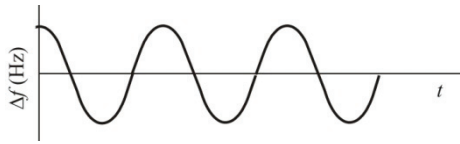
**Figure 20.18** Output of the comparison of the two signals in a Doppler DF system.

A sense antenna located in the center of the circle determines the true frequency. The response would be as shown in Figure 20.18. When the rotating antenna is moving toward the signal source, the difference frequency is positive, and when moving away, it is negative. In most modern implementations, a circular array of fixed antennas would be used as opposed to actually mechanically rotating an antenna. The effects of rotation can be achieved by electronically switching each antenna in the array in turn. The sense antenna is not physically needed since the output of all the antennas in the circular array can be combined in phase to accomplish this function.

The pattern for this Doppler DF array is the same as that shown in Figure 20.8 for the four-element Adcock VHF array except, of course, the pattern is rotating. A directional pattern as in Figure 20.7 can be created as well if the phases of the two antennas are connected in opposition. For Doppler DF signal processing, a directional pattern is not required, however.

## 20.3.3 Phase Interferometer System Overview

One popular technique for measuring the *angle of arrival* (AOA) of an incoming signal, and thereby determining its DOA, is *interferometry*. In this case the phase difference $\Delta\phi_{12}$ or time difference $\Delta t_{12}$ between two antennas is measured directly by some means. These two types of measurements produce the same result, the major difference being what is measured.

It is also possible to implement an active interferometer. Active interferometers emit a signal and measure the phase or time difference of the returned signal. This is a form of radar.

The phase interferometer measures the phase differences between two antennas, and the angle of arrival is deduced from this angle. The second type of interferometer measures the time of arrival difference of the signal at two antennas. To make this measurement, there must be some feature associated with the signal that can be used as a time mark, such as the leading edge of a radar pulse. Lacking such a feature the signals at the two antennas must be correlated against each other to determine this time difference. Where this correlation peaks is an indication of the time difference. This is called *arrival time interferometry*. We will now discuss the concepts involved with phase interferometry.
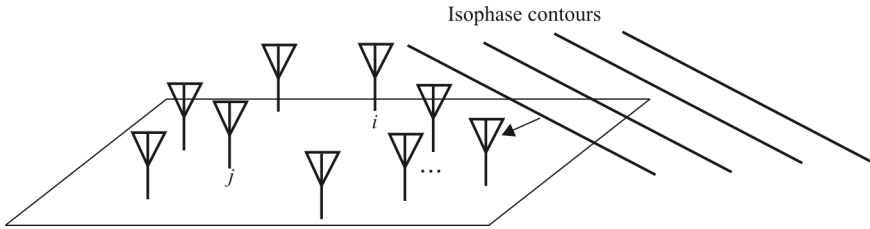
**Figure 20.19** Array of *M* sensors.

20.3.3.1 Phase Interferometry

Consider the arbitrary planar antenna array of *M* sensors illustrated in Figure 20.19. If $s(t)$ represents the signal emitted from a far-field source, then the outputs from *M* narrowband receiver channels connected to the output of these antennas at each time, $t \in \{1, 2, \ldots, K\}$, can be represented as

$$\vec{r}(t) = \vec{a}(\phi)s(t) + \vec{n}(t), \qquad t = 1, 2, \ldots, K \qquad (20.10)$$

where $\vec{r}(t)$ is an $M \times 1$ vector with complex elements, *K* is the number of samples taken (snapshots), and $\vec{n}(t)$ is an $M \times 1$ vector of uncorrelated antenna AWGN samples. $\vec{a}(\phi)$ is the $M \times 1$ complex vector representing the phase response of the array with a signal impinging on it from direction $\phi$.

An interferometer measures the phase differences from pairwise antenna elements. Usually one is designated as the reference antenna and the phase differences are computed from each of the other elements compared to that reference. In general, the estimated phase difference, $\hat{\phi}_{ij}$, between the *i*th element and *j*th element is found from

$$\hat{\phi}_{ij} = \arg\left( \frac{1}{K} \sum_{t=1}^{K} r_i(t) r_j^*(t) \right) \qquad (20.11)$$

The signal impinging on a second antenna displaced from an antenna as shown in Figure 20.20 must travel an extra distance of $d_1 = D\sin\phi$ compared with that antenna. This imposes an additional phase shift on the signal given by

$$\phi = \beta D \sin\phi \qquad (20.12)$$

As we describe later, (20.12) is used to compute the AOA, $\phi$.
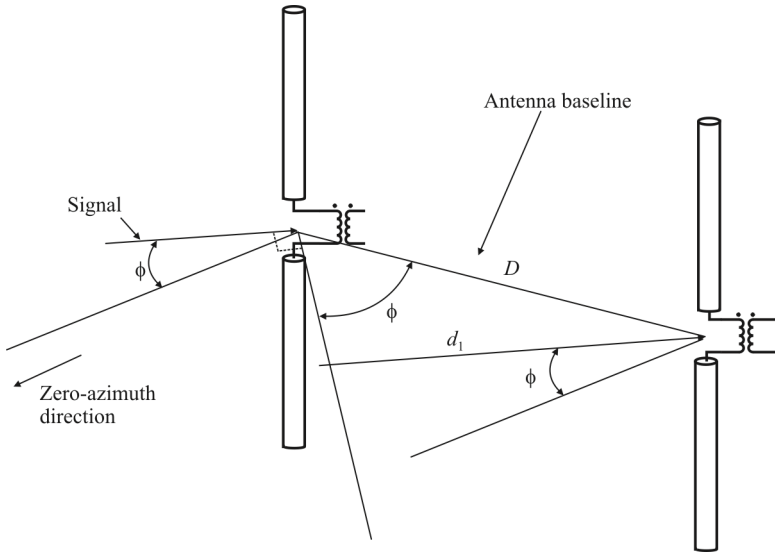
**Figure 20.20** Interferometer baseline.

# 20.4 Error Sources in Direction Finding Systems

Error sources in DF systems can be divided into two broad categories: (1) those external to the receiving system and (2) those internal to the receiving system. In this section we summarize the major sources of these errors, while the impacts on the specific DF techniques are covered in the appropriate sections to follow.

### 20.4.1 Polarization-Induced Error

Polarization errors can occur any time there is a mismatch between the polarization of the target signal and the receive antennas. This is normally manifest in a reduced signal level available for the (normally) vertical response of the antennas.

In some cases, however, polarization effects can cause DF errors even though there is no polarization mismatch between the target signal and the receive array. In the case of the Adcock DF as well as in the case of the Doppler DF, currents are induced on the outer conductor of the connecting coaxial cables between opposite antennas; these currents produce a secondary field, which results in additional error vectors with opposite sign at the terminals of the two antenna elements.

The antenna voltages in Figure 20.21 are
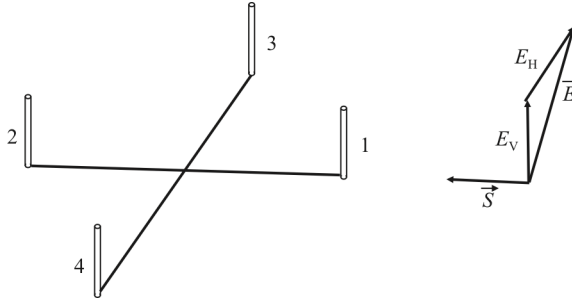
**Figure 20.21** Polarization error mechanism. Currents $(\vec{S})$ in the cable interconnecting antenna 1 with antenna 2 set up secondary fields $(\vec{E})$, which result in additional error vectors with opposite sign at the terminals of the two antenna elements.

$$
\begin{aligned}
V_1 &= E_V h_{\text{eff}} e^{+j\kappa} & V_2 &= E_V h_{\text{eff}} e^{-j\kappa} \\
V_3 &= E_V h_{\text{eff}} e^{+j\kappa} + E_H \cdot h & V_4 &= E_V h_{\text{eff}} e^{+j\kappa} - E_H \cdot h
\end{aligned} \tag{20.13}
$$

where

$h_{\text{eff}}$ is the effective height of the antenna
$h$ is the proportionality factor between the horizontal component and the antenna output voltage
$$\kappa = \frac{2\pi R}{\lambda} \sin\theta$$
$R$ is the array radius
$\theta$ is the elevation angle

### 20.4.2 DF Errors Caused by Incoherent Wave Interference

With incoherent interference, otherwise known as *cochannel interference*, two (or more) waves add as vectors (amplitude and phase), to produce unpredictable isophase and isoamplitude contours, for which producing accurate AOA estimates with traditional methods (those considered here) is very difficult. We show in Figure 20.22 a sketch of the impacts of two waves in space that are within 0.05 in amplitude (arbitrary units) and $10^\circ$ in separation. The isoamplitude contours are straight lines essentially parallel to the X-axis (a feature that is a function of the specific parameters chosen for this example), while the isophase contours form curves. For a phase measuring technique, depending on where in particular the receive antennas are located relative to these isophase contours, virtually any estimated AOA may emerge.
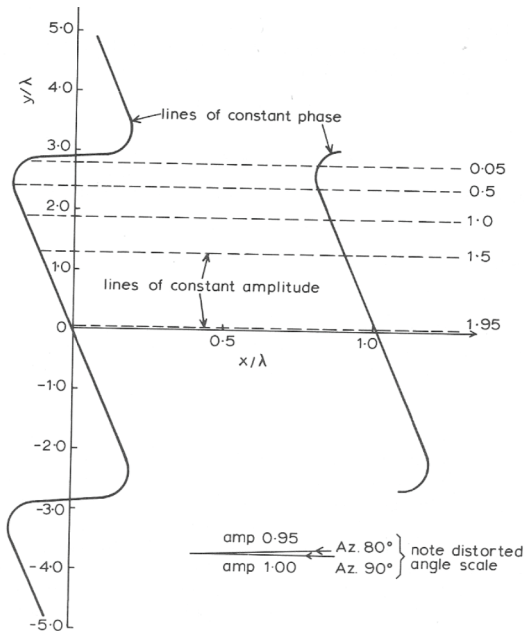
**Figure 20.22** Interfering waves. Wave 1: $0.95\angle80^\circ$ while Wave 2: $1.0\angle90^\circ$. (Source: [5], © 1991, Peter Peregrinus, Ltd. Reprinted with permission.)

Superresolution DF methods have been devised that can separate multiple incoherent (and sometimes coherent as well) waveforms in some cases, depending on the particular parameters. We do not consider them here. For a more thorough discussion see [6, 7].

### 20.4.3 DF Errors Caused by Coherent Wave Interference (Multipath)

When two (or more) coherent signals arrive at a receiver array from multiple directions, errors can be generated in computation of the DOA. Such multiple signals are usually the result of reflections of a target signal from multiple reflectors that see the target signal and are within sight of the receiver.

These signals arrive at the receiver with different amplitudes and different phases. In some cases, the amplitudes and phases of the reflected waves can be such that complete cancellation of the direct signals occurs. In most cases, however, the reflected waves have smaller amplitudes than the direct waves, although the phase angles are difficult to predict.

In any case, these coherent signals can severely impact the accuracy of the DOA computation, since receiver systems have difficulty separating reflected signals from the direct signal.

### 20.4.4 Modulation

The impacts of modulation on the target signals vary with the DF processing subsequent to the antenna. AM affects some techniques while FM/PM has no (or minimal) impact. In other configurations, AM has little impact while FM/PM can cause significant errors. Occasionally, all types of modulation have some impact.

Rarely are target signals CW in nature. Some type of modulation is almost always present, so the modulation impacts must be considered when designing receivers for DF applications.

### 20.4.5 Physical Antenna Arrangement

When antennas are not precisely placed in an antenna array, it usually causes errors to occur in the estimation of the AOAs estimated. Since array processing implies precise knowledge of where the antenna elements are in space, these errors lead directly to miscalculations in the AOA estimation.

### 20.4.6 Receiver Noise

RF noise is an omnipresent adversary in any communication problem, including EW receivers. It comes in a variety of forms, some from internal to an electronic system, others from external sources.

The predominant internal noise sources are agitated electrons that vibrate and in doing so emit energy that covers very broad bandwidths. This noise is referred to as *thermal noise*. This noise affects both the amplitude and phase of signals in EW receivers. The amplitude is affected directly in that the instantaneous value of noise voltage or current adds to the amplitude of the signal. Phase is effected primarily through the thermal phase noise associated with oscillators.

We have discussed thermal noise and its affects and measurement elsewhere herein. The effects of noise on the front end of DF receivers are no different from their effects on other receivers. The predominant measure of performance in noise is dictated by the SNR. To determine the performance in noise, noise levels are reflected to the input of the receiver, and the remainder of the receiver is assumed to be noise free.

### 20.4.7 Amplitude Matching and Phase Tracking

In those configurations that require multiple receivers, there are usually requirements imposed on how well the receivers track each other, in both
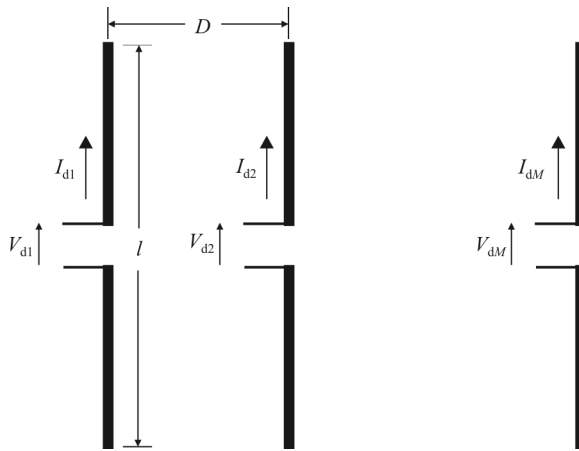
**Figure 20.23** Array of dipoles.

amplitude and phase responses. Often, real-time or non-real-time calibration is required so that these tracking parameters are at least known, if they cannot be eliminated altogether in the design.

## 20.4.8 Antenna Element Interaction

Antenna arrays are configurations of multiple (>1) antennas essentially collocated, or located close enough together that interaction between elements can be expected. That is certainly true for the antennas under consideration here. The antennas are all located within one or a few wavelengths of one another, and that places the antennas within the near field of other antennas [8].

Arrays of dipoles, monopoles, and loops are the most common for DF applications under consideration here. Some of these configurations tend to minimize the antenna interactions (e.g., the dipole array) while others cannot suppress the interactions (e.g., monopoles). An array of $M$ dipoles of length $l$ and separated by distance $D$ is shown in Figure 20.23.

A mutual coupling model of two dipoles is shown in Figure 20.24. Whenever two or more antenna elements are in close proximity to one another, they interact. This interaction is called *mutual coupling*. The element currents are not the same as they would be for an element in isolation (free space). A two-port model for two elements in Figure 20.24(a) interacting in this way is shown in Figure 20.24(b).

The impedances in Figure 20.24(b) are the port parameters, assuming that the two antennas form a two-port network. The two-port model is given by
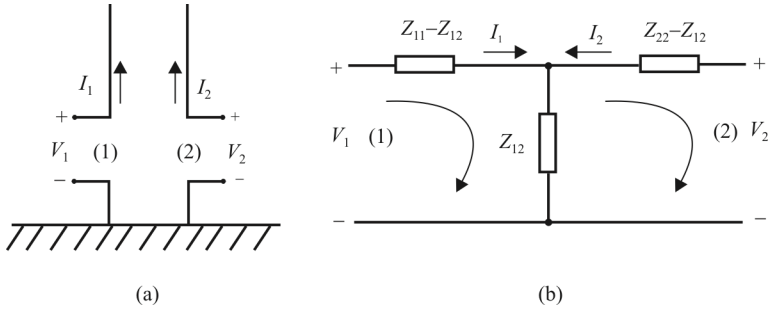
**Figure 20.24** Mutual coupling: (a) antenna configuration and (b) equivalent two-port model.

$$V_1 = Z_{11}I_1 + Z_{12}I_2$$
$$V_2 = Z_{21}I_1 + Z_{22}I_2$$

(20.14)

So $Z_{11}$ is found by measuring the voltage and current at port 1 with port 2 open circuited (or, since it is an antenna element, by removing it) since

$$Z_{11} = \left.\frac{U_1}{I_1}\right|_{I_2=0}$$

(20.15)

Likewise, $Z_{22}$ is determined by measuring the voltage and current at port 2 with the antenna at port 1 open circuited (or not there) since

$$Z_{22} = \left.\frac{V_2}{I_2}\right|_{I_1=0}$$

(20.16)

All of these measurements are, of course, frequency dependent and, in general, complex values.

Assuming that the network is symmetrical (this is certainly true for an array of dipoles, e.g.), then $Z_{21} = Z_{12}$. Either of these is found in the same way: $Z_{12}$ is found by measuring the voltage at port 1 when it is an open circuit ($I_1 = 0$) caused by a known current source at port 2 because

$$Z_{12} = \left.\frac{V_1}{I_2}\right|_{I_1=0}$$

(20.17)
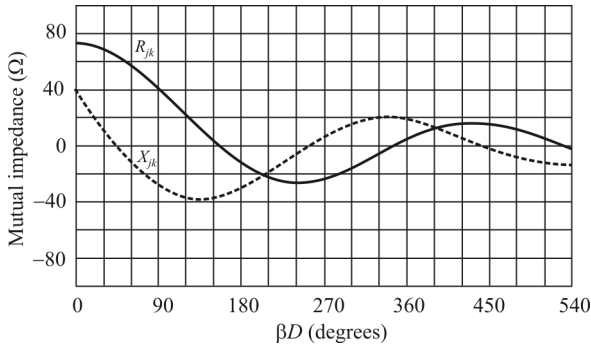
**Figure 20.25** Mutual impedance between two $\lambda/2$ dipoles at distance $D$ ($\beta D$ in degrees).

Notice with port 2 open circuited, the impedance seen looking into port 1 is $Z_{11} - Z_{12} + Z_{12} = Z_{11}$; similarly for port 2.

For an array with $M$ elements, all (or most) or the antenna elements will have an effect on all the others. Hence, the two-port analysis needs to be extended to $M$ ports. This is accomplished in a straightforward way and many textbooks are available that indicate how this is done. Also computer programs are available to assist in this process.

The magnitude of the mutual impedance between two elements depends on the antenna dimensions and on the distance between antenna elements. The real and imaginary components of the mutual impedance can be both positive and negative, and their maximum values decrease as the distance between elements, $D$, increases. The influence of very distant elements is negligible. Typical characteristics of the components of the mutual impedance $Z_{jk} = R_{jk} + jX_{jk}$ on the distance $D$ (multiplied by wavenumber) between two parallel $\lambda/2$ dipoles are depicted in Figure 20.25. The wavenumber is given by $\beta = 2\pi/\lambda$.

## 20.4.9 Antenna Height above Ground

Theoretically, the radiation resistance of an antenna does not vary with environmental conditions in the vicinity of the antenna. In practice, this is only true in free space—when there is nothing in the vicinity of the antenna for considerable distances.

We illustrated the effects in Figure 20.26, where the variation of the radiation resistance of a theoretical half-wave dipole with height above ground above a perfectly conducting ground plane is shown. We can see that the actual radiation resistance oscillates around the theoretical value of $73\Omega$. We can also see that the effect virtually disappears at heights greater than about 1 wavelength or so.
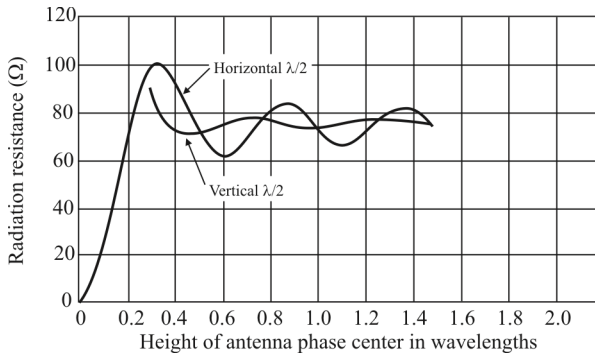
**Figure 20.26** Radiation resistance variation with height.

## 20.5 Adcock/Watson-Watt (Four-Element Adcock)

Lipsky analyzed the performance of the Adcock/Watson-Watt configuration [9]. The signals from the receivers shown in Figure 20.4 are given by

$$V_{EW} = k_{EW} \sin \phi \tag{20.18}$$

and

$$V_{NS} = k_{NS} \cos \phi \tag{20.19}$$

where $\phi$ is the AOA of the target signal, and, as above, $k_{EW}$ and $k_{NS}$ are the amplitude responses of the two channels through the receiver paths. The sense antenna is the sum of the responses of the other four antennas and is normally formed in that way—as the sum; typically a separate antenna is not included. The sense antenna is used to remove ambiguities in the AOA, and its amplitude response characteristics are not critical to this discussion.

The AOA is determined by finding the ratio of the E-W and N-S signals as

$$\frac{V_{EW}}{V_{NS}} = \frac{k_{EW} \sin \phi}{k_{NS} \cos \phi} = \frac{k_{EW}}{k_{NS}} \tan \phi \tag{20.20}$$

We assume that the amplitude characteristics before the receivers are ideal so that we can examine the receiver requirements on $k_{EW}$ and $k_{NS}$, not the antenna and related component characteristics.

From (20.20) we can see that

$$\phi = \tan^{-1} \frac{k_{NS}}{k_{EW}} \frac{V_{EW}}{V_{NS}} \tag{20.21}$$

and the DF system calculates an estimate of the value of $\phi$, which we will denote by $\hat{\phi}$. Ideally, $k_{NS} = k_{EW}$ for an error-free system.

The error in the estimate is then

$$\varepsilon = \hat{\phi} - \phi = \tan^{-1} \frac{k_{NS}}{k_{EW}} \frac{V_{EW}}{V_{NS}} - \phi = \tan^{-1} \frac{k_{NS}}{k_{EW}} \tan\phi - \phi \tag{20.22}$$

Let us denote $k_{NS}/k_{EW}$ by $X$:

$$X \triangleq \frac{k_{NS}}{k_{EW}}$$

so that

$$\varepsilon = \tan^{-1}(X \tan\phi) - \phi \tag{20.23}$$

The worst-case error is found by determining the maximum of (20.23), which is found by differentiation and setting the result to zero. Since, if $v$ is a function of $x$, $v(x)$, then from tables of derivatives we know that [10]

$$\frac{d \tan^{-1} v(x)}{dx} = [1 + v^2(x)]^{-1} \frac{dv(x)}{dx}$$

then

$$\frac{d\varepsilon}{d\phi} = \frac{d \tan^{-1}(X \tan\phi)}{dx} - 1$$

$$= X(1 + X^2 \tan^2\phi)^{-1} \frac{d \tan\phi}{d\phi} - 1$$

$$= \frac{X}{1 + X^2 \tan^2\phi} \sec^2\phi - 1 \tag{20.24}$$

Equating (20.24) to zero yields

$$\frac{d\varepsilon}{d\phi} = \frac{X \sec^2 \phi - 1 - X^2 \tan^2 \phi}{1 + X^2 \tan^2 \phi} = 0$$

so that the condition for a maximum becomes

$$X \sec^2 \phi - 1 - X^2 \tan^2 \phi = 0 \qquad (20.25)$$

which is a quadratic in $X$ as

$$(\tan^2 \phi) X^2 - (\sec^2 \phi) X + 1 = 0$$

so that

$$X = \frac{\sec^2 \phi \pm \sqrt{\sec^4 \phi - 4 \tan^2 \phi}}{2 \tan^2 \phi} \qquad (20.26)$$

But the Pythagorean formula for tangents and secants [11] says that $\tan^2 \phi = \sec^2 \phi - 1$. Making this substitution into (20.26) yields

$$X = \frac{\sec^2 \phi \pm \sqrt{\sec^4 \phi - 4 \sec^2 \phi + 4}}{2 \tan^2 \phi}$$
$$= \frac{\sec^2 \phi \pm (\sec^2 \phi - 2)}{2 \tan^2 \phi}$$

The plus sign in the numerator yields the trivial solution $X = 1$ so there is a minimum or maximum (minimum in this case) at $X = 1$ where $k_{EW} = k_{NS}$, which we already knew. The minus sign yields

$$X = \frac{2}{2 \tan^2 \phi} = \frac{1}{\tan^2 \phi}$$

so that

$$\phi = \tan^{-1}\left( \pm \frac{1}{\sqrt{X}} \right) \qquad (20.27)$$

Substituting (20.27) into (20.23) yields
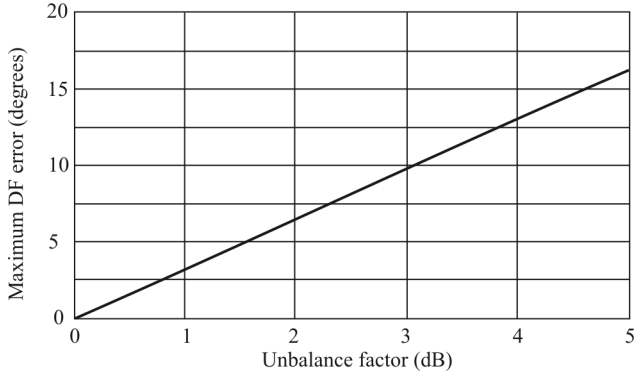
**Figure 20.27** Adcock/Watson-Watt maximum DF error.

$$\varepsilon = \tan^{-1}(X\tan\phi) - \tan^{-1}\left(\pm\frac{1}{\sqrt{X}}\right)$$

$$= \tan^{-1}\left(X\pm\frac{1}{\sqrt{X}}\right) - \tan^{-1}\frac{1}{\sqrt{X}}$$

$$= \tan^{-1}(\pm X^{1/2}) - \tan^{-1}X^{-1/2} \tag{20.28}$$

In the first quadrant, (20.28) yields

$$\varepsilon = \tan^{-1}X^{1/2} - \tan^{-1}X^{-1/2} \tag{20.29}$$

Equation (20.29) is plotted in Figure 20.27 when $X$ is expressed in decibels ($20\log_{10}X$ since $X$ is a voltage ratio). For example, if the channels are unbalanced by 1dB, the maximum DF error is about $3.5^\circ$.

## 20.5.1 Natural DF Error of the Adcock

For the Adcock/Watson-Watt DF only the approximation $\hat{\phi} \approx \phi$ is valid because of the sin and cos functions in the numerator and denominator of (20.5). The resulting error $\varepsilon_\phi = \hat{\phi} - \phi$ (natural DF error of the Adcock) disappears for $D \ll \lambda$. In the case of the four-element Adcock this error amounts to a maximum value of approximately $7^\circ$ (Figure 20.28) for $D/\lambda = 1/2$ while for $D/\lambda = 1/5$ it remains below $1^\circ$.

The maximum DF error for an *n*-antenna Adcock is determined with
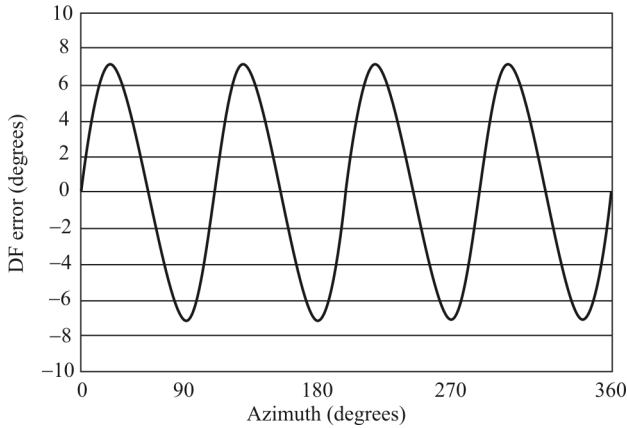
**Figure 20.28** Natural error of a four-element Adcock for $D = \lambda / 2$.

$$\varepsilon_\phi = \frac{2J_n(\kappa)}{\kappa J_1(\kappa)}$$

where

$n$ is the number of antennas

$$\kappa = \frac{2\pi R}{\lambda} \sin\theta$$

$\theta$ is the elevation angle
$J_n$ is the Bessel functions of order $n$

## 20.5.2 Adcock Direction Finding Errors Caused by Reflections (Coherent Wave Interference)

If two waves of the same frequency and comparable amplitudes are incident on an antenna array, a stationary field of interference is formed by the waves. This results in distortion of the lines of constant phase. These waves are both within the IF passband of the receiver and the receiver will react to the distorted constant phase lines. It becomes impossible for the receiver to properly separate the signals with the basic DF processing provided by the Adcock arrangement. This is referred to as *cochannel interference*, and the resulting DOA will be in error.

The amount of error produced is a function of the amplitude ratio of the two waves as well as the antenna aperture. Compared with narrow-aperture systems, a wide-aperture system in this case works more precisely (Figure 20.29). In the following, the improvement factor will be calculated. If the lines of constant phase
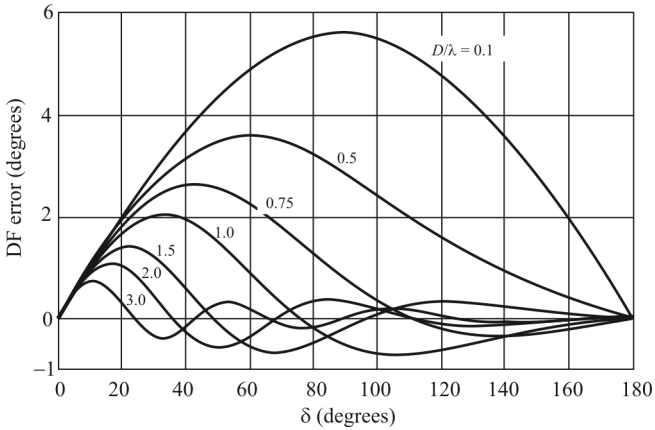
**Figure 20.29** Maximum DF error caused by a reflection as a function of the angle $\delta$ between the direct and the reflected wave. $\rho = 0.1$, $\theta_0 = 0°$.

are determined in a field of interference established by two waves, then the deviation of the tangent to these lines from the direction of the undisturbed lines gives the DF error of small base systems of infinitesimally small aperture given by

$$\varepsilon_\phi = \tan^{-1} \frac{\rho \cos \theta_0 \sin \delta}{1 + \rho \cos \theta_0 \cos \delta} \tag{20.30}$$

where

$\varepsilon_\phi$ is the DF error
$\rho$ is the amplitude ratio
$\delta$ is the azimuth difference between the two waves
$\theta_0$ is the phase difference between the two waves
$D / \lambda$ is the size of the baseline

From (20.30) we can approximate the error as

$$\varepsilon_\phi \approx \rho \cos \theta_0 \sin \delta \qquad \rho \ll 1, D / \lambda \ll 1 \tag{20.31}$$

## 20.5.3 Adcock Incoherent Interference

In the case of interference conditions with two waves, when the Watson-Watt processing can calculate the well-known parallelograms, often the angle of

incidence of each wave can be determined by measuring the parameters of the sides of the parallelogram obtained. This is the case, for example, when the bearings are displayed on a CRT. An operator can readily see the parallelogram and determine the two bearing angles.

If the difference in the level of interference is at least 6dB, the error in the azimuth of the stronger wave is less than $1^\circ$.

### 20.5.4 Adcock Polarization Error

In the case of an Adcock arrangement, from (20.13)

$$V_{12} = V_1 - V_2 = E_V h_{\text{eff}}\, j2\sin\kappa \qquad V_{34} = V_3 - V_4 = 2E_H k$$

The maximum error is given in the case of equal phase

$$\varepsilon_{\phi\max} = \tan^{-1}\left|\frac{V_{34}}{V_{12}}\right| = \tan^{-1}\left(\frac{E_H k}{E_V h_{\text{eff}}}\frac{1}{\sin\kappa}\right) \tag{20.32}$$

For $D = \lambda/2$, (20.32) gives $\varepsilon_{\phi\max} = 90^\circ$.

### 20.5.5 Adcock/Watson-Watt Errors Due to Receiver Noise

The variance of the DF error as a function of the receiver noise is given by

$$\sigma_\phi^2 = \overline{\varepsilon_\phi^2(t)} = \frac{1}{S_1/N} = \frac{1}{\left(\dfrac{W}{w}\right)_{\text{WW}}\gamma_{\text{WW}}}$$

where

$W$ is the bandwidth at the receiver input
$w$ is the smallest bandwidth of the total system
$\gamma_{\text{WW}}$ is the SNR

In most cases of interest to us, $W = w$ so the variance is given by

$$\sigma_\phi^2 = \frac{1}{\gamma_{\text{WW}}} \tag{20.33}$$
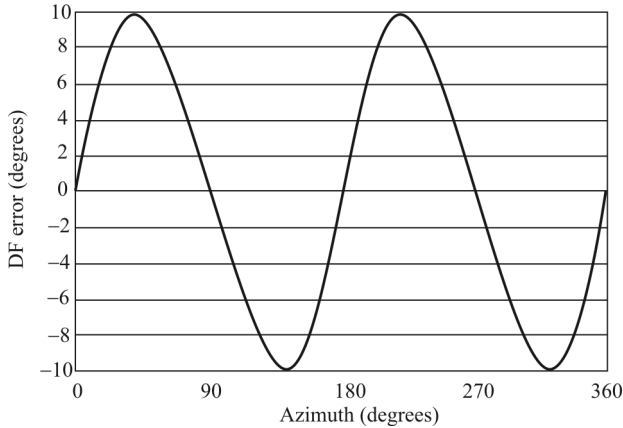
**Figure 20.30** DF error caused by amplitude error $\rho = \sqrt{2} \approx 3\,\text{dB}$.

## 20.5.6 Amplitude Matching with Adcock DF

From (20.3), amplitude mismatch errors with the Adcock DF can be determined from

$$\hat{\phi} = \tan^{-1} \frac{A_1 \sin(\kappa \sin\phi)}{A_2 \sin(\kappa \cos\phi)}$$

$$\varepsilon = \hat{\phi} - \phi \approx \tan^{-1}(\rho\tan\phi) - \phi \tag{20.34}$$

Equation (20.34) is plotted in Figure 20.30 for $\rho = A_1 / A_2 = \sqrt{2}$. We can see that even for a 3dB difference in amplitudes, the error caused by amplitude imbalance can be quite significant, approaching $10^{\circ}$ as the azimuth is traversed.

## 20.5.7 Phase Errors with the Adcock DF

To evaluate the effects of receiver phase tracking we must insert the time dependency into (20.20). The result is

$$\frac{V_{EW}}{V_{NS}} = \frac{k_{EW}}{k_{NS}} \frac{\sin\phi\cos(\omega t)}{\cos\phi\cos(\omega t + \delta_{\phi})} = \frac{k_{EW}}{k_{NS}} \tan\phi \frac{\cos(\omega t)}{\cos(\omega t + \delta_{\phi})} \tag{20.35}$$

where we have assigned all of the phase imbalance to the N-S channel. The value of this phase imbalance is denoted by $\delta_{\phi}$.

The error in the bearing estimation is given by
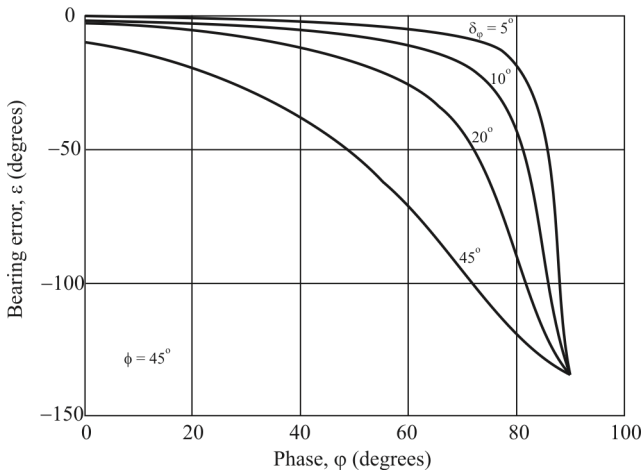
**Figure 20.31** Phase imbalance bearing error; $\phi = 45^\circ$.

$$\varepsilon = \hat{\phi} - \phi$$

with $\phi$ given by (20.21), where $k_{EW} = k_{NS}$, and $\hat{\phi}$ given by

$$\hat{\phi} = \tan^{-1}\left[\frac{k_{NS}}{k_{EW}}\frac{V_{EW}}{V_{NS}}\frac{\cos(\omega t + \delta_\phi)}{\cos(\omega t)}\right]_{k_{NS}=k_{EW}} \tag{20.36}$$

Thus

$$\varepsilon = \tan^{-1}\left[\frac{V_{EW}}{V_{NS}}\frac{\cos(\omega t + \delta_\phi)}{\cos(\omega t)}\right] - \tan^{-1}\left[\frac{V_{EW}}{V_{NS}}\right] \tag{20.37}$$

We can see immediately that the term containing the time dependence (and thus the phase imbalance) can produce large bearing errors at phase angles approaching $\omega t = n\pi/2, m3\pi/2$ (when $\delta_\phi \neq 0$) irrespective of the value of $\delta_\phi$ or $\phi$. Some representative characteristics are illustrated in Figure 20.31 for $\phi = 45^\circ$.

## 20.5.8 Adcock/Watson-Watt Modulation-Induced Errors

FM-induced errors do not occur in the multichannel Adcock DF since the amplitudes of the signals are used to derive the DF information.

As indicated in (20.1), we model the AM as multiplicative factors for the antenna signals. Thus

$$k'_{EW} = m(t)k_{EW}$$
$$k'_{NS} = m(t)k_{NS}$$

where $m(t)$ represents the amplitude modulation signal. Thus, when the ratio indicated in (20.20) is calculated, the effects of the modulation are cancelled. Channel amplitude imbalance impacts are as indicated previously.

### 20.5.9 Interaction of the Adcock Antenna Elements

Coupling is basically compensated due to the geometrical symmetry. There is, however, no absolute symmetry of the electromagnetic field—for example, a thick mast in the center. In this case of radiation couping, the differential voltages of a four-mast Adcock system can be expressed as

$$V_{EW} = \frac{j2A}{1+k}\sin(\kappa\sin\alpha) \qquad\qquad V_{NS} = \frac{j2A}{1+k}\sin(\kappa\cos\alpha)$$

Once the ratio of these two quantities is taken, the denominator with the coupling factor $k$ has no influence on the bearing.

### 20.5.10 Geometrical Errors of the Adcock Antenna

If the phase centers of the single antennas of a four-element Adcock are not in the correct position, the voltages are given by

$$V_{EW}(t) = A\sin\big[r_{EW}\beta\cos(\alpha - \alpha_{EW})\big]\cos\omega t \qquad (20.38)$$
$$V_{NS}(t) = A\sin\big[r_{NS}\beta\cos(\alpha - \alpha_{NS})\big]\cos[\omega t + \phi(\alpha)] \qquad (20.39)$$

where

$$\phi(\alpha) = -\vec{\beta}\bullet(\vec{r}_{MNS} - \vec{r}_{MEW})$$
$$\vec{\beta} = \frac{2\pi}{\lambda}\vec{e}_{wave}$$

The bearing error $\Delta\alpha$ depends, apart from the geometrical dimensions, also on the procedure of evaluation. Figure 20.32 shows the DF error of a non-rectangular antenna system.

(a)　　　　　　　　　　　　　　(b)
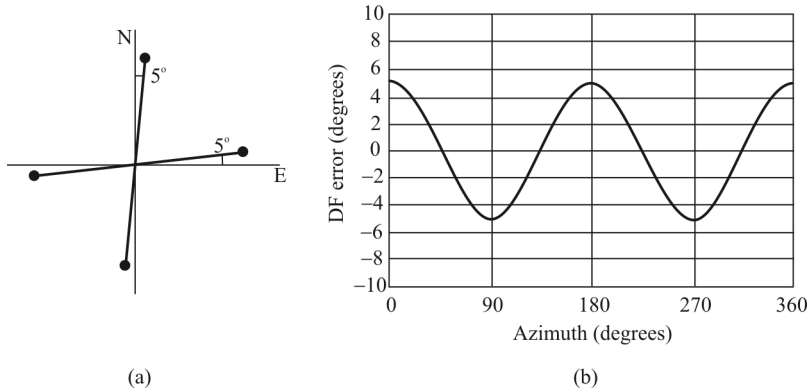
**Figure 20.32** Incorrect geometrical configuration and the resulting error. $\vec{r}_{\text{MNS}} = \vec{r}_{\text{MES}} = \vec{0}$, $r_{\text{NS}} = r_{\text{EW}}$, $\alpha_{\text{NS}} = 85^{\circ}$, $\alpha_{\text{EW}} = 5^{\circ}$.

## 20.6 PseudoDoppler Systems

An antenna, when rotating in a circle at a constant angular frequency $\omega_{\text{r}}$, modulates the phase and the frequency of the received signal. Once the signal has passed through the receiver and the demodulator, the DF value can be determined by comparison with a reference signal. In practice, the rotating antenna is realized by sequential switching of fixed antenna elements, which are spaced at equal intervals around the circle.

A pseudoDoppler antenna configuration with four antennas is diagrammed in Figure 20.33. The equivalent of a rotating commutator (could be mechanical for slower applications but is typically electronic) sequentially selects an antenna for sampling the incoming target signal that arrives at the antenna at an azimuth angle given by $\phi$ and an elevation angle denoted by $\theta$. The commutator is rotating at an angular velocity $\omega_{\text{r}}$, producing a tangential velocity of $v_{\text{T}}$ at a distance $R$ from the center of the array.

The RF signals from the antennas are converted to IF by a single-channel receiver. The IF signal is demodulated by an FM discriminator forming a phase detector. The signal from the discriminator takes the form shown in Figure 20.34 as the commutator is rotated between the antennas. The signal forms a series of impulses the strength of which are a function of the phase shift between the two adjacent antennas.

In the absence of noise, the time signal from the discriminator can be represented as [12]
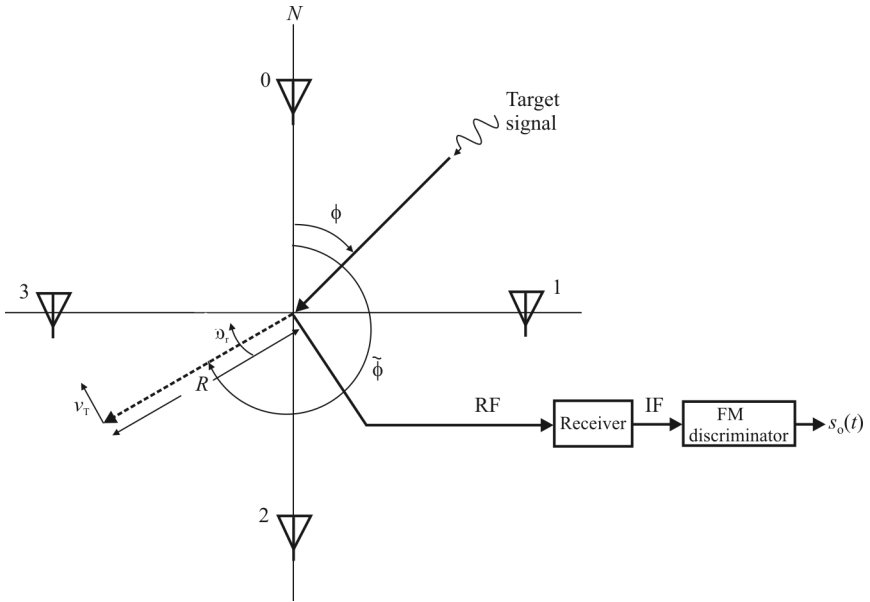
**Figure 20.33** PseudoDoppler antenna.
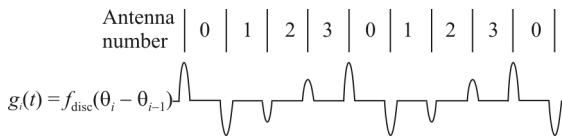


**Figure 20.34** PseudoDoppler antenna response.

$$s_o(t) = f_0 + \frac{v_T f_0}{c} \sin[\phi - \tilde{\phi}(t)] \sin\theta \qquad (20.40)$$

The second term on the rhs of (20.40) represents the Doppler shift caused by the commutation between the antenna elements.

When noise is included, the output of the discriminator is given by $r(t) = s_o(t) + n(t)$, where $n(t)$ represents zero mean AWGN. The estimate of the azimuth is given by value of $\tilde{\phi}(t)$ for which $r(t) = f_0$, where $f_0$ is known. Since $s_o(t) = f_0$ when $\tilde{\phi}(t) = \phi$ and $\tilde{\phi}(t) = \phi + \pi$, there is an ambiguity in the result. The ambiguity can be resolved by observing where the maximums and minimums of $r(t)$ occur. An estimate of $\theta$ is obtained by the peak-to-peak variation of $r(t)$.

The filtering of the discriminator output can be very narrow, corresponding to the frequency of commutation, usually a low rate. That makes the selectivity quite high, minimizing the effects of noise. The antenna sampling process, however, causes audible tones at the output that must somehow be filtered. We discuss these tones next.

### 20.6.1 Output Harmonics

Another representation of the signals at the antennas is given by [13]

$$e_A(t) = V_o \sin[\omega_0 t + \beta R \cos\phi \sin\theta] \qquad (20.41)$$

when $e(t) = V_0 \sin\omega_0 t$ is the target signal at the center of the array.

Since the antenna is rotated at $\omega_r$, we have $\phi = \omega_r t$ and

$$e_A(t) = V_0 \sin[\omega_0 t + \beta R \cos\omega_r t \sin\theta] \qquad (20.42)$$

Ignoring the effects of the elevation angle, the output of a phase detector with (20.42) as its input is given by

$$v_P(t) = \sin(\beta R \cos\omega_r t) \qquad (20.43)$$

Equation (20.43) can be represented as a Bessel function series with odd harmonics:

$$v_P(t) = 2[J_1(\beta R)\sin\omega_r t + J_3(\beta R)\sin 3\omega_r t + \ldots + J_{2n+1}(\beta R)\sin(2n+1)\omega_r t + \ldots] \quad (20.44)$$

We can see from (20.44) that the output is a collection of audio tones with frequencies at odd multiples of the commutation frequency. These tones will typically be heard by an operator listening to the output or be available for further processing by automated methods, where they are a nuisance (additional noise). In EW applications where the signal internals are important, a separate receiver outside of the commutation process (perhaps using only one of the antennas in a static mode) may be required.

## 20.6.2 Other Receiver Implications

Periodically sampled antennas provide an output with numerous AM sidebands around the received signal. Also, the FM created by periodic frequency shift of pseudoDoppler creates sidebands. These AM and FM sidebands are enough of a problem on their own, but they also interact since they are generated by the same phenomenon. Such sidebands and their interactions can cause the DOA to possess significant error when their amplitude is large. Filtering at appropriate points in the process can be used to minimize the sidebands.

The DOA computed with pseudoDoppler is sensitive to elevation angle. Accuracy decreases as elevation angle (measured from zenith) decreases because the instantaneous frequency shift decreases.

Since a single channel receiver is used in this implementation of a pseudoDoppler system, there are no channel matching requirements that must be met by the receiver.

AM modulation effects can be minimized by employing a limiter with the discriminator. Limiters affect the signal amplitudes only, leaving any frequency or phase modulation intact. It is the latter that is exploited with pseudoDoppler systems.

The targets for pseudoDoppler systems must be narrowband. Wideband signals propagating across the aperture of a Doppler array do not exhibit enough of a phase deviation at separate antennas, and the idea of measuring distinct phase shifts becomes difficult.

Measuring the phase in a single cycle $(0, 2\pi)$ of an RF signal is a very precise requirement. Antenna spacing and placement accuracy are critical for acceptable performance.

## 20.6.3 Polarization-Induced Errors

In the case of Doppler DF, from Figure 20.21 we can see that the maximum phase error is at positions 3 and 4

$$\varepsilon_{\varphi} = \tan^{-1} \frac{E_{\mathrm{H}} h}{E_{\mathrm{V}} h_{\mathrm{eff}}}$$

Then the maximum bearing error is obtained as

$$\varepsilon_{\phi max} = \frac{\varepsilon_{\phi max}}{\kappa} = \frac{1}{\kappa} \tan^{-1} \frac{E_{\mathrm{H}} h}{E_{\mathrm{V}} h_{\mathrm{eff}}} \approx \frac{1}{\kappa} \frac{E_{\mathrm{H}} h}{E_{\mathrm{V}} h_{\mathrm{eff}}} \tag{20.45}$$

### 20.6.4 Doppler Coherent Wave Interference

For the Doppler DF the error as a function of the radius $R$ can be expressed as

$$\varepsilon_{\phi} \approx \frac{2\rho \cos\theta_0 \cos\dfrac{\delta}{2}}{\beta R} J_1\left(2\beta R \sin\frac{\delta}{2}\right) \qquad \rho \ll 1 \tag{20.46}$$

By dividing (20.31) by (20.46) the improvement is obtained as a function of the azimuth difference

$$\frac{\beta R \sin\dfrac{\delta}{2}}{J_1\left(2\beta R \sin\dfrac{\delta}{2}\right)} = \frac{\xi}{J_1(2\xi)}$$

where $\xi = \beta R \sin(\delta/2)$. For small diameters $D \ll \lambda$ the error of the Doppler DF expressed as (20.46) approximates the error of small aperture systems given by (20.31) because $J_1(x) \approx x/2$ for $x \ll 1$. The improvement factor then becomes equal to unity.

### 20.6.5 Doppler Incoherent Interference

In the Doppler DF, the multiwave incidence causes errors, which are, however, significantly diminished both by the wide aperture effect and by averaging. If the level difference is at least 6 dB, the azimuth of the stronger wave is indicated with an error of less than $1^{\circ}$.

### 20.6.6 Doppler Errors Due to Receiver Noise

The errors caused by receiver (input reflected thermal) noise are given by

$$\sqrt{\overline{\varepsilon_\phi^2(t)}} = \frac{1}{\sqrt{2(S/N)_{AF}}} = \frac{1}{\pi \dfrac{D}{\lambda} \sqrt{\left(\dfrac{W}{w}\right)_{Dop}} \gamma}$$

where

$(S/N)_{AF}$ is the SNR after the frequency demodulator
$W$ is the bandwidth at the receiver input
$w$ is the smallest bandwidth of the total system
$\gamma$ is the RF SNR

## 20.6.7 Tracking and Matching for Doppler Direction Finding

Since the Doppler DF configuration we are considering is a single channel configuration (multiple channel topologies are also possible), there is only one channel to consider. By definition, channel tracking and matching errors do not occur in a single channel.

Variations with time, temperature, and other environmental conditions do, however, cause errors. These should be minimized, and perhaps the best way to do that is to maximize the amount of digital signal processing.

## 20.6.8 DF Errors Caused by the Group Delay of the Doppler DF Receiver

Amplitude or phase errors do not occur in the Doppler DF since it is a single-channel DF principle. However, the variation of the receiver group delay time diminishes the accuracy of the measurement by shifting the phase of the AF signal:

$$\delta_\phi = \omega_r \tau_{gr}$$

Since this error depends on the sense of rotation, it can be eliminated by taking two measurements, where the antenna elements are scanned both clockwise and counterclockwise:

$$\hat{\phi}_{CW} = \omega_r \tau_{gr} + \phi$$
$$\hat{\phi}_{CCW} = \omega_r \tau_{gr} - \phi$$

so that

$$\hat{\phi} = \frac{1}{2}(\hat{\phi}_{CW} - \hat{\phi}_{CCW})$$

### 20.6.9 Doppler DF Errors Caused by Modulation

Modulation errors occur in the Doppler DF with only one receiver. Without modulation, the signal from the discriminator can be expressed as

$$e(t) = A\cos[\omega_0 t + \varphi + \kappa\cos(\omega_r t - \alpha)] \tag{20.47}$$

where $\alpha$ is the angle the incoming wave makes with the x-axis, and $\varphi$ is an arbitrary phase offset. With FM, from (20.47) we have

$$e(t) = A\cos[\omega_0 t + \varphi + \zeta\int m(t)dt + \kappa\cos(\omega_r t - \alpha)] \tag{20.48}$$

where $m(t)$ denotes the modulating signal. The phase-demodulated signal is then obtained from (20.48) by differentiation of the argument in brackets and filtering to eliminate $\omega_0$ and the DC term, yielding

$$\varsigma_o(t) = \zeta m(t) - \kappa\omega_r \sin(\omega_r t - \alpha) \tag{20.49}$$

We can see that the FM directly changes the phase. With random modulation, the instantaneous phase is also random.

An estimate of $\alpha$ is provided by the first coefficient, $c_1$, of the Fourier transform of (20.49)

$$\hat{\alpha} = \frac{\pi}{2} - \arg(c_1) \tag{20.50}$$

The effects of these errors can be mitigated by

- Statistic disturbance is averaged; averaging the IF signal gives more sensitivity than averaging of the AF signals.
- Amplitude modulation is suppressed by a signal limiter.
- By using a two-channel receiver system, a special compensation technique can be applied to eliminate DF errors caused by frequency and phase modulation.
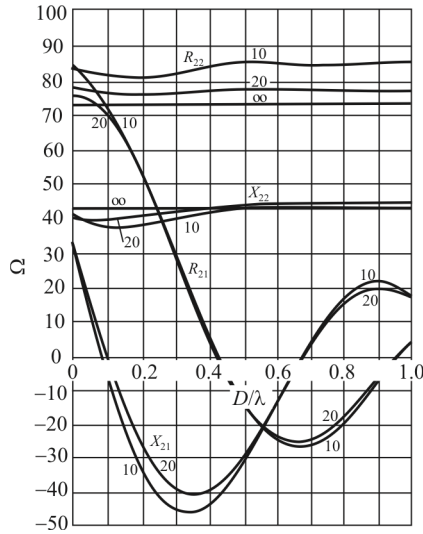
**Figure 20.35** Mutual impedance $Z_{21}$ and self-impedance $Z_{22}$ of two parallel dipoles as a function of $D/\lambda$, $l = \lambda/4$. Parameter $Z_2 \ln(Z_{21}/R) = 10, 20, \infty$.

## 20.6.10 Interaction of the Doppler Antenna Elements

The Doppler DF as a sequential procedure does not form differential voltages as does the Adcock [see (20.2)]; this principally leads to interaction errors. If only considering two antennas, the current induced into antenna 2 due to a current in antenna 1 is given by the ratio

$$\frac{I_2}{I_1} = -\frac{Z_{21}}{Z_2 + Z_{22}}$$

where

$Z_{21}$ is the mutual impedance

$Z_{22}$ is the self-impedance

$Z_2$ is the terminating impedance

$I_{1/2}$ is the current at the terminal of antenna 1/2

$D$ is the distance between the two dipoles

$l$ is the dipole length

$R$ is the radius of the antenna
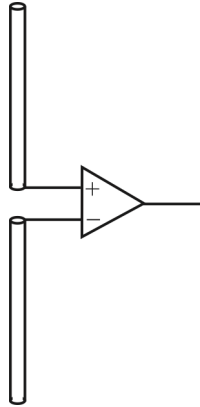
**Figure 20.36** Active dipole antenna.

**Example 20.1:** Figure 20.35 illustrates an example where

$$D/\lambda = 0.5, l/\lambda = 0.25, Z_2 = 50\Omega$$

so that

$$\frac{I_2}{I_1} \approx 0.2\angle 55^\circ$$

We see that the mutual impedances vary considerably with $D/\lambda$ whereas the self-impedances are relatively constant. $X_{21}$ starts out at small baselines as inductive, changing to capacitive at about $D/\lambda \sim 0.1$. It changes back to inductive at about $D/\lambda \sim 0.65$. The mutual resistance is negative over a region as well.

When using active antennas with a high-input impedance of the antenna amplifier, the coupling error is considerably reduced, since the current at the antenna terminals vanishes. As the maximum of the current on the rod then is shifted to the center of the upper and lower halves of the dipole, there will still be some interaction. Such an arrangement is illustrated in Figure 20.36.

## 20.6.11 Geometrical Errors of the Doppler Antenna

For a constant phase error $\xi_k$ of the $k$th antenna element we have
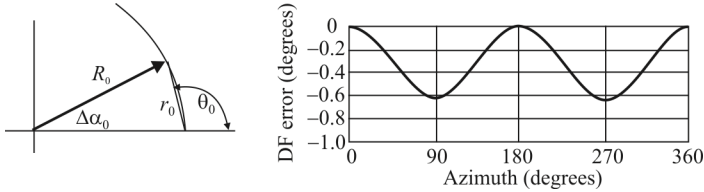
**Figure 20.37** Incorrect configuration of the antenna element 0 and the resulting DF error $(\Delta\alpha_0 = 5^\circ)$.

$$\Delta\alpha = \tan^{-1} \frac{\dfrac{2}{\kappa N}\displaystyle\sum_{k=0}^{N-1}\xi_k \sin\left(\dfrac{2\pi}{N}k-\alpha\right)}{1+\dfrac{2}{\kappa N}\displaystyle\sum_{k=0}^{N-1}\xi_k \cos\left(\dfrac{2\pi}{N}k-\alpha\right)} \qquad (20.51)$$

If the antenna element 0 alone is misplaced $(\xi_k = 0$ for $k \neq 0)$, then (20.51) can be reduced to

$$\Delta\alpha = -\tan^{-1}\frac{\dfrac{2}{\kappa N}\xi_0 \sin\alpha}{1+\dfrac{2}{\kappa N}\xi_0 \cos\alpha} \qquad (20.52)$$

$\xi_0$ depends on the azimuth for incorrect positioning of the antenna element:

$$\xi_0 = \beta r_0 \cos(\alpha - \theta_0)$$

Figure 20.37 illustrates an incorrect configuration of element 0 and the corresponding DF error.

## 20.7 Phase Interferometers

Phase interferometers compare the phase of the target signal at two ends of a baseline formed by two antennas. A simplified flow diagram for the phase interferometer is shown in Figure 20.38. The phase difference is a measure of the angle of arrival. A typical phase detector is shown in Figure 20.39, where a ring modulator is used. Its response to the phase difference, denoted with $\Delta\varphi$, between the two RF inputs $v_1(t)$ and $v_2(t)$, as manifest in the phase of the output, is shown in Figure 20.40.
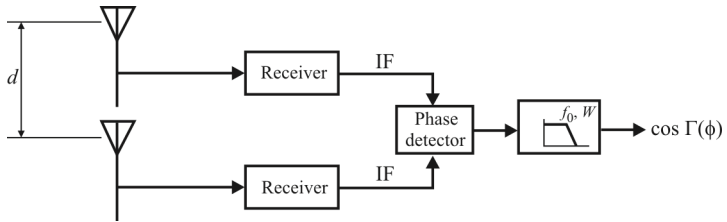
**Figure 20.38** Interferometer.
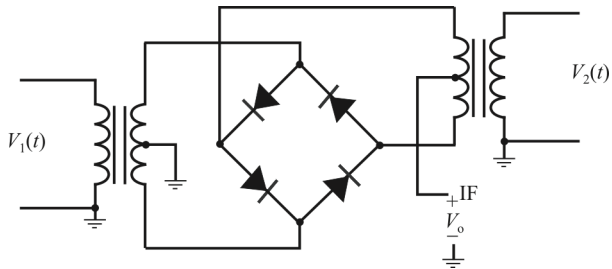


**Figure 20.39** Ring mixer as phase detector.
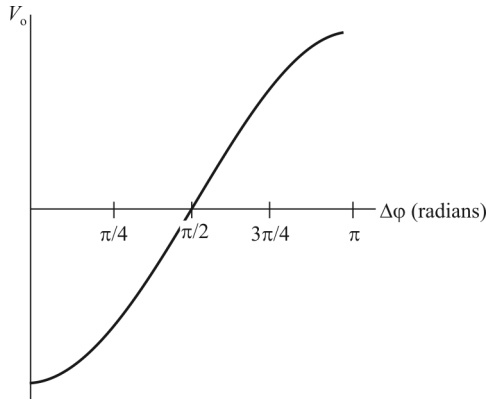
**Figure 20.40** Phase detector response.

Multipliers are also frequently used as phase detectors as illustrated in Figure 20.41. The concept in this case relies on the trigonometric relationship

$$f(t) = 2\sin(\omega t)\sin[\omega t + \Gamma(\phi)] = \cos[\omega t - \omega t - \Gamma(\phi)] - \cos[\omega t + \omega t + \Gamma(\phi)]$$
$$= \cos\Gamma(\phi) - \cos[2\omega t + \Gamma(\phi)] \qquad (20.53)$$

where $\Gamma(\phi)$ represents the impact of the azimuth angle on the phase of the IF signal. When (20.53) is lowpass filtered we get

$$g(t) = \cos\Gamma(\phi) \qquad (20.54)$$

Equation (20.54) applies to both Figures 20.38 and 20.41 as does the phase detector response characteristic shown in Figure 20.40. We thus have a way to estimate the azimuth AOA based on the difference in phase between the two signals from the antennas at the ends of the baseline, denoted by $\phi$.
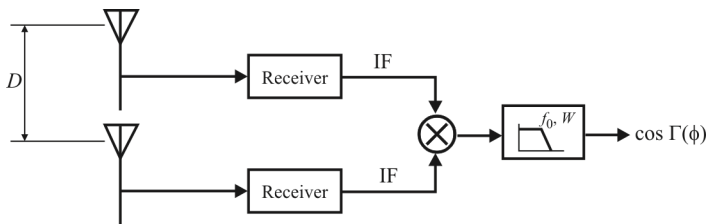


**Figure 20.41** Interferometer with a mixer as the phase detector.

Assume that the mean of $\varphi$ is zero so that we have [14]

$$\sigma_\varphi = \frac{\partial \varphi}{\partial \phi} \sigma_\phi \qquad (20.55)$$

The partial derivative in this expression can be calculated from (20.12) as

$$\frac{\partial \varphi}{\partial \phi} = \beta D \cos \phi \qquad (20.56)$$

which yields the expression for the standard deviation of the azimuth calculation as

$$\sigma_\varphi = \beta D \cos \varphi \sigma_\phi \qquad (20.57)$$

Thus, the standard deviation of the azimuth measurement is maximum when $\phi = 0$, or off the ends of the baseline. It is minimum for $\phi = \pi/2$, or orthogonal to the baseline.

The *Cramer-Rao lower bound* establishes the theoretical limits on how accurately parameters associated with signals can be measured when noise is present and taken into consideration. It is a measure of parameter estimation accuracy in the presence of white noise. White noise is an approximation to the input-reflected thermal noise in receivers and is usually a fairly good approximation. For example, the hissing noise that we hear sometimes from a radio when it is not tuned to a station, especially when the volume is turned up, is very close to white noise. The term *white* comes from the fact that white light contains all of the colors—white noise contains energy from all of the frequencies. For an interferometric line of position system, the Cramer-Rao bound $\sigma$ can be calculated to be

$$\sigma^2 = \left( \frac{E}{N_0} \right)^{-1} \qquad (20.58)$$

where $E$ is the signal energies at the two antennas (watt-seconds), assumed to be the same, and $N_0$ is the noise spectral density at the two antennas (watts per hertz), also assumed to be the same and independent of each other. We also assume for this equation to apply is that the angle of arrival, $\phi$, does not vary over the measurement interval.

Recall that $E = S$ (W) $T$ (seconds), and that $N$ (W) $= N_0$ (W/Hz) $W$ (Hz), where $N$ is the noise power and $W$ is the noise bandwidth, the latter assumed for

convenience here to be the IF bandwidth. After some trivial algebra, (20.58) can be put into a more usable form as

$$\sigma^2(\phi) = (\gamma TW)^{-1} \quad \text{rad}^2 \qquad (20.59)$$

with $\gamma$ being the SNR. Therefore, the variance is reduced (accuracy improved) by increasing the SNR, the integration time, or the measurement bandwidth or by some combination. Note, however, that increasing the bandwidth beyond the bandwidth of the SOI will decrease the SNR.

## 20.7.1 Four-Element Interferometer

The geometric relationships in this antenna system are shown in Figure 20.42. As above, $R$ is the radius of the array, while the azimuth AOA of the signal $s(t)$ is given as $\phi$, and the arrival angle of the signal in the vertical dimension (zenith) is $\theta$ relative to the plane of the array. The frequency of the signal is given as $f = c/\lambda$, the number of antenna elements $N = 4$, and $c$ is the speed of light. It is assumed that $R < \lambda/4$ so that phase ambiguities do not arise. Derivation of the expressions for determining $\phi$ and $\theta$ are provided in [15].

As indicated, the normal method of implementing phase interferometers is to measure the phase difference (or equivalently the TOA difference) between two signals impinging on two antennas forming a baseline. Typically the components, including receivers, measuring this phase difference are swapped in the process of determining the phase parameter [16] (Figure 20.43). This swapping, in principle, removes any phase errors caused in the receiver chains. The remaining source of error in the phase determining process is due to noise within the receiving chain. This noise is caused from thermal noise sources internal to the components themselves, since external noise (such as atmospheric, man-made, and so forth) are also removed by the antenna swapping.

Assuming no bias in the measurments (zero mean), the variance of the azimuth phase measurements is given by

$$\sigma_\phi^2 = \mathcal{E}\{\hat{\phi}^2 - \phi^2\}$$

The estimated RMS bearing error in this case can be expressed as [17]

$$\varepsilon = \frac{\varepsilon_\phi}{\beta D \cos\phi \sin\theta} \qquad (20.60)$$

where
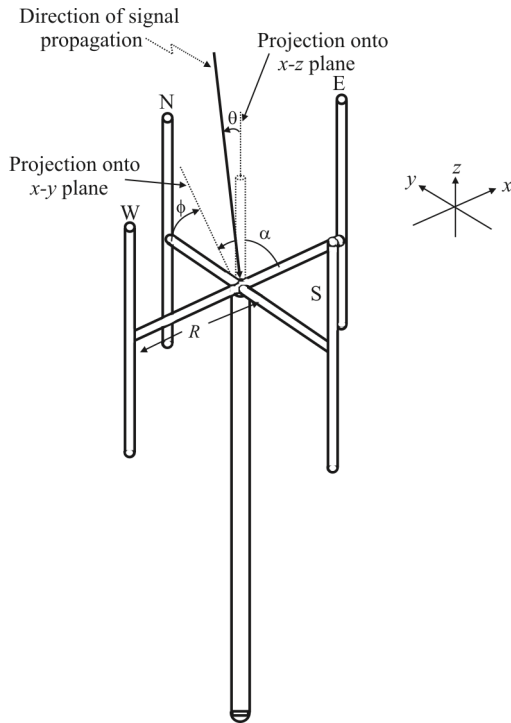
**Figure 20.42** Mast-mounted four-element Adcock array.
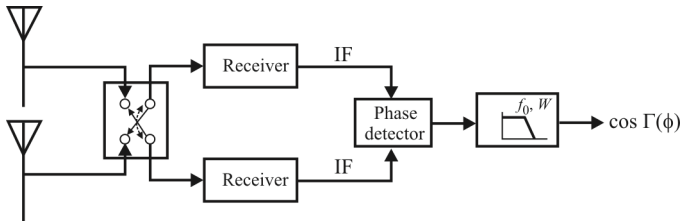
**Figure 20.43** Interferometer with antenna swapping (reversing).

$D$ is the baseline length

$\lambda$ is the wavelength

$\varepsilon_\phi$ is the estimated RMS phase error

$\phi$ is the azimuth angle of arrival

$\theta$ is the elevation angle of arrival (from zenith)

The phase error is a function of the SNR. Shown in Figure 20.44 is a diagram with a signal $E$, displayed as a phasor, at a phase angle $\delta$, where $\delta$ is perturbed by noise, $n_t$, to produce a phase error $\delta_\varepsilon$. The AWGN, $n_t$, has quadrature components, $n_i$ and $n_q$, the former of which is in phase with $E$ while the latter is in phase quadrature to signal vector $E$. As we see, the quadrature component, $n_q$, contributes to the phase error $\delta_\varepsilon$, while the in-phase component, $n_i$, does not. The total noise power is

$$n_t^2 = n_i^2 + n_q^2 \tag{20.61}$$

and we assume that $n_i = n_q$. Thus we have

$$n_t^2 = 2n_q^2 \tag{20.62}$$

For a high SNR,

$$\tan \delta_\varepsilon \approx \delta_\varepsilon = \frac{n_q}{|E|} \tag{20.63}$$

Denoting the total signal power by $S$, we have $|E| = \sqrt{S}$, and from (20.63) and (20.62)
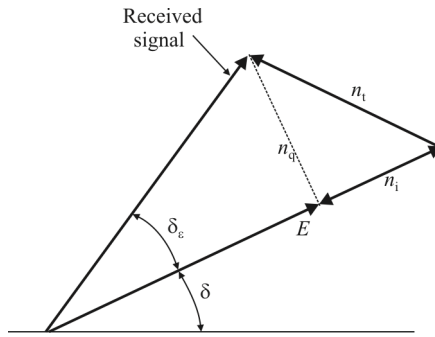
**Figure 20.44** Signal phasor with noise corruption.

$$\varepsilon_\phi = \sqrt{\frac{n_t^2}{2}} \frac{1}{\sqrt{S}}$$

$$= \frac{1}{\sqrt{2\gamma}} \quad \text{radians} \qquad (20.64)$$

where $\gamma$ is the SNR, because $n_t^2 = N$, where $N$ is the total noise power, and $\varepsilon_\phi$ is the phase error for one measurement. As mentioned, in phase interferometry, due to swapping of the channels, at least two independent phase measurements are made so that

$$\varepsilon_\phi = \frac{1}{\sqrt{\gamma}} \qquad (20.65)$$

for these two measurements assuming equal SNR values. With the reference phase at the center point of the baseline, the estimated azimuth angle error from (20.60) and (20.65) is

$$\varepsilon = \frac{1}{\beta D \cos\phi \sin\theta \sqrt{\gamma}} \quad \text{radians} \qquad (20.66)$$

Equation (20.66) is plotted in Figure 20.45 for several values of the parameters.

    We should remember that these results are for a single sample of the DF baseline (two actually once swapped). Other factors that impact DF accuracy include
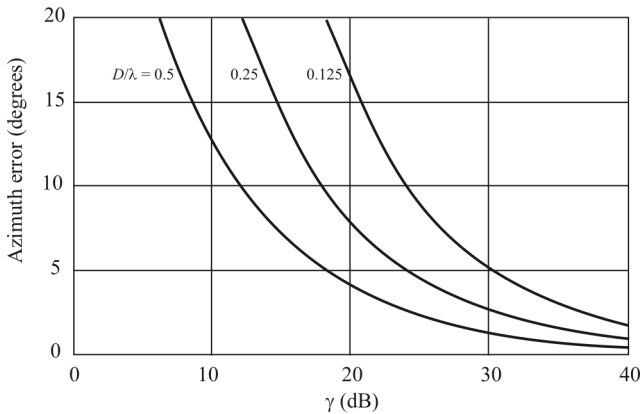
**Figure 20.45** Phase comparison bearing error. $\theta = 90^{\circ}$ (on the horizon) and $\phi = 0^{\circ}$ (baseline boresight).

- In general, the accuracy of an estimator in AWGN improves as the number of samples increases, typically as $1/\sqrt{M}$, where $M$ is the number of samples.
- The data in Figure 20.45 only applies when $D/\lambda \leq 1/2$. This is to ensure there is no ambiguity in the measurement. When physical space allows, much longer baselines are possible, which can substantially improve the accuracy, as long as there is a baseline available with $D/\lambda \leq 1/2$ for ambiguity resolution.

### 20.7.2 Modulation-Induced Errors

We can see from (20.53) that FM or PM on the target signal will cause perturbations in the instantaneous phase of the antenna signals and therefore the receiver IF signals from which the AOA is estimated. The effect will be the same as that indicated previously for pseudoDoppler DF. The phase offsets caused by the modulation will directly offset the measured bearing. For random modulations, which comprise the majority of target signals, averaging the measurements will decrease the impact of this error source.

AM, on the other hand, will have little effect on the AOA calculation since the phases of the signals are used for the estimate; amplitudes are not used. Any AM effects can be removed with a limiter.

### 20.7.3 Tracking Imbalance-Induced Errors

Since phase interferometry relies on phase accuracy for DF performance, amplitude imbalances have little effect. This can be seen from Figure 20.39 for the

ring mixer. As long as the input waveforms have adequate levels to turn the diodes on and off properly, the mixer works as expected.

On the other hand, phase imbalanced between the two channels will cause perturbations in the phase measurements and lead directly to AOA estimation errors, as can be expected from (20.53). In order to mitigate these effects, it is common practice to toggle the antennas and receivers, yielding half the measurements with one antenna/receiver arrangement and half from the other. See Figure 20.43. The phase tracking imbalance can be removed by differencing the average of the results.

### 20.7.4 Polarization-Induced Errors

The phenomenon that produces polarization-induced errors in Adcock and pseudoDoppler DF systems is not dominant in phase interferometers. The effects of the cable currents are certainly present, and the secondary fields are created. However, they do not impact the phase of the target signals, only their amplitudes. Therefore there is little impact of the AOA estimates.

Reduction in vertical signal levels due to polarization mismatch between the target signal and the antenna is also present, effectively lowering the SNR in the equations above.

### 20.7.5 Antenna Interaction-Induced Errors

Errors caused by the interaction of the antenna elements of an Adcock array for phase interferometry are constant. Such errors can be removed by calibration of the array, which is normal practice.

### 20.7.6 Geometrical Misplacement-Induced Errors

Geometry-induced errors are also constant and a function of the array configuration. They also can be removed by array calibration. One possible cause of variations in such errors is maintenance activities, such as the requirement to replace an antenna element. If the new element is not placed precisely where the old one was, errors occur in phase estimation.

### 20.7.7 Coherent Interference

As illustrated in Figure 20.22, coherent interference causes curvature of the wavefronts arriving at the receiver array. As the phase interferometer is sensitive to the difference in phase arrivals at the antennas, such curvature will cause bearing errors to be included in the AOA estimates. These errors are hard to predict and detect since they are inherent to the arriving signals. For a given frequency and geometrical configuration (principally by the reflecting sources) the

errors will be relatively constant and therefore unchanging. If the reflecting sources are moving (such as a passing vehicle or a street sign waving in the wind), this movement will be included in the phase characteristics of the signals and result in variations in the phase estimates. These changes may be detectable, and the resulting phase estimates removed from consideration in estimating the DOA.

### 20.7.8 Incoherent Interference

For phase interferometry, a technique sensitive to target signal phase, cochannel interference causes significant system degradation. Often the best that can be expected is to detect when cochannel interference is occurring and rejecting the collected data during that interval. (One technique for the detection of such cochannel interference is if the estimated bearings are varying wildly from one measurement to the next.)

## 20.8 Dual Channel Compressive Receivers for DF

The narrowband superheterodyne receivers discussed in the previous sections have limited applicability when the targets are modern wideband communication systems employing FHSS access methods. We have already discussed in Chapter 15 the applicability of scanning a superheterodyne receiver across the spectrum for the detection of FHSS signals. The same approach and limitations apply for DF as they do for detection for the scanning approach. In this section we review the application of wideband compressive receivers for this task [6].

Dual channel compressive receivers are shown in Figure 20.46. The phase difference of the signals in the two channels can be determined with a phase processor, notionally shown in Figure 20.46. This phase difference is a measure of the phase angle difference of the signals arriving at the input to the compressive receiver channels and is a measure of the angle of arrival of the signal at the two receiver antennas. For real-time direction finding, four such channels may be necessary. If close to real-time processing is adequate, then the inputs can be switched between two orthogonally arrayed antenna baselines, made up of four antennas. Alternately, only two receiver channels are required for real-time DF when a Butler matrix is used ahead of the receivers.

### 20.8.1 Phase Processor

The output of both channels is processed in a phase processor to determine the phase differential between channels. Selection of the phase processor architecture is driven by the wideband nature of both the RF and video characteristics of the signal. Further, the chosen phase processor implementation has a very low amplitude-to-phase coupling. As an example, a 1.6dB amplitude imbalance
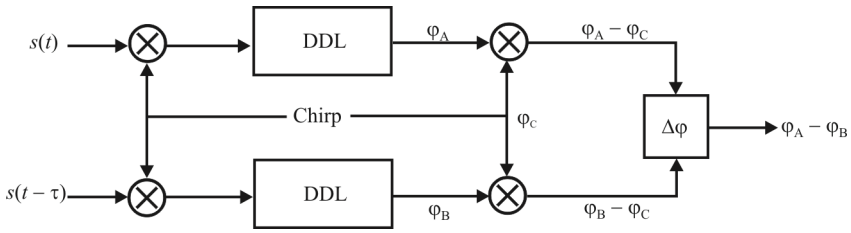
**Figure 20.46** Dual channel CxRx.

produces only a 1.2° phase measurement error. Figure 20.47 consists of two in-phase power dividers, a quadrature hybrid, a 180° hybrid, and four logarithmic detectors.

The magnitude of the signal $V_5$, which is a sum of two vectors $V_1$ and $V_2$, is given by

$$|V_5| = \sqrt{|V_1|^2 + |V_2|^2 - 2|V_1||V_2|\sin(\Delta\varphi)} \qquad (20.67)$$

where $\Delta\varphi$ is the phase angle between $U_1$ and $U_2$. Similarly

$$|V_6| = \sqrt{|V_1|^2 + |V_2|^2 + 2|V_1||V_2|\sin(\Delta\varphi)} \qquad (20.68)$$

$$|V_7| = \sqrt{|V_1|^2 + |V_2|^2 - 2|V_1||V_2|\cos(\Delta\varphi)} \qquad (20.69)$$

$$|V_8| = \sqrt{|V_1|^2 + |V_2|^2 + 2|V_1||V_2|\cos(\Delta\varphi)} \qquad (20.70)$$

For each frequency present at the input to the receiver, four detected signals are sampled and processed in the computer to determine the phase angle. It can be shown that, compared to other types of envelope detectors, the log-detector-based
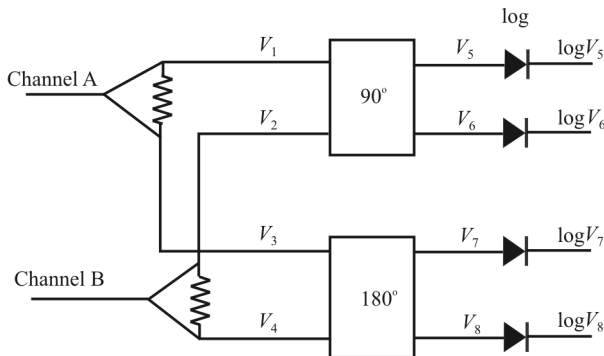


**Figure 20.47** Phase processor.

processor is the least sensitive to channel imbalance for angles near 45$^o$. This is commonly referred to as AM-to-PM conversion and is undesirable. As an example, for $\Delta\varphi = 45^o$ and an amplitude imbalance of 1.6 dB, the log amp-based system produces a phase error of 1.2$^o$. If a square law detector is used, the error is 12.6$^o$ and, for a linear detector, 4.6$^o$. Clearly the log detector is more desirable.

## 20.8.2 Phase Measurements

For some applications, the Fourier transform is not required. If low sidelobes are not required but the phase difference between two parallel channels must be determined, then at the final mixer output of the dual channel system shown in Figure 20.46, the phase difference is

$$\Delta\varphi = \varphi_A - \varphi_C - (\varphi_B - \varphi_C)$$
$$= \varphi_A - \varphi_B$$

so the final chirp multiplication is not required.

## 20.8.3 Butler Matrix

While the basic functioning of a dual channel compressive receiver for direction finding was presented in the last section, it only produced two channels of information at a time for this purpose. This is enough for a single DF baseline but some form of multiplexing is required if multiple (say 2) baselines are being considered. Two baselines provide enough information for instantaneous 360$^o$ coverage.

A Butler matrix configuration that works with a circular Adcock antenna array is shown in Figure 20.48 [18]. This is a phase comparison architecture. The output port labeled $n = 0$ is the reference signal. The signals from all four antennas arrive at output port 0 with the same phase. The north antenna output passes through the two bottom 180$^o$ hybrids with no phase shift to port zero. The east antenna output passes through the +90$^o$ phase shifter, is shifted –90$^o$ through the 90$^o$ hybrid, and passes through the bottom right hybrid with no phase shift for a net total of 0$^o$. The south antenna's signal passes through both the bottom two hybrids with no phase shift. The west antenna's signal reaches output port 0, bypassing through both the 90$^o$ hybrid and the bottom right hybrid with no phase shift.

Next consider the phase at the $n = 1$ output port. The signal from the north antenna reaches this port with no phase shift, passing directly through the bottom left hybrid and upper right hybrid. The signal from the east antenna reaches the $n = 1$ port by passing through the +90$^o$ phase shift and then directly through the upper two hybrids for a net +90$^o$ phase shift. The south antenna's signal reaches
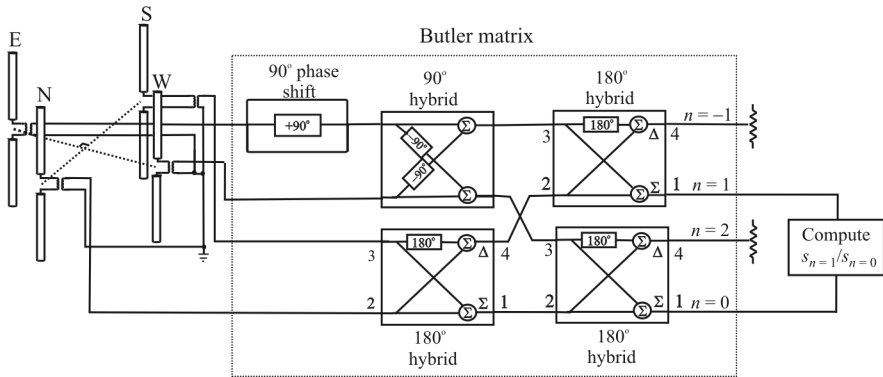
**Figure 20.48** Butler matrix. (Source: [18], ©Artech House, 2012. Reprinted with permission.)

the $n = 1$ port via $180^\circ$ phase shift in the bottom left hybrid and then directly through the upper right hybrid for a net $180^\circ$ phase shift. The west antenna's signal reaches the $n = 1$ port with $-90^\circ$ ($270^\circ$) phase shift through the $90^\circ$ hybrid and direct connection through the upper right hybrid for a total of $270^\circ$. The results are tabulated in Table 20.1.

With the configuration shown in Figure 20.48, instantaneous DOAs are available on every signal in the CxRx passband. This information, among other uses, can be used for sorting hop pulses based on those DOAs. The presumption is that the target cannot move fast enough from one hop to the next to significantly change the DOA at the receiving system.

## 20.8.4 Receiver Implications

It is not necessary to maintain absolute amplitude or phase to ensure accurate DF, but the relative values between channels must be stable. This implies that the variation with time and temperature must be minimized or at least that they track each other between channels. That means that the DDLs and mixers should be mounted on the same heat sink so that heat dissipation can track.

**Table 20.1** Phase Shifts through a Butler Matrix

| Antenna | Spatial Angle (°) | Electrical Phase Shift at Port | | | |
|---------|---------|---------|---------|---------|---------|
| | | $n = 0$ | $n = 1$ | $n = 2$ | $n = -1$ |
| N | 0 | $0^\circ$ | $0^\circ$ | $0^\circ$ | $0^\circ$ |
| E | 90 | $0^\circ$ | $90^\circ$ | $180^\circ$ | $270^\circ$ |
| S | 180 | $0^\circ$ | $180^\circ$ | $0^\circ$ | $180^\circ$ |
| W | 270 | $0^\circ$ | $270^\circ$ | $180^\circ$ | $90^\circ$ |

Source: [18].

## 20.9 Concluding Remarks

We discussed the major techniques for determining a DOA in this chapter: (1) the Adcock array with Watson-Watt processing, which is an amplitude comparison method; (2) the pseudoDoppler method, which measures frequency changes as an antenna rotates in a circle; and (3) interferometry where the phase or time difference at two physically separated antennas is measured. The basic operating principles were presented for these three techniques. In particular, the implications on the characteristics of receivers that are used for this function were considered.

In the second part of the chapter we discussed the error sources in these three methods and included the requirements on the receivers employed. Phase and gain tracking as well as thermal noise are the principal requirements for the receivers. We saw that some of the error sources produce considerable errors in the DOA computation.

We also considered the use of a compressive receiver for rapid DOA determination across a wide bandwidth. The relative amplitude and phase in the two CxRx channels must remain constant for accurate DF with a twin channel receiver.

# Appendix 20.A RMS and RSS in Error Analysis

Some people get confused whether to use *root-mean-squared* (RMS) *or root sum square* (RSS) values in error analysis. We explain their relationship to one another here. These two are closely related and are used to estimate the variation of some quantity about some typical behavior. However, they are used to answer different questions and are not alternatives to each other.

The sample standard deviation in statistics is an RSS

$$\sigma = \sqrt{\frac{1}{N}[(x_1 - \mu)^2 + (x_2 - \mu)^2 + \ldots + (x_N - \mu)^2]} \qquad (20.A.1)$$

where $\mu$ represents the sample mean value. We can see that we have obtained the sum of the squares, taken their mean (by dividing by $N$), and then taken the square root. This RMS represents a typical error of each of the $N$ measurements; it gives an estimate of how far each measurement is from $\mu$. This is not so much an *overall error* as it is a *typical error*. In a sense it is *a localized error*, where the concept of an average value has meaning (such as the addition of thermal noise to a measurement).

The RSS is closely related, differing only in that there is no division by $N$. This type of combination is used when we are combining sources of errors to come up with some sort of indication of overall error, not to determine a typical error for a sample, as we did above.

For example, suppose you are trying to pinpoint your latitude/longitude coordinates. Let's suppose that your uncertainty in the east-west measurement is 1 km, and the uncertainty in the north-south measurement is only 0.4 km, maybe because you have a very good sighting of the North Star. Notice that instead of having a circle of uncertainty around the location, you have an ellipse. How could you estimate the typical distance error in this case? It is

$$\sqrt{(1\,\text{km})^2 + (0.4\,\text{km})^2} = 1.08\,\text{km}$$

Notice that the total error is always larger than any of the individual errors, and it is dominated by the largest error source (in this example, the east-west error). If the two error sources were equal, then this calculation would have become $\sqrt{2} \times 1\ \text{km} = 1.41\ \text{km}$.

Finally, notice that this RSS, or addition in quadrature, requires that the error sources be uncorrelated. If they are correlated, then we should take this into account. For example, suppose that our error sources are

east-west:        1.0 km

north-south:    0.4 km

NE-SW:         0.1 km, where the N/S component of this error is always in the opposite direction as the 0.4 km error, and the E/W component of this error is uncorrelated with the 1.0 km error

In this case the calculation leads to

$$\sqrt{(1.0)^2 + [0.4 - 0.1\sin(\pi/8)]^2 + [0.1\cos(\pi/8)]^2} = 1.0353\,\text{km}$$

By including the diagonal NE-SW error, our total error decreased! This may seem surprising, but remember that a component of it is anti-correlated with one of our original error sources and partially cancelled it out. Notice that in order to treat correlated errors we require information about their correlations or covariances.

Sometimes this is difficult information to obtain, and sometimes there's good reason to expect that the error sources are uncorrelated, in which case the simple RSS or add-in-quadrature formula is used.

# References

[1]      Poisel, R. A., *Electronic Warfare Target Location Methods*, 2nd Ed., Norwood, MA: Artech House, 2012, Ch. 3.

[2]      Hammerle, R., "Factors Limiting the Accuracy of Doppler and Adcock Direction Finding Systems," *Digest of IEE Colloquium on Passive Direction Finding,* No. 31, January 1989, pp. 3/1–3/13.

[3]      Poisel, R. A., *Antenna Systems and Electronic Warfare Applications*, Norwood, MA: Artech House, 2012, Ch. 6.

[4]      Poisel, R. A., *Introduction to Communication Electronic Warfare Systems*, 2nd Ed., Norwood, MA: Artech House, 2008, Section 8.2.5.

[5]      Gething, P. J. D., *Radio Direction Finding and Superresolution*, London: Peter Peregrinus, Ltd., 1991, p. 42.

[6]      Poisel, R. A., *Electronic Warfare Target Location Methods,* 2nd Ed., Norwood, MA: Artech House, 2012.

[7]      Gething, P. J. D., *Radio Direction Finding and Superresolution*, London: Peter Peregrinus, Ltd., 1991, p. 42.

[8]      Poisel, R. A., *Antenna Systems and Electronic Warfare Applications*, Norwood, MA: Artech House, 2012, Chs. 9 and 10.

[9]      Lipsky, S. E., *Microwave Passive Direction Finding*, New York: Wiley, 1987.

[10]    Abramowitz, M., and I. A. Stegun, *Handbook of Mathematical Functions*, New York: Dover, 1965, Eq. 4.4.54, p. 82.

[11]    Abramowitz, M., and I. A. Stegun, *Handbook of Mathematical Functions*, New York: Dover, 1965, Eq. 4.3.11, p. 72.

[12]    Torrieri, D. J., *Principles of Secure Communication Systems*, Norwood, MA: Artech House, 1992, p. 362.

[13]    Jenkins, H. H., *Small-Aperture Radio Direction-Finding*, Norwood, MA: Artech House, 1991, p. 139.

[14]    Poisel, R. A., *Introduction to Communication Electronic Warfare Systems*, 2nd Ed., Norwood, MA: Artech House, 2008, p. 340.
[15]    Poisel, R. A., *Introduction to Communication Electronic Warfare Systems*, 2nd Ed., Norwood, MA: Artech House, 2008, Ch. 8.
[16]    Jenkins, H. H., *Small-Aperture Radio Direction-Finding*, Norwood, MA: Artech House, 1991, Ch. 5
[17]    Daniels, W. D., M. Churchman, R. Kyle, and W. Skudera, "Compressive Receiver Technology," *Microwave Journal*, April 1986, pp. 175–185.
[18]    Poisel, R. A., *Electronic Warfare Target Location Methods*, 2nd Ed., Norwood, MA: Artech House, 2012, p. 176.

# Acronyms

| | |
|---|---|
| AC | alternating current |
| ACT | acoustic charge transport |
| ADC | analog to digital converter |
| AFC | automatic frequency control |
| AGC | automatic gain control |
| AJ | anti-jamming |
| ALR | average likelihood ratio |
| AM | amplitude modulation |
| AOA | angle of arrival |
| APSK | amplitude phase shift key |
| ASIC | application specific integrated circuit |
| ASK | amplitude shift key |
| AWG | additive white Gaussian |
| AWGN | additive white Gaussian noise |
| | |
| BB | baseband |
| BER | bit error rate |
| BJT | bipolar junction transistor |
| BPAM | binary pulse amplitude modulation |
| BPF | bandpass filter |
| bps | bits per second |
| BPSK | binary phase shift key |
| BW | bandwidth |
| BWER | bandwidth enhancement ratio |
| | |
| $C/I$ | carrier to interference |
| C2 | command and control |
| CAE | computer-aided engineering |
| CDMA | code division multiple access |
| CE | common emitter |
| CFIR | compensating finite impulse response |
| CIC | cascaded integrated comb |
| CM | collection management |
| CMOS | complementary metal oxide semiconductor |
| CNR | carrier to noise ratio |
| COA | course of action |
| cps | chips per second |
| CRT | cathode ray tube |
| CS | common source |

| | |
|---|---|
| CW | continuous wave |
| CxRx | compressive receiver |
| | |
| DAC | digital to analog converter |
| dB | decibel |
| DC | direct current |
| DCO | digitally controlled oscillator |
| DCR | direct conversion radio |
| DDC | direct digital converter |
| DDL | dispersive delay line |
| DDR | digital drop receiver |
| DDS | digital data synthesizer |
| DF | direction finding |
| DFT | discrete Fourier transform |
| DMA | direct memory access |
| DNL | differential non-linearity |
| DOA | direction of arrival |
| DPSK | differential phase shift key |
| DSB | double sideband |
| DSL | digital subscriber line |
| DSP | digital signal processor |
| DSSS | direct sequence spread spectrum |
| | |
| EA | electronic attack |
| ECCM | electronic counter-counter measures |
| EDAC | error detection and correction |
| EM | electromagnetic |
| EMS | electromagnetic spectrum |
| ENOB | effective number of bits |
| EP | electronic protect |
| ES | electronic support |
| EW | electronic warfare |
| | |
| FBC | filter bank combiner |
| FCC | federal communications commission |
| FDD | frequency division duplex |
| FDM | frequency division multiplex |
| FDMA | frequency division multiple access |
| FEC | forward error correction |
| FET | field effect transistor |
| FFH | fast frequency hopping |
| FFHSS | fast frequency hopping spread spectrum |
| FFT | fast Fourier transform |

| | |
|---|---|
| FHSS | frequency hopping spread spectrum |
| FIR | finite impulse response |
| FM | frequency modulation |
| FSK | frequency shift keying |
| FT | Fourier transform |
| | |
| GaAs | gallium arsenide |
| GBW | gain bandwidth product |
| GHz | gigahertz ($10^9$ hertz) |
| GMSK | Gaussian filtered minimum shift keying |
| GSM | global system for mobile communications |
| | |
| HD3 | third order harmonic distortion |
| HF | high frequency |
| HT | Hilbert transform |
| Hz | hertz |
| | |
| IC | integrated circuit |
| ICI | inter-channel interference |
| IDT | interdigital transducer |
| IF | intermediate frequency |
| IFFT | inverse fast Fourier transform |
| IIP3 | third order input intercept point |
| IRR | image rejection ratio |
| IIR | infinite impulse response |
| IMD | intermodulation distortion |
| IMD3 | third-order intermodulation distortion |
| INL | integral nonlinearity |
| IO | information operations |
| IP | intercept point |
| ISI | inter-symbol interference |
| IVGA | input variable gain amplifier |
| IW | information warfare |
| | |
| JFET | junction field effect transistor |
| | |
| kHz | kilohertz ($10^3$ hertz) |
| | |
| LAN | local area network |
| LC | long convolver |
| LF | loop filter |
| LFSR | linear feedback shift register |
| LM | long multiplier |

| | |
|---|---|
| LMR | land mobile radio |
| LNA | low noise amplifier |
| LO | local oscillator |
| LOG | logarithmic |
| LP | lowpass |
| LPD | low probability of detection |
| LPE | low probability of exploitation |
| LPF | lowpass filter |
| LPI | low probability of intercept |
| LPTV | linear periodically time variant |
| lsb | least significant bit |
| LSB | lower sideband |
| LTE | long term evolution |
| LTI | linear time invariant |
| LTV | linear time variant |
| LUT | look-up table |
| | |
| MAC | multiplication and accumulation |
| MDS | minimum detectable signal |
| MEM | microelectromechanical |
| MESFET | metal-semiconductor field effect transistor |
| MFSK | multiple frequency shift keying |
| MHz | megahertz ($10^6$ hertz) |
| MIMI | multiple-input multiple-output |
| MOS | metal oxide semiconductor |
| MOSFET | metal oxide semiconductor field effect transistor |
| msb | most significant bit |
| MSK | minimum shift keying |
| MT | multitone |
| | |
| NAI | named area of interest |
| NB | narrowband |
| NCO | numerically controlled oscillator |
| NF | noise figure |
| NPO | negative-positive 0 ppm/°C |
| NPR | noise power ratio |
| | |
| OFDM | orthogonal frequency division multiplexing |
| OIP3 | third order output intercept point |
| OOK | on-off keying |
| OQPSK | offset quadrature phase shift keying |
| OVGA | output variable gain amplifier |

| | |
|---|---|
| PA | power amplifier |
| PAM | pulse amplitude modulation |
| PAN | personal area network |
| PBD | partial-band detection |
| PBN | partial band noise |
| PD | phase detector |
| pdf | probability density function |
| PLC | power-line communications |
| PLL | phase locked loop |
| PM | phase modulation |
| PMR | private mobile radio |
| PN | pseudo-noise |
| POI | probability of intercept |
| PP | peak-to-peak |
| ppm | parts per million |
| PROM | programmable read-only memory |
| psd | power spectral density |
| PSK | phase shift key |
| PSTN | public switched telephone network |
| PWD | pulse width demodulator |
| PWM | pulse width modulation |
| | |
| QAM | quadrature amplitude multiplex |
| QPSK | quadrature phase shift key |
| | |
| R&S | reconnaissance and surveillance |
| RAC | reflective array compressive |
| RCU | receiver control unit |
| RF | radio frequency |
| RFC | radio frequency choke |
| RFIC | radio frequency integrated circuit |
| RMS | root mean square |
| ROM | read-only memory |
| rps | radians per second |
| RSS | root-sum square |
| RSSI | received signal strength indicator |
| Rx | receiver |
| | |
| SAR | synthetic aperture radar |
| SAW | surface acoustic wave |
| SC | suppressed carrier |
| SDE | stochastic differential equation |
| SDMA | spatial division multiple access |

| SDR   | software defined radio |
| SDU   | spectral display unit |
| SFDR  | spur-free dynamic range |
| SFHSS | slow frequency hopping spread spectrum |
| SH    | shear horizontal |
| SHF   | slow frequency hopping |
| SHF   | super high frequencies |
| SI    | statistically independent |
| SINAD | signal to noise and distortion ratio |
| SIR   | specific information request |
| SLO   | swept local oscillator |
| SNR   | signal to noise ratio |
| SOI   | signal of interest |
| SOR   | specific operational requirements |
| SoS   | system on silicon |
| sps   | samples per second |
| SS    | spread spectrum |
| sss   | strict-sense stationary |

| T/H   | track and hold |
| TAI   | targeted areas of interest |
| TCXO  | temperature compensated crystal oscillator |
| TDD   | time division duplex |
| TDM   | time division multiplex |
| TDMA  | time division multiple access |
| THSS  | time hopping spread spectrum |
| TLT   | transmission line transformer |
| TOA   | time of arrival |
| TRF   | tuned radio frequency |
| TWT   | traveling wave tube |

| UHF   | ultra high frequency |
| USB   | upper sideband |
| UWB   | ultrawideband |

| VCO   | voltage controlled oscillator |
| VGA   | variable gain amplifier |
| VHF   | very high frequency |
| VLSI  | very large-scale integration |
| VSWR  | voltage standing wave ratio |

| WB    | wideband |
| WLAN  | wireless local area network |

wss        wide-sense stationary

# Index